

INDOLE ARYLATION IN TRYPTOPHAN
RESIDUES: DEVELOPMENT OF NEW
CHEMICAL METHODOLOGIES, SYNTHETIC
STUDIES AND BIOLOGICAL EVALUATION
OF MODIFIED PEPTIDES
VOLUME I

Lorena Mendive Tapia

TESIS CIENCIAS DE LA SALUD 2016-2017

Premios Enrique Fuentes Quintana de Tesis Doctorales

 funcas

PREMIOS
ENRIQUE
FUENTES
QUINTANA

2018

**INDOLE ARYLATION IN TRYPTOPHAN
RESIDUES: DEVELOPMENT OF NEW
CHEMICAL METHODOLOGIES,
SYNTHETIC STUDIES AND
BIOLOGICAL EVALUATION
OF MODIFIED PEPTIDES**

VOLUME I

Lorena Mendive Tapia

 funcas

Funcas

PATRONATO

ISIDRO FAINÉ CASAS
JOSÉ MARÍA MÉNDEZ ÁLVAREZ-CEDRÓN
FERNANDO CONLLEDO LANTERO
CARLOS EGEA KRAUEL
MIGUEL ÁNGEL ESCOTET ÁLVAREZ
AMADO FRANCO LAHOZ
MANUEL MENÉNDEZ MENÉNDEZ
PEDRO ANTONIO MERINO GARCÍA
ANTONIO PULIDO GUTIÉRREZ
VÍCTORIO VALLE SÁNCHEZ
GREGORIO VILLALABEITIA GALARRAGA

DIRECTOR GENERAL

CARLOS OCAÑA PÉREZ DE TUDELA

Impreso en España
Edita: Funcas

Caballero de Gracia, 28, 28013 - Madrid
© Funcas

Todos los derechos reservados. Queda prohibida la reproducción total o parcial de esta publicación, así como la edición de su contenido por medio de cualquier proceso reprográfico o fónico, electrónico o mecánico, especialmente imprenta, fotocopia, microfilm, *offset* o mimeógrafo, sin la previa autorización escrita del editor.

ISBN (obra completa): 978-84-17609-07-8
ISBN (volumen I): 978-84-17609-08-5
ISBN (digital): 978-84-17609-11-5
Depósito legal: M-38987-2018
Maquetación: Funcas
Imprime: Cecabank

Esta tesis doctoral ha sido distinguida con el
PREMIO ENRIQUE FUENTES QUINTANA DE TESIS DOCTORALES,
CATEGORÍA DE CIENCIAS DE LA SALUD,
en la convocatoria 2016-2017

Tesis doctoral presentada en la
Universitat de Barcelona
Departament de Química Orgànica

Directores de la tesis:
Rodolfo Lavilla Grifols
Fernando Albericio Palomera

A mi familia

*We had a lot of sorrow, a lot of fear, and a lot of shame.
But I never regretted it, and I never envied anyone...And if we
haven't had our misfortunes, we wouldn't have been better off.
It would have been worse. Because in that case, there wouldn't
have been any happiness. And there wouldn't have been any hope.*

Andrej Tarkovsky (Stalker, 1979)



VOLUME I



AGRADECIMIENTOS

Ya por fin llegando al final de este trayecto llamado tesis doctoral es inevitable echar un vistazo atrás para ver el recorrido. Partiendo de un objetivo inicial específico, este trabajo se ha ido conformando y creciendo en base a su entorno e inevitablemente ha ido adoptando las huellas de todos los que han pasado por ella. *Rodolfo y Fernando*, mis directores de tesis, y *Marc Vendrell*, supervisor durante mi estancia en Edimburgo, fueron los que marcaron el camino con su experiencia y buenas indicaciones. Agradecer al Instituto de Investigación Biomédica (IRB) y al Parque Científico de Barcelona (en especial a *Eva Poca*, *Esther Zurita*, *Marta Vilaseca*, *M^a del Mar Vilanova*, *Jesús García* y miembros de la administración IRB) y al Queen's Medical Research Institute (University of Edinburgh) por su apoyo para realizar este trabajo.

Gracias a mis compañeros de mi primer laboratorio durante la tesis (*Miriam*, *Marta*, *Iván*, *Vida*, *Ximena*, *Juan*, *Gerardo*, *Lidia*, *Ramón*, *Hortensia*, *Sveta*, *Ramón*, *Pau*), de Biosyner-UQC (*Unai*, *Marta M.*, *Marta B.*, *Sergi*, *Jose*, *Charo*, *Ulduz*, *Marc*, *Nicola*, *Kranti*, *Sara*, *Sandra*, *Arantxa*, *Esther*, *Samantha*), del nuevo ChemBiolab (*Helena*, *Laia*, *Jesús*, *Álex*) y de alrededores (*Alejandro*, *Patricia* y *Júlia*) por aportarme siempre buenos consejos, risas y apoyo cuando lo necesité, y también a *Marc V.* y *Antonio* por darme ese soplo de aire fresco edimburgués. *Gabriela*, *Jordi*, *Óscar*, *Albert*, gracias por todo lo compartido y por siempre estar allí, llueve o truene.

Familia, sois la constante que rige todos mis senderos, un maravilloso microcosmos que siempre está presente en mis pensamientos y al que debo agradecer cada paso que doy. *Benji*, gracias por ser mi guía, mi compañero de juegos, en este y en los nuevos caminos que nos vienen por delante.

VOLUME I

AGRADECIMIENTOS	13
ANNEX	21
ANNEX 1. ABBREVIATIONS AND ACRONYMS	23
ANNEX 2. TABLES OF REAGENTS FOR SOLID-PHASE PEPTIDE SYNTHESIS	24
INTRODUCTION AND OBJECTIVES	29
GENERAL INTRODUCTION	31
C-2 ARYLATION OF INDOLE THROUGH METAL-CATALYZED C-H ACTIVATION	39
PEPTIDE-BASED IMAGING PROBES	41
BIARYL PEPTIDIC TOPOLOGIES. STAPLED PEPTIDES	44
C-H OXIDATIVE MODIFICATION OF TRP-BASED DKPS	48
OBJECTIVES	50
REFERENCES	53
CHAPTER 1. C-2 ARYLATION OF TRP AMINO ACIDS THROUGH PD-CATALYZED C-H ACTIVATION	57
PUBLICATION I. Synthesis and biological evaluation of a postsynthetically modified Trp-based diketopiperazine	59
PUBLICATION II. Synthesis of C-2 arylated tryptophan amino acids and related compounds through palladium-catalyzed C–H activation	73
PUBLICATION III. Enhanced antimicrobial activity of a peptide derived from human lysozyme by arylation of its tryptophan residues	91
CHAPTER 2. SPACER-FREE TRP-BODIPY FLUOROGEN FOR PEPTIDE-BASED IMAGING PROBES	105
PUBLICATION IV. Spacer-free BODIPY fluorogens in antimicrobial peptides for direct imaging of fungal infection in human tissue	107

PUBLICATION V. A Trp-BODIPY cyclic peptide for fluorescence labelling of apoptotic bodies	129
PUBLICATION VI. A Trp-BODIPY fluorogenic amino acid to label peptides for enhanced live-cell fluorescence imaging	147
CHAPTER 3. BIARYL PEPTIDIC TOPOLOGIES THROUGH PD-CATALYZED C-H ACTIVATION REACTIONS BETWEEN TRP AND PHE/TYR RESIDUES	197
PUBLICATION VII. New peptide architectures through C–H activation stapling between tryptophan–phenylalanine/tyrosine residues	199
PUBLICATION VIII. Constrained cyclopeptides: biaryl formation through Pd-catalyzed C-H activation in peptides—structural control of the cyclization vs. cyclodimerization outcome	233
CHAPTER 4. CU(II) CROSS-DEHYDROGENATIVE CYCLIZATION OF TRP-BASED DKPS	251
PUBLICATION IX. Access to new scaffolds through cross dehydrogenative couplings on tryptophan-based diketopiperazines	253
RESULTS AND DISCUSSION	267
CHAPTER 1. C-2 ARYLATION OF TRP AMINO ACIDS THROUGH PD-CATALYZED C-H ACTIVATION	269
CHAPTER 2. SPACER-FREE TRP-BODIPY FLUOROGEN FOR PEPTIDE-BASED IMAGING PROBES	273
CHAPTER 3. BIARYL PEPTIDIC TOPOLOGIES THROUGH PD-CATALYZED C-H ACTIVATION REACTIONS BETWEEN TRP AND PHE/TYR RESIDUES	280
CHAPTER 4. CU(II) CROSS-DEHYDROGENATIVE CYCLIZATION OF TRP-BASED DKPS	289
REFERENCES	293
CONCLUSIONS (IN SPANISH)	295

PERSONAL CONTRIBUTION TO THE PUBLICATIONS (IN SPANISH)	301
---	------------

ANNEX 3. SUMMARY OF INTRODUCTION AND OBJECTIVES (IN SPANISH)	307
---	------------

VOLUME II

ANNEX 4. SUMMARY OF RESULTS AND DISCUSSION (IN SPANISH)	333
--	------------



ANNEX

ANNEX 1. ABBREVIATIONS AND ACRONYMS

AA	Amino acid	MDM2	Mouse double minute 2 homolog
ACN	Acetonitrile	Met	Metal
Act	Activator	MIC	Minimal inhibitory concentration
Ar	Aryl	MRI	Magnetic resonance imaging
BL2	Burkitt's lymphoma cells	MW	Microwave
BODIPY	4,4-Difluoro-4-bora-3a,4a-diaza-s-indacene	NMA	N-methylaniline
BQ	Benzoquinone	NMM	N-methylmorpholine
CD	Circular dichroism	NMR	Nuclear magnetic resonance
CDC	Cross-dehydrogenative coupling	2-NO₂BzOH	2-nitrobenzoic acid
CMD	Concerted metallation-deprotonation	NOE	Nuclear Overhauser effect
DCM	Dichloromethane	NOTA	2-[4,7-bis(carboxymethyl)-1,4,7-triazonan-1-yl]acetic acid
DDC	Sodium diethyldithiocarbamate	PBS	Phosphate buffered saline
DDQ	2,3-Dichloro-5,6-dicyano-1,4-benzoquinone	PC	Phosphatidylcholine
DIEA	N,N-diisopropylethylamine	PEG	Polyethylene glycol
DKP	Diketopiperazine	PET	Positron emission tomography
DLP	Dilauroyl peroxide	PG	Protecting group
DMF	N,N-Dimethylformamide	PIFA	Bis(trifluoroacetoxy)iodobenzene
DMSO	Dimethyl sulfoxide	PPI	Protein-protein interaction
DOTA	2-[4,7,10-tris(carboxymethyl)-1,4,7,10-tetrazacyclododec-1-yl]acetic acid	PS	Phosphatidylserine
DTBP	Di-tert-butyl peroxide	QY	Quantum yield
DTPA	Diethylenetriaminepentaacetic acid	RCM	Ring-closing metathesis
ε	Molar extinction coefficient	RFP	Red fluorescent protein
EC₅₀	Half maximal effective concentration	S_NAr	Aromatic nucleophilic substitution
Emac	Macrocyclization efficiency index	SPECT	Single-photon emission computed tomography
Eq	Equivalent	SPPS	Solid-phase peptide synthesis
FDA	Food and drug administration	TIS	Triisopropylsilane
GUV	Giant unilamellar vesicle	TBHP	Tert-butyl hydroperoxide
HPLC	High performance liquid chromatography	TEA	Triethylamine
HPLC-MS	High performance liquid chromatography-mass spectrometry	TFA	Trifluoroacetic acid
HUVEC	Human umbilical vein endothelial cells	THF	Tetrahydrofuran
IPA	Invasive pulmonary aspergillosis	tRNA	Transfer ribonucleic acid
KDa	Kilodalton		

ANNEX 2. TABLES OF REAGENTS FOR SOLID-PHASE PEPTIDE SYNTHESIS

Table 1.

Amino acid structures and nomenclatures

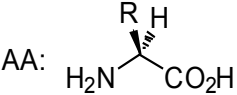

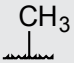
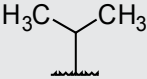
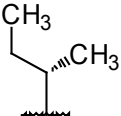
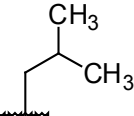
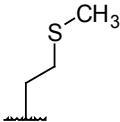
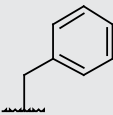
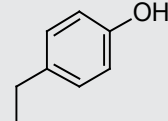
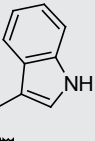
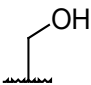
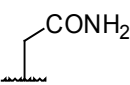
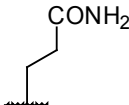
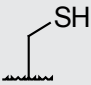
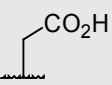
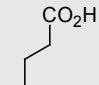
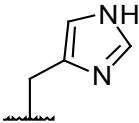
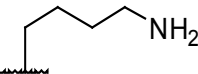
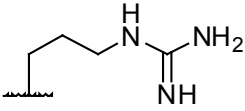
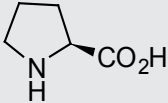
AA: 		
R:  AA: Glycine (Gly, G)	R:  AA: Alanine (Ala, A)	R:  AA: Valine (Val, V)
R:  AA: Isoleucine (Ile, I)	R:  AA: Leucine (Leu, L)	R:  AA: Methionine (Met, M)
R:  AA: Phenylalanine (Phe, F)	R:  AA: Tyrosine (Tyr, Y)	R:  AA: Tryptophan (Trp, W)
R:  AA: Serine (Ser, S)	R:  AA: Asparagine (Asn, N)	R:  AA: Glutamine (Gln, Q)
R:  AA: Cysteine (Cys, C)	R:  AA: Aspartic acid (Asp, D)	R:  AA: Glutamic acid (Glu, E)
R:  AA: Histidine (His, H)	R:  AA: Lysine (Lys, K)	R:  AA: Arginine (Arg, R)
	 AA: Proline (Pro, P)	

Table 2.

Protecting groups

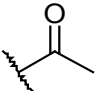
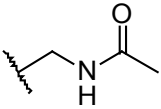
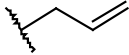
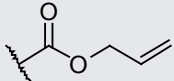
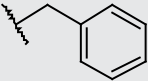
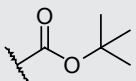
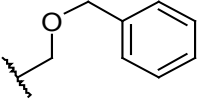
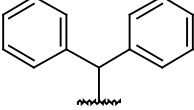
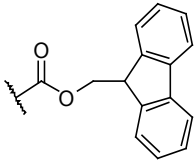
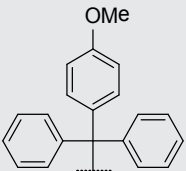
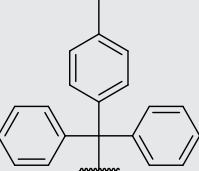
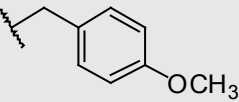
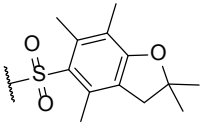
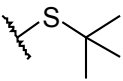
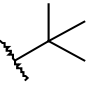
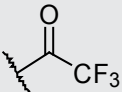
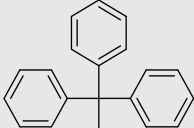
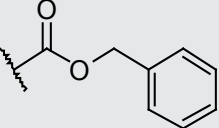
 <p>Acetyl (Ac)</p>	 <p>Acetamidomethyl (Acm)</p>	 <p>Allyl (Al)</p>
 <p>Allyloxycarbonyl (Alloc)</p>	 <p>Benzyl (Bn)</p>	 <p>tert-Butyloxycarbonyl (Boc)</p>
 <p>Benzyloxymethyl (Bom)</p>	 <p>Diphenylmethyl (Dpm)</p>	 <p>9-Fluorenylmethoxycarbonyl (Fmoc)</p>
 <p>Monomethoxytrityl (Mmt)</p>	 <p>4-Methyltrityl (Mtt)</p>	 <p>p-Methoxybenzyl (Mob)</p>
 <p>2,2,4,6,7-Pentamethyl-2,3-dihydrobenzofuran-5-sulfonyl (Pbf)</p>	 <p>tert-Butylmercapto (StBu)</p>	 <p>tert-Butyl (tBu)</p>
 <p>Trifluoroacetyl (Tfa)</p>	 <p>Trityl (Trt)</p>	 <p>Benzyloxycarbonyl (Z)</p>

Table 3.

Coupling reagents and additives

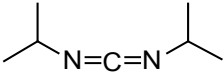
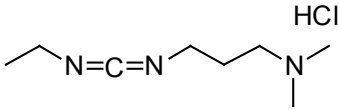
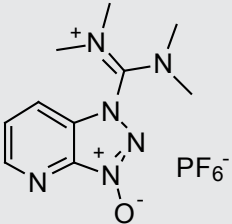
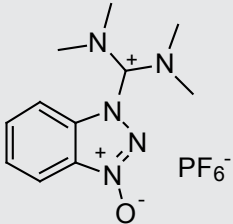
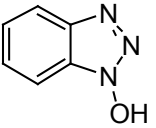
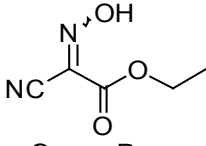
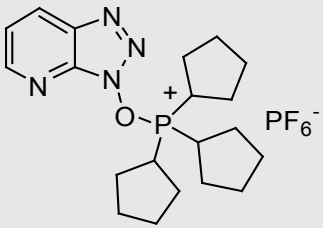
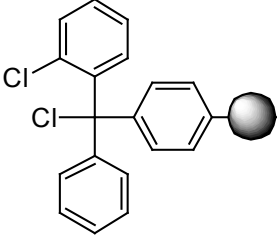
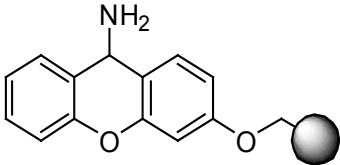
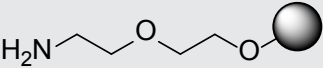
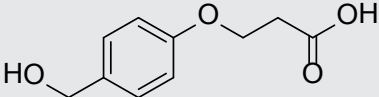
 <p><i>N,N'</i>-Diisopropylcarbodiimide (DIC)</p>	 <p><i>N</i>-(3-Dimethylaminopropyl)- <i>N'</i>-ethylcarbodiimide hydrochloride (EDC·HCl)</p>
 <p>1-[Bis(dimethylamino)methylene]-1<i>H</i>- 1,2,3-triazolo[4,5-<i>b</i>]pyridinium 3-oxide hexafluorophosphate (HATU)</p>	 <p>3-[Bis(dimethylamino)methyl]- 3<i>H</i>-benzotriazol-1-yl hexafluorophosphate (HBTU)</p>
 <p>1-Hydroxybenzotriazole (HOBt)</p>	 <p>OxymaPure</p>
 <p>(7-Azabenzotriazol-1-yloxy) tripyrrolidinophosphonium hexafluorophosphate (PyAOP)</p>	

Table 4.

Resins and linkers

 <p>2-Chlorotrityl chloride resin (2-CTC)</p>	 <p>Sieber amide resin</p>
 <p>TentaGel S-NH₂ resin</p>	 <p>3-(4-Hydroxymethylphenoxy) propionic linker (AB)</p>



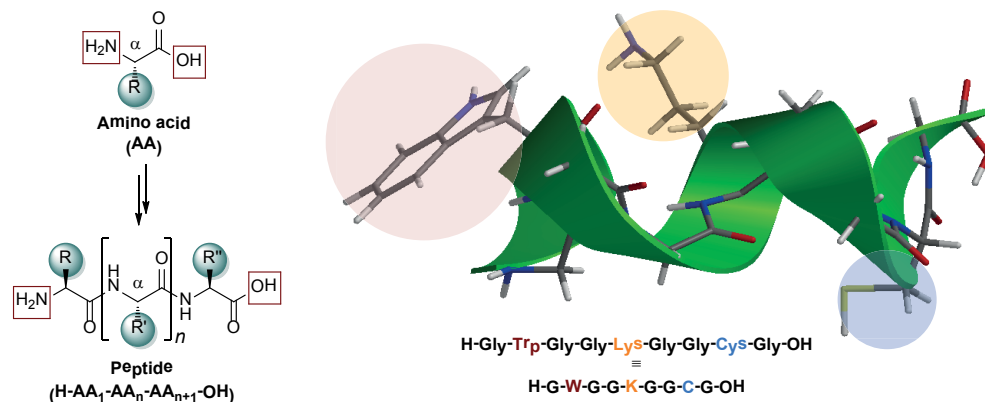
INTRODUCTION AND OBJECTIVES

GENERAL INTRODUCTION¹

Peptides are naturally occurring biopolymeric chains comprised of 100 or less amino acid monomers that play key roles in the regulation and function of a plethora of physiological and biochemical processes (*e.g.*, hormones, neurotransmitters, cytokines, growth factors, etc.) and represent important scaffolds in organic and medicinal chemistry (Sewald and Jakubke, 2002; Wade, 2010). Each residue contains an amine and a carboxylic acid function, along with a side-chain (R group) specific to each amino acid, and are linked together through amide bonds (Fig. 1). Basically, proteinogenic peptides and proteins are comprised of 20 different α -(L)-amino acids, which are designated by one/three letter codes, whereas synthetic peptides and many secondary metabolites of peptidic nature do not have this restriction. Thus, linear peptides are normally described with an N→C abbreviation code sequence and, if necessary, side-chain functionalities are also displayed in brackets.

Figure 1.

General representation of peptides (left) and illustrative example (right)



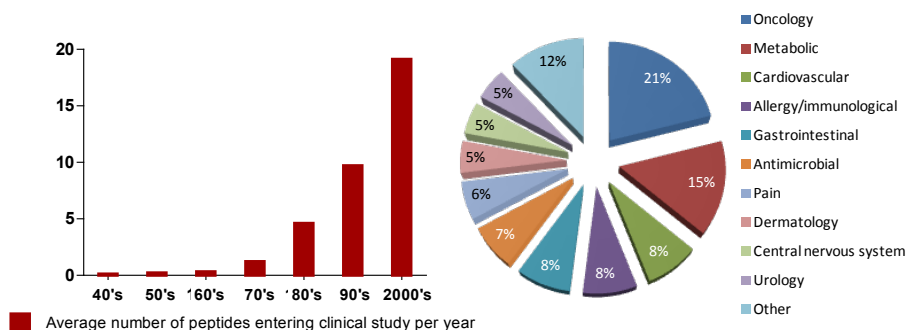
Source: Own elaboration.

¹ The present thesis has been developed at the Institute for Research in Biomedicine (IRB) located in the Parc Científic de Barcelona (PCB) (January 2013-December 2015) and in the Parc Científic de Barcelona (January 2016-December 2016). This work was supported by DGICYT—Spain (projects BQU-CTQ2012-30930 and CTQ2015-67870-P), Generalitat de Catalunya (2014 SGR 137) and Institute for Research in Biomedicine Barcelona (Spain). The PhD student has been supported by a “Formación de Profesorado Universitario” (FPU) fellowship from the Ministerio de Educación, Cultura y Deporte—Spain (MECD).

The use of peptides as therapeutics has emerged as a field in continuous expansion and a valuable source of new drugs (Fosgerau and Hoffmann, 2015; Tsomaia, 2015). The interest of peptides as therapeutic agents relies on their protein-like molecular topology and dimensions, which confer them great specificity, tolerability and potency towards biological targets (*e.g.*, protein-protein interactions, receptors, etc.). Since its outburst in the late 1990s and 2000s, the peptide market is growing steadily (Fig. 2, left). Thus, the global peptide therapeutic market was valued at US\$ 20.0 billion in 2015 and is estimated to reach US\$ 23.7 billion in 2020 (Transparency Market Research, 2015). In 2015, more than 60 US Food and Drug Administration (FDA)-approved peptide medicines were launched on the market, with other many in clinical and preclinical phases, being metabolic diseases and oncology the main therapeutic areas (Fig. 2, right). Some representative commercialized peptide drugs are disclosed in Table 1 (Kaspar and Reichert, 2013; Wishart *et al.*, 2006).

Figure 2.

Average number of peptides entering clinical study per year (left) and commercialized peptide drugs distributed by therapeutic areas from a 2012 report (right) (Tsomaia, 2015)



Source: Own elaboration.

The use of peptides as drugs has been hampered by their propensity to be degraded by proteases and then eliminated by the kidneys or liver (short circulating plasma half-life), also often displaying aggregation and low permeability to cross-membranes (the vast majority of peptides are directed towards extracellular targets). Indeed, few oral administrated peptide drugs are present in the market, being intravenous, subcutaneous or intramuscular administrations the preferential routes in order to avoid hepatic or gastrointestinal enzymatic early degradation (Diao and Meibohm, 2013). Nevertheless, peptide drugs are progressively being more sophisticated and new approaches and strategies are emerging in order to overcome these problems.

The production of therapeutic peptides is achieved through chemical synthesis, recombinant microorganisms or by extraction from their natural sources. Particularly, the

Table 1.

Selection of commercialized peptide drugs (1984-2014)

Company	Brand name	Generic name	Mechanism of action	FDA approval	Approved indication	Administration route
GlaxoSmithKline	Tanzeum*	Albiglutide	GLP-1 receptor agonist	2014	Type 2 diabetes	Subcutaneous
Novartis	Signifor*	Pasireotide	Somatostatin receptor agonist	2012	Cushing's disease	Subcutaneous, intramuscular
Ironwood Pharmaceuticals	Linzzess*	Linaclotide	GC-C receptor agonist	2012	Chronic constipation	Oral
Novo Nordisk	Victoza*	Liraglutide	GLP-1 receptor agonist	2010	Type 2 diabetes	Subcutaneous
Beaufour Ipsen	Somatuline Depot*	Lanreotide	Somatostatin receptors inhibition	2007	Acromegaly, Neuroendocrine tumors	Subcutaneous
Amylin	Symlin*	Pramlintide	Amylin analogue	2005	Type 1 and 2 diabetes	Subcutaneous
Roche/Trimeris	Fuzeon*	Enfuvirtide	HIV-1 fusion inhibition	2003	Antiretroviral (HIV-1 infection)	Subcutaneous
Ferring	Minirin*	Desmopressin	AVPR2 receptor agonist	2002	Antidiuretic	Oral/nasal
Sanofi	Lantus*	Insulin glargine	Insulin receptor agonist	2002	Lowering of glucose levels	Subcutaneous
Medicines Co.	Angiomax*	Bivalirudin	Thrombin inhibitor	2000	Anticoagulant	Intravenous
Schering	Integrilin*	Eptifibatide	Integrin- $\alpha_{IIb}\beta_3$ inhibitor	1998	Platelet aggregation inhibition	Intravenous
Sandoz	Neoral*	Cyclosporine	Lymphocytes inhibition	1995	Immunosuppressant	Oral
Abbott Laboratories	Lupron*	Leuprolide	GnRH agonist	1985	Prostate cancer symptoms	Subcutaneous, intramuscular

Notes: GLP: glucagon-like peptide; GC-C: guanylate cyclase-C; HIV: human immunodeficiency virus; AVPR: arginine vasopressin receptor; GnRH: gonadotropin-releasing hormone.

Source: Own elaboration.

chemical synthesis of peptides can be performed on solution, solid-phase or through hybrid approaches.

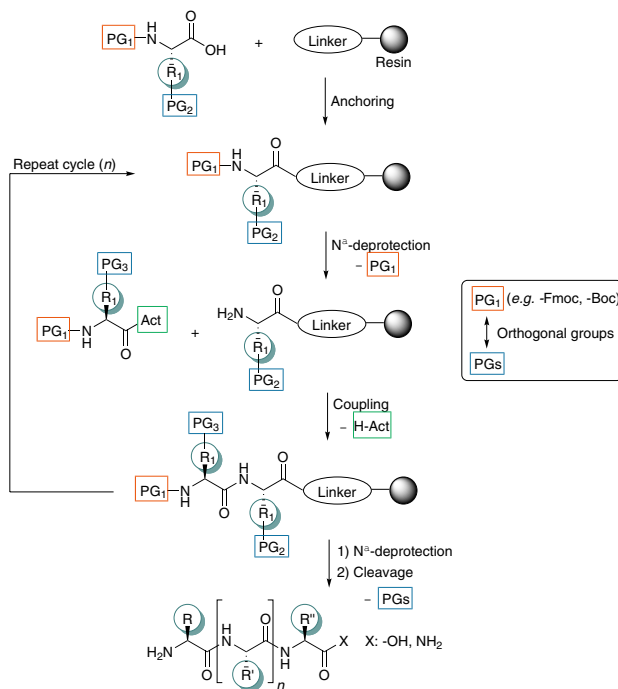
Solid-phase peptide synthesis (SPPS) is a methodology first described by Robert Bruce Merrifield in 1963, which consists on the covalent anchoring of a growing peptide sequence through its C-terminus carboxylic group to an insoluble polymeric resin via a linker functionality (Fig. 3). To form the amide bond, the nucleophilic amino function of the residue anchored to the resin needs to be deprotected in order to react with the carboxylic group of the second amino acid component, which is previously activated. In this manner, the anchored sequence is elongated by a series of N^α deprotection-coupling cycles. At the end of the synthesis,

the peptide is cleaved from the resin with concomitant removal of the existing side-chain protecting groups labile to the cleavage conditions. Depending on the N^α protecting group used, two main strategies of SPPS are described: Fmoc- (9-fluorenylmethoxycarbonyl-) and Boc- (*tert*-butoxycarbonyl-) based SPPS. For Fmoc-SPPS, piperidine is applied to remove the Fmoc-protecting group, whereas acidic conditions with trifluoroacetic acid (TFA) are used for the final peptide scission. Reactive side-chain functionalities are temporary protected with compatible or orthogonal groups (Isidro-Llobet, Alvarez and Albericio, 2009) capable to remain unaltered under Fmoc-protecting group removals, couplings conditions and, in some cases, cleavage of the peptide from the resin. The main advantage of solid-phase protocols over solution synthesis is the avoidance of purification steps during peptide elongation, as the excess of reagents and by-products are removed by simple elution. Besides, these syntheses can be performed manually or on automated solid-phase synthesizers.

The enhancement of the therapeutic utility of peptides and proteins can be tackled by a wide range of different strategies, based on specific modifications (*e.g.*, alterations based on metal coordination) (Mosquera *et al.*, 2013) in order to tune their functional or pharmacokinetic properties. Among other purposes, these changes are performed in order to increase the potency and/or selectivity for a specific substrate, modulate protein-protein interactions, design multifunctional peptides, target biological entities or visualize biological processes

Figure 3.

Schematic representation of SPPS. PGs: protecting groups; Act: activator



Source: Own elaboration.

(bioimaging). In general, these alterations can be performed on the amino and carboxylic terminal functions, side-chain positions, peptide backbone or by the entire replacement of specific amino acids. The site and method selection will be determined by the polipeptidic structure, function and specific purpose.

The increase of stability of peptides is normally correlated with better resistance to enzymatic degradation by minimizing peptidic bond cleavages. Strategies to increase stability include:

- Conformational restriction by cyclization, evolved from linkages between C-terminus to N-terminus, side-chain to N/C-terminus or side-chain to side-chain positions.
- Restriction of individual amino acid conformations that can favor the formation of turn structures by N^α-methylation, β-disubstitution or use of α, β-dehydro or cyclic (*e.g.*, proline) amino acids.
- Conjugation to polymers (*e.g.*, PEG) or polypeptide chains (*e.g.*, XTEN).
- Innovative formulations (*e.g.*, additives, encapsulation, implantable devices).
- Others: Hydrogen bond surrogates, D-amino acids, olefinic substitution, peptide mimetics, N-acetylation, C-amidation, carbonyl reduction, etc.

Selective modifications are also performed in order to modulate protein-protein interactions or increase the potency and/or selectivity by enhancing the molecular recognition for a specific receptor or substrate. Some approaches involve:

- Rigidification of a bioactive conformation for a specific target by the above mentioned cyclization modes. Particularly, stapled peptides, which are originated from selective non-amide bond connections between side-chains, have emerged as a breakthrough in the drug modulation field and several companies such as Aileron Therapeutics have developed therapeutic peptides based on this technique.
- Modification of the polipeptidic chain extension or sequence of residues.
- Replacement or modification of certain amino acids.

Regarding the use of unnatural amino acids, diverse strategies for the direct incorporation (genetically or chemically) of non-standard residues into peptides or proteins have been developed. Approaches focused on genetic code expansion in proteins are based on the site-specific incorporation of a non-proteinogenic amino acid (not genetically encoded) into a protein. This tool is based on the specific recognition of the unnatural amino acid in the cell by an orthogonal tRNA/aminoacyl tRNA synthase pair (from phylogenetically distant organisms) that directs its incorporation into a defined position in the encoded polypeptide chain, normally in response to a nonsense or frameshift codon located in the gene of interest. Numerous applications of this methodology have been reported regarding the exploration of protein structure and function as well as the regulation or change of protein activity (Chin, 2014; Davis and Chin, 2012; Xiao *et al.*, 2013; Wang *et al.*, 2001). Other methods for protein modification that do not alter the genetic code include: *in vitro* (cell-free) translation syntheses or the synthesis of proteins evolved from the replacement of a coded natural amino

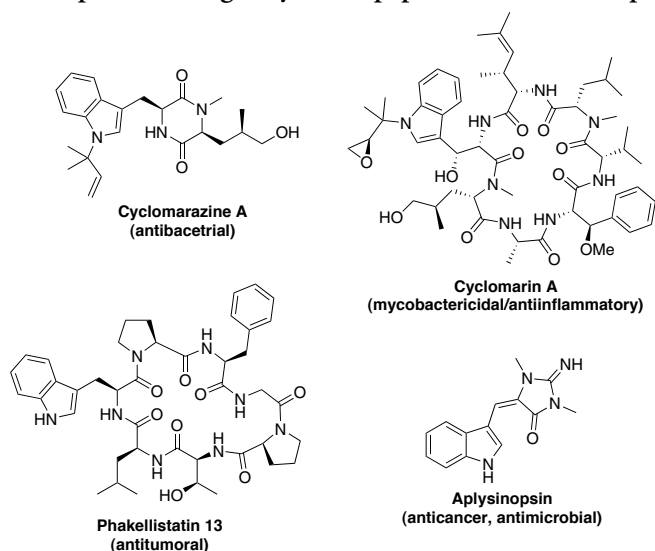
acid during translation by a similar non-proteinogenic amino acid via the cell incubation of this latter in the absence of the coded one (Hong, Kwon and Jewett, 2014). Site-specific chemical modifications on peptides can also be achieved by the direct incorporation of non-standard amino acids or site-selective modifications through chemical peptide syntheses in solution or solid-phase. Particularly, side-chain modification is carried out through different methodologies according to the functional group reactivity involved.

Indoles are π -excessive aromatic heterocyclic ring topologies present in many natural systems (Joule and Mills, 2010). Moreover, indole-containing molecules are valuable scaffolds widely found in drug discovery and in many other industrial applications (*e.g.*, dyes, herbicides, fungicides, perfumes, etc.) (Gribble, 2010). Particularly, tryptophan (Trp) is an essential indole-containing amino acid with key functional roles, present in many alkaloids, peptides and proteins (Fig. 4) (Alkhalaf, 2015; Higuchi and Kawasaki, 2005; Bialonska and Zjawiony, 2009). Although Trp is the lowest abundant member of the 20 canonical amino acids (around 1% in peptides and proteins), the high hydrophobicity and hydrogen-bond donor features of its side-chain enables interactions by non-covalent forces (*e.g.*, aromatic-aromatic, cation- π , etc.) with key roles in protein stability and recognition (Santiveri and Jiménez, 2010). Furthermore, the inherent reactivity of the indole moiety (*e.g.*, to electrophilic aromatic substitutions, oxidations, enzymatic modifications, etc.) makes Trp an interesting scaffold for chemical diversification.

Over the past decades, the development of methodologies based on transition metal-catalyzed cross-couplings for the formation of carbon-carbon or carbon-heteroatom bonds have brought significant advances in synthetic organic chemistry (De Meijere and Diederich,

Figure 4.

Representative examples of biologically active peptidic structures displaying Trp



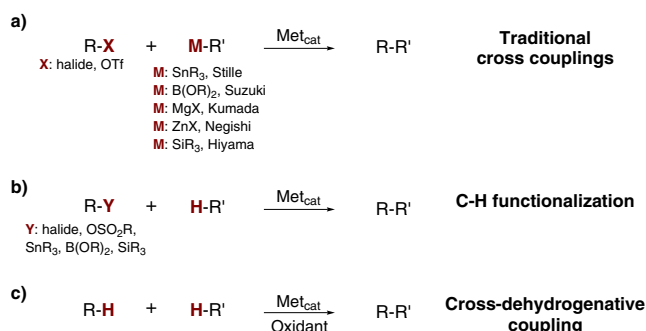
Source: Own elaboration.

2004). Classical cross-coupling methods for aryl-aryl bond formation rely on the reaction of an organometallic reagent (nucleophilic component) with a second compound containing an halide (or surrogate) substituent (electrophilic component). According to the transition metal source and the functional groups involved, different cross-coupling methods have been reported, including Stille, Suzuki, Kumada, Negishi and Hiyama reactions (Fig. 5a). These cross-couplings are frequently catalyzed by palladium (Ni, Ru and Ir, etc. are also reported) and in some cases in junction with a base (Suzuki and Hiyama couplings). The mechanism of these processes generally involves three main stages: oxidative addition, transmetallation (+isomerization) and reductive elimination (Fig. 6). First, the organic halide (R-X) coordinates the metal center through an oxidative addition to yield intermediate I, then the second coupling partner undergoes transmetallation to form intermediate II. Finally, reductive elimination of the two coupling reagents renders the R-R' product with concomitant regeneration of the catalyst. In some cases, an isomerization prior the reductive elimination occurs.

In the last decades, transition metal-catalyzed carbon-hydrogen (C-H) bond activation (or C-H functionalization) processes have undergone an explosive growth. In contrast to traditional methods, these reactions are based on the coupling of only one functionalized component, being the other partner a molecule reacting through a C-H bond (Yu and Shi, 2010). To overcome the ubiquity of C-H bonds, metal catalysis enables the selective activation of one C-H bond via the metal coordination (C-metal) and further functionalization by reaction with the electrophile (Fig. 5b). Thus, the chemical waste and the number of synthetic steps required for the C-C bond formation is reduced as the prefunctionalization of one coupling component is avoided. Moreover, double C-H activation processes (or cross-dehydrogenative couplings) rely on the selective construction of C-C linkages directly from two different C-H bonds under oxidative conditions (Fig. 5c). The main challenge of these methodologies again deals with the ubiquity of C-H bonds.

Figure 5.

Reported transition metal-catalyzed cross-coupling strategies for aryl-aryl bond formation

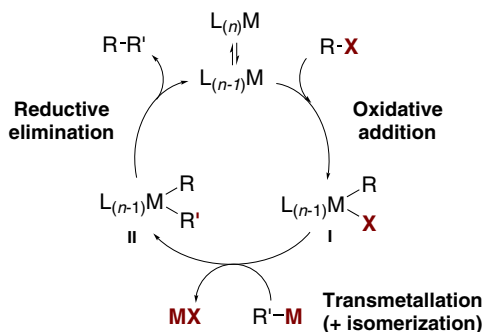


Source: Own elaboration.

C-H functionalization is a continuously growing field with remarkable applications in late-stage diversification and for the synthesis of biologically active compounds and other functional materials. Thus, since the first contributions reported in the end of the last century,

Figure 6.

General mechanism for traditional transition metal-catalyzed cross-coupling reactions

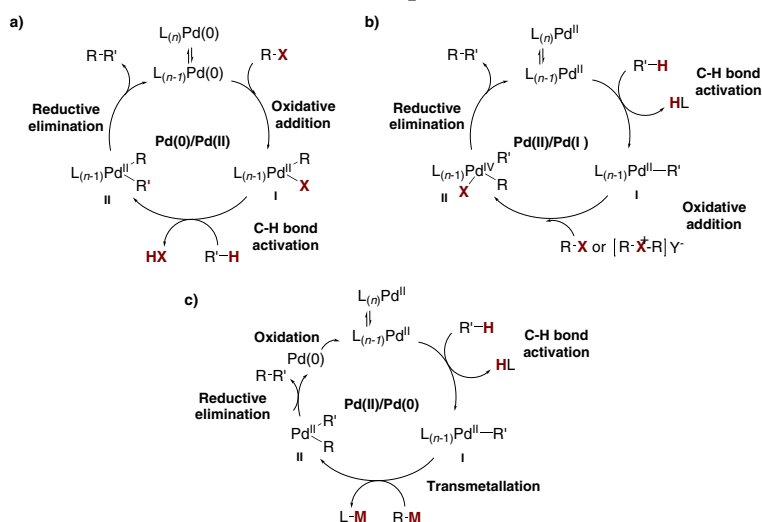


Source: Own elaboration.

the number of publications concerning C-H functionalization has significantly increased (Wencel-Delord and Glorius, 2013; White, 2012; Yamaguchi, Yamaguchi and Itami, 2012). Particularly, C-H arylations with Cu, Rh, Ru and Pd transition metals are reported, being the latter the most widely explored (Ackermann, 2009). Regarding the catalytic species involved and the reaction conditions (*e.g.*, substrate, solvent, ligands), there are three main general mechanisms reported for Pd-catalyzed C-H arylations (Fig. 7). The first mechanism shown in Fig. 7 is based on a Pd(0)/Pd(II) catalytic cycle. First, the cycle starts with the oxidative addition of R-X organic halide into the Pd(0) species to form Pd(II) intermediate I. Next, C-H

Figure 7.

General catalytic cycles for Pd-catalyzed C-H arylation reactions involving a) Pd(0)/Pd(II), b) Pd(II)/Pd(IV) or c) Pd(II)/Pd(0) species



Source: Own elaboration.

bond activation of R'-H takes place at the previous intermediate I by palladium coordination. Finally, C-C bond formation by reductive elimination from Pd(II) centre affords the R-R' compound with the recovery of Pd(0) species (Fig. 7a). The second catalytic cycle involves a Pd(II)/Pd(IV) mechanism (Fig. 7b). In this case, the electrophilic C-H bond activation of R'-H takes place first, followed by the oxidative addition of the organic halide to Pd(II) intermediate I to form the corresponding Pd(IV) species (II) and subsequent reductive elimination.

Additives such as Ag(I)-salts are reported to function as oxidants or halide scavengers to promote the reaction. Moreover, recently Larrosa and co-workers propose that Ag(I)-salts could carry out the C-H activation in Pd-catalyzed C-H functionalization reactions (Whitaker, Burés and Larrosa, 2016). Finally, the Pd(II)/Pd(0) catalytic cycle (Fig. 7c), mainly reported with boronic acids, includes an oxidant and is initiated by the electrophilic C-H bond activation of R'-H by the Pd(II) species, followed by a transmetalation with a metallic R-M derivative and subsequent reductive elimination to yield R-R' and Pd(0) species, which is oxidized to close the catalytic cycle.

In this context, we focused on the study of the following main topics:

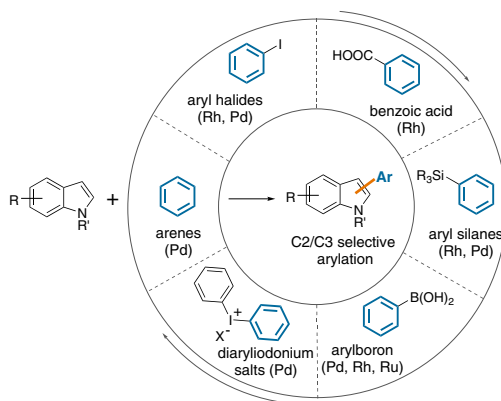
C-2 ARYLATION OF INDOLE THROUGH METAL-CATALYZED C-H ACTIVATION

Indole ring constitutes a class of nitrogen-containing heterocycle present in wide range of natural products and drugs. Therefore, the derivatization of this core arises as a powerful strategy for the modulation of the structure and bioactivity of potential pharmaceutical agents.

In this sense, 2-aryl indole derivatives appear as privileged scaffolds. As an alternative to standard methods, in the past few decades several strategies have been reported for the metal-catalyzed C-H arylation of indoles (Sandtorv, 2015; Yu and Shi, 2010). According to the nature

Figure 8.

Reported strategies of metal-catalyzed C-H arylation of indoles



Source: Own elaboration.

of the indole precursor, the coupling partner and the transition metal applied, the reported methodologies on this field can be classified in the following main groups: aryl halides (Rh, Pd), arenes (Pd), diaryliodonium salts (Pd), arylboron reagents (Pd, Rh, Ru), arylsilanes (Rh, Pd) and aromatic carboxylic acids (Rh) (Fig. 8).

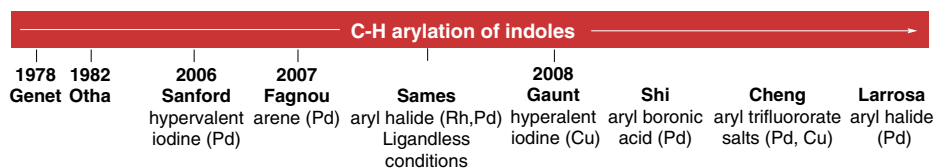
Some of the first pioneering work regarding the C-H activation of indoles appeared in the 80's with the work of Genet (Trost, Godleski and Genet, 1978) and Ohta (1989), among others (Fig. 9). Then, Grigg and co-workers disclosed in 1990 the first transition-metal catalyzed direct arylation of an indole with an aryl halide in an intramolecular mode using $\text{Pd}(\text{OAc})_2$ and PPh_3 as a ligand (Grigg *et al.*, 1990).

Nonetheless, it was not until the 2000s when this methodology showed a relevant progress (Fig. 9). Hence, in 2006 Sanford's group displayed a protocol under mild conditions with hypervalent iodine aryl iodonium salts and Pd(II) catalysis (Deprez *et al.*, 2006). Next, in 2007 Sames and co-workers presented a new arylation method for indoles with aryl halides, $\text{Pd}(\text{OAc})_2$ as the catalyst and CsOAc as a base under ligandless conditions (Wang, Gribkov and Sames, 2007). Interestingly, they evidenced a C-2/C-3 site-selectivity for the indole position according to the nature of the halide. Analogously to these results, in the same year Fagnou showed an oxidative methodology based on $\text{Pd}(\text{TFA})_2$ as catalyst directly connecting arenes to indoles (Stuart, Villemure and Fagnou, 2007). Moreover, in 2008 Gaunt described a copper(II) triflate-based arylation protocol of indoles with diaryliodonium triflates, where the protection of the NH-indole determines the C-2/C-3 indole selectivity (Phipps, Grimster and Gaunt, 2008).

Alternative coupling partners have also been published in the arylation of indole systems. Hence, Shi and co-workers (2008) arylated a series of indole derivatives with aryl boronic acids under $\text{Pd}(\text{OAc})_2$ catalysis, in an oxygen atmosphere in acetic acid (Yang *et al.*, 2008). The same year, Cheng's group showed the use of aryltrifluoroborate salts in the presence of $\text{Pd}(\text{OAc})_2$ and $\text{Cu}(\text{OAc})_2$ in air (Zhao, Zhang and Cheng, 2008). Overall, direct C-H activation protocols have emerged as a breakthrough in the field since these methodologies circumvent the use of prefunctionalized organometallic precursors.

Figure 9.

Historic diagram of the most illustrative intermolecular precedents on the C-H arylation of indoles



Source: Own elaboration.

Importantly, indole ring is present as part of the side-chain of Trp amino acid, which appears as a key amino acid due to its specific biological interactions together with its limited presence in peptides and proteins (around 1%) and its photo-electronic properties. By the

time where the present project thesis was developed, very few precedents on the direct C-2-arylation of Trp amino acid had been disclosed. The synthesis of 2-aryl-Trp derivatives by direct arylation was only reported by classical Pd-mediated cross-coupling methods using Suzuki–Miyaura type reactions or through Ru-based catalytic C-H bond formation processes (Ackermann and Lygin, 2011; Colletti *et al.*, 2000); none of them being ideal in terms of applicability and experimental requirements, since these protocols demanded the use of protected Trp amino acid under harsh coupling conditions.

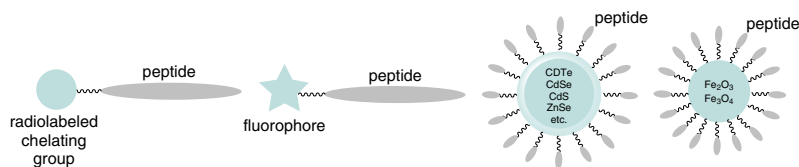
PEPTIDE-BASED IMAGING PROBES

Peptides are chemical entities allocated in a privileged chemical space, lying between small molecules and biopolymers. This fact renders them medium-size molecules with high specificity and potency to their respective targets, and then stressing the needs for a diversified and practical synthetic access. Moreover, peptides possess low intrinsic toxicity and immunogenicity and can be structurally modified to modulate their pharmacokinetics properties. Yet, in the vast majority of cases, only sequences displaying natural amino acids are prepared through SPPS.

Particularly, bioimaging based on peptides has established as valuable tool to target biological entities and visualize biological processes. To date, a largely variety of imaging agents have been developed using a range of different labeling techniques (Moss, Vavere and Azhdarinia, 2012; Lee, Xie and Chen, 2010): radioisotopes (*e.g.* ^{99m}Tc , ^{18}F , ^{64}Cu , ^{111}In , ^{123}I , ^{68}Ga , etc.) for PET and SPECT tomography techniques attaching a radiolabeled chelating polyaminopolycarboxylic group (*e.g.* DOTA, NOTA, DTPA, etc.), organic fluorophores or quantum dots (fluorescent semiconductor nanocrystals) for optical imaging, and magnetic nanoparticles (iron oxide nanoparticles) for MRI (Fig. 10). These different modalities can be used as complementary tools, and can be conveniently combined in multimodal techniques based on dual-labeled imaging agents.

Figure 10.

Common peptide-based imaging strategies upon labeling of a) radioisotopes, b) fluorophores, c) quantum-dots, d) iron-oxide nanoparticles

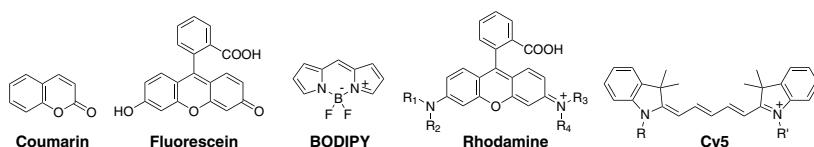


Source: Own elaboration.

Among them, fluorophore based optical imaging has emerged as a valuable technique due to its highly sensitive and nonradioactive features. A fluorophore is a molecule, typically an aromatic ring system with extended π conjugation, which absorbs photons of a specific wavelength and emits the energy at a longer range in the spectrum. It is characterized by

several indices, including the molar extinction coefficient (ϵ) and the quantum yield (QY), associated with absorption and fluorescence, respectively. The most popularly employed fluorophores are coumarin, fluorescein, BODIPY, rhodamine, and cyanine type dyes (Fig. 11), attached by different chemical tools to the selected molecule. In this respect, 4,4-difluoro-4-bora-3a,4a-diaza-s-indacene (BODIPY) scaffold has been extensively studied and a wide range of BODIPY derivatives have been described (Hong-Hermesdorf *et al.*, 2014; Vázquez-Romero *et al.*, 2013; Lee *et al.*, 2009) in numerous fluorescent imaging applications due to its excellent permeability and photophysical properties (Kowada, Maeda and Kikuchi, 2015).

Figure 11.
Commonly used fluorophores



Source: Own elaboration.

Whereas in long peptides and proteins, many preparation methods are usually based on the direct conjugation of the selected peptide to an adequate fluorophore via a chemical spacer (Brustad *et al.*, 2008; Beatty *et al.*, 2005), in short peptides this linkage can most probably affect important chemical sites and, as a result, alter the peptide molecular recognition properties. Therefore, there is a need for new approaches to incorporate fluorophores into peptides in a site-specific manner and without disrupting their inherent properties and activity. In the past few years it has been reported the use of unnatural amino acids as building blocks for the synthesis of fluorescent peptides or proteins. In these strategies, the fluorophore group can be introduced via the coupling to a modified chemical orthogonal residue of the sequence (and in a second step the excess labeling agent is removed prior to the visualization) or by the preparation of a fluorogenic amino acid and then incorporation of this building block into the sequence through chemical synthesis or other biosynthetic methods (Maity, Honcharenko and Strömberg, 2015; Koopmans *et al.*, 2013; Krueger and Imperiali, 2013). Particularly relevant is the work of the Imperiali's group on the development of environmentally-sensitive fluorescent amino acids for its incorporation in peptides or proteins (Socher and Imperiali, 2013; Venkatraman *et al.*, 2007; Sainlos and Imperiali, 2007).

In this context, we propose to study the following projects:

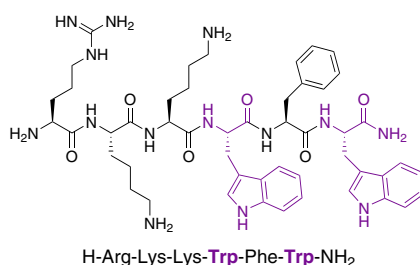
Antifungal peptide PAF26

PAF26 (López-García *et al.*, 2002) is a synthetic peptide which is known to act against invasive pulmonary aspergillosis (IPA), a fatal pulmonary infection with high mortality rates caused by the *Aspergillus Fumigatus* fungal pathogen (Fig. 12). Current diagnostic tools rely on culture analysis from different fluidic body samples but these methods can be hampered

by co-lateral difficulties (*e.g.*, airway contamination and diagnostic delays). For these reason, there has been an increasing demand on imaging probes that can afford *in situ* and real-time knowledge of the course of the infection. Antimicrobial peptides are a group of therapeutic agents that are active against a diverse spectrum of microorganisms. Many of them tend to accumulate in lipophilic intracellular compartments of microbial cell membranes. In the present case study, PAF26 is a hexapeptide formed by C-terminal hydrophobic (Trp–Phe–Trp) and N-terminal cationic (Arg–Lys–Lys) domains and this amphipaticity is closely related with its antifungal role as is crucial for the interaction with the fungal cell membrane, its internalization and transport inside the cell where it exert its function (Muñoz *et al.*, 2013).

Figure 12.

Antimicrobial peptide PAF26



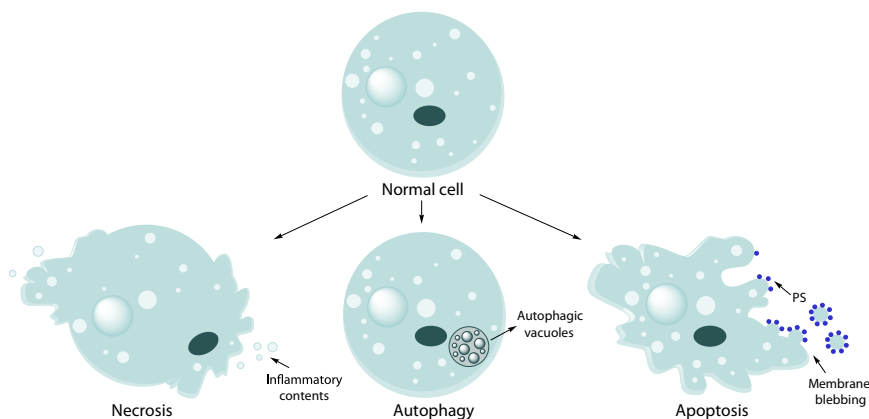
Source: Own elaboration.

Apoptotic cell death processes

Cell death is a functional mechanism in organisms that can be originated by natural or external factors (*e.g.*, infections or injuries). According to the morphological aspects and

Figure 13.

Different modes of cell death



Source: Own elaboration.

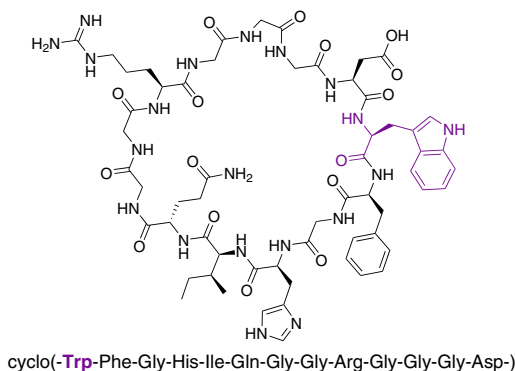
function, three main modes can be distinguished (Duprez *et al.*, 2009): apoptosis, autophagy and necrosis (Fig. 13). While necrosis is a non-programmed inflammatory cell death characterized by the loss of cell membrane integrity and release of the cellular contents to the exterior, apoptosis and autophagy are both programmed and regulated events which take place under specific signaling events. Autophagy features the degradation and recycling of cellular components within the dying cell in autophagic vacuoles. Apoptosis is characterized by the nuclear fragmentation and chromatin condensation. Besides, in early phases of apoptosis, membrane blebs are formed and subcellular structures (*i.e.*, apoptotic bodies) are released to the extracellular space in order to communicate with other cells. There is evidence that phosphatidylserine (PS) aminophospholipids are externalized to the outer face from the cell membrane and are also found in released apoptotic bodies. The recognition of these units by other molecules can be used to detect apoptotic processes.

In this sense, Annexin V is a 36-KDa protein well-reported as a marker of apoptosis (Nazari, Minai-Tehrani and Emamzadeh, 2014). Despite its popularity and extensive use, its high molecular weight, moderate permeability and dependence to high Ca^{2+} concentrations are limitations to have into consideration.

Lactadherin is a 47-KDa glycoprotein which mediates the phagocytosis of apoptotic cells by recognizing surface-exposed PS with a nanomolar affinity, in a Ca^{2+} -independent manner. Recently, Zheng and co-workers disclosed the synthesis of cyclic lactadherin mimics (cLacs) which recreate the disposition of the key amino acids involved on the lactadherin-PS interaction with Gly as linker spacers (Fig. 14) (Zheng *et al.*, 2011).

Figure 14.

cLac mimic reported by Zheng's group



Source: Own elaboration.

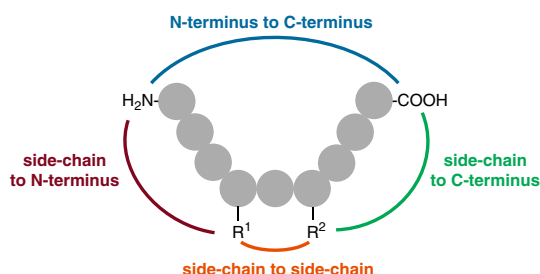
BIARYL PEPTIDIC TOPOLOGIES. STAPLED PEPTIDES

Peptides possess intrinsic properties (*e.g.*, protein-like molecular topology and dimensions) which make them a group of synthetically accessible entities with high selectivity, potency and low toxicity, qualities highly valuable for therapeutic agents. Nevertheless, their

success in the drug market has been hampered by their poor pharmacokinetic properties (metabolic instability and low permeability). In this regard, different constraining strategies are applied to generate more rigidified structures with improved metabolic stability and membrane permeability as well as stabilized secondary structure motives (Thapa *et al.*, 2014). According to the elements involved in the cyclization, the type of constraining can be distinguished in four subdivisions: i) N-terminus to C-terminus, ii) side-chain to one of their termini, iii) side-chain to side-chain and iv) complex cyclic compounds which are formed by a mixture of the previous linkages (Fig. 15).

Figure 15.

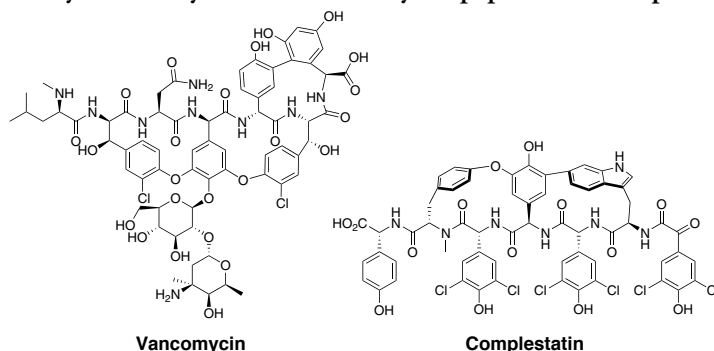
Common peptide cyclization strategies



Source: Own elaboration.

Macrocyclic drugs are large ring structures widely used for infectious diseases and in oncology (Giordanetto and Kihlberg, 2014), capable to modulate protein-protein interactions that are out of range for small molecules (Villar *et al.*, 2014). Moreover, these molecular entities are big enough to encapsulate compounds inside their cavities in a molecular recognition process based on non-covalent forces such as hydrophobic interactions (Ogoshi and Yamagishi, 2015). Nowadays, new techniques and computational tools (Heinis, 2015) are being developed for the generation of peptide-based macrocycles. In order to control the macrocycle-to-oligomer ratio, a series of key factors have to be considered when planning the strategy macrocyclization (Martí-Centelles *et al.*, 2015; Chouhan and James, 2013). On these systems, kinetic and thermodynamic factors are pivotal for the cyclization outcome. Thus, the use of high- or pseudo-high dilution conditions, on solution or the immobilization of the precursors on functional resins, will kinetically favor intramolecular processes vs. the formation of oligomer/polymeric products; alternatively, under thermodynamic control, the formation of the more stable species will be more energetically favored. Other intrinsic parameters such as the ring size or the proper conformational/configurational pre-organization that orientates the two reactive sites in a proper disposition, as well as specific intramolecular interactions (*e.g.*, hydrogen bonds) and experimental conditions (*e.g.*, solvent, reagents, temperature, etc.) can play a critical role in the cyclization. In this regard, James and Collins recently reported a quantitative index for the macrocyclization efficiency (Emac), which is proportional to the concentration and the yield of the reaction (Collins and James, 2012).

Biaryl and biaryl ether bismacrocyclic peptide-derived natural products (Feliu and Planas, 2005) such as vancomycin (Boger *et al.*, 1999) and complestatin (Wang *et al.*, 2010) are

Figure 16.**Examples of biaryl and biaryl ether bismacrocylic peptidic natural products**

Source: Own elaboration.

prominent examples of the wide range of naturally-occurring constrained bioactive peptides with potent bioactivity and prospective great value in drug discovery (Fig. 16).

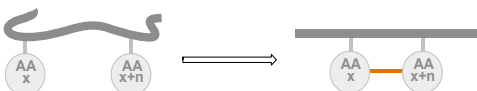
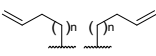
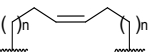
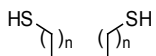
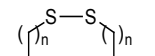
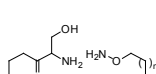
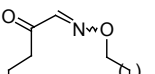
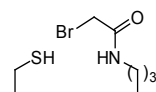
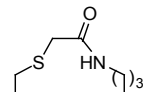
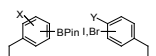
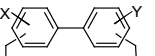
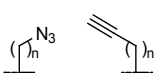
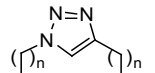
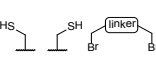
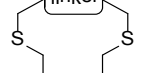
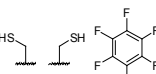
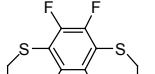
These compounds exhibit relevant biological activities, including proteasome inhibition, and antimicrobial or cytotoxic activities among others. Even so, the complexity of these structures has led to synthetically challenging syntheses where the biaryl or biaryl ether moiety formation rely on the preparation of diphenyl intermediates, intramolecular reactions involving Suzuki, Negishi and Stille cross-coupling reactions or S_NAr reactions. Therefore, the access to simplified scaffolds in order to access structural diversification to modulate their activity is of great relevance.

Stapled peptides (Lau *et al.*, 2015; Dharanipragada, 2013) are a type of constrained architectures that have recently emerged as a breakthrough in the peptide drug modulation. The stapled bond formation, formed by a non-amide side-chain to a side-chain covalent linkage, has been reported to confer improvements of the pharmacokinetic profile and conformational behavior in relevant peptides (Table 2) (Walensky and Bird, 2014; Verdine and Hilinski, 2012).

One of the first reports of the enhancement of the helicity and metabolic stability of a peptide by an stapling approach was firstly disclosed by Verdine and co-workers (Christian, Po and Verdine, 2000), who presented a RCM-stapling approach based on the pioneering studies previously reported by Grubbs (Blackwell and Grubbs, 1998) on olefin metathesis reaction with *O*-allyl serine/homoserine residues. This hydrocarbon-type stapling technique has been widely applied for PPI targets. One of the first examples of hydrocarbon stapling applied to a biological system was reported by Walensky and co-workers (Walensky *et al.*, 2004). On this work, stapled peptide variants of a BCL-2 domain, which is an apoptosis regulator protein, led to improvements on the pharmacokinetic and conformational behavior of these peptides. Other stapling approaches reported over the past several years with high potential include: disulfide bridges arising from natural cysteine side-chains (Góngora-Benítez, Tulla-Puche and Albericio, 2014), oxyme linkages from hydroxylamine and 1,2-aminoalcohol groups (Haney, Loch and Horne, 2011), thioether bond formation through the crosslinking between

Table 2.

Conventional peptide stapling techniques

native peptide flexible conformation				structured peptide restricted conformation		
Stapling linkage	Stapling reaction	Precursors	Stapling form	Natural AAs	Chemical stability	Structural versatility
olefine or hydrocarbon	RCM			X	✓	✓
disulfide	oxidation			✓	~	X
oxyme	oxidation + condensation			X	~	~
thioether	nucleophilic substitution			X	✓	X
biaryl	Suzuki cross-coupling			X	✓	✓
triazole	1,3-dipolar cycloaddition (click)			X	✓	✓
thioether (two-component stapling)	nucleophilic substitution			✓	✓	~
thioether (two-component stapling)	nucleophilic substitution			✓	✓	X

Source: Own elaboration.

a Cys residue and α -bromo amide side-chain (Brunel and Dawson, 2005), biaryl linkages involving borylated phenylalanine derivatives (Meyer *et al.*, 2012; Afonso, Feliu and Planas, 2011; Bois-Choussy, Cristau and Zhu, 2003; Carbonnelle and Zhu, 2000) and azide-alkyne cycloadditions (click reaction) (Scrima *et al.*, 2010). Additionally, two-component stapling techniques involve a bifunctional linker compound. Among them, thioether bond formation

has also been reported from the crosslinking between two Cys and dibromo-linkers (e.g., α,α' -dibromo-*m*-xylene) (Jo *et al.*, 2012) or through aromatic nucleophilic substitutions with perfluoroaromatic reactants (Spokoyny *et al.*, 2013). In another example of stapling application to biological targets, Lin and co-workers modulated the tumor suppressor activity of p53 protein by the inhibition of MDM2, which is a negative regulator protein of p53, overexpressed in cancer cells (Muppidi *et al.*, 2011). Thus, they reported a cysteine crosslinked peptide derivative based on a stapling with aryl linkers for the inhibition of the MDM2-p53 interaction.

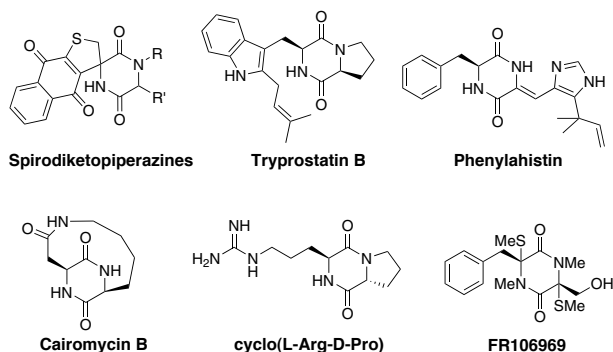
Each methodology has its own specific advantages and handicaps and the choice of the stapling method depends on the particularities of the case. Some of their drawbacks include: requirement of chemically modified *de novo* amino acids, chemical instability (that is the case of disulfide bridges) or difficult modulation to improve the structural versatility of the compounds generated. For this reason, peptide stapling is an emerging field of continuous growing.

C-H OXIDATIVE MODIFICATION OF TRP-BASED DKPS

2,5-Diketopiperazines (DKPs), formed by the cyclocondensation of two α -amino acids, are the smallest cyclic peptide derivatives found in nature. Their well-defined three-dimensional structure, their resistance to proteolysis, the presence of donor and acceptor groups for hydrogen bonding that favors their interaction with biological targets and their high structural diversity are valuable features for drug discovery (Cherkupally *et al.*, 2015; Ressurreição *et al.*, 2011). Is not surprising, therefore, that this core is widespread in biologically active natural products with a wide spectrum of biological properties (Borthwick, 2012). Some representative examples include: DNA-binding agents (e.g., spirodiketopiperazines), cell-cycle inhibitors (e.g., tryprostatin B), tubulin depolymerizing agents (e.g., phenylahistin), metalloproteinases inhibitors (e.g., thiol DKPs), antibiotics and antibacterials (e.g., cairomycin B),

Figure 17.

Representative examples of biologically active DKPs



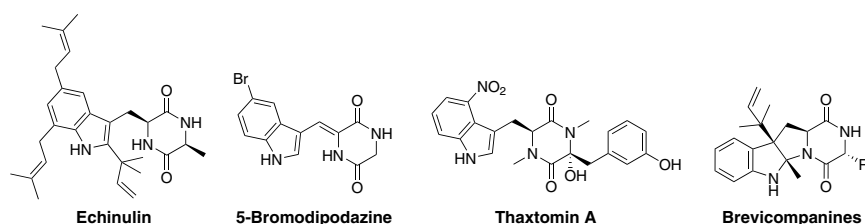
Source: Own elaboration.

antifungal agents [e.g., c(L-Arg-D-Pro)] and anti-inflammatory inhibitors (e.g., FR106969) (Fig. 17).

Besides Tryprostatin derivatives (Fig. 17), Trp residue is commonly found in a wide range of natural cyclo (AA-Trp) DKPs (Nishanth Kumar, Mohandas and Nambisan, 2014; Wang *et al.*, 2012; Klausmeyer *et al.*, 2005), including brevianamide F [c(L-Pro-L-Trp)], which has antibacterial and antifungal properties (Mehdi *et al.*, 2009), 5-bromodipodazine which display antifouling activity (Liao *et al.*, 2015) and also echinulins, thaxtomins, c(L-Phe-L-Trp), c(D-Leu-L-Trp) and annulated Trp-containing derivatives (e.g., brevicompanines) which have been shown to be phytotoxins or plant-growth regulators (Fig. 18) (Borthwick, 2012).

Figure 18.

Examples of biologically active cyclo (AA-Trp) DKPs

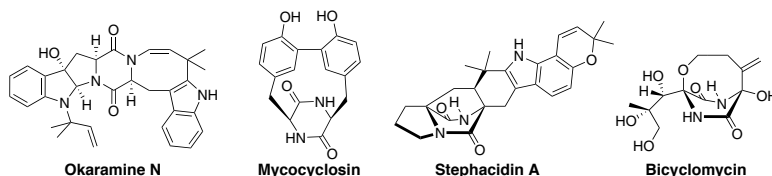


Source: Own elaboration.

Thanks to their innate reactivity, DKPs are privileged building blocks for diversification to access to structurally varied frameworks (Gonzalez *et al.*, 2012). In this regard, although bridged and polycyclic natural DKPs are extensively present in nature and constitute highly valuable scaffolds (Fig. 19), the synthesis of these cores represents a challenging issue and few precedents of direct DKPs cyclization approaches have been reported (Amatov *et al.*, 2015; Cochrane *et al.*, 2012; Lim, Gallucci and Rajanbabu, 2010; El Kaim *et al.*, 2007; Baran, Guerrero and Corey, 2003).

Figure 19.

Examples of biologically active bridged and polycyclic natural DKPs



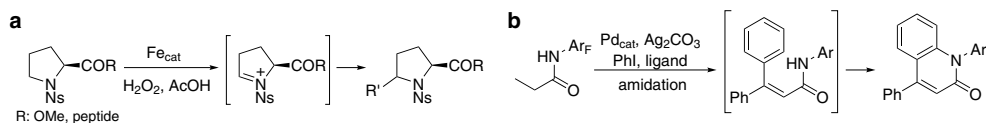
Source: Own elaboration.

The selective C-H oxidative modification of amino acids and peptides to form new C-C and C-N bonds appears an attractive and challenging tool for structural modification. Particularly inspiring to us, were the work of White and co-workers (Osberger *et al.*, 2016), who reported an iron catalyzed process based on the C(5)-H oxidative hydroxylation of proline

derivatives and subsequent functionalization via an iminium intermediate as a valuable precursor for further derivatization by the generation of C-C bonds; and the amidation process of Yu and co-workers (Deng *et al.*, 2014) based on oxidative palladium catalysis for the formation of new C-N bonds (Fig. 20).

Figure 20.

Examples of C-H oxidations. a) Iron catalyzed C(5)-H oxidation of proline, b) amidation by oxidative Pd catalysis



Source: Own elaboration.

Within the recent years, the selective construction of C–C linkages directly from two different C–H bonds under oxidative conditions, known as cross-dehydrogenative coupling (CDC), has attracted much attention (Girard, Knauber and Li, 2014; Yeung and Dong, 2011). These double C–H activation processes do not rely on the use of pre-functionalized starting materials, which reduces the number of synthetic steps required, and it is beneficial for the atom economy of the process. The main challenge of this methodology deals with the ubiquity of C–H bonds, being the selective functionalization of one type of C–H bond the major goal. Typically, CDCs involve the use of an oxidant (*e.g.*, O₂, peroxides TBHP, DDQ, PIFA, etc.) and, in many cases, are catalyzed by transition metals (*e.g.*, Cu Pd, Fe, Ag, Ru, etc.) for the connection of Csp³–H, Csp²–H, and even Csp³–H bonds with each other.

OBJECTIVES

In the present thesis we investigated the development of new methodologies for the selective and straightforward chemical modification of Trp amino acid either alone or in peptides. Specifically, we proposed the following main goals:

1) C-2 arylation of Trp amino acids through Pd-catalyzed C-H activation

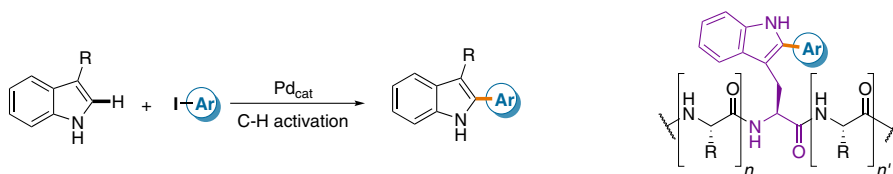
We want to develop a methodology based on a C–H activation protocol catalyzed by palladium to enable an intermolecular chemoselective C-arylation of Trp amino acid in the C-2 position of the free indole ring. Specifically, we proposed to:

- Undertake a previous optimization of the reaction conditions of a C–H activation process previously initiated in our group.
- Apply these conditions to the preparation of arylated analogues of brevianamide F.
- Study the direct C-arylation of tryptophan amino acid and related indole systems for the preparation of a small library of arylated indole compounds (Scheme 1, left).

- Study the applicability of C-2 arylated tryptophan residues in model peptide sequences (Scheme 1, right).
- Apply the methodology to selected bioactive peptides suitable for preparing libraries and evaluate their pharmacological activity against therapeutic targets.

Scheme 1.

Study regarding the Pd-catalyzed C-H arylation of the C-2 indole position of Trp amino acid and other related indole-containing structures



Source: Own elaboration.

2) Spacer-free Trp-BODIPY fluorogen for peptide-based imaging probes

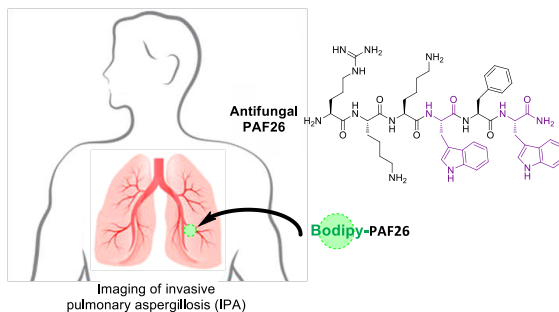
As no precedents of BODIPY-based Trp amino acids had been described in the literature, we envisioned the attachment of a BODIPY core directly into the C-2 indole position of the Trp amino acid, via the C-H activation protocol developed in chapter 1, for the synthesis of fluorophore-labeled relevant peptides for bioimaging applications. In particular, we planned to accomplish the following objectives:

- Synthesize a BODIPY-antifungal PAF26 derivative for cell imaging fungal infections.

We hypothesized that the replacement of a Trp residue with the fluorogenic Trp-BODIPY unit could render a novel probe for imaging fungal infections as it would not alter the chemical features of PAF26 (*i.e.*, charge balance, overall polarity, hydrogen bonding pattern) key for its activity (Scheme 2).

Scheme 2.

Strategy for imaging IPA fungal infection by a BODIPY-labeled PAF26 peptide



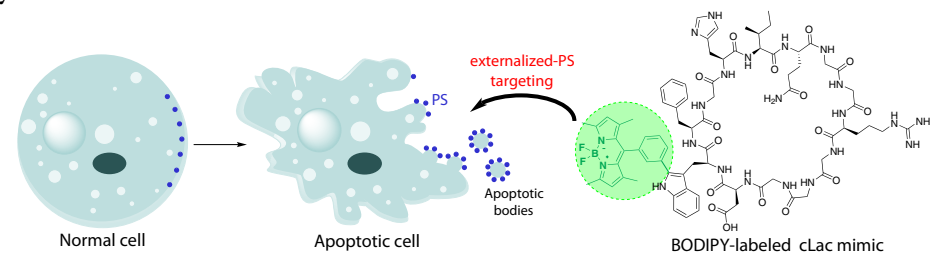
Source: Own elaboration.

- Synthesize a BODIPY-cyclic cLac mimic for cell imaging apoptosis.

Taking into account the recognition of cLac peptide to PS units disposed in apoptotic cell surfaces, it was proposed to replace the natural Trp of a cLac mimic with a Trp-BODIPY unit to exert the minimal impact on the original structure and obtain a synthetic noninvasive reagent for imaging apoptosis in a Ca^{2+} -independent manner (Scheme 3).

Scheme 3.

Strategy for imaging apoptotic cells based on the recognition of externalized PS units by a BODIPY-labeled cLac mimic



Source: Own elaboration.

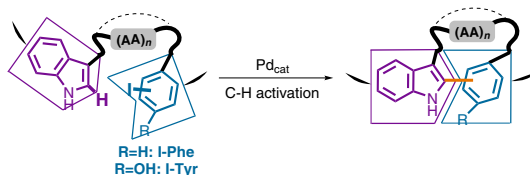
3) Biaryl peptidic topologies through Pd-catalyzed C-H activation reactions between Trp and Phe/Tyr residues

The third main goal of this work discloses the cyclization of peptides via the developed C-H activation protocol in chapter 1 (Scheme 4). Specifically, the pursued objectives in this section are the following:

- Undertake a systematic evaluation of the structural factors that determine the cyclization in peptides through the C-H activation process.
- Apply this methodology for the constraining of selected bioactive peptides suitable for preparing libraries and evaluate their pharmacological activity against therapeutic targets.
- Explore the access to novel complex peptide architectures.

Scheme 4.

Study of the peptide constraining between Phe/Tyr and Trp residues through C-H activation



Source: Own elaboration.

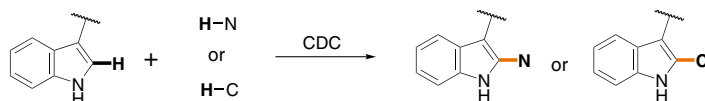
4) Cu(II) cross-dehydrogenative cyclization of Trp-based DKPs

The fourth main goal of the present thesis focuses on the study of intramolecular double C-H activation processes on Trp-containing peptides (Scheme 5). Specifically, we wanted to explore the following issues:

- The study of cross-dehydrogenative processes on Trp-containing diketopiperazines by a systematic screening of oxidants and reaction conditions.

Scheme 5.

Cross-dehydrogenative couplings of Trp-containing peptides



Source: Own elaboration.

REFERENCES

- MOSS, A. J.; VAVERE, A. L., and A. AZHDARINIA (2012), *Curr. Med. Chem.*, 19: 3255.
- ACKERMANN, L. (2009), *Modern Arylation Methods*; Wiley-VCH, Weinheim: Weinheim, 2009.
- ACKERMANN, L., and A. V. LYGIN (2011), *Org. Lett.*, 13: 3332.
- AFONSO, A.; FELIU, L., and M. PLANAS (2011), *Tetrahedron*, 67: 2238.
- ALKHALAF, L. M., and K. S. RYAN (2015), *Chem. Biol.*, 22: 317.
- AMATOV, T.; POHL, R.; ČÍSAŘOVÁ, I., and U. JAHN (2015), *Angew. Chem. Int. Ed.*, 54: 12153.
- BARAN, P. S.; GUERRERO, C. A., and E. J. COREY (2003), *J. Am. Chem. Soc.*, 125: 5628.
- BEATTY, K. E.; XIE, F.; WANG, Q., and D. A. TYRRELL (2005), *J. Am. Chem. Soc.*, 127: 14150.
- BIALONSKA, D., and J. K. ZJAWIONY (2009), *Mar. Drugs*, 7: 166.
- BLACKWELL, H. E., and R. H. GRUBBS (1998), *Angew. Chem. Int. Ed.*, 37: 3281.
- BOGER, D. L.; MIYAZAKI, S.; KIM, S. H.; WU, J. H.; CASTLE, S. L.; LOISELEUR, O., and Q. JIN (1999), *J. Am. Chem. Soc.*, 121: 10004.
- BOIS-CHOUSSY, M.; CRISTAU, P., and J. ZHU (2003), *Angew. Chem. Int. Ed.*, 42: 4238.
- BORTHWICK, A. D. (2012), *Chem. Rev.*, 112: 3641.
- BRUNEL, F. M., and P. E. DAWSON (2005), *Chem. Commun.*: 2552.
- BRUSTAD, E. M.; LEMKE, E. A.; SCHULTZ, P. G., and A. A. DENIZ (2008), *J. Am. Chem. Soc.*, 130: 17664.
- CARBONNELLE, A.-C., and J. ZHU (2000), *Org. Lett.*, 2: 3477.
- CHERKUPALLY, P.; RAMESH, S.; JAD, Y. E.; GOVENDER, T.; KRUGER, H. G.; TORRE, B. G. DE LA, and F. ALBERICIO (2015), *In Privileged Scaffolds in Medicinal Chemistry: Design, Synthesis, Evaluation*; Bräse, S., Ed.; Royal Society of Chemistry, Cambridge: United Kingdom, 2015: 400–407.
- CHIN, J. W. (2014), *Annu. Rev. Biochem.*, 83: 379.
- CHOUHAN, G., and K. JAMES (2013), *Org. Lett.*, 15: 1206.

- COCHRANE, J. R.; WHITE, J. M.; WILLE, U., and C. A. HUTTON (2012), *Org. Lett.*, 14: 2402.
- COLLETTI, S. L.; LI, C.; FISHER, M. H.; WYVRATT, M. J., and P. T. MEINKE, P. T. (2000), *Tetrahedron Lett.*, 41: 7825.
- COLLINS, J. C., and K. JAMES (2012), *Med. Chem. Commun.*, 3: 1489.
- DAVIS, L., and J. W. CHIN (2012), *Nat. Rev. Mol. Cell Biol.*, 13: 168.
- DE MEIJERE, A., and F. DIEDERICH (2004), *Metal-Catalyzed Cross-Coupling Reactions*, Vol. 1, 2nd ed.; DE MEIJERE, A., DIEDERICH, F., Eds.; Wiley-VCH, Weinheim, 2004.
- DENG, Y.; GONG, W.; HE, J., and J. Q. YU (2014), *Angew. Chem. Int. Ed.*, 53: 6692.
- DEPREZ, N. R.; KALYANI, D.; KRAUSE, A., and M. S. SANFORD (2006), *J. Am. Chem. Soc.*, 128: 4972.
- DHARANIPRAGADA, R. (2013), *Futur. Med. Chem.*, 5: 831.
- DIAO, L., and B. MEIBOHM (2013), *Clin. Pharmacokinet.*, 52: 855.
- DUPREZ, L.; WIRAWAN, E.; BERGHE, T. VANDEN, and P. VANDENABEELE (2009), *Microbes Infect.*, 11: 1050.
- EL KAIM, L.; GAGEAT, M.; GAULTIER, L., and L. GRIMAUD (2007), *Synlett*, 500.
- FELIU, L., and M. PLANAS (2005), *Int. J. Pept. Res. Ther.*, 11: 53.
- FOSGERAU, K., and T. HOFFMANN (2015), *Drug Discov. Today*, 20: 122.
- GIORDANETTO, F., and J. KIHLEBERG (2014), *J. Med. Chem.*, 57: 278.
- GIRARD, S. A.; KNAUBER, T., and C. LI (2014), *In From C-H to C-C Bonds: Cross-Dehydrogenative-Coupling*; LI, CH.-J., Ed.; The Royal Society of Chemistry: United Kingdom: 1–32.
- GONZALEZ, J. F.; ORTIN, I.; DE LA CUESTA, E., J. C. MENENDEZ (2012), *Chem. Soc. Rev.*, 41: 6902.
- GRIBBLE, G. W. (2010), *Topics in Heterocyclic Chemistry, Heterocyclic Scaffolds II: Reactions and Applications of Indoles*, Vol. 26; GRIBBLE, G. W., Ed.; Springer-Verlag Berlin Heidelberg: New York, 2010.
- GRIGG, R.; SRIDHARAN, V.; STEVENSON, P.; SUKIRTHALINGAM, S., and T. WORAKUN (1990), *Tetrahedron*, 46: 4003.
- GÓNGORA-BENÍTEZ, M.; TULLA-PUCHE, J., and F. ALBERICIO (2014), *Chem. Rev.*, 114: 901.
- HANEY, C. M.; LOCH, M. T., and W. S. HORNE (2011), *Chem. Commun.*, 47: 10915.
- HEINIS, C. (2014), *Nat. Chem. Biol.*, 10: 696.
- HIGUCHI, K., and T. KAWASAKI (2005), *Nat. Prod. Rep.*, 22: 761.
- HONG, S. H.; KWON, Y.-C., and M. C. JEWETT (2014), *Front. Chem.*, 2: 34.
- HONG-HERMESDORF, A.; MIETHKE, M.; GALLAHER, S. D.; KROPAT, J.; DODANI, S. C.; CHAN, J.; BARUPALA, D.; DOMAILLE, D. W.; SHIRASAKI, D. I.; LOO, J. A.; WEBER, P. K.; PETT-RIDGE, J.; STEMMLER, T. L.; CHANG, C. J., and S. S. MERCHANT (2014), *Nat. Chem. Biol.*, 10: 1034.
- ISIDRO-LLOBET, A.; ALVAREZ, M., and F. ALBERICIO (2009), *Chem. Rev.*, 109: 2455.
- JO, H.; MEINHARDT, N.; WU, Y.; KULKARNI, S.; HU, X.; LOW, K. E.; DAVIES, P. L.; DEGRADO, W. F., and D. C. GREENBAUM (2012), *J. Am. Chem. Soc.*, 134: 17704.
- JOULE, J. A., and K. MILLS (2010), *Heterocyclic Chemistry*, 5th ed.; John Wiley & Sons: Chichester.
- KASPAR, A. A., and J. M. REICHERT (2013), *Drug Discov. Today*, 18: 807.
- KLAUSMEYER, P.; MCCLOUD, T. G.; TUCKER, K. D.; CARDELLINA, J. H., and R. H. SHOEMAKER. (2005), *J. Nat. Prod.*, 68: 1300.
- KOOPMANS, T.; VAN HAREN, M.; VAN UFFORD, L. Q.; BEEKMAN, J. M., and N. I. MARTIN (2013), *Bioorganic Med. Chem.*, 21: 553.
- KOWADA, T.; MAEDA, H., and K. KIKUCHI (2015), *Chem. Soc. Rev.*, 44: 4953.
- KRUEGER, A. T., and B. IMPERIALI (2013), *ChemBioChem*, 14: 788.

- LAU, Y. H.; DE ANDRADE, P.; WU, Y., and D. R. SPRING (2015), *Chem. Soc. Rev.*, 44: 91.
- LEE, J. S.; KANG, N. Y.; YUN, K. K.; SAMANTA, A.; FENG, S.; HYEONG, K. K.; VENDRELL, M.; JUNG, H. P., and Y. T. CHANG (2009), *J. Am. Chem. Soc.*, 131: 10077.
- LEE, S.; XIE, J., and X. CHEN (2010), *Chem. Rev.*, 110: 3087.
- LIAO, S.; XU, Y.; TANG, Y.; WANG, J.; ZHOU, X.; XU, L., and Y. LIU (2015), *RSC Adv.*, 5: 51020.
- LIM, H. J.; GALLUCCI, J. C., and T. V. RAJANBABU (2010), *Org. Lett.*, 12: 2162.
- LÓPEZ-GARCÍA, B.; PÉREZ-PAYÁ, E.; JOSE, F., and J. F. MARCOS (2002), *Appl. Environ. Microbiol.*, 68: 2453.
- MAITY, J.; HONCHARENKO, D., and R. STRÖMBERG (2015), *Tetrahedron Lett.*, 56: 4780.
- MARTÍ-CENTELLES, V.; PANDEY, M. D.; BURGUETE, M. I., and S. V. LUIS (2015), *Chem. Rev.*, 115: 8736.
- MEHDI, R. B. A.; SHAABAN, K. A.; REBAI, I. K.; SMAOUI, S.; BEJAR, S., and L. MELLOULI (2009), *Nat. Prod. Res.*, 23: 1095.
- MERRIFIELD, R. B. (1963), *J. Am. Chem. Soc.*, 85: 2149.
- MEYER, F.-M.; COLLINS, J. C.; BORIN, B.; BRADOW, J.; LIRAS, S.; LIMBERAKIS, C.; MATHIOWETZ, A. M.; PHILIPPE, L.; PRICE, D.; SONG, K., and K. JAMES (2012), *J. Org. Chem.*, 77: 3099.
- MOSQUERA, J.; JIMÉNEZ-BALSA, A.; DODERO, V. I.; VÁZQUEZ, M. E., and J. L. MASCAREÑAS (2013), *Nat. Commun.*, 4:1874; DOI: 10.1038/ncomms2825.
- MUPPIDI, A.; WANG, Z.; LI, X.; CHEN, J., and Q. LIN (2011), *Chem. Commun.*, 47: 9396.
- MUÑOZ, A.; HARRIES, E.; CONTRERAS-VALENZUELA, A.; CARMONA, L.; READ, N. D., and J. F. MARCOS (2013), *PLoS One*, 8: e54813.
- NAZARI, M.; MINAI-TEHRANI, A., and R. EMAMZADEH (2014), *Rsc Adv.*, 4: 45128.
- NISHANTH KUMAR, S.; MOHANDAS, C., and B. NAMBIAN (2014), *Peptides*, 53: 48.
- OGOSHI, T., and T. YAMAGISHI (2015), *In Pillararenes*; OGOSHI, T., Ed.; The Royal Society of Chemistry: United Kingdom: 1–22.
- OHTA, A. (1989), *Chem. Pharm. Bull.*, 37: 1477.
- OSBERGER, T. J.; ROGNES, D. C.; KOHRT, J. T.; STEPAN, A. F., and M. C. WHITE (2016), *Nature*, 537: 214.
- PHIPPS, R. J.; GRIMSTER, N. P., and M. J. GAUNT (2008), *J. Am. Chem. Soc.*, 130: 8172.
- RESSURREIÇÃO, A. S. M.; DELATOCHE, R.; GENNARI, C., and U. PIARULLI (2011), *Eur. J. Org. Chem.*, 217.
- SAINLOS, M., and B. IMPERIALI (2007), *Nat. Protoc.*, 2: 3210.
- SANDTORV, A. H. (2015), *Adv. Synth. Catal.*, 357: 2403.
- SANTIVERI, C. M., and M. A. JIMÉNEZ (2010), *Pept. Sci.*, 94: 779.
- SCHAFMEISTER, C. E.; PO, J., and G. L. VERDINE (2000), *J. Am. Chem. Soc.*, 122: 5891.
- SCRIMA, M.; LE CHEVALIER-ISAAD, A.; ROVERO, P.; PAPINI, A. M.; CHOREV, M., and A. M. D'URSI (2010), *European J. Org. Chem.*, 446.
- SEWALD, N., and H.-D. JAKUBKE (2002), *Peptides: Chemistry and Biology*; Wiley-VCH, Weinheim.
- SOCHER, E., and B. IMPERIALI (2013), *ChemBioChem*, 14: 53.
- SPOKOYNY, A. M.; ZOU, Y.; LING, J. J.; YU, H.; LIN, Y., and B. L. PENTELUTE (2013), *J. Am. Chem. Soc.*, 135: 5946.
- STUART, D. R.; VILLEMURE, E., and K. FAGNOU (2007), *J. Am. Chem. Soc.*, 129: 12072.
- THAPA, P.; ESPIRITU, M. J.; CABALTEJA, C., and J.-P. BINGHAM (2014), *Int. J. Pept. Res. Ther.*, 20: 545.
- TRANSPARENCY MARKET RESEARCH (2015), *Peptide Therapeutics Market - Global Industry Analysis, Size, Share, Growth, Trends and Forecast 2014-2020*.

- TROST, B. M.; GODLESKI, S. a. and J. P. GENET (1978), *J. Am. Chem. Soc.*, 100: 3930.
- TSOMAIA, N. (2015), *Eur. J. Med. Chem.*, 94: 459.
- VENKATRAMAN, P.; NGUYEN, T. T.; SAINLOS, M.; BILSEL, O.; CHITTA, S.; IMPERIALI, B., and L. J. STERN (2007), *Nat. Chem. Biol.*, 3: 222.
- VERDINE, G. L., and G. J. HILINSKI (2012), *In Methods in Enzymology*; WITTRIP, K. D., VERDINE, G. L., Eds.; Elsevier Inc.: United States of America, Vol. 503: 3–33.
- VILLAR, E. A.; BEGLOV, D.; CHENNAMADHAVUNI, S.; PORCO JR, J. A.; KOZAKOV, D.; VAJDA, S., and A. WHITTY (2014), *Nat. Chem. Biol.*, 10: 723.
- VÁZQUEZ-ROMERO, A.; KIELLAND, N.; ARÉVALO, M. J.; PRECIADO, S.; MELLANBY, R. J.; FENG, Y.; LAVILLA, R., and M. VENDRELL (2013), *J. Am. Chem. Soc.*, 135: 16018.
- WADE, L. G. J. (2010), *In Organic Chemistry. Chapter 24: Amino acids, peptides, and proteins*: 1153–1199.
- WALENSKY, L. D., and G. H. BIRD (2014), *J. Med. Chem.*, 57: 6275.
- WALENSKY, L. D.; KUNG, A. L.; ESCHER, I.; MALIA, T. J.; BARBUTO, S.; WRIGHT, R. D.; WAGNER, G.; VERDINE, G. L., and s. J. KORSMEYER (2004), *Science*, 305: 1466.
- Wang, F.-Z.; Huang, Z.; Shi, X.-F.; Chen, Y.-C.; Zhang, W.-M.; Tian, X. P.; Li, J., and S. Zhang (2012), *Bioorg. Med. Chem. Lett.*, 22: 7265.
- WANG, L.; BROCK, A.; HERBERICH, B., and P. G. SCHULTZ (2001), *Science*, 292: 498.
- WANG, X.; GRIBKOV, D. V., and D. SAMES (2007), *J. Org. Chem.*, 72: 1476.
- WANG, Z.; BOIS-CHOUSSEY, M.; JIA, Y., and J. ZHU (2010), *Angew. Chem. Int. Ed.*, 49, 2018.
- WENCEL-DELDOR, J., and F. GLORIUS (2013), *Nat. Chem.*, 5: 369.
- WHITAKER, D.; BURÉS, J., and I. LARROSA (2016), *J. Am. Chem. Soc.*, 138: 8384.
- WHITE, M. C. (2012), *Synlett*, 23: 2746.
- WISHART, D. S.; KNOX, C.; GUO, A. C.; SHRIVASTAVA, S.; HASSANALI, M.; STOTHARD, P.; CHANG, Z., and J. WOOLSEY (2006), *Nucleic Acids Res.*, 34: D668.
- XIAO, H.; CHATTERJEE, A.; CHOI, S.-H.; BAJJURI, K. M.; SINHA, S. C., and P. G. SCHULTZ (2013), *Angew. Chem. Int. Ed.*, 52: 14080.
- YAMAGUCHI, J.; YAMAGUCHI, A. D., and K. ITAMI (2012), *Angew. Chem. Int. Ed.*, 51: 2.
- YANG, S. D.; SUN, C. L.; FANG, Z.; LI, B. J.; LI, Y. Z., and Z. J. SHI (2008), *Angew. Chem. Int. Ed.*, 47: 1473.
- YEUNG, C. S., and V. M. DONG (2011), *Chem. Rev.*, 111: 1215.
- YU, J.-Q., and Z. SHI (2010), *Topics in Current Chemistry, C-H activation*, vol 292; YU, J.-Q., SHI, Z., Eds.; Springer: Berlin Heidelberg.
- ZHAO, J.; ZHANG, Y., and K. CHENG (2008), *J. Org. Chem.*, 2008, 73: 7428.
- ZHENG, H.; WANG, F.; WANG, Q., and J. GAO (2011), *J. Am. Chem. Soc.*, 133: 15280.



1

C-2 ARYLATION OF TRP AMINO ACIDS THROUGH PD-CATALYZED C-H ACTIVATION

PUBLICATION I.

Synthesis and biological evaluation of a postsynthetically modified Trp-based diketopiperazine

Sara Preciado,^a Lorena Mendive-Tapia,^b Carolina Torres-García,^c Rubí Zamudio-Vázquez,^{b, d} Vanessa Soto-Cerrato,^c Ricardo Pérez-Tomás,^c Fernando Albericio,^{b, c, d, f} Ernesto Nicolás,^c and Rodolfo Lavilla^{a, g}

Medicinal Chemical Communications, 2013, 4, 1171-1174.

- a) Barcelona Science Park, Baldiri Reixac 10-12, 08028 Barcelona, Spain.
- b) Institute for Research in Biomedicine, Barcelona Science Park, Baldiri Reixac 10-12, 08028 Barcelona, Spain.
- c) Department of Organic Chemistry, Faculty of Chemistry, University of Barcelona, Martí I Franquès 1-11, 08028 Barcelona, Spain.
- d) CIBER-BBN, Networking Centre on Bioengineering Biomaterials and Nanomedicine, Barcelona Science Park, Baldiri Reixac 10, 08028 Barcelona, Spain.
- e) Department of Patology and Experimental Therapeutics, Faculty of Medicine, University of Barcelona, Feixa Llarga s/n, Pavelló de Govern, 08907 L'Hospitalet, Barcelona, Spain.
- f) School of Chemistry, University of KwaZulu-Natal, 4001-Durban, South Africa.
- g) Laboratory of Organic Chemistry, Faculty of Pharmacy, University of Barcelona, Avda. Joan XXII s.n., 08028 Barcelona, Spain.

Synthesis and biological evaluation of a post-synthetically modified Trp-based diketopiperazine†

Cite this: *Med. Chem. Commun.*, 2013, 4, 1171

Sara Preciado,^a Lorena Mendive-Tapia,^b Carolina Torres-García,^c Rubí Zamudio-Vázquez,^{bd} Vanessa Soto-Cerrato,^e Ricardo Pérez-Tomás,^e Fernando Albericio,^{*bcd} Ernesto Nicolás^{*c} and Rodolfo Lavilla^{*ag}

Received 23rd November 2012
Accepted 7th June 2013

DOI: 10.1039/c3md20353k

www.rsc.org/medchemcomm

A series of C2-arylated analogues of the diketopiperazine brevianamide F has been synthesized using a mild Pd-catalyzed CH-activation procedure. Biological evaluation of the new derivatives in different cell lines shows that this modification is responsible for the remarkable change in activity, turning a mild antibiotic and antifungal natural product (brevianamide F) into novel antitumoral compounds. Furthermore, the approach stated represents a new straightforward and versatile methodology with promising applications in peptidomimetics and medicinal chemistry.

2,5-Diketopiperazines (DKPs) are the smallest cyclic peptides known. Their characteristic heterocyclic system is present in several natural products with biological properties such as antitumor, antimicrobial, and antiviral activities, as well as modulation of enzymes, receptors and biochemical mediators.¹ Regarding their chemical and physical properties, worth noting are their resistance to proteolysis, conformational rigidity and the presence of donor and acceptor groups for hydrogen bonding which favours the interaction with biological targets. The abovementioned features often result in suitable pharmacokinetic profiles, converting these structures into promising scaffolds for the development of new drugs.² On the other hand, the indole ring is one of the most commonly found heterocycles in medicinal chemistry, being present also in many natural products, especially as tryptophan (Trp) derivatives, and is considered a privileged substructure.³

A relevant example, where these two important substructures coexist, is brevianamide F [1, cyclo-(L-Trp-L-Pro), Fig. 1],⁴ which

has antibacterial and antifungal properties, and it has been used in the treatment of cardiovascular dysfunction⁵ and in cognitive enhancement.⁶ In addition, the structurally related tryprostatins A and B (2 and 3 respectively, Fig. 1), diketopiperazines featuring a prenyl moiety at C2 of the indole ring, exhibit cytotoxicity towards various cancer cell lines, the latter residue being essential for their biological activity.⁷ In this context, we explored the chemical modifications of DKP 1 to prepare arylated compounds 4 and determine the impact of the aryl group on the biological activity of the derivatized brevianamides (Fig. 1).

The development of new synthetic methodologies for the selective and straightforward chemical modification of peptides and natural products is a scientific challenge. Particularly, the introduction of aromatic rings into the indole nucleus to modulate the structure and bioactivity of selected peptides is becoming an important issue.⁸ In this context, two strategies have been developed to date: preliminary preparation of arylated-Trp residues by standard methods, and metal-catalyzed couplings from derivatized indole precursors, none of them being ideal in terms of feasibility and atom-step economies. Recently, a new synthetic methodology has been developed, which can solve these problems if properly applied: the metal-catalyzed C-C coupling through direct C-H activation.^{9,10} These

^aBarcelona Science Park, Baldori Reixac 10-12, 08028 Barcelona, Spain. E-mail: rlavilla@pcb.ub.es; Tel: +34-934037106

^bInstitute for Research in Biomedicine, Barcelona Science Park, Baldori Reixac 10-12, 08028 Barcelona, Spain

^cDepartment of Organic Chemistry, Faculty of Chemistry, University of Barcelona, Martí I Franqués 1-11, 08028 Barcelona, Spain

^dCIBER-BBN, Networking Centre on Bioengineering Biomaterials and Nanomedicine, Barcelona Science Park, Baldori Reixac 10, 08028 Barcelona, Spain

^eDepartment of Pathology and Experimental Therapeutics, Faculty of Medicine, University of Barcelona, Feixa Larga s/n, Pavelló de Govern. 08907 L'Hospitalet, Barcelona, Spain

^fSchool of Chemistry, University of KwaZulu-Natal, 4001-Durban, South Africa

^gLaboratory of Organic Chemistry, Faculty of Pharmacy, University of Barcelona, Avda. Joan XXII s.n., 08028 Barcelona, Spain

† Electronic supplementary information (ESI) available: Experimental procedures including spectra for all final compounds and biological assays. See DOI: 10.1039/c3md20353k

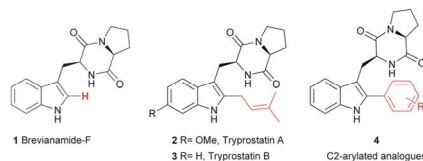


Fig. 1 Tryptophan containing diketopiperazines.

reactions allow the straightforward linkage of aryl groups (from haloarenes) to unsubstituted positions of aromatic rings, and have revolutionized the design and preparation of a wide range of organic compounds.

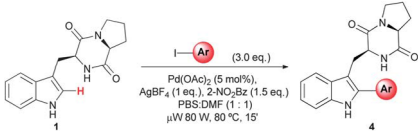
Aiming to confer either new or enhanced biological properties with respect to the parent compound, we have designed and synthesized a variety of DKPs 4 arylated at C2 of the indole ring (Fig. 1). The proposed route involves an efficient access to brevianamide F followed by a mild Pd-catalyzed C–H activation procedure. DKP 1 is a suitable probe to perform modifications at the indole system, as it is a small molecule that features stereogenic centres and bears amide groups, known to stabilize palladium intermediates. Ideally, the new derivatives should be obtained in a short and versatile synthetic sequence, allowing in principle the preparation of libraries of analogues by introduction of diverse structural, electronic and functional group variations on a single presynthesized peptide. In sharp contrast, strategies described in the literature to obtain a related collection of tryprostatin derivatives require long multistep approaches.^{7,11}

Brevianamide F (1, Scheme 1) was prepared following a solid-phase approach recently developed in our laboratory¹² that consists of anchoring Fmoc-Trp-OAllyl through its side chain to an aminomethyl resin previously functionalized with dihydropyran-2-yl groups using 4-[(3,4-dihydro-2H-pyran-2-yl)methoxy]benzoic acid (PPTS in DCE at 80 °C), deprotection of the C-terminal carboxylic group [Pd(PPh₃)₄/PhSiH₃ in DMF], coupling of H-Pro-OMe (PyBOP/DIEA in DMF), deprotection of the N-terminal amino function with piperidine in DMF, resulting in the concomitant DKP formation. Final cleavage of the peptide from the resin (TFA–mDMB–DCM [5 : 5 : 90 v/v]) conveniently affords the desired DKP 1 in a 56% overall yield (Scheme 1).

With respect to the arylation reaction of indoles, modern fundamental discoveries have paved the way to robust and reliable methodologies.¹³ Recently, this technique has also been used for the arylation of Trp and peptides containing this amino acid.¹⁴ Although solid-phase arylations tested upon resin-linked brevianamide (see structures in Scheme 1) were unproductive, the solution phase approach was successful. After exploring different conditions (combinations of solvents, additives, temperatures and reaction times), the C2 arylated compounds 4 were obtained through palladium-catalyzed reaction with

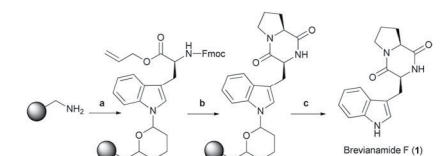
iodoareenes. Surprisingly, the first experiments under our standard conditions¹⁴ (Pd(OAc)₂, AgBF₄, *o*-NO₂Bz in DMF) showed a considerable degree of epimerization. This problem was conveniently suppressed with the use of microwave irradiation as the heat source, and the combination of PBS–DMF (1 : 1) as the solvent, carrying the transformation at 80 °C in only 15 min, with total conversion and stereochemical purity. The participation of other solvents or combinations thereof (DMF, DMSO, PBS), the use of higher temperatures or longer reaction times led to different degrees of epimerization, as shown in their respective HPLC profiles. Incidentally, in an elegant work, Cook *et al.* showed that the natural stereochemistry in tryprostatins is a requisite for antitumoral activity.⁷ In this way, both electron-donor and electron-withdrawing substituents at *ortho*, *meta* and *para* positions on the aryl iodide allowed the reaction, leading to the corresponding arylated compounds 4a–o cleanly and in convenient yields through this mild Pd-catalyzed C–H activation protocol (Table 1). Transformations involving *p*-iodoarenes were more efficient than the corresponding *m*- and *o*-substrates, where the electron-donor substituents lead to higher yields. A low reactivity was noticed when the highly deactivated *m,m*-bis-CF₃-iodoaryl group was tested, although the desired adduct could be isolated in a 13% yield (entry 13, Table 1). Also when a double C–H activation was attempted using two equivalents of 1 and *p*-diiodobenzene, the expected disubstituted product was obtained in the same range as the monosubstituted 4n (7% yield, entry 14, Table 1). Furthermore, the use of heterocyclic arenes such as 2-iodothiophene was explored, affording compound 4o with the usual high conversion, however difficulties in the purification resulted in an isolated yield of 9%

Table 1 Arylation of brevianamide F (1)



Entry	Ar-I	Compound	Yield ^a (%)
1	<i>p</i> -I-C ₆ H ₄ -CH ₃	4a	84
2	<i>p</i> -I-C ₆ H ₄ -OCH ₃	4b	86
3	<i>p</i> -I-C ₆ H ₄ -CF ₃	4c	73
4	<i>p</i> -I-C ₆ H ₄ -Cl	4d	72
5	<i>p</i> -I-C ₆ H ₄ -CO ₂ CH ₃	4e	95
6	<i>o</i> -I-C ₆ H ₄ -OCH ₃	4f	70
7	<i>o</i> -I-C ₆ H ₄ -CF ₃	4g	45 ^b
8	<i>o</i> -I-C ₆ H ₄ -Cl	4h	54
9	<i>m</i> -I-C ₆ H ₄ -OCH ₃	4i	73
10	<i>m</i> -I-C ₆ H ₄ -CF ₃	4j	51
11	<i>m</i> -I-C ₆ H ₄ -Cl	4k	71
12	<i>m</i> -I-C ₆ H ₄ -CO ₂ CH ₃	4l	40
13	<i>m,m</i> -I-C ₆ H ₄ -(CF ₃) ₂	4m	13 ^b
14	<i>p</i> -I-C ₆ H ₄ -I	4n	7
15	2-Iodothiophene	4o	9

^a Isolated yield. ^b An additional irradiation cycle was performed.



Scheme 1 Solid-phase synthesis of brevianamide F. Reagents and conditions: (a) (i) 4-[(3,4-dihydro-2H-pyran-2-yl)methoxy] benzoic acid (3 eq.), DIPCDI (3 eq.), Oxyma™ (3 eq.), DCM, 1 h; (ii) Fmoc-(S)-Trp-OAllyl (1.5 eq.), PPTS (2.3 eq.), DCE, 80 °C, 16 h (76%, two steps); (b) (i) Pd(PPh₃)₄ (0.4 eq.), PhSiH₃ (48 eq.), DCM, 30 min (2×), (ii) H-Pro-OMe-HCl (3 eq.), PyBOP (3 eq.), DIEA (9 eq.), DCM, 1 h (3×), (iii) 20% piperidine in DMF, 10 min (2×); (c) TFA–mDMB/DCM (0.5/0.5/9) (3×). 74% overall yield from the amino-acyl resin.

Concise Article

View Article Online
MedChemComm

(entry 15, Table 1). In this way a combinatorial set of C2 arylated brevianamide F derivatives was readily prepared (Fig. 2).

Regarding the biological studies, first the antiproliferative activity of the *p*-substituted compounds **4a–e** was evaluated against four human cancer cell lines: lung carcinoma A-549 cells, breast adenocarcinoma SK-BR-3 cells, colon adenocarcinoma HT-29 cells and cervical adenocarcinoma HeLa cells (see ESI†). Although low or moderate activity was determined for all compounds against the first three cell lines, a remarkable cytotoxicity in HeLa cells is observed for compounds **4c** ($26 \pm 4 \mu\text{M}$) and **4d** ($52 \pm 9 \mu\text{M}$), in comparison with brevianamide F (**1**), which is almost inactive ($>200 \mu\text{M}$) (Fig. 3).

These initial results were followed by the activity determination of the rest of the derivatives, in analogous experiments using puromycin as a cytotoxic control. Thus, the antiproliferative activity of compounds **4f–o** was tested in HeLa and HT-29 cells. Compounds bearing an *ortho*-substituent (**4f–h**) were in the same range of activity as compounds **4c** and **4d**. In addition, the *m,m*-disubstituted compound **4m** shows also moderate cytotoxic activity in HT-29 cells, in the μM range. Furthermore, to assess the impact of the diketopiperazine stereochemistry on the biological activity,⁷ three stereoisomers of **4c** arising from D-amino acids were prepared by standard arylation of the corresponding NH-diketopiperazine precursors. These new compounds (**4c'** and **4c''**, Fig. 4) were generated

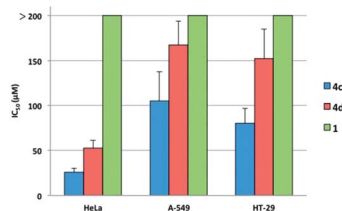


Fig. 3 Cytotoxicity evaluation of compounds **4c** and **4d** compared with brevianamide F (**1**). IC₅₀ (μM) in different cell lines for each compound.

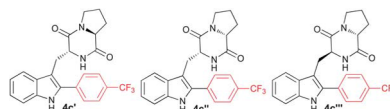


Fig. 4 Stereoisomeric **4c**-derivatives.

selectively as the Pd-mediated C–H activation proceeds without epimerization of the α -hydrogens. Only, DKP **4c'** showed antitumoral activity, comparable to the parent analogue **4c**. With respect to the mechanism of action, it was determined that neither **4c** nor **4c''** had effects on cell cycle arrest (see ESI†), therefore excluding cytostatic activity.¹⁵

Conclusions

Some of the novel C2-arylated brevianamide F analogues synthesized through our methodology showed antitumoral activity in the μM range, dramatically changing the properties of the parent compound. In spite of the moderate potency observed, our findings constitute a proof of concept since a structural modification upon an indole moiety modifies the bioactivity profile of the Trp-containing biomolecule. Thus, a mild antibiotic DKP is converted into a series of antitumoral compounds through a single-step straightforward transformation. The reported methodology enables the ensuing SAR studies, as the introduction of different substituents at distinct positions of the phenyl ring is feasible. Our approach is useful to generate active compounds in a combinatorial fashion and, therefore, can be appropriate for drug discovery purposes, opening the door to similar approaches involving more complex peptides. Remarkably, the synthetic access to these tryptostatin A mimetics is much shorter than reported syntheses. Work along this line is being carried out in our laboratories.

Experimental section

General procedure for the C2 arylation of the tryptophan residue in brevianamide F

Brevianamide **1** (ref. 12) (214 mg, 1 eq.), aryl iodide (3 eq.), AgBF₄ (1 eq.), 2-nitrobenzoic acid (1.5 eq.) and Pd(OAc)₂ (5%

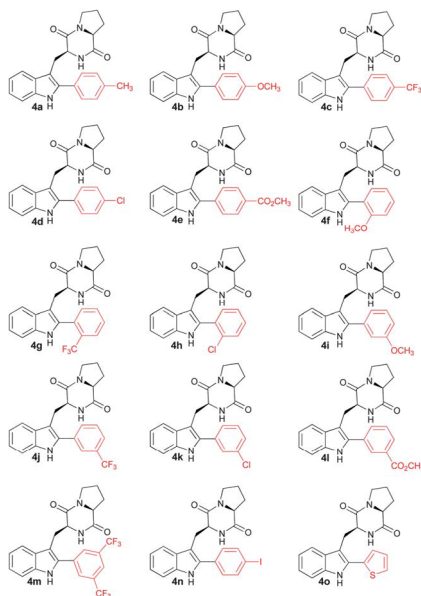


Fig. 2 C2-arylated brevianamide F derivatives.

mol) were placed in a microwave reactor vessel in a 1 : 1 mixture of PBS–DMF (total volume of 1200 μ L). The mixture was heated under microwave irradiation (80 W) at 80 °C for 15 min. In some cases, an additional irradiation cycle, adding AgBF_4 (1 eq.) and $\text{Pd}(\text{OAc})_2$ (5% eq.), was necessary in order to obtain a good conversion. Ethyl acetate (60 mL) was added and the resulting suspension was filtered through Celite. The filtrate was successively washed with aqueous saturated solutions of NH_4Cl (3×20 mL), NaHCO_3 (3×20 mL) and brine (3×20 mL), then the organic phase was dried over Na_2SO_4 , filtered and the solvent was removed under vacuum. The crude extract was purified by flash chromatography on silica gel to obtain **4** as a pure product.

Acknowledgements

This work has been partially financed by CICYT (BQU-CTQ2012-30930), FIS (PI10/00338), Generalitat de Catalunya (2009SGR 1024), the Institute for Research in Biomedicine Barcelona (IRB Barcelona), and the Barcelona Science Park. R.Z.-V. is supported by a "La Caixa-IRB Barcelona" grant.

Notes and references

- (a) A. S. M. Ressurreição, R. Delatouche, C. Gennari and U. Piarulli, *Eur. J. Org. Chem.*, 2011, 217–228; (b) A. D. Borthwick, *Chem. Rev.*, 2012, **112**, 3641–3716.
- N. Sewald and H.-D. Jakubke, in *Peptides: Chemistry and Biology*, Wiley-VCH, Verlag GmbH, Darmstadt (Germany), 2002.
- (a) F. Rodrigues de Sa Alves, E. J. Barreiro and C. A. M. Fraga, *Mini-Rev. Med. Chem.*, 2009, **9**, 782–793; (b) H. Zhao, A. C. Donnelly, B. R. Kusuma, G. E. L. Brandt, D. Brown, R. A. Rajewski, G. Vielhauer, J. Holzbeierlein, M. S. Cohen and B. S. J. Blagg, *J. Med. Chem.*, 2011, **54**, 3839–3853; (c) T. O. Painter, L. Wang, S. Majumder, X.-Q. Xie and K. M. Brummond, *ACS Comb. Sci.*, 2011, **13**, 166–174.
- R. B. A. Mehdi, K. A. Shaaban, I. K. Rebai, S. Smaoui, S. Bejar and L. Mellouli, *Nat. Prod. Res.*, 2009, **23**, 1095–1107, and references cited therein.
- H. Jamie, G. Kilian, K. Dyason and P. J. Milne, *J. Pharm. Pharmacol.*, 2002, **54**, 1659–1665.
- N. Tsuruoka, Y. Beppu, H. Kouda and H. Watanabe, JP. Pat., 296164, 2009.
- H. D. Jain, C. Zhang, S. Zhou, H. Zhou, J. Ma, X. Liu, X. Liao, A. M. Deveau, C. M. Dieckhaus, M. A. Jhonson, K. S. Smith, T. L. Macdonald, H. Kakeya, H. Osada and J. M. Cook, *Bioorg. Med. Chem.*, 2008, **16**, 4626–4651; incidentally, in this work the preparation of a phenyl-DKP (**4**, R = H, Fig. 1) through a long sequence is reported, but its bioactivity was not determined, probably due to the scarcity of the obtained material.
- For the pioneering work of Hruby in this field, including the synthesis of a C2-arylated Trp derivative through a multistep sequence, see: W. Wang, M. Cai, C. Xiong, J. Zhang, D. Trivedi and V. J. Hruby, *Tetrahedron*, 2002, **58**, 7365–7374.
- For recent reviews, see: (a) D. Alberico, M. E. Scott and M. Lautens, *Chem. Rev.*, 2007, **107**, 174–238; (b) X. Chen, K. M. Engle, D.-H. Wang and J.-Q. Yu, *Angew. Chem., Int. Ed.*, 2009, **48**, 5094–5115; (c) P. Mendoza and A. Echavarren in *Modern Arylation Methods*, ed. L. Ackermann, Wiley-VCH, Weinheim, 2009, pp. 363–399; (d) G. P. McGlacken and L. M. Bateman, *Chem. Soc. Rev.*, 2009, **38**, 2447–2464; (e) H. Li, C.-L. Sun, M. Yu, D.-G. Yu, B.-J. Li and Z.-J. Shi, *Chem.-Eur. J.*, 2011, **17**, 3593–3597.
- For C–H arylation of indoles, see: (a) E. M. Beck and M. J. Gaunt, in *C–H Activation, Topics in Current Chemistry* 292, ed. J.-Q. Yu and Z. Shi, Springer-Verlag, Heidelberg, 2010, pp. 87–121; (b) N. Lebrasseur and I. Larrosa, *Adv. Heterocycl. Chem.*, 2012, **105**, 309–351.
- E. Caballero, C. Avendaño and J. C. Menéndez, *J. Org. Chem.*, 2003, **68**, 6944–6951.
- C. Torres-García, M. Díaz, D. Blasi, I. Farras, I. Fernandez, X. Ariza, J. Farras, P. Lloyd-Williams, M. Royo and E. Nicolas, *Int. J. Pept. Res. Ther.*, 2012, **18**, 7–19.
- (a) N. Lebrasseur and I. Larrosa, *J. Am. Chem. Soc.*, 2008, **130**, 2926–2927; (b) R. J. Phipps, N. P. Grimster and M. J. Gaunt, *J. Am. Chem. Soc.*, 2008, **130**, 8172–8174.
- J. Ruiz-Rodríguez, F. Albericio and R. Lavilla, *Chem.-Eur. J.*, 2010, **16**, 1124–1127.
- Although there are clear differences in antitumoral potency, depending on the stereochemical and substitution patterns, strictly speaking a nonspecific mechanism of action, such as a membrane disruption, cannot be ruled out.

Supporting Information

Synthesis and Biological Evaluation of a Postsynthetically Modified Trp-Based Diketopiperazine

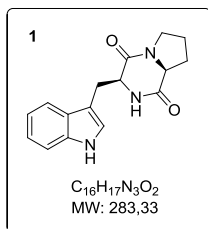
The following data is a selection of the content of the Supporting Information. Full supplementary information including general experimentation, procedures, compound characterization and biological evaluation is available in the Supporting Information in electronic format.

Table of Contents

<i>Experimental procedures and characterization data for selected compounds</i>	<i>67</i>
<i>Spectroscopic data for selected compounds</i>	<i>69</i>
<i>Biological Evaluation.</i>	<i>71</i>

Experimental procedures and characterization data for selected compounds

Solid-Phase Synthesis of Brevianamide F (1)



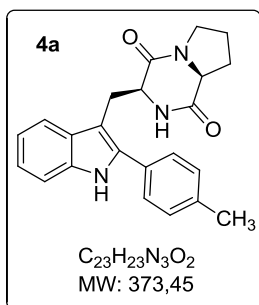
Aminomethyl-polystyrene resin (0.37 mmol g^{-1} , 5 g, 1.85 mmol) was introduced into a polypropylene syringe fitted with a porous polystyrene frit and was washed successively with DCM (10×30s), TFA (40% v/v) in DCM (1×1 min and 2×10 min), DCM (5×30s), DIEA (5% v/v) in DCM (6×2 min), DCM (5×30s), DMF (5×30s) and DCM (5×30s). 4-[[3,4-Dihydro-2H-pyran-2-yl)methoxy]benzoic acid (1.30 g, 5.55 mmol), DIPCDI (0.85 mL, 5.49 mmol) and ethyl cyanoglyoxyl-2-oxime (0.7 g, 5.55 mmol) in DCM (40 mL) were then added and the mixture was allowed to stand for 1 h at rt with occasional manual stirring. The resin was then washed with DCM (5×30s). Fmoc-Trp-OAI (1.3 g, 2.79 mmol) and PPTS (1.1 g, 4.38 mmol) in DCE were then added to the handle-resin and the suspension was shaken at 80 °C for 16 h in an Advanced Chemtech PLS 4x4 organic synthesizer. After cooling to rt the aminoacyl-resin was washed successively with DCM (5×30s), DMF (5×30s) and MeOH (5×30s). Spectrophotometric quantification of the dibenzofulvene-piperidine adduct indicated a 76% yield for amino acid coupling. After washing with DMF (5×30s) and DCM (5×30s) this resin was placed under Ar and Pd(PPh₃)₄ (0.86 g, 0.74 mmol) and PhSiH₃ (11 mL, 89.24 mmol) in DCM (40 mL) were added. The mixture was shaken for 30 min at rt, filtered and washed with DCM (8×30s). A second treatment with Pd(PPh₃)₄ and PhSiH₃ in DCM was then carried out. After filtration the resin was washed successively with DCM (8×30s), diethyl dithiocarbamate (5% v/v) in DMF (2×5 min), DMF (5×1 min), DCM (5×30s) and DMF (5×30s). The resin was then treated with H-Pro-OMe-HCl (0.72 g, 5.57 mmol), PyBOP (2.90 g, 5.57 mmol) and DIEA (3 mL, 17.22 mmol) in DMF (40 mL) for 60 min with occasional manual stirring. The resin was washed with DCM (5×30s) and DMF (5×30s). This coupling reaction and washing cycle was then repeated twice using the same quantities of reagents and solvents. The resulting resin was treated with piperidine (20% v/v) in DMF (2×10 min), was washed with DMF (5×30s) and DCM (5×30s) and dried. Cleavage of the product from the resin was brought about by treatment with TFA/*m*DMB/DCM (5:5:90 v/v) (3×10 min) and the collected washings were submitted to solvent removal. The crude product was washed with hexanes and the remaining solid was centrifuged (10 min at 6000 rpm) and filtered, affording **1** as a foamy white solid (0.37 g, 71 %).

¹H-NMR (400 MHz, DMSO-*d*₆) δ 1.37 (m, 1H), 1.64 (m, 2H), 1.95 (m, 1H), 3.08 (dd, *J* = 14.9, 5.7 Hz, 1H), 3.26 (m, 2H), 3.39 (m, 1H), 4.04 (bt, *J* = 8.3 Hz, 1H), 4.29 (bt, *J* = 4.9 Hz, 1H), 6.95 (bt, *J* = 7.5 Hz, 1H), 7.05 (bt, *J* = 7.5 Hz, 1H), 7.18 (d, *J* = 2.1 Hz, 1H), 7.32 (d, *J* = 8.2 Hz, 1H), 7.56 (d, *J* = 7.9 Hz, 1H), 7.72 (s, 1H), 10.9 (s, 1H) ppm. **¹³C-NMR** (100 MHz, DMSO-*d*₆): δ 21.9, 25.8, 27.7, 44.6, 55.3, 58.4, 109.3, 111.2, 118.2, 118.7, 120.9, 124.4, 127.4, 136.0, 165.5, 169.1 ppm. **IR** (KBr, cm⁻¹) ν = 3290.93, 3262, 2873.42, 1675.84, 1654.62, 1620.88, 1457.92, 1451.17, 1428.99, 1341.25, 1301.72, 1242.9, 1223.61, 1109.83, 738.60, 693.28, 681.71, 642.18, 563.11, 431.98 cm⁻¹. **HRMS (ESI)** calcd for C₁₆H₁₈N₃O₂ (M+H)⁺ 284.1399, found 284.1394.

General procedure for the C2 arylation of the indole residue in brevianamide F:

Unless stated otherwise, Brevianamide F (1 equiv), aryl iodide (3 equiv), AgBF_4 (1 equiv), 2-nitrobenzoic acid (1.5 equiv) and $\text{Pd}(\text{OAc})_2$ (5 % equiv) were placed in a microwave reactor vessel in a 1:1 mixture of DMF:PBS (total volume of 1200 μL). The mixture was heated under microwave irradiation (80 W) at 80°C for 15 min. When detailed, a second irradiation cycle (15 min) was performed, adding extra AgBF_4 (1 equiv) and $\text{Pd}(\text{OAc})_2$ (5 % equiv). Ethyl acetate (60 mL) was added and the resulting suspension was filtered through Celite. The filtrate was successively washed with aqueous saturated solutions of $\text{NH}_4\text{Cl}_{\text{sat}}$ (3x20 mL), $\text{NaHCO}_3_{\text{sat}}$ (3x20 mL) and brine (3x20 mL), then the organic phase was dried over Na_2SO_4 , filtered and the solvent was removed under vacuum. Unless otherwise quoted, the crude extract was purified by flash chromatography on silica gel (hexane/ethyl acetate) to obtain **4** as a pure product.

(3*S*,8*aS*)-3-((2-(*p*-Tolyl)-1*H*-indol-3-yl)methyl)hexahydropyrrolo[1,2-*a*]pyrazine-1,4-dione (**4a**)



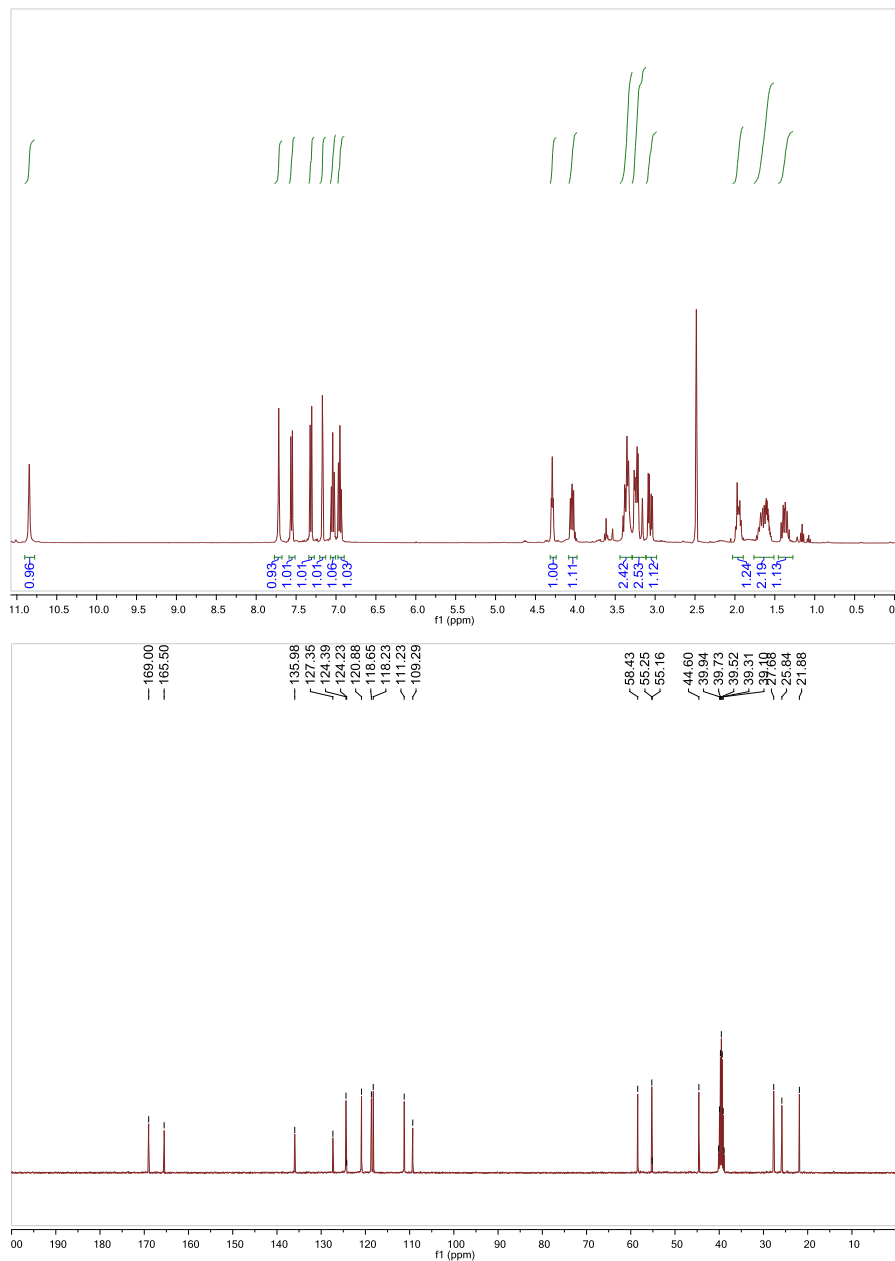
Compound **4a** was prepared according to the general procedure using 1-iodo-4-methylbenzene (492.8 mg, 2.26 mmol). The crude product was purified by flash chromatography on silica using methyl *tert*-butyl ether (MTBE) to obtain **4a** as a white solid (235.3 mg, 84 %).

$^1\text{H-NMR}$ (400 MHz, CDCl_3): δ 8.26 (s, 1H), 7.59 (d, $J = 7.9$ Hz, 1H), 7.45 (d, $J = 8.0$ Hz, 2H), 7.40 (d, $J = 8.1$ Hz, 1H), 7.28 (s, 1H), 7.23 (dd, $J = 8.1, 1.1$ Hz, 1H), 7.19 – 7.13 (m, 1H), 5.46 (s, 1H), 4.36 (d, $J = 9.3$ Hz, 1H), 3.98 (s, 1H), 3.88 (dd, $J = 15.2, 3.7$ Hz, 1H), 3.58 (tt, $J = 11.5, 10.3$ Hz, 2H), 3.21 (dd, $J = 15.2, 11.6$ Hz, 1H), 2.40 (s, 3H), 2.31 – 2.24 (m, 1H), 2.00 (dd, $J = 14.3, 7.8$ Hz, 2H), 1.91 – 1.82 (m, 1H) ppm. **$^{13}\text{C-NMR}$** (100 MHz, CDCl_3): 169.33, 165.74, 138.21, 136.75, 136.04, 129.79, 129.23, 128.32, 128.21, 122.66, 120.12, 118.39, 111.35, 105.67, 59.10, 54.54, 45.35, 28.14, 25.50, 22.57, 21.23 ppm. **IR** (Film, cm^{-1}) $\nu = 3365.84, 3282.56, 3051.96, 2975.09, 2949.47, 2923.84, 2879.00, 1668.33, 1463.35, 1424.91, 1303.20, 1258.36, 1104.63, 1014.95, 912.46, 829.18, 739.50, 656.23$ cm^{-1} . **HRMS** (ESI) m/z calcd 374,1790 ($\text{C}_{23}\text{H}_{24}\text{N}_3\text{O}_2$) found 374.1873 ($\text{M}+\text{H}$) $^+$.

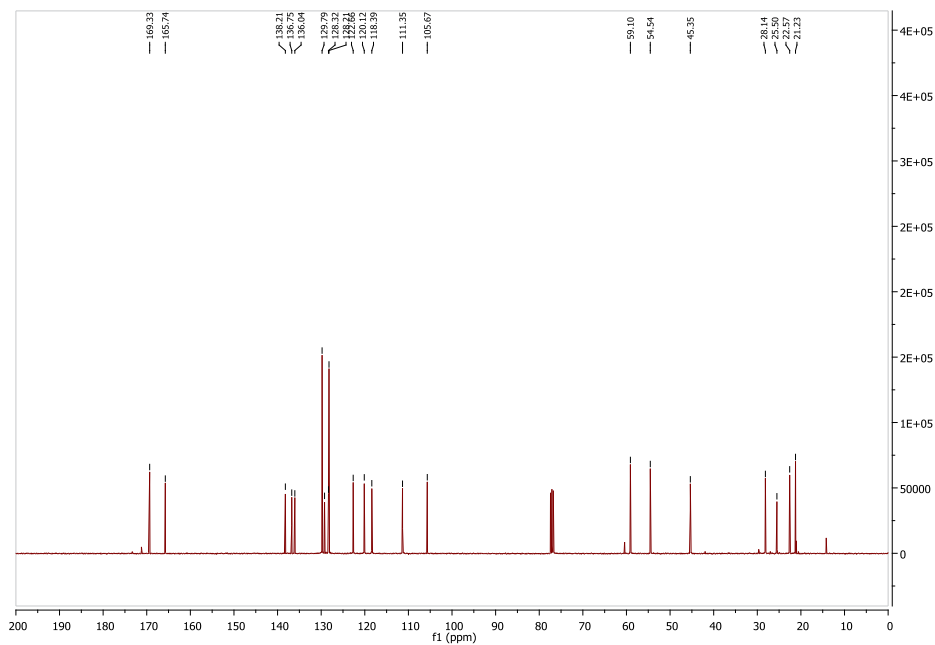
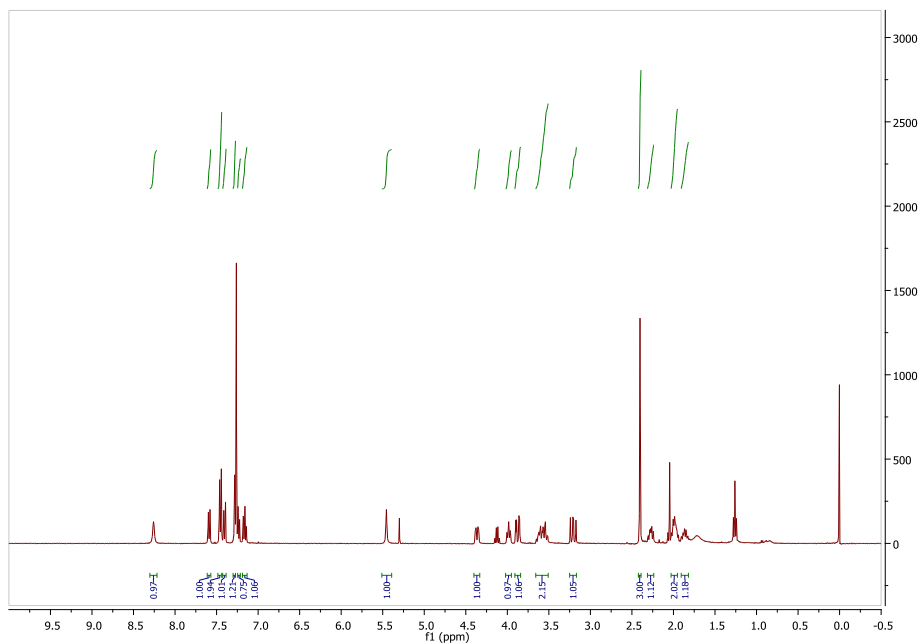
Spectroscopic data for selected compounds

NMR spectra are available in the supporting information in electronic format.

Brevianamide F (1)



(3S,8aS)-3-((2-(*p*-Tolyl)-1*H*-indol-3-yl)methyl)hexahydropyrrolo[1,2-*a*]pyrazine-1,4-dione (4a)



Biological Evaluation.

Cytotoxicity assay for compounds 4a-o

Table 1. Cytotoxicity evaluation (IC_{50} , $\mu M \pm SD^1$) of compounds **4a-e** and a reference compound (brevianamide F, **1**) against selected tumor cell lines.

Cell line	4a	4b	4c	4d	4e	1
HeLa	135.0 \pm 9.0	157.2 \pm 12.7	25.8 \pm 4.2	52.2 \pm 9.2	>200	>200
A-549	149.7 \pm 24.4	>200	104.6 \pm 33.2	167.2 \pm 26.3	>200	>200
SK-BR-3	>200	>200	127.2 \pm 43.7	>200	>200	>200
HT-29	>200	191.3 \pm 24.4	80.4 \pm 16.2	152.1 \pm 32.9	>200	>200

¹ SD: standard deviation. All experiments were independently performed at least three times.

Table 2. Cytotoxicity evaluation (IC_{50} , $\mu M \pm SD^1$) of compounds **4a-o** and a reference compound (puromycin) against selected tumor cell lines.

Compound	HeLa cells	HT-29 cells
4a	160.2 \pm 9.2	214.9 \pm 10.0
4b	193.8 \pm 10.7	205.3 \pm 7.0
4c	62.0 \pm 11.5	118.5 \pm 7.7
4d	81.8 \pm 12.0	184.3 \pm 7.8
4e	208.7 \pm 17.8	204.1 \pm 10.5
4f	82.2 \pm 12.0	143.0 \pm 15.7
4g	82.4 \pm 18.6	153.7 \pm 12.4
4h	66.7 \pm 17.4	144.2 \pm 13.2
4i	172.1 \pm 25.8	200.3 \pm 9.9
4j	255.4 \pm 11.8	187.8 \pm 6.9
4k	174.6 \pm 18.5	200.3 \pm 12.7
4l	190.3 \pm 19.6	177.6 \pm 14.2
4m	160.3 \pm 23.7	64.2 \pm 15.8
4n	146.6 \pm 13.3	170.8 \pm 8.6
4o	170.1 \pm 11.5	177.6 \pm 15.2
Puromycin	0.7 \pm 0.1	3.6 \pm 1.2

¹ SD: standard deviation. All experiments were independently performed at least three times.

Cell Viability Assay for compounds **4c-4c'''**

Table 3. Cell viability assay (IC_{50} , $\mu M \pm SD^1$) for compounds **4c-4c'''** at 72h treatment (μM).

Compound	MDA-MB-231	Cal27	A549
4c	161.27 ± 10.53	182.14 ± 7.7	179.61 ± 8.34
4c'	$>200 \mu M$	$>200 \mu M$	$>200 \mu M$
4c''	161.35 ± 8.24	137.72 ± 29.20	185.92 ± 12.75
4c'''	$>200 \mu M$	$>200 \mu M$	$>200 \mu M$

PUBLICATION II.

Synthesis of C-2 arylated tryptophan amino acids and related compounds through palladium-catalyzed C–H activation

Sara Preciado,^{#, a} Lorena Mendive-Tapia,^{#, b, c} Fernando Albericio,^{b, c, d, e} and Rodolfo Lavilla^{a, f}

[#] Both researchers have contributed equally to this work.

The Journal of Organic Chemistry, 2013, 78, 8129-8135.

a) Barcelona Science Park, Baldiri Reixac 10-12, 08028 Barcelona, Spain.

b) Institute for Research in Biomedicine, Barcelona Science Park, Baldiri Reixac 10-12, 08028 Barcelona, Spain.

c) Department of Organic Chemistry, University of Barcelona, Martí i Franquès 1-11, 08028 Barcelona, Spain.

d) CIBER-BBN, Networking Centre on Bioengineering Biomaterials and Nanomedicine, Barcelona Science Park, Baldiri Reixac 10, 08028 Barcelona, Spain.

e) School of Chemistry, University of KwaZulu-Natal, 4001-Durban, South Africa.

f) Laboratory of Organic Chemistry, Faculty of Pharmacy, University of Barcelona, Avda. Joan XXII s.n. 08028 Barcelona, Spain.

Synthesis of C-2 Arylated Tryptophan Amino Acids and Related Compounds through Palladium-Catalyzed C–H Activation

Sara Preciado,^{†,▽} Lorena Mendive-Tapia,^{‡,§,▽} Fernando Albericio,^{*,‡,§,||,⊥} and Rodolfo Lavilla^{*,†,#}

[†]Barcelona Science Park, Baldiri Reixac 10-12, 08028 Barcelona, Spain

[‡]Institute for Research in Biomedicine, Barcelona Science Park, Baldiri Reixac 10-12, 08028 Barcelona, Spain

[§]Department of Organic Chemistry, University of Barcelona, Martí i Franqués 1-11, 08028 Barcelona, Spain

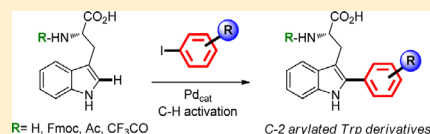
^{||}CIBER-BBN, Networking Centre on Bioengineering Biomaterials and Nanomedicine, Barcelona Science Park, Baldiri Reixac 10, 08028 Barcelona, Spain

[⊥]School of Chemistry, University of KwaZulu-Natal, 4001-Durban, South Africa

[#]Laboratory of Organic Chemistry, Faculty of Pharmacy, University of Barcelona, Avda. Joan XXII s.n. 08028 Barcelona, Spain

Supporting Information

ABSTRACT: Tryptophan (Trp) and tryptophan derivatives are C2-arylated. A C–H activation process allows the preparation of both protected and unprotected arylated-Trp amino acids, directly from the amino acid precursor and aryl iodides. The obtained compounds are suitable for standard solid-phase peptide synthesis.



Although tryptophan (Trp) shows a low relative abundance in peptide and protein sequences (around 1% of the overall amino acids), its presence is of crucial importance for the activity of these molecules. Furthermore, Trp is a common precursor to a wide range of biologically active compounds (natural products and drugs), and its structural, chemical, and biological roles make it an ideal site for selective chemical modifications. The access to modified Trp peptides would provide novel and useful applications in organic chemistry, drug discovery, and medicinal chemistry.¹ Furthermore, it would open the possibility of preparing new chemically modified peptides that are potentially useful in chemical biology. Right now, this goal is only achievable through *de novo* synthesis of the non-natural amino acid, by means of long stepwise syntheses,² with the exception of C- and N-allylations, which have been reported through Pd-catalyzed transformations.³

Indole, the heterocyclic residue of Trp, is probably one of the most abundant heterocycles in nature. Owing to the great structural diversity of biologically active indoles, it is not surprising that this ring system has become an important structural component in many pharmaceutical agents. Substituted indoles have been referred to as “privileged substructures” since they appear in many scaffolds capable of binding a variety of different receptors with high affinity.⁴ Incidentally, the 2-arylindole moiety has gained relevance in medicinal chemistry and is considered a common scaffold.⁵ Interestingly, the synthetic access to related drugs relies on its previous preparation. For well over a hundred years, the synthesis and functionalization of indoles has been a major area of focus for synthetic organic chemists, and numerous methods for the preparation of indoles have been described.⁶

Thus, the development of new synthetic methodologies for the selective chemical modification of Trp is of major importance. Particularly, the introduction of aromatic moieties into the indole ring of the Trp to modulate the structure and bioactivity of the selected biomolecules might be a challenging issue. Recently, the metal-catalyzed C–C coupling through direct C–H activation⁷ for the functionalization of indoles has been extensively studied.⁸

Particularly relevant to our research was Larrosa’s methodology for indole arylation using Pd(OAc)₂, Ag₂O, and *o*-nitrobenzoic acid (2-NO₂BzOH) in DMF.^{8c} In this context, we described C-2 arylation of indoles in Trp derivatives and peptides through a Pd-catalyzed C–H activation protocol, allowing the preparation of a variety of peptide sequences with modified Trp moieties (Figure 1a).^{9,10} In this work, it was determined that unprotected Trp was not reactive under the original conditions, and only the *N*^ε-acetyl tryptophan methyl ester (Ac-Trp-OMe) could be properly arylated, using high-temperature microwave (MW) activation.¹¹ As the Ac is not a friendly group to mask the amino function, applicability of that methodology for the preparation of some peptides containing modified Trp units was restricted and, therefore, prompted us to tackle this problem (Figure 1b). Thus, a more convenient *N*-protecting group was tested next, and the *N*^ε-trifluoroacetyl (Tfa) Trp 1a could be successfully arylated (Table 1, entry 1). Although this group can be hydrolytically removed in solution, it was reluctant to standard deprotection methods in the solid phase,¹² which is the method of choice for the preparation of peptides.

Received: May 2, 2013

Published: July 18, 2013

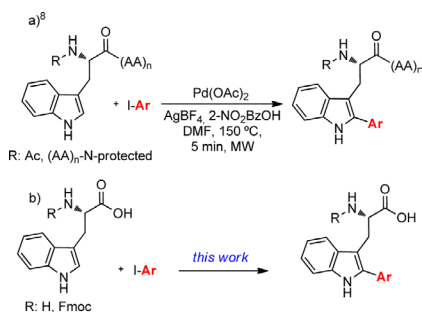


Figure 1. Arylation of indole in Trp derivatives.

As a starting point, we analyzed the reaction of native Trp **1b** using our standard conditions (2-NO₂-BzOH, 150 °C, MW), but the arylated product was obtained just in traces in a complex mixture (Table 1, entry 2). Satisfactorily, the use of TFA alone (1 equiv) afforded 75% in 20 min (Table 1, entry 3). This result encouraged us to optimize the process using this acid, which apparently removes the incompatibility of a free amino group. In this regard, TFA is more convenient than other carboxylic acids, as it is water-soluble, has a low boiling point, and, therefore, can be conveniently removed, not hampering the stability and purification of the final products. Although traces of the acid could remain in the crude residue after standard evaporation, the use of TFA constitutes a practical improvement for this transformation, as it does not require chromatographic methods for the removal of the acid input. Also, it is evident that working at temperatures well below 150 °C is essential to keep the integrity of the Trp amino acids. Working at 90 °C under the same conditions allowed us to reduce the amount of aryl iodide while slightly increasing the conversion (87%, Table 1, entry 4). However, a slightly higher temperature (100 °C) resulted in a less efficient transformation

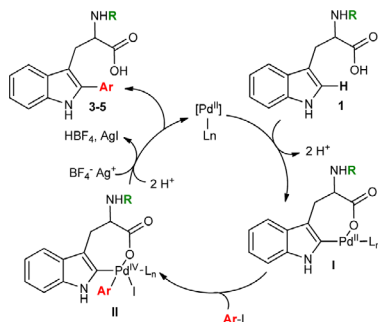
(Table 1, entry 5), probably fixing the practical limit of this reaction. Interestingly, the absence of an external acidic source still allowed the arylation process, although in lower conversion (Table 1, entry 6). Interestingly, a key parameter was the amount of Ag⁺ salt present. Thus, using an excess of the Ag⁺ salt (Table 1, entry 7) gave a practically quantitative reaction. Next, the Fmoc-Trp-OH derivative **1c**, which can be used directly in a solid-phase peptide synthesis, was assayed to be arylated (Table 1, entry 8), and again the use of 2 equiv of AgBF₄ afforded a quantitative transformation.¹³ Incidentally, these optimized conditions lead to a total conversion of Tfa-Trp-OH derivative **1a** into **3** (Table 1, entry 9). Excess of TFA (up to 4 equiv) did not improve the yields, whereas the use of Ag₂CO₃ or different Pd sources [Pd(TFA)₂] was not beneficial. On the other hand, the presence of additives (LiCl, Cs₂CO₃, K₂CO₃) was detrimental to the reaction, leading to lower conversions.

A hypothetical mechanism for this C–H activation may proceed through a catalytic cycle involving Pd(II)/Pd(IV) species, taking into account the intramolecular coordination of the carboxylic acid moiety and the facilitated formation of the putative palladacycle (Scheme 1).^{7a,14} However, alternative Pd(0)/Pd(II) pathways could also be considered in this context, starting with the Pd insertion into the C–I bond, the C–H activation taking place upon the metalated intermediate.^{7c,8c} The role of silver salts and carboxylic acids seems to be critical for the fate of the catalytic cycle. First, coordination of Trp derivative **1** to the Pd^{II} species may evolve through indole palladation, presumably by a concerted metalation deprotonation mechanism¹⁵ to generate Pd^{II} complex **I**. Insertion of this intermediate upon the C–I bond of the aryl halide by oxidative addition yields the palladium(IV) complex **II**, and then silver cation (I) acts as a halide scavenger, removing the iodide and setting up the reductive elimination to release the arylated products **3–5** and regenerate the Pd(II) catalyst.¹⁶ Additionally, TFA is acidic enough (pK_a = 0.23) to protonate the amino group of the unprotected Trp, avoiding in this way an unproductive amino acid coordination.¹⁷

Table 1. Selected Optimization Results for the Arylation of Tryptophans (**1**) under Microwave Irradiation^a

entry	R	T (°C)	time (min)	acid ^b	AgBF ₄ (equiv)	I-Ar (equiv)	conv (%) ^c
1	Tfa ^d	150	5	2-NO ₂ -BzOH	1.0	4.0	76
2	H	150	15	2-NO ₂ -BzOH	1.0	4.0	<5
3	H	80	20	TFA	1.0	3.0	75
4 ^e	H	90	20	TFA	1.0	1.5	87
5	H	100	20	TFA	1.0	1.5	78
6	H	100	20		1.0	1.5	49
7	H	90	20	TFA	2.0	1.5	>99
8	Fmoc	90	20	TFA	2.0	1.5	>99
9	Tfa	90	20	TFA	2.0	1.5	>99

^aUnless otherwise noted, all reactions were carried out using 5 mol % Pd(OAc)₂ and 1.0 equiv of Trp in a 0.2 M solution. ^b1.5 equiv of 2-NO₂-BzOH (entries 1 and 2) and 1.0 equiv of TFA were used. ^cConversion measured by HPLC. ^dTfa = trifluoroacetyl. ^eThese reactions were also tested using PBS/DMF (1:1) as a solvent, and other silver salts, without any relevant improvement.

Scheme 1. Proposed Mechanism for the Reaction of Trp Amino Acid with Aryl Iodides

Furthermore, the trifluoroacetate anion can also coordinate with the metal to render it more electrophilic and also take part in the deprotonation and proton transfer steps. DMF seems to be very suitable for this process as it dissolves all the reactants involved and is also a ligand, capable to stabilize palladium intermediates as well.

We next examined the scope of the reaction with a variety of differently substituted aryl iodides. As shown in Table 2,

Table 2. C-2 Arylation of Fmoc-Trp-OH Amino Acid 1c

entry	I-Ar	compound	yield (%) ^a
1	C ₆ H ₅ -	5a	56
2 ^b	C ₆ H ₅ -	5a'	51
3	<i>p</i> -NO ₂ -C ₆ H ₄ -	5b	91
4	<i>p</i> -MeO-C ₆ H ₄ -	5c	68
5	<i>p</i> -Br-C ₆ H ₄ -	5d	62
6	<i>m</i> -CF ₃ -C ₆ H ₄ -	5e	59
7	<i>o</i> -F-C ₆ H ₄ -	5f	77
8	<i>p</i> -Me-C ₆ H ₄ -	5g	81
9	<i>p</i> -MeO-C ₆ H ₄ -	5h	63
10	1-pyrenyl	5i	66
11	2-thienyl		^c

^aYields are of the isolated pure material. ^bOpposite absolute stereochemistry (R). ^cConversion lower than 15%; the thienyl-Trp was detected (¹H NMR, HPLC-MS) but not purified.

excellent yields are obtained in the reaction of Fmoc-Trp-OH with several aryl iodides. Both electron-withdrawing (5b–5f) and electron-donating substituents (5g–5h) are suitable groups for this transformation. Furthermore, a rather hindered pyrenyl fluorophore was introduced (5i), which would allow the synthesis of labeled Trp-containing peptides.¹⁸ With respect to heterocyclic iodides, although an α -thienyl residue can be attached to the Trp-2 position, the reactivity was low and purification problems precluded the isolation of the corresponding adduct (Table 2, entry 11). In this way, an array of

arylated Fmoc-Trp derivatives were prepared in a direct manner with useful yields (Table 2) in scalable procedures (up to 500 mg of the Fmoc-Trp-OH was successfully arylated). Interestingly, the mild conditions allowed us to preserve the stereochemical integrity of the parent amino acid. Thus, the *S* and *R* enantiomers of the Fmoc-Trp-OH were separately subjected to the arylation reaction to yield compounds 5a and 5a', respectively (entries 1 and 2, Table 2), whose chromatographic behavior (chiral HPLC, see the Supporting Information) confirmed the conservation of the initial absolute stereochemistry.¹⁹

To prove the suitability for standard solid-phase peptide synthesis of the arylated-Trp amino acids, two peptide sequences were chosen as proof of principle (Table 3). The

Table 3. Solid-Phase Synthesis of Peptide Sequences Containing Arylated-Trp Amino Acids

entry	peptide	compound
1	H-Met-Gly-Trp(C2- <i>p</i> -methylphenyl)-Ala-OH	6
2	H-Trp-Gly-Trp(C2- <i>p</i> -methylphenyl)-Ala-OH	7

syntheses were performed using Fmoc-based SPPS on a 2-chlorotrityl chloride resin and standard coupling protocol. *N*-Terminal peptide chain elongation was carried out by anchoring the *N*⁶-Fmoc protected amino acids with DIC/OxymaPure, followed by Fmoc deprotection in an iterative manner. Finally, sequences 6–7 were cleaved from the resin with 5% TFA in DCM, affording the corresponding peptides in high yield and purity (more than 99%), as determined by integration of the chromatographic peak areas of RP-HPLC-ESMS. The direct introduction of the Fmoc-arylated amino acid 5f on the solid phase is very efficient and also overcomes the limitation encountered in previous studies regarding sequences containing sulfur-amino acids (Met or Cys). It also allows the selective preparation of arylated Trp peptides in sequences with multiple Trp units.⁹

As the carboxylic acid moiety in Trp seems to actively promote the arylation by coordination with the palladium species, we extended this methodology to a series of indole-carboxylic acids having the CO₂H linked to the heteroaromatic ring by spacers of different lengths (1–4 bonds, Table 4). In this way, the corresponding arylated compounds 8–12 were obtained in high yields. However, remarkably, the indole 3-

Table 4. C-2 Arylation of Indole-Carboxylic Acids and Tryptamines

entry	R	compound	yield (%) ^a
1	CO ₂ H	8	79
2	CH ₂ CO ₂ H	9	75
3	CH ₂ CH ₂ CO ₂ H	10	74
4	CH ₂ CH ₂ CH ₂ CO ₂ H	11	48 ^b
5	CH ₂ CH ₂ NH ₂	12	73
6	CH ₂ CH ₂ NHAc		

^aYields are of the isolated pure material. ^bThe reaction was carried out using two MW cycles, without adding TFA.

carboxylic acid was not reactive under these conditions, and the expected adduct was not detected. Incidentally, indoleacetic acid is a natural plant hormone involved in growth and development, and indolebutyric acid is a synthetic and metabolically more stable analogue.²⁰ Taking into account the potential bioactivity of derivatives 8–10, it is relevant to note the easy access to these compounds. Furthermore, compound 10 is also a patented IL-8 receptor antagonist,^{21,22} whereas the other two phenyl-indole carboxylic acids 8 and 9 also showed interesting biological properties.²³ Interestingly, their preparation is reported through long stepwise synthetic sequences. Using our methodology, a more direct synthetic approach to this family of compounds can be feasible using cheap common indole precursors and a variety of commercially available aryl iodides in just one step.

Analogously, tryptamine was arylated under these acidic conditions (1 equiv TFA) to yield compound 11, as expected in a low conversion (16%). However, when operating in the absence of TFA, an improved transformation (48%, Table 4, entry 5) was determined, suggesting that, in this case, the aminopalladacycle was an intermediate en route of the final compound.²⁴ In agreement with previous results,⁹ the *N*-acetyltryptamine was satisfactorily arylated to yield derivative 12 (73%). This compound was prepared in higher yields and under much milder conditions than previously reported in a distinct C–H activation protocol.²⁵ Overall, the process is effective upon Trp, indole carboxylic acids, indole amines and amides. It has to be stated that, although different coordination modes are feasible depending on the substrate, TFA protonation allows the arylation of the free amino acids, which was not possible in the previous protocol.⁹ Presumably, the formation of palladium–amino acid complexes is inhibited in these conditions, leading to productive catalytic cycles.

In conclusion, we have developed a synthetic methodology to α -arylated indoles in Trp, tryptamines, and β -substituted indole carboxylic acids, which is simple, high-yielding, versatile, and mild enough to allow the efficient transformation of biomolecules. Remarkably, the intramolecular ligand effect of the carboxylic acid seems to facilitate the process, as the conditions are milder than many C–H arylations previously reported upon 3-substituted indoles. Application of the newly synthesized amino acid derivatives to the preparation of modified Trp-containing peptides through solid-phase methodology has shown to be efficient.

■ EXPERIMENTAL SECTION

Reactions were monitored by RP-HPLC-ESMS at 220 nm and thin-layer chromatography using Merck silica gel 60 F254 TLC glass plates and visualized with UV at 254 nm. Chromatographic purification was performed with flash chromatography on silica 60A, 35–70 nm from SDS. Yields refer to chromatographically pure compounds. NMR spectra were recorded on a 400 spectrometer, operating at 400 MHz for ¹H, 100 MHz for ¹³C, and 376 MHz for ¹⁹F. Chemical shifts (δ) are reported in parts per million. Multiplicities refer to the following abbreviations: s = singlet, d = doublet, t = triplet, dd = double doublet, dt = double triplet, q = quartet, p = pentuplet, and m = multiplet. IR spectra were obtained with an FTIR spectrometer and are reported in cm^{−1}. HRMS (ESI positive) were obtained with a linear ion trap mass analyzer. Optical rotation was performed using MeOH as solvent. All microwave reactions were carried out in 10 mL sealed glass tubes in a focused monomode microwave oven ("Discover" by CEM Corporation) featured with a surface sensor for internal temperature determination. Cooling was provided by compressed air ventilating the microwave chamber S3 during the reaction. The chiral chromatography was performed in a linear gradient of CH₃CN

(+0.1% TFA) into H₂O (+0.1% TFA) from 50% to 90% CH₃CN, and a chiral HPLC column (Chiralpak ia, Amylose tris(3,5-dimethyl-phenylcarbamate) immobilized on 5 μ m silica gel, 250 \times 2 mm).

Preparation of (S)-3-(1*H*-indol-3-yl)-2-(2,2,2-trifluoroacetamido)propanoic Acid (1a).²⁶ Compound 1a was prepared using amino acid 1b (1.0 g, 5.0 mmol). The system was purged with N₂, and the amino acid was dissolved in anhydrous MeOH (4.5 mL). With stirring, NEt₃ (696.5 μ L, 5.0 mmol) was added, followed by ethyl trifluoroacetate (1.5 mL, 12.8 mmol) after 5 min. The reaction was left under vigorous agitation at r.t. for 24 h. The solvent was removed under vacuum, and the crude product was dissolved in H₂O (46 mL) and acidified with concentrated HCl (1 mL). The precipitate was filtered by a filter plate, leaving 1a as a white solid (1.22 g, 81%). ¹H NMR (400 MHz, DMSO): δ 10.84 (d, *J* = 2.5 Hz, 1H), 9.74 (d, *J* = 8.1 Hz, 1H), 7.53 (d, *J* = 7.8 Hz, 1H), 7.32 (d, *J* = 8.1 Hz, 1H), 7.12 (d, *J* = 2.3 Hz, 1H), 7.08–7.02 (m, 1H), 6.97 (t, *J* = 7.4 Hz, 1H), 4.49 (ddd, *J* = 10.3, 7.9, 4.3 Hz, 1H), 3.30 (dd, *J* = 14.8, 4.4 Hz, 3H), 3.14 (dd, *J* = 14.8, 10.3 Hz, 1H) ppm. ¹³C NMR (100 MHz, DMSO): δ 172.2, 157.3–156.6 (m), 136.5, 127.4, 124.0, 121.5, 120.5, 118.9, 118.4, 117.6, 114.8, 111.9, 110.1, 110.0, 54.1, 26.4 ppm.

Preparation of 1-iodopyrene (2b).²⁷ Compound 2b was prepared using 1-aminopyrene (973 mg, 4.47 mmol), which was suspended in aqueous HCl solution (3 M, 25 mL) with vigorous stirring at 0 °C. A solution of NaNO₂ (308.4 mg, 4.47 mmol) in H₂O (1.5 mL) was added in small portions. After 5 min, a solution of KI (742.4 mg, 4.47 mmol) in H₂O (3 mL) was added to the reaction mixture. The ice bath was removed, and the reaction mixture was stirred for 2 h at r.t. and then heated to 60 °C for 1 h. The crude product was separated by filtration, dissolved in ether, and washed with a concentrated solution of Na₂SO₃. The ether solution was dried with MgSO₄ and concentrated under vacuum. The resulting product was purified by flash chromatography on silica gel (hexane/ethyl acetate) to obtain 1-iodopyrene 2b as a white yellowish solid (598.8 mg, 41%). ¹H NMR (400 MHz, CDCl₃): δ 8.37 (d, *J* = 8.1 Hz, 1H), 8.16 (d, *J* = 9.2 Hz, 1H), 8.11–8.06 (m, 2H), 8.01–7.94 (m, 2H), 7.93–7.85 (m, 2H), 7.72 (d, *J* = 8.1 Hz, 1H) ppm.

General Procedure for the C2 Arylation of Trp Amino Acids (3–5). Unless stated otherwise, Trp amino acid (1a–1c) (0.117 mmol, 1 equiv), aryl iodide (1.5 equiv), AgBF₄ (2 equiv), TFA (1.0 equiv), and Pd(OAc)₂ (5% mol) were placed in a microwave reactor vessel in dry DMF (600 μ L). The mixture was heated under microwave irradiation (250 W) at 90 °C for 20 min. Ethyl acetate (20 mL) was added, the resulting suspension was filtered through Celite, and the solvent was removed under vacuum. Unless otherwise quoted, the crude extract was purified by flash chromatography on silica gel (hexane/ethyl acetate) to obtain 3–5 as a pure product. Fractions containing the arylated tryptophans were collected, and the solvent was removed under reduced pressure. The residue was dissolved in CH₃CN/H₂O and lyophilized for 24 h to yield the pure product.

(S)-3-(2-(*p*-Tolyl)-1*H*-indol-3-yl)-2-(2,2,2-trifluoroacetamido)propanoic Acid (3). Starting from amino acid 1a (100 mg, 0.333 mmol) and 4-iodotoluene (110 mg, 0.500 mmol). Pale oil (65.9 mg, 51%). ¹H NMR (400 MHz, DMSO): δ 11.16 (s, 1H), 9.77 (d, *J* = 8.2 Hz, 1H), 7.62 (d, *J* = 8.0 Hz, 1H), 7.54–7.51 (m, 2H), 7.30 (td, *J* = 7.9, 0.9 Hz, 3H), 7.06 (ddd, *J* = 8.1, 7.0, 1.1 Hz, 1H), 6.96 (ddd, *J* = 8.0, 7.0, 1.0 Hz, 1H), 4.51 (td, *J* = 8.7, 5.1 Hz, 1H), 3.47 (dd, *J* = 14.7, 5.1 Hz, 1H), 3.32–3.23 (m, 1H), 2.35 (s, 3H) ppm. ¹³C NMR (100 MHz, DMSO): δ 171.3, 156.0, 155.7, 136.6, 135.5, 135.1, 129.6, 129.0, 128.6, 127.6, 121.1, 118.5, 118.4, 116.9, 114.0, 110.8, 106.7, 53.8, 25.8, 20.6 ppm. IR (film, cm^{−1}): ν = 3378.65, 3301.78, 2930.25, 1693.95 cm^{−1}. HRMS (ESI): *m/z* calcd 391.12640 (C₂₀H₁₈F₃N₂O₃), found 391.12592 (M + H)⁺.

(S)-2-Amino-3-(2-(*p*-tolyl)-1*H*-indol-3-yl)propanoic Acid (4). Starting from amino acid 1b (50.0 mg, 0.245 mmol) and 4-iodotoluene (80.2 mg, 0.368 mmol). The crude product was purified by flash chromatography on silica using hexane/ethyl acetate and then DCM/EtOH. Pale oil (39.9 mg, 56%). ¹H NMR (400 MHz, DMSO): δ 11.20 (s, 1H), 7.62 (d, *J* = 7.8 Hz, 1H), 7.55 (d, *J* = 7.8 Hz, 2H), 7.34 (d, *J* = 8.0 Hz, 1H), 7.27 (d, *J* = 7.8 Hz, 2H), 7.08 (t, *J* = 7.5 Hz, 1H), 6.99 (t, *J* = 7.4 Hz, 1H), 3.68 (t, *J* = 7.2 Hz, 1H), 3.44 (dd, *J* = 14.9, 6.2 Hz,

1H), 3.10 (dd, $J = 14.8, 8.4$ Hz, 1H), 2.34 (s, 3H) ppm. ^{13}C NMR (100 MHz, DMSO): δ 170.9, 137.2, 136.4, 136.1, 130.2, 129.6, 129.1, 128.5, 121.8, 119.2, 119.0, 111.5, 106.5, 54.7, 27.5, 21.3 ppm. IR (film, cm^{-1}): $\nu = 3404.27, 3231.32, 3051.96, 2962.28, 2923.84, 1706.76$ cm^{-1} . HRMS (ESI): m/z calcd 295.14410 ($\text{C}_{18}\text{H}_{19}\text{N}_2\text{O}_2$), found 295.14381 ($\text{M} + \text{H}^+$).

(S)-2-(((9H-Fluoren-9-yl)methoxy)carbonyl)amino)-3-(2-phenyl-1H-indol-3-yl)propanoic Acid (**5a**). Starting from amino acid **1c** (50.0 mg, 0.117 mmol) and iodobenzene (26.2 μL , 0.234 mmol). Pale oil (32.9 mg, 56%). Scale-up: Starting from amino acid **1c** (0.5 g, 1.17 mmol) and iodobenzene (200 μL , 1.75 mmol) in dry DMF (2 mL). The general microwave process was performed six times, all the reaction mixtures were collected altogether, and the resulting crude was treated according to the general procedure. Pale oil (1.98 g, 56%). ^1H NMR (400 MHz, DMSO): δ 12.62 (s, 1H), 11.20 (s, 1H), 7.88–7.84 (m, 2H), 7.78 (d, $J = 8.6$ Hz, 1H), 7.72–7.60 (m, 5H), 7.47 (t, $J = 7.7$ Hz, 2H), 7.41–7.32 (m, 4H), 7.28 (td, $J = 7.4, 1.1$ Hz, 1H), 7.23 (td, $J = 7.5, 1.1$ Hz, 1H), 7.10–7.05 (m, 1H), 6.97 (ddd, $J = 8.0, 6.9, 1.0$ Hz, 1H), 4.31 (td, $J = 8.6, 5.8$ Hz, 1H), 4.15–4.06 (m, 3H), 3.40–3.34 (m, 1H), 3.18 (dd, $J = 14.6, 8.7$ Hz, 1H) ppm. IR (film, cm^{-1}): $\nu = 3372.24, 3321.00, 3051.96, 2955.87, 1693.95$ cm^{-1} . RP-HPLC-ESMS: m/z (%) 503.22 ($\text{M} + \text{H}^+$). $[\alpha]_{\text{D}}^{20} -5.9$ (c 0.48, MeOH).

(R)-2-(((9H-Fluoren-9-yl)methoxy)carbonyl)amino)-3-(2-phenyl-1H-indol-3-yl)propanoic Acid (**5a'**). Starting from amino acid **1c** (50.0 mg, 0.117 mmol) and iodobenzene (26.2 μL , 0.234 mmol). Pale oil (29.9 mg, 51%). ^1H NMR (400 MHz, DMSO): δ 12.64 (s, 1H), 11.20 (s, 1H), 7.86 (d, $J = 7.6$ Hz, 2H), 7.78 (d, $J = 8.6$ Hz, 1H), 7.72–7.60 (m, 5H), 7.47 (t, $J = 7.7$ Hz, 2H), 7.41–7.32 (m, 4H), 7.28 (td, $J = 7.5, 1.2$ Hz, 1H), 7.23 (td, $J = 7.5, 1.2$ Hz, 1H), 7.10–7.05 (m, 1H), 6.98 (t, $J = 7.4$ Hz, 1H), 4.31 (td, $J = 8.5, 5.7$ Hz, 1H), 4.15–4.06 (m, 3H), 3.37 (dd, $J = 14.5, 5.8$ Hz, 1H), 3.19 (dd, $J = 14.6, 8.7$ Hz, 1H) ppm. ^{13}C NMR (100 MHz, DMSO): δ 174.0, 156.3, 144.2, 144.12, 141.07, 136.3, 135.6, 133.2, 129.4, 129.1, 128.4, 128.05, 128.03, 127.8, 127.5, 125.8, 121.9, 120.5, 119.5, 119.2, 111.5, 108.4, 66.2, 55.7, 47.0, 27.4 ppm. IR (film, cm^{-1}): $\nu = 3372.24, 3321.00, 3051.96, 2955.87, 1693.95$ cm^{-1} . HRMS (ESI): m/z calcd 503.19653 ($\text{C}_{23}\text{H}_{26}\text{N}_2\text{O}_4$), found 503.19761 ($\text{M} + \text{H}^+$). $[\alpha]_{\text{D}}^{20} +13.2$ (c 0.27, MeOH).

(S)-2-(((9H-Fluoren-9-yl)methoxy)carbonyl)amino)-3-(2-(4-nitrophenyl)-1H-indol-3-yl)propanoic Acid (**5b**). Starting from amino acid **1c** (100 mg, 0.234 mmol) and 4-iodo-4-nitrobenzene (89.4 mg, 0.352 mmol). Pale oil (116.7 mg, 91%). ^1H NMR (400 MHz, DMSO- d_6): δ 11.50 (s, 1H), 8.31–8.26 (m, 2H), 7.96–7.92 (m, 2H), 7.86 (d, $J = 7.6$ Hz, 2H), 7.79 (d, $J = 8.8$ Hz, 1H), 7.75 (d, $J = 8.1$ Hz, 1H), 7.60 (dd, $J = 7.5, 4.5$ Hz, 2H), 7.41–7.36 (m, 3H), 7.29–7.20 (m, 2H), 7.19–7.13 (m, 1H), 7.03 (t, $J = 7.5$ Hz, 1H), 4.31 (td, $J = 8.8, 5.3$ Hz, 1H), 4.17–4.00 (m, 3H), 3.51–3.39 (m, 2H) ppm. ^{13}C NMR (100 MHz, DMSO- d_6): δ 173.31, 155.87, 145.92, 143.76, 143.65, 140.65, 139.32, 136.56, 132.78, 128.85, 128.52, 127.62, 127.01, 125.28, 123.87, 122.81, 120.07, 119.52, 119.34, 111.48, 111.10, 65.73, 54.99, 46.50, 26.92 ppm. IR (film, cm^{-1}): $\nu = 3404.27, 3327.40, 3058.36, 2943.06, 2917.44, 1700.36, 1508.19, 1348.04, 848.40, 733.10$ cm^{-1} . RP-HPLC-ESMS: m/z (%) calcd 548.1816 ($\text{C}_{25}\text{H}_{26}\text{N}_3\text{O}_6$), found 548.18268 ($\text{M} + \text{H}^+$). $[\alpha]_{\text{D}}^{20} -21.8$ (c 0.50, MeOH).

(S)-2-(((9H-Fluoren-9-yl)methoxy)carbonyl)amino)-3-(2-(4-methoxyphenyl)-1H-indol-3-yl)propanoic Acid (**5c**). Starting from amino acid **1c** (50 mg, 0.117 mmol) and methyl 4-iodobenzoate (46.1 mg, 0.176 mmol). Pale oil (44.8 mg, 68%). ^1H NMR (400 MHz, CDCl_3): δ 8.00 (s, 1H), 7.63 (dd, $J = 33.5, 7.4$ Hz, 3H), 7.43–7.28 (m, 7H), 7.23–7.17 (m, 2H), 7.16–7.11 (m, 1H), 7.10–7.05 (m, 1H), 6.88–6.83 (m, 2H), 5.04 (d, $J = 7.9$ Hz, 1H), 4.55 (q, $J = 6.8$ Hz, 1H), 4.18–4.07 (m, 2H), 4.01 (t, $J = 7.3$ Hz, 1H), 3.70 (s, 3H), 3.43 (qd, $J = 14.9, 6.3$ Hz, 2H) ppm. ^{13}C NMR (100 MHz, CDCl_3): δ 175.9, 166.8, 159.5, 143.8, 143.79, 143.72, 141.2, 136.0, 135.5, 135.0, 130.2, 129.7, 129.3, 128.1, 127.7, 127.0, 125.1, 123.2, 122.3, 120.5, 120.2, 119.91, 119.89, 119.2, 114.5, 111.1, 110.9, 108.2, 106.1, 67.1, 55.3, 54.4, 52.3, 47.0 ppm. IR (film, cm^{-1}): $\nu = 3410.68, 3340.21, 3058.36, 2949.47, 1713.17, 1693.95$ cm^{-1} . HRMS (ESI): m/z calcd 561.20201 ($\text{C}_{34}\text{H}_{38}\text{N}_2\text{O}_6$), found 561.20365 ($\text{M} + \text{H}^+$). $[\alpha]_{\text{D}}^{20} -15.9$ (c 0.51, MeOH).

(S)-2-(((9H-Fluoren-9-yl)methoxy)carbonyl)amino)-3-(2-(4-bromophenyl)-1H-indol-3-yl)propanoic Acid (**5d**). Starting from amino acid **1c** (50.0 mg, 0.117 mmol) and 1-bromo-4-iodobenzene (50.8 mg, 0.176 mmol). Pale oil (42.5 mg, 62%). ^1H NMR (400 MHz, CDCl_3): δ 8.02 (s, 1H), 7.72–7.65 (m, 2H), 7.64–7.57 (m, 1H), 7.44–7.36 (m, 4H), 7.37–7.27 (m, 2H), 7.29–7.21 (m, 3H), 7.26–7.17 (m, 2H), 7.16 (d, $J = 7.9$ Hz, 1H), 7.09 (t, $J = 7.4$ Hz, 1H), 5.04 (d, $J = 8.0$ Hz, 1H), 4.57 (q, $J = 6.5$ Hz, 1H), 4.22–4.00 (m, 3H), 3.45 (qd, $J = 14.9, 6.0$ Hz, 2H) ppm. ^{13}C NMR (100 MHz, CDCl_3): δ 176.1, 155.7, 143.73, 143.67, 141.25, 141.23, 135.7, 135.2, 131.6, 129.9, 129.0, 127.7, 127.0, 125.2, 122.9, 122.3, 120.4, 119.9, 119.0, 111.1, 107.2, 67.1, 54.3, 46.9, 26.8 ppm. IR (film, cm^{-1}): $\nu = 3378.65, 3314.59, 3058.36, 2949.47, 1687.54$ cm^{-1} . HRMS (ESI): m/z calcd 581.10705 ($\text{C}_{32}\text{H}_{32}\text{BrN}_2\text{O}_4$), found 581.10888 ($\text{M} + \text{H}^+$). $[\alpha]_{\text{D}}^{20} -8.1$ (c 0.50, MeOH).

(S)-2-(((9H-Fluoren-9-yl)methoxy)carbonyl)amino)-3-(2-(3-(trifluoromethyl)phenyl)-1H-indol-3-yl)propanoic Acid (**5e**). Starting from amino acid **1c** (50.0 mg, 0.117 mmol) and 1-iodo-3-(trifluoromethyl)benzene (25.9 μL , 0.176 mmol). Pale oil (39.4 mg, 59%). ^1H NMR (400 MHz, DMSO): δ 12.67 (s, 1H), 11.39 (s, 1H), 8.01–7.95 (m, 2H), 7.89–7.79 (m, 3H), 7.74 (d, $J = 8.1$ Hz, 1H), 7.72–7.69 (m, 2H), 7.61 (dd, $J = 11.1, 7.5$ Hz, 2H), 7.41–7.35 (m, 3H), 7.30–7.20 (m, 2H), 7.12 (t, $J = 7.8$ Hz, 1H), 7.00 (t, $J = 7.5$ Hz, 1H), 4.30 (td, $J = 8.6, 5.6$ Hz, 1H), 4.15–4.04 (m, 3H), 3.40 (dd, $J = 14.6, 5.7$ Hz, 2H), 3.23 (dd, $J = 14.7, 8.7$ Hz, 1H) ppm. ^{19}F NMR (376 MHz, DMSO): δ -61.07 ppm. ^{13}C NMR (100 MHz, DMSO): δ 173.8, 156.3, 144.2, 144.1, 141.1, 136.5, 134.1, 133.7, 132.2, 130.22, 130.16, 129.3, 128.05, 128.03, 127.5, 125.7, 124.60, 124.56, 124.3, 122.5, 120.5, 119.8, 119.5, 111.7, 109.7, 66.2, 55.5, 46.9, 27.3 ppm. IR (film, cm^{-1}): $\nu = 3391.46, 3314.59, 3064.77, 2949.47, 1706.76$ cm^{-1} . HRMS (ESI): m/z calcd 571.18392 ($\text{C}_{33}\text{H}_{32}\text{F}_3\text{N}_2\text{O}_4$), found 571.18559 ($\text{M} + \text{H}^+$). $[\alpha]_{\text{D}}^{20} -12.1$ (c 0.50, MeOH).

(S)-2-(((9H-Fluoren-9-yl)methoxy)carbonyl)amino)-3-(2-(2-fluorophenyl)-1H-indol-3-yl)propanoic Acid (**5f**). Starting from amino acid **1c** (100 mg, 0.234 mmol) and 2-fluoroiodobenzene (41.4 μL , 0.351 mmol). Pale oil (121.8 mg, 77%). ^1H NMR (400 MHz, CDCl_3): δ 8.16 (s, 1H), 7.68 (d, $J = 7.6$ Hz, 2H), 7.62 (d, $J = 7.9$ Hz, 1H), 7.44–7.25 (m, 8H), 7.24–7.20 (m, 1H), 7.17–7.04 (m, 4H), 5.07 (d, $J = 8.1$ Hz, 1H), 4.63–4.53 (m, 1H), 4.21–4.06 (m, 2H), 4.03 (t, $J = 7.4$ Hz, 1H), 3.48–3.30 (m, 2H) ppm. ^{19}F NMR (376 MHz, CDCl_3): δ -114.0 to -114.2 ppm. ^{13}C NMR (100 MHz, CDCl_3): δ 175.8, 158.7, 155.9, 144.0, 141.4, 136.1, 131.5, 130.6, 130.5, 130.3, 127.8, 127.2, 125.3, 124.84, 124.81, 123.1, 120.4, 120.1, 119.1, 116.6, 116.4, 111.2, 108.9, 67.3, 54.3, 47.1, 27.2. IR (film, cm^{-1}): $\nu = 3415.92, 3334.19, 3062.16, 2924.47, 1715.77$ cm^{-1} . HRMS (ESI): m/z calcd 521.18711 ($\text{C}_{33}\text{H}_{32}\text{FN}_2\text{O}_4$), found 521.18728 ($\text{M} + \text{H}^+$). $[\alpha]_{\text{D}}^{20} -2.9$ (c 0.50, MeOH).

(S)-2-(((9H-Fluoren-9-yl)methoxy)carbonyl)amino)-3-(2-(p-tolyl)-1H-indol-3-yl)propanoic Acid (**5g**). Starting from amino acid **1c** (100 mg, 0.234 mmol) and 4-iodotoluene (76.7 mg, 0.351 mmol). Pale oil (97.4 mg, 81%). ^1H NMR (400 MHz, CDCl_3): δ 8.03 (s, 1H), 7.69–7.65 (m, 2H), 7.59 (d, $J = 7.9$ Hz, 1H), 7.41–7.27 (m, 8H), 7.21–7.19 (m, 1H), 7.16–7.08 (m, 3H), 7.09–7.05 (m, 1H), 5.02 (d, $J = 7.9$ Hz, 1H), 4.54 (q, $J = 6.9$ Hz, 1H), 4.16–4.05 (m, 2H), 4.00 (t, $J = 7.2$ Hz, 1H), 3.54–3.35 (m, 3H), 2.26 (s, 3H) ppm. ^{13}C NMR (100 MHz, CDCl_3): δ 175.8, 155.8, 143.8, 143.7, 141.2, 138.2, 136.64, 135.60, 129.7, 129.6, 129.0, 128.3, 127.7, 127.6, 127.1, 127.0, 125.2, 122.5, 120.2, 120.0, 119.9, 118.7, 110.9, 106.4, 67.1, 54.5, 47.0, 26.8, 21.2 ppm. IR (film, cm^{-1}): $\nu = 3385.05, 3314.59, 3051.96, 2949.47, 1693.95$ cm^{-1} . HRMS (ESI): m/z calcd 517.21218 ($\text{C}_{33}\text{H}_{38}\text{N}_2\text{O}_4$), found 517.21356 ($\text{M} + \text{H}^+$). $[\alpha]_{\text{D}}^{20} -9.9$ (c 0.50, MeOH).

(S)-2-(((9H-Fluoren-9-yl)methoxy)carbonyl)amino)-3-(2-(4-methoxyphenyl)-1H-indol-3-yl)propanoic Acid (**5h**). Starting from amino acid **1c** (50.0 mg, 0.117 mmol) and 4-iodoanisole (41.2 mg, 0.176 mmol). Pale oil (39.0 mg, 63%). ^1H NMR (400 MHz, CDCl_3): δ 8.18 (s, 1H), 7.98–7.94 (m, 2H), 7.71–7.61 (m, 3H), 7.48 (d, $J = 8.3$ Hz, 2H), 7.42–7.28 (m, 5H), 7.23–7.16 (m, 3H), 7.09 (t, $J = 7.5$ Hz, 1H), 5.15 (d, $J = 8.4$ Hz, 1H), 4.60 (q, $J = 6.6, 6.1$ Hz, 1H), 4.18–4.07 (m, 2H), 3.99 (t, $J = 7.3$ Hz, 1H), 3.80 (s, 3H), 3.59–3.42 (m, 2H) ppm. ^{13}C NMR (100 MHz, CDCl_3): δ 175.2, 158.5, 154.8, 142.8,

142.7, 140.19, 140.17, 134.5, 129.2, 128.7, 127.1, 126.6, 126.0, 124.2, 123.9, 121.3, 119.1, 118.90, 118.87, 117.6, 113.5, 109.9, 107.1, 105.1, 66.1, 54.2, 53.5, 51.2, 46.0 ppm. IR (film, cm^{-1}): $\nu = 3365.84, 3308.19, 3051.96, 2923.84, 1693.95 \text{ cm}^{-1}$. HRMS (ESI): m/z calcd 533.20710 ($\text{C}_{33}\text{H}_{28}\text{N}_2\text{O}_5$), found 533.20867 ($M + H$). $[\alpha]_D^{20} -9.8$ (c 0.45, MeOH).

(S)-2-((((9H-Fluoren-9-yl)methoxy)carbonyl)amino)-3-(2-(pyren-1-yl)-1H-indol-3-yl)propanoic Acid (**5i**). Starting from amino acid **1c** (100 mg, 0.234 mmol) and 1-iodopyrene **2b** (115 mg, 0.352 mmol). Pale oil (94.2 mg, 66%). ^1H NMR (400 MHz, DMSO): δ 12.36 (s, 1H), 11.46 (s, 1H), 8.36–8.21 (m, 6H), 8.17–8.07 (m, 4H), 7.95 (d, $J = 9.2 \text{ Hz}$, 1H), 7.86 (d, $J = 7.6 \text{ Hz}$, 2H), 7.79 (d, $J = 7.9 \text{ Hz}$, 1H), 7.52 (t, $J = 7.1 \text{ Hz}$, 2H), 7.44–7.35 (m, 4H), 7.27–7.15 (m, 3H), 7.09 (t, $J = 7.4 \text{ Hz}$, 1H), 4.13 (q, $J = 7.8 \text{ Hz}$, 1H), 4.01–3.78 (m, 3H), 3.12 (s, 2H) ppm. ^{13}C NMR (100 MHz, DMSO): δ 173.2, 155.5, 143.7, 140.6, 136.2, 134.8, 130.8, 130.7, 130.4, 129.4, 128.8, 128.2, 128.0, 127.8, 127.7, 127.5, 127.3, 127.0, 126.4, 125.4, 125.3, 125.2, 124.5, 124.0, 123.8, 121.3, 120.0, 118.89, 118.86, 111.1, 109.8, 65.5, 54.8, 46.4, 26.8 ppm. IR (film, cm^{-1}): $\nu = 3417.33, 3308.19, 3043.35, 2923.54, 1714.91 \text{ cm}^{-1}$. HRMS (ESI): m/z calcd 627.22783 ($\text{C}_{47}\text{H}_{30}\text{N}_2\text{O}_5$), found 627.23025 ($M + H$). $[\alpha]_D^{20} +7.6$ (c 0.13, MeOH).

2-(2-Phenyl-1H-indol-3-yl)acetic Acid (8**)**.²⁸ Starting from 2-(1H-indol-3-yl)acetic acid (42.0 mg, 0.240 mmol) and iodobenzene (40.3 μL , 0.360 mmol). Pale oil (47.8 mg, 79%). ^1H NMR (400 MHz, CDCl_3): δ 8.10 (s, 1H), 7.60 (ddt, $J = 7.8, 1.5, 0.7 \text{ Hz}$, 1H), 7.57–7.54 (m, 2H), 7.46–7.36 (m, 2H), 7.35–7.30 (m, 2H), 7.21–7.12 (m, 1H), 7.14–7.05 (m, 1H), 3.80 (s, 2H) ppm. HRMS (ESI): m/z calcd 252.10191 ($\text{C}_{16}\text{H}_{13}\text{NO}_2$), found 252.10168 ($M + H$).

3-(2-Phenyl-1H-indol-3-yl)propanoic Acid (9**)**.²⁹ Starting from 3-(1H-indol-3-yl)propanoic acid (45.4 mg, 0.240 mmol) and iodobenzene (41.1 μL , 0.360 mmol). Pale oil (47.6 mg, 75%). ^1H NMR (400 MHz, CDCl_3): δ 7.96 (s, 1H), 7.58–7.55 (m, 1H), 7.48–7.45 (m, 2H), 7.43–7.38 (m, 2H), 7.33–7.28 (m, 2H), 7.15 (ddd, $J = 8.1, 7.1, 1.2 \text{ Hz}$, 1H), 7.08 (ddd, $J = 8.1, 7.1, 1.1 \text{ Hz}$, 1H), 3.21–3.16 (m, 2H), 2.68–2.63 (m, 2H) ppm. HRMS (ESI): m/z calcd 266.11756 ($\text{C}_{17}\text{H}_{15}\text{NO}_2$), found 266.11729 ($M + H$).

4-(2-Phenyl-1H-indol-3-yl)butanoic Acid (10**)**.³⁰ Starting from 4-(1H-indol-3-yl)butanoic acid (83.7 mg, 0.412 mmol) and iodobenzene (69.2 μL , 0.618 mmol). Pale oil (84.8 mg, 74%). ^1H NMR (400 MHz, CDCl_3): δ 7.97 (s, 1H), 7.57 (ddt, $J = 7.8, 1.2, 0.7 \text{ Hz}$, 1H), 7.49–7.46 (m, 2H), 7.41–7.35 (m, 2H), 7.31–7.25 (m, 2H), 7.16–7.10 (m, 1H), 7.07 (ddt, $J = 7.9, 6.9, 0.7 \text{ Hz}$, 1H), 2.91–2.87 (m, 2H), 2.33 (t, $J = 7.3 \text{ Hz}$, 2H), 2.03–1.94 (m, 2H) ppm. HRMS (ESI): m/z calcd 280.13321 ($\text{C}_{18}\text{H}_{17}\text{NO}_2$), found 280.13287 ($M + H$).

2-(2-Phenyl-1H-indol-3-yl)ethanamine (11**)**.³¹ Tryptamine (76.9 mg, 0.480 mmol), iodobenzene (80.6 μL , 0.720 mmol), AgBF_4 (186.9 mg, 0.960 mmol), and $\text{Pd}(\text{OAc})_2$ (5.4 mg, 0.024 mmol) were placed in a microwave reactor vessel in dry DMF (2.4 mL). The mixture was heated under microwave irradiation (250 W) at 90 °C for 20 min. HPLC/MS analysis showed 29% of compound **11**. Incidentally, iodobenzene (80.6 μL , 0.720 mmol) and $\text{Pd}(\text{OAc})_2$ (5.4 mg, 0.024 mmol) were added, and a second irradiation cycle was performed (250 W) at 90 °C for 20 min, thus increasing the conversion up to 89%, as shown in the HPLC/MS. Ethyl acetate (30 mL) was added, the resulting suspension was filtered through Celite, and the solvent was removed under vacuum. The crude product was purified by flash chromatography on silica using hexane/ethyl acetate and then DCM/MeOH to obtain **11** as an oil (54.4 mg, 48%). ^1H NMR (400 MHz, DMSO): δ 11.30 (s, 1H), 7.79 (s, 2H), 7.63–7.59 (m, 3H), 7.52 (t, $J = 7.6 \text{ Hz}$, 2H), 7.44–7.35 (m, 2H), 7.15–7.10 (m, 1H), 7.08–7.02 (m, 1H), 3.15–3.09 (m, 2H), 3.09–2.98 (m, 2H) ppm. RP-HPLC-ESMS: m/z (%) 237.12 ($M + H$).

N-(2-(2-Phenyl-1H-indol-3-yl)ethyl)acetamide (12**)**.³² Starting from N-(2-(1H-indol-3-yl)ethyl)acetamide (98.0 mg, 0.485 mmol) and iodobenzene (80.6 μL , 0.720 mmol). Yellow solid (103.1 mg, 73%). ^1H NMR (400 MHz, CDCl_3): δ 8.28 (s, 1H), 7.56 (d, $J = 7.9 \text{ Hz}$, 1H), 7.52–7.45 (m, 2H), 7.38 (t, $J = 7.7 \text{ Hz}$, 2H), 7.33–7.26 (m, 2H), 7.17–7.12 (m, 1H), 7.09–7.05 (m, 1H), 5.41 (s, 1H), 3.46 (q, $J = 6.5 \text{ Hz}$, 2H), 3.04 (t, $J = 6.8 \text{ Hz}$, 2H), 1.67 (s, 3H) ppm. RP-HPLC-ESMS: 279.12 ($M + H$).

General Procedure for SPPS. All peptides were manually synthesized in polystyrene syringes fitted with a polyethylene porous disc. The synthesis of the peptides were performed using Fmoc-based SPPS on a 2-chlorotriyl chloride resin. Solvents and soluble reagents were removed by suction. The Fmoc group was removed with piperidine-DMF (1:4, v/v) (1 \times 1 min, 2 \times 5 min). Peptide synthesis transformations and washes were performed at r.t.

Resin Loading. Fmoc-XX-OH (1 equiv) was attached to the resin (1 equiv) with DIPEA (3 equiv) in DCM at r.t. for 10 min and then DIPEA (7 equiv) for 40 min. The remaining trityl groups were capped, adding 0.8 μL of MeOH/mg resin for 10 min. After that, the resin was filtered and washed with DCM (4 \times 1 min) and DMF (4 \times 1 min). The loading of the resin was determined by titration of the Fmoc group.³³

Peptide Elongation. After the Fmoc group was eliminated, the resin was washed with DMF (4 \times 1 min), DCM (3 \times 1 min), and DMF (4 \times 1 min). Amino acid coupling: Fmoc-XX-OH (3 equiv) was incorporated with a 5 min preactivation with DIPCDI (3 equiv) and OxymaPure (3 equiv) in DMF for 1h. The completion of the coupling was monitored with the ninhydrin test (free amine group).³⁴ The resin was then filtered and washed with DCM (4 \times 1 min) and DMF (4 \times 1 min), and the Fmoc group was eliminated.

Final Cleavage. The resin bound peptide was treated with 5% TFA in DCM (5 \times 1 min). The resin was washed with DCM, and the combined eluates were evaporated under vacuum. The residue was then dissolved in $\text{ACN}/\text{H}_2\text{O}$ and lyophilized, furnishing the corresponding peptide.

H-Met-Gly-Trp(C2-p-methylphenyl)-Ala-OH (6**)**. Starting from 150 mg of 2-chlorotriyl resin (0.92 mmol/g). Pale solid (purity > 99%, HPLC). ^1H NMR (400 MHz, DMSO d_6): δ 12.51 (s, 1H), 11.09 (s, 1H), 8.53 (t, $J = 5.6 \text{ Hz}$, 1H), 8.20–8.07 (m, 5H), 7.74 (d, $J = 7.9 \text{ Hz}$, 1H), 7.58 (d, $J = 8.0 \text{ Hz}$, 2H), 7.31–7.28 (m, 2H), 7.10–7.02 (m, 1H), 6.97 (t, $J = 7.5 \text{ Hz}$, 1H), 4.76 (q, $J = 7.6 \text{ Hz}$, 1H), 4.13 (p, $J = 7.2 \text{ Hz}$, 1H), 3.85 (m, 1H), 3.78 (dd, $J = 16.8, 5.4 \text{ Hz}$, 1H), 3.60 (dd, $J = 16.8, 5.7 \text{ Hz}$, 1H), 3.26 (dd, $J = 14.5, 5.7 \text{ Hz}$, 1H), 3.05 (dd, $J = 14.5, 7.9 \text{ Hz}$, 1H), 2.48 (m, 2H), 2.37 (s, 3H), 2.03 (s, 3H), 1.99–1.88 (m, 2H), 1.22 (d, $J = 7.2 \text{ Hz}$, 3H) ppm. ^{13}C NMR (100 MHz, DMSO): δ 173.6, 170.7, 168.2, 167.5, 136.6, 135.8, 135.5, 129.9, 129.2, 129.0, 128.1, 121.2, 119.2, 118.5, 110.9, 107.0, 53.7, 51.5, 47.5, 41.6, 30.9, 28.3, 28.0, 20.8, 17.3, 14.4 ppm. HRMS (ESI): m/z calcd 554.2432 ($\text{C}_{28}\text{H}_{33}\text{N}_5\text{O}_5\text{S}$), found 554.2429 ($M + H$).

H-Trp-Gly-Trp(C2-p-methylphenyl)-Ala-OH (7**)**. Starting from 150 mg of 2-chlorotriyl resin (0.92 mmol/g). Pale solid (purity > 99%, HPLC). ^1H NMR (400 MHz, DMSO d_6): δ 11.10 (s, 1H), 10.98 (d, $J = 2.5 \text{ Hz}$, 1H), 8.72 (t, $J = 5.5 \text{ Hz}$, 1H), 8.16 (dd, $J = 8.0, 5.8 \text{ Hz}$, 2H), 7.97 (m, 3H), 7.75 (d, $J = 7.9 \text{ Hz}$, 1H), 7.68–7.63 (m, 1H), 7.60–7.54 (m, 2H), 7.36 (d, $J = 8.1, 1\text{H}$), 7.29 (d, $J = 7.8 \text{ Hz}$, 2H), 7.19 (m, 1H), 7.08 (dddd, $J = 8.1, 6.9, 5.8, 1.2 \text{ Hz}$, 2H), 6.98 (dddd, $J = 8.0, 7.0, 4.4, 1.1 \text{ Hz}$, 2H), 4.79 (td, $J = 8.3, 5.6 \text{ Hz}$, 1H), 4.14 (p, $J = 7.2 \text{ Hz}$, 1H), 4.00 (m, 1H), 3.90 (dd, $J = 16.9, 5.9 \text{ Hz}$, 1H), 3.45 (dd, $J = 16.9, 5.0 \text{ Hz}$, 1H), 3.23 (ddd, $J = 35.5, 14.7, 5.2 \text{ Hz}$, 2H), 3.04 (m, 2H), 2.36 (s, 3H), 1.22 (d, $J = 7.3 \text{ Hz}$, 3H) ppm. ^{13}C NMR (100 MHz, DMSO): δ 173.6, 170.8, 168.6, 167.5, 136.6, 136.3, 135.8, 135.6, 130.0, 129.2, 129.0, 128.1, 127.0, 125.0, 121.2, 119.2, 118.5, 118.4, 111.5, 110.9, 107.0, 106.8, 53.6, 52.5, 47.6, 41.8, 27.52 (2 C), 20.8, 17.3 ppm. HRMS (ESI): m/z calcd 609.2820 ($\text{C}_{34}\text{H}_{36}\text{N}_6\text{O}_5$), found 609.2820 ($M + H$).

■ ASSOCIATED CONTENT

● Supporting Information

Spectral and analytical data: copies of the ^1H , ^{13}C , and ^{19}F NMR spectra for all new compounds and chiral HPLC profiles of **5a** and **5a'**. This material is available free of charge via the Internet at <http://pubs.acs.org>.

■ AUTHOR INFORMATION

Corresponding Author

*E-mail: fernando.albericio@irbbarcelona.org (F.A.), rlavilla@pcb.ub.es (R.L.).

Author Contributions

†Both researchers have contributed equally to this work.

Notes

The authors declare no competing financial interest.

■ ACKNOWLEDGMENTS

This work was supported by DGICYT – Spain (project BQU-CTQ2012-30930) and Generalitat de Catalunya (project 2009SGR 1024).

■ REFERENCES

- (1) (a) Yuki, E. T.; Wilmut, C. M. *Curr. Opin. Chem. Biol.* **2012**, *16*, 54–59. (b) Abu, T. N.; Jensen, L. M. R.; Yuki, E. T.; Geng, J.; Liu, A.; Wilmut, C. M.; Davidson, V. L. *Proc. Natl. Acad. Sci. U.S.A.* **2011**, *108*, 16956–16961.
- (2) For the synthesis of a C2-arylated Trp derivative through a multistep sequence, see: Wang, W.; Cai, M.; Xiong, C.; Zhang, J.; Trivedi, D.; Hruby, V. J. *Tetrahedron* **2002**, *58*, 7365–7374.
- (3) For Pd-catalyzed allylations on Trp derivatives, see: (a) Yokoyama, Y.; Hikawa, H.; Mitsuhashi, M.; Uyama, A.; Hiroki, Y.; Murakami, Y. *Eur. J. Org. Chem.* **2004**, 1244–1253. (b) Hikawa, H.; Yokoyama, Y. *Org. Biomol. Chem.* **2011**, 4044–4050.
- (4) (a) Rodrigues de Sa Alves, F.; Barreiro, E. J.; Fraga, C. A. M. *Mini-Rev. Med. Chem.* **2009**, *9*, 782–793. (b) Zhao, H.; Donnelly, A. C.; Kusuma, B. R.; Brandt, G. E. L.; Brown, D.; Rajewski, R. A.; Vielhauer, G.; Holzbeierlein, J.; Cohen, M. S.; Blagg, B. S. J. *J. Med. Chem.* **2011**, *54*, 3839–3853. (c) Painter, T. O.; Wang, L.; Majumder, S.; Xie, X.-Q.; Brummond, K. M. *ACS Comb. Sci.* **2011**, *13*, 166–174.
- (5) (a) Johansson, H.; Jorgensen, T. B.; Gloriam, D. E.; Braeuner-Osborne, H.; Pedersen, D. S. *RSC Adv.* **2013**, *3*, 945–960. (b) Gloriam, D. E.; Wellendorph, P.; Johansen, L. D.; Thomsen, A. R. B.; Phonekeo, K.; Pedersen, D. S.; Braeuner-Osborne, H. *Chem. Biol.* **2011**, *18*, 1489–1498.
- (6) Humphrey, G. R.; Kuether, J. T. *Chem. Rev.* **2006**, *106*, 2875–2911.
- (7) For selected reviews, see: (a) Ackermann, L. *Chem. Rev.* **2011**, *111*, 1315–1345. (b) McMurray, L.; O'Hara, F. O.; Gaunt, M. *Chem. Soc. Rev.* **2011**, *40*, 1885–1898. (c) Wencel-Delord, J.; Dröge, T.; Liu, F.; Glorius, F. *Chem. Soc. Rev.* **2011**, *40*, 4740–4761. (d) Chen, X.; Engle, K. M.; Wang, D.-H.; Yu, J.-Q. *Angew. Chem., Int. Ed.* **2009**, *48*, 5094–5115. (e) Albericio, D.; Scott, M. E.; Lautens, M. *Chem. Rev.* **2007**, *107*, 174–238. (f) Mendoza, P.; Echavarren, A. In *Modern Arylation Methods*; Ackermann, L., Ed.; Wiley-VCH: Weinheim, 2009; pp 363–399.
- (8) For C–H arylation of indoles, see: (a) Beck, E. M.; Gaunt, M. J. In *C–H Activation*; Yu, J.-Q.; Shi, Z., Eds.; Topics in Current Chemistry; Springer-Verlag: Heidelberg, 2010; Vol. 292, pp 87–121. (b) Lebrasseur, N.; Larrosa, I. *Adv. Heterocycl. Chem.* **2012**, *105*, 309–351. (c) Lebrasseur, N.; Larrosa, I. *J. Am. Chem. Soc.* **2008**, *130*, 2926–2927.
- (9) Ruiz-Rodríguez, J.; Albericio, F.; Lavilla, R. *Chem.—Eur. J.* **2010**, *16*, 1124–1127.
- (10) For a recent peptide macrocyclization via Pd-catalyzed C–H arylation of the side chains of Trp with iodo-containing amino acids, see: Dong, H.; Limberakis, C.; Liras, S.; Price, D.; James, K. *Chem. Commun.* **2012**, 48, 11644–11646.
- (11) Sharma, A.; Vacchani, D.; Van der Eycken, E. *Chem.—Eur. J.* **2013**, *19*, 1158–1168.
- (12) Hughes, A. B. Ed. *Amino Acids, Peptides and Proteins in Organic Chemistry: Building Blocks, Catalysis and Coupling Chemistry*; Wiley-VCH Verlag GmbH & Co. KGaA: Weinheim, Germany, 2011; Vol. 3.
- (13) For previous stepwise syntheses of racemic 2-aryltryptophans, see: (a) Majchrzak, M. W.; Zobel, J. N.; Obradovich, D. J. *Synth. Commun.* **1997**, *27*, 3201–3211. (b) Balsamini, C.; Diamantini, G.; Duranti, A.; Spadoni, G.; Tontini, A. *Synthesis* **1995**, *4*, 370–372.
- (14) (a) Chiong, H. A.; Pham, Q.-N.; Daugulis, O. *J. Am. Chem. Soc.* **2007**, *129*, 9879–9884. (b) Thirunavukkarasu, V. S.; Parthasarathy, K.; Cheng, C.-H. *Angew. Chem., Int. Ed.* **2008**, *47*, 9462–9465.
- (15) (a) Garcia-Cuadrado, D.; de Mendoza, P.; Braga, A. A. C.; Maseras, F.; Echavarren, A. M. *J. Am. Chem. Soc.* **2007**, *129*, 6880–6886. (b) Gorelsky, S. I.; Lapointe, D.; Fagnou, K. *J. Am. Chem. Soc.* **2008**, *130*, 10848–10849 and references cited therein.
- (16) Weibel, J.-M.; Blanc, A.; Pale, P. *Chem. Rev.* **2008**, *108*, 3149–3173.
- (17) The Trp free amino acid may form stable Pd complexes that quench the reaction. For instance, see: Beck, W. *Pure Appl. Chem.* **1988**, *60*, 1357–1362.
- (18) (a) For a fluorescent Trp surrogate, see: Moroz, Y. S.; Binder, W.; Nygren, P.; Caputo, G. A.; Korendovych, I. V. *Chem. Commun.* **2013**, 49, 490–492. (b) The pyrenyl group is commonly used as a protein fluorophore, attached to cysteine: Kouyama, T.; Mihashi, K. *Eur. J. Biochem.* **1981**, *114*, 33–38.
- (19) Although the HPLC profiles are slightly overlapped and a low level of racemization cannot be excluded, the incorporation of these amino acids into peptides through SPSS (see below) does not show evidence of diastereomer formation, therefore, indicating that the racemization in the Pd-catalyzed reaction, if any, should be minimal.
- (20) (a) Strader, L. C.; Bartel, B. *Mol. Plant* **2011**, *4*, 477–86. (b) Labavitch, J. M. *Proc. - Plant Growth Regul. Soc. Am.* **1999**, *26*, 13–14.
- (21) Paquet, J.-L.; Barth, M.; Pruneau, D.; Dodey, P. *PCT Int. Appl. WO* 2001038305 A2 20010531, 2001.
- (22) (a) 2-Arylated indole butyric acids are also found in other applications: Slade, R.; Klimova, Y.; Halter, R. J.; Yungai, A. J.; Weiner, W. S.; Walton, R. J.; Willardsen, J. A.; Anderson, M. B.; Zavitz, K. U.S. *Pat. Appl. Publ. US* 20080249135 A1 20081009, 2008. (b) Rolland, C.; Gonalbes, R.; Nicolai, E.; Paugam, M.-F.; Coussy, L.; Barbosa, F.; Horvath, D.; Revah, F. *J. Med. Chem.* **2005**, *48*, 6563–6574.
- (23) For some relevant examples: (a) Arisawa, M.; Kasaya, Y.; Obata, T.; Sasaki, T.; Ito, M.; Abe, H.; Ito, Y.; Yamano, A.; Shuto, S. *ACS Med. Chem. Lett.* **2011**, *2*, 353–357. (b) Girisha, M.; Badiger, J.; Purohit, M. G.; Thippeswamy, B. S.; Patil, B. M. *Indian J. Heterocycl. Chem.* **2008**, *17*, 275–276. (c) Yang, Z.; Reiling, S.; Nieduzak, T. R.; Mathew, R. M.; Jackson, S.; Harris, K. J. *PCT Int. Appl. WO* 2008014186 A1 20080131, 2008.
- (24) For instance, see: Vicente, J.; Saura-Llamas, I.; García-López, J.-A. *Organometallics* **2009**, *28*, 448–464.
- (25) Wang, X.; Gribkov, D. V.; Sames, D. *J. Org. Chem.* **2007**, *72*, 1476–1479.
- (26) Chambers, J. J.; Kurrasch-Orbaugh, D. M.; Parker, M. A.; Nichols, D. E. *J. Med. Chem.* **2001**, *44*, 1003–1010.
- (27) Rivera, E.; Belletete, M.; Zhu, X. X.; Durocher, G.; Giasson, R. *Polymer* **2002**, *43*, 5059–5068.
- (28) Arisawa, M.; Kasaya, Y.; Obata, T.; Sasaki, T.; Nakamura, T.; Araki, T.; Yamamoto, K.; Sasaki, A.; Yamano, A.; Ito, M.; Abe, H.; Ito, Y.; Shuto, S. *J. Med. Chem.* **2012**, *55*, 8152–8163.
- (29) Jennings, L. D.; Foreman, K. W.; Rush, T. S., III; Tsao, D. H. H.; Mosyak, L.; Kincaid, S. L.; Sukhdeo, M. N.; Sutherland, A. G.; Ding, W.; Kenny, C. H.; Sabus, C. L.; Liu, H.; Dushin, E. G.; Moghazeh, S. L.; Labthavikul, P.; Petersen, P. J.; Tuckmand, M.; Ruzind, A. V. *Bioorg. Med. Chem.* **2004**, *12*, S115–S131.
- (30) Saleha, S.; Khan, N. H.; Siddiqui, A. A.; Kidwai, M. M. *Indian J. Chem., Sect. B* **1978**, *16B*, 1122–1124.
- (31) Bunders, C. A.; Minvielle, M. J.; Worthington, R. J.; Ortiz, M.; Cavanagh, J.; Melander, C. *J. Am. Chem. Soc.* **2011**, *133*, 20160–20163.
- (32) Wang, X.; Gribkov, D. V.; Sames, D. *J. Org. Chem.* **2007**, *72*, 1476–1479.
- (33) Chan, W.; White, P. D., Eds. *Fmoc Solid Phase Peptide Synthesis*; Oxford University Press: New York, 2000.
- (34) Kaiser, E.; Colclough, R. L.; Bossinger, C. D.; Cook, P. I. *Anal. Biochem.* **1970**, *34*, 595–598.

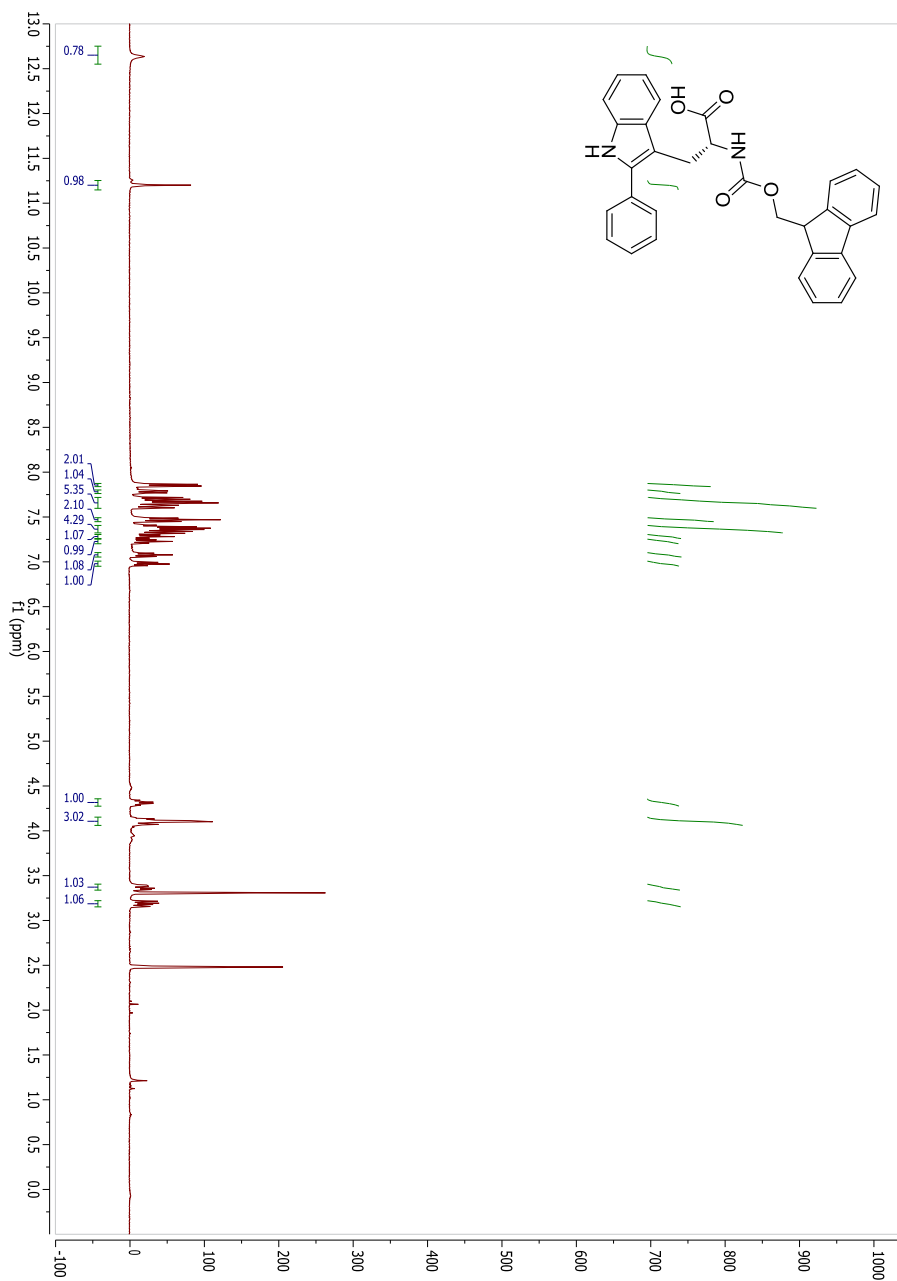
Supporting Information

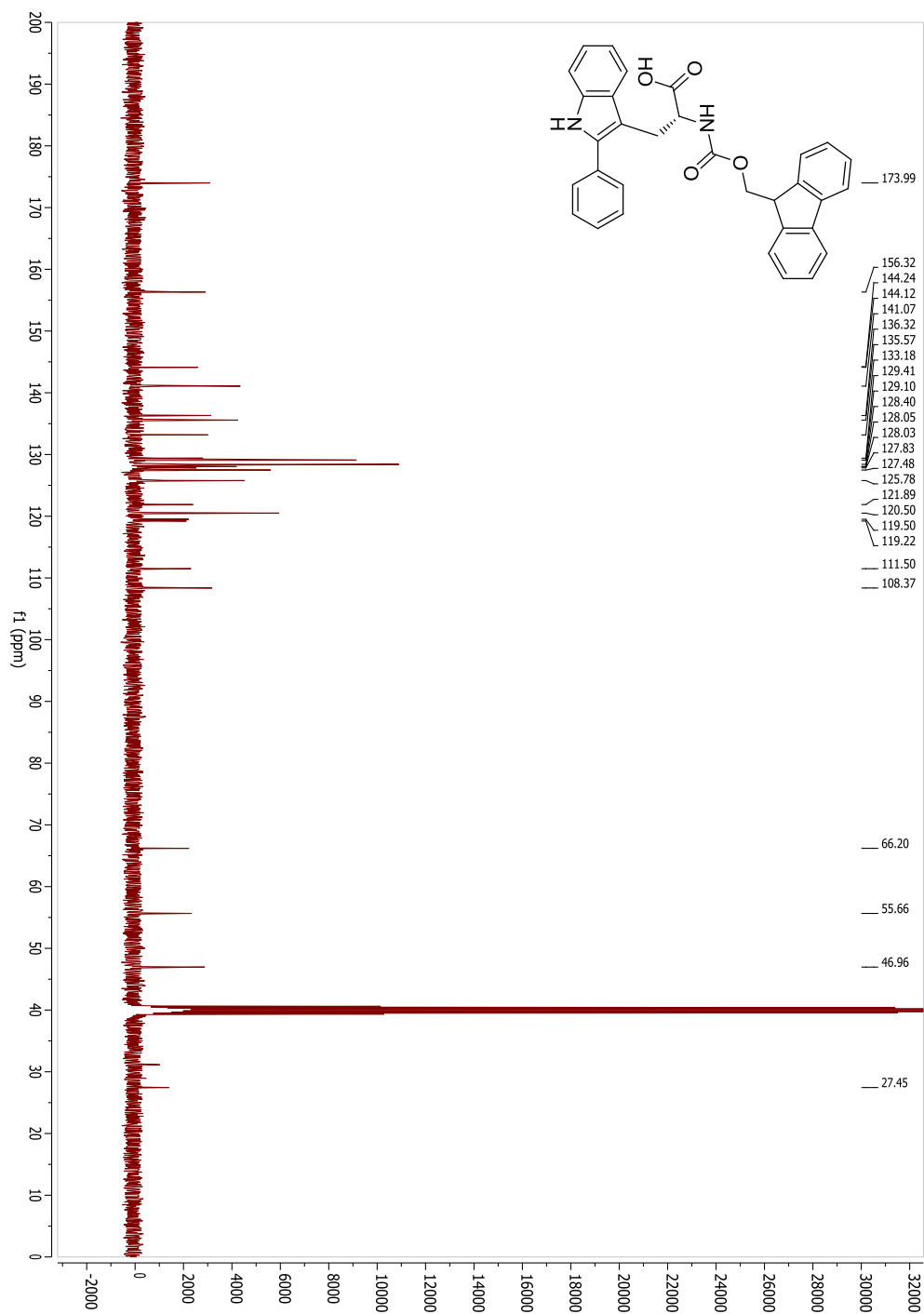
Synthesis of C-2 Arylated Tryptophan Amino Acids and Related Compounds through Palladium Catalyzed C-H Activation

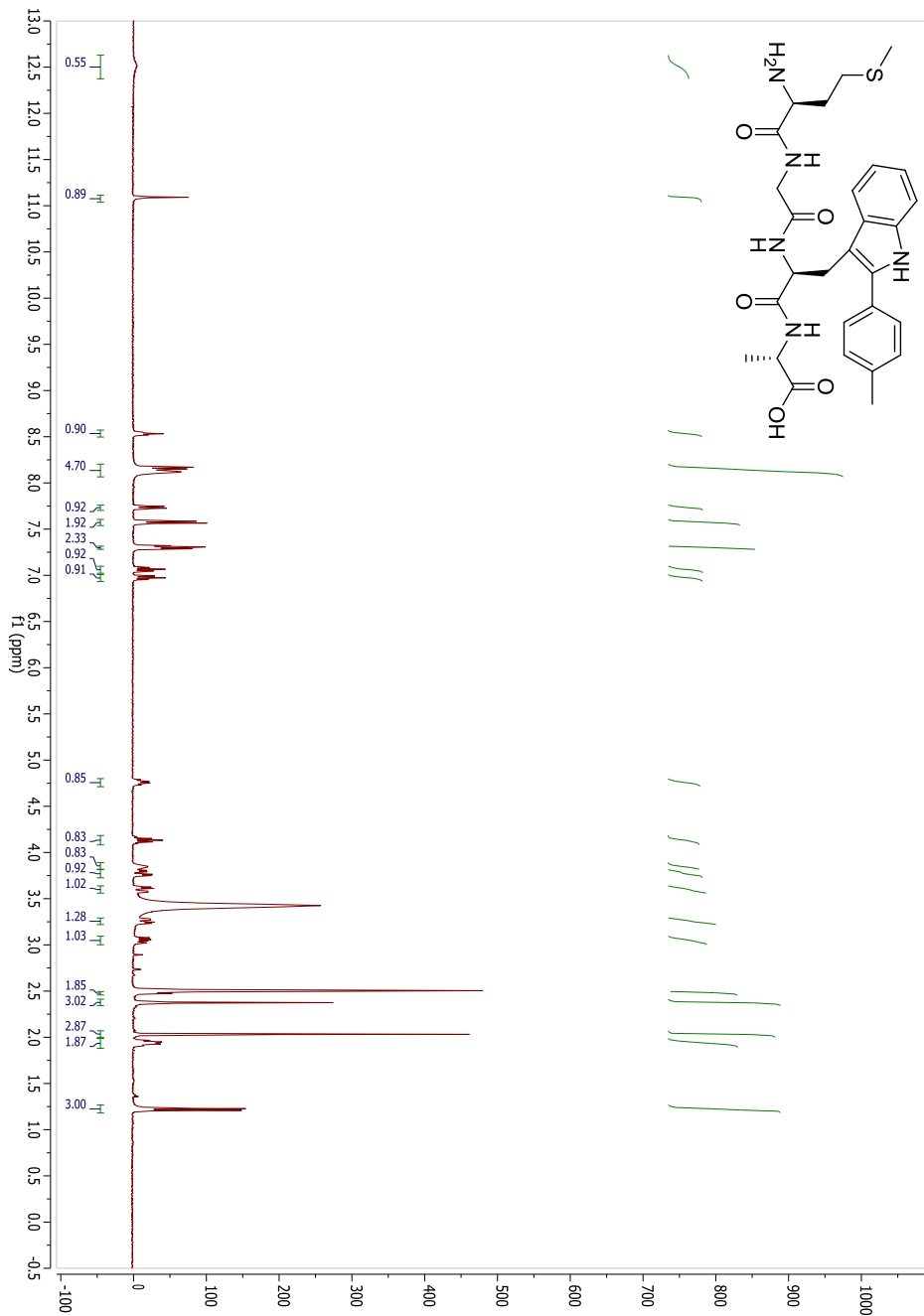
The following data is a selection of the content of the Supporting Information. Full supplementary information including NMR spectra and chromatographic analysis is available in the Supporting Information in electronic format.

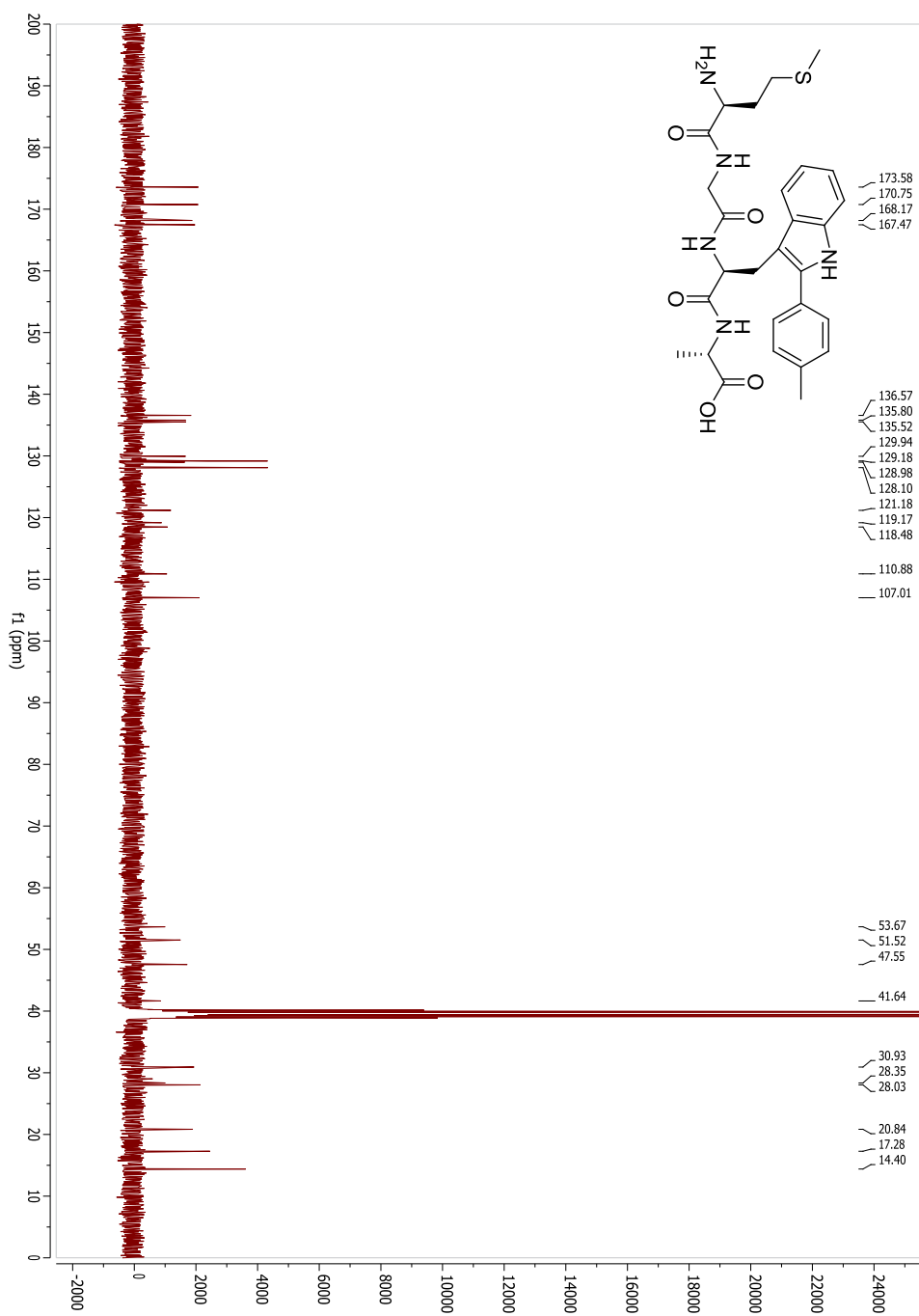
NMR spectra for selected compounds

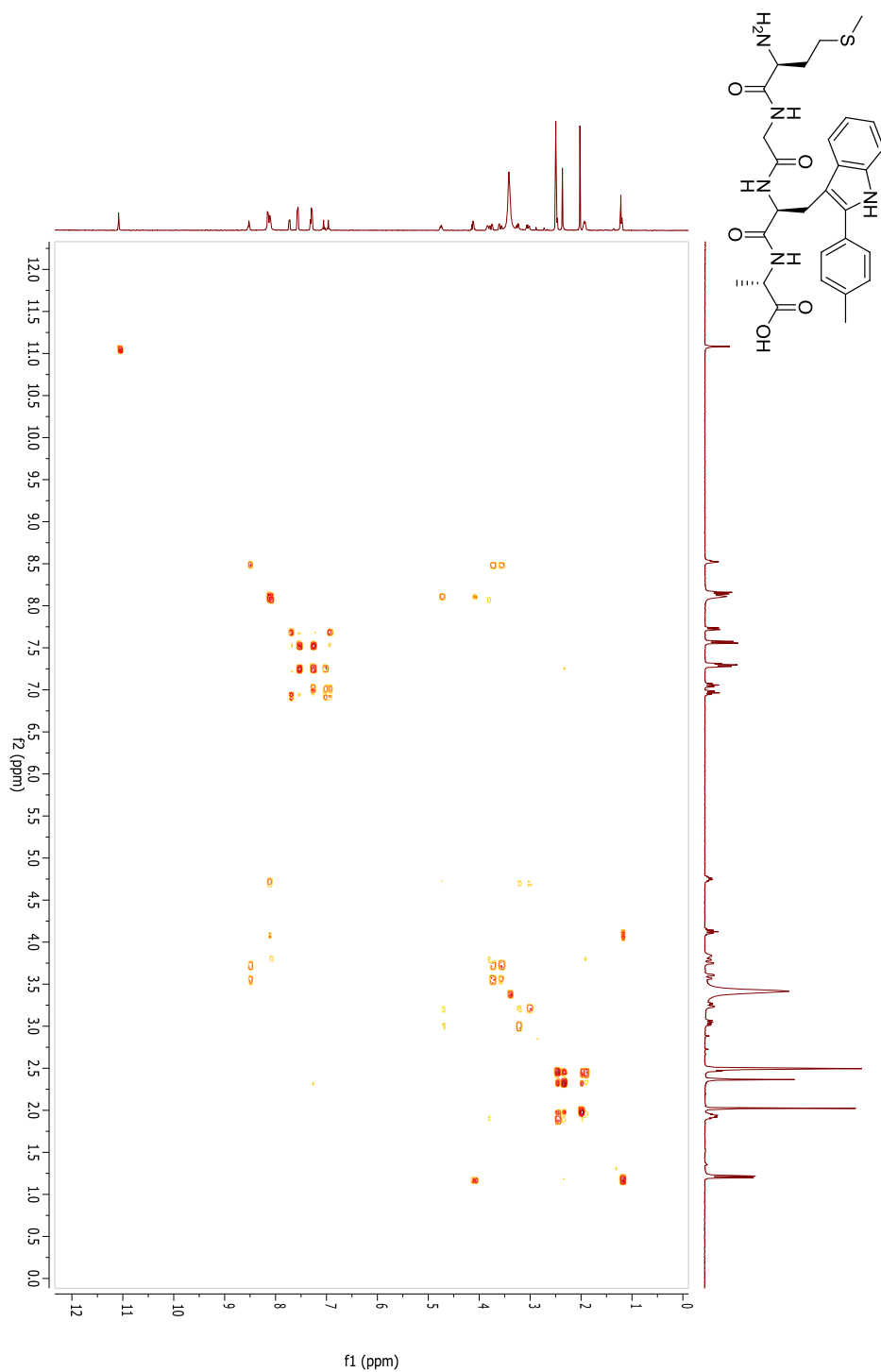
(*R*)-2-((((9*H*-Fluoren-9-yl)methoxy)carbonyl)amino)-3-(2-phenyl-1*H*-indol-3-yl)propanoic acid (**5a'**)

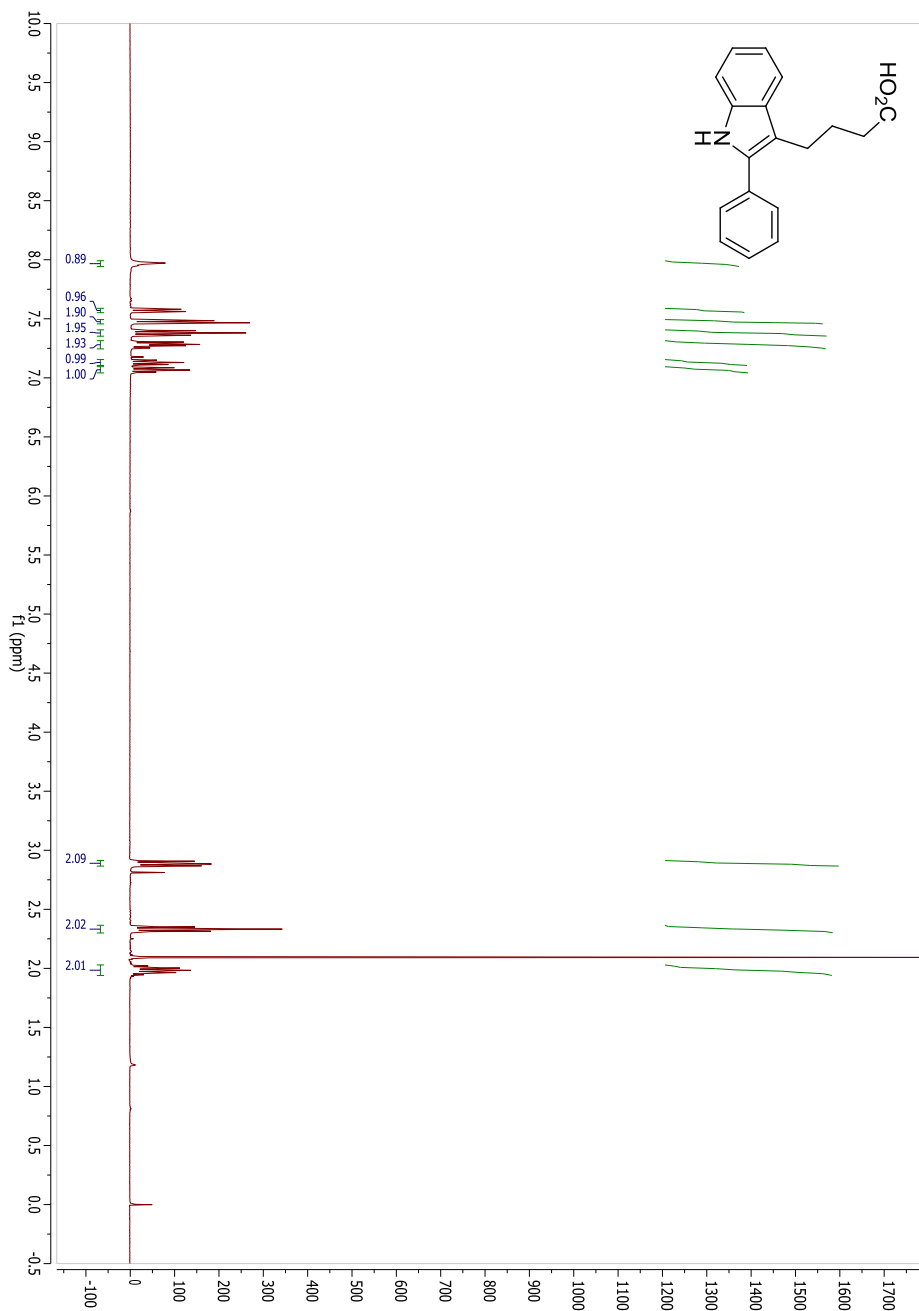




H-Met-Gly-Trp(C2-*p*-methylphenyl)-Ala-OH (6)





4-(2-Phenyl-1*H*-indol-3-yl)butanoic acid (10)

PUBLICATION III.

Enhanced antimicrobial activity of a peptide derived from human lysozyme by arylation of its tryptophan residues

Rodrigo González,^a Lorena Mendive-Tapia,^{b, c, d} María B. Pastrian,^a Fernando Albericio,^{b, c, d, e} Rodolfo Lavilla,^f Osvaldo Cascone,^a and Nancy B. Iannucci^a

Journal of Peptide Science, 2016, 22, 123-128.

- a) Cathedra of Biotechnology, School of Pharmacy and Biochemistry, UBA, and NANOBIOTEC, UBA-CONICET, Junín 956, (1113), Buenos Aires, Argentina.
- b) Department of Organic Chemistry, School of Chemistry, University of Barcelona, Martí i Franquès 1-11, 08028, Barcelona, Spain.
- c) Institute for Research in Biomedicine, Barcelona Science Park, Baldiri Reixac 10, 08028, Barcelona, Spain.
- d) CIBER-BBN, Networking Centre on Bioengineering, Biomaterials and Nanomedicine, Barcelona Science Park, Baldiri Reixac 10, 08028, Barcelona, Spain.
- e) School of Chemistry and Physics, University of KwaZulu-Natal, Westville Campus, University Road, Westville, 4001, Durban, South Africa.
- f) Laboratory of Organic Chemistry, Faculty of Pharmacy, University of Barcelona, Barcelona Science Park, Baldiri Reixac 10-12, 08028, Barcelona, Spain.

Research Article

Journal of
Peptide Science

Received: 24 October 2015

Revised: 3 December 2015

Accepted: 14 December 2015

Published online in Wiley Online Library

(wileyonlinelibrary.com) DOI 10.1002/psc.2850



Enhanced antimicrobial activity of a peptide derived from human lysozyme by arylation of its tryptophan residues

Rodrigo González,^a Lorena Mendive-Tapia,^{b,c,d} María B Pastrian,^a
Fernando Albericio,^{b,c,d,e} Rodolfo Lavilla,^{f,*} Osvaldo Cascone^{a,*}
and Nancy B Iannucci^a

Antimicrobial peptides are valuable agents to fight antibiotic resistance. These amphipathic species display positively charged and hydrophobic amino acids. Here, we enhance the local hydrophobicity of a model peptide derived from human lysozyme (107RKVVWWRNR115) by arylation of its tryptophan (Trp) residues, which renders a positive effect on *Staphylococcus aureus* and *Staphylococcus epidermidis* growth inhibition. This site-selective modification was accessed by solid-phase peptide synthesis using the non-proteinogenic amino acid 2-aryltryptophan, generated by direct C-H activation from protected Trp. The modification brought about a relevant increase in growth inhibition: *S. aureus* was fully inhibited by arylation of Trp 112 and by only 10% by arylation of Trp 109 or 111, respect to the non-arylated peptide. On the other hand, *S. epidermidis* was fully inhibited by the three arylated peptides and the parent peptide. The minimum inhibitory concentration was significantly reduced for *S. aureus* depending on the arylation site. Copyright © 2016 European Peptide Society and John Wiley & Sons, Ltd.

Additional Supporting information may be found in the online version of this article at the publisher's website.

Keywords: peptide; human lysozyme; arylation; tryptophan; antimicrobial activity

Introduction

According to the World Health Organization priority programs, microbial resistance is a threat for public health because of the possible re-emergence of past diseases. The therapeutic management of infections caused by resistant microorganisms is a challenging issue in medicine, mainly because of the exhaustion of the classical antibiotic arsenal. In this way, the development of new entities targeting cell components difficult to modify to generate resistance (such as the cell membrane) represents a strategic approach for the pharmaceutical industry [1].

In this context, the fragment 107–115 of the C-terminus of the human lysozyme possesses a relevant antimicrobial activity [2,3]. The attributes of antimicrobial peptides are the presence of positively charged and hydrophobic amino acids and an amphiphilic helical conformation. There are many precedents in the literature, which illustrate that these features give rise to antimicrobial peptide–membrane interactions with subsequent bacterial membrane disruption [4]. They exert their destructive power by variety of mechanisms including the generation of pores; therefore arguably, the development of microbial resistance should be extremely difficult. The anchorage of an antimicrobial peptide to the bacterial membrane depends on its amphipathic character [1,5]. The substitution of amino acids in a peptide with known antimicrobial activity can dramatically affect its biological activity [6]. Consequently, when alanine in positions 108 and 111 of this peptide are replaced by lysine and tryptophan (Trp), respectively, the antimicrobial activity against *Escherichia coli* and

Staphylococcus aureus is enhanced by fourfold and 20-fold, respectively [7,8]. Accordingly, its bioactivity could be enhanced by locally increasing its hydrophobicity.

* Correspondence to: Rodolfo Lavilla, Laboratory of Organic Chemistry, Faculty of Pharmacy, University of Barcelona, Barcelona Science Park, Baldri Reixac 10-12, 08028, Barcelona, Spain. E-mail: rlavilla@pcb.ub.es

* Osvaldo Cascone, Cathedra of Biotechnology, School of Pharmacy and Biochemistry, UBA, and NANOBIOTEC, UBA-CONICET, Junín 956, (1113) Buenos Aires, Argentina. E-mail: osvaldocascone@yahoo.com.ar

This paper is dedicated to the memory of Prof. Nancy B. Iannucci, a dear friend and an exceptional scholar.

a Cathedra of Biotechnology, School of Pharmacy and Biochemistry, UBA, and NANOBIOTEC, UBA-CONICET, Junín 956, (1113), Buenos Aires, Argentina

b Department of Organic Chemistry, School of Chemistry, University of Barcelona, Martí i Franqués 1-11, 08028, Barcelona, Spain

c Institute for Research in Biomedicine, Barcelona Science Park, Baldri Reixac 10, 08028, Barcelona, Spain

d CIBER-BBN, Networking Centre on Bioengineering, Biomaterials and Nanomedicine, Barcelona Science Park, Baldri Reixac 10, 08028, Barcelona, Spain

e School of Chemistry and Physics, University of KwaZulu-Natal, Westville Campus, University Road, Westville, 4001, Durban, South Africa

f Laboratory of Organic Chemistry, Faculty of Pharmacy, University of Barcelona, Barcelona Science Park, Baldri Reixac 10-12, 08028, Barcelona, Spain

In this respect, the site-selective arylation of hydrophobic residues appears as the method of choice to perform such modification. Using state of the art C-H activation transformations [9] upon indole substrates via palladium-catalyzed processes [10], we have recently developed methods for the selective arylation of Trp residues in peptides at C-2indole [11]. This protocol has been extended to a new stapling technique for Trp-Phe peptides [12]. In these transformations, we can introduce a variety of diversely substituted aryl groups in N-protected Trp, and the ensuing adducts are suitable for solid-phase peptide synthesis [13]. This formal post-synthetic modification has important structural consequences, directly altering the physicochemical properties and, more importantly, the biological activity of the adducts [14]. In this context, it has recently been described that the antifungal activity of the natural product aureobasidin can be improved through the functionalization of phenylalanine residues by iridium-catalyzed borylation [15].

The aim of this paper was to enhance the hydrophobicity of the antimicrobial peptide RKWVWWRNR by programmed and selective arylation of its Trp residues directly from the leader sequence. We planned to assess this effect on the antimicrobial activity against two microorganisms of clinical relevance (*S. aureus* and *Staphylococcus epidermidis*). 2-Arylated Trp was prepared in a protected form, amenable to solid-phase peptide synthesis as previously described through Pd-catalyzed C-H activation from Fmoc-Trp and 2-iodobenzene [13] and directly used to synthesize three peptides, each with an aryl-Trp residue at positions 109, 111 or 112, respectively.

Materials and Methods

Reagents and microorganisms

N α -Fmoc-Trp, iodobenzene, palladium (II) acetate and N,N-dimethylformamide anhydrous (DMF) were from Aldrich. Fmoc-Rink-Amide AM resin was from Iris-Biotech. O-benzotriazole-N,N',N''-tetramethyl-uronium-hexafluoro-phosphate (HBTU) and 2-(1H-7-azabenzotriazol-1-yl)-1,1,3,3-tetramethyluroniumhexafluorophosphate (HATU) were from Fluorochem. N,N-dimethylformamide was from Panreac AppliChem. N,N-diisopropylethylamine (DIEA) and silicagel were from Merck Biosciences. Müller-Hinton culture medium was from Oxoid. Bacterial strains *S. aureus* ATCC 29213 and *S. epidermidis* ATCC 12228 were from The American Type Culture Collection (Manassas, VA, USA).

Tryptophan arylation

The arylation of the indolic C2 of Trp was carried out by activation of this carbon catalyzed by palladium as described by Ruiz-Rodríguez *et al.* [11] and Preciado *et al.* [13]. Briefly, the N α -Fmoc-Trp, activated with Pd(OAc)₂ was treated with iodobenzene in a microwave at 90° C and purified by flash chromatography on silicagel as described by Preciado *et al.* [14]. The product was identified by nuclear magnetic resonance and electrospray mass spectrometry, and the yield was 56% (see Supporting Information for details).

Synthesis of arylated peptides

The preparation of 2-aryl-N α -Fmoc-Trp was performed as described from 4-iodobenzene and N α -Fmoc-Trp [1]. The resulting arylated amino acid was used in solid-phase peptide synthesis without any special requirement. The solid-phase method was performed

according to Kates and Albericio [16]. Fmoc chemistry and Fmoc-Rink-Amide AM resin were used. HBTU and DIEA were used as coupling reagents for arginine, alanine, Trp, valine and asparagine. According to previous observations, HATU and DIEA were used for aryl Trp coupling to ensure its total incorporation. After side-chains removal, peptides were cleaved from the resin with trifluoroacetic acid/water/triisopropylsilane. Purification of peptides was performed by RP-HPLC. Identification was carried out by MALDI-MS and MALDI-MS/MS (see Supporting Information for details).

Scanning electron microscopy

Samples were fixed with 1% glutaraldehyde in 0.1 M cacodylate buffer, pH 7.0, for 10 min, then were dehydrated with ethanol washes (50–100% ethanol) and immersed in ethanol/hexamethyldisilazane (1 : 1) and 100% hexamethyldisilazane for 60 min. Afterwards, samples were dried, mounted on scanning electron microscope (SEM) stubs and coated immediately in a sputter coater with gold/palladium (Cressington Scientific Instruments). The microographies were obtained with a Zeiss Supra 40 scanning electron microscope.

Growth inhibition assay

Bacteria from –80 °C frozen glycerol stock were grown in Müller-Hinton (MH) agar plates for 16 h at 37 °C. Individual colonies were inoculated in Erlenmeyer flasks containing 50 ml MA broth and incubated at 37 °C and 200 RPM until a density of 1×10^5 CFU/ml was reached. Bacteria suspensions were diluted to 2.0×10^5 CFU/ml with 2X MA broth for the assay.

The 0.5 ml peptide solutions were twofold diluted with water from 2.50 to 0.16 mg/ml and filter sterilized through 0.22 μ m filters. Sterile peptide dilutions were then mixed with the same volume of 2X MH medium containing 2.0×10^5 CFU/ml and incubated at 37 °C for 21 h in sterile capped glass tubes. Bacterial growth was determined by measuring the absorbance at 600 nm. Positive control (100% growth) was performed in absence of peptide (0.5 ml of sterile water), and negative control was carried out in absence of bacteria (0.5 ml 2X MH broth).

Minimum inhibitory concentration (MIC) determination

Minimum inhibitory concentration determination was performed based on a micro-dilution assay [17]. Briefly, 100 μ l of 2.0 mg/ml peptide sterile solution in water was diluted twofold with 2X MH broth in well 1 and twofold serially diluted with MH broth up to well 12.

One-hundred microliter of bacterial suspension containing 2.0×10^5 CFU/ml in MH broth was added to each well, and plates were incubated for 16–20 h at 37 °C. Growth was measured at 600 nm in a FlexStation 3 Multi-Mode Microplate Reader. A positive control without peptide (100% growth) and a negative control without bacteria (0% growth) were included in the assay.

Minimum inhibitory concentration is defined as the minimum concentration of peptide producing total inhibition of the growth under these conditions. Each peptide was assayed in triplicate.

Hemolysis assay

Hemolysis was performed using human red blood cells (RBC), basally as described by Helmerhorst *et al.* [18]. Briefly, RBC from heparinized blood were washed three times with phosphate-buffered saline (PBS) and resuspended at 0.5% in the same buffer. 500 μ l of peptide

solution in concentrations of 15, 50 and 125 µg/ml was added to equal volume of RBC suspension. After 1 h at 37 °C, the mixture was centrifuged at 2800 rpm for 5 min, and the absorbance of the supernatant at 414 nm was measured. PBS and 1% Triton X-100 in water were the negative and positive controls, respectively. The hemolysis percentage was calculated by the formula:

$$\left[\frac{(A_{\text{peptide}} - A_{\text{PBS}})}{A_{\text{Triton}} - A_{\text{PBS}}} \right] \times 100$$

Results and Discussion

We efficiently synthesized all three peptides selectively mono-phenylated at indole position 2 of each Trp (see Figure 1). Once the peptides were prepared, the purification and spectroscopic analyses confirmed the expected structures (see Supporting Information).

Table 1 shows the sequences of the leader peptide, the K108-W111 intermediary sequence **1** and the three aryl-peptides **2**, **3** and **4**, each with one phenyl-Trp respectively.

Table 1. Peptides used in this work		
Sequence ^a	Formula ^b	Name
RAWVAWRNR-NH ₂	107–115 hLZ	Leader
RKWVWWRNR-NH ₂	[K ¹⁰⁸ W ¹¹¹] 107–115 hLZ	1
RKW(Ar)VWWRNR-NH ₂	[K ¹⁰⁸ W(Ar) ¹⁰⁹ W ¹¹¹] 107–115 hLZ	2
RKWVW(Ar)WRNR-NH ₂	[K ¹⁰⁸ W(Ar) ¹¹¹] 107–115 hLZ	3
RKWVWV(Ar)RNR-NH ₂	[K ¹⁰⁸ W ¹¹¹ W(Ar) ¹¹²] 107–115 hLZ	4

^aR, arginine; A, alanine; W, tryptophan; W(Ar), 2-phenyltryptophan; V, valine; N, asparagine; -NH₂, amidated C-terminal group.
^bhLZ, human lysozyme.

Table 2. Characterization of the peptides used in this work		
Peptide ^a	RT ^b (min)	Experimental MW ^c (theoretical)
1	4.7	1384.79 (1384.76)
2	5.2	1461.05 (1460.86)
3	5.2	1461.02 (1460.86)
4	5.2	1461.07 (1460.86)

^aPurities of the pure peptides are around 94–98% according to HPLC profiles (see SI).
^bRT, retention time.
^cMW, molecular mass weight.

Table 2 shows the results of the characterization by RP-HPLC and MALDI-MS for the intermediary peptide and the three aryl-peptides.

The retention time of the aryl-peptides **2**, **3** and **4** in RP-HPLC was longer than that of the non-arylated intermediary peptide **1**, thus evidencing the increase in hydrophobicity because of the addition of a phenyl group. Besides, the experimental molecular weight matched with that of the theoretical one, and the sequence analysis by MALDI-MS/MS allowed identifying unambiguously the Trp in the preselected position. Next, we tackled the biological assays of the antimicrobial activity of these compounds. To this end, we performed growth inhibition assays and MIC determination of each arylated peptide and compared the results with those obtained with the parent non-arylated peptide **1** (Figure 1).

Figure 2 shows the results of the inhibition assays performed on the microorganisms studied, where different degrees of inhibition are evident. Full inhibition of *S. epidermidis* growth was evidenced regardless of which Trp was arylated. Moreover, the non-arylated intermediary peptide **1** was almost equally active. In contrast, for the more pathogenic *S. aureus*, the arylation of Trp 109 or 111 (peptides **2** and **3**, respectively) caused little effect on the antimicrobial activity of the intermediary peptide, whereas arylation at position 112 (peptide **4**) brought about a relevant increase in the antimicrobial activity of the intermediary peptide **1**.

Preliminary calculations showed that the molecular mechanics optimized geometries (Merck Molecular Force Field implemented in a Spartan'14 suite) of the arylated peptides display a common conserved structure, similar to that of the native peptide, sharing relatively close hydrogen bond networks and helical motifs (see Supporting Information). The newly incorporated phenyl group does not seem to modify the preferred conformation of the biomolecules drastically, but rather is preferentially located outward in the periphery in all three arylated peptides. Simultaneously, the incorporated hydrophobic aryl moiety should moderately increase the LogP, thus partially justifying the observed effects. Although more refined computational approaches, for instance Molecular Dynamics, may bring a better understanding of the structural features of the aryl-peptides, at this point, it may be risky to rely mainly on conformational factors taking into account the variety of mechanisms of action for antimicrobial peptides, as stated earlier [1,4,5]. We took an empirical approach as the starting point and future experimentation (polyarylated peptides, exploration of other sequences/residues, and Molecular Dynamic simulations) will shed more light in these issues.

Figure 3 shows the SEM pictures of *S. aureus* and *S. epidermidis* treated with the phenyl-peptides synthesized, where the damage in the microbial membrane due to the treatment can be seen.

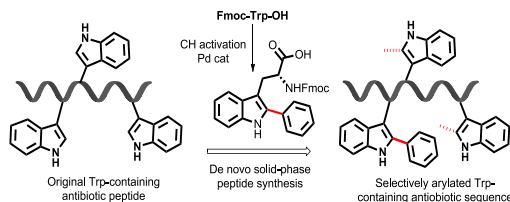


Figure 1. Synthetic approach for the selective arylation of the antimicrobial peptide RKWVWWRNR.

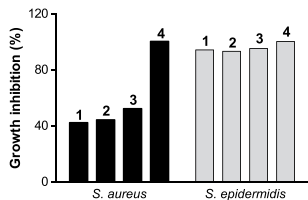


Figure 2. Inhibition assay at 0.1 mg/ml of the non-arylated intermediary peptide 1 and aryl-peptides at tryptophan (Trp) 109, Trp 111 and Trp 112 (peptides 2, 3 and 4, respectively) on *Staphylococcus aureus* and *Staphylococcus epidermidis*. Results are expressed as percentage.

A similar membrane disruption effect was demonstrated by Tan *et al.* [19] working with Gram negative bacteria and peptides with positive charge and different hydrophobicity degree.

Table 3 shows the MICs of the phenyl-peptides compared with those of the leader peptide and peptide 1, against the two microorganisms studied. In *S. aureus* ATCC 29213, the MIC decreased twofold with peptide 2 and fourfold with peptides 3 and 4 respect to peptide 1. In *S. epidermidis*, the arylation of Trp 109 (peptide 2) brought about no changes in the MIC, while arylation of Trp 111 or Trp 112 (peptides 3 and 4, respectively) decreased it by twofold respect to peptide 1. In all cases, arylation of Trp of peptide 1 brought about a significant decrease in the MIC, but the inhibition degree was different if the arylated Trp was in positions 109 or 111–112. Moreover, the arylation of Trp in these peptides increased their antimicrobial activity, reaching MICs compatible with an effective therapeutic window and evidencing their excellent possibilities as active pharmaceutical ingredients for renovation of antimicrobial agents.

The results of the hemolysis assay shown in Table 4 are similar to those obtained with the intermediary peptide and become significant only at concentrations higher than tenfold their MICs, thus

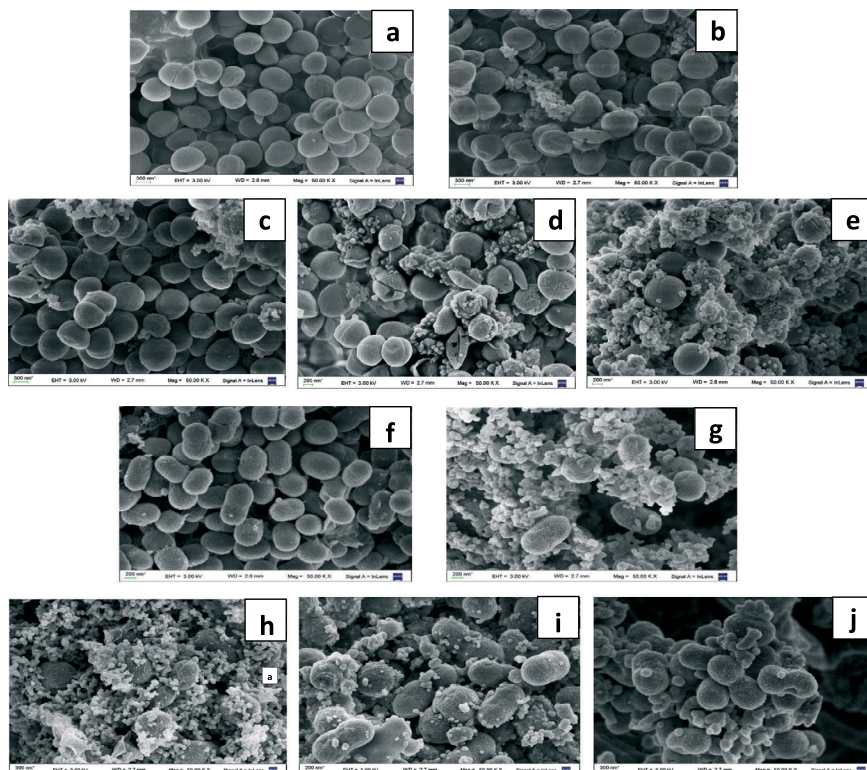


Figure 3. Pictures of microorganisms treated with the antimicrobial peptides assayed in this work. (A) *Staphylococcus aureus* ATCC 29213. a) Control without peptide; b) Peptide 1; c) Peptide 2; d) Peptide 3; e) Peptide 4. (B) *Staphylococcus epidermidis* ATCC 12228. f) Control without peptide; g) Peptide 1; h) Peptide 2; i) Peptide 3; j) Peptide 4. All experimentation was performed at a peptide concentration of 60 μ M (see Supporting Information).

ANTIMICROBIAL ACTIVITY ENHANCEMENT BY TRYPTOPHAN ARYLATION

Table 3. Minimum inhibitory concentration (MIC) of the peptides used in this work

Peptide	Staphylococcus aureus ATCC 29213		Staphylococcus epidermidis ATCC 12228	
	µg/ml	µM	µg/ml	µM
Leader	250	206	ND ^a	
1	16	11	8	5
2	8	5	8	5
3	4	3	4	3
4	4	3	4	3

^aND, not determined.**Table 4.** Hemolysis percentage of aryl-peptides at 15, 50 and 125 µg/ml

Peptide	15 µg/ml	50 µg/ml	125 µg/ml
1	2.6	5.4	30.7
2	2.7	6.1	30.9
3	2.7	5.8	31.6
4	2.9	5.6	29.8

evidencing the safety of the arylated peptides towards human red blood cells.

There are some relevant precedents in the literature regarding the effect of arylated histidines in antimicrobial peptides [20,21]; herein, we disclose a new methodology based on the preparation of an arylated Trp-peptide through C-H activation, leading to enhancement of its antimicrobial activity. This may open the door to further transformations of this type, aimed to improve the pharmacological action without disrupting the existing amphipathic nature of the peptide, but locally increasing the lipophilicity of specific residues. Although the herein described proof of concept has only explored the introduction of a naked phenyl group, access to peptides displaying diversely substituted aryl groups using the same methodology is open. To date, most biomolecule modifications of this type involve conjugation reactions that severely decrease the polarity of the original peptide by generating amide bonds from amino and acid groups present in the precursor peptide.

Conclusions

We have shown that the arylation of Trp-containing microbial peptides results in meaningful improvements of their biological activity, while keeping the hemolysis low. It is remarkable that a slight increment in the molecular weight (~5%) results in a four-fold decrease in the MIC, suggesting additional interactions between the extra aromatic group and the target. Importantly, because the microbial membranes are the biological targets of aryl-peptides, the possibility of generating resistance is seriously compromised. Thus, the eventual therapeutic use of these agents may display relevant advantages over conventional antibiotics to combat resistance. This proof of concept can open new avenues in the development of novel amphipathic peptides based on differently arylated Trp residues.

Acknowledgements

This work was supported by DGICYT – Spain (project BQU-CTQ2012-30930), Generalitat de Catalunya (2014 SGR 137), Institute for Research in Biomedicine Barcelona (Spain) and Ministerio de Salud de la República Argentina. An FPU fellowship for L.M.T. from the Ministerio de Educación, Cultura y Deporte– Spain (MECD) is acknowledged.

References

- Blair JMA, Webber MA, Baylay AJ, Ogbolu DO, Piddock LJV. Molecular mechanisms of antibiotic resistance. *Nat. Rev. Microbiol.* 2016; **13**: 42–51.
- Pellegrini A, Thomas U, Bramaz N, Klausner S, Hunziker P, von Fellenberg R. Identification and isolation of a bactericidal domain in chicken egg white lysozyme. *J. Appl. Microbiol.* 1997; **82**: 372–378.
- Ibrahim HR, Thomas U, Pellegrini A. A helix-loop-helix peptide at the upper lip of the active site cleft of lysozyme confers potent antimicrobial activity with membrane permeabilization action. *J. Biol. Chem.* 2001; **276**: 43767–43774.
- Sato H, Feix JB. Peptide-membrane interactions and mechanisms of membrane destruction by amphipathic alpha-helical antimicrobial peptides. *Biochim. Biophys. Acta* 2006; **1758**: 1245–1256.
- Aisenbrey C, Bechinger B. Molecular packing of amphipathic peptides on the surface of lipid membranes. *Langmuir* 2014; **30**: 10374–10383.
- Pérez-Payá E, Houghten RA, Blondelle SE. Determination of the secondary structure of selected melittin analogues with different hemolytic activities. *Biochem. J.* 1994; **299**: 587–591.
- González R, Albericio F, Cascone O, Iannucci NB. Improved antimicrobial activity of h-lysozyme (107–115) by rational Ala substitution. *J. Pept. Sci.* 2010; **16**: 424–429.
- Iannucci NB, Curto LM, Albericio F, Cascone O, Delfino JM. Structural glance into a novel anti-staphylococcal peptide. *Biopolymers: Pept. Sci.* 2013; **102**: 49–57.
- Yu JQ, Shi Z. *Topics in Current Chemistry, C-H activation*, Vol. **292**, Springer: Berlin Heidelberg, 2010.
- Lebrasseur N, Larrosa I. *Adv. Heterocycl. Chem. In Recent Advances in the C2 and C3 Regioselective Direct Arylation of Indoles*, Vol. **105**, Academic Press: New York, 2012 Chapter 4: 309–351.
- Ruiz-Rodríguez J, Albericio F, Lavilla R. Postsynthetic modification of peptides: chemoselective C-arylation of tryptophan residues. *Chem. Eur. J.* 2010; **16**: 1124–1127.
- Mendive-Tapia L, Preciado S, García J, Ramón R, Kielland N, Albericio F, Lavilla R. New peptide architectures through C-H activation stapling between tryptophan-phenylalanine/tyrosine residues. *Nat. Commun.* 2015; **6**: 7160. DOI: 10.1038/ncomms8160.
- Preciado S, Mendive-Tapia L, Albericio F, Lavilla R. Synthesis of C-2 arylated tryptophan amino acids and related compounds through palladium catalyzed C-H activation. *J. Org. Chem.* 2013; **78**: 8129–8135.
- Preciado S, Mendive-Tapia L, Torres-García C, Zamudio-Vázquez R, Soto-Cerrato V, Pérez-Tomás R, Albericio F, Nicolás E, Lavilla R. Synthesis and biological evaluation of a postsynthetically modified Trp-based diketopiperazine. *Med. Chem. Comm.* 2013; **4**: 1171–1174.
- Wuts PGM, Simons LJ, Metzger BP, Sterling RC, Slightom JL, Elhammer AP. Generation of broad-spectrum antifungal drug candidates from the natural product compound aureobasidin A. *ACS Med. Chem. Lett.* 2015; **6**: 645–649.
- Kates SA, Albericio F. In *Solid Phase Synthesis. A Practical Guide*, (ed.) : New York, 2000.
- Wiegand I, Hilpert K, Hancock REW. Agar and broth dilution methods to determine the minimal inhibitory concentration (MIC) of antimicrobial substances. *Nat. Protoc.* 2008; **3**: 163–175.
- Helmerhorst EJ, Reijnders IM, van't Hoff W, Veerman ECI, Nieuw Amerongen AV. A critical comparison of the hemolytic and fungicidal activities of cationic antimicrobial peptides. *FEBS Lett.* 1999; **449**: 105–110.
- Tan J, Huang J, Huang Y, Chen Y. Effects of single amino acid substitution on the biophysical properties and biological activities of an amphipathic α -helical antibacterial peptide against Gram-negative bacteria. *Molecules* 2014; **19**: 10803–10817.
- Ng-Choi I, Soler M, Cerezo V, Badosa E, Montesinos E, Planas M, Feliu L. Solid-phase synthesis of 5-arylhistidine-containing peptides with

- antimicrobial activity through a microwave-assisted Suzuki-Miyaura cross-coupling. *Eur. J. Org. Chem.* 2012; **2012**: 4321–4332.
- 21 We may consider also the arylation of peptide-like compounds, taking place in non-amino acidic moieties: a) Grotenbreg GM, Buizert AEM, Llamas-Saiz AL, Spalburg E, Van Hooft PAV, de Neeling AJ, Noort D, van Raaij MJ, van der Marel GA, Overkleeft HS, Overhand M. β -turn modified Gramicidin S analogues containing arylated sugar amino acids display antimicrobial and hemolytic activity comparable to the natural product. *J. Am. Chem. Soc.* 2006; **128**: 7559–7565; b) Wales SM, Hammer KA, Somphol K, Kemker I, Schröder DC, Tague AJ, Brkic Z, King AM, Lyras D, Riley TV, Bremner JB,

Keller PA, Pyne SG. Synthesis and antimicrobial activity of binaphthyl-based, functionalized oxazole and thiazole peptidomimetics. *Org. Biomol. Chem.* 2015; **13**: 10813–10824.

Supporting Information

Additional Supporting information may be found in the online version of this article at the publisher's website.

Supporting Information

Enhanced antimicrobial activity of a peptide derived from human lysozyme by arylation of its tryptophan residues

The following data is a selection of the content of the Supporting Information. Full supplementary information including general experimentation, procedures and compound characterization is available in the Supporting Information in electronic format.

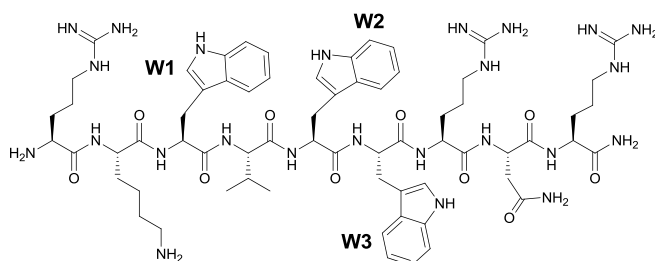
Table of Contents

<i>Synthesis of arylated peptides</i>	<i>101</i>
<i>RP-HPLC chromatograms of pure arylated peptides 1-4.....</i>	<i>102</i>
<i>Minimized geometries of the native peptide and the arylated derivatives generated by the Spartan '14 suite (molecular mechanics, MMFF94)⁷</i>	<i>103</i>

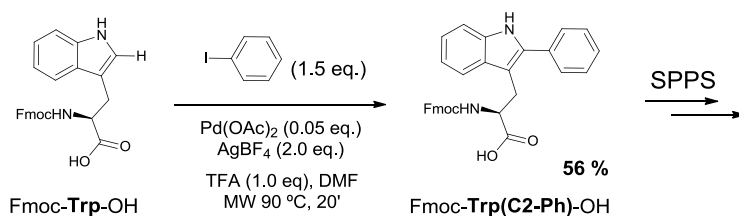
Synthesis of arylated peptides

The preparation of 2-aryl- $N\alpha$ -Fmoc-tryptophan was performed as described from 4-iodobenzene and $N\alpha$ -Fmoc-tryptophan (Preciado et al., 2013).¹ The resulting arylated amino acid was used in solid-phase peptide synthesis without any special requirement.

The solid-phase method was performed according to Kates and Albericio, (2000).⁴ Fmoc chemistry and Fmoc-Rink-Amide AM resin were used. O-Benzotriazole- N,N,N',N' -tetramethyluronium-hexafluoro-phosphate (HBTU) and N,N -diisopropylethylamine (DIEA) were used as coupling reagents for arginine, alanine, tryptophan, valine and asparagine, while 2-(1H-7-azabenzotriazol-1-yl)-1,1,3,3-tetramethyl uronium hexafluorophosphate (HATU) and DIEA were used for aryl tryptophan. After side-chains removal, peptides were cleaved from the resin with trifluoroacetic acid (TFA)/water/triisopropylsilane (TIS). Purification of peptides was performed by RP-HPLC. Identification was carried out by MALDI-MS and MALDI-MS/MS.



Native Peptide H-Arg-Lys-Trp-Val-Trp-Trp-Arg-Asn-Arg-NH₂ (1)



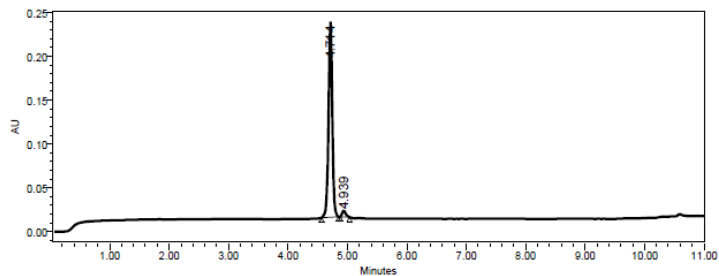
W1-Ar H-Arg-Lys-Trp(C2-Ph)-Val-Trp-Trp-Arg-Asn-Arg-NH₂ (2)

W2-Ar H-Arg-Lys-Trp-Val-Trp(C2-Ph)-Trp-Arg-Asn-Arg-NH₂ (3)

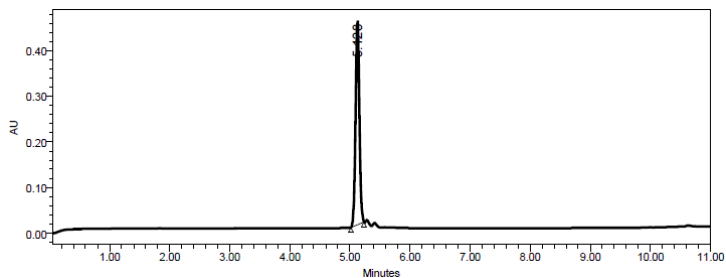
W3-Ar H-Arg-Lys-Trp-Val-Trp-Trp(C2-Ph)-Arg-Asn-Arg-NH₂ (4)

RP-HPLC chromatograms of pure arylated peptides 1-4

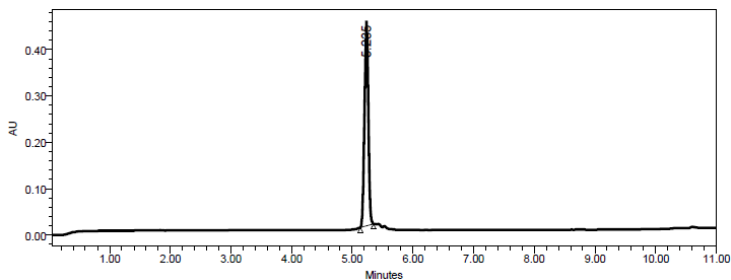
H-Arg-Lys-Trp-Val-Trp-Trp-Arg-Asn-Arg-NH₂ (1)



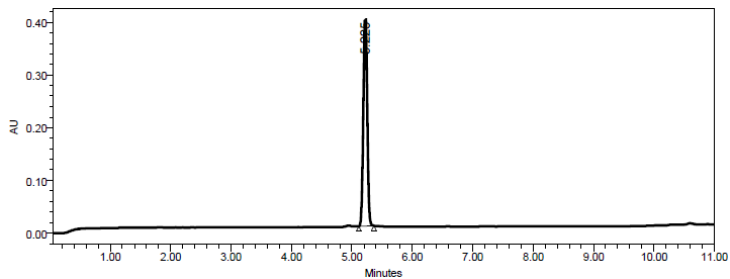
H-Arg-Lys-Trp(C2-Ph)-Val-Trp-Trp-Arg-Asn-Arg-NH₂ (2)



H-Arg-Lys-Trp-Val-Trp(C2-Ph)-Trp-Arg-Asn-Arg-NH₂ (3)



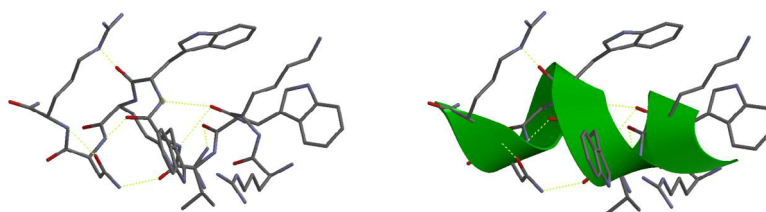
H-Arg-Lys-Trp-Val-Trp-Trp(C2-Ph)-Arg-Asn-Arg-NH₂ (4)



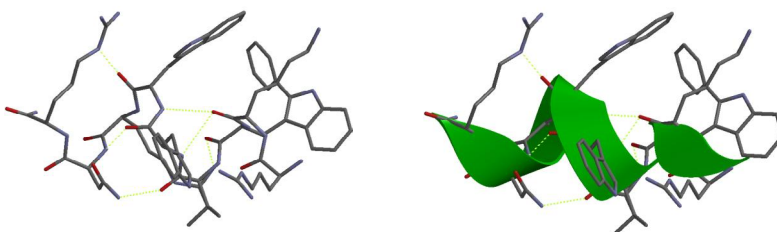
Gradient was 5-60% of B. Solvent A (0.045 % TFA in H₂O) and solvent B (0.036 % TFA in ACN), in 8 min. Elution was monitored at 254 nm and the flow rate was 1.0 mL/min.

Minimized geometries of the native peptide and the arylated derivatives generated by the Spartan '14 suite (molecular mechanics, MMFF94)⁷

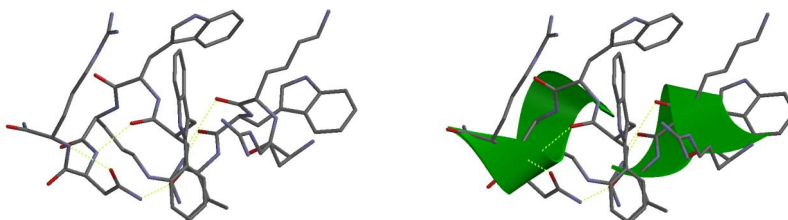
1- Native Peptide: RKWVWWRNR-NH₂



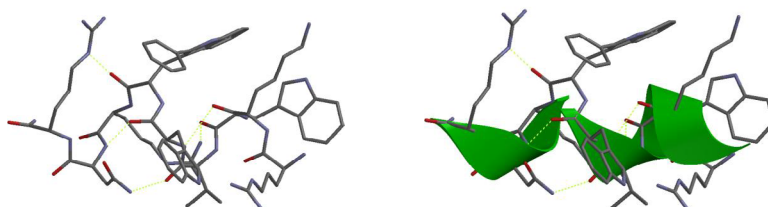
2- W1Ar: RKW(Ar)VWWRNR-NH₂



3- W2Ar: RKWVW(Ar)WRNR-NH₂



4- W3-Ar: RKWVWW(Ar)RNR-NH₂



Hydrogens omitted for clarity. Left section: hydrogen bonds shown in yellow. Right section: ribbons in green. No significant changes were observed when the optimization was done with semi-empirical methods.



2

SPACER-FREE TRP-BODIPY FLUOROGEN FOR PEPTIDE-BASED IMAGING PROBES

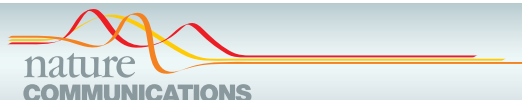
PUBLICATION IV.

Spacer-free BODIPY fluorogens in antimicrobial peptides for direct imaging of fungal infection in human tissue

Lorena Mendive-Tapia,^a Can Zhao,^b Ahsan R. Akram,^c Sara Preciado,^a Fernando Albericio,^{a, d, e, f} Martin Lee,^g Alan Serrels,^g Nicola Kielland,^h Nick D. Read,^b Rodolfo Lavilla,^{e, h} and Marc Vendrell^c

Nature Communications, 2016, 7:10940. DOI: 10.1038/ncomms10940.

- a) Institute for Research in Biomedicine, Barcelona Science Park, Baldiri Reixac 10-12, Barcelona 08028, Spain.
- b) Manchester Fungal Infection Group, Institute of Inflammation and Repair, University of Manchester, CTF Building, Grafton St, Manchester M13 9NT, UK.
- c) MRC/UoE Centre for Inflammation Research, University of Edinburgh, 47 Little France Crescent, Edinburgh EH16 4TJ, UK.
- d) Department Organic Chemistry, University of Barcelona, Martí i Franquès 1-11, Barcelona 08028, Spain.
- e) CIBER-BBN, Networking Centre for Bioengineering, Biomaterials and Nanomedicine, Baldiri Reixac 10-12, Barcelona 08028, Spain.
- f) School of Chemistry, University of KwaZulu-Natal, Durban 4001, South Africa.
- g) Edinburgh Cancer Research Centre, University of Edinburgh, Crewe South Road, Edinburgh EH4 2XR, UK.
- h) Laboratory of Organic Chemistry, Faculty of Pharmacy, University of Barcelona, Barcelona Science Park, Baldiri Reixac 10-12, Barcelona 08028, Spain.



ARTICLE

Received 31 Jul 2015 | Accepted 3 Feb 2016 | Published 9 Mar 2016

DOI: 10.1038/ncomms10940

OPEN

Spacer-free BODIPY fluorogens in antimicrobial peptides for direct imaging of fungal infection in human tissue

Lorena Mendive-Tapia¹, Can Zhao², Ahsan R. Akram³, Sara Preciado¹, Fernando Albericio^{1,4,5,6}, Martin Lee⁷, Alan Serrels⁷, Nicola Kielland⁸, Nick D. Read², Rodolfo Lavilla^{5,8} & Marc Vendrell³

Fluorescent antimicrobial peptides are promising structures for *in situ*, real-time imaging of fungal infection. Here we report a fluorogenic probe to image *Aspergillus fumigatus* directly in human pulmonary tissue. We have developed a fluorogenic Trp-BODIPY amino acid with a spacer-free C-C linkage between Trp and a BODIPY fluorogen, which shows remarkable fluorescence enhancement in hydrophobic microenvironments. The incorporation of our fluorogenic amino acid in short antimicrobial peptides does not impair their selectivity for fungal cells, and enables rapid and direct fungal imaging without any washing steps. We have optimized the stability of our probes in human samples to perform multi-photon imaging of *A. fumigatus* in *ex vivo* human tissue. The incorporation of our unique BODIPY fluorogen in biologically relevant peptides will accelerate the development of novel imaging probes with high sensitivity and specificity.

¹Institute for Research in Biomedicine, Barcelona Science Park, Baldri Reixac 10-12, Barcelona 08028, Spain. ²Manchester Fungal Infection Group, Institute of Inflammation and Repair, University of Manchester, CTF Building, Grafton St, Manchester M13 9NT, UK. ³MRC/UoE Centre for Inflammation Research, University of Edinburgh, 47 Little France Crescent, Edinburgh EH16 4TJ, UK. ⁴Department Organic Chemistry, University of Barcelona, Martí i Franqués 1-11, Barcelona 08028, Spain. ⁵CIBER-BBN, Networking Centre for Bioengineering, Biomaterials and Nanomedicine, Baldri Reixac 10-12, Barcelona 08028, Spain. ⁶School of Chemistry, University of KwaZulu-Natal, Durban 4001, South Africa. ⁷Edinburgh Cancer Research Centre, University of Edinburgh, Crewe South Road, Edinburgh EH4 2XR, UK. ⁸Laboratory of Organic Chemistry, Faculty of Pharmacy, University of Barcelona, Barcelona Science Park, Baldri Reixac 10-12, Barcelona 08028, Spain. Correspondence and requests for materials should be addressed to R.L. (email: rlavilla@pcb.ub.es) or to M.V. (email: mvendrel@staffmail.ed.ac.uk).

ARTICLE

NATURE COMMUNICATIONS | DOI: 10.1038/ncomms10940

Invasive pulmonary aspergillosis (IPA) is a highly fatal disease in immunocompromised patients. IPA results from the infection with the fungal pathogen *Aspergillus fumigatus*, and it is a frequent cause of fungal pneumonia with mortality rates up to 40% (ref. 1). Current diagnostic approaches for IPA rely on histological analysis, cultures from bronchoalveolar lavage fluid and sampling peripheral blood². These methods are fraught with problems of upper airway contamination and diagnostic delays, by which time the disease may have progressed or been treated empirically with inappropriate drugs. Moreover, blood markers are unlikely to provide useful information about events deep in pulmonary tissue, especially in patients with multi-system disease, such as immunosuppressed patients affected by IPA. These limitations of current diagnostic tools have prompted the development of imaging probes that can provide *in situ* and real-time information on the progression of infection^{3–6}. Fluorescent probes based on antibiotics and antimicrobial peptides are chemical entities with enormous potential for imaging infection sites due to their high selectivity for microbial cell structures over mammalian cells^{7–11}. van Oosten *et al.*¹² recently reported a near-infrared fluorescently labelled vancomycin for real-time *in vivo* imaging of bacterial infections in a mouse mycosis model. Similarly, Thiberville and co-workers have described fluorescein-conjugated peptides to visualize fungal biofilms in immunosuppressed rats using fibre-based microendoscopy¹³. These probes have been prepared by conjugating peptides of interest to suitable fluorophores via chemical spacers. While such approaches have been useful to functionalise long peptides or proteins¹⁴, alternative strategies are needed for shorter peptides, where relevant modifications can compromise their specificity. Our group and others have studied the mechanism of action of Peptide AntiFungal 26 (PAF26), a synthetic antimicrobial hexapeptide with high affinity for fungal cells and selectivity over bacterial and mammalian cells^{15,16}. We envisaged that fluorescent analogues of PAF26 would enable imaging of fungal infection sites provided that the main recognition features of PAF26 remained unaffected after labelling. However, the incorporation of fluorophores in short antimicrobial peptides is challenging as chemical modifications are likely to alter the distribution of positive charges as well as their amphipathic character. PAF26 has a highly conserved sequence with a C-terminal hydrophobic domain (Trp-Phe-Trp) and an N-terminal cationic domain (Arg-Lys-Lys) that are essential to exert its antifungal action. Site-specific peptide labelling can be achieved by incorporation of amino acids with bio-orthogonal^{17–20} or fluorogenic groups^{21–23}. Fluorogenic amino acids are advantageous in that they provide high signal-to-noise ratios without the need for washing or additional labelling steps. A number of fluorogenic amino acids have been reported^{24–26}, but most exhibit inherent limitations as fluorophores (for example, short emission wavelengths, low extinction coefficients and compromised cell permeability). We have developed a spacer-free fluorogenic amino acid based on the 4,4-difluoro-4-bora-3a,4a-diaza-s-indacene (BODIPY) scaffold, and incorporated it in the hydrophobic domain of PAF26 to maintain the recognition features of the peptide while providing an excellent reporter of the interaction with fungal cells. This innovative approach has rendered fluorogenic BODIPY-labelled antimicrobial peptides as highly stable probes to image *A. fumigatus* directly in *ex vivo* human tissue.

Results

Design and synthesis of a Trp-BODIPY fluorogenic amino acid. BODIPY is a fluorescent structure with excellent cell permeability and photophysical properties^{27,28}. Moreover, the

BODIPY scaffold can be derivatized with radioisotopes to prepare multimodal agents for both optical imaging and positron emission tomography^{29,30}, enabling quantitative whole-body imaging with high sensitivity^{31,32}. Multimodal agents, which are designed to be compatible with complementary imaging modalities, are excellent tools to achieve good spatial resolution and specificity without compromising high sensitivity³³. Despite the numerous BODIPY derivatives described to date^{34–38}, there are no reports of BODIPY-based fluorogenic amino acids. Environmentally sensitive fluorogens can be prepared by direct conjugation of the BODIPY core to electron-rich groups leading to photo-induced electron transfer quenching^{39–41}. We envisaged that the direct coupling of the indole group of Trp to the BODIPY core would render a fluorogenic amino acid with potential to replace Trp in the preparation of fluorogenic antimicrobial peptides. Our group has recently described some Pd-catalysed C–H activation^{42–44} as an efficient way to arylate the indole C₂ position⁴⁵ of Trp and prepare Trp-derivatized peptides and peptidomimetics^{46–48}. In this way, we synthesized two BODIPY iodide derivatives (1 and 2, Fig. 1a) in good yields using our recently developed procedures and assessed their reactivity in Pd-catalysed C₂-arylation of Fmoc-Trp-OH. Notably, only the conjugate 3 was obtained from the *m*-iodophenyl-BODIPY (2)⁴⁹, while the corresponding *p*-iodophenyl 1 was unreactive, reflecting electronic preferences (Fig. 1a and Supplementary Discussion). We further optimized the gram-scale synthesis of 3 using microwave-assisted irradiation to readily isolate the fluorogenic amino acid as a solid stable compound with 74% yield, suitably protected to be directly used in solid-phase peptide synthesis (SPPS).

Synthesis and evaluation of fluorogenic antifungal peptides.

The amino acid 3 displayed characteristic absorption and emission wavelengths of BODIPY probes as well as very high extinction coefficients (Fig. 1a, Supplementary Figs 1,2). Next we evaluated the properties of 3 as a fluorogenic probe and its potential to report interactions of antimicrobial peptides with fungal cells. Many antimicrobial peptides, including PAF26, recognize molecular components of the microbial cell membrane and accumulate in lipophilic intracellular compartments. Therefore, we examined the fluorescence spectra of 3 in phospholipid bilayer membranes that mimic such microenvironments. As shown in Fig. 1b, the BODIPY core embedded in 3 displayed remarkable fluorogenic behaviour with strong fluorescence emission upon binding to phospholipid membranes. In view of the properties of 3 as a fluorogenic surrogate of Trp, we prepared fluorogenic derivatives of PAF26 by SPPS. Since the sequence of PAF26 (4, Fig. 2a) contains two Trp residues, we synthesized all three possible combinations (5–7, Fig. 2a) to assess the impact of the amino acid 3 at different positions of the antimicrobial peptide. The amino acid 3 proved to be fully compatible with SPPS as it tolerates standard Fmoc deprotection and coupling conditions as well as mildly acidic (that is, 1% trifluoroacetic acid) cleavage cocktails for acid-labile solid supports (for example, Sieber amide and chlorotriyl-based polystyrene resins) without observing any degradation (Supplementary Methods and Supplementary Fig. 20). Being mildly acidic conditions harmless to the BODIPY core⁵⁰, peptides 5–7 were prepared using conventional SPPS protocols in a Sieber amide polystyrene resin. Molecular simulation models of both labelled and non-labelled peptides corroborated that the introduction of BODIPY scaffolds in the hydrophobic domain of PAF26 did not disrupt the conformation and hydrogen bonding pattern of the original peptide (Supplementary Fig. 3). Next we determined the activity of the peptides 4–7 in *A. fumigatus* as well as in

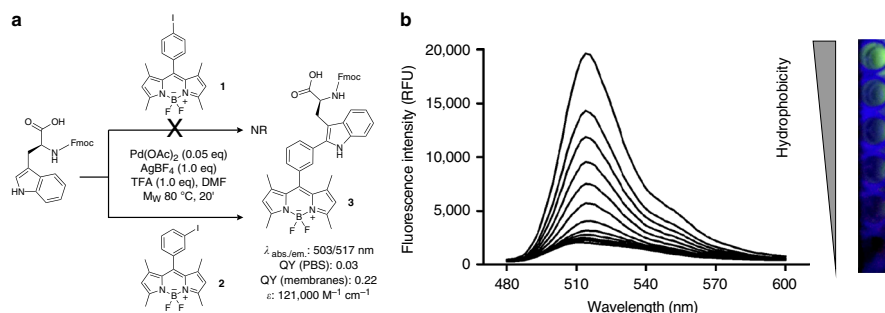


Figure 1 | A Trp-BODIPY fluorogenic amino acid. (a) Synthetic scheme and spectral properties of the Trp-BODIPY fluorogenic amino acid **3** (NR: no reaction). (b) The amino acid **3** displays strong fluorogenic behaviour in phospholipid membranes. Spectra of compound **3** (10 μ M) were recorded after incubation with PC:cholesterol (7:1) liposome suspensions in PBS ranging from 3.75 to 0.004 mg ml⁻¹ of PC in two-fold serial dilutions, λ_{exc} : 450 nm. PBS alone was used as a negative control for a non-hydrophobic environment. On the right-hand side, pictures of the fluorescence emission of **3** under excitation with a 365 nm UV-lamp in PC:cholesterol liposome suspensions with increasing PC content (from top to bottom: 3.75, 1.88, 0.94, 0.47, 0.23 and 0 (only PBS) mg ml⁻¹ of PC).

bacterial strains and human RBCs as an indication of their affinity for both microbial and human cells. We included *Klebsiella pneumoniae*, *Escherichia coli* and *Pseudomonas aeruginosa* as clinically relevant bacterial strains commonly found in hospitalized pulmonary infections⁵¹. Likewise, we tested the activity of **4–7** in human RBCs, because positively charged peptides are potential haemolytic agents⁵². Remarkably, the incorporation of **3** in the hydrophobic domain of PAF26 rendered peptides (**5–7**) with slightly higher affinity for *A. fumigatus* than the non-labelled PAF26 peptide (**4**) (Fig. 2b and Supplementary Fig. 4). The marginal activity of PAF26 in bacterial and human cells was also maintained in all fluorogenic analogues (Fig. 2b, Supplementary Figs 5,6). Altogether, these results validate the direct C-C conjugation of BODIPY fluorogens to the C₂ position of the indole ring of Trp as a novel labelling approach with minimal interference in the molecular recognition properties of PAF26 while providing a suitable tag to report the interaction with *A. fumigatus*.

Imaging *Aspergillus fumigatus* in co-culture with human cells. Peptides **5–7** exhibited similar spectral properties to **3** with an equally strong fluorogenic behaviour in phospholipid membranes (Fig. 2c and Supplementary Fig. 7). Double-labelled peptide **7** displayed a weaker fluorescence response than mono-labelled peptides (**5, 6**), partially due to the self-quenching derived from two neighbouring BODIPY fluorophores. In view of the excellent properties of **5–7** as fungi-targeting fluorogenic peptides, we evaluated them as live cell imaging agents of *A. fumigatus*. Peptides **5** and **6** brightly stained fungal cells, whereas **7** showed significantly weaker fluorescence, in accordance with its lower fluorogenicity (Fig. 2c). As negative controls, we assessed the activity and imaging properties of fluorogenic derivatives of PAF26 replacing some of the key residues for their interaction with fungal cells⁵³. Peptide **5a**, which lacks the hydrophilic domain of PAF26, showed poor activity and staining in *A. fumigatus* (Supplementary Fig. 8). Similar results were obtained when we examined the activity and staining properties of the single BODIPY amino acid **3** (Supplementary Fig. 8). We also synthesized peptide **5b**, including less non-polar residues in the hydrophobic domain, which exhibited reduced activity and brightness in *A. fumigatus* (Supplementary Fig. 8). These observations confirmed the importance of embedding

the amino acid **3** within the full amphipathic sequence of PAF26 in order to efficiently interact with the cell membrane of *A. fumigatus*.

We further used peptide **5** to image live *A. fumigatus* in co-cultures with human lung epithelial cells. As shown in Fig. 2d, the fluorogenic properties of **5** enabled direct live fungal cell imaging without the need of any washing steps. Furthermore, we counterstained lung epithelial cells with the red fluorescent dye Syto82 and performed plot profile analysis to confirm that **5** specifically labelled *A. fumigatus* without staining human lung epithelial cells (Fig. 2d).

Probe optimization for direct *ex vivo* tissue imaging. Direct tissue imaging of infection sites is often hampered by the high concentration of proteolytic enzymes⁵⁴, which can compromise the integrity of imaging agents. Hence, we decided to examine the chemical stability of peptide **5** in human bronchoalveolar lavages from patients with acute respiratory distress syndrome to assess the potential for *ex vivo* human tissue imaging. The linear peptide **5** was rapidly degraded in human lavages with a half-life shorter than 60 min (Fig. 3a, Supplementary Figs 9,10). To enhance the stability required for direct *ex vivo* imaging in human pulmonary tissue, we synthesized **8** as the corresponding BODIPY-labelled cyclic analogue (Fig. 3b). Cyclic peptides do not contain free N- and C-terminal groups, leading to increased resistance to degradation by proteases^{55,56}. We synthesized compound **8** using 2-chlorotriptyl polystyrene resin, which enabled the preparation and subsequent cleavage of the protected linear peptide under mild acidic conditions (Supplementary Fig. 11). Head-to-tail cyclization was performed in solution with 87% yield using HATU as the coupling reagent. We optimized the reaction conditions to remove all the protecting groups without affecting the BODIPY scaffold. Reduction of the protected peptide in H₂ atmosphere with Pd(OH)₂/C using mild acidic conditions led to the desired product with yields around 60% and purities over 90%. The peptide **8** showed around two-fold enhanced affinity for fungal cells compared with peptide **5**, and maintained very high selectivity over bacteria and human cells (Fig. 2b). A similar activity profile was observed for peptide **9**, the non-labelled analogue of peptide **8** (Supplementary Fig. 8). Peptide **9** showed slightly enhanced affinity for *A. fumigatus* when compared with

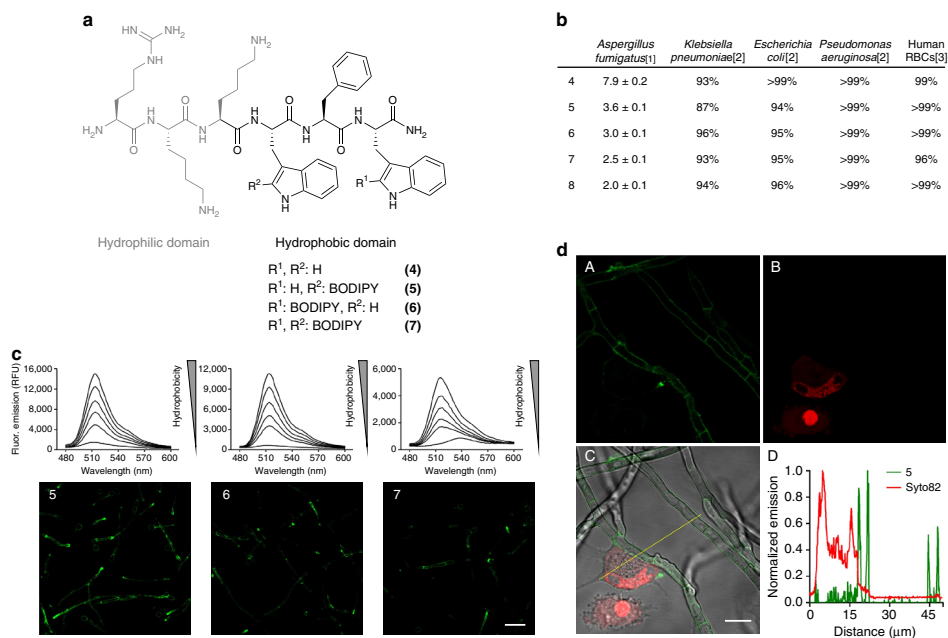


Figure 2 | Fluorogenic peptides for live cell imaging of *A. fumigatus* in co-culture with human lung epithelial cells. (a) Chemical structures of non-labelled and fluorogenic linear peptides (4–7), highlighting the two conserved hydrophilic (grey) and hydrophobic (black) domains of Peptide Antifungal 26 (PAF26). (b) Activity of antimicrobial peptides in *A. fumigatus*, several bacterial strains and in human RBCs.[1] IC₅₀ (μM) values represented as means ± s.e.m. from n = 3, [2] cell viability upon 16 h incubation with 4–8 at their respective IC₅₀ concentrations (n = 3), [3] cell viability upon 1 h incubation with 4–8 at their respective IC₅₀ concentrations (n = 3). (c) Fluorogenic behaviour of 5–7 (10 μM) in phosphatidylcholine (PC):cholesterol (7:1) liposome suspensions in PBS ranging from 3.75 to 0.004 mg ml⁻¹ of PC in two-fold serial dilutions (λ_{exc}: 450 nm), and wash-free live cell images of *A. fumigatus* at 37 °C using fluorescence confocal microscopy after incubation with peptides 5–7 (5 μM). Scale bar, 20 μm. (d) Peptide 5 (5 μM, green) and Syto82 (2.5 μM, red counterstain for lung epithelial cells) were incubated in co-cultures of *A. fumigatus* and human lung A549 epithelial cells and imaged under a fluorescence confocal microscope at 37 °C without any washing steps. Fluorescence staining of 5 (A), Syto82 (B), merged (C) and plot profile analysis (D) of peptide 5 (green) and Syto82 (red) from image C. Scale bar, 10 μm.

the linear PAF26 sequence (4), and maintained high selectivity over bacteria and human RBCs (Supplementary Fig. 8). These observations are in line with the fact that peptide cyclization can restrict conformational flexibility, which often leads to enhanced affinity and activity⁵⁷. Preliminary NMR analysis of 8 showed no evidence of relevant structural modifications with respect to the non-labelled peptide 9, in agreement with molecular simulations (Supplementary Fig. 3). Importantly, the peptide 8 remained intact after 24 h in human bronchoalveolar lavages from patients with acute respiratory distress syndrome (Fig. 3a, Supplementary Figs 9,10). The peptide 8 also displayed stronger fluorogenic response than the linear peptides (5,6) and remarkable fluorescence emission in phospholipid membranes with quantum yields reaching 30% (Supplementary Figs 12,13). In addition to *A. fumigatus*, we examined the ability of peptide 8 to stain different fungal strains (Supplementary Fig. 14). While we observed slight differences in fluorescence intensity between strains, peptide 8 stained most fungal cells, indicating its potential as a probe for imaging fungal infection sites of variable origin. We also employed 8 to image *A. fumigatus* that had been pre-treated or not with an excess of non-labelled PAF26 (4) (Supplementary

Fig. 15 and Supplementary Movies 1,2). Cells that were pre-treated with compound 4 showed significantly lower staining when exposed to the same concentration of peptide 8, confirming the specificity of our fluorogenic cyclic structure. We also confirmed that the peptide 8 brightly stained *A. fumigatus* in co-cultures with human lung epithelial cells (Supplementary Fig. 16). All these observations assert the cyclic peptide 8 as a fluorogenic probe with high stability in lavage samples from patients with multi-system respiratory disease and potential for direct *ex vivo* imaging of *A. fumigatus* in human pulmonary tissue.

Ex vivo imaging of *Aspergillus fumigatus* in human tissue. Next we employed the peptide 8 for high-resolution imaging of *A. fumigatus*. Time-lapse imaging showed the fluorogenic response of 8 upon interaction with the fungal cell membrane and after being internalized and accumulated in lipid-rich intracellular compartments (Fig. 3d and Supplementary Movie 3). The kinetic analysis shows that the peptide 8 labelled fungal cells very rapidly, within few minutes after addition of the probe and

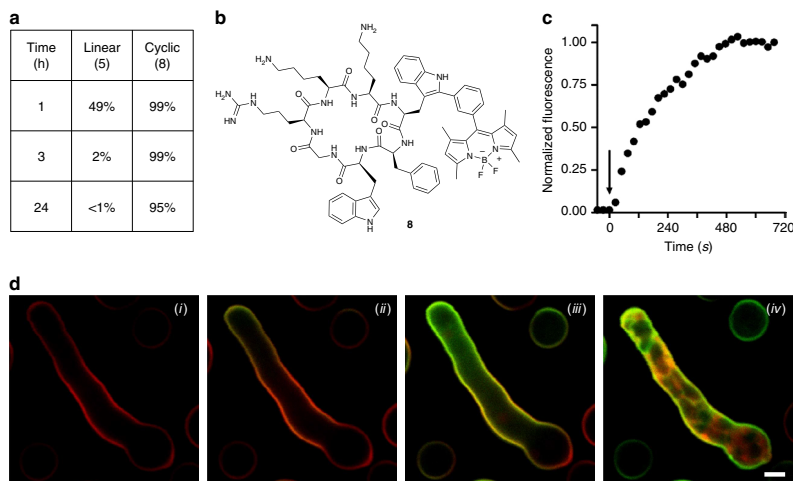


Figure 3 | The cyclic peptide **8 is a highly stable fluorogenic agent for high-resolution imaging of *A. fumigatus*.** (a) Comparative chemical stability of mono-labelled BODIPY linear (**5**) and cyclic (**8**) PAF26 analogues in human bronchoalveolar lavage samples from patients with acute respiratory distress syndrome. (b) Chemical structure of the cyclic BODIPY-labelled peptide **8**. (c) Kinetic analysis (from time-lapse imaging in d) of the fluorescence signal of compound **8** (2 μ M) in the cell membrane of *A. fumigatus* (arrow points at the addition time for compound **8**). (d) Time-lapse high-resolution imaging of *A. fumigatus* upon incubation with a cell membrane counterstain (red) and compound **8** (2 μ M, green) for 0 min (i), 1 min (ii), 3 min (iii) and 10 min (iv) (see Supplementary Movie 3). Scale bar, 2.5 μ m.

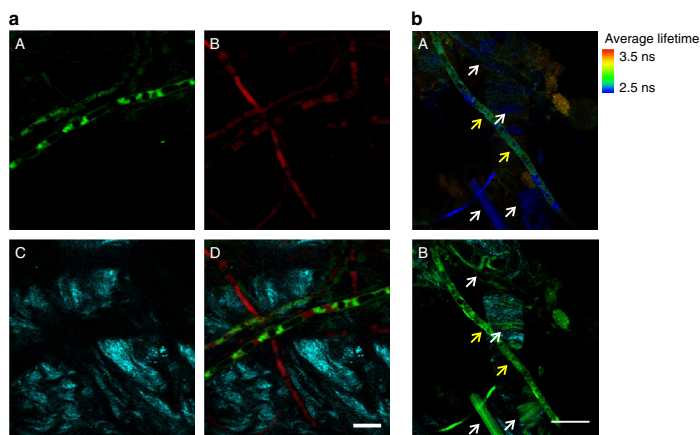


Figure 4 | Multi-photon fluorescence microscopy of ex vivo human pulmonary tissue after incubation with RFP-expressing *A. fumigatus*. (a) Multi-photon microscope images from peptide **8** (5 μ M) (A), RFP-expressing *A. fumigatus* (B), second harmonic generation from collagen fibres (C) and merged (D) in ex vivo human lung tissue. Scale bar, 10 μ m. (b) (A) Fluorescence lifetime image of **8**-stained *A. fumigatus* in ex vivo human lung tissue. White arrows point autofluorescent tissue structures and yellow arrows point **8**-stained fungal cells. (B) Corresponding fluorescence image of **8**-stained *A. fumigatus* (green) and collagen fibres (second harmonic generation, cyan) for the fluorescence lifetime image in A. Scale bar, 20 μ m.

without requiring any washing steps (Fig. 3c). Moreover, the peptide **8** showed no cytotoxicity in lung epithelial cells, even at high concentrations (Supplementary Fig. 17). In view of these properties, we employed the peptide **8** for direct imaging of

A. fumigatus in human pulmonary tissue using multi-photon microscopy. In order to confirm the specific staining of **8**, we employed a transgenic strain of *A. fumigatus* expressing red fluorescent protein (RFP) in the cytoplasm. As shown in Fig. 4a,

the peptide **8** (green) clearly stained RFP-expressing *A. fumigatus* (red), which confirmed the selectivity of our probe. Multi-photon excitation enabled the acquisition of second harmonic generation (cyan) from the collagen structures of the fibrillar network of human pulmonary tissue. Furthermore, the examination of these samples by fluorescence lifetime imaging revealed that autofluorescent human tissue structures (for example, collagen and elastin)⁵⁸, which could potentially overlap with the emission of BODIPY fluorogens, are readily distinguished from **8**-stained *A. fumigatus* by their fluorescence lifetimes (Fig. 4b). Altogether, these results validate our fluorogenic BODIPY-labelled cyclic peptide **8** as a highly stable imaging agent for direct and straightforward visualization of *A. fumigatus* in human tissue.

Discussion

Peptides are excellent scaffolds for the development of imaging agents due to the highly specific molecular interactions with their respective targets. Since most peptides do not contain chemical groups that enable their direct visualization, they often need to be modified with reporters (for example, fluorophores) or reactive groups (for example, aldehydes, azides, alkynes and tetrazines) for further derivatization⁵⁹. Unnatural amino acids containing bio-orthogonal tags can be incorporated at specific sites of peptide sequences by SPPS⁶⁰. Likewise, the incorporation of genetically encoded unnatural amino acids in response to nonsense or frameshift codons has opened the possibility to synthesize protein and peptide structures with reactive groups for subsequent modification⁶¹. Bio-orthogonal approaches typically involve two-step labelling processes including a conjugation reaction (for example, 'click' chemistry) followed by the removal of excess labelling agent. Recent advances in bio-orthogonal chemistry have led to fluorogenic labelling agents that emit a signal only after conjugation, thus reducing background fluorescence and washing steps^{62,63}. Alternatively, and most commonly, peptides are derivatized by incorporation of fluorophores into their sequence so they can be directly used for imaging. Since fluorophores are typically bulkier structures, it is imperative that they are introduced at specific positions of the sequence without impairing the molecular recognition properties of the peptide. Many conjugation methods to attach fluorophores to peptides involve a chemical spacer and rely on the reactivity of polar groups (that is, amines, carboxylic acids, thiols, alcohols); however, these modifications often disrupt the hydrogen bonding pattern of the original peptide, having a detrimental effect on its biological properties.

In the present work, we have engineered a methodology to prepare fluorogenic peptides that relies on a unique Trp-BODIPY derivative (**3**, Fig. 1), which mimics the molecular interactions of the native Trp. The incorporation of a BODIPY group into the C₂ position of Trp via a spacer-free C-C linkage does not affect the conformation and molecular interactions of the native amino acid, and introduces a fluorogenic tag that emits only in hydrophobic environments (Fig. 1). To assess the compatibility of our approach with SPPS and validate its utility to prepare peptide-based agents for imaging of fungal infection, we derivatized the antimicrobial hexapeptide PAF26, which shows high affinity for the membrane of fungal cells. PAF26 is an amphipathic peptide with highly conserved C-terminal hydrophobic and N-terminal cationic domains that are essential to exert its antifungal action¹⁶. Therefore, the derivatization of PAF26 is not straightforward since conventional labelling might alter the distribution of positive charges or its amphipathic character, resulting in a loss of activity and selectivity.

Analogues of PAF26 incorporating the fluorogenic amino acid **3** at specific sites in their sequence were prepared by SPPS and showed no impairment of the affinity and selectivity of the

original peptide for fungal cells (Fig. 2). Our fluorogenic peptides were used for real-time imaging of several fungal pathogens, namely *Fusarium oxysporum*, *Candida albicans*, *Cryptococcus neoformans* and *A. fumigatus*, suggesting a potential common target for different fungal strains (Supplementary Fig. 14). Given that *A. fumigatus* is the fungal pathogen responsible for IPA, a highly fatal disease in immunocompromised patients, we focused our imaging studies in this fungal strain.

Notably, the minimal fluorescence background in aqueous media and strong fluorogenic behaviour of our probes enabled their use for direct and wash-free imaging of *A. fumigatus* (Fig. 2). Competition experiments with the corresponding non-labelled analogues and comparative studies with non-antifungal negative controls—lacking key residues for the interaction at fungal cells—confirmed the specificity of our PAF26-derived fluorogenic peptides (Supplementary Figs 8,15).

A major advantage of our methodology is its wide applicability to bioconjugation and peptide chemistry. The fluorogenic amino acid **3** and its peptide derivatives are compatible with most Fmoc-based SPPS protocols as they tolerate standard deprotection and coupling conditions as well as mildly acidic (that is, 1% trifluoroacetic acid) cleavage cocktails without observing any degradation. Whereas the precise impact of the amino acid **3** in the molecular recognition properties of labelled sequences needs to be examined on a case-by-case basis, we observed similar activities for labelled and non-labelled peptides in a relatively broad range of short antimicrobial sequences, which confirms the ability of the Trp-BODIPY amino acid **3** to behave as a Trp surrogate (Fig. 2 and Supplementary Fig. 8).

With these peptides being promising imaging agents for *in situ* detection of fungal pathogens in clinically relevant samples, we optimized their chemical stability to image *A. fumigatus* in *ex vivo* human pulmonary tissue. Our optimization studies yielded peptide **8** as a highly fluorogenic cyclic structure with bright fluorescence emission in fungal cells and excellent chemical integrity in samples with high proteolytic activity (Fig. 3 and Supplementary Figs 9,16). The excellent properties of **8** enabled its use in multi-photon and lifetime imaging for the direct visualization of *A. fumigatus* in *ex vivo* human tissue and its discrimination from autofluorescent tissue structures (Fig. 4).

Given that the fluorogenic amino acid **3** can be readily incorporated and has general applicability to both linear and cyclic peptides, we envisage that the introduction of our spacer-free BODIPY fluorogen in relevant peptides will become a transformative methodology to develop peptide-based imaging probes with high sensitivity and specificity. Furthermore, the extension of our methodology to other aromatic amino acids will create numerous opportunities for minimally invasive peptide tagging using synthetically available building blocks.

Methods

Chemical synthesis and characterization. Synthetic procedures and chemical characterization (NMR and high-performance liquid chromatography analysis) for all the probes are included in the Supplementary Information (Supplementary Figs 18–25).

In vitro spectral measurements. Spectroscopic and quantum yield data were recorded on a Synergy HT spectrophotometer (Biotek). Compounds were dissolved at the indicated concentrations and spectra were recorded at room temperature. Spectra are represented as means from at least two independent experiments with $n = 3$. Quantum yields were calculated by measuring the integrated emission area of the fluorescence spectra and comparing it to the area measured for fluorescein in basic ethanol as reference (QY: 0.97). Phosphatidylcoline (PC)-based liposome suspensions were purchased from Clodronateliposomes (Netherlands) and were prepared as previously reported⁶⁴.

IC₅₀ determination in *Aspergillus fumigatus*. The *A. fumigatus* (strain CEA10, source: FGSC A1163) was grown on Vogel's medium at 37 °C for 5 days before

the spores (conidia) were harvested. Peptides 4–8 were incubated at different concentrations with *A. fumigatus* conidia to reach a final volume of 100 μ l per well. The final conidia concentration was 5×10^5 cells ml^{-1} in 10% Vogel's medium. After 24 h incubation at 37 °C in 96 well-plates, fungal growth was determined by measuring OD_{610nm} in a spectrophotometer. IC₅₀ values were determined using four parameter logistic regression. Data is represented as means \pm s.e.m from at least three independent experiments with $n = 3$.

Cell culture of fungal strains. *Neurospora crassa* (strain 74-OR23-1VA, source: FGSC 2489) was grown on standard Vogel's agar (Vogel, 1956) at 25 °C under constant artificial light for 5 days. Conidia were collected using sterile dH₂O and then diluted in 20% Vogel's liquid medium for imaging. *F. oxysporum* (strain 4287, source: FGSC 9935) was grown in liquid potato dextrose broth (PDB) at 28 °C with shaking. Conidia were re-suspended in 20% Vogel's liquid medium and imaged after incubation for 12 h at 30 °C. *Can. albicans* (strain SC5314, source: ATCC MYA-2876) was grown on yeast peptone dextrose liquid medium at 30 °C for 12 h with shaking and then diluted using minimal medium (0.7% yeast nitrogen base plus 2% glucose) before imaging. *Cry. neoformans* (strain H99, source: FGSC 9487) was grown on yeast peptone dextrose agar at 30 °C for 3 days. To collect the cells for imaging, a single colony 1–2 mm in diameter was re-suspended in PBS and washed once with fresh PBS before imaging.

In vitro measurements of antimicrobial activity. *P. aeruginosa* (ATCC 47085), *K. pneumoniae* (ATCC BAA1706) and *E. coli* (ATCC 25922) were grown on Lysogeny Broth (LB) agar plates and stored at 4 °C. For assays, a single colony of bacteria was taken into 10 mL liquid broth and incubated at 37 °C for 16 h. Cultures were centrifuged at 4,000 r.p.m. for 5 min and the pellet was re-suspended in 1 mL of fresh PBS and washed three times. Cultures were reconstituted to 1.0 OD_{595nm}, then diluted 1:1,000 and incubated with compounds 4–8 at the indicated concentrations (that is, concentrations matching the IC₅₀ values in *A. fumigatus* for all compounds, except for compounds 3 and 5a where a top concentration of 20 μ M was used). Cell viability was monitored over 16 h by measuring OD_{600nm} in a spectrophotometer. Data is represented as % of cell viability as means from at least two independent experiments with $n = 3$.

Determination of haemolytic activity. Erythrocytes were isolated from freshly drawn, anticoagulated human blood and diluted in PBS (1:5). An amount of 50 μ l of erythrocyte suspension was added to 50 μ l of compounds 4–8 at the indicated concentrations (that is, concentrations matching the IC₅₀ values in *A. fumigatus* for all compounds, except for compounds 3 and 5a where a top concentration of 20 μ M was used). 0.2% Triton X-100 was used as positive control and PBS as negative control. The plate was incubated at 37 °C for 1 h, each well was diluted with 150 μ l of PBS and the plate was centrifuged at 1,200g for 15 min. A total of 100 μ l of the supernatant from each well was transferred to a fresh plate, and the absorbance at 550 nm was measured in a microplate reader. Data is represented as % of cell viability as means from three independent experiments with $n = 3$.

Confocal microscopy of *Aspergillus fumigatus* and human cells. Human lung A549 epithelial cells (ATCC CCL-185) were grown using DMEM supplemented with 10% fetal bovine serum (FBS), antibiotics (100 U ml^{-1} penicillin and 100 mg ml^{-1} streptomycin) and 2 mM L-glutamine in a humidified atmosphere at 37 °C with 5% CO₂. A549 cells were regularly passaged in T-75 cell culture flasks. *A. fumigatus* was grown on standard Vogel's agar at 37 °C for 5 days. Conidia were collected using 0.05% Tween 80, re-suspended in 20% Vogel's liquid medium and incubated for 12 h at 25 °C. For co-cultures, human lung epithelial cells were plated on glass chamber slides Lab-Tek II (Nunc) 2 days before imaging and incubated for 16 h with *A. fumigatus* conidia reaching 75–90% confluence on the day of the experiment. For imaging experiments, cells were incubated for 15 min at 37 °C with compounds 5–8 (5 μ M for compounds 5–7 and 2 μ M for compound 8) and imaged without washing in phenol red-free DMEM under a Zeiss LSM 510 META fluorescence confocal microscope equipped with a live cell imaging stage. Fluorescence and bright-field images were acquired using $\times 40$ or $\times 63$ oil objectives. Fluorescent probes were excited with 488 nm (compounds 5–8) or 543 nm (Syto82) lasers. Confocal microscopy images were analysed and processed with ImageJ. Quantitative analysis of mean fluorescence intensities in competition experiments was performed with Imaaris by calculating the mean intensity of each hyphae as independent regions of interests. For competition assays, all images were acquired and analysed using exactly the same conditions.

Chemical stability in human bronchoalveolar lavages. Peptides 5 and 8 (20 μ M) were dissolved in human bronchoalveolar lavage samples (total volume: 100 μ l) and incubated at 37 °C for the indicated times. Samples were injected into an high-performance liquid chromatography Agilent 1100 separations module connected to a UV detector with a Discovery C₁₈ column (5 μ m, 4.6 \times 50 mm). Matrix-assisted laser desorption/ionization data was recorded on a Bruker Ultraflex mass spectrometer using sinapinic acid as the matrix.

Multi-photon imaging in ex vivo human tissue. *Ex vivo* human lung tissue experiments were approved by the NHS Lothian Tissue Governance Committee and Regional Ethics Committee (REC reference: ref. 13/ES/0126). Human lung tissue was obtained from the periphery (non-cancerous) region of patients undergoing resection for lung cancer. A 1 cm² tissue was inflated with optimum cutting temperature formulation and stored at -80 °C. Embedded tissue was cryosectioned at 10 μ m intervals and fixed onto glass slides for imaging. RFP-expressing *A. fumigatus* conidia were grown overnight at 37 °C the day before the experiments and incubated with human lung tissue sections for 2–3 h before imaging. For multi-photon imaging experiments, the cyclic peptide 8 was used at a concentration of 5 μ M. A custom-built multi-photon microscope was used to acquire second harmonic generation (SHG) and two-photon fluorescence images. Briefly, a picoEmerald (APE) laser provided both a tunable pump laser (720–990 nm, 7 ps, 80 MHz repetition rate) and a spatially overlapped Stokes laser (1064 nm, 5–6 ps and 80 MHz repetition rate). GFP two-photon fluorescence signals were filtered using the following series of filters: FF520-Di02, FF483/639-Di01 and ET500/40m. RFP two-photon fluorescence signals were filtered using FF520-Di02, FF757-Di01 and FF01-609/181, and SHG signals were filtered using FF520-Di02, FF483/639-Di01 and FF01-466/40. Fluorescence lifetime images were acquired by connecting the relevant detector to a PicoHarp 300 (Picoquant, Berlin) and configuring the PMT for photon counting mode for TCSPC-FLIM. SHG and GFP images were taken with the laser tuned to 950 nm and RFP images were recorded using a 1,064 nm laser. Lifetime images were recorded at 20 mW with a 10 μ s pixel dwell using the SymPhoTime software (Picoquant). All images were analysed and processed using ImageJ.

References

- Chai, L. Y. & Hsu, L. Y. Recent advances in invasive pulmonary aspergillosis. *Curr. Opin. Pulm. Med.* **17**, 160–166 (2011).
- Azoulay, E. & Afeesa, B. Diagnostic criteria for invasive pulmonary aspergillosis in critically ill patients. *Am. J. Respir. Crit. Care Med.* **186**, 8–10 (2012).
- Zhao, M. *et al.* Spatial-temporal imaging of bacterial infection and antibiotic response in intact animals. *Proc. Natl Acad. Sci. USA* **98**, 9814–9818 (2001).
- Leevy, W. M. *et al.* Optical imaging of bacterial infection in living mice using a fluorescent near-infrared molecular probe. *J. Am. Chem. Soc.* **128**, 16476–16477 (2006).
- Leevy, W. M. *et al.* Noninvasive optical imaging of staphylococcus aureus bacterial infection in living mice using a Bis-dipicolylamine-Zinc(II) affinity group conjugated to a near-infrared fluorophore. *Bioconjug. Chem.* **19**, 686–692 (2008).
- Xie, X. *et al.* Rapid point-of-care detection of the tuberculosis pathogen using a BlaC-specific fluorogenic probe. *Nat. Chem.* **4**, 802–809 (2012).
- Panizzi, P. *et al.* In vivo detection of *Staphylococcus aureus* endocarditis by targeting pathogen-specific prothrombin activation. *Nat. Med.* **17**, 1142–1146 (2011).
- Shi, H. *et al.* Engineering the stereochemistry of cephalosporin for specific detection of pathogenic carbenapenem-expressing bacteria. *Angew. Chem. Int. Ed. Engl.* **53**, 8113–8116 (2014).
- Cheng, Y. *et al.* Fluorogenic probes with substitutions at the 2 and 7 positions of cephalosporin are highly BlaC-specific for rapid *Mycobacterium tuberculosis* detection. *Angew. Chem. Int. Ed. Engl.* **53**, 9360–9364 (2014).
- Welling, M. M. *et al.* Development of a hybrid tracer for SPECT and optical imaging of bacterial infections. *Bioconjug. Chem.* **26**, 839–849 (2015).
- Akram, A. R. *et al.* A labelled-ubiquitin antimicrobial peptide for immediate in situ optical detection of live bacteria in human alveolar lung tissue. *Chem. Sci.* **6**, 6971–6979 (2015).
- van Oosten, M. *et al.* Real-time in vivo imaging of invasive- and biomaterial-associated bacterial infections using fluorescently labelled vancomycin. *Nat. Commun.* **4**, 2584 (2013).
- Morisse, H. *et al.* In vivo molecular microimaging of pulmonary aspergillosis. *Med. Mycol.* **51**, 352–360 (2013).
- Zhou, Q. *et al.* Bioconjugation by native chemical tagging of C-H bonds. *J. Am. Chem. Soc.* **135**, 12994–12997 (2013).
- Lopez-Garcia, B., Perez-Paya, E. & Marcos, J. F. Identification of novel hexapeptides bioactive against phytopathogenic fungi through screening of a synthetic peptide combinatorial library. *Appl. Environ. Microbiol.* **68**, 2453–2460 (2002).
- Muñoz, A. *et al.* Two functional motifs define the interaction, internalization and toxicity of the cell-penetrating antifungal peptide PAF26 on fungal cells. *PLoS ONE* **8**, e54813 (2013).
- Beatty, K. E., Xie, F., Wang, Q. & Tirrell, D. A. Selective dye-labelling of newly synthesized proteins in bacterial cells. *J. Am. Chem. Soc.* **127**, 14150–14151 (2005).
- Carriço, I. S., Carlson, B. L. & Bertozzi, C. R. Introducing genetically encoded aldehydes into proteins. *Nat. Chem. Biol.* **3**, 321–322 (2007).
- Brustad, E. M., Lemke, E. A., Schultz, P. G. & Deniz, A. A. A general and efficient method for the site-specific dual-labelling of proteins for single molecule fluorescence resonance energy transfer. *J. Am. Chem. Soc.* **130**, 17664–17665 (2008).
- Lang, K. *et al.* Genetically encoded norbornene directs site-specific cellular protein labelling via a rapid bioorthogonal reaction. *Nat. Chem.* **4**, 298–304 (2012).

ARTICLE

NATURE COMMUNICATIONS | DOI: 10.1038/ncomms10940

21. Venkatraman, P. *et al.* Fluorogenic probes for monitoring peptide binding to class II MHC proteins in living cells. *Nat. Chem. Biol.* **3**, 222–228 (2007).
22. Lee, H. S., Guo, J., Lemke, E. A., Dimla, R. D. & Schultz, P. G. Genetic incorporation of a small, environmentally sensitive, fluorescent probe into proteins in *Saccharomyces cerevisiae*. *J. Am. Chem. Soc.* **131**, 12921–12923 (2009).
23. Lukinavičius, G. *et al.* A near-infrared fluorophore for live-cell super-resolution microscopy of cellular proteins. *Nat. Chem.* **5**, 132–139 (2013).
24. Vazquez, M. E., Blanco, J. B. & Imperiali, B. Photophysics and biological applications of the environment-sensitive fluorophore 6-N,N-dimethylamino-2,3-naphthalimide. *J. Am. Chem. Soc.* **127**, 1300–1306 (2005).
25. Loving, G. & Imperiali, B. A versatile amino acid analogue of the solvatochromic fluorophore 4-N,N-dimethylamino-1,8-naphthalimide: a powerful tool for the study of dynamic protein interactions. *J. Am. Chem. Soc.* **130**, 13630–13638 (2008).
26. Ge, J., Li, L. & Yao, S. Q. A self-immobilizing and fluorogenic unnatural amino acid that mimics phosphotyrosine. *Chem. Commun.* **47**, 10939–10941 (2011).
27. Loudet, A. & Burgess, K. BODIPY dyes and their derivatives: syntheses and spectroscopic properties. *Chem. Rev.* **107**, 4891–4932 (2007).
28. Boens, N., Leen, V. & Dehaen, W. Fluorescent indicators based on BODIPY. *Chem. Soc. Rev.* **41**, 1130–1172 (2012).
29. Li, Z. *et al.* Rapid aqueous [¹⁸F]-labeling of a BODIPY dye for positron emission tomography/fluorescence dual modality imaging. *Chem. Commun.* **47**, 9324–9327 (2011).
30. Hendricks, J. A. *et al.* Synthesis of [¹⁸F]-BODIPY: bifunctional reporter for hybrid optical/positron emission tomography imaging. *Angew. Chem. Int. Ed. Engl.* **51**, 4603–4606 (2012).
31. Holland, J. P. *et al.* Annotating MYC status with 89Zr-transferrin imaging. *Nat. Med.* **18**, 1586–1591 (2012).
32. Thorek, D. L., Ogirala, A., Beattie, B. J. & Grimm, J. Quantitative imaging of disease signatures through radioactive decay signal conversion. *Nat. Med.* **19**, 1345–1350 (2013).
33. Kircher, M. F. *et al.* A brain tumor molecular imaging strategy using a new triple-modality MRI-photoacoustic-Raman nanoparticle. *Nat. Med.* **18**, 829–834 (2012).
34. Miller, E. W., Zeng, L., Domaille, D. W. & Chang, C. J. Preparation and use of Coppersensor-1, a synthetic fluorophore for live-cell copper imaging. *Nat. Protoc.* **1**, 824–827 (2006).
35. Lee, J. S. *et al.* Synthesis of a BODIPY library and its application to the development of live cell glucagon imaging probe. *J. Am. Chem. Soc.* **131**, 10077–10082 (2009).
36. Zhai, D., Lee, S. C., Vendrell, M., Leong, L. P. & Chang, Y. T. Synthesis of a novel BODIPY library and its application in the discovery of a fructose sensor. *ACS Comb. Sci.* **14**, 81–84 (2012).
37. Vazquez-Romero, A. *et al.* Multicomponent reactions for *de novo* synthesis of BODIPY probes: *in vivo* imaging of phagocytic macrophages. *J. Am. Chem. Soc.* **135**, 16018–16021 (2013).
38. Hong-Hermesdorf, A. *et al.* Subcellular metal imaging identifies dynamic sites of Cu accumulation in *Chlamydomonas*. *Nat. Chem. Biol.* **10**, 1034–1042 (2014).
39. Sunahara, H., Urano, Y., Kojima, H. & Nagano, T. Design and synthesis of a library of BODIPY-based environmental polarity sensors utilizing photoinduced electron-transfer-controlled fluorescence ON/OFF switching. *J. Am. Chem. Soc.* **129**, 5597–5604 (2007).
40. Bura, T., Retailleau, P., Ulrich, G. & Ziesler, R. Highly substituted BODIPY dyes with spectroscopic features sensitive to the environment. *J. Org. Chem.* **76**, 1109–1117 (2011).
41. Er, J. C. *et al.* MegaStokes BODIPY-triazoles as environmentally sensitive turn-on fluorescent dyes. *Chem. Sci.* **4**, 2168–2176 (2013).
42. White, M. C. C-H bond functionalization & synthesis in the 21st century: a brief history and prospectus. *Synlett* **23**, 2746–2748 (2012).
43. Ackermann, L. Carboxylate-assisted transition-metal-catalyzed C-H bond functionalizations: mechanism and scope. *Chem. Rev.* **111**, 1315–1345 (2011).
44. Chen, X., Engle, K. M., Wang, D. H. & Yu, J. Q. Palladium(II)-catalyzed C-H activation/C-C cross-coupling reactions: versatility and practicality. *Angew. Chem. Int. Ed. Engl.* **48**, 5094–5115 (2009).
45. Lebrasseur, N. & Larrosa, I. Room temperature and phosphine free palladium catalyzed direct C-2 arylation of indoles. *J. Am. Chem. Soc.* **130**, 2926–2927 (2008).
46. Ruiz-Rodríguez, J., Albericio, F. & Lavilla, R. Postsynthetic modification of peptides: chemoselective C-arylation of tryptophan residues. *Chem. Eur. J.* **16**, 1124–1127 (2010).
47. Preciado, S., Mendive-Tapia, L., Albericio, F. & Lavilla, R. Synthesis of C-2 arylated tryptophan amino acids and related compounds through palladium-catalyzed C-H activation. *J. Org. Chem.* **78**, 8129–8135 (2013).
48. Mendive-Tapia, L. *et al.* New peptide architectures through C-H activation stapling between tryptophan-phenylalanine/tyrosine residues. *Nat. Commun.* **6**, 7160 (2015).
49. Li, L. *et al.* Influence of the number and substitution position of phenyl groups on the aggregation-enhanced emission of benzene-cored luminogens. *Chem. Commun.* **51**, 4830–4833 (2015).
50. Vendrell, M. *et al.* Solid-phase synthesis of BODIPY dyes and development of an immunoglobulin fluorescent sensor. *Chem. Commun.* **47**, 8424–8426 (2011).
51. Lynch, 3rd J. P. Hospital-acquired pneumonia: risk factors, microbiology, and treatment. *Chest* **119**, 373S–384S (2001).
52. Hamuro, Y., Schneider, J. P. & DeGrado, W. F. *De novo* design of antibacterial β -peptides. *J. Am. Chem. Soc.* **121**, 12200–12201 (1999).
53. Muñoz, A. *et al.* Understanding the mechanism of action of cell-penetrating antifungal peptides using the rationally designed hexapeptide PAF26 as a model. *Fungal Biol. Rev.* **26**, 146–155 (2013).
54. Nishimura, J. *et al.* Potent antimycobacterial activity of mouse secretory leukocyte protease inhibitor. *J. Immunol.* **180**, 4032–4039 (2008).
55. White, C. & Yudin, A. K. Contemporary strategies for peptide macrocyclization. *Nat. Chem.* **3**, 509–524 (2011).
56. Hill, T. A., Shepherd, N. E., Dinness, F. & Fairlie, D. P. Constraining cyclic peptides to mimic protein structure motifs. *Angew. Chem. Int. Ed. Engl.* **53**, 13020–13041 (2014).
57. Glas, A. *et al.* Constrained peptides with target-adapted cross-links as inhibitors of a pathogenic protein-protein interaction. *Angew. Chem. Int. Ed. Engl.* **53**, 2489–2493 (2014).
58. Newton, R. C. *et al.* Imaging parenchymal lung diseases with confocal endomicroscopy. *Respir. Med.* **106**, 127–137 (2012).
59. Schumacher, D. & Hackenberger, C. P. R. More than add-on: chemoselective reactions for the synthesis of functional peptides and proteins. *Curr. Opin. Chem. Biol.* **22**, 62–69 (2014).
60. Zhao, L. *et al.* Synthesis of a cytotoxic amanitin for bioorthogonal conjugation. *ChemBiochem* **16**, 1420–1425 (2015).
61. Liu, W., Brock, A., Chen, S., Chen, S. & Schultz, P. G. Genetic incorporation of unnatural amino acids into proteins in mammalian cells. *Nat. Methods* **4**, 239–244 (2007).
62. Shien, P. *et al.* CalFluors: a universal motif for fluorogenic azide probes across the visible spectrum. *J. Am. Chem. Soc.* **137**, 7145–7151 (2015).
63. Meimets, L. G., Carlson, J. C., Giedt, R. J., Kohler, R. H. & Weissleder, R. Ultrafluorogenic coumarin-tetrazine probes for real-time biological imaging. *Angew. Chem. Int. Ed. Engl.* **53**, 7531–7534 (2014).
64. van Rooijen, N. & van Nieuwenegem, R. Elimination of phagocytic cells in the spleen after intravenous injection of liposome-encapsulated dichloromethylene disphosphonate. *Cell Tissue Res.* **238**, 355–358 (1984).

Acknowledgements

L.M.-T. acknowledges the support of MECED—Spain in the form of a FPU Scholarship. A.S. and M.L. acknowledge the support of CRUK (C157/A15703 (A.S.) and C10195/A18075 (M.L.)). R.L. acknowledges the support of DGICYT-Spain (CTQ2015-67870-P) and Generalitat de Catalunya (2014 SGR 137). M.V. acknowledges the support of the Medical Research Council and the FP7 Marie Curie Integration Grant (333847). We acknowledge Dr Andrew Conway-Morris (University of Cambridge) for providing samples of human bronchoalveolar lavage and Dr Kevin Dhalliwal (University of Edinburgh) for providing samples of *ex vivo* human lung tissue. All experiments employing human samples were conducted with approval from the NHS Lothian Regional Ethics Committee and the NHS Lothian SAHSC Biosource. We dedicate this article to the memory of Prof. Enrique Pérez-Payá for his contribution to the discovery of antimicrobial peptides.

Author contributions

L.M.-T., S.P. and N.K. performed all compound syntheses and chemical characterization; C.Z. and N.D.R. designed the *in vitro* experiments with fungal cells; C.Z., A.R.A. and M.V. performed *in vitro* spectral and biological characterization, imaging experiments and analysed the data; M.L. and A.S. set up multi-photon and lifetime imaging experiments in *ex vivo* human lung tissue; F.A., R.L. and M.V. designed the chemical syntheses of the probes. All authors discussed the results and commented on the manuscript. R.L. and M.V. conceived and co-supervised the overall project; M.V. wrote the paper.

Additional information

Supplementary Information accompanies this paper at <http://www.nature.com/naturecommunications>

Competing financial interests: The authors declare competing financial interests: University of Edinburgh has filed an invention disclosure form to protect part of the technology described in the study.

Reprints and permission information is available online at <http://npg.nature.com/reprintsandpermissions/>

How to cite this article: Mendive-Tapia, L. *et al.* Spacer-free BODIPY fluorogens in antimicrobial peptides for direct imaging of fungal infection in human tissue. *Nat. Commun.* 7:10940 doi: 10.1038/ncomms10940 (2016).



This work is licensed under a Creative Commons Attribution 4.0 International License. The images or other third party material in this article are included in the article's Creative Commons license, unless indicated otherwise in the credit line; if the material is not included under the Creative Commons license, users will need to obtain permission from the license holder to reproduce the material. To view a copy of this license, visit <http://creativecommons.org/licenses/by/4.0/>

Supporting Information

Spacer-free BODIPY fluorogens in antimicrobial peptides for direct imaging of fungal infection in human tissue

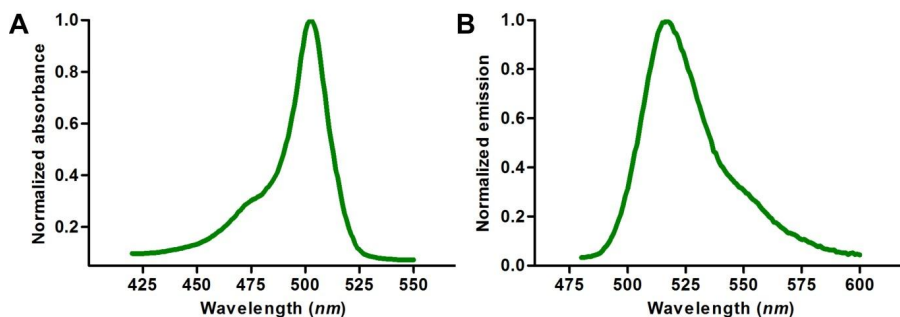
The following data is a selection of the content of the Supporting Information. Full supplementary information including supplementary figures, notes, discussion and methods is available in the Supporting Information in electronic format.

Table of Contents

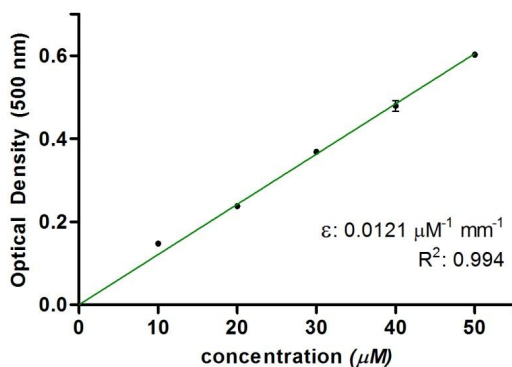
Selected Supplementary Figures	121
Spectral properties of compound 3.....	121
Molecular simulation models of labelled and non-labelled peptides.	122
Antimicrobial and haemolysis assays.	123
Stability assays.....	124
Fluorescence emission of peptides upon incubation with <i>A. fumigatus</i>	125
Competition experiments between 8 and PAF26 (4).	125
Cell viability assays.	126
Selected Supplementary Methods.....	127
Experimental procedures and characterisation data of selected compounds.	127

Selected Supplementary Figures

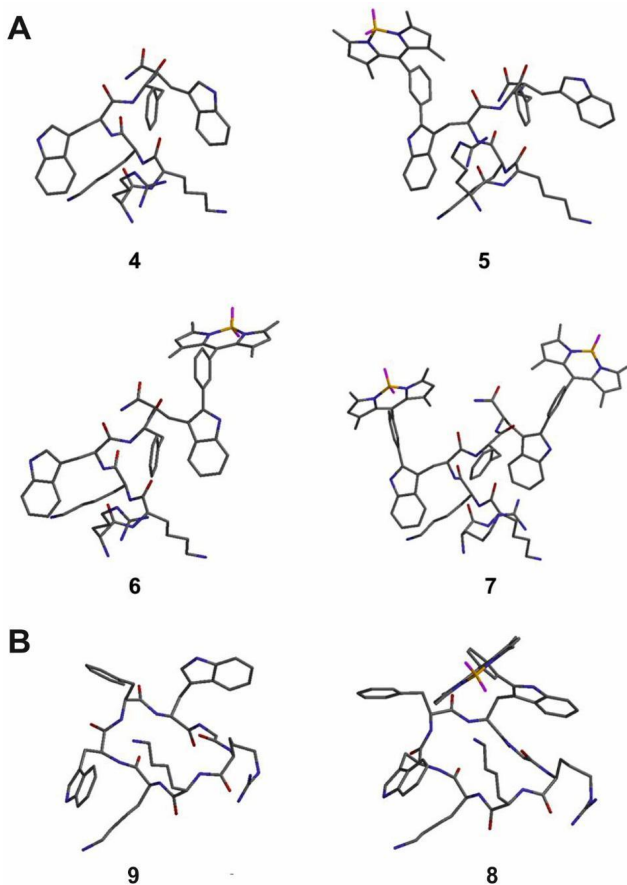
Spectral properties of compound **3**.



Supplementary Figure 1. Spectral characterisation of **3.** A) Absorbance and B) emission spectra (λ_{exc} : 450 nm) of compound **3**.

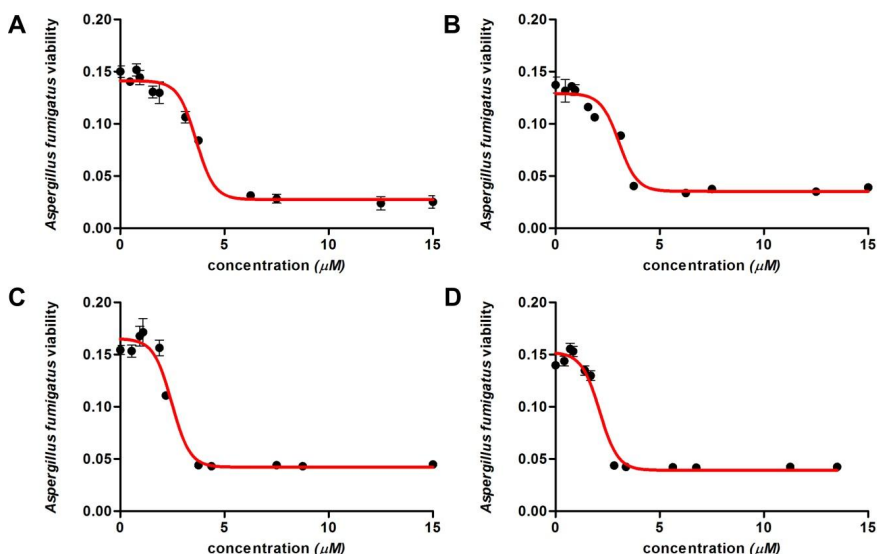


Supplementary Figure 2. Determination of extinction coefficient of **3**. Solutions of **3** were prepared in ethanol and their optical densities were measured at 500 nm in a NanoDrop 1000 spectrophotometer. Data represented as means \pm s.e.m. ($n=3$).

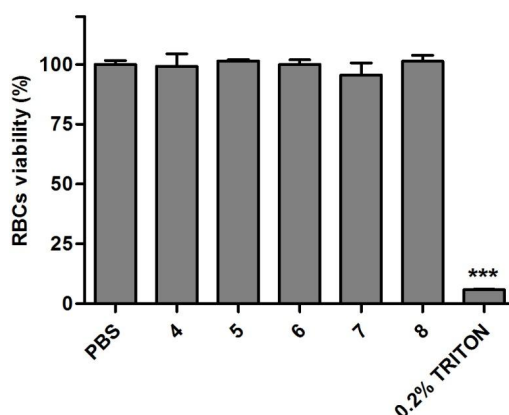
Molecular simulation models of labelled and non-labelled peptides.

Supplementary Figure 3. A) Optimised geometries of fluorogenic linear peptides **5-7** and the corresponding non-labelled linear peptide **4**. B) Optimised geometries of the fluorogenic cyclic peptide **8** and the corresponding non-labelled cyclic peptide **9** (for structure see Supplementary Fig. 8). All simulations were generated by the Spartan '14 suite using Molecular Mechanics (MMFF94) and Semi-Empirical (AM1) methods.*

* Spartan'14 for Windows, Macintosh and Linux, version 1.1.4, wavefunction, inc. www.wavefun.com.

Antimicrobial and haemolysis assays.

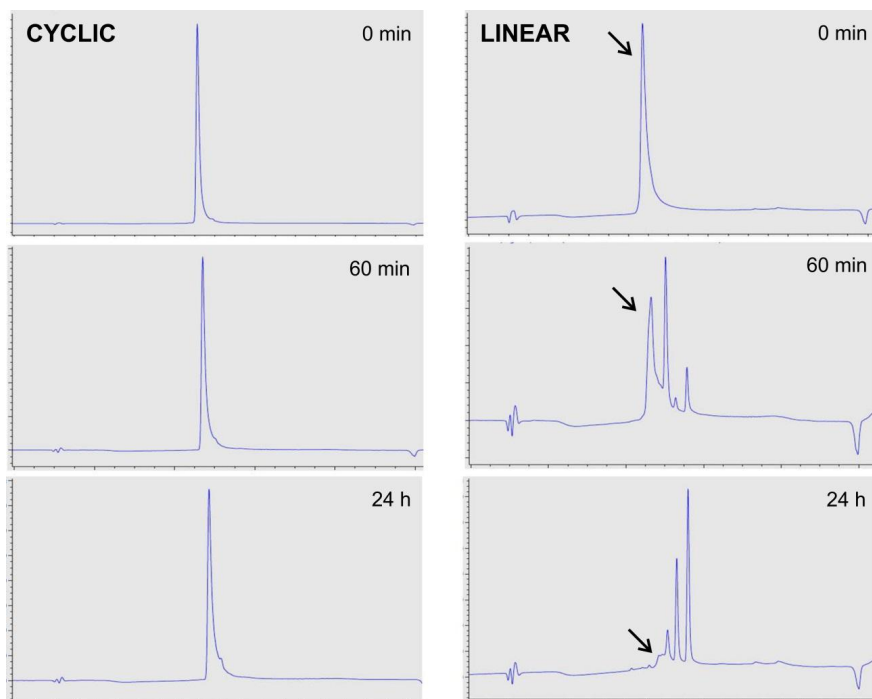
Supplementary Figure 4. Determination of IC_{50} values of BODIPY-labelled peptides 5-8 in *A. fumigatus*. Cell viability plots and non-linear regressions for peptides 5 (A), 6 (B), 7 (C) and 8 (D). Peptides were incubated at different concentrations with *A. fumigatus* conidia to reach a final volume of 100 μL per well. The final conidia concentration was 5×10^5 cells/mL in 10% Vogel's medium. After 24 h incubation at 37 °C in 96 well-plates, fungal growth was determined by measuring the optical density at 610 nm. The IC_{50} values were determined using four parameter logistic regression. Data represented as means \pm s.e.m ($n=3$).



Supplementary Figure 6. Haemolytic activity of peptides 4-8 in human red blood cells (RBCs). Peptides 4-8 and Triton X-100 (0.2% as positive control) were incubated with human RBCs at 37 °C and their viability was assessed after 1 h. Data represented as means \pm s.d. ($n=3$). *** for $p < 0.001$

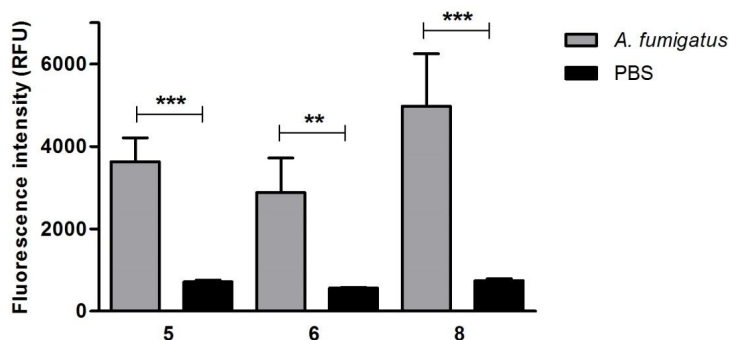
was determined as a statistically significant difference between the cell viabilities in PBS (phosphate buffer saline) and in Triton X-100.

Stability assays.



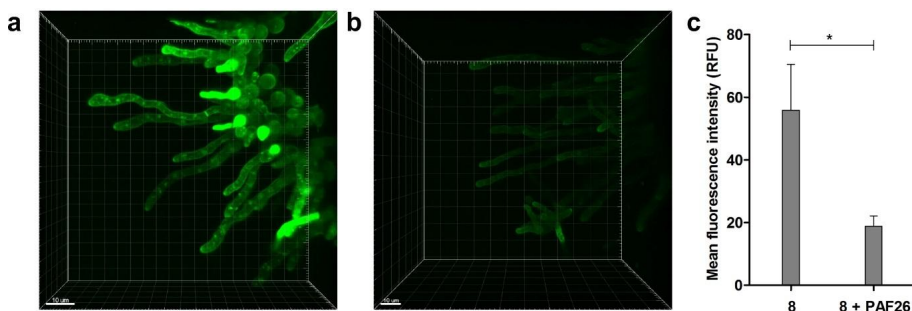
Supplementary Figure 9. Stability of cyclic (8) and linear (5) mono-BODIPY labelled peptides in human bronchoalveolar lavage samples from patients with acute respiratory distress syndrome. Peptides were incubated in human bronchoalveolar lavage samples at 37 °C and analysed by HPLC at the time points indicated. Arrows point at the peaks corresponding to the intact linear peptide.

Fluorescence emission of peptides upon incubation with *A. fumigatus*



Supplementary Figure 13. Fluorescence emission of mono-BODIPY labelled peptides 5, 6 (linear) and 8 (cyclic) upon incubation with *A. fumigatus*. Peptides 5, 6, and 8 were incubated in PBS (phosphate buffer saline) alone or in suspensions of *A. fumigatus* in PBS (λ_{exc} : 485 nm; λ_{em} : 515 nm). Data represented as means \pm s.d. ($n=3$). ** for $p < 0.01$ and *** for $p < 0.005$ were determined as statistically significant differences between the fluorescence emission values in PBS and in suspensions of *A. fumigatus* in PBS.

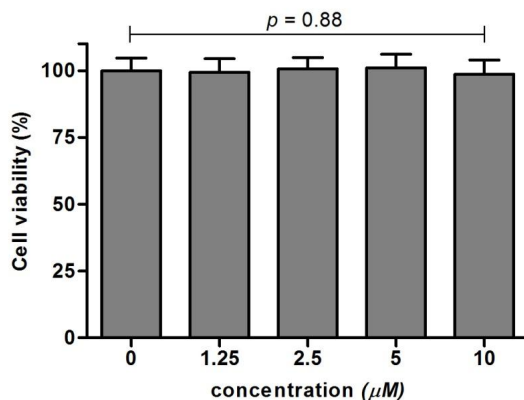
Competition experiments between 8 and PAF26 (4).



Supplementary Figure 15. Fluorescence images of *A. fumigatus* after incubation with the peptide 8 without and with pre-treatment of PAF26 (4). Peptide 8 (2 μM) was incubated for 15 min in *A. fumigatus* that had been not pre-treated (a) or pre-treated with PAF26 (3 μM) for 30 min (b). Images were taken under a confocal microscope at 37 $^{\circ}\text{C}$. For 3D representations, see Supplementary Movies 1 and 2. Scale bar: 10 μm . c) Mean fluorescence intensity values were determined using the software Imaris (for details, see Methods) and represented as means \pm SD. * for $p < 0.05$ was determined as a statistically significant difference between PAF26 pre-treated and not pre-treated *A. fumigatus*.

Cell viability assays.

Cell viability was determined with a TACS® MTT Cell Proliferation assay (Trevigen) according to the manufacturer's instructions. Briefly, human lung A549 epithelial cells were plated on 96-well plates the day before the experiment, reaching 90-95% confluence on the day of the experiment. The peptide **8** was added to the cells at different concentrations (0, 1.25, 2.5, 5 and 10 μM) and incubated at 37 °C for 4 h. After 4 h, cells were washed, treated according to the manufacturer's instructions and their absorbance values (570 nm) were measured in a Synergy HT spectrophotometer (Biotek). Cell viability data was normalised to the proliferation of cells without addition of the peptide **8**.



Supplementary Figure 17. Cell proliferation assays. Viability of human lung A549 epithelial cells after incubation with different concentrations of the peptide **8**. Data represented as means \pm s.d. with $n=4$. No significant differences ($p > 0.05$) were determined between the control and any of the treatments.

Selected Supplementary Methods

Experimental procedures and characterisation data of selected compounds.

4,4-Difluoro-8-(3-iodophenyl)-1,3,5,7-tetramethyl-4-bora-3a,4a-diaza-s-indacene (**2**).

3-iodobenzaldehyde (500 mg, 2.2 mmol) was dissolved in anhydride DCM (50 mL) under N₂. Then, 2,4-dimethylpyrrole (492 μ L, 4.8 mmol) and three drops of TFA were added and the reaction was stirred overnight at r.t. in N₂ atmosphere or until the consumption of the aldehyde was complete (TLC). DDQ (490 mg, 2.2 mmol) dissolved in DCM (20 mL) was added dropwise (10–15 min) to the reaction mixture and the reaction was stirred for 15 min at r.t. Finally, TEA (4 mL, 45 mmol) and BF₃OEt₂ (4 mL, 30 mmol) were added and the mixture stirred for 3 h. Workup was done by diluting with DCM (50 mL) and washing with H₂O (4 x 100 mL). The organic layers were combined, dried over sodium sulfate, filtered and concentrated under vacuum. The crude was purified via flash column chromatography using and DCM/hexane gradient on silica gel. The expected compound was isolated as a red amorphous solid (401 mg, 41%).

Characterisation data: ¹H NMR (400 MHz, CDCl₃): δ 7.76 (dt, *J* = 7.7, 1.5 Hz, 1H), 7.62 (t, *J* = 1.6 Hz, 1H), 7.24 – 7.20 (m, 1H), 7.19 – 7.14 (m, 1H), 5.92 (s, 2H), 2.48 (d, *J* = 1.3 Hz, 6H), 1.36 (s, 6H); ¹³C NMR (100 MHz, CDCl₃): δ 155.9, 142.9, 139.3, 138.0, 137.1, 136.8, 130.7, 127.3, 121.5, 94.3, 14.7, 14.6 (one quaternary carbon signal not seen); HRMS (*m/z*): [M+H]⁺ calcd. for C₁₉H₁₈BF₂IN₂, 451.0654; found, 451.0651.

Fmoc-Trp(C2-BODIPY)-OH (**3**).

Fmoc-Trp-OH (100 mg, 0.234 mmol), **2** (1.5 eq., 158 mg, 0.352 mmol), AgBF₄ (1.0 eq., 46 mg, 0.234 mmol), TFA (1.0 eq., 18 μ L, 0.234 mmol) and Pd(OAc)₂ (0.05 eq., 2.6 mg, 0.0117 mmol) were placed in a microwave reactor vessel in 1.8 mL DMF. The mixture was heated under microwave irradiation (250 W) at 80°C for 20 min. EtOAc was added and the resulting suspension was filtered through Celite and concentrated under vacuum. The resulting crude was purified by flash column chromatography using and EtOAc/hexane gradient on silica gel. The expected adduct was isolated as a red solid (130 mg, 74%).

Characterisation data: ¹H NMR (400 MHz, CDCl₃): δ 8.12 (s, 1H), 7.69 – 7.56 (m, 4H), 7.48 (t, *J* = 7.7 Hz, 1H), 7.41 (t, *J* = 1.7 Hz, 1H), 7.37 (d, *J* = 4.9 Hz, 2H), 7.30 (t, *J* = 8.0 Hz, 3H), 7.25 – 7.21 (m, 1H), 7.20 – 7.13 (m, 3H), 7.07 (ddd, *J* = 8.0, 7.0, 1.1 Hz, 1H), 5.90 (s, 1H), 5.87 (s, 1H), 5.09 (d, *J* = 8.0 Hz, 1H), 4.55 (d, *J* = 7.5 Hz, 1H), 4.17 (q, *J* = 10.3, 9.4 Hz, 2H), 4.01 (s, 1H), 3.44 – 3.37 (m, 1H), 3.37 – 3.28 (m, 1H), 2.47 (s, 3H), 2.46 (s, 3H), 1.38 (s, 3H), 1.35 (s, 3H); ¹³C NMR (100 MHz, CDCl₃): δ 174.8, 163.1, 156.0, 155.9, 143.9, 143.2, 141.4, 140.7, 136.1, 136.0, 135.1, 133.9, 131.5, 130.1, 129.1, 128.8, 127.9, 127.8, 127.2, 125.2, 123.2, 121.6, 120.5, 120.1, 119.3, 111.2, 108.2, 67.2, 47.2, 36.9, 28.0, 14.8, 14.7; HRMS (*m/z*): [M+Na]⁺ calcd. for C₄₅H₃₉BF₂N₄O₄, 771.2930; found, 771.2925.

General procedures for SPPS. All peptides were manually synthesized in polystyrene syringes fitted with a polyethylene porous disc using Fmoc-based SPPS. Solvents and soluble reagents were removed by suction. The Fmoc group was removed with piperidine-DMF (1:4) (1 x 1 min, 2 x 5 min). Peptide synthesis transformations and washings were performed at r.t.

Resin loading (only for 2-chlorotrityl polystyrene resin). Fmoc-AA-OH (1 eq.) was attached to the resin (1 eq.) with DIPEA (3 eq.) in DCM at r.t for 10 min and then DIPEA (7.0 eq.) for 40 min. The remaining trityl groups were capped adding 0.8 μ L MeOH/mg resin for 10 minutes. After that, the resin was filtered and washed with DCM (4 x 1 min), DMF (4 x 1 min). The loading of the resin was determined by titration of the Fmoc group. Peptide elongation. After the Fmoc group was removed, the resin was washed with DMF (4 x 1 min), DCM (3 x 1 min), DMF (4 x 1 min). Unless otherwise noted, standard coupling procedures used DIC (3 eq.) and OxymaPure (3 eq.) in DMF for 1 h and 5-min of pre-activation. The completion of the coupling was monitored by the Kaiser test. Then, the resin was filtered and washed with DCM (4 x 1 min) and DMF (4 x 1 min). Final cleavage (for Sieber amide and for 2-chlorotrityl polystyrene resins). The resin bound peptide was treated for 5 times with 1% TFA in DCM (1 min in each treatment) and washed with DCM. The combined filtered mixtures were poured over DCM and evaporated under vacuum. Then, the residue was dissolved in ACN:H₂O and lyophilised.

Cyclo(Arg-Lys-Lys-Trp(C2-BODIPY)-Phe-Trp-Gly) (8). The synthesis was performed on 91 mg of 2-chlorotrityl polystyrene resin (0.94 mmol/g). Amino acid **3** (1.5 eq.) was incorporated with PyBOP (1.5 eq.), HOBt (1.5 eq.) and DIPEA (2.0 eq.) in DMF for 1 h. Other Fmoc amino acids (3 eq.) were incorporated with a 5 min pre-activation with DIC (3 eq.) and OxymaPure (3 eq.) in DMF for 1 h. After cleavage as described above, the protected linear peptide (119 mg, 0.073 mmol) was dissolved in 1.3 mL of DMF (0.055 M). DIPEA (2.5 eq., 32 μ L, 0.182 mmol) and HATU (1.0 eq., 28 mg, 0.073 mmol) were added. The solution was stirred at r.t. until the cyclisation was complete (approx. 2 h). The cyclic peptide was precipitated by adding H₂O to the solution. The precipitate was washed with H₂O, decanted and dried, obtaining 109 mg of crude protected cyclic peptide (87% yield). The crude protected macrocycle (108 mg, 0.067 mmol) and 20% Pd(OH)₂-C (54 mg) were dissolved in 5% HCOOH/MeOH (10.8 mL), previously purged with Ar. Then, the reaction flask was flushed again with Ar, evacuated and filled with H₂. The reaction mixture was stirred under H₂ for 72 h (H₂ balloons were refilled periodically during the reaction along with re-addition of Pd(OH)₂-C (4 times). The catalyst was removed by filtration and the filtrate was evaporated to afford 46 mg of the crude deprotected peptide. The final peptide was purified by PoraPak Rxn RP 60 cc reverse phase column. Mobile phase: ACN (0.1% HCOOH)/H₂O (0.1% HCOOH). Pure fractions were lyophilised furnishing the corresponding peptide.

Red powder (30 mg).

Characterisation data: ¹H NMR (600 MHz, CD₃OD): δ 8.55 (s, 3H), 7.89 – 7.84 (m, 1H), 7.71 (t, J = 7.7 Hz, 1H), 7.65 (d, J = 7.8 Hz, 1H), 7.60 – 7.55 (m, 2H), 7.42 (dt, J = 8.1, 0.9 Hz, 1H), 7.40 – 7.36 (m, 2H), 7.18 – 7.12 (m, 5H), 7.11 (s, 1H), 7.06 (m, 3H), 6.94 (m, 1H), 6.10 (s, 1H), 6.06 (s, 1H), 4.45 (t, J = 7.4 Hz, 1H), 4.32 (d, J = 10.5 Hz, 1H), 4.25 (m, 1H), 4.17 – 4.07 (m, 2H), 4.04 (d, J = 16.5 Hz, 1H), 4.00 (m, 1H), 3.63 (dd, J = 14.9, 9.5 Hz, 1H), 3.51 – 3.45 (m, 1H), 3.38 (m, 1H), 3.30 (1H), 3.27 – 3.23 (m, 2H), 3.15 (dd, J = 14.2, 7.5 Hz, 1H), 3.10 (dd, J = 14.0, 5.9 Hz, 1H), 2.90 (td, J = 8.6, 4.2 Hz, 2H), 2.72 (t, J = 7.7 Hz, 2H), 2.63 (dd, J = 14.2, 8.5 Hz, 1H), 2.51 (s, 3H), 2.50 (s, 3H), 2.09 – 1.88 (m, 4H), 1.76 (m, 1H), 1.67 (m, 3H), 1.52 (m, 7H), 1.48 – 1.41 (m, 4H), 1.37 (m, 2H), 1.26 – 1.14 (m, 2H); HPLC: tR: 4.45 min (98% purity); HRMS (m/z): [M+H]⁺ calcd. for C₇₀H₈₆BF₂N₁₆O₇, 1311.6926; found, 1311.6864.

PUBLICATION V.**A Trp-BODIPY cyclic peptide for fluorescence labelling of apoptotic bodies**

Ramon Subiros-Funosas,^{*,a} Lorena Mendive-Tapia,^{*,b} Jesus Sot,^c John D. Pound,^a Nicole Barth,^a Yaiza Varela,^c Felix M. Goñi,^c Margaret Paterson,^a Christopher D. Gregory,^a Fernando Albericio,^{b,d} Ian Dransfield,^a Rodolfo Lavilla,^{d,e} and Marc Vendrell^a

[#]Both researchers have contributed equally to this work.

Chemical Communications. Accepted for publication, ahead of print. DOI: 10.1039/c6cc07879f.

- a) MRC/UoE Centre for Inflammation Research, The University of Edinburgh, 47 Little France Crescent, EH16 4TJ Edinburgh, United Kingdom.
- b) Department of Inorganic and Organic Chemistry, University of Barcelona, Martí i Franquès 1-11, 08028 Barcelona, Spain.
- c) Instituto Biofisika, Universidad del País Vasco (UPV/EHU), Campus de Leioa, Barrio Sarriena s/n, 48940 Leioa, Bizkaia, Spain.
- d) CIBER-BBN, Networking Centre on Bioengineering, Biomaterials and Nanomedicine, Baldiri Reixac 10-12, 08028 Barcelona, Spain.
- e) Laboratory of Organic Chemistry, Faculty of Pharmacy, University of Barcelona, Baldiri Reixac 10-12, 08028 Barcelona, Spain.



ChemComm

COMMUNICATION

View Article Online
View Journal

Cite this: DOI: 10.1039/c6cc07879f

Received 28th September 2016,
Accepted 13th December 2016

DOI: 10.1039/c6cc07879f

www.rsc.org/chemcomm

A Trp-BODIPY cyclic peptide for fluorescence labelling of apoptotic bodies†

Ramon Subiros-Funosas,^{‡,a} Lorena Mendive-Tapia,^{‡,b} Jesus Sot,^c John D. Pound,^a Nicole Barth,^a Yaiza Varela,^c Felix M. Goñi,^c Margaret Paterson,^a Christopher D. Gregory,^a Fernando Albericio,^{bd} Ian Dransfield,^a Rodolfo Lavilla^{*de} and Marc Vendrell^{*a}

The rational design and synthesis of a Trp-BODIPY cyclic peptide for the fluorescent labelling of apoptotic bodies is described. Affinity assays, confocal microscopy and flow cytometry analysis confirmed the binding of the peptide to negatively-charged phospholipids associated with apoptosis, and its applicability for the detection and characterisation of subcellular structures released by apoptotic cells.

Apoptosis is a process of programmed cell death taking place after severe cellular damage following specific signalling events. In early stages of apoptosis, molecules of phosphatidylserine (PS) are translocated to the outer face of the plasma membrane. Recent studies provide evidence that apoptotic cells release subcellular structures to the extracellular space in order to communicate with other cells.^{1–5} These structures are membranous components that can be classified as exosomes, apoptotic vesicles and apoptotic bodies. Whereas exosomes, which range in size from 20–100 nm, are secreted by multivesicular endosomes upon fusion with the plasma membrane, apoptotic vesicles (100–1000 nm) and apoptotic bodies (>1000 nm) are expelled directly from the plasma membrane to the extracellular space. Although their precise mechanisms of action remain elusive, these structures play critical roles in many biological processes, such as coagulation, inflammation, tumour progression, cell adhesion or transfer of signalling components and genetic information. For instance, recent studies have validated tumour exosomes as important mediators in defining pre-metastatic niches.^{6,7} As a result,

subcellular vesicles secreted by apoptotic cells might become valuable biomarkers for monitoring and diagnosing several pathological conditions, which has prompted the development of novel methods for their detection and characterisation.⁸ One defining characteristic of apoptotic bodies is the presentation of negatively-charged phospholipids, such as PS, in high amounts. This feature has been exploited to design chemical reagents to monitor apoptosis in cells.^{9–11} Annexin V, a 36 kDa protein with high binding affinity to PS, has been widely used to monitor cell death *in vitro*.¹² However, Annexin V-based labelling is limited by its high molecular weight, the formation of membrane lattices and its dependence on high concentrations of Ca²⁺, which are incompatible with many physiological environments. We envisaged that the development of probes for labelling apoptotic bodies in a Ca²⁺-independent manner would represent a significant advancement in the field.

Lactadherin is a β sheet-rich glycoprotein (43 kDa) that acts as a bridge between phagocytic receptors (e.g. $\alpha_v\beta_3$) and apoptotic cells by binding at externalised PS in a Ca²⁺-independent manner. Based on the disposition of lactadherin residues upon binding to PS, Zheng and co-workers condensed its fundamental amino acids to prepare lactadherin-like small cyclic peptides (cLac-1, Fig. 1).¹³ We envisioned that fluorescent probes of the cLac family might be useful tools for labelling PS-rich apoptotic bodies, given their high sensitivity and suitability for imaging assays.^{14,15} However, most labelling methods alter the molecular properties of small peptides. Our group has optimized C-H activation methodologies^{16–19} and pioneered the Trp-BODIPY fluorogenic amino acid for non-perturbative labelling of peptide sequences.²⁰ The Trp-BODIPY amino acid emits fluorescence once labelled peptides bind to their corresponding targets, which leads to the rigidification and fluorescence enhancement of the Trp-BODIPY fluorophore (Fig. S1 in ESI†).²⁰ Since the cLac-1 peptide contains one Trp in its original sequence, we prepared a fluorescent cyclic peptide (cLac-BODIPY) for binding to PS-rich vesicles by replacing the Trp of cLac-1 with the Trp-BODIPY amino acid (Fig. 1). Using this approach, we examined cLac-BODIPY as a novel probe to fluorescently label apoptotic bodies in a Ca²⁺-independent manner.

^a MRC/UoE Centre for Inflammation Research, The University of Edinburgh,

47 Little France Crescent, EH16 4TJ Edinburgh, UK. E-mail: marc.vendrell@ed.ac.uk

^b Department of Inorganic and Organic Chemistry, University of Barcelona, Martí i Franquès 1-11, 08028 Barcelona, Spain^c Instituto Biofísica (CSIC, UPV/EHU) and Departamento de Bioquímica, Universidad del País Vasco, Campus de Leioa, Barrio de Sarriena s/n, 48940 Leioa, Bizkaia, Spain^d CIBER-BBN, Networking Centre on Bioengineering, Biomaterials and Nanomedicine, Baldori Reixac 10-12, 08028 Barcelona, Spain^e Laboratory of Organic Chemistry, Faculty of Pharmacy, University of Barcelona, Baldori Reixac 10-12, 08028 Barcelona, Spain. E-mail: rlavilla@ub.edu

† Electronic supplementary information (ESI) available. See DOI: 10.1039/c6cc07879f

‡ These authors contributed equally to this work.

Communication

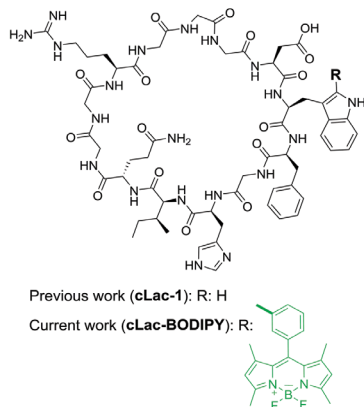


Fig. 1 Chemical structures of peptide-based lactadherin mimics related to previous and the current work.

We designed the synthesis of **cLac-BODIPY** in solid-phase by selecting appropriate orthogonal protecting groups and using 2-chlorotriethylchloride polystyrene resin as the solid support, in order to cleave the peptide under mild acidic conditions without affecting the BODIPY core (Scheme 1).^{21,22} We used Mmt as the protective group for His and the NO₂ group for Arg because they can be removed by mild acidic treatment and hydrogenation respectively,²³ and Gln was introduced without any side-chain protection. Furthermore, in order to maximize the efficiency of the cyclisation, we designed a head-to-tail solid-phase approach by anchoring the peptide through the side chain of the Asp residue, while protecting the C-terminal carboxylic acid as an allylic ester. The peptide elongation was performed using standard conditions,^{24–26} followed by on-bead cyclisation. The partially-protected peptide was isolated after treatment with TFA:DCM (1:99), and **cLac-BODIPY** was obtained in very high purities (>99%) after catalytic hydrogenation and reverse-phase HPLC purification (Fig. S2 and S3 in ESI†).

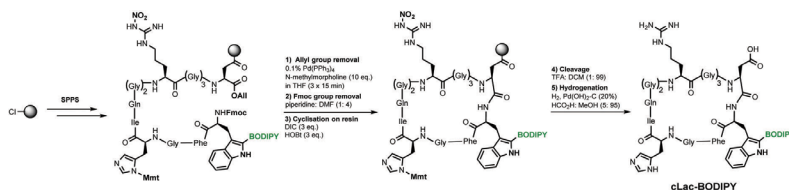
In order to assess the properties of **cLac-BODIPY** and its affinity for PS, we measured the fluorescence spectra of

cLac-BODIPY upon incubation with layers of constant lipid content and different ratios of PS and phosphatidylcholine (PC). As shown in Fig. 2, **cLac-BODIPY** displayed a dose-dependent increase of the fluorescence emission after interaction with PS, with low emission in films containing only PC.

cLac-BODIPY showed a remarkable fluorescence quantum yield upon binding to PS (0.46) due to the fluorogenic behaviour of the Trp-BODIPY reporter. Furthermore, we assessed the fluorescence emission of **cLac-BODIPY** after incubation with PS-containing lipid layers in the presence and absence of Ca²⁺. Unlike Annexin V, the interaction between **cLac-BODIPY** and PS did not show any dependence on Ca²⁺, which confirms the applicability of **cLac-BODIPY** to recognise PS-rich vesicles under most physiological conditions (Fig. 2 and Fig. S4 in ESI†).

In view of the excellent features of **cLac-BODIPY** as a fluorescent reporter for PS-rich environments, we examined its physico-chemical properties in lipid–aqueous interfaces. First, we determined the tensioactive potential of **cLac-BODIPY** by measuring the surface pressure of lipid–aqueous mixtures at different concentrations of the probe. **cLac-BODIPY** displayed remarkable tensioactivity and was able to form monolayers in the air–water interphase with a saturation pressure (π_s) of 20.4 mN m^{−1} (Table 1 and Fig. S5 in ESI†). We compared the behaviour of **cLac-BODIPY** with the non-labelled peptide **cLac-1** under the same experimental conditions, and observed that **cLac-BODIPY** displayed significantly stronger tensioactivity (Fig. S5 in ESI†), suggesting its suitability to monitor biomolecular changes in these interphases. These results also confirm that the BODIPY fluorophore is an optimal scaffold for reporting molecular events associated with lipid-rich environments.^{27–29}

Next we quantified the binding affinity of **cLac-BODIPY** for different phospholipids by determining the critical surface pressure of **cLac-BODIPY** in lipid monolayers with different composition. **cLac-BODIPY** incorporated into PS-containing monolayers (PC:PS, 7:3) with a critical pressure of 42 mN m^{−1}, with 15% lower affinity (36 mN m^{−1}) in PC-only monolayers (Table 1 and Fig. S6 in ESI†). We extended the analysis to other negatively-charged phospholipids (e.g. phosphatidylglycine (PG), cardiolipin) that are associated with apoptotic processes,³⁰ and observed the increased binding of **cLac-BODIPY** for monolayers containing these lipids over PC-only monolayers (Fig. S7 in ESI†). This pattern suggests the preferential binding of **cLac-BODIPY** to labelling subcellular structures derived from apoptotic cells. We also examined the specificity of these interactions by



Scheme 1 Chemical synthetic approach for the solid-phase synthesis of the **cLac-BODIPY**.

ChemComm

View Article Online

Communication

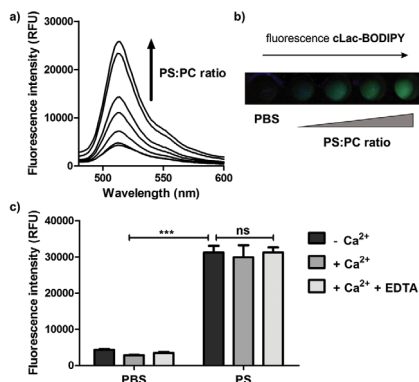


Fig. 2 (a) Fluorescence spectra of **cLac-BODIPY** in films with constant lipid content and increasing PS:PC ratios. QY (100% PS): 0.46, QY (100% PC): 0.08. (b) Fluorescence emission of **cLac-BODIPY** under 365 nm in solutions with different PS:PC ratios and PBS as a blank. (c) Ca^{2+} -independent binding between **cLac-BODIPY** and PS ([CaCl_2]: 2 mM, [EDTA]: 2.5 mM). *** for $p < 0.001$, ns for $p > 0.05$.

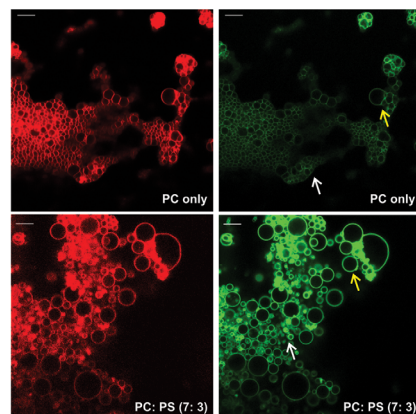


Fig. 3 Confocal fluorescence microscopy images of giant unilamellar vesicles (GUVs) containing PC-only or PC:PS (7:3) after co-staining with lissamine-rhodamine-PE (red, lipid stain) and **cLac-BODIPY** (green, 2 μM). White and yellow arrows point at vesicles of similar size in PC only and PC:PS (7:3) GUVs. Scale bar: 10 μm .

Table 1 Critical surface pressure quantification assays in lipid monolayers

	π_s (mN m^{-1})	π_c (mN m^{-1})	Decrease π_c vs. PS^a	
			PC	PG
cLac-BODIPY	20.4	42.0	15%	<1%
cLac-1	5.0	30.3	16%	<1%

^a Relative decrease in π_c values when comparing PC:PS (7:3) monolayers (PS) to PC monolayers (PC) or PC:PG (7:3) monolayers (PG; phosphatidylglycine).

analysing the behaviour of the non-labelled peptide **cLac-1**. Notably, the relative binding pattern of **cLac-1** to the different phospholipids closely correlated with that observed for **cLac-BODIPY** (Table 1 and Fig. S7 in ESI†). This minimal impairment in the lipid recognition ability of the **cLac-1** peptide indicates that the BODIPY fluorogen is optimally positioned within the cLac peptide sequence. Altogether, these results confirm the preferential binding of **cLac-BODIPY** to lipid domains found in structures released by apoptotic cells.

We employed **cLac-BODIPY** in fluorescence microscopy experiments with PS-containing vesicles as well as other lipidated vesicles. We prepared giant unilamellar vesicles (GUVs) containing PC-only or PC:PS (7:3), and incubated them with the same concentration of **cLac-BODIPY** and lissamine-rhodamine-PE as a generic lipid stain. As shown in Fig. 3, **cLac-BODIPY** displayed significantly brighter staining in vesicles containing PC:PS (7:3) than in vesicles with only PC. This observation is in agreement with our results from the *in vitro* assays in lipid monolayers and confirms the applicability of **cLac-BODIPY** for the fluorescence labelling of apoptotic bodies.

Finally, we examined **cLac-BODIPY** as a fluorescent probe for labelling subcellular structures derived from apoptotic human cells. We induced apoptosis in Burkitt's lymphoma (BL2) cells by irradiation with UV light and subsequent culture, and isolated the apoptotic bodies. First we incubated the apoptotic bodies with different concentrations of **cLac-BODIPY** and analysed the fluorescence labelling by flow cytometry (Fig. 4a and b). **cLac-BODIPY** showed dose-dependent staining, with significant labelling even at low concentrations (Fig. S8 in ESI†). Flow cytometry assays confirmed that most apoptotic bodies stained with **cLac-BODIPY** were also stained with Annexin V, suggesting the interaction with PS as the responsible for the fluorescence labelling of apoptotic bodies using **cLac-BODIPY** (Fig. 4c). Furthermore, we employed fluorescence microscopy to visualize subcellular bodies derived from apoptotic human A549 cells (Fig. S9 in ESI†).

In summary, we have synthesized a fluorescent cyclic peptide (**cLac-BODIPY**) to label apoptotic bodies by including the fluorogenic Trp-BODIPY amino acid into a short lactadherin-like peptide sequence. **cLac-BODIPY** shows remarkable fluorescence emission only after binding to phosphatidylserine and, unlike Annexin V, displays strong binding in a Ca^{2+} independent-manner. *In vitro* assays in lipid monolayers indicate the suitability of the Trp-BODIPY fluorogen to report changes in the composition of lipid-aqueous interphases, and validated the selectivity of **cLac-BODIPY** for PS-rich vesicles using fluorescence confocal microscopy. Flow cytometry experiments using **cLac-BODIPY** confirmed the labelling of apoptotic bodies from BL2 human lymphoma cells, creating new opportunities to monitor, profile and characterise these subcellular structures in multiple biological contexts.

Communication

View Article Online

ChemComm

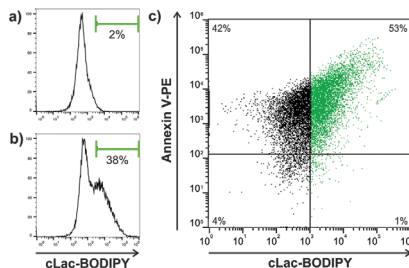


Fig. 4 Flow cytometry analysis of apoptotic bodies from BL2 cells. Histograms of apoptotic bodies incubated without (a) and with cLac-BODIPY (2.5 μ M) (b). (c) Dot plot of apoptotic bodies treated with cLac-BODIPY (X-axis, green) and Annexin V-PE (Y-axis) showing the double staining.

R. S.-F. acknowledges a MSCA Individual Fellowship (659046). L. M.-T. acknowledges a FPU Scholarship (MECD-Spain). F. M. G. acknowledges FEDER-Mineco (BFU 2015-66306-P) and the Basque Gov. (IT849-13). R. L. acknowledges DGICYT-Spain (BQU-CTQ2015-67870-P) and Generalitat de Catalunya (2014 SGR 137). C. D. G., J. D. P. and M. P. acknowledge Bloodwise. M. V. acknowledges the Medical Research Council, the Marie Curie Integration Grant (333847), and the Biotechnology and Biological Sciences Research Council (BB/M025160/1). The authors thank Luxembourg Bio Technologies, Ltd (Rehovot) for the kind supply of OxymaPure and derived reagents.

Notes and references

- 1 C. Théry, M. Ostrowski and E. Segura, *Nat. Rev. Immunol.*, 2009, **9**, 581.
- 2 E. Van Der Pol, A. N. Böling, P. Harrison, A. Sturk and R. Nieuwland, *Pharmacol. Rev.*, 2012, **64**, 676.
- 3 S. Mathivanan, H. Ji and R. J. Simpson, *J. Proteomics*, 2010, **73**, 1907.
- 4 E. Cocucci, G. Racchetti and J. Meldolesi, *Trends Cell Biol.*, 2009, **19**, 43.
- 5 J. Ratajczak, M. Wysocki, F. Hayek, A. Janowska-Wieczorek and M. Z. Ratajczak, *Leukemia*, 2006, **20**, 1487.
- 6 A. Hoshino, B. Costa-Silva, T.-L. Shen, G. Rodrigues, A. Hashimoto, M. Tesic Mark, H. Molina, S. Kohsaka, A. Di Giannatale, S. Ceder, S. Singh, C. Williams, N. Soplop, K. Uryu, L. Pharmed, T. King, L. Bojmar, A. E. Davies, Y. Ararso, T. Zhang, H. Zhang, J. Hernandez, J. M. Weiss, V. D. Dumont-Cole, K. Kramer, L. H. Wexler, A. Narendran, G. K. Schwartz, J. H. Healey, P. Sandstrom, K. Jørgen Latori, E. H. Kure, P. M. Grandgenett, M. A. Hollingsworth, M. de Sousa, S. Kaur, M. Jain, K. Mallya, S. K. Batra, W. R. Jarnagin, M. S. Brady, O. Fodstad, V. Muller, K. Pantel, A. J. Minn, M. J. Bissell, B. A. Garcia, Y. Kang, V. K. Rajasekhar, C. M. Ghajar, I. Matei, H. Peinado, J. Bromberg and D. Lyden, *Nature*, 2015, **527**, 329.
- 7 H. Peinado, M. Aleck, S. Lavotshkin, I. Matei, B. Costa-silva, G. Moreno-bueno, M. Hergueta-redondo, C. Williams, G. Garcia-santos, C. M. Ghajar, A. Nitadori-hoshino, C. Hoffman, K. Badal, B. A. Garcia, M. K. Callahan, J. Yuan, V. R. Martins, J. Skog, R. N. Kaplan, M. S. Brady, J. D. Wolchok, P. B. Chapman and Y. Kang, *Nat. Med.*, 2012, **18**, 883.
- 8 J. Ko, E. Carpenter and D. Issadore, *Analyst*, 2016, **141**, 450.
- 9 A. Neves and K. M. Brindle, *J. Nucl. Med.*, 2014, **55**, 1.
- 10 K. Schutters and C. Reutelingsperger, *Apoptosis*, 2010, **15**, 1072.
- 11 Y. S. Cho, K. M. Kim, D. Lee, W. J. Kim and K. H. Han, *Chem. - Asian J.*, 2013, **8**, 755.
- 12 M. Nazari, A. Minaei-Tehrani and R. Emamzadeh, *RSC Adv.*, 2014, **4**, 45128.
- 13 H. Zheng, F. Wang, Q. Wang and J. Gao, *J. Am. Chem. Soc.*, 2011, **133**, 15280.
- 14 J. S. Lee, M. Vendrell and Y.-T. Chang, *Curr. Opin. Chem. Biol.*, 2011, **15**, 760.
- 15 M. Vendrell, A. Samanta, S.-W. Yun and Y.-T. Chang, *Org. Biomol. Chem.*, 2011, **9**, 4760.
- 16 L. Mendive-Tapia, S. Preciado, J. Garcia, R. Ramón, N. Kielland, F. Albericio and R. Lavilla, *Nat. Commun.*, 2015, **6**, 7160.
- 17 S. Preciado, L. Mendive-Tapia, F. Albericio and R. Lavilla, *J. Org. Chem.*, 2013, **78**, 8129.
- 18 S. Preciado, L. Mendive-Tapia, C. Torres-Garcia, R. Zamudio-Vázquez, V. Soto-Cerrato, R. Pérez-Tomás, F. Albericio, E. Nicolás and R. Lavilla, *MedChemComm*, 2013, **4**, 1171.
- 19 J. Ruiz-Rodríguez, F. Albericio and R. Lavilla, *Chem. - Eur. J.*, 2010, **16**, 1124.
- 20 L. Mendive-Tapia, C. Zhao, A. R. Akram, S. Preciado, F. Albericio, M. Lee, A. Serrels, N. Kielland, N. D. Read, R. Lavilla and M. Vendrell, *Nat. Commun.*, 2016, **7**, 10940.
- 21 M. Vendrell, G. G. Krishna, K. K. Ghosh, D. Zhai, J.-S. Lee, Q. Zhu, Y. H. Yau, S. G. Shochat, H. Kim, J. Chung and Y.-T. Chang, *Chem. Commun.*, 2011, **47**, 8424.
- 22 J. C. Er, M. K. Tang, C. G. Chia, H. Liew, M. Vendrell and Y.-T. Chang, *Chem. Sci.*, 2013, **4**, 2168.
- 23 A. Isidro-Llobet, M. Alvarez and F. Albericio, *Chem. Rev.*, 2009, **109**, 2455.
- 24 M. Vendrell, E. Angulo, V. Casado, C. Lluis, R. Franco, F. Albericio and M. Royo, *J. Med. Chem.*, 2007, **50**, 3062.
- 25 F. Yraola, R. Ventura, M. Vendrell, A. Colombo, J.-C. Fernández, N. de la Figuera, D. Fernández-Fórner, M. Royo, P. Forn and F. Albericio, *QSAR Comb. Sci.*, 2004, **23**, 145.
- 26 R. Subiros-Funosas, R. Prohens, R. Barbas, A. El-Faham and F. Albericio, *Chem. - Eur. J.*, 2009, **15**, 9394.
- 27 S. W. Yun, C. Leong, D. Zhai, Y. L. Tan, L. Lim, X. Bi, J. J. Lee, H. J. Kim, N. Y. Kang, S. H. Ng, L. W. Stanton and Y.-T. Chang, *Proc. Natl. Acad. Sci. U. S. A.*, 2012, **109**, 10214.
- 28 J. C. Er, M. Vendrell, M. K. Tang, D. Zhai and Y.-T. Chang, *ACS Comb. Sci.*, 2013, **15**, 452.
- 29 J. O. Flores-Rizo, I. Esnal, C. A. Osorio-Martínez, C. F. Gómez-Durán, J. Bañuelos, I. López Arbeloa, K. H. Pannell, A. J. Metta-Magaña and E. Peña-Cabrera, *J. Org. Chem.*, 2013, **78**, 5867.
- 30 V. Manganelli, A. Capozzi, S. Recalchi, M. Signore, V. Mattei, T. Garofalo, R. Misasi, M. Degli Esposti and M. Sorice, *J. Immunol. Res.*, 2015, **2015**, 847985.

Supporting Information

A Trp-BODIPY cyclic peptide for fluorescence labelling of apoptotic bodies

The following data is a selection of the content of the Supporting Information. Full supplementary information including general experimentation, procedures, NMR spectra and supplementary figures is available in the Supporting Information in electronic format.

Table of Contents

<i>Selected Experimental Section</i>	<i>137</i>
<i>Selected NMR spectra.....</i>	<i>140</i>
<i>Selected Supplementary Figures</i>	<i>145</i>

Selected Experimental Section

General procedures for SPPS

All peptides were manually synthesized in polystyrene syringes fitted with a polyethylene porous disc using Fmoc-based SPPS. Solvents and soluble reagents were removed by suction. The Fmoc group was removed with piperidine: DMF (1: 4) (1 × 1 min, 2 × 5 min). Peptide synthesis transformations and washings were performed at r.t.

Resin loading. Fmoc-Asp-OAllyl (1 eq.) was attached to the resin (1 eq.) with DIPEA (3 eq.) in DCM at r.t. for 10 min and then DIPEA (7 eq.) for 40 min. The remaining trityl groups were capped adding 0.8 $\mu\text{L MeOH mg}^{-1}$ resin for 10 min. The resin was filtered and washed with DCM (4 × 1 min), DMF (4 × 1 min). The loading of the resin was determined by titration of the Fmoc group.

Peptide elongation. After the Fmoc group was removed with piperidine: DMF (1: 4) (1 × 1 min, 2 × 5 min), the resin was washed with DMF (4 × 1 min), DCM (3 × 1 min), DMF (4 × 1 min). Unless otherwise noted, standard coupling procedure with DIC (3 eq.) and OxymaPure (3 eq.) in DMF for 1 h and 5 min of pre-activation was carried out. The completion of the coupling was monitored with the Kaiser test. Then, the resin was filtered and washed with DCM (4 × 1 min) and DMF (4 × 1 min) and was ready for the elongation with the next Fmoc amino acid.

Final cleavage. The resin bound peptide was treated repeated times with TFA: DCM (1: 99) for 1 min in each treatment and washed with DCM. The combined filtered mixtures were poured over DCM and evaporated under vacuum. The residue was precipitated in Et_2O , dissolved in ACN: H_2O and lyophilised.

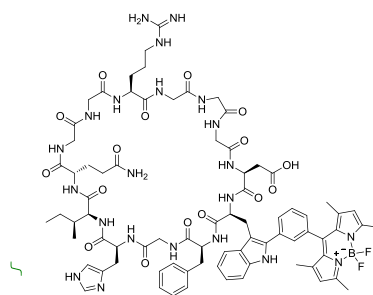
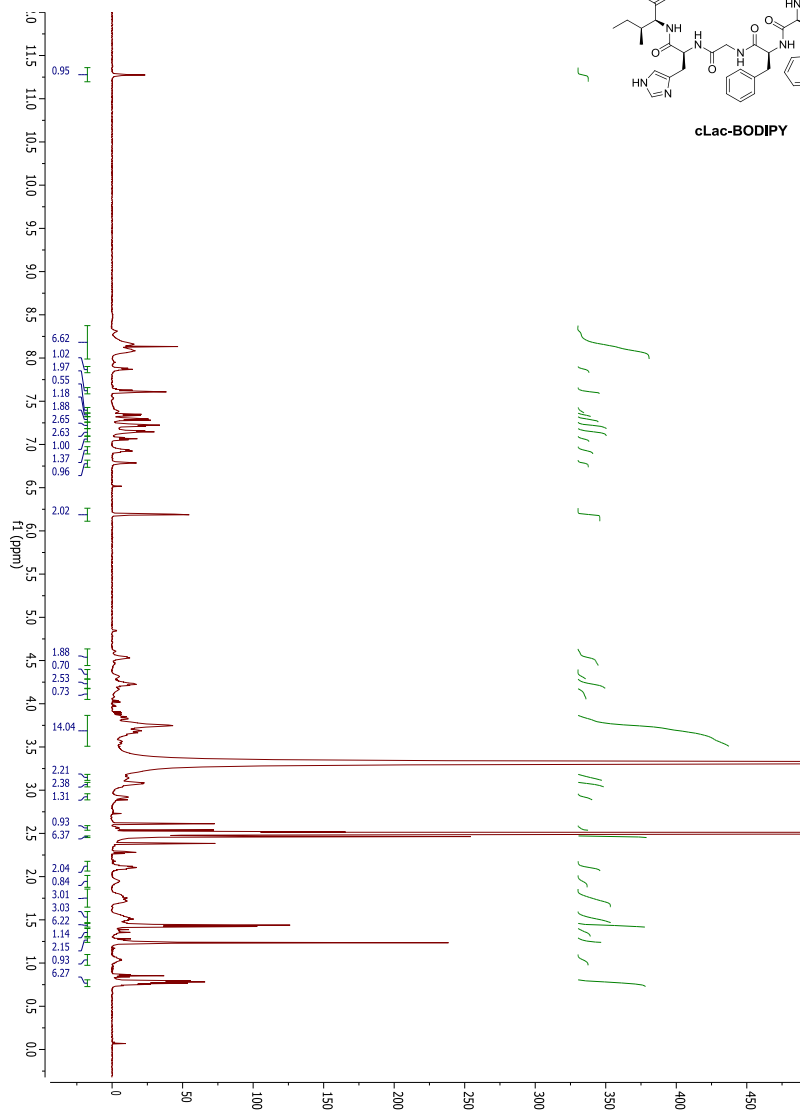
cLac-BODIPY. Starting from 750 mg of 2-chlorotrityl PS resin (0.3 mmol g^{-1}).

Amino acid coupling. Fmoc-Trp(BODIPY)-OH^[1] (1.5 eq.) was incorporated with HBTU (1.2 eq.), HOBt (1.2 eq.) and DIEA (2.4 eq.) in DMF for 1 h. The other amino acids Fmoc-AA-OH (3 eq.) were incorporated with a 5 min pre-activation with DIC (3 eq.) and OxymaPure (3 eq.) in DMF for 1 h. Fmoc-AA-OH: Fmoc-Asp-Oallyl, Fmoc-Gly-OH, Fmoc-Arg(NO₂)-OH, Fmoc-Gln-OH, Fmoc-Ile-OH, Fmoc-His(Mmt)-OH, Fmoc-Phe-OH. Peptide cyclisation. The C-terminal allyl ester group of the aspartic acid was removed after addition of the last amino acid with Pd(PPh₃)₄ (26 mg, 0.023 mmol, 0.1 eq.) and N-methylmorpholine (244 μL , 2.25 mmol, 10 eq.) in THF for 1 h at r.t (3 x 15 min). The head-to-tail cyclization was performed by removal of the N-terminal Fmoc group before addition of DIC (96 μL , 0.548 mmol, 3 eq.) and HOBt (75 mg, 0.548 mmol, 3 eq.) in DMF at r.t. for 5 h. Peptide cleavage. The resin bound peptide was treated repeated times with the TFA cocktail obtaining 69 mg of cyclic peptide crude (60% purity by HPLC-MS). Removal of nitro group. The crude protected peptide (69 mg, 0.041 mmol) and 20% Pd(OH)₂-C (34 mg) were dissolved in HCO₂H: DMF: H₂O (5: 47.5: 47.5) (10 mL) and the reaction flask was flushed with Ar, evacuated and filled with H₂. The reaction mixture was stirred under balloon pressure of H₂ for 32 h (H₂ was refilled periodically during the reaction along with re-addition of Pd(OH)₂-C (2 X). The catalyst was removed through filtration with Celite and the filtrate was evaporated *in vacuo* to afford 64 mg of the crude peptide (70% purity by HPLC-MS, 69% yield). Peptide purification. A highly pure fraction of the totally deprotected cyclic peptide was obtained by semi-preparative RP-HPLC (XBRIDGETM, C₁₈, 5 μM OBD 19 x 150 mm column. The pure fractions were lyophilised rendering the corresponding peptide as a

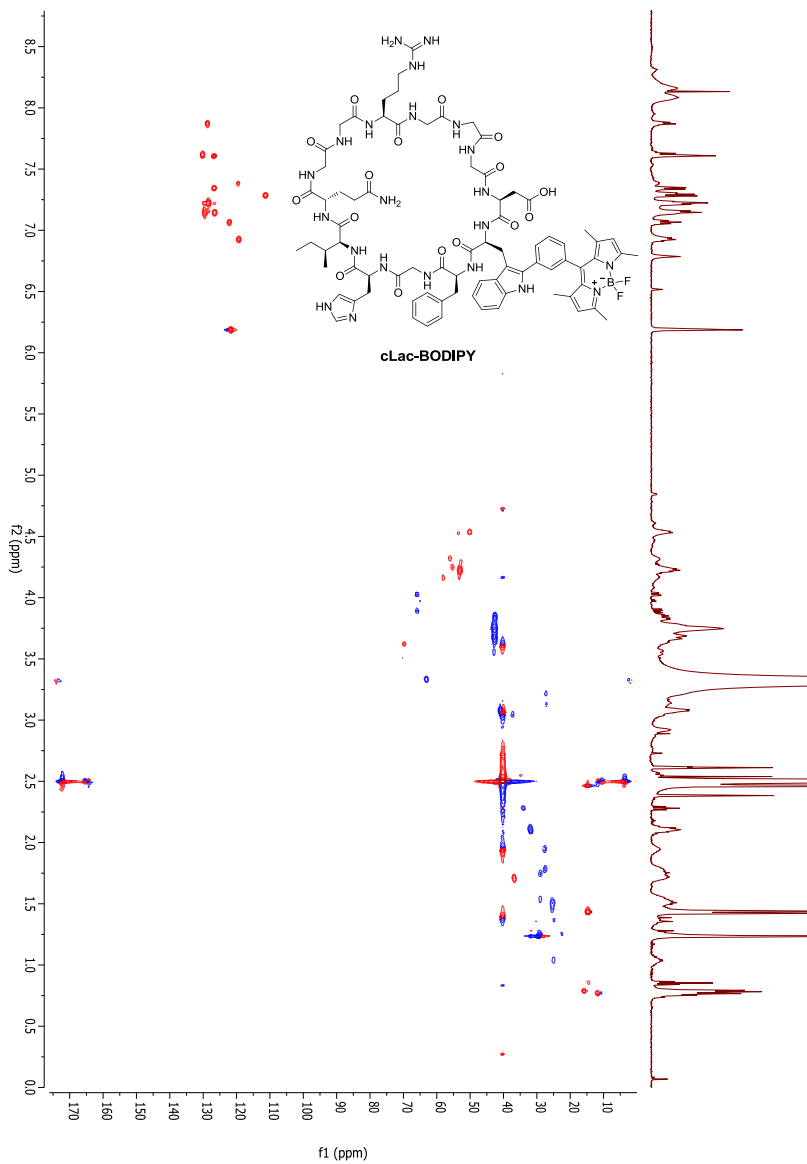
¹H NMR (600 MHz, DMSO-*d*₆): δ 11.27 (s, 1H), 8.37 – 7.99 (m, 7H), 7.90 – 7.83 (m, 1H), 7.66 – 7.59 (m, 2H), 7.43 – 7.36 (m, 1H), 7.34 (dd, *J* = 7.6, 1.5 Hz, 1H), 7.32 – 7.26 (m, 2H), 7.26 – 7.18 (m, 3H), 7.15 (t, *J* = 7.2 Hz, 3H), 7.07 (t, *J* = 7.4 Hz, 1H), 6.92 (t, *J* = 8.3 Hz, 1H), 6.79 (s, 1H), 6.19 (d, *J* = 4.5 Hz, 2H), 4.63 – 4.44 (m, 2H), 4.40 – 4.29 (m, 1H), 4.28 – 4.18 (m, 3H), 4.17 – 4.05 (m, 1H), 3.87 – 3.51 (m, 14H), 3.18 – 3.11 (m, 2H), 3.09 – 3.04 (m, 2H), 2.96 – 2.89 (m, 1H), 2.56 (m, 1H), 2.47 – 2.45 (m, 6H), 2.18 – 2.06 (m, 2H), 1.95 (s, 1H), 1.86 – 1.65 (m, 3H), 1.60 – 1.47 (m, 3H), 1.43 (d, *J* = 9.4 Hz, 6H), 1.40 – 1.31 (m, 1H), 1.29 – 1.24 (m, 2H), 1.04 (m, 1H), 0.81 – 0.73 (m, 6H) ppm. **HRMS** (ESI) (*m/z*): [M+H]⁺ calcd. for C₇₈H₉₇O₁₆ N₂₂BF₂, 1646.7509; found, 1646.7509.

Selected NMR spectra

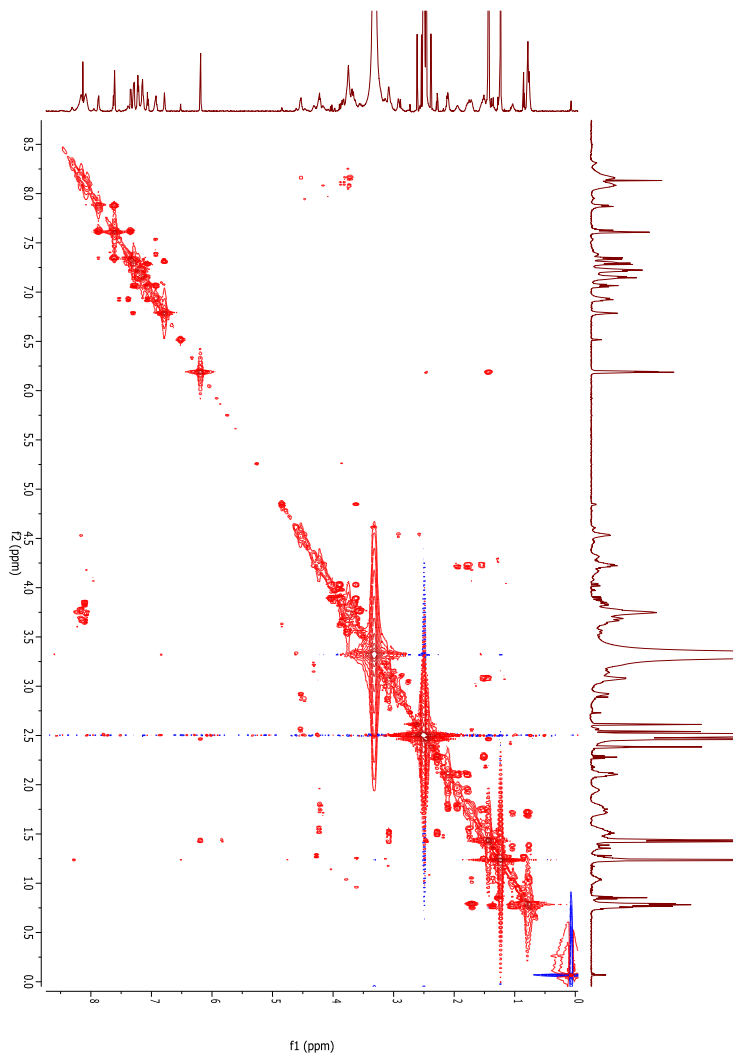
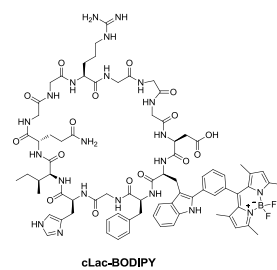
¹H-NMR of cLac-BODIPY



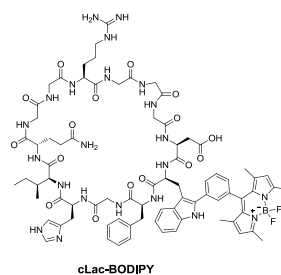
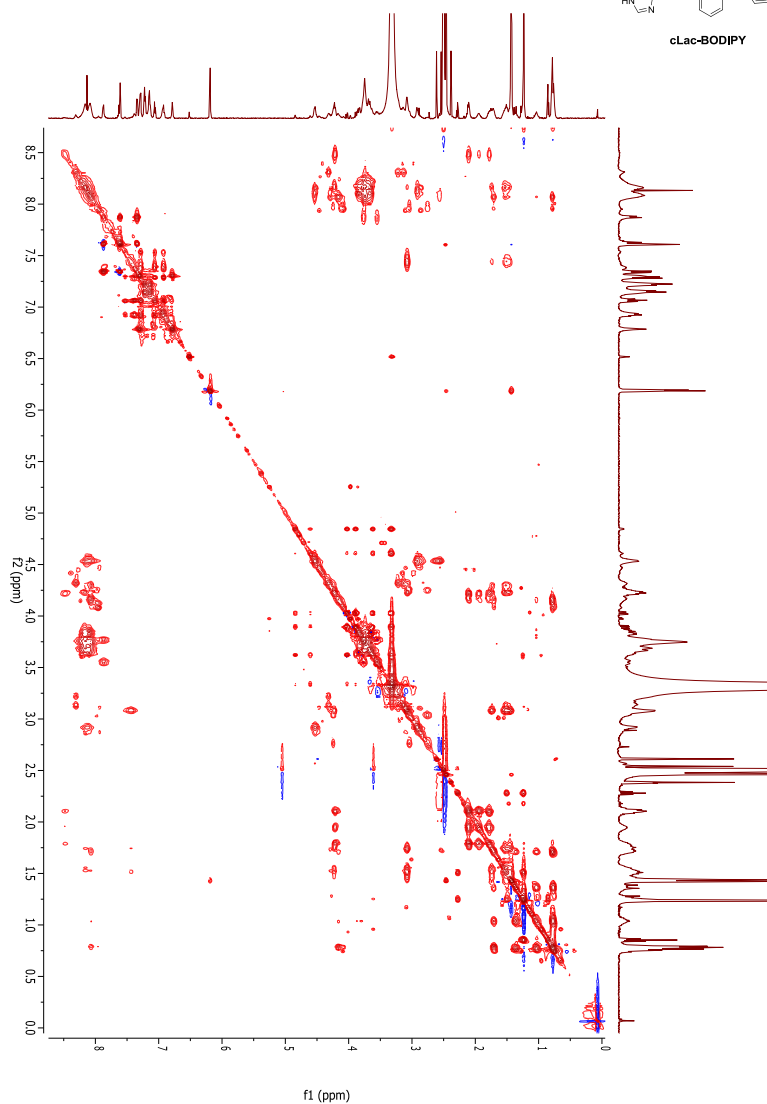
cLac-BODIPY

HSQC-NMR of **cLac-BODIPY**

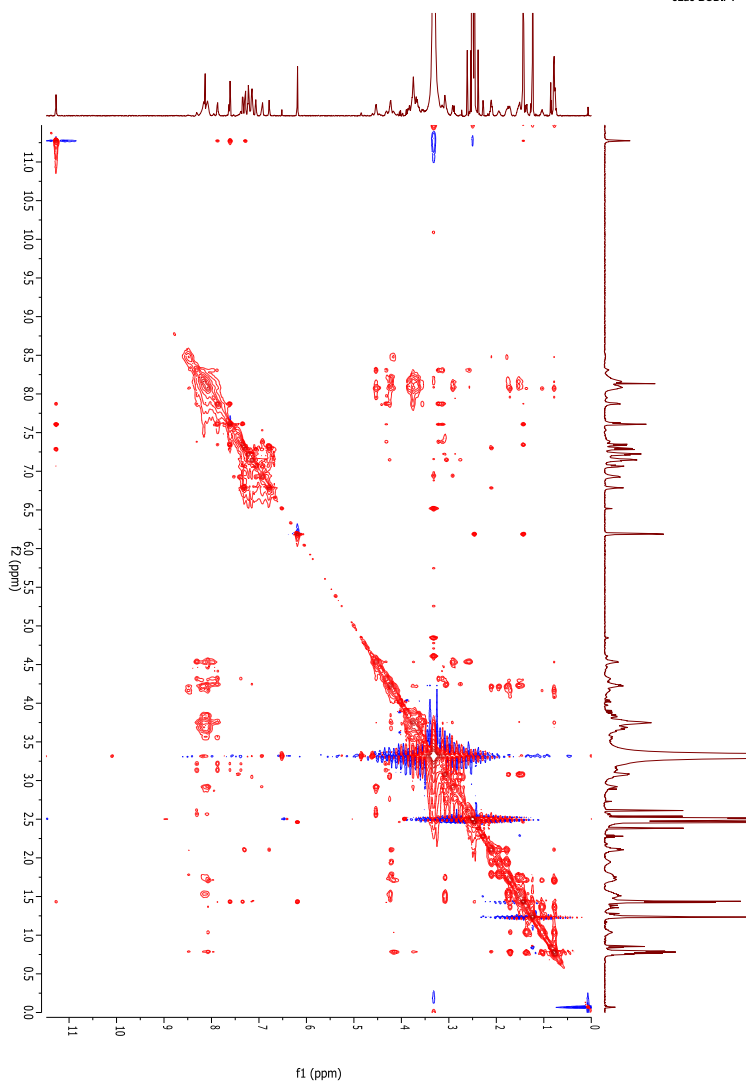
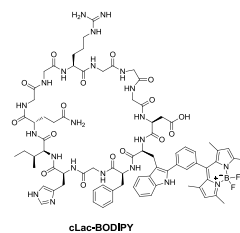
COSY-NMR of cLac-BODIPY



TOCSY-NMR of cLac-BODIPY



NOESY-NMR of cLac-BODIPY



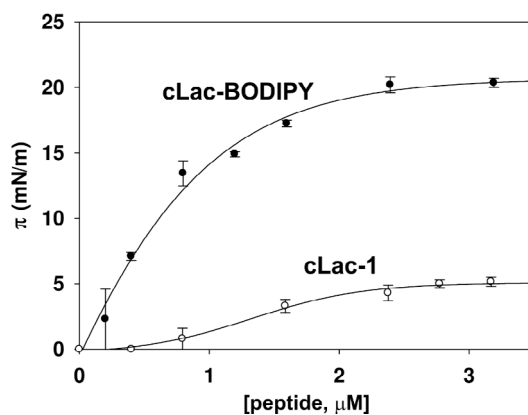
Selected Supplementary Figures

Figure S4. Determination of the tensioactivity of **cLac-1** and **cLac-BODIPY**. **cLac-BODIPY** shows high tensioactivity with a saturation pressure (π_s) of 20.4 mN m⁻¹ and a saturation concentration (C_s) of 3 μ M. The π_s for **cLac-1** is 5 mN m⁻¹. Values represented as means and error bars as SD ($n = 3$).

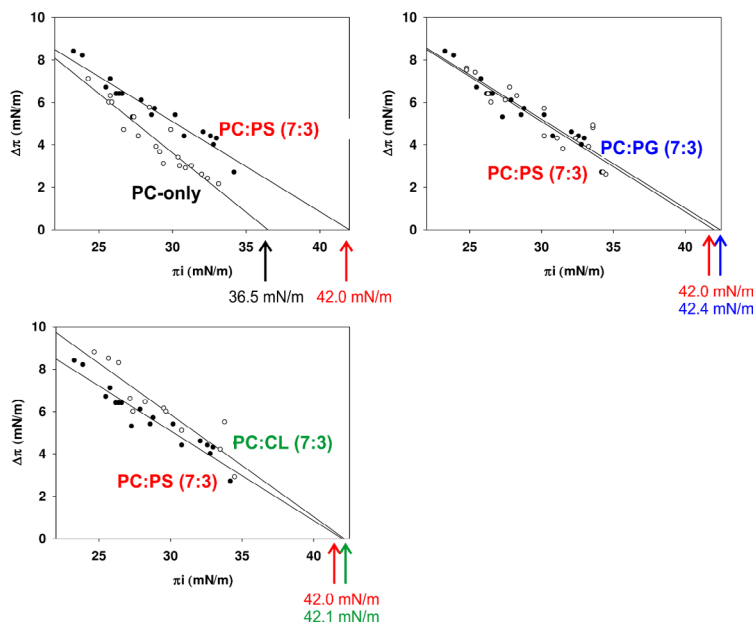


Figure S5. Quantitative binding assays of **cLac-BODIPY** to monolayers with variable lipid composition. Arrows point at the π_c values for every lipid composition. PC: phosphatidylcholine, PS: phosphatidylserine, PG: phosphatidylglycine, CL: cardiolipin. Values represented as means from $n = 3$.

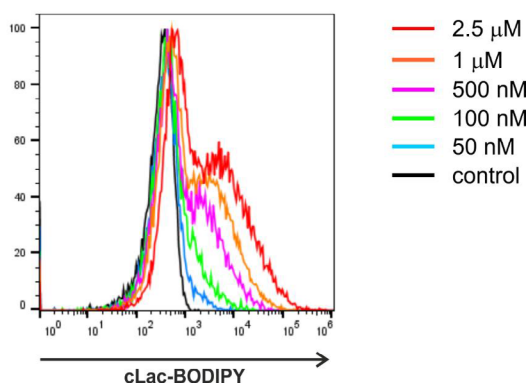


Figure S7. Flow cytometry analysis of the fluorescence labelling of apoptotic bodies after incubation with different concentrations of **cLac-BODIPY**.

PUBLICATION VI.

A Trp-BODIPY fluorogenic amino acid to label peptides for enhanced live-cell fluorescence imaging

Lorena Mendive-Tapia,^{#, a} Ramon Subiros-Funosas,^{#, b} Can Zhao,^{#, c} Fernando Albericio,^{a, d} Nick D. Read,^c Rodolfo Lavilla,^{d, e} and Marc Vendrell^b

[#]These authors contributed equally to this work.

Nature Protocols. Accepted for publication. Under editorial processing.

- a) Department of Inorganic and Organic Chemistry, University of Barcelona. Martí i Franquès 1-11, 08028 Barcelona, Spain.
- b) MRC/UoE Centre for Inflammation Research, The University of Edinburgh, 47 Little France Crescent, EH16 4TJ Edinburgh, United Kingdom.
- c) Manchester Fungal Infection Group, Division of Infection, Immunity and Respiratory Medicine, University of Manchester. CTF Building, Grafton St., M13 9NT Manchester, United Kingdom.
- d) Networking Centre for Bioengineering, Biomaterials and Nanomedicine (CIBER-BBN). Baldiri Reixac 10-12, 08028 Barcelona, Spain.
- e) Laboratory of Organic Chemistry, Faculty of Pharmacy, University of Barcelona, Barcelona Science Park, Baldiri Reixac 10-12, 08028 Barcelona, Spain.

A Trp-BODIPY fluorogenic amino acid to label peptides for enhanced live-cell fluorescence imaging

Lorena Mendive-Tapia,^{1,‡} Ramon Subiros-Funosas,^{2,‡} Can Zhao,^{3,‡} Fernando Albericio,^{1,4} Nick D. Read,³ Rodolfo Lavilla,^{4,5,*} Marc Vendrell^{2,*}

1. Department of Inorganic and Organic Chemistry, University of Barcelona. Martí i Franqués 1-11, 08028 Barcelona, Spain.

2. MRC/UoE Centre for Inflammation Research, The University of Edinburgh. 47 Little France Crescent, EH16 4TJ Edinburgh, United Kingdom. Tel: +44 1312426685. Fax: +44 1312426578. Website: www.dynafluors.co.uk. E-mail: marc.vendrell@ed.ac.uk

3. Manchester Fungal Infection Group, Division of Infection, Immunity and Respiratory Medicine, University of Manchester. CTF Building, Grafton St., M13 9NT Manchester, United Kingdom.

4. Networking Centre for Bioengineering, Biomaterials and Nanomedicine (CIBER-BBN). Baldiri Reixac 10-12, 08028 Barcelona, Spain.

5. Laboratory of Organic Chemistry, Faculty of Pharmacy, University of Barcelona, Barcelona Science Park. Baldiri Reixac 10-12, 08028 Barcelona, Spain. Tel: +34 934037106. E-mail: rlavilla@ub.edu.

‡ These authors contributed equally to the work.

Keywords: fluorescent probes, peptides, SPPS, microscopy, bioconjugation, unnatural amino acids.

Abstract

This protocol describes the preparation of the Trp-based fluorogenic amino acid Fmoc-Trp(C₂-BODIPY)-OH (**1**) and its incorporation into peptides for live-cell fluorescence imaging. The amino acid **1** contains a BODIPY core attached to Trp *via* a spacer-free C-C linkage, mimicking the molecular interactions of Trp while introducing a fluorogenic label for wash-free imaging. The amino acid **1** can be prepared in 3-4 d, and employed for the solid-phase synthesis of fluorogenic peptides (6-7 d). We have used this technology to prepare the fluorogenic antimicrobial peptide **BODIPY-cPAF26**, which shows high chemical stability and minimal disruption of cellular activity when compared to the unlabeled sequence (3-4 d). We used **BODIPY-cPAF26** for wash-free imaging of fungal pathogens, including real-time visualization of *Aspergillus fumigatus* (5 d culturing, 1-2 d imaging). One major advantage of this protocol is the applicability to most sequences, enabling the preparation of many peptide-based probes for enhanced fluorescence imaging.

INTRODUCTION

Peptides are excellent molecular frameworks for the generation of imaging agents because they bind with high affinity and specificity to their respective targets. However, most peptides cannot be directly visualized using fluorescence imaging as they lack proper reporter groups and need to be modified with fluorophores or reactive tags for further derivatization.¹ A milestone in peptide and protein labeling has been the development of genetically encoded unnatural amino acids, which can be incorporated in response to nonsense or frameshift codons to embed suitable bioorthogonal groups at specific sites of peptides and proteins.² Some of the recent advances in this field towards fluorescence imaging applications include the genetic encoding of norbornene amino acids, which can rapidly and specifically couple to tetrazine-containing fluorophores for protein labeling,³ or the optimization of orthogonal variants of the inverse-electron-demand Diels-Alder cycloaddition reaction for dual color live-cell imaging and super-resolution microscopy.^{4, 5}

In addition to synthetic biology strategies, many unnatural amino acids are available as building blocks to expand the chemical diversity within peptide sequences using solid-phase peptide synthesis (SPPS).^{6, 7} These include unnatural amino acids with chemical groups (e.g. azides, alkynes, alkenes) amenable for two-step labeling processes. Once peptides containing these amino acids are synthesized, they are coupled to a suitable fluorophore (for instance, using 'click' chemistry) and then the excess labeling agent is washed out prior to image acquisition. This approach has proven

useful for many different applications,⁸⁻¹¹ although the need for washing steps might hamper its translation to in vivo and real-time imaging. Recent progress in the preparation of bioorthogonal fluorophores has rendered labels with bright fluorescence emission after the conjugation reaction to reduce fluorescence background and minimize the washing steps.¹²⁻¹⁴ Moreover, further development of synthetic methodologies to diversify amino acids and peptides¹⁵⁻¹⁷ will create opportunities for direct fluorescence labeling and in situ imaging studies.

Most commonly, peptides are readily labeled by attaching a fluorophore to a residue in the peptide sequence, yielding fluorescent conjugates that can be directly used for imaging. However, fluorophores are bulky structures and can impair the molecular recognition properties of the native peptide, therefore it is important to introduce them at appropriate positions within the sequence. Most fluorophores are incorporated into peptides by reaction with terminal or side-chain chemical groups (e.g. amines, carboxylic acids, thiols) from polar residues or through chemical spacers.¹⁸⁻²⁰ Because these modifications can disrupt the hydrogen bonding pattern of the original peptide and have a detrimental effect on the biological properties of the fluorescent conjugate,²¹ there is a demand for new technologies to incorporate fluorophores into peptides without affecting their inherent activity and, ideally, with suitable spectral properties for live-cell imaging applications.

Overview of the procedure.

A schematic flowchart outlining the procedures described in this protocol and their expected timing is shown in Figure 1. We have developed a new methodology to synthesize fluorogenic peptides that relies on a unique Fmoc-Trp(C₂-BODIPY)-OH amino acid (**1**),²² which can be prepared by attaching a BODIPY fluorophore to the C₂ position of Trp *via* a spacer-free C-C linkage (Steps 1-35). The amino acid **1** mimics the molecular interactions of the native Trp while introducing a convenient fluorogenic label for live-cell imaging. The fluorogenic amino acid **1** shows high chemical stability (Steps 36-37), excitation and emission spectra in the visible range, and remarkable fluorescence enhancement in hydrophobic environments (i.e. when the peptide is binding to its target), which facilitates wash-free imaging experiments. We have validated the amino acid **1** to prepare peptide-based imaging probes by derivatizing the antimicrobial peptide PAF26,²³ which shows high affinity and selectivity for fungal cells. We synthesized the fluorogenic analogue of PAF26 (**BODIPY-cPAF26**) by conventional SPPS, simply using the amino acid **1** instead of the natural Trp (Steps 38-89). The **BODIPY-cPAF26** peptide shows high resistance to proteolysis (Steps 90-94), strong fluorogenic response in hydrophobic environments (Steps 95-106) and no impairment of the activity and selectivity of the native peptide in human and fungal cells (Steps 107-131 and 132-162). Finally,

we used **BODIPY-cPAF26** for fluorescence live-cell imaging of several fungal pathogens (Steps 163-206) and real-time imaging of *Aspergillus fumigatus* (Steps 207-219), one of the most life-threatening human fungal pathogens.

Figure 1.

Advantages and limitations of the procedure.

A major advantage of this procedure is its general applicability as it can be used to prepare fluorogenic analogues of most peptide sequences. The amino acid **1** is compatible with Fmoc-based SPPS protocols, tolerates standard deprotection and coupling conditions as well as mild acid-based deprotection strategy without observing degradation of the BODIPY fluorophore.^{24, 25} Notably, careful design of the protecting group scheme is needed to ensure full orthogonality with the BODIPY structure [e.g. in the synthesis of **BODIPY-cPAF26**, we used Fmoc-Lys(Z)-OH instead of Fmoc-Lys(Boc)-OH and Fmoc-Arg(NO₂)-OH instead of Fmoc-Arg(Pbf)-OH]. Besides, the exact impact of the Trp-BODIPY on the biomolecular properties of the labeled peptides needs to be examined on a case-by-case basis, although most of the bioactive peptides examined so far have shown similar activity patterns between labeled and non-labeled sequences.²²

Regarding the spectral properties, the amino acid **1** has both excitation and emission maximum wavelengths in the green region of the visible spectra ($\lambda_{\text{exc.}} \sim 500 \text{ nm}$, $\lambda_{\text{em.}} \sim 520 \text{ nm}$), being ideally suited for conventional GFP/FITC filters found in most spectrophotometers, flow cytometers, confocal microscopes and other imaging equipment. This is an important advantage over naphthalene, coumarin and dansyl-based fluorescent amino acids for SPPS,²⁶⁻²⁹ which display shorter excitation and emission wavelengths with relatively long Stokes shifts. Extensive work in this field has been performed by Imperiali and co-workers, who developed environmentally-sensitive fluorescent amino acids as reporters of protein-protein interactions.³⁰⁻³³ These amino acids are mostly based on the naphthalimide scaffold, with remarkable fluorescence enhancements in hydrophobic environments, excitation wavelengths around 400-450 nm and extinction coefficients around 10^3 to $10^4 \text{ M}^{-1} \text{ cm}^{-1}$.^{34, 35} Whereas the emission enhancement of the amino acid **1** might be slightly lower than for naphthalimide-based amino acids, its high extinction coefficient (i.e. around one order of magnitude higher) results in overall stronger brightness. The strong fluorogenic behaviour of the amino acid **1** core enables the use of the labeled peptides directly for live-cell imaging in wash-free conditions and without any additional labeling steps, unlike peptides containing unnatural amino

acids with reactive orthogonal groups. This represents a major advantage for imaging experiments where dynamic processes in living cells need to be monitored in real time.

This procedure is currently limited to preparing fluorogenic peptides or small proteins that are accessible via semi-synthetic approaches or by SPPS. Future investigation will be necessary to incorporate the amino acid **1** into full-length proteins using the ribosomal machinery (e.g. chemical acylation of suppressor tRNA, exploitation of orthogonal tRNA/aminoacyl-tRNA synthetase pairs).

Experimental design and crucial parameters.

Fmoc-Trp(C₂-BODIPY)-OH: chemical synthesis, fluorescence properties and shelf life.

We designed the synthesis of the amino acid **1** as the Fmoc-protected compound so that it could be readily used for the synthesis of medium-sized peptides by conventional SPPS. The BODIPY fluorophore was selected because of its compact structure and excellent spectral photophysical properties,^{36,37} and was incorporated into the C₂ position of Trp in a spacer-free C-C linkage to maintain the main recognition features of the labeled peptides (e.g. charge balance, overall polarity, H-bond pattern). The retrosynthetic analysis of the amino acid **1** involves the arylation of the *m*-iodophenyl-BODIPY (**3**) on the unsubstituted C₂ position of Fmoc-Trp-OH (**2**) by Pd-catalyzed C-H activation³⁸⁻⁴⁰ using our recently developed methodology (Figure 2).¹⁶ The *m*-iodophenyl-BODIPY (**3**) can be prepared by acid-catalyzed condensation of the *m*-iodobenzaldehyde (**4**) with two equivalents of 2,4-dimethylpyrrole (**5**), followed by DDQ oxidation and BF₃ complexation. Notably, all the starting materials needed for the synthesis of the amino acid **1** (i.e. compounds **2**, **4** and **5**) are commercially available.

Figure 2.

Following similar reported procedures,⁴¹ compounds **4** and **5** were mixed under TFA catalysis to yield the expected adduct with loss of a water molecule after stirring at r.t. for 22 h in anhydrous DCM (Note: in our hands, the synthetic yields did not significantly improve in the presence of dehydrating agents, such as 4Å molecular sieves). Next, DDQ was added to the crude mixture with continuous stirring for 15 min, followed by addition of an excess of Et₃N and BF₃·Et₂O. The resulting dark green solution was stirred at r.t. for 4.5 h to render compound **3** as the major product in a crude form. Liquid-liquid extraction followed by flash chromatography over silica gel afforded the compound **3** with synthetic yields (over the 3 steps) around 30%. Of note, we observed slightly lower synthetic yields when this reaction was scaled up over 200 mg scale. Next, the *m*-iodophenyl-

BODIPY **3** was subjected to Pd-catalyzed arylation of Fmoc-Trp-OH (**2**) to afford the desired Fmoc-Trp(C₂-BODIPY)-OH (**1**) (Figure 3a).⁴²⁻⁴⁴ The amino acid **2**, a slight excess of *m*-iodophenyl-BODIPY **3** (1.5 eq.), AgBF₄ (1.0 eq.), TFA (1.0 eq.) as the acid source, and catalytic Pd(OAc)₂ (0.05 eq.) were dissolved in DMF and subjected to microwave irradiation for 20 min at 80 °C. The amino acid **1** was isolated by normal-phase chromatography over silica gel with synthetic yields around 70 %. Initial attempts to scale-up this reaction resulted in decreased recovery yields, however parallelization of the procedure is convenient and reproducible. Notably, transformations under conventional heating require higher temperatures and lead to more complex crude mixtures, due to the limited stability of the Fmoc and BODIPY groups under these conditions.

Figure 3.

The amino acid **1** displays excitation and emission maximum wavelengths in the green region of the visible spectra ($\lambda_{\text{exc.}}$: 503 nm, $\lambda_{\text{em.}}$: 517 nm) (Figure 3b). These spectral properties are optimal for its use in most spectrophotometers, flow cytometers and confocal microscopes, since these are generally equipped with excitation sources and emission filters matching the spectral properties of GFP or FITC ($\lambda_{\text{exc.}}$ ~ 490 nm, $\lambda_{\text{em.}}$ ~ 520 nm). Furthermore, we examined the chemical integrity of the amino acid **1** in different conditions to determine the optimal storage conditions as well as its shelf life (Figure 3c and Supplementary Figures 1-2). The amino acid **1** is completely stable when stored in the dark as a solid, even at r.t., for up to 4 months (i.e. this was the longest time point measured at the time of submission). We also examined its chemical integrity in DCM, MeOH and DMF as common solvents used in peptide synthesis. The amino acid is fully stable in solutions of DCM and MeOH for up to 4 months, but loses the Fmoc group when it is stored in DMF for long periods of time at r.t. (13% degradation after 1 month, 45% after 2 months and 93% after 4 months), in agreement with previous reports on the stability of Fmoc-protected amino acids.⁴⁵ Altogether, these results confirm that the amino acid **1** can be shipped and employed as most Fmoc-protected amino acids, and even stored for several months in DMF at 4 °C or -20 °C.

Fluorogenic antimicrobial peptides: solid-phase synthesis, fluorogenic behaviour and biological characterization.

Fluorescent antimicrobial peptides are promising tools for imaging infectious pathogens, given their selectivity for microbes over mammalian cells.^{46, 47} Our group and others have studied the mechanism of action of Peptide AntiFungal 26 (PAF26), an antimicrobial hexapeptide with high affinity for fungal cells. PAF26 (H-RKKFW-NH₂) has a short and conserved sequence with hydrophobic and cationic domains that are indispensable for its cellular activity.⁴⁸ We envisioned that fluorogenic PAF26 analogues in which the natural Trp was replaced by the amino acid **1** would retain the activity and selectivity of the original sequence for fungal cells while incorporating a suitable label for fluorescence imaging. Furthermore, since cyclic peptides show increased resistance to proteases⁴⁹ (such as those secreted by infective pathogens), we designed the synthesis of a cyclic fluorogenic peptide (**BODIPY-cPAF26**, Figures 4 and 5a) based on the sequence of PAF26. **BODIPY-cPAF26** was synthesized using 2-chlorotrityl polystyrene resin and Fmoc-based SPPS protocols (Figure 4).

Figure 4.

As building blocks, we used the amino acid **1** as well as Fmoc-Gly-OH, Fmoc-Phe-OH, Fmoc-Trp-OH, Fmoc-Lys(Z)-OH and Fmoc-Arg(NO₂)-OH, which are fully orthogonal to the mildly acidic cleavage conditions [TFA: DCM (1: 99)] and enabled the isolation of the fully protected cyclic peptide without damaging the BODIPY core. In the synthesis of **BODIPY-cPAF26**, we incorporated all the amino acids (3 eq.) using conventional DIC and OxymaPure, whereas the amino acid **1** was introduced using a moderate excess (1.5 eq.), and PyBOP, HOBt and DIPEA as coupling reagents. The acidic cleavage rendered the protected linear peptide, which was cyclized by treatment with DIPEA and HATU in DMF with over 80% yields after precipitation in H₂O. Final hydrogenolysis and purification by semi-preparative HPLC afforded the **BODIPY-cPAF26** peptide in very high purities (> 99%). Typically, the overall yields for the synthesis of the peptide **BODIPY-cPAF26** are around 20-25% (~10 mg product per ~45 mg of resin).

Next, we compared the antimicrobial activity of PAF26 and **BODIPY-cPAF26**, and determined their IC₅₀ values in two different fungal species (*Neurospora crassa* and *Aspergillus fumigatus*). *N. crassa* is an experimental model organism for filamentous fungi,⁵⁰ whereas *A. fumigatus* is a fungal pathogen related to multiple human diseases, the most lethal of which is invasive pulmonary aspergillosis (IPA) with around 200,000 deaths per year.⁵¹ Notably, **BODIPY-cPAF26** did not

impair the antifungal activity of the original sequence, with slightly higher affinity for both fungal species than the unlabeled PAF26 peptide (Figure 5b and Supplementary Table 1). We also examined the fluorescence response of **BODIPY-cPAF26** in phospholipid liposomes mimicking the microenvironments in cell membranes. Fluorescence spectra of **BODIPY-cPAF26** were recorded upon incubation with liposome suspensions of phosphatidylcholine (PC): cholesterol (7: 1) in phosphate buffer saline (PBS) with increasing concentrations of PC. As shown in Figure 5c, **BODIPY-cPAF26** displayed strong fluorogenic behavior, with quantum yields slightly over 30% after binding to phospholipid membranes (Supplementary Table 2). Finally, we evaluated the cytotoxicity of **BODIPY-cPAF26** in A549 lung epithelial cells as an indication of their poor affinity for human cells. We did not detect significant differences in the viability of A549 cells with or without incubation of **BODIPY-cPAF26** for several hours, even at relatively high concentrations (Figure 5d). Altogether, these results corroborate the suitability of the fluorogenic amino acid **1** as a Trp surrogate with minimal interference in the recognition properties of peptide sequences, while providing a suitable reporter to visualize molecular interactions using fluorescence-based techniques.

Figure 5.

Because imaging infection sites using peptide-based probes can be hindered by the presence of proteolytic enzymes, we examined the chemical integrity of **BODIPY-cPAF26** in proteolytic environments, and compared its degradation to the unlabeled PAF26. Both peptides were incubated at the same concentration in a protease cocktail for over 24 h, and time-course analysis was performed by HPLC-MS. Being a cyclic peptide, **BODIPY-cPAF26** showed high stability to proteases, with marginal degradation after 24 h incubation (Supplementary Figures 3-4). In the same experimental conditions, the unlabeled linear peptide PAF26 was mostly degraded with only 20% of intact peptide left after 24 h.

Live-cell fluorescence imaging of fungal pathogens, including *A. fumigatus*.

In view of the excellent properties of **BODIPY-cPAF26** as a highly stable and fluorogenic peptide to report the interaction with fungal cells, we employed it for live-cell imaging in different fungal species. In addition to *N. crassa* and *A. fumigatus*, we also examined the staining of **BODIPY-cPAF26** in other fungal pathogens, namely *Cryptococcus neoformans*, *Fusarium oxysporum* and *Candida albicans*. **BODIPY-cPAF26** showed bright staining in all the species, suggesting a potential common target for different fungi (Figure 6). Notably, the fluorogenic behaviour of **BODIPY-cPAF26** enables live-cell imaging by simple incubation with the cells, in a single step and

without the need for any washing protocols. This procedure represents an important advantage over imaging procedures with fluorescent peptides that are labeled using alternative procedures (e.g. ‘click’ fluorophores used in two-step labeling procedures, ‘always-on’ fluorophores that require washing).

Figure 6.

Since *A. fumigatus* is the fungal pathogen responsible for IPA, a life-threatening disease in immunocompromised patients,⁵¹ we performed further studies to visualize the dynamic interaction between **BODIPY-cPAF26** and living cells of *A. fumigatus*. Germlings of *A. fumigatus* were pre-incubated with a red fluorescent probe that first stained the whole plasma membrane and then intracellular vacuoles. Before the red membrane stain was internalized, we added **BODIPY-cPAF26** to the cells and acquired time-course fluorescence images at high magnification to overlay the green signal from **BODIPY-cPAF26** and the red signal from the counterstain (Figure 7 and Supplementary Video 1). After 20 seconds of its addition, **BODIPY-cPAF26** stained the plasma membrane in the apical region of the germling cells. In the following minutes, the green fluorescence signal moved towards the base of the germling, while the red counterstain started to accumulate in intracellular vacuolar organelles. These results validate our procedure using the amino acid Fmoc-Trp(C₂-BODIPY)-OH (**1**) as an efficient chemical strategy to prepare fluorogenic peptides for enhanced fluorescence live-cell imaging without any washing steps. As a proof-of-concept, we have synthesized **BODIPY-cPAF26** as a stable, cyclic antimicrobial peptide for imaging dynamic processes in living fungal pathogens.

Figure 7.

MATERIALS

! CAUTION All organic solvents and bases are flammable, toxic and harmful by inhalation, ingestion or skin contact. Coupling reagents and additives are flammable and irritant. For these and other toxic, corrosive and/or irritant reagents, laboratory coat, gloves and safety goggles should be worn. All synthetic operations should be performed in a chemical fume hood.

REAGENTS

- Deionized water (dH₂O)
- Sterile water (Baxter, cat. no. UKF7114, stored at r.t.) (r.t.: 20-25 °C)
- Celite (Sigma-Aldrich, cat. no. 22138, stored at r.t.)
- Silica gel 60 Å (Carlo Erba, cat. no. P2000027, stored at r.t.)
- 2-Chlorotriyl chloride polystyrene resin (2-CTC-PS; Iris Biotech GMBH, cat. no. BR-1060, stored at r.t.)
- Dichloromethane (DCM; Scharlab, cat. no. CL0331, stored at r.t.)
- Anhydrous dichloromethane (DCM_{anh}; Sigma-Aldrich, cat. no. 494453, stored at r.t.)
- Hexane (Scharlab, cat. no. HE0228, stored at r.t.)
- Toluene (J.T. Baker, cat. no. 8078, stored at r.t.)
- Ethyl acetate (AcOEt; Scharlab, cat. no. AC0143, stored at r.t.)
- *N,N*-Dimethylformamide (DMF; Panreac Applichem, cat. no. 161785.1612, stored at r.t.)
- Anhydrous *N,N*-Dimethylformamide (DMF_{anh}; Sigma-Aldrich, cat. no. 227056, stored at r.t.)
- *N,N*-Diisopropylethylamine (DIPEA; Sigma-Aldrich, cat. no. 496218, stored at r.t.)
- *N_ε*-(9-Fluorenylmethyloxycarbonyl)-L-glycine (Fmoc-Gly-OH; Iris Biotech GMBH, cat. no. FAA1050, stored at 4 °C)
- *N_ε*-(9-Fluorenylmethyloxycarbonyl)-L-tryptophan (Fmoc-Trp-OH; Sigma-Aldrich, cat. no. 47637, stored at 4 °C)
- *N_ε*-(9-Fluorenylmethyloxycarbonyl)-L-phenylalanine (Fmoc-Phe-OH; Iris Biotech GMBH, cat. no. FAA1175, stored at 4 °C)
- *N_ε*-(9-Fluorenylmethyloxycarbonyl)-*N_ε*-(benzyloxycarbonyl)-L-lysine (Fmoc-Lys(Z)-OH; Sigma-Aldrich, cat. no. 47577, stored at 4 °C)
- *N_ε*-(9-Fluorenylmethyloxycarbonyl)-*N_ε*-(nitro)-L-arginine (Fmoc-Arg(NO₂)-OH; Sigma-Aldrich, cat. no. 47527, stored at 4 °C)
- Methanol (MeOH; Sigma-Aldrich, cat. no. 65542, stored at r.t.)
- Acetonitrile (ACN; Scharlab, cat. no. AC0333, stored at r.t.)
- Formic acid (FA; Merck Millipore, cat. no. 100264, stored at r.t.)
- Trifluoroacetic acid (TFA; Fluorochem, cat. no. 001271, stored at r.t.) **! CAUTION** Toxic and corrosive
- Piperidine (Carlo Erba; cat. no. P0660216, stored at r.t.)
- Ethyl (hydroxyimino)cynoacetate (OxymaPure; Luxembourg Bio Technologies, stored at r.t.)
- (Benzotriazol-1-yloxy)tripyrrolidinophosphonium hexafluorophosphate (PyBOP; Novabiochem, cat. no. 8510090, stored at 4 °C)
- 1-Hydroxybenzotriazole (HOBt; Carboxynth, cat. no. FH02087, stored at 4 °C) **! CAUTION** Explosive, if dry. Always use as the monohydrate form and keep away from heat sources.
- (1-[Bis(dimethylamino)methylene]-1H-1,2,3-triazolo[4,5-b]pyridinium 3-oxid hexafluorophosphate) (HATU; Fluorochem, cat. no. 023926, stored at 4 °C) **! CAUTION** Irritant
- Palladium hydroxide on activated charcoal (Pd(OH)₂-C; Sigma-Aldrich, cat. no. 76063, stored at r.t.)
- 3-Iodobenzaldehyde (Apollo Scientific, cat. no. OR8221, stored at 4 °C) **! CAUTION** Irritant
- 2,4-Dimethylpyrrole (Sigma-Aldrich, cat. no. 390836, stored at 4 °C) **! CAUTION** Irritant
- 2,3-Dichloro-5,6-dicyano-*p*-benzoquinone (DDQ; Sigma-Aldrich, cat. no. D60400, stored at 4 °C) **! CAUTION** Toxic
- Triethylamine (TEA; Sigma-Aldrich, cat. no. T0886, stored at r.t.)
- Boron trifluoride diethyl etherate (BF₃·OEt₂; Sigma-Aldrich, cat. no. 175501, stored at 4 °C) **! CAUTION** Flammable, toxic and corrosive
- Anhydrous sodium sulfate (Na₂SO₄_{anh}; Panreac Applichem, cat. no. 191716.1211, stored at r.t.)
- Palladium acetate (Pd(OAc)₂; Sigma-Aldrich, cat. no. 205869, stored at r.t.) **! CAUTION** Irritant and causes skin corrosion
- Silver tetrafluoroborate (AgBF₄; Sigma-Aldrich, cat. no. 208361, stored at r.t.) **! CAUTION** Corrosive and harmful.
- Ethanol absolute (VWR, cat. no. 20821.330, stored at r.t.)
- Sodium phosphate dibasic heptahydrate (Sigma Aldrich, cat. no. S9390, stored at r.t.)
- Citric acid monohydrate (Sigma Aldrich, cat. no. C-1909, stored at r.t.)
- Sodium hydroxide (Fisher, cat. no. S/4840/60, stored at r.t.)
- *N,N'*-Diisopropylcarbodiimide (DIC; Sigma-Aldrich, cat. no. D125407, stored at 4 °C)
- Fluorescein (Sigma-Aldrich, cat. no. 32615, stored at r.t.)
- Protease from *Streptomyces Griseus* type XIV (Sigma Aldrich, cat. no. P5147, stored at -20 °C)
- PAF26 peptide (H-RKKWFW-NH₂; Genscript, lot no. P10271403, stored at 4 °C)
- Dimethyl sulfoxide for molecular biology (Sigma Life Sciences, cat. no. D8418, stored at r.t.)
- Dulbecco's Phosphate Buffered Saline (DPBS; Gibco, Life Technologies, cat. no. 14040-091, stored at r.t.)
- MTT reagent (Trevigen, MTT Cell Proliferation assay kit, cat. no. 4890-25-01; stored at 4 °C)
- Detergent reagent for MTT assay (Trevigen, MTT Cell Proliferation assay kit, cat. no. 4890-25-02, stored at r.t.)
- RPMI Cell Media 1640 (Gibco, Life Technologies, cat. no. 31870-025, stored at 4 °C)
- Phosphatidylcholine: cholesterol (7: 1) liposomes (Clodronate Liposomes, 10 mL PBS liposomes, stored at 4 °C)
- Heat inactivated Fetal Bovine Serum (FBS; Gibco Life Technologies, cat. no. 10500-064, stored at -20 °C)
- Penicillin-Streptomycin (Pen Strep; Gibco Life Technologies, cat. no. 15140-122, stored at -20 °C)
- L-Glutamine (L-Glu; Gibco Life Technologies, cat. no. 25030-024, stored at -20 °C)
- 0.05% (w/v) Trypsin-EDTA (Gibco Life Technologies, cat. no. 25300-054, stored at -20 °C)
- Sucrose (Sigma-Aldrich, cat. no. S0389, stored at r.t.)
- Oxoid™ Agar technical (Thermo Fisher Scientific, cat. no. LP0013B, stored at r.t.)
- Sodium citrate dihydrate (Sigma-Aldrich, cat. no. 71402, stored at r.t.)
- Potassium phosphate monobasic (KH₂PO₄; Sigma-Aldrich, cat. no. P5655, stored at r.t.)
- Ammonium nitrate (NH₄NO₃; Fluka, cat. no. A9642, stored at r.t.)
- Magnesium sulfate heptahydrate (MgSO₄ · 7 H₂O; Sigma-Aldrich, cat. no. M2773, stored at r.t.)
- Calcium chloride dihydrate (CaCl₂ · 2H₂O; Sigma-Aldrich, cat. no. C3306, stored at r.t.)
- Citric acid (Sigma-Aldrich, cat. no. P5655, stored at r.t.)

- Zinc sulfate heptahydrate ($\text{ZnSO}_4 \cdot 7 \text{H}_2\text{O}$; Sigma-Aldrich, cat. no. Z0251, stored at r.t.)
- Ammonium iron (II) sulfate hexahydrate ($(\text{NH}_4)_2\text{Fe}(\text{SO}_4)_2 \cdot 6 \text{H}_2\text{O}$; Sigma-Aldrich, cat. no. 09719, stored at r.t.)
- Copper (II) sulfate pentahydrate ($\text{CuSO}_4 \cdot 5 \text{H}_2\text{O}$; Sigma-Aldrich, cat. no. C8072, stored at r.t.)
- Manganese (II) sulfate monohydrate ($\text{MnSO}_4 \cdot \text{H}_2\text{O}$; Sigma-Aldrich, cat. no. M7899, stored at r.t.)
- Boric acid (H_3BO_3 ; Sigma-Aldrich, cat. no. B6768, stored at r.t.)
- Sodium molybdate dihydrate ($\text{Na}_2\text{MoO}_4 \cdot 2 \text{H}_2\text{O}$; Sigma-Aldrich, cat. no. M1651, stored at r.t.)
- D-biotin (SUPELCO, cat. no. 47868, stored at 4 °C)
- UltraPure™ Glycerol (Thermo Fisher Scientific, cat. no. 15514011, stored at r.t.)
- Oxoid™ Sabouraud (SAB) dextrose liquid medium (Thermo Fisher Scientific, cat. no. CM0147, stored at r.t.)
- Oxoid™ Sabouraud dextrose agar (Thermo Fisher Scientific, cat. no. CM0041, stored at r.t.)
- Oxoid™ Potato dextrose agar (PDA; Thermo Fisher Scientific, cat. no. CM0139, stored at r.t.)
- Potato dextrose broth (PDB; CONDA, cat. no. 1261, stored at r.t.)
- Tween80 (Sigma-Aldrich, cat. no. P4780, stored at r.t.)
- Red counter stain (TMR-PAF96, TAMRA-AAAWFW-NH₂; Genscript, stored at 4 °C)
- High level disinfectant (Chemgene HLD₄L, stored at r.t.)
- A549 cells (ATCC, cat. no. A549-ATCC CCL-185, stocks stored at -80 °C or -125 °C)
- Fungal cells: *Neurospora crassa* (strain 74-OR23-1V A, source: FGSC 2489), *Aspergillus fumigatus* (strain CEA10, source: FGSC A1163), *Cryptococcus neoformans* (strain H99, source: FGSC 9487), *Fusarium oxysporum* (strain 4287, source: FGSC 9935).

LABWARE AND EQUIPMENT

- Set of micropipettes (200-1000, 20-200 and 2-20 µL, Gilson)
- Pipette disposable universal tips (5-200 and 100-1000 µL, Daslab)
- Teflon stick
- 6 mL polystyrene syringes cartridge with polyethylene porous disc (Agilent technologies)
- Spatula
- Timer
- 50 mL polypropylene centrifuge tubes with screwcaps (VWR)
- 15 mL polypropylene conical tubes (Corning)
- 75 cm² polystyrene cell culture flasks with canted neck (Corning, cat. no. 430720U)
- 50 mL polystyrene disposable pipette basins (Fisherbrand, cat. no. 13-681-502)
- Pipet aid PIPETBOY acu 2 (Integra, cat. no. 155000)
- 96-well tissue culture plates, black, flat bottom with lid (Falcon, cat. no. 353376)
- 96-well cell culture plates, flat bottom with low-evaporation lid, polystyrene (Costar, cat. no. 3595)
- Plastic syringes (Terumo or BD Plastipak, hypodermic Syringes without needle)
- Needles (BD Microlance, 21 G)
- 1.5 mL microcentrifuge tubes (VWR)
- Plastic (Agilent technologies) and Teflon (Biotage) stopcocks
- Glass vials (7 x 50 mm, VWR)
- Filters (0.45 µm, PVDF hydrophilic) (Millipore)
- Latex (VWR) or nitrile gloves (GEN-X, Kisher Biotech)
- Plastic septa (Φ 14.9 mm and Φ 30.7 mm, Saint-Gobain Performance Plastics)
- Parafilm
- Round-bottom flasks
- Plastic funnels
- Separatory funnels
- Conical flasks
- Glass Pasteur pipettes (VWR)
- Plastic Pasteur pipettes (VWR)
- Cotton
- Stirring bars
- Aluminium TLC plates (Silica gel 60 F₂₅₄ 20 × 20 cm, Merck KGaA)
- Fritted glass funnels (Φ 55 mm, grade 4, Duran)
- Adapter flask funnels
- 10 mL capped reaction vessels (CEM, cat. no. 19.909050)
- CEM Discover SP microwave synthesizer with Synergy software (CEM)
- RediSep R_f frits for RediSep 25 g cartridges (Teledyne ISCO, cat. no. 60-5237-053)
- Syringe filters (25 mm polypropylene 0.45 µm, Phenex, cat. no. AF7-1101-12)
- Columns for ISCO flash chromatography: Silica HP RediSep R_f 40 g flash columns, cat. no. 69-2203-347; Silica HP RediSep R_f 30 g flash column, cat. no. 69-2203-345 (Teledyne ISCO)
- 60 mL polystyrene syringe cartridge with polyethylene porous disc for flash chromatography (Agilent technologies)
- CombiFlash purification system (Teledyne ISCO)
- Rotary evaporator (Laborota 4003, Heidolph)
- Analytical balance (AB204-S, Mettler Toledo)
- Orbital platform shaker (Unimax 1010, Heidolph)
- Magnetic stirrer (IKA RCT Basic S1 Werke Safety Control Magnetic Hotplate Stirrer)
- UBD heating block (Grant)
- pH-meter (CyberScan pH 510, Eutech)
- Thermoblock shaker (Eppendorf Thermomixer)
- Vortex mixer (BV1000, Benchmark Scientific)
- Multichannel electronic pipette (Rainin E4 XLS 12-channel, 20-200 µL LTS, Mettler-Toledo)
- Multichannel electronic pipette tips (Rainin Tips LTS, 200 µL, GP-L200F, Mettler-Toledo)

- Cell counter (ChemoMetec A/S, Nucleocounter)
- Lyophilizer (Virtis Freezemobile)
- Centrifuge for peptide synthesis (Beckman Allegra 21R)
- Centrifuge for cell culture (Sanyo Mistrall 3000i)
- Sonicator (Clifton Ultrasonic bath)
- Water bath (Aqualine AL18, Lauda)
- Vacuum pump
- High-performance liquid chromatography system (HPLC): Waters 2695 separations module, Waters 2996 photodiode array detector
- HPLC system coupled to mass spectrometer (HPLC-MS): Waters 2695 separations module, Waters 2996 photodiode array detector. The MS spectrometer contains an electrospray ionization source (Micromass ZQ) and the MassLynx 4.1 software.
- Semi-preparative HPLC: Waters 2707 autosampler, Waters 2489 detector, Waters fraction collector III and software ChromeScope.
- HPLC vials (300 μ L polypropylene plastic, Waters)
- Nuclear Magnetic Resonance spectrometers (NMR): Varian Mercury 400 MHz or Bruker Avance III 600 MHz
- High-resolution mass spectrometer (HRMS): LTQ-FT Ultra (Thermo Scientific)
- Class-II microbiological safety cabinet (Biomat2)
- Synergy H1 hybrid spectrophotometer (Gen5 2.01 analysis software, Biotek).
- Cell incubator (Panasonic Incusafe)
- Inverse microscope (Olympus CK2)
- Cell culture flasks (TC Flask T25 stand, Vent. Cap, SARSTEDT, cat. no. 83.3910.002)
- Inoculation loop (10 μ L, blue, sterile, Greiner bio-one, cat. no. 731171)
- Glass flat bottom flasks (250 mL, PYREX®)
- Foam plug for flask (50 \times 38 mm, King Scientific, cat. no. FS5038)
- 8-well chamber (μ -Slide, ibiTreat, V2.0, sterilized, ibidi GmbH, cat. no. 80826)
- Miracloth (Merck Calbiochem, cat. no. 475855)
- Sterile disposable Petri dishes (9 cm, Thermo Scientific, cat. no.101IRR)
- Haemocytometer (Profondeur, 0.200 mm, 0.0625 mm², Fuchs-Rosenthal, SUPERIOR MARIENFELD)
- Lens cleaning tissue (Whatman105, 100 \times 150 mm, GE Healthcare, cat. no. 2105-841)
- Aluminum foil (45 cm, Terinex)
- 3M Micropore surgical-tape (Micropore)
- TriStar LB941 multimode microplate reader (BertholdTech)
- Inverted confocal fluorescent microscope (Leica SP8) with temperature control unit (550W, the Cube E5CN-H) and environmental control box
- Autoclave (AL02-01, Advantage-Lab)
- Refrigerated incubator (Model MIR-153, 126 L, Sanyo)
- Shaking incubator (Innova 4400, New Brunswick)

REAGENT SETUP

Piperidine solution Prepare a minimum of 110 mL of piperidine: DMF (1:4) solution. This should be freshly prepared.

! CAUTION Piperidine is toxic by inhalation. It must be handled with care inside the fume hood.

Sample preparation for analytical HPLC and HPLC-MS Dissolve an aliquot of the crude or the final products in ACN: H₂O (1:1) or in MeOH and then transfer into an HPLC vial. Aliquots containing other organic solvents must be first evaporated and redissolved in MeOH. Filter, when appropriate, through a 0.45 μ m filter to remove any insoluble material. Typically, 5-50 μ L volume injections are used for HPLC analysis.

5 mM DMSO solutions of BODIPY-cPAF26 and PAF26 peptides Dissolve 1.0 mg of each peptide in DMSO (152 μ L for BODIPY-cPAF26, 210 μ L for PAF26) and store at -20 °C. In order to avoid several freeze-thaw cycles, DMSO stocks should be ideally stored in small multiple aliquots.

! CAUTION DMSO is highly toxic. Gloves must be worn at all times to avoid contact with skin.

1 μ M fluorescein in 0.1 N NaOH in EtOH Prepare a 10 mM solution of fluorescein in DMSO by weighing 3.3 mg and dissolving them in 1 mL of DMSO. Weigh 40 mg NaOH in a 15 mL conical tube and dissolve in 10 mL EtOH. Dilute the 10 mM fluorescein solution in 0.1 N NaOH in EtOH to a final concentration of 1 μ M. This solution can be stored at r.t. in the dark for several days.

! CAUTION NaOH is very corrosive; hence protective equipment (goggles, gloves and lab coat) should be worn when handling this chemical.

Citric acid/phosphate buffer (pH 7.1). Weigh 1 g of citric acid monohydrate in a 50 mL centrifuge tube and dissolve in 50 mL sterile H₂O. On a separate tube, weigh 2.7 g dibasic sodium phosphate heptahydrate and dissolve in 50 mL sterile H₂O. Mix 21.9 mL of phosphate solution with 3.1 mL of citric acid solution and dilute to a total of 50 mL with sterile H₂O. Adjust pH with the help of a pH meter to 7.1. This buffer solution can be stored at 4 °C for several months.

Protease cocktail solutions Weigh 1.5 mg protease type XIV in a 1.5 mL microcentrifuge tube and dissolve in 1.5 mL citric acid/phosphate buffer (pH 7.1) to reach a 1 mg mL⁻¹ stock solution. Dilute the stock solution in the same buffer to a final concentration of 1 μ g mL⁻¹. The protease cocktail should be prepared freshly before use.

Cell culture media Mix 500 mL RPMI cell media 1640, 50 mL FBS, 5 mL Pen Strep and 5 mL L-Glu in a sterile environment. The resulting media can be filtered using disposable bottle top filters with PES membranes, and stored at 4 °C for 2-3 months.

▲ CRITICAL STEP Cell culture experiments must be performed in sterile conditions inside a class-II microbiological safety cabinet.

Vogel's sucrose minimal medium Prepare solid Vogel's sucrose minimal agar medium according to **Tables 1-3**, adding 2% (w/v) agar before autoclaving without any pH adjustment (pH ~ 5.8). To prepare liquid Vogel's sucrose minimal medium, follow the same recipe excluding agar addition (autoclave and store at r.t.).

SAB dextrose liquid medium Dissolve 30 g of SAB liquid medium in 1 L dH₂O (autoclave and store at r.t.).

SAB dextrose agar Dissolve 65 g of SAB agar in 1 L dH₂O (autoclave and store at r.t.).

PDA medium Dissolve 40 g of PDA agar in 1 L dH₂O (autoclave and store at r.t.).

PDB medium Dissolve 26.5 g of PDB medium in 1 L dH₂O. Mix well and dissolve by heating with frequent agitation until complete dissolution. Boil for 1 min if needed (autoclave and store at r.t.).

! CAUTION Do not place materials that are not autoclave safe in autoclave (non-heat resistant plastics and glass) as they will melt or shatter during sterilization cycle. Fill the container up to 2/3 of the maximum volume and always loose the lid of the bottles before autoclaving.

▲ **CRITICAL STEP** Autoclave all media on the same day solutions are prepared.

Table 1.

Table 2.

Table 3.

Preparation of agar flasks for culturing fungal cells Sterile solid agar medium is heated up and melted using a conventional microwave oven and poured (10 – 15 mL) into sterile T25 cell culture flasks. Tighten the lids, lay the flasks down and let the agar cool down at r.t. Store the flasks at 4 °C in a sealed plastic bag for future use.

▲ **CRITICAL STEP** This experiment must be performed in sterile conditions inside a class-II microbiological safety cabinet.

EQUIPMENT SETUP

Manual peptide-synthesis manifold Place a vacuum manifold in the fume hood and connect it to the vacuum line including a trap. Use polystyrene syringe cartridges with polyethylene porous discs to retain the resins, and hold them on the manifold with two-way stopcocks. Cap all unused inlets with plastic septa. Use a Teflon stick for manual stirring.

Thermoblock shaker Before incubating samples for protease degradation assays, the thermoblock shaker must be equilibrated at 37 °C. Once equilibrated, microcentrifuge tubes containing samples are covered in aluminium foil and shaken at 950 rpm and 37 °C for the indicated times.

Spectrophotometer Settings for fluorescence readings: monochromator-based, excitation: 450 nm, emission: 480-600 nm with 1 nm resolution, gain: 90-100. Settings for absorbance readings: 420-550 nm with 1 nm resolution or single endpoint measurements.

HPLC-based analysis and purification See Table 4 and Table 5.

Table 4.

Table 5.

Autoclave Autoclave all samples at 121 °C for 18 min without any drying cycles. Autoclave any lab ware/equipment (pipette tips etc.) at 121 °C for 15 min with a 15 min drying cycle and fast exhaust.

! CAUTION Do not place materials that are not autoclave safe in autoclave (non-heat resistant plastics and glass) as they will melt or shatter during sterilization cycle. Fill the container up to 2/3 of the maximum volume and always loose the lid of the bottles before autoclaving.

Confocal microscopy We used a Leica TCS SP8 laser scanning confocal microscope with a tunable white light laser (WLL, 450-750 nm), photomultiplier tubes (PMT), hybrid GaAsP (HyD) detectors and a 63× water immersion objective (HC PL APO UVIS CS2, 1.4 N.A.) for fluorescence live-cell imaging. For live-cell imaging of different fungal species (steps 199-206), we used one excitation wavelength (496 nm, laser intensity: 20%) from the WLL source (power level: 70%) and the emission was detected between 505 and 550 nm. A transmitted light detector was used for brightfield image acquisition (gain 355, offset 0%).

For time-lapse high resolution imaging (steps 207-219), we used two different excitation wavelengths (i.e. 496 nm (laser intensity: 25%) and 570 nm (laser intensity: 10 %) from the WLL (power level: 70%) and two emission bands (i.e. 505-550 nm (green) and 585-650 nm (red)). The transmitted light detector was used with the same settings as above. Images for time-lapse movies were acquired at 5 sec intervals. All images were acquired in a 1024 × 1024 pixel format and a scanning speed of 400 Hz. The pixel size of all images was 39.95 × 39.95 nm².

PROCEDURE**Synthesis of 4,4-difluoro-8-(3-iodophenyl)-1,3,5,7-tetramethyl-4-bora-3a,4a-diaza-s-indacene (*m*-iodophenyl-BODIPY (3), Figure 8) • TIMING 32 h**

- 1| Weigh 500 mg 3-iodobenzaldehyde (1.0 eq., 2.2 mmol) in a 250 mL round-bottom flask containing a magnetic stirring bar (egg-shaped stirring bar 25 × 10 mm).
- 2| Cap the flask with a plastic septum (Ø 30.7 mm) and add 50 mL of anhydrous DCM with a 60 mL syringe under N₂ stream on a magnetic stirrer (stirring mot.: 70 % of full power).
- 3| Add 500 µL 2,4-dimethylpyrrole (2.2 eq., 4.7 mmol) with a 1 mL syringe under N₂ stream.
- 4| Add 4 drops (15 µL) TFA with a 1-mL syringe under N₂ stream. The solution turns orange.
- 5| Stir the reaction mixture under N₂ stream at r.t. for 30 min (stirring mot.: 70 % of full power).
- 6| Remove the N₂ stream and stir the reaction mixture under N₂ atmosphere at r.t. for 22 h (stirring mot.: 70 % of full power). The solution turns dark red.
- 7| Monitor the consumption of 3-iodobenzaldehyde and the formation of a new product by sampling an aliquot from the reaction mixture and performing analysis by TLC or HPLC.
- 8| Weigh 490 mg DDQ (1.0 eq., 2.2 mmol) in a 50 mL conical flask and add 30 mL anhydrous DCM.
- 9| Shake and sonicate the resulting yellow suspension until it is almost completely dissolved.
- 10| Add dropwise (for ~ 10 min) the solution from step 9 to the reaction mixture with a syringe under N₂ stream (stirring mot.: 80 % of full power).
- 11| Rinse the conical flask with 2 mL anhydrous DCM and transfer the solution to the reaction mixture (for ~ 5 min).
- 12| Stir the reaction mixture under N₂ for 5 min.
- 13| Remove the N₂ stream and stir the reaction mixture under N₂ atmosphere for 10 min.
- 14| Add dropwise 4 mL TEA (45.0 eq., 97.0 mmol) with a syringe and under N₂ stream. The solution turns dark green.
- 15| Add dropwise (for ~ 3 min) 4 mL BF₃·OEt₂ (30.0 equivalents, 64.7 mmol) with a syringe and under N₂ stream.
- 16| Stir the reaction mixture under N₂ for 3 min; then, remove the stream and stir the reaction mixture under N₂ atmosphere for 4 h 30 min.
- 17| Monitor the formation of the new product by sampling the reaction mixture and performing analysis by TLC or HPLC (DCM: hexane (1: 1), R_f ~ 0.2-0.3).
- 18| Remove the septum and transfer the reaction mixture into a 250 mL separatory funnel containing deionized H₂O (50 mL). Rinse the reaction flask with 20 mL DCM.
- 19| Place a stopper on the separatory funnel and shake vigorously 10 times. Remove the stopper, transfer the organic layer into a 250 mL conical flask and discard the aqueous layer into another 250 mL container. Transfer the organic layer in the separatory funnel and repeat the step with 50 mL deionized H₂O.
- 20| Combine the aqueous layers and back-extract with 20 mL of DCM. Combine the organic layers, transfer them into a 250 mL conical flask and add 4 spatula tips of anhydrous Na₂SO₄.
- 21| Filter the solution into a 250 mL round-bottom flask through a funnel containing a small piece of glass wool at the bottom. Rinse the reaction flask with 20 mL DCM.
- 22| Remove the solvent under reduced pressure (water bath max. T: 40 °C) using a rotary evaporator.
- **PAUSE POINT** For storage, cap the flask and store the crude mixture at 4 °C.
- 23| Purify compound **3** (DCM: hexane (1: 1), R_f ~ 0.2) by flash column chromatography (Silica RediSep R_f 40 g flash column CV 53.9 mL - 40 mL/min) using DCM: hexane gradient and dual-wavelength detection (254 and 360 nm). For loading, dissolve the crude in 10 mL DCM in a round-bottom flask and add two spatula tips of silica. Then, remove the solvent under reduced pressure (water bath max. T: 30 °C) using a rotary evaporator. Transfer the silica-adsorbed crude mixture into a 60 mL polystyrene syringe cartridge and load into a CombiFlash purification system. Run the flash column chromatography with DCM: hexane at 40 mL min⁻¹ and collect 12 mL fractions. Typically, compound **3** elutes with DCM: hexane (88: 12). The compound **3** might crystallize in some of the collection tubes.

? TROUBLESHOOTING

- 24| Identify the fractions containing the compound **3** by sampling aliquots from the collected tubes and analyzing them by HPLC.

- 25| Combine the pure fractions into a 100 mL round-bottom flask and remove the solvent under reduced pressure (water bath max. T: 40 °C) using a rotary evaporator to render a red solid.

? TROUBLESHOOTING

- **PAUSE POINT** For storage, cap the flask and store compound **3** at 4 °C.

Figure 8.**Synthesis of Fmoc-Trp(C₂-BODIPY)-OH (1) (Figure 9) • TIMING 5 h**

- 26| Weigh 3.3 mg Pd(OAc)₂ (0.05 eq., 0.02 mmol), 57.1 mg AgBF₄ (1.0 eq., 0.29 mmol) and 125 mg Fmoc-Trp-OH (1.0 eq., 0.29 mmol) and transfer them as solids into a 10 mL microwave reaction vessel.
- 27| Add a magnetic stirring bar (cylindrical stirring bar 10 × 3 mm).
- 28| Place 198 mg compound **3** (1.5 eq., 0.44 mmol) in a 5 mL round-bottom flask and transfer to the microwave reaction vessel with DMF (1.2 mL in 100 μ L portions) using a micropipette. Shake the resulting solution.
- 29| Add 22 μ L (0.29 mmol) TFA with a micropipette and close the reaction vessel with a microwave cap.
- 30| Sonicate the solution for 10 seconds.
- 31| Place the reaction mixture under microwave irradiation (250 W) at 80 °C for 20 min in a CEM Discover microwave. Monitor the formation of compound **1** by sampling an aliquot from the crude mixture and performing analysis by HPLC.
- ? TROUBLESHOOTING**
- 32| Pack a pad of Celite into a fritted glass funnel and wash it twice with 25 mL EtOAc.
- 33| Load the crude reaction mixture with a glass pipette.
- 34| Rinse the reaction vessel with 25 mL EtOAc and add the solution to the glass funnel. Filter through Celite using vacuum and collect the filtrates in a 100 mL round-bottom flask. Wash twice with 17 mL EtOAc. Evaporate the solvent under reduced pressure at 43 °C using a rotary evaporator (add portions of toluene to enhance DMF removal).
- PAUSE POINT** For storage, cap the flask and store the crude mixture at 4 °C.
- 35| Purify compound **1** (EtOAc, R_f ~ 0.3) by flash column chromatography (Silica RediSep R_f 12 g flash column CV 16.8 mL - 30 mL min⁻¹) using a EtOAc: hexane gradient and dual-wavelength detection (254 and 306 nm). For loading, dissolve the crude in 15 mL EtOAc in a round-bottom flask and add two spatula tips of silica. Then, remove the solvent under reduced pressure (water bath max. T: 40 °C) using a rotary evaporator. Transfer the silica-adsorbed crude mixture into a 60 mL polystyrene syringe cartridge and load into a CombiFlash purification system. Run the flash column chromatography with EtOAc: hexane at 30 mL min⁻¹ and collect 12 mL fractions. Typically, compound **3** elutes with EtOAc: hexane (3: 7). When 40 g columns are used, the product elutes with EtOAc: hexane (1: 1). Compound **1** is isolated as a red amorphous solid.

Figure 9.

Stability analysis of the amino acid **1 • TIMING 1 h (analysis of samples stored for up to 4 months)**

- 36| For stability analysis as a solid, weigh 5 mg of the amino acid **1** in a 2 mL glass vial and wrap in aluminium foil. For stability analysis in solution: weigh 2.2 mg of the amino acid **1** in a 50 mL centrifuge tube and dissolve in 30 mL DCM, MeOH or DMF to reach 0.1 M concentration. Aliquot the solution in 3 separate 15 mL conical tubes (10 mL each, for 3 different T) and wrap them in aluminium foil.
- 37| Store samples at r.t., 4 °C or -20 °C. At the indicated time points, sample aliquots (spatula tip for solid, 50 μ L for solutions), dilute in MeOH (50 μ L) and analyze by HPLC-MS.
- ? TROUBLESHOOTING**

Solid-phase peptide synthesis of BODIPY-cPAF26 (Figure 10) • TIMING 165 h

Resin preparation • TIMING 15 min

- 38| Weigh 46 mg of 2-CTC-PS resin into a 6 mL polystyrene syringe with polyethylene porous disc. Place it in the vacuum manifold using a two-way stopcock.
- 39| Swell the resin with DCM with gentle agitation using a Teflon stick (2 × 4 mL × 15 s).

Coupling of the first amino acid to the resin • TIMING 1.25 h

- 40| Calculate the amount of the first amino acid (Fmoc-Gly-OH) to achieve a loading capacity around 1 mmol g⁻¹ [i.e. mass of resin (g) × 1 mmol g⁻¹ × amino acid molecular weight (g mol⁻¹)] (Table 6).
- 41| Weigh 14 mg of Fmoc-Gly-OH in a 1.5 mL microcentrifuge tube. Add 0.5 mL DCM and 24 μ L DIPEA. Shake for a few seconds until it dissolves completely and add the solution to the syringe followed by manual stirring using a Teflon stick. Wash the microcentrifuge tube with 0.5 mL DCM and add them to the syringe followed by manual stirring using a Teflon stick.
- 42| Shake the syringe in an orbital shaker for 10 min at 200 rpm (4 g).
- 43| Add 55 μ L DIPEA without filtering and shake the syringe in an orbital shaker for 40 min (200 rpm).
- 44| Add 36 μ L MeOH (0.8 μ L MeOH per mg resin) to the resin without filtering to cap unreacted groups. Shake the syringe in an orbital shaker for 10 min at (200 rpm).
- 45| Put the syringe in the vacuum manifold and drain the resin.

Fmoc removal • TIMING 15 min

- 46| Wash the resin thoroughly with DCM (4 × 3 mL × 10 s) and DMF (4 × 3 mL × 10 s), and apply vacuum to drain the resin after each wash.

47| Add piperidine: DMF (1: 4) solution to remove the Fmoc protecting group ($1 \times 5 \text{ mL} \times 1 \text{ min} + 2 \times 5 \text{ mL} \times 5 \text{ min}$). For each wash, gently shake with the Teflon stick and the drain the resin under vacuum.

Coupling of second amino acid and subsequent peptide elongation • TIMING 9 h

48| Calculate the amount of the second amino acid and the coupling reagents (Fmoc-Trp-OH, DIC and OxymaPure) needed on the basis of the amount of resin and functionalization (i.e. mass of resin (g) $\times 1 \text{ mmol g}^{-1} \times 3 \text{ eq.} \times \text{reagent molecular weight (g mol}^{-1})$) (Table 6).

49| Weigh the amino acid and OxymaPure as calculated in step 48 in a 1.5 mL microcentrifuge tube.

50| Wash the resin thoroughly with DCM ($4 \times 3 \text{ mL} \times 10 \text{ s}$) and DMF ($4 \times 3 \text{ mL} \times 10 \text{ s}$), and apply vacuum to drain the resin after each wash.

51| Dissolve the reagents from step 49 in 0.5 mL DMF, add 21 μL DIC and shake the resulting solution for 5 min.

52| Add the resulting activated amino acid solution to the resin and gently shake with the Teflon stick for 4 min.

53| Shake the syringe in an orbital shaker for 56 min at 200 rpm and then drain the resin. Wash the resin as in step 50.

54| Run a Kaiser test⁵² to assess the extent of the peptide coupling.

? TROUBLESHOOTING

55| Repeat steps 48-54 for coupling all following amino acid (i.e. Fmoc-Phe-OH) and steps 46-47 for Fmoc removal.

■ **PAUSE POINT** Peptide elongation can be paused at any point after the incorporation of the third amino acid. Pausing after the incorporation of the second amino acid is not recommended due to the potential formation of diketopiperazines.⁵³ Storing the peptide as Fmoc-protected is not recommended, because partial Fmoc removal can lead to re-incorporation of the fluorenylmethyl moiety to the free amine group giving the corresponding secondary amine. For storage, wash the resin 3 times with DCM or DMF (5 mL each), wrap the syringe in aluminium foil and store at r.t.

Coupling of amino acid 1 • TIMING 1.25 h

56| Calculate the amount of amino acid and coupling reagents (1, HOBt, PyBOP and DIPEA) needed on the basis of the amount of resin and functionalization (i.e. mass of resin (g) $\times 1 \text{ mmol g}^{-1} \times 1.5$ or 2 eq. $\times \text{reagent molecular weight (g mol}^{-1})$) (Table 6).

57| Weigh the amino acid and HOBt as calculated in step 56 in a 1.5 mL microcentrifuge tube. Separately, weigh PyBOP in a separate 1.5 mL microcentrifuge tube.

58| Wash the resin thoroughly with DCM ($4 \times 3 \text{ mL} \times 10 \text{ s}$) and DMF ($4 \times 3 \text{ mL} \times 10 \text{ s}$), and apply vacuum to drain the resin after each wash.

59| Dissolve PyBOP from step 57 in 0.1 mL DMF.

60| Dissolve the reagents from step 57 in 0.4 mL DMF. Add 16 μL DIPEA (2 eq.) and the PyBOP solution from step 59. Shake the resulting solution for 2 s, add it to the resin and gently shake with the Teflon stick for 4 min.

61| Shake the syringe in an orbital shaker for 56 min (200 rpm) and then drain the resin. Wash as in step 58.

62| Run a Kaiser test⁵² to assess the extent of the coupling.

? TROUBLESHOOTING

■ **PAUSE POINT** For storage, wash and drain the resin 3 times with DCM (5 mL each), and wrap the syringe in aluminium foil and store at r.t.

Table 6.

Cleavage of the linear protected peptide from the resin • TIMING 1 h

63| Wash the resin thoroughly with DCM ($4 \times 3 \text{ mL} \times 10 \text{ s}$) and DMF ($4 \times 3 \text{ mL} \times 10 \text{ s}$), and apply vacuum to drain the resin after each wash.

! **CAUTION** Always use a Teflon two-way stopcock when working with TFA.

64| Add 3 mL of a freshly prepared TFA: DCM (1: 99) solution to the resin. Shake gently with a Teflon stick for 1 min.

Collect the filtrates in a 100 mL round-bottom flask with 30 mL DCM. Keep constant stirring of the solution in a magnetic stirrer (egg-shaped stirring bar 2 cm \times 1 cm, stirring mot.: 60% of full power). Wash the resin with DCM (3 mL \times 5 s) and collect the filtrates in the same flask.

65| Repeat step 64 another 4 times with an additional final wash with DCM (3 mL \times 5 s), collecting all the filtrates in the same flask.

66| Remove the solvent under reduced pressure (water bath max. T: 40 °C) using a rotary evaporator.

▲ **CRITICAL STEP** Low acidic conditions and short reaction times are critical to preserve the integrity of the BODIPY fluorophore.

67| Dissolve the crude in 14 mL ACN: H₂O (1:1), adding first ACN and then H₂O in a 50 mL polypropylene centrifuge tube.

Solvent removal from the crude peptide • TIMING 24 h

68| Freeze the crude peptide solution using liquid N₂. Lyophilize for 24 h, wrapping the glass container in aluminium foil.

69| Sample a small aliquot of the peptide crude, dissolve in ACN: H₂O (1: 1) and analyze by HPLC to check the crude purity.

Figure 10.

Cyclization of the protected peptide • TIMING 3 h

70| Weigh 14 mg of HATU (1.0 eq., 0.04 mmol) in the 50 mL centrifuge tube from step 68 with 61 mg of linear protected peptide (0.04 mmol).

71| Dissolve the compounds in 0.9 mL DMF and add 16 µL DIPEA (2.5 eq., 0.09 mmol).

72| Stir the solution for 2 h at r.t. on a magnetic stirrer (cylindrical stirring bar 8 × 3 mm, stirring mot.: 80% of full power). Sample a small aliquot of the peptide crude, dissolve in ACN: H₂O (1: 1) and analyze by HPLC to confirm the reaction is completed.

73| Add dropwise 12 mL of cold H₂O to precipitate the protected peptide.

74| Vortex the mixture for 1 min, centrifuge for 5 min at 4,000 rpm and carefully decant H₂O.

75| Repeat steps 73-74 another 2 times.

Lyophilization of the cyclic protected peptide • TIMING 24 h

76| Re-dissolve the protected peptide in 8 mL ACN: H₂O (1: 1). Freeze the crude peptide solution using liquid N₂. Lyophilize for 24 h, wrapping the glass container in aluminium foil.

77| Sample a small aliquot of the peptide crude, dissolve in ACN: H₂O (1: 1) and analyze by HPLC to check the crude purity.

■ **PAUSE POINT** For storage, wrap the centrifuge tube in aluminium foil and store at 4 °C.

Hydrogenation reaction (Figure 11) • TIMING 49 h

78| Weigh 45 mg of protected **BODIPY-cPAF26** peptide from step 76 (1.0 eq., 0.03 mmol) and 23 mg of Pd(OH)₂-C in a 25 mL round-bottom flask containing a magnetic stir bar (cylindrical stirring bar 10 × 3 mm).

? TROUBLESHOOTING

79| Cap the flask with a plastic septum (Φ 14.9 mm). Evacuate and backfill the flask with Ar or N₂.

80| Add 4.5 mL of freshly prepared MeOH: FA (95: 5) with a syringe and purge for 5 min.

81| Connect a balloon filled with H₂ to the system through a needle and purge the flask with H₂.

82| Stir the reaction mixture under H₂ atmosphere on a magnetic stirrer at r.t. for 48 h (stirring mot.: 80% of full power). Refill the H₂ balloon periodically along with re-addition of Pd(OH)₂-C (3 times overall).

! **CAUTION** H₂ is a highly flammable gas. H₂ gas must be always handled inside a ventilated fume hood.

83| Filter the solution through a glass Pasteur pipette containing Celite and a tiny piece of cotton at the bottom. Wash with 3 mL MeOH to ensure complete elution of the peptide.

84| Remove the solvent under reduced pressure (water bath max. T: 40 °C) using a rotary evaporator.

Purification of the BODIPY-cPAF26 peptide • TIMING 51 h

85| Dissolve 25 mg of the crude **BODIPY-cPAF26** peptide from step 84 in 1.5 mL ACN: H₂O (1: 1). Heating for a few minutes in a water bath at 40 °C or sonication help to dissolve the sample.

86| Filter the solution through a 0.45 µm syringe filter into a 3 mL vial for semi-preparative HPLC purification. Rinse the round-bottom flask with 0.5 mL ACN: H₂O (1: 1), filter and transfer to the same vial.

87| Inject 500 µL sample to the semi-preparative HPLC. **BODIPY-cPAF26** elutes around t_R: 12-14 min (ACN: H₂O (4:6)). Collect the pure **BODIPY-cPAF26** peptide in a 50 mL centrifuge tube (~ 30 mL per injection).

88| Repeat step 87 three times.

89| Combine all the pure fractions. Freeze them using liquid N₂ and lyophilize for 48 h, wrapping the glass container in aluminium foil.

Figure 11.

Proteolytic stability of BODIPY-cPAF26 and PAF26 peptides • TIMING 25 h

90| Aliquot 20 µL of 5 mM DMSO solutions of **BODIPY-cPAF26** and PAF26 peptides in 2 separate 1.5 mL microcentrifuge tubes.

91| Dilute both peptides in 480 µL protease cocktail (1 µg mL⁻¹, pH 7.1) to reach 200 µM final concentration.

- 92| Vortex the solutions. Aliquot samples (62 μL) for the first time point ($t = 0$), precipitate the proteins by microcentrifugation (4 °C, 13,000 rpm), and analyze the supernatants by HPLC-MS.
- 93| Place the solutions in the pre-heated thermoblock shaker at 37 °C (see Equipment setup). Shake the tubes at 950 rpm and take aliquots (62 μL) at the indicated time points (i.e. 0.25 h, 1 h, 4 h, 8 h and 24 h).
- 94| Precipitate the proteins by microcentrifugation (4 °C, 13,000 rpm), and analyze the supernatants by HPLC-MS.

? TROUBLESHOOTING

Fluorogenic behaviour of BODIPY-cPAF26 in phospholipid membranes • TIMING 1.5 h

- 95| Dilute the 5 mM DMSO solution of **BODIPY-cPAF26** (40 μL) in DMSO (40 μL) to reach 2.5 mM final concentration.
- 96| Vortex the phosphatidylcholine (PC): cholesterol (7: 1) liposome suspension in PBS (7.5 mg mL⁻¹ PC) for 10 seconds.
- ▲ **CRITICAL STEP** Liposome suspensions must be used at r.t. and stored at 4 °C, but cannot be frozen.
- 97| Dilute the 7.5 mg mL⁻¹ PC liposome suspension in 2-fold serial dilutions (495 μL in 1.5 mL microcentrifuge tubes) using DPBS. 10 serial dilutions are prepared, ranging from 3.75 mg mL⁻¹ PC (2-fold dilution) to 0.007 mg mL⁻¹ PC (1024-fold dilution). Prepare a blank sample with only DPBS (495 μL in 1.5 mL microcentrifuge tube).
- 98| Add 5 μL of 2.5 mM **BODIPY-cPAF26** to all liposome suspensions and also to the DPBS blank to reach 25 μM final concentrations.
- 99| Vortex all the liposome suspensions and the DPBS blank for 10 seconds.
- 100| Transfer 150 μL ($\times 3$) from every suspension onto separate wells of a 96-well black plate with flat bottom and lid. Include 3 wells (150 μL each) of 1 μM fluorescein in 0.1 N basic EtOH as a reference for the quantum yield measurements.
- 101| Incubate the plate for 15 min at r.t. in the dark.
- ▲ **CRITICAL STEP** Do not incubate **BODIPY-cPAF26** with liposomes for longer than 30 min as sedimentation can lead to inaccurate measurements.
- 102| Measure fluorescence emission spectra for the 96-well black plate using a Synergy H1 spectrophotometer. Excitation wavelength: 450 nm, emission range: 480-600 nm (every 1 nm).
- 103| Transfer samples to a 96-well polystyrene transparent plate using a multichannel pipette. Include 3 wells (150 μL each) of DPBS as a reference for background measurements.
- 104| Measure absorbance spectra of the 96-well transparent plate using a Synergy H1 spectrophotometer. Absorbance range: 420-550 nm (every 1 nm).
- 105| Transfer **BODIPY-cPAF26** suspensions with high liposome content, low liposome content, DPBS blank as well as fluorescein in basic EtOH into 2 mL glass vials.
- 106| Irradiate the glass vials with 365 nm light using a hand-held UV-lamp. Differences in fluorescence intensity of **BODIPY-cPAF26** can be detected by naked eye (Figure 12).
- ! **CAUTION** Exposure to UV radiation can cause skin or eye burns; hence protective equipment (goggles, gloves and lab coat) should be worn.

? TROUBLESHOOTING

Figure 12.

Cytotoxicity of BODIPY-cPAF26 in A549 human lung epithelial cells • TIMING 42 h

- ▲ **CRITICAL STEP** Cell culture experiments must be performed in sterile conditions using a class-II microbiological safety cabinet. All reagents (media, DPBS, Trypsin-EDTA) and pipette tips must be sterile.
- 107| Use a running culture of A549 cells, typically one T-75 cell culture flask with 25 mL full media (see Reagent setup) incubated at 37 °C in 5% CO₂.
- 108| Check confluency and morphology of the cells under a microscope.
- ▲ **CRITICAL STEP** Live A549 cells should be adhered to the flask. If most cells are floating or with signs of contamination (e.g. bacteria, cloudy media), discard culture and use a new batch.
- 109| Remove and discard media with a 25 mL plastic pipette.
- 110| Gently add 10 mL Ca²⁺-free DPBS to wash the cells and discard with a 10 mL plastic pipette.
- 111| Add 1 mL Trypsin-EDTA to the flask, rock gently to cover all the surface and incubate for 3 min at 37 °C in 5% CO₂.
- ? **TROUBLESHOOTING**
- 112| Take the flask out of the incubator, tap gently to detach cells, add 10 mL media to the flask and transfer the cell suspension to a 50 mL centrifuge tube.
- 113| Sample a 50 μL aliquot for cell counting.
- 114| Determine the number of cells using a cell counter. In fully confluent flasks of A549 cells, counts are typically $\sim 0.5\text{--}2 \times 10^6$ cells mL⁻¹, depending on their manipulation.
- 115| Centrifuge the cell suspension (5 min, 20 °C, 350 rpm).

116| Discard the supernatant and resuspend the cell pellet in 1 mL media. Calculate the amount of cells needed for the cytotoxicity assay depending on the wells to be used (25,000 cells/well). In a standard assay with 6 different conditions and 4 replicates (total 24 wells), around 6×10^5 cells are needed.

117| Dilute the cell suspension in media to achieve a final concentration of 2.5×10^5 cells mL⁻¹, and place the cell suspension in a 50 mL pipette basin.

118| Plate cells (100 µL/well) in sterile 96-well flat bottom polystyrene clear plates with lid using a multichannel pipette. Discard remaining cells following biological waste disposal regulations.

119| Incubate the plate(s) for 16 h at 37 °C in 5% CO₂.

120| Check confluency and morphology of the cells under a microscope.

? TROUBLESHOOTING

121| Dilute 5 mM **BODIPY-cPAF26** solution in DMSO to 1 mM in a 1.5 mL microcentrifuge tube (4 µL of 5 mM solution plus 16 µL DMSO).

122| Prepare another 3 dilutions from 1 mM **BODIPY-cPAF26** in DMSO (2-fold serial dilutions) in separate 1.5 mL microcentrifuge tubes to obtain 0.5 mM, 0.25 mM and 0.125 mM DMSO solutions.

123| Dilute the 4 DMSO solutions in cell culture media (9 µL of DMSO solutions plus 90 µL media) to obtain 90 µM, 45 µM, 22.5 µM, and 11.25 µM solutions of **BODIPY-cPAF26**. Prepare an additional blank solution with 9 µL of DPBS plus 90 µL media.

124| Add 12.4 µL of the solutions to the cells in the 96-well plate to reach a final concentration of **BODIPY-cPAF26** of 10 µM, 5 µM, 2.5 µM, and 1.25 µM. As negative controls add 12.4 µL of DPBS solution, and for positive controls, remove media from the wells and 112 µL DMSO to the cells.

125| Rock the plate(s) gently and incubate the cells for 4 h at 37 °C in 5% CO₂.

126| Dilute an appropriate volume of MTT reagent with media (2.3-fold dilution, a minimum of 30 µL solution/well is required), and place the solution in a 50 mL pipette basin.

127| Add 30 µL MTT solution in media to each well using a multichannel pipette.

128| Rock the plate(s) gently and incubate the cells for 4 h at 37 °C in 5% CO₂.

▲ **CRITICAL STEP** Under the microscope, check the progression of the MTT reaction by observing the precipitation of a dark solid in the cells.

? TROUBLESHOOTING

129| Place detergent reagent in a 50 mL pipette basin (a minimum of 100 µL detergent/well is required).

130| Add 100 µL detergent to each well using a multichannel pipette. Rock gently the plate, wrap it in aluminium foil and keep at r.t. for a minimum of 2 h.

■ **PAUSE POINT** At this point, the experiment can be paused and the plate can be kept at r.t. overnight.

▲ **CRITICAL STEP** Typically, 2-4 h incubation with detergent are enough but overnight incubation is recommended to ensure full solubilization.

131| Measure absorbance at 570 nm and 650 nm (background signal) of the 96-well transparent plate using a Synergy H1 spectrophotometer. Wells with high cell viability values (DPBS negative control) are dark-colored while wells with low cell viability (full DMSO positive control) are yellow-colored (**Figure 13**). Absorbance values should be between 0.5 and 1.5 AU.

? TROUBLESHOOTING

Figure 13.

Culture of fungal species • **TIMING 121 h**

Culture of *N. crassa* • **TIMING 121 h**

▲ **CRITICAL STEP** Culturing of the 5 different fungal species (steps 132-151) must be performed under sterile conditions using a class-II microbiological safety cabinet. All reagents and pipette tips must be sterile. Cultures of the multiple species can be performed in parallel to maximize time efficiency.

132| Streak *N. crassa* spores from a stock culture (stored at -20 °C) using a sterile inoculation loop onto the surface of solid Vogel's sucrose minimal agar medium within a T25 cell culture flask.

133| Incubate the flask at 25 °C in the refrigerated incubator under 15 W 'warm white' light for 5 days.

? TROUBLESHOOTING

134| Add 1.5 mL sterile dH₂O to the flask, shake gently and recover the suspension containing fungal cells with a P1000 micropipette. Filter the suspension through folded Miracloth (4 layers) into a sterile 1.5 mL microcentrifuge tube.

135| Remove a 4 µL-aliquot of the cell suspension and transfer to a haemocytometer to count the spores.

■ **PAUSE POINT** The *N. crassa* conidial suspension in sterile dH₂O can be stored for up to 4 days at 4 °C.

▲ **CRITICAL STEP** After 4 days, *N. crassa* conidia must be discarded following biological waste disposal regulations. All inoculations should be performed from original stock cultures and not from sub-cultures to reduce the possibility of cultures acquiring new mutations.

Culture of *A. fumigatus* • TIMING 73 h

136| Vortex the stock suspension of *A. fumigatus* conidia (stored at 4 °C) to produce a homogeneous cell suspension.

137| Add 50 µL of the homogeneous cell suspension onto the surface of solid Vogel's sucrose minimal agar medium within a T25 cell culture flasks and spread the conidia over the agar surface with a sterile inoculation loop.

138| Incubate the flask at 37 °C in the dark for 3 days.

? TROUBLESHOOTING

139| Prepare 0.05 % (v/v) Tween 80 in sterile dH₂O and add 1.5 mL of it to the flask, shake gently and recover the suspension with a P1000 micropipette.

140| Remove a 4 µL-aliquot of the cell suspension and transfer to a haemocytometer to count the spores.

■ **PAUSE POINT** *A. fumigatus* conidial suspension in sterile dH₂O can be stored for up to one month at 4 °C.

▲ **CRITICAL STEP** After one month, *A. fumigatus* conidia must be discarded following biological waste disposal regulations. All inoculations should be performed from original stock cultures and not from sub-cultures to reduce the possibility of cultures acquiring new mutations.

Culture of *C. neoformans* • TIMING 73 h

141| Thaw an aliquot of *C. neoformans* stock suspension (stored at -80 °C) and gently streak onto 15 mL SAB agar medium within a 9 cm Petri dish.

142| Seal the plate with Micropore tape, and place it inverted in an incubator at 30 °C for 3 days.

? TROUBLESHOOTING

■ **PAUSE POINT** Petri dishes containing *C. neoformans* colonies can be stored for up to one month at 4 °C.

▲ **CRITICAL STEP** After one month, *C. neoformans* colonies must be discarded following biological waste disposal regulations. All inoculations should be performed from original stock cultures and not from sub-cultures to reduce the possibility of cultures acquiring new mutations.

Culture of *F. oxysporum* • TIMING 121 h

143| Vortex the stock suspension of *F. oxysporum* microconidia (stored at -80 °C) to produce a homogeneous cell suspension.

144| Add 50 µL of the homogeneous cell suspension to a sterile glass flat-bottom flask with 20 mL liquid PDB medium.

145| Plug the flask with a sterile foam plug and seal the flask with aluminium foil. Incubate the flask on a shaking incubator at 28 °C for 5 days (170 rpm).

? TROUBLESHOOTING

146| Filter the cell suspension through folded Miracloth (4 layers) and transfer into a sterile 50 mL centrifuge tube.

147| Centrifuge the suspension (10 min, r.t., 4,000 rpm) and discard the supernatant.

148| Re-suspend the pellet in 2 mL sterile dH₂O and transfer with a P1000 micropipette into a 2 mL microcentrifuge tube.

149| Remove a 4 µL-aliquot of the cell suspension and transfer to a haemocytometer to count the spores.

■ **PAUSE POINT** *F. oxysporum* conidia suspension in sterile dH₂O can be stored for up to one month at 4 °C.

▲ **CRITICAL STEP** After one month, *F. oxysporum* conidia must be discarded following biological waste disposal regulations. All inoculations should be performed from original stock cultures and not from sub-cultures to reduce the possibility of cultures acquiring new mutations.

Culture of *C. albicans* • TIMING 73 h

150| Thaw an aliquot of *C. albicans* stock suspension (stored at -80 °C) and gently streak onto 15 mL PDA medium within a 9 cm Petri dish.

151| Seal the plate, and place it inverted in an incubator at 30 °C for 3 days.

? TROUBLESHOOTING

■ **PAUSE POINT** Petri dishes containing *C. albicans* colonies can be stored for up to one month at 4 °C.

▲ **CRITICAL STEP** After one month, *C. albicans* colonies must be discarded following biological waste disposal regulations. All inoculations should be performed from original stock cultures and not from sub-cultures to reduce the possibility of cultures acquiring new mutations.

Antifungal activity measurements of BODIPY-cPAF26 and PAF26 peptides in *N. crassa* and *A. fumigatus* • TIMING 26 h

- 152| Dilute 5 mM **BODIPY-cPAF26** or **PAF26** solution in DMSO to 1 mM in a 1.5 mL microcentrifuge tube (20 μ L of 5 mM solution plus 80 μ L DMSO).
- 153| Prepare another 2 dilutions from 1 mM **BODIPY-cPAF26** or **PAF26** in DMSO in separate 1.5 mL microcentrifuge tubes to obtain 30 μ M (30 μ L of 1 mM peptide and 970 μ L dH₂O) and 25 μ M (25 μ L of 1 mM peptide and 975 μ L dH₂O) solutions.
- 154| Add 100 μ L of 30 μ M peptide into each of the wells (A1-G1) of a transparent U-bottom 96-well plate (Figure 14a).
- 155| Add 100 μ L of 25 μ M peptide into each of the wells (A2-G2) of a transparent U-bottom 96-well plate (Figure 14a).
- 156| Add 100 μ L of sterile dH₂O into each of the wells (D1, H1, D2 and H2) and 50 μ L of sterile dH₂O into each of the rest of the wells.
- 157| Perform 2-fold serial dilutions of 30 μ M peptide (step 153) using a multichannel electronic pipette by transferring 50 μ L from column 1 into column 3 and then 5 and so on. Discard the 50 μ L taken from column 11 (Figure 14b).
- 158| Perform 2-fold serial dilutions of 25 μ M peptide (step 153) using a multichannel electronic pipette by transferring 50 μ L from column 2 into column 4 and then 6 and so on. Discard the 50 μ L taken from column 10. (Figure 14c).
- 159| Dilute an appropriate volume of conidial suspension from step 134 (*N. crassa*) or step 139 (*A. fumigatus*) with 5 mL solution of liquid Vogel's sucrose minimal medium in dH₂O (1: 4). Vortex the suspension and place in a 50 mL pipette basin.
- 160| Add 50 μ L conidial suspension into each well using a multichannel pipette (excluding wells in rows D and H). For the wells that are considered as 'blanks', add 50 μ L of a solution of liquid Vogel's sucrose minimal medium in dH₂O (1: 4) to wells in row D and H and achieve a final volume of 100 μ L/well (Figure 14d).
- ▲ **CRITICAL STEP** The addition of the conidia to the wells of the 96-well plate must be performed quickly to avoid any settlement of the conidia in the pipette basin.
- 161| Put the lid on the plate and wrap it in aluminium foil. Incubate for 24 h at 37 °C (*A. fumigatus*) or at 25 °C (*N. crassa*).

Figure 14.

■ **PAUSE POINT** At this point, the experiment can be paused as the plate(s) needs to be incubated overnight.

- 162| Measure optical density at 610 nm using a spectrophotometer. Optical density values for the control group (conidia alone) should be ~ 0.1-0.2 AU. IC₅₀ values are determined by four-parameter logistic regression analysis.

? TROUBLESHOOTING

Preparation of fungal cells for live-cell fluorescence imaging • **TIMING 21.5 h**

Preparing *N. crassa* conidial germlings for imaging • **TIMING 4.5 h**

▲ **CRITICAL STEP** The preparation of fungal cells for imaging (steps 163-189) must be performed under sterile conditions using a class-II microbiological safety cabinet. All reagents and pipette tips must be sterile. Preparation of the multiple species can be performed in parallel to maximize time efficiency.

- 163| Vortex the cell suspension of *N. crassa* conidia from step 134.

- 164| Dilute *N. crassa* conidia to 10⁵ cells mL⁻¹ with 2 mL of solution of liquid Vogel's sucrose minimal medium in dH₂O (1: 4).

- 165| Vortex the diluted suspension and transfer with a P200 micropipette to an 8-well chamber (200 μ L/well).

- 166| Place the chamber in a refrigerated incubator for 4 h at 25 °C in the dark.

▲ **CRITICAL STEP** A dilution of liquid Vogel's sucrose minimal medium in dH₂O (1: 4) must be used instead of 100% liquid Vogel's sucrose minimal medium to produce *N. crassa* as conidial germlings and avoid the formation of mature hyphae, which are not suitable for single cell imaging.

Preparing *A. fumigatus* conidial germlings for imaging • **TIMING 25 h**

- 167| Vortex the cell suspension of *A. fumigatus* conidia from step 139.

- 168| Dilute *A. fumigatus* conidia to 10⁵ cells mL⁻¹ with 2 mL of solution of liquid Vogel's sucrose minimal medium in dH₂O (1: 4).

- 169| Vortex the diluted suspension and transfer with a P200 micropipette to an 8-well chamber (200 μ L/well).

- 170| Place the chamber in a refrigerated incubator for 24 h at 25 °C in the dark.

▲ **CRITICAL STEP** A dilution of liquid Vogel's sucrose minimal medium in dH₂O (1: 4) must be used instead of 100% liquid Vogel's sucrose minimal medium to produce *A. fumigatus* as conidial germlings and avoid the formation of mature hyphae, which are not suitable for single cell imaging.

Preparing *C. neoformans* cells for imaging • **TIMING 21.5 h**

- 171| Transfer 3-4 colonies of *C. neoformans* from step 142 into a sterile glass flat-bottom flask with 10 mL liquid SAB medium.
- 172| Plug the flask with a sterile foam plug and seal the flask with aluminium foil. Incubate the flask on a shaking incubator at 37 °C for 20 h (170 rpm).
- 173| Filter the cell suspension through folded Miracloth (4 layers) and transfer into a sterile 50 mL centrifuge tube.
- 174| Centrifuge the suspension (5 min, r.t., 4,000 rpm) and discard the supernatant.
- 175| Re-suspend the pellet in 2 mL sterile dH₂O and transfer into a 2 mL microcentrifuge tube.
- 176| Remove a 4 µL-aliquot of the cell suspension and transfer to a haemocytometer to count the spores.
- 177| Dilute *C. neoformans* conidia to 5×10^5 cells mL⁻¹ in sterile dH₂O.
- 178| Vortex the diluted suspension and transfer with a P200 micropipette to an 8-well chamber (200 µL/well).
- 179| Incubate the chamber at r.t. for 30 min before use.

▲ **CRITICAL STEP** The chamber containing *C. neoformans* cells must be handled carefully as they will not adhere to the bottom of the 8-well chamber as well as the other fungal species.

? TROUBLESHOOTING

Preparing *F. oxysporum* cells for imaging • TIMING 9 h

- 180| Dilute *F. oxysporum* microconidial suspension from step 148 to 5×10^5 cells mL⁻¹ with 2 mL 1% (v/v) PDB medium.
- 181| Vortex the diluted cell suspension and transfer with a P200 micropipette to an 8-well chamber (200 µL/well).
- 182| Place the chamber in a refrigerated incubator at 25 °C under 15 W 'warm white' light for 8 h before use.

Preparing *C. albicans* cells for imaging • TIMING 13.5 h

- 183| Transfer one single colony of *C. albicans* from step 151 into a sterile glass flat-bottom flask containing 15 mL PDB medium.
- 184| Plug the flask with a sterile foam plug and seal the flask with aluminium foil. Incubate the flask on a shaking incubator at 30 °C for 12 h (170 rpm).
- 185| Filter the suspension through folded Miracloth (4 layers) and transfer into a sterile 50 mL centrifuge tube.
- 186| Remove a 4 µL-aliquot of the cell suspension and transfer to a haemocytometer to count the yeast cells.
- 187| Dilute the *C. albicans* cells to 5×10^5 cells mL⁻¹ in PDB medium.
- 188| Vortex the diluted cell suspension and transfer with a P200 micropipette to an 8-well chamber (200 µL/well).
- 189| Incubate the chamber at r.t. for 30 min before use.

▲ **CRITICAL STEP** The chamber containing *C. albicans* cells must be handled carefully as they will not adhere to the bottom of the 8-well chamber as well as the other fungal species.

? TROUBLESHOOTING

General setup of the fluorescence confocal microscope for live-cell imaging • TIMING 30 min

- 190| Switch on the laser(s) and set the stage temperature as required.
- 191| Adjust the WLL laser power to 70 %.
- 192| Clean the 63× water immersion objective with lens cleaning tissue.
- 193| Set the excitation beam wavelength(s), laser intensity(ies) and emission wavelength(s) as required.
- ▲ **CRITICAL STEP** Due to the high sensitivity of HyD detectors, it is important to set the laser intensity at a low level (~10 %) to avoid damaging to the detectors.
- 194| During imaging experiments, place the 8-well chamber on the microscope stage, focus the sample using the eyepieces and select the region of interest to image.

? TROUBLESHOOTING

- 195| Adjust the Z-position as well as gain and offset for each channel.
- 196| At this point, individual images can be captured or successive images can be recorded in a time course by setting the interval time between image capture and the overall length of the imaging period as appropriate.
- 197| Save the experimental data to appropriate folders and export images as .tif images.
- 198| Remove the sample and clean the objective. Cool down the laser(s) and switch them off.

Live-cell fluorescence imaging of fungal cells using BODIPY-cPAF26 • TIMING 45 min

- 199| Prepare samples as described in steps 163-166 (*N. crassa*), 167-170 (*A. fumigatus*), 171-179 (*C. neoformans*), 180-182 (*F. oxysporum*) and 183-189 (*C. albicans*).
- 200| Dilute 5 mM BODIPY-cPAF26 DMSO stock in sterile dH₂O to achieve a final 10 µM solution using a 1.5 mL microcentrifuge tube (2 µL of 5 mM solution and 998 µL dH₂O).
- 201| Using a P200 micropipette, carefully remove 40 µL of the 200 µL medium from one well of the 8-well chamber.
- 202| Add 40 µL of the solution prepared in step 200 to achieve a 2 µM final concentration of BODIPY-cPAF26.

203| Incubate the cells with **BODIPY-cPAF26** for 10 min at r.t.

▲ **CRITICAL STEP** Cells must be handled carefully to minimize cell detachment from the bottom of the well.

204| Acquire images as required. Live-cell imaging can be performed up to 60 min without causing obvious deleterious effects to the cells. However, immediate imaging following **BODIPY-cPAF26** treatment is highly recommended.

205| After acquisition, save the files to an appropriate location and subsequently back up the files at an appropriate time to prevent any data loss.

206| Discard cells following biological waste disposal regulations.

■ **PAUSE POINT** After acquisition, images can be analyzed at any time.

Real-time fluorescence imaging of *A. fumigatus* using **BODIPY-cPAF26** • **TIMING 1 h**

207| Prepare samples as described in steps 167-170.

208| Prepare a 5 mM DMSO stock solution of the red counterstain (TAMRA-PAF96) using a 1.5 mL microcentrifuge tube (4.8 mg in 1 mL DMSO).

209| Dilute the 5 mM red counterstain DMSO stock solution in sterile dH₂O to achieve a final 20 μ M solution in a 1.5 mL microcentrifuge tube (4 μ L of 5 mM solution and 996 μ L dH₂O).

210| Using a P200 micropipette, carefully remove 40 μ L of the 200 μ L medium from a well of the 8-well chamber.

211| Add 40 μ L of the solution prepared in step 208 to achieve a 5 μ M final concentration of the red counterstain.

212| Incubate the cells with 5 μ M red counterstain for 10 min at r.t.

▲ **CRITICAL STEP** To maximize the cell membrane localization of the red counterstain with minimal internalization at the time of addition of **BODIPY-cPAF26**, we recommend performing steps 201-212 one well at a time.

213| Using a P200 micropipette, carefully remove 160 μ L of the 200 μ L medium from the well of the 8-well chamber and add 160 μ L of a fresh solution of liquid Vogel's sucrose minimal medium in dH₂O (1: 4).

▲ **CRITICAL STEP** Cells must be handled carefully to minimize any cell detachment from the bottom of the well.

214| Using a P200 micropipette, carefully remove 40 μ L of the 200 μ L medium from the well of the 8-well chamber and place the chamber on the stage of the confocal microscope.

215| Identify a region of interest containing one or more red-stained cells. Re-adjust the Z-position for optimal focus.

216| Using a P200 micropipette, gently add 40 μ L of the solution prepared in step 200 to achieve a 2 μ M final concentration of **BODIPY-cPAF26**.

217| Acquire a series of images in a time course (recommended interval time between images: 5 sec).

? **TROUBLESHOOTING**

218| After acquisition, back up the files to prevent any data loss.

219| Discard cells following biological waste disposal regulations.

■ **PAUSE POINT** After acquisition, images can be analyzed at any time.

? **TROUBLESHOOTING**

Troubleshooting advice can be found in **Table 7**.

Table 7.

• **TIMING**

Synthesis of *m*-iodophenyl-BODIPY (3): Steps 1-25

Steps 1-7, Condensation of 3-iodobenzaldehyde and 2,4-dimethylpyrrole: 23 h

Steps 8-13, Oxidation: 1 h

Steps 14-17, BF₃·Et₂O coordination: 5 h

Steps 18-22, Work-up: 1 h

Steps 23-25, Purification: 2 h

Synthesis of Fmoc-Trp(C₂-BODIPY)-OH (1): Steps 26-35

Steps 26-31, Fmoc-Trp-OH arylation with compound 3: 1 h

Steps 32-34, Work-up: 1 h

Steps 35, Purification: 3 h

Stability analysis of the amino acid 1: Steps 36-37

Steps 36-37, HPLC analysis: 1 h

Solid-phase peptide synthesis of BODIPY-cPAF26: Steps 38-69

Steps 38-39, Resin preparation: 15 min

Steps 40-45, Coupling of the first amino acid to the resin: 1.25 h

Steps 46-47, Fmoc removal: 15 min

Steps 48-55, Coupling of second amino acid and peptide elongation: 9 h

Steps 56-62, Coupling of amino acid **1**: 1.25 h

Steps 63-67, Cleavage of the linear protected peptide from the resin: 1 h

Steps 68-69, Solvent removal from the crude peptide: 24 h

Peptide cyclization: Steps 70-77

Steps 70-75, Cyclization of the protected peptide: 3 h

Steps 76-77, Lyophilization of the cyclic protected peptide: 24 h

Hydrogenation reaction: Steps 78-84

Steps 78-82, Hydrogenation reaction: 48 h

Steps 83-84, Work-up: 1 h

Purification of the BODIPY-cPAF26 peptide: Steps 85-89

Steps 85-88, HPLC purification: 3 h

Step 89, Solvent removal and isolation of **BODIPY-cPAF26**: 48 h

Proteolytic stability of BODIPY-cPAF26 and PAF26 peptides: Steps 90-94

Steps 90-92, Sample preparation: 1 h

Steps 93-94, Incubation and HPLC analysis: 24 h

Fluorogenic response of BODIPY-cPAF26 in phospholipid membranes: Steps 95-106

Steps 95-101, Sample preparation: 1 h

Steps 102-106, Spectroscopic measurements: 30 min

Cytotoxicity of BODIPY-cPAF26 in A549 human lung epithelial cells: Steps 107-131

Steps 107-118, Cell counting and plating: 1 h

Steps 119-120, Overnight cell incubation: 16 h

Steps 121-123, Preparation of **BODIPY-cPAF26** and control solutions: 1 h

Steps 124-125, Incubation of cells with compounds: 4 h

Steps 126-131, MTT cell viability assay: 20 h

Culture of fungal species: Steps 132-151 (can be performed in parallel)

Steps 132-135, Culture of *N. crassa*: 121 h

Steps 136-140, Culture of *A. fumigatus*: 73 h

Steps 141-142, Culture of *C. neoformans*: 73 h

Steps 143-149, Culture of *F. oxysporum*: 121 h

Steps 150-151, Culture of *C. albicans*: 73 h

Antifungal activity measurements of BODIPY-cPAF26 and PAF26 peptides in *N. crassa* and *A. fumigatus*: Steps 152-162

Steps 152-153, Peptide dilutions: 30 min

Steps 154-160, Plate preparation: 1 h

Steps 161-162, Overnight incubation and measurements: 24.5 h

Preparation of fungal cells for live-cell fluorescence imaging: Steps 163-189 (can be performed in parallel)

Steps 163-166, Preparation of *N. crassa* cells: 4.5 h

Steps 167-170, Preparation of *A. fumigatus* cells: 25 h

Steps 171-179, Preparation of *C. neoformans* cells: 21.5 h

Steps 180-182, Preparation of *F. oxysporum* cells: 9 h

Steps 183-189, Preparation of *C. albicans* cells: 13.5 h

General setup of the fluorescence confocal microscope for live-cell imaging: Steps 190-198

Steps 190-198, Microscope set-up: 30 min

Live-cell fluorescence imaging of fungal cells using BODIPY-cPAF26: Steps 199-206

Steps 199-202, Sample preparation: 15 min

Steps 203-206, Incubation of **BODIPY-cPAF26** and image acquisition: 30 min

Real-time fluorescence imaging of *A. fumigatus* using BODIPY-cPAF26: Steps 207-219

Steps 207-213, Sample preparation and incubation of counterstain: 30 min

Steps 214-219, Incubation of **BODIPY-cPAF26** and image acquisition: 30 min

ANTICIPATED RESULTS

Fluorescence properties of the amino acid **1 and the peptide BODIPY-cPAF26.** Both the amino acid **1** and the peptide **BODIPY-cPAF26** display excitation and emission maximum wavelengths in the green region of the visible spectra ($\lambda_{exc.} \sim 500$ nm, $\lambda_{em.} \sim 520$ nm), making them compatible with GFP/FITC filters in most equipments (Figure 3). **BODIPY-cPAF26** displays strong fluorogenic behavior, with quantum yields over 30 % in phospholipid membranes and negligible fluorescence in aqueous media (Figures 5 and 12).

Fluorescence live-cell imaging of fungal cells and real-time imaging of *A. fumigatus* using the peptide BODIPY-cPAF26. We employed the peptide BODIPY-cPAF26 for confocal fluorescence imaging of several fungal pathogens, including *N. crassa*, *A. fumigatus*, *C. neoformans*, *F. oxysporum* and *C. albicans*. The fluorogenic behavior of BODIPY-cPAF26 enables direct live-cell imaging by simple incubation of the peptide with the fungal cells, in a single step and without the need for any washing (Figure 6). We also performed real-time imaging experiments using BODIPY-cPAF26 in *A. fumigatus* (Figure 7). Time-course fluorescence imaging at high magnification show staining of the cells a few seconds after the addition of BODIPY-cPAF26 to the media, and its preferential localization in the fungal cell membranes.

Characterization data for *m*-iodophenyl-BODIPY (3).

Red powder, 234 mg (98 % purity, 24 % yield). HPLC t_R = 8.0 min (Gradient_2, Table 4).

^1H NMR (CDCl_3 , 400 MHz): δ 7.76 (dt, J = 7.7, 1.5 Hz, 1H), 7.62 (t, J = 1.6 Hz, 1H), 7.24 – 7.20 (m, 1H), 7.19 – 7.14 (m, 1H), 5.92 (s, 2H), 2.48 (d, J = 1.3 Hz, 6H), 1.36 (s, 6H).

^{13}C NMR (CDCl_3 , 100 MHz): δ 155.9, 142.9, 139.3, 138.0, 137.1, 136.8, 130.7, 127.3, 121.5, 94.3, 14.7, 14.6 (one quaternary carbon signal not seen).

HRMS (m/z): $[\text{M}+\text{H}]^+$ calcd. for $\text{C}_{19}\text{H}_{18}\text{BF}_2\text{IN}_2$, 451.0654; found: 451.0651.

Characterization data for Fmoc-Trp(C_2 -BODIPY)-OH (1).

Red powder, 122 mg (> 99 % purity, 56% yield). HPLC t_R = 7.0 min (Gradient_2, Table 4).

^1H NMR (CDCl_3 , 400 MHz): δ 8.12 (s, 1H), 7.69 – 7.56 (m, 4H), 7.48 (t, J = 7.7 Hz, 1H), 7.41 (t, J = 1.7 Hz, 1H), 7.37 (d, J = 4.9 Hz, 2H), 7.30 (t, J = 8.0 Hz, 3H), 7.25 – 7.21 (m, 1H), 7.20 – 7.13 (m, 3H), 7.07 (ddd, J = 8.0, 7.0, 1.1 Hz, 1H), 5.90 (s, 1H), 5.87 (s, 1H), 5.09 (d, J = 8.0 Hz, 1H), 4.55 (d, J = 7.5 Hz, 1H), 4.17 (q, J = 10.3, 9.4 Hz, 2H), 4.01 (s, 1H), 3.44 – 3.37 (m, 1H), 3.37 – 3.28 (m, 1H), 2.47 (s, 3H), 2.46 (s, 3H), 1.38 (s, 3H), 1.35 (s, 3H).

^{13}C NMR (CDCl_3 , 100 MHz): δ 174.8, 163.1, 156.0, 155.9, 143.9, 143.2, 141.4, 140.7, 136.1, 136.0, 135.1, 133.9, 131.5, 130.1, 129.1, 128.8, 127.9, 127.8, 127.2, 125.2, 123.2, 121.6, 120.5, 120.1, 119.3, 111.2, 108.2, 67.2, 47.2, 36.9, 28.0, 14.8, 14.7.

HRMS (m/z): $[\text{M}+\text{Na}]^+$ calcd. for $\text{C}_{45}\text{H}_{39}\text{BF}_2\text{N}_4\text{O}_4$, 771.2930; found: 771.2925.

Characterization data for H-Arg(NO_2)-Lys(Z)-Lys(Z)-Trp(C_2 -BODIPY)-Phe-Trp-Gly-OH.

Red powder, 61 mg (90 % purity, 75 % yield).

HPLC-MS (m/z): $[\text{M}+\text{H}]^+$ calcd for $\text{C}_{86}\text{H}_{98}\text{BF}_2\text{N}_{17}\text{O}_{14}$, 1642.6, found 1643.2.

Characterization data for cyclo(Arg(NO_2)-Lys(Z)-Lys(Z)-Trp(C_2 -BODIPY)-Phe-Trp-Gly).

Red powder, 53 mg (88 % purity, 77 % yield).

HPLC-MS (m/z): $[\text{M}+\text{H}]^+$ calcd for $\text{C}_{86}\text{H}_{96}\text{BF}_2\text{N}_{17}\text{O}_{13}$, 1624.6, found 1626.2.

Characterization data for the BODIPY-cPAF26 peptide.

Crude form: red powder, 25 mg (85 % purity, 58 % yield)

Pure form: red powder, 9.2 mg (> 99 % purity, 25 % yield). HPLC t_R = 5.8 min (Gradient_1, Table 4).

^1H NMR (CD_3OD , 600 MHz): δ 8.55 (s, 3H), 7.89 – 7.84 (m, 1H), 7.71 (t, J = 7.7 Hz, 1H), 7.65 (d, J = 7.8 Hz, 1H), 7.60 – 7.55 (m, 2H), 7.42 (dt, J = 8.1, 0.9 Hz, 1H), 7.40 – 7.36 (m, 2H), 7.18 – 7.12 (m, 5H), 7.11 (s, 1H), 7.06 (m, 3H), 6.94 (m, 1H), 6.10 (s, 1H), 6.06 (s, 1H), 4.45 (t, J = 7.4 Hz, 1H), 4.32 (d, J = 10.5 Hz, 1H), 4.25 (m, 1H), 4.17 – 4.07 (m, 2H), 4.04 (d, J = 16.5 Hz, 1H), 4.00 (m, 1H), 3.63 (dd, J = 14.9, 9.5 Hz, 1H), 3.51 – 3.45 (m, 1H), 3.38 (m, 1H), 3.30 (1H), 3.27 – 3.23 (m, 2H), 3.15 (dd, J = 14.2, 7.5 Hz, 1H), 3.10 (dd, J = 14.0, 5.9 Hz, 1H), 2.90 (td, J = 8.6, 4.2 Hz, 2H), 2.72 (t, J = 7.7 Hz, 2H), 2.63 (dd, J = 14.2, 8.5 Hz, 1H), 2.51 (s, 3H), 2.50 (s, 3H), 2.09 – 1.88 (m, 4H), 1.76 (m, 1H), 1.67 (m, 3H), 1.52 (m, 7H), 1.48 – 1.41 (m, 4H), 1.37 (m, 2H), 1.26 – 1.14 (m, 2H).

HRMS (m/z): $[\text{M}+\text{H}]^+$ calcd for $\text{C}_{70}\text{H}_{85}\text{BF}_2\text{N}_{16}\text{O}_7$, 1311.6926, found 1311.6864.

Acknowledgements

L. M.-T. acknowledges the support of MEC-D- Spain for a FPU Scholarship. R. S.-F. acknowledges the support of a MSCA Individual Fellowship (659046). R. L. acknowledges the support of DGICYT-Spain (CTQ2015-67870-P) and Generalitat de Catalunya (2014 SGR 137). M. V.

acknowledges the support of the Medical Research Council, the Marie Curie Integration Grant (333847), and the Biotechnology and Biological Sciences Research Council (BB/M025160/1). The authors thank Luxembourg Bio Technologies, Ltd. (Rehovot) for the kind supply of OxymaPure and derived reagents.

Author contributions

L. M.-T. performed all compound syntheses and chemical characterization; R. S.-F. performed in vitro spectral and biological characterization; C. Z. and N. D. R. designed and performed the experiments with fungal cells; F. A., R. L. and M. V. designed the chemical syntheses; R. L. and M. V. supervised the project; M. V. analyzed the data and wrote the paper. All authors discussed the results and commented on the manuscript.

Competing financial interests

The authors declare competing financial interests (see HTML version of this article for details).

Figures with Figure Legends

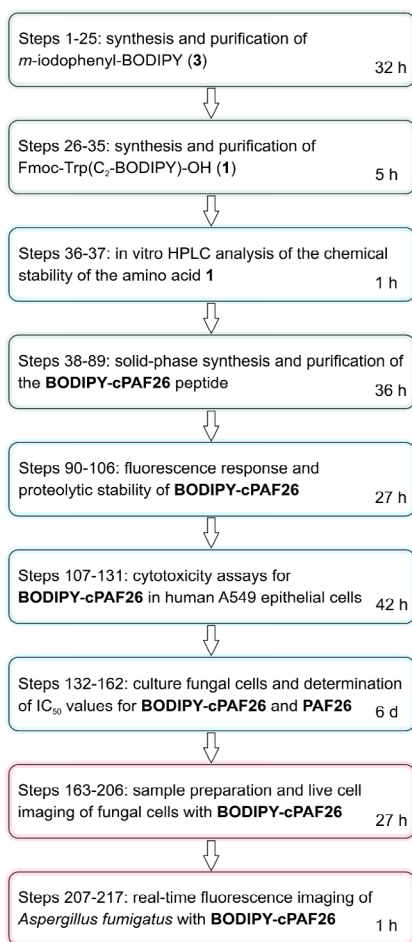


Figure 1. Flowchart outlining all the experimental procedures described in this protocol, which includes chemical synthesis (yellow), in vitro characterization (blue) and fluorescence imaging assays (red).

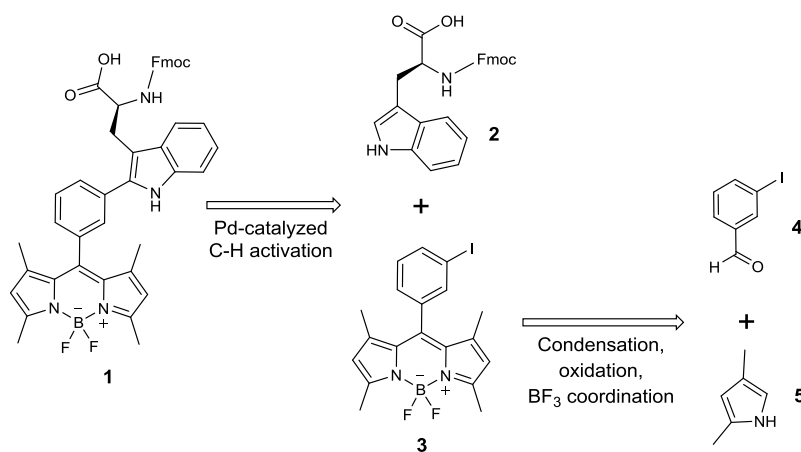


Figure 2. Retrosynthetic analysis of the amino acid Fmoc-Trp(C₂-BODIPY)-OH (**1**).

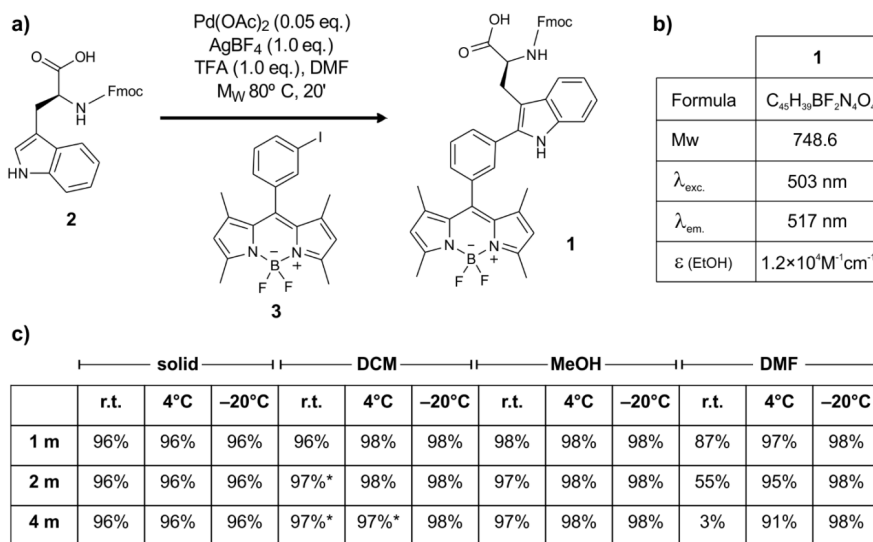


Figure 3. Synthesis and chemical characterization of amino acid Fmoc-Trp(C₂-BODIPY)-OH (1**).** a) Preparation of the amino acid **1** from Fmoc-Trp-OH (**2**) and *m*-iodophenyl-BODIPY (**3**). b) Spectral properties of the amino acid **1**. c) Long-term stability (as determined by HPLC analysis) of the amino acid **1** as solid and in solution (0.1 M) at different temperatures. *: determined after redissolving due to solvent evaporation.

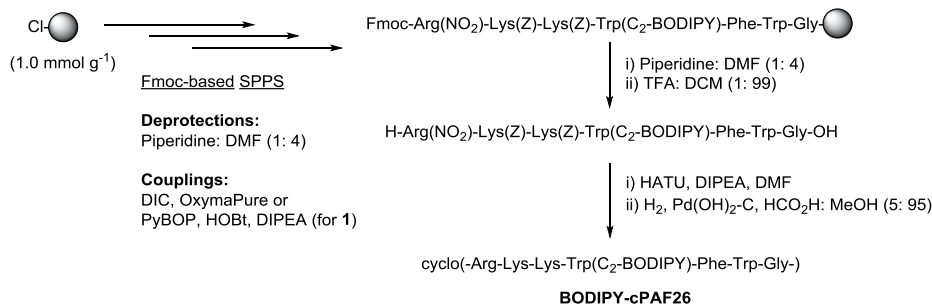


Figure 4. Synthetic scheme for the preparation of **BODIPY-cPAF26** on solid-phase.

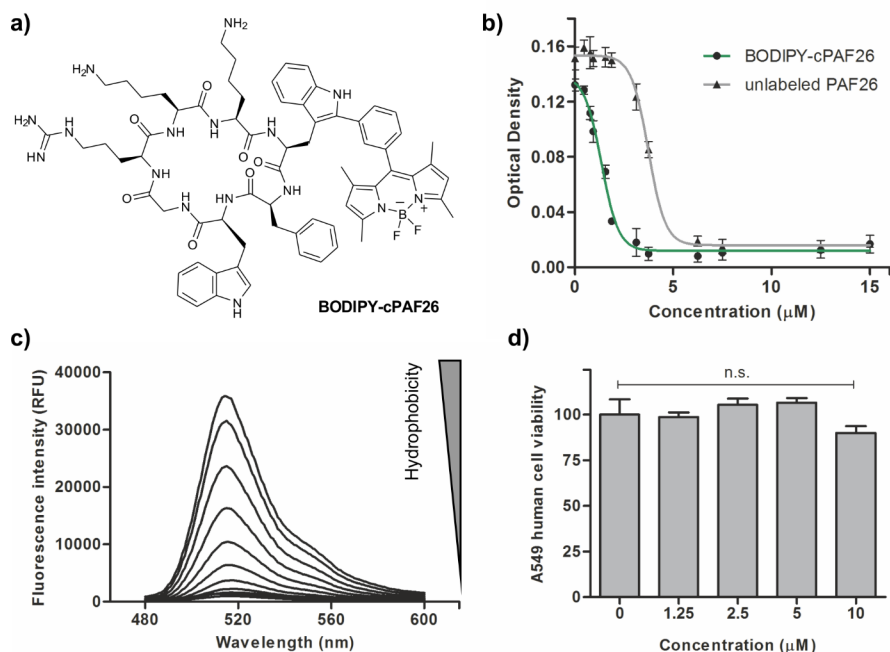


Figure 5. **BODIPY-cPAF26** is a fluorogenic peptide with high affinity for fungal cells. a) Chemical structure of **BODIPY-cPAF26**. b) Cell viability plots and non-linear regressions for **BODIPY-cPAF26** and unlabeled PAF26 in *N. crassa*. Both peptides were incubated at the same concentrations with *N. crassa* conidia, and after 24 h at 25 °C fungal growth was determined by measuring the optical density at 610 nm. Data represented as means ± s.d. (n=3). c) Fluorescence spectra of **BODIPY-cPAF26** after incubation with liposome suspensions of PC: cholesterol (7:1) in PBS ranging from 3.75 mg mL⁻¹ to 0.007 mg mL⁻¹ of PC in 2-fold serial dilutions, λ_{exc.}: 450 nm. d) Viability of human lung A549 epithelial cells after incubation with different concentrations of

BODIPY-cPAF26. Data represented as means \pm s.d. (n=4). No significant differences ($p > 0.05$) were found between untreated cells and any of the treatments.

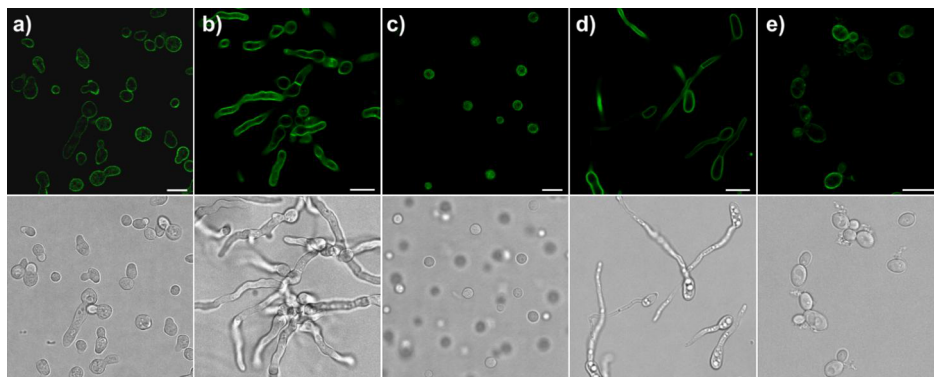


Figure 6. BODIPY-cPAF26 stains various fungal species, including several fungal pathogens. Confocal live-cell images (*top*: fluorescence, *bottom*: bright field) of different fungal species after incubation with **BODIPY-cPAF26** (2 μ M for a-d, 10 μ M for e,) for 10 min, without any washing steps. a) *N. crassa*, b) *A. fumigatus*, c) *C. neoformans*, d) *F. oxysporum* and e) *C. albicans*. Scale bar: 10 μ m.

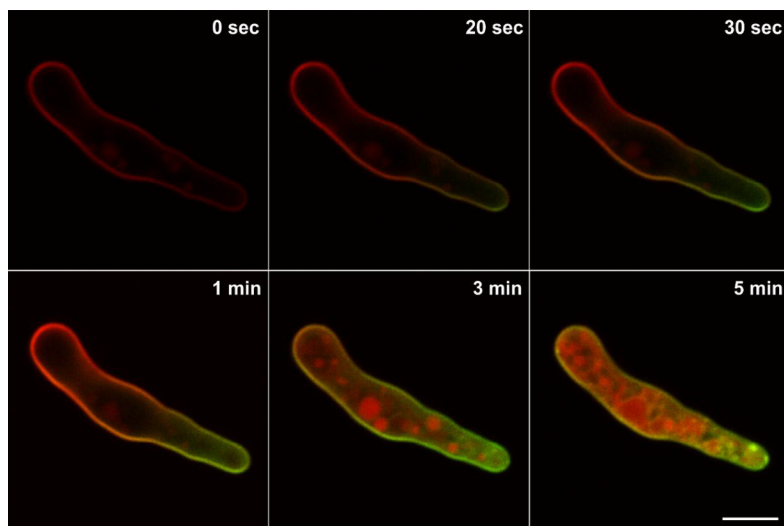


Figure 7. Time-course fluorescence imaging of *A. fumigatus* with BODIPY-cPAF26. High-resolution fluorescence confocal images of the fungal pathogen *A. fumigatus* after incubation with a cell membrane counterstain (red) and following direct addition of **BODIPY-cPAF26** (2 μ M, green) without any washing steps. **BODIPY-cPAF26** initially interacts rapidly with the apical plasma

membrane of *A. fumigatus*, then its staining moves towards the base of the germling cell within a few minutes (see Supplementary Video 1). Scale bar: 5 μm .

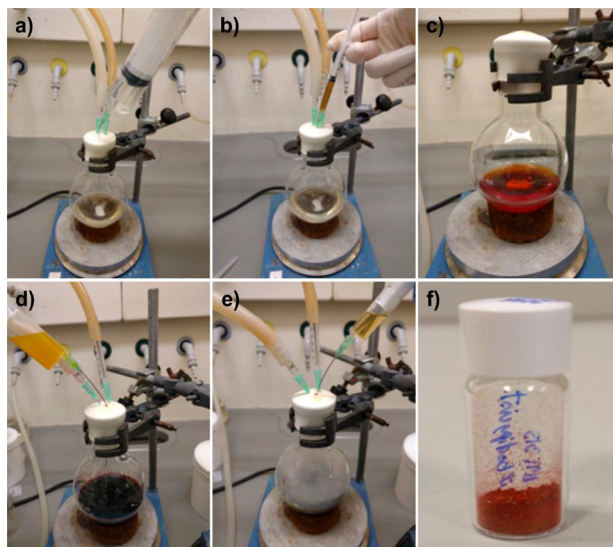


Figure 8. Time-course illustration of the reaction set-up for the synthesis of compound **3** under N_2 . a) Addition of anhydrous DCM, b) addition of 2,4-dimethylpyrrole, c) resulting solution after addition of TFA, d) slow addition of DDQ, e) addition of $\text{BF}_3 \cdot \text{OEt}_2$ to the TEA-containing mixture, f) isolated pure compound **3**.

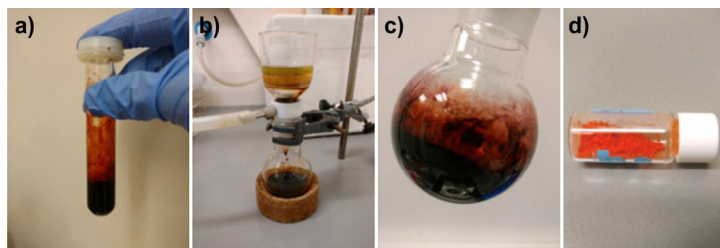


Figure 9. Time-course illustration of the reaction set-up for the synthesis of the amino acid **1**. a) Reaction vessel after microwave irradiation, b) filtration of the crude reaction through Celite under vacuum, c) crude mixture prior to purification, d) isolated pure amino acid **1**.

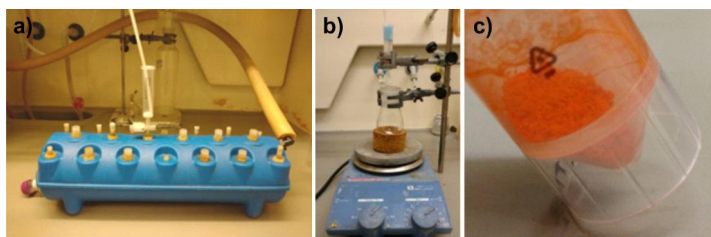


Figure 10. Setup for the solid-phase synthesis of **BODIPY-cPAF26**. a) Manifold for manual SPPS, b) experimental set-up for cleavage of the resin, c) crude protected peptide after lyophilization.

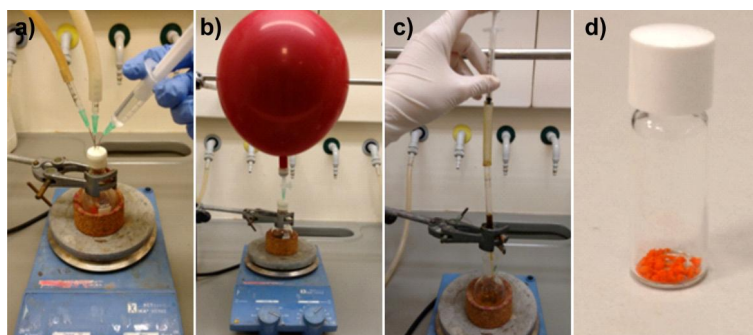


Figure 11. Experimental setup for the hydrogenation of the cyclic protected peptide. a) Purge under N_2 stream, b) hydrogenation reaction under H_2 at atmospheric pressure, c) filtration of crude solution through a glass Pasteur pipette, d) final pure **BODIPY-cPAF26** after semi-preparative HPLC purification.

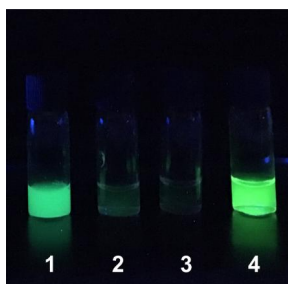
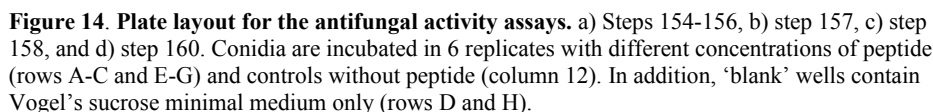
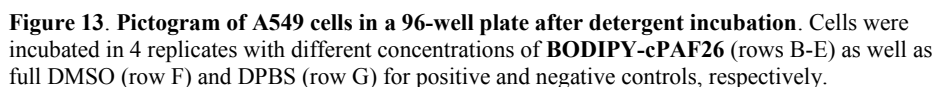


Figure 12. Pictograms of **BODIPY-cPAF26** and fluorescein under excitation with 365 nm light using a hand-held UV lamp. 1) **BODIPY-cPAF26** (10 μM) in high concentration of liposomes, 2) **BODIPY-cPAF26** (10 μM) in low concentration of liposomes, 3) **BODIPY-cPAF26** (10 μM) in DPBS, 4) fluorescein (4 μM) in basic EtOH.



Tables

Table 1. Composition of Vogel's trace element solution (store at 4 °C).

Citric acid · H ₂ O	5 g
ZnSO ₄ · 7 H ₂ O	5 g
(NH ₄) ₂ Fe(SO ₄) ₂ · 6 H ₂ O	1 g
CuSO ₄ · 5 H ₂ O	250 mg
MnSO ₄ · H ₂ O	50 mg
H ₃ BO ₃	50 mg
Na ₂ MoO ₄ · 2H ₂ O	50 mg
dH ₂ O	1 L

Table 2| Composition of Vogel's salts 50X stock solution (store at 4 °C).

Sodium citrate · 2 H ₂ O	127 g
KH ₂ PO ₄	250 g
NH ₄ NO ₃	100 g
MgSO ₄ · 7 H ₂ O	10 g
CaCl ₂ · 2 H ₂ O	5 g
Vogel's trace element solution (see Table 1)	5 mL
Biotin solution (0.5 % (w/v) of d-biotin in dH ₂ O)	5 mL
dH ₂ O	1 L

Table 3| Composition of solid Vogel's sucrose minimal agar medium.

Vogel's salts 50X stock solution (see Table 2)	20 mL
Sucrose	20 g
Agar	20 g
dH ₂ O	1 L

Table 4| HPLC conditions for the analysis of crude mixtures and purified compounds.

Equipment	HPLC	HPLC-MS
Column	XBridge BEH 130 C18 reverse-phase column 4.6 × 100 mm (3.5 µm)	Phenomenex Gemini C18 110A reverse-phase column 4.6 × 50 mm (particle size 3.5 µm)
Solvents	A: H ₂ O (0.045 % TFA (v/v)) B: ACN (0.036 % TFA (v/v))	A: H ₂ O (0.1 % FA (v/v)) B: ACN (0.1 % FA (v/v))
Flow rate	1 mL min ⁻¹	1 mL min ⁻¹
Gradient_1	5-100% (v/v) B over 8 min; 100% (v/v) B over 3 min; 100-5% (v/v) B over 0.5 min; 5% (v/v) B over 3 min	0-100% (v/v) B over 8 min; 100 % (v/v) over 3 min; 100- 0% (v/v) B over 0.5 min; 0% (v/v) B over 2.5 min
Gradient_2	50-100% (v/v) B over 8 min; 100% (v/v) (v/v) B over 3 min; 100-50% (v/v) B over 0.5 min; 50% (v/v) B over 3 min	-
Injection volume	2-15 µL	10-50 µL
Detection wavelengths	210-400 nm	210-600 nm

Table 5 | Semi-preparative HPLC conditions for the purification of compounds.

Column	Jupiter C12 reverse-phase column 21.2 × 100 mm (10 μm), Proteo 90 Å, Ax (Phenomenex)
Solvents	A: H ₂ O (0.1 % TFA (v/v)) B: ACN (0.05 % TFA (v/v))
Flow rate	16 mL min ⁻¹
Gradient	0–35% (v/v) B over 5 min; 35–55% (v/v) B over 18 min; 100–0% (v/v) B over 1 min; 0% (v/v) B over 1 min
Injection volume	500 μL
Detection wavelengths	220 and 310 nm

Table 6 | Reagents needed for the solid-phase peptide synthesis of **BODIPY-cPAF26**.

Resin weight: 45.0 mg		Loading capacity: 1 mmol g ⁻¹		
Reagent	Equivalents	Molecular weight	Density	Quantity
Fmoc-Gly-OH	1.0	297.3 g mol ⁻¹	-	13 mg
DIPEA	3.0	129.2 g mol ⁻¹	0.742 g mL ⁻¹	24 μL
DIPEA	7.0	129.2 g mol ⁻¹	0.742 g mL ⁻¹	55 μL
Fmoc-Trp-OH	3.0	426.5 g mol ⁻¹	-	57 mg
Fmoc-Phe-OH	3.0	387.4 g mol ⁻¹	-	52 mg
Fmoc-Lys(Z)-OH	3.0	502.6 g mol ⁻¹	-	68 mg
Fmoc-Arg(NO ₂)-OH	3.0	441.4 g mol ⁻¹	-	60 mg
DIC	3.0	126.2 g mol ⁻¹	0.815 g mL ⁻¹	21 μL
OxymaPure	3.0	142.1 g mol ⁻¹	-	19 mg
Fmoc-Trp(C ₂ -BODIPY)-OH	1.5	748.6 g mol ⁻¹	-	51 mg
PyBOP	1.5	520.4 g mol ⁻¹	-	35 mg
HOBt (hydrate)	1.5	153.1 g mol ⁻¹	-	10 mg
DIPEA	2.0	129.2 g mol ⁻¹	0.742 g mL ⁻¹	16 μL

Table 7 | Troubleshooting.

Step(s)	Problem	Possible reason	Possible solution
23	Compound 3 is eluted with only hexane during column chromatography	Incorrect equilibration of the purification system or traces of DCM remaining after evaporation	Combine all fractions in a round-bottom flask to remove the solvent and repeat the purification steps
25	Low recovery yield after column chromatography	Compound 3 co-elutes with some byproducts	Combine impure fractions in a round-bottom flask, remove the solvent and crystallize compound 3 in DCM: hexane (1: 6)
31	Low conversion in the	Crude impurities or large scale may decrease the	Add more Pd(OAc) ₂ and AgBF ₄ and perform an

	formation of compound 1	synthetic yield	additional microwave irradiation cycle
37	Samples of amino acid 1 in solution dry out	Low boiling point of the solvent used	Re-dissolve the dry sample in MeOH and analyze by HPLC-MS
54	Positive Kaiser test	Partial amino acid incorporation	Repeat the coupling. Alternatively, employ longer reaction times (16 h) or reaction conditions from steps 48-52
54, 62	Unclear result in Kaiser test	Partial amino acid incorporation or too many resin beads used for the test	Repeat the test with less resin beads. If still unclear, cleave a small portion of the resin and analyze it by HPLC. If the incorporation of the amino acid is partial, repeat the coupling.
62	Positive Kaiser test	Partial amino acid incorporation	Repeat the coupling using 0.5 eq. of amino acid 1 , HOBT and PyBOP and 1 eq. DIPEA
62	Abnormal color in Kaiser test	The BODIPY fluorophore gives intense yellow color	Repeat the test with less resin beads
82	BODIPY-cPAF26 peptide not formed and/or formation of byproducts	Low catalyst efficiency	Repeat the hydrogenation reaction with a different source/batch of Pd(OH) ₂ -C
82	BODIPY-cPAF26 peptide not detected	Incomplete removal of the NO ₂ protecting group	Repeat the hydrogenation for a longer time, refilling the H ₂ balloon and with re-addition of Pd(OH) ₂ -C
94	Minor degradation observed for PAF26	Low protease concentration	Increase the pH of the buffer to 7.5-7.8 with sodium dibasic phosphate to speed up the degradation
106	No differences in fluorescence between different liposome suspensions	Wrong concentration of BODIPY-cPAF26 or liposome suspensions	Repeat the preparation of the liposome dilutions in DPBS, ensuring all samples are properly vortexed
106	Fluorescein shows little fluorescence emission	pH of the solution is not adequate	Basify the solution with basic EtOH (0.1 N NaOH) or repeat the sample preparation
111	A549 cells do not detach from cell culture flask	The proteolytic activity of trypsin is reduced	Incubate for longer time (5 min). Alternatively, wash the cells again with 10 mL Ca ²⁺ -free DPBS and use a fresh batch of Trypsin-EDTA

120	A549 cells are not adhered to the bottom of the plate(s) or there are signs of contamination	Inadequate manipulation of the cells	Discard plate(s) and use a fresh batch of cells and reagents (i.e. media, DPBS, Trypsin-EDTA)
128	Dark precipitate is not observed in the cells	The MTT reaction is slow	Incubate the cells for longer time, typically another 2 h
131	Absorbance values are too low	Cell number per cell is too low or incubation times are too short	Repeat the experiment with more cells/well or increase the MTT reagent and detergent incubation times
131	Absorbance values are too high	Cell number per well is too high	Decrease cell density when plating
131	High standard deviation between replicates	Inaccurate plating or pipetting	Increase accuracy of cell plating and check the performance of pipettes
133, 138, 142, 145, 151	Fungal cells do not grow properly or there are signs of contamination	Fungus in stock culture is dead or mutated. Poor microbiological technique or growth medium recipe was not followed correctly	Discard flasks. Prepare new cultures using a new batch of medium. Inoculate with a fresh stock culture. Check that the temperature of incubation is correct
162	High variability in absorbance values between replicates	Inaccurate preparation of the 96 well-plate	Confirm the multichannel pipette is working well for all the channels
162	Absorbance values are too low	Not enough cells have been transferred to the 96 well-plate	Gently homogenize the cell suspension during the plating to avoid any cell settlement in the pipette basin
179,189	<i>C. neoformans</i> or <i>C. albicans</i> detach from the bottom of the chamber	Sudden movement of the chamber	Discard cells if they have been treated with peptide. If untreated, leave them in the incubator for further 30 min and avoid sudden movements
194	Fluorescence is not detected during image acquisition	Laser intensity is too low or laser is switched off	Check the laser is switched on and adjust its intensity appropriately
217	Red-stained cell(s) have disappeared from the field of view after the addition of BODIPY-cPAF26	Cells have detached during the addition of BODIPY-cPAF26	Move to another well and, when gently adding BODIPY-cPAF26 , place the pipette tip close to the media surface to minimize any movement generated by impact of the droplet

Additional information

Supplementary Information is available in the online version of the paper.

References

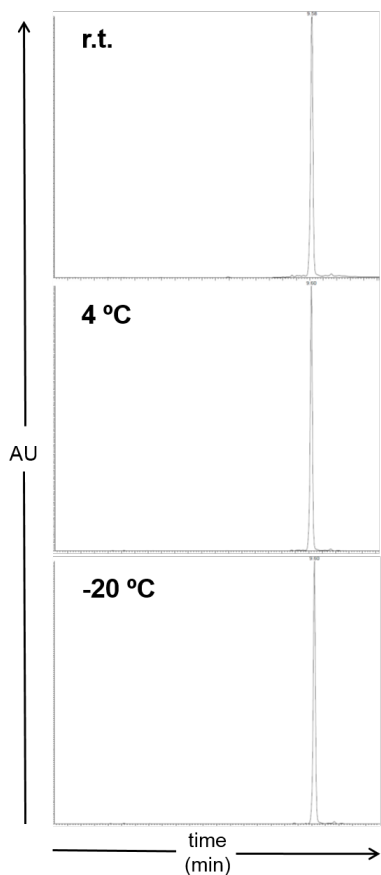
1. For a recent review, see: Schumacher, D. & Hackenberger, C.P. More than add-on: chemoselective reactions for the synthesis of functional peptides and proteins. *Curr. Opin. Chem. Biol.* **22**, 62-69 (2014).
2. Liu, W., Brock, A., Chen, S., Chen, S. & Schultz, P.G. Genetic incorporation of unnatural amino acids into proteins in mammalian cells. *Nat. Methods* **4**, 239-244 (2007).
3. Lang, K. *et al.* Genetically encoded norbornene directs site-specific cellular protein labelling via a rapid bioorthogonal reaction. *Nat. Chem.* **4**, 298-304 (2012).
4. Nikic, I. *et al.* Minimal tags for rapid dual-color live-cell labeling and super-resolution microscopy. *Angew. Chem. Int. Ed. Engl.* **53**, 2245-2249 (2014).
5. Nikic, I., Kang, J. H., Girona, G.E., Aramburu, I. V. & Lemke, E. A. Labeling proteins on live mammalian cells using click chemistry. *Nat. Protoc.* **10**, 780-791 (2015).
6. Vendrell, M. *et al.* Novel ergopeptides as dual ligands for adenosine and dopamine receptors. *J. Med. Chem.* **50**, 3062-3069 (2007).
7. Zhao, L. *et al.* Synthesis of a cytotoxic amanitin for bioorthogonal conjugation. *Chembiochem* **16**, 1420-1425 (2015).
8. Reiner, T. *et al.* Accurate measurement of pancreatic islet beta-cell mass using a second-generation fluorescent exendin-4 analog. *Proc. Natl. Acad. Sci. U. S. A.* **108**, 12815-12820 (2011).
9. Demeter, O. *et al.* A double-clicking bis-azide fluorogenic dye for bioorthogonal self-labeling peptide tags. *Chem. Eur. J.* **22**, 6382-6388 (2016).
10. Gentil, G. P. *et al.* Synthesis and evaluation of fluorescent Pam3Cys peptide conjugates. *Bioorg. Med. Chem. Lett.* **26**, 3641-3645 (2016).
11. Lee, J. S., Vendrell, M. & Chang, Y.-T. Diversity-oriented optical imaging probe development. *Curr. Opin. Chem. Biol.* **15**, 760-767 (2011).
12. Carlson, J. C., Meimetis, L. G., Hilderbrand, S. A. & Weissleder, R. BODIPY-tetrazine derivatives as superbright bioorthogonal turn-on probes. *Angew. Chem. Int. Ed. Engl.* **52**, 6917-6920 (2013).
13. Meimetis, L. G., Carlson, J. C., Giedt, R. J., Kohler, R. H. & Weissleder, R. Ultrafluorogenic coumarin-tetrazine probes for real-time biological imaging. *Angew. Chem. Int. Ed. Engl.* **53**, 7531-7534 (2014).
14. Shieh, P. *et al.* CalFluors: a universal motif for fluorogenic azide probes across the visible spectrum. *J. Am. Chem. Soc.* **137**, 7145-7151 (2015).
15. Ban, H., Gavriluk, J. & Barbas, C. F., 3rd Tyrosine bioconjugation through aqueous ene-type reactions: a click-like reaction for tyrosine. *J. Am. Chem. Soc.* **132**, 1523-1525 (2010).
16. Mendive-Tapia, L. *et al.* New peptide architectures through C-H activation stapling between tryptophan-phenylalanine/tyrosine residues. *Nat. Commun.* **6**, 7160 (2015).
17. Osberger, T. J., Rogness, D. C., Kohrt, J. T., Stepan, A. F. & White, M. C. Oxidative diversification of amino acids and peptides by small-molecule iron catalysis. *Nature*, doi: 10.1038/nature18941 (2016).
18. Zwanziger, D. *et al.* Novel chemically modified analogues of neuropeptide Y for tumor targeting. *Bioconjug. Chem.* **19**, 1430-1438 (2008).
19. Sibrian-Vazquez, M. *et al.* Synthesis and properties of cell-targeted Zn(II)-phthalocyanine-peptide conjugates. *Bioconjug. Chem.* **18**, 410-420 (2007).

20. Vendrell, M., Samanta, A., Yun, S.-W. & Chang, Y.-T. Synthesis and characterization of a cell-permeable near-infrared fluorescent deoxyglucose analogue for cancer cell imaging. *Org. Biomol. Chem.* **9**, 4760-4762 (2011).
21. Reiner, T. *et al.* Near-infrared fluorescent probe for imaging of pancreatic beta cells. *Bioconjug. Chem.* **21**, 1362-1368 (2010).
22. Mendive-Tapia, L. *et al.* Spacer-free BODIPY fluorogens in antimicrobial peptides for direct imaging of fungal infection in human tissue. *Nat. Commun.* **7**, 10940 (2016).
23. Lopez-Garcia, B., Perez-Paya, E. & Marcos, J. F. Identification of novel hexapeptides bioactive against phytopathogenic fungi through screening of a synthetic peptide combinatorial library. *Appl. Environ. Microbiol.* **68**, 2453-2460 (2002).
24. Vendrell, M. *et al.* Solid-phase synthesis of BODIPY dyes and development of an immunoglobulin fluorescent sensor. *Chem. Commun.* **47**, 8424-8426 (2011).
25. Yraola, F. *et al.* A re-evaluation on the use of Rink, BAL and PAL resins and linkers. *QSAR Comb. Sci.* **23**, 145-152 (2004).
26. Turcatti, G. *et al.* Characterization of non-peptide antagonist and peptide agonist binding sites of the NK1 receptor with fluorescent ligands. *J. Biol. Chem.* **272**, 21167-21175 (1997).
27. Cohen, B. E. *et al.* Probing protein electrostatics with a synthetic fluorescent amino acid. *Science* **296**, 1700-1703 (2002).
28. Koopmans, T., van Haren, M., van Ufford, L. Q., Beekman, J. M. & Martin, N. I. A concise preparation of the fluorescent amino acid L-(7-hydroxycoumarin-4-yl) ethylglycine and extension of its utility in solid phase peptide synthesis. *Bioorg. Med. Chem.* **21**, 553-559 (2013).
29. Ge, J., Li, L. & Yao, S. Q. A self-immobilizing and fluorogenic unnatural amino acid that mimics phosphotyrosine. *Chem. Commun.* **47**, 10939-10941 (2011).
30. Nitz, M., Mezo, A. R., Ali, M. H. & Imperiali, B. Enantioselective synthesis and application of the highly fluorescent and environment-sensitive amino acid 6-(2-dimethylaminonaphthoyl) alanine (DANA). *Chem. Commun.*, 1912-1913 (2002).
31. Vazquez, E. M., Rothman, D. M. & Imperiali, B. A new environment-sensitive fluorescent amino acid for Fmoc-based solid phase peptide synthesis. *Org. Biomol. Chem.* **2**, 1965-1966 (2004).
32. Sainlos, M. & Imperiali, B. Tools for investigating peptide-protein interactions: peptide incorporation of environment-sensitive fluorophores through SPPS-based 'building block' approach. *Nat. Protoc.* **2**, 3210-3218 (2007).
33. Venkatraman, P. *et al.* Fluorogenic probes for monitoring peptide binding to class II MHC proteins in living cells. *Nat. Chem. Biol.* **3**, 222-228 (2007).
34. Vazquez, M. E., Blanco, J. B. & Imperiali, B. Photophysics and biological applications of the environment-sensitive fluorophore 6-N,N-dimethylamino-2,3-naphthalimide. *J. Am. Chem. Soc.* **127**, 1300-1306 (2005).
35. Loving, G. & Imperiali, B. A versatile amino acid analogue of the solvatochromic fluorophore 4-N,N-dimethylamino-1,8-naphthalimide: a powerful tool for the study of dynamic protein interactions. *J. Am. Chem. Soc.* **130**, 13630-13638 (2008).
36. Kowada, T., Maeda, H. & Kikuchi, K. BODIPY-based probes for the fluorescence imaging of biomolecules in living cells. *Chem. Soc. Rev.* **44**, 4953-4972 (2015).
37. Loudet, A. & Burgess, K. BODIPY dyes and their derivatives: syntheses and spectroscopic properties. *Chem. Rev.* **107**, 4891-4932 (2007).
38. Ackermann, L. Carboxylate-assisted transition-metal-catalyzed C-H bond functionalizations: mechanism and scope. *Chem. Rev.* **111**, 1315-1345 (2011).
39. Chen, X., Engle, K. M., Wang, D. H. & Yu, J. Q. Palladium(II)-catalyzed C-H activation/C-C cross-coupling reactions: versatility and practicality. *Angew. Chem. Int. Ed. Engl.* **48**, 5094-5115 (2009).
40. Lebrasseur, N. & Larrosa, I. Room temperature and phosphine free palladium catalyzed direct C-2 arylation of indoles. *J. Am. Chem. Soc.* **130**, 2926-2927 (2008).

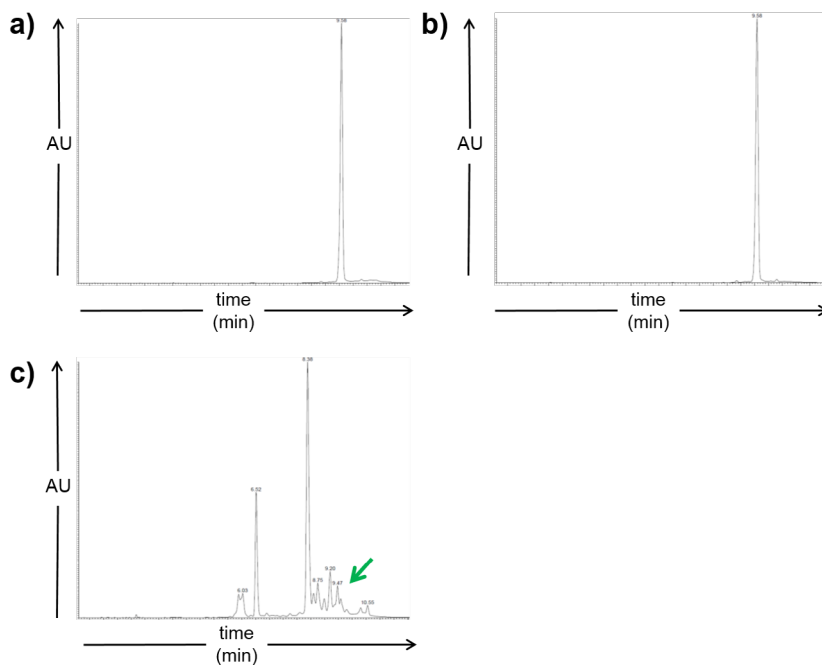
41. Basaric, N. *et al.* Synthesis and spectroscopic characterisation of BODIPY based fluorescent off-on indicators with low affinity for calcium. *Org Biomol Chem* **3**, 2755-2761 (2005).
42. Ruiz-Rodriguez, J., Albericio, F. & Lavilla, R. Postsynthetic modification of peptides: chemoselective C-arylation of tryptophan residues. *Chemistry* **16**, 1124-1127 (2010).
43. Preciado, S., Mendive-Tapia, L., Albericio, F. & Lavilla, R. Synthesis of C-2 arylated tryptophan amino acids and related compounds through palladium-catalyzed C-H activation. *J. Org. Chem.* **78**, 8129-8135 (2013).
44. Zhu, Y., Bauer, M., Ploog, J. & Ackermann, L. Late-stage diversification of peptides by metal-free C-H arylation. *Chemistry* **20**, 13099-13102 (2014).
45. Atherton, E., Bury, C., Sheppard, R. C. & Williams, B. J. Stability of fluorenylmethoxycarbonylamino groups in peptide synthesis. Cleavage by hydrogenolysis and by dipolar aprotic solvents. *Tet. Lett.* 3041-3042 (1979).
46. Welling, M. M. *et al.* Development of a hybrid tracer for SPECT and optical imaging of bacterial infections. *Bioconjug. Chem.* **26**, 839-849 (2015).
47. Akram, A. R. *et al.* A labelled-ubiquicidin antimicrobial peptide for immediate in situ optical detection of live bacteria in human alveolar lung tissue. *Chem. Sci.* **6**, 6971-6979 (2015).
48. Munoz, A. *et al.* Two functional motifs define the interaction, internalization and toxicity of the cell-penetrating antifungal peptide PAF26 on fungal cells. *PLoS One* **8**, e54813 (2013).
49. White, C. J. & Yudin, A. K. Contemporary strategies for peptide macrocyclization. *Nat. Chem.* **3**, 509-524 (2011).
50. Davis, R. H. & Perkins, D. D. Timeline: Neurospora: a model of model microbes. *Nat. Rev. Genet.* **3**, 397-403 (2002).
51. Brown, G. D. *et al.* Hidden killers: human fungal infections. *Sci. Transl. Med.* **4**, 165rv113 (2012).
52. Kaiser, E., Collescott, R.L., Bossinger, C. D. & Cook, P. I. Color test for detection of free terminal amino groups in the solid-phase synthesis of peptides. *Anal. Biochem.* **34**, 595-598 (1970).
53. Gisin, B. F. & Merrifield, R. B. Carboxyl-catalyzed intramolecular aminolysis. Side reaction in solid-phase peptide synthesis. *J. Am. Chem. Soc.* **94**, 3102-3016 (1972).

Supporting Information

A Trp-BODIPY fluorogenic amino acid to label peptides for enhanced live-cell fluorescence imaging

Supplementary Information

Supplementary Figure 1. Analysis of the long-term stability of the amino acid 1 when stored as a solid at different temperatures. HPLC-MS traces of the amino acid 1 after being stored in the dark for 4 months at r.t., 4 °C, and -20 °C. UV detection: 500 nm.



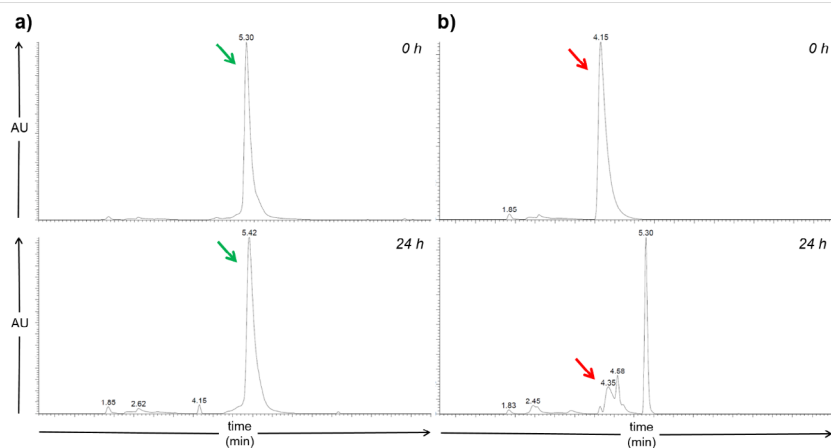
Supplementary Figure 2. Analysis of the long-term stability of the amino acid 1 when dissolved in organic solvents at different temperatures. HPLC-MS traces of the amino acid 1 after being stored in the dark for 4 months in: a) DCM at -20 °C, b) MeOH at 4 °C, c) DMF at r.t. In c), the green arrow points at the remaining amino acid 1 and the main peaks correspond to Fmoc-deprotection side products. UV detection: 500 nm.

Supplementary Table 1. Cellular activity of BODIPY-cPAF26 and PAF26 in different fungal species. Cell viability was measured after 16 h incubation with different concentrations of **BODIPY-cPAF26** or PAF26 peptides at 25 °C for *N. crassa* or 37 °C for *A. fumigatus*. IC₅₀ values (μM) are represented as means ± s.d. (n=3).

	IC ₅₀ (<i>N. crassa</i>)	IC ₅₀ (<i>A. fumigatus</i>)
BODIPY-cPAF26	1.4 ± 0.1	2.2 ± 0.1
PAF26	3.7 ± 0.1	7.9 ± 0.3

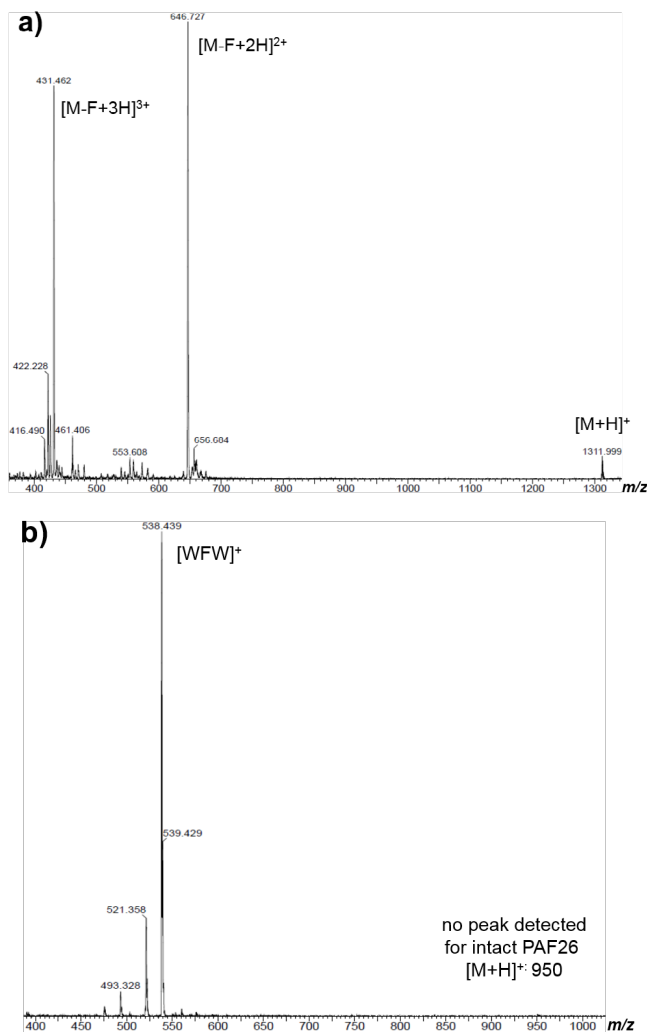
Supplementary Table 2. Fluorescence quantum yields of BODIPY-cPAF26 in PC: cholesterol (7: 1) liposome suspensions in PBS with increasing hydrophobicity. PBS alone was used as a negative control. Quantum yields were determined by comparing the integrated emission area of the fluorescence spectra to the emission area of fluorescein in basic EtOH (QY: 0.97), λ_{exc.}: 450 nm. Data represented as means ± s.d. (n=3).

PC (mg mL ⁻¹) content on liposomes	Quantum yield
3.75	0.32 ± 0.04
1.88	0.27 ± 0.04
0.94	0.20 ± 0.02
0.47	0.14 ± 0.02
0.23	0.09 ± 0.01
0.12	0.06 ± 0.01
0.06	0.04 ± 0.01
0.03	0.02 ± 0.004
0.02	0.02 ± 0.003
0.007	0.01 ± 0.002
PBS	0.01 ± 0.002



Time (h)	Purity (% of intact peptide left)	
	BODIPY-cPAF26	Unlabeled PAF26
0.25	99%	83%
1	99%	79%
4	99%	73%
8	99%	63%
24	98%	20%

Supplementary Figure 3. Time-course analysis of the chemical integrity of BODIPY-cPAF26 and unlabeled linear PAF26 in proteolytic environments. HPLC traces of BODIPY-cPAF26 (a) and unlabeled PAF26 (b) before incubation (*top*) and after incubation (*bottom*) at a concentration of 200 μM in a protease cocktail (1 mg L^{-1}). Green arrows point at the peaks of intact BODIPY-cPAF26 and red arrows point at intact PAF26. UV detection: 280 nm. Purities were determined by integration of the peak areas in respective HPLC chromatograms at 280 nm.



Supplementary Figure 4. Electrospray analysis of BODIPY-cPAF26 and unlabeled PAF26 after 24 h incubation in a protease cocktail. Both peptides (200 μ M) were incubated in 1 mg L⁻¹ of the protease cocktail, and their respective mass spectra were recorded on a Waters Micromass ZQ mass spectrometer (ESI positive mode). a) MS analysis of **BODIPY-cPAF26** (exact mass: 1311 Da); b) MS analysis of unlabeled PAF26 (exact mass: 949 Da).

Supplementary Video 1. Time-course high-resolution imaging of *A. fumigatus* upon treatment with BODIPY-cPAF26. *A. fumigatus* were pre-treated with a cell membrane counterstain (*red*) and imaged under the confocal microscope. Cells were then treated with **BODIPY-cPAF26** (2 μ M, *green*) and further imaged without any washing steps. The movie shows the rapid fluorogenic response of **BODIPY-cPAF26** upon interaction with the cell membrane of *A. fumigatus*. Scale bar: 5 μ m.



3

**BIARYL PEPTIDIC TOPOLOGIES THROUGH
PD-CATALYZED C-H ACTIVATION REACTIONS
BETWEEN TRP AND PHE/TYR RESIDUES**

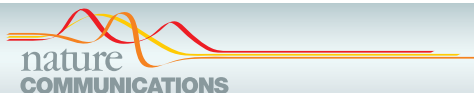
PUBLICATION VII.

New peptide architectures through C–H activation stapling between tryptophan–phenylalanine/tyrosine residues

Lorena Mendive-Tapia,^{a, b, c} Sara Preciado,^b Jesús García,^a Rosario Ramón,^d Nicola Kielland,^d Fernando Albericio,^{a, b, c, e} and Rodolfo Lavilla^{d, f}

Nature Communications, 2015, 6:7160. DOI: 10.1038/ncomms8160.

- a) Institute for Research in Biomedicine, Barcelona Science Park, Baldiri Reixac 10-12, 08028 Barcelona, Spain.
- b) Department Organic Chemistry, University of Barcelona, Martí i Franquès 1-11, 08028 Barcelona, Spain.
- c) CIBER-BBN, Networking Centre for Bioengineering, Biomaterials and Nanomedicine, Baldiri Reixac 10-12, Barcelona 08028, Spain.
- d) Barcelona Science Park, Baldiri Reixac 10-12, 08028 Barcelona, Spain.
- e) School of Chemistry, Yachay Tech, Yachay City of Knowledge, 100119 Urcuqui, Ecuador.
- f) Laboratory of Organic Chemistry, Faculty of Pharmacy, University of Barcelona, Avda. Joan XXII s.n., 08028 Barcelona, Spain.



ARTICLE

Received 5 Nov 2014 | Accepted 10 Apr 2015 | Published 21 May 2015

DOI: 10.1038/ncomms8160

OPEN

New peptide architectures through C-H activation stapling between tryptophan-phenylalanine/tyrosine residues

Lorena Mendive-Tapia^{1,2,3}, Sara Preciado², Jesús García¹, Rosario Ramón⁴, Nicola Kielland⁴, Fernando Albericio^{1,2,3,5} & Rodolfo Lavilla^{4,6}

Natural peptides show high degrees of specificity in their biological action. However, their therapeutical profile is severely limited by their conformational freedom and metabolic instability. Stapled peptides constitute a solution to these problems and access to these structures lies on a limited number of reactions involving the use of non-natural amino acids. Here, we describe a synthetic strategy for the preparation of unique constrained peptides featuring a covalent bond between tryptophan and phenylalanine or tyrosine residues. The preparation of such peptides is achieved in solution and on solid phase directly from the corresponding sequences having an iodo-aryl amino acid through an intramolecular palladium-catalysed C-H activation process. Moreover, complex topologies arise from the internal stapling of cyclopeptides and double intramolecular arylations within a linear peptide. Finally, as a proof of principle, we report the application to this new stapling method to relevant biologically active compounds.

¹Institute for Research in Biomedicine, Barcelona Science Park, Baldri Reixac 10-12, 08028 Barcelona, Spain. ²Department of Organic Chemistry, University of Barcelona, Martí i Franqués 1-11, 08028 Barcelona, Spain. ³CIBER-BBN, Networking Centre on Bioengineering, Biomaterials and Nanomedicine. ⁴Barcelona Science Park, Baldri Reixac 10-12, 08028 Barcelona, Spain. ⁵School of Chemistry, Yachay Tech, Yachay City of Knowledge, 100119 Urcuqui, Ecuador. ⁶Laboratory of Organic Chemistry, Faculty of Pharmacy, University of Barcelona, Avda. Joan XXII s.n., 08028 Barcelona, Spain. Correspondence and requests for materials should be addressed to F.A. (email: albericio@irbbbarcelona.org) or to R.L. (email: rlavilla@pcb.ub.es).

ARTICLE

NATURE COMMUNICATIONS | DOI: 10.1038/ncomms8160

Peptides are attracting great attention as therapeutics since they combine the high selectivity, potency and low toxicity of biologics with advantages such as the conformational restrictions and the reduced costs characteristic of small molecular entities^{1,2}. In addition to the large number of commercialized peptides, many others are also found in clinical phases, thereby demonstrating their validity and application as active pharmaceutical ingredients³. However, the general use of peptides as drugs is severely hampered by their poor pharmacokinetic features. In this regard, it is widely believed that the characterization of protein–protein interactions, a fundamental issue in deciphering biological pathways, is better tackled through structurally defined small peptides with specific sequences. Therefore, there is a need for peptides with new topological architectures; however, these are difficult to obtain even using modern synthetic procedures^{4,5}. To address these problems, general strategies for peptide macrocyclization have been developed to improve the properties (cell penetration, stability, selectivity and so on) and enhance the potential of peptides as therapeutics and bioprobes, with a special focus on poorly tractable targets^{6–8}. In this context, peptides constrained via a non-amide sidechain-to-sidechain linkage (stapled peptides) provide a new structural paradigm because the conformational stabilized species display remarkably stronger biological activity. In this regard, the pioneering work of Verdine *et al.*^{9,10} on the

basis of all-hydrocarbon staples through olefin metathesis represents a breakthrough in the field.

So far, stapled peptides are generated through a variety of strategies¹¹, the main being the use of cysteine side chains to form disulfide bridges¹² and thioether formation (crosslinking with α,α' -dibromo-*m*-xylene¹³ or aromatic nucleophilic substitutions with perfluoroaromatic reactants¹⁴); or with functionalized non-natural amino acids by means of biaryl linkages involving the borylated phenylalanine derivatives^{15–18}, ring-closing metathesis¹⁹ and azide–alkyne cycloadditions (click chemistry)²⁰, and so on, usually in expensive and long stepwise syntheses. A comparative table summarizes the major strengths and weaknesses of the main conventional stapling strategies (Fig. 1a). Owing to the increasing interest in stapled peptides and other conformationally restricted structures, many efforts have been made to develop new practical and general preparative methods for their generation.

There is a considerable concern regarding the efficiency of synthetic aspects with respect to the preparation of complex bioactive compounds. In this context, the function-oriented synthesis approach to target simplified, although biologically meaningful, fragments of complex chemical entities is relevant, as it leads to practical syntheses of new specific drugs and probes, also in the field of peptides²¹.

Tryptophan (Trp) has a low relative abundance in peptide and protein sequences ($\approx 1\%$ of the amino acids); however, its presence is critical for the activity of these biomolecules. Therefore, the development of new synthetic methods for the selective and straightforward chemical modification of Trp is highly significant²².

Recently, metal-catalysed C–C coupling through direct C–H activation^{23–29} has become a fundamental process in modern organic syntheses, allowing the straightforward preparation of a plethora of new structural types. In this respect, the functionalization of indoles using this approach has been extensively examined^{30,31}, including studies described in (refs 28, 32–35) among others. Particularly relevant to our research was the methodology of Larrosa for indole arylation using Pd(OAc)₂ in acidic media³⁶. In particular, although the Pd-mediated C-2 arylation of Trp has been reported^{37–39}, it has not yet been applied to staple true peptides. We recently disclosed the direct C-2 arylation of indoles in Trp-containing peptidic sequences in an intermolecular manner, without additional requirements³⁷. Although the alternative *N*-arylation processes are conceivable, such Ullmann-type reactions take place normally with Cu and Pd catalysts, in the latter case usually requiring strong bases⁴⁰. No experimental evidence of these transformations have been recorded in our systems. The main restriction is that lower conversions are obtained for sequences that comprise methionine, cysteine or histidine residues, presumably because of selective hydrolysis of the peptide bond catalysed by bidentate palladium coordination; on-going experiments along this line show that working in nonaqueous solvents allows reasonable arylations (unpublished results). Later we reported on the arylation of Trp-diketopiperazines⁴¹ and related transformations of Trp derivatives, leading to the generation of Fmoc-protected arylated Trps that are amenable to direct incorporation in solid-phase peptide synthesis (SPPS)⁴². These processes work well with *N*-protected peptides in dimethylformamide (DMF) or in aqueous environments.

In this work, we present a new stapling methodology involving Trp and Phe(Tyr) through a Pd-catalysed C–H activation process. The method is versatile, allowing the formation of constrained peptides of different ring sizes, amenable to solution- and solid-phase synthesis and can lead to the direct preparation of biologically meaningful peptide derivatives.

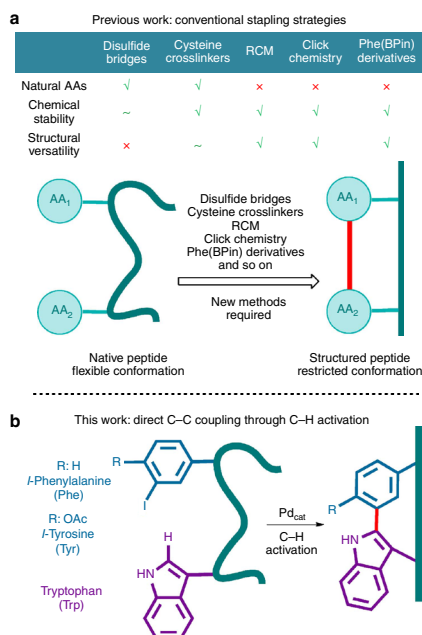
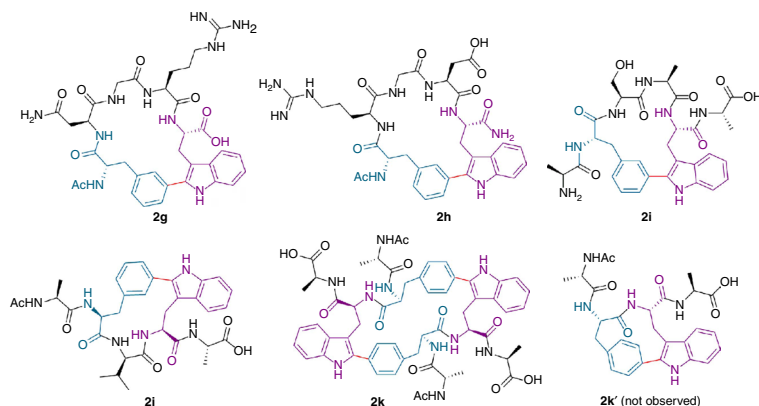


Figure 1 | Formation of stapled peptides. (a) Conventional stapling methods. (b) Phe/Tyr–Trp stapling via a selective Pd-catalysed C–H arylation process.

Table 1 | Results for the stapled bond formation of peptides 1 under microwave irradiation.

Entry	<i>n</i>	Linear peptide (1)	Coupling conditions ^a	Stapled peptide	Conv. (%) ^b
1	1	Ac-Ala- <i>m</i> -I-Phe-Ala-Trp-Ala-OH (1a)	A	2a	38
2	2	Ac-Ala- <i>m</i> -I-Phe-Ala-Ala-Trp-Ala-OH (1b)	A	2b	100
3	3	Ac-Ala- <i>m</i> -I-Phe-Ala-Ala-Ala-Trp-Ala-OH (1c)	A	2c	100
4	1	Ac-Ala- <i>m</i> -I-Tyr-Ala-Trp-Ala-OH (1d)	A	2d	100
5	2	Ac-Ala- <i>m</i> -I-Tyr-Ala-Ala-Trp-Ala-OH (1e)	A	2e	100
6	3	Ac-Ala- <i>m</i> -I-Tyr-Ala-Ala-Ala-Trp-Ala-OH (1f)	A	2f	100
7	3	Ac- <i>m</i> -I-Phe-Asn-Gly-Arg-Trp-NH ₂ (1g)	B	2g	77
8	3	Ac- <i>m</i> -I-Phe-Arg-Gly-Asp-Trp-NH ₂ (1h)	B	2h	70
9	2	H-Ala- <i>m</i> -I-Phe-Ser-Ala-Trp-Ala-OH (1i)	B	2i	39 [†]
10	1	Ac-Ala- <i>m</i> -I-Phe-Val-Trp-Ala-OH (1j)	B	2j	71
11	0	Ac-Ala- <i>p</i> -I-Phe-Trp-Ala-OH (1k)	B	2k [‡]	60

Conv, conversion; HPLC-MS, high-performance liquid chromatography-mass spectrometry; MW, microwave.
^aCoupling conditions (A): 5 mol % Pd(OAc)₂, 1.0 eq. of AgBF₄, 1.5 eq. of 2-NO₂BzOH in DMF:PBS (1:1), MW 80 °C, 15 min. (B) 5 mol % Pd(OAc)₂, 2.0 eq. of AgBF₄, 1.0 eq. of TFA in DMF, MW 90 °C, 20 min.
^bConversion: estimated yield (HPLC-MS).
[†]Additional MW irradiation cycles were necessary to obtain the desired product as the main compound (HPLC-MS).
[‡]Cyclodimer **2k** was obtained in place of the putative monomeric structure **2k'**.

**Figure 2 | Structure of isolated locked peptides 2g–2k.** Schematic representation: Phe (blue), Trp (purple) and staple bond (red).

Results

Preliminary studies. Here we present a one-step process for the synthesis of Trp–Phe(Tyr)-stapled peptides directly from commercially available precursors. The method is based on an intramolecular Pd-catalyzed C–H activation reaction between a Trp residue and an iodo-phenylalanine (or tyrosine) unit (Fig. 1b).

After a preliminary modelling study, we established the structural features for the intramolecular C–H arylation, placing the iodo-substituent for Phe or Tyr amino acids in the *meta* position. The preferential distances between these latter residues and Trp ranged from one to three amino acids in a series of linear N-terminal-acetylated sequences.

The initial experiments were carried out using the conditions previously applied in the arylation of the Trp diketopiperazine:⁴¹ Overall, 5 mol % Pd(OAc)₂, AgBF₄ (1.0 eq.) and *o*-nitrobenzoic acid (2-NO₂BzOH) (1.5 eq.) in PBS:DMF (1:1) under microwave (MW) irradiation at 80 °C for 15 min (Table 1, entries 1–6). These preliminary observations suggested that these arrangements are suitable for stapled peptide formation, affording good to excellent conversions for Trp–Phe(Tyr) staples located at *i*–*i*+2, *i*–*i*+3 and *i*–*i*+4 positions (Table 1, entries 1–6). Furthermore, a series of representative sequences displaying from one to three amino acids between Trp and *m*-iodinated Phe were constrained in useful yields (Table 1, entries 7–10; Fig. 2; see Supplementary Fig. 1), in an

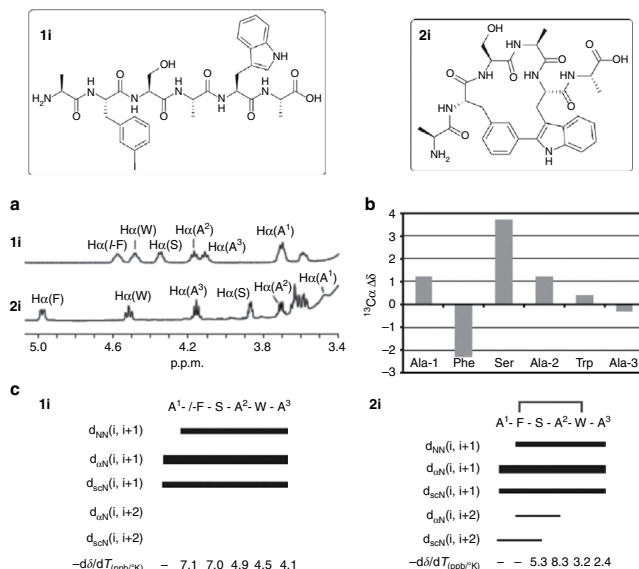


Figure 3 | Peptide NMR spectra comparison between stapled peptide **2i and its linear counterpart **1i**.** (a) NMR H_α region of peptide **2i** and its linear precursor **1i**. (b) Plot of the $^{13}\text{C}_\alpha$ chemical shift differences ($^{13}\text{C}_\alpha \Delta\delta_{\text{cyclic-linear}}$) between stapled peptide **2i** and its linear counterpart **1i**. (c) Summary of NOE connectivity and temperature coefficients of the NH amide protons ($\Delta\delta/\Delta T$) of peptide **1i** (bottom left) and **2i** (bottom right). The thickness of the bars reflects the intensity of the NOEs, that is, weak (—), medium (▬) and strong (■). *I*-F: *m*-iodophenylalanine.

anhydrous medium using trifluoroacetic acid (TFA) as the acid, applying the optimized conditions previously reported for the preparation of Fmoc-protected arylated Trps⁴². Although these transformations may lead to atropisomeric diastereomers, only one stereochemically defined structure was observed in each case. Of note is the successful application of this technique to stapled peptides containing the Asn-Gly-Arg (-NGR-) and Arg-Gly-Asp (-RGD-) tumour-homing signalling sequences (**2g** and **2h**, Table 1, entries 7 and 8, respectively).

Preliminary studies on the capacity of the RGD-containing compound **2h** and its linear precursor **1h** to inhibit cellular adhesion showed that these substances act selectively as antagonists for the $\alpha v\beta 3$ in front of $\alpha v\beta 5$ integrin receptors; compound **2h** showing a moderate EC_{50} (6 μM) is more active than its linear precursor (**1h**, 26 μM , see Biochemical and Cellular Studies in Supplementary Methods). Compound **2h** is considerably less potent than ctenilgite, not surprisingly as this drug has been thoroughly optimized. However, it has to be considered that even linear analogues display a much lower potency (10–10³ times, depending on the targeted integrin) than the parent ctenilgite^{43,44}. These preliminary results clearly show that this stapling technique preserves the activity of the natural sequence, while improving its potency, in line with pioneering experiments in macrocyclization techniques for medchem peptide development^{45,46}.

We next tackled the preparation of the more challenging locked peptide $i-i+1$. Three sequences with adjacent Trp—(ortho-, meta- or para)-I-Phe were synthesized. A constrained C–C linked structure was obtained for the meta-derivative (60%),

although it could not be properly characterized. With respect to the ortho analogue, only the reduced peptide was detected. Interestingly, the para-I-Phe peptide **1k** was successfully reacted under the usual conditions to yield cyclodimer **2k** (60%, Table 1, entry 11; see Supplementary Figs 2 and 3). Presumably, the putative monomeric structure **2k'** would be highly strained (molecular models display a nonplanar phenyl ring, see Supplementary Fig. 4) and the process evolves through a ditopic pathway, in a remarkable demonstration of the process versatility.

A detailed nuclear magnetic resonance (NMR) study was performed on dimethylsulphoxide to analyse the conformational behaviour of the peptides synthesized. The NMR spectra of linear sequences **1g–1j** were indicative of flexible, unstructured peptides. H_α and $^{13}\text{C}_\alpha$ chemical shifts displayed values typical for random coil, and the NH temperature coefficients and $^3\text{J}(\text{H}_\alpha\text{NH})$ couplings were within the range expected for unstructured peptides⁴⁷.

Staple bond formation caused a substantial modification of the peptide NMR spectra. Compared with their linear precursors, peptides **2g–2j** showed larger H_α chemical shift dispersion (Fig. 3a and Supplementary Figs 5–7), indicating less conformational flexibility. However, broad resonances were observed at 25 °C for some backbone NH protons, suggesting that peptides **2g–2j** show some flexibility. Significant differences in $^{13}\text{C}_\alpha$ chemical shifts were observed between stapled peptides **2g–2j** and their linear counterparts **1g–1j** (Fig. 3b and Supplementary Figs 5–7). The temperature dependence of the amide NH groups was also significantly affected by staple formation (Fig. 3c and Supplementary Figs 5–7). Stapled peptides showed a wider distribution of $\Delta\delta/\Delta T$ values within the amino-acid sequence and

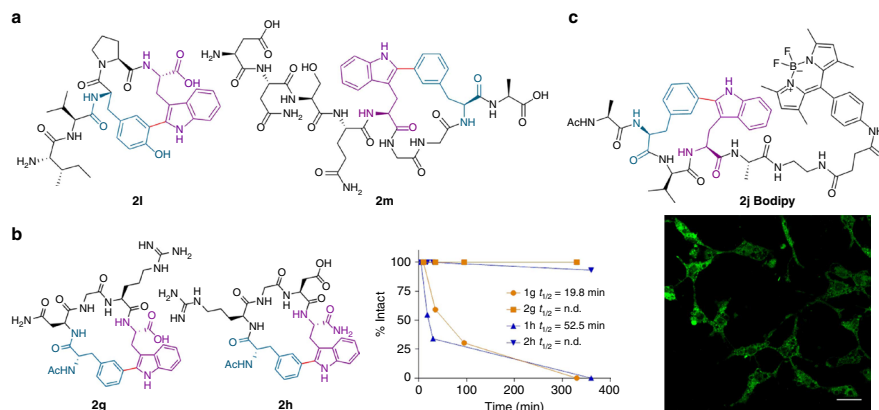


Figure 4 | Bioactive stapled peptides, biochemical and cellular studies. (a) Structure of stapled peptides **2l** (valorphin analogue) and **2m** (baratin analogue). (b) Proteolytic degradation assay of stapled peptides **2g** and **2h** and their linear precursors **1g** and **1h**. (c) Structure of labelled-stapled peptide **2j Bodipy** (left) and the corresponding confocal microscopy image of SH-SY5Y cells treated with compound **2j Bodipy** (750 nM). Scale bar, 25 μ m (right).

also featured values characteristic of solvent-shielded NH groups (lower than -3 ppb/K). NOE connectivity was also affected by staple formation. In the case of peptides **2h**, **2i** and **2j**, several nonsequential NOEs indicated that the peptides were constrained by intramolecular cyclization (Fig. 3c and Supplementary Figs 6 and 7). Incidentally, we detect all $N_{\text{indole-H}}$ atoms, and also we find the corresponding indole C α positions consequently substituted, therefore ruling out any interference by *N*-arylation processes. The aryl-aryl moieties show NOE correlations consistent with a defined single configuration in each case, which matches with the arrangement predicted from molecular modelling.

Moreover, circular dichroism measurements of stapled peptides **2g** and **2h** were performed in order to detect evidence of secondary structure and were then compared with their linear precursors **1g** and **1h**, respectively (See Supplementary Figs 8–11). Stapled peptides **2** show a positive maximum at ~ 190 nm and minimum peaks at 206 nm, which indicate some levels of structuring. In contrast, linear peptides exhibit a more flattened profile typical of a flexible unfolded structure.

Extension to biologically relevant peptides. To further explore the potential of the methodology, we planned to make the stapled analogues of known linear bioactive peptides, and at the same time test the influence of new features, such as the presence of proline (Pro) in the sequence, the overall length of the chain (up to nine amino acids) and the possibility of performing the C–H arylation on the solid phase, which enables the transformation of unprotected *N*-terminal peptides. In this way, we prepared the stapled version of an active valorphin analogue⁴⁸, which is a potent dipeptidyl peptidase III inhibitor, displaying Pro in a five amino-acid sequence containing also Trp and Tyr (see Supplementary Fig. 12). Interestingly, this peptide is closely related to spinorphin, an endogenous antinociceptive peptide, a potent and noncompetitive antagonist at the ATP-activated human P2X₃ receptor⁴⁹. The SPPS method was used to synthesize the Fmoc-protected sequence, which was intramolecularly arylated on resin. Subsequent *N*-terminal

deprotection and cleavage, successfully afforded the stapled peptide **2l** (Fig. 4a). This solid-phase protocol is fully compatible with the Pd chemistry involved and, interestingly, allows the preparation of arylated sequences having unprotected terminal amino groups. Furthermore, baratin⁵⁰, a neurostimulating peptide, was stapled following a related procedure. In this way, the standard SPPS protocol was interrupted to perform the on-resin C–H activation step, to be continued with the incorporation of the final four amino acids. Afterwards, deprotection and cleavage afforded the desired derivative **2m** (Fig. 4a, see Supplementary Methods and Supplementary Fig. 12).

Next, we determined the proteolytic stability of a couple of meaningful stapled peptides, in comparison with their respective linear counterparts. We followed a chymotrypsin-based protocol, previously used to evaluate stapled peptides⁵¹. Plotting the HPLC-MS profiles of the couples **2g/1g** and **2h/1h** (Fig. 4b, also Supplementary Figs 13–15) clearly shows an almost total protection of the stapled peptides towards enzymatic degradation, after 5–6 h, whereas the linear precursors suffered a rapid hydrolytic cleavage to remove the *N*-terminal amino acid, and completely disappeared after this time lapse.

Finally, we studied the controlled labelling of the stapled peptides. The goal was to selectively attach a fluorophore to the C-terminal amino acid to trace cellular permeabilization and localization. Thus, we linked a Bodipy residue to cyclopeptide **2j** through an amino spacer (the novel Bodipy construct was designed and prepared for this purpose, see Supplementary Fig. 16 and Supplementary Methods), to get the desired labelled-stapled peptide **2j Bodipy** (Fig. 4c) in a convenient manner. This compound exhibits low cytotoxicity at 750 nM after 24 h of incubation in SH-SY5Y cells (MTT assay; see Supplementary Fig. 17), and this concentration was used for the cell penetration studies. In a preliminary flow cytometry experiment (fluorescence-activated cell sorting assay), SH-SY5Y cells resulted in brightly stained sections on incubation for 30 min (see Supplementary Fig. 18). The cells treated in this manner were analysed using confocal microscopy. The stapled peptide **2j Bodipy** was localized both in the membrane and in the cytoplasmic region (Fig. 4c). Incidentally, the Bodipy-labelled

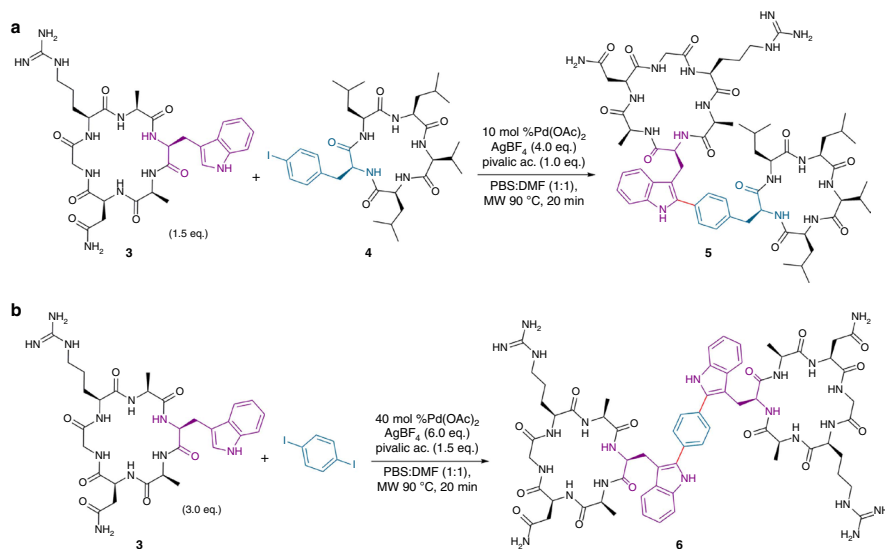


Figure 5 | Macrocyclic conjugation via C-H activation. (a) Intermolecular conjugation of NGR cyclopeptide **3** with the sansalvamide derivative **4** via C-H activation. (b) Double conjugation of the NGR cyclopeptide **3** with 1,4-diodobenzene.

linear precursor **1j** Bodipy also penetrates into cells in a comparable extent; however, there are appreciable differences in toxicity and cell permeability with respect to the stapled analogue (see Supplementary Figs 19 and 20). Overall, these results enable the performance of systematic bioimaging studies on these compounds.

Intermolecular peptide conjugation through C-H activation.

Chemical conjugation can effectively link drugs to carriers, and this technique is routinely used to modify biologics, especially antibodies with therapeutic indications⁵². We next explored peptide-peptide conjugation via C-H activation to achieve bismacrocyclic peptide constructs linked through a nonhydrolysable bond.

Peptides that inhibit the new blood vessel growth (angiogenesis) have become a promising tool for treating cancer. In this context, it has been reported that cyclic forms of NGR-containing sequences (tumour-homing peptides) lead to an improvement of the anticancer activity of an associated drug⁵³. We selected the previously studied Asn-Gly-Arg (NGR) array and synthesized the corresponding Trp-containing macrocycle **3** to be conjugated to a synthetic *p*-I-Phe-cyclopeptide derivative of the cyclic desipeptide sansalvamide **4** (Fig. 5a), a natural product whose synthetic analogues have demonstrated significant anticancer activity⁵⁴. Using a standard Pd-catalysed reaction in an aqueous medium of PBS-DMF, the two partners were successfully coupled to yield the C-C conjugate **5** (Fig. 5a).

In a second example, the conjugation of two units of the NGR Trp-containing cyclopeptide **3** with a 1,4-diodobenzene connector via a double C-H arylation was achieved. Again, the process yielded the expected bis-NGR-adduct **6** in a single step (Fig. 5b).

To evaluate the effects of macrocyclic conjugation, the NMR spectra of conjugated peptide **5** and its cyclic precursors **3** and **4** were compared (see Supplementary Fig. 21). After conjugation, small shifts were observed in the H_α resonances of the sansalvamide **4** analogue. In contrast, the H_α chemical shifts of the NGR-containing cycle were almost identical in peptides **5** and **3**. Comparison of ¹³C_α chemical shifts showed that in both cycles the larger ¹³C_α chemical shift change corresponded to the residue involved in the intermolecular bond formation: Trp (1.2 p.p.m.) in the NGR-containing cycle and Phe (0.6 p.p.m.) in the sansalvamide **4** derivative. More modest changes were observed in the ¹³C_α of the remaining amino acids. The resemblance of the H_α and ¹³C_α chemical shifts, which are highly sensitive to conformational changes, suggests that conjugation provided a minimal perturbation of the overall structures of peptides **3** and **4**. The NMR analysis was extended to peptide **6** and its precursor **3**. The effects of conjugation in the H_α and C_α resonances are shown in Supplementary Fig. 22.

Unfortunately, in preliminary biological studies evaluating the conjugated peptide **5** and its macrocycle precursors **3** and **4** against several cancer cell lines, only the cyclopeptide **4** showed activity (IC₅₀ < 10 μM). Nevertheless, the protocol seems general and offers new possibilities for peptide-based conjugation.

Stapled cyclopeptides. We then explored access to complex topologies, focusing on the synthesis of bicyclic peptide chemotypes. In a first approach, the synthesis of a stapled cyclopeptide was attempted by promoting the usual C-H arylation through an intramolecular Trp-I-Phe interaction. Preliminary studies showed that alanine (Ala) hexapeptides containing a *m*-I-Phe and Trp units, respectively, placed at positions *i* - *i* + 2 and *i* - *i* + 3 afforded the corresponding macrocycles after routine amide

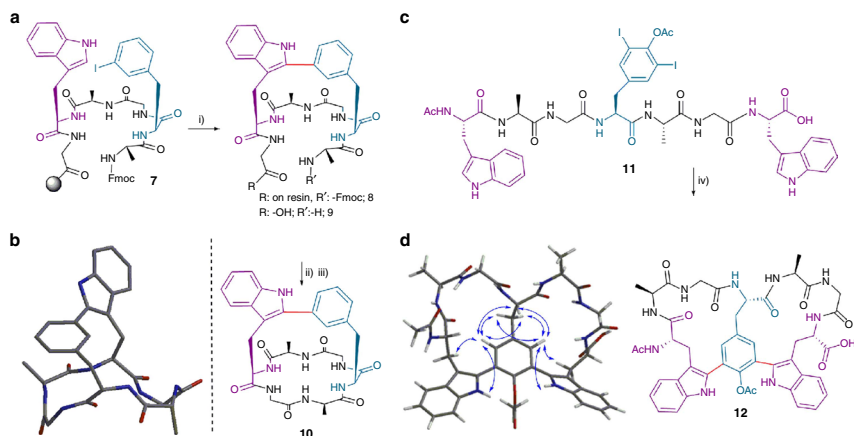


Figure 6 | Synthesis of macrobicyclic peptides 10 and 12. (a) Synthesis of macrobicyclic peptide 10 through solid-phase stapling. Reaction conditions: (i) $\text{Pd}(\text{OAc})_2$ (0.05 eq.), AgBF_4 (1.0 eq.), 2- NO_2BzOH (1.5 eq.), DMF, MW 90 °C, 20 min; (ii) (1) 1% sodium diethyldithiocarbamate (DDC) in DMF, (2) Piperidine-DMF (1:4; 1 \times 1 min, 2 \times 5 min). (3) TFA-TIS- H_2O (95:2.5:2.5), rt, 1 h; (iii) PyAOP (2.0 eq.), DIEA (6.0 eq.), DMF, rt, 1.5 h. (b) Minimized geometry of compound 10 generated by the Spartan '14 suite. Hydrogens omitted for clarity. (c) Double C-H arylation to cyclic biaryl 12 (25% conversion, estimated by HPLC). Reaction conditions: (iv) 40 mol % $\text{Pd}(\text{OAc})_2$, AgBF_4 (6.0 eq.), pivalic ac. (1.5 eq.), DMF, MW 90 °C, 20 min. (d) Minimized geometry of compound 12 generated by Spartan '14 suite showing the diagnostic NOE correlations (blue arrows).

coupling in quantitative yields; however, the subsequent intramolecular C-H arylations did not take place under the standard conditions, probably because of a highly restricted conformation. Remarkably, when the stapling on the linear sequence anchored to the resin 7 was carried out first on the solid phase, we obtained the corresponding NH-free amino terminal-stapled peptide 9 after cleavage from resin. Finally, we isolated the desired bicyclic compound 10 by amide cyclization (Fig. 6a,b). Furthermore, in this way, we overcame the relative limitation of irreversible protection of the N-terminal amino group, as previously reported³⁷. Incidentally, preliminary results showed that increasing the $\text{Pd}(\text{OAc})_2$ amount up to 0.2 eq. gave acceptable intermolecular arylations for NH-free amino terminal sequences (data not shown). The stapled cyclopeptide 10 was prepared in a suitable manner, involving a solid-phase arylation, thus facilitating the purification step, followed by a routine peptide coupling. This protocol may enable the synthesis of further derivatives of this attractive and unexplored structural class.

The ^1H NMR spectrum of the linear stapled peptide 9 was characterized by a large chemical shift dispersion of the NH and H_α resonances. Bicyclopeptide 10 showed a slightly larger chemical shift range for the H_α protons, as expected for a more rigid and structured peptide. Backbone cyclization was also reflected in a large splitting of the methylene H_α atoms of Gly-1 and H_β atoms of Phe. In the case of peptide 9, the chemical shift difference between the two geminal protons was <0.2 (H_α , Gly-1) and 0.1 (H_β , Phe) p.p.m., whereas for peptide 10 this difference increased to >0.9 (H_α , Gly-1) and >0.7 (H_β , Phe) p.p.m. Backbone cyclization was further evidenced by significant changes in $^{13}\text{C}_\alpha$ chemical shifts and in the temperature coefficients of amide NH (Supplementary Fig. 23).

Double stapling of linear peptides. Biaryl bismacroyclic peptide-derived natural products such as vancomycin⁵⁵ and complestatin⁵⁶ display very interesting bioactivity profiles and

as synthetic targets they are extremely difficult to prepare⁵⁷. Thus, the development of new methodologies to access simplified scaffolds is crucial to enable structural diversification, thereby allowing practical medicinal chemistry and biological studies. Hence, it was envisioned that intramolecular double C-H arylation of a sequence containing a diiodinated Tyr (commercially available) flanked by two Trp units would give rise to bicyclic peptide topologies with adjacent biaryl moieties in a straightforward manner. In order to establish the conditions for this transformation, we performed some preliminary experiments where the intermolecular C-H activation of a Ac-*m,m'*-1,1-Tyr(OAc)-OH unit with 2.0 eq. of Ac-Trp-OH was tested. An increase in the amount of the Pd catalyst (40%) and AgBF_4 (6.0 eq.)⁵⁸ and use of a mild excess of pivalic acid resulted in a productive reaction (see Supplementary Methods). Next, we designed the linear peptide sequence 11 (Fig. 6c), which was synthesized in a straightforward manner on the solid phase. Using the previous C-H activation conditions for the diiodoTyr, we successfully obtained the double stapled peptide 12 directly from the corresponding linear precursor in one step in a 25% HPLC conversion, together with monoarylated cycles and dehalogenated derivatives, which were probably produced in competitive processes (Fig. 6c). This remarkable result is the proof of principle that even these complex peptidic topologies are accessible through the present methodology. The ^1H NMR spectrum of the double stapled peptide 12 is characterized by a wide chemical shift range for the NH and H_α protons (see Supplementary Fig. 134). The observed pattern of NOEs, summarized in Fig. 6d, indicates that each side of the Tyr aromatic ring faces a distinct Trp-Ala-Gly motif.

As an optimization of this methodology, we have developed the exclusive use of standard proteinogenic amino acids (Tyr), which, once coupled, are modified *in situ*, thus simplifying the protocol and rendering it considerably more affordable. In this way, the corresponding linear precursor of peptide 11 can be obtained

ARTICLE

NATURE COMMUNICATIONS | DOI: 10.1038/ncomms8160

through routine amide couplings followed by on-resin iodination of the Tyr residue to yield derivative **11** (41% conversion, unoptimized, see Supplementary Fig. 24)⁵⁹. This remarkable result enables the direct synthesis of bicyclopeptide **12** to be performed on solid-phase from commercially available reagents in a single sequence.

Discussion

Metal-catalysed arylations through C–H activation are suitable processes to gain access to minimalistic staples (two-electron) in relevant Trp-containing peptide sequences directly from Trp and iodo-phenylalanine (-tyrosine) precursors. The validation of the methodology includes the analysis of the scope of the transformation, compatibility with other amino acids and the applicability to SPPS. This approach has also been applied to constrain biologically active signalling sequences. In an intermolecular mode, the process efficiently links two Trp peptides to a benzene connector and is also useful to conjugate peptides through a C–C bond. All compounds showed a structured nature, as revealed by spectroscopic characterization. Finally, we have developed a simple protocol for the straightforward access to novel peptide topologies such as dimeric macrocycles, stapled bicyclopeptides and biaryl–biaryl species (see Supplementary Figs 4 and 25) from the corresponding linear precursors in only one step. These findings open up general access to a variety of novel constrained peptidic chemotypes, and we believe that this breakthrough will make a significant contribution to the development of a broad range of applications for peptides in biological and medicinal chemistry.

Methods

General. For abbreviations and detailed experimental procedures see Supplementary Methods. For NMR analysis of the compounds, see Supplementary Figs 26–148 and Supplementary Tables 1–40.

Peptide synthesis. All peptides were manually synthesized on a 2-Chlorotrityl, H-Rink-Amide Chemmatrix or TentGel S NH₂ resin using standard Fmoc chemistry for SPPS.

Linear peptide cyclization. The free-amine free-acid linear peptide (1.0 eq.) was dissolved in ACN/DMF or DMF (0.001–0.003 M) and N,N-diisopropylethylamine (DIEA) (6.0 eq.) and the corresponding coupling agents (1.5–3.0 eq., benzotriazol-1-yl-oxytrypirrolidinophosphonium hexafluorophosphate (PyBOP) with hydroxybenzotriazole (HOBt) or 1-[Bis(dimethylamino)methylene]-1H-1,2,3-triazolo[4,5-b]pyridinium 3-oxid hexafluorophosphate (HATU) and O-(benzotriazol-1-yl)-N,N,N',N'-tetramethyluronium tetrafluoroborate (TBTU) or (7-azabenzotriazol-1-yloxy)trypirrolidinophosphonium hexafluorophosphate (PyAOP)) were added. The solution was stirred at r.t. until the cyclization was complete (1–3 h). Workup was performed by extraction with aqueous solutions of NH₄Cl_{sat} and NaHCO₃^{sat}. Organic layers were combined, dried over anhydrous sodium sulfate, filtered and concentrated under vacuum. When remaining protecting groups were present, the macrocycle was treated with a 95% TFA, 2.5% triisopropylsilane (TIS) and 2.5% H₂O cocktail (3 h), washed with Et₂O, dissolved in ACN/H₂O and lyophilized to furnish the corresponding deprotected peptide. When necessary, the macrocycle was purified by flash column chromatography on silica gel or semipreparative RP-HPLC.

General protocol for the stapled bond formation in solution. The linear peptide (50 mg), AgBF₄ (2.0 eq.), trifluoroacetic acid (1.0 eq.) and Pd(OAc)₂ (0.05 eq.) were placed in a MW reactor vessel in DMF (1.2 ml). The mixture was heated under MW irradiation (250 W) at 90 °C for 20 min. The residue was filtered and purified using semipreparative RP-HPLC. This process was scaled up to 0.907 mmol of peptide, affording the stapled/locked peptides **2g–2k** in isolated yields ranging from 1 to 32%.

Procedure for the single macrocycle conjugation. Cyclopeptide **4** (40.0 mg, 0.056 mmol), cyclopeptide **3** (55.3 mg, 0.084 mmol, 1.5 eq.), AgBF₄ (43.8 mg, 0.225 mmol, 4.0 eq.), pivalic acid (5.7 mg, 0.056 mmol, 1.0 eq.) and Pd(OAc)₂ (1.4 mg, 0.077 mmol, 0.1 eq.) were placed in a MW reactor vessel in 2 ml of PBS:DMF (1:1). The mixture was heated under MW irradiation (250 W) at 90 °C for 20 min. The irradiation cycle was repeated after adding a new portion of Pd(OAc)₂ and AgBF₄. The residue was filtered and partially purified in a Porapak Rxn reverse phase column (1.63 mg, 2% estimated using HPLC-MS). A pure fraction was obtained using analytical RP-HPLC to yield pure conjugate **5**.

Procedure for the double macrocycle conjugation. 1,4-diiodobenzene (35 mg, 0.106 mmol), macrocycle **3** (209 mg, 0.318 mmol, 3.0 eq.), AgBF₄ (124 mg, 0.637 mmol, 6.0 eq.), pivalic acid (16.3 mg, 0.159 mmol, 1.5 eq.) and Pd(OAc)₂ (9.5 mg, 0.042 mmol, 0.4 eq.) were placed in a MW reactor vessel in 2 ml of PBS:DMF (1:1). The mixture was heated under MW irradiation (250 W) at 90 °C for 20 min. The crude product was filtered, and the workup was carried out by washing with AcOEt and then precipitating by adding ACN to the aqueous phase. The resulting precipitate was washed with ACN, decanted and dried, obtaining 159 mg of crude product (pale solid, 42% estimated using HPLC-MS). A pure fraction was obtained with semipreparative RP-HPLC to yield pure conjugate **6**.

Typical procedure for the stapled cyclopeptide formation on the solid phase. Once sequence **7** was synthesized on a TentGel S NH₂ resin via an AB linker, the peptide anchored to the resin (139 mg, 0.145 mmol), AgBF₄ (28 mg, 0.144 mmol, 1.0 eq.), 2-nitrobenzoic acid (36 mg, 0.215 mmol, 1.5 eq.) and Pd(OAc)₂ (1.6 mg, 7.1 μmol, 0.05 eq.) in DMF (2 ml) was placed in a MW reactor vessel. The mixture was heated under MW irradiation (250 W) at 90 °C for 20 min. Eight more batches were carried out following the same procedure and were then combined. The resin was treated with 1% DDC in DMF and the Fmoc group was removed. The peptide was cleaved from the resin with a 95% TFA, 2.5% TIS and 2.5% H₂O cocktail (1 h), yielding the stapled sequence **9** (85% purity, estimated using HPLC-MS). Finally, the stapled peptide **9** was cyclized (see above for standard cyclization procedure) and the crude product was purified using semipreparative RP-HPLC to yield bicyclopeptide **10** (pale solid, 18% unoptimized).

One-step double arylation to biaryl–biaryl stapled peptide. Linear peptide **11** (50 mg, 0.044 mmol), AgBF₄ (51 mg, 0.262 mmol, 6.0 eq.), pivalic acid (6.7 mg, 0.066 mmol, 1.5 eq.) and Pd(OAc)₂ (3.9 mg, 0.018 mmol, 0.4 eq.) were placed in a MW reactor vessel in DMF (500 μl). The mixture was heated under MW irradiation (250 W) at 90 °C for 20 min. Three more batches were carried out following the same procedure and then filtered and combined (25% conversion, estimated using HPLC-MS). A pure fraction of bicyclopeptide **12** was isolated using semipreparative RP-HPLC.

References

- Ramakers, B. E. I., van Hest, J. C. M. & Löwik, D. W. P. M. Molecular tools for the construction of peptide-based materials. *Chem. Soc. Rev.* **43**, 2743–2756 (2014).
- Craik, D. J., Fairlie, D. P., Liras, S. & Price, D. The future of peptide-based drugs. *Chem. Biol. Drug Des.* **81**, 136–147 (2013).
- Albericio, F. & Kruger, H. G. Therapeutic peptides. *Future Med. Chem.* **4**, 1527–1531 (2012).
- Lawson, K. V., Rose, T. E. & Harman, P. G. Template-constrained macrocyclic peptides prepared from native, unprotected precursors. *Proc. Natl. Acad. Sci. USA* **110**, E3753–E3760 (2013).
- Marsault, E. *et al.* Efficient parallel synthesis of macrocyclic peptidomimetics. *Bioorg. Med. Chem. Lett.* **18**, 4731–4735 (2008).
- Royo-Gracia, S., Gaus, K. & Sewald, N. Synthesis of chemically modified bioactive peptides: recent advances, challenges and developments for medicinal chemistry. *Future Med. Chem.* **1**, 1289–1310 (2009).
- White, C. J. & Yudin, A. K. Contemporary strategies for peptide macrocyclization. *Nat. Chem.* **3**, 509–524 (2011).
- Heinis, C. Tools and rules for macrocycles. *Nat. Chem. Biol.* **10**, 696–698 (2014).
- Verdine, G. L. & Hilinski, G. J. Stapled peptides for intracellular drug targets. *Methods Enzymol.* **503**, 3–33, 2012).
- Walensky, L. D. & Bird, G. H. Hydrocarbon-stapled peptides: principles, practice, and progress. *J. Med. Chem.* **57**, 6275–6288 (2014).
- Lau, Y. H., de Andrade, P., Wu, Y. & Spring, D. R. Peptide stapling techniques based on different macrocyclisation chemistries. *Chem. Soc. Rev.* **44**, 91–102 (2015).
- Góngora-Benítez, M., Tulla-Puche, J. & Albericio, F. Multifaceted roles of disulfide bonds. Peptides as therapeutics. *Chem. Rev.* **114**, 901–926 (2014).
- Jo, H. *et al.* Development of α -helical calpain probes by mimicking a natural protein–protein interaction. *J. Am. Chem. Soc.* **134**, 17704–17713 (2012).
- Spokoiny, A. M. *et al.* A perfluoroaryl–cysteine SNAr chemistry approach to unprotected peptide stapling. *J. Am. Chem. Soc.* **135**, 5946–5949 (2013).
- Bois-Choussy, M., Cristau, P. & Zhu, J. Total synthesis of an atropidiastereomer of RP-66453 and determination of its absolute configuration. *Angew. Chem. Int. Ed.* **42**, 4238–4241 (2003).
- Carbannelle, A.-C. & Zhu, J. A novel synthesis of biaryl-containing macrocycles by a domino miyaura arylboronate formation: intramolecular suzuki reaction. *Org. Lett.* **2**, 3477–3480 (2000).
- Afonso, A., Felici, L. & Planas, M. Solid-phase synthesis of biaryl cyclic peptides by borylation and microwave-assisted intramolecular Suzuki–Miyaura reaction. *Tetrahedron* **67**, 2238–2245 (2011).

18. Meyer, F.-M. *et al.* Biaryl-bridged macrocyclic peptides: conformational constraint via carbogenic fusion of natural amino acid side chains. *J. Org. Chem.* **77**, 3099–3114 (2012).
19. Blackwell, H. E. & Grubbs, R. H. Highly efficient synthesis of covalently cross-linked peptide helices by ring-closing metathesis. *Angew. Chem. Int. Ed.* **37**, 3281–3284 (1998).
20. Dharanipragada, R. New modalities in conformationally constrained peptides for potency, selectivity and cell permeation. *Future Med. Chem.* **5**, 831–849 (2013).
21. Wender, P. A. Toward the ideal synthesis and molecular function through synthesis-informed design. *Nat. Prod. Rep.* **31**, 433–440 (2014).
22. Sletten, E. M. & Bertozzi, C. R. Bioorthogonal chemistry: fishing for selectivity in a sea of functionality. *Angew. Chem. Int. Ed.* **48**, 6974–6998 (2009).
23. Yu, J.-Q. & Shi, Z. *Topics in Current Chemistry* 384 (Springer, 2010).
24. Seecurn, C. C. J., Kitching, M. O., Colacot, T. J. & Snickus, V. Palladium-catalyzed cross-coupling: a historical contextual perspective to the 2010 Nobel Prize. *Angew. Chem. Int. Ed.* **51**, 5062–5086 (2012).
25. Ackermann, L. Carboxylate-assisted transition-metal-catalyzed C-H bond functionalizations: mechanism and scope. *Chem. Rev.* **111**, 1315–1345 (2011).
26. McMurray, L., O'Hara, F. & Gaunt, M. J. Recent developments in natural product synthesis using metal-catalyzed C-H bond functionalisation. *Chem. Soc. Rev.* **40**, 1885–1898 (2011).
27. Wencel-Delord, J., Dröge, T., Liu, F. & Glorius, F. Towards mild metal-catalyzed C-H bond activation. *Chem. Soc. Rev.* **40**, 4740–4761 (2011).
28. Daugulis, O., Do, H. & Shabashov, D. Palladium- and copper-catalyzed arylation of carbon-hydrogen bonds. *Acc. Chem. Res.* **42**, 1074–1086 (2009).
29. Noisier, F. M. & Brimble, M. A. C–H functionalization in the synthesis of amino acids and peptides. *Chem. Rev.* **114**, 8775–8806 (2014).
30. Rossi, R., Bellina, F., Lessi, M. & Manzini, C. Cross-Coupling of heteroarenes by C-H functionalization: recent progress towards direct arylation and heteroarylation reactions involving heteroarenes containing one heteroatom. *Adv. Synth. Catal.* **356**, 17–117 (2014).
31. Lebrasseur, N. & Larrosa, I. Recent advances in the C2 and C3 regioselective direct arylation of indoles. *Adv. Heterocycl. Chem.* **105**, 309–351 (2012).
32. Liégault, B., Petrov, I., Goresky, S. I. & Fagnou, K. Modulating reactivity and induction selectivity in palladium-catalyzed heteroaromatic direct arylation through the use of a chloride activating/blocking group. *J. Org. Chem.* **75**, 1047–1060 (2010).
33. Wang, X., Gribkov, D. V. & Sames, D. Phosphine-free palladium-catalyzed C-H bond arylation of free (N-H)-indoles and pyrroles. *J. Org. Chem.* **72**, 1476–1479 (2007).
34. Phipps, R. J., Grimster, N. P. & Gaunt, M. J. Cu(II)-catalyzed direct and site-selective arylation of indoles under mild conditions. *J. Am. Chem. Soc.* **130**, 8172–8174 (2008).
35. Islam, S. & Larrosa, I. "On water", phosphine-free palladium-catalyzed room temperature C-H arylation of indoles. *Chem. Eur. J.* **19**, 15093–15096 (2013).
36. Lebrasseur, N. & Larrosa, I. Room temperature and phosphine free palladium catalyzed direct C-2 arylation of indoles. *J. Am. Chem. Soc.* **130**, 2926–2927 (2008).
37. Ruiz-Rodríguez, J., Albericio, F. & Lavilla, R. Postsynthetic modification of peptides: chemoselective C-arylation of tryptophan residues. *Chem. Eur. J.* **16**, 1124–1127 (2010).
38. Williams, T. J., Reay, A. J., Whitwood, A. C. & Fairlamb, I. J. S. A mild and selective Pd-mediated methodology for the synthesis of highly fluorescent 2-arylated tryptophans and tryptophan-containing peptides: a catalytic role for Pd(0) nanoparticles? *Chem. Commun.* **50**, 3052–3054 (2014).
39. Dong, H., Limberakis, C., Liras, S., Price, D. & James, K. Peptide macrocyclization via palladium-catalyzed chemoselective indole C-2 arylation. *Chem. Commun.* **48**, 11644–11646 (2012).
40. Monguchi, Y., Marumoto, T., Takamatsu, H., Sawama, Y. & Sajiki, H. Palladium on carbon-catalyzed one-pot N-arylindole synthesis: intramolecular aromatic amination, aromatization, and intermolecular aromatic amination. *Adv. Synth. Catal.* **356**, 1866–1872 (2014).
41. Preciado, S. *et al.* Synthesis and biological evaluation of a post-synthetically modified Trp-based diketopiperazine. *Med. Chem. Comm.* **4**, 1171–1174 (2013).
42. Preciado, S., Mendive-Tapia, L., Albericio, F. & Lavilla, R. Synthesis of C-2 arylated tryptophan amino acids and related compounds through palladium-catalyzed C-H activation. *J. Org. Chem.* **78**, 8129–8135 (2013).
43. Mas-moruno, C., Rechenmacher, F. & Kessler, H. Cilengitide: the first anti-angiogenic small molecule drug candidate. Design, synthesis and clinical evaluation. *Anticancer Agents Med. Chem.* **10**, 753–768 (2010).
44. Weide, T., Modlinger, A. & Kessler, H. Spatial screening for the identification of the bioactive conformation of integrin ligands. *Top. Curr. Chem.* **272**, 1–50 (2007).
45. Boger, D. L. & Myers, J. B. Design and synthesis of a conformational analogue of deoxybouvardin. *J. Org. Chem.* **56**, 5385–5390 (1991).
46. Jackson, S. *et al.* Template-constrained cyclic peptides: design of high-affinity ligands for GPIIb/IIIa. *J. Am. Chem. Soc.* **116**, 3220–3230 (1994).
47. Dyson, H. J. & Wright, P. E. Nuclear Magnetic Resonance methods for elucidation of structure and dynamics in disordered states. *Methods Enzymol.* **339**, 258–270 (2001).
48. Chiba, T. *et al.* Inhibition of recombinant dipeptidyl peptidase III by synthetic hemorphin-like peptides. *Peptides* **24**, 773–778 (2003).
49. Jung, K.-Y. *et al.* Structure - activity relationship studies of spinorphin as a potent and selective human 2P2X3 receptor antagonist. *J. Med. Chem.* **50**, 4543–4547 (2007).
50. Nässel, D. R., Persson, M. G. S. & Muren, J. E. Baratin, a nonamidated neurostimulating neuropeptide, isolated from cockroach brain: distribution and actions in the cockroach and locust nervous systems. *J. Comp. Neurol.* **286**, 267–286 (2000).
51. Bird, G. H. *et al.* Hydrocarbon double-stapling remedies the proteolytic instability of a lengthy peptide therapeutic. *Proc. Natl. Acad. Sci. USA* **107**, 14093–14098 (2010).
52. Du, A. W. & Stenzel, M. H. Drug carriers for the delivery of therapeutic peptides. *Biomacromolecules* **15**, 1097–1114 (2014).
53. Colombo, G. *et al.* Structure-activity relationships of linear and cyclic peptides containing the NGR tumor-homing motif. *J. Biol. Chem.* **277**, 47891–47897 (2002).
54. Pan, P.-S. *et al.* A comprehensive study of Sansalvamide A derivatives: the structure-activity relationships of 78 derivatives in two pancreatic cancer cell lines. *Bioorg. Med. Chem.* **17**, 5806–5825 (2009).
55. Boger, D. L. *et al.* Total synthesis of the vancomycin aglycon. *J. Am. Chem. Soc.* **121**, 10004–10011 (1999).
56. Wang, Z., Bois-Choussy, M., Jia, Y. & Zhu, J. Total synthesis of complestatin (chloroepitriptin II). *Angew. Chem. Int. Ed.* **49**, 2018–2022 (2010).
57. Feliu, L. & Planas, M. Cyclic peptides containing biaryl and biaryl ether linkages. *Int. J. Pept. Res. Ther.* **11**, 53–97 (2005).
58. Arroniz, C., Denis, J. G., Ironmonger, A., Rassias, G. & Larrosa, I. An organic cation as a silver(i) analogue for the arylation of sp² and sp³ C-H bonds with iodoarenes. *Chem. Sci.* **5**, 3509–3514 (2014).
59. Arsequell, G. *et al.* First aromatic electrophilic iodination reaction on the solid-phase: iodination of bioactive peptides. *Tetrahedron Lett.* **39**, 7393–7396 (1998).

Acknowledgements

This work was supported by DGICYT–Spain (project BQU-CTQ2012-30930), Generalitat de Catalunya (2014 SGR 137) and Institute for Research in Biomedicine Barcelona (Spain). We acknowledge an FPU fellowship for L.M.-T. from the Ministerio de Educación, Cultura y Deporte–Spain (MECD). NMR instruments were made available by the Scientific and Technological Centre of the University of Barcelona (CCIT UB). Dr M. J. Macías, Dr M. Vilaseca, Dr M. Teixidó and J. García (IRB Barcelona), Dr F. Mitjans (BioLeitat), Dr M. Royo (Barcelona Science Park) and Professors R. Pérez-Tomás and V. Soto-Cerrato (U. Barcelona) are gratefully acknowledged for useful suggestions and for the biological assays.

Author contributions

L.M.-T., F.A. and R.L. wrote the manuscript. L.M.-T., S.P., N.K. and R.R. performed the experiments, compound characterization and data analysis. J.G. performed the NMR studies. R.L. and F.A. supervised the research and evaluated all the data.


Additional information

Supplementary Information accompanies this paper at <http://www.nature.com/naturecommunications>

Competing financial interests: The authors declare no competing financial interests.

Reprints and permission information is available online at <http://npg.nature.com/reprintsandpermissions/>

How to cite this article: Mendive-Tapia, L. *et al.* New peptide architectures through C-H activation stapling between tryptophan–phenylalanine/tyrosine residues. *Nat. Commun.* 6:7160 doi: 10.1038/ncomms8160 (2015).

 This work is licensed under a Creative Commons Attribution 4.0 International License. The images or other third party material in this article are included in the article's Creative Commons license, unless indicated otherwise in the credit line; if the material is not included under the Creative Commons license, users will need to obtain permission from the license holder to reproduce the material. To view a copy of this license, visit <http://creativecommons.org/licenses/by/4.0/>

Supporting Information

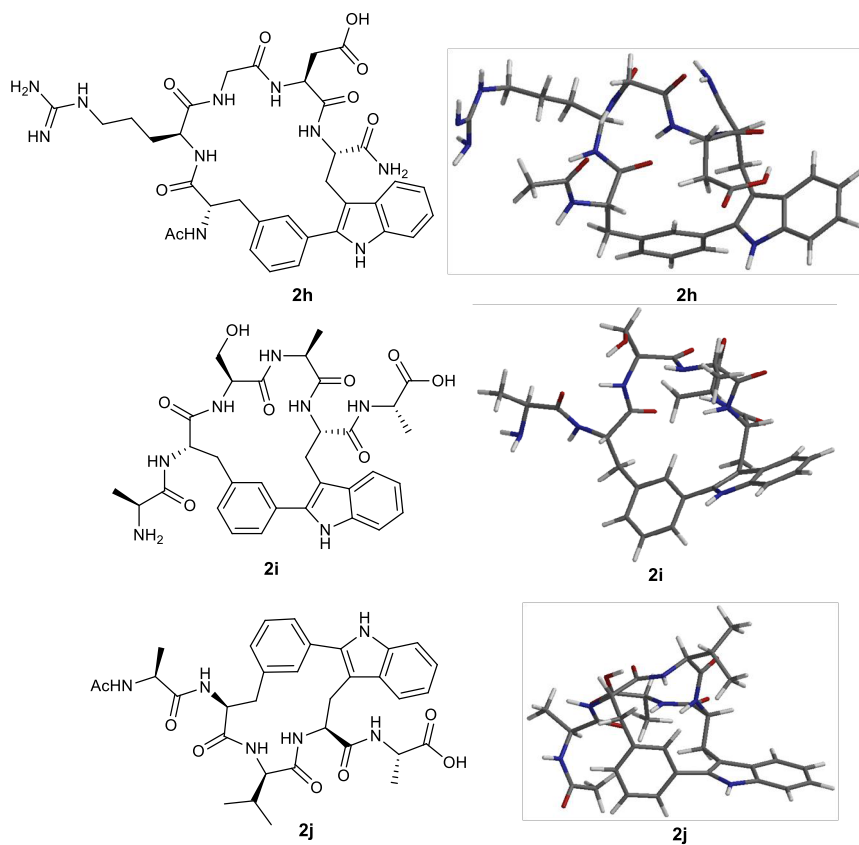
New peptide architectures through C–H activation stapling between tryptophan–phenylalanine/tyrosine residues

The following data is a selection of the content of the Supporting Information. Full supplementary figures, tables and methods are available in the Supporting Information in electronic format.

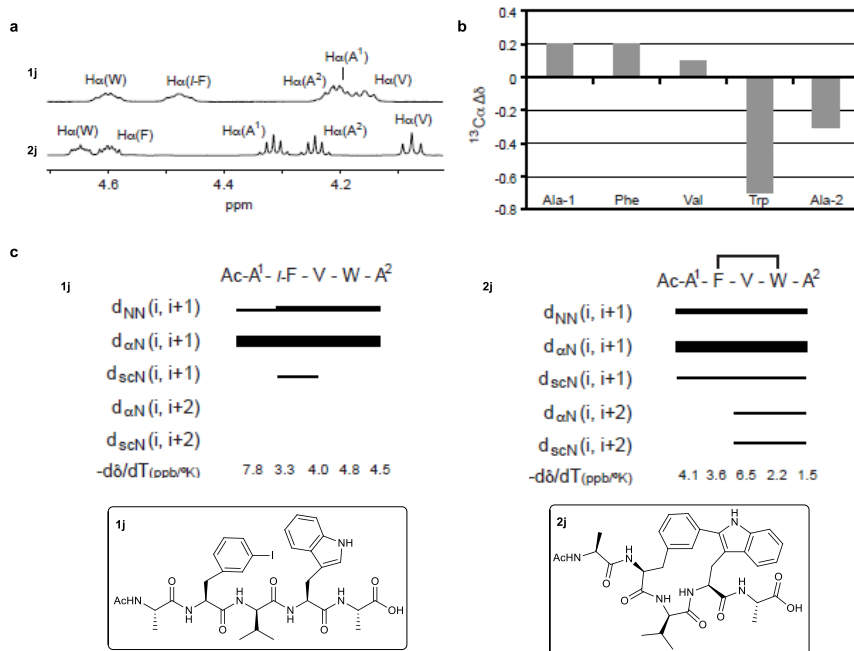
Table of Contents

<i>Selected supplementary figures and tables.....</i>	<i>213</i>
<i>Selected supplementary methods.....</i>	<i>229</i>

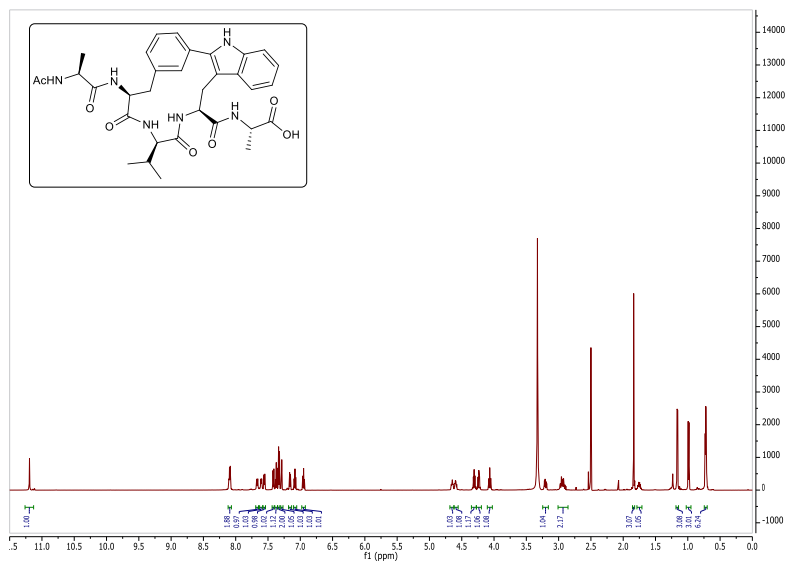
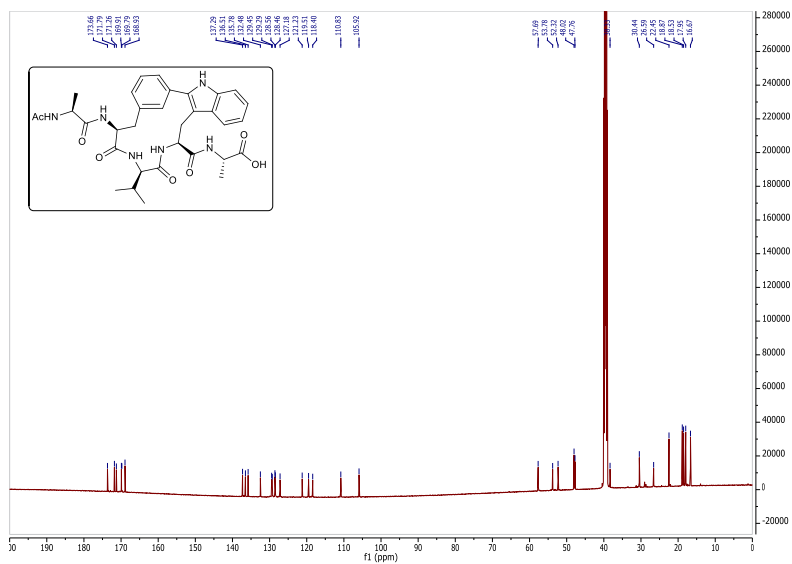
Selected supplementary figures and tables

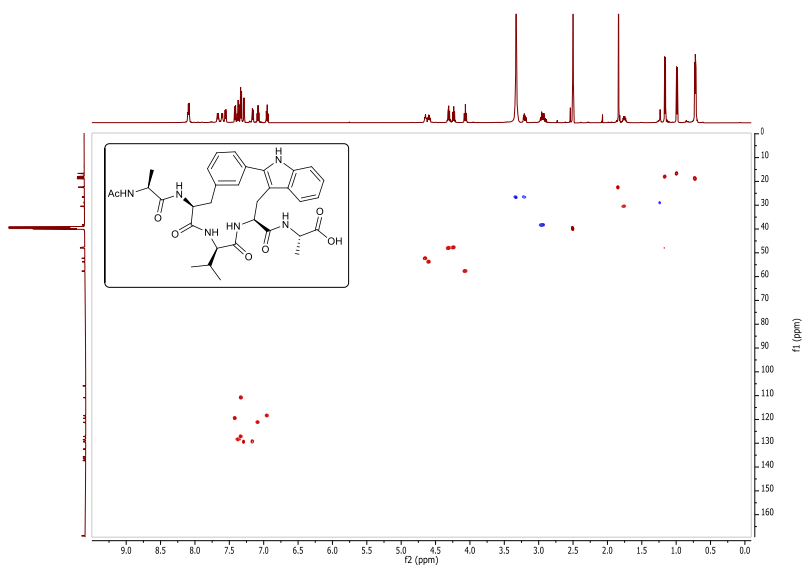


Supplementary Figure 1 | Minimized geometries of compounds 2h-j generated by the Spartan '14 suite (molecular mechanics, MMFF94).⁸

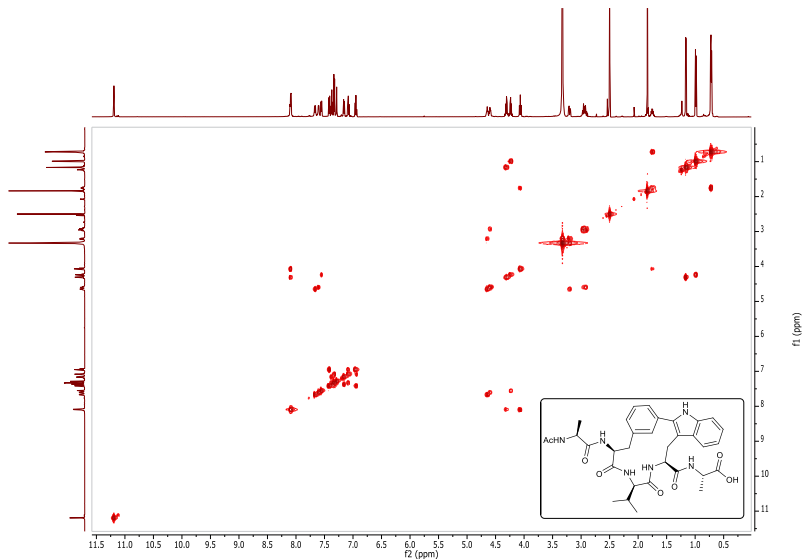


Supplementary Figure 7 | Peptide NMR spectra comparison between compounds 2j and 1j. a, NMR H_{α} region of peptide 2j and its linear precursor 1j. **b,** Plot of the $^{13}C_{\alpha}$ chemical shift differences ($^{13}C_{\alpha} \Delta\delta_{cyclic-linear}$) between stapled peptide 2j and its linear counterpart 1j (bottom left) and 2j (bottom right). The thickness of the bars reflects the intensity of the NOEs, i.e. weak (—), medium (▬) and strong (▮). *I-F*: *m*-iodophenylalanine.

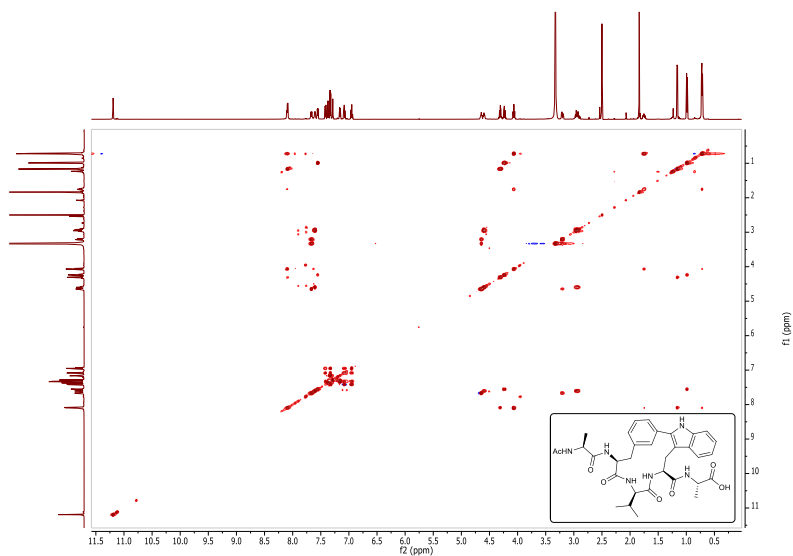
Supplementary Figure 74 | ¹H NMR spectrum of compound Ac-Ala-(Cyclo-*m*)-[Phe-Val-Trp]-Ala-OH (**2j**).Supplementary Figure 75 | ¹³C NMR spectrum of compound Ac-Ala-(Cyclo-*m*)-[Phe-Val-Trp]-Ala-OH (**2j**).



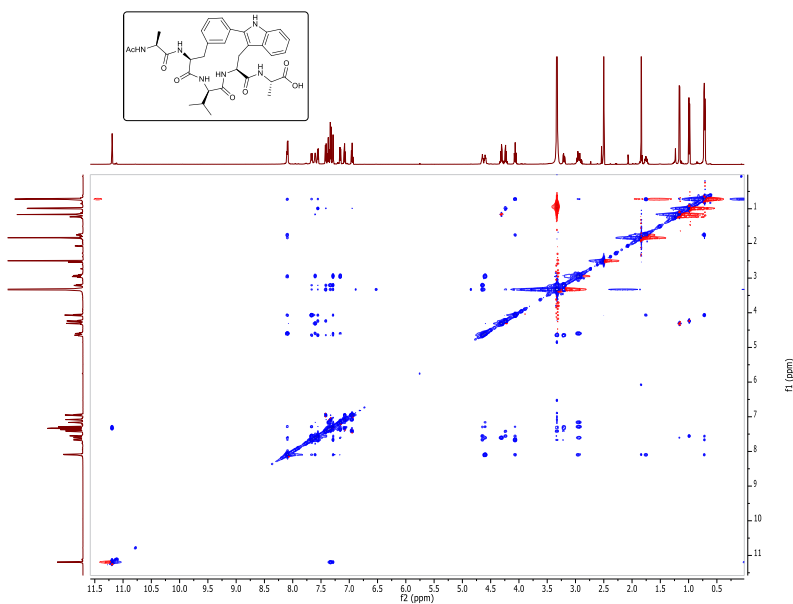
Supplementary Figure 76 | ^1H - ^{13}C HSQC NMR spectrum of compound Ac-Ala-(Cyclo-*m*)-[Phe-Val-Trp]-Ala-OH (2j).



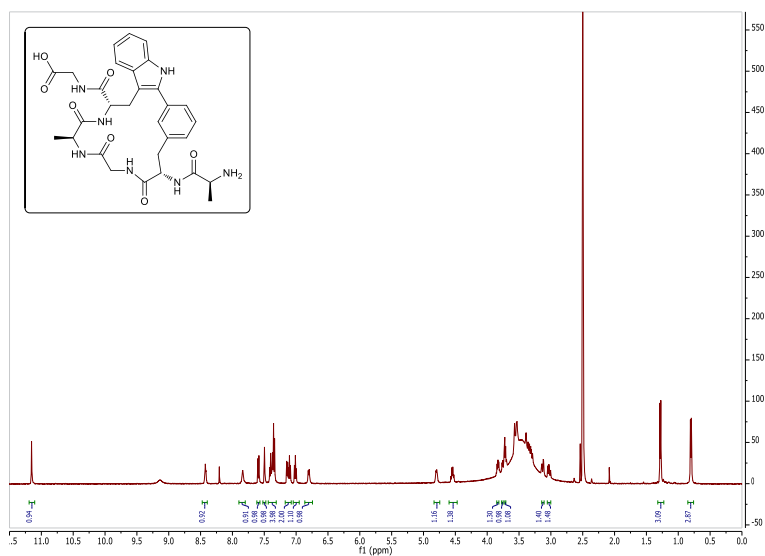
Supplementary Figure 77 | COSY NMR spectrum of compound Ac-Ala-(Cyclo-*m*)-[Phe-Val-Trp]-Ala-OH (2j).



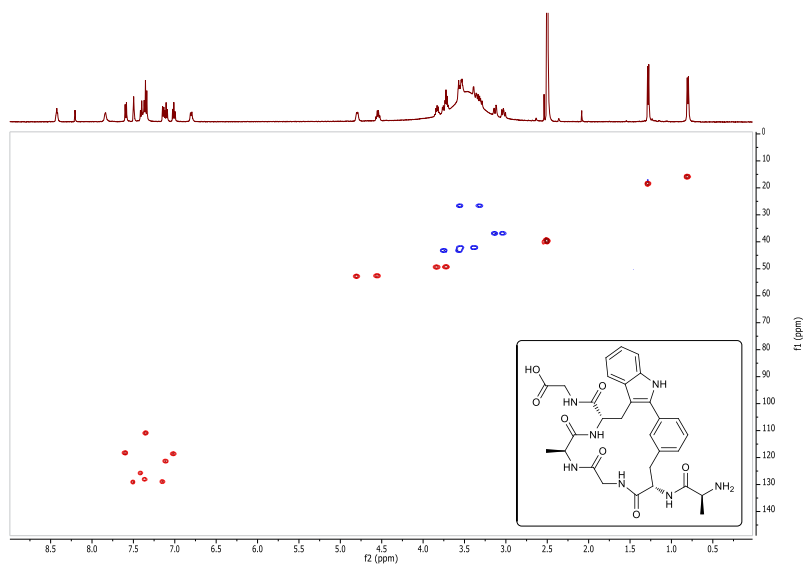
Supplementary Figure 78 | TOCSY NMR spectrum of compound **Ac-Ala-(Cyclo-*m*)-[Phe-Val-Trp]-Ala-OH (2j)**.



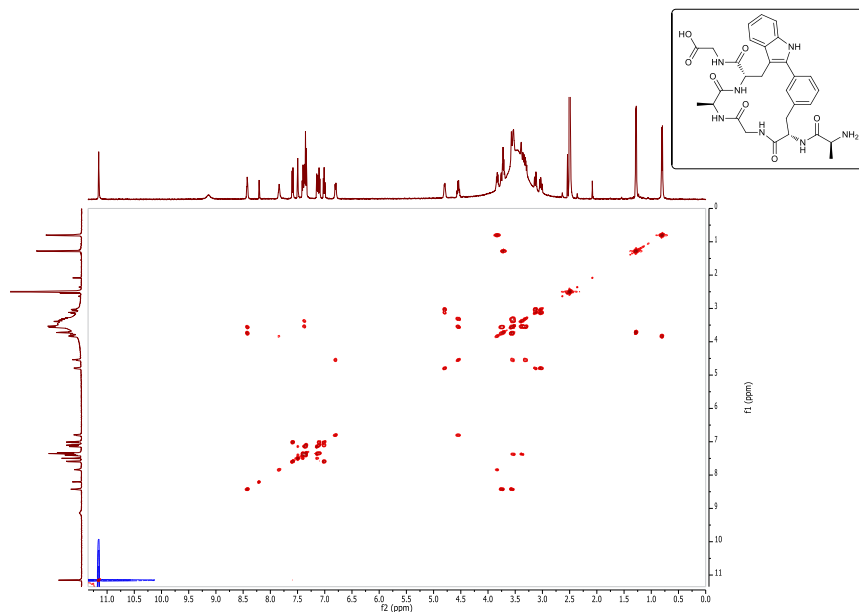
Supplementary Figure 79 | NOESY NMR spectrum of compound **Ac-Ala-(Cyclo-*m*)-[Phe-Val-Trp]-Ala-OH (2j)**.



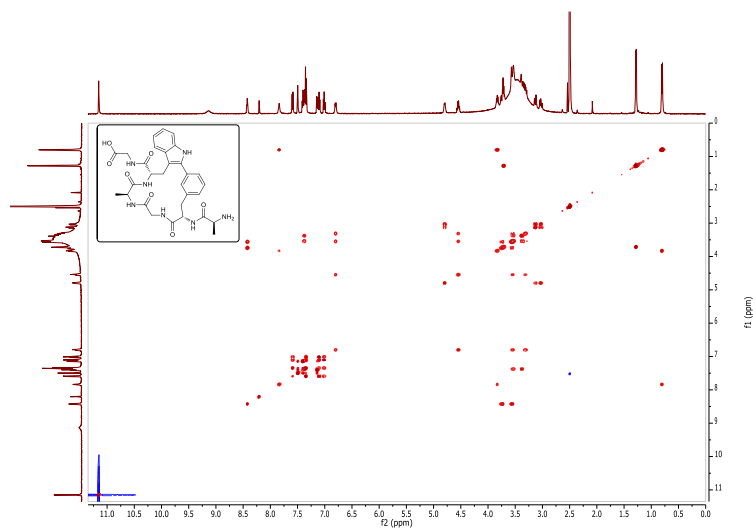
Supplementary Figure 117 | ¹H NMR spectrum of compound H-Ala-(Cyclo-*m*)-[Phe-Gly-Ala-Trp]-Gly-OH (9).



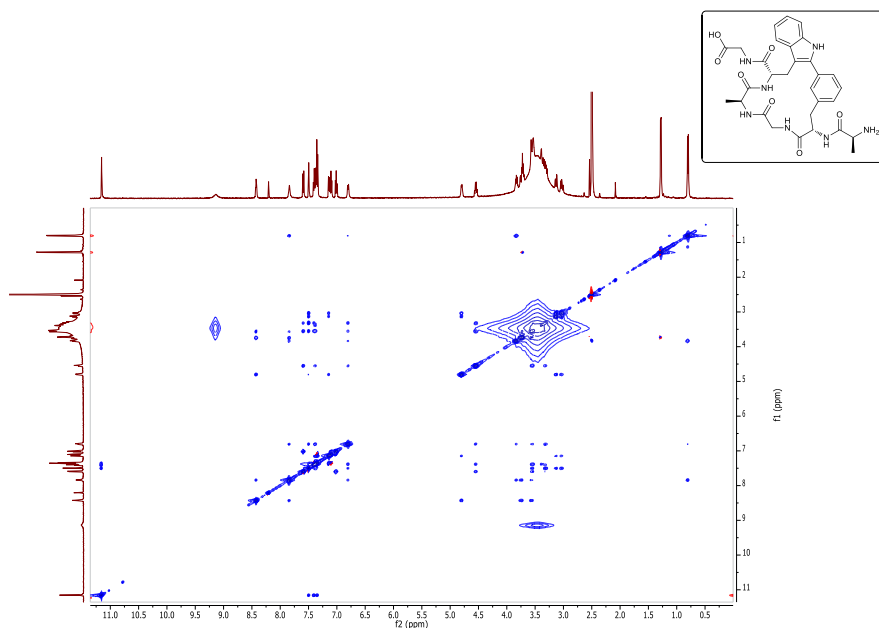
Supplementary Figure 118 | ¹H-¹³C HSQC NMR spectrum of compound H-Ala-(Cyclo-*m*)-[Phe-Gly-Ala-Trp]-Gly-OH (9).



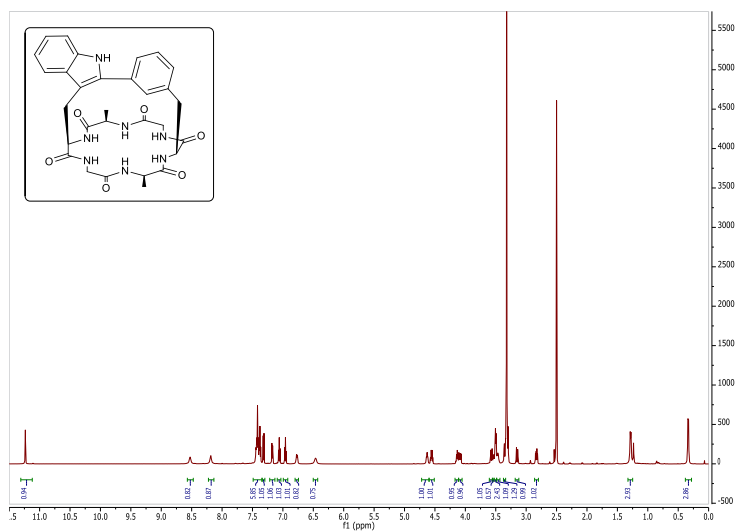
Supplementary Figure 119 | COSY NMR spectrum of compound H-Ala-(Cyclo-*m*)-[Phe-Gly-Ala-Trp]-Gly-OH (9).

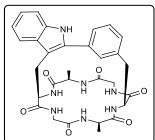


Supplementary Figure 120 | TOCSY NMR spectrum of compound H-Ala-(Cyclo-*m*)-[Phe-Gly-Ala-Trp]-Gly-OH (9).

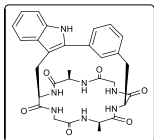


Supplementary Figure 121 | NOESY NMR spectrum of compound H-Ala-(Cyclo-*m*)-[Phe-Gly-Ala-Trp]-Gly-OH (9).

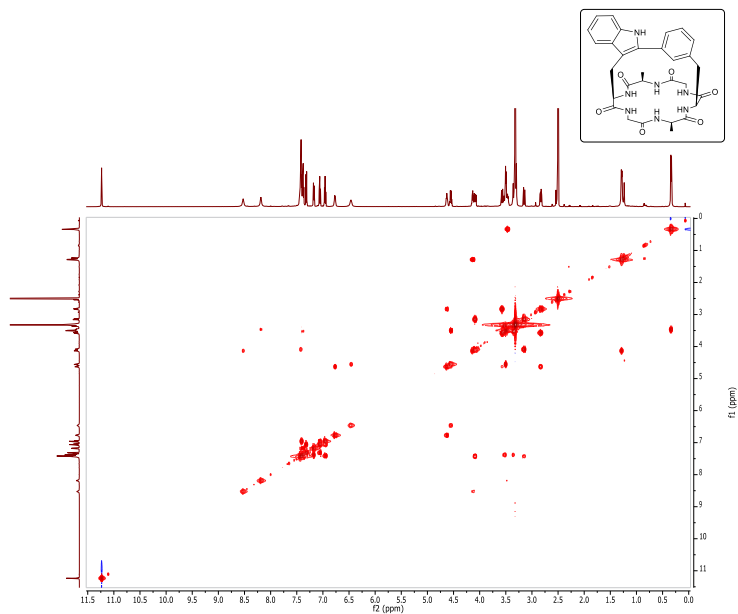




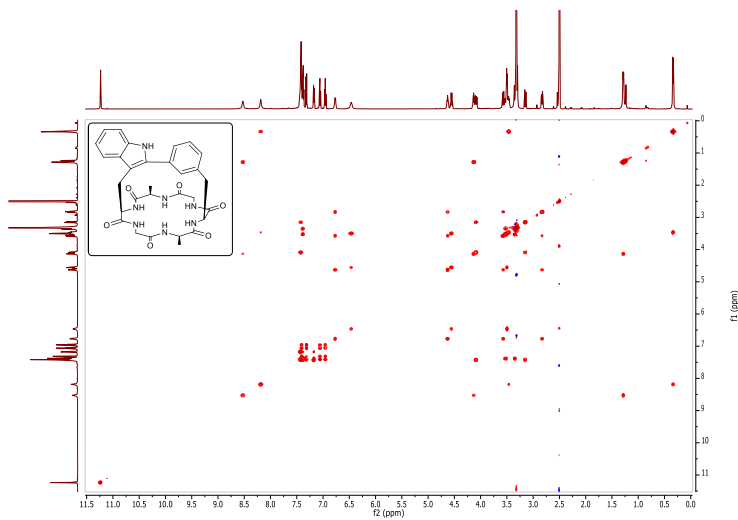
Supplementary Figure 123 | ^{13}C NMR spectrum of compound Cyclo[-Ala-(Cyclo-*m*)-[Phe-Gly-Ala-Trp]-Gly-] (10).



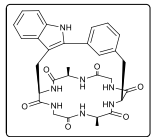
Supplementary Figure 124 | ^1H - ^{13}C HSQC NMR spectrum of compound Cyclo[-Ala-(Cyclo-*m*)-[Phe-Gly-Ala-Trp]-Gly-] (10).



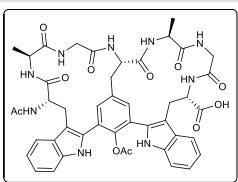
Supplementary Figure 125 | COSY NMR spectrum of compound Cyclo[-Ala-(Cyclo-*m*)-[Phe-Gly-Ala-Trp]-Gly-] (10).



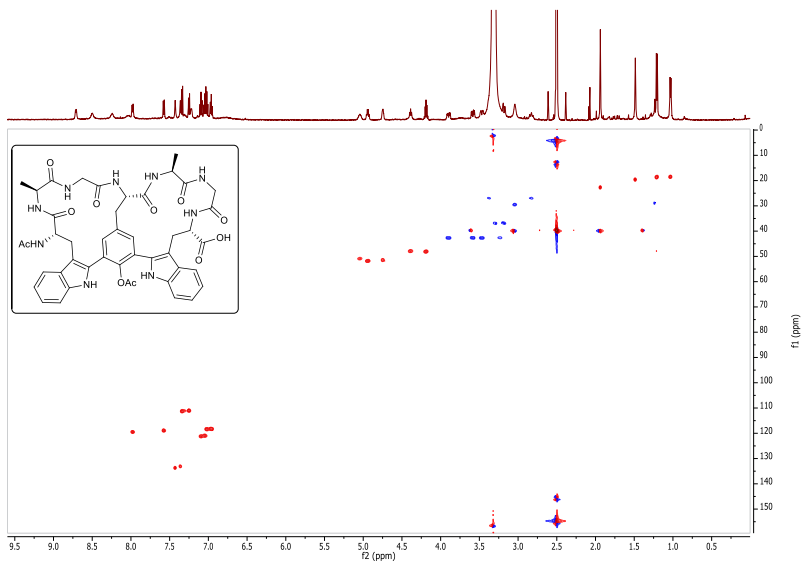
Supplementary Figure 126 | TOCSY NMR spectrum of compound Cyclo[-Ala-(Cyclo-*m*)-[Phe-Gly-Ala-Trp]-Gly-] (10).



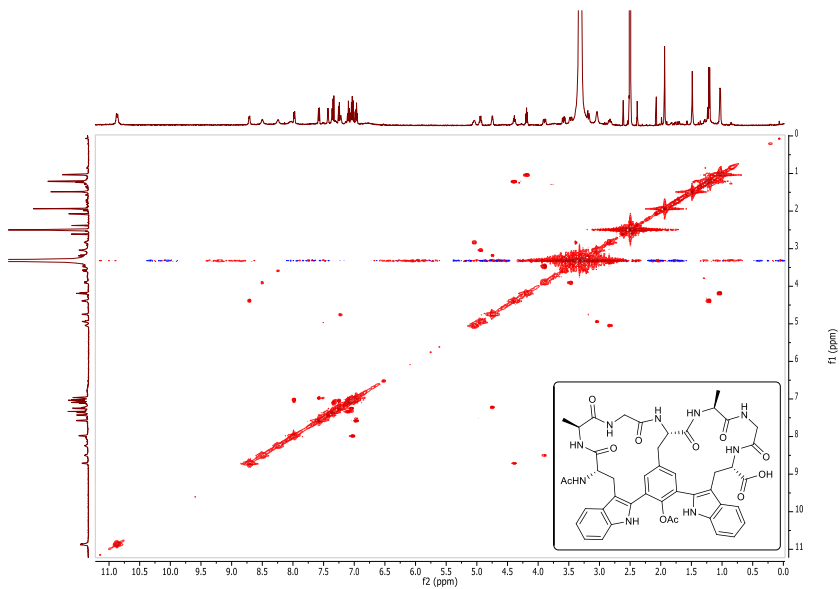
(10).



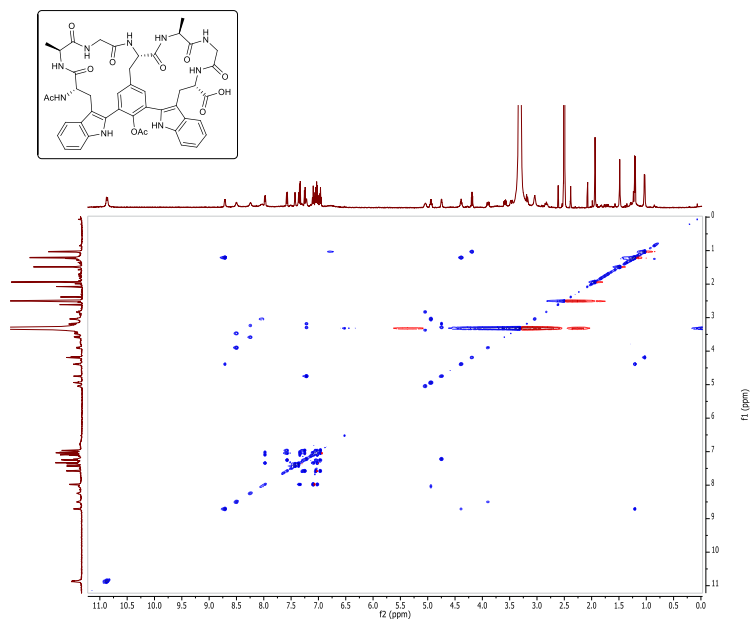
[Tyr(OAc)-Ala-Gly-Trp]-OH (12).



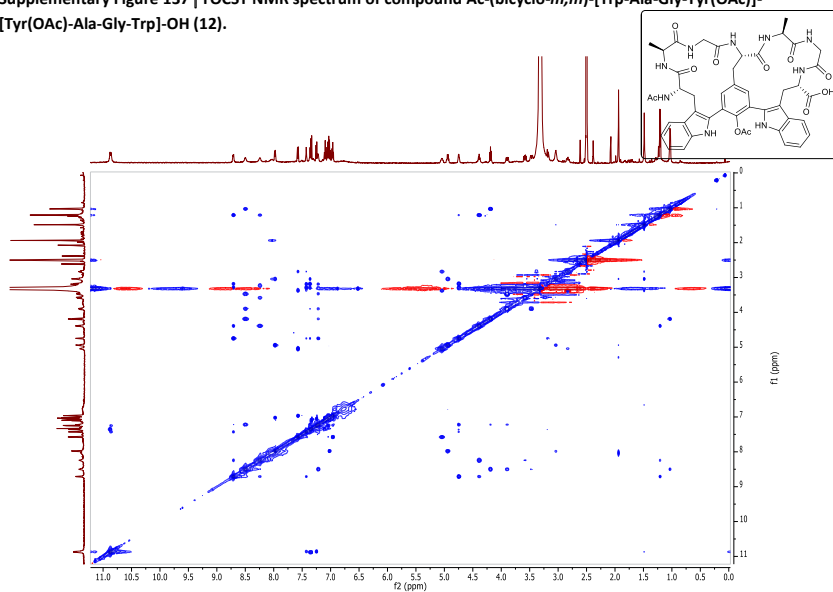
Supplementary Figure 135 | ^1H - ^{13}C HSQC NMR spectrum of compound Ac-(bicyclo-*m,m*)-[Trp-Ala-Gly-Tyr(OAc)]-[Tyr(OAc)-Ala-Gly-Trp]-OH (12).



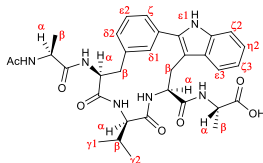
Supplementary Figure 136 | COSY NMR spectrum of compound Ac-(bicyclo-*m,m*)-[Trp-Ala-Gly-Tyr(OAc)]-[Tyr(OAc)-Ala-Gly-Trp]-OH (12).



Supplementary Figure 137 | TOSY NMR spectrum of compound **Ac-[bicyclo-*m,m*]-[Trp-Ala-Gly-Tyr(OAc)]-[Tyr(OAc)-Ala-Gly-Trp]-OH (12)**.



Supplementary Figure 138 | NOESY NMR spectrum of compound **Ac-[bicyclo-*m,m*]-[Trp-Ala-Gly-Tyr(OAc)]-[Tyr(OAc)-Ala-Gly-Trp]-OH (12)**.

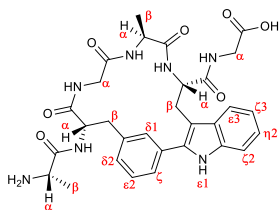


2j (¹ H)	δ (ppm)												
AA	NH	α	β	δ1	δ2	ε2	ζ	ε1	ζ2	η2	ζ3	ε3	γ
Ala1	8.09	4.31	1.16	-	-	-	-	-	-	-	-	-	-
<i>m</i> - <i>t</i> -Phe	7.60	4.60	2.93	7.29	7.16	7.37	7.33	-	-	-	-	-	-
Val	8.09	4.07	1.75	-	-	-	-	-	-	-	-	-	0.72
Trp	7.67	4.65	3.34/3.20	-	-	-	-	11.19	7.33	7.08	6.95	7.42	-
Ala2	7.56	4.24	0.99	-	-	-	-	-	-	-	-	-	-

Supplementary Table 15 | ¹H chemical shifts assignments of compound Ac-Ala-(Cyclo-*m*)-[Phe-Val-Trp]-Ala-OH (2j).

2j (¹³ C)	δ (ppm)												
AA	α	β	δ1	δ2	ε2	ζ	ζ2	η2	ζ3	ε3	γ		
Ala1	47.7	17.7	-	-	-	-	-	-	-	-	-	-	-
<i>m</i> - <i>t</i> -Phe	53.4	38.0	129.1	128.9	128.1	126.8	-	-	-	-	-	-	-
Val	57.4	30.1	-	-	-	-	-	-	-	-	-	-	18.5
Trp	52.0	26.2	-	-	-	-	110.5	120.9	118.0	119.2	-	-	-
Ala2	47.4	16.4	-	-	-	-	-	-	-	-	-	-	-

Supplementary Table 16 | ¹³C chemical shifts assignments of compound Ac-Ala-(Cyclo-*m*)-[Phe-Val-Trp]-Ala-OH (2j).

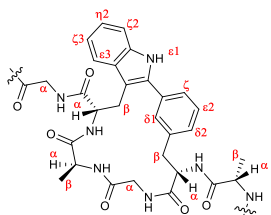


9 (¹ H)	δ (ppm)												
AA	NH	α	β	δ1	δ2	ε2	ζ	ε1	ζ2	η2	ζ3	ε3	
Ala1	-	3.71	1.28	-	-	-	-	-	-	-	-	-	-
<i>m</i> - <i>t</i> -Phe	9.14	4.79	3.14/3.03	7.50	7.14	7.35	7.40	-	-	-	-	-	-
Gly1	8.43	3.76/3.57	-	-	-	-	-	-	-	-	-	-	-
Ala2	7.84	3.83	0.80	-	-	-	-	-	-	-	-	-	-
Trp	6.80	4.55	3.56/3.32	-	-	-	-	11.15	7.34	7.11	7.01	7.59	-
Gly2	7.38	3.55/3.38	-	-	-	-	-	-	-	-	-	-	-

Supplementary Table 33 | ¹H chemical shifts assignments of compound H-Ala-(Cyclo-*m*)-[Phe-Gly-Ala-Trp]-Gly-OH (9).

9 (¹³ C)	δ (ppm)												
AA	α	β	δ1	δ2	ε2	ζ	ζ2	η2	ζ3	ε3			
Ala1	49.2	18.3	-	-	-	-	-	-	-	-	-	-	-
<i>m</i> - <i>t</i> -Phe	52.7	36.8	129.0	128.9	128.0	128.7	-	-	-	-	-	-	-
Gly1	43.1	-	-	-	-	-	-	-	-	-	-	-	-
Ala2	49.3	15.8	-	-	-	-	-	-	-	-	-	-	-
Trp	52.4	26.6	-	-	-	-	110.9	121.3	118.5	118.2	-	-	-
Gly2	42.1	-	-	-	-	-	-	-	-	-	-	-	-

Supplementary Table 34 | ¹³C chemical shifts assignments of compound H-Ala-(Cyclo-*m*)-[Phe-Gly-Ala-Trp]-Gly-OH (9).

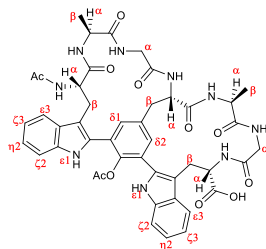


10 (¹ H)		δ (ppm)										
AA	NH	α	β	δ1	δ2	ε2	ζ	ε1	ζ2	η2	ζ3	ε3
Ala1	8.53	4.14	1.28	-	-	-	-	-	-	-	-	-
<i>m</i> - <i>l</i> -Phe	6.77	4.63	3.57/2.83	7.42	7.17	7.38	7.44	-	-	-	-	-
Gly1	7.39	4.09/3.15	-	-	-	-	-	-	-	-	-	-
Ala2	8.19	3.47	0.34	-	-	-	-	-	-	-	-	-
Trp	6.46	4.55	3.50	-	-	-	-	11.2	7.32	7.06	6.96	7.41
Gly2	7.38	3.54/3.35	-	-	-	-	-	-	-	-	-	-

Supplementary Table 35 | ¹H chemical shifts assignments of compound Cyclo[-Ala-(Cyclo-*m*)-[Phe-Gly-Ala-Trp]-Gly-] (10).

10 (¹³ C)		δ (ppm)										
AA	α	β	δ1	δ2	ε2	ζ	ζ2	η2	ζ3	ε3		
Ala1	49.2	16.2	-	-	-	-	-	-	-	-	-	-
<i>m</i> - <i>l</i> -Phe	51.0	35.6	129.9	129.8	128.0	126.5	-	-	-	-	-	-
Gly1	42.9	-	-	-	-	-	-	-	-	-	-	-
Ala2	50.9	15.0	-	-	-	-	-	-	-	-	-	-
Trp	48.5	24.8	-	-	-	-	110.8	121.0	118.2	118.2	-	-
Gly2	43.1	-	-	-	-	-	-	-	-	-	-	-

Supplementary Table 36 | ¹³C chemical shifts assignments of compound Cyclo[-Ala-(Cyclo-*m*)-[Phe-Gly-Ala-Trp]-Gly-] (10).



12 (¹ H)		δ (ppm)								
AA	NH	α	β	δ1	δ2	ε1	ζ2	η2	ζ3	ε3
Trp1	8.03	4.94	3.04	-	-	10.87	7.34	7.09	7.03	7.98
Ala1	6.79	4.19	1.03	-	-	-	-	-	-	-
Gly1	8.50	3.90/3.47	-	-	-	-	-	-	-	-
Tyr	7.22	4.75	3.30/3.19	7.43	7.36	-	-	-	-	-
Ala2	8.71	4.39	1.21	-	-	-	-	-	-	-
Gly2	8.24	3.58/3.24	-	-	-	-	-	-	-	-
Trp2	6.79	5.04	3.38/2.83	-	-	10.87	7.25	7.03	6.96	7.58

Supplementary Table 39 | ¹H chemical shifts assignments of compound Ac-(bicyclo-*m,m*)-[Trp-Ala-Gly-Tyr(OAc)]-[Tyr(OAc)-Ala-Gly-Trp]-OH (12).

12 (¹³ C)		δ (ppm)							
AA	α	β	δ1	δ2	ζ2	η2	ζ3	ε3	
Trp1	51.5	29.2	-	-	111.0	120.9	118.1	119.2	
Ala1	47.8	18.2	-	-	-	-	-	-	
Gly1	42.4	-	-	-	-	-	-	-	
Tyr	51.2	36.6	132.8	133.4	-	-	-	-	
Ala2	47.6	18.4	-	-	-	-	-	-	
Gly2	42.4	-	-	-	-	-	-	-	
Trp2	50.6	26.7	-	-	110.8	120.7	118.0	118.7	

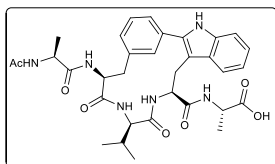
Supplementary Table 40 | ¹³C chemical shifts assignments of compound Ac-(bicyclo-*m,m*)-[Trp-Ala-Gly-Tyr(OAc)]-[Tyr(OAc)-Ala-Gly-Trp]-OH (12).

Selected supplementary methods

General procedure for the C-H activation process of peptides 2g-2k

Unless stated otherwise, the linear peptide (50 mg), AgBF_4 (2.0 eq.), trifluoroacetic acid (1.0 eq.) and $\text{Pd}(\text{OAc})_2$ (0.05 eq.) were placed in a microwave reactor vessel in DMF. The mixture was heated under microwave irradiation (250 W) at 90 °C for 20 min. The residue was filtered and purified by semi-preparative RP-HPLC (XBRIDGE™ BEH 130, C18, 5 μM OBD 19x50 mm column) [solvent A (0.1% FA in H_2O) and solvent B (0.1% FA in ACN)], in 10 min, flux: 20 mL·min⁻¹, detection at $\lambda=220$ nm.

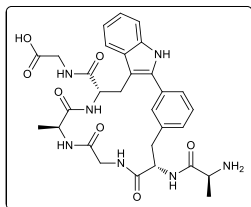
Ac-Ala-(Cyclo-*m*)-[Phe-Val-Trp]-Ala-OH (2j). Starting from peptide **1j** (207 mg, 0.374 mmol)



(71% conversion, estimated by HPLC-MS). Semi-preparative RP-HPLC gradient: 20-40% of B. Pale solid (55.2 mg, 32%). **¹H NMR** (600 MHz, $\text{DMSO}-d_6$): δ 11.19 (s, 1H), 8.09 (m, 2H), 7.67 (d, J = 9.6 Hz, 1H), 7.60 (d, J = 7.3 Hz, 1H), 7.56 (d, J = 7.0 Hz, 1H), 7.42

(d, J = 8.0 Hz, 1H), 7.37 (t, J = 7.5 Hz, 1H), 7.33 (dd, J = 7.9, 1.3 Hz, 2H), 7.29 (t, J = 1.7 Hz, 1H), 7.16 (dt, J = 7.5, 1.5 Hz, 1H), 7.08 (ddd, J = 8.1, 6.9, 1.1 Hz, 1H), 6.95 (ddd, J = 7.9, 6.9, 1.1 Hz, 1H), 4.65 (ddd, J = 9.7, 6.4, 3.2 Hz, 1H), 4.60 (ddd, J = 8.8, 7.2, 4.4 Hz, 1H), 4.31 (p, J = 7.2 Hz, 1H), 4.24 (p, J = 7.3 Hz, 1H), 4.07 (t, J = 9.5 Hz, 1H), 3.34 (1H), 3.20 (dd, J = 14.7, 6.6 Hz, 1H), 3.01 – 2.85 (m, 2H), 1.84 (s, 3H), 1.75 (m, 1H), 1.16 (d, J = 7.1 Hz, 3H), 0.99 (d, J = 7.3 Hz, 3H), 0.72 (dd, J = 6.7, 4.3 Hz, 6H) ppm. **¹³C NMR** (151 MHz, $\text{DMSO}-d_6$): δ 173.66, 171.79, 171.26, 169.91, 169.79, 168.93, 137.29, 136.51, 135.78, 132.48, 129.45, 129.29, 128.56, 128.46, 127.18, 121.23, 119.51, 118.40, 110.83, 105.92, 57.69, 53.78, 52.32, 48.02, 47.76, 38.33, 30.44, 26.59, 22.45, 18.87, 18.53, 17.95, 16.67 ppm. **IR** (Film, cm^{-1}) ν = 3295.37, 3051.96, 2962.28, 1642.70, 1617.08, 1514.59 cm^{-1} . **HRMS** (ESI) (m/z): $[\text{M}+\text{H}]^+$ calcd. for $\text{C}_{33}\text{H}_{40}\text{N}_6\text{O}_7$, 633.30312; found, 633.30487.

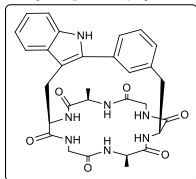
H-Ala-(Cyclo-*m*)-[Phe-Gly-Ala-Trp]-Gly-OH (9). *AB linker incorporation for TentaGel S NH₂*



resin. AB linker (3.0 eq.) was attached to the resin (1.0 eq.) with DIPCDI (3.0 eq.), OxymaPure (3.0 eq.) in DMF at r.t for 1h. *First*

amino acid incorporation. Fmoc-Gly-OH (4.0 eq.) was attached to the resin (1.0 eq.) with DIPCDI (2.0 eq.), DMAP (0.4 eq.) in DCM at r.t (1 x 2h, 1 x 16h). *End-capping of resin to block any remaining unreacted active resin sites.* Anhydride acetic (5.0 eq.) and DIEA (5.0 eq.) in DMF were added for 30 min. *Peptide elongation.* Fmoc-XX-OH (3.0 eq.) were incorporated with a 5-min pre-activation with DIPCDI (3.0 eq.) and OxymaPure (3.0 eq.) in DMF for 1h. Fmoc-XX-OH: Fmoc-Trp-OH, Fmoc-Ala-OH, Fmoc-Gly-OH. Fmoc-*m*-Phe-OH (1.5 eq.) was incorporated with HBTU (1.5 eq.), HOBT (1.5 eq.) and DIEA (3.0 eq.) in DMF for 1h. *Stapled bond formation on solid-phase.* The resulting peptide **7** anchored to the resin (139 mg, 0.145 mmol), AgBF₄ (28 mg, 0.144 mmol, 1.0 eq.), 2-nitrobenzoic acid (36 mg, 0.215 mmol, 1.5 eq.) and Pd(OAc)₂ (1.6 mg, 7.1 μmol, 0.05 eq.) were placed in a microwave reactor vessel in 2 mL of DMF. The mixture was heated under microwave irradiation (250 W) at 90 °C for 20 min. Eight more batches were carried out following the same procedure and were combined. The peptide **8** anchored to the resin was treated with 1% DDC in DMF and after removing the Fmoc group it was cleaved from the resin with a 95% TFA, 2.5% TIS, 2.5% H₂O cocktail (1h). (85% purity, estimated by HPLC-MS). **¹H NMR** (500 MHz, DMSO-*d*₆): δ 11.15 (s, 1H), 8.43 (t, *J* = 5.1 Hz, 1H), 7.84 (s, 1H), 7.59 (d, *J* = 7.9 Hz, 1H), 7.50 (s, 1H), 7.41-7.35 (m, 4H), 7.17 – 7.08 (m, 2H), 7.01 (t, *J* = 7.4 Hz, 1H), 6.80 (d, *J* = 8.4 Hz, 1H), 4.83 – 4.74 (m, 1H), 4.55 (q, *J* = 8.2 Hz, 1H), 3.83 (m, 1H), 3.76 (m, 1H), 3.71 (m, 1H), 3.57 – 3.53 (m, 3H), 3.38-3.32 (m, 2H), 3.14 – 3.11 (m, 1H), 3.03 (dd, *J* = 13.5, 8.8 Hz, 1H), 1.28 (d, *J* = 6.9 Hz, 3H), 0.80 (d, *J* = 7.2 Hz, 3H) ppm. **IR** (Film, cm⁻¹) ν = 3288.97, 3051.96, 2923.84, 1649.11, 1527.40 cm⁻¹. **HRMS** (ESI) (*m/z*): [M+H]⁺ calcd. for C₃₀H₃₅N₇O₇, 606.26707; found, 606.26754.

Cyclo[-Ala-(Cyclo-*m*)-[Phe-Gly-Ala-Trp]-Gly-] (10). The free-amine free-acid stapled peptide **9**

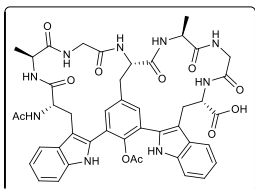


(92.2 mg, 0.152 mmol) was dissolved in 152 mL of DMF (0.001 M) and DIEA (6.0 eq.) and PyAOP (2.0 eq.) were added. The solution was stirred at r.t until the cyclization was complete (1.5h). DMF was removed under vacuum, and the crude was dissolved in EtOAc and extracted with NH₄Cl_{sat}

and NaHCO_{3sat}. Organic layers were combined, dried over sodium sulfate, filtered and concentrated under vacuum. The crude was purified by semi-preparative RP-HPLC (XBRIDGETM BEH 130, C18,

5 μ M OBD 19x50 mm column) [solvent A (0.1% FA in H₂O) and solvent B (0.1% FA in ACN)], in 10 min, flux: 20 mL·min⁻¹, detection at λ =220 nm (gradient: 20-30% of B). Pale solid (16.0 mg, 18%). **¹H NMR** (600 MHz, DMSO-*d*₆): δ 11.23 (s, 1H), 8.53 (s, 1H), 8.19 (s, 1H), 7.49 – 7.35 (m, 6H), 7.32 (d, *J* = 8.0 Hz, 1H), 7.17 (dt, *J* = 7.7, 1.4 Hz, 1H), 7.06 (ddd, *J* = 8.0, 6.9, 1.2 Hz, 1H), 6.96 (ddd, *J* = 8.0, 6.8, 1.0 Hz, 1H), 6.77 (d, *J* = 8.9 Hz, 1H), 6.46 (s, 1H), 4.72 – 4.60 (m, 1H), 4.55 (dt, *J* = 8.6, 6.7 Hz, 1H), 4.14 (m, 1H), 4.11 – 4.05 (m, 1H), 3.57 (dd, *J* = 13.4, 1.9 Hz, 1H), 3.54 (d, *J* = 4.9 Hz, 1H), 3.50 (m, 2H), 3.49 – 3.43 (m, 1H), 3.37 – 3.34 (m, 1H), 3.15 (dd, *J* = 14.1, 2.6 Hz, 1H), 2.83 (dd, *J* = 13.7, 6.7 Hz, 1H), 1.28 (d, *J* = 7.4 Hz, 3H), 0.34 (d, *J* = 7.3 Hz, 3H) ppm. **¹³C NMR** (151 MHz, DMSO-*d*₆): δ 171.42, 171.41, 170.82, 170.71, 169.08, 168.56, 136.02, 135.69, 135.66, 133.76, 130.16, 130.11, 129.65, 128.24, 126.79, 121.22, 118.51, 118.45, 111.02, 105.66, 51.27, 51.18, 49.44, 48.72, 43.31, 43.18, 35.90, 25.07, 16.43, 15.23 ppm. **IR** (Film, cm⁻¹) ν = 3378.65, 3301.78, 3051.96, 2930.25, 1649.11, 1533.81 cm⁻¹. **HRMS** (ESI) (*m/z*): [*M*+*H*]⁺ calcd. for C₃₀H₃₃N₇O₆, 588.25651; found, 588.25770.

Ac-(bicyclo-*m,m*)-[Trp-Ala-Gly-Tyr(OAc)]-[Tyr(OAc)-Ala-Gly-Trp]-OH (12). The linear peptide **11** (50 mg, 0.044 mmol), AgBF₄ (51 mg, 0.262 mmol, 6.0 eq.), pivalic acid (6.7 mg, 0.066 mmol, 1.5 eq.) and Pd(OAc)₂ (3.9 mg, 0.018 mmol, 0.4 eq.) were placed in a microwave reactor vessel in 500 μ L of DMF. The mixture was heated under microwave irradiation (250 W) at 90 °C for 20 min. Three more batches were carried out following the same procedure. All the crudes were filtered and combined (25% conversion, estimated by HPLC-MS). The crude was purified by semi-preparative RP-HPLC (XBRIDGETM BEH 130, C18, 5 μ M OBD 19x50 mm column, [solvent A (0.1% FA in H₂O) and solvent B (0.1% FA in ACN)], in 10 min, flux: 20 mL·min⁻¹, detection at λ =220 nm, gradient: 25-30% of B. **¹H NMR** (600 MHz, DMSO-*d*₆): δ 10.87 (d, *J* = 12.6 Hz, 2H), 8.71 (d, *J* = 8.0 Hz, 1H), 8.50 (s, 1H), 8.24 (s, 1H), 8.03 (m, 1H), 7.98 (d, *J* = 8.0 Hz, 1H), 7.58 (d, *J* = 8.0 Hz, 1H), 7.43 (s, 1H), 7.38 – 7.32 (m, 2H), 7.25 (d, *J* = 8.2 Hz, 1H), 7.22 (d, *J* = 7.0 Hz, 1H), 7.09 (ddd, *J* = 8.1, 6.9, 1.1 Hz, 1H), 7.03 (dt, *J* = 15.7, 7.6 Hz, 2H), 6.96 (t, *J* = 7.8 Hz, 1H), 6.79 (2H), 5.04 (m, 1H), 4.94 (q, *J* = 7.4 Hz, 1H), 4.75 (m, 1H), 4.43 – 4.35 (m, 1H), 4.19 (p,



$J = 6.9$ Hz, 1H), 3.90 (dd, $J = 17.0, 7.1$ Hz, 1H), 3.58 (dd, $J = 16.7, 7.0$ Hz, 1H), 3.51 – 3.44 (m, 1H), 3.38 (1H), 3.30 (1H), 3.24 (1H), 3.19 (m, 1H), 3.04 (s, 2H), 2.83 (t, $J = 13.2$ Hz, 1H), 1.94 (s, 3H), 1.49 (s, 3H), 1.21 (d, $J = 7.2$ Hz, 3H), 1.03 (d, $J = 7.0$ Hz, 3H) ppm. **HRMS** (ESI) (m/z): $[M+H]^+$ calcd. for $C_{45}H_{47}N_9O_{11}$, 890.34678; found, 890.34796.

PUBLICATION VIII.

Constrained cyclopeptides: biaryl formation through Pd-catalyzed C-H activation in peptides—structural control of the cyclization vs. cyclodimerization outcome

Lorena Mendive-Tapia,^a Alexandra Bertran,^a Jesús García,^a Gerardo Acosta,^b Fernando Albericio,^{b, c, d} and Rodolfo Lavilla^{b, e}

Chemistry – A European Journal, 2016, 22, 13114-13119.

- a) Institute for Research in Biomedicine, Barcelona Science Park, Baldiri Reixac 10-12, 08028 Barcelona (Spain).
- b) CIBER-BBN, Networking Centre for Bioengineering, Biomaterials and Nanomedicine, Barcelona Science Park, Baldiri Reixac 10-12, 08028 Barcelona (Spain).
- c) Department Organic Chemistry, University of Barcelona, Martí i Franquès 1-11, 08028 Barcelona (Spain).
- d) School of Chemistry, University of KwaZulu-Natal, 4001-Durban (South Africa).
- e) Laboratory of Organic Chemistry, Faculty of Pharmacy, University of Barcelona, Barcelona Science Park Baldiri Reixac 10-12, 08028 Barcelona (Spain).

Macrocycles

Constrained Cyclopeptides: Biaryl Formation through Pd-Catalyzed C–H Activation in Peptides—Structural Control of the Cyclization vs. Cyclodimerization Outcome

Lorena Mendive-Tapia,^[a] Alexandra Bertran,^[a] Jesús García,^[a] Gerardo Acosta,^[b] Fernando Albericio,^[b, c, d] and Rodolfo Lavilla^{*,[b, e]}

Abstract: A series of short tryptophan-phenylalanine peptides containing an iodo substituent on the phenyl ring was subjected to Pd-catalyzed CH activation reactions to give the corresponding aryl-indole coupled products. Two types of adducts were generated: cyclomonomer and cyclodimeric peptides; no evidence of oligo- or polymerization products was detected. Contrary to standard peptide macrocycliza-

tions, the factors controlling the fate of the reaction are the number of amino acids between the aromatic residues and the regiochemistry of the parent iodo derivative, independent of both the concentration and the cyclization mode. The method is general and allows access to novel biaryl peptidic topologies, which have been fully characterized.

Introduction

Peptides display ideal features for exploring the biological space associated with complex biomolecules such as chemical diversity, molecular topology and dimensions, and high selectivity is often achieved with these chemical entities. However, their metabolic stability is generally low, which limits their use as drugs, and their conformational flexibility normally leads to reduced affinity to the target. Cyclopeptides are naturally occurring substances displaying large rings often exhibiting improved properties.^[1] Recently, the groups of Heins^[2] and Whitty^[3] have reviewed the ways peptide-based macrocycles bind to proteins and the development of new techniques and computational tools for the generation of these macrocycles. There is a wide range of different strategies to perform the

macrocyclization,^[4] in which competing poly(oligo)merization^[5] may be limited through high-dilution conditions or solid-phase cyclization. The efficiency of the process is determined by several key parameters, such as concentration, structure and pre-organization of the linear precursors, solvent and ring size, which can all play a critical role in the control of the macrocycle-to-oligomer ratio.^[6] In this respect, Kappe studied the influence of the ring size in a copper-catalyzed dipolar cycloaddition (CuAAC) macrocyclization of linear peptoids.^[7] In addition, the concept of stapled peptides has recently emerged as a breakthrough in their use as drugs. The intramolecular constriction in these modified biomolecules normally improves the pharmacokinetic profile and the conformational behavior.^[8] The main stapling methods so far described include cysteine modification, ring-closing metathesis and click chemistry.^[9] Although efficient, these approaches require the use of two chemically modified de novo amino acids. On the other hand, peptides containing biaryl linkages constitute attractive targets because they display potent bioactivities; however, they are synthetically challenging.^[10] In this context, we have disclosed an alternative constraining method involving the coupling of an iodo-phenylalanine/tyrosine (Phe/Tyr) moiety with the 2-position of the indole nucleus of a neighboring tryptophan (Trp) residue, to yield an aryl-aryl peptidic adduct in a palladium-catalyzed C–H activation reaction.^[11–13] The scope of the reaction is general with the exception of peptidic sequences containing metal-coordinating amino acids (cysteine, methionine, histidine) as we reported.^[12a] Recently, Ackermann and co-workers developed a new arylation method that proceeds at much lower temperatures using arylodonium species, which is particularly suitable for intermolecular arylations.^[14] By following our protocol, a variety of peptidic macrocycles of several lengths and topologies have been prepared. These studies

[a] L. Mendive-Tapia, A. Bertran, Dr. J. García
Institute for Research in Biomedicine, Barcelona Science Park
Baldri Reixac 10–12, 08028 Barcelona (Spain)

[b] G. Acosta, Prof. F. Albericio, Prof. R. Lavilla
CIBER-BBN, Networking Centre in Bioengineering,
Biomaterials and Nanomedicine, Barcelona Science Park
Baldri Reixac 10–12, 08028 Barcelona (Spain)

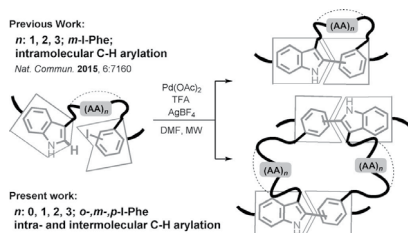
[c] Prof. F. Albericio
Department of Organic Chemistry, University of Barcelona
Martí i Franqués 1–11, 08028 Barcelona (Spain)

[d] Prof. F. Albericio
School of Chemistry, University of KwaZulu-Natal
4001-Durban (South Africa)

[e] Prof. R. Lavilla
Laboratory of Organic Chemistry, Faculty of Pharmacy
University of Barcelona, Barcelona Science Park
Baldri Reixac 10–12, 08028 Barcelona (Spain)
E-mail: rlavilla@pcb.ub.es

Supporting information and ORCID of the author for this article is available on the WWW under <http://dx.doi.org/10.1002/chem.201601832>.

have involved *meta*-regiochemistry in the aryl iodide, rendering almost exclusively the cyclic peptide through an intramolecular C–H arylation reaction. Here, with the aim of obtaining highly constrained cyclic peptides and determining the factors controlling the fate of the chemical transformation, we report a systematic study of I-Phe/Trp coupling processes involving shorter spacers and also alternative regiochemistries for the aryl iodide unit. The main factors determining the outcome of the reaction and novel chemotypes arising from these transformations are discussed (Scheme 1).



Scheme 1. Palladium-catalyzed cyclization between Phe-Trp containing peptides.

Results and Discussion

ortho-Regiochemistry

We first evaluated the impact of an *ortho*-regiochemistry in the aryl iodide residue in the outcome of the C–H coupling. For this purpose, linear sequences were first manually prepared by solid-phase peptide synthesis (SPPS) with either none or one alanine (Ala) residue between the Trp and *o*-iodo-Phe amino acids. When the C–H coupling was attempted under our standard conditions, only reduction of the carbon–halogen bond was observed. This behavior may reflect the high strain that

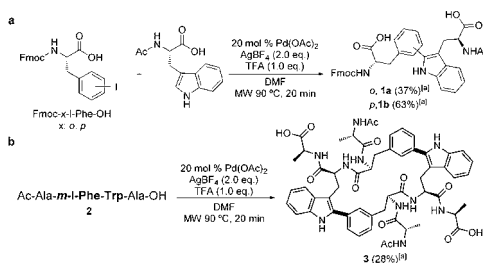
would arise in an *ortho*-biaryl cyclopeptide, with the consequent difficulty in the cyclization. Interestingly, the intermolecular reaction between the single residues Fmoc-*o*-I-Phe-OH and Ac-Trp-OH successfully yielded the corresponding Trp-Phe adduct **1a**, as seen in previous work on *meta/para*-aryl iodide derivatives, although the process proceeds with a slightly lower reactivity than that observed for those described derivatives.^[12a] This is probably due to steric hindrance associated with the *ortho*-disposition; consistently, the *para*-derivative analogue **1b** (Scheme 2a) was produced in higher yield.

meta-Regiochemistry

We recently reported access to a variety of biaryl cyclic peptides ranging from one to three amino acids between *m*-I-Phe and Trp residues through a selective intramolecular C–H activation reaction.^[12a] In an analogous manner, we tackled the chemistry of adjacent Phe-Trp residues. In this way, an Ala-containing tetrapeptide featuring contiguous *m*-I-Phe and Trp units was reacted under the usual conditions. Consistently, the arylation evolved to yield the cyclodimeric structure **3** (28% estimated yield based on the HPLC profile, Scheme 2b), with no trace of either the putative cyclic peptide or oligo(poly)merization species being detected. Furthermore, we have not detected any racemization on the peptide stereogenic centers, and neither was atropoisomerism related to the new aryl–aryl bond observed, which is a trend always seen throughout the rest of the studies. Detailed high-resolution mass spectrometry analyses were performed to unambiguously distinguish the cyclic monomer from the cyclic dimer products (see the Supporting Information).

para-Regiochemistry

Peptides **4**, with an increasing number of amino acids between Trp and *p*-I-Phe units, were prepared by using SPPS. As previously reported by our group, reaction of the adjacent Phe and Trp containing sequence (**4a**) again resulted in the exclusive formation of the cyclodimeric peptide **5a** (Table 1, entry 1;



Scheme 2. Intermolecular C–H arylation of a) (*o/p*-I)Phe unit and b) cyclodimer formation from adjacent (*m*-I)Phe-Trp. [a] Estimated yield based on the HPLC-MS profile.

Table 1. Influence of the number of residues between *p*-I-Phe and Trp residues in the palladium-catalyzed C–H arylation^[a]

Entry	Peptide sequence ^[b]	Cyclodimeric peptide ^[c]	Cyclic peptide ^[c]
1	A-(<i>p</i> -I)F-W-A (4a)	(5a) (60%)	n.d. ^[d]
2	(<i>p</i> -I)F-A-W-K (4b)	(5b) (54%)	n.d.
3	A-(<i>p</i> -I)F-K-G-W-A (4c)	(5c) (23%)	(5c') (51%)
4	A-(<i>p</i> -I)F-R-K-G-W-A (4d) ^[e]	n.d.	(5d') (81%)

[a] Coupling conditions: 20 mol% Pd(OAc)₂, AgBF₄ (2.0 equiv), TFA (1.0 equiv) in DMF (0.10–0.25 M peptide concentration), MW 90 °C, 20 min. [b] A: alanine, F: phenylalanine, G: glycine, K: lysine, R: arginine, W: tryptophan. [c] Conversions estimated based on HPLC-MS analysis. [d] n.d.: not detected. [e] A second irradiation cycle was performed.

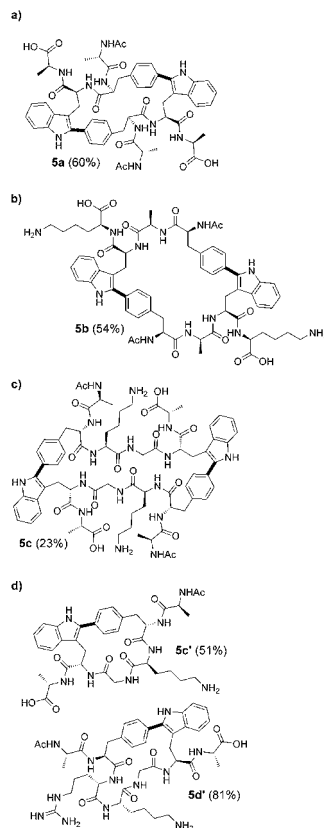
Figure 1).^[15] The inclusion of one amino acid residue between the Trp and Phe units (**4b**) did not alter this tendency, and the corresponding cyclodimer **5b** was selectively generated (Table 1, entry 2; Figure 1). Remarkably, when the chain length was increased up to two residues (peptide **4c**), both cyclodimeric **5c** (23% estimated conversion based on HPLC analysis) and cyclic **5c'** (51%) species were formed in meaningful extents (Table 1, entry 3; Figure 1). Furthermore, the presence of three amino acids (peptide **4d**) resulted in the exclusive generation of the corresponding cyclic derivative **5d'** (Table 1, entry 4; Figure 1) after Pd-catalyzed arylation.

Incidentally, in some cases when the reactions evolve predominantly through the cyclodimeric pathway, traces of cyclotrimeric species were also detected by HPLC-MS analysis. Nevertheless, no evidence of polymerization was observed.

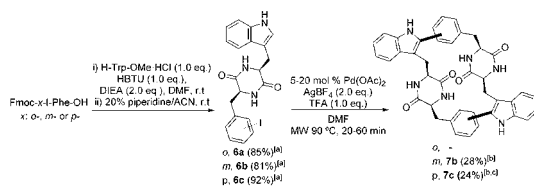
Likely, the first intermolecular process leads to intermediate species, which may be preorganized through Pd-to-amide coordination thus favoring the subsequent cyclization by an intramolecular C–H arylation, then leading to cyclodimers.

Typically, standard peptide macrocyclizations have to be carried out at high dilution conditions (<1 mM), which is a drawback in terms of solvent economy. However, in all of our experiments, the cyclodimer-to-cyclic peptide ratio seems to be independent of the concentration, which is moderately high (0.10–0.25 M); the structure of the parent peptide and the regiochemistry of the I-Phe unit tend to control the fate of the reaction. Additional experiments carried out at lower concentrations (1 mM) gave essentially unreacted substrates. With respect to solid-phase cyclizations (the alternative way to achieve high dilution conditions, then favoring intramolecular interactions), a series of I-Phe-(Ala)_n-Trp sequences were subjected to analogous Pd-catalyzed couplings on low functionalized TentaGel resins. The same trends were observed, with cyclodimerization being the only outcome of the reaction (see the Supporting Information).

We then focused our attention in 2,5-diketopiperazines (DKPs), the smallest cyclopeptides, which are present in numerous natural products and constitute attractive scaffolds for the development of new drugs.^[16] For the synthesis of these compounds, we reacted the commercially available H-Trp-OMe-HCl and Fmoc-x-I-Phe-OH (x: *o*, *m*, *p*) through a standard amide coupling with HBTU (1.0 equiv) and DIEA (2.0 equiv) to form the corresponding dipeptide, with the iodo substituent


Figure 1. C–C linked structures resulted from C–H arylations of linear peptides containing *p*-I-Phe and Trp residues located at different distances a) *ii*+1; b) *ii*+2; c) *ii*+3; d) *ii*+4.

placed at *ortho*, *meta* or *para* positions, respectively. This substrate was then suspended in 20% piperidine/ACN solution to remove the N-terminal Fmoc protecting group with subsequent spontaneous DKP formation. Finally, the resulting DKPs **6a–c** were subjected to our reported Pd-catalyzed C–H activation protocol to yield the corresponding cyclodimeric products **7b–c** from the *m,p*-regiochemistries (24 and 28% yield, respectively; Scheme 3), whereas the *o*-derivative afforded only reduction of the carbon–halogen bond and neither cyclodimeric nor cyclic products could be detected.



Scheme 3. Synthesis of dimeric Phe-Trp DKPs **7b** and **7c**. [a] Isolated yields. [b] Estimated yields based on HPLC-MS analysis. [c] A second irradiation cycle was performed.

James and Collins recently reported a quantitative index for the macrocyclization efficiency (Emac), which is proportional to the concentration and the yield of the reaction.^[17] To assess the practicality of our macrocyclization protocol, we calculated the Emac values for a range of representative macrocyclic peptides disclosed so far with our methodology. The calculated indexes (between 6.5 and 7.7, see the Supporting Information) are within the range of the previously reported Emac dataset^[17] and rank among the most productive processes of these types.

All the synthesized cyclopeptides were unequivocally characterized by HRMS and NMR spectroscopy. Most compounds show well-defined signals compatible with flexible conformations. Cyclodimeric peptides **5a–c** were fully assigned by NMR spectroscopic analysis and showed a C_2 -symmetric structure. Aromatic ring flipping was observed for Phe residues in all peptides. Rapid reorientation around the C β –O bond renders the H δ 1/H δ 2 protons on one side and the He1/He2 protons on the other side, being equivalent on the NMR timescale.

On the other hand, peptide **5a** displayed sharp peaks at 298 K whereas many resonances of peptides **5b** and **5c** appeared as broad signals at this temperature. On increasing the temperature, a clear sharpening on the ^1H resonances of cyclodimers **5b** and **5c** was observed. This behavior is indicative of exchange broadening effects, suggesting that backbone flexibility increases with the size of the polypeptide chain. The ^1H NMR spectra of macrocycles **5c'** and **5d'** were characterized by a significant chemical shift dispersion of the amide NH (in some cases resonating around 8.0 ppm or higher) and H α resonances. As in the case of peptides **5a–c**, ring flipping is rapid on the NMR timescale, resulting in chemical shift averaging, yielding only two resonances for the four Phe aromatic protons, one for the two H δ 1/H δ 2 protons and the second one for the two He1/He2 protons (see the Supporting Information). Finally, the ^1H NMR spectra of DKP cyclodimers **7b** and **7c** were well resolved and consistent with the symmetric and rigid nature of these molecules. Cyclodimer formation was characterized by a large diastereotopic splitting of geminal H β protons (for additional comments on this section see the Supporting Information).

Interestingly, the small cyclodimeric DKPs **7b** and **7c** display two different topologies (square and rhomboid, respectively) defined by the regioisomeric pattern of the phenyl moiety (Figure 2a). On the other hand, cyclodimers **5b** and **5c** possess

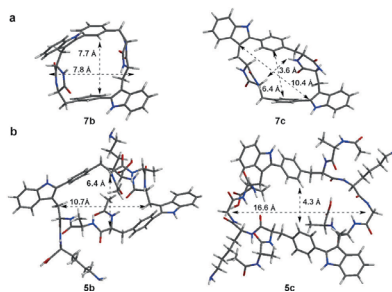


Figure 2. Minimized geometries of compounds a) **7b** and **7c** b) **5b** and **5c** generated by using the Spartan '14 suite (Molecular Mechanics + Semiempirical methods).

larger cavity diameters in the range of known macrocycles such as cyclodextrins (Figure 2b). These cyclic oligosaccharides can encapsulate a broad range of compounds inside their hydrophobic cavity.^[18] Consequently, our novel peptidic architectures could be envisioned as possible host compounds for flat guests. In preliminary experiments, estradiol was selected as potential guest. Modest increments of host absorbance were detected with a progressive increase of the estradiol molar fraction and, importantly, a typical saturation curve was obtained for both compounds at high molar guest fractions, suggesting the existence of molecular recognition events (see the Supporting Information).^[19]

The controlled formation of cyclopeptides or cyclodimers, depending on the structure of the parent peptides, prompted us to rationalize this remarkable behavior. In this respect, we have to mention the recent work of Houk, James, and co-workers, in which a related system was analyzed.^[5a] They clearly related the ease of formation of the macrocyclic structures with their strain energy. With these results in mind, we performed a preliminary assessment of the relative stability of meaningful models of the smaller cyclic/cyclodimer pairs ($n=0, 1$).^[20] After the optimization of the geometries for a series of representative Phe-Trp derivatives by molecular mechanics (MMFF) and

semiempirical methods (PM3, see the Supporting Information), we had a rough qualitative estimation of the stabilities for these compounds.

We noticed the following trends: (i) *ortho*-derivatives always gave strained cyclic species. (ii) *meta*-regiochemistries led, in the adjacent Trp-Phe construct, to highly strained cyclic species, and to an energetically more reasonable cyclodimer; only the latter was experimentally obtained. In a larger substrate with a glycine spacer between the Phe and Trp units, the cyclopeptides and the cyclodimer are comparable in energy, with the former being isolated, whereas the latter is not observed. In cases in which the enthalpy barrier to formation of both species are in the same range, it may be considered that with the cyclopeptide being energetically accessible, its formation may be faster (in a single irreversible process) than the stepwise ring closure leading to a larger macrocycle (cyclodimer). (iii) Regarding the *para*-isomers, for both directly linked Trp-Phe systems and those featuring one Gly spacer, the cyclic species are highly unstable, displaying distorted nonplanar benzene rings, whereas the cyclodimeric structure is energetically favorable and its formation is thus justified. Overall, this rough estimation seems to be in line with previous findings,^[19] and accounts for the experimental observations. A more detailed study involving larger substrates and the reaction barriers leading to the cyclized compounds is expected to be extremely challenging, taking into consideration the conformational landscape of the cyclopeptides and the complexity of the Pd-catalyzed process.

Conclusion

We have established the structural factors controlling the fate of intramolecular C–H arylation in a series of Phe-Trp peptides leading to cycles or to cyclodimers. Overall, short spacers lead to cyclodimers (*i, i+1-meta/para*; *i, i+2-para*) and longer linkages (*i, i+4-meta/para*) or intermediate *meta* substrates render cyclopeptides, whereas in one case (*i, i+3-para*) both species are produced to similar extents. These practical rules conveniently chart the synthesis of these species. Furthermore, novel chemotypes of the highly constrained biaryl-cyclic and cyclodimeric peptides have been disclosed. Overall, these studies clearly show that in biaryl peptidic sequences, the fate of the cyclization or cyclodimerization is mainly due to structural features rather than regulated by experimental factors. The preparation of new biaryl cyclopeptides could be achieved by following these lines.

Experimental Section

General information

Reactions were monitored by HPLC-MS at 220 nm with a HPLC Waters Alliance HT comprising a pump (Edwards RV12) with degasser, an autosampler and a diode array detector. Flow from the column was split to a MS spectrometer. The MS detector was configured with an electrospray ionization source (micromass ZQ4000) and nitrogen was used as the nebulizer gas. Mass scans were acquired in positive ion mode, and linear gradients of ACN (+0.05%

formic acid) into H₂O (+0.1% formic acid) were run at a flow rate of 1.6 mL min⁻¹ over 3.5 min. Data acquisition was performed with MassLynx software. High-resolution mass spectrometry analyses were conducted with an LTQ-FT Ultra (Thermo Scientific) spectrometer with a NanoESI positive ionization. Data was acquired with Xcalibur software, vs.2.0SR2 (ThermoScientific) and elemental compositions from experimental exact mass monoisotopic values were obtained with a dedicated algorithm integrated in Xcalibur. All microwave reactions were carried out in 10 mL sealed glass tubes in a focused mono-mode microwave oven ("Discover" by CEM Corporation) with a surface sensor for internal temperature determination. Cooling was provided by compressed air ventilating the microwave chamber during the reaction. When stated, final crude material was purified with a semipreparative RP-HPLC with a RP-HPLC XBRIDGETM Prep C18, 5 μ m OBD 19 \times 50 mm column, a Waters Delta 600 system comprising a sample manager (Waters 2700), a controller (Waters 600), a dual λ absorbance detector (Waters 2487), a fraction collector II, and a software system controller (MassLynx). Linear gradients of ACN (+0.05% formic acid) into H₂O (+0.1% formic acid) were run at a flow rate of 16 mL min⁻¹ over 20 min. Otherwise, the final crude material was purified by flash column chromatography Combi Flash ISCO RF provided with dual UV detection. Normal mode: crude residue and silica media were suspended in DCM, concentrated, and the resultant solid samples were eluted on a RediSepRf silica column. Reverse mode: crude residues and Celite were suspended in DCM, concentrated, and the resultant solid samples were eluted on a RediSepRf GOLD C18 column. NMR spectra of peptides in [D₆]DMSO were acquired with a Varian Mercury 400 MHz, Bruker DMX-500 MHz, or Bruker Avance III 600 MHz spectrometer, with the latter equipped with a TCI cryoprobe. The spectra were referenced relative to the residual DMSO signal (¹H, 2.49 ppm; ¹³C, 39.5 ppm). For peptides **5a-c** and **7b-c**, ¹H resonances were unequivocally assigned by two-dimensional NMR experiments (COSY, TOCSY and NOESY and/or ROESY). The ¹³C resonances were straightforwardly assigned on the basis of the cross-correlations observed in the ¹H-¹³C HSQC spectra. Mixing times for TOCSY spectra were 70 ms, for NOESY spectra 300–450 ms and for ROESY experiments were 200 ms. Chemical shifts (δ) are reported in ppm. Multiplicities are abbreviated: s = singlet, d = doublet, t = triplet, dd = double doublet, dt = double triplet, q = quartet and m = multiplet. HRMS (ESI positive) were obtained with a LTQ-FT Ultra (Thermo Scientific) mass spectrometer. IR spectra were obtained with a Thermo Nicolet NEXUS.

General procedure for the synthesis of compounds 1a–b

Fmoc-Phe(x-I)-OH (x: *o* or *p*) (1.0 equiv), Ac-Trp-OH (1.0 equiv), AgBF₄ (2.0 equiv), trifluoroacetic acid (1.0 equiv) and Pd(OAc)₂ (0.20 equiv) were placed in a microwave reactor vessel in DMF. The mixture was heated under microwave irradiation (250 W) at 90 °C for 20 min. Then, further Pd(OAc)₂ (0.20 equiv) and AgBF₄ (2.0 equiv) were added and a second irradiation cycle was performed. The resulting suspension was filtered through Celite and the filtrate was evaporated under vacuum. The crude residue was purified by flash chromatography on Silica using DCM/EtOH to obtain the final product **1** (37–63% isolated yield) as a pale solid.

General procedure for the C–H arylation process of peptides **3** and **5**

The linear peptide (1.0 equiv), AgBF₄ (2.0 equiv), trifluoroacetic acid (1.0 equiv) and Pd(OAc)₂ (0.20 equiv) were placed in a microwave reactor vessel in DMF. The mixture was heated under microwave irradiation (250 W) at 90 °C for 20 min. The resulting suspension was

filtered through Celite and the filtrate was evaporated under vacuum (23–81 % HPLC-MS conversions). An analytically pure sample was obtained by purification of the crude residue by semi-preparative RP-HPLC to properly characterize the products **3** and **5** (XBRIDGE™ Prep C18, 5 μ m OBD 19 \times 50 mm column) [solvent A (0.1% formic acid in H₂O) and solvent B (0.1% formic acid in ACN)], in 10 min, flux: 20 mL min⁻¹, detection at λ = 220 nm.

General procedure for the synthesis of DKPs **6a–c**

Compounds **6a–c** were prepared by using Fmoc-Phe(x)-OH (x: o, m or p) (1.0 equiv), H-Trp-OMe-HCl (1.0 equiv), HBTU (1.0 equiv) and DIEA (2.0 equiv), which were dissolved in DMF. The pale-yellow solution was stirred at r.t. for 24 h followed by evaporation under vacuum. The obtained suspension was dissolved in ethyl acetate and washed with sat. aq. NaHCO₃ (x3). The organic phase was then dried over Na₂SO₄, filtered and the solvent was removed under vacuum to give the desired dipeptide. The resulting white solid was suspended in 20% piperidine/ACN and stirred for 20 h. The resulting suspension was concentrated under vacuum and diethyl ether was added over the solid. The suspension was stirred for 10 min, filtered and washed with diethyl ether (x3). The white solid obtained was dried to yield the corresponding pure product **6** (81–92% isolated yield).

General procedure for the synthesis of cyclodimeric DKPs **7b–c**

Compound **6b–c** (1.0 equiv), AgBF₄ (2.0 equiv), trifluoroacetic acid (1.0 equiv) and Pd(OAc)₂ (0.05 equiv) were dissolved in DMF and placed in a microwave reactor vessel. The mixture was heated under microwave irradiation (250W) at 90 °C for 20 min. The resulting suspension was filtered through Celite and the filtrate was evaporated under vacuum (24–28% HPLC-MS conversions). An analytically pure sample was obtained by purification of the crude residue by semi-preparative RP-HPLC or flash chromatography on Celite using H₂O (0.1% formic acid)/ACN (0.1% formic acid) to properly characterize the products **7b–c**.

Acknowledgements

This work was supported by DGICYT-Spain (project CTQ2015-67870-P) and Generalitat de Catalunya (2014 SGR 137). We acknowledge an FPU fellowship for L. M.-T. from the Ministerio de Educación, Cultura y Deporte-Spain. NMR instruments were made available by the Scientific and Technological Centre of the University of Barcelona (CCIT UB). Professor M. Bradley (U. Edinburgh), Profs. M. L. Pérez, F. J. Luque, Dr. C. Estarellas (U. Barcelona), and Dr. M. Vilaseca (IRB Barcelona) are thanked for useful suggestions and support.

Keywords: biaryls • C–H activation • cyclization • palladium • peptides

- [1] a) S. Royo-Gracia, K. Gaus, N. Sewald, *Future Med. Chem.* **2009**, *1*, 1289–1310; b) D. J. Craik, D. P. Fairlie, S. Liras, D. Price, *Chem. Biol. Drug Des.* **2013**, *81*, 136–147; c) T. A. Hill, N. E. Shepherd, F. Diness, D. P. Fairlie, *Angew. Chem. Int. Ed.* **2014**, *53*, 13020–13041; *Angew. Chem.* **2014**, *126*, 13234–13257; d) P. Thapa, M. J. Espiritu, C. Cabaletta, J. P. Bingham, *Int. J. Pept. Res. Ther.* **2014**, *20*, 545–551; e) F. Giordanetto, J. Kihlberg, *J. Med. Chem.* **2014**, *57*, 278–295.

- [2] C. Heinis, *Nat. Chem. Biol.* **2014**, *10*, 696–698.
[3] E. A. Villar, D. Beglov, S. Chennamadhavuni, J. A. Porco, D. Kozakov, S. Vajda, A. Whitty, *Nat. Chem. Biol.* **2014**, *10*, 723–732.
[4] a) V. Marti-Centelles, M. D. Pandey, M. I. Burguete, S. V. Luis, *Chem. Rev.* **2015**, *115*, 8736–8834 and references included therein; b) A. Dalla Cort, J. G. Ercolani, A. L. Iamelli, L. Mandolini, P. J. Mencarelli, *J. Am. Chem. Soc.* **1994**, *116*, 7081–7087; c) D. B. Amabilino, P. L. Anelli, P. R. Ashton, G. R. Brown, E. Córdova, L. A. Godínez, W. Hayes, A. E. Kaifer, D. Philp, A. M. Z. Slawin, N. Spencer, J. F. Stoddart, M. S. Tolley, D. J. Williams, *J. Am. Chem. Soc.* **1995**, *117*, 11142–11170; d) R. Jasti, J. Bhattacharjee, J. B. Neaton, C. R. Bertozzi, *J. Am. Chem. Soc.* **2008**, *130*, 17646–17647; e) B. Qin, W. Q. Ong, R. Ye, Z. Du, X. Chen, Y. Yan, K. Zhang, H. Su, H. Zeng, *Chem. Commun.* **2011**, *47*, 5419–5421.
[5] a) A. R. Bogdan, S. V. Jerome, K. N. Houk, K. James, *J. Am. Chem. Soc.* **2012**, *134*, 2127–2138; b) A. Thakkar, T. B. Trinh, D. Pei, *ACS Comb. Sci.* **2013**, *15*, 120–129.
[6] a) B. J. Larsen, B. Z. Sun, P. Nagorny, *Org. Lett.* **2013**, *15*, 2998–3001; b) G. Chouhan, K. James, *Org. Lett.* **2013**, *15*, 1206–1209.
[7] C. E. M. Salvador, B. Pieber, P. M. Neu, A. Torvisco, C. K. Z. Andrade, C. O. Kappe, *J. Org. Chem.* **2015**, *80*, 4590–4602.
[8] a) G. L. Verdine, G. J. Hilinski, *Methods Enzymol.* **2012**, *503*, 3–33; b) L. D. Walensky, G. H. Bird, *J. Med. Chem.* **2014**, *57*, 6275–6288.
[9] a) H. E. Blackwell, R. H. Grubbs, *Angew. Chem. Int. Ed.* **1998**, *37*, 3281–3284; *Angew. Chem.* **1998**, *110*, 3469–3472; b) C. J. White, A. K. Yudin, *Nat. Chem.* **2011**, *3*, 509–524; c) R. Dharanipragada, *Future Med. Chem.* **2013**, *5*, 831–849; d) M. Góngora-Benítez, J. Tulla-Puche, F. Albericio, *Chem. Rev.* **2014**, *114*, 901–926; e) Y. H. Lau, P. de Andrade, Y. Wu, D. R. Spring, *Chem. Soc. Rev.* **2015**, *44*, 91–102.
[10] a) A. Montero, F. Albericio, M. Royo, B. Herradon, *Org. Lett.* **2004**, *6*, 4089–4092; b) L. Felli, M. Planas, *Int. J. Pept. Res. Ther.* **2005**, *11*, 53–97; c) F.-M. Meyer, J. C. Collins, B. Borin, J. Bradov, S. Liras, C. Limberakis, A. M. Mathiowetz, L. Philippe, D. Price, K. Song, K. James, *J. Org. Chem.* **2012**, *77*, 3099–3114; d) Also see: M. Bois-Choussy, P. Cristau, J. Zhu, *Angew. Chem. Int. Ed.* **2003**, *42*, 4238–4424; *Angew. Chem.* **2003**, *115*, 4370–4373.
[11] For an overview, see: a) *Topics in Current Chemistry*, Vol. 292, C-H Activation (Eds.: J.-Q. Yu, Z. Shi, Springer, Berlin Heidelberg, **2010**); b) M. C. White, *Synlett* **2012**, 2746–2748.
[12] a) J. Ruiz-Rodríguez, F. Albericio, R. Lavilla, *Chem. Eur. J.* **2010**, *16*, 1124–1127; b) S. Preciado, L. Mendive-Tapia, F. Albericio, R. Lavilla, *J. Org. Chem.* **2013**, *78*, 8129–8813; c) L. Mendive-Tapia, S. Preciado, J. García, R. Ramón, N. Kießland, F. Albericio, R. Lavilla, *Nat. Commun.* **2015**, *6*, 7160.
[13] Also see: a) H. Dong, C. Limberakis, S. Liras, D. Price, K. James, *Chem. Commun.* **2012**, *48*, 11644–11646; b) F. M. Noisier, M. A. Brimble, *Chem. Rev.* **2014**, *114*, 8775–8806.
[14] a) Y. Zhu, M. Bauer, J. Plog, L. Ackermann, *Chem. Eur. J.* **2014**, *20*, 13099–13102; b) Y. Zhu, M. Bauer, L. Ackermann, *Chem. Eur. J.* **2015**, *21*, 9980–9983.
[15] Incidentally, this result prompted the systematic evaluation of the cyclization/cyclodimerization studies. The cyclodimeric compound was previously reported in ref. [12c].
[16] P. Cherkupally, S. Ramesh, Y. E. Jad, T. Govender, H. G. Kruger, B. G. de La Torre, F. Albericio, in *Privileged Scaffolds in Medicinal Chemistry—Design, Synthesis Evaluation* (Eds.: S. Brasse), Royal Society of Chemistry, Cambridge, **2015**, pp. 398–438 and references cited therein.
[17] J. C. Collins, K. James, *Med. Chem. Commun.* **2012**, *3*, 1489–1495.
[18] For instance, see J. Sejlitz, *Chem. Rev.* **1998**, *98*, 1743–1753.
[19] As negative control, the absorbance of estradiol alone does not show saturation at increasing concentrations. Furthermore, it is very close to zero at the wavelengths relevant for measuring the molecular recognition (see the Supporting Information).
[20] For higher analogues, the structures show a more complex conformational landscape, making it more difficult to obtain meaningful data.

Received: April 19, 2016
Published online on August 4, 2016

Supporting Information

Constrained Cyclopeptides: Biaryl Formation through Pd-Catalyzed C H Activation in Peptides—Structural Control of the Cyclization vs. Cyclodimerization Outcome

The following data is a selection of the content of the Supporting Information. Full supplementary information including general experimentation, procedures and compound characterization is available in the Supporting Information in electronic format.

Table of Contents

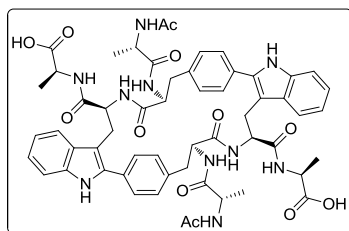
<i>Selected experimental procedures and peptide characterization.....</i>	<i>243</i>
<i>Selected NMR spectra</i>	<i>244</i>
<i>Selected ¹H and ¹³C chemical shifts assignments.....</i>	<i>249</i>
<i>Preliminary calculations on the relative stabilities of the cyclic/cyclodimeric peptides after the Pd-catalyzed CH activation reaction</i>	<i>250</i>

Selected experimental procedures and peptide characterization

General procedure for the C-H activation process of peptides 3 and 5

Unless stated otherwise, the linear peptide, AgBF_4 (2.0 eq.), trifluoroacetic acid (1.0 eq.) and $\text{Pd}(\text{OAc})_2$ (0.20 eq.) were placed in a microwave reactor vessel in DMF. The mixture was heated under microwave irradiation (250 W) at 90 °C for 20 min. The resulting suspension was filtered through Celite and the filtrate was evaporated under vacuum. The crude residue was purified by semi-preparative RP-HPLC (XBRIDGE™ Prep C18, 5 μM OBD 19 x 50 mm column) [solvent A (0.1% FA in H_2O) and solvent B (0.1% FA in ACN)], in 10 min, flux: 20 $\text{mL}\cdot\text{min}^{-1}$, detection at $\lambda=220$ nm.

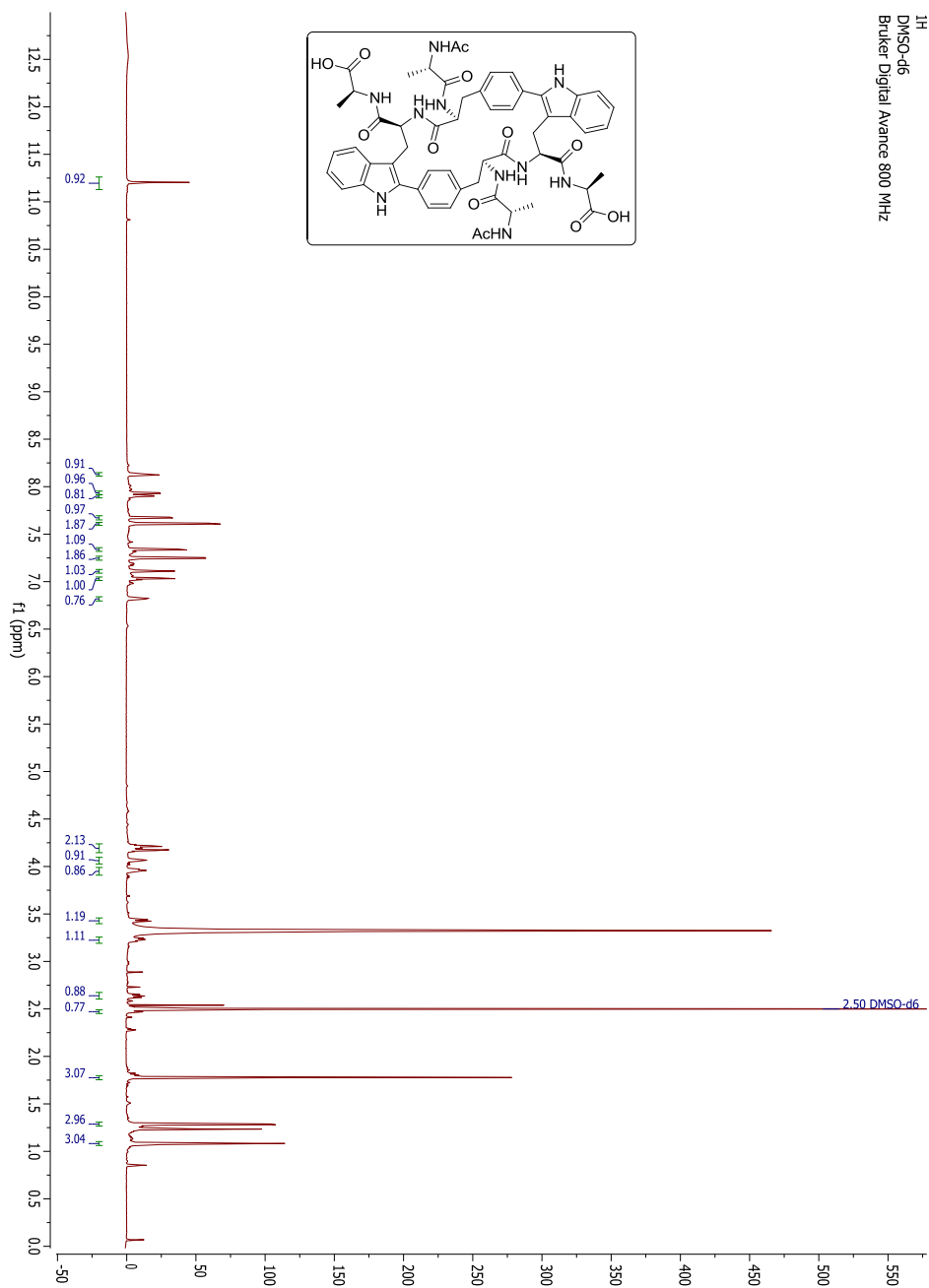
(Cyclo-*p,p*)bis-[Phe-Trp]-(Ac-Ala-Phe-Trp-Ala-OH) (5a). Starting from peptide **4a** (600 mg, 0.907 mmol) (60% conversion estimated by HPLC-MS). An analytically pure sample was obtained by semi-preparative RP-HPLC purification. Gradient: 25-30% of B (pale solid). **¹H**

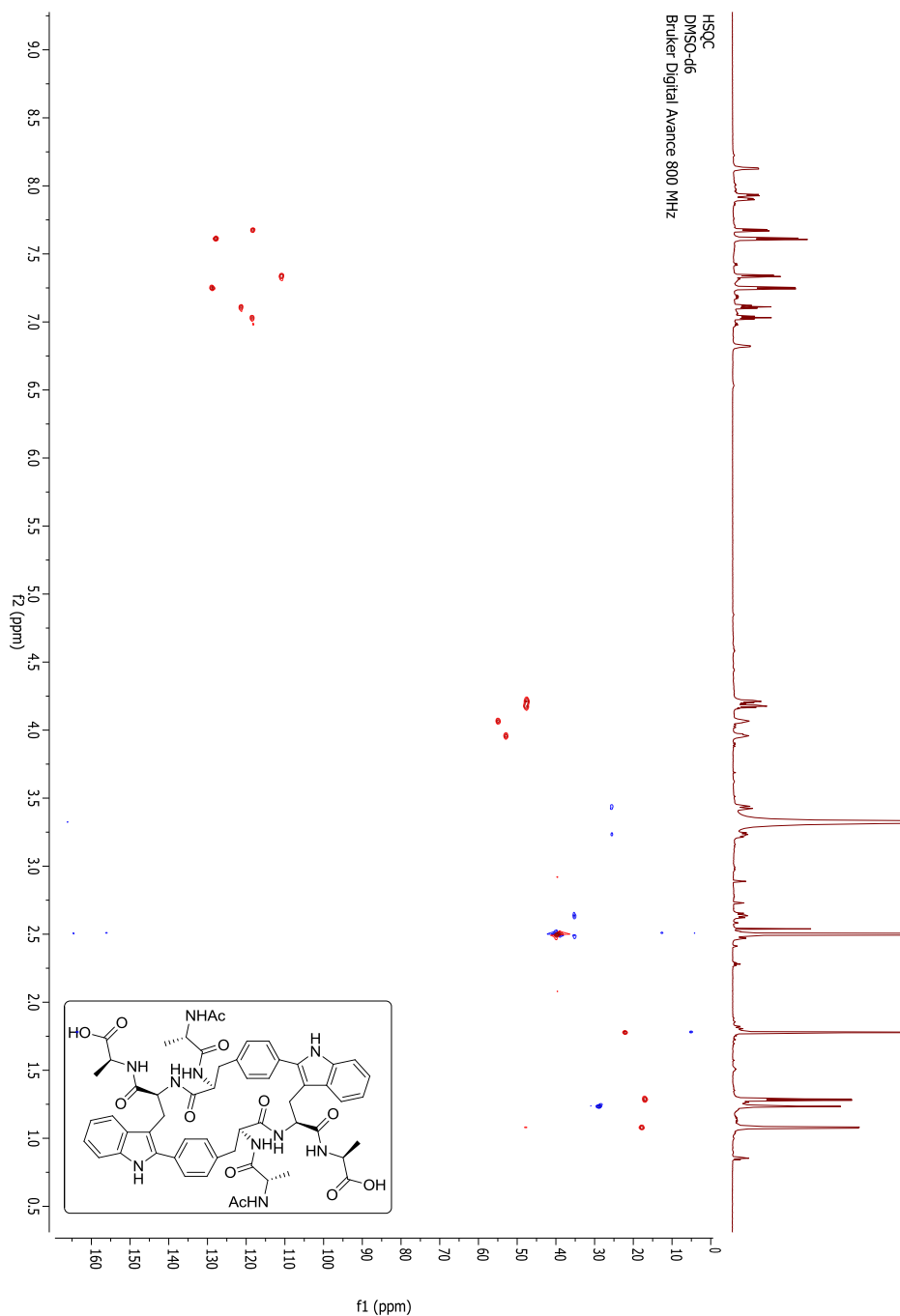


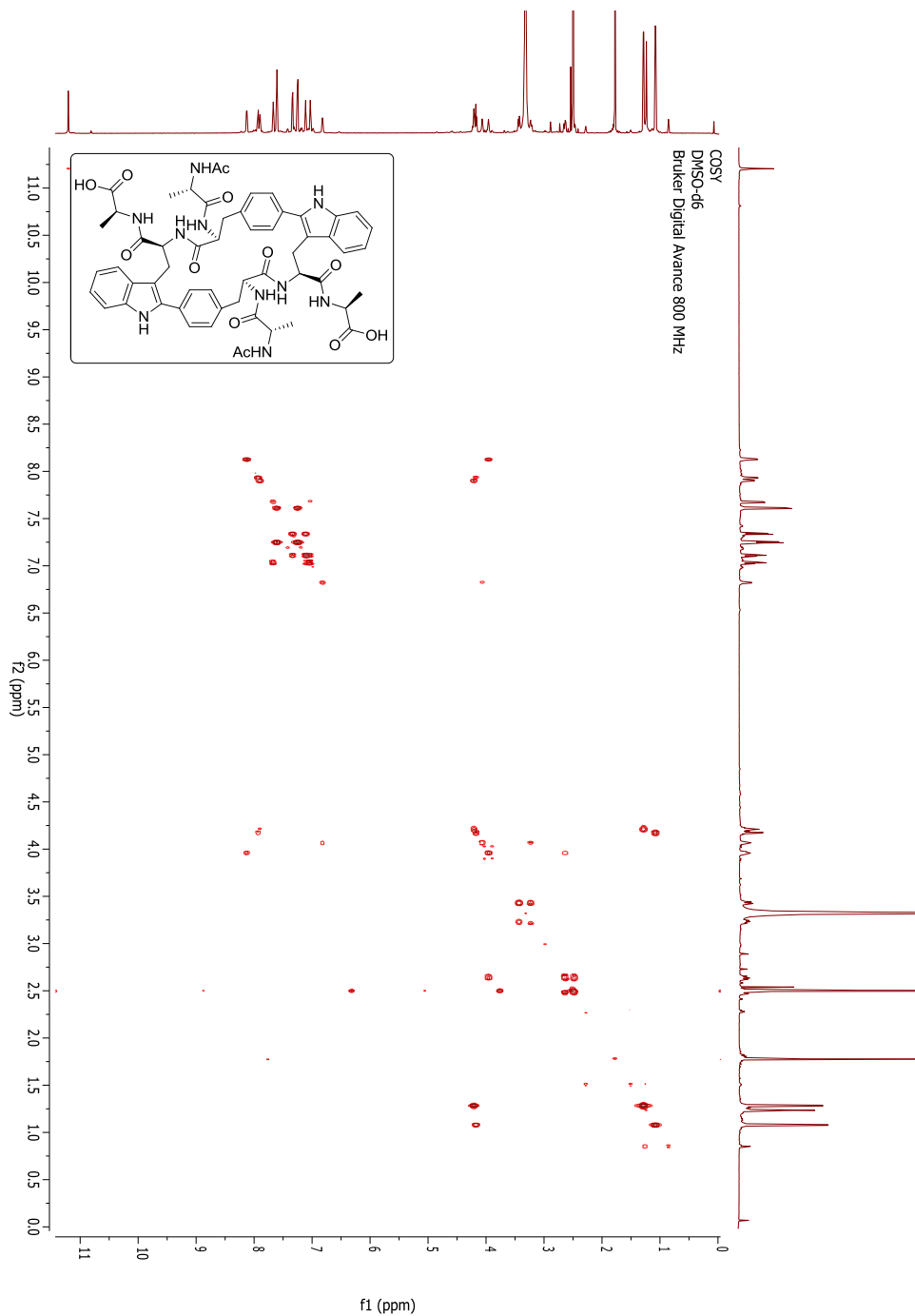
NMR (800 MHz, $[\text{D}_6]\text{DMSO}$): δ 11.20 (s, 1H), 8.13 (d, $J = 7.7$ Hz, 1H), 7.93 (d, $J = 7.3$ Hz, 1H), 7.90 (d, $J = 7.0$ Hz, 1H), 7.67 (d, $J = 7.9$ Hz, 1H), 7.61 (d, $J = 7.6$ Hz, 2H), 7.34 (d, $J = 7.9$ Hz, 1H), 7.25 (d, $J = 7.7$ Hz, 2H), 7.11 (t, $J = 7.5$ Hz, 1H), 7.03 (t, $J = 7.5$ Hz, 1H), 6.82 (d, $J = 6.9$ Hz, 1H), 4.24 – 4.15 (dp, $J = 28.2$, 7.1

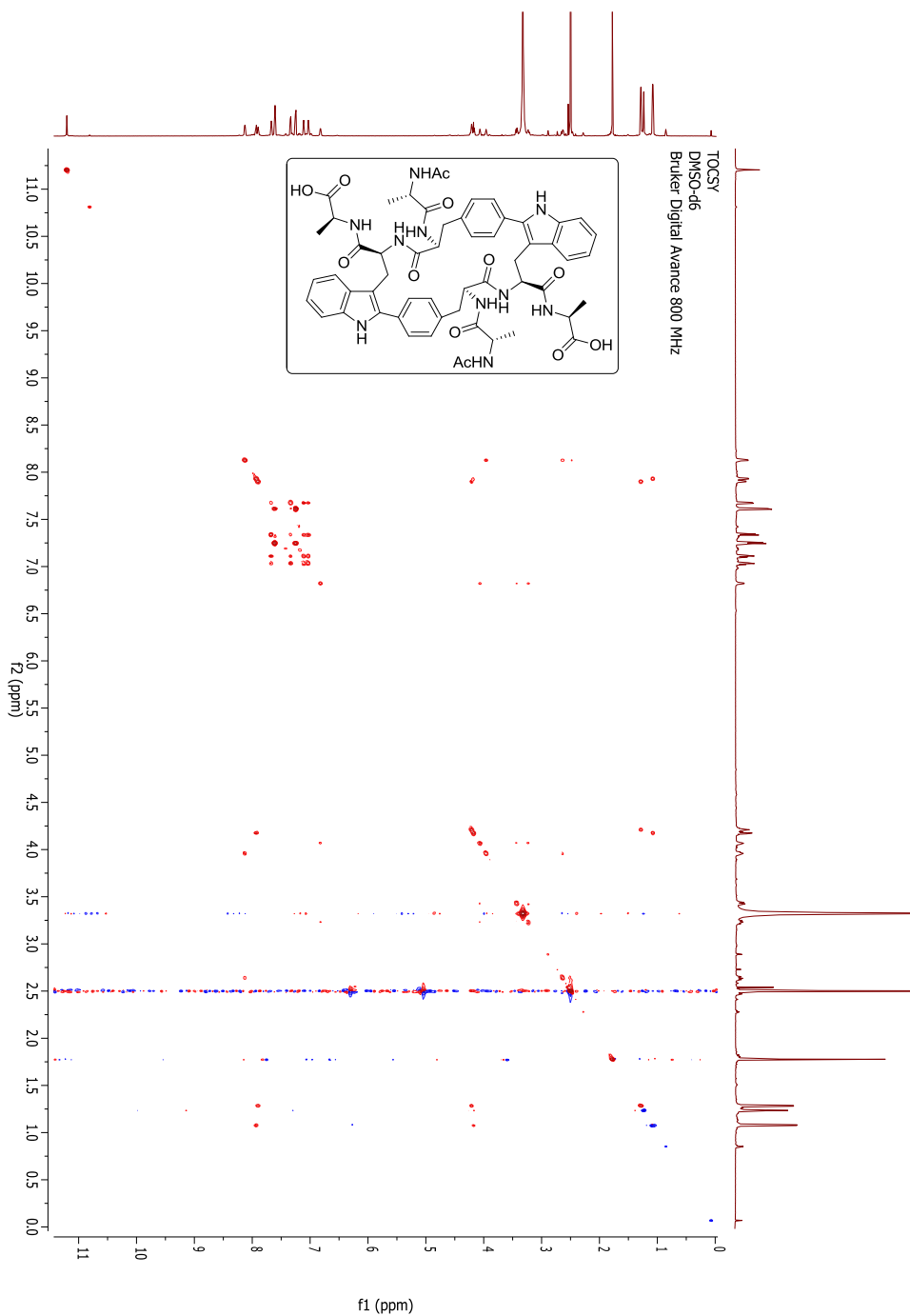
Hz, 2H), 4.07 (ddd, $J = 10.4$, 6.9, 3.8 Hz, 1H), 3.96 (m, 1H), 3.43 (dd, $J = 15.1$, 3.7 Hz, 1H), 3.23 (dd, $J = 15.2$, 9.4 Hz, 1H), 2.64 (dd, $J = 15.1$, 10.6 Hz, 1H), 2.48 (m, 1H), 1.78 (s, 3H), 1.28 (d, $J = 7.3$ Hz, 3H), 1.08 (d, $J = 7.0$ Hz, 3H) ppm. **IR** (Film, cm^{-1}): $\nu = 3404.27$, 2911.03, 1655.52 cm^{-1} . **HPLC-MS**: t_R 2.32 min (gradient 5-100% ACN). **HRMS (ESI)** (m/z): $[\text{M}+\text{H}]^+$ calcd. for $\text{C}_{56}\text{H}_{62}\text{N}_{10}\text{O}_{12}$, 1067.4621; found, 1067.4624.

Selected NMR spectra

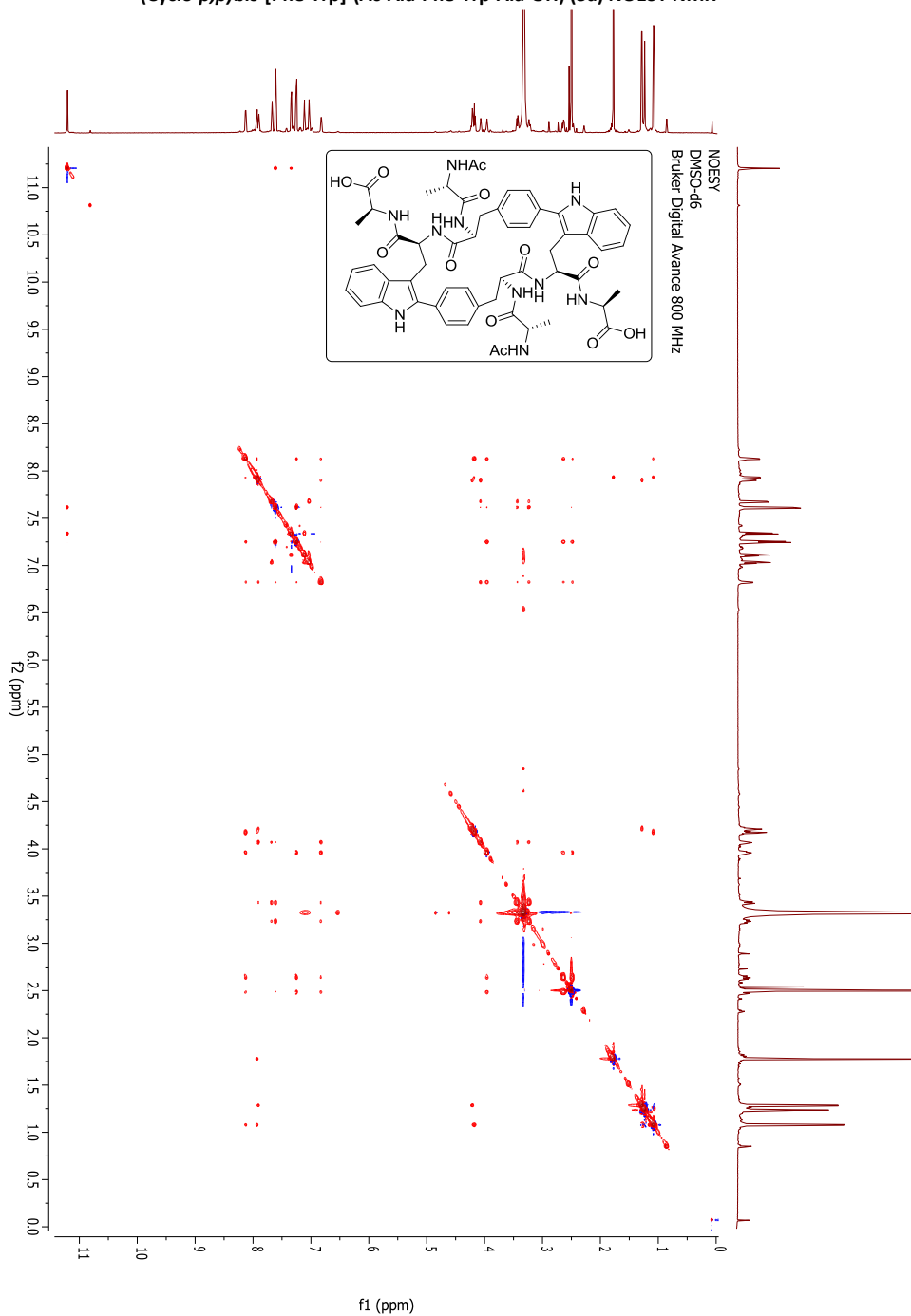
(Cyclo-*p,p*)-bis-[Phe-Trp]-(Ac-Ala-Phe-Trp-Ala-OH) (5a) ^1H NMR

(Cyclo-*p,p*)bis-[Phe-Trp]-(Ac-Ala-Phe-Trp-Ala-OH) (5a) ^1H - ^{13}C HSQC NMR

(Cyclo-*p,p*)-bis-[Phe-Trp]-(Ac-Ala-Phe-Trp-Ala-OH) (5a) COSY NMR

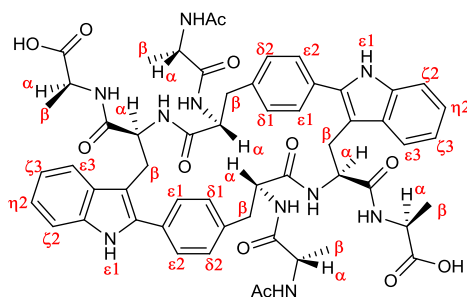
(Cyclo-*p,p*)bis-[Phe-Trp]-(Ac-Ala-Phe-Trp-Ala-OH) (5a) TOCSY NMR

(Cyclo-*p,p*)-bis-[Phe-Trp]-(Ac-Ala-Phe-Trp-Ala-OH) (5a) NOESY NMR



Selected ^1H and ^{13}C chemical shifts assignments

Due to the symmetric nature of dimeric peptides, both peptide moieties are chemically equivalent and have identical NMR signals.

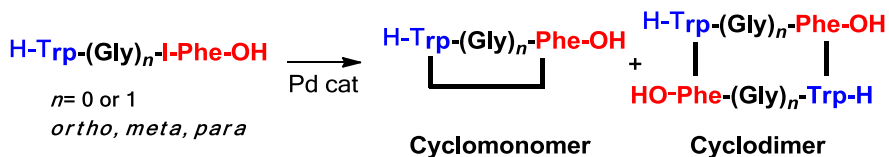


5a (^1H)		δ (ppm)									
AA	NH	α	β	$\delta 1$	$\delta 2$	$\epsilon 2$	$\epsilon 1$	$\zeta 2$	$\eta 2$	$\zeta 3$	$\epsilon 3$
Ala1	7.93	4.18	1.08	-	-	-	-	-	-	-	-
<i>p</i> -I-Phe	8.13	3.96	2.64/2.48	7.25	7.25	7.61	7.61	-	-	-	-
Trp	6.82	4.07	3.43/3.43	-	-	-	11.20	7.34	7.11	7.03	7.67
Ala2	7.90	4.21	1.28	-	-	-	-	-	-	-	-

5a (¹³ C)			δ (ppm)							
AA	α	β	δ1	δ2	ε2	ε1	ζ2	η2	ζ3	ε3
Ala1	47.7	17.8	-	-	-	-	-	-	-	-
<i>p</i> -I-Phe	52.9	35.2	128.8	128.8	127.9	127.9	-	-	-	-
Trp	54.9	25.6	-	-	-	-	110.9	121.4	118.5	118.3
Ala2	47.5	17.0	-	-	-	-	-	-	-	-

Preliminary calculations on the relative stabilities of the cyclic/cyclodimeric peptides after the Pd-catalyzed CH activation reaction

Estimation of the stabilities of the putative cyclic and cyclodimeric peptides arising from the Pd-catalyzed C-H activation upon the parent Trp-(Gly)_n-(l)Phe peptides, displaying different spacer lengths ($n = 0$ or 1) and regiochemistries (*ortho*, *meta* and *para*).



Data referring to the equilibrium geometries of the products, optimized through molecular mechanics (MMFF) and semiempirical methods (PM3), implemented in a Spartan suite.⁴ For the sake of comparison, and as a rule of thumb, the cyclodimers may account for twice the enthalpy barrier to formation of their cyclic counterparts.

SIZE/Regio	CYCLOMONOMER calc. Enthalpy barrier to fotation (kJ/mol)	CYCLOMONOMER exp. Detection	CYCLODIMER calc. Enthalpy barrier to formation (kJ/mol)	CYCLODIMER exp. Detection
0-ortho	-58.451	×	-222.670	×
0-meta	-74.395	×	-283.809	ISOLATED
0-para	-26.863	×	-286.967	ISOLATED
1-ortho	-237.066	×	-709.951	×
1-meta	-273.213	ISOLATED	-708.951	×
1-para	-251.280	×	-737.138	ISOLATED



4

CU(II) CROSS-DEHYDROGENATIVE CYCLIZATION OF TRP-BASED DKPS

PUBLICATION IX.

Access to new scaffolds through cross dehydrogenative couplings on tryptophan-based diketopiperazines

Lorena Mendive-Tapia,^a Arantxa Albornoz Grados,^a Alexandra Bertran,^a Fernando Albericio,^{a, b, c} and Rodolfo Lavilla^{b, d}

Manuscript in preparation.

- a) Department Inorganic and Organic Chemistry, University of Barcelona, Martí i Franquès 1-11, 08028 Barcelona, Spain.
- b) CIBER-BBN, Networking Centre for Bioengineering, Biomaterials and Nanomedicine, Barcelona Science Park, Baldiri Reixac 10-12, 08028 Barcelona, Spain.
- c) School of Chemistry & Physics, University of KwaZulu-Natal, Durban, South Africa.
- d) Laboratory of Organic Chemistry, Faculty of Pharmacy, University of Barcelona, Barcelona Science Park, Baldiri Reixac 10-12, 08028 Barcelona, Spain.

Access to new scaffolds through cross dehydrogenative couplings on tryptophan-based diketopiperazines

Received 00th January 20xx,
Accepted 00th January 20xx

Lorena Mendive-Tapia,^a Arantxa Albornoz Grados,^a Alexandra Bertran,^a Fernando Albericio,^{a,b,c}
Rodolfo Lavilla^{b,d,*}

www.rsc.org/

We report the direct access to two structurally distinct tryptophan-based diketopiperazine scaffolds through selective C-C or C-N intramolecular dehydrogenative couplings. The outcome of the reaction depends on the choice of the oxidant source.

2,5-Diketopiperazines (DKPs), formed by the cyclocondensation of two α -amino acids, are the smallest cyclic peptide derivatives found in nature. Their well-defined 3D structure, their resistance to proteolysis, the presence of donor and acceptor groups for H bonding that favors their interaction with biological targets and their high structural diversity have fueled its presence in many drug discovery programs.^{1,2} Furthermore, this core is widespread in biologically active natural products with a wide spectrum of biological properties.³ Specifically, Trp residue is commonly found in a wide range of natural cyclo (Trp-Xaa) DKPs exhibiting potent and selective bioactivity (Fig. 1).^{4–7}

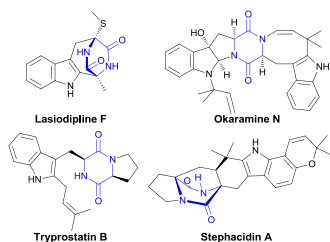
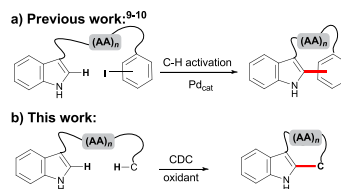


Figure 1 Representative examples of biologically active natural Trp-DKPs.

The site-selective modification of amino acids and peptides through C-H activation is an attractive and efficient tool for structural modification.⁸ In this respect, we have developed a Pd-catalyzed C-H activation protocol for the inter- or intramolecular arylation of Trp amino acid in peptides via the coupling of iodoarenes (e.g. l-phenylalanine residue) to the C-2 indole position of Trp (Scheme 1a).^{9–11} Recently, the selective construction of C-C linkages directly from two different C-H bonds under oxidative conditions, known as cross-dehydrogenative coupling (CDC), has attracted much attention.^{12–14} These reactions do not rely on the use of pre-functionalized starting materials, which reduces the number of synthetic steps required, and are beneficial for the atom and step economy of the processes. The main challenge of this methodology deals with the ubiquity of C-H bonds, being the selectivity the major goal. In this context, we want to explore the functionalization of Trp-containing peptide substrates at the indole moiety via intramolecular CDCs (Scheme 1b).

First oxidations upon the simple substrate c(Phe-Trp) DKP **1a** involved a variety of oxidant sources (Pd(OAc)₂, TBH, FeCl₃, PIFA or BQ, DLP, MnO₂, DTBP; see SI, Table S1) and led to detectable traces of a triply oxidized compound. Gratifyingly, DDQ improved the yield (25% HPLC-MS conversion) and allowed the isolation and structural assignment of the desired product **2a** (Scheme 2). Analogously, the *ortho*-iodinated derivative **1b** gave the corresponding product **2b**. These remarkable structures embody a polycyclic highly conjugated



Scheme 1 C₂-H indole modification of Trp. a) Previous work on the Pd catalyzed C-H activation; b) direct C-C coupling through CDC.

^a Department of Inorganic and Organic Chemistry, University of Barcelona, Martí i Franquès 1-11, 08028 Barcelona, Spain.

^b CIBER-BBN, Networking Centre on Bioengineering, Biomaterials and Nanomedicine, Baldori Reixac 10-12, 08028 Barcelona, Spain.

^c School of Chemistry & Physics, University of KwaZulu-Natal, Durban, South Africa

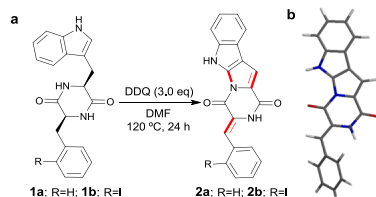
^d Laboratory of Organic Chemistry, Faculty of Pharmacy, University of Barcelona, Barcelona Science Park, Baldori Reixac 10-12, 08028 Barcelona, Spain.

* To whom correspondence should be addressed: rlavilla@ub.edu

Electronic Supplementary Information (ESI) available: see DOI: 10.1039/x0xx00000x

COMMUNICATION

Journal Name



Scheme 2 a) c(Phe-Trp) DKP (**1a-b**) oxidative coupling with DDQ. b) Minimized geometry of the oxidized product **2a** generated by Spartan '14 suite. Red Bonds mark the oxidative transformations.

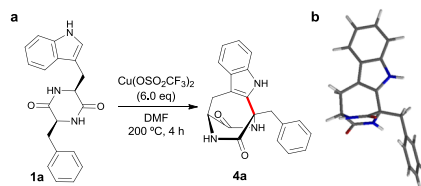
DKP, featuring a diacylated pyrroloindole core, present in pyrroindomycin antibiotics;¹⁵ this heteroaromatic scaffold and the more common dihydro analog are accessible through multi-step synthesis.¹⁶ These compounds likely arise from a complex cascade reaction involving a double C α -C β dehydrogenation (Trp and Phe) terminated by an oxidative C-N bond formation between the C-2 indole position and the α N group from the same Trp moiety. The synthesis of α,β -dehydroamino acid derivatives^{17,18} and, in general, enamides¹⁹ from amino acid/amine precursors has previously been disclosed, although often involving multi-step procedures. For a somewhat related precedent it is worth to mention the amidation process of Yu and co-workers²⁰ based on oxidative palladium catalysis. Although the overall yields are modest, this remarkable transformation, involving a tandem α,β -dehydrogenation/C-N cyclization reaction, affords a constrained previously unknown pyrroloindol DKPs chemotype in just one step. Considering other C-N cyclization processes disclosed in the literature,²¹⁻²⁵ mainly involving Cu(II), Pd(II) or Ir(III)-type oxidants, a new series of oxidative conditions were tested with the aim to optimize this new cyclization (Table 1).

Table 1 Oxidative screening upon c(Phe-Trp) diketopiperazine **1b**.^a

Entry	Oxidant (eq)	Additive (eq)	2a ^b	3a	4a
1 ^b	PhI(OAc) ₂ (1.1)	-	-	-	-
2	PdCl ₂ (3.0)	2,5-lutidine (6.0) Ag ₂ CO ₃ (3.0)	-	19	5
3	CuCl ₂ (6.0)	-	-	-	-
4	Cu(OAc) ₂ (6.0)	-	14	59	3
5	Cu(OCOCF ₃) ₂ (6.0)	-	1	42	28
6	Cu(OSO ₂ CF ₃) ₂ (6.0)	-	-	4	71

^a 30 mg of DKP (0.09 mmol), C:0.2-0.3M, DMF, T: 200 °C, 4h. ^b T: r.t., HFIP. Values are given in (%).

Treatment with PhI(OAc)₂ (Table 1, entry 1), PdCl₂ with 2,5-lutidine and Ag₂CO₃ (Table 1, entry 2) or CuCl₂ (Table 1, entry 3) were basically unproductive. Interestingly, when other Cu(II)-based oxidants²⁶ were used, in addition to the pyrroloindole **2a** and the double dehydrogenated DKP **3a**, we detected the C-C bridged singly oxidized compound **4a** in different ratios, depending on the counteranion. Thus, the formation of the CDC product **4a** gradually increased from 3% with acetate, to 28% with trifluoroacetate to finally reach a suitable 71% when using triflate (Table 1, entries 4-6). The screening of different cooxidants or reaction conditions (adding acid or 2,5-lutidine, see Table S2 in SI) did not lead to any improvement. Thus, the oxidative treatment with Cu(OSO₂CF₃)₂ in DMF at high temperature, enabled the isolation and characterization of the bridged DKP **4a** originated from the selective dehydrogenative C-C cyclization between the C₂-H indole of Trp and the C α -H of Phe (Scheme 3). Very few examples of this bridged DKP architecture are reported in the literature, either obtained from natural sources or through long-stepwise syntheses. Incidentally, some of them display relevant bioactivity, are important intermediates in heterocyclic synthesis and relevant scaffolds in medicinal chemistry.²⁷⁻³¹ Related to this transformation, recently Huo³² has disclosed the formation of iminium species from α -aminoacyl substrates, usually N-protected, using different oxidative systems. Noteworthy, White³⁶ reported an iron catalyzed process leading to the C(5)-H hydroxylation of proline residues in peptide structures without interfering the C α position. Furthermore, she was able to functionalize these oxidized positions via the corresponding iminium intermediate. Previously, Moeller³⁷ had disclosed an electrochemical oxidation of peptide-related substrates with similar selectivity. All three approaches finally trapped these iminium moieties with a variety of heteroatom- or aromatic-based nucleophiles; incidentally the intermolecular attack of indole has been described.³² We latter extended our chemistry to the c(Gly-Trp) DKP **1c** and screen the reaction conditions to find that the use of Cu(OCOCF₃)₂ (4.0 eq), TFA (4.0 eq) in DMF, under MW irradiation at 120 °C in 30 min was the most suitable and general protocol, although in some particular cases leads to lower yields (see SI, Table S3). Then, we analyze the scope of the cross-dehydrogenative reaction scanning other Trp-containing DKPs (Table 2, Fig. 2). Hence, a variety of



Scheme 3 a) c(Phe-Trp) DKP (**1a**) oxidative coupling with Cu(OSO₂CF₃)₂ to afford compound **4a**. b) Minimized geometry of the product generated by Spartan '14 suite.

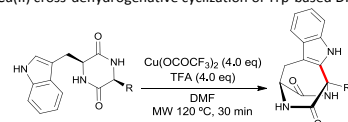
c(AA-Trp) DKPs resulted reactive, including those having aromatic and non-polar residues, showing variable conversions by HPLC-MS (Table 2, Fig. 2, entries 1-4). Interestingly, Asp(^tBu)-containing DKP **1f** underwent *in situ* deprotection and decarboxylation to yield the oxidized c(Ala-Trp) **4e**, which in this case was suitably isolated and characterized (Table 2, entries 5; Fig. 2, for a mechanistic rationale see Fig. S2 in SI). Remarkably, stereoisomeric Brevianamides [c(D/L-Pro-D/L-Trp)] with different configurations were stereospecifically oxidized, showing slightly different reactivities. Thus, the stereoisomers with the same configuration for both residues (L-Pro-L-Trp and D-Pro-D-Trp) showed better conversions than the counterpart displaying and alternative L-D configuration (Table 2, entries 6-8; Fig. 2). These reactions always occur with retention of configuration at the stereogenic centre of the Trp unit whereas the Pro center may evolve with retention or inversion depending on the initial stereochemistry. The CDC

resulted also compatible with a Z-protected Lys residue, although in lower extension likely due to competitive oxidations (Table 2, entry 9; Fig. 4). This tendency was also detected in other cases. Trp-DKPs having other amino acid partners (oxidation prone or functionalized such as Met, Ser, Tyr, Glu, Arg, Asn) resulted unproductive under these conditions. Model linear Trp-containing dipeptidic systems decomposed presumably due to oxidative hydrolytic processes (HPLC-MS evidences), highlighting the need of a cyclic substrate. This conformational restriction may favour intramolecular evolution towards a bridged derivative, although intermolecular indole additions have been described for simplified glycine derivatives.^{32,34,38}

A mechanistic proposal for the dehydrogenative oxidative coupling was proposed (Scheme 2). This hypothesis, in agreement with the experimental observations, was based on the formation of an N-iminium intermediate generated from the Cu(II) oxidation (two equivalents), and subsequent cyclization via the nucleophilic attack of the Trp indole ring. Considering that DKPs **1** have two almost equivalent C-H bonds, the corresponding N-iminium intermediates may be generated at similar rates, then the C-C bond selectivity in this reaction may be attributed to a formal 1,4-hydride shift which isomerizes the unproductive iminium ion into the reactive one en route for the bridged DKPs **4** (see SI).³⁹ We have also determined the stereochemical integrity of the stereogenic center at the Trp center and as a consequence, products from DKPs 1-A and 1-B give rise to enantiomeric bridged derivatives (4-A and 4-B). Alternatively, stereoisomers 1-B and 1-C, having opposite configuration at the variable amino acid α -C stereogenic center (AA), would provide the same iminium species (II) therefore leading to the same oxidized product (4-B). In the particular case of Pro-containing DKPs **4g-h**, the C-H abstraction occurs at the weakest α -C(2) rather than the C(5) position, in agreement with their bond dissociation enthalpies.⁴⁰ White and co-workers revert this preferential trend by careful selection of the iron catalyst.³⁶

To confirm the mechanistic hypothesis, additional experiments were carried out on the oxidized DKPs stereoisomers **4g-h** (Fig. 3). In circular dichroism measurements in MeOH (Fig. 3a), the

Table 2 Cu(II) cross-dehydrogenative cyclization of Trp-based DKPs.^a



Entry	c(AA-Trp) DKP	AA-Trp ^b	Oxidized DKP	Conv. (yield) (%)
1	1a	Phe-Trp	4a	32 (30)
2	1c	Gly-Trp	4c	68 (33)
3	1d	Leu-Trp	4d	36 (20)
4	1e	Ala-Trp	4e	46 ^c
5	1f	Asp(^t Bu)-Trp ^d	4e	75 (43)
6	1g	L-Pro-L-Trp	4g	73 (60)
7	1h	D-Pro-D-Trp	4h	92 (71)
8	1i	L-Pro-D-Trp	4h	54 (17)
9	1j	Lys(Z)-Trp ^e	4i	30 (20)

^a DKP (0.2M).^b Unless stated, (L) configuration.^c It suffers a decarboxylation rendering the Ala derivative.^d Isolation not feasible (see SI).^e Cu(OSO₂CF₃)₂ source was used instead to reduce the extent of competitive C α -C β dehydrogenations.

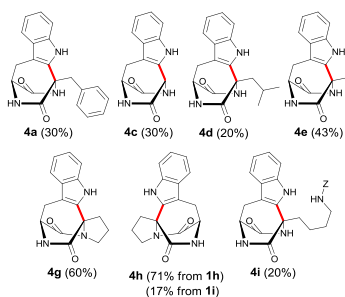
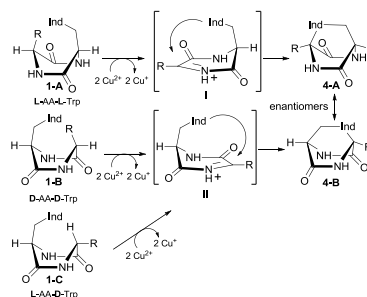


Figure 2 Cu(II) cross-dehydrogenative oxidized bicyclic DKPs **4a-i**.



Scheme 4 Mechanistic proposal for Cu(II) cross-dehydrogenative cyclization of DKPs.

product **4g** from the L-Pro-L-Trp DKP (**1g**) showed a positive Cotton effect, whereas the counterparts from D-Pro-D-Trp and L-Pro-D-Trp (**1h** and **1i**, respectively) displayed identical profiles, opposite to compound **4g** (Fig. 3a). Additional chiral HPLC analysis (Fig. 3b-e, see SI for details) positively support this relationship and additionally demonstrate the retention of configuration at the Trp stereogenic centre. In summary we have disclosed novel CDC processes for the selective formation of C-C and C-N bonds on unprotected Trp-DKPs in a straightforward manner. Although the yields are modest, the cyclization step prevails in these substrates over the routine dehydrogenations or hydrolytic degradations and give direct access to fused and bridged DKP frameworks with relevant presence in medicinal and natural product chemistry.

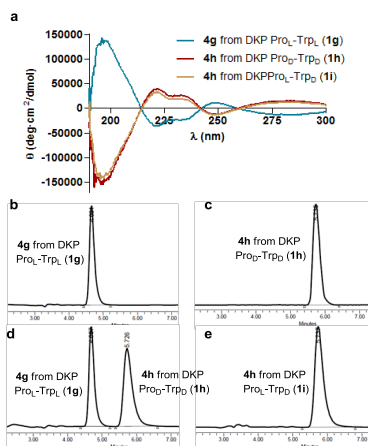


Figure 3 a) Circular dichroism spectra of oxidized c(Pro-Trp) DKPs **4g-i** at 0.3 mM in MeOH. Chiral chromatograms of compounds b) **4g** from **1g**, c) **4h** from **1h**, d) co-elution of **4g** and **4h** from **1g** and **1h**, respectively, e) **4h** from **1i**.

Notes and references

- P. Cherkupally, S. Ramesh, Y. E. Jad, T. Govender, H. G. Kruger, B. G. de la Torre and F. Albericio, in *Privileged Scaffolds in Medicinal Chemistry: Design, Synthesis, Evaluation*, ed. S. Bräse, Royal Society of Chemistry, Cambridge, United Kingdom, 2015, pp. 400–407.
- A. S. M. Ressurreição, R. Delatouche, C. Gennari and U. Piarulli, *Eur. J. Org. Chem.*, 2011, 217–228.
- A. D. Borthwick, *Chem. Rev.*, 2012, **112**, 3641–3716.
- S. Liao, Y. Xu, Y. Tang, J. Wang, X. Zhou, L. Xu and Y. Liu, *RSC Adv.*, 2015, **5**, 51020–51026.
- S. Nishanth Kumar, C. Mohandas and B. Nambisan, *Peptides*, 2014, **53**, 48–58.
- F.-Z. Wang, Z. Huang, X.-F. Shi, Y.-C. Chen, W.-M. Zhang, X. P. Tian, J. Li and S. Zhang, *Bioorg. Med. Chem. Lett.*, 2012, **22**, 7265–7267.
- P. Klausmeyer, T. G. McCloud, K. D. Tucker, J. H. Cardellina and R. H. Shoemaker, *J. Nat. Prod.*, 2005, **68**, 1300–1302.
- F. M. Noisier and M. A. Brimble, *Chem. Rev.*, 2014, **114**, 8775–8806.
- L. Mendive-Tapia, S. Preciado, J. García, R. Ramón, N. Kielland, F. Albericio and R. Lavilla, *Nat. Commun.*, Published online May, 2015; DOI:10.1038/ncomms8160.
- L. Mendive-Tapia, A. Bertran, J. García and G. Acosta, *Chem. Eur. J.*, 2016, **22**, 13114–13119 and references cited therein.
- A. F. M. Noisier, J. García, I. A. Ionut and F. Albericio, *Angew. Chem. Int. Ed.*, 2016, **55**, xx–xx and references cited therein.
- S. A. Girard, T. Knauber and C. Li, in *From C-H to C-C Bonds: Cross-Dehydrogenative-Coupling*, ed. Ch.-J. Li, The Royal Society of Chemistry, United Kingdom, 2014, pp. 1–32.
- C. S. Yeung and V. M. Dong, *Chem. Rev.*, 2011, **111**, 1215–1292.
- C. Liu, J. Yuan, M. Gao, S. Tang, W. Li, R. Shi and A. Lei, *Chem. Rev.*, 2015, **115**, 12138–12204.
- W. Ding, D. R. Williams, P. Northcote, M. M. Siegel, R. Tsao, J. Ashcroft, G. O. Morton, M. Alluri, D. Abbanat, W. M. Maiese and G. A. Ellestad, *J. Antibiot. (Tokyo)*, 1994, **47**, 1250–1257.
- A. Coste, M. Tourni, K. Wright, V. Razafimahaleo, F. Couty, J. Marrot and G. Evano, *Org. Lett.*, 2008, **10**, 3841–3844 and references cited therein.
- J. Jiang, Z. Ma and S. L. Castle, *Tetrahedron*, 2015, **71**, 5431–5451.
- H. Kaur, A. M. Heapy and M. A. Brimble, *Org. Biomol. Chem.*, 2011, **9**, 5897–5907.
- T. Kuranaga, Y. Sesoko and M. Inoue, *Nat. Prod. Rep.*, 2014, **31**, 514–32.
- Y. Deng, W. Gong, J. He and J. Q. Yu, *Angew. Chem. Int. Ed.*, 2014, **53**, 6692–6695.
- K. Takamatsu, K. Hirano, T. Satoh and M. Miura, *J. Org. Chem.*, 2015, **80**, 3242–3249.
- Y. P. He, C. Zhang, M. Fan, Z. Wu and D. Ma, *Org. Lett.*, 2015, **17**, 496–499.
- R. Narayan, S. Manna and A. P. Antonchick, *Synlett*, 2015, **26**, 1785–1803.
- Xiaoqiang Wang, Y. Jin, Y. Zhao, L. Zhu and H. Fu, *Org. Lett.*, 2012, **14**, 452–455.
- G. Brasche and S. L. Buchwald, *Angew. Chemie - Int. Ed.*, 2008, **47**, 1932–1934.
- S. E. Allen, R. R. Walvoord, R. Padilla-Salinas and M. C. Kozlowski, *Chem. Rev.*, 2013, **113**, 6234–6458.
- W. Wei, N. Jiang, Y. N. Mei, Y. L. Chu, H. M. Ge, Y. C. Song, S. W. Ng and R. X. Tan, *Phytochemistry*, 2014, **100**, 103–109.
- R. Holl, D. Schepmann, R. Fröhlich, R. Grünert, P. J. Bednarski and B. Wünsch, *J. Med. Chem.*, 2009, **52**, 2126–2137.
- G. Lazarovits, J. Hill, R. R. King and L. A. Calhoun, *Can. J. Microbiol.*, 2004, **50**, 121–126.
- D. Orain, R. Denay, G. Koch and R. Giger, *Org. Lett.*, 2002, **4**, 4709–4712.
- J. Gelin, J. Mortier and J. Moyroud, *J. Org. Chem.*, 1993, **58**, 3473–3475.
- C. Huo, J. Dong, Y. Su, J. Tang and F. Chen, *Chem. Commun.*, 2016, **52**, 13341–13344 and references cited therein.
- C. Huo, F. Chen, Y. Yuan, H. Xie and Y. Wang, *Org. Lett.*, 2015, **17**, 5028–5031.
- C. Huo, C. Wang, M. Wu, X. Jia, H. Xie and Y. Yuan, *Adv. Synth. Catal.*, 2014, **356**, 411–415.
- C. Huo, Y. Yuan, M. Wu, X. Jia, X. Wang, F. Chen and J. Tang, *Angew. Chem. Int. Ed.*, 2014, **53**, 13544–13547.
- T. J. Osberger, D. C. Rogness, J. T. Kohrt, A. F. Stepan and M. C. White, *Nature*, 2016, **537**, 214–219.
- H. Sun, C. Martin, D. Kesselring, R. Keller and K. D. Moeller, *J. Am. Chem. Soc.*, 2006, **128**, 13761–13771.
- J. Liu, Y. Wang, L. Yu, C. Huo, X. Wang and X. Jia, *Adv. Synth. Catal.*, 2014, **356**, 3214–3218.
- E. W. Warnhoff, *J. Chem. Soc., Chem. Commun.*, 1976, 517–518.
- A. Rauk, D. Yu, J. Taylor, G. V. Shustov, D. A. Block and D. A. Armstrong, *Biochemistry*, 1999, **38**, 9089–9096.

Supporting Information

Access to new scaffolds through cross dehydrogenative couplings on tryptophan-based diketopiperazines

The following data is a selection of the content of the Supporting Information. Full supplementary information including general experimentation, procedures and compound characterization is available in the Supporting Information in electronic format.

Table of Contents

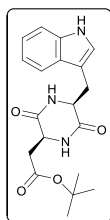
<i>Selected experimental procedures and peptide characterization</i>	<i>261</i>
<i>Oxidative screening experiments. Supplementary tables.....</i>	<i>265</i>

Selected experimental procedures and peptide characterization

General procedure for the synthesis of 2,5-Diketopiperazines 1a-j

Unless stated otherwise, all DKPs were synthesized using the following procedure. Fmoc-AA-OH (1.0 eq), H-Trp-OMe-HCl (1.0 eq), HBTU (1.0 eq) and DIEA (2.0 eq) were dissolved in DMF and the solution was stirred at r.t. for 24 h followed by evaporation under vacuum. The resulting suspension was dissolved in ethyl acetate and washed with saturated aqueous solution of NaHCO_3 ($\times 5$). Then, the organic phase was dried over Na_2SO_4 , filtered and the solvent was removed under vacuum obtaining the desired dipeptide. The resulting white solid was suspended in 20% piperidine/ACN and stirred for 16 h. The resulting suspension was concentrated under vacuum and washed with diethyl ether ($\times 5$). The white solid obtained was dried to yield the corresponding pure product (66-93% isolated yields). Cyclo(Pro-Trp) stereoisomers **1f-h** were prepared according to a previously published procedure on brevianamide arylation disclosed by the group.¹

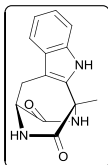
Cyclo[Asp(^tBu)-Trp] (1f). Compound **1f** was prepared using Fmoc-Asp(^tBu)-OH (2.47 g, 6.00 mmol, 1.0 eq), following the general procedure for the synthesis of DKPs to obtain the desired product as a pale yellow solid (2.18 g, 66%). ¹H NMR (400 MHz, DMSO- d_6): δ 10.92 (s, 1H), 7.98 (s, 1H), 7.76 (s, 1H), 7.55 (d, J = 7.9 Hz, 1H), 7.33 (d, J = 8.1 Hz, 1H), 7.10 (d, J = 2.3 Hz, 1H), 7.05 (t, J = 7.1 Hz, 1H), 6.94 (t, J = 7.1 Hz, 1H), 4.16 (t, J = 4.2 Hz, 1H), 3.97 (t, J = 6.2 Hz, 1H), 3.22 (dd, J = 14.5, 4.9 Hz, 1H), 3.08 (dd, J = 14.6, 4.5 Hz, 1H), 1.95 (dd, J = 16.4, 5.5 Hz, 1H), 1.50 (dd, J = 16.4, 6.9 Hz, 1H), 1.32 (s, J = 4.3 Hz, 9H) ppm. ¹³C NMR (100 MHz, DMSO- d_6): δ 169.1, 167.3, 166.6, 135.9, 127.5, 124.5, 120.9, 118.8, 118.4, 111.2, 108.6, 80.1, 55.1, 51.0, 44.3, 27.7, 23.1 ppm.



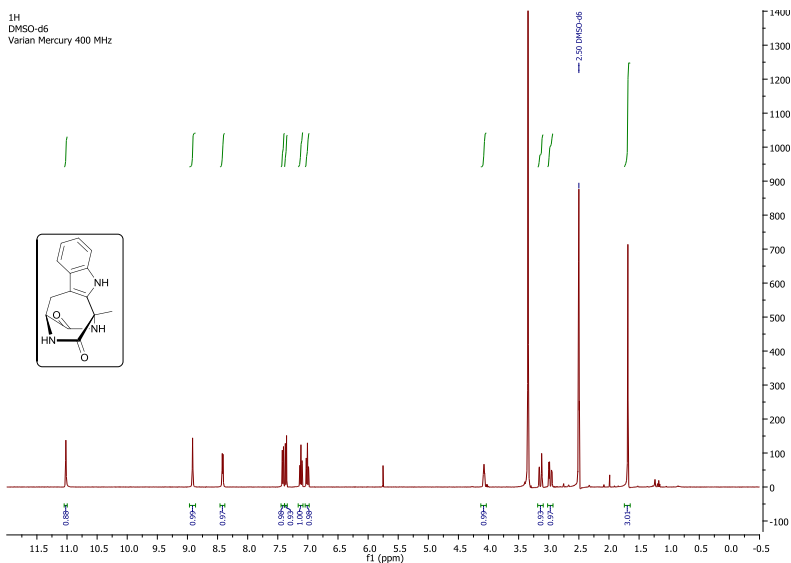
General procedure for the cross-dehydrogenative coupling (CDC) of DKPs 1a-j

Unless stated otherwise, cyclo(AA-Trp) (0.2 mmol, 1.0 eq) and $\text{Cu}(\text{OCOCF}_3)_2$ (4.0 eq) were placed in a microwave reactor vessel and dissolved in DMF (1 mL). Afterwards, TFA (4.0 eq) was added to the solution and the mixture was heated under microwave irradiation (250 W) at 120 °C for 30 min. The resulting crude was diluted in ethyl acetate, filtered through Celite and evaporated under vacuum. Then, the crude was dissolved again in ethyl acetate and washed with NaCl ($\times 3$); the aqueous solution was back-extracted. Then, all the organic layers were mixed, dried over Mg_2SO_4 , filtered and concentrated under vacuum. The crude was purified by flash chromatography on silica using DCM/DCM:MeOH (8:2) to yield the pure products **1a-j**.

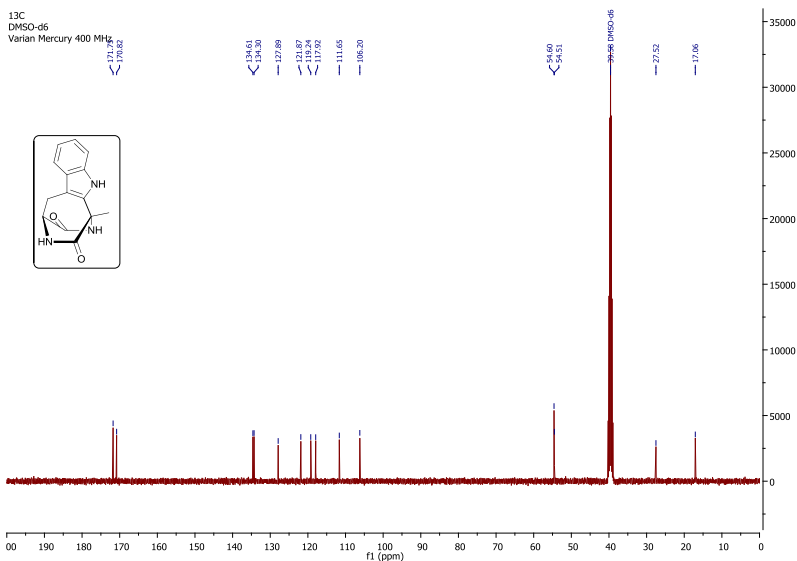
Oxidized cyclo[Asp(^tBu)-Trp] (4e). Compound **4e** was prepared using compound **1f** (73 mg, 0.204 mmol, 1.0 eq), following the general procedure for the synthesis of oxidized DKPs to obtain the pure product **4e** as a brown-orange solid (15.2 mg, 43%). ¹H NMR (400 MHz, DMSO-d₆): δ 11.02 (s, 1H), 8.91 (s, 1H), 8.42 (d, *J* = 5.1 Hz, 1H), 7.42 (d, *J* = 7.8 Hz, 1H), 7.36 (d, *J* = 8.1, 1H), 7.12 (ddd, *J* = 8.2, 7.0, 1.2 Hz, 1H), 7.01 (ddd, *J* = 7.9, 7.1, 1.1 Hz, 1H), 4.07 (m, 1H), 3.14 (dd, *J* = 16.9, 2.5 Hz, 1H), 2.97 (dd, *J* = 16.9, 4.6 Hz, 1H), 1.69 (s, 3H) ppm. ¹³C NMR (100 MHz, DMSO-d₆): δ 171.8, 170.8, 134.6, 134.3, 127.9, 121.9, 119.2, 117.9, 111.7, 106.2, 54.6, 54.5, 27.5, 17.1 ppm. HRMS (ESI): (M: C₁₄H₁₃O₂N₃) *m/z* calcd 256.1086, found 256.1085 (M+H)⁺.



1H
DMSO-d6
Varian Mercury 400 MHz

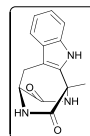


¹³C
DMSO-d₆
Varian Mercury 400 MHz

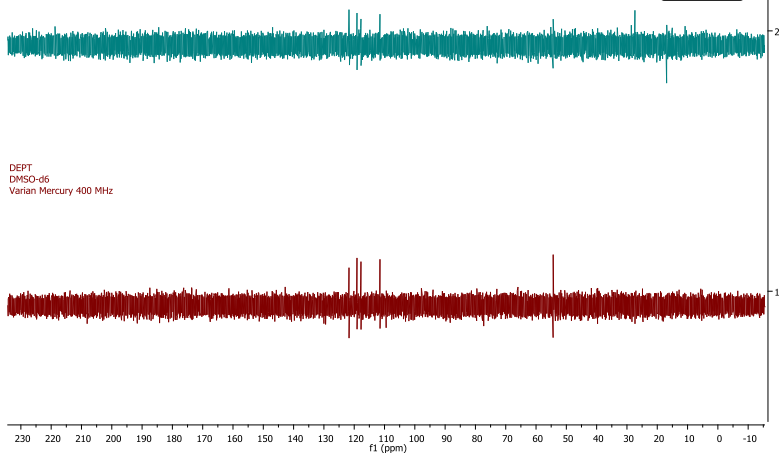


Oxidized cyclo[Asp(^tBu)-Trp] (4e) DEPT NMR

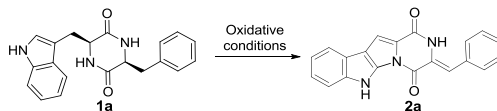
DEPT
DMSO-d₆
Varian Mercury 400 MHz



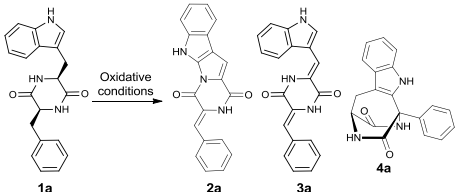
DEPT
DMSO-d₆
Varian Mercury 400 MHz



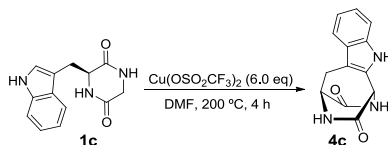
Oxidative screening experiments. Supplementary tables

Table S1. First oxidative screening upon c(Phe-Trp) diketopiperazine **1a**.

T (°C)	Oxidant (eq)	Solvent	Time (h)	2a (HPLC-MS conversion %)
120	TBH (3.0)	1-buthanol	26	-
RT	FeCl ₃ (3.0)	CH ₂ Cl ₂	24	-
RT	PIFA (3.0)	DMSO	23	-
120	BQ (3.0)	DMF	25	-
reflux	DLP (3.0)	CH ₂ Cl ₂ :H ₂ O (1:0.2)	30	-
170	DLP (3.0)	DMSO	24	< 5
77	MnO ₂ (100)	AcOEt	20	< 5
70	DTBP (3.0)	CHCl ₃ :DMF (1:0.1)	18	-
140	DTBP (4.0)	DMF	48	< 5
140	DTBP:FeCl ₃ (4.0:0.2)	DMF	24	-
120	DDQ:FeCl ₃ (3.0:0.1)	DMF	37	16
80	DDQ (3.0)	^t BuOH	27	-
120	DDQ (3.0)	DMF	39	25

Table S2. Oxidative screening upon c(Phe-Trp) diketopiperazine **1a**.^a


Entry	Oxidant (eq)	Additive (eq)	Time	2a ^b	3a	4a
1 ^b	PhI(OAc) ₂ (1.1)	-	4 h	-	-	-
2	PdCl ₂ (3.0)	2,5-lutidine (6.0) Ag ₂ CO ₃ (3.0)	4 h	-	19	5
3	CuCl ₂ (6.0)	-	4 h	-	-	-
4	Cu(OAc) ₂ (6.0)	-	4 h	14	59	3
5	Cu(OCOCF ₃) ₂	-	4 h	1	42	28
6	Cu(OSO ₂ CF ₃) ₂	-	4 h	-	4	71
7	Cu(OAc) ₂ (6.0)	DDQ (1.0)	4 h	3	45	4
8	Mn(OAc) ₃ (6.0)	DDQ (1.0)	4 h	-	12	4
9	Mn(OAc) ₃ (6.0)	Cu(OAc) ₂ (1.0)	4 h	-	6	20
10	MnO ₂ (6.0)	Cu(OAc) ₂ (1.0)	4 h	-	-	-
11	Cu(OAc) ₂ (6.0)	TFA (3.0)	4 h	-	32	31
12	Cu(OAc) ₂ (6.0)	2,5-lutidine (6.0)	4 h	1	44	4

^a 30 mg of DKP (0.09 mmol), C: 0.2-0.3M, DMF, T: 200 °C, ^b T: r.t., HFIP. ^c Values are given in (%).**Table S3.** Optimization of Cu(II)-based oxidation upon c(Gly-Trp) diketopiperazine **1c**.^a

T (°C)	Oxidant (eq)	Additive (eq)	Solvent	Time	Product (%) ^b
200	Cu(OCOCF ₃) ₂ (6.0)	-	DMF	4 h	90
200	Cu(OAc) ₂ (6.0)	-	DMF	4 h	75
200	Cu(OSO ₂ CF ₃) ₂ (6.0)	-	DMF	4 h	40
200	Cu(OCOCF ₃) ₂ (6.0)	-	DMF	2 h	74
200	Cu(OCOCF ₃) ₂ (4.0)	-	DMF	4 h	70
150	Cu(OCOCF ₃) ₂ (6.0)	-	DMF	16 h	68
150 (MW)	Cu(OCOCF ₃) ₂ (6.0)	-	DMF	30 min	49
150 (MW)	Cu(OCOCF ₃) ₂ (2.0)	TFA (4.0)	DMF	30 min	66
150 (MW)	Cu(OCOCF ₃) ₂ (2.0)	-	DMF	30 min	54
120 (MW)	Cu(OCOCF ₃) ₂ (2.0)	TFA (4.0)	DMF	30 min	69
120 (MW)	Cu(OCOCF ₃) ₂ (4.0)	TFA (4.0)	DMF	30 min	92
120 (MW)	Cu(OCOCF ₃) ₂ (4.0)	TFA (2.0)	DMF	30 min	86

^a 30 mg of DKP (0.12 mmol) , C: 0.2 M. ^b Conversion estimated by HPLC-MS. ^c C: 0.4 M.



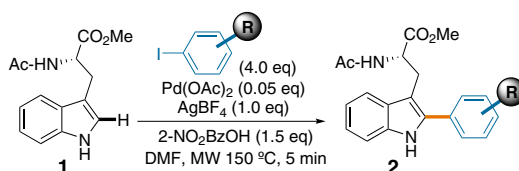
RESULTS AND DISCUSSION

CHAPTER 1. C-2 ARYLATION OF TRP AMINO ACIDS THROUGH PD-CATALYZED C-H ACTIVATION

Particularly inspiring to our research was Larrosa's methodology using $\text{Pd}(\text{OAc})_2$, Ag_2O , and *o*-nitrobenzoic acid ($2\text{-NO}_2\text{BzOH}$) in DMF for the coupling of aryl iodides to indoles (Lebrasseur and Larrosa, 2008). Based on these precedents, some preliminary studies on the C-2 arylation of Trp amino acid were undertaken in our group by Dr. Javier Ruíz (Ruiz-Rodríguez, Albericio and Lavilla, 2010). On these experiments, N^α -acetyl tryptophan methyl ester (Ac-Trp-OMe) (**1**) was conveniently arylated with several aryl iodides in moderate to high yields (Fig. 21). The process took place under MW irradiation with I-Ar (4.0 eq), $\text{Pd}(\text{Pac})_2$ (0.05 eq), AgBF_4 (1.0 eq), $2\text{-NO}_2\text{BzOH}$ (1.5 eq) in DMF at 150°C . Incidentally, unprotected Trp resulted not reactive under these conditions, and only use of acetyl protecting group for the N-terminal amino function under drastic conditions enabled efficient arylations.

Figure 21.

C-2 arylation of Trp amino acid through a C-H activation process catalyzed by palladium



Source: Own elaboration.

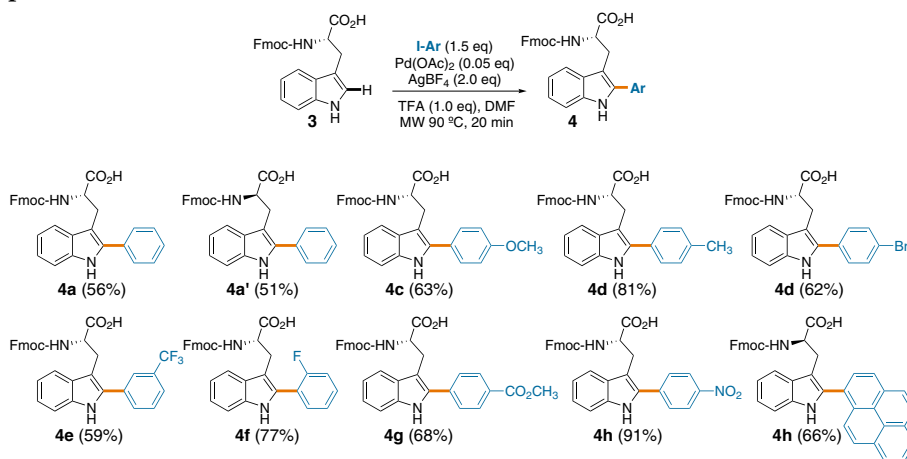
In collaboration with Dr. Sara Preciado, we explored different conditions (combinations of solvents, additives, temperatures and reaction times) and employed an optimized protocol for the arylation of Trp-Pro diketopiperazines (brevianamide F). This modification afforded a series of arylated derivatives with low or moderate antitumoral activity against four human cancer cell lines in comparison with brevianamide F, which is almost inactive.

Next, we initiated a new project in order to expand the scope of this C-H activation protocol. For this purpose, unprotected Trp amino acid was employed as starting point to optimize the process. After an exhaustive screening of the conditions, the unprotected amino acid was successfully arylated with different aryl halides (*i.e.*, 4-iodotoluene, 4-iodoanisole, methyl-4-iodobenzoate), under MW irradiation with I-Ar (1.5 eq), $\text{Pd}(\text{Pac})_2$ (0.05 eq), AgBF_4 (2.0 eq), TFA (1.0 eq) in DMF at 90°C in good conversions (higher than 75%). Afterwards,

alternative N^α protecting groups for Trp (-Fmoc, -Tfa) were tested under the new conditions. Hence, the commercially available Fmoc-Trp-OH (**3**) was arylated with a range of different aryl iodides with both electron-withdrawing and electron-donating substituents in useful yields (Fig. 22). It is noticeable that the location of the iodine atom can be programmed, giving rise to *ortho*, *meta* and *para* aryl derivatives. Remarkably, the insertion of the hindered pyrenyl fluorophore was achieved through this methodology, enabling potential applications in peptide labeling (Fig. 22, compound **4h**).

Figure 22.

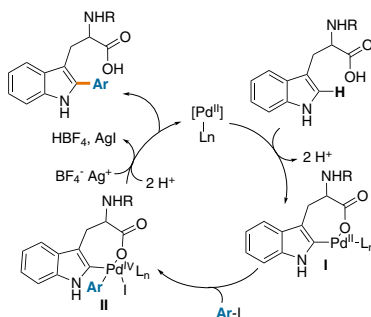
C-2 arylation of Trp amino acid through a C-H activation process catalyzed by palladium



Source: Own elaboration.

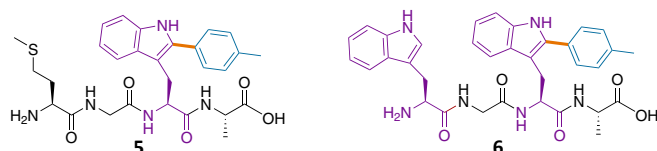
To confirm that the mild conditions applied suitably preserved the stereochemical integrity of the parent amino acid, the chromatographic behavior of the corresponding arylated products of (*S*) and (*R*) Fmoc-Trp amino acid (**4a** and **4a'**, respectively) was analyzed by chiral HPLC.

Based on the reported literature and the experimental observations, a hypothetical mechanism based on a Pd(II)/Pd(IV) catalytic cycle was proposed (Fig. 23). First, the intramolecular ligand effect of the carboxylic function would promote the indole palladation to form a Pd(II) complex **I** through a concerted metallation-deprotonation pathway (CMD). This CMD was based on numerous precedents of metal/base-promoted C-H bond functionalization (Lapointe and Fagnou, 2010), including the mechanistic studies disclosed by Echavarren on catalytic direct functionalization of arenes (García-Cuadrado *et al.*, 2006). Then, subsequent insertion of this intermediate upon the C-I bond of the aryl halide by oxidative addition would yield the Pd(IV) complex **II**. Finally, silver cation (**I**) would act as an halide scavenger, removing the iodide and setting up the reductive elimination to release the corresponding arylated product **IV** and regenerate the Pd(II) catalyst. Remarkably, the intramolecular ligand effect of the carboxylic acid seems to facilitate the process.

Figure 23.**Proposed mechanism for the reaction of Trp amino acid with aryl iodides**

Source: Own elaboration.

In the initial stages of the project, one of the main drawbacks of the C-H arylation processes based on Pd catalysis was the restriction of using metal-coordinating amino acids (methionine, cysteine or histidine), as the bidentate palladium coordination to these nucleophilic residues catalyses the selective hydrolysis of peptide bonds (Parac and Kostic, 1996; Zhu *et al.*, 1994). To deal with this limitation, the intermolecular C-H arylation of Trp in linear peptides containing metal-coordinating amino acids was attempted using different solvents and protecting groups for these residues: cys (-Mob, -Dpm, S'Bu, -Acm, -'Bu), His (-Trt, -3-Bom), but only traces of the corresponding arylated products, with concomitant partial or total elimination of the protecting groups, could be afforded. Only in the case of Met, significant proportions of arylation after two irradiation cycles were detected by HPLC-MS (54% of arylated product). Nevertheless, the direct incorporation of Fmoc-Trp(C₂-Ar)-OH **4** in SPPS, enabled the straightforward preparation of Trp-arylated peptide sequences containing problematic amino acids (**5** and **6**), overcoming in this way this previous limitation. Furthermore, this protocol enabled the synthesis of model N-terminal unprotected peptide sequences containing multiple Trp amino acids (Fig. 24).

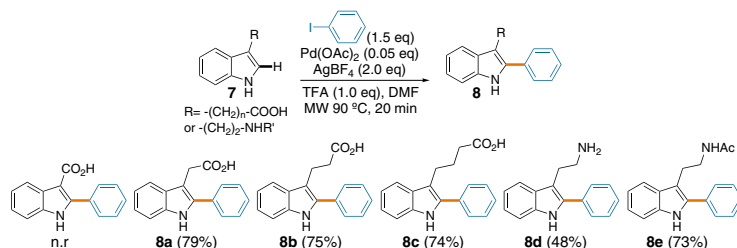
Figure 24.**Solid-phase synthesis of peptide sequences 5 and 6 containing arylated-Trp Amino Acids**H-Met-Gly-Trp(C₂-*p*-methylphenyl)-Ala-OHH-Trp-Gly-Trp(C₂-*p*-methylphenyl)-Ala-OH

Source: Own elaboration.

To further demonstrate the potential applicability of the process, a series of tryptamines and indole-carboxylic acids (**7**) having the acidic functionality linked to the heteroaromatic ring by different length spacers were C-2 arylated in good yields (Fig. 25).

Figure 25.

C-2 arylation of indole-carboxylic acids and tryptamines



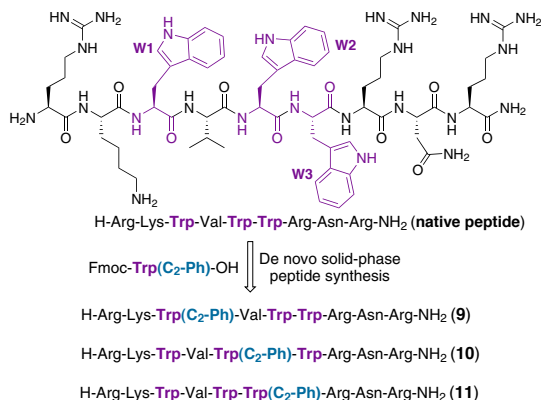
Source: Own elaboration.

Worthy of note is the potential bioactivity of these new arylated derivatives whose precursors possess valuable biological functions as they constitute natural plant hormones or analogues involved in growth and development (Strader and Bartel, 2011; Kasaya *et al.*, 2011; Girisha *et al.*, 2008; Labavitch, 1999). In preliminary assays, the arylated compounds were tested as plant hormone agonists in calluses. Despite initial growth evidences were observed for some analogues, these results could not be maintained in the following generations.

At present, antimicrobial peptides have emerged as potentially valuable therapeutic agents due to the progressive increase antibiotic resistance. This class of peptides includes both positively charged and hydrophobic amino acids and this amphipaticity is believed to be the cause of their bioactivity as it allows peptide-membrane interactions that eventually lead to the bacterial membrane disruption. In this sense, site-selective modifications in order to locally enhance the hydrophobicity of these species can have a positive impact on their potency. Specifically, the methodology developed in the present thesis provides an alternative tool for the site-selective arylation of hydrophobic residues such as Trp.

Figure 26.

Synthetic approach for the selective arylation of the antimicrobial peptide RKWVWWRNR



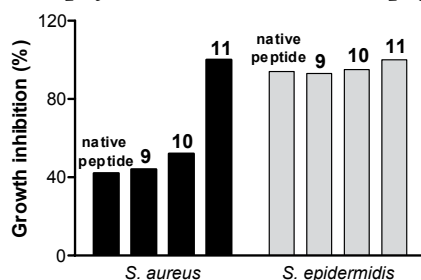
Source: Own elaboration.

As proof of concept, it was proposed to enhance the antimicrobial activity of a peptide derived from the fragment 107–115 of the C-terminus of the human lysozyme (107RKWVWWRNR115) by arylation of its tryptophan residues. Fmoc-Trp(C2-phenyl)-OH **4a** was prepared by direct arylation of Fmoc-Trp-OH with iodobenzene and directly used to synthesize through standard SPPS the three possible arylated peptides **9–11**, each with an aryl-Trp residue at positions 109, 111 or 112, respectively (Fig. 26).

Then, growth inhibition assays against *Staphylococcus aureus* and *Staphylococcus epidermidis* microorganisms were carried out (Fig. 27). Overall, *S. aureus* was fully inhibited by arylation of Trp 112 (**11**) and by only 10% by arylation of Trp 109 (**9**) or 111 (**10**), respect to the non-arylated peptide. On the other hand, *S. epidermidis* was fully inhibited by the three arylated peptides and the parent native peptide. The minimum inhibitory concentration (MIC) was significantly reduced for *S. Aureus* (up to four-fold) depending on the arylation site and hemolysis percentage become significant only at concentrations higher than ten-fold their MICs, indicating their safety towards red blood cells. These results open the door to the evaluation of further modifications by the incorporation of other Fmoc-Trp(C₂-Ar)-OH having different substituents on the phenyl ring.

Figure 27.

Inhibition assay at 0.1 mg/ml of the non-arylated intermediary peptide (native peptide) and aryl-peptides at Trp 109, Trp 111 and Trp 112 (peptides **9**, **10** and **11**, respectively) on *Staphylococcus aureus* and *Staphylococcus epidermidis*



Source: Own elaboration.

CHAPTER 2. SPACER-FREE TRP-BODIPY FLUOROGEN FOR PEPTIDE-BASED IMAGING PROBES

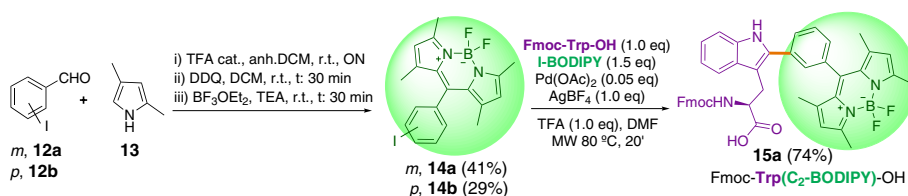
Based on related BODIPY syntheses reported in the literature, two novel BODIPY iodide derivatives were synthesized via the condensation of iodobenzaldehyde having the halogen group in *meta* (**12a**) or *para* (**12b**) positions, respectively, with two units of 2,4-dimethylpyrrole **13** followed by DDQ oxidation and BF₃ complexation to afford compounds **14a** and **14b**. Next, these iodide derivatives were reacted with the commercially available N^α Fmoc-protected Trp amino acid through the C-H arylation process disclosed by our group (Fig. 28). Interestingly, the *m*-iodophenyl derivative **14a** led to the corresponding arylated Trp amino acid **15a** in a 74% yield, whereas the *p*-iodophenyl analogue **14b** resulted unreactive. Presumably, when the insertion of the electrophilic indole-Pd(II) intermediate into the C-I bond takes place, the

electron-withdrawing BODIPY group exerts a stronger deactivating effect when is located in the *para* position, thus diffculting the interaction.

Spectroscopic experiments showed a strong fluorescence emission of Fmoc-Trp(C₂-BODIPY)-OH **15a** in hydrophobic environments that could mimic phospholipid bilayer membranes. Having this environmentally sensitive fluorescence behavior in mind, the direct application of this new fluorogenic amino acid in the labeling of relevant peptides was studied.

Figure 28.

Synthesis of Fmoc-Trp(C₂-BODIPY)-OH **15a**



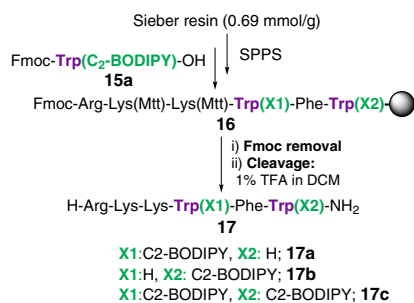
Source: Own elaboration.

Spacer-free BODIPY-antimicrobial peptide PAF26 for cell imaging of fungal infections

The preparation of a novel BODIPY-containing antifungal PAF26 peptide was achieved via the direct incorporation of Fmoc-(C₂-BODIPY)-OH fluorogenic amino acid **15a** in SPPS synthesis (Fig. 29). Importantly, the instability of the BODIPY core to acidic media was a critical point which had to be carefully contemplated during the synthetic design. As a carboxamide group was desired at the C-terminal end of the peptide, the synthesis was performed on Sieber amide resin and the amino acids were introduced through standard conditions using DIC and OxymaPure coupling reagents. Arg and Lys amino acids are normally employed with Pbf and Boc side-chain protecting groups, respectively. Nonetheless, due to the strong acidic conditions required to remove these groups (>50% TFA) alternative conditions and protecting groups were required. In the case of Arg, the non-protected side-chain version (Fmoc-Arg-OH) was used and several coupling treatments with DIC and HOBt without pre-activation were necessary for a quantitative coupling. Regarding the Lys residues, in a first attempt, Alloc protecting group was used to protect the side-chains but the reductive conditions necessary to eliminate this group [Pd(PPh₃)₄, PhSiH₃ in DCM] compromised the integrity of the BODIPY core. Alternatively, Mtt enabled the use of low acidic conditions sufficient to ensure the integrity of the BODIPY group. After elongation of the Mtt-containing peptide sequence **16**, the scission of the peptide from the resin was carried out under mild acidic conditions (that is 1% TFA) with concomitant removal of Mtt groups. In this manner, the three possible BODIPY-labeled sequences (BODIPY-Trp1, Trp2; Trp1, BODIPY-Trp2; BODIPY-Trp1, BODIPY-Trp2) **17a-c** could be obtained, allowing the selective labeling of a fluorescent probe with no need of chemical spacers and maintaining unaltered the amphipatic character necessary for the peptide antifungal activity (Fig. 29).

Figure 29.

Solid-phase synthesis of fluorescent linear peptide analogues 17a-c of PAF26



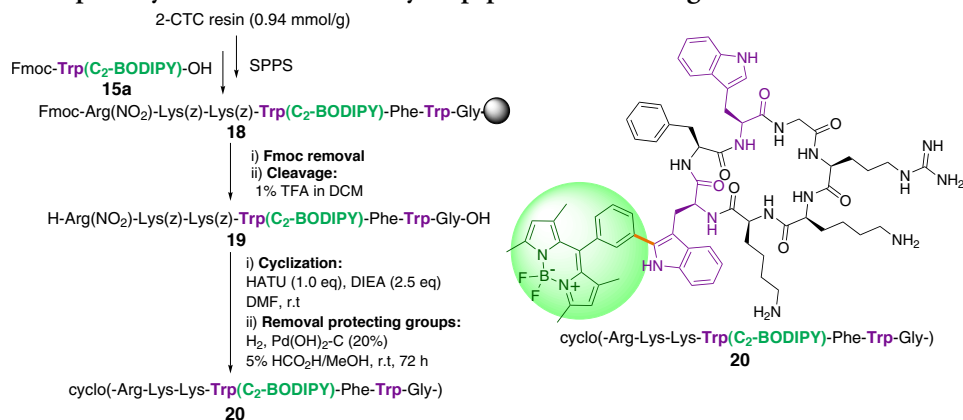
Source: Own elaboration.

AA	PG	Removal conditions	BODIPY stability
Arg	Pbf	> 50% TFA	X
	-	-	✓
Lys	Boc	> 50% TFA	X
	Alloc	Pd(PPh ₃) ₄ , PhSiH ₃	X
	Mtt	< 5% TFA	✓

In order to enhance the stability towards proteases, the preparation of a BODIPY-labeled cyclic analogue was also carried out (Fig. 30). The synthesis was performed on 2-CTC resin in order to cleave the peptide from resin under mild TFA conditions and perform the subsequent cyclization in solution. To avoid side-reactions during the head-to-tail ring-closing, Arg and Lys side-chains were introduced with nitro and carboxybenzyl orthogonal protecting groups, respectively. The fully elongated linear sequence **18** was cleaved from the resin with 1% of TFA and the resulting protected linear peptide **19** was cyclized in solution using HATU as the coupling reagent. Then, reduction in H₂ atmosphere with Pd(OH)₂/C and formic acid yielded the corresponding final cyclic version of PAF26 peptide **20**.

Figure 30.

Solid-phase synthesis of fluorescent cyclic peptide PAF26 analogue 20



Source: Own elaboration.

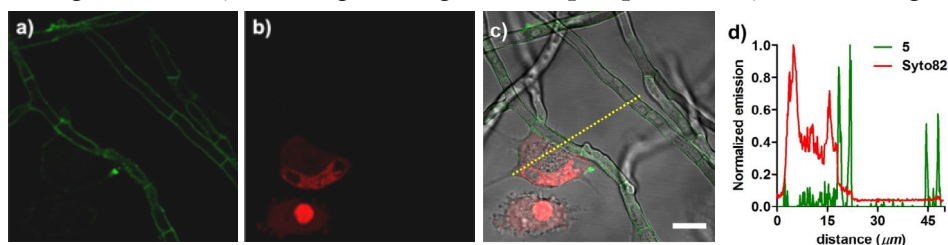
The cytotoxic activity of derivatives **17a-c** and **20** was assayed in *Aspergillus Fumigatus* fungus as well as in several bacterial strains commonly found in pulmonary infections and in human mature red blood cells. Notably, both linear and cyclic BODIPY-labeled peptides

displayed affinity for *A. Fumigatus*, even slightly higher than the non-labeled derivatives. Furthermore, only a marginal activity in bacterial and human cells was displayed by all fluorogenic analogues.

In vitro imaging of *A. Fumigatus* in co-cultures with human lung epithelial cells showed that the peptides specifically labeled *A. Fumigatus* without staining human cells (Fig. 31). Remarkably, there is no need of any washing steps as the fluorogenic behavior of these BODIPY-labeled peptides is dependent of hydrophobic environments and, therefore, the strong fluorescence emission only appears upon binding to phospholipid fungal membranes. Additionally, the fluorescent cyclic peptide analogue **20** was also tested against other fungal strains, demonstrating its versatility to stain fungal infections of different origin.

Figure 31.

Fluorescence confocal microscopy of co-cultures of *A. fumigatus* and human lung A549 epithelial cells. Fluorescence staining of a) linear BODIPY-labeled peptide analogue 17a, b) Syto82 lung, c) merged and d) plot profile analysis from image c



Source: Own elaboration.

Moreover, a high-resolution time-lapse imaging experiment with compound **20** showed the mode of action of the peptide in fungal cells. After the interaction with the fungal cell membrane, the peptide internalizes and accumulates in lipid-rich intracellular compartments of cell membrane within few minutes after the addition. Incidentally, other BODIPY-labeled PAF26 analogues lacking key-containing amino acids were tested as negative controls to prove the importance of the nature and amphipatic character of PAF26 for the interaction with the fungal cell membrane. Furthermore, the cyclic version **20** was also used for direct and selective *ex vivo* imaging using multi-photon microscopy in human pulmonary tissue of a transgenic strain of *A. Fumigatus* expressing red fluorescent protein (RFP) as a control in the cytoplasm.

Recently, a more exhaustive examination of the experimental procedure, including the cell fluorescence imaging experiments, was carried out for the elaboration of a detailed protocol (under revision) that describes the synthesis of the Fmoc-Trp(C₂-BODIPY)-OH to label the corresponding fluorogenic PAF26 and other relevant sequences.

Apoptotic cell imaging with a Spacer-free BODIPY-lactadherin mimic

In the context of labeling the lactadherin mimic peptide (see above), and having in mind the instability of BODIPY core to acidic medium, two approaches were attempted to

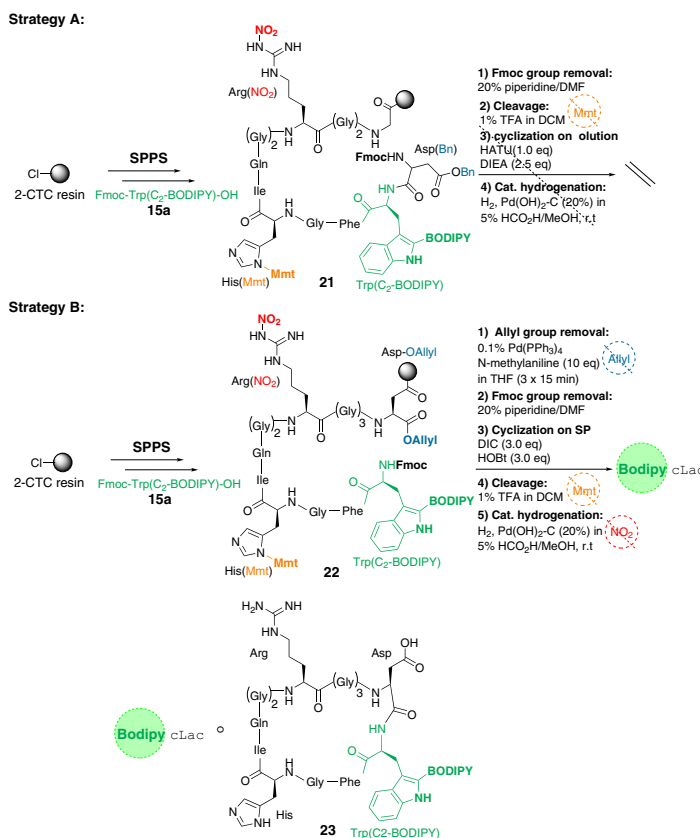
find the most appropriate cyclization mode and combination of orthogonal protecting groups for the mildly acidic cleavage conditions (Fig. 32).

The first strategy (A) was based on a head-to-tail cyclization in solution between the Asp and the adjacent Gly residue, anchoring the linear peptide sequence **21** to a 2-CTC resin through this latter residue. Side-chains were protected with the Mmt group for His, the nitro group for Arg and the benzyl group for Asp, which are removed by mild acidic treatment (Mmt) and catalytic hydrogenation (nitro, benzyl), respectively. Once the linear protected sequence **21** was fully elongated, a mild TFA solution enabled to cleave the peptide from resin with concomitant Mmt protecting group removal from His residue. Attempts to carry out the cyclization of the resulting linear peptide in solution with several coupling reagents (i.e. HATU, PyAOP) resulted unproductive.

The second strategy (B) involved a head-to-tail cyclization on solid-phase between the Asp and the adjacent Trp(BODIPY) residue. The peptide **22** was anchored to a 2-CTC

Figure 32.

Synthetic approaches for the solid-phase synthesis of the BODIPY-labeled cLac mimic



resin through the side-chain of Asp amino acid, protecting the C-terminal carboxylic acid as an allylic ester. As in the first strategy, His and Arg side-chains were protected with Mmt and nitro protecting groups, respectively, and the peptide sequence was elongated through standard solid-phase couplings.

Taking into consideration that in the previous reported synthesis of BODIPY-labeled PAF26 for fungal infection detection, the reductive conditions necessary to eliminate the Alloc protecting group ($\text{Pd}(\text{PPh}_3)_4$, PhSiH_3 in DCM) compromised the integrity of the BODIPY core, different nucleophiles (*i.e.*, N-methylmorpholine, N-methylaniline, water) had to be tested for the palladium-catalyzed removal of the allyl group. Finally, palladium catalysis with N-methylaniline in THF resulted fully compatible for the BODIPY group (Table 3).

Table 3.

Reductive removal conditions for side-chain protecting groups

AA	PG	Removal conditions	BODIPY stability
Lys	Alloc	$\text{Pd}(\text{PPh}_3)_4$, PhSiH_3	X
Asp	Allyl	$\text{Pd}(\text{PPh}_3)_4$, H_2O	X
		$\text{Pd}(\text{PPh}_3)_4$, NMM	X
		$\text{Pd}(\text{PPh}_3)_4$, NMA	✓

Source: Own elaboration.

Once allyl and Fmoc protecting groups were eliminated from the terminal residues, the cyclization on solid-phase was carried out with DIC coupling reagent in DMF (other attempts with other coupling reagents under basic conditions were unsuccessful). Afterwards, cleavage of the cyclic peptide from resin under mild acidic conditions and subsequent catalytic hydrogenation to remove the nitro group afforded the desired BODIPY-cLac derivative **23** (78% purity prior to semi-preparative HPLC purification).

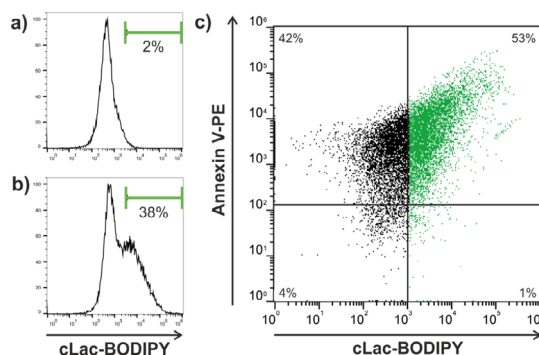
Next, studies focused on the validation of this new fluorophore-labeled cLac derivative as a non-invasive reagent for imaging apoptotic bodies were performed.

With the aim to evaluate its affinity to PS, preliminary *in vitro* spectroscopic experiments incubating the labeled peptide **23** with PS/PC (phosphatidylcholine)-containing lipid films evidenced that the peptide fluorescence emission is sensitive to PS, showing a very low emission only with PC. Importantly, unlike Annexin V, this recognition is Ca^{2+} -independent. This lipid affinity was also supported in parallel tensioactivity measurement experiments by the determination of the surface pressure in lipid-aqueous interfaces at different peptide concentrations. Incidentally, this recognition trend has also been determined in other negatively-charged phospholipids directly related to apoptotic processes.

In view of these promising results, confocal fluorescence imaging and flow cytometry experiments were undertaken. Flow cytometry assays confirmed the peptide specificity for exposed PS in apoptotic bodies isolated from apoptotic human Burkitt lymphoma (BL2) cells in a dose-dependent manner and showing the same staining profile in co-stained experiments with Annexin V (Fig. 33).

Figure 33.

Flow cytometry analysis of apoptotic bodies from BL2 cells. a) Histograms of apoptotic bodies without (top) and with peptide (2.5 μM) (bottom), c) Dot plot chart of apoptotic bodies after co-staining with peptide (X-axis) and Annexin V-PE (Y-axis) showing the double staining

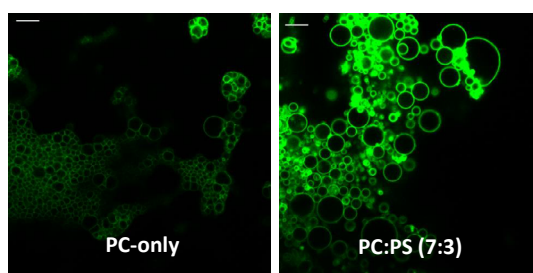


Source: Own elaboration.

In additional confocal microscopy experiments, incubation of the BODIPY-cLac peptide 23 with prepared PS-containing giant unilamellar vesicles (GUVs) showed a brighter staining than vesicles with only PC (Fig. 34).

Figure 34.

Confocal fluorescence microscopy images of giant unilamellar vesicles (GUVs) containing PC-only or PC:PS (7:3) after incubation with peptide (2 μM)



Source: Own elaboration.

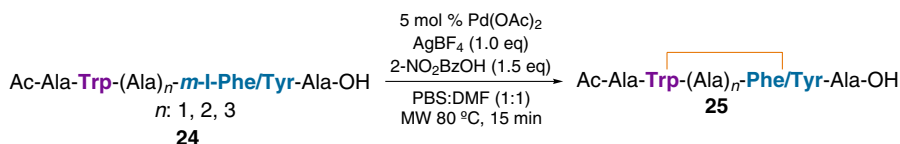
Interestingly, although no selective staining could be observed on partially apoptotic neutrophil cells, the BODIPY-antimicrobial peptide analogue **20** synthesized for the previously commented cell imaging application to fungal infections (Fig. 30) did allow selective detection of apoptosis in neutrophil experiments, with no-binding to viable cells. On-going studies to elucidate the structural factors and the mechanism of action which determine this selective staining for apoptotic bodies are being carried out.

CHAPTER 3. BIARYL PEPTIDIC TOPOLOGIES THROUGH Pd-CATALYZED C-H ACTIVATION REACTIONS BETWEEN TRP AND PHE/TYR RESIDUES

A few years ago initial studies of an alternative peptide constraining were undertaken in the group. Thus, model Ala-containing linear peptide sequences (**24**) were directly constrained by a linkage of a Trp residue and a *m*-I-Phe or *p*-I-Tyr unit via an intramolecular C-H activation process with Pd(OAc)₂, AgBF₄ and *o*-2-NO₂BzOH in PBS:DMF (1:1) under MW irradiation (Fig. 35). Good to excellent conversions were obtained for Trp (*i*)-Phe(Tyr) staples located at (*i,i*+2), (*i,i*+3) and (*i,i*+4) positions (**25**). Although preliminary NMR studies confirmed the peptide cyclization, the similarity of the amino acids, the high insolubility and the low amount of isolated product avoided any further structural characterization.

Figure 35.

C-H activation stapling in Ala-containing linear peptides between Trp and *m*-I-Phe or *p*-I-Tyr residues

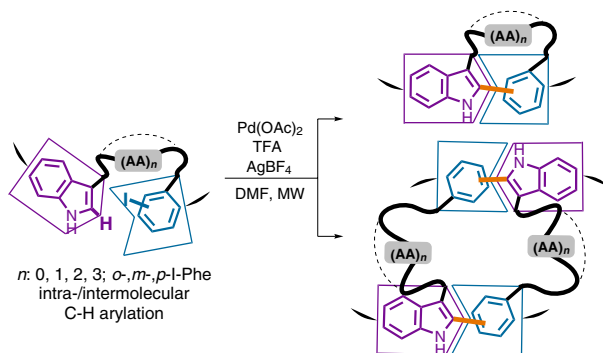


Source: Own elaboration.

In order to further continue the initial experiments on the C-H arylation applied on peptides, a more exhaustive evaluation of the structural factors (*i.e.*, peptide length, number of spacers between Trp and I-Phe/Tyr residues, regiochemistry of the aryl iodide unit, amino acid sequence and concentration) that dictate the outcome of the cyclization was initiated. Thus, the optimized protocol disclosed in chapter 1 was examined in a representative set of peptides sequences containing diverse amino acids (Scheme 6).

Scheme 6.

Study of the cyclization between Phe-Trp containing peptides through C-H activation



Source: Own elaboration.

Meta-Regiochemistry

First, linear peptide sequences (**26**) with an increasing number of amino acids (*n*) between the Trp and *m*-I-Phe residues were prepared through standard SPPS protocols on 2-CTC resin (Table 4, Fig. 36). When Ala containing tetrapeptide **26a** featuring contiguous *m*-I-Phe and Trp residues was tested (Table 4, entry 1), the corresponding cyclodimeric product **27a** was formed in a double intermolecular C-H arylation process with no traces of racemization or oligo(poly)merization species (Table 4, entry 1; Fig. 36a). Presumably, the corresponding putative monomeric structure would be highly strained (molecular models generated by Spartan program display a non-planar phenyl ring). On the contrary, for linear sequences **26b-e** featuring one to three amino acids between Trp and *m*-iodinated Phe residues (Table 4, entries 2-5), the C-H arylation reaction yielded selectively the stapled peptide bond formation to afford compounds **27b-e** in an intramolecular process (Table 4, entries 2-5; Fig. 36b-d). In all cases, only one stereochemically defined structure was obtained.

Table 4.

Influence of the number of residues (*n*) between *m*-I-Phe and Trp residues in the palladium-catalyzed C-H arylation^a

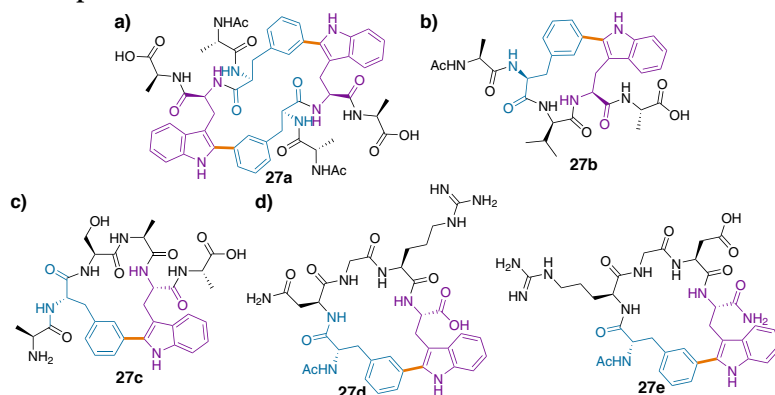
Entry	<i>i, i+n</i>	Linear peptide (26)	Cyclodimeric peptide	Stapled peptide	HPLC-MS conversion (%)
1	<i>i, i+1</i>	Ac-Ala- <i>m</i> -I-Phe-Trp-Ala-OH (26a)	27a	n.d. ^b	48
2	<i>i, i+2</i>	Ac-Ala- <i>m</i> -I-Phe-Val-Trp-Ala-OH (26b)	n.d.	27b	71
3	<i>i, i+3</i>	H-Ala- <i>m</i> -I-Phe-Ser-Ala-Trp-Ala-OH (26c)	n.d.	27c	39 ^c
4	<i>i, i+4</i>	Ac- <i>m</i> -I-Phe-Asn-Gly-Arg-Trp-NH ₂ (26d)	n.d.	27d	77
5	<i>i, i+4</i>	Ac- <i>m</i> -I-Phe-Arg-Gly-Asp-Trp-NH ₂ (26e)	n.d.	27e	70

Note: ^a 5 mol % Pd(OAc)₂, AgBF₄ (2.0 eq), TFA (1.0 eq), DMF, MW 90 °C, 20 min. ^b n.d.: not detected. ^c Additional MW irradiation cycles were necessary to obtain the desired compound as the main product (HPLC-MS).

Source: Own elaboration.

Figure 36.

C-C linked structures resulted from C-H arylations of linear peptides 26a-e containing *m*-I-Phe and Trp residues located at different distances a) *i, i+1*; b) *i, i+2*; c) *i, i+3*; d) *i, i+4*



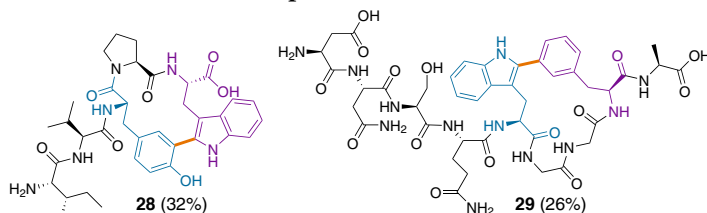
Source: Own elaboration.

It is worthy to highlight the successful application of this technique to prepare stapled peptides containing the NGR- and RGD- tumor homing signaling sequences (**27d** and **27e**, respectively). In cellular adhesion inhibition assays in HUVEC cells, the stapled form of RGD-containing compound resulted a selective antagonist for the $\alpha\text{v}\beta 3$ (in front of $\alpha\text{v}\beta 5$) integrin receptor with a moderate EC_{50} (6 μM), being more active than its linear precursor **26e** (26 μM).

To further explore the potential of the methodology, the stapling of known linear bioactive peptides was carried out directly on solid-phase (Fig. 37). In this way, the constrained version of an active valorphin analogue, which is a potent dipeptidyl peptidase III inhibitor (Muppidi *et al.*, 2011), was accomplished though the intramolecular C-H arylation on resin between 3-I-Tyr and Trp residues once the peptide sequence was fully elongated on a TentaGel S-NH₂ type resin. Afterwards, the stapled product was cleaved from resin applying a standard protocol to afford peptide **28**. Furthermore, baratin (Nässel, Persson and Muren, 2000), a neurostimulating peptide, was stapled following a related procedure to yield compound **29**. In this case, the incorporation of four additional amino acids after the stapled bond formation enabled the extension of the chain up to 9 residues. In this manner, the previous limitation regarding the preparation of unprotected N-terminal peptides could be overcome.

Figure 37.

Cyclic derivatives of valorphin (left) and baratin (right) bioactive peptides originated from direct C-H activation on solid-phase



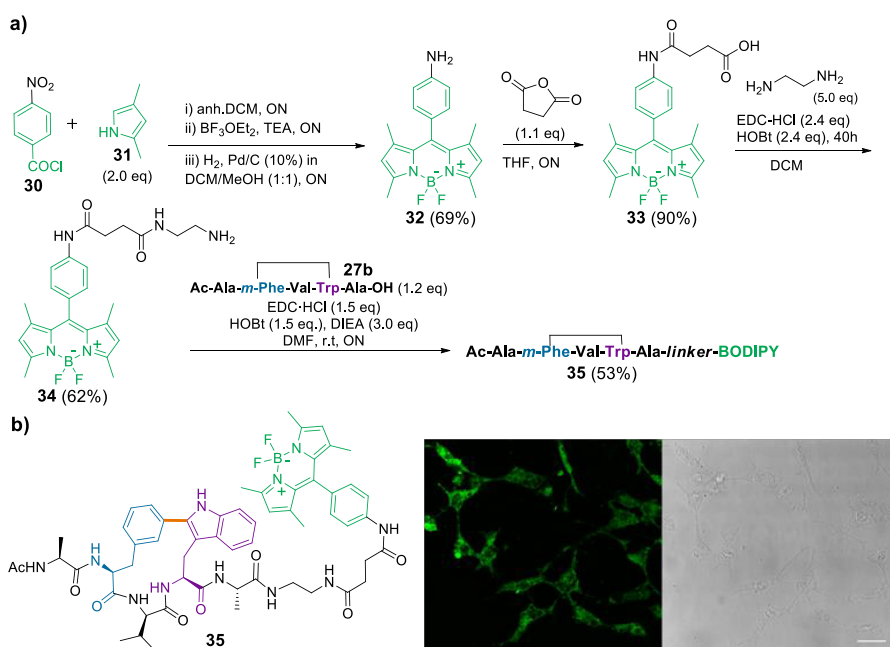
Source: Own elaboration.

A detailed NMR study was performed on dimethylsulphoxide ($\text{DMSO}-d_6$) to corroborate the selective C-C linkage and analyze the conformational behavior of the synthesized peptides. The NMR spectra of stapled peptides **27b-e** were in agreement with the existence of a defined single conformation. Moreover, these stapled peptides showed larger H_α chemical shift dispersions compared with their linear counterparts **26b-e**, indicating less conformational flexibility. Several non-sequential NOEs confirmed the intramolecular cyclization. Additionally, circular dichroism (CD) measurements of stapled peptides **27d** and **27e** showed profiles clearly indicative of some level of structuring. In contrast, linear peptides **26d** and **26e** exhibited a more flattened profile typical of a flexible unfolded structure. As a preliminary evaluation of the application of these stapled peptides in biological systems, the proteolytic stability of stapled peptides **27d** and **27e** was evaluated following a chymotrypsin-based protocol. HPLC-MS analysis showed a remarkable stability of the stapled forms, whereas the corresponding linear analogues suffered from a rapid hydrolytic cleavage in a few hours.

Next, the labeling of stapled peptide **27b** with a novel bodipy fluorophore **33** thorough an amino spacer to the terminal amino acid was carried out (Fig. 38a). In SH-SY5Y cells, the labeled stapled peptide **35** displayed low citotoxicity at 750 nM after 24 h of incubation. Besides, flow cytometry and confocal experiments in these cells, the peptide **35** stained both the membrane and the cytoplasmatic region (Fig. 38b).

Figure 38.

a) Synthesis of labeled-stapled peptide **35**, b) structure of peptide **35** (left) and the corresponding confocal microscopy image of SH-SY5Y cells treated with compound **35** (750 nM). Scale bar, 25 mm (right)

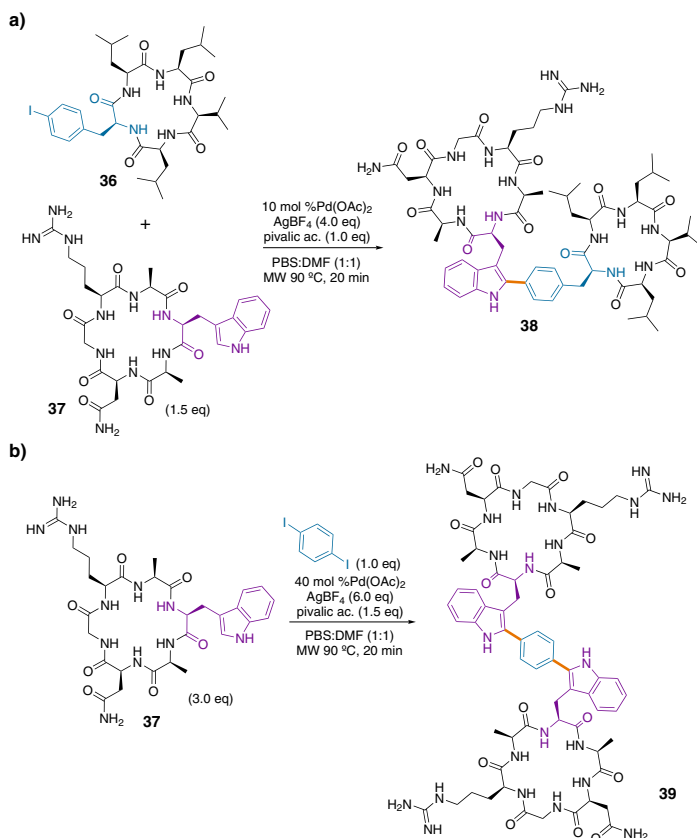


Source: Own elaboration.

To further demonstrate the feasibility and applicability of the methodology, the preparation of a couple of macrocyclic conjugates was tackled (Fig. 39). As a proof of concept, the intermolecular connection of a *p*-I-Phe-containing derivative of a drug (Sansalvamide A depsipeptide (Pan *et al.*, 2009)) (**36**) with a signaling peptide (**37**) to yield the macrocyclic conjugate **38** (Fig. 39a) was studied and successfully achieved. Unfortunately, the conjugate **38** was not biologically active. Next, the conjugation of Trp-containing macrocycles **37** (cyclic NGR signaling peptide) via a double C-H arylation process with a 1,4-diiodobenzene unit (Fig. 39b) led to conjugate **39**, suggesting the potential of this technique in biological multivalency.

Figure 39.

Macrocyclic conjugation via C–H activation. (a) Intermolecular conjugation of NGR cyclopeptide 37 with the sansalvamide derivative 36 via C–H activation. (b) Double conjugation of the NGR cyclopeptide 37 with 1,4-diiodobenzene



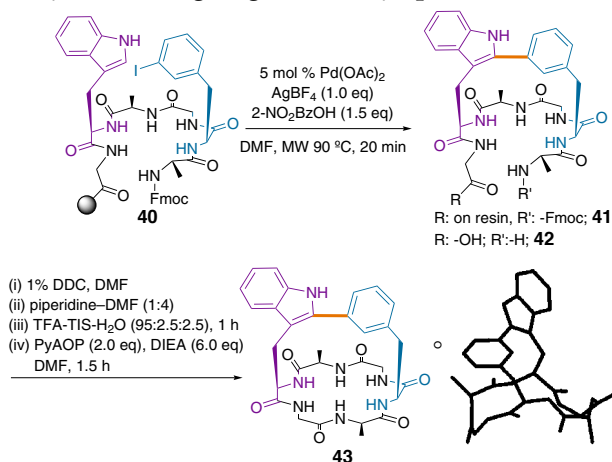
Source: Own elaboration.

In the light of these results, the access to more complex topologies was explored. Hence, the novel bicyclic bridged peptide **43** was generated from an internal stapling of the linear sequence **40** on solid-phase (85% purity, estimated by HPLC-MS, after the C–H arylation) and subsequent N-terminal C-terminal amide cyclization on solution (Fig. 40). Incidentally, the stapling to the directly cyclized forms with meta and *para* iodinated-Phe (*i*) and the Trp residue at (*i*,*i*+3) and (*i*,*i*+4), respectively, resulted totally unproductive, presumably because of conformational restrictions.

Regarding the complex vancomycin-like structures, an alternative bicyclic chemotype was also tackled from a double intramolecular C–H arylation within a linear peptide containing a commercially available diiodinated Tyr and two Trp units (Fig. 41). The optimization of the

Figure 40.

Synthesis of macrobicyclic peptide **43** through solid-phase stapling and its minimized geometry (bottom right) generated by Spartan '14 suite

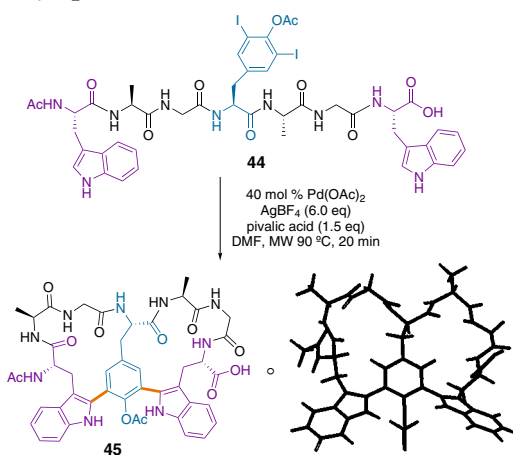


Source: Own elaboration.

conditions was performed on a model system, involving Ac-*m,m*-I-Tyr(OAc)-OH unit and two equivalents of Ac-Trp-OH, and led to an increase of the palladium catalyst (40 mol %) and AgBF₄ (6.0 eq) and also to the use of mild excess of pivalic acid (1.5 eq). With these conditions, different linear peptide sequences modifying the relative position of Tyr and Trps were tested. Finally, the corresponding diarylated bicyclic product **45** evolved from a double

Figure 41.

Double C-H arylation to form cyclic biaryl **45** and its minimized geometry (bottom right) generated by Spartan '14 suite



Source: Own elaboration.

(*i,i*+3) stapling of the linear peptide **44** (25% HPLC-MS conversion). This strategy could open the door to the access of simplified bismacrocylic structural analogues of biologically relevant compounds in a straightforward manner from simple linear peptidic sequences prepared through SPPS out of commercially available amino acids.

Ortho-Regiochemistry

Next, linear peptide sequences **46** with either one or none Ala units between the Trp and *o*-I-Phe residues were prepared as usual through standard SPPS protocols on 2-CTC resin. Disappointingly, when the C-H activation protocol was attempted on solution to the cleaved N-terminal acetylated sequences, only reduction of the carbon-halogen bond was detected (Table 5, entries 1-2). Minimized geometries generated by Spartan computational program supported this experimental observation as high strained cyclic peptides would arise from these geometries.

Table 5.

Palladium-catalyzed C-H arylation attempt to linear peptides with (n) residues between *o*-I-Phe and Trp residues^a

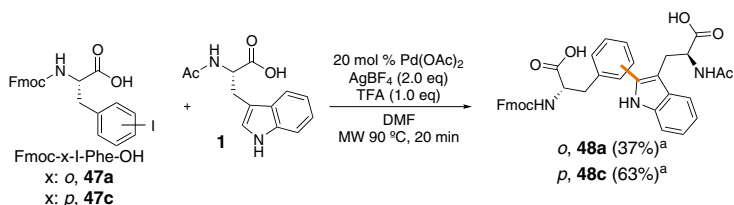
Entry	<i>i,i</i> +n	Linear peptide (46)	Cyclodimeric peptide	Cyclic peptide
1	<i>i, i</i> + 1	Ac-Ala- <i>o</i> -I-Phe-Trp-Ala-OH (46a)	n.db	n.d
2	<i>i, i</i> + 2	Ac-Ala- <i>o</i> -I-Phe-Ala-Trp-Ala-OH (46b)	n.d	n.d

Note: ^a 20 mol % Pd(OAc)₂, AgBF₄ (2.0 eq), TFA (1.0 eq), DMF, MW 90 °C, 20 min. ^b n.d: not detected.
Source: Own elaboration.

Interestingly, the intermolecular reaction between the commercially available Fmoc-*o*-I-Phe-OH **47a** and Ac-Trp-OH **1** successfully yielded the corresponding Trp-Phe adduct **48a**, although with a lower reactivity than the parent *para*-aryl iodide derivative **48c** (Fig. 42).

Figure 42.

Intermolecular C-H arylation of Ac-Trp-OH (**1**) with Fmoc-(*o/p*-I)Phe-OH (**47a/c**).^[a]
Estimated yield based on the HPLC-MS profile



Source: Own elaboration.

Para-Regiochemistry

To further complete the evaluation of the structural factors that determine the cyclization/cyclodimerization outcome of the C-H activation, a series of *p*-iodinated peptide sequences (**49a-d**), with an increasing number of amino acids (*n*) between Trp and *p*-I-Phe units, were prepared by using SPPS (Table 6, Fig. 43).

Hence, adjacent Phe and Trp residues led exclusively to the cyclodimeric formation (**50a**) in an analogous manner than the parent *meta*-iodinated peptide (Table 6, entry 1; Fig. 43a). The inclusion of one residue did not alter the cyclodimeric outcome of the reaction (Table 6, entry 2; Fig. 43b). Interestingly, when the number was increased up to two residues, both cyclodimeric (**50c**) and stapled (**50c'**) species were generated in meaningful extension (Table 6, entry 3; Fig. 43c). Furthermore, the presence of three residues resulted in the exclusive generation of the corresponding stapled bond derivative **50d** (Table 6, entry 4; Fig. 43d). Rough estimations of the stabilities by Spartan molecular modeling software were in agreement with the experimental observations. Importantly, high-resolution mass spectrometry analyses were pivotal to distinguish cyclic monomers from the cyclic dimer products. Incidentally, parallel C-H arylations performed directly on low-functionalized TentaGel S-NH₂ resin led to the same cyclodimerization trends, ruling out concentration effects.

Table 6.

Influence of the number of residues (n) between *p*-I-Phe and Trp residues in the palladium-catalyzed C-H arylation

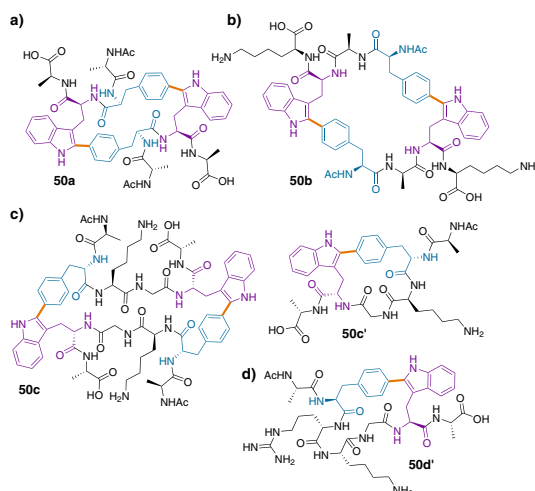
Entry	<i>i,i+n</i>	Linear peptide (49)	Cyclodimeric peptide	Stapled peptide	HPLC-MS conversion (%)
1	<i>i,i+1</i>	Ac-Ala- <i>p</i> -I-Phe-Trp-Ala-OH (49a)	50a	n.d. ^a	60
2	<i>i,i+2</i>	Ac- <i>p</i> -I-Phe-Ala-Trp-Lys-OH (49b)	50b	n.d.	54
3	<i>i,i+3</i>	Ac-Ala- <i>p</i> -I-Phe-Lys-Gly-Trp-Ala-OH (49c)	50c	50c'	23 / 51
4	<i>i,i+4</i>	Ac-Ala- <i>p</i> -I-Phe-Arg-Lys-Gly-Trp-Ala-OH (49d)	n.d.	50d	81 ^c

Note: ^a 20 mol % Pd(OAc)₂, AgBF₄ (2.0 eq), TFA (1.0 eq), DMF, MW 90 °C, 20 min. ^b n.d: not detected. ^c Additional MW irradiation cycle.

Source: Own elaboration.

Figure 43.

C-C linked structures resulted from C-H arylations of linear peptides 49a-d containing *p*-I-Phe and Trp residues located at different distances a) *i,i+1*; b) *i,i+2*; c) *i,i+3*; d) *i,i+4*



Source: Own elaboration.

All the *para*-derivatives **50a-d** were characterized by NMR. Remarkably, an aromatic ring flipping was observed for Phe residues in all peptides; as a consequence, a chemical shift averaging yields only two resonances for the four Phe aromatic protons on the NMR timescale. Additionally, compounds **50b** and **50c** exhibit wide signals at 298K, due to exchange broadening effects, which become sharper as the temperature increases, suggesting that the backbone flexibility increases with the size of the cyclodimer.

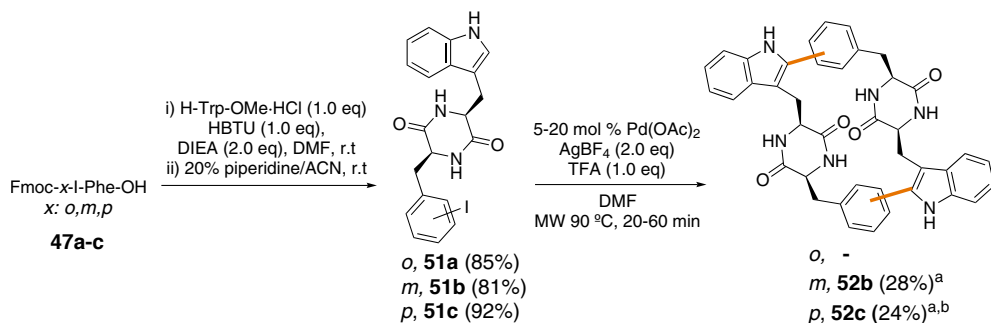
Cyclodimers **50b** and **50c** were envisioned as possible host compounds for flat guests due to their large cavity diameters. In preliminary experiments undertaken in MeOH, the model steroid estradiol was selected as possible guest. Modest increments of host absorbance were measured upon progressively increase of the guest molar fraction. A saturation curve was obtained at high molar guest fractions, showing evidence of molecular recognition.

Overall, cyclodimer-to-cyclic peptide ratio is independent of the concentration, which is considerably high (0.10-0.25 M). To assess the practicality of the macrocyclization protocol, the Emac values for a range of representative macrocyclic peptides were determined (between 6.5 and 7.7) and found to be within the range of previously reported Emac dataset for related reactions.

Finally, special interest was devoted to a singular case-study: the selective coupling of the smallest cyclopeptides known as 2,5-diketopiperazines (DKPs), which are natural products with a potential value as scaffolds in drug discovery (Cherkupally *et al.*, 2015). First, commercially available H-Trp-OMe•HCl and Fmoc-x-I-Phe-OH (x: *o*, *m*, *p*) were reacted through a standard amide coupling with HBTU and DIEA and then suspended in 20% piperidine/ACN solution to yield the corresponding *o,m,p*-iodinated DKPs **51a-c**. Then, the DKPs were subjected to the Pd-catalyzed C-H activation to yield the corresponding cyclodimeric products **52b-c** from the *m,p*-regiochemistries, whereas the *o*-derivative **51a** afforded only reduction of the carbon-halogen bond (Fig. 44).

Figure 44.

Synthesis of dimeric Phe-Trp DKPs **52b and **52c**.** ^[a] Estimated yields based on HPLC-MS analysis. ^[b] A second irradiation cycle was performed

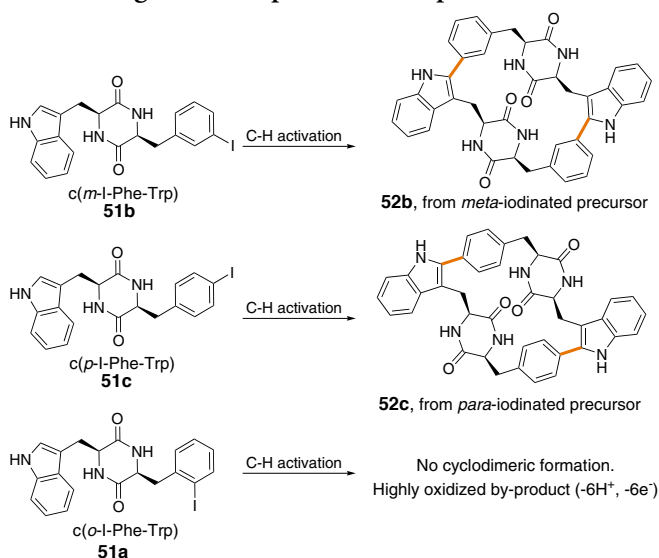


CHAPTER 4. CU(II) CROSS-DEHYDROGENATIVE CYCLIZATION OF TRP-BASED DKPs

Recently, the DKP functionalization has been explored in our group. In 2013, we employed the C-H activation protocol disclosed in the present thesis for the arylation of Trp-DKP brevianamide F in the C-2 indole position of Trp (chapter 1). Besides, in the previous disclosed chapter 3, *o,m,p*-iodinated DKPs **51a-c** were subjected to the developed Pd-catalyzed C-H activation process to yield the corresponding cyclodimeric products **52b-c** from the *m,p*-regiochemistries. Interestingly, the *o*-derivative **51a** afforded the reduction of the carbon-halogen bond as the main product, together with an unknown highly oxidized by-product detectable by HPLC-MS (Fig. 45). This intriguing result prompted us to further investigate the nature of this new process.

Figure 45.

Synthesis of dimeric Phe-Trp DKPs **52b-c** (chapter 3). C-H activation conditions: 5-20 mol % Pd(OAc)₂, AgBF₄ (2.0 eq), TFA (1.0 eq), DMF, MW 90 °C, 20-60 min



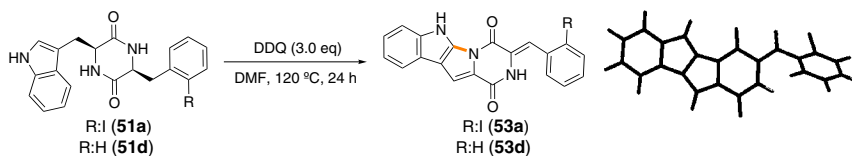
Source: Own elaboration.

In order to isolate the by-product and assign its structure, a screening of different oxidative conditions upon the simple scaffold c(Phe-Trp) DKP **51d** was initiated. The use of stoichiometric amounts of different oxidant sources (*i.e.*, TBHP, FeCl₃, PIFA or BQ, DLP, MnO₂, DTBP), from r.t to 170°C, in different solvents and reaction times, led only to detectable product traces by HPLC-MS. Gratifyingly, DDQ proved to be the best oxidant (25% HPLC-MS conversion) and, with these conditions in hand, the desired product was successfully isolated and characterized. HRMS and NMR experiments were in agreement with a structure of a polycyclic highly conjugated DKP (**53d**) showing a triply oxidation. This was originated from a double C_α-C_β dehydrogenation (Trp and Phe) and a C-N bond

formation between the C-2 indole position and the α N group from the same Trp moiety. Analogous results were obtained with the *ortho* iodinated *c(o*-I-Phe-Trp) DKP derivative **51a** (Fig. 46).

Figure 46.

c(Phe-Trp) DKP oxidative coupling with DDQ and minimized geometry of the oxidized chemotype **53a** (right) generated by Spartan '14 suite

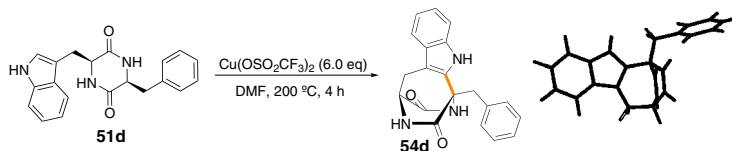


Source: Own elaboration.

The synthesis of α,β -dehydroamino acid derivatives (Jiang and Ma, 2015; Kaur, Heapy and Brimble, 2011) and, in general, enamides (Kuranaga, Sesoko and Inoue, 2014) from amino acid/amine precursors has previously been disclosed, although often involving multi-step procedures. This remarkable transformation involving a tandem C-N cyclization/ α,β -dehydrogenation reaction affords a constrained previously unknown pyrroloindol DKPs chemotype in just one step. Although the reaction is unprecedented, this process presents some serious limitations in terms of scope, isolation and yields. Taking into account other C-N cyclization processes disclosed in the literature (Takamatsu *et al.*, 2015; He *et al.*, 2015; Narayan, Manna and Antonchick, 2015; Xiaoqiang *et al.*, 2012; Brasche and Buchwald, 2008) mainly based on Cu(II), Pd(II) or I(III)-type oxidants, a new series of oxidative conditions were tested with the aim to optimize this new cyclization. Interestingly, the oxidative treatment with $\text{Cu}(\text{OSO}_2\text{CF}_3)_2$ enabled the isolation and characterization of an alternative mono-oxidized bicyclic compound (**54d**), evolved from the dehydrogenative C-C cyclization between the C-2 indole of Trp and the C^α of Phe (Fig. 47).

Figure 47.

c(Phe-Trp) DKP oxidative coupling with $\text{Cu}(\text{OSO}_2\text{CF}_3)_2$ and the minimized geometry of product **54d** (right) generated by Spartan '14 suite



Source: Own elaboration.

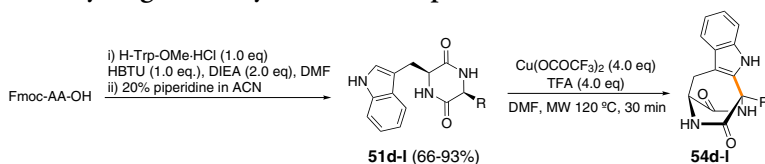
Very few, but remarkable examples are reported of these highly C-C strained DKP architectures, only obtained from isolation as metabolites from fungal cultures or through long-stepwise synthesis (Wei *et al.*, 2014; Holl *et al.*, 2009; Lazarovits *et al.*, 2004; Orain *et al.*,

2002; Gelin, Mortier and Moyroud, 1993). Notably, an intermolecular copper(I) chloride-catalyzed aerobic oxidative arylation of glycine derivatives with indoles was previously reported (Huo *et al.*, 2014); nonetheless, these conditions resulted unproductive for our DKP system.

In view of this promising result, a final optimization was undertaken upon the more simplified c(Gly-Trp) DKP **51e**. With these latter optimized conditions [that is $\text{Cu}(\text{OCOFC}_3)_2$ (4.0 eq), TFA (4.0 eq) in DMF, under MW irradiation at 120 °C in 30 min], the scope of the cross-dehydrogenative coupling reaction was studied in other Trp-containing DKPs, which were synthesized following an analogous procedure to the previously disclosed in chapter 3. Hence, a variety of c(AA-Trp) DKPs (**51d-l**) resulted compatible, including aromatic, non-polar and polar residues, showing variable conversions by HPLC-MS (Table 7, Fig. 48).

Table 7.

Cu(II) cross-dehydrogenative cyclization of Trp-based DKPs^a



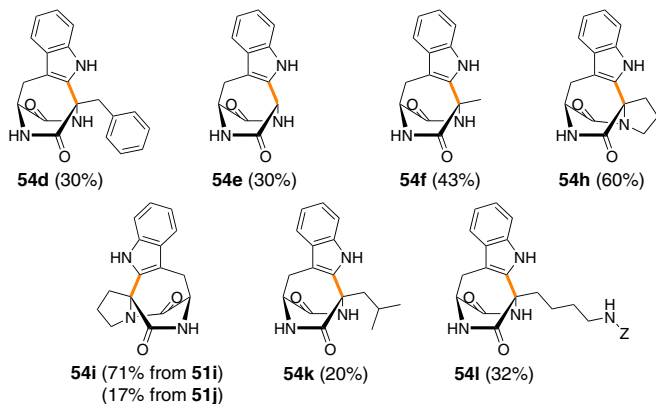
Entry	c(AA-Trp) DKP	AA-Trp ^b	Oxidized DKP	Yield (%)
1	51d	Phe-Trp	54d	30
2	51e	Gly-Trp	54e	30
3	51f	Ala-Trp	54f	not isolated
4	51g	Asp(tBu)-Trp	54f	43
5	51h	L-Pro- L-Trp	54h	60
6	51i	D-Pro-D-Trp	54i	71
7	51j	L-Pro-D-Trp	54i	17
8	51k	Leu-Trp	54k	20
9	51l	Lys(z)-Trp ^c	54l	32

Notes: ^a DKP (C:0.2M). ^b Unless stated, (L) configuration. ^c $\text{Cu}(\text{OSO}_2\text{CF}_3)_2$ source was used instead to reduce the extent of competitive C_α - C_β dehydrogenations.

Source: Own elaboration.

Interestingly, Asp(tBu)-containing DKP **51g** underwent decarboxylation to yield the oxidized c(Ala-Trp) **54f**, in a higher conversion than the corresponding Ala-containing-DKP **51f** (Table 7, entries 3 and 4; Fig. 48). Additionally, different configurations of the relevant brevianamide F [c(LPro-L-Trp)] were conveniently oxidized, showing similar (although not identical) reactivities. Thus, the stereoisomers with the same configuration for both residues [L-Pro-L-Trp (**51h**) and D-Pro-D-Trp (**51i**)] showed better conversions than the counterpart displaying an alternative L-D configuration (**51j**) (Table 7, entries 5-7; Fig. 48). The CDC resulted also compatible with Phe, Leu and protected Lys residues, although in lower extension due to competitive secondary side-oxidations such as C_α - C_β dehydrogenations

Figure 48.

Cu(II) cross-dehydrogenations to yield bicyclic DKPs **54d-l**

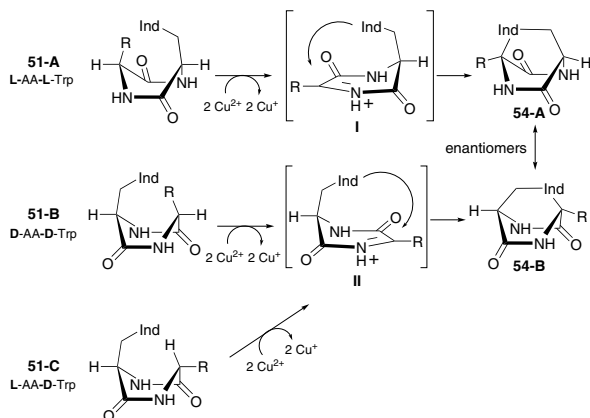
Source: Own elaboration.

(Table 7, entries 1, 8 and 9; Fig. 48). Remarkably, Trp-DKPs having other amino acid partners (*i.e.*, Met, Ser, Tyr, Glu, Arg, Asn) resulted unproductive for the CDC transformation.

A mechanistic proposal for the dehydrogenative coupling was envisioned (scheme 7). This mechanism is based on the formation of an N-iminium intermediate generated from the oxidation by two equivalents of Cu(II), and subsequent cyclization by the nucleophilic attack of the Trp indole ring (single-electron transfer processes to form radicalary intermediates may be involved). As a consequence, products from DKPs **51-A** and **51-B** give rise to enantiomeric bridged derivatives (**54-A** and **54-B**). Alternatively, stereoisomers **51-B** and **51-C**, having opposite configuration at the variable amino acid α -C stereogenic center (AA), would provide the same iminium species (II) therefore leading to the same oxidized product (**54-B**).

Scheme 7.

Mechanistic proposal for Cu(II) cross-dehydrogenative cyclization of DKPs

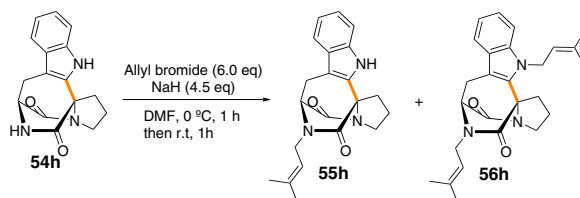


Source: Own elaboration.

To reinforce this hypothesis, additional experiments based on circular dichroism measurements, polarimetry and chiral chromatography analysis were carried out to the oxidized c(Pro-Trp) DKPs stereoisomers **54h-i**. Prenylated indole-based natural products, widely spread in terrestrial and marine organisms, display diverse biological activities which are directly related with their prenyl moiety (Li, 2010). In a preliminary experiment, with the aim to explore the chemical derivatization of these novel constrained DKPs, oxidized cyclo(ProL-TrpL) (**54h**) was prenylated by N-H deprotonation with NaH (4.5 eq) and subsequent addition of allyl bromide (5.0 eq) under an Ar atmosphere in DMF, affording a mixture of mono (**55h**) and diprenylated (**56h**) products (Fig. 49).

Figure 49.

Prenylation of oxidized cyclo(Pro_L-Trp_L) **54h**



Source: Own elaboration.

Overall, this study has led to dehydrogenative coupling processes for the selective formation of C-C and C-N linkages on Trp-DKPs in a straightforward manner. Despite the limited scope of the reaction, this method can serve as a valuable approach to access fused and bridged DKPs frameworks with potential biological activity features.

REFERENCES

- ARISAWA, M.; KASAYA, Y.; OBATA, T.; SASAKI, T.; ITO, M.; ABE, H.; ITO, Y.; YAMANO, A., and S. SHUTO (2011), *ACS. MED. CHEM. LETT.*, 2: 353.
- BRASCHE, G., and S. L. Buchwald (2008), *Angew. Chemie - Int. Ed.*, 47: 1932.
- CHERKUPALLY, P.; RAMESH, S.; JAD, Y. E.; GOVENDER, T.; KRUGER, H. G., and F. DE LA TORRE (2015), *Privileged Scaffolds in Medicinal Chemistry: Design, Synthesis, Evaluation*, in BRÄSE, S., Ed.; Royal Society of Chemistry, Cambridge: United Kingdom: 398–438 and references cited therein.
- GARCÍA-CUADRADO, D.; BRAGA, A. A. C.; F. MASERAS, F., and A. M. ECHAVARREN (2006), *J. Am. Chem. Soc.*, 128: 1066.
- GELIN, J.; MORTIER, J., and J. J. MOYROUD (1993), *J. J. Org. Chem.*, 58: 3473.
- GIRISHA, M.; BADIGER, J.; PUROHIT, M. G.; THIPPESWAMY, B. S., and B. M. PATIL (2008), *Indian J. Heterocycl. Chem.*, 17: 275.
- HE, Y. P.; ZHANG, C.; FAN, M.; WU, Z., and D. MA (2015), *Org. Lett.*, 17: 496.
- HOLL, R.; SCHEPMANN, D.; FRÖHLICH, R.; GRÜNERT, R.; BEDNARSKI, P. J., and B. WÜNSCH (2009), *B. J. Med. Chem.*, 52: 2126.
- HUO, C.; WANG, C.; WU, M.; JIA, X.; XIE, H., and Y. YUAN (2014), *Adv. Synth. Catal.*, 356: 411.

- JIANG, J.; MA, Z., and S. L. CASTLE (2015), *Tetrahedron*, 71: 5431.
- KAUR, H.; HEAPY, A. M., and M. A. BRIMBLE (2011), *Org. Biomol. Chem.*, 9: 5897.
- KURANAGA, T.; SESOKO, Y., and M. INOUE (2014), *Nat. Prod. Rep.*, 31: 514.
- LABAVITCH, J. M. (1999), *Proc. - Plant Growth Regul. Soc. Am.*, 26: 13.
- LAPOINTE, D., and K. FAGNOU (2010), *Chem. Lett.*, 39: 1118.
- LAZAROVITS, G.; HILL, J.; KING, R. R., and L. A. CALHOUN (2004), *Can. J. Microbiol.*, 50: 121.
- LEBRASSEUR, N., and I. LARROSA (2008), *J. Am. Chem. Soc.*, 130: 2926.
- LI, S.-M. (2010), *Nat. Prod. Rep.*, 27: 57.
- MUPPIDI, A.; WANG, Z.; LI, X.; CHEN, J., and Q. LIN (2011), *Chem. Commun*, 47: 9396.
- NARAYAN, R.; MANNA, S., and A. P. ANTONCHICK (2015), *Synlett*, 26: 1785.
- NÄSSEL, D. R.; PERSSON, M. G. S., and J. E. MUREN (2000), *J. Comp. Neurol.*, 422: 267.
- ORAIN, D.; DENAY, R.; KOCH, G., and R. GIGER (2002), *Org. Lett.*, 4: 4709.
- PAN, P.-S.; VASKO, R. C.; LAPERA, S. A.; JOHNSON, V. A.; SELLERS, R. P.; LIN, C.-C.; PAN, C.-M.; DAVIS, M. R.; ARDI, V. C., and S. R. McALPINE (2009), *Bioorg. Med. Chem.*, 17: 5806.
- PARAC, T. N., and N. M. KOSTIC (1996), *J. Am. Chem. Soc.*, 118: 51.
- RUIZ-RODRÍGUEZ, J.; ALBERICIO, F., and R. LAVILLA (2010), *Chem. Eur. J.*, 16: 1124.
- STRADER, L. C., and B. BARTEL (2011), *Mol. Plant*, 4: 477.
- TAKAMATSU, K.; HIRANO, K.; SATOH, T., and M. MIURA (2015), *J. Org. Chem.*, 80: 3242.
- WANG, X.; JIN, Y.; ZHAO, Y.; ZHU, L., and H. FU (2012), *Org. Lett.*, 14: 452.
- WEI, W.; JIANG, N.; MEI, Y. N.; CHU, Y. L.; GE, H. M.; SONG, Y. C.; NG, S. W., and R. X. Tan (2014), *Phytochemistry*, 100: 103.
- ZHU, L.; QIN, L.; PARAC, T. N., and N. M. KOSTIC (1994), *J. Am. Chem. Soc.*, 116: 5218.



CONCLUSIONS (IN SPANISH)

CONCLUSIONES

En esta tesis se ha investigado el desarrollo de nuevas metodologías para la modificación postsintética del aminoácido Trp. De acuerdo a los resultados obtenidos, se pueden extraer las siguientes conclusiones:

Capítulo 1. Arilación en C-2 del aminoácido Trp a través de activación C-H catalizada por paladio.

- Se ha optimizado un método de arilación en C-2 del grupo indol, basado en un proceso de activación C-H catalizado por paladio. Esta metodología es versátil; así se han podido arilar indoles de Trp, triptaminas y ácidos carboxílicos de indol β -substituidos. En especial, se ha arilado de manera directa el aminoácido comercial Fmoc-Trp-OH con diferentes iodoarilos sustituidos con grupos tanto electrón-dadores como electrón-atrayentes.
- Se ha llevado a cabo la arilación selectiva en C-2 de indol de la dicetopiperazina natural brevianamida F, obteniendo así una serie de miméticos de triprostatina con moderada actividad antitumoral.
- Se ha propuesto un posible mecanismo basado en un ciclo catalítico Pd(II)/Pd(IV), en el que un efecto de coordinación intramolecular del ácido del Trp parece favorecer el proceso con la formación del correspondiente paladaciclo. La presencia de ácidos carboxílicos y sales de plata Ag⁺ parecen ser claves para la reacción.
- Los derivados arilados de Trp preparados, Fmoc-Trp(C₂-Ar)-OH, se pueden aplicar directamente en síntesis en fase sólida. Así, se han podido preparar péptidos modificados a través de síntesis rutinarias con agentes de acoplamiento y condiciones estándar, pudiendo dirigir la arilación selectiva del residuo en secuencias con diversas unidades de Trp presentes y de acuerdo a la disposición del sustituyente yodo en el anillo (*orto*, *meta* o *para*).
- Como prueba de concepto, uno de los Trp arilados sintetizados se ha aplicado en fase sólida para la selectiva arilación de residuos de Trp de un péptido antimicrobiano, obteniendo así mejoras en su actividad biológica.

Capítulo 2. Aminoácido fluorógeno Trp-BODIPY para sondas de visualización basadas en péptidos.

- Se ha sintetizado un triptófano fluorógeno basado en el grupo BODIPY, vía el proceso de activación C-H desarrollado en el capítulo 1, con el fin de preparar agentes peptídicos para visualizar procesos biológicos. De este modo, se ofrece una alternativa a otros métodos de conjugación existentes basados en el uso de espaciadores químicos y en modificaciones de funciones químicas de aminoácidos, las cuales pueden ser clave para la actividad del péptido. Así, este aminoácido se ha aplicado directamente en fase sólida para la síntesis de dos péptidos fluorogénicos con interés terapéutico.
- Se ha sintetizado una serie de derivados fluorogénicos del péptido antifúngico PAF26 con la finalidad de visualizar infecciones fúngicas de diversos patógenos. El correspondiente análogo cíclico y fluorógeno de PAF26 ha permitido la visualización *ex vivo* del patógeno *A. Fumigatus* en tejido pulmonar humano. Esta estrategia permite mantener la anfipaticidad y distribución de cargas del péptido PAF26, esencial para su actividad y selectividad, ya que la incorporación del fluoróforo BODIPY no afecta a la conformación ni a las interacciones moleculares del Trp. Además, PAF26-BODIPY solo emite señal de fluorescencia en entornos hidrofóbicos; ello permite la visualización directa (*imaging*) sin la necesidad de llevar a cabo lavados previos.
- Se ha sintetizado el péptido cíclico fluorescente cLac-BODIPY para la detección de apoptosis, basado en la incorporación del grupo BODIPY a una secuencia peptídica simplificada de lactaderina. Experimentos de citometría de flujo y microscopía confocal han descartado la selectiva afinidad de este compuesto por células apoptóticas pero sí se ha confirmado el reconocimiento de cuerpos apoptóticos producidos por células tipo BL2. cLac-BODIPY solo muestra emisión de fluorescencia cuando se une a unidades de PS presentes en cuerpos apoptóticos. Esta fluorescencia es independiente de Ca^{2+} , lo cual es una mejora respecto a Annexin V, una proteína ampliamente utilizada para monitorizar apoptosis celular.

Capítulo 3. Topologías biaril-peptídicas a través de reacciones C-H catalizadas por paladio entre residuos de Trp y Phe/Tyr.

- Se ha aplicado la metodología desarrollada en el capítulo 1 para el acceso a estructuras tipo *grapa* (*staple*), directamente a partir de secuencias lineales precursoras que contengan Trp y I-Phe/I-Tyr en un proceso de activación C-H. Este protocolo se ha podido aplicar tanto en solución como en fase sólida, obteniendo resultados análogos, y sobre un rango diverso de aminoácidos con cadenas laterales de diferente naturaleza. De este modo, se han sintetizado péptidos *grapados* de secuencias con interés biológico.
- Se han determinado los factores que determinan la ciclación/ciclodimerización de la reacción, los cuales son básicamente estructurales. En líneas generales, espaciadores cortos dan lugar a estructuras ciclodiméricas (*i*, *i+1-meta/para*; *i*, *i+2-para*) y espa-

ciadores más largos (*i, i+4-meta/para*) o sustratos intermedios en meta dan lugar a ciclopéptidos en un proceso intramolecular. En un caso, (*i, i+3-para*) se producen ambas formas en una extensión similar.

- Esta metodología permite obtener un amplio rango de diferentes topologías. Así, se han obtenido péptidos *grapa*, conjugados macrocíclicos, macrociclos diméricos, biciclopéptidos que incluyen una ciclación tipo *grapa* y otra ciclación N-terminal/C-terminal y biciclopéptidos formados por dos ciclaciones tipo *grapa* en una sola etapa sintética. Estos métodos pueden servir de base para futuras aproximaciones con el fin de acceder en pocas etapas sintéticas a análogos estructurales simplificados de compuestos cíclicos o bicíclicos biológicamente relevantes, a partir de secuencias lineales preparadas en fase sólida con aminoácidos comercialmente asequibles.

Capítulo 4. Ciclación de acoplamiento cruzado deshidrogenativa mediada por Cu(II) de dicetopiperazinas basadas en Trp.

- Se ha desarrollado una metodología basada en reacciones de acoplamiento deshidrogenativo para la formación selectiva de enlaces C-C o C-N en dicetopiperazinas que contengan Trp. Concretamente, se ha accedido a dos tipos de topologías a partir de la correspondiente dicetopiperazina en un solo paso, de acuerdo a la naturaleza del oxidante utilizado. La formación del nuevo enlace tiene lugar vía una ciclación deshidrogenativa entre el C-2 de indol de Trp y el grupo N^a del mismo Trp o el C^a del aminoácido adyacente; dicha ciclación es favorable respecto otras deshidrogenaciones o degradaciones hidrolíticas que podrían esperarse en estas condiciones.
- Respecto la reacción deshidrogenativa para la ciclación a través de un nuevo enlace C-C, se ha planteado un mecanismo hipotético que evolucionaría a través de un intermedio de iminio, el cual se ha contrastado con experimentos de polarimetría, DC y HPLC quiral.
- Pese al restringido alcance de estas reacciones, las topologías formadas constituyen arquetipos con potencial interés terapéutico.



PERSONAL CONTRIBUTION TO THE PUBLICATIONS (IN SPANISH)

CONTRIBUCIÓN PERSONAL A LAS PUBLICACIONES PRESENTADAS

Publicación I. Synthesis and biological evaluation of a postsynthetically modified Trp-based diketopiperazine

Sara Preciado, Lorena Mendive-Tapia, Carolina Torres-García, Rubí Zamudio-Vázquez, Vanessa Soto-Cerrato, Ricardo Pérez-Tomás, Fernando Albericio, Ernesto Nicolás, Rodolfo Lavilla.

Medicinal Chemical Communications, 2013, 4, 1171-1174.

En este trabajo he colaborado en el estudio y diseño de los compuestos que constituyen la publicación y he sintetizado la mayor parte de los compuestos finales a través de la reacción de arilación C-H sobre brevianamida F. Así mismo, he llevado a cabo la caracterización de los productos sintetizados por mi parte así como la elucidación estructural de los mismos por métodos espectroscópicos. He participado en la escritura del manuscrito.

Publicación II. Synthesis of C-2 arylated tryptophan amino acids and related compounds through palladium-catalyzed C-H activation

Sara Preciado[#], Lorena Mendive-Tapia[#], Fernando Albericio, Rodolfo Lavilla. [#] Ambos investigadores han contribuido de manera similar a este trabajo.

The Journal of Organic Chemistry, 2013, 78, 8129-8135.

En este trabajo he colaborado en el estudio y diseño de los compuestos que constituyen la publicación. He realizado gran parte de los experimentos de optimización y síntesis de la reacción de arilación C-H sobre el aminoácido Trp y otros indoles y he ejecutado los correspondientes experimentos en fase sólida. Así mismo, he llevado a cabo la caracterización de los productos sintetizados por mi parte así como la elucidación estructural de los mismos por métodos espectroscópicos. He participado en la escritura del manuscrito.

Publicación III. Enhanced antimicrobial activity of a peptide derived from human lysozyme by arylation of its tryptophan residues

Rodrigo González, Lorena Mendive-Tapia, María B. Pastrian, Fernando Albericio, Rodolfo Lavilla, Osvaldo Cascone, Nancy B. Iannucci.

Journal of Peptide Science, 2016, 22, 123-128.

Mi aportación en este trabajo ha consistido en la realización del precursor arilado de Trp a gran escala para su uso directo en la síntesis en fase sólida de las secuencias peptídicas. Así mismo, he llevado a cabo la caracterización del Trp arilado así como la elucidación estructural del mismo por métodos espectroscópicos. He participado en la escritura del manuscrito.

Publicación IV. Spacer-free BODIPY fluorogens in antimicrobial peptides for direct imaging of fungal infection in human tissue

Lorena Mendive-Tapia, Can Zhao, Ahsan R. Akram, Sara Preciado, Fernando Albericio, Martin Lee, Alan Serrels, Nicola Kielland, Nick D. Read, Rodolfo Lavilla, Marc Vendrell.

Nature Communications, 2016, 7:10940. DOI: 10.1038/ncomms10940.

En este trabajo he llevado a cabo el diseño, exploración y ejecución de las síntesis químicas correspondientes a la preparación del aminoácido fluorescente Fmoc-Trp(C2-BODIPY)-OH y de todos los péptidos del trabajo. Así mismo, he realizado la caracterización de los productos sintetizados así como la elucidación estructural de los mismos por métodos espectroscópicos. He participado en la escritura del manuscrito.

Publicación V. A Trp-BODIPY cyclic peptide for fluorescence labeling of apoptotic bodies

Ramon Subiros-Funosas[#], Lorena Mendive-Tapia[#], Jesus Sot, John D. Pound, Nicole Barth, Yaiza Varela, Felix M. Goñi, Margaret Paterson, Christopher D. Gregory, Fernando Albericio, Ian Dransfield, Rodolfo Lavilla, Marc Vendrell. [#]Ambos investigadores han contribuido de manera similar a este trabajo.

Chemical Communications. Aceptado para publicación. DOI: 10.1039/c6cc07879f.

Mi contribución ha consistido en el diseño y ejecución de las propuestas sintéticas para la preparación del péptido cíclico fluorescente BODIPY-cLac, presentado en este trabajo, y su correspondiente análogo no fluorescente. Así mismo, he llevado a cabo sus correspondientes caracterizaciones y elucidaciones estructurales por métodos espectroscópicos. He ejecutado los primeros experimentos in vitro para la evaluación de las propiedades de BODIPY-cLac (variación de la fluorescencia respecto la concentración o entornos hidrofóbicos y determinación del rendimiento cuántico) y de su afinidad por PS. He efectuado estudios

preliminares por citometría de flujo y microscopía de fluorescencia con células y vesículas aisladas. He participado en la escritura del manuscrito.

Publicación VI. A Trp-BODIPY fluorogenic amino acid to label peptides for enhanced live-cell fluorescence imaging

Lorena Mendive-Tapia[#], Ramon Subiros-Funosas[#], Can Zhao[#], Fernando Albericio, Nick D. Read, Rodolfo Lavilla, Marc Vendrell. [#]Ambos investigadores han contribuido de manera similar a este trabajo.

Nature Protocols. Aceptado para publicación, en proceso editorial.

En relación a la parte experimental, he elaborado un análisis más exhaustivo de la síntesis de Fmoc-Trp(C₂-BODIPY)-OH y de péptidos que contienen este residuo fluorogénico para así reportar dichos procedimientos en forma de protocolo. He participado en la escritura del manuscrito.

Adicionalmente este trabajo también ha dado lugar a una patente:

Patente. Fluorogenic compounds, process of preparation thereof and methods of use.

Marc Vendrell, Ramón Subiros-Funosas, Lorena Mendive-Tapia, Fernando Albericio, Rodolfo Lavilla, Nick D. Read. WO 2016207626 (PCT/GB2016/051864).

Publicación VII. New peptide architectures through C–H activation stapling between tryptophan phenylalanine/tyrosine residues

Lorena Mendive-Tapia, Sara Preciado, Jesús García, Rosario Ramón, Nicola Kielland, Fernando Albericio, Rodolfo Lavilla.

Nature Communications, 2015, 6: 7160. DOI: 10.1038/ncomms8160.

Tras el descubrimiento inicial por parte de la Dra. Sara Preciado de la aplicabilidad de la metodología de arilación C-H en secuencias peptídicas modelo, mi contribución en este trabajo ha consistido en el estudio, diseño y ejecución de las síntesis de los compuestos que constituyen el trabajo. He realizado la síntesis de todos los compuestos a excepción del único péptido modelo fluorescente presentado en este trabajo. Así mismo, los correspondientes experimentos *in vitro* sobre este último compuesto los llevé a cabo en colaboración con el Dr. Nicola Kielland. He llevado a cabo la caracterización de todos los productos sintetizados así como la elucidación estructural de los mismos por métodos espectroscópicos. También he realizado los ensayos de degradación proteolítica sobre los péptidos *grapados*, los experimentos de dicroísmo circular y el análisis computacional de las estructuras. He participado en la escritura del manuscrito.

Publicación VIII. Constrained cyclopeptides: biaryl formation through Pd-catalyzed C-H activation in peptides—structural control of the cyclization vs. cyclodimerization outcome

Lorena Mendive-Tapia, Alexandra Bertran, Jesús García, Gerardo Acosta, Fernando Albericio, Rodolfo Lavilla.

Chemistry – A European Journal, 2016, 22, 13114-13119.

Mi aportación en este trabajo ha consistido en el diseño y ejecución de las síntesis de todos los compuestos que constituyen el artículo a excepción de los compuestos formados por dicetopiperazinas. He llevado a cabo la caracterización de todos los productos sintetizados así como la elucidación estructural de los mismos por métodos espectroscópicos y de análisis computacional, y he realizado los estudios preliminares de reconocimiento molecular sobre estructuras diméricas. He participado en la escritura del manuscrito.

Publicación IX. Access to new scaffolds through cross dehydrogenative couplings on tryptophan-based diketopiperazines

Lorena Mendive-Tapia, Arantxa Albornoz Grados, Alexandra Bertran, Fernando Albericio, Rodolfo Lavilla.

Manuscrito en preparación.

En este trabajo he llevado a cabo el diseño y ejecución de las síntesis de todos los compuestos que constituyen el trabajo a excepción del derivado de dicetopiperazina compuesto por Trp y Leu. He llevado a cabo la optimización de las condiciones de reacción para la obtención de las dicetopiperazinas cicladas a través del nuevo enlace C-C y he efectuado la caracterización de todos los productos sintetizados así como la elucidación estructural de los mismos por métodos espectroscópicos y de análisis computacional. Además, he realizado los experimentos de dicroísmo circular y resolución por HPLC quiral para el estudio del mecanismo propuesto. He participado en la escritura del manuscrito.



ANNEX 3. SUMMARY OF INTRODUCTION AND OBJECTIVES (IN SPANISH)

INTRODUCCIÓN GENERAL

Se definen los péptidos como cadenas naturales biopoliméricas de hasta unos 100 aminoácidos o menos, que juegan papeles cruciales en la regulación y función de una gran variedad de procesos fisiológicos (ej. hormonas, neurotransmisores, factores de crecimiento, etcétera), y representan arquetipos importantes en química orgánica y médica (Sewald y Jakubke, 2002; Wade, 2010). Cada residuo contiene un grupo funcional amino y un grupo ácido carboxílico, junto con una cadena lateral específica para cada aminoácido, y están conectados entre sí a través de enlaces tipo amida.

El uso de péptidos como agentes terapéuticos es un campo en continuo crecimiento y una fuente valiosa de nuevos fármacos (Fosgerau y Hoffmann, 2015; Tsomaia, 2015). Este interés se debe en parte a sus dimensiones y topología molecular, cercanas a las de proteínas, las cuales les confieren elevada especificidad, tolerabilidad y potencia frente a objetivos biológicos (ej. interacciones proteína-proteína, receptores, etc.). El mercado de agentes peptídicos se halla en continuo crecimiento. Así, en 2015 el mercado global de péptidos terapéuticos alcanzó los 20.000 millones de dólares y se estima que este valor alcance los 23.700 millones en 2020 (Transparency Market Research, 2016). En 2015, más de 60 péptidos aprobados por la Agencia de Alimentos y Medicamentos FDA llegaron al mercado (con otros muchos en fases clínicas y preclínicas), siendo las enfermedades metabólicas y oncología sus principales áreas terapéuticas. El uso de péptidos como fármacos, sin embargo, se ha visto dificultado por su tendencia a ser degradados por enzimas para posteriormente ser eliminados a través de los riñones o el hígado, mostrando también agregación o baja permeabilidad para cruzar membranas. Muy pocos son los fármacos peptídicos en el mercado que se administran oralmente, siendo las rutas preferentes de administración intravenosa, subcutánea o intramuscular para así evitar la prematura degradación enzimática (Diao y Meibohm, 2013). No obstante, los fármacos basados en péptidos se van optimizando progresivamente y están emergiendo nuevas estrategias con el fin de superar estas limitaciones.

La producción de péptidos terapéuticos se puede realizar a través de síntesis química, microorganismos recombinantes o mediante extracción de fuentes naturales. En particular, la síntesis química de péptidos se puede efectuar en solución, en fase sólida o a través de estrategias que combinen las dos anteriores.

El aumento de la utilidad terapéutica de péptidos y proteínas se puede llevar a cabo a través de un amplio repertorio de diferentes estrategias basadas en modificaciones específicas para modular sus propiedades funcionales o farmacocinéticas. Entre otros propósitos, estos cambios se efectúan con el fin de incrementar la potencia y/o selectividad para un sustrato

específico, modular interacciones tipo proteína-proteína, diseñar péptidos multifuncionales, reconocer entidades biológicas o visualizar procesos biológicos. En general, estas modificaciones se pueden realizar sobre los grupos funcionales terminales amino o ácido, las cadenas laterales, el esqueleto peptídico o por medio de la sustitución de un aminoácido específico. La ubicación de este cambio y el método de selección estarán determinados por la estructura polipeptídica, la función biológica y el objetivo concreto que se persigue. Respecto al uso de aminoácidos no naturales, existen diversas estrategias para su incorporación directa (genética o químicamente) en péptidos o proteínas. Las aproximaciones basadas en la expansión del código genético consisten en la incorporación selectiva de un aminoácido no proteinogénico (no codificado genéticamente) en un péptido o proteína (Chin, 2014; Davis y Chin, 2012; Xiao *et al.*, 2013; Wang *et al.*, 2001; Hong, Kwon y Jewett, 2014). La modificación selectiva en péptidos también se puede efectuar a través de síntesis química para lograr la introducción directa de aminoácidos no estándares o con alteraciones específicas.

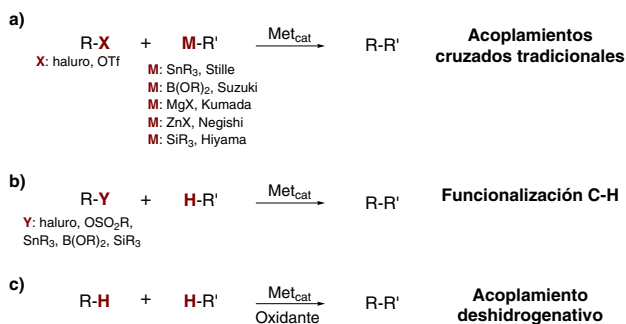
Los indoles son heterociclos aromáticos π excedentes presentes en muchos sistemas naturales (Joule y Mills, 2010). Muchas moléculas que contienen anillos de indol representan arquetipos estructurales de gran interés, con gran repercusión en el desarrollo de fármacos y en otras aplicaciones industriales (ej. colorantes, herbicidas, fungicidas, perfumes, etc.) (Gribble, 2010). En particular, el triptófano (Trp) es un aminoácido esencial que contiene un anillo de indol en su cadena lateral con papeles funcionales clave, presente en muchos alcaloides, péptidos y proteínas (Alkhalaf y Ryan, 2015; Higuchi y Kawasaki, 2005; Bialonska y Zjawiony, 2009). Pese a que Trp es el menos abundante de los 20 aminoácidos canónicos (alrededor de un 1% en péptidos y proteínas), su elevada hidrofobicidad y características dadoras de puentes de hidrógeno de su cadena lateral permiten interacciones por fuerzas no covalentes (ej. aromático-aromático, π -catión, etc.) con funciones clave en el reconocimiento y estabilización de proteínas (Santiveri y Jiménez, 2010). Además, la inherente reactividad del grupo indol (ej. a sustituciones electrofílicas aromáticas, oxidaciones, modificaciones enzimáticas, etc.) hacen del Trp un sustrato interesante para su diversificación química.

En las últimas décadas, el desarrollo de metodologías basadas en acoplamientos cruzados catalizados por metales de transición para la formación de enlaces carbono-carbono o carbono-heteroátomo ha aportado avances significativos a la química orgánica sintética (De Meijere y Diederich, 2004). Los métodos clásicos de acoplamiento cruzado para la formación de enlaces arilo-arilo consisten en la reacción de un agente organometálico (componente nucleofílico) con un segundo compuesto que contenga un sustituyente haluro o similar (componente electrofílico, Fig. 50a). De acuerdo al metal de transición y a los grupos funcionales involucrados, se han descrito diferentes métodos, incluyendo reacciones de Stille, Suzuki, Kumada, Negishi y Hiyama. Estos acoplamientos son usualmente catalizados por Pd (Ni, Ru, Ir, etc. también se han reportado) y en algunos casos en conjunción con una base.

Recientemente, los procesos de activación de enlace carbono-hidrógeno (C-H) (o funcionalización C-H) catalizados por metal han experimentado un rápido crecimiento. En contraste con los métodos tradicionales, estos procesos se basan en el acoplamiento de solo un componente funcionalizado, siendo el otro componente una molécula que reacciona a través de un enlace C-H (Yu y Shi, 2010). Con el fin de lidiar con la ubicuidad de los enlaces C-H, la catálisis por metales permite la activación selectiva de un enlace C-H vía coordinación del

Figura 50.

Estrategias descritas para la formación de uniones arilo-arilo a través de reacciones de acoplamiento cruzado catalizadas por metales



Fuente: Elaboración propia.

metal (C-metal) y posterior funcionalización a través de la reacción con un electrófilo (Fig. 50b). De este modo, se reducen los residuos contaminantes químicos y el número de etapas sintéticas necesarias para la formación del enlace C-C ya que se evita la funcionalización de uno de los componentes. Adicionalmente, los procesos de doble activación C-H (o reacciones de acoplamiento deshidrogenativo) se fundamentan en la construcción selectiva de uniones C-C, directamente a partir de dos enlaces C-H diferentes, bajo condiciones oxidantes (Fig. 50c). El principal problema en estos procesos es, de nuevo, la ubicuidad de los enlaces C-H.

La funcionalización C-H es un campo en continuo crecimiento con aplicaciones destacadas en la síntesis de compuestos biológicamente activos y otros materiales funcionales. Así, desde las primeras contribuciones reportadas a finales del siglo pasado, el número de publicaciones concernientes a la funcionalización C-H se ha incrementado significativamente (Wencel-Delord y Glorius, 2013; White, 2012; Yamaguchi, Yamaguchi e Itami, 2012). En particular, se han reportado arilaciones C-H con Cu, Rh, Ru y Pd, siendo este último el más ampliamente explorado (Ackermann, 2009).

En este contexto, en la presente tesis nos centramos en el estudio de los siguientes temas principales:

ARILACIÓN EN C-2 DE INDOL A TRAVÉS DE ACTIVACIÓN C-H CATALIZADA POR METALES

La derivatización a través de la arilación en C-2 de indol constituye una estrategia atractiva para la modulación de la estructura y la bioactividad de potenciales agentes farmacológicos. En contraposición a métodos estándar, en las últimas décadas se han reportado diversas estrategias para la arilación de indoles a través de activación C-H catalizada por metales (Sandtorv, 2015; Yu y Shi, 2010).

Algunos de los trabajos pioneros referentes a la activación C-H de indoles aparecieron en la década de los 80 con el trabajo de Genet (1978) (Trost, Godleski y Genet, 1978) y Ohta (1989), entre otros. Posteriormente, Grigg y colaboradores presentaron en 1990 la primera arilación directa catalizada por metales con un iodoarilo en un proceso intramolecular usando $\text{Pd}(\text{OAc})_2$ y PPh_3 como ligando (Grigg *et al.*, 1990). No obstante, no fue hasta la década de los 2000 cuando esta metodología realmente mostró un progreso relevante. Así, en 2006 el grupo de Sanford describió un protocolo bajo condiciones suaves con sales de aril yodonio y catálisis con $\text{Pd}(\text{II})$ (Deprez *et al.*, 2006). Después, en 2007 Sames y colaboradores presentaron un nuevo método de arilación para indoles con iodoarilos, mediado por $\text{Pd}(\text{OAc})_2$ como catalizador y CsOAc como base, en las que evidenciaron una selectividad de las posiciones C-2/C-3 indólicas en función del tipo de ligando utilizado (Wang, Gribkov y Sames, 2007). De manera análoga, el mismo año el grupo de Fagnou mostró una metodología oxidativa basada en el uso de $\text{Pd}(\text{TFA})_2$ como catalizador para la conexión directa de arenos a indoles (Stuart, Villemure y Fagnou, 2007). En 2008, Gaunt describió un protocolo basado en $\text{Cu}(\text{OTf})_2$ para la arilación de indoles con triflatos diarylyodonio, donde la protección del NH-indólico determina la selectividad C-2/C-3 de indol (Phipps, Grimster y Gaunt, 2008). Alternativamente, también se han publicado otros agentes de acoplamiento para la arilación de sistemas indólicos. Así, Shi y colaboradores (2008) arilaron una serie de derivados de indol con ácidos aril borónicos bajo catálisis con $\text{Pd}(\text{OAc})_2$, en presencia de atmósfera de oxígeno y ácido acético (Yang, 2008). El mismo año, el grupo de Cheng describió el uso de sales de ariltrifluoroboronato en presencia de $\text{Pd}(\text{OAc})_2$, $\text{Cu}(\text{OAc})_2$ y aire (Zhao, Zhang y Cheng, 2008).

En el momento en el que el presente proyecto se empezó a desarrollar se habían reportado escasos precedentes referentes a la directa arilación en C-2 de indol en Trp. La síntesis de derivados 2-aril-Trp por arilación directa solo se había descrito mediante metodologías clásicas de acoplamiento cruzado mediadas por paladio a través de reacciones de Suzuki-Miyaura o procesos de formación de enlace C-H catalizados por Ru (Ackermann y Lygin, 2011; Colletti, 2000); aunque ninguna de ellas era ideal en términos de aplicabilidad y condiciones experimentales, ya que dichos protocolos requerían el uso de Trp protegido y condiciones de reacción drásticas.

SONDAS DE VISUALIZACIÓN BASADAS EN PÉPTIDOS

Los péptidos son entidades químicas que ocupan un espacio químico privilegiado, localizado entre moléculas pequeñas y biopolímeros. Esto confiere moléculas de tamaño medio con gran especificidad y potencia respecto dianas moleculares. Además, los péptidos poseen de manera inherente baja toxicidad e inmunogenicidad y pueden ser estructuralmente modificados para modular sus propiedades farmacocinéticas.

En particular, las sondas de visualización basadas en péptidos se han establecido como herramientas de gran interés para dirigirse a entidades biológicas y así visualizar procesos. Entre las diferentes aproximaciones de visualización, las sondas basadas en agentes fluorogénicos han emergido como técnicas de gran interés debido a sus propiedades no radioactivas y altamente sensibles. En este sentido, el grupo 4,4-difluoro-4-bora-3a,4a-diaza-

s-indaceno (BODIPY) ha sido extensamente estudiado y se han descrito un amplio rango de derivados basados en este grupo en numerosas aplicaciones de visualización (Hong-Hermesdorf *et al.*, 2014; Vázquez-Romero *et al.*, 2013; Lee *et al.*, 2009) debido a sus excelentes propiedades fotofísicas y de permeabilidad (Kowada, Maeda y Kikuchi, 2015).

Actualmente, existe la necesidad de nuevas aproximaciones para la incorporación de fluoróforos en péptidos, de una manera específica y sin alterar sus propiedades intrínsecas ni su actividad. En los últimos años, se ha reportado el uso de aminoácidos no naturales como precursores para la síntesis de péptidos o proteínas fluorescentes. En dichas estrategias, el grupo fluorogénico puede ser introducido mediante acoplamiento a un residuo modificado de la secuencia con una funcionalidad química ortogonal o por medio de la preparación de un aminoácido fluorogénico y posterior incorporación de éste en la secuencia a través de síntesis química o por otros métodos biosintéticos (Maity, Honcharenko y Strömberg, 2015; Koopmans *et al.*, 2013; Krueger y Imperiali, 2013). Particularmente relevante es el trabajo del grupo de Imperiali sobre el desarrollo de aminoácidos fluorescentes sensibles al entorno para su incorporación en péptidos o proteínas (Socher y Imperiali, 2013; Venkatraman *et al.*, 2007; Sainlos y Imperiali, 2007).

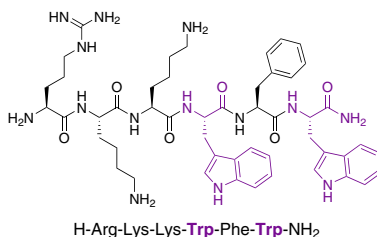
En este contexto, nos propusimos estudiar los siguientes proyectos:

Péptido antifúngico PAF26

PAF26 (López-García *et al.*, 2002) es un péptido sintético que actúa contra la aspergilosis pulmonar invasiva, una infección pulmonar grave con tasas de mortalidad elevadas causada por el patógeno fúngico *Aspergillus Fumigatus* (Fig. 51). Las herramientas diagnósticas utilizadas actualmente consisten en análisis de cultivos de diferentes muestras de fluidos biológicos, pero estos métodos pueden verse obstaculizados por dificultades colaterales (ej. contaminación de las vías respiratorias, crecimiento lento del microorganismo, etc.). Por esta razón, existe la demanda de sondas que permitan el conocimiento *in situ* y a tiempo real del curso de la infección. Por otra parte, la anfipaticidad de PAF26 está estrechamente relacionada con su papel antifúngico, ya que es crucial para la interacción con la membrana

Figura 51.

Péptido antimicrobiano PAF26



Fuente: Elaboración propia.

celular fúngica, su internalización y transporte dentro de la célula donde ejerce su función (Muñoz *et al.*, 2013).

Procesos de muerte celular apoptóticos.

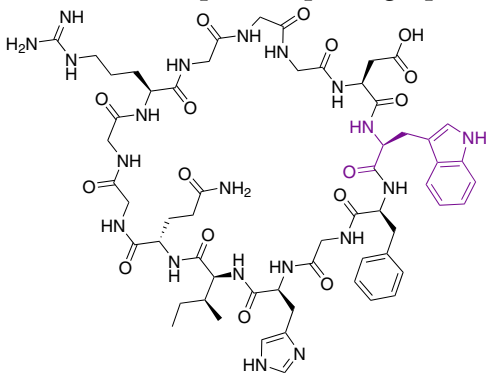
La muerte celular es un mecanismo funcional en organismos que puede ser originado por factores naturales o externos (ej. infecciones o daños estructurales). De acuerdo a los aspectos morfológicos y función, se pueden diferenciar tres grandes modos de muerte celular (Duprez *et al.*, 2009): apoptosis, autofagia y necrosis.

En estadios tempranos de apoptosis, se forman protuberancias y se liberan estructuras subcelulares (cuerpos apoptóticos) al espacio extracelular con el fin de establecer comunicación con otras células. Además, existe la evidencia que unidades de fosfatidilserina (PS) son externalizadas en la cara externa de la membrana celular y también en cuerpos apoptóticos secretados por la misma célula. El reconocimiento de estas unidades por otras moléculas puede ser utilizado para la detección de procesos apoptóticos. Anexina V es una proteína de 36-KDa reportada como marcador de apoptosis (Nazari, Minai-Tehrani y Emamzadeh, 2014). Pese a su popularidad y extenso uso, su elevado peso molecular, permeabilidad moderada y dependencia a concentraciones elevadas de Ca^{2+} son limitaciones que tienen que ser consideradas.

La lactaderina es una glicoproteína de 47-KDa que media la fagocitosis de células apoptóticas a través del reconocimiento de unidades de PS expuestas superficialmente, con una afinidad nanomolar y de manera independiente a Ca^{2+} . Recientemente, el grupo de Zheng describió la preparación de un mimético cíclico de lactaderina (cLac), el cual recrea la disposición de los aminoácidos clave involucrados en la interacción lactaderina-PS (Fig. 52) (Zheng *et al.*, 2011).

Figura 52.

Mimético cíclico de lactaderina reportado por el grupo de Zheng



c(-Trp-Phe-Gly-His-Ile-Gln-Gly-Gly-Arg-Gly-Gly-Gly-Asp-)

Fuente: Elaboración propia.

TOPOLOGÍAS BIARIL PEPTÍDICAS. PÉPTIDOS GRAPA

Los péptidos poseen una serie de propiedades intrínsecas que hacen de ellos un grupo de entidades moleculares sintéticamente accesibles con elevada selectividad, potencia y baja toxicidad, cualidades muy valoradas en la generación de agentes terapéuticos. No obstante, su éxito en el mercado farmacéutico se ha visto dificultado por sus pobres propiedades farmacocinéticas (inestabilidad metabólica y baja permeabilidad). En este sentido, se aplican diferentes estrategias de constreñimiento con el fin de generar estructuras más rígidas con mejoras en su estabilidad metabólica y permeabilidad. En función de los elementos involucrados en la ciclación, el tipo de constricción se puede clasificar en cuatro categorías: i) N-terminal con C-terminal, ii) cadena lateral con uno de los extremos, iii) cadena lateral con cadena lateral y iv) compuestos cíclicos formados por dos o más de los anteriores modos de ciclación.

Los productos naturales peptídicos derivados de bismacrociclos biaril y biaril éter (Feliu y Planas, 2005), tales como vancomicina (Boger *et al.*, 1999) y complestatina (Wang *et al.*, 2010), son ejemplos destacados del amplio rango de ciclopéptidos presentes en la naturaleza con elevada bioactividad y valor para el descubrimiento de nuevos fármacos. Aún así, la complejidad de estas estructuras conlleva preparaciones sintéticamente desafiantes donde la formación de las subestructuras de biaril o biaril éter se fundamentan en la preparación de intermedios biarílicos a través de reacciones intramoleculares tipo Suzuki, Negishi o Stille o bien mediante sustituciones nucleofílicas aromáticas. Así pues, el acceso a topologías simplificadas con el fin de explorar la diversificación estructural para modular su actividad constituye un campo de gran interés.

Los péptidos grapa (Lau *et al.*, 2015; Dharanipragada, 2013) son un tipo de arquitecturas restringidas estructuralmente que han emergido recientemente en la modulación de fármacos peptídicos. Se ha reportado que la formación de la grapa, formada por un enlace no amídico entre cadenas laterales, puede conferir mejoras en aspectos conformacionales y farmacocinético de péptidos relevantes (Walensky y Bird, 2014; Verdine y Hilinski, 2012).

Una de las primeras referencias sobre el aumento de la helicidad y estabilidad metabólica de un péptido gracias a esta aproximación fue reportada por el grupo de Verdine (Christian, Po y Verdine, 2000), el cual presentó una metodología basada en RCM, inspirada en los estudios pioneros previamente reportados por el grupo de Grubbs (Blackwell y Grubbs, 1998), y ampliamente aplicada en interacciones proteína-proteína. Otras técnicas para la formación de péptidos grapa reportadas incluyen: puentes disulfuro a partir de cadenas laterales de cisteínas naturales (Góngora-Benítez, Tulla-Puche y Albericio, 2014), uniones tipo oxima a través de la reacción de grupos hidroxilamina con 1,2-aminoalcoholes previamente oxidados a los correspondientes glioxil aldehídos (Haney, Loch y Horne, 2011), formación de enlaces tioéter vía la conexión entre unidades de Cys y cadenas laterales α -bromo amida (Brunel y Dawson, 2005), conectividades biarílicas que involucran derivados borilados de fenilalanina (Meyer *et al.*, 2012; Afonso, Feliu y Planas, 2011; Bois-Choussy, Cristau y Zhu, 2003; Carbonnelle y Zhu, 2000) y cicloadiciones azida-alquino (click) (Scrima *et al.*, 2010). Cada metodología tiene sus ventajas y desventajas específicas; la elección del método dependerá de las particularidades de cada caso. Algunos de los inconvenientes incluyen: síntesis de aminoácidos químicamente

modificados, inestabilidad química, o difícil modulación estructural para mejorar la versatilidad de los compuestos generados. Por esta razón, la formación de péptidos grapa es un campo emergente en continuo crecimiento y desarrollo.

MODIFICACIÓN OXIDATIVA C-H DE DKPS BASADAS EN TRP

2,5-Diketopiperazinas (DKPs), formadas por la ciclocondensación de dos α -aminoácidos, constituyen los derivados cíclicos peptídicos más pequeños en la naturaleza. Su estructura tridimensional bien definida, su resistencia a proteólisis, la presencia de grupos dadores y aceptores para la formación de puentes hidrógeno que favorece su interacción con objetivos biológicos y su elevada diversidad estructural son características valiosas para el desarrollo de fármacos (Cherkupally *et al.*, 2015; Ressurreição *et al.*, 2011). Es lógico, pues, que este arquetipo se encuentre ampliamente extendido en productos naturales con un diverso espectro de propiedades biológicas (Borthwick, 2012).

Trp es un residuo que comúnmente se encuentra en DKPs c(AA-Trp) naturales (Nishanth, Mohandas y Nambisan, 2014; Wang *et al.*, 2012; Klausmeyer *et al.*, 2005), incluyendo brevianamida F [c(L-Pro-L-Trp)], la cual posee propiedades antibacterianas y antifúngicas (Mehdi *et al.*, 2009). Gracias a su inherente reactividad, las DKPs son sustratos privilegiados para acceder a topologías estructuralmente diversas (Gonzalez *et al.*, 2012). En este sentido, aunque las DKPs naturales policíclicas se encuentran ampliamente presentes en la naturaleza y constituyen estructuras de potencial interés, su síntesis representa un desafío sintético y se han descrito muy pocos precedentes de metodologías para la directa ciclación de DKPs (Amatov *et al.*, 2015; Cochrane *et al.*, 2012; Lim, Gallucci y Rajanbabu, 2010; El Kaim *et al.*, 2007; Baran, Guerrero y Corey, 2003).

La modificación oxidativa C-H de aminoácidos y péptidos para formar nuevos enlaces C-C o C-N es una herramienta atractiva para su diversificación estructural. Recientemente, la construcción selectiva de uniones C-C directamente a partir de dos enlaces C-H bajo condiciones oxidativas, conocido como reacciones de acoplamiento deshidrogenativo, ha atraído mucho interés (Girard, Knauber y Li, 2014; Yeung y Dong, 2011). Estas reacciones no requieren el uso de materiales de partida prefuncionalizados, lo cual reduce el número de etapas sintéticas necesarias, y también es beneficioso para la economía atómica del proceso. El principal reto de estas metodologías concierne la ubicuidad de los enlaces C-H, siendo la selectiva funcionalización de un enlace C-H el principal objetivo. Típicamente, estas reacciones implican el uso de un oxidante (ej. O_2 , peróxidos, DDQ, etc.) y, en muchos casos, están catalizadas por metales de transición (ej. Cu Pd, Fe, Ag, Ru, etc.) para la conexión de carbonos tipo Csp-H, Csp₂-H, e incluso Csp₃-H.

OBJETIVOS

En la presente tesis hemos investigado el desarrollo de nuevas metodologías para la modificación (arilación) selectiva del aminoácido Trp ya sea aislado o en secuencias peptídicas. Específicamente, nos propusimos los siguientes objetivos:

1) Arilación en C-2 del aminoácido Trp a través de un proceso de activación C-H mediado por paladio

Queremos desarrollar una metodología basada en un protocolo de activación C-H catalizado por paladio que permita la selectiva arilación intermolecular del aminoácido Trp en la posición C-2 del anillo de indol desprotegido. En concreto, pretendemos estudiar:

- Llevar a cabo una adaptación al Trp de las condiciones de reacción del proceso de activación C-H desarrolladas para el indol.
- Aplicar estas condiciones a la preparación de análogos arilados de brevianamida F.
- Estudiar la arilación directa del aminoácido Trp y de otros sistemas de indol relacionados para la preparación de una pequeña librería de compuestos.
- Estudiar la incorporación de aminoácidos de Trp arilados en C-2 de indol en secuencias peptídicas modelo.
- Aplicar la metodología a péptidos bioactivos y evaluar su actividad farmacológica contra determinadas dianas terapéuticas.

2) Aminoácido fluorógeno Trp-BODIPY para sondas de visualización basadas en péptidos

Al no haber precedentes en la literatura de aminoácidos de Trp basados en BODIPY, nos planteamos la unión de este grupo en la posición C-2 de indol, mediante el protocolo de activación C-H desarrollado en el capítulo 1, para la síntesis de péptidos fluorogénicos relevantes. En particular, abordamos los siguientes objetivos:

- Sintetizar un derivado con BODIPY del péptido antifúngico PAF26 para visualizar infecciones fúngicas en células.

Propusimos que el reemplazo de un residuo de Trp por el fluorógeno Trp-BODIPY podría dar lugar a una nueva sonda para visualizar infecciones fúngicas, puesto que no alteraría las propiedades químicas de PAF26 (ej. balance de cargas, polaridad global, patrón de puentes de hidrógeno, etc.) claves para su actividad.

- Sintetizar un mimético cíclico de lactaderina con BODIPY para visualizar apoptosis en células. Basándonos en la reportada interacción del péptido cLac por unidades de PS localizadas en la superficie de células apoptóticas, se propuso reemplazar el residuo de Trp por Trp-BODIPY para así ejercer el mínimo impacto en la estructura original y obtener un agente no invasivo para visualizar apoptosis con independencia de Ca^{2+} .

3) Topologías biaril peptídicas a través de reacciones de activación C-H mediadas por paladio entre residuos de Trp y Phe/Tyr

El tercer principal objetivo de este trabajo se basa en la ciclación de péptidos a través del protocolo de activación C-H desarrollado en el capítulo 1. Específicamente, se planteó:

- Realizar una evaluación sistemática de los factores estructurales que determinan la ciclación en péptidos mediante el proceso de activación C-H.
- Aplicar esta metodología para ciclar péptidos bioactivos y evaluar su actividad farmacológica frente a determinadas dianas terapéuticas.
- Explorar el acceso a nuevas y complejas arquitecturas peptídicas.

4) Ciclación de acoplamiento cruzado deshidrogenativa mediada por Cu(II) de dicetopiperazinas basadas en Trp

El cuarto principal objetivo de la presente tesis se centra en el estudio de procesos intramoleculares de doble activación C-H sobre péptidos con Trp. En particular, queremos explorar procesos de acoplamiento cruzado deshidrogenativo en dicetopiperazinas que contengan Trp a través de un análisis sistemático de oxidantes y condiciones de reacción.

REFERENCIAS

- ACKERMANN, L. (2009), *Modern Arylation Methods*, Wiley-VCH, Weinheim: Weinheim.
- ACKERMANN, L., y A. V. LYGIN (2011), *Org. Lett.*, 13: 3332.
- AFONSO, A.; FELIU, L., y M. PLANAS (2011), *Tetrahedron*, 67: 2238.
- ALKHALAF, L. M., y K. S. RYAN (2015), *Chem. Biol.*, 22: 317.
- AMATOV, T.; POHL, R.; ČÍSAŘOVÁ, I. y U. JAHN (2015), *Angew. Chem. Int. Ed.*, 54: 12153.
- BARAN, P. S.; GUERRERO, C. A., y E. J. COREY (2003), *J. Am. Chem. Soc.*, 125: 5628.
- BIALONSKA, D., y J. K. ZJAWIONY (2009), *Mar. Drugs*, 7: 166.
- BLACKWELL, H. E., y R. H. GRUBBS (1998), *Angew. Chem. Int. Ed.*, 37: 3281.
- BOGER, D. L.; MIYAZAKI, S.; KIM, S. H.; WU, J. H.; CASTLE, S. L.; LOISELEUR, O., y Q. JIN (1999), *J. Am. Chem. Soc.*, 121: 10004.
- BOIS-CHOUSSY, M.; CRISTAU, P., y J. ZHU (2003), *Angew. Chem. Int. Ed.*, 42: 4238.
- BORTHWICK, A. D. (2012), *Chem. Rev.*, 112: 3641.
- BRUNEL, F. M., y P. E. DAWSON (2005), *Chem. Commun.*, 2552.
- CARBONNELLE, A.-C., y J. ZHU (2000), *Org. Lett.*, 2: 3477.
- CHERKUPALLY, P.; RAMESH, S.; JAD, Y. E.; GOVENDER, T.; KRUGER, H. G.; TORRE, B. G. DE LA, y F. ALBERICIO (2015), *In Privileged Scaffolds in Medicinal Chemistry: Design, Synthesis, Evaluation*; BRÅSE, S., Ed.; Royal Society of Chemistry, Cambridge: United Kingdom: 400–407.
- CHIN, J. W. (2014), *Annu. Rev. Biochem.*, 83: 379.
- COCHRANE, J. R.; WHITE, J. M.; WILLE, U., y C. A. HUTTON (2012), *Org. Lett.*, 14: 2402.
- COLLETTI, S. L.; LI, C.; FISHER, M. H.; WYVRATT, M. J., y P. T. Meinke (2000), *Tetrahedron Lett.*, 41: 7825.
- DAVIS, L., y J. W. CHIN (2012), *Nat. Rev. Mol. Cell Biol.*, 13: 168.
- DE MEIJERE, A., y F. DIEDERICH (2004), *Metal-Catalyzed Cross-Coupling Reactions*, Vol. 1, 2nd ed.; DE MEIJERE, A., DIEDERICH, F., Eds., Wiley-VCH, Weinheim, 2004.
- DEPREZ, N. R.; KALYANI, D.; KRAUSE, A., y M. S. SANFORD (2006), *J. Am. Chem. Soc.*, 128: 4972.

- DHARANIPRAGADA, R. (2013), *Futur. Med. Chem.*, 5: 831.
- DIAO, L., y B. MEIBOHM (2013), *Clin. Pharmacokinet.*, 52: 855.
- DUPREZ, L.; WIRAWAN, E.; BERGHE, T. VANDEN, y P. VANDENABEELE (2009), *Microbes Infect.*, 11: 1050.
- EL KAIM, L.; GAGEAT, M.; GAULTIER, L., y L. GRIMAUD (2005), *Synlett*, 500.
- FELIU, L., y M. PLANAS (2005), *Int. J. Pept. Res. Ther.*, 11: 53.
- FOSGERAU, K., y T. HOFFMANN (2015), *Drug Discov. Today*, 20: 122.
- GIRARD, S. A.; KNAUBER, T., C. LI (2014), In *From C-H to C-C Bonds: Cross-Dehydrogenative-Coupling*; LI, CH.-J., Ed.; The Royal Society of Chemistry: United Kindom: 1–32.
- GONZALEZ, J. F.; ORTIN, I.; DE LA CUESTA, E., y J. C. MENENDEZ (2012), *Chem. Soc. Rev.*, 41: 6902.
- GRIBBLE, G. W. (2010), *Topics in Heterocyclic Chemistry, Heterocyclic Scaffolds II: Reactions and Applications of Indoles*, Vol. 26; GRIBBLE, G. W., Ed.; Springer-Verlag Berlin Heidelberg: New York.
- GRIGG, R.; SRIDHARAN, V.; STEVENSON, P.; SUKIRTHALINGAM, S., y T. WORAKUN (1990), *Tetrahedron*, 46: 4003.
- GÓNGORA-BENÍTEZ, M.; TULLA-PUCHE, J., y F. ALBERICIO (2014), *Chem. Rev.*, 114: 901.
- HANEY, C. M.; LOCH, M. T., y W. S. HORNE (2011), *Chem. Commun.*, 47: 10915.
- HIGUCHI, K., y T. KAWASAKI (2005), *Nat. Prod. Rep.*, 22: 761.
- HONG, S. H.; KWON, Y.-C., y M. C. JEWETT (2014), *Front. Chem.*, 2: 34.
- HONG-HERMESDORF, A.; MIETHKE, M.; GALLAHER, S. D.; KROPAT, J.; DODANI, S. C.; CHAN, J.; BARUPALA, D.; DOMAILLE, D. W.; SHIRASAKI, D. I.; LOO, J. A.; WEBER, P. K.; PETT-RIDGE, J.; STEMMLER, T. L.; CHANG, C. J., y S. S. MERCHANT (2014), *Nat. Chem. Biol.*, 10: 1034.
- JOULE, J. A., y K. MILLS (2010), *Heterocyclic Chemistry*, 5th ed.; John Wiley & Sons: Chichester.
- KLAUSMEYER, P.; MCCLOUD, T. G.; TUCKER, K. D.; CARDELLINA, J. H., y R. H. SHOEMAKER (2005), *J. Nat. Prod.*, 68: 1300.
- KOOPMANS, T.; VAN HAREN, M.; VAN UFFORD, L. Q.; BEEKMAN, J. M., y N. I. MARTIN (2013), *Bioorganic Med. Chem.*, 21: 553.
- KOWADA, T.; MAEDA, H., y K. KIKUCHI (2015), *Chem. Soc. Rev.*, 44: 4953.
- Krueger, A. T., y B. Imperiali (2013), *ChemBioChem*, 14: 788.
- LAU, Y. H.; DE ANDRADE, P.; WU, Y., y D. R. SPRING (2015), *Chem. Soc. Rev.*, 44: 91.
- Lee, J. S.; Kang, N. Y.; Yun, K. K.; Samanta, A.; Feng, S.; Hyeong, K. K.; Vendrell, M.; Jung, H. P., e Y. T. Chang (2009), *J. Am. Chem. Soc.*, 131: 10077.
- LIM, H. J.; GALLUCCI, J. C., y T. V. RAJANBABU (2010), *Org. Lett.*, 12: 2162.
- LÓPEZ-GARCÍA, B.; PÉREZ-PAYÁ, E.; JOSE, F., y J. F. MARCOS (2002), *Appl. Environ. Microbiol.*, 68: 2453.
- MAITY, J.; HONCHARENKO, D., y R. STRÖMBERG (2015), *Tetrahedron Lett.*, 56: 4780.
- MEHDI, R. B. A.; SHAABAN, K. A.; REBAI, I. K.; SMAOUI, S.; BEJAR, S., y L. MELLOULI (2009), *Nat. Prod. Res.*, 23: 1095.
- MEYER, F.-M.; COLLINS, J. C.; BORIN, B.; BRADOW, J.; LIRAS, S.; LIMBERAKIS, C.; MATHIOWETZ, A. M.; PHILIPPE, L.; PRICE, D.; SONG, K., y K. James (2012), *J. Org. Chem.*, 77: 3099.
- MUÑOZ, A.; HARRIES, E.; CONTRERAS-VALENZUELA, A.; CARMONA, L.; READ, N. D., y J. F. MARCOS (2013), *PLoS One*, 8: e54813.
- NAZARI, M.; MINAI-TEHRANI, A., y R. EMAMZADEH (2014), *Rsc Adv.*, 4: 45128.
- NISHANTH KUMAR, S.; MOHANDAS, C., y B. NAMBISAN (2014), *Peptides*, 53: 48.

- OHTA, A. (1989), *Chem. Pharm. Bull.*, 37: 1477.
- PHIPPS, R. J.; GRIMSTER, N. P., y M. J. GAUNT (2008), *J. Am. Chem. Soc.*, 130: 8172.
- RESSURREIÇÃO, A. S. M.; DELATOUCHE, R.; GENNARI, C., y U. PIARULLI (2011), *Eur. J. Org. Chem.*, 217.
- SAINLOS, M., y B. IMPERIALI (2007), *Nat. Protoc.*, 2: 3210.
- SANDTORV, A. H. (2015), *Adv. Synth. Catal.*, 357: 2403.
- SANTIVERI, C. M., y M. A. JIMÉNEZ (2010), *Pept. Sci.*, 94: 779.
- SCHAFMEISTER, C. E.; PO, J., y G. L. VERDINE (2000), *J. Am. Chem. Soc.*, 122: 5891.
- SCRIMA, M.; LE CHEVALIER-ISAAD, A.; ROVERO, P.; PAPINI, A. M.; CHOREV, M., y A. M. D'URSI (2010), *European J. Org. Chem.*, 446.
- SEWALD, N., y H.-D. Jakubke (2002), *Peptides : Chemistry and Biology*; Wiley-VCH, Weinheim.
- SOCHER, E., y B. IMPERIALI (2013), *ChemBioChem*, 14: 53.
- STUART, D. R.; VILLEMURE, E., y K. FAGNOU (2007), *J. Am. Chem. Soc.*, 129: 12072.
- TRANSPARENCY MARKET RESEARCH (2016), *Peptide Therapeutics Market - Global Industry Analysis, Size, Share, Growth, Trends and Forecast 2014 - 2020*.
- TROST, B. M.; GODLESKI, S. A., y J. P. GENET (1978), *J. Am. Chem. Soc.*, 100: 3930.
- TSOMAIA, N. (2015), *Eur. J. Med. Chem.*, 94: 459.
- VENKATRAMAN, P.; NGUYEN, T. T.; SAINLOS, M.; BILSEL, O.; CHITTA, S.; IMPERIALI, B., y L. J. STERN (2007), *Nat. Chem. Biol.*, 3: 222.
- VERDINE, G. L., y G. J. HILINSKI (2012), *In Methods in Enzymology*; WITTRIP, K. D., VERDINE, G. L., Eds.; Elsevier Inc.: United States of America, Vol. 503: 3–33.
- VÁZQUEZ-ROMERO, A.; KIELLAND, N.; ARÉVALO, M. J.; PRECIADO, S.; MELLANBY, R. J.; FENG, Y.; LAVILLA, R., y M. VENDRELL (2013), *J. Am. Chem. Soc.*, 135: 16018.
- WADE, L. G. J. (2010), *In Organic Chemistry. Chapter 24: Amino acids, peptides, and proteins*: 1153–1199.
- WALENSKY, L. D., y G. H. BIRD (2014), *J. Med. Chem.*, 57: 6275.
- WANG, F.-Z.; HUANG, Z.; SHI, X.-F.; CHEN, Y.-C.; ZHANG, W.-M.; TIAN, X. P.; LI, J., y S. ZHANG (2012), *Bioorg. Med. Chem. Lett.*, 22: 7265.
- WANG, L.; BROCK, A.; HERBERICH, B., y P. G. SCHULTZ (2001), *Science*, 292: 498.
- WANG, X.; GRIBKOV, D. V., y D. SAMES (2007), *J. Org. Chem.*, 72: 1476.
- WANG, Z.; BOIS-CHOUSSEY, M.; JIA, Y., J. ZHU (2010), *Angew. Chem. Int. Ed.*, 49: 2018.
- WENCEL-DELDORF, J., F. GLORIUS (2013), *Nat. Chem.*, 5: 369.
- WHITE, M. C. (2012), *Synlett*, 23: 2746.
- XIAO, H.; CHATTERJEE, A.; CHOI, S.-H.; BAJJURI, K. M.; SINHA, S. C., y P. G. SCHULTZ (2013), *Angew. Chem. Int. Ed.*, 52: 14080.
- YAMAGUCHI, J.; YAMAGUCHI, A. D., y K. ITAMI (2012), *Angew. Chem. Int. Ed.*, 51: 2.
- YANG, S. D.; SUN, C. L.; FANG, Z.; LI, B. J.; LI, Y. Z., y Z. J. SHI (2008), *Angew. Chem. Int. Ed.*, 47: 1473.
- YEUNG, C. S., y V. M. DONG (2011), *Chem. Rev.*, 111: 1215.
- YU, J.-Q., y Z. SHI (2010), *Topics in Current Chemistry, C-H activation*, vol 292; Yu, J.-Q., SHI, Z., Eds.; Springer: Berlin Heidelberg.
- ZHAO, J.; ZHANG, Y., y K. CHENG (2008), *J. Org. Chem.*, 73: 7428.
- ZHENG, H.; WANG, F.; WANG, Q., y J. GAO (2011), *J. Am. Chem. Soc.*, 133: 15280.

 funcas

PREMIOS
ENRIQUE
FUENTES
QUINTANA

2018

Pedidos e información:

Funcas

Caballero de Gracia, 28

28013 Madrid

Teléfono: 91 596 54 81

Fax: 91 596 57 96

publica@funcas.es

www.funcas.es

P.V.P.: Edición papel, 12€ (IVA incluido)

P.V.P.: Edición digital, gratuita

ISBN 978-84-17609-11-5



TESIS CIENCIAS DE LA SALUD 2016-2017

Premios Enrique Fuentes Quintana de Tesis Doctorales

INDOLE ARYLATION IN TRYPTOPHAN RESIDUES: DEVELOPMENT OF NEW CHEMICAL METHODOLOGIES, SYNTHETIC STUDIES AND BIOLOGICAL EVALUATION OF MODIFIED PEPTIDES VOLUME II

Lorena Mendive Tapia

TESIS CIENCIAS DE LA SALUD 2016-2017

Premios Enrique Fuentes Quintana de Tesis Doctorales



**INDOLE ARYLATION IN TRYPTOPHAN
RESIDUES: DEVELOPMENT OF NEW
CHEMICAL METHODOLOGIES,
SYNTHETIC STUDIES AND
BIOLOGICAL EVALUATION
OF MODIFIED PEPTIDES**

VOLUME II

Lorena Mendive Tapia

Funcas

PATRONATO

ISIDRO FAINÉ CASAS
JOSÉ MARÍA MÉNDEZ ÁLVAREZ-CEDRÓN
FERNANDO CONLLEDO LANTERO
CARLOS EGEA KRAUEL
MIGUEL ÁNGEL ESCOTET ÁLVAREZ
AMADO FRANCO LAHOZ
MANUEL MENÉNDEZ MENÉNDEZ
PEDRO ANTONIO MERINO GARCÍA
ANTONIO PULIDO GUTIÉRREZ
VÍCTORIO VALLE SÁNCHEZ
GREGORIO VILLALABEITIA GALARRAGA

DIRECTOR GENERAL

CARLOS OCAÑA PÉREZ DE TUDELA

Impreso en España
Edita: Funcas

Caballero de Gracia, 28, 28013 - Madrid
© Funcas

Todos los derechos reservados. Queda prohibida la reproducción total o parcial de esta publicación, así como la edición de su contenido por medio de cualquier proceso reprográfico o fónico, electrónico o mecánico, especialmente imprenta, fotocopia, microfilm, *offset* o mimeógrafo, sin la previa autorización escrita del editor.

ISBN (obra completa): 978-84-17609-07-8
ISBN (volumen II): 978-84-17609-09-2
ISBN (digital): 978-84-17609-12-2
Depósito legal: M-38987-2018
Maquetación: Funcas
Imprime: Cecabank

Esta tesis doctoral ha sido distinguida con el
PREMIO ENRIQUE FUENTES QUINTANA DE TESIS DOCTORALES,
CATEGORÍA DE CIENCIAS DE LA SALUD,
en la convocatoria 2016-2017

Tesis doctoral presentada en la
Universitat de Barcelona
Departament de Química Orgànica

Directores de la tesis:
Rodolfo Lavilla Grifols
Fernando Albericio Palomera

VOLUME I

AGRADECIMIENTOS	13
ANNEX	21
ANNEX 1. ABBREVIATIONS AND ACRONYMS	23
ANNEX 2. TABLES OF REAGENTS FOR SOLID-PHASE PEPTIDE SYNTHESIS	24
INTRODUCTION AND OBJECTIVES	29
GENERAL INTRODUCTION	31
C-2 ARYLATION OF INDOLE THROUGH METAL-CATALYZED C-H ACTIVATION	39
PEPTIDE-BASED IMAGING PROBES	41
BIARYL PEPTIDIC TOPOLOGIES. STAPLED PEPTIDES	44
C-H OXIDATIVE MODIFICATION OF TRP-BASED DKPS	48
OBJECTIVES	50
REFERENCES	53
CHAPTER 1. C-2 ARYLATION OF TRP AMINO ACIDS THROUGH PD-CATALYZED C-H ACTIVATION	57
PUBLICATION I. Synthesis and biological evaluation of a postsynthetically modified Trp-based diketopiperazine	59
PUBLICATION II. Synthesis of C-2 arylated tryptophan amino acids and related compounds through palladium-catalyzed C–H activation	73
PUBLICATION III. Enhanced antimicrobial activity of a peptide derived from human lysozyme by arylation of its tryptophan residues	91
CHAPTER 2. SPACER-FREE TRP-BODIPY FLUOROGEN FOR PEPTIDE-BASED IMAGING PROBES	105
PUBLICATION IV. Spacer-free BODIPY fluorogens in antimicrobial peptides for direct imaging of fungal infection in human tissue	107

PUBLICATION V. A Trp-BODIPY cyclic peptide for fluorescence labelling of apoptotic bodies	129
PUBLICATION VI. A Trp-BODIPY fluorogenic amino acid to label peptides for enhanced live-cell fluorescence imaging	147
CHAPTER 3. BIARYL PEPTIDIC TOPOLOGIES THROUGH PD-CATALYZED C-H ACTIVATION REACTIONS BETWEEN TRP AND PHE/TYR RESIDUES	197
PUBLICATION VII. New peptide architectures through C–H activation stapling between tryptophan–phenylalanine/tyrosine residues	199
PUBLICATION VIII. Constrained cyclopeptides: biaryl formation through Pd-catalyzed C-H activation in peptides—structural control of the cyclization vs. cyclodimerization outcome	233
CHAPTER 4. CU(II) CROSS-DEHYDROGENATIVE CYCLIZATION OF TRP-BASED DKPS	251
PUBLICATION IX. Access to new scaffolds through cross dehydrogenative couplings on tryptophan-based diketopiperazines	253
RESULTS AND DISCUSSION	267
CHAPTER 1. C-2 ARYLATION OF TRP AMINO ACIDS THROUGH PD-CATALYZED C-H ACTIVATION	269
CHAPTER 2. SPACER-FREE TRP-BODIPY FLUOROGEN FOR PEPTIDE-BASED IMAGING PROBES	273
CHAPTER 3. BIARYL PEPTIDIC TOPOLOGIES THROUGH PD-CATALYZED C-H ACTIVATION REACTIONS BETWEEN TRP AND PHE/TYR RESIDUES	280
CHAPTER 4. CU(II) CROSS-DEHYDROGENATIVE CYCLIZATION OF TRP-BASED DKPS	289
REFERENCES	293
CONCLUSIONS (IN SPANISH)	295

PERSONAL CONTRIBUTION TO THE PUBLICATIONS (IN SPANISH)	301
---	------------

ANNEX 3. SUMMARY OF INTRODUCTION AND OBJECTIVES (IN SPANISH)	307
---	------------

VOLUME II

ANNEX 4. SUMMARY OF RESULTS AND DISCUSSION (IN SPANISH)	333
--	------------



VOLUME II



ANNEX 4. SUMMARY OF RESULTS AND DISCUSSION (IN SPANISH)

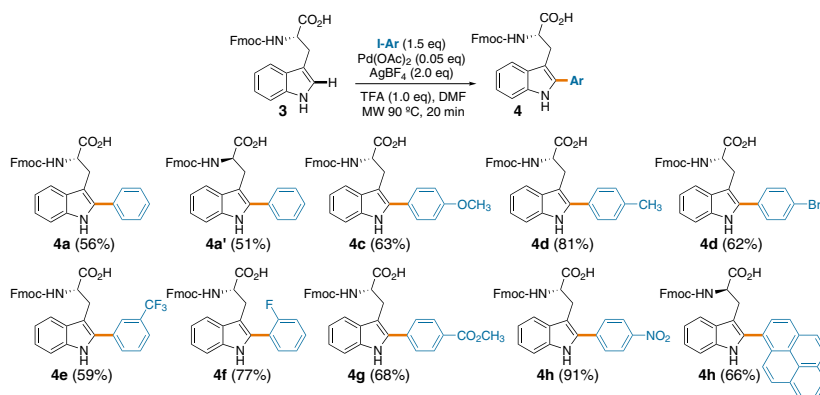
CAPÍTULO 1. ARILACIÓN EN C-2 DEL AMINOÁCIDO TRP A TRAVÉS DE ACTIVACIÓN C-H CATALIZADA POR PALADIO

En base a los precedentes establecidos, previamente se llevaron a cabo una serie de estudios preliminares de arilación en C-2 de indol del aminoácido Trp por el Dr. Javier Ruíz. En estos experimentos, el triptófano en forma de éster metílico y protegido en el extremo amino terminal con el grupo acetilo (Ac-Trp-OMe) (**1**) fue convenientemente arilado con diversos iodoarilos en rendimientos moderados o altos. Este proceso se llevó a cabo bajo irradiación de microondas con I-Ar (4.0 eq), Pd(PAc)₂ (0.05 eq), AgBF₄ (1.0 eq), 2-NO₂BzOH (1.5 eq) en DMF a 150 °C. El triptófano en su forma totalmente desprotegida resultó no ser apto para estas condiciones.

En colaboración con la Dra. Sara Preciado, exploramos diferentes condiciones (combinaciones de disolventes, aditivos, temperaturas y tiempos de reacción) y aplicamos un protocolo optimizado para la arilación de dicetopierazinas Trp-Pro (brevianamida F). Esta modificación dio lugar a una serie de derivados arilados con baja o moderada actividad antitumoral en cuatro líneas celulares de cáncer humano en comparación con brevianamida F, la cual resultó ser casi inactiva.

Figura 53.

Arilación en C-2 de aminoácido mediante activación C-H catalizada por paladio



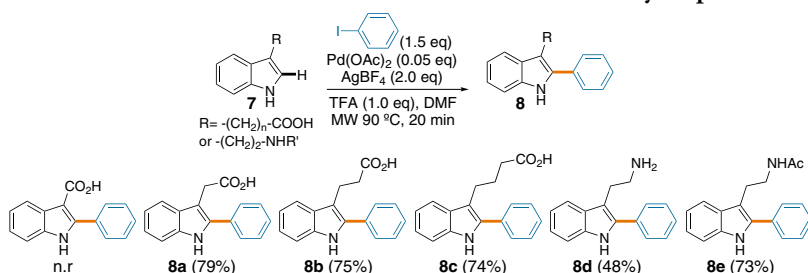
Fuente: Elaboración propia.

A continuación, iniciamos un nuevo proyecto con el fin de expandir el alcance de este protocolo de activación C-H. Así, el Fmoc-Trp-OH (**3**), comercialmente asequible, fue arilado con un amplio rango de diferentes iodoarilos tanto sustituidos con grupos electrón-dadores como electrón-atrayentes en rendimientos útiles (Fig. 53).

Es de destacar que la localización del sustituyente de yodo puede ser programada, dando lugar a *orto*, *meta* o *para* derivados arilados. Además, la incorporación de Fmoc-Trp(C₂-Ar)-OH directamente en fase sólida permite la preparación de secuencias peptídicas con un Trp arilado que estén desprotegidas en su extremo N-terminal y que

Figura 54.

Arilación en C-2 de indol de ácidos carboxílicos de indol y triptaminas

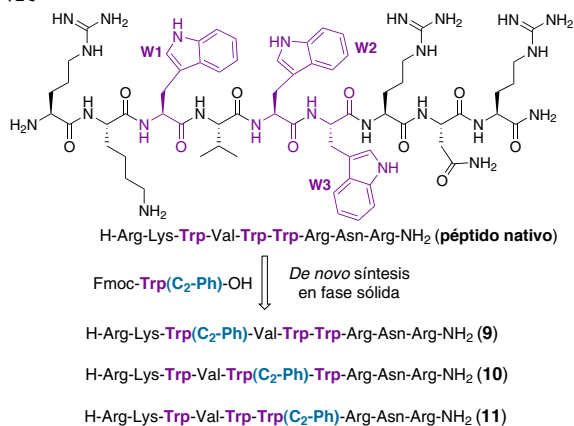


Fuente: Elaboración propia.

contengan diversos residuos de Trp. Con el fin de demostrar la potencial aplicabilidad del proceso, se arilaron en la posición C-2 de indol una serie de triptaminas y ácidos carboxílicos de indol (**7**), con la función ácida unida al anillo heteroaromático por diferentes espaciadores

Figura 55.

Estrategia sintética para la arilación selectiva del péptido antimicrobiano RKWVWWRNR



Fuente: Elaboración propia.

con buenos rendimientos (Fig. 54). Es de destacar la potencial bioactividad de estos nuevos derivados, cuyos precursores constituyen hormonas de plantas naturales o análogos involucrados en el crecimiento y desarrollo.⁷⁻¹⁰ En ensayos preliminares, los compuestos arilados se analizaron como agonistas de hormonas de plantas en callos. Pese a las evidencias iniciales de crecimiento que se observaron para algunos análogos, estos resultados no se mantuvieron en las siguientes generaciones.

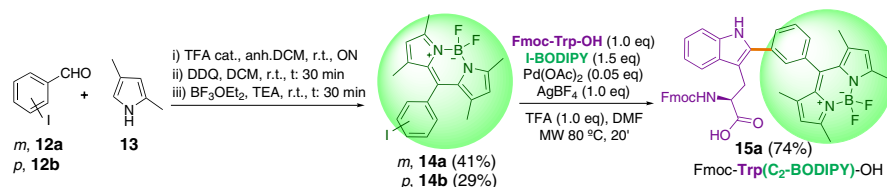
Como prueba de concepto, se propuso aumentar la actividad antimicrobiana de un péptido derivado del fragmento 107-115 del extremo C-terminal de la lisozima humana (107RKWVWWRNR115) mediante la arilación de sus residuos de Trp. El Fmoc-Trp(C₂-phenyl)-OH (**4a**) fue preparado a través de la arilación de Fmoc-Trp-OH con iodobenceno y su posterior incorporación en fase sólida permitió la síntesis de los tres posibles péptidos arilados en Trp (**9-11**) (Fig. 55). A continuación, se realizaron ensayos de inhibición de crecimiento en los microorganismos *Staphylococcus aureus* y *Staphylococcus epidermidis*. *S. aureus* fue totalmente inhibido en el caso del péptido arilado en la posición 112 (**11**), y solo un 10% cuando la arilación se realizó en los Trps 109 (**9**) o 111 (**10**), respecto al péptido no arilado. Por otro lado, *S. epidermidis* fue totalmente inhibido por los tres péptidos arilados así como por el péptido nativo.

CAPÍTULO 2. AMINOÁCIDO FLUORÓGENICO TRP-BODIPY PARA SONDAS DE VISUALIZACIÓN BASADAS EN PÉPTIDOS

En base a las síntesis de compuestos con BODIPY descritas en la literatura, se sintetizaron dos derivados con iodo-BODIPY a través la condensación de iodobenzaldehído con el sustituyente de iodo posicionado en *meta* (**12a**) o *para* (**12b**), respectivamente, con dos unidades de 2,4-dimetilpirrol (**13**), seguidos de la oxidación con DDQ y la complejación con BF₃ para dar lugar a los compuestos **14a** y **14b**. A continuación, estos derivados iodados se hicieron reaccionar con el Trp protegido en su extremo N-terminal con el grupo Fmoc, comercialmente asequible, a través del proceso de arilación C-H desarrollado por nuestro grupo (Fig. 56). Es de destacar que el derivado *m*-iodofenilo (**14a**) dio lugar al correspondiente Trp arilado con un rendimiento del 74%, mientras que la reacción con el análogo con el iodo posicionado en *para* (**14b**) resultó ser improductiva.

Figura 56.

Síntesis de Fmoc-Trp(C₂-BODIPY)-OH **15a**



Fuente: Elaboración propia.

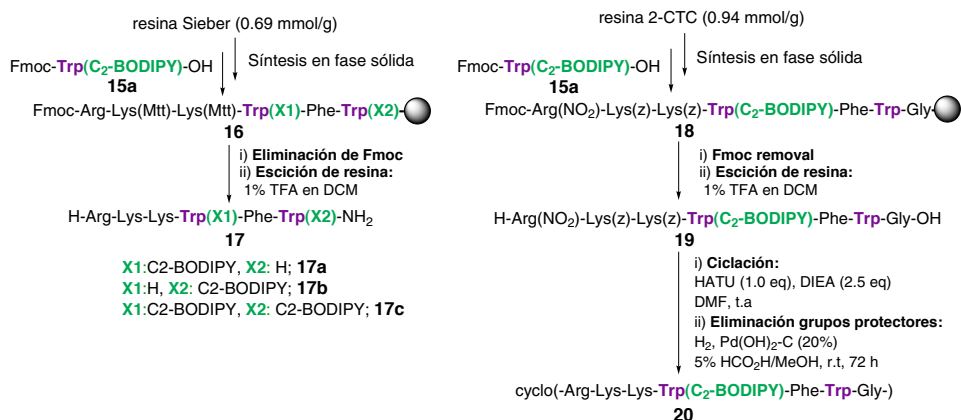
Experimentos espectroscópicos mostraron una fuerte emisión de fluorescencia de Fmoc-Trp(C₂-BODIPY)-OH **15a** en ambientes hidrofóbicos que podrían emular membranas de bicapas de fosfolípidos. Teniendo esta consideración en mente, se estudió la aplicación directa de este aminoácido fluorogénico para el marcaje de péptidos relevantes.

Derivados fluorogénicos del péptido antimicrobiano PAF26 para visualizar infecciones fúngicas

La preparación del péptido antifúngico PAF26-BODIPY se llevó a cabo mediante la incorporación directa del aminoácido fluorogénico Fmoc-(C₂-BODIPY)-OH (**15a**) en la síntesis en fase sólida (Fig. 57, izquierda). La inestabilidad del grupo BODIPY a medios ácidos fue un punto clave que fue cuidadosamente contemplado durante el diseño sintético. Con el fin de aumentar la estabilidad frente a proteasas, también se llevó a cabo la preparación de un análogo cíclico (Fig. 57, derecha).

Figura 57.

Síntesis en fase sólida de los análogos fluorescentes lineales (17a-c) y cíclico (20) del péptido PAF26



Fuente: Elaboración propia.

La actividad citotóxica de los derivados **17a-c** y **20** se ensayó frente al hongo *Aspergillus Fumigatus* así como en diversas cepas bacterianas comúnmente encontradas en infecciones pulmonares y en glóbulos rojos humanos. Notablemente, tanto los derivados lineales como el cíclico mostraron afinidad por *A. Fumigatus*, incluso ligeramente superior a la del análogo no etiquetado con el grupo fluorescente. Es más, sólo se observó una actividad marginal en células humanas o bacterianas para todos los derivados fluorogénicos.

La visualización *in vitro* de *A. Fumigatus* en co-cultivos con células epiteliales de pulmón mostró que los péptidos sintetizados específicamente marcan *A. Fumigatus* sin marcar las células humanas. No hay necesidad de etapas previas de lavado para la visualización ya que

el comportamiento fluorogénico de estos péptidos es dependiente del entorno hidrofóbico y, en consecuencia, la intensa emisión por fluorescencia solo aparece tras la interacción con las membranas fosfolipídicas de hongos. Adicionalmente, el análogo cíclico fluorescente **20** fue también analizado frente otras cepas fúngicas, demostrando su versatilidad para marcar infecciones fúngicas de diferente origen, y también se usó para la visualización directa y selectiva *ex vivo* usando microscopia multifotónica en tejido pulmonar humano de una cepa transgénica de *A. Fumigatus*.

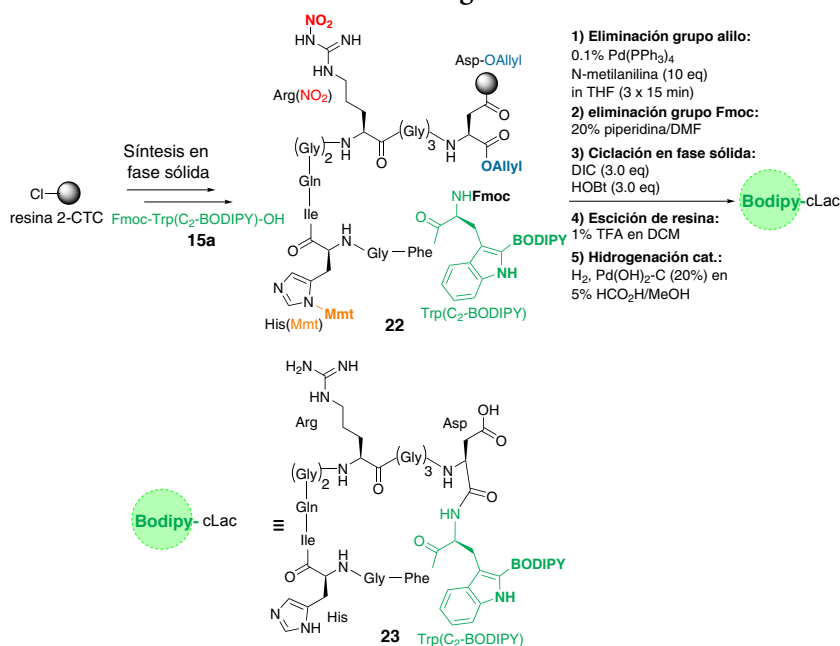
Visualización de apoptosis con un mimético fluorescente cíclico de lactaderina

En el contexto de marcaje del mimético peptídico de lactaderina, y teniendo presente la inestabilidad del grupo BODIPY a medios ácidos, se probaron diversas estrategias para encontrar el modo de ciclación y la combinación de grupos protectores ortogonales apropiados a las condiciones de escisión del péptido de la resina. Finalmente, se obtuvo el derivado fluorogénico de cLac a través de la ruta sintética mostrada en la Figura 58.

Con el objetivo de evaluar su afinidad con PS, en experimentos *in vitro* incubando el péptido fluorescente **23** en láminas lipídicas con diferentes proporciones de PS/PC se determinó que la emisión de fluorescencia del péptido es sensible a PS, mostrando una emisión muy baja solo con PC. A diferencia de Anexina V, este reconocimiento es independiente de Ca^{2+} . La afinidad lipídica también fue corroborada en experimentos de medida de tensoactividad

Figura 58.

Síntesis en fase sólida del derivado fluorogénico de cLac



Fuente: Elaboración propia.

mediante la determinación de la presión superficial en interfases lípido-acuosas a diferentes concentraciones del péptido. Ensayos de citometría de flujo confirmaron la especificidad del péptido por unidades de PS expuestas en cuerpos apoptóticos aislados de células humanas tipo BL2, mostrando el mismo tipo de perfil que Anexina V. También, en experimentos de microscopía confocal incubando el péptido BODIPY-cLac **23** con vesículas con PS se observó una mayor fluorescencia que en vesículas con solo PC.

CAPÍTULO 3. TOPOLOGÍAS BIARIL-PEPTÍDICAS A TRAVÉS DE REACCIONES C-H CATALIZADAS POR PALADIO ENTRE RESIDUOS DE TRP Y PHE/TYR

Con la finalidad de estudiar la arilación C-H en péptidos, se llevó a cabo una evaluación sistemática de los factores estructurales (longitud del péptido, número de aminoácidos entre Trp y I-Phe/Tyr, regioquímica de la unidad de iodoarilo, secuencia y concentración) que dictan el resultado de la ciclación. Así, el protocolo optimizado desarrollado en el capítulo 1 fue examinado en una serie representativa de secuencias peptídicas que contuvieran diversos aminoácidos (tabla 8).

Tabla 8.

Influencia del número de residuos (n) entre los residuos de m-I-Phe y Trp en la arilación C-H mediada por paladio^a

<i>i, i+n</i>	Péptido lineal (26)	Péptido ciclodímero	Péptido grapado	Conversión HPLC-MS (%)
<i>i, i+1</i>	Ac-Ala- <i>m</i> -I-Phe-Trp-Ala-OH (26a)	27a	n.d ^b	48
<i>i, i+2</i>	Ac-Ala- <i>m</i> -I-Phe-Val-Trp-Ala-OH (26b)	n.d	27b	71
<i>i, i+3</i>	H-Ala- <i>m</i> -I-Phe-Ser-Ala-Trp-Ala-OH (26c)	n.d	27c	39 ^c
<i>i, i+4</i>	Ac- <i>m</i> -I-Phe-Asn-Gly-Arg-Trp-NH ₂ (26d)	n.d	27d	77
<i>i, i+4</i>	Ac- <i>m</i> -I-Phe-Arg-Gly-Asp-Trp-NH ₂ (26e)	n.d	27e	70

Notas: ^a 5 mol % Pd(OAc)₂, AgBF₄ (2.0 eq), TFA (1.0 eq), DMF, MW 90 °C, 20 min. ^b n.d: no detectado. ^c Ciclo adicional de irradiación por microondas.

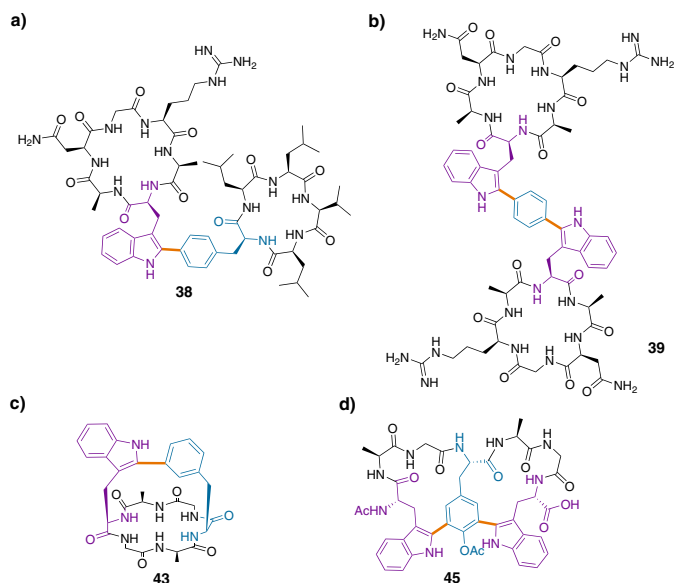
Fuente: Elaboración propia.

Cuando el protocolo de activación C-H se aplicó a secuencias con el sustituyente yodo localizado en la posición *orto*, solo se detectó reducción del enlace carbono-halógeno. Cabe destacar la exitosa aplicación de esta técnica para preparar péptidos grapa que contengan las secuencias de señalización tumoral de NGR y RGD (**27d** y **27e**, respectivamente). En ensayos de inhibición de adhesión celular en células HUVEC, la correspondiente forma grapada del péptido con NGR resultó ser un agonista selectivo para el receptor de integrina $\alpha v \beta 3$ (frente a $\alpha v \beta 5$), con una actividad EC₅₀ moderada (6 μ M) y siendo más potente que su precursor lineal **26e** (26 μ M). Adicionalmente, también se prepararon las correspondientes formas grapadas en fase sólida de dos péptidos con relevancia biológica y se abordó la preparación de compuestos peptídicos más complejos. Como prueba de concepto, se llevó a cabo la conexión intermolecular de un derivado del depsipéptido sansalvamide A (**36**), que tuviera un residuo de *p*-I-Phe, con un péptido de señalización (**37**) para dar el macrociclo conjugado **38**

(Fig. 59a). Este conjugado, no obstante, resultó inactivo. También se conjugaron dos péptidos de señalización (37) a través de una doble arilación C-H con una unidad de 1,4-diiodobenceno (Fig. 59b) para formar el compuesto 39 (Fig. 59b). A la luz de estos resultados, se exploró el acceso a topologías más complejas. Así, se generó el péptido puente bicíclico 43 aplicando directamente el proceso de activación C-H en fase sólida sobre la correspondiente secuencia precursora lineal seguido de una ciclación de los extremos terminales en solución (Fig. 59c).

Figura 59.

Proceso de activación C-H para la (a) conjugación intermolecular del ciclopeptido NGR (37) con un derivado de sansalvamáida (36), (b) doble conjugación del ciclopeptido (37) con una unidad de 1,4-diiodobenceno, (c) síntesis del péptido macrobicclico (43), (d) síntesis del péptido macrobicclico (45)



Fuente: Elaboración propia.

También, se preparó un quemotipo bicíclico fusionado a partir de una doble arilación C-H intramolecular sobre una secuencia precursora lineal que contenía un residuo de tirosina diiodada y dos unidades de triptófano (Fig. 59d).

Para completar la evaluación de los factores estructurales que determinan la ciclación o ciclodimerización de la reacción de activación C-H, se aplicó el protocolo sobre una serie de secuencias peptídicas *para*-iodadas (49a-d) con un número creciente de residuos (n) entre las unidades de Trp y p-I-Phe (Tabla 9) y se determinaron los requerimientos para una u otra evolución.

Recientemente, se ha explorado la funcionalización de DKPs en nuestro grupo (Fig. 60). Así, varias DKPs *o,m,p*-yodadas 51a-c se hicieron reaccionar en condiciones de la activación C-H desarrollada en el capítulo 1 para dar lugar a los correspondientes productos

Tabla 9.

Influencia del número de residuos (n) entre los residuos de *p*-I-Phe y Trp en la arilación C-H mediada por paladio^a

<i>i, i+n</i>	Péptido lineal (26)	Péptido ciclodímero	Péptido grapado	Conversión HPLC-MS (%)
<i>i, i+1</i>	Ac-Ala- <i>p</i> -I-Phe-Trp-Ala-OH (49a)	50a	n.d. ^a	60
<i>i, i+2</i>	Ac- <i>p</i> -I-Phe-Ala-Trp-Lys-OH (49b)	50b	n.d	54
<i>i, i+3</i>	Ac-Ala- <i>p</i> -I-Phe-Lys-Gly-Trp-Ala-OH (49c)	50c	50c ^b	23 / 51
<i>i, i+4</i>	Ac-Ala- <i>p</i> -I-Phe-Arg-Lys-Gly-Trp-Ala-OH (49d)	n.d	50d	81 ^c

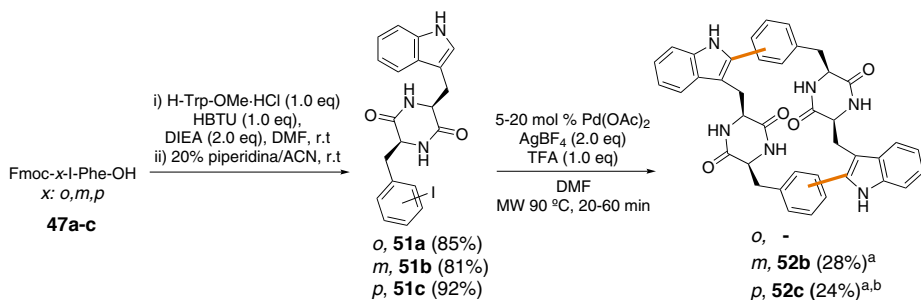
Notas: ^a 20 mol % Pd(OAc)₂, AgBF₄ (2.0 eq), TFA (1.0 eq), DMF, MW 90 °C, 20 min. ^b n.d: no detectado. ^c Ciclo adicional de irradiación de microondas

Fuente: Elaboración propia.

ciclodiméricos **52b-c** a partir de las regioquímicas *meta* y *para*, respectivamente. En este contexto, la reacción con el *orto*-derivado **51a** dio lugar a la reducción del enlace carbono-halógeno como principal producto junto con otra especie altamente oxidada detectable por espectrometría de masas. Este intrigante resultado nos empujó a investigar la naturaleza de este nuevo proceso en último capítulo de la presente tesis.

Figura 60.

Síntesis de DKPs diméricas **52b** y **52c**. ^[a] Rendimientos estimados en base al análisis de HPLC-MS. ^[b] Se efectuó un segundo ciclo de irradiación



Fuente: Elaboración propia.

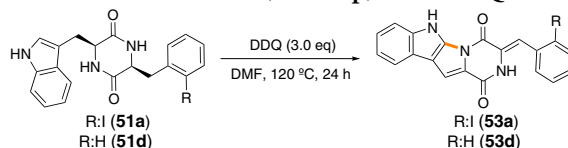
CAPÍTULO 4. CICLACIÓN DE ACOPLAMIENTO CRUZADO DESHIDROGENATIVA MEDIADA POR CU(II) DE DICETOPIPERAZINAS BASADAS EN TRP

Para poder aislar el subproducto y asignar la estructura del producto altamente oxidado detectado en la anterior reacción, se efectuó un estudio de diferentes condiciones oxidativas sobre el sustrato de DKP c(Phe-Trp) **51d**. El oxidante DDQ demostró ser el reactivo de elección y, con estas condiciones, el producto deseado fue convenientemente aislado y caracterizado. Los experimentos de espectrometría de masas y resonancia magnética permitieron la asignación estructural de la DKP policíclica altamente conjugada (**53d**) mostrando una triple oxidación (Fig. 61). Esta estructura se origina a través de una doble deshidrogenación

C $_{\alpha}$ -C $_{\beta}$ (Trp y Phe) y la formación de un enlace C-N entre la posición C-2 de indol y el grupo $^{\alpha}$ N del mismo residuo de Trp. Resultados análogos se obtuvieron con el derivado de DKP *orto* iodado c(*o*-I-Phe-Trp) **51a** (Fig. 61).

Figura 61.

Tratamiento oxidativo sobre la DKP c(Phe-Trp) con DDQ

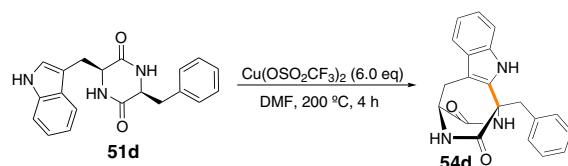


Fuente: Elaboración propia.

Teniendo en cuenta otros procesos de ciclación C-N descritos en la literatura, principalmente referidos al uso de oxidantes basados en Cu(II), Pd(II) o I(III), se ensayaron una serie de nuevas condiciones con el objetivo de optimizar esta nueva ciclación. El tratamiento oxidativo con Cu(OTf)₂ permitió el aislamiento y caracterización de un compuesto bicíclico diferente (**54d**), originado de una ciclación C-C deshidrogenativa entre la posición C-2 de indol de Trp y el C $^{\alpha}$ de Phe (Fig. 62).

Figura 62.

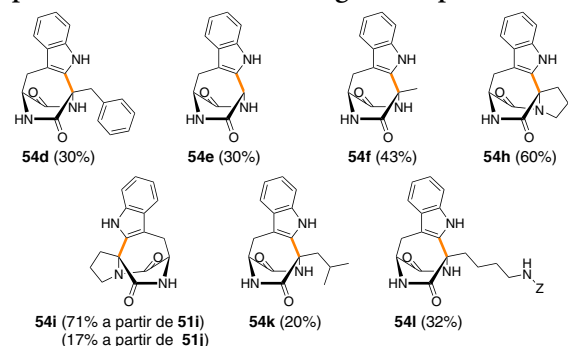
Tratamiento oxidativo sobre la DPC c(Phe-Trp) con Cu(OSO₂CF₃)₂



Fuente: Elaboración propia.

Figura 63.

Ciclación de acoplamiento cruzado deshidrogenativa para obtener las DKPs 54d-l



Fuente: Elaboración propia.

En vista de este resultado prometedor, se llevó a cabo una última optimización sobre la DKP c(Gly-Trp) **51e**. Con estas condiciones [Cu(OCOCF₃)₂ (4.0 eq), TFA (4.0 eq) en DMF, irradiación de microondas a 120 °C en 30 min], el alcance de esta reacción se extendió a otras DKPs conteniendo Trp. Así, una variedad de DKPs c(AA-Trp) (**51d-l**) resultaron reactivas en el proceso, incluyendo sustratos con residuos aromáticos, no-polares y polares, conduciendo a los correspondientes derivados oxidados **54d-l** (Fig. 63).



FULL SUPPORTING INFORMATION PUBLICATION I

Electronic Supplementary Material (ESI) for Medicinal Chemistry Communications
This journal is © The Royal Society of Chemistry 2013

Electronic Supplementary Information

Synthesis and Biological Evaluation of a Postsynthetically Modified Trp-Based Diketopiperazine

*Sara Preciado, Lorena Mendive-Tapia, Carolina Torres-García, Rubí
Zamudio-Vázquez, Vanessa Soto, Ricardo Pérez, Fernando
Albericio, Ernesto Nicolás, and Rodolfo Lavilla*

Electronic Supplementary Material (ESI) for Medicinal Chemistry Communications
This journal is © The Royal Society of Chemistry 2013

Table of Contents

General experimental information. Page 2.

Experimental procedures and characterization data for compounds. Page 2.

Spectroscopic data. Page 16.

Biological evaluation. Page 38.

Supporting Information

General experimental information.

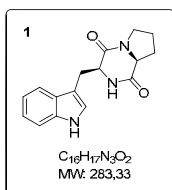
Unless stated otherwise, all reactions were carried out under argon atmosphere in dried glassware. Commercially available reactants were used without further purification. Thin-layer chromatography was performed on pre-coated Merk silica gel 60 F254 plates and visualized under a UV lamp. ^1H and ^{13}C NMR spectra were recorded on a Varian Mercury 400 (at 400 MHz and 100 MHz respectively). Unless otherwise quoted, NMR spectra were recorded in CDCl_3 solution with TMS as an internal reference. Data for ^1H -NMR spectra are reported as follows: chemical shift (δ ppm), multiplicity, integration and coupling constants (Hz). Data for ^{13}C -NMR spectra are reported in terms of chemical shift (δ ppm). Signals were assigned as far as possible by means of two-dimensional NMR spectroscopy: ^1H - ^1H -COSY, ^1H - ^{13}C -COSY (HSQC: Heteronuclear Single Quantum Coherence) and long-range ^1H - ^{13}C -COSY (HMBC: Heteronuclear Multiple Bond Connectivity). IR spectra were recorded using a Thermo Nicolet Nexus spectrometer and are reported in frequency of absorption (cm^{-1}). High Resolution Mass Spectrometry was performed by the University of Barcelona Mass Spectrometry Service.

Abbreviations

Abbreviation used for amino acids and designations of peptides follow the rules of the IUPAC-IUB Commission of Biochemical Nomenclature in *J. Biol. Chem.* 247, 977-983 (1982). The following additional abbreviations are used: ACN: acetonitrile, DMF: *N,N*-dimethylformamide, DCM: dichloromethane, Fmoc: 9*H*-fluorenylmethoxycarbonyl, DIPEA: *N,N*-diisopropylethylamine, DIPCDI: *N,N'*-diisopropylcarbodiimide, Et₂O: diethyl ether, HOAt: 1-hydroxy-7-azabenzotriazole, HOBt: Hydroxybenzotriazole, TFA: trifluoroacetic acid, TIS: triisopropylsilane. RP-HPLC: reverse-phase high performance liquid chromatography, HRMS: high-resolution mass spectrometry, NMR: nuclear magnetic resonance, SPPS: solid-phase peptide synthesis, IR: infrared spectroscopy.

Experimental procedures and characterization data for compounds

Solid-Phase Synthesis of Brevianamide F (1)



Aminomethyl-polystyrene resin (0.37 mmol^{-1} , 5 g, 1.85 mmol) was introduced into a polypropylene syringe fitted with a porous polystyrene frit and was washed successively with DCM (10×30s), TFA (40% v/v) in DCM (1×1 min and 2×10 min), DCM (5×30s), DIEA (5% v/v) in DCM (6×2 min), DCM (5×30s), DMF (5×30s) and DCM (5×30s). 4-[(3,4-Dihydro-2*H*-pyran-2-yl)methoxy]benzoic acid (1.30 g, 5.55 mmol), DIPCDI (0.85 mL, 5.49 mmol) and ethyl cyanoglyoxyl-2-oxime (0.7 g, 5.55 mmol) in DCM (40 mL) were then added and the mixture was

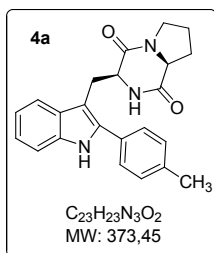
Electronic Supplementary Material (ESI) for Medicinal Chemistry Communications
This journal is © The Royal Society of Chemistry 2013

allowed to stand for 1 h at rt with occasional manual stirring. The resin was then washed with DCM (5×30s). Fmoc-Trp-OAl (1.3 g, 2.79 mmol) and PPTS (1.1 g, 4.38 mmol) in DCE were then added to the handle-resin and the suspension was shaken at 80 °C for 16 h in an Advanced Chemtech PLS 4x4 organic synthesizer. After cooling to rt the aminoacyl-resin was washed successively with DCM (5×30s), DMF (5×30s) and MeOH (5×30s). Spectrophotometric quantification of the dibenzofulvene-piperidine adduct indicated a 76% yield for amino acid coupling. After washing with DMF (5×30s) and DCM (5×30s) this resin was placed under Ar and Pd(PPh₃)₄ (0.86 g, 0.74 mmol) and PhSiH₃ (11 mL, 89.24 mmol) in DCM (40 mL) were added. The mixture was shaken for 30 min at rt, filtered and washed with DCM (8×30s). A second treatment with Pd(PPh₃)₄ and PhSiH₃ in DCM was then carried out. After filtration the resin was washed successively with DCM (8×30s), diethyl dithiocarbamate (5% v/v) in DMF (2×5 min), DMF (5×1 min), DCM (5×30s) and DMF (5×30s). The resin was then treated with H-Pro-OMe-HCl (0.72 g, 5.57 mmol), PyBOP (2.90 g, 5.57 mmol) and DIEA (3 mL, 17.22 mmol) in DMF (40 mL) for 60 min with occasional manual stirring. The resin was washed with DCM (5×30s) and DMF (5×30s). This coupling reaction and washing cycle was then repeated twice using the same quantities of reagents and solvents. The resulting resin was treated with piperidine (20% v/v) in DMF (2×10 min), was washed with DMF (5×30s) and DCM (5×30s) and dried. Cleavage of the product from the resin was brought about by treatment with TFA/*m*DMB/DCM (5:5:90 v/v) (3×10 min) and the collected washings were submitted to solvent removal. The crude product was washed with hexanes and the remaining solid was centrifuged (10 min at 6000 rpm) and filtered, affording **1** as a foamy white solid (0.37 g, 71 %).

¹H-NMR (400 MHz, DMSO-d₆) δ 1.37 (m, 1H), 1.64 (m, 2H), 1.95 (m, 1H), 3.08 (dd, *J* = 14.9, 5.7 Hz, 1H), 3.26 (m, 2H), 3.39 (m, 1H), 4.04 (bt, *J* = 8.3 Hz, 1H), 4.29 (bt, *J* = 4.9 Hz, 1H), 6.95 (bt, *J* = 7.5 Hz, 1H), 7.05 (bt, *J* = 7.5 Hz, 1H), 7.18 (d, *J* = 2.1 Hz, 1H), 7.32 (d, *J* = 8.2 Hz, 1H), 7.56 (d, *J* = 7.9 Hz, 1H), 7.72 (s, 1H), 10.9 (s, 1H) ppm. ¹³C-NMR (100 MHz, DMSO-d₆): δ 21.9, 25.8, 27.7, 44.6, 55.3, 58.4, 109.3, 111.2, 118.2, 118.7, 120.9, 124.4, 127.4, 136.0, 165.5, 169.1 ppm. IR (KBr, cm⁻¹) ν = 3290.93, 3262, 2873.42, 1675.84, 1654.62, 1620.88, 1457.92, 1451.17, 1428.99, 1341.25, 1301.72, 1242.9, 1223.61, 1109.83, 738.60, 693.28, 681.71, 642.18, 563.11, 431.98 cm⁻¹. HRMS (ESI) calcd for C₁₆H₁₈N₃O₂ (M+H)⁺ 284.1399, found 284.1394.

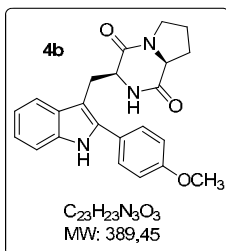
General procedure for the C2 arylation of the indole residue in brevianamide F:

Unless stated otherwise, Brevianamide F (1 equiv), aryl iodide (3 equiv), AgBF₄ (1 equiv), 2-nitrobenzoic acid (1.5 equiv) and Pd(OAc)₂ (5 % equiv) were placed in a microwave reactor vessel in a 1:1 mixture of DMF:PBS (total volume of 1200 μL). The mixture was heated under microwave irradiation (80 W) at 80°C for 15 min. When detailed, a second irradiation cycle (15 min) was performed, adding extra AgBF₄ (1 equiv) and Pd(OAc)₂ (5 % equiv). Ethyl acetate (60 mL) was added and the resulting suspension was filtered through Celite. The filtrate was successively washed with aqueous saturated solutions of NH₄Cl_{sat} (3x20 mL), NaHCO_{3 sat} (3x20 mL) and brine (3x20 mL), then the organic phase was dried over Na₂SO₄, filtered and the solvent was removed under vacuum. Unless otherwise quoted, the crude extract was purified by flash chromatography on silica gel (hexane/ethyl acetate) to obtain **4** as a pure product.

(3S,8aS)-3-((2-(*p*-Tolyl)-1*H*-indol-3-yl)methyl)hexahydropyrrolo[1,2-*a*]pyrazine-1,4-dione (4a)

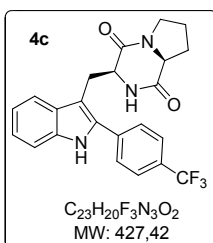
Compound **4a** was prepared according to the general procedure using 1-iodo-4-methylbenzene (492.8 mg, 2.26 mmol). The crude product was purified by flash chromatography on silica using methyl *tert*-butyl ether (MTBE) to obtain **4a** as a white solid (235.3 mg, 84 %).

¹H-NMR (400 MHz, $CDCl_3$): δ 8.26 (s, 1H), 7.59 (d, J = 7.9 Hz, 1H), 7.45 (d, J = 8.0 Hz, 2H), 7.40 (d, J = 8.1 Hz, 1H), 7.28 (s, 1H), 7.23 (dd, J = 8.1, 1.1 Hz, 1H), 7.19 – 7.13 (m, 1H), 5.46 (s, 1H), 4.36 (d, J = 9.3 Hz, 1H), 3.98 (s, 1H), 3.88 (dd, J = 15.2, 3.7 Hz, 1H), 3.58 (tt, J = 11.5, 10.3 Hz, 2H), 3.21 (dd, J = 15.2, 11.6 Hz, 1H), 2.40 (s, 3H), 2.31 – 2.24 (m, 1H), 2.00 (dd, J = 14.3, 7.8 Hz, 2H), 1.91 – 1.82 (m, 1H) ppm. **¹³C-NMR** (100 MHz, $CDCl_3$): 169.33, 165.74, 138.21, 136.75, 136.04, 129.79, 129.23, 128.32, 128.21, 122.66, 120.12, 118.39, 111.35, 105.67, 59.10, 54.54, 45.35, 28.14, 25.50, 22.57, 21.23 ppm. **IR** (Film, cm^{-1}) ν = 3365.84, 3282.56, 3051.96, 2975.09, 2949.47, 2923.84, 2879.00, 1668.33, 1463.35, 1424.91, 1303.20, 1258.36, 1104.63, 1014.95, 912.46, 829.18, 739.50, 656.23 cm^{-1} . **HRMS** (ESI) m/z calcd 374,1790 ($C_{23}H_{24}N_3O_2$) found 374.1873 ($M+H$)⁺.

(3S,8aS)-3-((2-(4-Methoxyphenyl)-1*H*-indol-3-yl)methyl)hexahydropyrrolo[1,2-*a*]pyrazine-1,4-dione (4b)

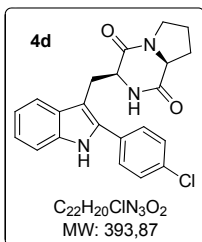
Compound **4b** was prepared according to the general procedure using 1-iodo-4-methylbenzene (528.9 mg, 2.26 mmol). The crude product was purified by flash chromatography on silica using methyl *tert*-butyl ether (MTBE) to obtain **4b** as a white solid (251.2 mg, 86 %).

¹H-NMR (400 MHz, $CDCl_3$): δ 9.05 (s, 1H), 7.55 (d, J = 7.8 Hz, 1H), 7.38 – 7.30 (m, 3H), 7.16 (dt, J = 14.9, 7.2 Hz, 2H), 6.80 (d, J = 8.5 Hz, 2H), 5.45 (s, 1H), 4.29 (d, J = 8.6 Hz, 1H), 3.90 (t, J = 7.8 Hz, 1H), 3.80 (dd, J = 15.1, 3.7 Hz, 1H), 3.74 (s, 3H), 3.51 (dt, J = 20.6, 6.5 Hz, 2H), 3.13 (dd, J = 15.1, 11.4 Hz, 1H), 2.20 (dd, J = 15.1, 8.9 Hz, 1H), 1.93 (dd, J = 16.9, 7.8 Hz, 2H), 1.84 – 1.74 (m, 1H) ppm. **¹³C-NMR** (100 MHz, $CDCl_3$): 169.33, 165.74, 159.50, 136.68, 136.02, 129.64, 128.30, 124.47, 122.49, 120.04, 118.31, 114.48, 111.36, 105.29, 59.08, 55.30, 54.52, 45.34, 28.12, 25.48, 22.56 ppm. **IR** (Film, cm^{-1}) ν = 3359.43, 3288.97, 3058.36, 2949.47, 2930.25, 2891.81, 2827.76, 1674.73, 1508.19, 1456.94, 1431.32, 1309.61, 1283.99, 1245.55, 1175.09, 1111.03, 1021.35, 835.59, 745.91 cm^{-1} . **HRMS** (ESI) m/z calcd 390,1739 ($C_{23}H_{24}N_3O_3$) found 390.1825 ($M+H$)⁺.

(3S,8aS)-3-((2-(4-(Trifluoromethyl)phenyl)-1H-indol-3-yl)methyl)hexahydropyrrolo[1,2-a]pyrazine-1,4-dione (4c)

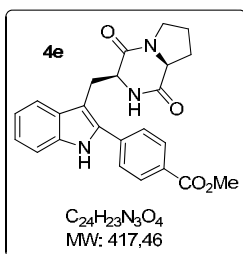
Compound **4c** was prepared according to the general procedure using 1-iodo-4-(trifluoromethyl)benzene (333 μ L, 2.26 mmol). The crude product was purified by flash chromatography on silica using methyl *tert*-butyl ether (MTBE) to obtain **4c** as a white solid (236.4 mg, 73%).

1H -NMR (400 MHz, $CDCl_3$): δ 8.42 (s, 1H), 7.69 (q, J = 8.6 Hz, 4H), 7.62 (d, J = 7.9 Hz, 1H), 7.43 (d, J = 8.1 Hz, 1H), 7.32 – 7.27 (m, 1H), 7.19 (t, J = 7.5 Hz, 1H), 5.41 (s, 1H), 4.38 (dd, J = 11.5, 2.8 Hz, 1H), 4.01 (t, J = 7.5 Hz, 1H), 3.91 (dd, J = 15.3, 3.9 Hz, 1H), 3.67 – 3.52 (m, 2H), 3.20 (dd, J = 15.3, 11.5 Hz, 2H), 2.29 (dt, J = 10.2, 7.0 Hz, 1H), 2.05 – 1.95 (m, 2H), 1.88 (dt, J = 9.0, 7.9 Hz, 1H) ppm. **^{13}C -NMR** (100 MHz, $CDCl_3$): δ 169.38, 165.44, 136.46, 135.71, 134.93, 129.89 (q, J = 32.7 Hz), 128.47, 128.08, 125.96, 125.93, 123.88 (q, J = 272.2 Hz), 123.53, 120.56, 118.75, 111.66, 107.24, 59.11, 54.43, 45.41, 28.18, 25.72, 22.50 ppm. **IR** (Film, cm^{-1}) ν = 3365.84, 3269.75, 3058.36, 2930.25, 2872.60, 1668.33, 1617.08, 1424.91, 1335.23, 1168.68, 1123.84, 1059.79, 1008.54, 912.46, 841.99, 733.10 cm^{-1} . **HRMS** (ESI) m/z calcd 428,1508 ($C_{23}H_{21}F_3N_3O_2$) found 428.1574 ($M+H$) $^+$.

(3S,8aS)-3-((2-(4-Chlorophenyl)-1H-indol-3-yl)methyl)hexahydropyrrolo[1,2-a]pyrazine-1,4-dione (4d)

Compound **4d** was prepared according to the general procedure using 1-chloro-4-iodobenzene (540.3 mg, 2.26 mmol). The crude product was purified by flash chromatography on silica using methyl *tert*-butyl ether (MTBE) to obtain **4d** as a white solid (213.7 mg, 72 %).

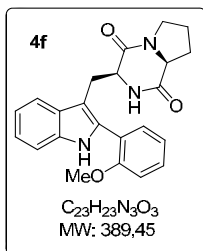
1H -NMR (400 MHz, $CDCl_3$): δ 8.29 (s, 1H), 7.60 (d, J = 8.0 Hz, 1H), 7.52 – 7.47 (m, 2H), 7.46 – 7.39 (m, 3H), 7.28 (dd, J = 7.1, 1.1 Hz, 1H), 7.25 (dd, J = 3.1, 0.8 Hz, 1H), 7.20 – 7.15 (m, 1H), 5.42 (s, 1H), 4.36 (dd, J = 11.5, 2.5 Hz, 1H), 4.00 (t, J = 7.4 Hz, 1H), 3.87 (dd, J = 15.2, 3.8 Hz, 1H), 3.58 (tdd, J = 11.9, 10.4, 5.8 Hz, 2H), 3.17 (dd, J = 15.2, 11.5 Hz, 1H), 2.35 – 2.25 (m, 1H), 2.03 – 1.94 (m, 2H), 1.92 – 1.83 (m, 1H) ppm. **^{13}C -NMR** (100 MHz, $CDCl_3$): 169.36, 165.51, 136.16, 135.36, 134.29, 130.56, 129.53, 129.33, 128.16, 123.20, 120.46, 118.61, 111.45, 106.52, 59.13, 54.42, 45.40, 28.19, 25.63, 22.55 ppm. **IR** (Film, cm^{-1}) ν = 3365.84, 3282.56, 3051.96, 2930.25, 2872.60, 1668.33, 1488.97, 1456.94, 1431.32, 1303.20, 1264.77, 1091.81, 1008.54, 829.18, 733.10 cm^{-1} . **HRMS** (ESI) m/z calcd 393,1244 ($C_{22}H_{20}ClN_3O_2$) found 394.1321 ($M+H$) $^+$.

Methyl 4-(3-(((3S,8aS)-1,4-dioxooctahydropyrrolo[1,2-a]pyrazin-3-yl)methyl)-1H-indol-2-yl)benzoate (4e)

Compound **4e** was prepared according to the general procedure using methyl 4-iodobenzoate (592.2 mg, 2.26 mmol). The crude product was purified by flash chromatography on silica using methyl *tert*-butyl ether (MTBE) to obtain **4e** as a white pale solid (298.3 mg, 95 %).

¹H-NMR (400 MHz, CDCl₃): δ 8.40 (s, 1H), 8.12 (d, *J* = 8.3 Hz, 2H), 7.65 (d, *J* = 8.3 Hz, 2H), 7.61 (d, *J* = 8.0 Hz, 1H), 7.43 (d, *J* = 8.1 Hz, 1H), 7.29 (d, *J* = 7.2 Hz, 1H), 7.18 (t, *J* = 7.4 Hz, 1H), 5.40 (s, 1H), 4.37 (d, *J* = 8.7 Hz, 1H), 3.99 (t, *J* = 7.8 Hz, 1H),

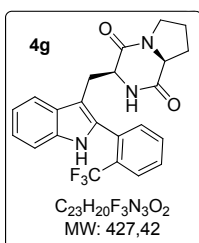
3.95 (s, 3H), 3.91 (d, *J* = 3.8 Hz, 1H), 3.67 – 3.52 (m, 2H), 3.23 (dd, *J* = 15.2, 11.5 Hz, 1H), 2.33 – 2.24 (m, 1H), 2.03 – 1.95 (m, 2H), 1.87 (dt, *J* = 15.4, 7.8 Hz, 1H) ppm. **¹³C-NMR** (100 MHz, CDCl₃): δ 169.35, 166.52, 165.43, 136.53, 136.33, 135.12, 130.41, 129.62, 128.32, 127.94, 123.63, 120.65, 118.79, 111.48, 107.68, 59.15, 54.45, 52.28, 45.40, 28.23, 25.73, 22.58 ppm. **IR** (Film, cm⁻¹) ν = 3378.27, 3282.17, 3064.34, 2949.02, 2878.55, 2840.11, 1718.96, 1667.71, 1603.64, 1430.66, 1276.90, 1110.33, 1007.83, 854.07, 770.78, 738.75, 687.50 cm⁻¹. **HRMS** (ESI) *m/z* calcd 418,1689 (C₂₃H₂₄N₃O₃) found 418.1768 (M+H)⁺.

(3S,8aS)-3-((2-(2-Methoxyphenyl)-1H-indol-3-yl)methyl)hexahydropyrrolo[1,2-a]pyrazine-1,4-dione (4f)

Compound **4f** was prepared according to the general procedure using 2-iodoanisole, 98 % (300.8 μL, 2.26 mmol). The crude product was purified by flash chromatography on silica using 100 % ethyl acetate to obtain **4f** as a pale solid (204.9 mg, 70 %).

¹H NMR (400 MHz, CDCl₃): δ 8.30 (s, 1H), 7.61 (d, *J* = 8.1 Hz, 1H), 7.46 – 7.34 (m, 3H), 7.26 – 7.22 (m, 1H), 7.19 – 7.12 (m, 1H), 7.06 (dd, *J* = 12.1, 4.7 Hz, 2H), 6.03 (s, 1H), 4.40 (d, *J* = 9.4 Hz, 1H), 4.00 (t, *J* = 8.1 Hz, 1H), 3.89 (s, 3H), 3.79 (dd, *J* = 15.1, 3.5 Hz, 1H), 3.56 (dt, *J* = 12.3, 8.9 Hz, 2H), 2.89 (dd, *J* = 15.1, 11.8 Hz, 1H), 2.32 –

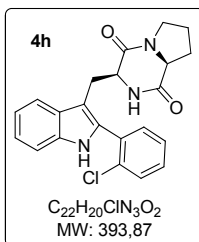
2.22 (m, 1H), 1.99 (ddd, *J* = 23.5, 13.1, 7.5 Hz, 2H), 1.91 – 1.80 (m, 1H) ppm. **¹³C NMR** (100 MHz, CDCl₃): δ 169.40, 166.14, 157.42, 136.16, 133.69, 132.05, 130.62, 127.41, 122.66, 121.05, 120.77, 119.90, 118.61, 111.26, 110.01, 59.30, 55.73, 54.41, 45.47, 28.19, 25.77, 22.85 ppm. **IR** (Film, cm⁻¹) ν = 3301.78, 3051.96, 2955.87, 2879.00, 2834.16, 1661.92 cm⁻¹. **HRMS** (ESI) *m/z* calcd 390.1812 (C₂₃H₂₃N₃O₃) found 390.1817 (M+H)⁺.

(3S,8aS)-3-((2-(2-(Trifluoromethyl)phenyl)-1H-indol-3-yl)methyl)hexahydropyrrolo[1,2-a]pyrazine-1,4-dione (4g)

Compound **4g** was prepared according to the general procedure using 1-(trifluoromethyl)-2-iodobenzene, 99 % (321.4 μ L, 2.26 mmol). A second irradiation cycle was performed. The crude product was purified by flash chromatography on silica using 100 % ethyl acetate to obtain **4g** as a pale solid (146.2 mg, 45%).

¹H NMR (400 MHz, $CDCl_3$): δ 8.39 (s, 1H), 7.83 (d, J = 7.5 Hz, 1H), 7.67 – 7.55 (m, 3H), 7.51 (d, J = 7.4 Hz, 1H), 7.42 (d, J = 8.0 Hz, 1H), 7.31 – 7.23 (m, 1H), 7.19 (t, J = 7.4 Hz, 1H), 5.50 (s, 1H), 4.28 (d, J = 11.0 Hz, 1H), 3.98 (t, J = 7.6 Hz, 1H), 3.70 (dd, J = 15.2, 3.5 Hz, 1H),

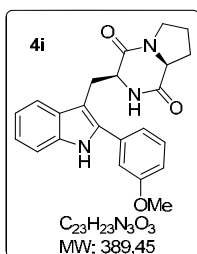
3.62 – 3.41 (m, 2H), 2.89 (dd, J = 15.0, 11.9 Hz, 1H), 2.35 – 2.21 (m, 1H), 1.98 (dd, J = 16.2, 7.9 Hz, 2H), 1.84 (dd, J = 18.4, 10.1 Hz, 1H) ppm. **¹³C NMR** (100 MHz, $CDCl_3$): δ 169.30, 165.72, 136.01, 133.71, 133.47, 132.28, 130.44, 130.15, 129.86, 129.47, 127.36, 126.90, 123.43, 120.66, 118.76, 111.52, 108.56, 59.28, 54.53, 45.52, 28.36, 25.78, 22.75. **IR** (Film, cm^{-1}) ν = 3385.05, 3276.16, 3051.96, 2962.28, 2917.44, 2879.00, 2846.98, 1668.33 cm^{-1} . **HRMS** (ESI) m/z calcd 428.1580 ($C_{23}H_{20}F_3N_3O_2$) found 428.1587 ($M+H$)⁺.

(3S,8aS)-3-((2-(2-Chlorophenyl)-1H-indol-3-yl)methyl)hexahydropyrrolo[1,2-a]pyrazine-1,4-dione (4h)

Compound **4h** was prepared according to the general procedure using 1-chloro-2-iodobenzene (276.6 μ L, 2.26 mmol). The crude product was purified by flash chromatography on silica using 100 % ethyl acetate to obtain **4h** as a pale solid (161.3 mg, 54 %).

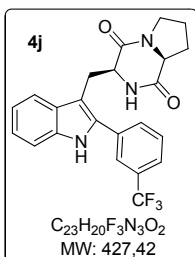
¹H NMR (400 MHz, $CDCl_3$): δ 8.30 (s, 1H), 7.63 (d, J = 8.0 Hz, 1H), 7.53 (d, J = 7.7 Hz, 1H), 7.46 – 7.33 (m, 4H), 7.29 (d, J = 7.5 Hz, 1H), 7.19 (t, J = 7.4 Hz, 1H), 5.56 (s, 1H), 4.31 (d, J = 11.2 Hz, 1H), 3.99 (t, J = 7.8 Hz, 1H), 3.75 (dd, J = 15.1, 3.7 Hz, 1H), 3.66 – 3.45 (m, 2H), 2.91 (dd, J = 15.1, 11.8 Hz, 1H), 2.34 – 2.18 (m, 1H), 2.03 – 1.91 (m,

2H), 1.85 (dd, J = 18.4, 10.2 Hz, 1H) ppm. **¹³C NMR** (100 MHz, $CDCl_3$): δ 169.33, 165.76, 136.19, 134.42, 134.03, 132.67, 131.13, 130.55, 130.24, 127.29, 127.26, 123.23, 120.35, 118.80, 111.58, 108.19, 59.25, 54.41, 45.47, 28.28, 25.85, 22.72 ppm. **IR** (Film, cm^{-1}) ν = 3372.24, 3282.56, 3051.96, 2975.09, 2955.87, 2930.25, 2879.00, 1668.33 cm^{-1} . **HRMS** (ESI) m/z calcd 394.1317 ($C_{22}H_{20}ClN_3O_2$) found 394.1323 ($M+H$)⁺.

(3S,8aS)-3-((2-(2-Methoxyphenyl)-1H-indol-3-yl)methyl)hexahydropyrrolo[1,2-a]pyrazine-1,4-dione (4i)

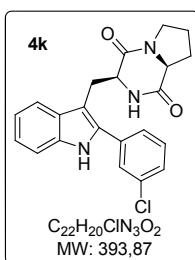
Compound **4i** was prepared according to the general procedure using 3-iodoanisole, 99 % (272.6 μ L, 2.26 mmol). The crude product was purified by flash chromatography on silica using 100 % ethyl acetate to obtain **4i** as a pale solid (214.4 mg, 73 %).

^1H NMR (400 MHz, CDCl_3): δ 8.25 (s, 1H), 7.59 (d, J = 8.0 Hz, 1H), 7.42 – 7.35 (m, 2H), 7.27 (d, J = 1.1 Hz, 1H), 7.25 – 7.22 (m, 1H), 7.19 – 7.12 (m, 2H), 7.10 – 7.06 (m, 1H), 6.95 – 6.91 (m, 1H), 5.45 (s, 1H), 4.36 (d, J = 9.0 Hz, 1H), 3.99 (t, J = 7.5 Hz, 1H), 3.89 (dd, J = 15.2, 3.8 Hz, 1H), 3.85 (s, 3H), 3.65 – 3.50 (m, 2H), 3.27 – 3.21 (m, 1H), 3.18 (s, 1H), 2.33 – 2.21 (m, 1H), 2.01 – 1.78 (m, 3H) ppm. **^{13}C NMR** (100 MHz, CDCl_3): δ 169.41, 165.77, 160.10, 136.47, 136.09, 133.55, 130.38, 128.43, 123.10, 120.77, 120.43, 118.66, 113.99, 113.99, 111.44, 106.44, 59.24, 55.45, 54.69, 45.48, 28.32, 25.71, 22.70 ppm. **IR** (Film, cm^{-1}) ν = 3365.84, 3282.56, 3058.36, 2962.28, 2930.25, 2879.00, 2834.16, 1668.33 cm^{-1} . **HRMS** (ESI) m/z calcd 390.1812 ($\text{C}_{23}\text{H}_{23}\text{N}_3\text{O}_3$) found 390.1818 ($\text{M}+\text{H}$) $^+$.

(3S,8aS)-3-((2-(3-(Trifluoromethyl)phenyl)-1H-indol-3-yl)methyl)hexahydropyrrolo[1,2-a]pyrazine-1,4-dione (4j)

Compound **4j** was prepared according to the general procedure using 3-iodobenzotrifluoride, 99 % (333.3 μ L, 2.26 mmol). The crude product was purified by flash chromatography on silica using 100 % ethyl acetate to obtain **4j** as a pale solid (164.7 mg, 51 %).

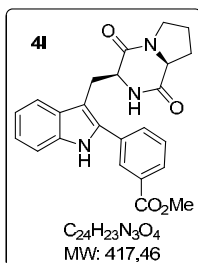
^1H NMR (400 MHz, CDCl_3): δ 8.44 (s, 1H), 7.81 (s, 1H), 7.77 (d, J = 7.6 Hz, 1H), 7.68 – 7.56 (m, 3H), 7.45 – 7.41 (m, 1H), 7.31 – 7.26 (m, 1H), 7.22 – 7.16 (m, 1H), 5.45 (s, 1H), 4.45 – 4.34 (m, 1H), 4.02 (t, J = 7.6 Hz, 1H), 3.89 (dt, J = 9.2, 4.6 Hz, 1H), 3.68 – 3.50 (m, 2H), 3.20 – 3.13 (m, 1H), 2.34 – 2.23 (m, 1H), 2.03 – 1.81 (m, 3H) ppm. **^{13}C NMR** (100 MHz, CDCl_3): δ 169.47, 165.53, 136.41, 135.02, 133.13, 131.69, 131.68 (q, J = 32.5 Hz), 129.87, 128.27, 125.05, 125.05, 123.92 (q, J = 272.6 Hz), 123.71, 120.81, 118.92, 111.64, 107.42, 59.30, 54.61, 45.54, 28.40, 25.95, 22.68 ppm. **IR** (Film, cm^{-1}) ν = 3372.24, 3269.75, 3064.77, 2962.28, 2930.25, 2879.00, 1668.33 cm^{-1} . **HRMS** (ESI) m/z calcd 428.1580 ($\text{C}_{23}\text{H}_{20}\text{F}_3\text{N}_3\text{O}_2$) found 428.1589 ($\text{M}+\text{H}$) $^+$.

(3S,8aS)-3-((2-(3-Chlorophenyl)-1H-indol-3-yl)methyl)hexahydropyrrolo[1,2-a]pyrazine-1,4-dione (4k)

Compound **4k** was prepared according to the general procedure using 3-chloriodobenzene, 98 % (286.3 μ L, 2.26 mmol). The crude product was purified by flash chromatography on silica using 100 % ethyl acetate to obtain **4k** as a pale solid (211.9 mg, 71 %).

1H NMR (400 MHz, $CDCl_3$): δ 8.32 (s, 1H), 7.60 (d, J = 8.0 Hz, 1H), 7.55 (t, J = 1.5 Hz, 1H), 7.48 – 7.34 (m, 4H), 7.28 – 7.25 (m, 1H), 7.20 – 7.15 (m, 1H), 5.42 (s, 1H), 4.39 (dd, J = 11.6, 2.6 Hz, 1H), 4.01 (t, J = 7.5 Hz, 1H), 3.89 (dd, J = 15.2, 3.8 Hz, 1H), 3.59 (tdd, J = 11.8, 10.3, 5.8 Hz, 2H), 3.24 – 3.14 (m, 1H), 2.34 – 2.24 (m, 1H), 2.06 – 1.80 (m, 3H) ppm. **^{13}C NMR** (100 MHz, $CDCl_3$): δ 169.49, 165.63, 136.26,

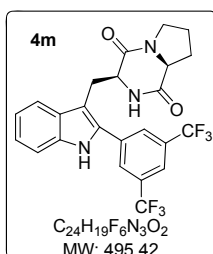
135.29, 135.12, 134.02, 130.65, 128.63, 128.37, 128.32, 126.60, 123.64, 120.79, 118.93, 111.55, 107.29, 59.33, 54.61, 45.57, 28.41, 25.81, 22.75 ppm. **IR** (Film, cm^{-1}) ν = 3365.84, 3269.75, 3051.96, 2962.28, 2923.84, 2872.60, 1668.33 cm^{-1} . **HRMS** (ESI) m/z calcd 394.1317 ($C_{22}H_{20}ClN_3O_2$) found 394.1325 ($M+H$)⁺.

Methyl 3-3-((3S,8aS)-1,4-dioxooctahydropyrrolo[1,2-a]pyrazin-3-yl)methyl)-1H-indol-2-yl)benzoate (4l)

Compound **4l** was prepared according to the general procedure using methyl-3-iodobenzoate, 97 % (306.2 mg, 1.13 mmol). The crude product was purified by flash chromatography on silica using 100 % ethyl acetate to obtain **4l** as a pale solid (62.6 mg, 40 %).

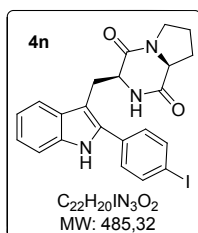
1H NMR (400 MHz, $CDCl_3$): δ 8.39 (s, 1H), 8.23 (s, 1H), 8.06 (d, J = 7.8 Hz, 1H), 7.78 (d, J = 7.7 Hz, 1H), 7.61 (d, J = 7.9 Hz, 1H), 7.56 (t, J = 7.8 Hz, 1H), 7.43 (d, J = 8.2 Hz, 1H), 7.29 (d, J = 7.1 Hz, 1H), 7.18 (t, J = 7.5 Hz, 1H), 5.45 (s, 1H), 4.39 (d, J = 8.9 Hz, 1H), 4.00 (t, J = 7.8 Hz, 1H), 3.95 (s, 3H), 3.91 (dd, J = 15.3, 3.7 Hz, 1H), 3.69 – 3.50

(m, 2H), 3.21 (dd, J = 15.8, 11.0 Hz, 1H), 2.35 – 2.23 (m, 1H), 2.03 – 1.81 (m, 3H) ppm. **^{13}C NMR** (100 MHz, $CDCl_3$): δ 169.48, 166.63, 165.64, 136.28, 135.51, 132.71, 132.60, 131.36, 129.56, 129.51, 129.31, 128.40, 123.58, 120.77, 118.90, 111.54, 107.21, 59.33, 54.66, 52.55, 45.57, 28.42, 25.85, 22.75 ppm. **IR** (Film, cm^{-1}) ν = 3372.24, 3282.56, 3058.36, 2949.47, 2923.84, 2885.41, 2846.98, 1725.98, 1661.92 cm^{-1} . **HRMS** (ESI) m/z calcd 418.1761 ($C_{24}H_{23}N_3O_4$) found 418.1770 ($M+H$)⁺.

(3S,8aS)-3-((2-(3,5-bis(trifluoromethyl)phenyl)-1H-indol-3-yl)methyl)hexahydropyrrolo[1,2-a]pyrazine-1,4-dione (4m)

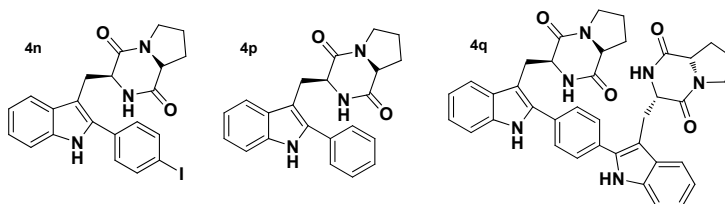
Compound **4m** was prepared according to the general procedure using 3,5-bis(trifluoromethyl)iodobenzene (409.4 μ L, 2.26 mmol). A second irradiation cycle was performed. The crude product was purified by flash chromatography on silica using 80-95 % ethyl acetate to obtain **4m** as a pale solid (48.4 mg, 13 %).

1H NMR (400 MHz, $CDCl_3$): δ 8.92 (s, 1H), 8.04 – 8.00 (m, 2H), 7.87 (s, 1H), 7.61 (d, J = 8.0 Hz, 1H), 7.41 (d, J = 8.2 Hz, 1H), 7.32 – 7.15 (m, 2H), 5.50 (s, 1H), 4.50 – 4.37 (m, 1H), 4.03 (t, J = 7.5 Hz, 1H), 3.90 (dd, J = 15.3, 4.1 Hz, 1H), 3.68 – 3.48 (m, 2H), 3.15 (dd, J = 15.3, 11.2 Hz, 1H), 2.31 (ddd, J = 13.0, 10.9, 6.8 Hz, 1H), 2.02 – 1.80 (m, 3H) ppm. **^{13}C NMR** (100 MHz, $CDCl_3$): δ 169.43, 165.22, 136.69, 134.50, 133.39, 132.64 (q, J = 33.6 Hz), 128.28, 128.25, 128.08, 124.28, 123.16 (q, J = 273.1 Hz), 121.10, 119.14, 111.79, 108.58, 59.30, 54.61, 45.57, 28.52, 26.34, 22.59 ppm. **IR** (Film, cm^{-1}) ν = 3376.92, 3263.35, 3064.77, 2962.28, 2930.25, 2891.81, 1674.73 cm^{-1} . **HRMS** (ESI) m/z calcd 496.1454 ($C_{24}H_{19}F_6N_3O_2$) found 496.1458 ($M+H$) $^+$.

(3S,8aS)-3-((2-(4-iodophenyl)-1H-indol-3-yl)methyl)hexahydropyrrolo[1,2-a]pyrazine-1,4-dione (4n)

mL) and brine (3x30 mL).

Compound **4n** was prepared using 1,4-diiodobenzene, 99 % (748.6 mg, 2.27 mmol). Brevianamide F (2 equiv), aryl iodide (3 equiv), $AgBF_4$ (2 equiv), 2-nitrobenzoic acid (3 equiv) and $Pd(OAc)_2$ (10 % equiv) were placed in a microwave reactor vessel in a 1:1 mixture of DMF:PBS (total volume of 2400 μ L). Analysis by RP-HPLC-ESMS showed a mixture of compounds **4n**, **4p** and **4q** in a 1.1:1:2 range. Ethyl acetate (100 mL) was added and the resulting suspension was filtered through Celite. The filtrate was successively washed with aqueous saturated solutions of NH_4Cl_{sat} (3x30 mL), $NaHCO_3_{sat}$ (3x30

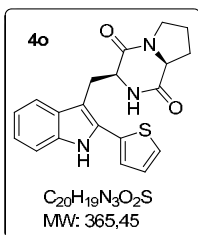


Electronic Supplementary Material (ESI) for Medicinal Chemistry Communications
This journal is © The Royal Society of Chemistry 2013

The crude product was purified by flash chromatography on silica using 80-90 % ethyl acetate to obtain **4n** as a pale solid (53.1 mg, 7.2%).

¹H NMR (400 MHz, CDCl₃): δ 8.64 (s, 1H), 7.76 – 7.71 (m, 2H), 7.59 (t, *J* = 7.2 Hz, 1H), 7.39 (t, *J* = 6.9 Hz, 1H), 7.29 – 7.22 (m, 3H), 7.20 – 7.10 (m, 1H), 5.41 (s, 1H), 4.35 (dd, *J* = 11.5, 2.7 Hz, 1H), 4.04 – 3.92 (m, 1H), 3.90 – 3.79 (m, 1H), 3.68 – 3.46 (m, 2H), 3.16 (dd, *J* = 15.2, 11.5 Hz, 1H), 2.35 – 2.23 (m, 1H), 2.03 – 1.77 (m, 3H) ppm. ¹³C NMR (100 MHz, CDCl₃): δ 169.49, 165.63, 138.42, 136.30, 135.49, 131.72, 130.01, 128.38, 123.44, 120.67, 118.78, 111.56, 106.87, 94.27, 59.28, 54.54, 45.54, 28.35, 25.77, 22.72 ppm. IR (Film, cm⁻¹) *v* = 3365.84, 3282.56, 3058.36, 2962.28, 2917.44, 2879.00, 1655.52 cm⁻¹. HRMS (ESI) *m/z* calcd 486.0673 (C₂₂H₂₀N₃O₂) found 486.0683 (M+H)⁺.

(3S,8aS)-3-((2-(2-Iodothiophene)-1*H*-indol-3-yl)methyl)hexahydropyrrolo[1,2-*a*]pyrazine-1,4-dione (4o**)**



Compound **4o** was prepared using 2-iodothiophene, 98 % (255.4 μL, 1.13 mmol). A second irradiation cycle was performed. Ethyl acetate (140 mL) was added and the resulting suspension was filtered through Celite. The filtrate was successively washed with aqueous saturated solutions of NH₄Cl_{sat} (3x60 mL), NaHCO_{3 sat} (3x60 mL) and brine (3x60 mL). The crude product was purified by flash chromatography on silica using 100 % ethyl acetate to obtain **4o** as a pale solid (23.7 mg, 8.6 %).

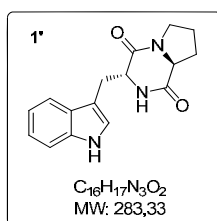
¹H NMR (400 MHz, CDCl₃): δ 8.28 (s, 1H), 7.58 (d, *J* = 7.9 Hz, 1H), 7.41 – 7.37 (m, 2H), 7.30 (dd, *J* = 3.6, 1.1 Hz, 1H), 7.27 (d, *J* = 1.1 Hz, 1H), 7.26 – 7.23 (m, 1H), 7.19 – 7.12 (m, 2H), 5.58 (s, 1H), 4.43 (d, *J* = 11.9 Hz, 1H), 4.04 (t, *J* = 7.4 Hz, 1H), 3.92 (dd, *J* = 15.3, 3.7 Hz, 1H), 3.73 – 3.51 (m, 2H), 3.29 (dd, *J* = 15.3, 11.5 Hz, 1H), 2.39 – 2.24 (m, 1H), 2.10 – 1.99 (m, 2H), 1.96 – 1.75 (m, 1H) ppm. ¹³C NMR (100 MHz, CDCl₃): δ 169.59, 165.66, 136.15, 133.64, 130.15, 128.67, 128.09, 126.14, 125.80, 123.54, 120.76, 118.54, 111.35, 107.37, 59.31, 54.92, 45.57, 28.43, 25.99, 22.76 ppm. IR (Film, cm⁻¹) *v* = 3365.84, 3276.16, 3109.61, 2949.47, 2917.44, 2879.00, 2846.98, 1661.92 cm⁻¹. HRMS (ESI) *m/z* calcd 366.1271 (C₂₀H₁₉N₃O₂S) found 366.1275 (M+H)⁺.

Synthesis of arylated diketopiperazines **4c'-**4c'''****

These compounds were prepared by arylation of the corresponding cycloTrp-Pro derivatives **1**, which in turn were synthesized by condensation of suitable Trp and Pro precursors.

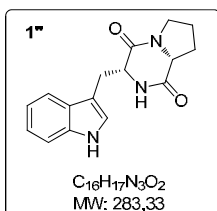
General procedure for the synthesis of the diketopiperazines 1'-1'''

Z-Trp-OH (L or D) (1 equiv), H-Pro-OMe-HCl (L or D) (1 equiv), HOBt (1 equiv) and EDC-HCl (1 equiv) were suspended in ACN (30 mL). Then, DIEA (1.5 equiv) was added and the mixture was stirred during 2 h at rt. The solvent was removed and ethyl acetate (30 mL) was added. The organic phase was washed successively with a saturated solution of NaHCO₃ (2 × 30 mL), 5 % HCl (2 × 30 mL) and brine (2 × 30 mL) and the resulting organic solution was dried with MgSO₄. After filtration and solvent removal, the residue was dissolved in MeOH (60 mL) and was added 10% Pd/C (10 mol %). Then this mixture was stirred vigorously under H₂ at rt overnight. Finally, the corresponding product **1c'-1c'''** was obtained by filtration through Celite and the solvent was removed under vacuum.

(3R,8aS)-3-((1H-indol-3-yl)methyl)hexahydropyrrolo[1,2-*a*]pyrazine-1,4-dione (1')

Compound **1'** was prepared according to the general procedure using Z-D-Trp-OH (2.11 g, 6.24 mmol) and H-L-Pro-OMe-HCl (1.03 g, 6.24 mmol). After filtration through Celite the solvent was removed affording a foamy white solid (**1'**) (1.42, 80 %).

¹H NMR (400 MHz, CDCl₃): δ 8.38 (s, 1H), 7.54 (dd, *J* = 8.1, 1.3 Hz, 1H), 7.33 – 7.24 (m, 1H), 7.12 (ddd, *J* = 8.2, 7.0, 1.2 Hz, 1H), 7.05 (ddd, *J* = 8.0, 7.0, 1.1 Hz, 1H), 6.95 (d, *J* = 2.4 Hz, 1H), 6.24 (d, *J* = 4.3 Hz, 1H), 4.16 (dt, *J* = 5.8, 4.1 Hz, 1H), 3.54 – 3.39 (m, 1H), 3.34 (dd, *J* = 14.6, 5.9 Hz, 1H), 3.16 – 3.03 (m, 2H), 2.73 (dd, *J* = 10.8, 6.4 Hz, 1H), 2.05 – 1.92 (m, 1H), 1.81 – 1.72 (m, 1H), 1.67 – 1.55 (m, 1H), 1.43 – 1.27 (m, 1H) ppm. ¹³C NMR (100 MHz, CDCl₃): δ 169.86, 165.81, 136.48, 127.30, 124.51, 122.78, 120.16, 119.21, 111.55, 109.65, 58.67, 58.18, 45.39, 30.95, 29.25, 21.85 ppm. IR (Film, cm⁻¹) *v* = 3269.75, 3077.58, 2923.84, 2879.00, 1649.11, 1456.94, 1341.64, 1296.80, 1091.81, 906.05, 726.69 cm⁻¹. HRMS (ESI) calcd 284.13935 (C₁₆H₁₈N₃O₂), found 284.13904 (M+H)⁺.

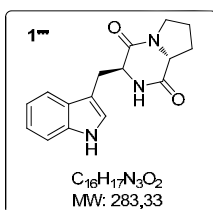
(3R,8aR)-3-((1H-indol-3-yl)methyl)hexahydropyrrolo[1,2-*a*]pyrazine-1,4-dione (1'')

Compound **1''** was prepared according to the general procedure using Z-D-Trp-OH (1.74 g, 5.14 mmol) and H-D-Pro-OMe-HCl (0.85 g, 5.14 mmol). After filtration through Celite the solvent was removed affording a foamy white solid (**1''**) (1.20 g, 83 %).

¹H NMR (400 MHz, CDCl₃): δ 8.25 (s, 1H), 7.52 (dt, *J* = 8.0, 0.9 Hz, 1H), 7.36 – 7.27 (m, 1H), 7.21 – 7.11 (m, 1H), 7.09 – 6.99 (m, 2H), 5.71 (s, 1H), 4.35 – 4.23 (m, 1H), 4.05 – 3.94 (m, 1H), 3.69 (ddd, *J* = 15.0, 3.8, 1.1 Hz, 1H), 3.62 – 3.44 (m, 2H), 2.91 (dd, *J* = 15.1,

10.8 Hz, 1H), 2.31 – 2.18 (m, 1H), 1.97 – 1.88 (m, 2H), 1.87 – 1.76 (m, 1H) ppm. ^{13}C NMR (100 MHz, CDCl_3): δ 169.66, 165.83, 136.97, 127.02, 123.64, 123.07, 120.29, 118.80, 111.86, 110.22, 59.53, 54.89, 45.72, 28.61, 27.15, 22.92 ppm. IR (Film, cm^{-1}) ν = 3282.56, 3051.96, 2955.87, 2917.44, 2872.60, 1655.52, 1456.94, 1424.91, 1341.64, 1296.80, 1528.36, 1219.93, 1098.22, 1008.54, 912.46, 803.56, 739.50 cm^{-1} . HRMS (ESI) calcd 284.13935 ($\text{C}_{16}\text{H}_{18}\text{N}_3\text{O}_2$), found 284.13905 ($\text{M}+\text{H}$) $^+$.

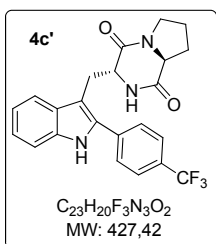
(3S,8aR)-3-((1H-indol-3-yl)methyl)hexahydropyrrolo[1,2-a]pyrazine-1,4-dione (1'')



Compound **1'** was prepared according to the general procedure using Z-L-Trp-OH (0.82 g, 2.43 mmol) and H-D-Pro-OMe-HCl (0.41 g, 2.45 mmol). After filtration through Celite the solvent was removed affording a foamy white solid (**1'**) (0.56 g, 81 %).

^1H NMR (400 MHz, CDCl_3): δ 8.29 (s, 1H), 7.54 (ddt, J = 7.9, 1.4, 0.7 Hz, 1H), 7.33 – 7.24 (m, 1H), 7.09 (dddd, J = 28.2, 8.1, 7.1, 1.1 Hz, 2H), 6.96 (d, J = 2.4 Hz, 1H), 6.12 (d, J = 3.8 Hz, 1H), 4.20 – 4.10 (m, 1H), 3.53 – 3.38 (m, 1H), 3.34 (dd, J = 14.6, 6.0 Hz, 1H), 3.16 – 3.03 (m, 2H), 2.74 (dd, J = 10.9, 6.3 Hz, 1H), 2.04 – 1.94 (m, 1H), 1.81 – 1.72 (m, 1H), 1.65 – 1.57 (m, 1H), 1.41 – 1.27 (m, 1H). ppm. ^{13}C NMR (101 MHz, CDCl_3): δ 169.86, 165.81, 136.48, 127.30, 124.51, 122.78, 120.16, 119.21, 111.55, 109.65, 58.67, 58.18, 45.39, 30.95, 29.25, 21.85 ppm. IR (Film, cm^{-1}) ν = 3295.37, 3064.77, 2917.44, 2878.60, 1668.33, 1450.53, 1341.64, 1290.39, 1258.36, 1187.90, 1104.63, 1008.54, 906.05, 803.56, 739.50, 656.23 cm^{-1} . HRMS (ESI) calcd 284.13935 ($\text{C}_{16}\text{H}_{18}\text{N}_3\text{O}_2$), found 284.13919 ($\text{M}+\text{H}$) $^+$.

(3R,8aS)-3-((2-(4-(Trifluoromethyl)phenyl)-1H-indol-3-yl)methyl)hexahydropyrrolo[1,2-a]pyrazine-1,4-dione (4c')

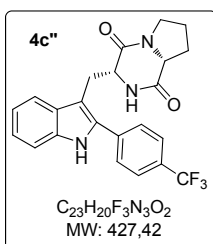


Compound **4c'** was prepared according to the general procedure using 1-iodo-4-(trifluoromethyl)benzene (340 μL , 2.26 mmol). The crude product was purified by flash chromatography on silica using 100 % ethyl acetate to obtain **4c'** as a pale solid (135.4 mg, 42 %).

^1H -NMR (400 MHz, CDCl_3): 8.90 (s, 1H), 7.53 (s, 1H), 7.50 (d, J = 5.4 Hz, 4H), 7.30 (s, 1H), 7.14 (t, J = 7.6 Hz, 1H), 7.04 (t, J = 7.6 Hz, 1H), 5.79 (s, 1H), 4.05 (q, J = 7.0, 5.5 Hz, 1H), 3.36 (dt, J = 21.1, 7.5 Hz, 2H), 3.26 (dd, J = 14.6, 5.4 Hz, 1H), 3.04 (t, J = 10.9 Hz, 1H), 2.75 (dd, J = 10.7, 6.5 Hz, 1H), 1.91 (p, J = 6.5, 6.0 Hz, 1H), 1.79 – 1.67 (m, 1H), 1.56 (qd, J = 11.5, 6.7 Hz, 1H), 1.38 – 1.24 (m, 1H) ppm. ^{13}C -NMR (100 MHz, CDCl_3): δ 168.82, 165.52,

136.30, 136.20, 135.95, 130.32, 129.99, 129.67, 129.01, 128.34, 125.93, 125.88, 125.41, 123.34, 122.71, 120.45, 119.44, 111.46, 107.47, 58.31, 57.82, 45.36, 29.30, 29.00, 21.73 ppm. IR (Film, cm^{-1}) ν = 3231.32, 3058.36, 2936.65, 2872.60, 1668.33 cm^{-1} . HRMS (ESI) m/z calcd 428.15804 ($\text{C}_{23}\text{H}_{21}\text{F}_3\text{N}_3\text{O}_2$), found 428.15815 ($\text{M}+\text{H}$)⁺.

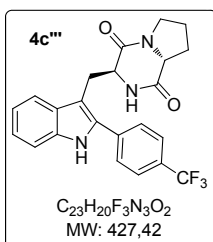
(3*R*,8*aR*)-3-((2-(4-(Trifluoromethyl)phenyl)-1*H*-indol-3-yl)methyl)hexahydropyrrolo[1,2-*a*]pyrazine-1,4-dione (4*c''*)



Compound 4*c''* was prepared according to the general procedure using 1-iodo-4-(trifluoromethyl)benzene (340 μL , 2.26 mmol). The crude product was purified by flash chromatography on silica using 92 % ethyl acetate to obtain 4*c''* as a pale solid (168.0 mg, 52 %).

¹H-NMR (400 MHz, CDCl_3): δ 8.35 (s, 1H), 7.63 (t, J = 8.1 Hz, 4H), 7.55 (dd, J = 7.9, 1.0 Hz, 1H), 7.36 (dt, J = 8.2, 0.8 Hz, 1H), 7.25 – 7.17 (m, 1H), 7.12 (ddd, J = 8.0, 7.1, 1.0 Hz, 1H), 5.34 (s, 1H), 4.42 – 4.20 (m, 1H), 3.98 – 3.90 (m, 1H), 3.84 (dd, J = 15.3, 3.8 Hz, 1H), 3.61 – 3.43 (m, 2H), 3.17 – 3.09 (m, 1H), 2.26 – 2.17 (m, 1H), 1.98 – 1.86 (m, 2H), 1.85 – 1.74 (m, 1H) ppm. ¹³C-NMR (100 MHz, CDCl_3): δ 169.53, 165.53, 136.43, 135.80, 134.93, 130.55, 130.23, 128.60, 128.37, 126.42, 126.38, 126.35, 126.31, 125.39, 123.93, 122.69, 120.98, 119.03, 111.64, 107.91, 59.34, 54.57, 45.58, 28.41, 25.88, 22.75 ppm. IR (Film, cm^{-1}) ν = 3365.84, 3269.75, 3058.36, 2949.47, 2879.00, 1661.92 cm^{-1} . HRMS (ESI) m/z calcd 428.15804 ($\text{C}_{23}\text{H}_{21}\text{F}_3\text{N}_3\text{O}_2$), found 428.15807 ($\text{M}+\text{H}$)⁺.

(3*S*,8*aR*)-3-((2-(4-(Trifluoromethyl)phenyl)-1*H*-indol-3-yl)methyl)hexahydropyrrolo[1,2-*a*]pyrazine-1,4-dione (4*c'''*)



Compound 4*c'''* was prepared according to the general procedure using 1-iodo-4-(trifluoromethyl)benzene (170 μL , 1.13 mmol). The crude product was purified by flash chromatography on silica using 97 % ethyl acetate to obtain 4*c'''* as a pale solid (89.8 mg, 56 %).

¹H-NMR (400 MHz, CDCl_3): δ 8.38 (s, 1H), 7.64 – 7.60 (m, 2H), 7.59 – 7.52 (m, 3H), 7.34 – 7.30 (m, 1H), 7.21 – 7.16 (m, 1H), 7.11 (ddd, J = 8.0, 7.0, 1.1 Hz, 1H), 5.46 – 5.32 (m, 1H), 4.19 – 4.09 (m, 1H), 3.48 – 3.36 (m, 2H), 3.32 (dd, J = 14.7, 4.9 Hz, 1H), 3.08 (ddd, J = 12.1, 9.4, 2.7 Hz, 1H), 2.71 (dd, J = 10.8, 6.4 Hz, 1H), 2.00 – 1.91 (m, 1H), 1.83 – 1.71 (m, 1H), 1.68 – 1.56 (m, 1H), 1.41 – 1.26 (m, 1H) ppm. ¹³C-NMR (100 MHz, CDCl_3): δ 168.35, 165.07,

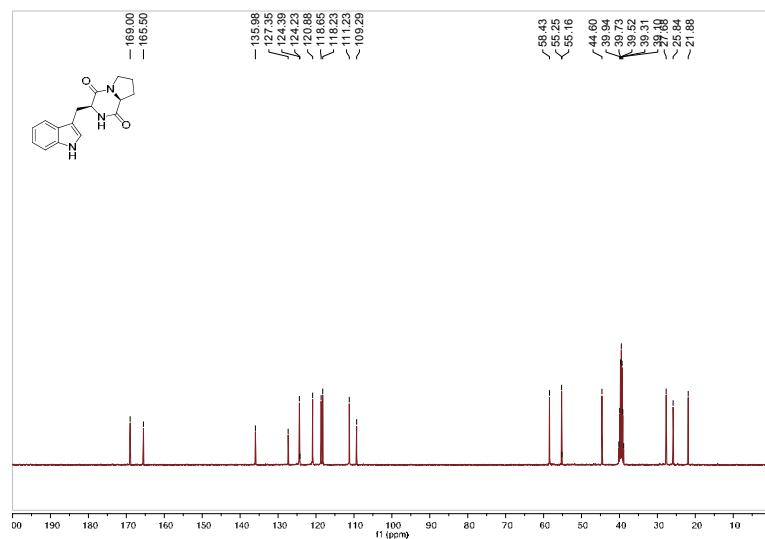
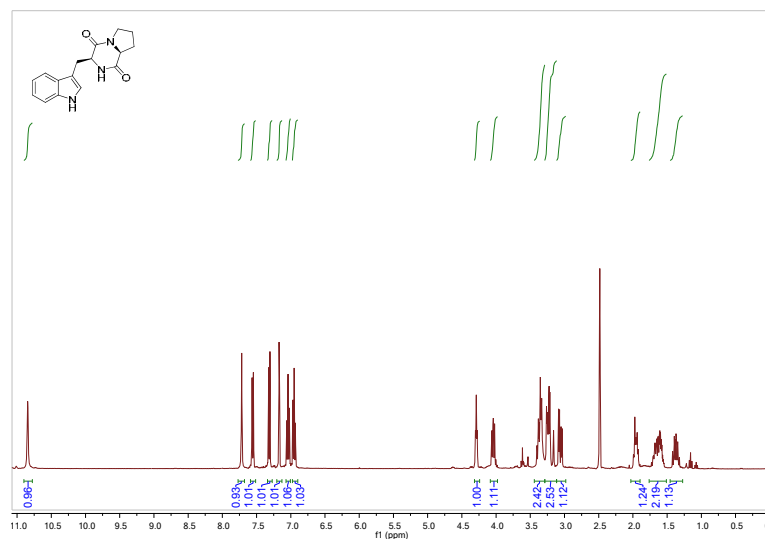
Electronic Supplementary Material (ESI) for Medicinal Chemistry Communications
This journal is © The Royal Society of Chemistry 2013

135.85, 135.79, 135.70, 130.28, 129.95, 128.71, 128.03, 125.85, 125.82, 125.78, 125.74, 123.25, 120.34, 119.26, 111.00, 107.32, 58.16, 57.51, 45.06, 29.04, 28.75, 21.42 ppm. **IR** (Film, cm^{-1}) ν = 3244.13, 2949.47, 2872.60, 1668.33 cm^{-1} . **HRMS** (ESI) m/z calcd 428.15804 ($\text{C}_{23}\text{H}_{21}\text{F}_3\text{N}_3\text{O}_2$), found 428.15780 ($\text{M}+\text{H}$)⁺.

Electronic Supplementary Material (ESI) for Medicinal Chemistry Communications
This journal is © The Royal Society of Chemistry 2013

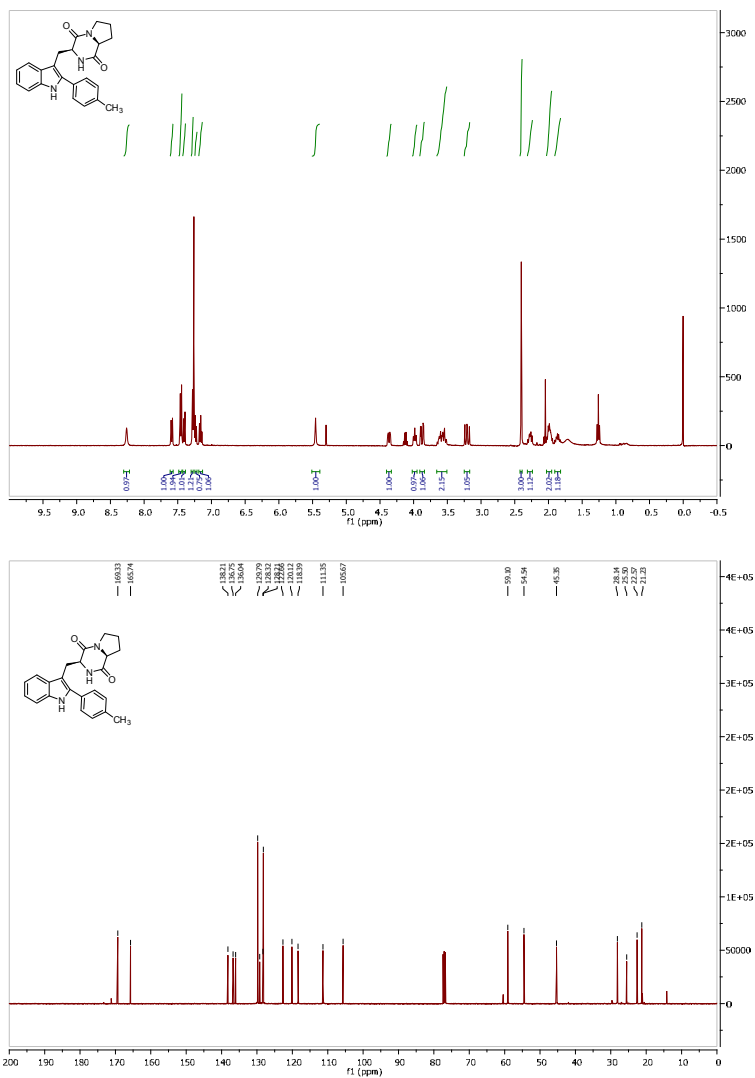
Spectroscopic data

Brevianamide F (1)



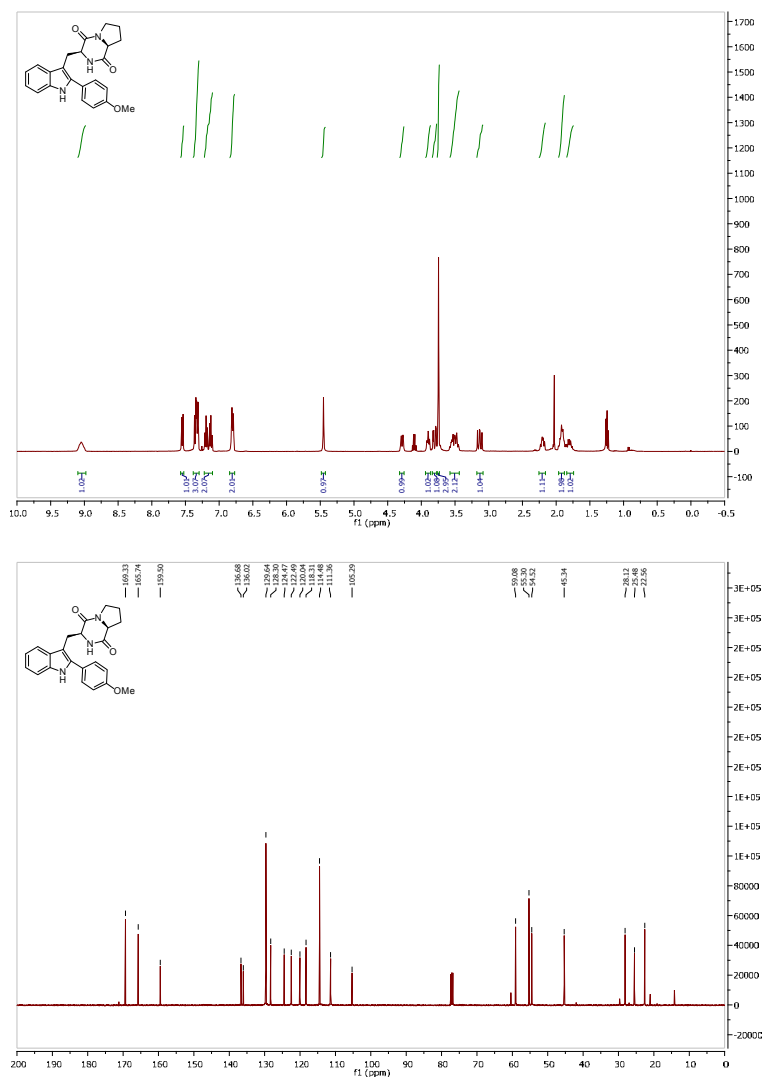
Electronic Supplementary Material (ESI) for Medicinal Chemistry Communications
This journal is © The Royal Society of Chemistry 2013

(3S,8aS)-3-((2-(*p*-Tolyl)-1*H*-indol-3-yl)methyl)hexahydropyrrolo[1,2-*a*]pyrazine-1,4-dione (4a)



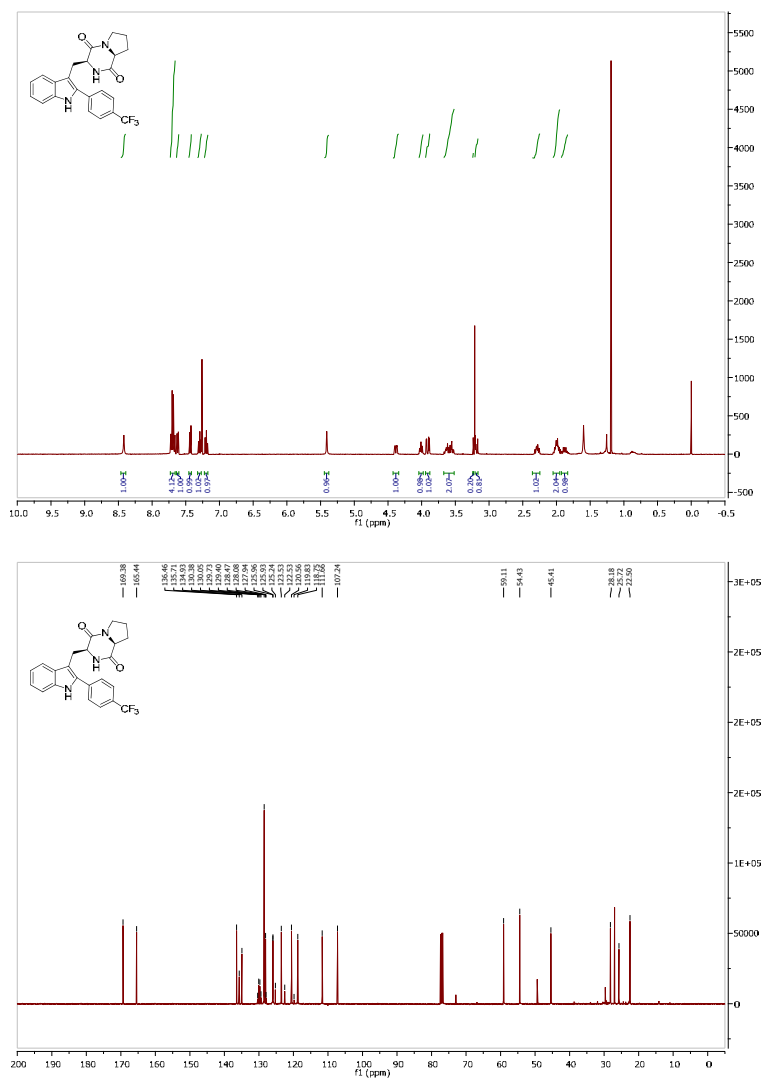
Electronic Supplementary Material (ESI) for Medicinal Chemistry Communications
This journal is © The Royal Society of Chemistry 2013

(3S,8aS)-3-((2-(4-Methoxyphenyl)-1H-indol-3-yl)methyl)hexahydropyrrolo[1,2-a]pyrazine-1,4-dione (4b)



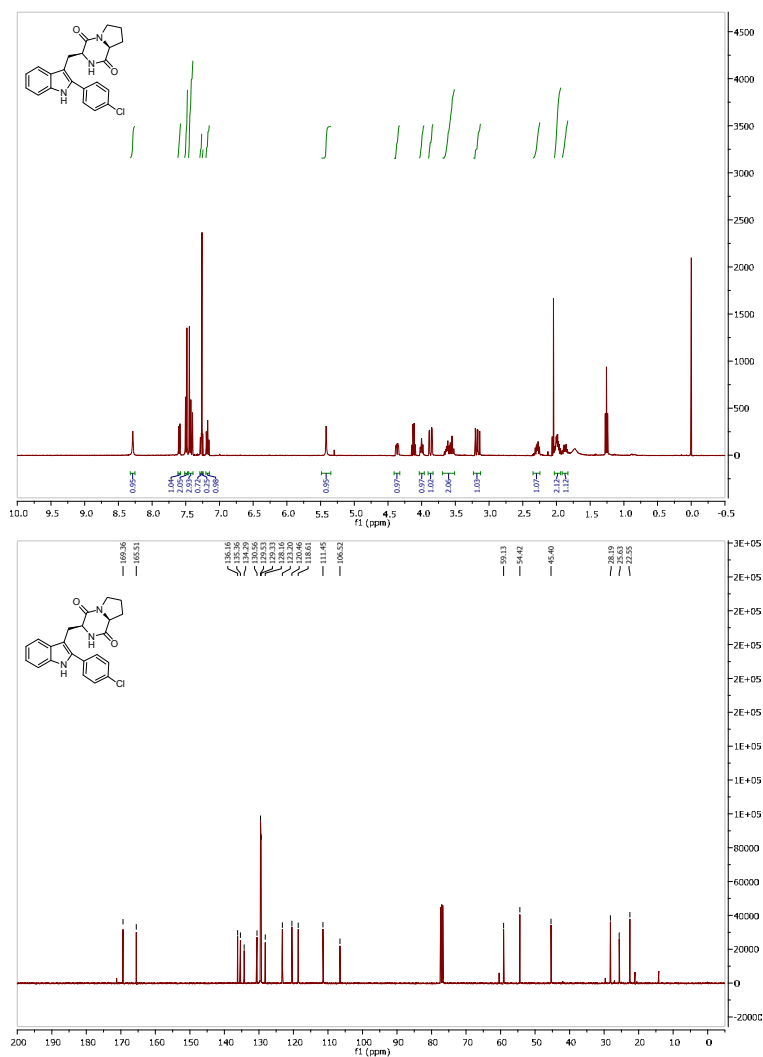
Electronic Supplementary Material (ESI) for Medicinal Chemistry Communications
This journal is © The Royal Society of Chemistry 2013

(3S,8aS)-3-((2-(4-(Trifluoromethyl)phenyl)-1H-indol-3-yl)methyl)hexahydropyrrolo[1,2-a]pyrazine-1,4-dione (4c)



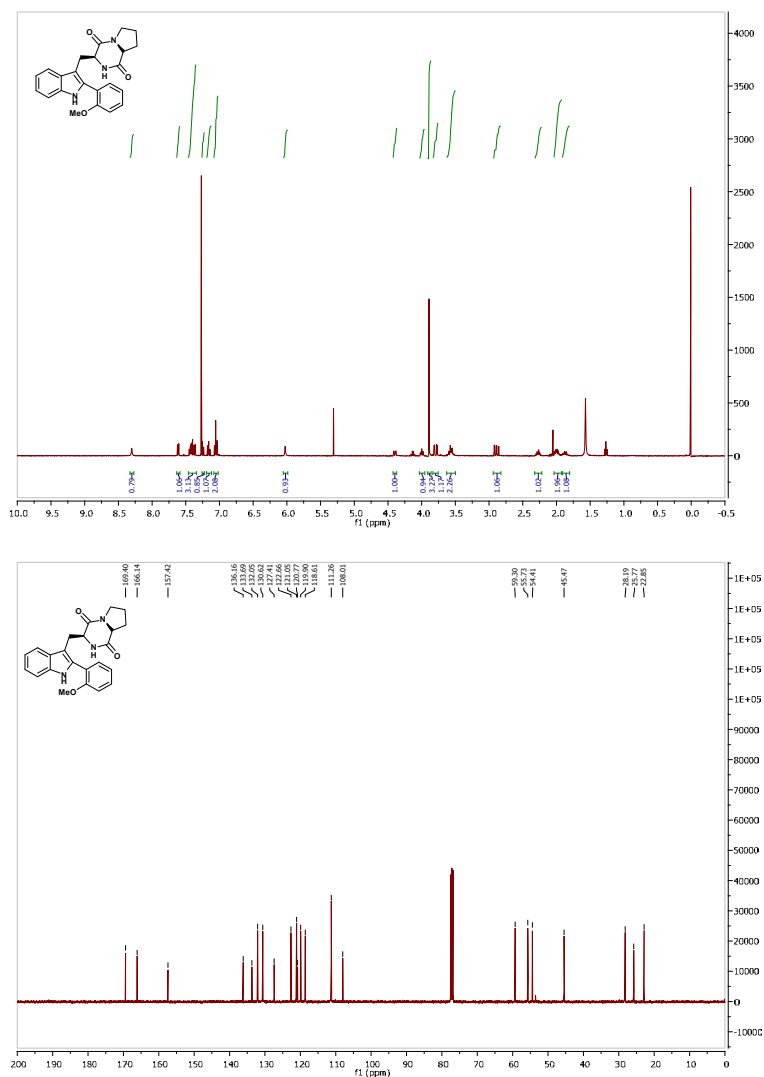
Electronic Supplementary Material (ESI) for Medicinal Chemistry Communications
This journal is © The Royal Society of Chemistry 2013

(3S,8aS)-3-((2-(4-Chlorophenyl)-1H-indol-3-yl)methyl)hexahydropyrrolo[1,2-a]pyrazine-1,4-dione (4d)



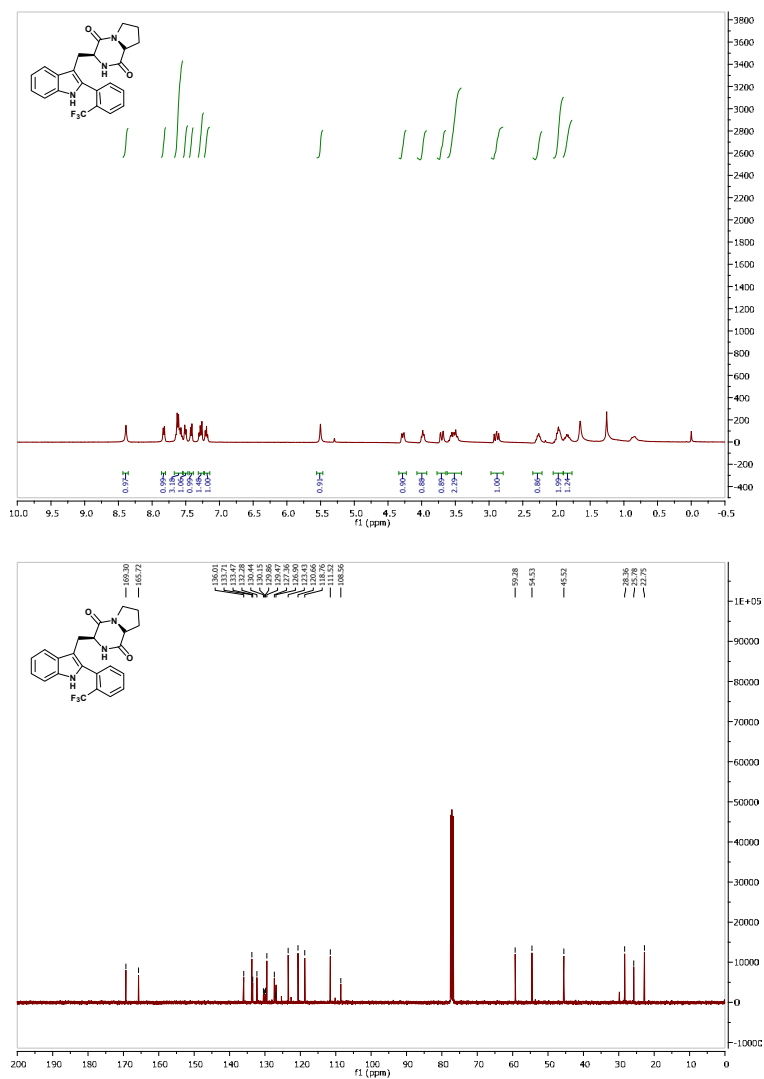
Electronic Supplementary Material (ESI) for Medicinal Chemistry Communications
This journal is © The Royal Society of Chemistry 2013

(3S,8aS)-3-((2-(2-Methoxyphenyl)-1*H*-indol-3-yl)methyl)hexahydropyrrolo[1,2-a]pyrazine-1,4-dione (4f)



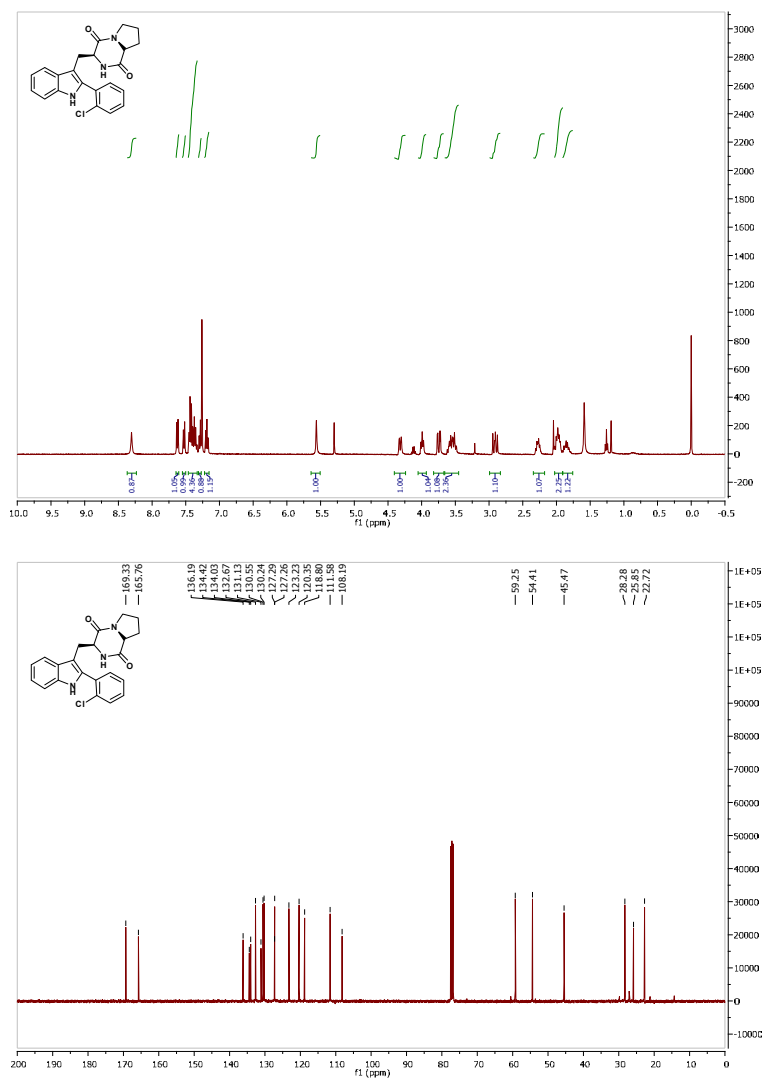
Electronic Supplementary Material (ESI) for Medicinal Chemistry Communications
This journal is © The Royal Society of Chemistry 2013

(3S,8aS)-3-((2-(2-(Trifluoromethyl)phenyl)-1H-indol-3-yl)methyl)hexahydropyrrolo[1,2-a]pyrazine-1,4-dione (4g)



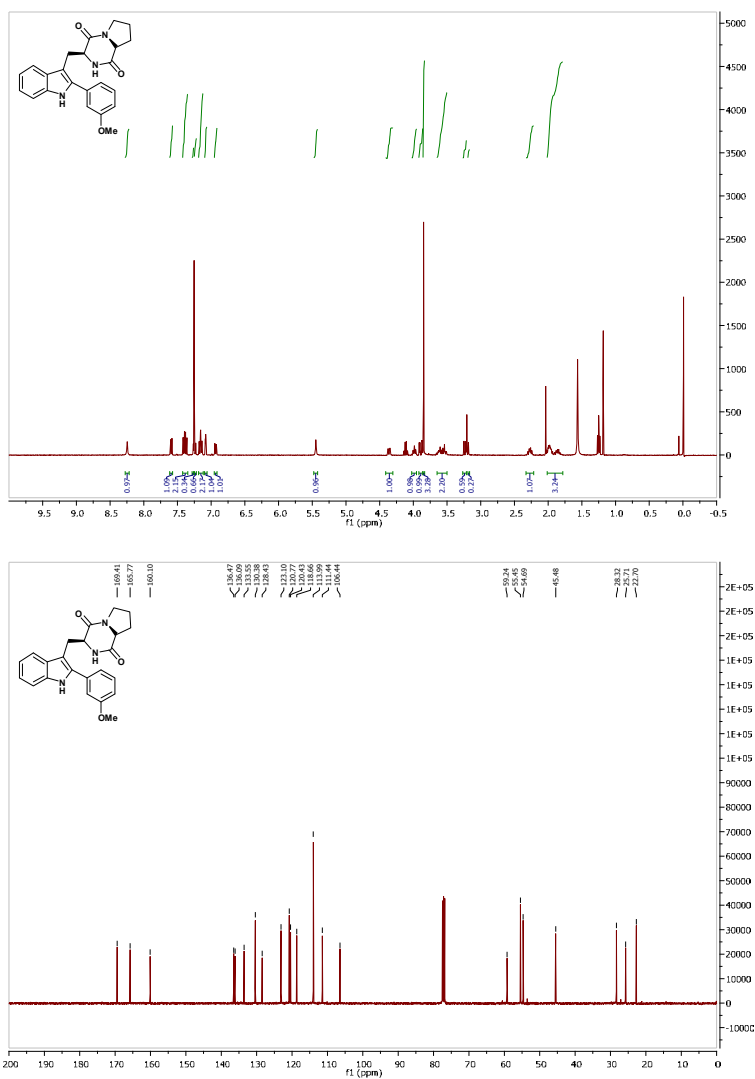
Electronic Supplementary Material (ESI) for Medicinal Chemistry Communications
This journal is © The Royal Society of Chemistry 2013

(3S,8aS)-3-((2-(2-Chlorophenyl)-1H-indol-3-yl)methyl)hexahydropyrrolo[1,2-a]pyrazine-1,4-dione (4h)



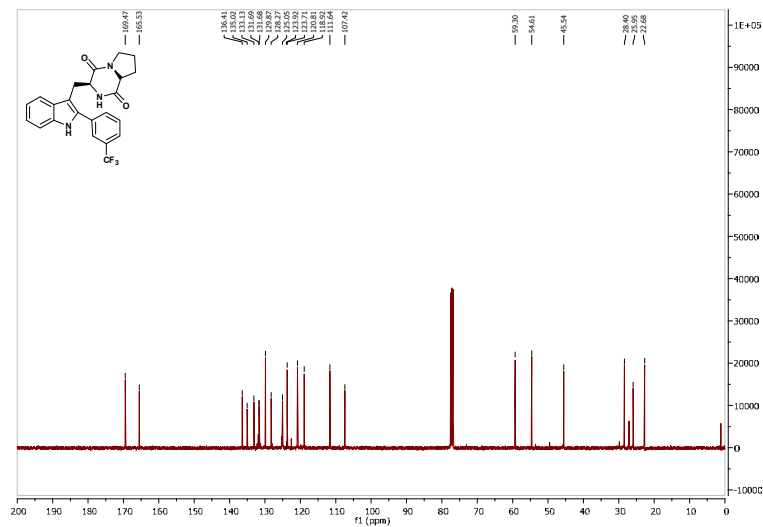
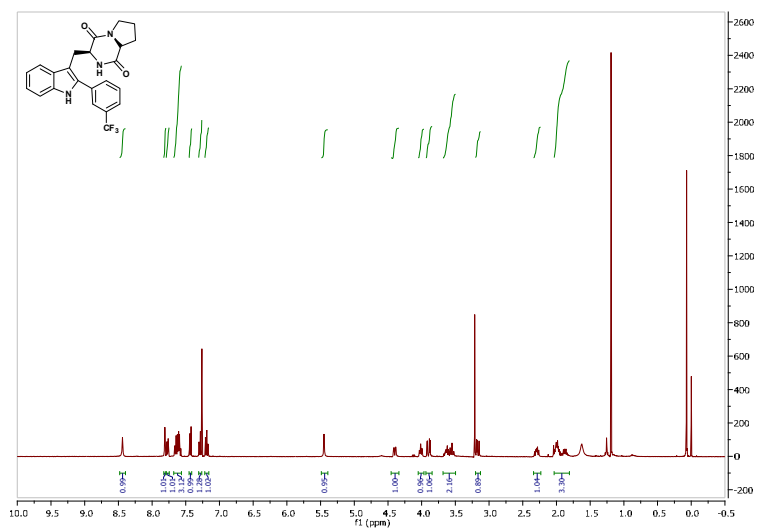
Electronic Supplementary Material (ESI) for Medicinal Chemistry Communications
This journal is © The Royal Society of Chemistry 2013

(3S,8aS)-3-((2-(3-Methoxyphenyl)-1*H*-indol-3-yl)methyl)hexahydropyrrolo[1,2-a]pyrazine-1,4-dione (4i)



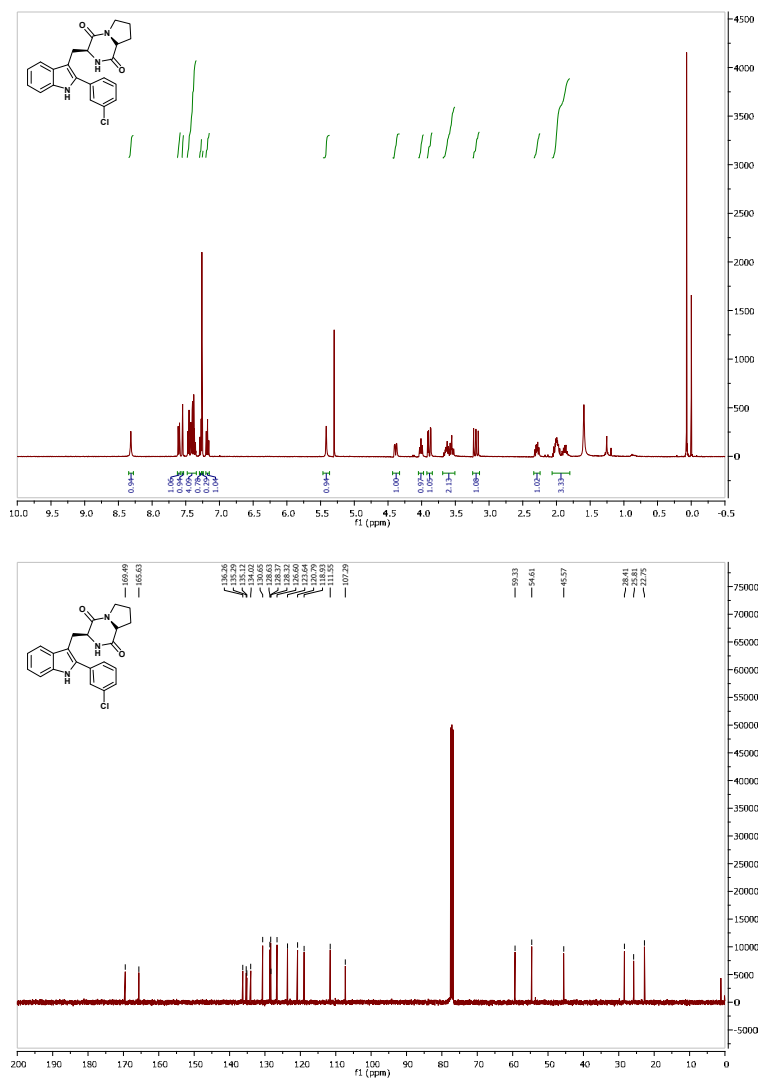
Electronic Supplementary Material (ESI) for Medicinal Chemistry Communications
This journal is © The Royal Society of Chemistry 2013

(3S,8aS)-3-((2-(3-(Trifluoromethyl)phenyl)-1*H*-indol-3-yl)methyl)hexahydropyrrolo[1,2-*a*]pyrazine-1,4-dione (4j**)**



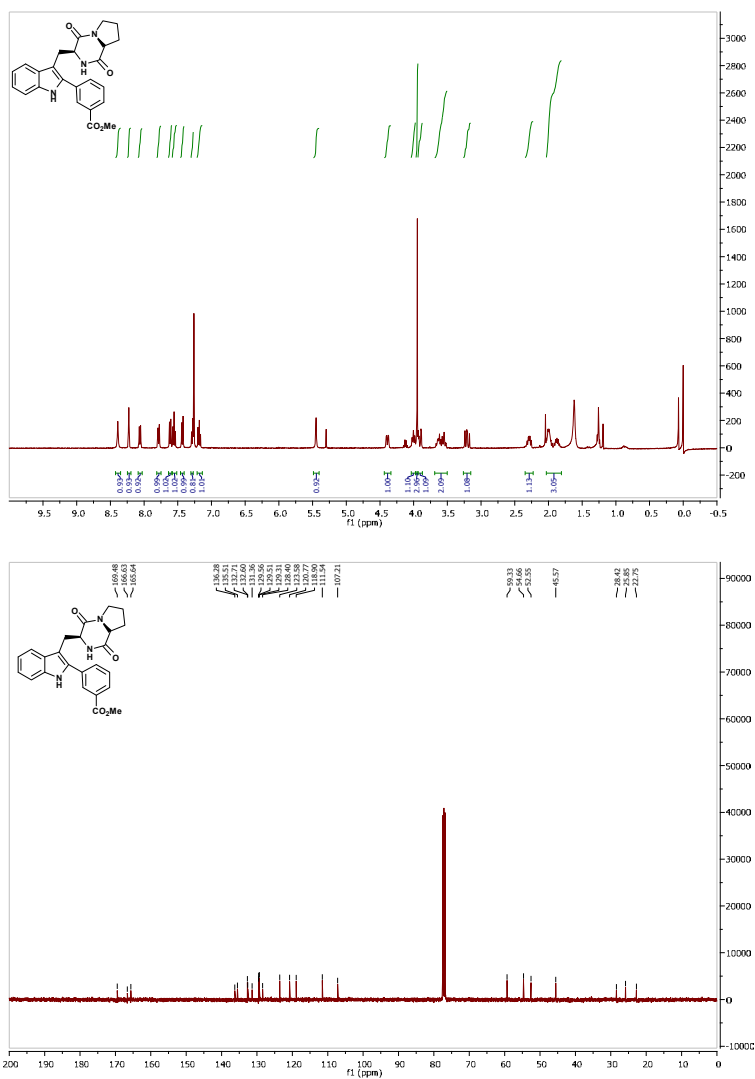
Electronic Supplementary Material (ESI) for Medicinal Chemistry Communications
This journal is © The Royal Society of Chemistry 2013

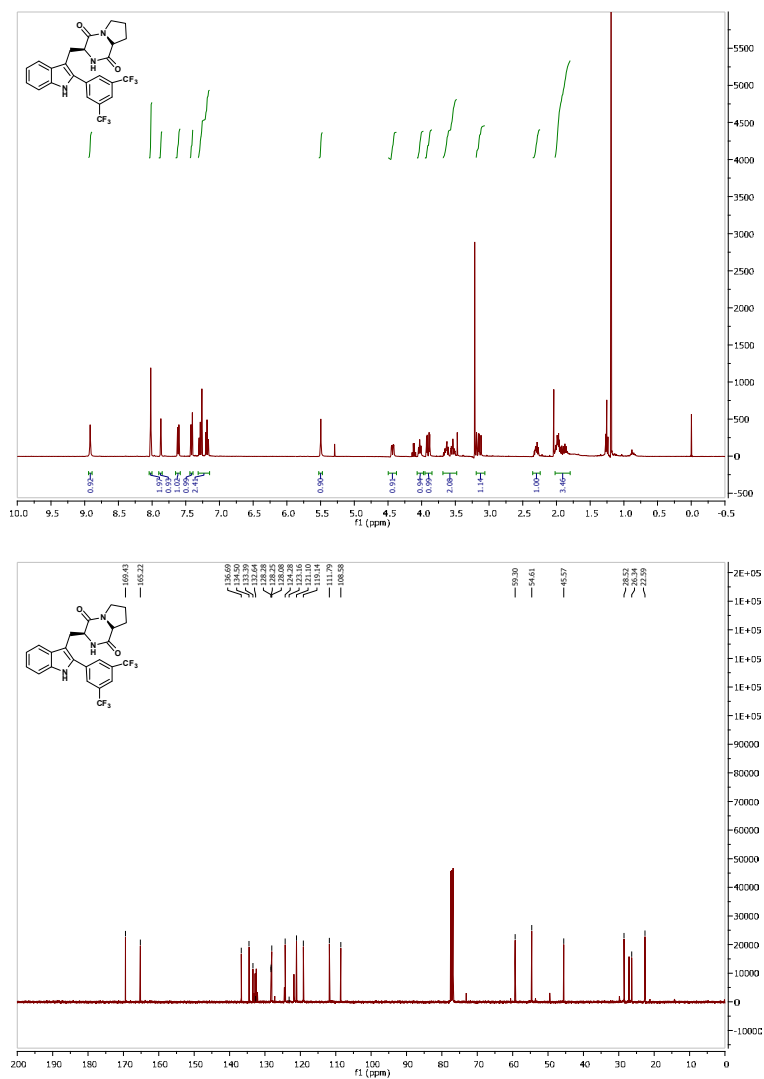
(3S,8aS)-3-((2-(3-Chlorophenyl)-1H-indol-3-yl)methyl)hexahydropyrrolo[1,2-a]pyrazine-1,4-dione (4k)



Electronic Supplementary Material (ESI) for Medicinal Chemistry Communications
This journal is © The Royal Society of Chemistry 2013

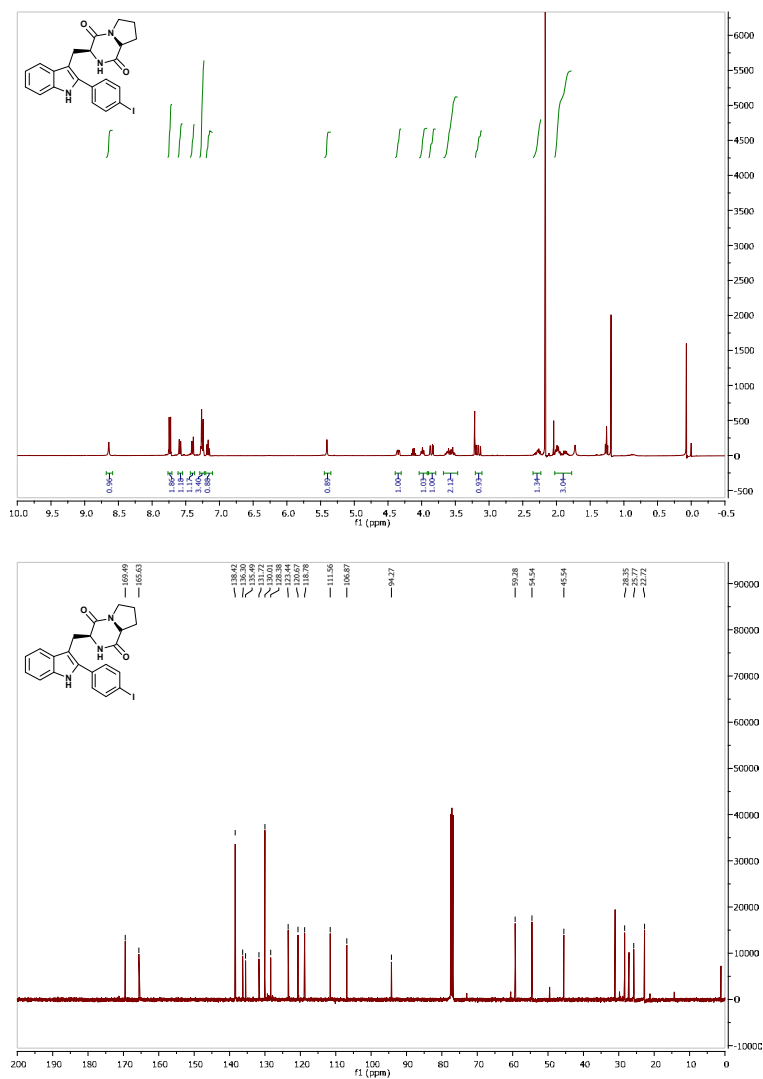
Methyl 3-(3-(((3*S*,8*aS*)-1,4-dioxooctahydropyrrolo[1,2-*a*]pyrazin-3-yl)methyl)-1*H*-indol-2-yl)benzoate (41)



(3S,8aS)-3-((2-(3,5-bis(trifluoromethyl)phenyl)-1*H*-indol-3-yl)methyl)hexahydropyrrolo[1,2-*a*]pyrazine-1,4-dione (4m)

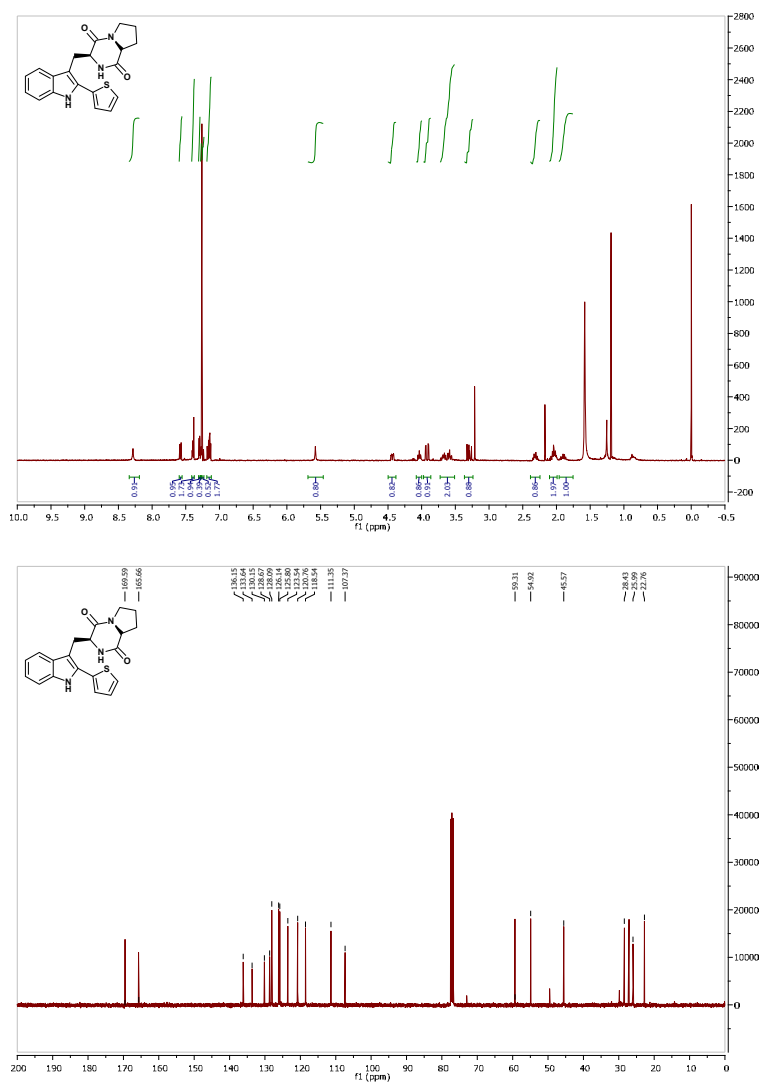
Electronic Supplementary Material (ESI) for Medicinal Chemistry Communications
This journal is © The Royal Society of Chemistry 2013

(3S,8aS)-3-((2-(4-iodophenyl)-1H-indol-3-yl)methyl)hexahydropyrrolo[1,2-a]pyrazine-1,4-dione (4n)



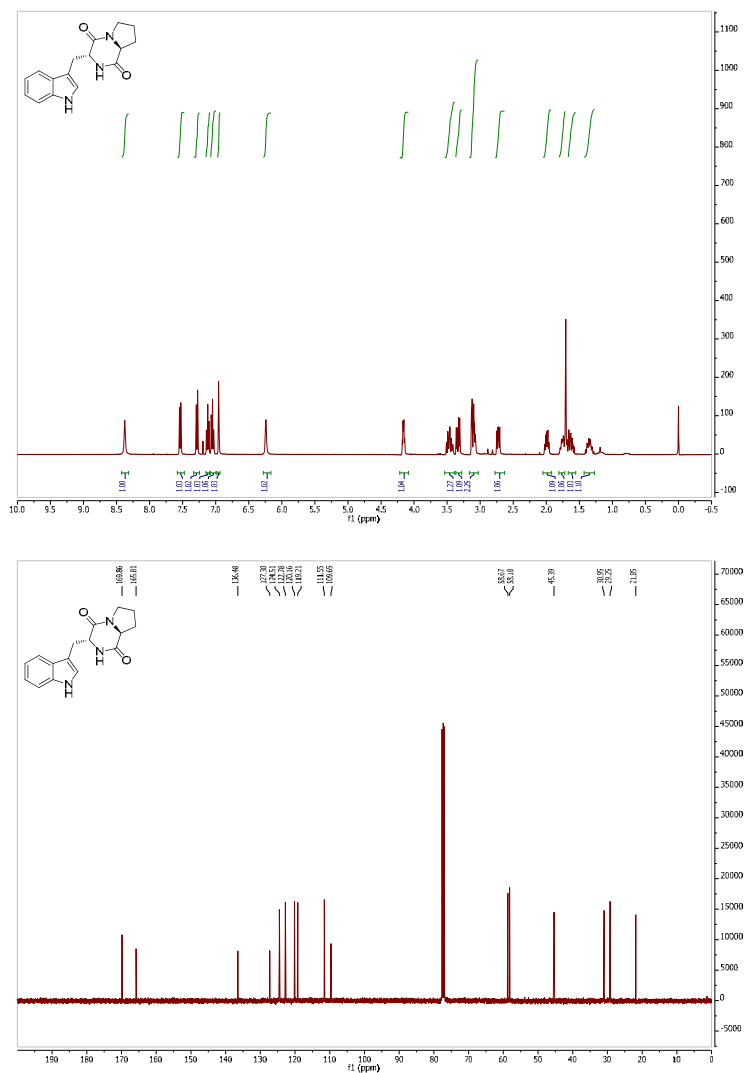
Electronic Supplementary Material (ESI) for Medicinal Chemistry Communications
This journal is © The Royal Society of Chemistry 2013

(3S,8aS)-3-((2-(2-iodothiophene)-1*H*-indol-3-yl)methyl)hexahydropyrrolo[1,2-*a*]pyrazine-1,4-dione (4o)



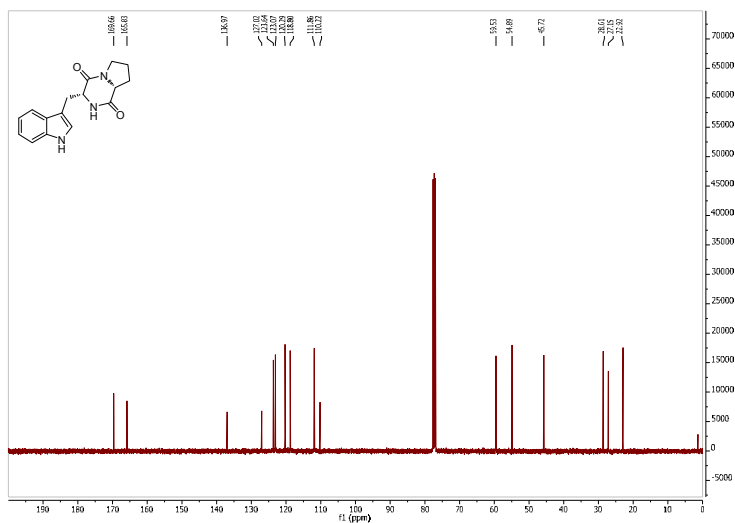
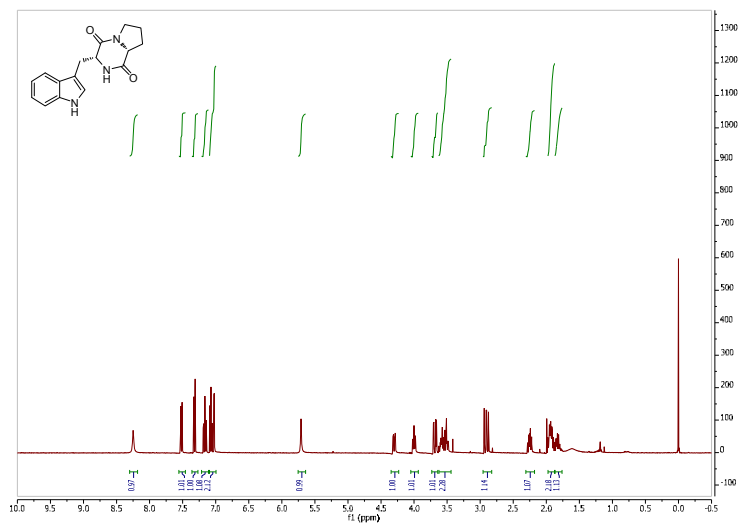
Electronic Supplementary Material (ESI) for Medicinal Chemistry Communications
This journal is © The Royal Society of Chemistry 2013

(3*R*,8*aS*)-3-((1*H*-indol-3-yl)methyl)hexahydropyrrolo[1,2-*a*]pyrazine-1,4-dione (1')



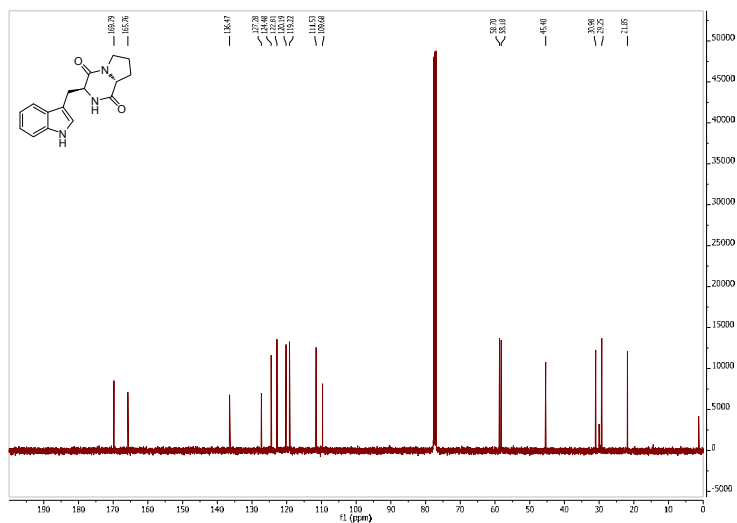
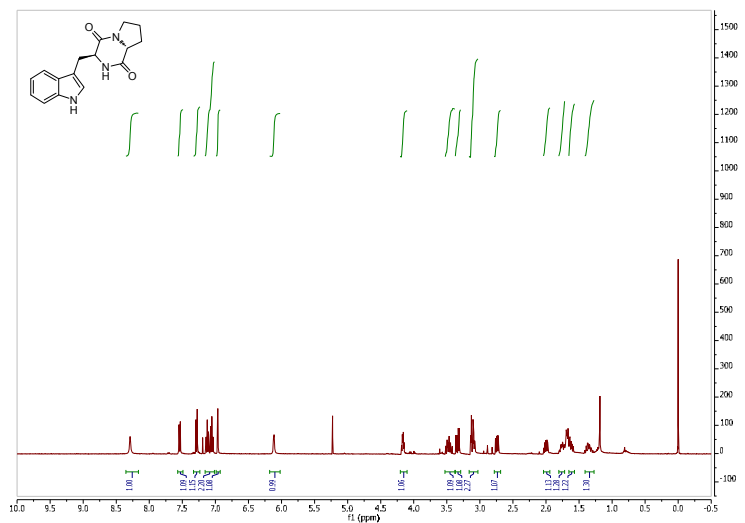
Electronic Supplementary Material (ESI) for Medicinal Chemistry Communications
This journal is © The Royal Society of Chemistry 2013

(3R,8aR)-3-((1H-indol-3-yl)methyl)hexahydropyrrolo[1,2-a]pyrazine-1,4-dione (1'')



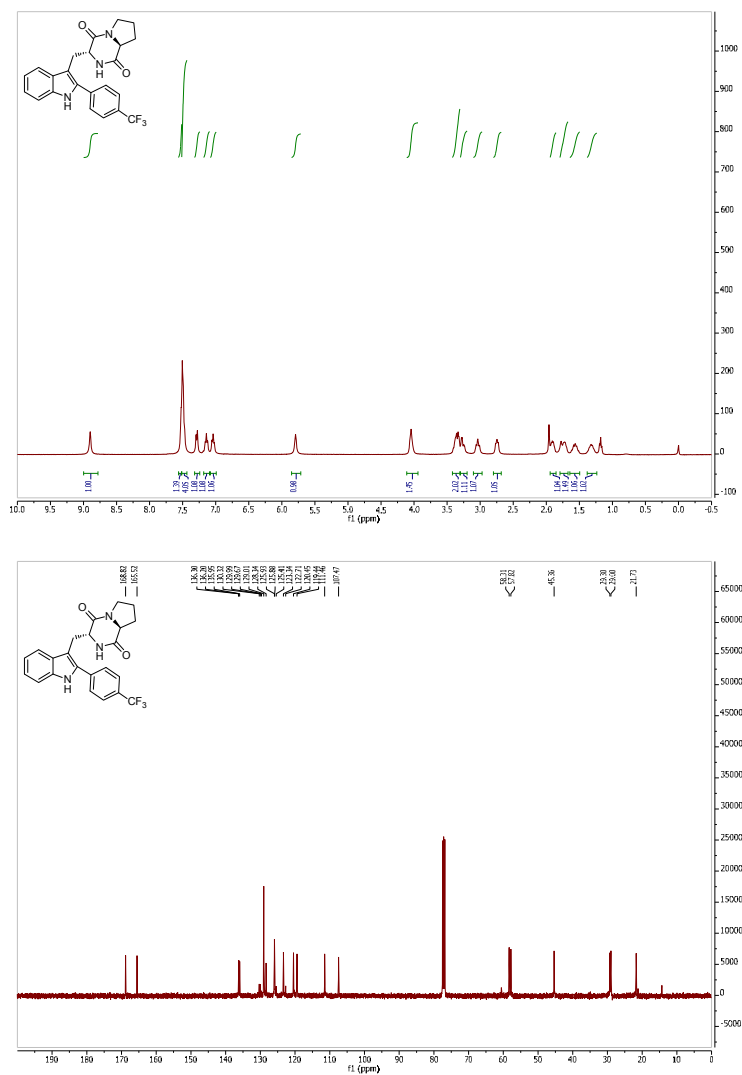
Electronic Supplementary Material (ESI) for Medicinal Chemistry Communications
This journal is © The Royal Society of Chemistry 2013

(3S,8aR)-3-((1H-indol-3-yl)methyl)hexahydropyrrolo[1,2-a]pyrazine-1,4-dione (1''')



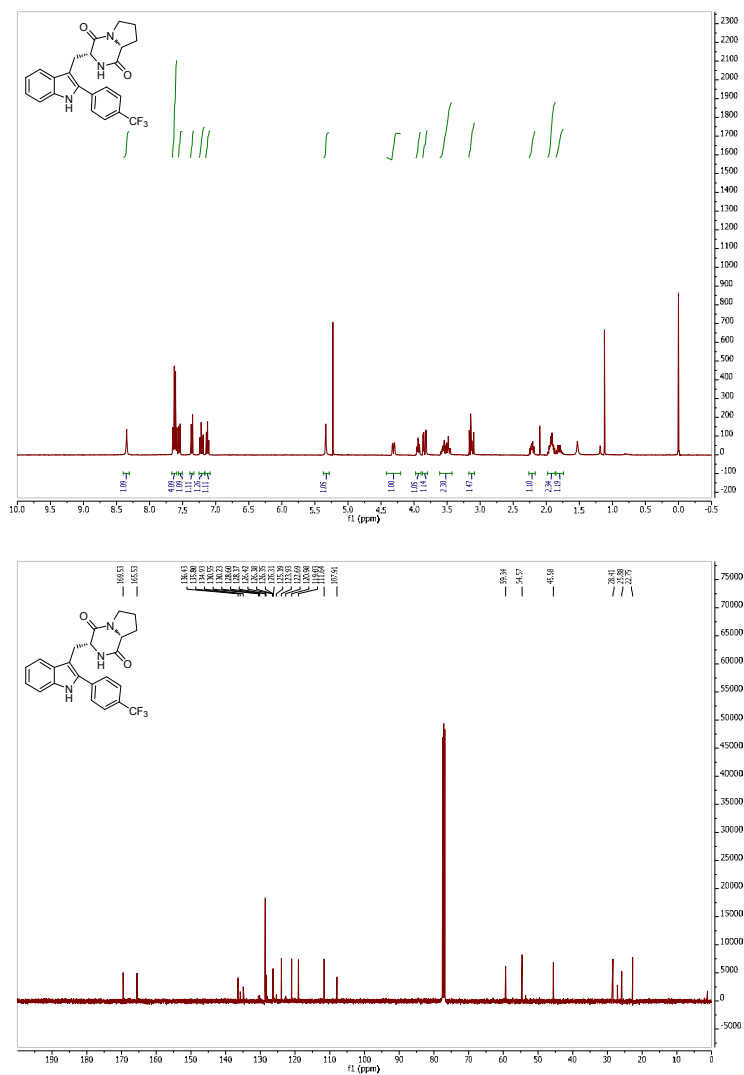
Electronic Supplementary Material (ESI) for Medicinal Chemistry Communications
This journal is © The Royal Society of Chemistry 2013

(3*R*,8*aS*)-3-((2-(4-(Trifluoromethyl)phenyl)-1*H*-indol-3-yl)methyl)hexahydropyrrolo[1,2-*a*]pyrazine-1,4-dione (4*c'*)



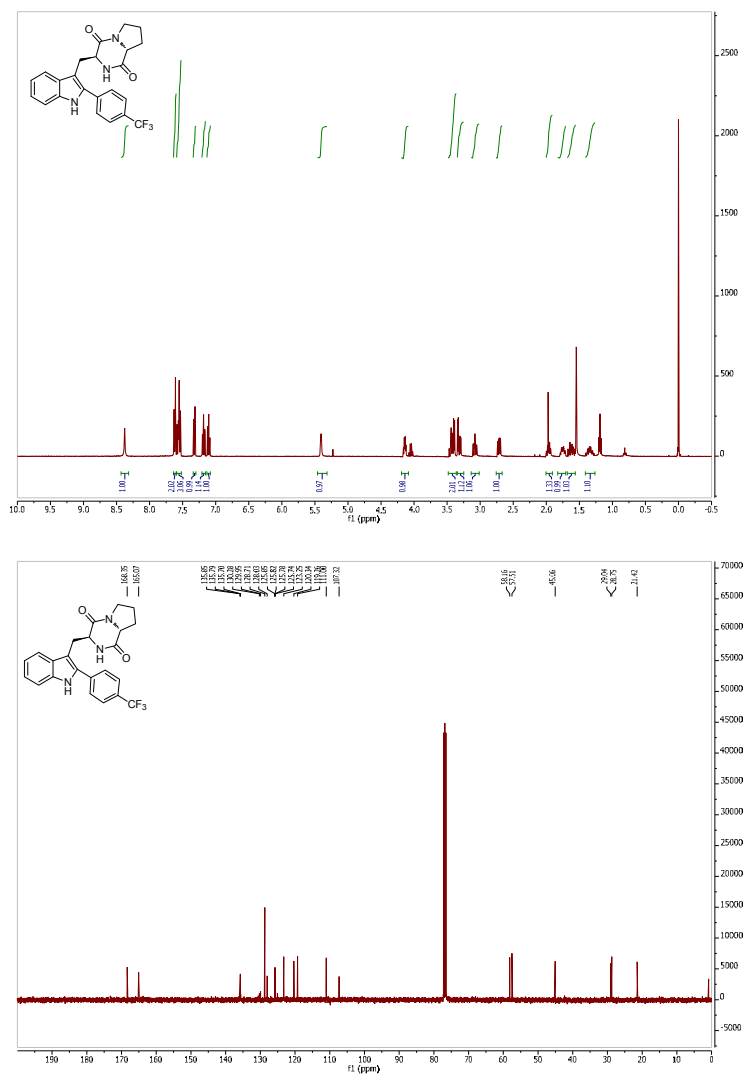
Electronic Supplementary Material (ESI) for Medicinal Chemistry Communications
This journal is © The Royal Society of Chemistry 2013

(3*R*,8*aR*)-3-((2-(4-(Trifluoromethyl)phenyl)-1*H*-indol-3-yl)methyl)hexahydropyrrolo[1,2-*a*]pyrazine-1,4-dione (4*c''*)



Electronic Supplementary Material (ESI) for Medicinal Chemistry Communications
This journal is © The Royal Society of Chemistry 2013

(3S,8aR)-3-((2-(4-(Trifluoromethyl)phenyl)-1H-indol-3-yl)methyl)hexahydropyrrolo[1,2-a]pyrazine-1,4-dione (4c'')



Biological Evaluation.

In vitro cell growth inhibitory activity

The synthesized compounds **4a-e** were evaluated for their antiproliferative activities against four human cancer cell lines: cervical adenocarcinoma HeLa cells, lung carcinoma A-549 cells, breast adenocarcinoma SK-BR-3 cells and colon adenocarcinoma HT-29 cells. In the assays the cells were exposed to the compounds *in vitro* and IC₅₀ values calculated from dose-response relationships following quantitation of the surviving cells by the standard MTT test. The IC₅₀ values are summarized in **tables 1 and 2**.

Cytotoxicity assay compounds 4a-4e

The four human cell lines were obtained from the American Type Culture Collection (ATCC). The HeLa cervical adenocarcinoma cells were grown in DMEM, A-549 lung carcinoma cells in F-12K Medium and SK-BR-3 breast adenocarcinoma and HT-29 colon adenocarcinoma cells in McCoy's 5a Medium Modified, all of them supplemented with 10% fetal bovine serum (FBS), 2 mM L-glutamine and antibiotics. Cells were subcultured twice a week and maintained at 37 °C in a humidified atmosphere containing 5% CO₂.

Normally growing cells were plated at 5x10³ cells/well into 96-well plates and incubated for 24 h at 37 °C to allow attachment to the plate surface. Samples were then added for initial screening at 200 μM, 100 μM and 50 μM dissolved in a DMSO-PBS vehicle (less than 1% in culture medium). Any drug showing <50% cell survival at 200 μM was further tested using appropriate drug concentrations to determine its IC₅₀. Drugs were run in triplicate or greater and control wells contained appropriate percentages of vehicle.

After 72 h exposure, the antitumor effect was measured using a solution of MTT (3-(4,5-Dimethylthiazol-2-yl)-2,5-diphenyltetrazolium bromide), which is bio-reduced by viable cells into formazan. The formed crystals were solubilized using DMSO and the amount of formazan was measured by reading the absorbance at 570 nm. The amount of formazan present was proportional to the number of living cells in culture. The absorbance of wells containing only the MTT reagent (the plate blank) was subtracted from all wells.

The IC₅₀ values were determined by dose response curve analysis and statistical analysis using GraphPad Prism software version 5.0a.

Table 1. Cytotoxicity evaluation (IC_{50} , $\mu M \pm SD^1$) of compounds **4a-e** and a reference compound (brevinamide F, **1**) against selected tumor cell lines.

Cell line	4a	4b	4c	4d	4e	1
HeLa	135.0 \pm 9.0	157.2 \pm 12.7	25.8 \pm 4.2	52.2 \pm 9.2	>200	>200
A-549	149.7 \pm 24.4	>200	104.6 \pm 33.2	167.2 \pm 26.3	>200	>200
SK-BR-3	>200	>200	127.2 \pm 43.7	>200	>200	>200
HT-29	>200	191.3 \pm 24.4	80.4 \pm 16.2	152.1 \pm 32.9	>200	>200

¹ SD: standard deviation. All experiments were independently performed at least three times.**Cytotoxicity assay compounds 4a-o**

The human cell lines were obtained from the American Type Culture Collection (ATCC). The HeLa cervical adenocarcinoma cells were grown in DMEM and HT-29 colon adenocarcinoma cells in McCoy's 5a Medium Modified, both of them supplemented with 10% fetal bovine serum (FBS), 2 mM *L*-glutamine and antibiotics. Cells were subcultured twice a week and maintained at 37 °C in a humidified atmosphere containing 5% CO₂.

Normally growing cells were plated at 1×10^4 cells/well into 96-well plates and incubated for 24 h at 37 °C to allow attachment to the plate surface. Samples were then added in ten different concentrations dissolved in a DMSO-PBS vehicle (less than 1% in culture medium) to determine their IC_{50} . Drugs were run in triplicate or greater and control wells contained appropriate percentages of vehicle.

After 24 h exposure, the antitumor effect was measured using a solution of MTT (3-(4,5-Dimethylthiazol-2-yl)-2,5-diphenyltetrazolium bromide), which is bio-reduced by viable cells into formazan. The formed crystals were solubilized using DMSO and the amount of formazan was measured by reading the absorbance at 570 nm. The amount of formazan present was proportional to the number of living cells in culture. The absorbance of wells containing only the MTT reagent (the plate blank) was subtracted from all wells.

The IC_{50} values were determined by dose response curve analysis and statistical analysis using GraphPad Prism software version 5.0a.

Table 2. Cytotoxicity evaluation (IC_{50} , $\mu M \pm SD^1$) of compounds **4a-o** and a reference compound (puromycin) against selected tumor cell lines.

Compound	HeLa cells	HT-29 cells
4a	160.2 \pm 9.2	214.9 \pm 10.0
4b	193.8 \pm 10.7	205.3 \pm 7.0
4c	62.0 \pm 11.5	118.5 \pm 7.7
4d	81.8 \pm 12.0	184.3 \pm 7.8
4e	208.7 \pm 17.8	204.1 \pm 10.5
4f	82.2 \pm 12.0	143.0 \pm 15.7
4g	82.4 \pm 18.6	153.7 \pm 12.4
4h	66.7 \pm 17.4	144.2 \pm 13.2
4i	172.1 \pm 25.8	200.3 \pm 9.9
4j	255.4 \pm 11.8	187.8 \pm 6.9
4k	174.6 \pm 18.5	200.3 \pm 12.7
4l	190.3 \pm 19.6	177.6 \pm 14.2
4m	160.3 \pm 23.7	64.2 \pm 15.8
4n	146.6 \pm 13.3	170.8 \pm 8.6
4o	170.1 \pm 11.5	177.6 \pm 15.2
Puromycin	0.7 \pm 0.1	3.6 \pm 1.2

¹ SD: standard deviation. All experiments were independently performed at least three times.**Cell lines and Culture Conditions**

Human lung carcinoma (A549) and human mammary adenocarcinoma (MDA-MB-231) cell lines were purchased from the American Type Culture Collection (ATCC, Manassas, VA). Human oral squamous carcinoma cells (Cal27) were kindly provided by Dr. Silvio Gutkind (Oral and Pharyngeal Cancer Branch, National Institute of Dental and Craniofacial Research, NIH, Bethesda, USA). A549 and Cal27 cells were cultured in DMEM medium and MDA-MB-231 cells in DMEM:F12 medium (1:1, Biological Industries, Beit Haemek, Israel) supplemented with 10% heat-inactivated foetal bovine serum (FBS; Life Technologies, Carlsbad, CA), 100 U/mL penicillin, 100 μ g/mL streptomycin, and 2 mM L- glutamine, all from Biological Industries. Cells were grown at 37°C in a 5% CO₂ atmosphere.

Cell Viability Assay for compounds 4c-4c''

Cells (1×10^5 cells/mL) were seeded in 96-well plates and allowed to grow for 24 h. Afterwards, they were treated with all compounds at different concentrations, ranging from 1.56 to 200 μ M, to calculate the inhibitory concentration of 50% of cell population (IC_{50}). Cell viability was determined by MTT assay. After a 72h-treatment, 10 μ M of 3-(4, 5-dimethylthiazol-2-yl)-2,5-diphenyltetrazolium bromide (MTT, Sigma-Aldrich) was added to each well for an additional 4 h. DMSO was added in control cells. Media was aspirated and the blue MTT formazan precipitate was dissolved in 100 μ l of DMSO. The absorbance at 570 nm was measured on a multiwell plate reader. Cell viability was expressed as a percentage of control cells, and data are shown as the mean value \pm S.D. of three independent experiments performed in duplicate. IC_{50} values were calculated with GraphPad Prism 5 software. The IC_{50} values are summarized in table 3.

Table 3. Cell viability assay (IC_{50} , μ M \pm SD¹) for compounds 4c-4c''' at 72h treatment (μ M).

Compound	MDA-MB-231	Cal27	A549
4c	161.27 \pm 10.53	182.14 \pm 7.7	179.61 \pm 8.34
4c'	>200 μ M	>200 μ M	>200 μ M
4c''	161.35 \pm 8.24	137.72 \pm 29.20	185.92 \pm 12.75
4c'''	>200 μ M	>200 μ M	>200 μ M

Cell Cycle Analysis for compounds 4c and 4c''

Cells (2.5×10^4 cells/mL) were seeded in 6-well plates and allowed to grow for 24 h. Then, FBS depletion was performed during 24 h to synchronize the cell culture. Cells were treated with IC_{50} values of different compounds for 6, 24 and 48 h in the presence of FBS. After treatment, cells were trypsinized, collected and centrifuged at 300g for 5 min. Cells were washed with PBS and centrifuged again at the same conditions. Then, cells were resuspended in 100 μ l PBS and added drop-wise into a tube containing 1 ml of ice cold 70% ethanol while vortexing. Cells were kept at -20°C at least overnight. Ethanol-fixed cells (400 μ l) were centrifuged at 300 g for 5 min, washed with PBS and centrifuged again. Cell pellet was resuspended in 200 μ l of Muse™ Cell Cycle Reagent (Millipore, Billerica, MA) and incubated for 30 min at room temperature protected from light. FACS analysis was performed using a Muse™ Cell Analyzer cytometer (Millipore). The results for cell cycle analysis are summarized in tables 4 and 5, respectively.

Table 4. Cell cycle analysis of compound **4c**.

Compound 4c	G0/G1	S	G2/M
0h	64.37 ± 3.11	16.92 ± 0.67	18.67 ± 2.72
6h	47.30 ± 0.42	23.70 ± 0.00	29.00 ± 0.42
24h	60.30 ± 0.28	18.05 ± 0.35	21.65 ± 0.07
48h	61.22 ± 0.73	17.65 ± 0.66	21.07 ± 0.63

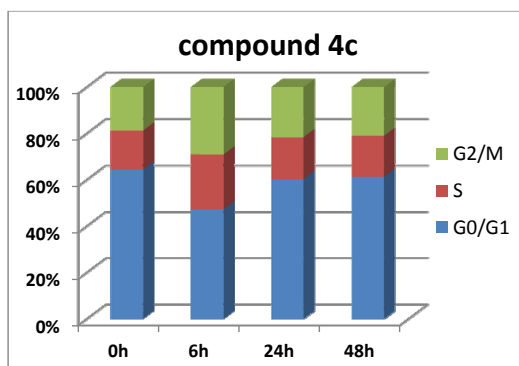
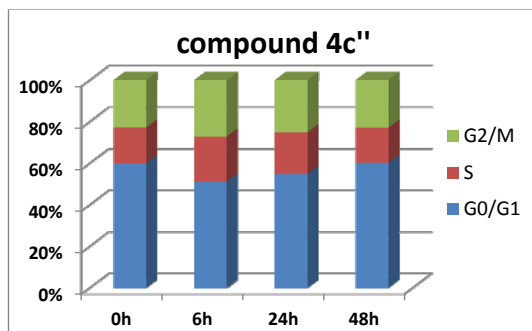


Table 5. Cell cycle analysis of compound **4c''**.

Compound 4c''	G0/G1	S	G2/M
0h	60.40 ± 0.94	17.30 ± 1.86	23.00 ± 0.61
6h	51.10 ± 0.42	21.65 ± 0.49	27.25 ± 0.07
24h	54.80 ± 1.13	20.05 ± 0.07	25.10 ± 1.13
48h	60.15 ± 0.89	16.95 ± 0.48	22.87 ± 0.63

Electronic Supplementary Material (ESI) for Medicinal Chemistry Communications
This journal is © The Royal Society of Chemistry 2013





FULL SUPPORTING INFORMATION PUBLICATION II

Supporting Information

Synthesis of C-2 Arylated Tryptophan Amino Acids and Related Compounds through Palladium Catalyzed C-H Activation

Sara Preciado, Lorena Mendive-Tapia, Fernando Albericio and Rodolfo
Lavilla**

Table of Contents

Abbreviations. Page S1.

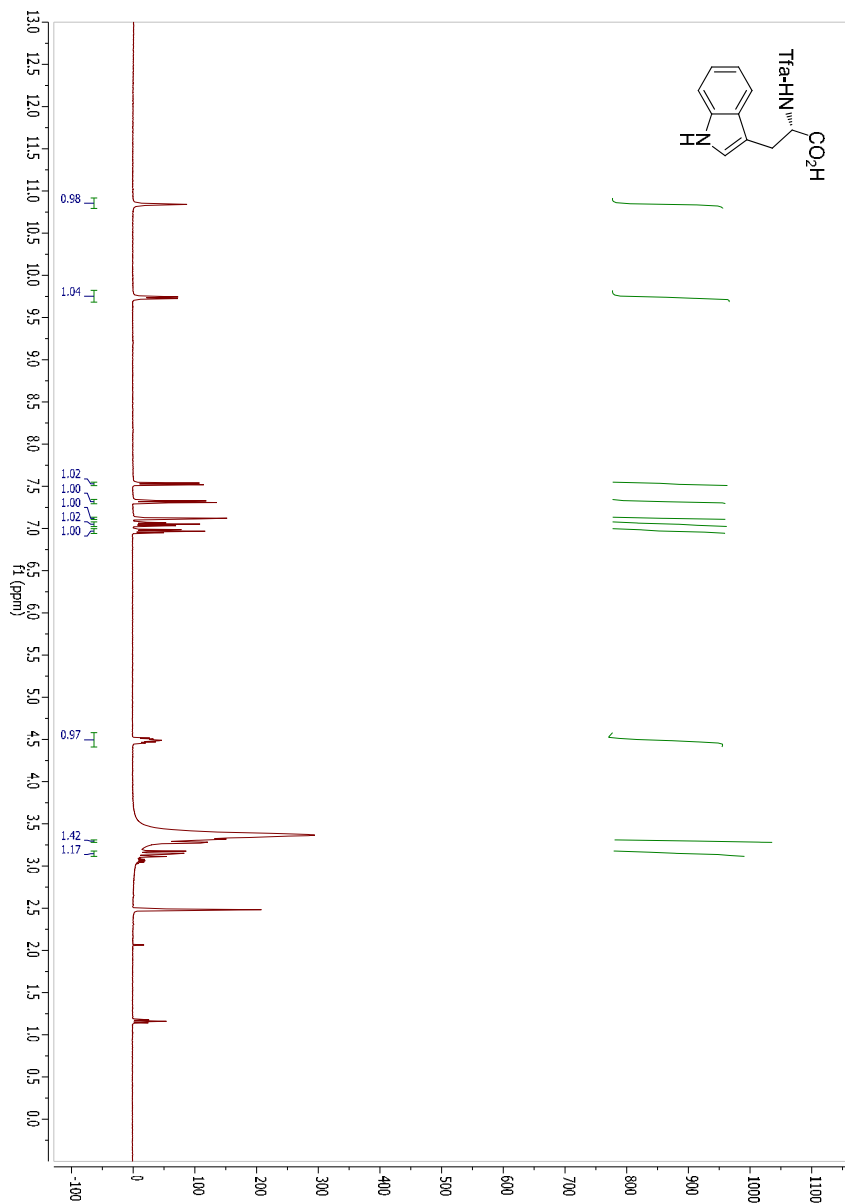
Spectroscopic data. Page S2.

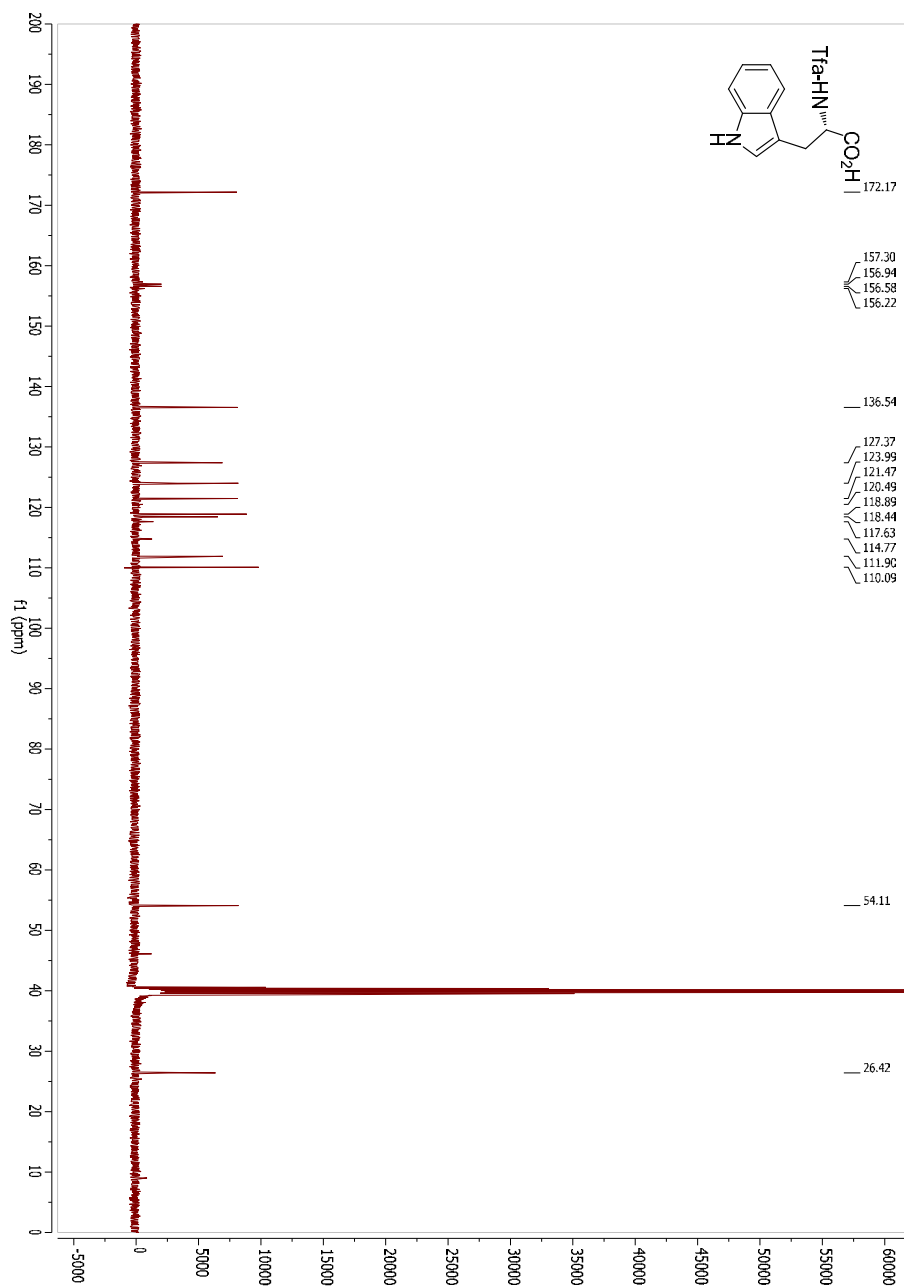
Chromatographic analysis of 5a and 5a'. Page S41.

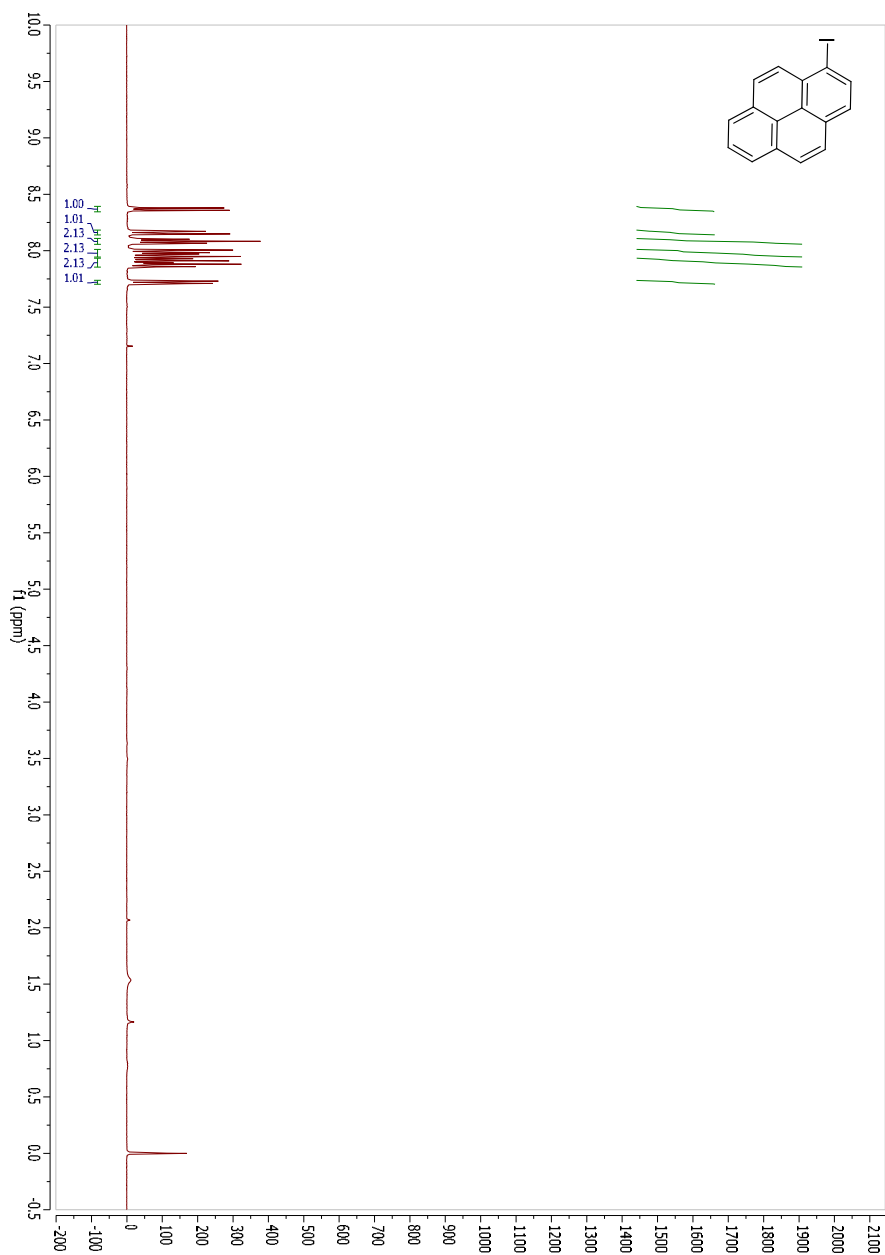
Supporting Information

Abbreviations

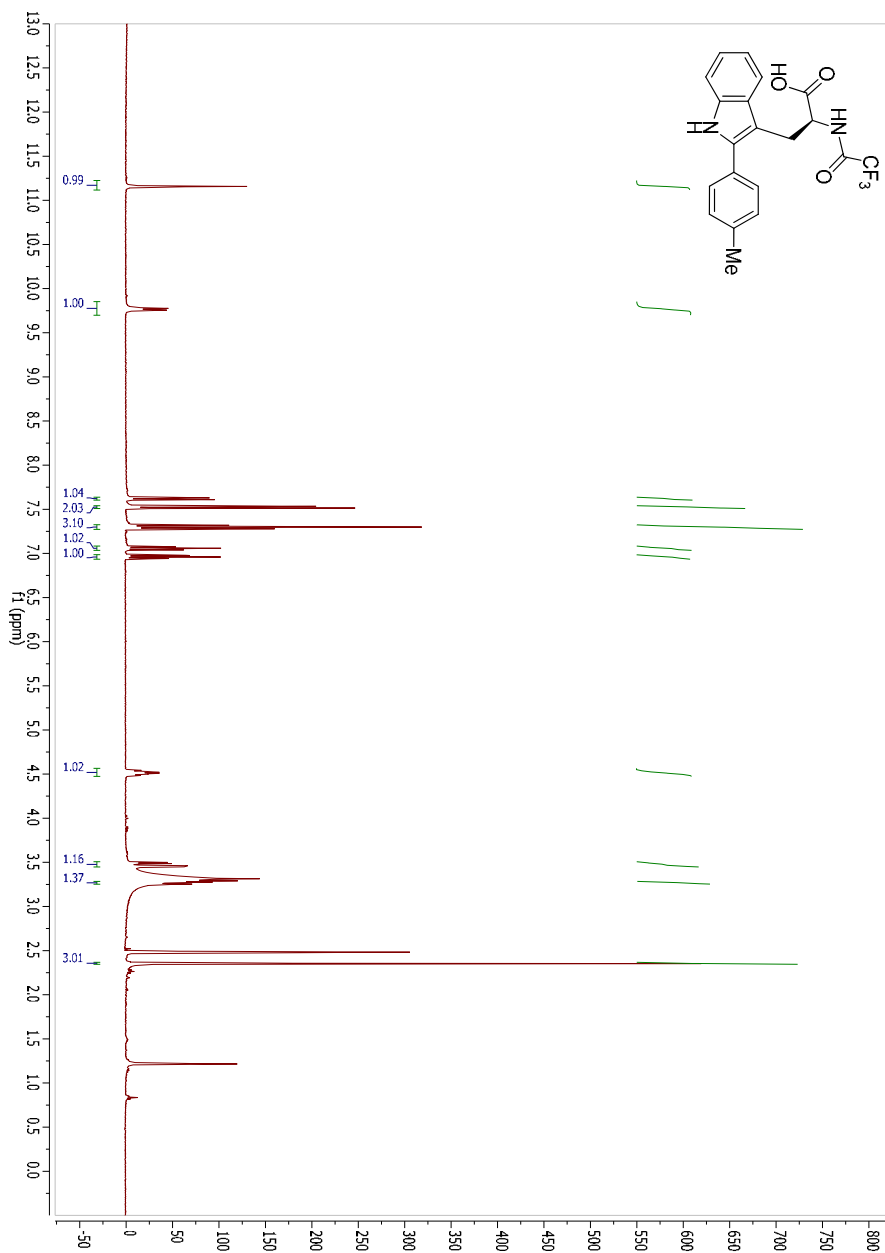
Abbreviation used for amino acids and designations of peptides follow the rules of the IUPAC-IUB Commission of Biochemical Nomenclature in *J. Biol. Chem.* 247, 977-983 (1982). The following additional abbreviations are used: DMF: *N,N*-dimethylformamide, DCM: dichloromethane, Fmoc: 9*H*-fluorenylmethyloxycarbonyl, Tfa: trifluoroacetyl, TFA: trifluoroacetic acid, SPPS: solid phase peptide synthesis, DIPEA: *N,N*-diisopropylethylamine, DIPCdi: *N,N*-diisopropylcarbodiimide, RP-HPLC-ESMS: reverse-phase high performance liquid chromatography electrospray mass spectrometry, HRMS: high-resolution mass spectrometry, NMR: nuclear magnetic resonance, SPPS: solid-phase peptide synthesis, IR: infrared spectroscopy.

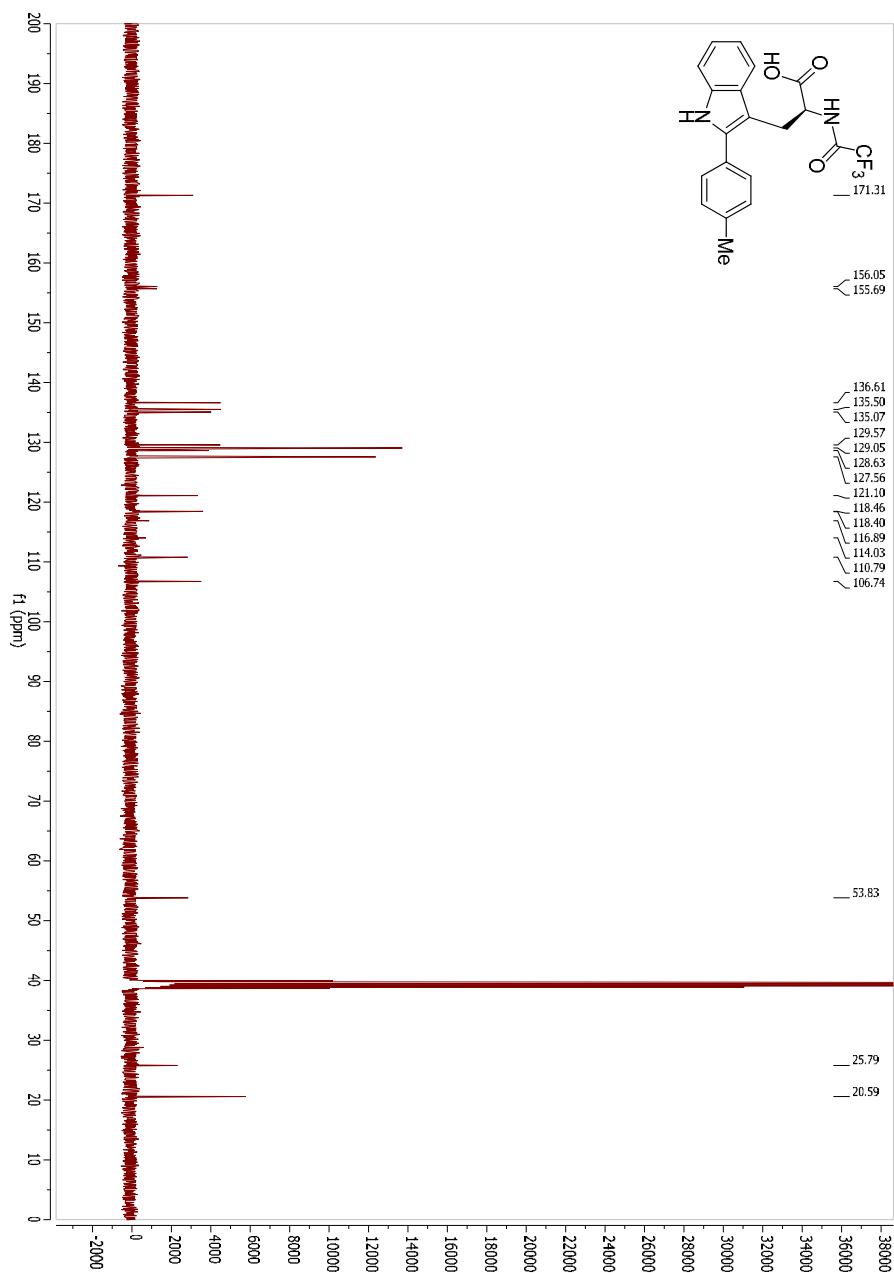
Spectroscopic data**(S)-3-(1*H*-Indol-3-yl)-2-(2,2,2-trifluoroacetamido)propanoic acid (1a)**

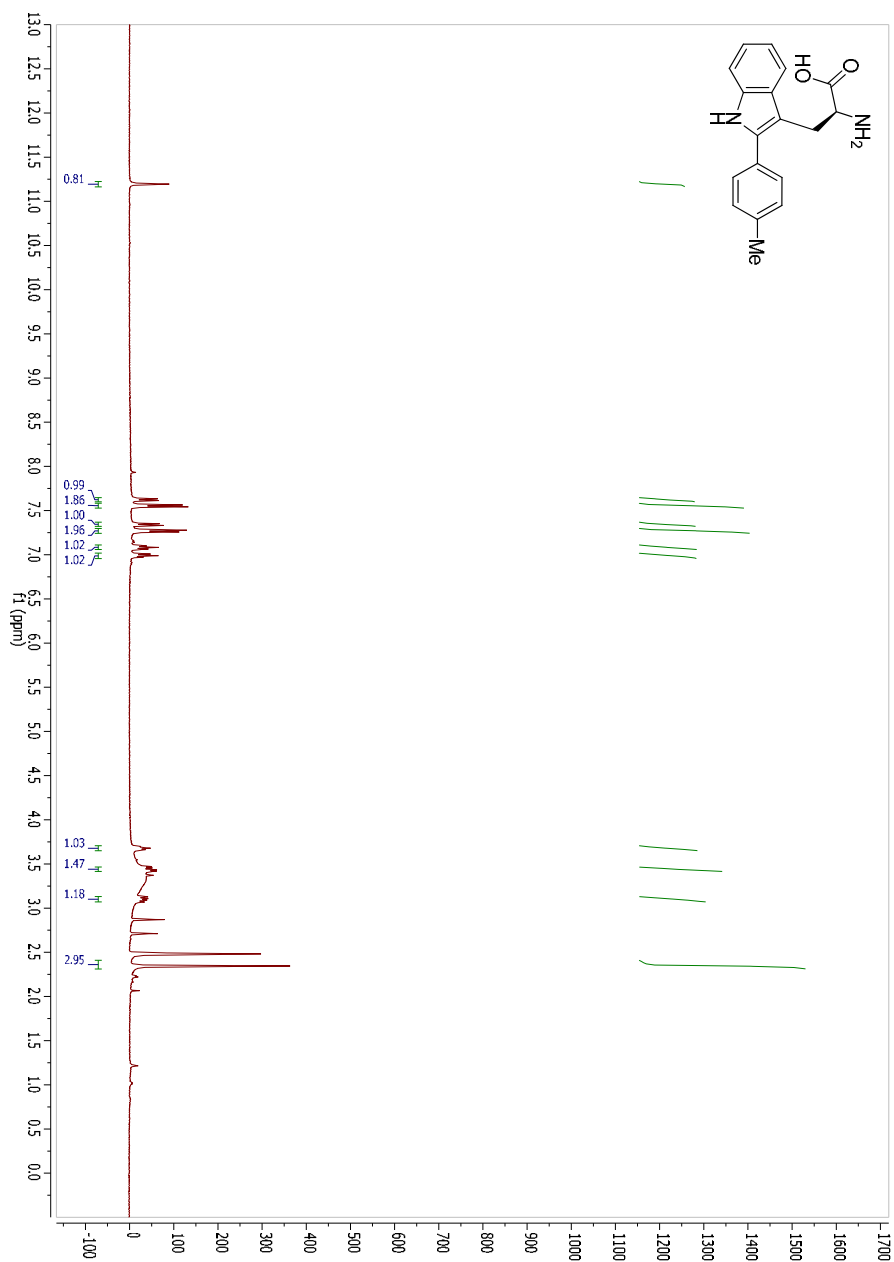


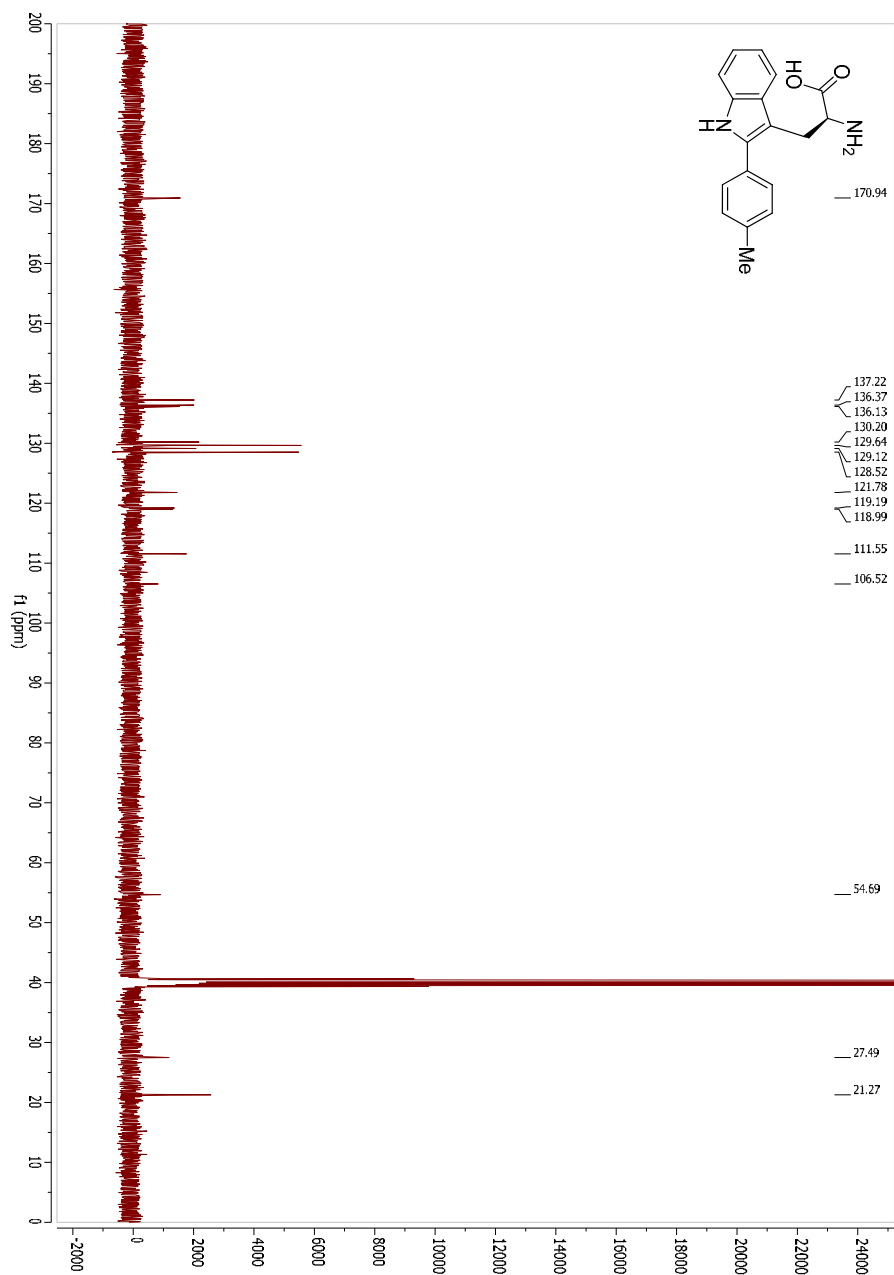
1-Iodopyrene (2b)

(S)-3-(2-phenyl-1*H*-indol-3-yl)-2-(2,2,2-trifluoroacetamido)propanoic acid (3)

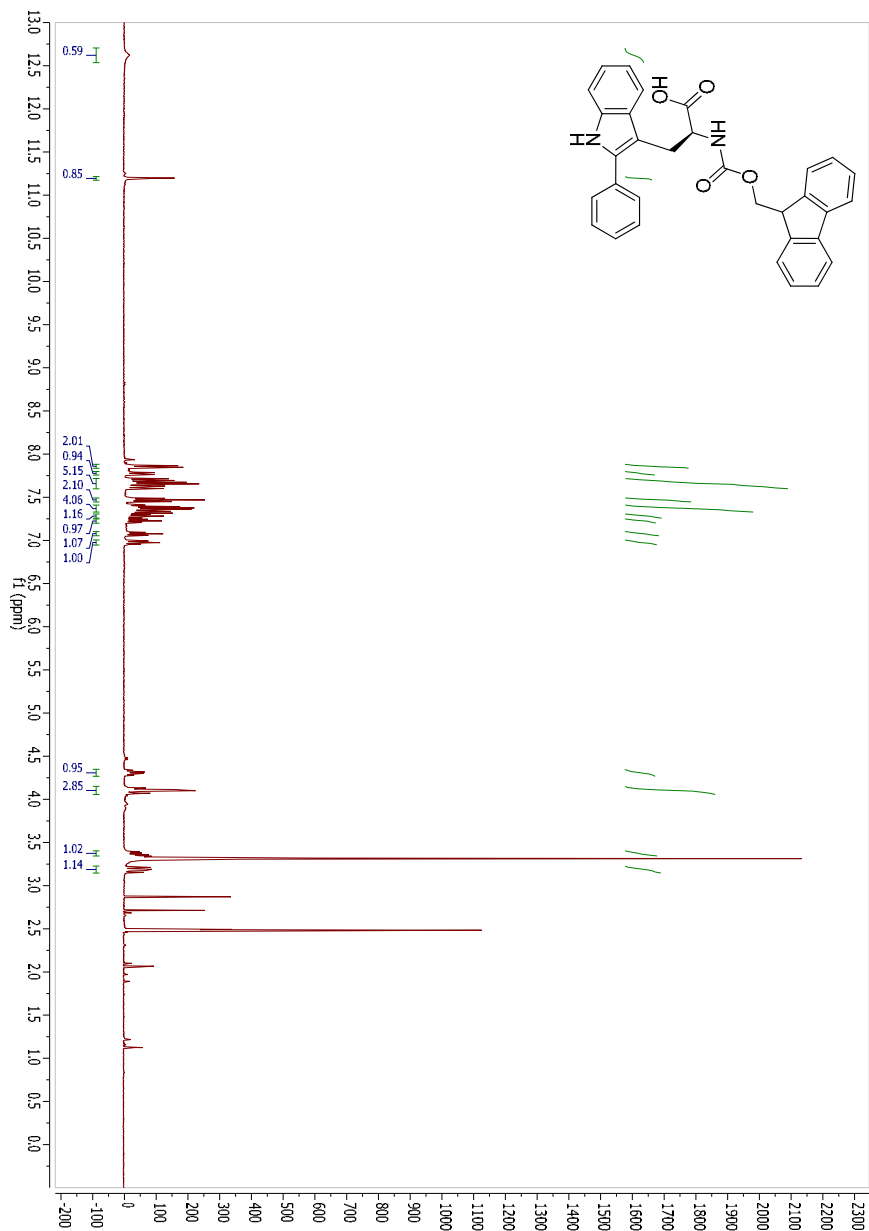




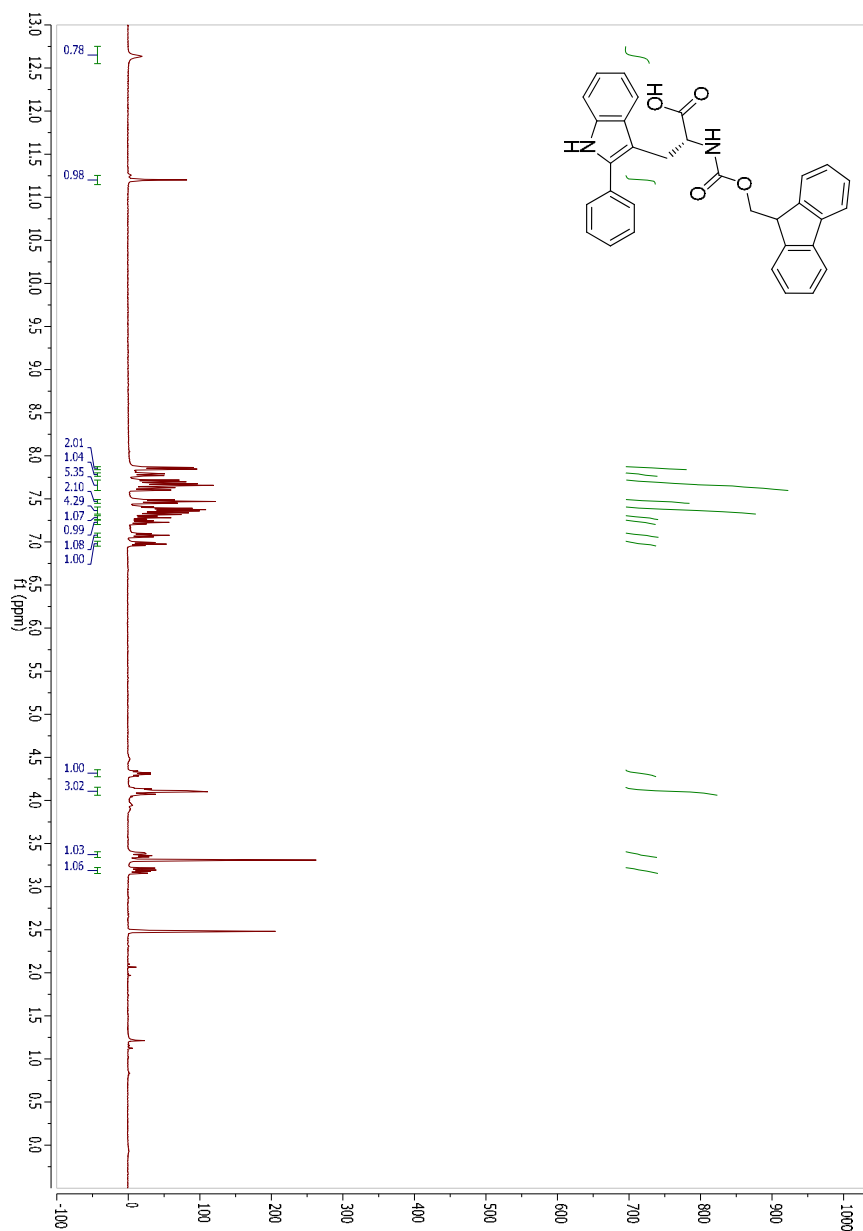
(S)-2-amino-3-(2-*p*-tolyl-1*H*-indol-3-yl)propanoic acid (4)

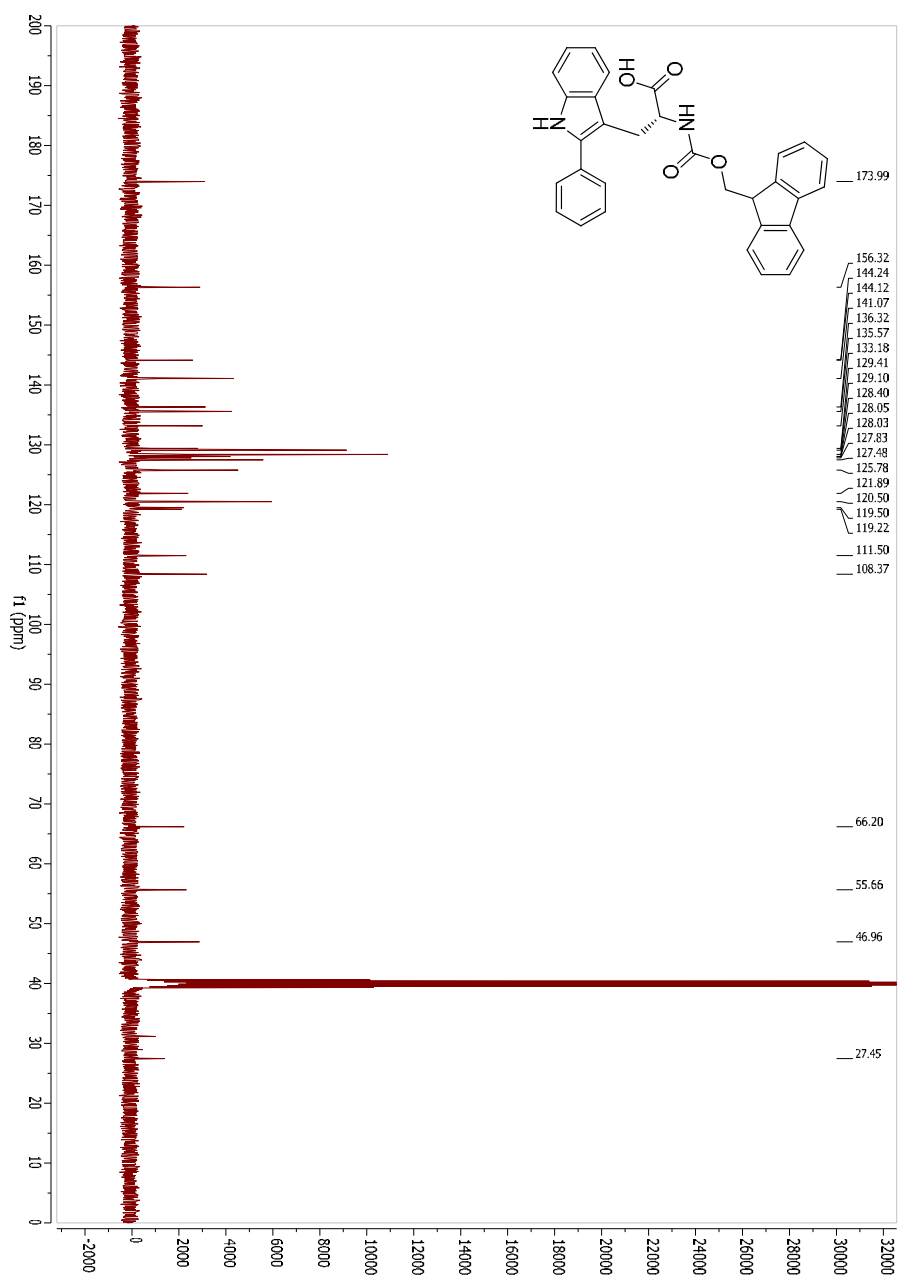


(S)-2-(((9H-Fluoren-9-yl)methoxy)carbonyl)amino)-3-(2-phenyl-1H-indol-3-yl)propanoic acid (5a)

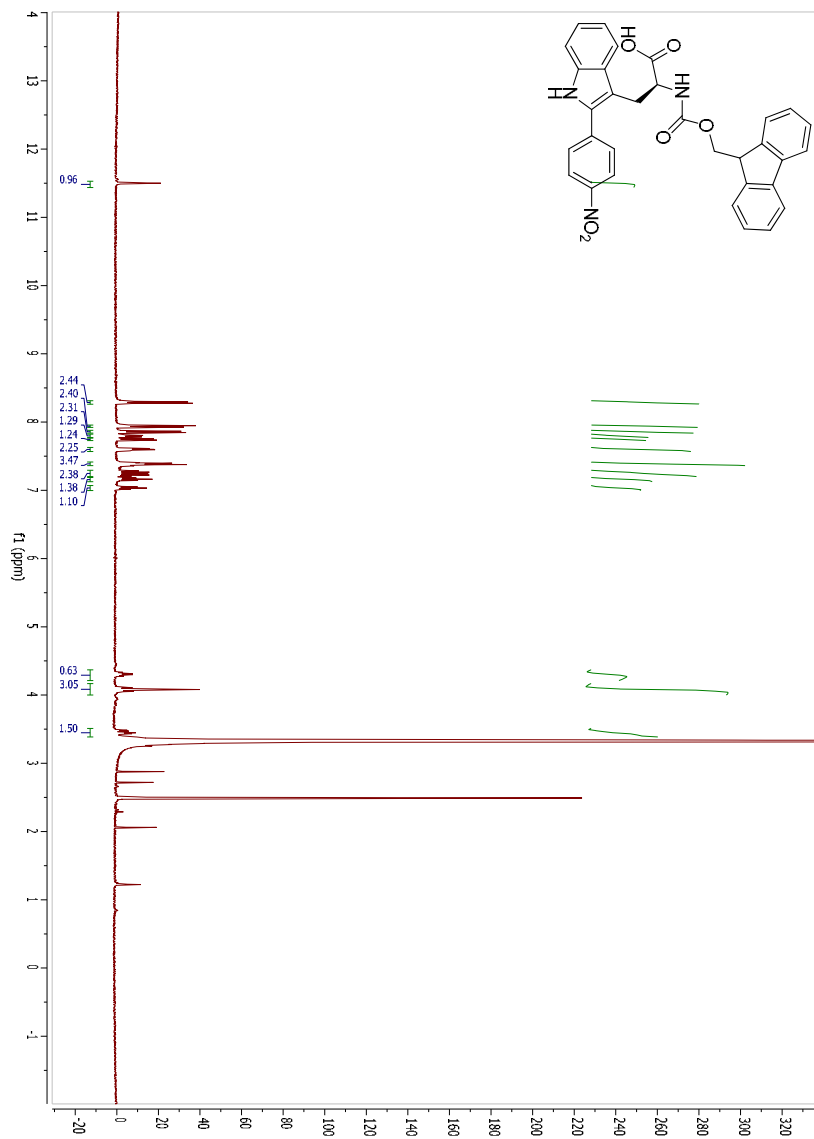


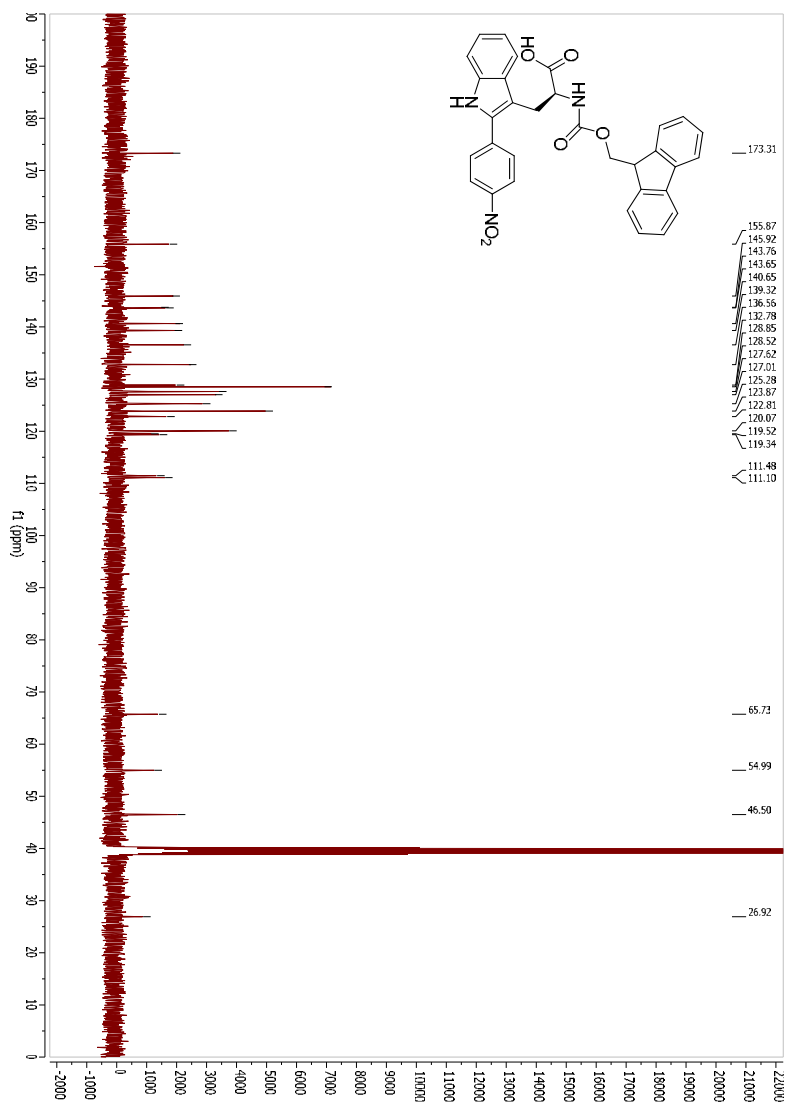
(*R*)-2-(((9*H*-Fluoren-9-yl)methoxy)carbonyl)amino)-3-(2-phenyl-1*H*-indol-3-yl)propanoic acid (5a'**)**



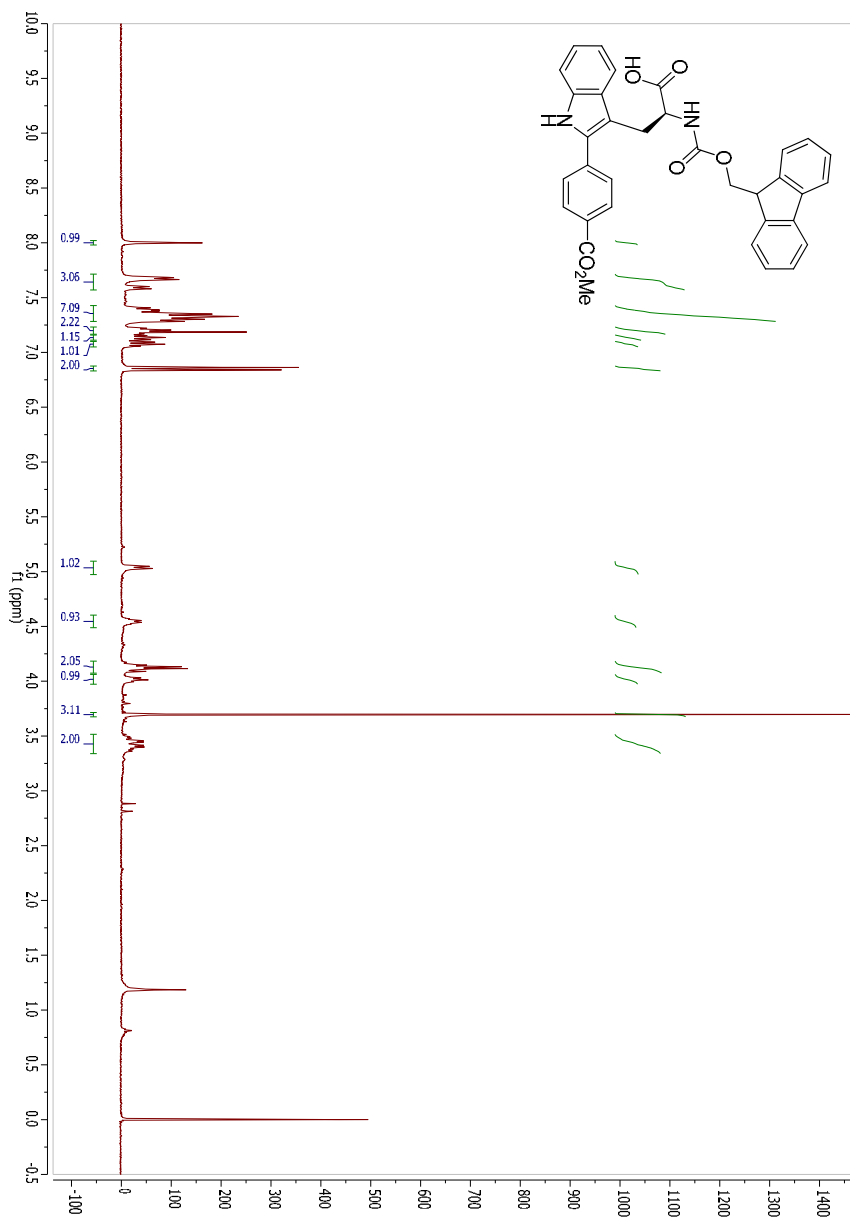


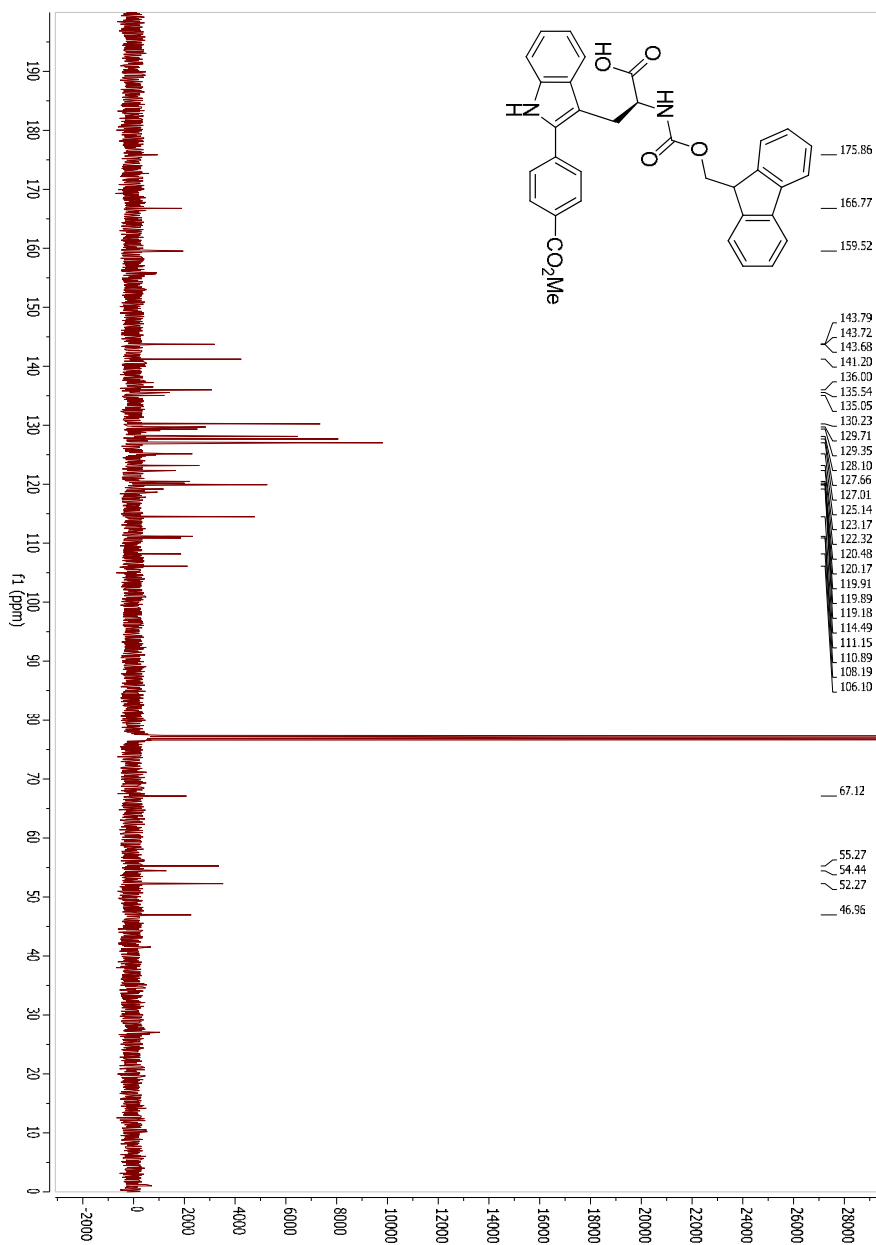
(S)-2-(((9H-Fluoren-9-yl)methoxy)carbonyl)amino)-3-(2-(4-nitrophenyl)-1H-indol-3-yl)propanoic acid (5b)



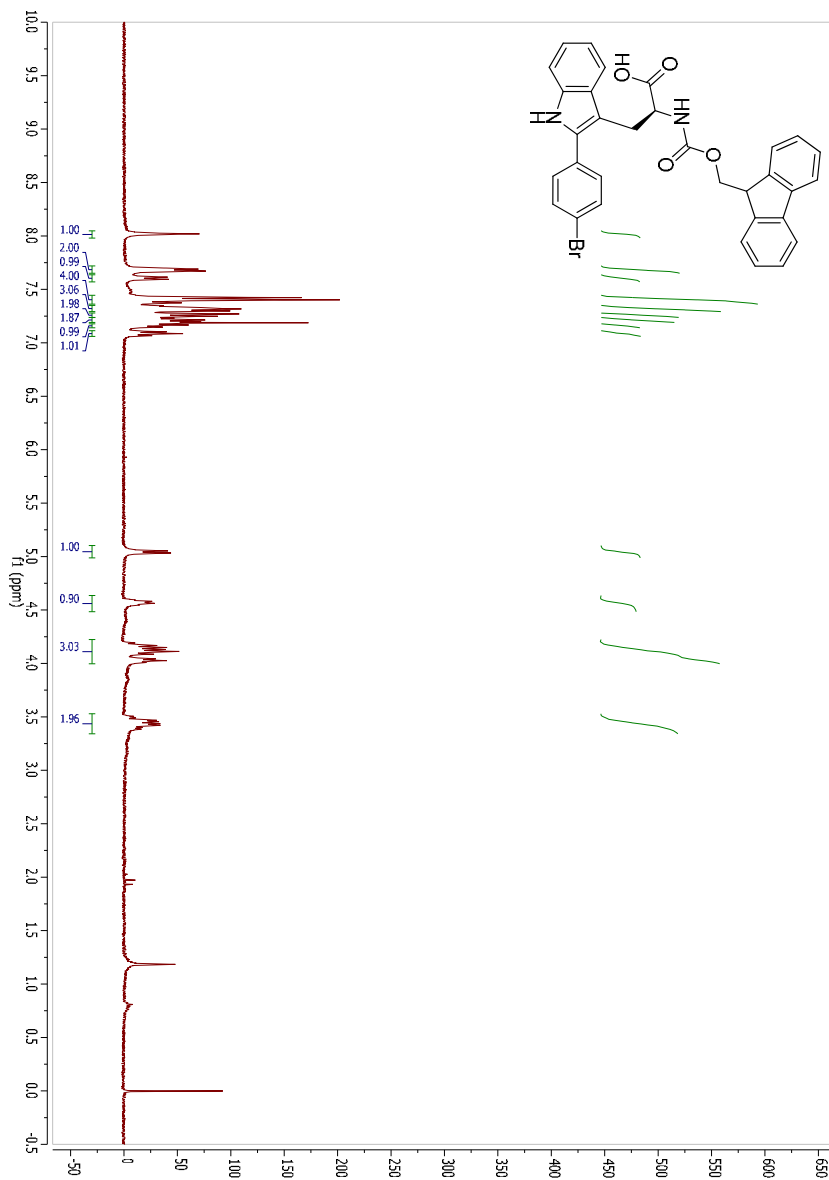


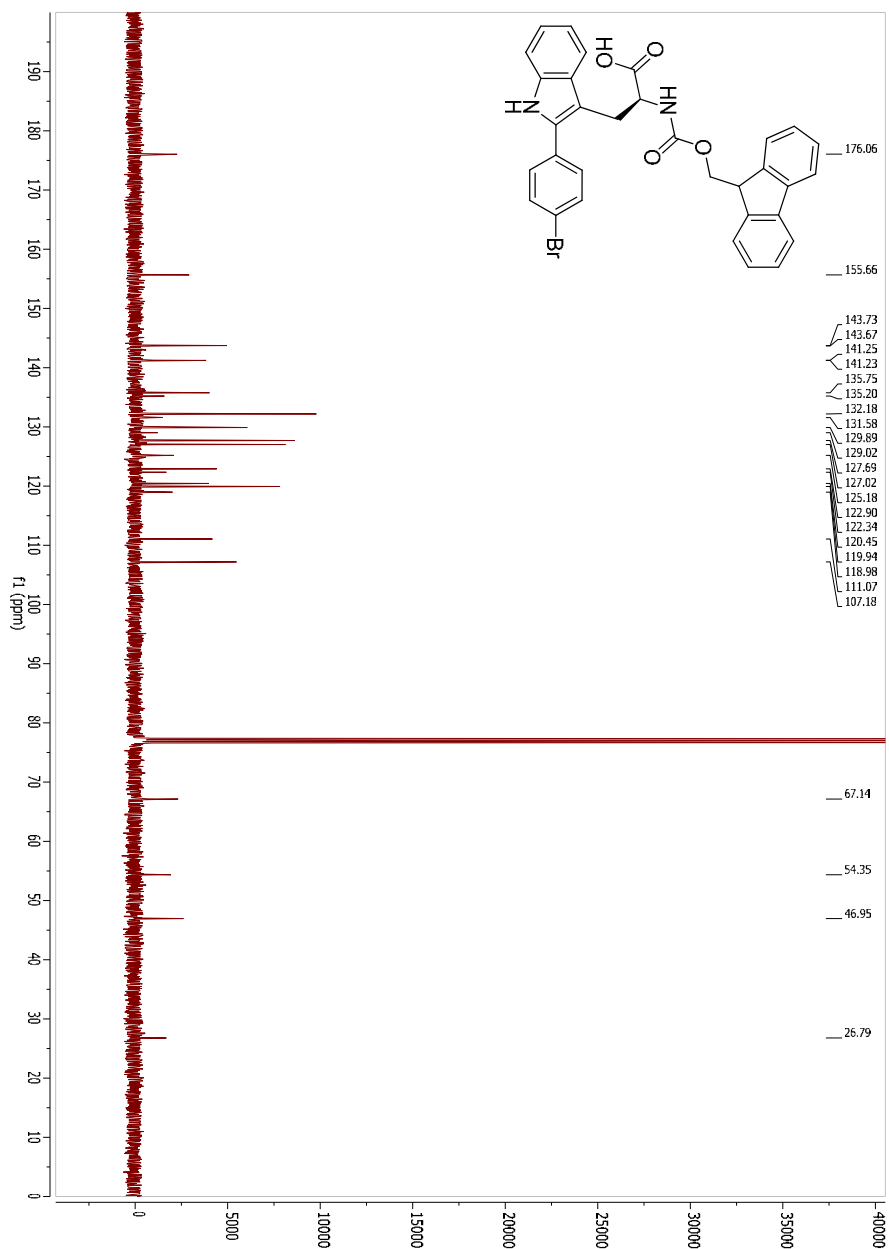
(S)-2-(((9H-Fluoren-9-yl)methoxy)carbonyl)amino)-3-(2-(4-(methoxycarbonyl)phenyl)-1H-indol-3-yl)propanoic acid (5c)



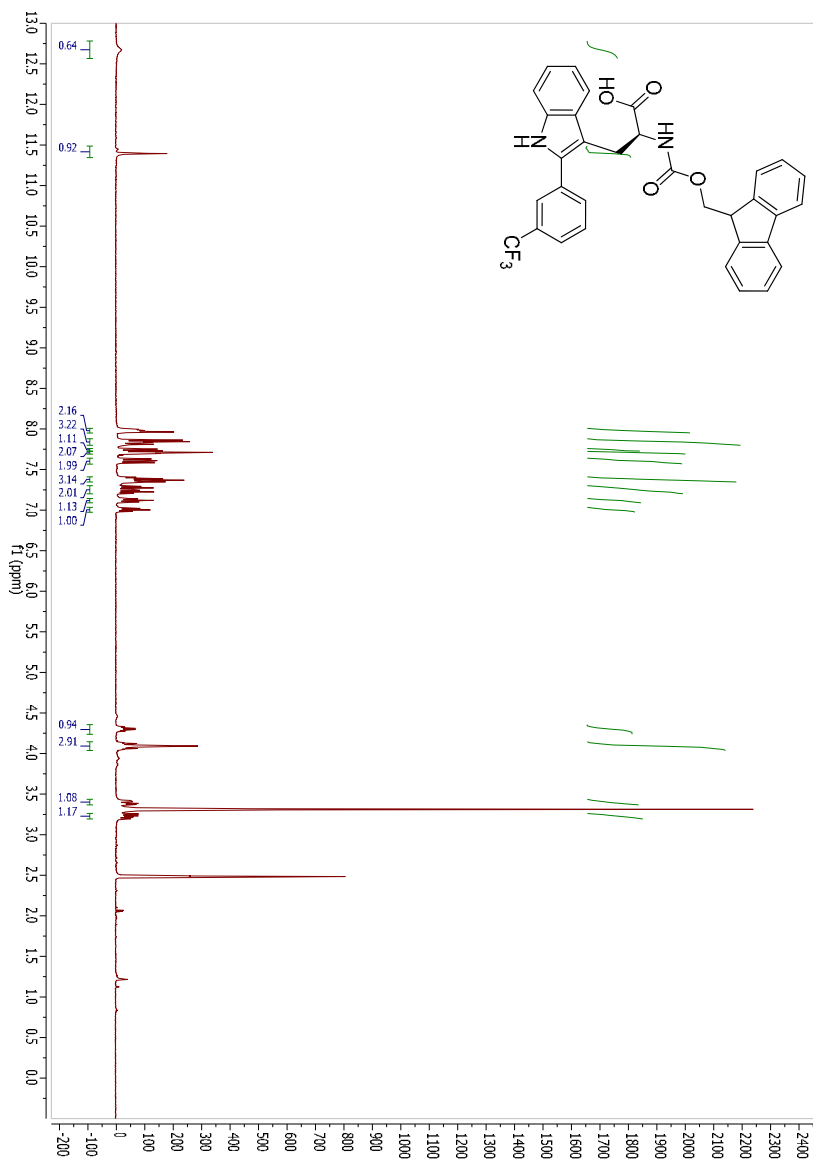


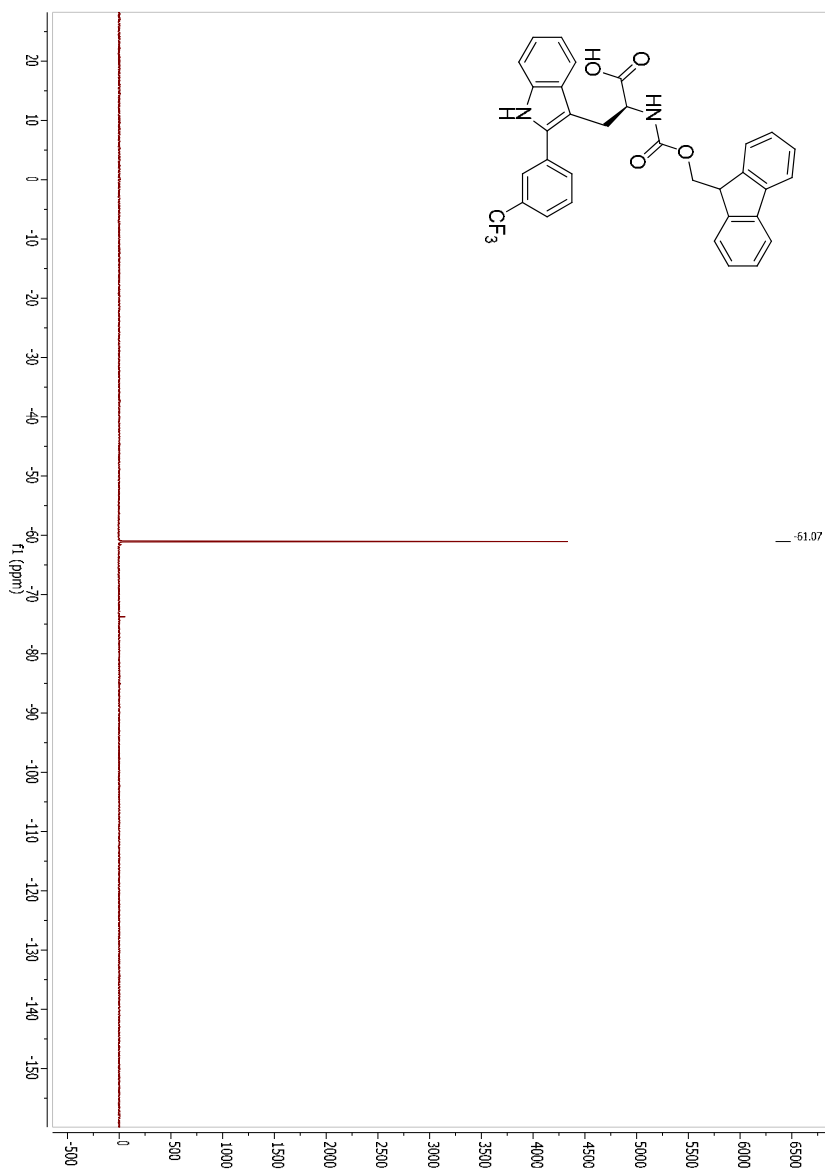
(S)-2-(((9H-Fluoren-9-yl)methoxy)carbonyl)amino)-3-(2-(4-bromophenyl)-1H-indol-3-yl)propanoic acid (5d)

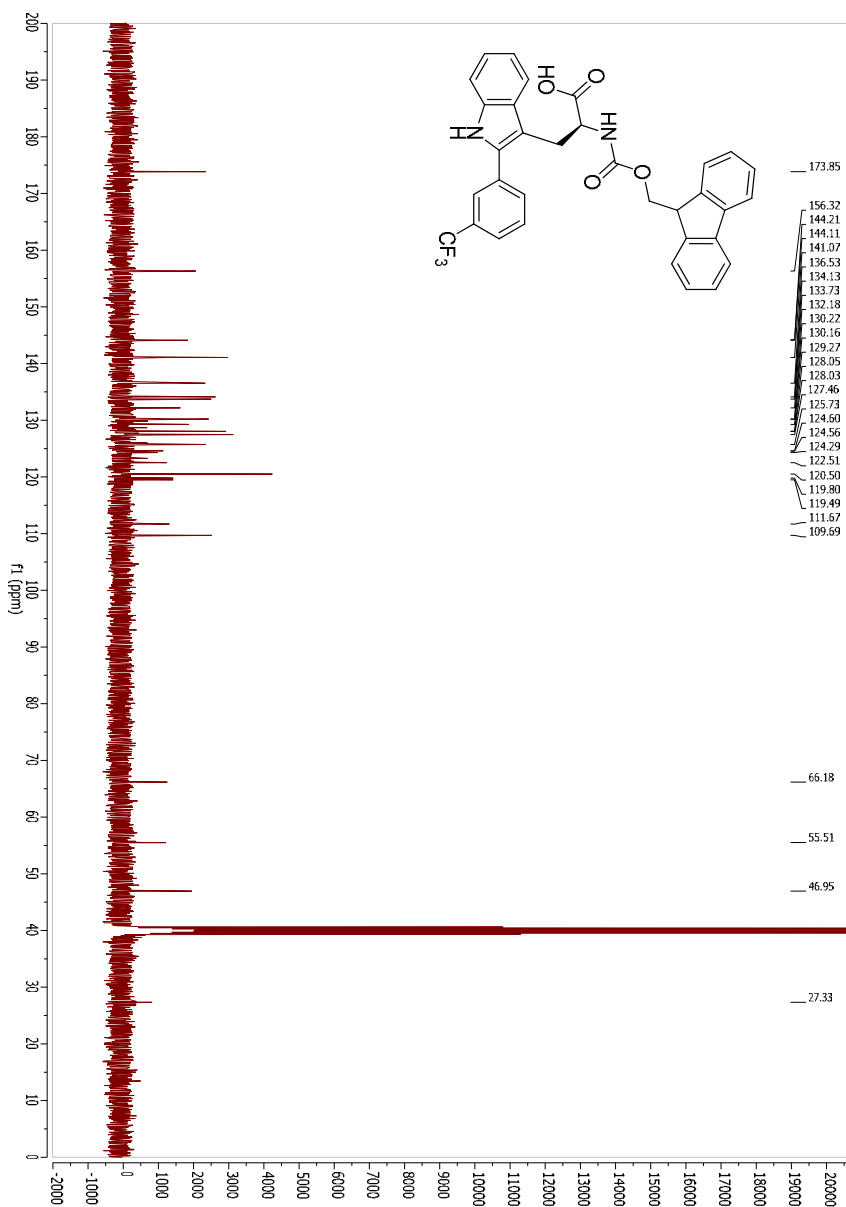




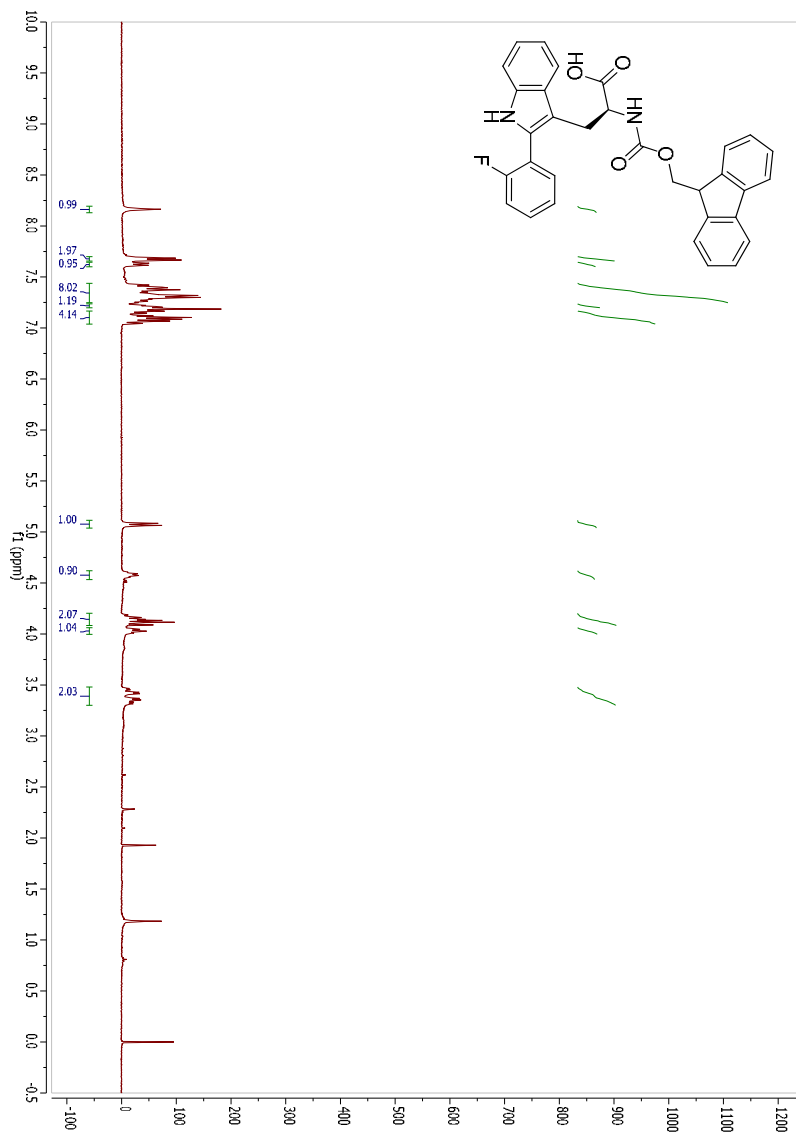
(S)-2-(((9H-Fluoren-9-yl)methoxy)carbonyl)amino)-3-(2-(3-(trifluoromethyl)phenyl)-1H-indol-3-yl)propanoic acid (5e)

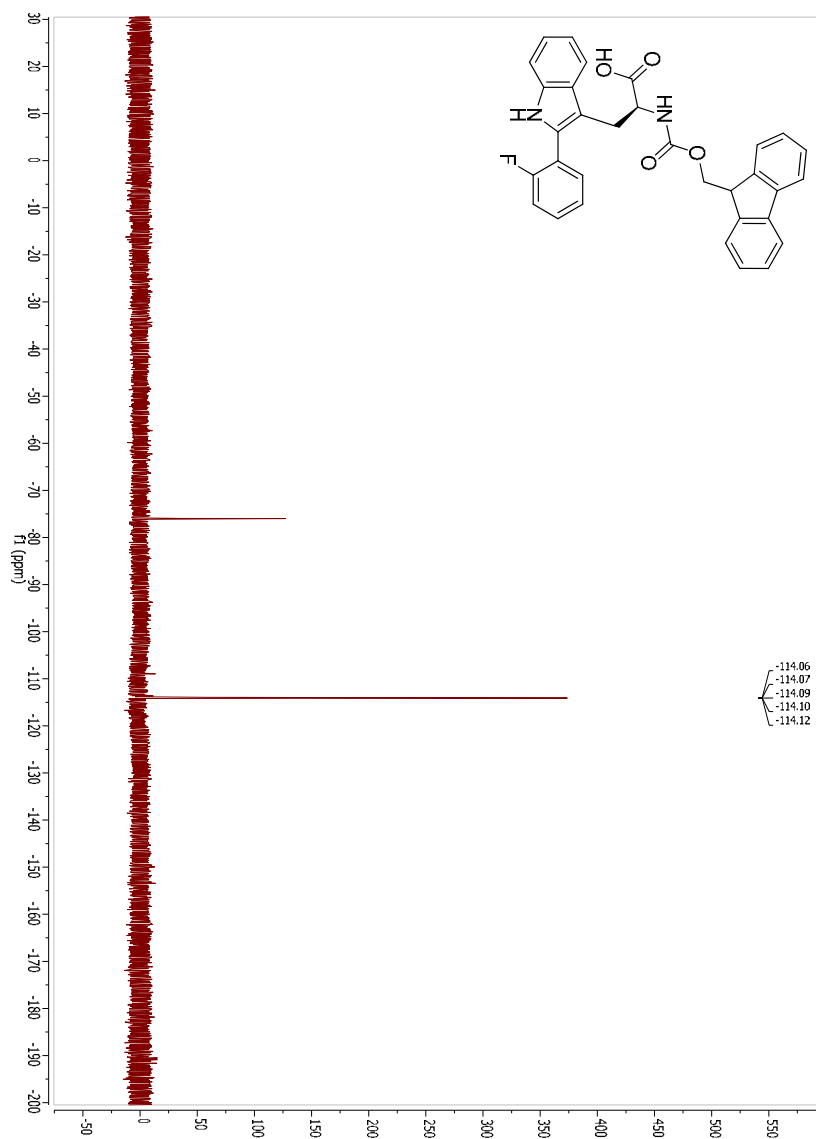


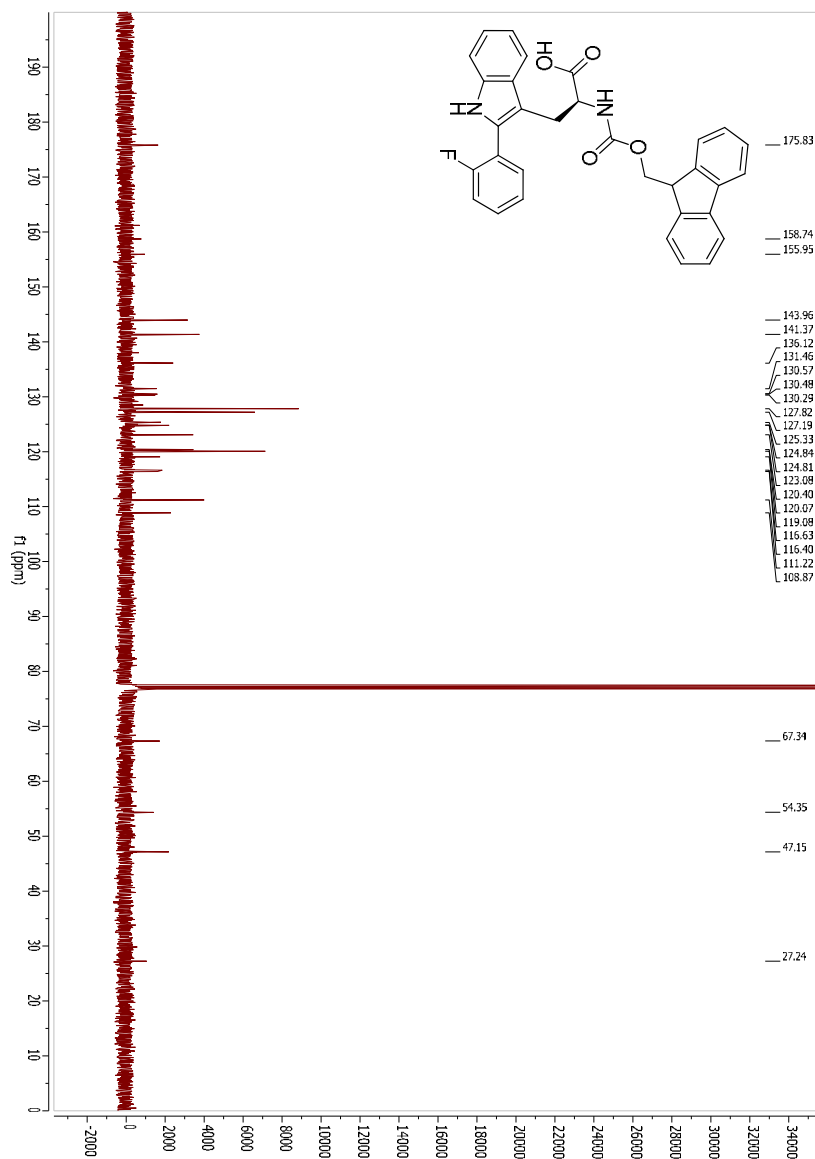




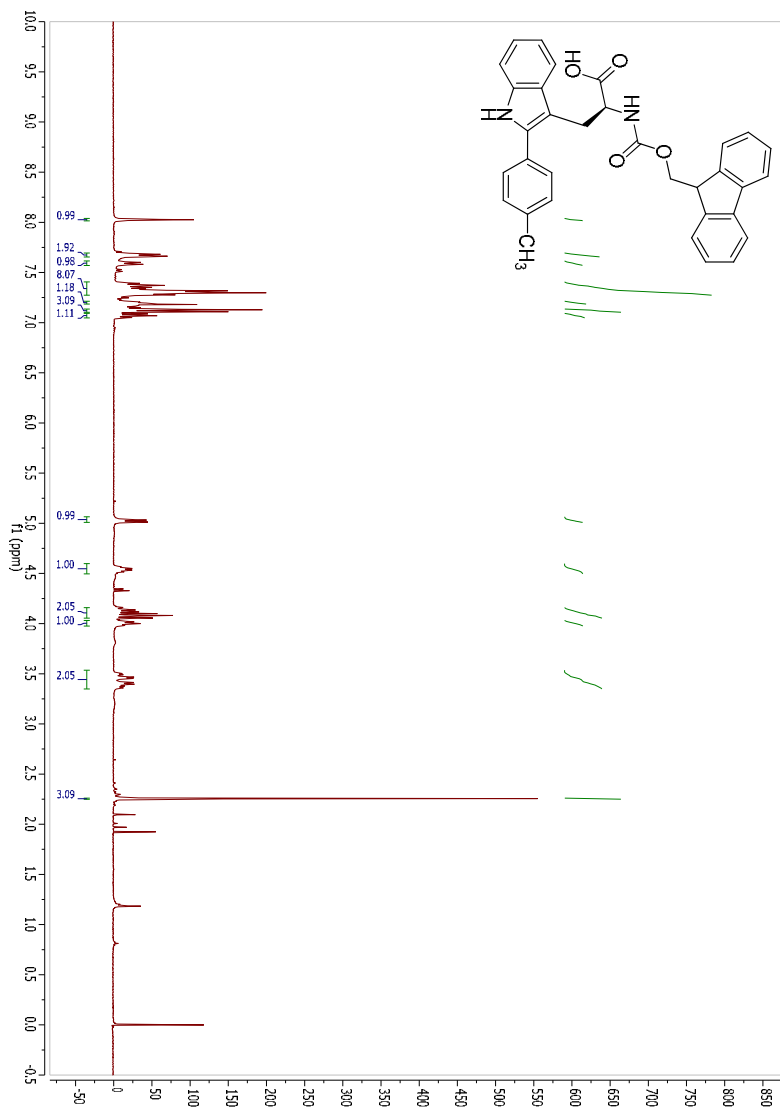
(S)-2-(((9H-Fluoren-9-yl)methoxy)carbonyl)amino)-3-(2-(2-fluorophenyl)-1H-indol-3-yl)propanoic acid (5f)

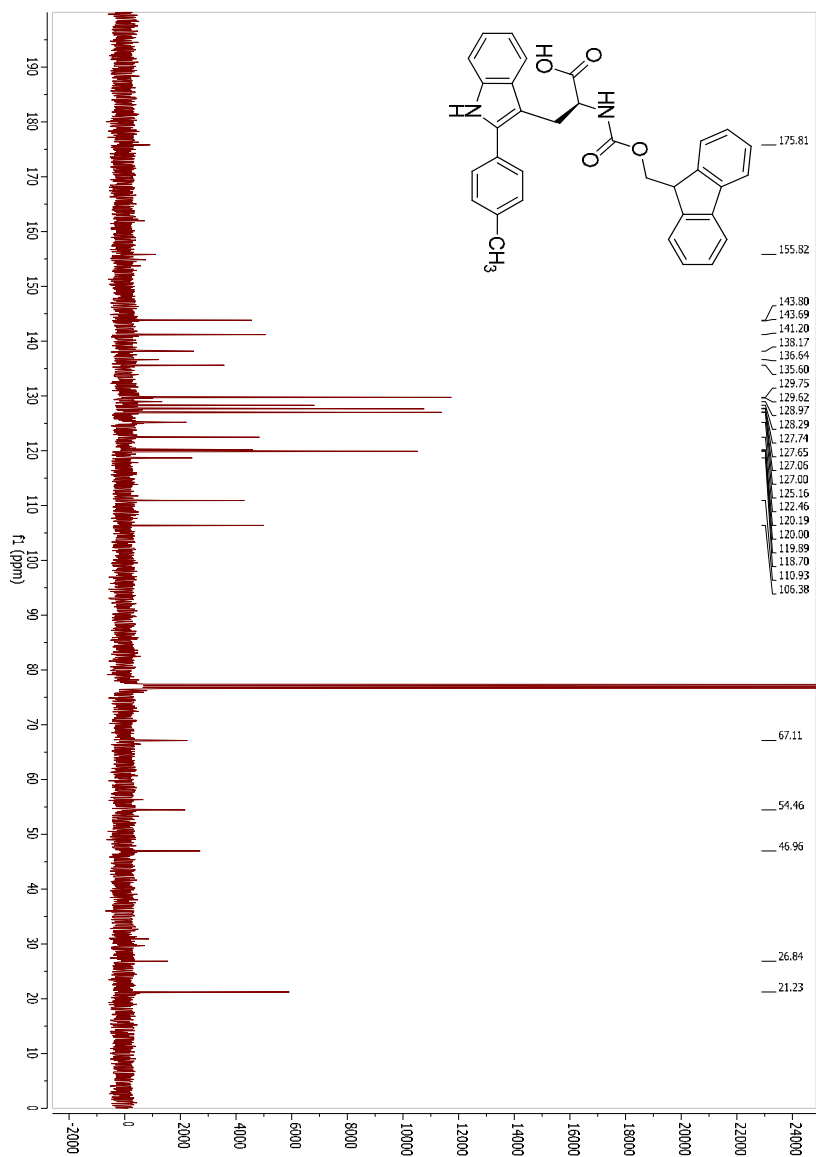




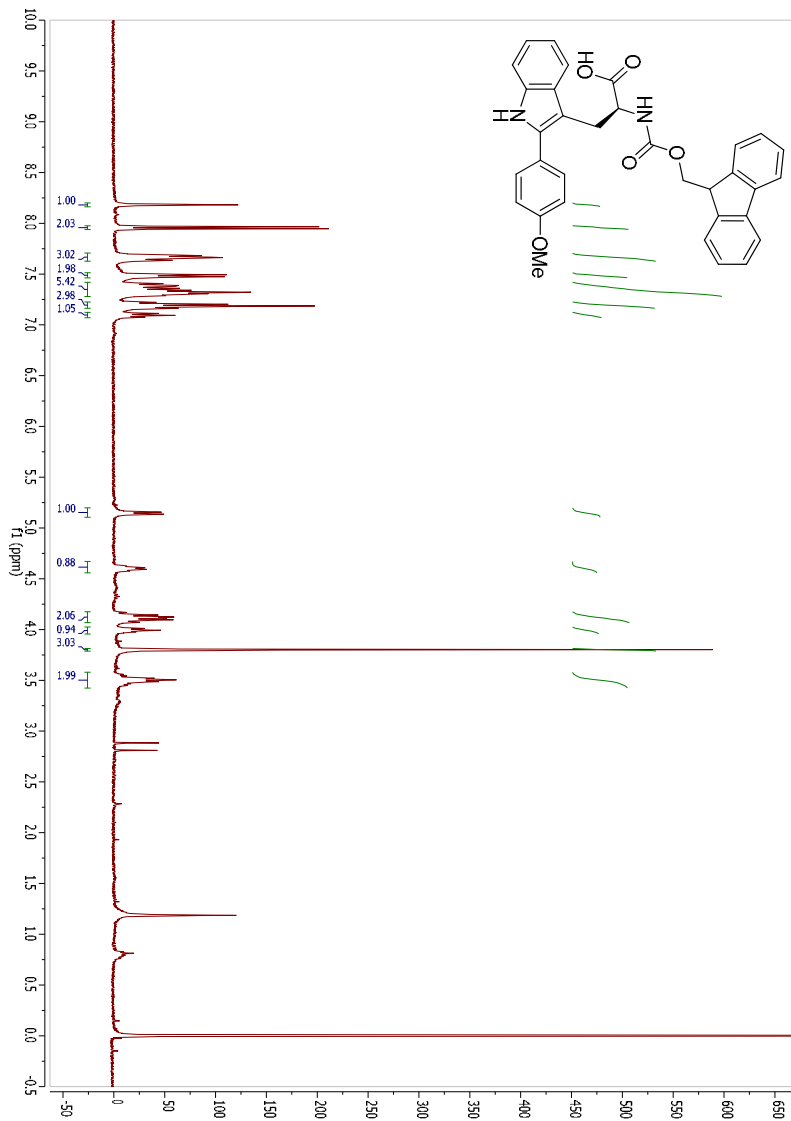


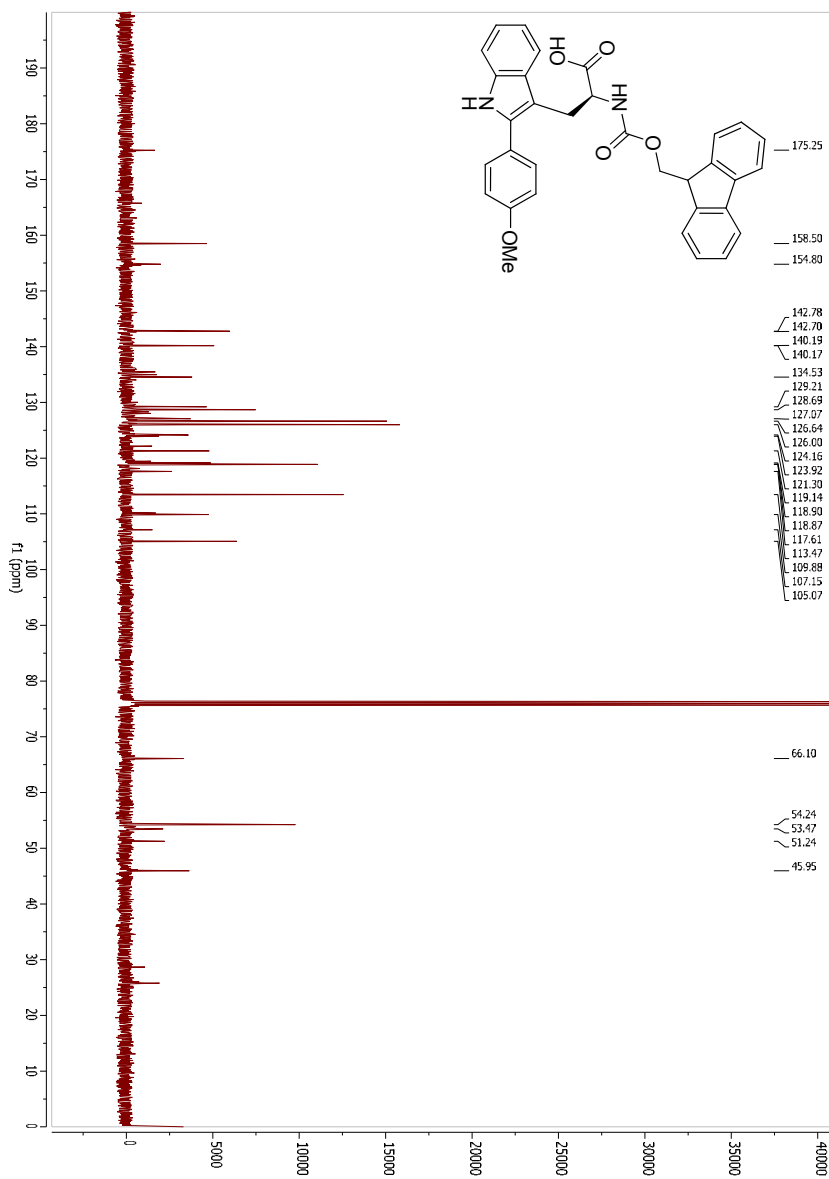
(S)-2-(((9H-Fluoren-9-yl)methoxy)carbonyl)amino)-3-(2-(*p*-tolyl)-1*H*-indol-3-yl)propanoic acid (5g)



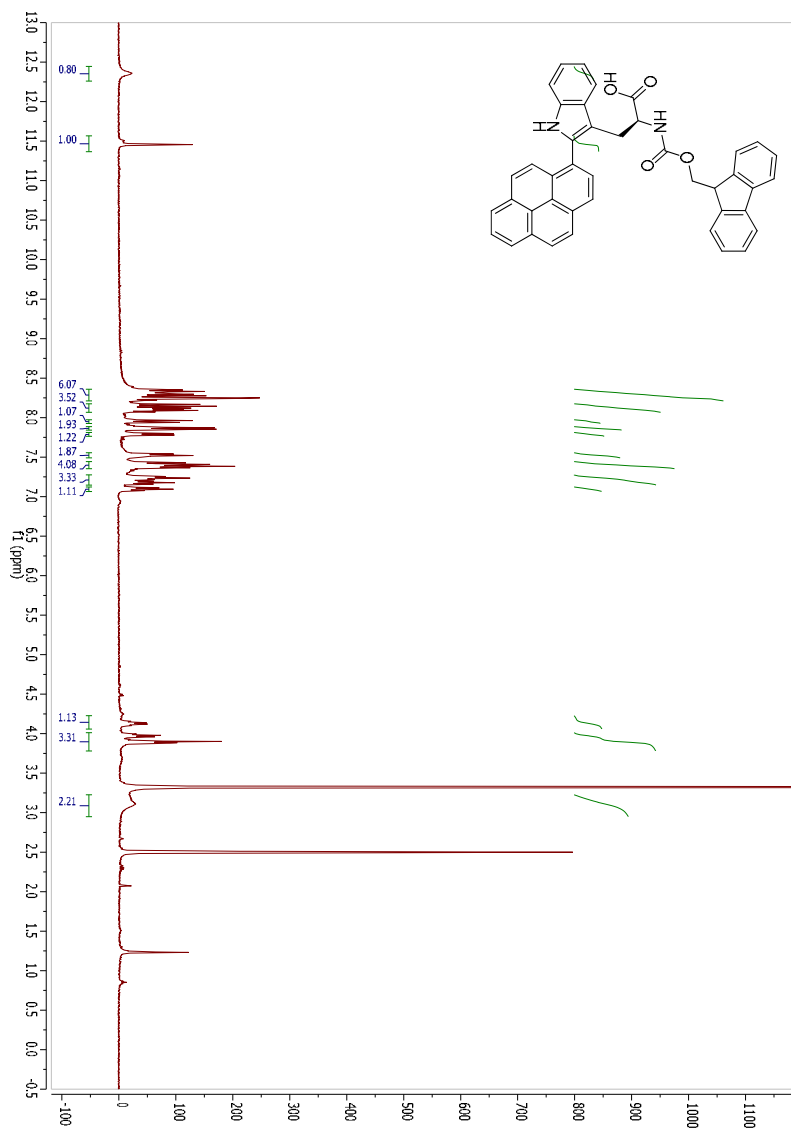


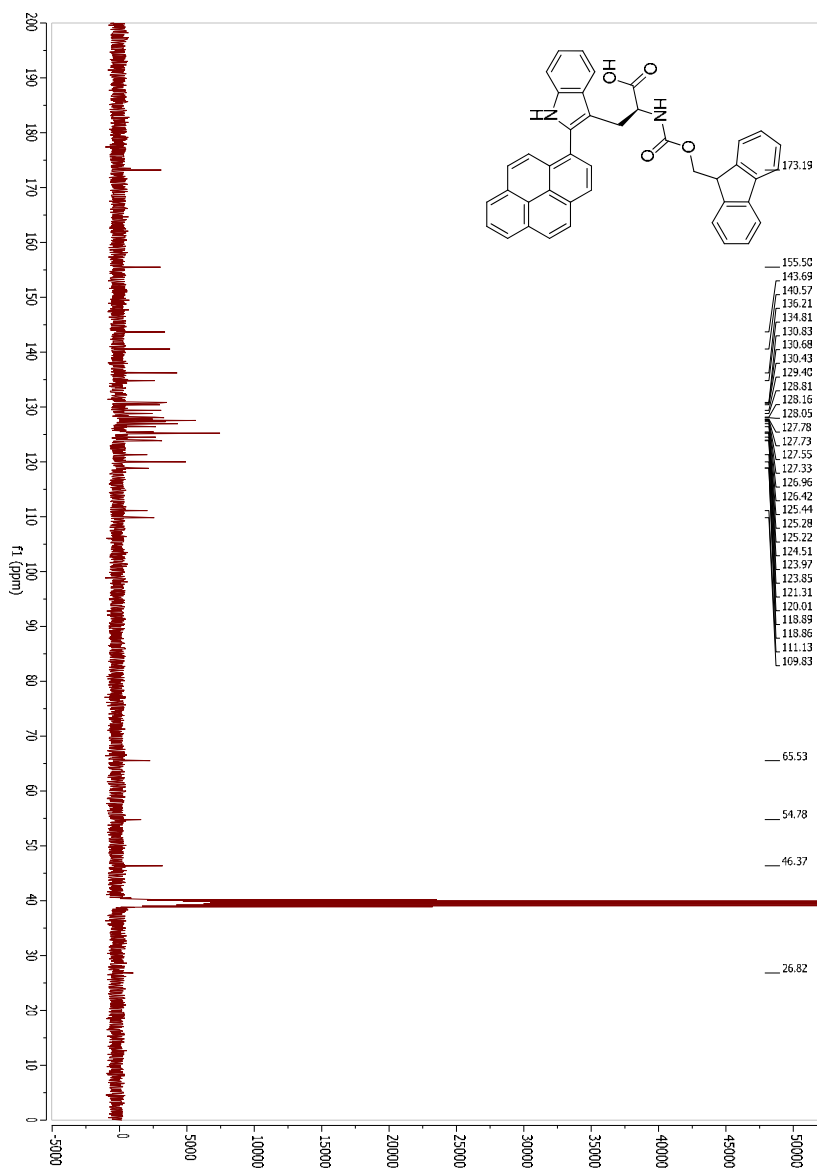
(S)-2-((((9H-Fluoren-9-yl)methoxy)carbonyl)amino)-3-(2-(4-methoxyphenyl)-1H-indol-3-yl)propanoic acid (5h)

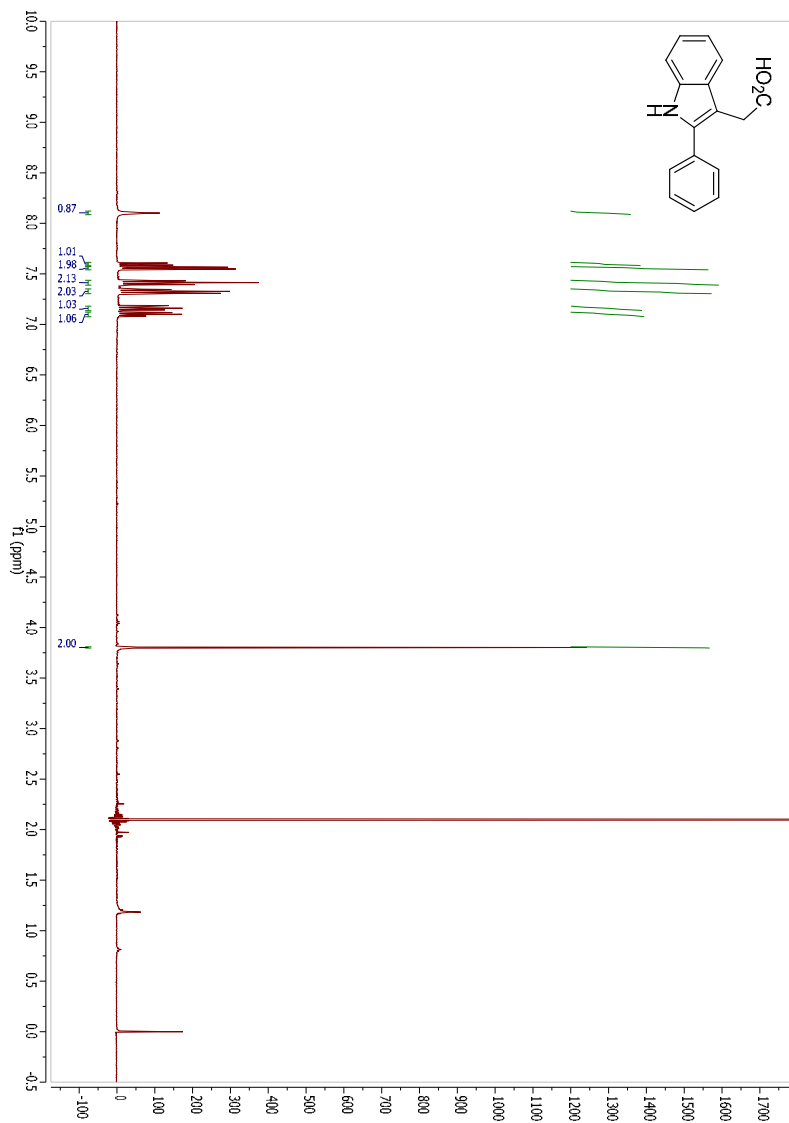


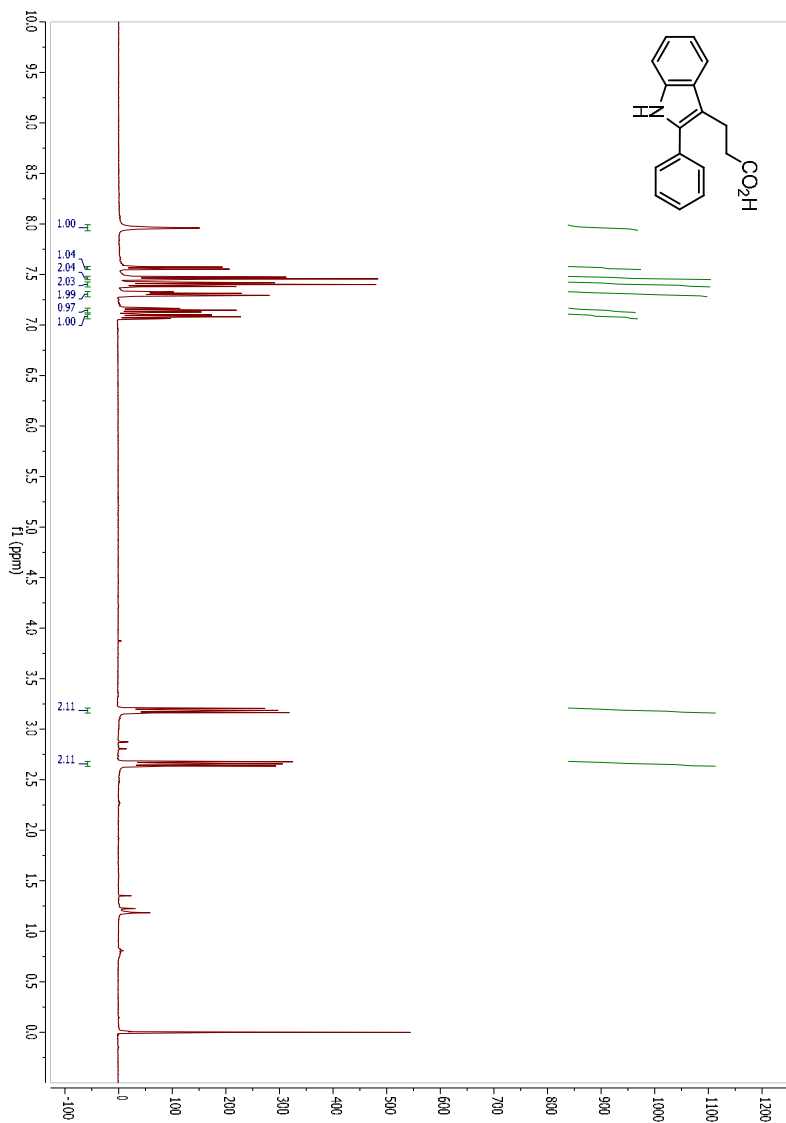


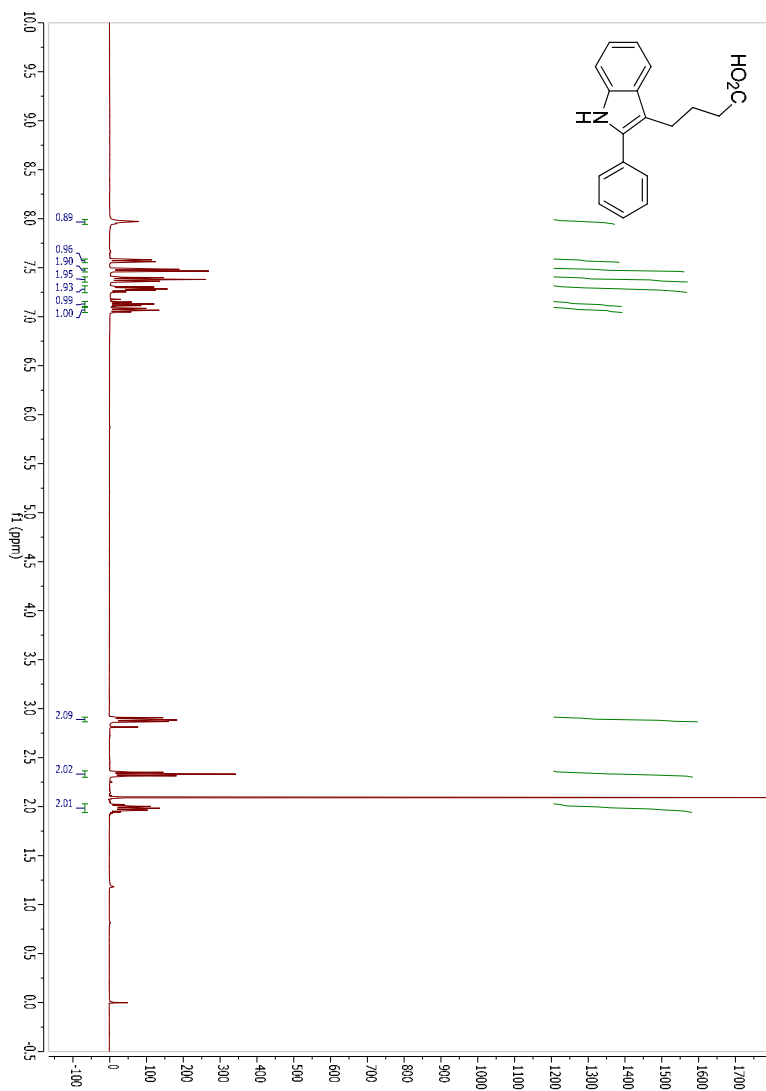
(S)-2-(((9H-Fluoren-9-yl)methoxy)carbonyl)amino)-3-(2-(pyren-1-yl)-1H-indol-3-yl)propanoic acid (5i)

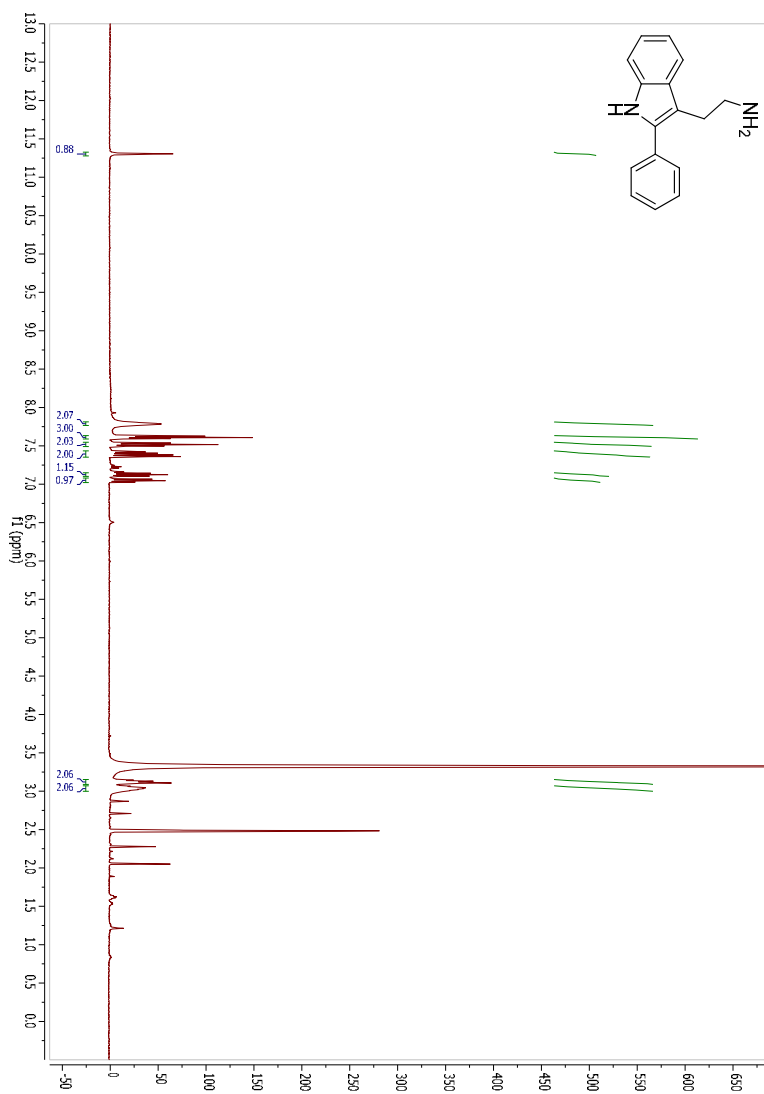


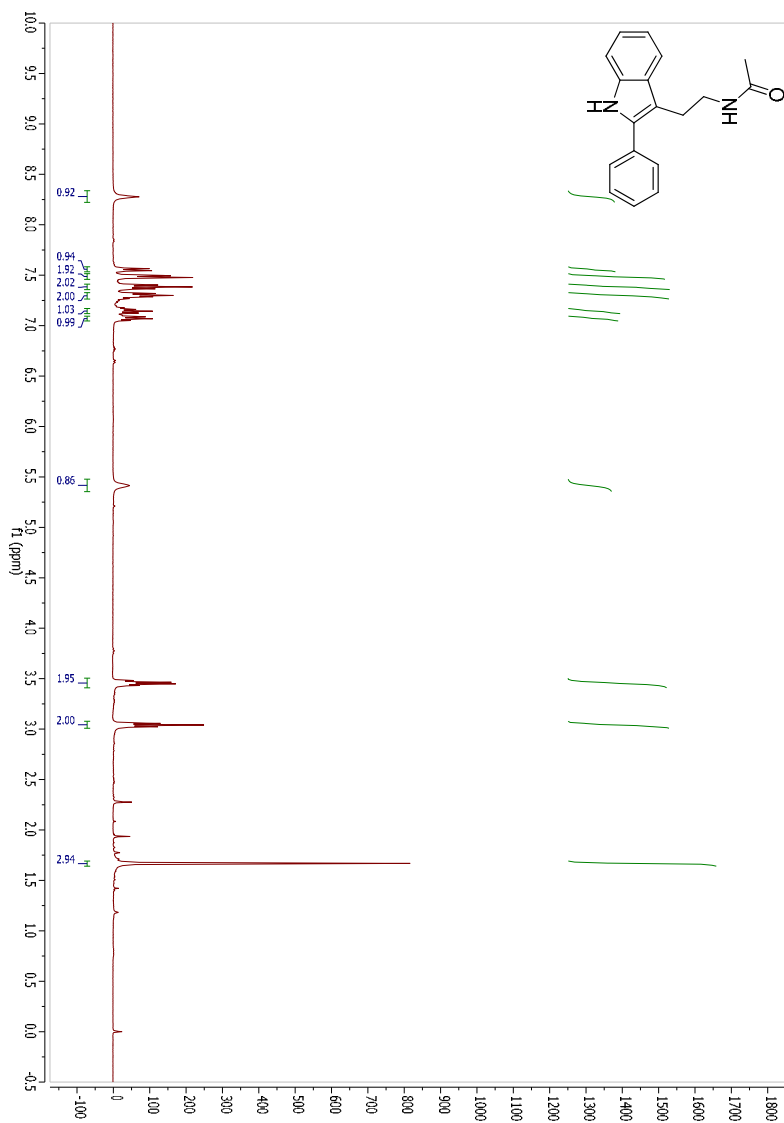


2-(2-Phenyl-1*H*-indol-3-yl)acetic acid (8)

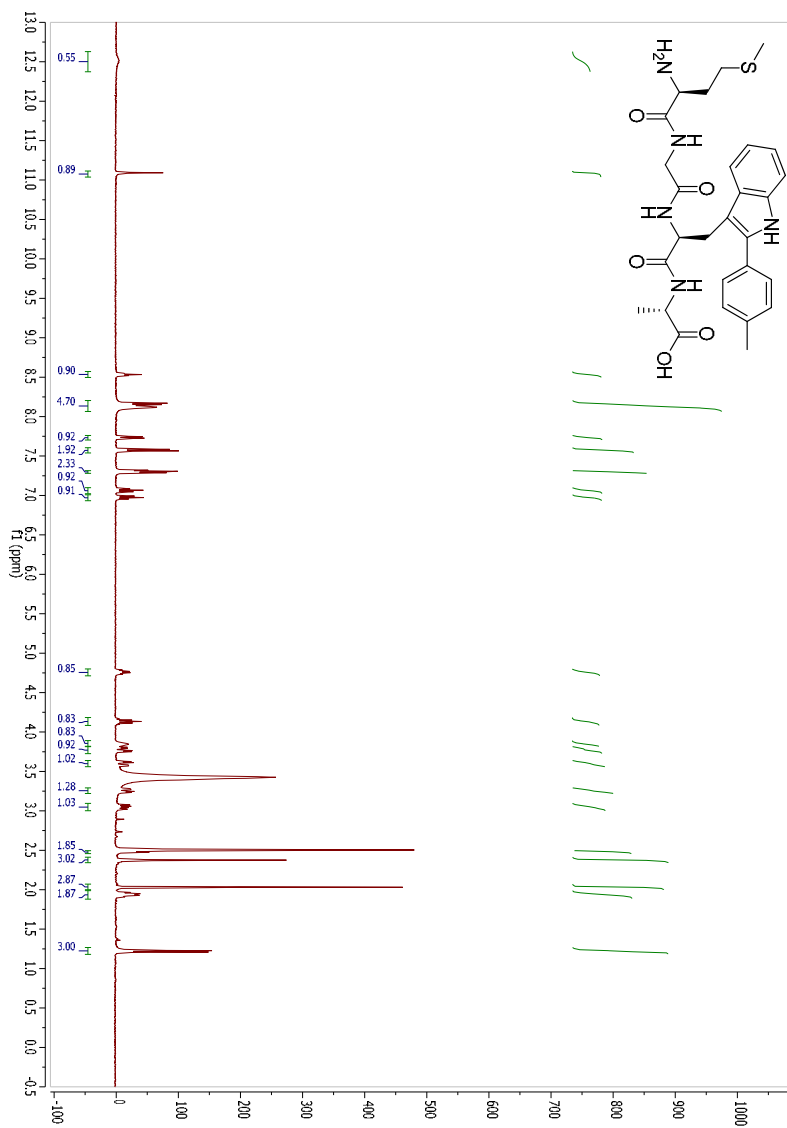
3-(2-Phenyl-1*H*-indol-3-yl)propanoic acid (9)

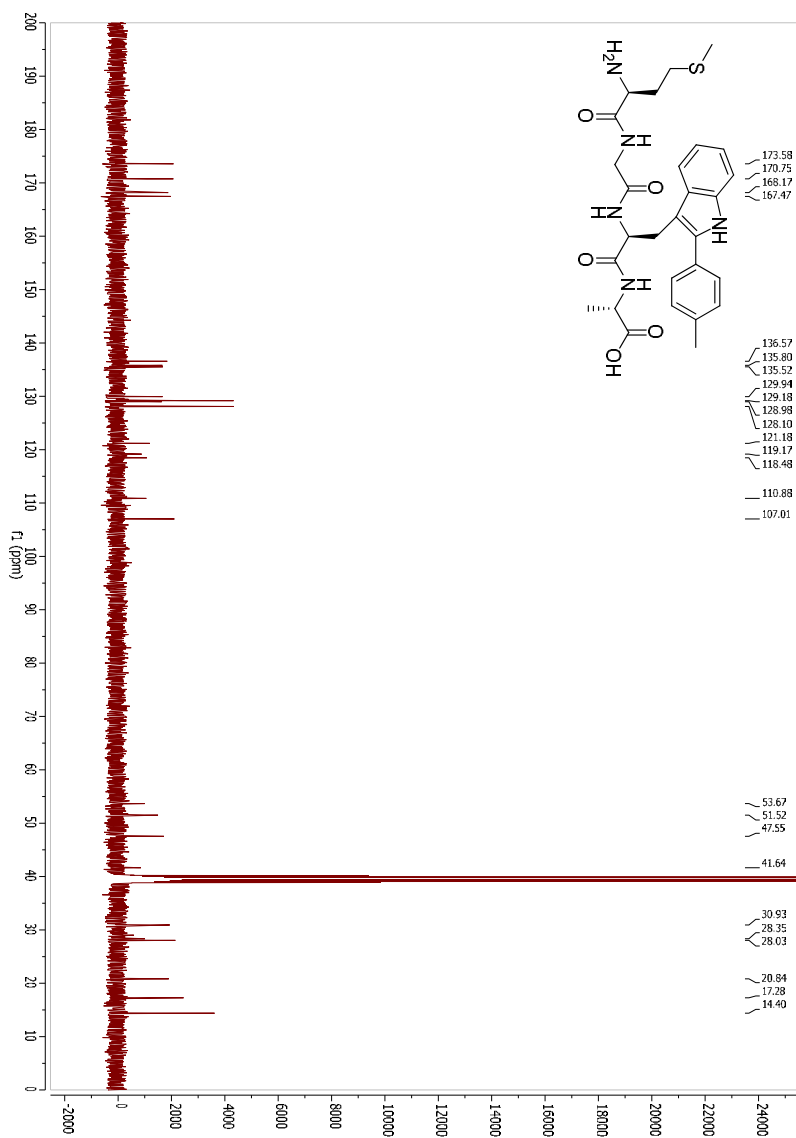
4-(2-Phenyl-1*H*-indol-3-yl)butanoic acid (10)

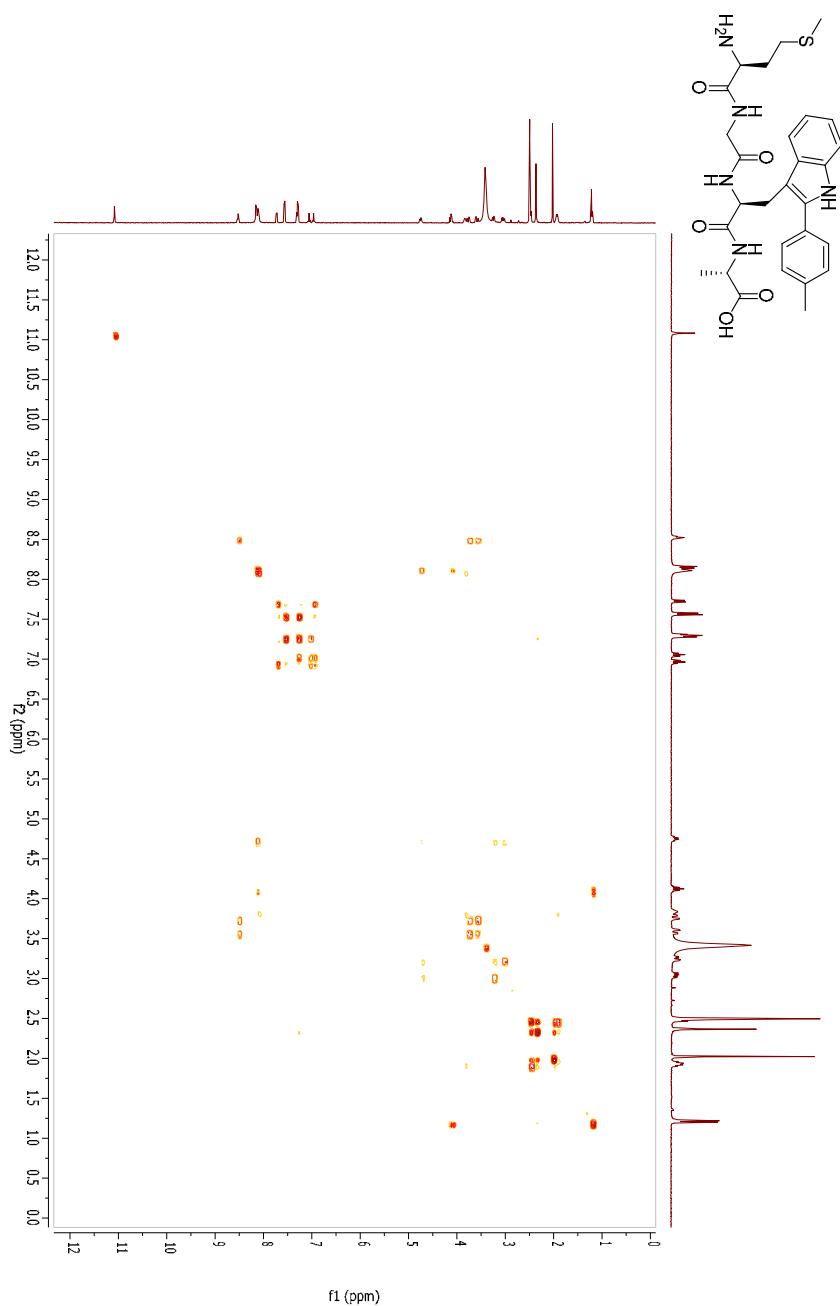
2-(2-Phenyl-1*H*-indol-3-yl)ethanamine (11)

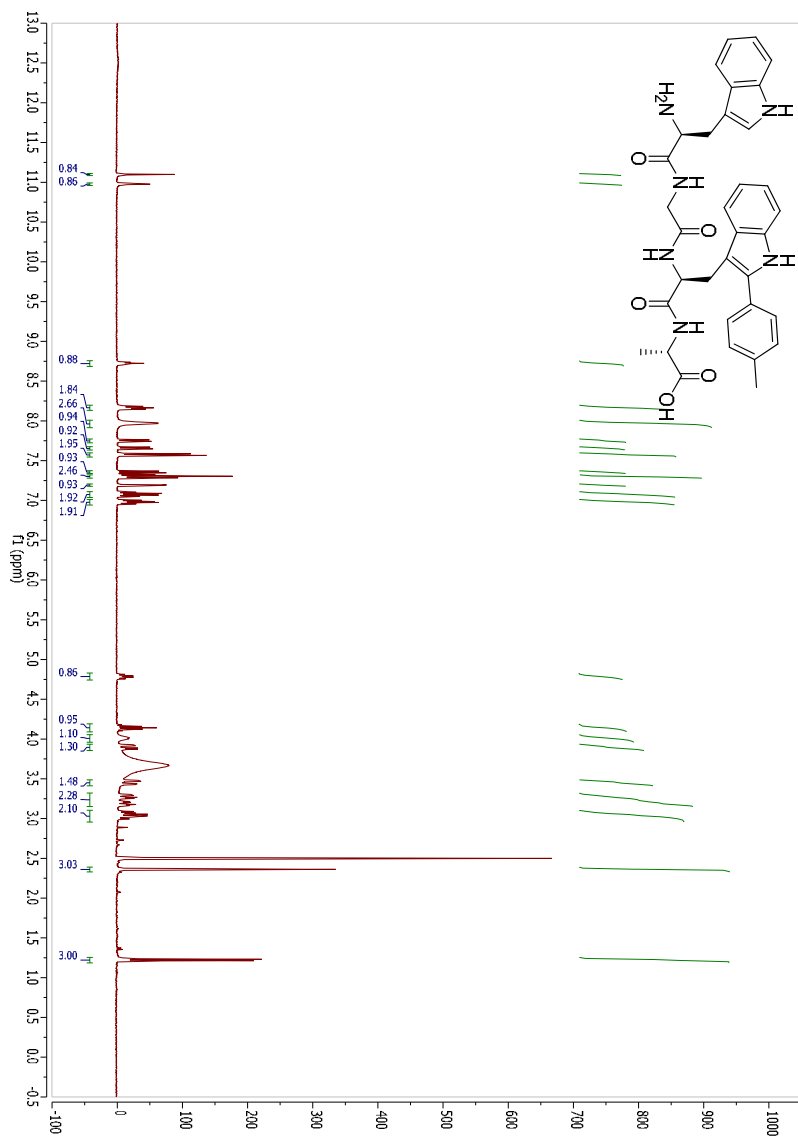
***N*-(2-(2-Phenyl-1*H*-indol-3-yl)ethyl)acetamide (12)**

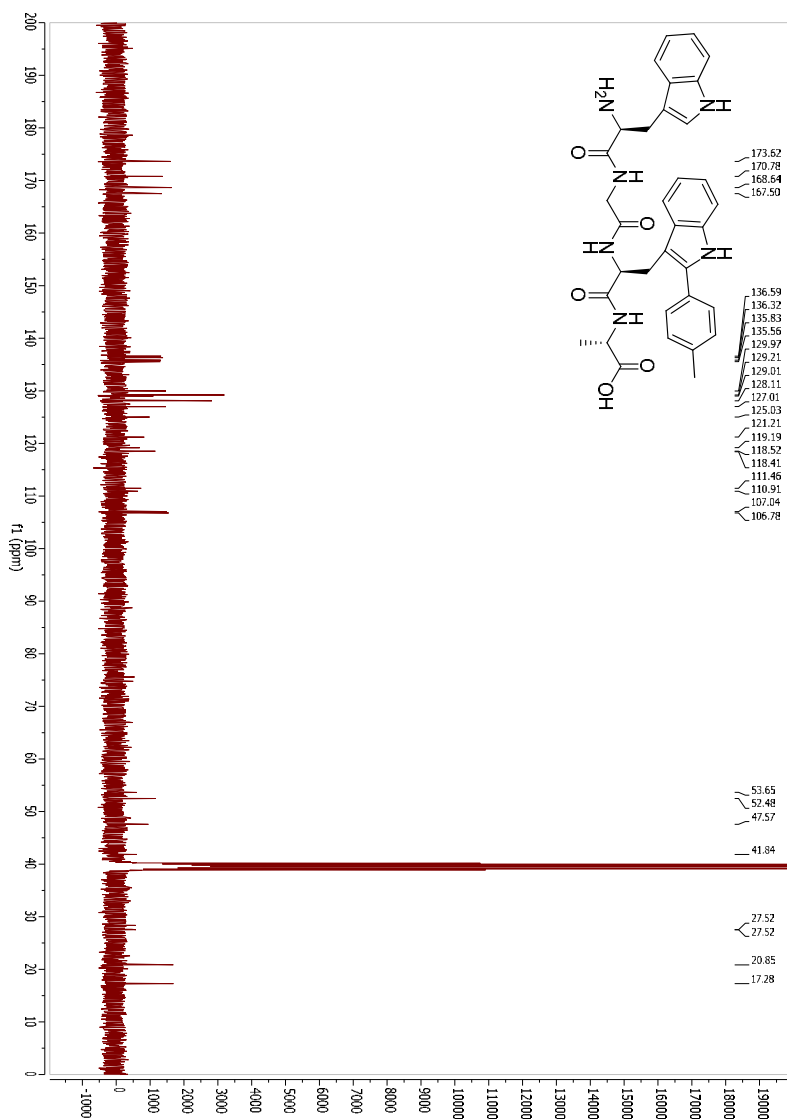
H-Met-Gly-Trp(C2-*p*-methylphenyl)-Ala-OH (6)

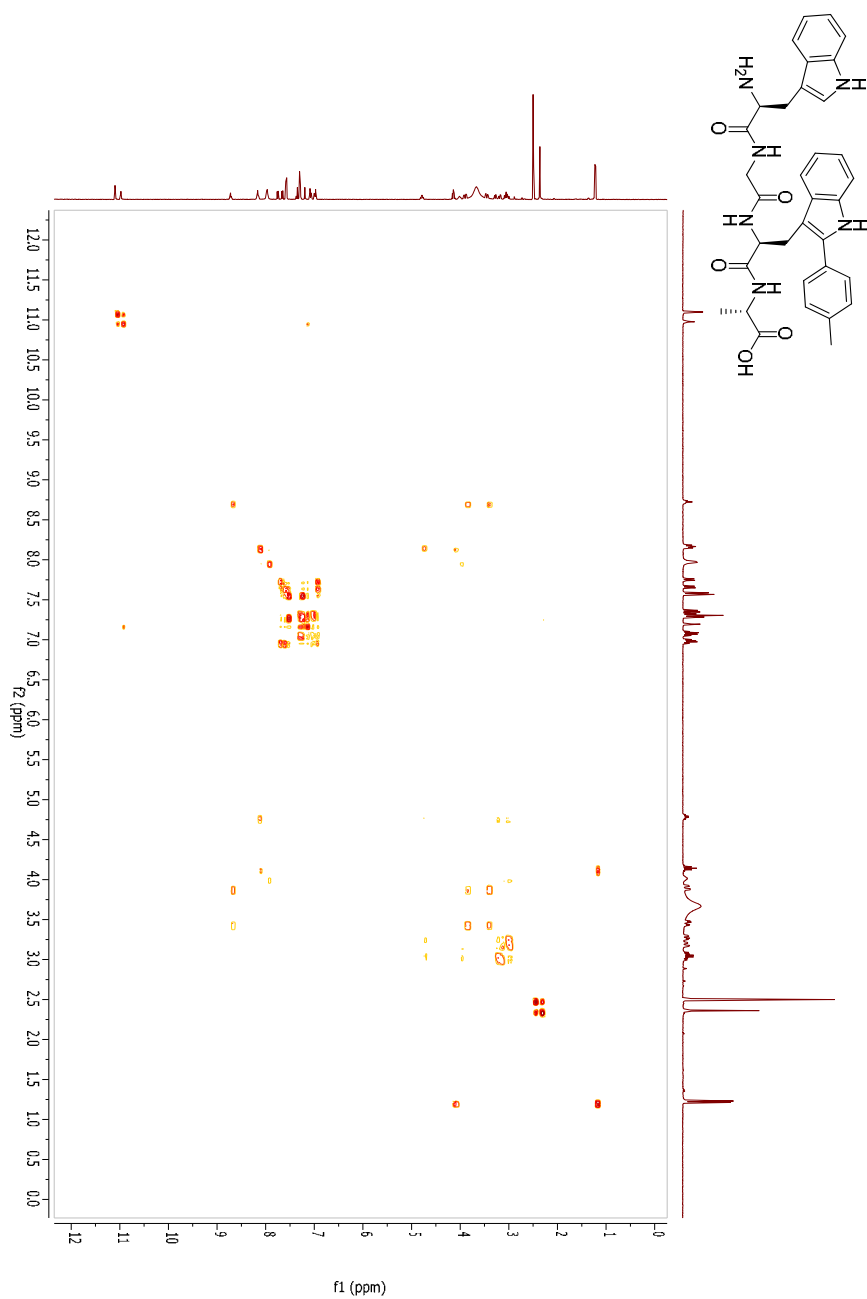






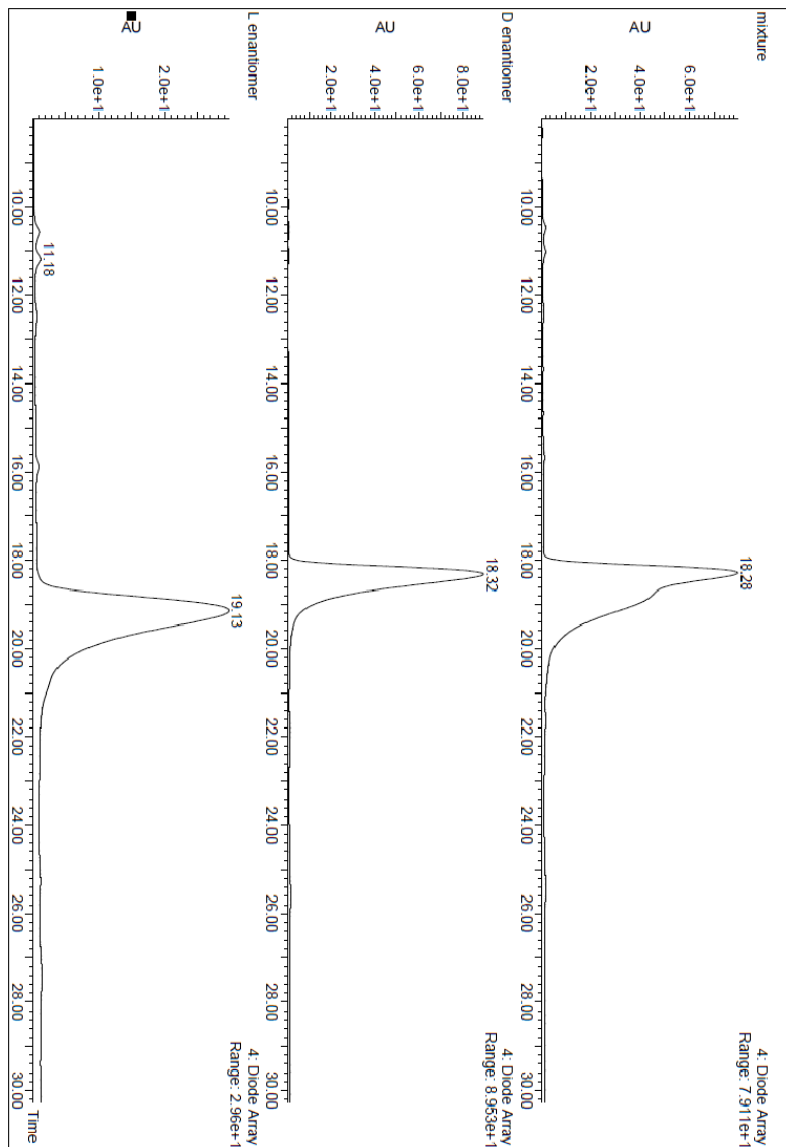
H-Trp-Gly-Trp(C2-*p*-methylphenyl)-Ala-OH (7)





Chromatographic analysis of 5a and 5a'.

Chiral column HPLC:





FULL SUPPORTING INFORMATION PUBLICATION III

Electronic Supplementary Information

Enhanced antimicrobial activity of a peptide derived from human lysozyme by arylation of its tryptophan residues

*Rodrigo González, Lorena Mendive-Tapia, María B. Pastrian,
Fernando Albericio, Rodolfo Lavilla Osvaldo Cascone and Nancy B.
Iannucci*

General experimental information

Commercially available reactants were used without further purification. Reactions were monitored by HPLC-MS at 220 nm using a HPLC Waters Alliance HT comprising a pump (Edwards RV12) with degasser, an autosampler and a diode array detector. Flow from the column was split to a MS spectrometer. The MS detector was configured with an electrospray ionization source (micromass ZQ4000) and nitrogen was used as the nebulizer gas. Data acquisition was performed with MassLynx software. Microwave reactions were carried out in 10 mL sealed glass tubes in a focused mono-mode microwave oven ("Discover" by CEM Corporation) featured with a surface sensor for internal temperature determination. Cooling was provided by compressed air ventilating the microwave chamber during the reaction. When stated, the final crude was purified via flash column chromatography Combi Flash ISCO RF provided with dual UV detection. ^1H NMR spectrum was recorded on a Varian Mercury 400 at 400 MHz in DMSO solution with TMS as an internal reference. Data for ^1H -NMR spectra are reported as follows: chemical shift (δ ppm), multiplicity, integration and coupling constants (Hz). Multiplicities are referred by the following abbreviations: s = singlet, d = doublet, t = triplet, dd = doublet of doublets, td = triplet of doublets, ddd = double doublet of doublets and m = multiplet. IR spectra were recorded using a Thermo Nicolet Nexus spectrometer and are reported in frequency of absorption (cm^{-1}). High Resolution Mass Spectrometry was performed by the University of Barcelona Mass Spectrometry Service.

Abbreviations

Abbreviation used for amino acids and designations of peptides follow the rules of the IUPAC-IUB Commission of Biochemical Nomenclature in *J. Biol. Chem.* 247, 977-983 (1982). The following additional abbreviations are used: DMF: *N,N*-dimethylformamide, ACN: acetonitrile, Fmoc: 9*H*-fluorenylmethyloxycarbonyl, TFA: trifluoroacetic acid, Trp/W: tryptophan, Phe/F: phenylalanine, Arg/R: arginine, Ala/A: alanine, W, tryptophan, Val/V: valine, Asn/N: asparagine, RP-HPLC-ESMS: reverse phase-high performance liquid chromatography-electro spray mass spectrometry, NMR: nuclear magnetic resonance, SPPS: solid-phase peptide synthesis, IR: infrared spectroscopy.

Reagents and microorganisms

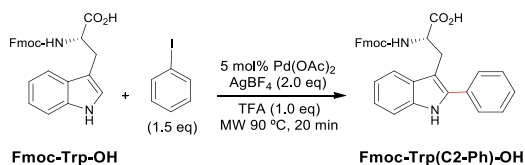
$\text{N}\alpha$ -Fmoc-tryptophan, iodobenzene, palladium (II) acetate and *N,N*-dimethylformamide anhydrous (DMF) were from Aldrich, Fmoc-Rink-Amide AM resin was from Iris-Biotech. *O*-benzotriazole-*N,N,N',N'*-tetramethyl-uronium-hexafluoro-phosphate (HBTU) and 2-(1*H*-7-

azabenzotriazol-1-yl)-1,1,3,3,-tetramethyl uronium hexafluorophosphate (HATU) were from Fluorochem. N,N-dimethylformamide was from Panreac AppliChem. N,N-diisopropylethylamine (DIEA) and silicagel were from Merck Biosciences.

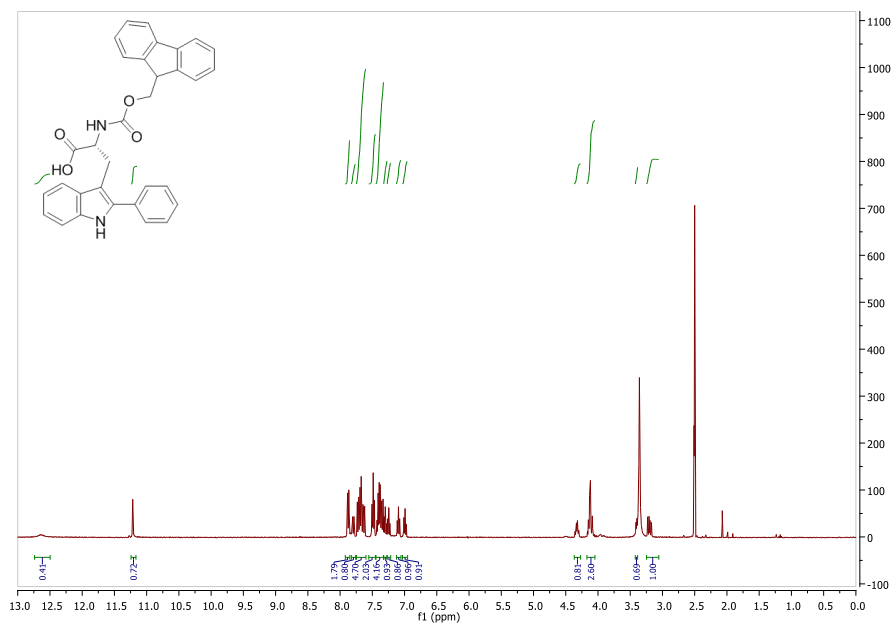
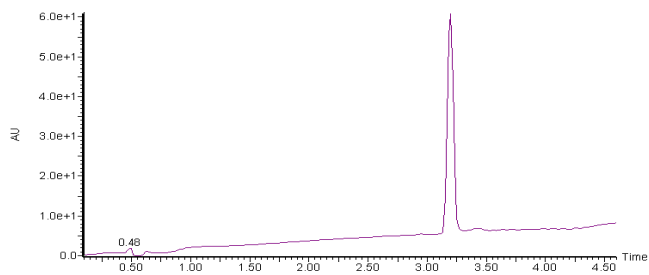
Müller-Hinton culture medium was from Oxoid. Bacterial strains *S. aureus* ATCC 29213 and *S. epidermidis* ATCC 12228 were from The American Type Culture Collection (Manassas, VA, USA).

Tryptophan arylation

The arylation of the indolic C2 of tryptophan was carried out by activation of this carbon catalyzed by palladium as described by Ruiz-Rodríguez et al.¹ and Preciado-Gallego et al.² Briefly, the Nα-Fmoc-tryptophan, activated with Pd(OAc)₂ was treated with iodobenzene in a microwave at 90° C and purified by flash chromatography on silicagel as described by Preciado-Gallego et al. (2013).³ The product was identified by nuclear magnetic resonance (NMR) and electrospray mass spectrometry (ESMS) and the yield was 56 %.



Fmoc-Trp(C2-Ph)-OH. Fmoc-Trp-OH (0.5 g, 1.17 mmol, 1 eq.), iodobenzene (1.5 eq.), AgBF₄ (2 eq.), TFA (1.0 eq.) and Pd(OAc)₂ (5 % mol) were placed in a microwave reactor vessel in dry DMF (2 mL). The mixture was heated under microwave irradiation (250 W) at 90 °C for 20 min. This microwave process was performed up to six times and all the reaction mixtures were collected altogether. Ethyl acetate (20 mL) was added and the resulting suspension was filtered through Celite and the solvent was removed under vacuum. The crude extract was purified by flash column chromatography on silica gel (hexane/ethyl acetate). Fractions containing the arylated tryptophan were collected and the solvent was removed under reduced pressure. Finally, the residue was dissolved in ACN/H₂O and lyophilized for 24 h to yield the pure product Fmoc-Trp(C2-Ph)-OH as a solid (1.98 g, 56 %). ¹H-NMR (400 MHz, DMSO): δ 12.62 (s, 1H), 11.20 (s, 1H), 7.88 – 7.84 (m, 2H), 7.78 (d, *J* = 8.6 Hz, 1H), 7.72 – 7.60 (m, 5H), 7.47 (t, *J* = 7.7 Hz, 2H), 7.41 – 7.32 (m, 4H), 7.28 (td, *J* = 7.4, 1.1 Hz, 1H), 7.23 (td, *J* = 7.5, 1.1 Hz, 1H), 7.10 – 7.05 (m, 1H), 6.97 (ddd, *J* = 8.0, 6.9, 1.0 Hz, 1H), 4.31 (td, *J* = 8.6, 5.8 Hz, 1H), 4.15 – 4.06 (m, 3H), 3.40 – 3.34 (m, 1H), 3.18 (dd, *J* = 14.6, 8.7 Hz, 1H) ppm. IR (Film, cm⁻¹) *v* = 3372.24, 3321.00, 3051.96, 2955.87, 1693.95 cm⁻¹. RP-HPLC-ESMS: *m/z* (%): 503.22 (M+H)⁺. [α]_D²⁰ -5.9 (c 0.48, MeOH).

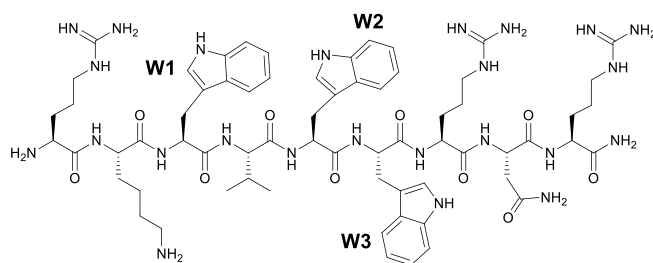
(S)-2-(((9H-Fluoren-9-yl)methoxy)carbonyl)amino)-3-(2-phenyl-1H-indol-3-yl)propanoic acid**¹H NMR****(S)-2-(((9H-Fluoren-9-yl)methoxy)carbonyl)amino)-3-(2-phenyl-1H-indol-3-yl)propanoic acid****RP-HPLC chromatogram.**

Gradient was 5-100% of B. Solvent A (0.1 % FA in H₂O) and solvent B (0.05 % FA in ACN), in 3.5 min. Elution was monitored at 254 nm and the flow rate was 1.6 mL/min.

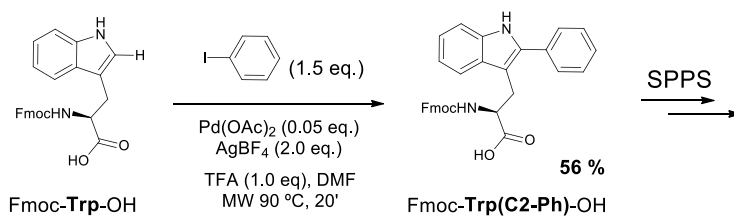
Synthesis of arylated peptides

The preparation of 2-aryl- α -Fmoc-tryptophan was performed as described from 4-iodobenzene and α -Fmoc-tryptophan (Preciado et al., 2013).¹ The resulting arylated amino acid was used in solid-phase peptide synthesis without any special requirement.

The solid-phase method was performed according to Kates and Albericio, (2000).⁴ Fmoc chemistry and Fmoc-Rink-Amide AM resin were used. O-Benzotriazole- N,N,N',N' -tetramethyluronium-hexafluoro-phosphate (HBTU) and N,N -diisopropylethylamine (DIEA) were used as coupling reagents for arginine, alanine, tryptophan, valine and asparagine, while 2-(1H-7-azabenzotriazol-1-yl)-1,1,3,3-tetramethyl uronium hexafluorophosphate (HATU) and DIEA were used for aryl tryptophan. After side-chains removal, peptides were cleaved from the resin with trifluoroacetic acid (TFA)/water/triisopropylsilane (TIS). Purification of peptides was performed by RP-HPLC. Identification was carried out by MALDI-MS and MALDI-MS/MS.



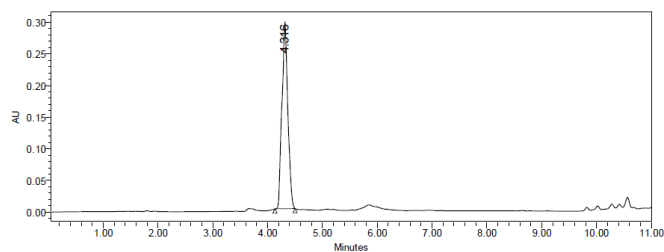
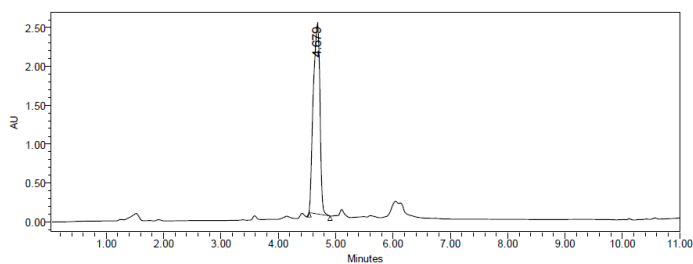
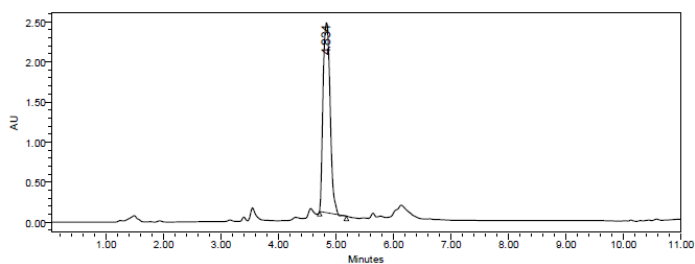
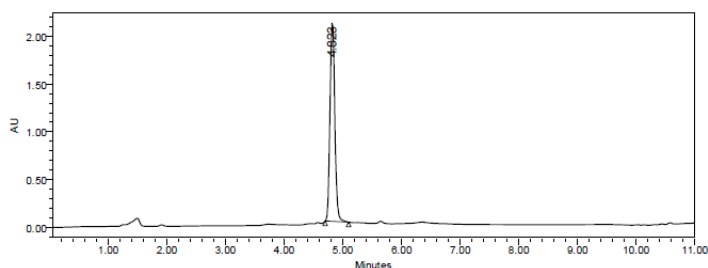
Native Peptide H-Arg-Lys-Trp-Val-Trp-Trp-Arg-Asn-Arg-NH₂ (1)



W1-Ar H-Arg-Lys-Trp(C2-Ph)-Val-Trp-Trp-Arg-Asn-Arg-NH₂ (2)

W2-Ar H-Arg-Lys-Trp-Val-Trp(C2-Ph)-Trp-Arg-Asn-Arg-NH₂ (3)

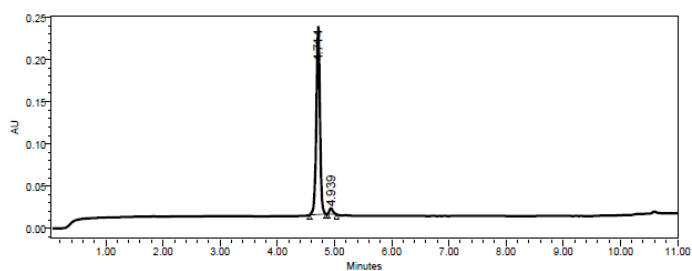
W3-Ar H-Arg-Lys-Trp-Val-Trp-Trp(C2-Ph)-Arg-Asn-Arg-NH₂ (4)

RP-HPLC chromatograms of crude arylated peptides 1-4**H-Arg-Lys-Trp-Val-Trp-Trp-Arg-Asn-Arg-NH₂ (1)****H-Arg-Lys-Trp(C2-Ph)-Val-Trp-Trp-Arg-Asn-Arg-NH₂ (2)****H-Arg-Lys-Trp-Val-Trp(C2-Ph)-Trp-Arg-Asn-Arg-NH₂ (3)****H-Arg-Lys-Trp-Val-Trp-Trp(C2-Ph)-Arg-Asn-Arg-NH₂ (4)**

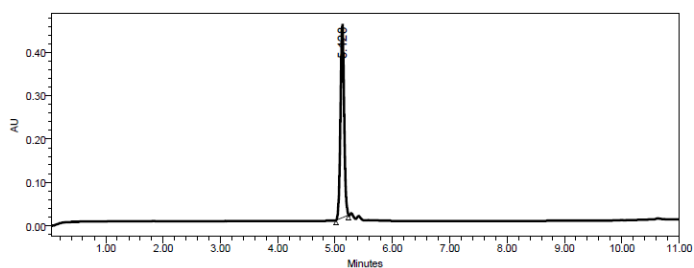
Gradient was 5-60% of B. Solvent A (0.045 % TFA in H₂O) and solvent B (0.036 % TFA in ACN), in 8 min. Elution was monitored at 220 nm and the flow rate was 1.0 mL/min.

RP-HPLC chromatograms of pure arylated peptides 1-4

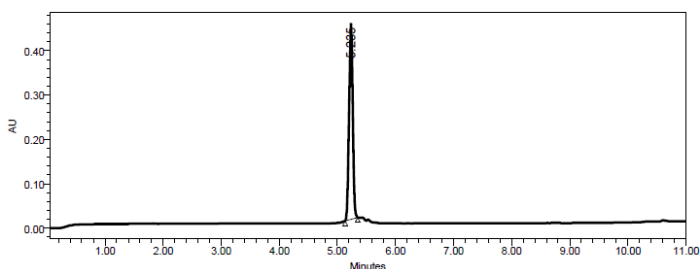
H-Arg-Lys-Trp-Val-Trp-Trp-Arg-Asn-Arg-NH₂ (1)



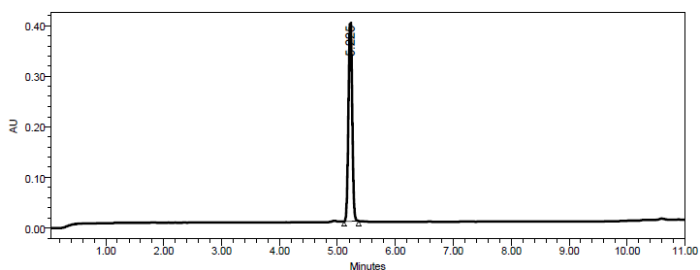
H-Arg-Lys-Trp(C2-Ph)-Val-Trp-Trp-Arg-Asn-Arg-NH₂ (2)



H-Arg-Lys-Trp-Val-Trp(C2-Ph)-Trp-Arg-Asn-Arg-NH₂ (3)



H-Arg-Lys-Trp-Val-Trp-Trp(C2-Ph)-Arg-Asn-Arg-NH₂ (4)

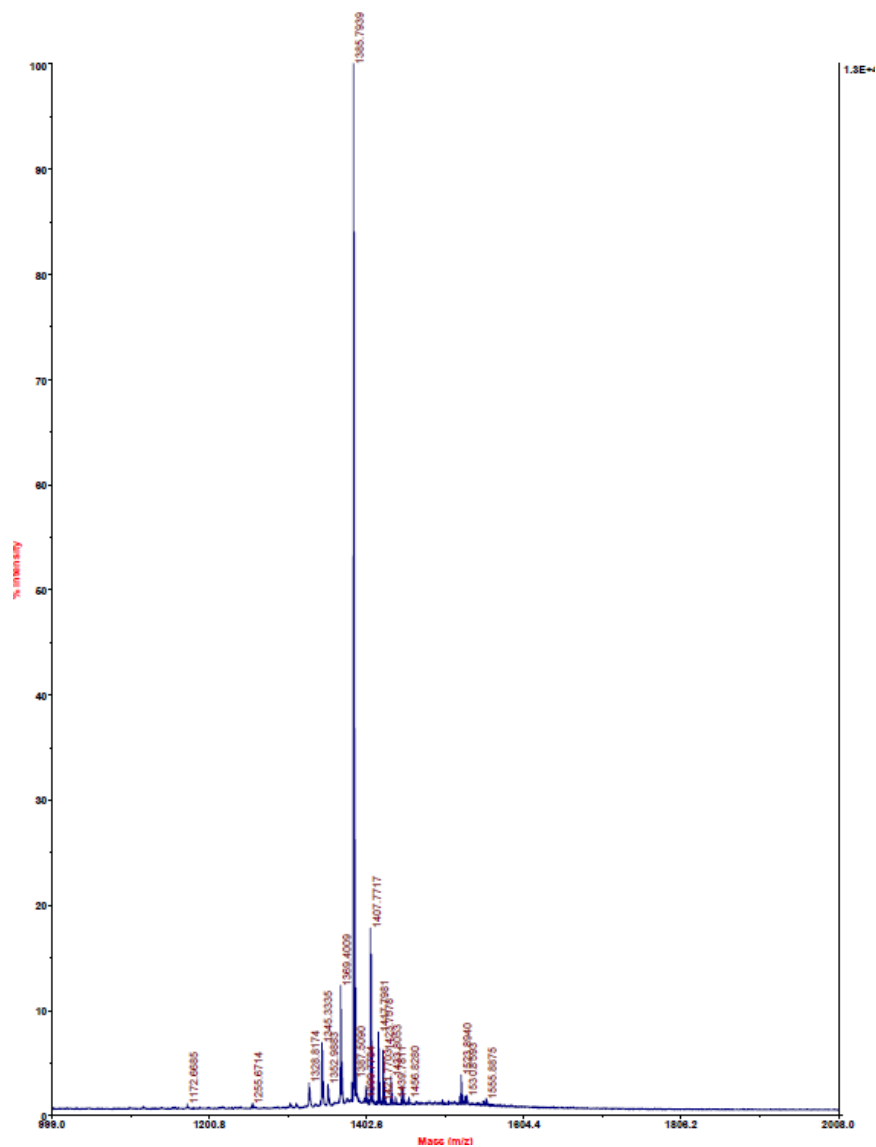


Gradient was 5-60% of B. Solvent A (0.045 % TFA in H₂O) and solvent B (0.036 % TFA in ACN), in 8 min. Elution was monitored at 254 nm and the flow rate was 1.0 mL/min.

MALDI spectra of arylated peptides 1-4

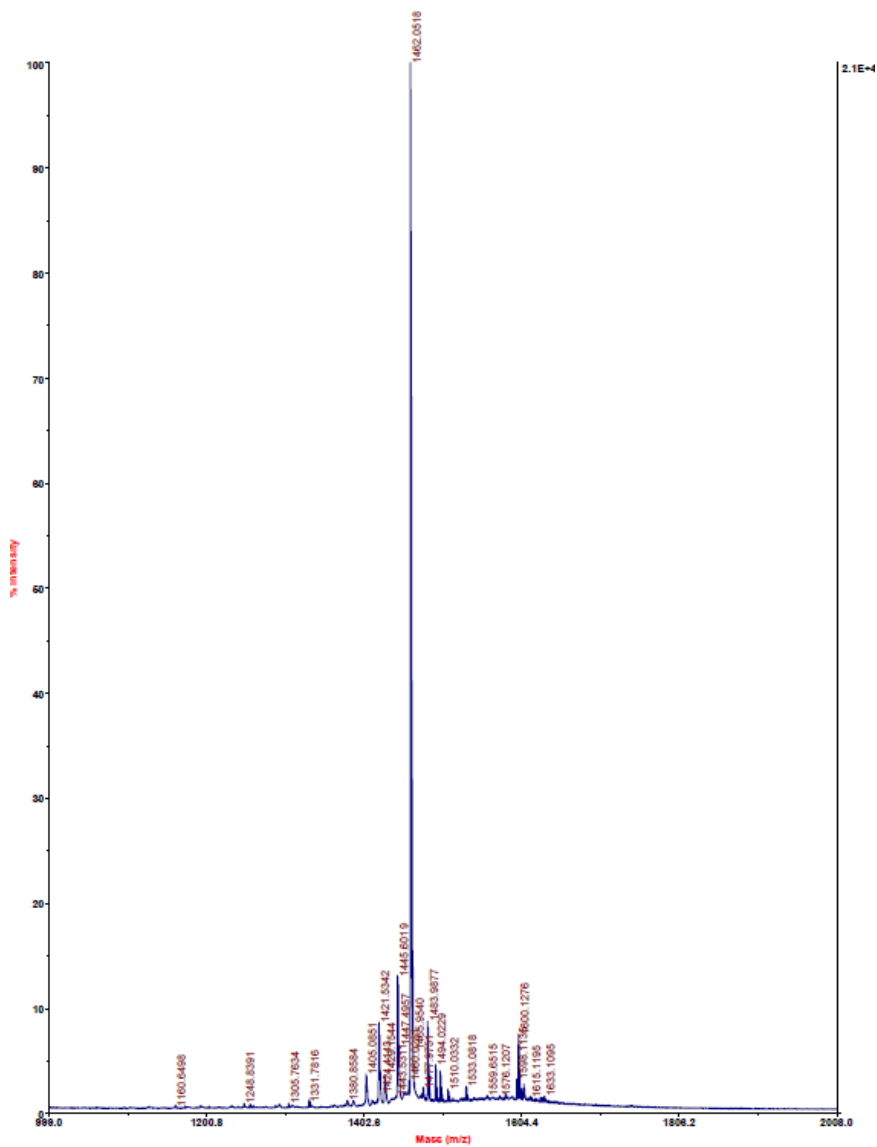
H-Arg-Lys-Trp-Val-Trp-Trp-Arg-Asn-Arg-NH₂ (**1**)

4700 Reflector Spec #1[BP = 1385.8, 13051]



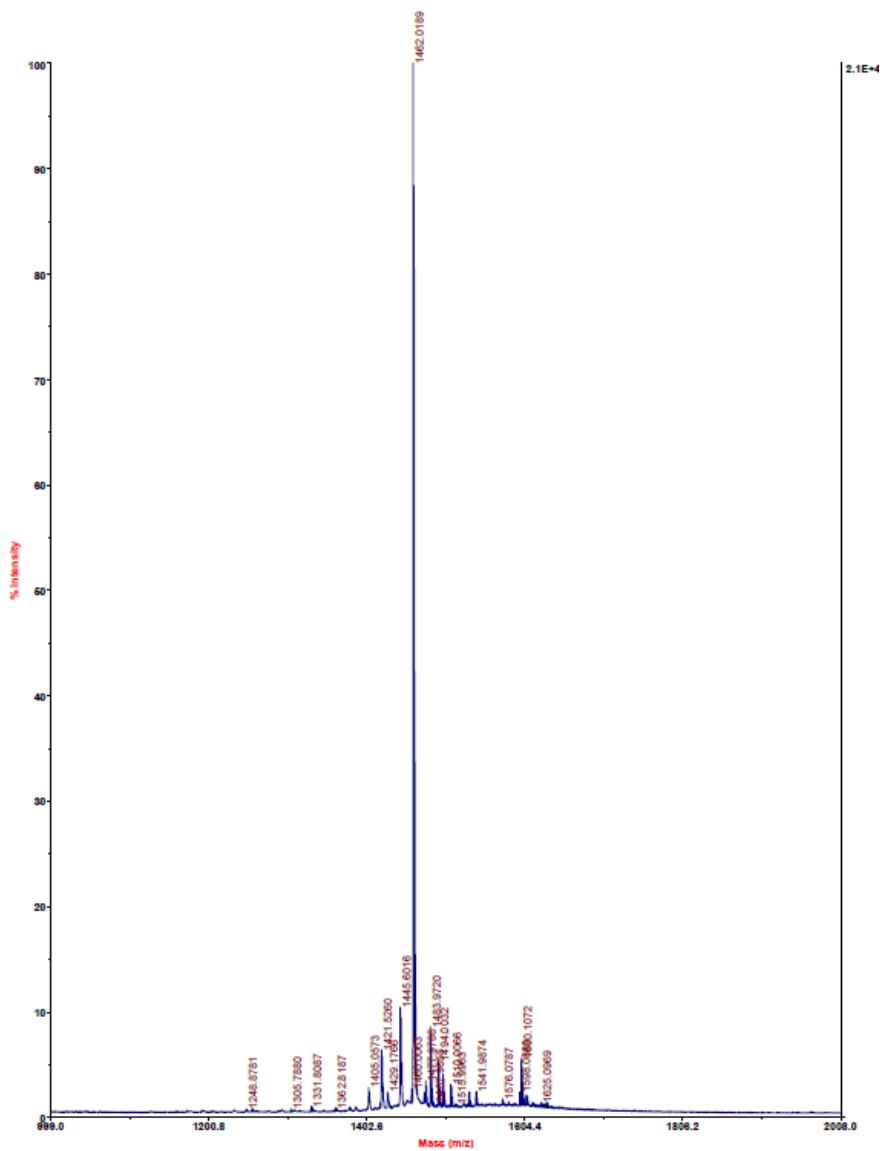
H-Arg-Lys-Trp(C2-Ph)-Val-Trp-Trp-Arg-Asn-Arg-NH₂ (2)

4700 Reflector Spec #1[BP = 1462.1, 20804]



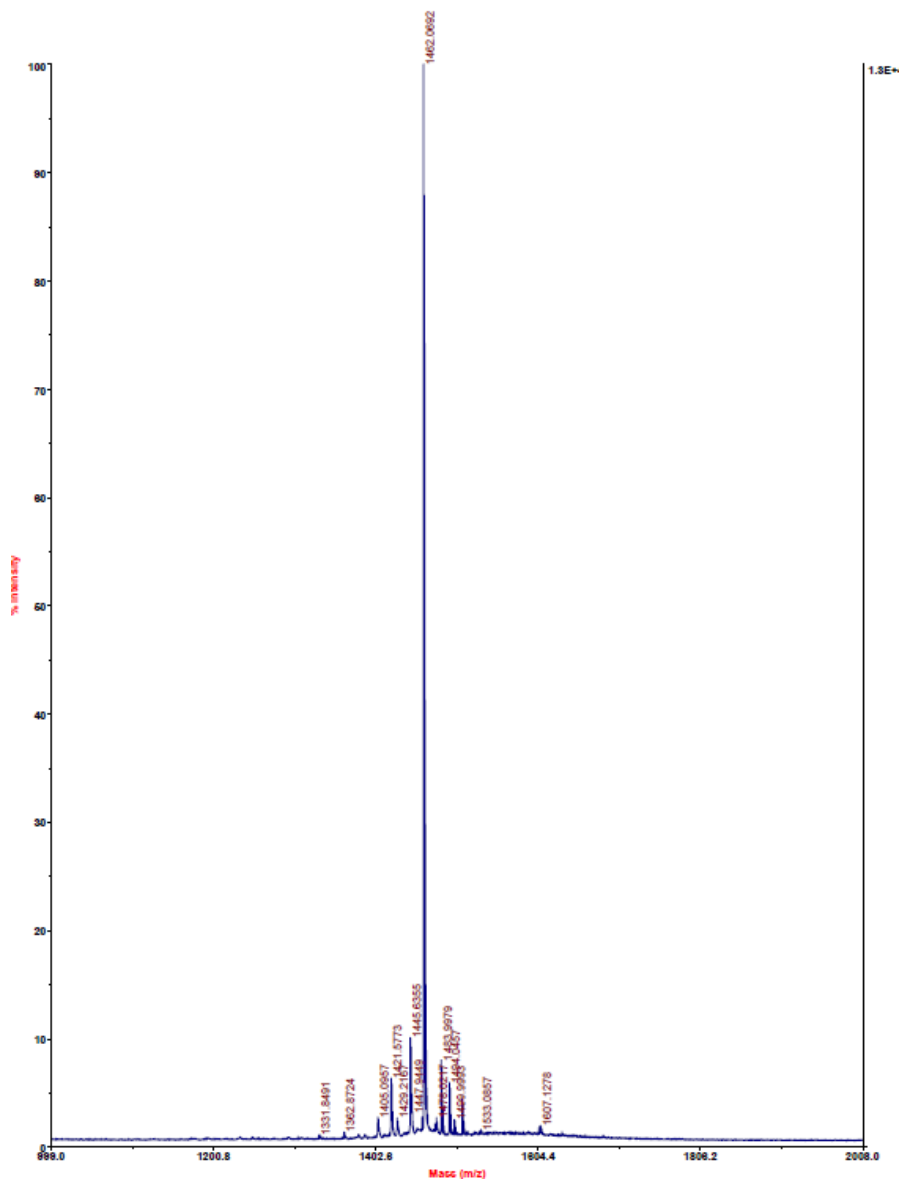
H-Arg-Lys-Trp-Val-Trp(C2-Ph)-Trp-Arg-Asn-Arg-NH₂ (3)

4700 Reflector Spec #1[BP = 1462.0, 21365]



H-Arg-Lys-Trp-Val-Trp-Trp(C2-Ph)-Arg-Asn-Arg-NH₂ (4)

4700 Reflector Spec #1[BP = 1462.1, 13051]



Detailed experimental procedures for the biological assays

Growth inhibition assay

Bacteria were grown in Müller-Hinton broth until a density of 1×10^8 CFU/mL was reached. A final bacteria concentration of $1-5 \times 10^5$ CFU/mL was used.

Peptide solutions in concentrations of 2.5 to 0.1 mg/mL, were mixed with the same volume of 2X Müller-Hinton medium and incubated at 37° C for 21 h in serial two-fold dilutions. Bacterial growth was determined by measuring the absorbance at 620 nm. Positive control (100 % growth) was performed in absence of peptide and negative control was carried out in absence of bacteria.

Minimum inhibitory concentration (MIC) determination

MIC determination was performed by the micro-dilution assay (Wiegand et al., 2008).⁵ Briefly, decreasing amounts of peptides (from 0.5 mg to 0.5 µg) were incubated with a bacterial inoculum in exponential growing phase, in Müller-Hinton culture medium. After 12 h at 37° C, the absorbance at 600 nm was measured. A positive control without peptide (100 % growth) and a negative control without bacteria (0 % growth) were also carried out.

MIC is defined as the minimum concentration of peptide producing total inhibition of the growth under these conditions. Each peptide was assayed in triplicate.

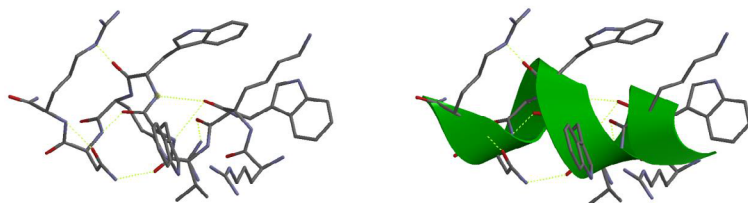
Hemolysis assay

It was performed on human red blood cells (RBC), basically as described by Helmerhorst et al. (1999).⁶ Briefly, RBC from heparinized blood were washed three times with phosphate-buffered saline (PBS) and resuspended at 0.5 % in PBS. The peptide solution, in concentrations of 15, 50 and 125 µg/mL was added to equal volume of RBC suspension. After 1 h at 37° C, the mixture was centrifuged at 2800 rpm for 5 min and the absorbance of the supernatant at 414 nm was measured. PBS and Triton X-100 were the negative and positive controls, respectively. The hemolysis percentage was calculated by the formula:

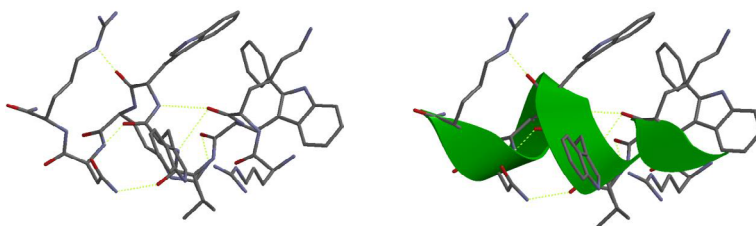
$$[(A_{\text{peptide}} - A_{\text{PBS}}) / (A_{\text{Triton}} - A_{\text{PBS}})] \times 100$$

Minimized geometries of the native peptide and the arylated derivatives generated by the Spartan '14 suite (molecular mechanics, MMFF94)⁷

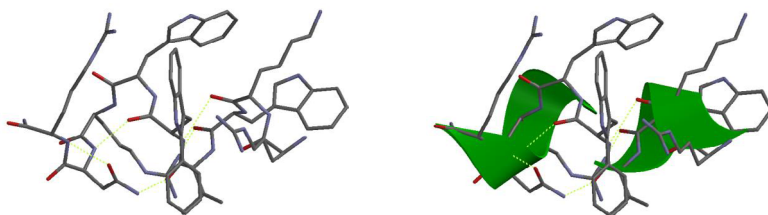
1- Native Peptide: RKWVWVRNR-NH₂



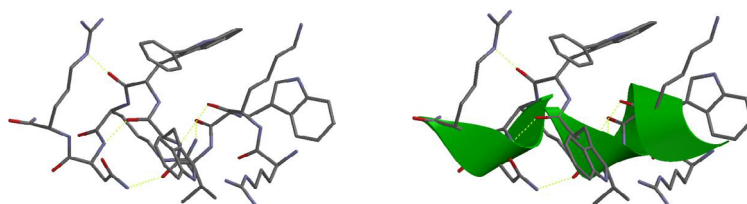
2- W1Ar: RKW(Ar)VWVRNR-NH₂



3- W2Ar: RKWVW(Ar)VRNR-NH₂



4- W3-Ar: RKWVWW(Ar)VRNR-NH₂



Hydrogens omitted for clarity. Left section: hydrogen bonds shown in yellow. Right section: ribbons in green. No significant changes were observed when the optimization was done with semi-empirical methods.

Bibliography

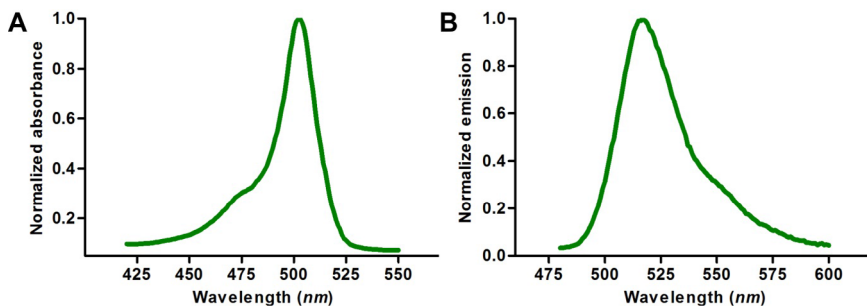
1. J. Ruiz-Rodríguez, F. Albericio and R. Lavilla, *Chem. Eur. J.* 2010, **16**, 1124-1127.
2. S. Preciado, L. Mendive-Tapia, C. Torres-García, R. Zamudio-Vázquez, V. Soto-Cerrato, R. Pérez-Tomás, F. Albericio, E. Nicolás and R. Lavilla, *Med. Chem. Comm.*, 2013, **4**, 1171-1174.
3. S. Preciado, L. Mendive-Tapia, F. Albericio and R. Lavilla, *J. Org. Chem.*, 2013, **78**, 8129-8135.
4. Kates, S. A.; Albericio, F. In *Solid Phase Synthesis. A Practical Guide*; Eds. Marcel Dekker: New York, 2000.
5. I. Wiegand, K. Hilpert and R. E. W. Hancock, *Nat. Protoc.* 2008, **3**, 163-175
6. E. J. Helmerhorst, I. M. Reijnders, W. van't Hoff, E. C. I. Veerman and A. V. Nieuw Amerongen, *FEBS Lett.* 1999, **449**, 105-110.
7. Spartan'14 for Windows, Macintosh and Linux, version 1.1.4, wavefunction, inc. www.wavefun.com.



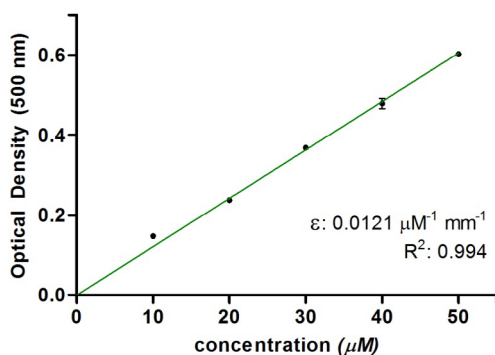
FULL SUPPORTING INFORMATION PUBLICATION IV

Supplementary Figures

Spectral properties of compound 3.

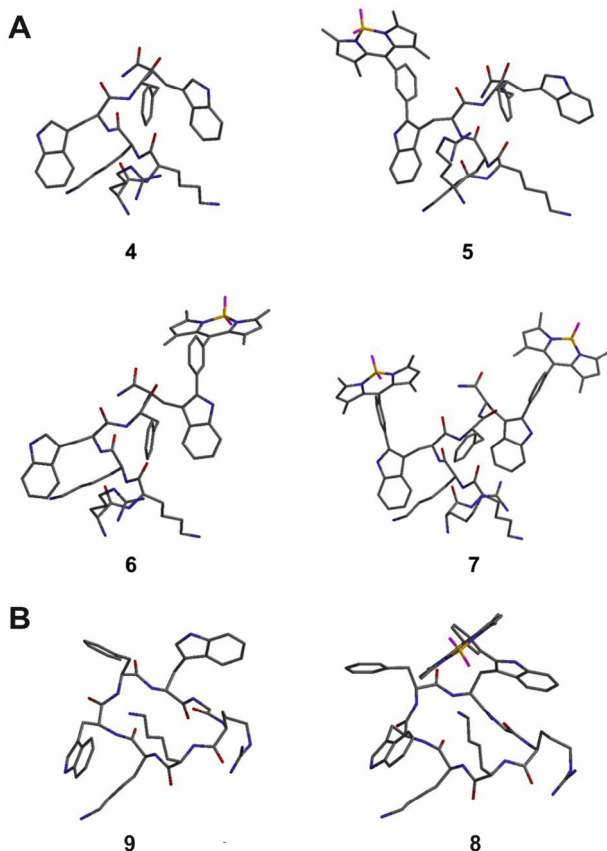


Supplementary Figure 1. Spectral characterisation of the amino acid 3. A) Absorbance and B) emission spectra ($\lambda_{exc.}$: 450 nm) of compound 3.



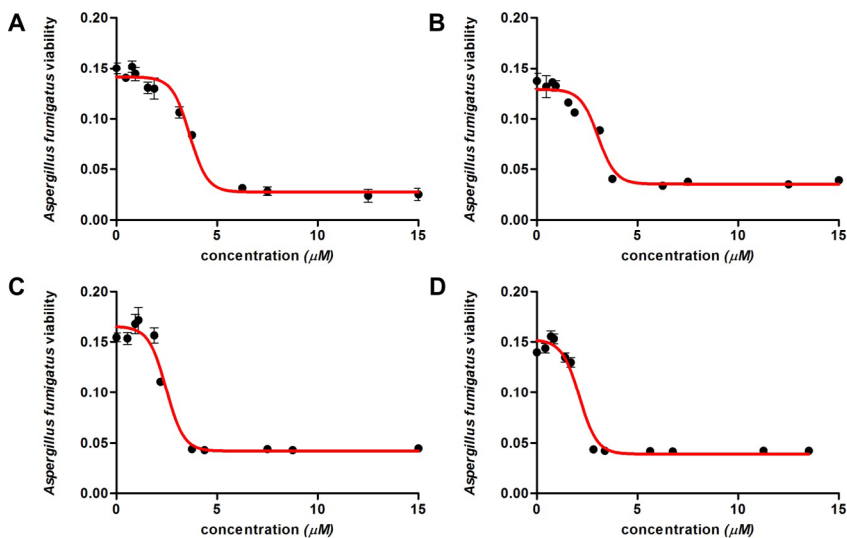
Supplementary Figure 2. Determination of the extinction coefficient of the amino acid 3. Solutions of 3 were prepared in ethanol and their optical densities were measured at 500 nm in a NanoDrop 1000 spectrophotometer. Data represented as means \pm s.e.m. ($n=3$).

Molecular simulation models of labelled and non-labelled peptides.

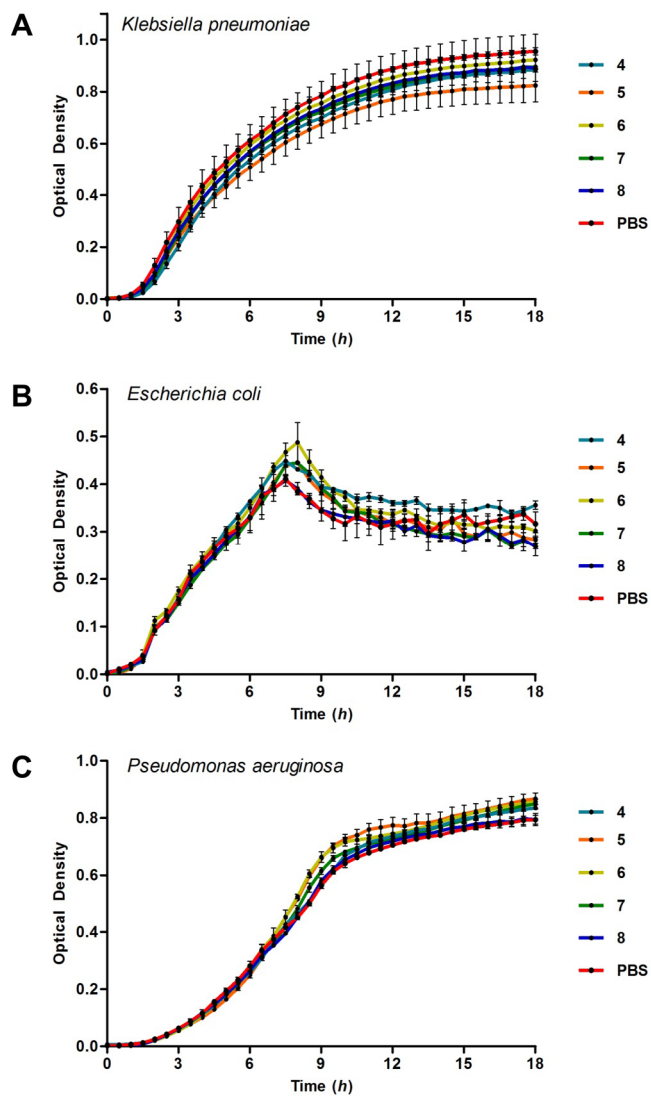


Supplementary Figure 3. A) Optimised geometries of fluorogenic linear peptides **5-7** and the corresponding non-labelled linear peptide **4**. B) Optimised geometries of the fluorogenic cyclic peptide **8** and the corresponding non-labelled cyclic peptide **9** (for structure see Supplementary Fig. 8). All simulations were generated by the Spartan '14 suite using Molecular Mechanics (MMFF94) and Semi-Empirical (AM1) methods.*

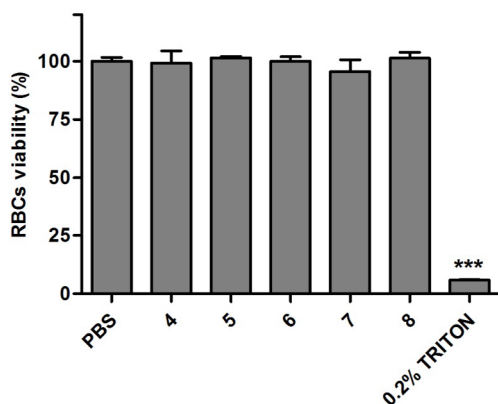
* Spartan'14 for Windows, Macintosh and Linux, version 1.1.4, wavefunction, inc. www.wavefun.com.

Antimicrobial and haemolysis assays.

Supplementary Figure 4. Determination of IC_{50} values of BODIPY-labelled peptides 5-8 in *A. fumigatus*. Cell viability plots and non-linear regressions for peptides 5 (A), 6 (B), 7 (C) and 8 (D). Peptides were incubated at different concentrations with *A. fumigatus* conidia to reach a final volume of 100 μL per well. The final conidia concentration was 5×10^5 cells/mL in 10% Vogel's medium. After 24 h incubation at 37 °C in 96 well-plates, fungal growth was determined by measuring the optical density at 610 nm. The IC_{50} values were determined using four parameter logistic regression. Data represented as means \pm s.e.m ($n=3$).

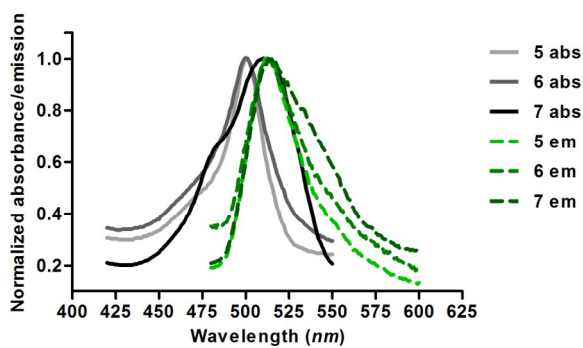


Supplementary Figure 5. Activity of peptides 4-8 in different bacterial strains. Peptides were added to the *Klebsiella pneumoniae* (A), *Escherichia coli* (B) and *Pseudomonas aeruginosa* (C), and their viability (optical density at 595 nm) was monitored at 37 °C for 16 h. Data represented as means \pm s.d. ($n=3$).



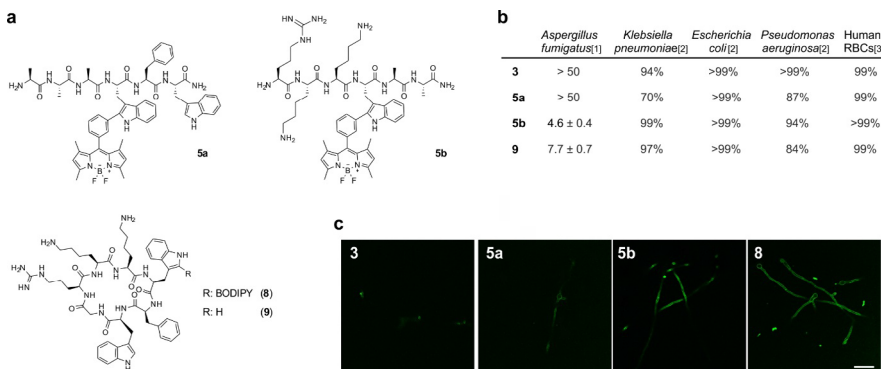
Supplementary Figure 6. Haemolytic activity of peptides 4-8 in human red blood cells (RBCs).

Peptides **4-8** and Triton X-100 (0.2% as positive control) were incubated with human RBCs at 37 °C and their viability was assessed after 1 h. Data represented as means \pm s.d. ($n=3$). *** for $p < 0.001$ was determined as a statistically significant difference between the cell viabilities in PBS (phosphate buffer saline) and in Triton X-100.

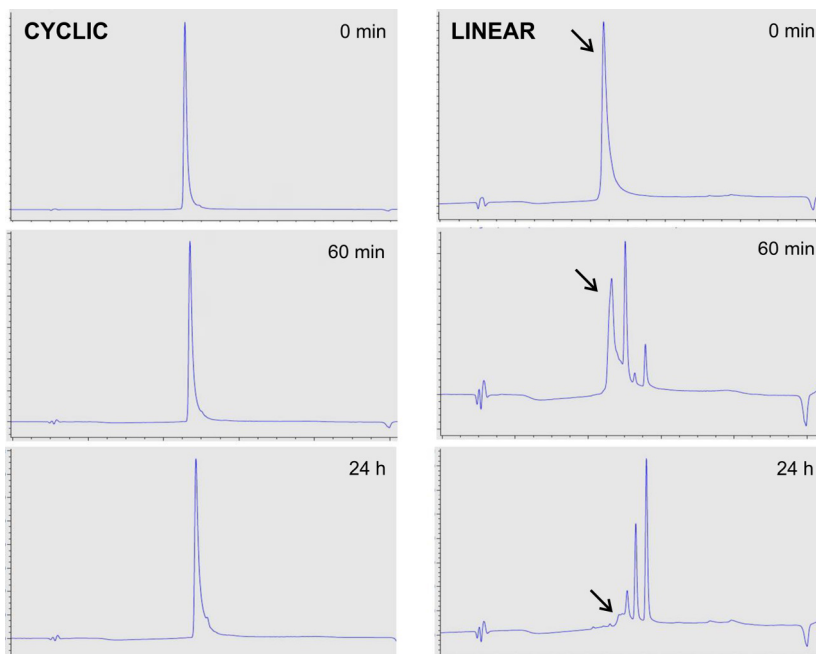
Spectral properties of peptides 5-7.

Supplementary Figure 7. Spectral characterisation of peptides 5, 6 and 7. Absorbance (solid lines) and emission (dashed lines) spectra ($\lambda_{exc.}$: 450 nm) of peptides **5-7** in PBS (phosphate buffer saline).

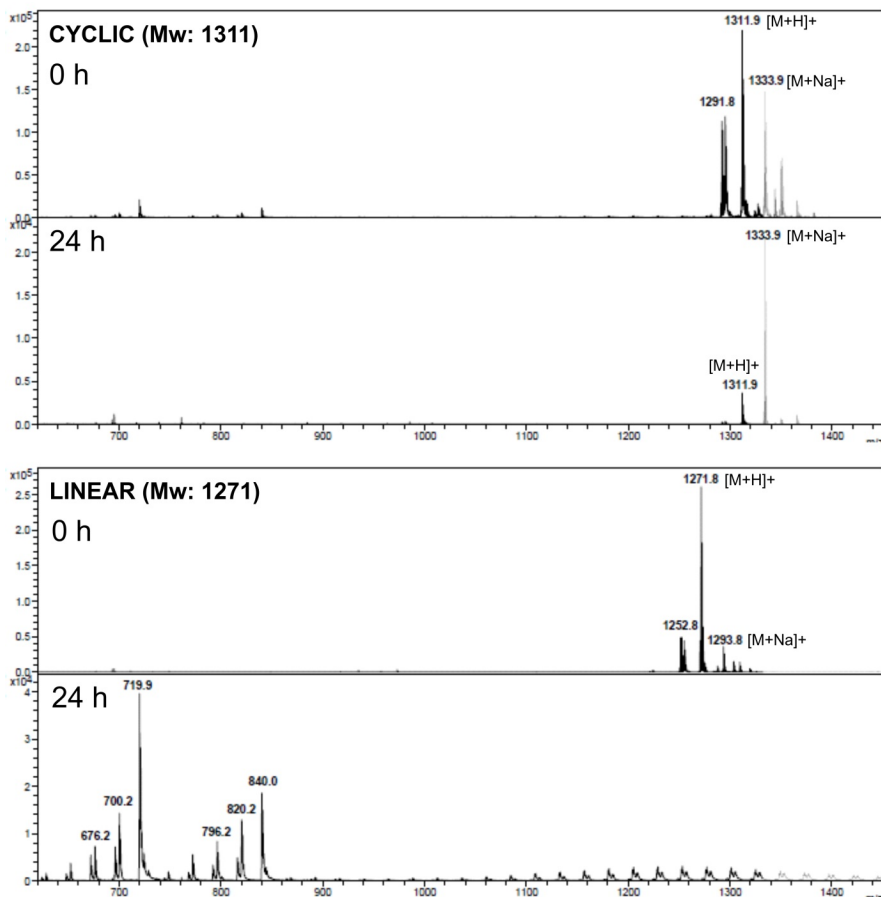
Characterisation of compounds 3, 5a, 5b and 9.



Supplementary Figure 8. Characterisation of the amino acid 3 and peptides 5a, 5b and 9 for live cell imaging of *A. fumigatus*. a) Chemical structures of fluorogenic linear (**5a**, **5b**) and cyclic peptides (**8**, **9**). b) Activity in *A. fumigatus*, several bacterial strains and in human red blood cells (RBCs).[1] IC₅₀ (μM) values as means ± s.e.m. (n=3), [2] cell viability upon 16 h incubation with **3**, **5a**, **5b** or **9** at their respective IC₅₀ concentrations or 20 μM for compounds **3** and **5a** (n=3), [3] cell viability upon 1 h incubation with **3**, **5a**, **5b** or **9** at their respective IC₅₀ concentrations or 20 μM for compounds **3** and **5a** (n=3). c) Wash-free fluorescent live cell images of *A. fumigatus* at 37 °C using confocal microscopy after incubation with peptides with **3**, **5a**, **5b** or **8** (all at 2 μM). Scale bar: 20 μm.

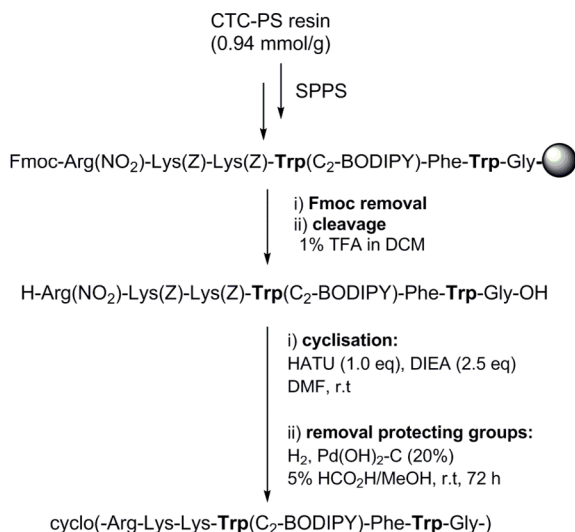
Stability assays.

Supplementary Figure 9. Stability of cyclic (8) and linear (5) mono-BODIPY labelled peptides in human bronchoalveolar lavage samples from patients with acute respiratory distress syndrome. Peptides were incubated in human bronchoalveolar lavage samples at 37 °C and analysed by HPLC at the time points indicated. Arrows point at the peaks corresponding to the intact linear peptide.

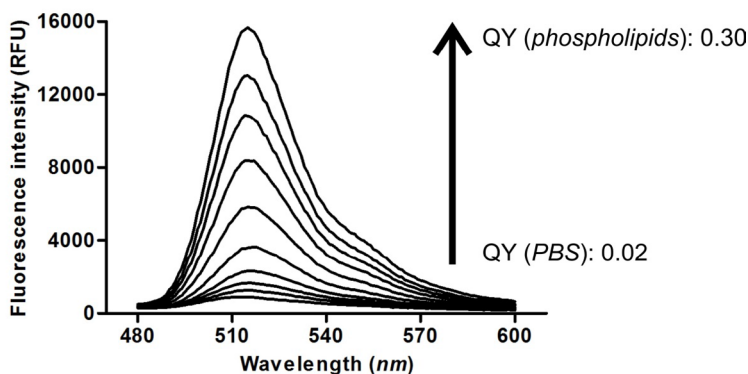


Supplementary Figure 10. MALDI analysis of cyclic (8) and linear (5) mono-BODIPY labelled peptides in bronchoalveolar lavage samples from patients with acute respiratory distress syndrome. Peptides were incubated in human bronchoalveolar lavage samples at 37 °C and analysed by MALDI at the time points indicated.

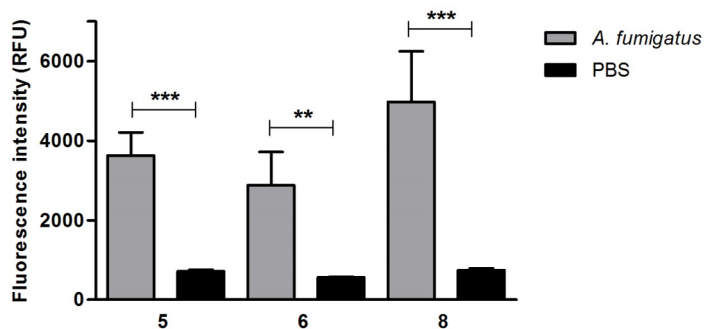
Synthesis and spectral properties of peptide 8.



Supplementary Figure 11. Synthetic scheme for the cyclic peptide 8.

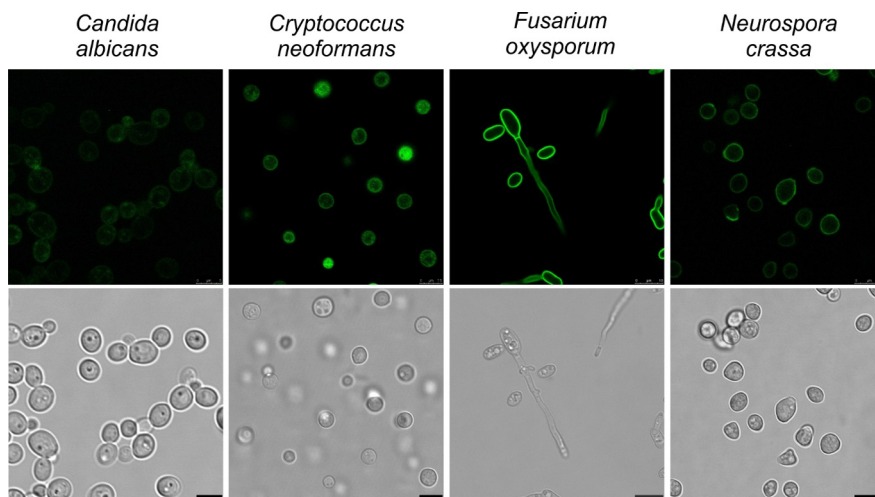


Supplementary Figure 12. Fluorogenic behaviour of the cyclic peptide 8 in phospholipid membranes. Spectra of peptide 8 were recorded after incubation with phosphatidylcholine:cholesterol (7:1) liposomes suspensions in phosphate buffer saline (PBS) ranging from 3.75 mg mL⁻¹ to 0.004 mg mL⁻¹ of PC in 2-fold serial dilutions, $\lambda_{exc.}$: 450 nm. Quantum yields were determined using fluorescein in basic ethanol as the reference (QY: 0.97).^[1]



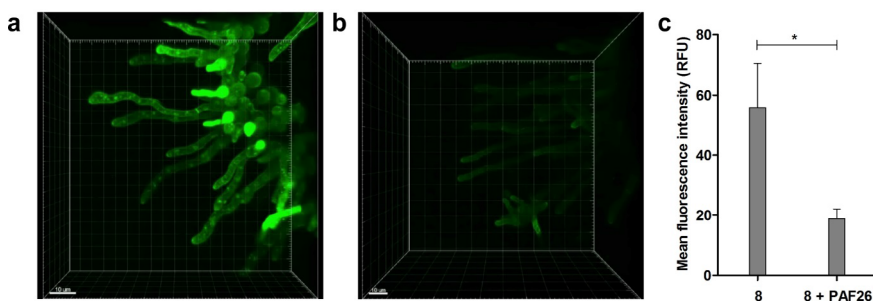
Supplementary Figure 13. Fluorescence emission of mono-BODIPY labelled peptides 5, 6 (linear) and 8 (cyclic) upon incubation with *A. fumigatus*. Peptides 5, 6, and 8 were incubated in PBS (phosphate buffer saline) alone or in suspensions of *A. fumigatus* in PBS ($\lambda_{exc.}$: 485 nm; $\lambda_{em.}$: 515 nm). Data represented as means \pm s.d. ($n=3$). ** for $p < 0.01$ and *** for $p < 0.005$ were determined as statistically significant differences between the fluorescence emission values in PBS and in suspensions of *A. fumigatus* in PBS.

Confocal microscopy images of different fungal species.



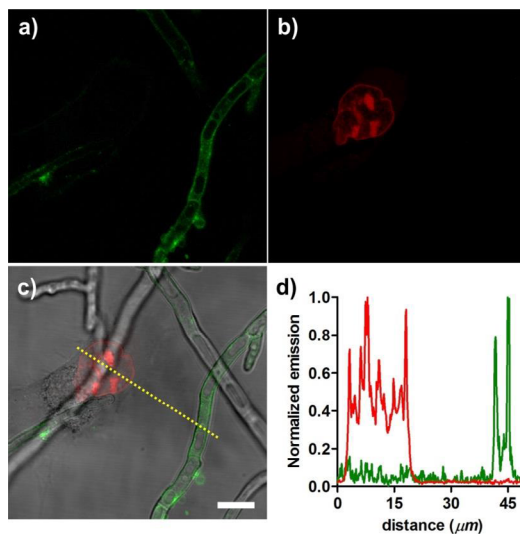
Supplementary Figure 14. Live cell imaging of fungal cells after incubation with the peptide 8.

Peptide **8** was used at 2 μM for all fungi except *C. albicans* for which 10 μM was used. Fluorescence (*top*) and corresponding brightfield (*bottom*) images were acquired under a confocal microscope at r.t.. Scale bars: *C. albicans*: 5 μm ; *C. neoformans*: 7.5 μm ; *F. oxysporum* and *N. crassa*: 10 μm .

Competition experiments between 8 and PAF26 (4).

Supplementary Figure 15. Fluorescence images of *A. fumigatus* after incubation with the peptide 8 without and with pre-treatment of PAF26 (4). Peptide 8 (2 μ M) was incubated for 15 min with *A. fumigatus* that had not been pre-treated (a) or had been pre-treated with PAF26 (3 μ M) for 30 min at 37°C (b). Images were captured under a confocal microscope at r.t. For 3D projections, see Supplementary Movies 1 and 2. Scale bars: 10 μ m. c) Mean fluorescence intensity values were determined using the software Imaris and represented as means \pm s.d. ($n=3$). * for $p < 0.05$ was determined as a statistically significant difference between PAF26 pre-treated and not pre-treated *A. fumigatus*.

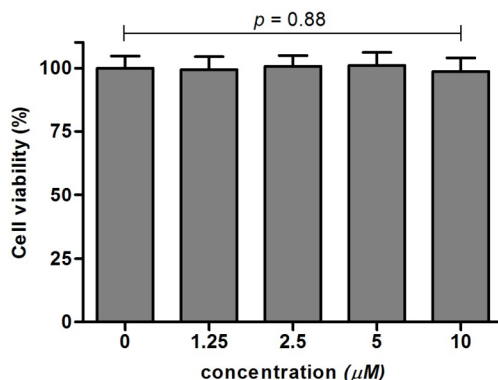
Confocal microscopy images of *Aspergillus fumigatus*.



Supplementary Figure 16. Live cell imaging of *A. fumigatus* in co-cultures with human lung A549 epithelial cells after treatment with the peptide 8. Peptide 8 (2 μM, green) and Syto82 (2.5 μM, red counterstain for human lung cells) were incubated in co-cultures and imaged without washing under a confocal microscope at 37 °C. Fluorescence staining of 8 (a), Syto82 (b) and merged (c). (d) Plot profile analysis of the staining from 8 (green) and Syto82 (red) shown in the merged image. Scale bar: 10 μm.

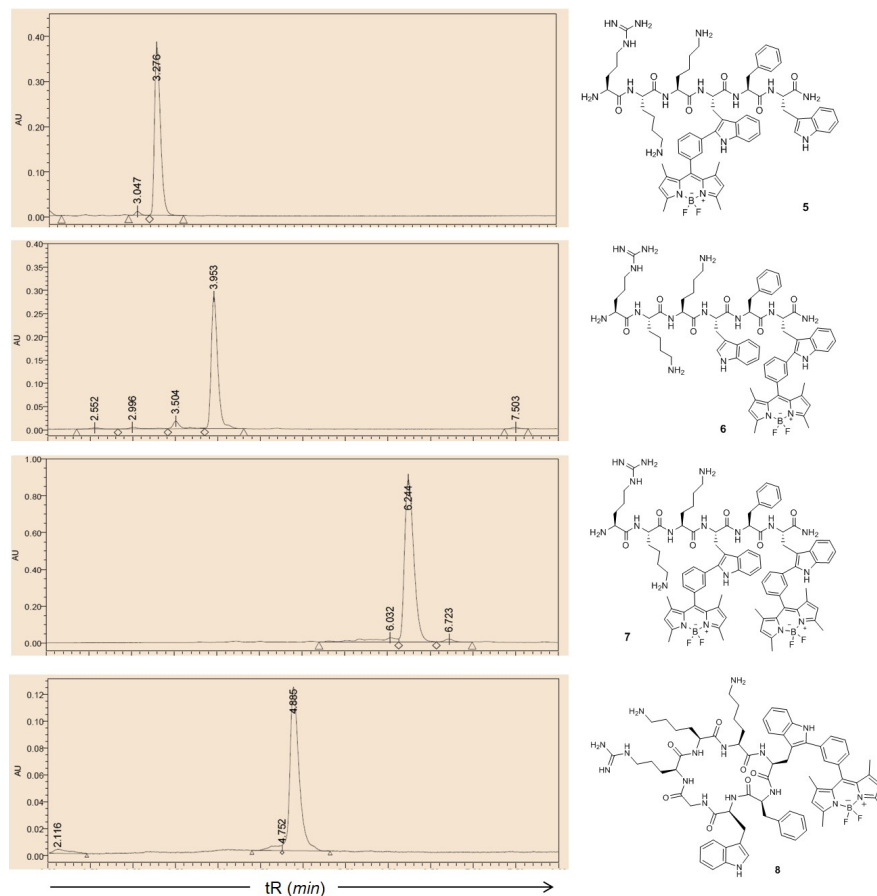
Cell viability assays.

Cell viability was determined with a TACS® MTT Cell Proliferation assay (Trevigen) according to the manufacturer's instructions. Briefly, human lung A549 epithelial cells were plated on 96-well plates the day before the experiment, reaching 90-95% confluence on the day of the experiment. The peptide **8** was added to the cells at different concentrations (0, 1.25, 2.5, 5 and 10 μM) and incubated at 37 °C for 4 h. After 4 h, cells were washed, treated according to the manufacturer's instructions and their absorbance values (570 nm) were measured in a Synergy HT spectrophotometer (Biotek). Cell viability data was normalised to the proliferation of cells without addition of the peptide **8**.

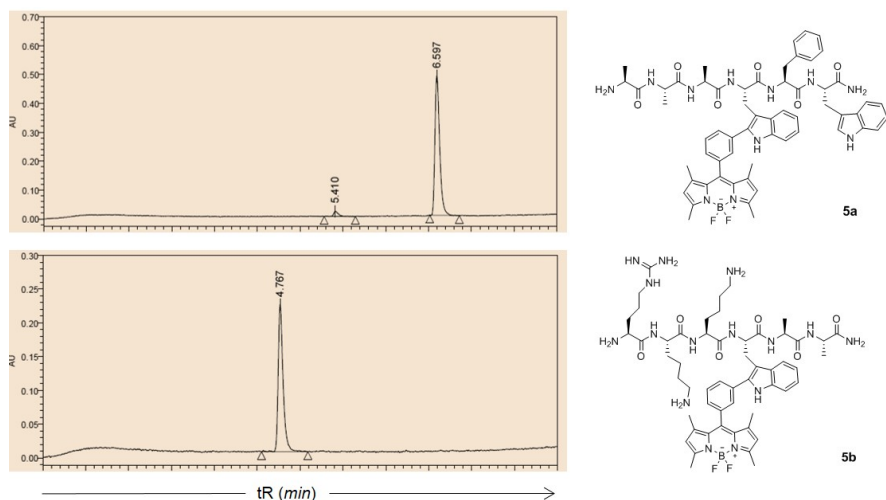


Supplementary Figure 17. Cell proliferation assays. Viability of human lung A549 epithelial cells after incubation with different concentrations of the peptide **8**. Data represented as means \pm s.d. ($n=4$). No significant differences ($p > 0.05$) were determined between the control and any of the treatments.

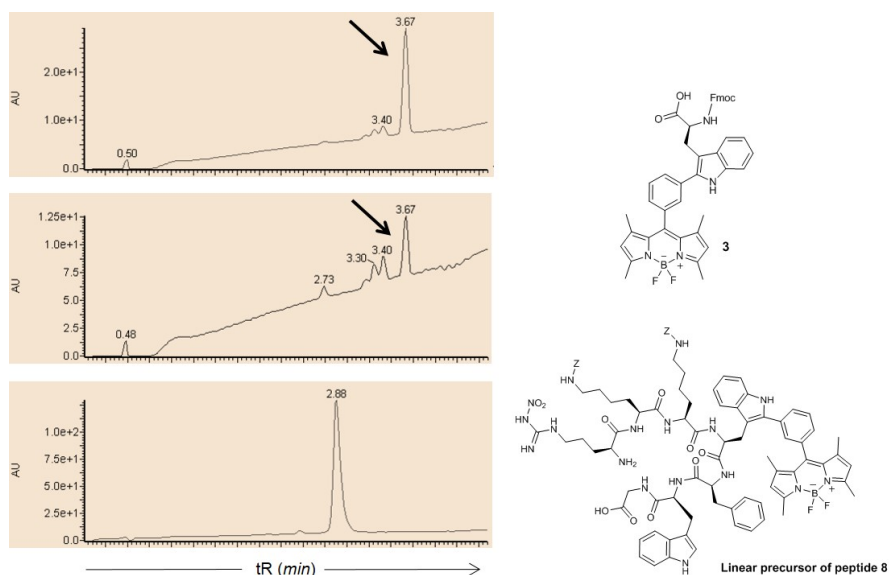
Chemical characterisation data.



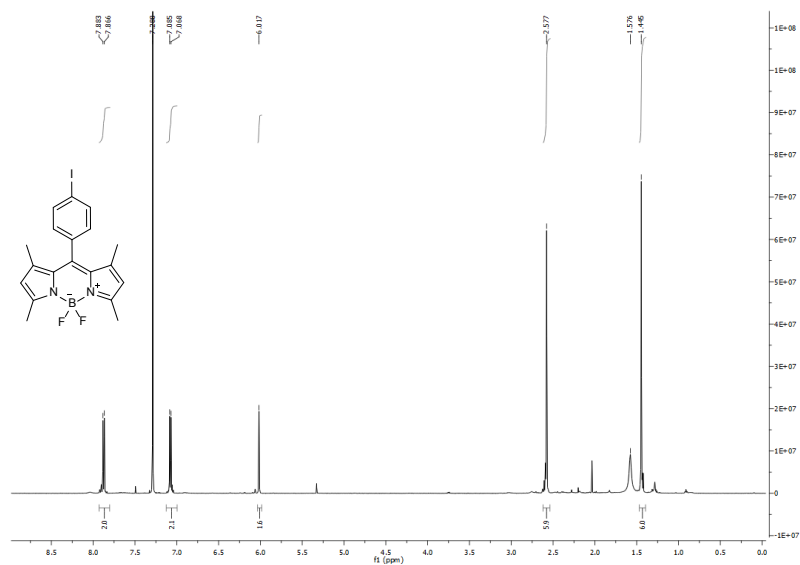
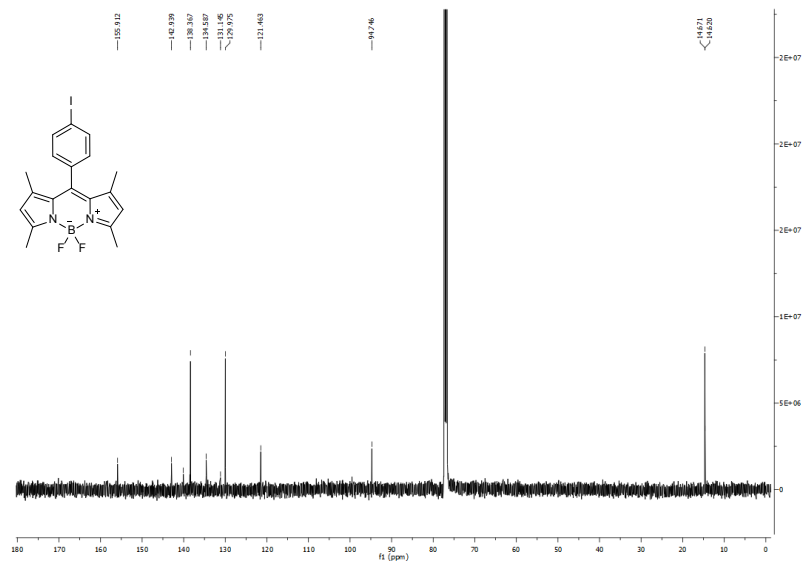
Supplementary Figure 18. HPLC analysis of BODIPY-labelled peptides 5-8.



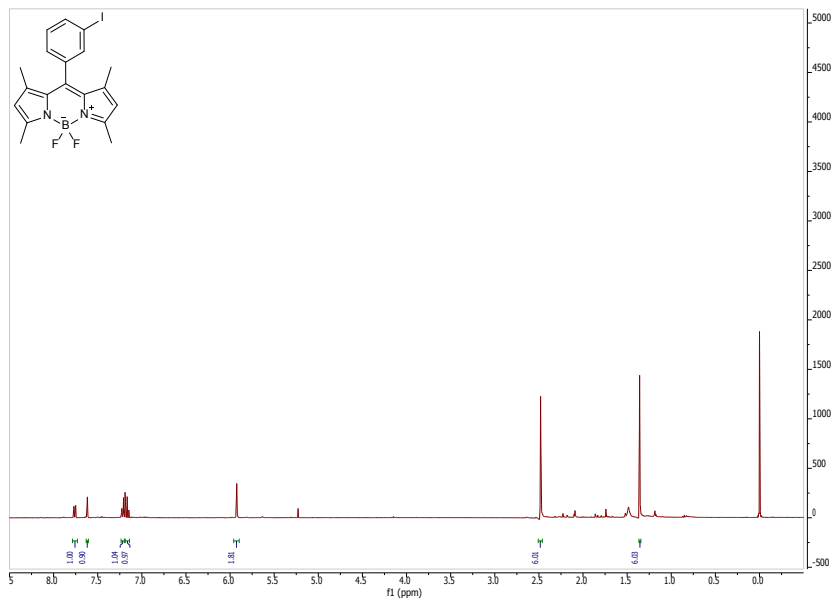
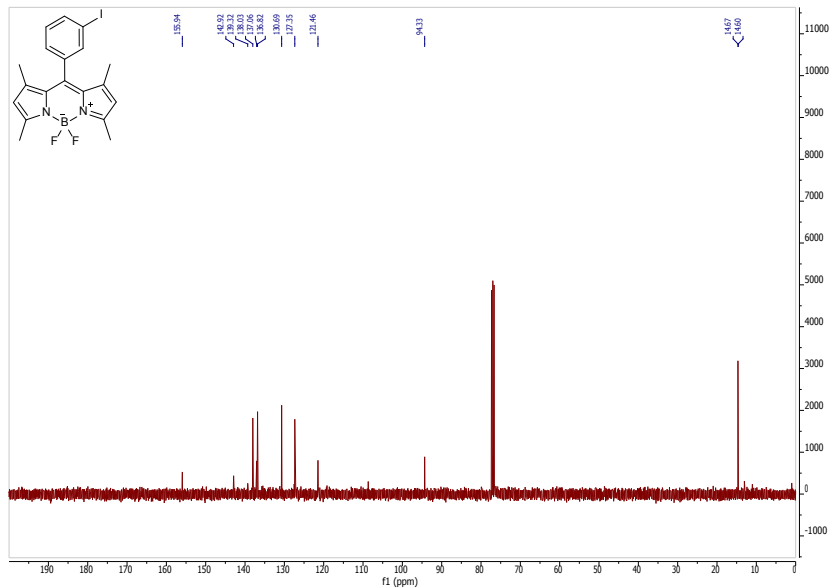
Supplementary Figure 19. HPLC analysis of BODIPY-labelled peptides **5a** and **5b**.



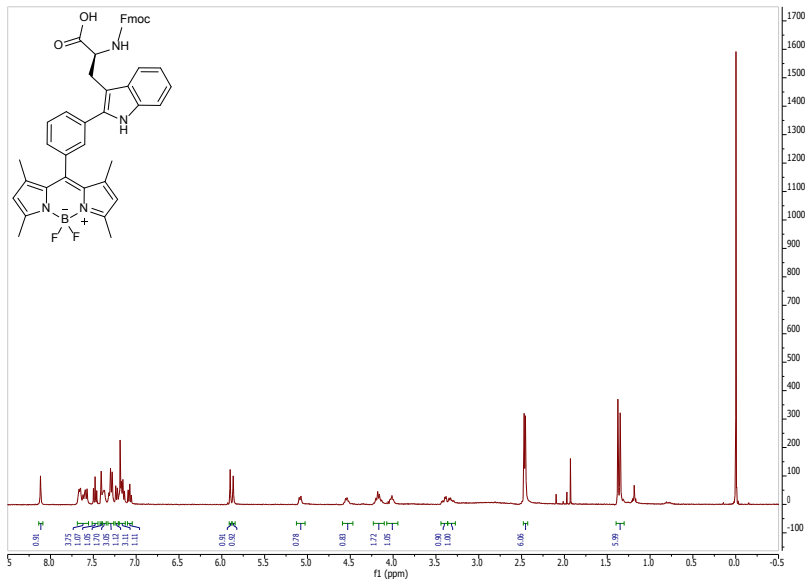
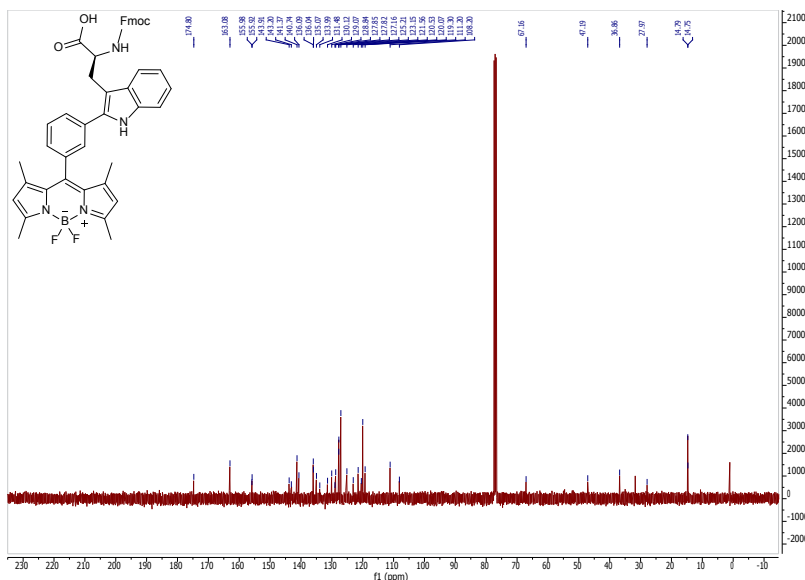
Supplementary Figure 20. Stability studies of BODIPY derivatives. HPLC analysis of Fmoc-Trp(C₂-BODIPY)-OH (**3**) in TFA:DCM (1:99) at r.t. after 10 min (83% purity) (*top panel*), Fmoc-Trp(C₂-BODIPY)-OH (**3**) in TFA:DCM (1:9) at r.t. after 30 min (46% purity) (*mid panel*), crude BODIPY-labelled linear precursor of the cyclic peptide **8** directly after cleavage from the resin with TFA:DCM (1:99) at r.t. (*bottom panel*) (98% purity). Black arrows in top and mid panels point at the peak corresponding to the amino acid **3**.

¹H NMR (CDCl₃)¹³C NMR (CDCl₃)

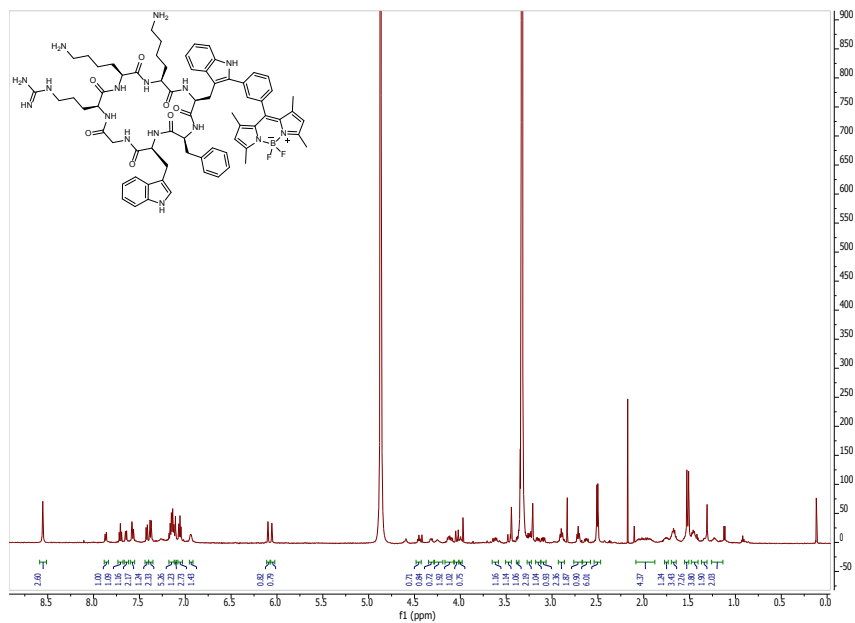
Supplementary Figure 21. NMR characterisation of 4,4-difluoro-8-(4-iodophenyl)-3,5-dimethyl-4-bora-3a,4a-diaza-s-indacene (**1**).

¹H NMR (CDCl₃)¹³C NMR (CDCl₃)

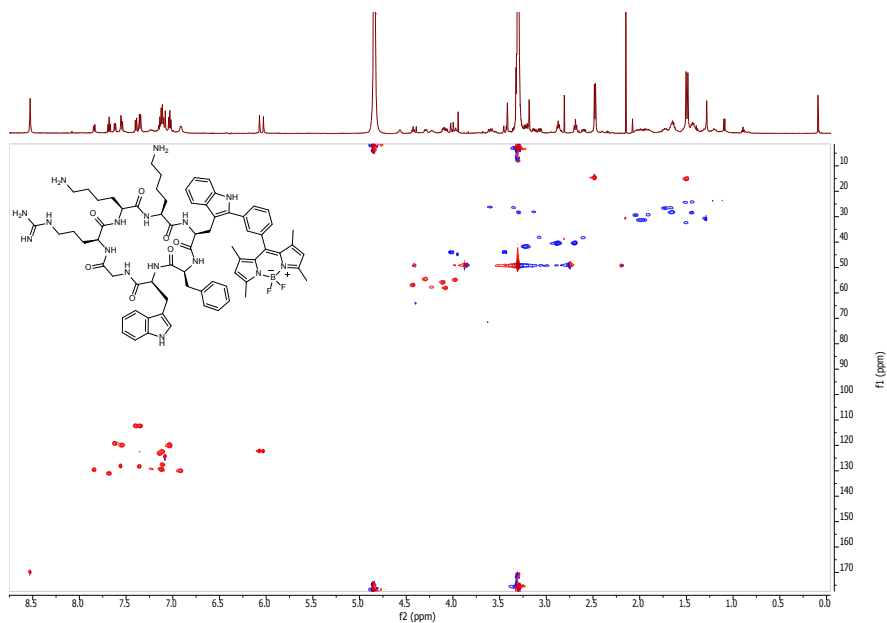
Supplementary Figure 22. NMR characterisation of 4,4-difluoro-8-(3-iodophenyl)-3,5-dimethyl-4-bora-3*a*,4*a*-diazas-indacene (**2**).

¹H NMR (CDCl₃) ^{13}C NMR (CDCl_3)

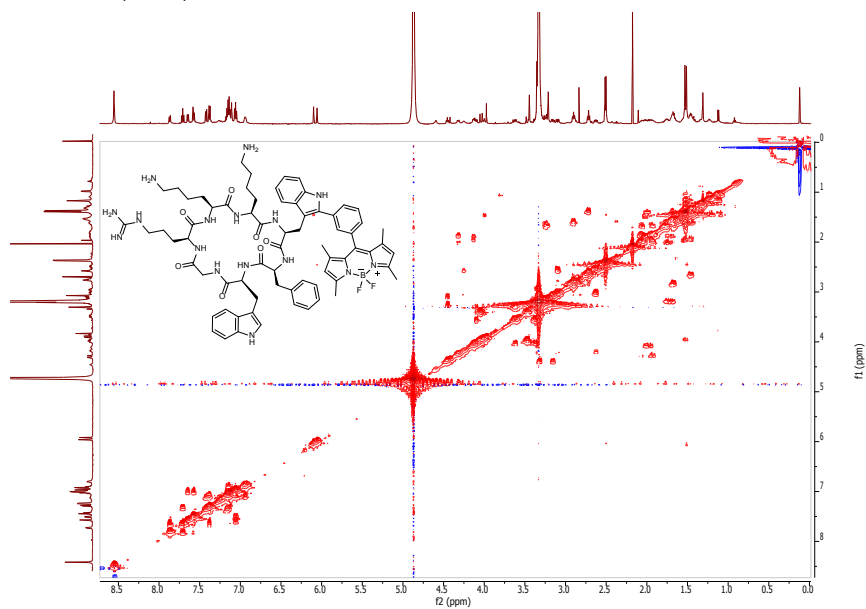
Supplementary Figure 23. NMR characterisation of Fmoc-Trp(C₂-BODIPY)-OH (**3**).

¹H NMR (MeOD)

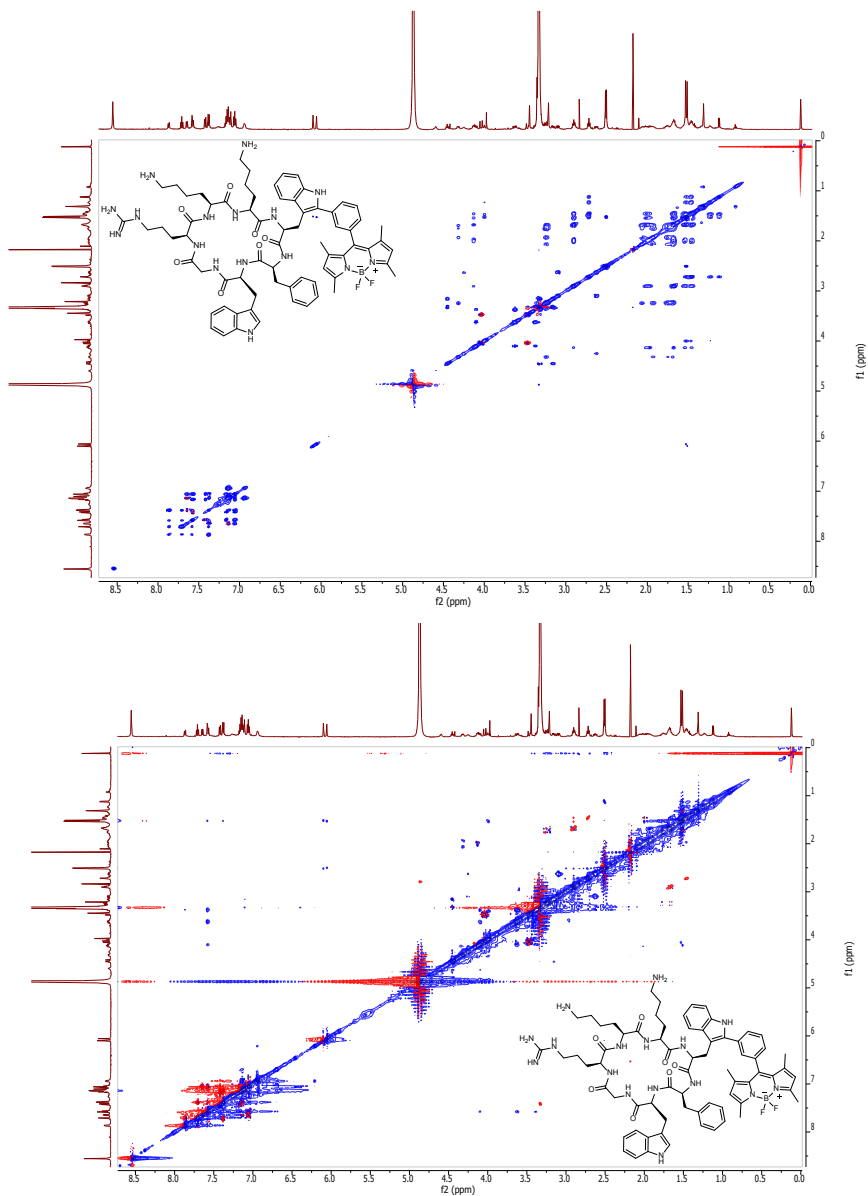
HSQC NMR (MeOD)



COSY NMR (MeOD)

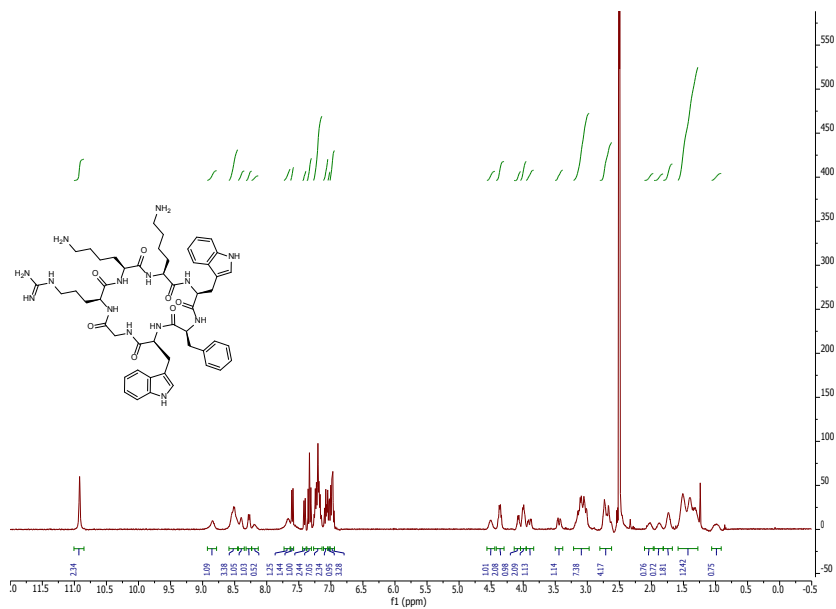


TOCSY NMR (MeOD)

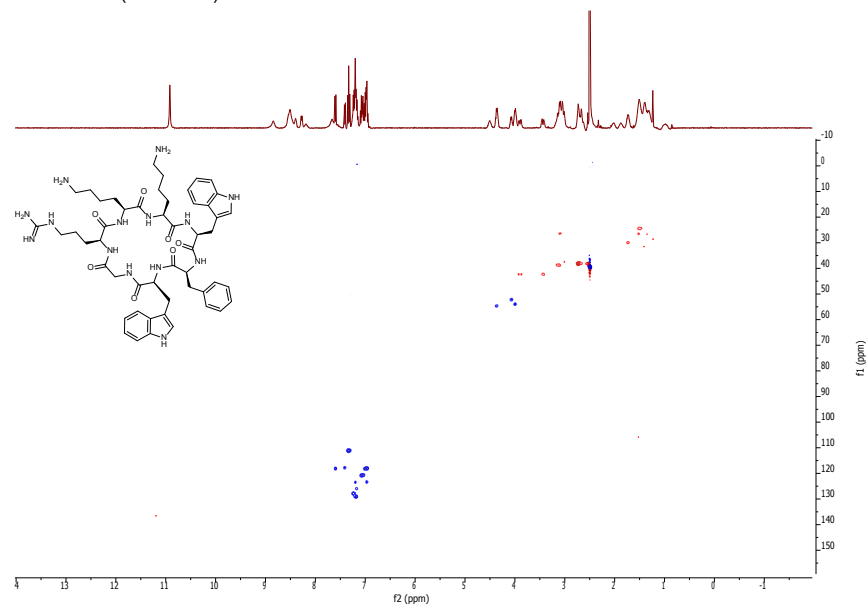


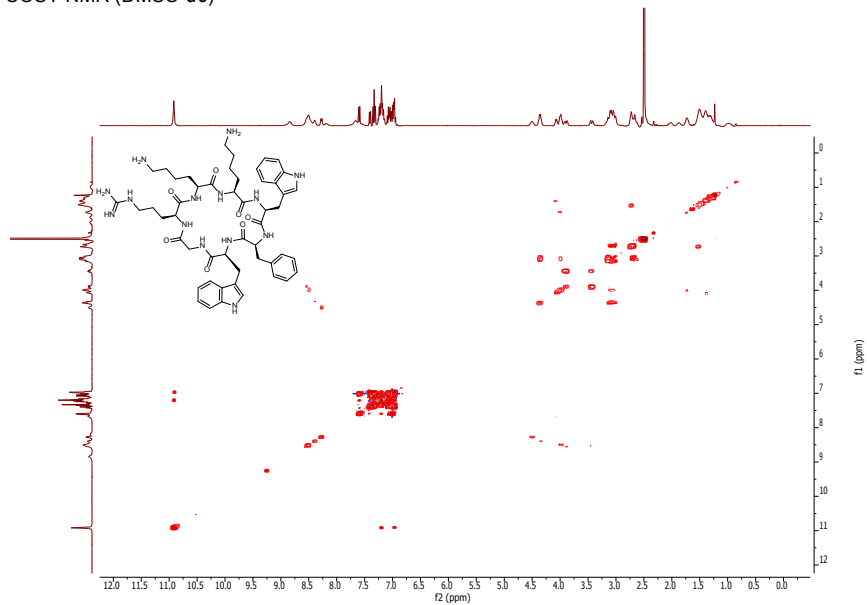
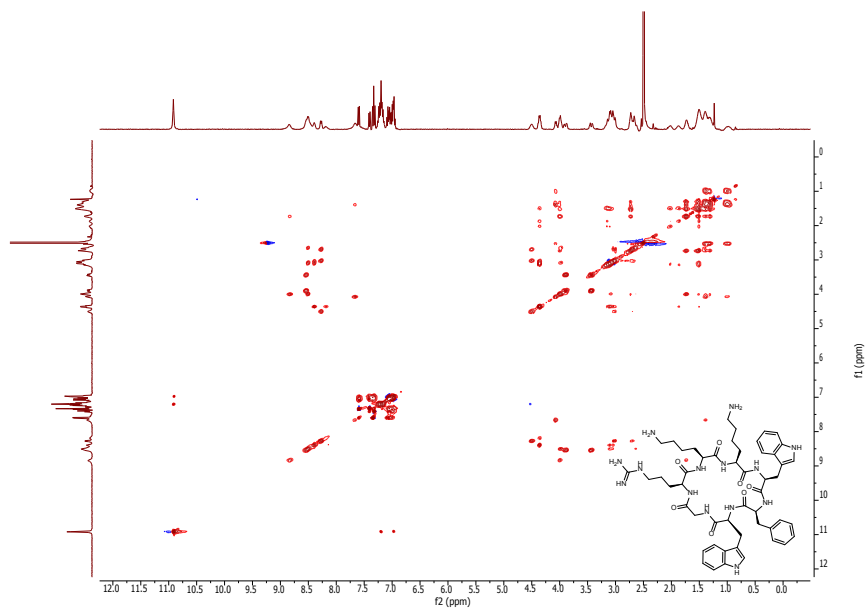
Supplementary Figure 24. NMR characterisation of cyclo(Arg-Lys-Lys-Trp(C₂-BODIPY)-Phe-Trp-Gly) (8).

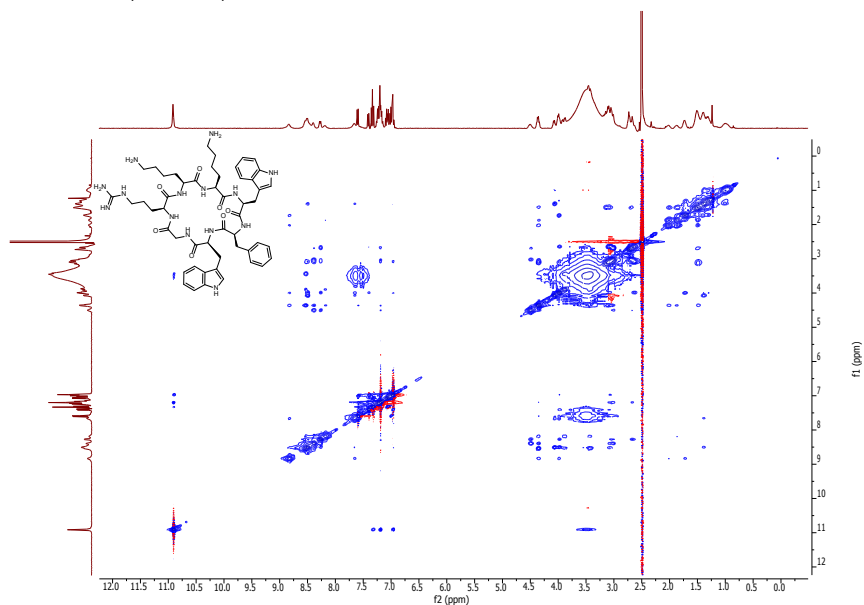
¹H-NMR (DMSO-d₆)



HSQC NMR (DMSO-d₆)



COSY NMR (DMSO-*d*₆)TOCSY NMR (DMSO-*d*₆)

NOESY NMR (DMSO-*d*6)**Supplementary Figure 25.** NMR characterisation of cyclo(Arg-Lys-Lys-Trp-Phe-Trp-Gly) (**9**).

Supplementary Discussion

Considerations about the influence of the aryl iodide substitution pattern.

Initially, we explored the interaction of Fmoc-Trp-OH with the *p*-iodophenyl-BODIPY **1**^[2] under similar conditions reported for this type of reactions^[3] [5 mol% Pd(OAc)₂, **1** (4.0 eq.), AgBF₄ (1.0 eq.) and *o*-nitrobenzoic acid (1.5 eq.) in DMF under microwave irradiation at 150 °C for 5 min]. Under these conditions, no reaction occurred. We then decided to test the *m*-iodophenyl-BODIPY **2** under the same reaction conditions and we observed the formation of the desired product (**3**). Next, we performed the reaction of Fmoc-Trp-OH with **2** applying an optimised arylation protocol^[4] [5 mol% Pd(OAc)₂, **2** (1.5 eq.), AgBF₄ (1.0 eq.) and TFA (1.5 eq.) in DMF under microwave irradiation at 80 °C for 20 min], which afforded the expected product **3** in 74% yield. The derivative **3** was recovered as a stable orange solid and properly characterised.

A plausible explanation lies in the nature of the arylation mechanism. Considering that the process is likely to involve a Pd(II)/Pd(IV) catalytic cycle, the C-H activation step may take place first to yield indole-Pd(II) species, where the oxidative addition to the Ar-I bond should occur, to be followed by the reductive elimination leading to the biaryl release and the regeneration of the catalyst.^[5,6] As the intermediate Pd(II) species are quite electrophilic, it is reasonable to think that electron-rich aryl halides will insert faster than deactivated derivatives. Therefore, BODIPY groups, which are considered electron-withdrawing, should exert a stronger deactivating effect in para position and a milder one in meta position, thus facilitating the insertion of Pd(II) species into the C-I bond in the latter case.^[7] Recent experimental results in similar reactions seem to support this hypothesis.^[8]

Supplementary Methods

General experimental information.

Unless stated otherwise, all reactions were carried out under argon in dried glassware. Commercially available reactants were used without further purification. Thin-layer chromatography was conducted on Merck silica gel 60 F254 sheets and visualized by UV (254 nm and 365 nm). Silica gel (particle size 35–70 μm) was used for flash column chromatography. HPLC analysis were performed on an Agilent 1100 separations module connected to a multiwavelength UV detection system using Discovery or Symmetry columns (C₁₈, 5 μm , 4.6 \times 150 mm), unless otherwise stated. NMR spectra were recorded on 400 or 500 MHz spectrometers. Chemical shifts (δ) are reported in ppm. Multiplicities are referred by the following abbreviations: s = singlet, d = doublet, t = triplet, dd = double doublet, dt = double triplet and m = multiplet. HRMS (ESI positive) were obtained with a LTQ-FT Ultra (Thermo Scientific) mass spectrometer. MALDI analysis was performed on a Bruker Ultraflex mass spectrometer. All microwave reactions were carried out in 10 mL sealed glass tubes in a focused mono-mode microwave oven ("Discover" by CEM Corporation) featured with a surface sensor for internal temperature determination. Cooling was provided by compressed air ventilating the microwave chamber during the reaction. When stated, the final crude was purified via flash column chromatography CombiFlash ISCO RF provided with dual UV detection.

Experimental procedures and characterisation data.**4,4-Difluoro-8-(4-iodophenyl)-1,3,5,7-tetramethyl-4-bora-3a,4a-diaza-s-indacene (1).**

4-iodobenzaldehyde (500 mg, 2.2 mmol) was dissolved in anhydride DCM (50 mL) under N₂. Then, 2,4-dimethylpyrrole (492 μ L, 4.8 mmol) and 2 drops of TFA were added and the reaction was stirred overnight at r.t in N₂ atmosphere or until the consumption of the aldehyde was complete (TLC). DDQ (490 mg, 2.2 mmol) dissolved in DCM (20 mL) was added dropwise (10-15 min) to the reaction mixture and the reaction was stirred for 15 min at r.t. Finally, TEA (4 mL, 45 mmol) and BF₃OEt₂ (4 mL, 30 mmol) were added and the mixture stirred for 3 h. Workup was done by diluting with DCM (50 mL) and washing with H₂O (4 x 100 mL). The organic layers were combined, dried over sodium sulphate, filtered and concentrated under vacuum. The crude was purified via flash column chromatography using and DCM/hexane gradient on silica gel. The expected compound was isolated as a red amorphous solid (290 mg, 29%).

Characterisation data: ¹H NMR (500 MHz, CDCl₃): δ 7.87 (d, J = 8.5 Hz, 2H), 7.08 (d, J = 8.5 Hz, 2H), 6.02 (s, 2H), 2.58 (s, 6H), 1.45 (s, 6H); ¹³C NMR (125 MHz, CDCl₃): δ 155.9, 142.9, 138.3, 134.6, 131.1, 130.0, 121.5, 94.7, 14.7, 14.6; HRMS (m/z): [M+H]⁺ calcd. for C₁₉H₁₈BF₂IN₂, 451.0654; found, 451.0651.

4,4-Difluoro-8-(3-iodophenyl)-1,3,5,7-tetramethyl-4-bora-3a,4a-diaza-s-indacene (2).

3-iodobenzaldehyde (500 mg, 2.2 mmol) was dissolved in anhydride DCM (50 mL) under N₂. Then, 2,4-dimethylpyrrole (492 μ L, 4.8 mmol) and three drops of TFA were added and the reaction was stirred overnight at r.t in N₂ atmosphere or until the consumption of the aldehyde was complete (TLC). DDQ (490 mg, 2.2 mmol) dissolved in DCM (20 mL) was added dropwise (10-15 min) to the reaction mixture and the reaction was stirred for 15 min at r.t. Finally, TEA (4 mL, 45 mmol) and BF₃OEt₂ (4 mL, 30 mmol) were added and the mixture stirred for 3 h. Workup was done by diluting with DCM (50 mL) and washing with H₂O (4 x 100 mL). The organic layers were combined, dried over sodium sulfate, filtered and concentrated under vacuum. The crude was purified via flash column chromatography using and DCM/hexane gradient on silica gel. The expected compound was isolated as a red amorphous solid (401 mg, 41%).

Characterisation data: ¹H NMR (400 MHz, CDCl₃): δ 7.76 (dt, J = 7.7, 1.5 Hz, 1H), 7.62 (t, J = 1.6 Hz, 1H), 7.24 – 7.20 (m, 1H), 7.19 – 7.14 (m, 1H), 5.92 (s, 2H), 2.48 (d, J = 1.3 Hz, 6H), 1.36 (s, 6H); ¹³C NMR (100 MHz, CDCl₃): δ 155.9, 142.9, 139.3, 138.0, 137.1, 136.8, 130.7, 127.3, 121.5, 94.3, 14.7, 14.6 (one quaternary carbon signal not seen); HRMS (m/z): [M+H]⁺ calcd. for C₁₉H₁₈BF₂IN₂, 451.0654; found, 451.0651.

Fmoc-Trp(C₂-BODIPY)-OH (3).

Fmoc-Trp-OH (100 mg, 0.234 mmol), **2** (1.5 eq., 158 mg, 0.352 mmol), AgBF₄ (1.0 eq., 46 mg, 0.234 mmol), TFA (1.0 eq., 18 μ L, 0.234 mmol) and Pd(OAc)₂ (0.05 eq., 2.6 mg, 0.0117 mmol) were placed in a microwave reactor vessel in 1.8 mL DMF. The mixture was heated under microwave irradiation (250 W) at 80°C for 20 min. EtOAc was added and the resulting suspension was filtered through Celite and concentrated under vacuum. The resulting crude was purified by flash column chromatography using and EtOAc/hexane gradient on silica gel. The expected adduct was isolated as a red solid (130 mg, 74%).

Characterisation data: ¹H NMR (400 MHz, CDCl₃): δ 8.12 (s, 1H), 7.69 – 7.56 (m, 4H), 7.48 (t, J = 7.7 Hz, 1H), 7.41 (t, J = 1.7 Hz, 1H), 7.37 (d, J = 4.9 Hz, 2H), 7.30 (t, J = 8.0 Hz, 3H), 7.25 – 7.21 (m, 1H), 7.20 – 7.13 (m, 3H), 7.07 (ddd, J = 8.0, 7.0, 1.1 Hz, 1H), 5.90 (s, 1H), 5.87 (s, 1H), 5.09 (d, J = 8.0 Hz, 1H), 4.55 (d, J = 7.5 Hz, 1H), 4.17 (q, J = 10.3, 9.4 Hz, 2H), 4.01 (s, 1H), 3.44 – 3.37 (m, 1H), 3.37 – 3.28 (m, 1H), 2.47 (s, 3H), 2.46 (s, 3H), 1.38 (s, 3H), 1.35 (s, 3H); ¹³C NMR (100 MHz, CDCl₃): δ 174.8, 163.1, 156.0, 155.9, 143.9, 143.2, 141.4, 140.7, 136.1, 136.0, 135.1, 133.9, 131.5, 130.1, 129.1, 128.8, 127.9, 127.8, 127.2, 125.2, 123.2, 121.6, 120.5, 120.1, 119.3, 111.2, 108.2, 67.2, 47.2, 36.9, 28.0, 14.8, 14.7; HRMS (m/z): [M+Na]⁺ calcd. for C₄₅H₃₉BF₂N₄O₄, 771.2930; found, 771.2925.

General procedures for SPPS. All peptides were manually synthesized in polystyrene syringes fitted with a polyethylene porous disc using Fmoc-based SPPS. Solvents and soluble reagents were removed by suction. The Fmoc group was removed with piperidine-DMF (1:4) (1 \times 1 min, 2 \times 5 min). Peptide synthesis transformations and washings were performed at r.t.

Resin loading (only for 2-chlorotriyl polystyrene resin). Fmoc-AA-OH (1 eq.) was attached to the resin (1 eq.) with DIPEA (3 eq.) in DCM at r.t for 10 min and then DIPEA (7.0 eq.) for 40 min. The remaining trityl groups were capped adding 0.8 μ L MeOH/mg resin for 10 minutes. After that, the resin was filtered and washed with DCM (4 \times 1 min), DMF (4 \times 1 min). The loading of the resin was determined by titration of the Fmoc group. Peptide elongation. After the Fmoc group was removed, the resin was washed with DMF (4 \times 1 min), DCM (3 \times 1 min), DMF (4 \times 1 min). Unless otherwise noted, standard coupling procedures used DIC (3 eq.) and OxymaPure (3 eq.) in DMF for 1 h and 5-min of pre-activation. The completion of the coupling was monitored by the Kaiser test.^[9] Then, the resin was filtered and washed with DCM (4 \times 1 min) and DMF (4 \times 1 min). Final cleavage (for Sieber amide and for 2-chlorotriyl polystyrene resins). The resin bound peptide was treated for 5 times with 1% TFA in DCM (1 min in each treatment) and washed with DCM. The combined filtered mixtures were poured over DCM and evaporated under vacuum. Then, the residue was dissolved in ACN:H₂O and liophilised.

General procedures for linear peptides 4-7. Syntheses were performed on Sieber amide resin (0.69 mmol/g). Amino acid **3** (1.5 eq.) was incorporated with a 5-min pre-activation using DIC (1.5 eq.) and OxymaPure (1.5 eq.) in DMF for 1h. For Fmoc-Arg-OH (3 eq.), we performed several treatments (up to 9) with DIC (3 eq.) and HOBt (3 eq.) in DMF for 15 min without pre-activation. The rest of amino acids (Fmoc-AA-OH, 3 eq.) were incorporated with a 5-min pre-activation with DIC (3 eq.) and OxymaPure (3 eq.) in DMF for 1 h. Peptides were purified by semi-preparative RP-HPLC (XBRIDGE™ BEH 130,

C₁₈, 5 μ M OBD 19 \times 50 mm column). Mobile phase: ACN (0.1% HCOOH)/H₂O (0.1% HCOOH); flow rate: 20 mL/min. Pure fractions were lyophilised furnishing the corresponding peptides.

H-Arg-Lys-Lys-Trp-Phe-Trp-NH₂ (4). Synthesised as previously reported.^[10]

White powder (5.0 mg).

Characterisation data: HPLC: t_R : 3.37 min (95% purity); HRMS (m/z): [M+H]⁺ calcd. for C₄₉H₆₇N₁₃O₇, 950.5365; found, 950.5364.

H-Arg-Lys-Lys-Trp(C₂-BODIPY)-Phe-Trp-NH₂ (5).

Red powder (3.6 mg).

Characterisation data: HPLC: t_R : 3.28 min (90% purity); HRMS (m/z): [M+H]⁺ calcd. for C₆₈H₈₅BF₂N₁₆O₆, 1271.6977; found, 1271.6947.

H-Ala-Ala-Ala-Trp(C₂-BODIPY)-Phe-Trp-NH₂ (5a).

Red powder (20 mg).

Characterisation data: HPLC: t_R : 6.60 min (96% purity). HRMS (m/z): [M+H]⁺ calcd. for C₅₉H₆₄BF₂N₁₁O₆: 1072.5175; found, 1072.5183.

H-Arg-Lys-Lys-Trp(C₂-BODIPY)-Ala-Ala-NH₂ (5b).

Red powder (7 mg).

Characterisation data: HPLC: t_R : 4.77 min (99% purity). HRMS (m/z): [M+H]⁺ calcd. for C₅₄H₇₆BF₂N₁₅O₆: 1080.6237; found, 1080.6250.

H-Arg-Lys-Lys-Trp-Phe-Trp(C₂-BODIPY)-NH₂ (6).

Red powder (1.8 mg).

Characterisation data: HPLC: t_R : 3.95 min (90% purity); HRMS (m/z): [M+H]⁺ calcd. for C₆₈H₈₅BF₂N₁₆O₆, 1271.6977; found: 1271.6937.

H-Arg-Lys-Lys-Trp(C₂-BODIPY)-Phe-Trp(C₂-BODIPY)-NH₂ (7).

Red powder (16.8 mg).

Characterisation data: HPLC: t_R : 6.24 min (91% purity); HRMS (m/z): [M+H]⁺ calcd. for C₈₇H₁₀₃B₂F₄N₁₈O₆, 1593.8449; found, 1593.8532.

Cyclo(Arg-Lys-Lys-Trp(C₂-BODIPY)-Phe-Trp-Gly) (8). The synthesis was performed on 91 mg of 2-chlorotriyl polystyrene resin (0.94 mmol/g). Amino acid **3** (1.5 eq.) was incorporated with PyBOP (1.5 eq.), HOBT (1.5 eq.) and DIPEA (2.0 eq.) in DMF for 1 h. Other Fmoc amino acids (3 eq.) were incorporated with a 5 min pre-activation with DIC (3 eq.) and OxymaPure (3 eq.) in DMF for 1 h. After cleavage as described above, the protected linear peptide (119 mg, 0.073 mmol) was dissolved in 1.3 mL of DMF (0.055 M). DIPEA (2.5 eq., 32 μ L, 0.182 mmol) and HATU (1.0 eq., 28 mg, 0.073 mmol) were added. The solution was stirred at r.t. until the cyclisation was complete (approx. 2 h). The cyclic peptide was precipitated by adding H₂O to the solution. The precipitate was washed with H₂O, decanted and dried, obtaining 109 mg of crude protected cyclic peptide (87% yield). The crude protected macrocycle (108 mg, 0.067 mmol) and 20% Pd(OH)₂-C (54 mg) were dissolved in 5% HCOOH/MeOH (10.8 mL), previously purged with Ar. Then, the reaction flask was flushed again with Ar, evacuated and filled with H₂. The reaction mixture was stirred under H₂ for 72 h (H₂ balloons were refilled periodically during the reaction along with re-addition of Pd(OH)₂-C (4 times). The catalyst was removed by filtration

and the filtrate was evaporated to afford 46 mg of the crude deprotected peptide. The final peptide was purified by PoraPak Rxn RP 60 cc reverse phase column. Mobile phase: ACN (0.1% HCOOH)/H₂O (0.1% HCOOH). Pure fractions were lyophilised furnishing the corresponding peptide.

Red powder (30 mg).

Characterisation data: ¹H NMR (600 MHz, CD₃OD): δ 8.55 (s, 3H), 7.89 – 7.84 (m, 1H), 7.71 (t, *J* = 7.7 Hz, 1H), 7.65 (d, *J* = 7.8 Hz, 1H), 7.60 – 7.55 (m, 2H), 7.42 (dt, *J* = 8.1, 0.9 Hz, 1H), 7.40 – 7.36 (m, 2H), 7.18 – 7.12 (m, 5H), 7.11 (s, 1H), 7.06 (m, 3H), 6.94 (m, 1H), 6.10 (s, 1H), 6.06 (s, 1H), 4.45 (t, *J* = 7.4 Hz, 1H), 4.32 (d, *J* = 10.5 Hz, 1H), 4.25 (m, 1H), 4.17 – 4.07 (m, 2H), 4.04 (d, *J* = 16.5 Hz, 1H), 4.00 (m, 1H), 3.63 (dd, *J* = 14.9, 9.5 Hz, 1H), 3.51 – 3.45 (m, 1H), 3.38 (m, 1H), 3.30 (1H), 3.27 – 3.23 (m, 2H), 3.15 (dd, *J* = 14.2, 7.5 Hz, 1H), 3.10 (dd, *J* = 14.0, 5.9 Hz, 1H), 2.90 (td, *J* = 8.6, 4.2 Hz, 2H), 2.72 (t, *J* = 7.7 Hz, 2H), 2.63 (dd, *J* = 14.2, 8.5 Hz, 1H), 2.51 (s, 3H), 2.50 (s, 3H), 2.09 – 1.88 (m, 4H), 1.76 (m, 1H), 1.67 (m, 3H), 1.52 (m, 7H), 1.48 – 1.41 (m, 4H), 1.37 (m, 2H), 1.26 – 1.14 (m, 2H); HPLC: *t*_R 4.45 min (98% purity); HRMS (*m/z*): [*M*+*H*]⁺ calcd. for C₇₀H₈₆BF₂N₁₆O₇, 1311.6926; found, 1311.6864.

Cyclo(Arg-Lys-Lys-Trp-Phe-Trp-Gly) (9). The synthesis was performed on 500 mg of 2-chlorotrityl polystyrene resin (1.0 mmol/g). Fmoc amino acids (3 eq.) were incorporated with a 5-min pre-activation with DIC (3 eq.) and OxymaPure (3 eq.) in DMF for 1 h. After cleavage as described above, the fully protected linear peptide (300 mg, 0.18 mmol) was dissolved in 3.5 mL of DMF (0.052 M). DIPEA (2.5 eq., 79 μ L, 0.18 mmol) and HATU (1.0 eq., 69 mg, 0.18 mmol) were added. The solution was stirred at r.t until the cyclisation was complete (2 h). The cyclic peptide was precipitated by adding H₂O to the solution and the precipitate was washed with H₂O, decanted and dried. The protected linear peptide was dissolved in TFA:TIS:H₂O (95:2.5:2.5) and the solution was stirred at r.t. for 2 h. The resulting solution was evaporated under vacuum, washed with Et₂O, dissolved in ACN:H₂O and lyophilised to afford 231 mg of the crude peptide (72% yield). 145 mg of peptide were purified by PoraPak Rxn RP 60 cc reverse phase column. Mobile phase: ACN (0.1% HCOOH)/H₂O (0.1% HCOOH). Pure fractions were lyophilised furnishing the corresponding pure cyclic peptide.

White powder (51 mg).

Characterisation data: ¹H NMR (600 MHz, DMSO-*d*₆): δ 10.92 (s, 2H), 8.92 – 8.78 (m, 1H), 8.59 – 8.45 (m, 3H), 8.44 – 8.35 (m, 1H), 8.27 (d, *J* = 8.4 Hz, 1H), 8.23 – 8.13 (m, 1H), 7.73 – 7.63 (m, 1H), 7.60 (d, *J* = 7.9 Hz, 1H), 7.41 (d, *J* = 7.9 Hz, 1H), 7.38 – 7.29 (m, 1H), 7.26 – 7.13 (m, 7H), 7.11 – 7.04 (m, 2H), 7.02 (dd, *J* = 3.9, 1.1 Hz, 1H), 7.01 – 6.94 (m, 3H), 4.56 – 4.44 (m, 1H), 4.36 (q, *J* = 6.9 Hz, 2H), 4.14 – 4.04 (m, 1H), 4.00 (q, *J* = 6.7 Hz, 2H), 3.90 (dd, *J* = 16.9, 6.0 Hz, 1H), 3.50 – 3.38 (m, 1H), 3.21 – 2.97 (m, 7H), 2.80 – 2.62 (m, 4H), 2.10 – 1.97 (m, 1H), 1.95 – 1.81 (m, 1H), 1.81 – 1.67 (m, 2H), 1.58 – 1.27 (m, 12H), 1.06 – 0.91 (m, 1H); HPLC: *t*_R 1.55 min (98% purity); HRMS (*m/z*): [*M*]⁺ calcd. for C₅₁H₆₈N₁₄O₇, 988.5395; found, 988.5387.

Supplementary References

- [1] Seybold, P. G., Gouterman, M. & Callis, J. Calorimetric, photometric and lifetime determinations of fluorescence yields of fluorescein dyes. *Photochem. Photobiol.* **9**, 229-242 (1969).
- [2] Tahtaoui, C. et al. Convenient Method To Access New 4,4-Dialkoxy- and 4,4-Diaryloxy-diaza-s-indacene Dyes: Synthesis and Spectroscopic Evaluation. *J. Org. Chem.* **72**, 269-272 (2007).
- [3] Ruiz-Rodriguez, J., Albericio, F. & Lavilla, R. Postsynthetic Modification of Peptides: Chemoselective C-Arylation of Tryptophan Residues. *Chem. Eur. J.* **16**, 1124-1127 (2010).
- [4] Preciado, S., Mendive-Tapia, L., Albericio F. & Lavilla, R. Synthesis of C-2 Arylated Tryptophan Amino Acids and Related Compounds through Palladium-Catalyzed C-H Activation. *J. Org. Chem.* **78**, 8129-8135 (2013).
- [5] Ackermann, L. Carboxylate-Assisted Transition-Metal-Catalyzed C-H Bond Functionalizations: Mechanism and Scope. *Chem. Rev.* **111**, 1315-1345 (2011).
- [6] Chiong, H. A., Pham Q. & Daugulis, O. Two Methods for Direct ortho-Arylation of Benzoic Acids. *J. Am. Chem. Soc.* **129**, 9879-9884 (2007).
- [7] Yu, J. Q. & Shi, Z. C-H Activation. *Topics in Current Chemistry*, Springer, Berlin Heidelberg (2010).
- [8] Feng, J., Lu, G., Lv, M. & Cai, C. Palladium catalyzed direct C-2 arylation of indoles. *J. Organomet. Chem.* **761**, 28-31 (2014).
- [9] Kaiser, E., Colescott, R. L., Bossinger C. D. & Cook, P. I. Color test for detection of free terminal amino groups in the solid-phase synthesis of peptides. *Anal. Biochem.* **34**, 595-598 (1970).
- [10] Lopez-Garcia, B., Perez-Paya, E. & Marcos, J. F. Identification of novel hexapeptides bioactive against phytopathogenic fungi through screening of a synthetic peptide combinatorial library. *Appl. Environ. Microbiol.* **68**, 2453-2460 (2002).



FULL SUPPORTING INFORMATION PUBLICATION V

Electronic Supplementary Material (ESI) for ChemComm.
This journal is © The Royal Society of Chemistry 2016

Electronic Supplementary Information

A Trp-BODIPY cyclic peptide for fluorescence labelling of apoptotic bodies

Ramon Subiros-Funosas, Lorena Mendive-Tapia, Jesus Sot, John D. Pound,
Nicole Barth, Yaiza Varela, Felix M. Goñi, Margaret Paterson, Christopher D.
Gregory, Fernando Albericio, Ian Dransfield, Rodolfo Lavilla, Marc Vendrell

Table of Contents

Materials and Methods. *Page S2.*

Experimental Section. *Page S4.*

NMR spectra. *Page S11.*

Supplementary Figures. *Page S21.*

References. *Page S27.*

Materials and Methods

Fmoc-amino acids were obtained from Iris Biotech GmbH (Fmoc-Gly-OH, Fmoc-Ile-OH, Fmoc-Phe-OH), Chem-Impex International [Fmoc-Asp-OAllyl, Fmoc-Gln-OH, Fmoc-His(Mmt)-OH] and Sigma-Aldrich [Fmoc-Arg(NO₂)-OH]. Resins and HBTU were obtained from Iris Biotech GmbH. HOBt was purchased from Carbosynth. Pd-based catalysts and bases were obtained from Sigma-Aldrich. All reagents were used without further purification unless otherwise stated. All microwave reactions were carried out in 10 mL sealed glass tubes in a focused mono-mode microwave oven ("Discover" by CEM Corporation) featured with a surface sensor for internal temperature determination. Cooling was provided by compressed air ventilating the microwave chamber during the reaction. Spectroscopic data and quantum yield data were measured on a Synergy HT spectrophotometer (Biotek), and the data analysis was performed using GraphPad Prism 5.0.

Reactions were monitored by HPLC-MS at 220 nm using a HPLC Waters Alliance HT comprising a pump (Edwards RV12) with degasser, an autosampler, a YMC-Pack ODS-AQ, 50 × 4.6 mm, S-3 μm column and a diode array detector. Eluents: H₂O (0.1% FA) and ACN (0.1% FA). Flow: 1.6 mL min⁻¹. The MS detector was configured with an electrospray ionization source (Micromass ZQ4000) and nitrogen was used as the nebulizer gas. Data acquisition was performed with MassLynx software. HRMS (ESI positive) were obtained in a LTQ-FT Ultra (Thermo Scientific) mass spectrometer. NMR spectra were recorded on Bruker Avance-III 600 MHz spectrometer in DMSO-*d*₆ at 308 K. Chemical shifts (δ) are reported in ppm. Multiplicities are referred by the following abbreviations: s = singlet, d = doublet, t = triplet, dd = double

doublet, ddd = double double doublet, dt = double triplet, q= quartet and m = multiplet.

General procedures for SPPS

All peptides were manually synthesized in polystyrene syringes fitted with a polyethylene porous disc using Fmoc-based SPPS. Solvents and soluble reagents were removed by suction. The Fmoc group was removed with piperidine: DMF (1: 4) (1 × 1 min, 2 × 5 min). Peptide synthesis transformations and washings were performed at r.t.

Resin loading. Fmoc-Asp-OAllyl (1 eq.) was attached to the resin (1 eq.) with DIPEA (3 eq.) in DCM at r.t. for 10 min and then DIPEA (7 eq.) for 40 min. The remaining trityl groups were capped adding 0.8 μL MeOH mg^{-1} resin for 10 min. The resin was filtered and washed with DCM (4 × 1 min), DMF (4 × 1 min). The loading of the resin was determined by titration of the Fmoc group.

Peptide elongation. After the Fmoc group was removed with piperidine: DMF (1: 4) (1 × 1 min, 2 × 5 min), the resin was washed with DMF (4 × 1 min), DCM (3 × 1 min), DMF (4 × 1 min). Unless otherwise noted, standard coupling procedure with DIC (3 eq.) and OxymaPure (3 eq.) in DMF for 1 h and 5 min of pre-activation was carried out. The completion of the coupling was monitored with the Kaiser test. Then, the resin was filtered and washed with DCM (4 × 1 min) and DMF (4 × 1 min) and was ready for the elongation with the next Fmoc amino acid.

Final cleavage. The resin bound peptide was treated 5 times with TFA: DCM (1: 99) for 1 min in each treatment and washed with DCM. The combined filtered mixtures were poured over DCM and evaporated under vacuum. The residue was precipitated in Et₂O, dissolved in ACN: H₂O and lyophilised.

Experimental Section

Chemical synthesis.

cLac-1. Starting from 750 mg of 2-chlorotrityl PS resin (0.3 mmol g⁻¹). Amino acid coupling. Fmoc-AA-OH (3 eq.) were incorporated with a 5 min pre-activation with DIC (3 eq.) and OxymaPure (3 eq.) in DMF for 1 h. Fmoc-AA-OH: Fmoc-Asp-OAllyl, Fmoc-Gly-OH, Fmoc-Arg(NO₂)-OH, Fmoc-Gln-OH, Fmoc-Ile-OH, Fmoc-His(Mmt)-OH, Fmoc-Phe-OH, Fmoc-Trp(Boc)-OH. Peptide cyclisation. The C-terminal allyl ester group of the aspartic acid was removed after addition of the last amino acid with Pd(PPh₃)₄ (26 mg, 0.023 mmol, 0.1 eq.) and N-methylmorpholine (244 µL, 2.25 mmol, 10 eq.) in THF for 1 h at r.t. (3 × 15 min). The head-to-tail cyclization was performed by removal of the *N*-terminal Fmoc group before addition of PyAOP (352 mg, 0.674 mmol, 3 eq.), HOAt (92 mg, 0.674 mmol, 3 eq.) and DIPEA (235 µL, 1.35 mmol, 6 eq.) in DMF at r.t for 1 h. Peptide cleavage. The resin bound peptide was treated repeated times with the TFA cocktail obtaining 210 mg of cyclic peptide crude (87% purity by HPLC-MS). Removal of nitro group. The crude protected peptide (210 mg, 0.153 mmol) and 20% Pd(OH)₂-C (105 mg) were dissolved in HCO₂H: DMF: H₂O (5: 47.5: 47.5) (10 mL) and the reaction flask was flushed with Ar, evacuated and filled with H₂. The reaction mixture was stirred under balloon pressure of H₂ for 48 h (H₂ was refilled periodically during the reaction along with re-addition of Pd(OH)₂-C (2 X). The catalyst was removed through filtration with Celite and the filtrate was evaporated *in vacuo* to afford 164 mg of the crude peptide (83% purity by HPLC-MS, 75% yield). Peptide purification. A highly pure fraction of the totally deprotected cyclic peptide was obtained by semi-preparative RP-HPLC (XBRIDGE™, C₁₈, 5 µm OBD 19 × 150 mm

column). The pure fractions were lyophilised rendering the pure peptide as a white solid (>99% purity by HPLC-MS).

¹H NMR (600 MHz, DMSO-*d*₆): δ 10.70 (s, 1H), 8.61 (m, 1H), 8.46 – 8.31 (m, 3H), 8.23 (s, 1H), 8.18 (s, 1H), 8.15 (s, 1H), 8.06 (s, 1H), 7.99 (s, 1H), 7.88 (s, 1H), 7.71 – 7.59 (m, 1H), 7.57 – 7.51 (m, 1H), 7.41 (d, *J* = 8.0 Hz, 1H), 7.31 – 7.27 (m, 3H), 7.25 – 7.20 (m, 4H), 7.07 (s, 1H), 7.03 (ddd, *J* = 8.1, 7.0, 1.2 Hz, 1H), 6.96 (ddd, *J* = 7.9, 6.9, 1.1 Hz, 1H), 6.83 (s, 1H), 6.74 (s, 1H), 4.57 (q, *J* = 7.1 Hz, 1H), 4.42 (q, *J* = 6.3 Hz, 2H), 4.33 (s, 1H), 4.27 (td, *J* = 8.3, 5.0 Hz, 1H), 4.18 (q, *J* = 7.8, 7.1 Hz, 1H), 4.10 (t, *J* = 7.4 Hz, 1H), 3.91 (dd, *J* = 16.9, 6.1 Hz, 1H), 3.79 – 3.68 (m, 9H), 3.65 – 3.61 (m, 1H), 3.55 – 3.50 (m, 1H), 3.11 – 3.03 (m, 2H), 2.99 (dd, *J* = 14.7, 4.6 Hz, 2H), 2.96 – 2.87 (m, 3H), 2.81 (dd, *J* = 15.0, 9.2 Hz, 1H), 2.76 – 2.65 (m, 1H), 2.46 (1H), 2.15 – 2.00 (m, 2H), 1.99 – 1.88 (m, 1H), 1.83 – 1.70 (m, 3H), 1.65 – 1.55 (m, 1H), 1.54 – 1.42 (m, 2H), 1.40 – 1.27 (m, 1H), 1.07 – 0.94 (m, 1H), 0.80 – 0.75 (m, 6H) ppm. **HRMS** (ESI) (*m/z*): [M+H]⁺ calcd. for C₅₉H₈₀O₁₆N₂₀, 1324.6056; found, 1324.6046.

cLac-BODIPY. Starting from 750 mg of 2-chlorotriptyl PS resin (0.3 mmol g⁻¹).

Amino acid coupling. Fmoc-Trp(BODIPY)-OH^[1] (1.5 eq.) was incorporated with HBTU (1.2 eq.), HOBT (1.2 eq.) and DIEA (2.4 eq.) in DMF for 1 h. The other amino acids Fmoc-AA-OH (3 eq.) were incorporated with a 5 min pre-activation with DIC (3 eq.) and OxymaPure (3 eq.) in DMF for 1 h. Fmoc-AA-OH: Fmoc-Asp-Oallyl, Fmoc-Gly-OH, Fmoc-Arg(NO₂)-OH, Fmoc-Gln-OH, Fmoc-Ile-OH, Fmoc-His(Mmt)-OH, Fmoc-Phe-OH. Peptide cyclisation. The C-terminal allyl ester group of the aspartic acid was removed after addition of the last amino acid with Pd(PPh₃)₄ (26 mg, 0.023 mmol, 0.1 eq.) and N-methylmorpholine (244 μL, 2.25 mmol, 10 eq.) in THF for 1 h at r.t (3 x 15 min). The head-to-tail

cyclization was performed by removal of the *N*-terminal Fmoc group before addition of DIC (96 μ L, 0.548 mmol, 3 eq.) and HOBt (75 mg, 0.548 mmol, 3 eq.) in DMF at r.t. for 5 h. Peptide cleavage. The resin bound peptide was treated repeated times with the TFA cocktail obtaining 69 mg of cyclic peptide crude (60% purity by HPLC-MS). Removal of nitro group. The crude protected peptide (69 mg, 0.041 mmol) and 20% Pd(OH)₂-C (34 mg) were dissolved in HCO₂H: DMF: H₂O (5: 47.5: 47.5) (10 mL) and the reaction flask was flushed with Ar, evacuated and filled with H₂. The reaction mixture was stirred under balloon pressure of H₂ for 32 h (H₂ was refilled periodically during the reaction along with re-addition of Pd(OH)₂-C (2 X). The catalyst was removed through filtration with Celite and the filtrate was evaporated *in vacuo* to afford 64 mg of the crude peptide (70% purity by HPLC-MS, 69% yield). Peptide purification. A highly pure fraction of the totally deprotected cyclic peptide was obtained by semi-preparative RP-HPLC (XBRIDGE™, C₁₈, 5 μ M OBD 19 \times 150 mm column). The pure fractions were lyophilised rendering the corresponding peptide as a red solid (>99% purity by HPLC-MS).

¹H NMR (600 MHz, DMSO-*d*₆): δ 11.27 (s, 1H), 8.37 – 7.99 (m, 7H), 7.90 – 7.83 (m, 1H), 7.66 – 7.59 (m, 2H), 7.43 – 7.36 (m, 1H), 7.34 (dd, *J* = 7.6, 1.5 Hz, 1H), 7.32 – 7.26 (m, 2H), 7.26 – 7.18 (m, 3H), 7.15 (t, *J* = 7.2 Hz, 3H), 7.07 (t, *J* = 7.4 Hz, 1H), 6.92 (t, *J* = 8.3 Hz, 1H), 6.79 (s, 1H), 6.19 (d, *J* = 4.5 Hz, 2H), 4.63 – 4.44 (m, 2H), 4.40 – 4.29 (m, 1H), 4.28 – 4.18 (m, 3H), 4.17 – 4.05 (m, 1H), 3.87 – 3.51 (m, 14H), 3.18 – 3.11 (m, 2H), 3.09 – 3.04 (m, 2H), 2.96 – 2.89 (m, 1H), 2.56 (m, 1H), 2.47 – 2.45 (m, 6H), 2.18 – 2.06 (m, 2H), 1.95 (s, 1H), 1.86 – 1.65 (m, 3H), 1.60 – 1.47 (m, 3H), 1.43 (d, *J* = 9.4 Hz, 6H), 1.40 – 1.31 (m, 1H), 1.29 – 1.24 (m, 2H), 1.04 (m, 1H), 0.81 – 0.73 (m, 6H) ppm. **HRMS** (ESI) (*m/z*): [*M*+H]⁺ calcd. for C₇₈H₉₇O₁₆ N₂₂BF₂, 1646.7509; found, 1646.7509.

Spectral characterisation.

PS and PC stock solutions were prepared by solubilisation in EtOH at a concentration of 1 mg mL⁻¹. 96-well plates were filled with 100 µL of different PS/PC solutions to form films after evaporation of EtOH at r.t. overnight. PS/PC-coated plates were incubated with **cLac-BODIPY** (5 µM) for 1 h at 37 °C in the dark. Quantum yields were determined by measuring the integrated emission area of the fluorescence spectra and comparing it to the area measured for fluorescein in 0.1 M NaOH when excited at 450 nm (QY: 0.92).^[2] Quantum yields were calculated using the equation:

$$\Phi_{sample} = \Phi_{reference} \left(\frac{F_{sample}}{F_{reference}} \right) \left(\frac{Abs^{reference}}{Abs^{sample}} \right) \left(\frac{\eta^{sample}}{\eta^{reference}} \right)^2$$

where F represents the area of fluorescent emission, η is the refractive index of the solvent, and Abs is absorbance at the excitation wavelength selected (i.e. 450 nm). Emission was integrated between 480 and 600 nm.

Surface pressure measurements.

DOPS, eggPG and Liss-Rho-DOPE were purchased from Avanti Polar Lipids (Alabaster, Alabama, U.S.A.). eggPC was purchased from Lipid Products (South Nutfield, UK). Surface pressure assays were performed with a DeltaPi-4 tensiometer (Kibron, Helsinki, Finland). Langmuir lipid monolayers at the air-water interface were used as a model membrane system to study lipid-peptide interaction. Surface pressure experiments were carried out with a DeltaPi-4 at 22°C with constant stirring. The aqueous phase consisted of 1.25 mL of 25 mM HEPES, 150 mM NaCl (pH 7.4). Lipids dissolved in chloroform: methanol (2: 1), eggPC, DOPS and eggPG were spread gently over the surface until the desired initial surface pressure was attained. The peptides were injected with a micropipette through a hole connected to the subphase. The increment in

surface pressure was recorded until a stable signal was obtained. Values of critical pressure (π_c) were determined by linear regression using the values over the saturation pressure (π_s).

Confocal microscopy.

Electroformation of Giant Unilamellar Vesicles. GUV formation took place with aid of a TG330 function generator (Thurlby Thandar Instruments, Huntingdon, UK). GUVs were prepared by electroformation on a pair of platinum (Pt) wires by a method first developed by Angelova and Dimitrov,^[3,4] modified as described previously.^[5] Lipid stock solutions were prepared in 2:1 (v/v) chloroform/methanol at 0.2 mg mL⁻¹. Labelling was carried out by pre-mixing the fluorescent probes with the lipids in organic solvent. We used Liss-Rho-DOPE as marker for lipid membranes. The average concentration of individual fluorescent probes in each sample was 0.2 mol%. 2.5 μ L lipid mixtures containing the fluorescent probes were deposited on Pt wires. The Pt wires were placed under vacuum for 2 h to completely remove the organic solvent. The sample was covered to avoid light exposure and allowed to precipitate onto the Pt wires for 5 min. One side of the chamber was then sealed with a coverslip. 500 μ L assay buffer, prepared with high-purity water (Millipore SuperQ) heated at 37°C was added to the chamber until it covered the Pt wires and connected to a TG330 function generator. AC field was applied in three steps, all of them performed at 37°C: 1), frequency 500 Hz, amplitude 220 mV (35 V/m) for 5 min; 2), frequency 500 Hz, amplitude 1900 mV (313 V/m) for 20 min; 3), frequency 500 Hz, amplitude 5.3 V (870 V/m) for 90 min. The temperatures used for GUV formation correspond to those at which the different membranes display a single fluid phase.

Confocal microscopy of GUVs. Nikon D-eclipse C1 confocal system (Nikon corporation, Tokyo, Japan) was used for GUV imaging, treating the images using the software EZ-C1 3.20 (Nikon Inc., Melville, N.Y.). The excitation wavelengths were 488 nm for **cLac-BODIPY** and 561 nm for Liss-Rho-DOPE. Fluorescence emission was retrieved at 500-530 for **cLac-BODIPY** and at 573-613 for Liss-Rho-PE. cLac-BODIPY was used at $3.3 \mu\text{g mL}^{-1}$ to study the labelling of the GUVs. All experiments were performed at 22 °C.

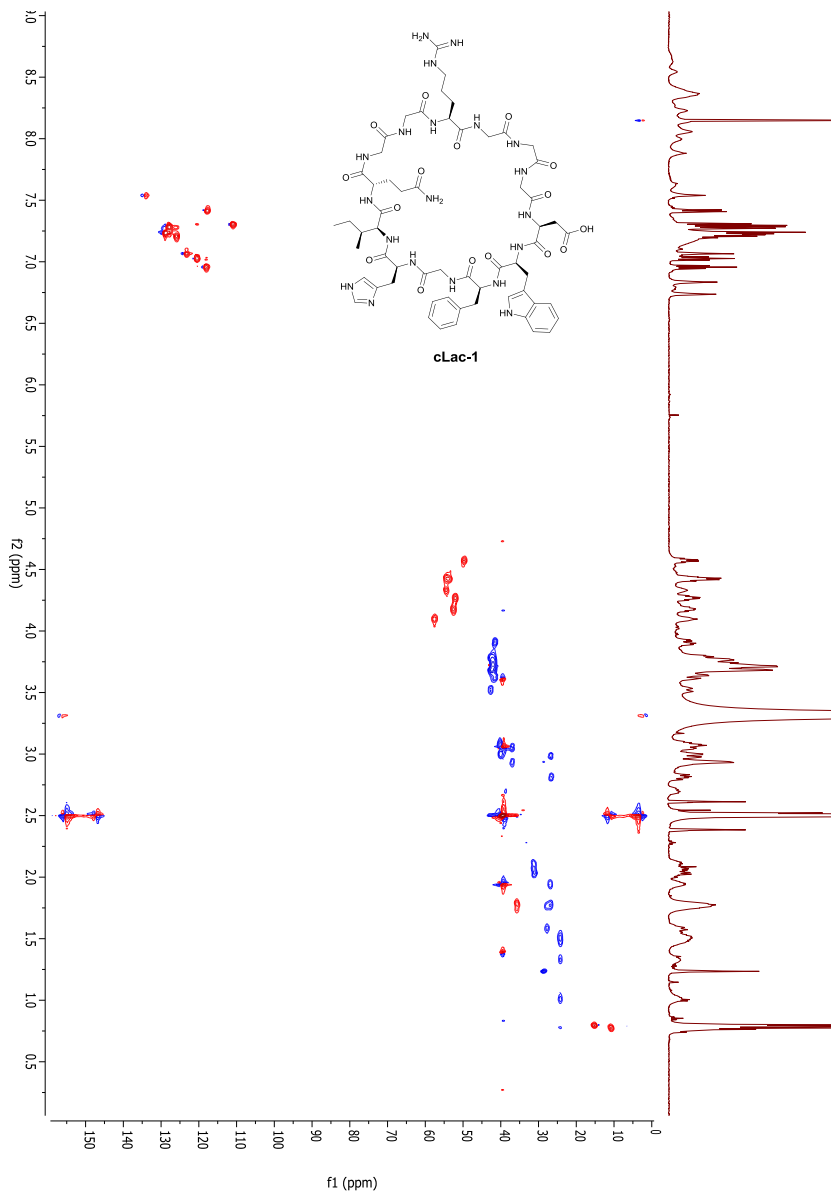
Confocal microscopy of cells. Human lung A549 epithelial cells (ATCC CCL-185) were grown using Dulbecco's Modified Eagle Medium (DMEM) supplemented with 10% fetal bovine serum (FBS), antibiotics (100 U mL^{-1} penicillin and 100 mg mL^{-1} streptomycin) and 2 mM L-glutamine in a humidified atmosphere at 37 °C with 5% CO₂. A549 cells were regularly passaged in T-75 cell culture flasks and plated on glass chamber slides Lab-Tek™ II (Nunc) the day before imaging. For imaging experiments, cells were treated with TNF- α (10 ng mL^{-1}) and flavopiridol (500 nM) for 6 h to induce apoptosis as previously reported,^[6] and incubated for 15 min with **cLac-BODIPY** ($1 \mu\text{M}$). Fluorescence and brightfield images were acquired under a Zeiss LSM 510 META confocal microscope equipped with a live cell imaging stage and a 63X oil objective, and analysed and processed with ImageJ.

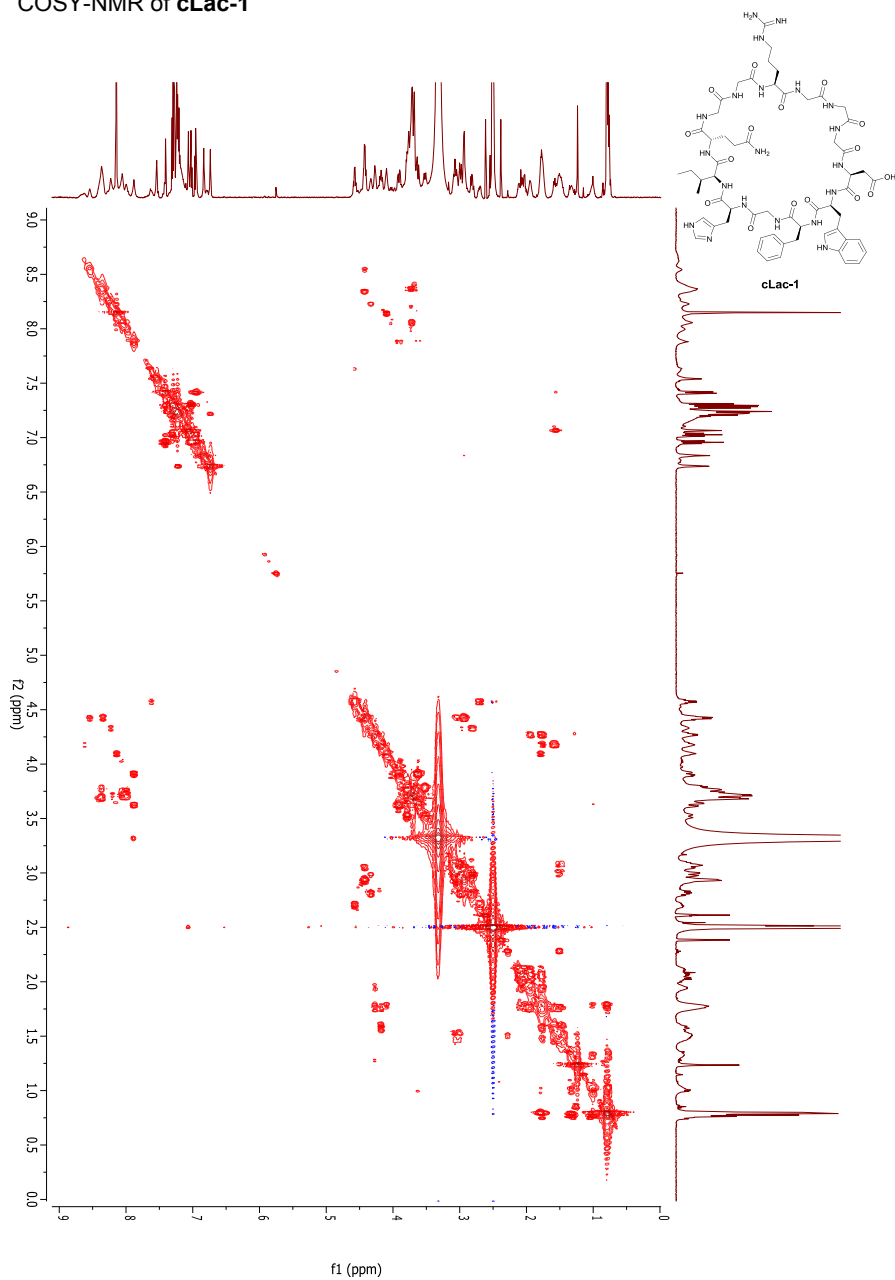
Flow cytometry.

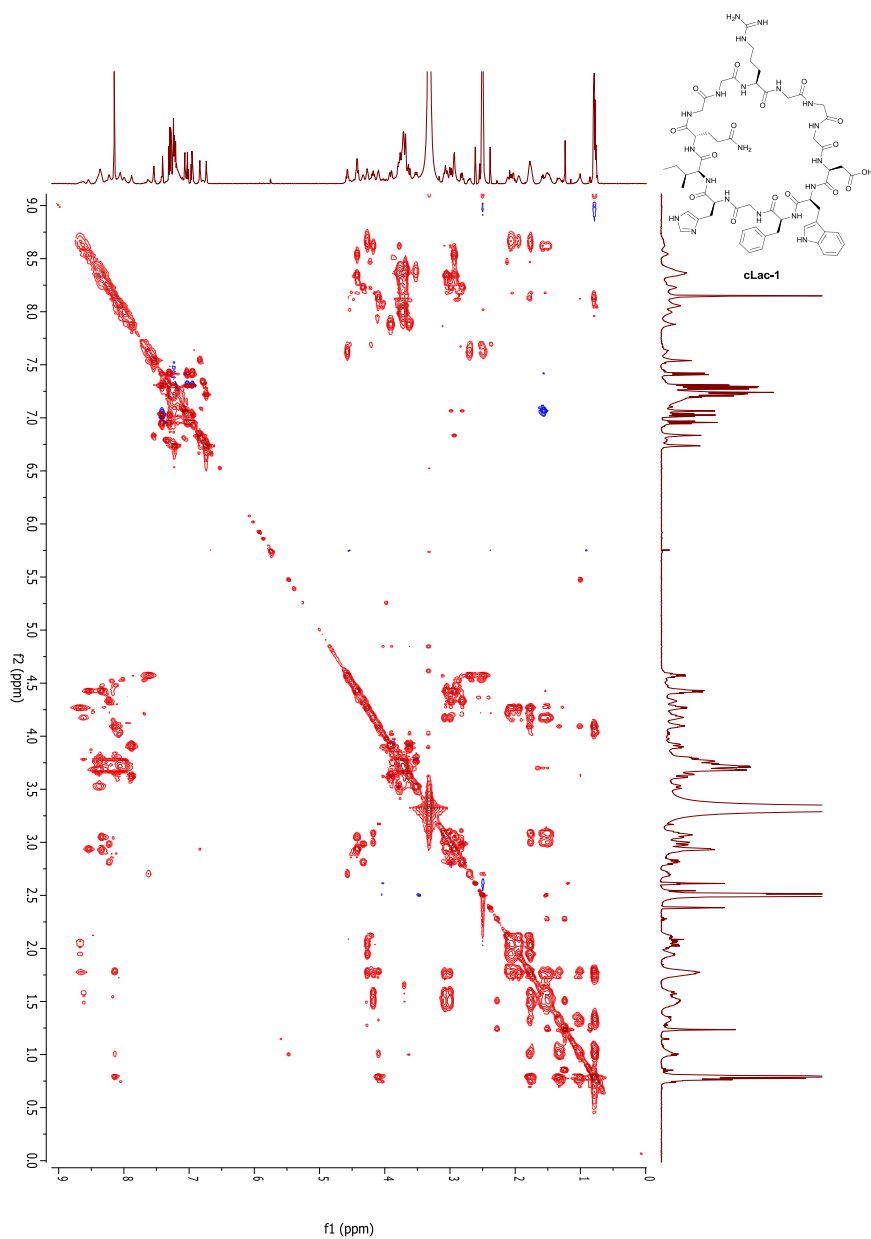
Subcellular material was obtained from supernatants of the human Burkitt lymphoma cell line BL2 undergoing UV-induced apoptosis. Exponentially growing cells were centrifuged and resuspended in culture medium passed through a $0.1 \mu\text{m}$ PVDF filter (Millipore) then exposed to a UV-B dose of 300 mJ per cm^2 . After reculture for 5 h, cells were centrifuged at 25 xg for 1 h at 4 °C,

and the supernatant was filtered through a 5 μm mesh filter (PluriSelect Life Sciences, Leipzig, Germany) to exclude residual cells. Binding of **cLac-BODIPY** and PE-labelled Annexin V (Invitrogen) was analysed by flow cytometry after excitation with a 488 nm laser using emission filters at 530 ± 30 nm and 574 ± 26 nm respectively, with appropriate electronic compensation for channel spillover. Data acquisition was carried out using a dual laser Attune acoustic focusing cytometer (Thermo Fisher Scientific Inc, Waltham, MA, USA) with post-acquisition data analysis using Flowjo software (Flowjo, Ashland, OR, USA).

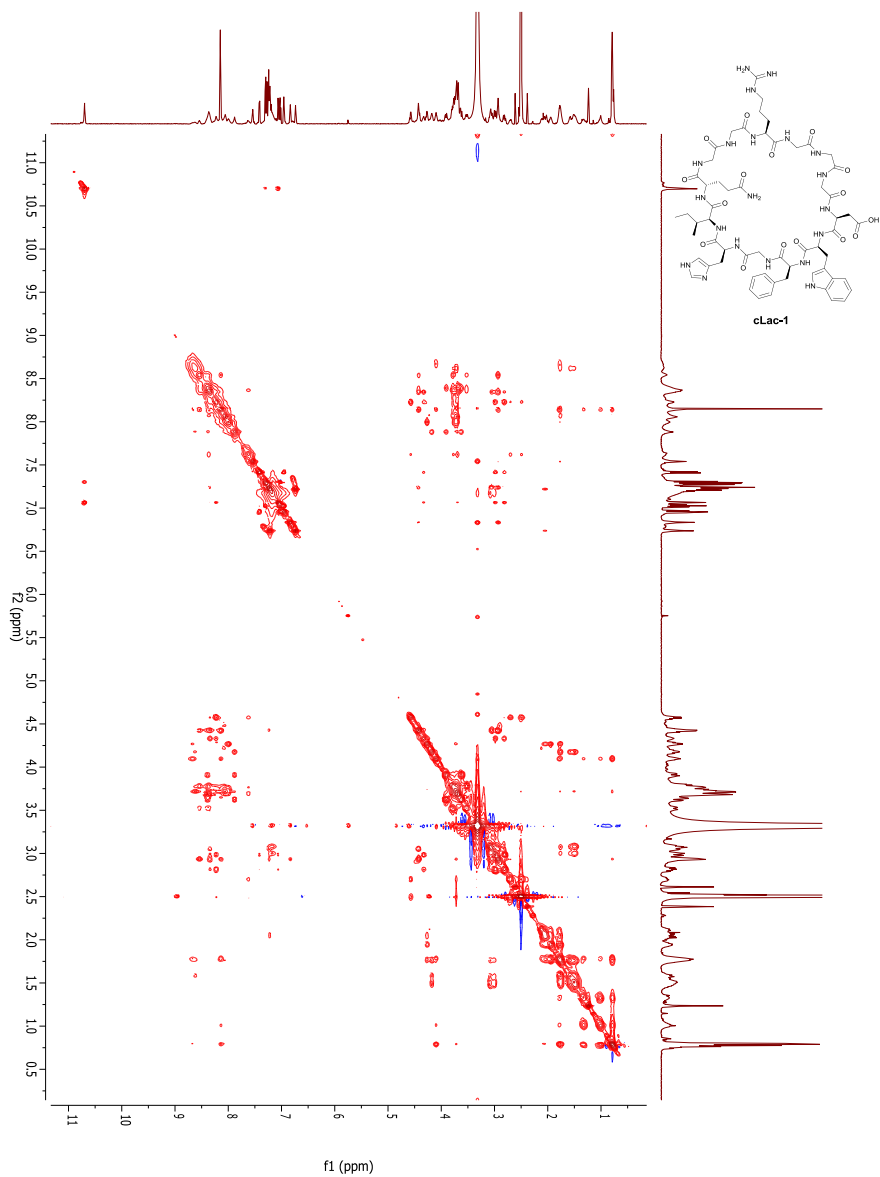
HSQC-NMR of cLac-1



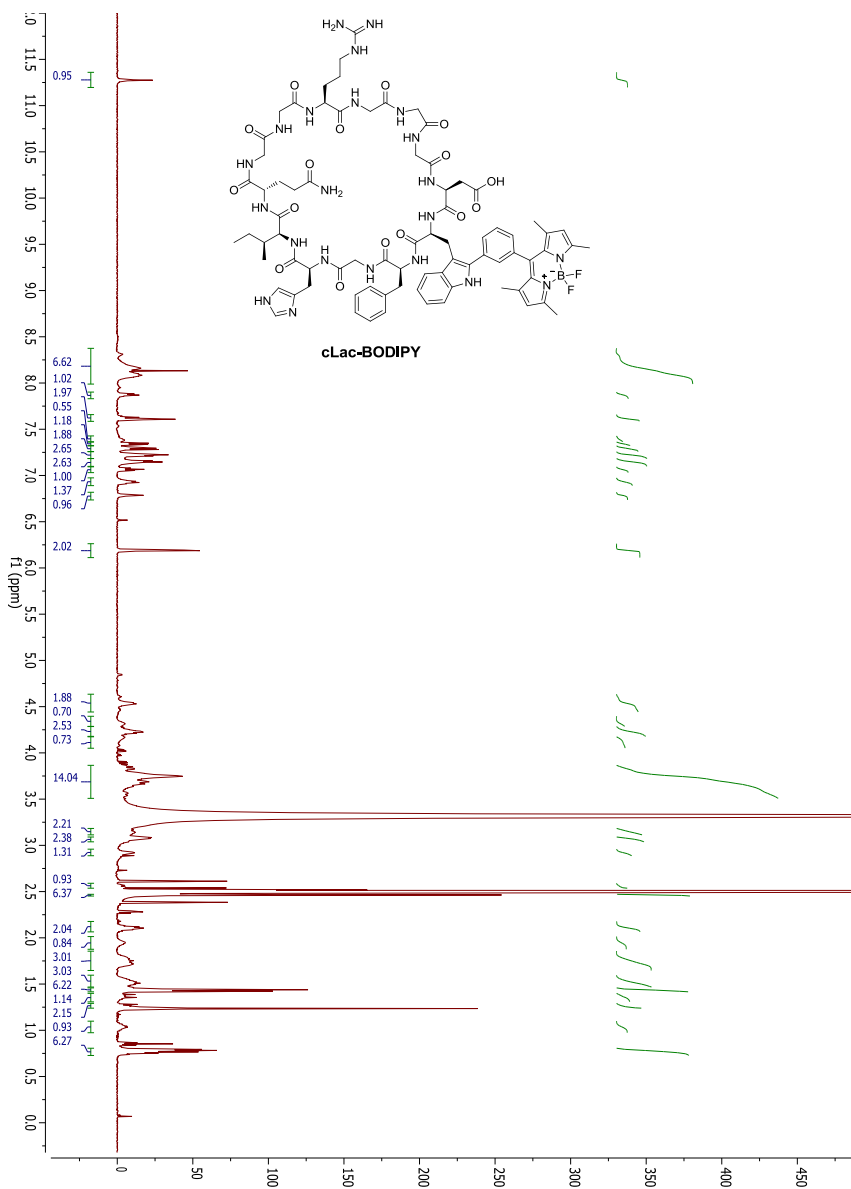
COSY-NMR of **cLac-1**

TOCSY-NMR of **cLac-1**

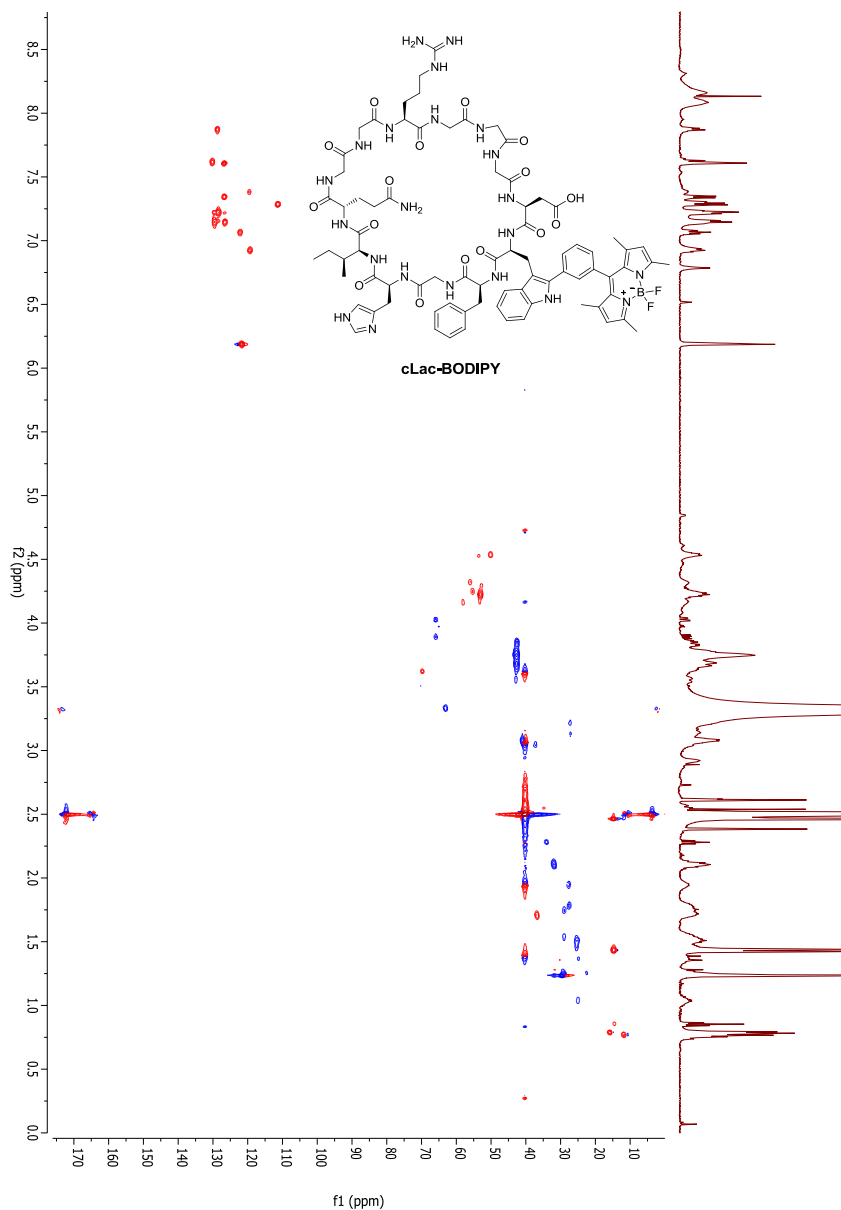
NOESY-NMR of cLac-1



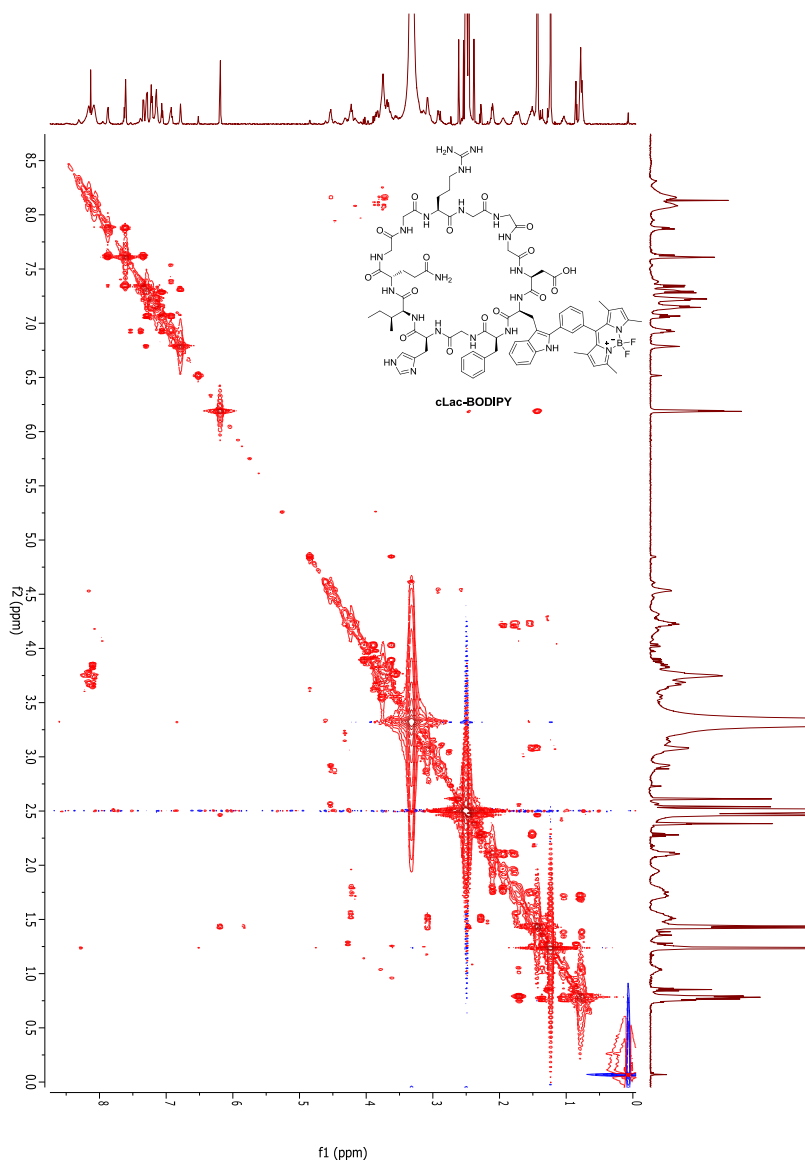
¹H-NMR of cLac-BODIPY



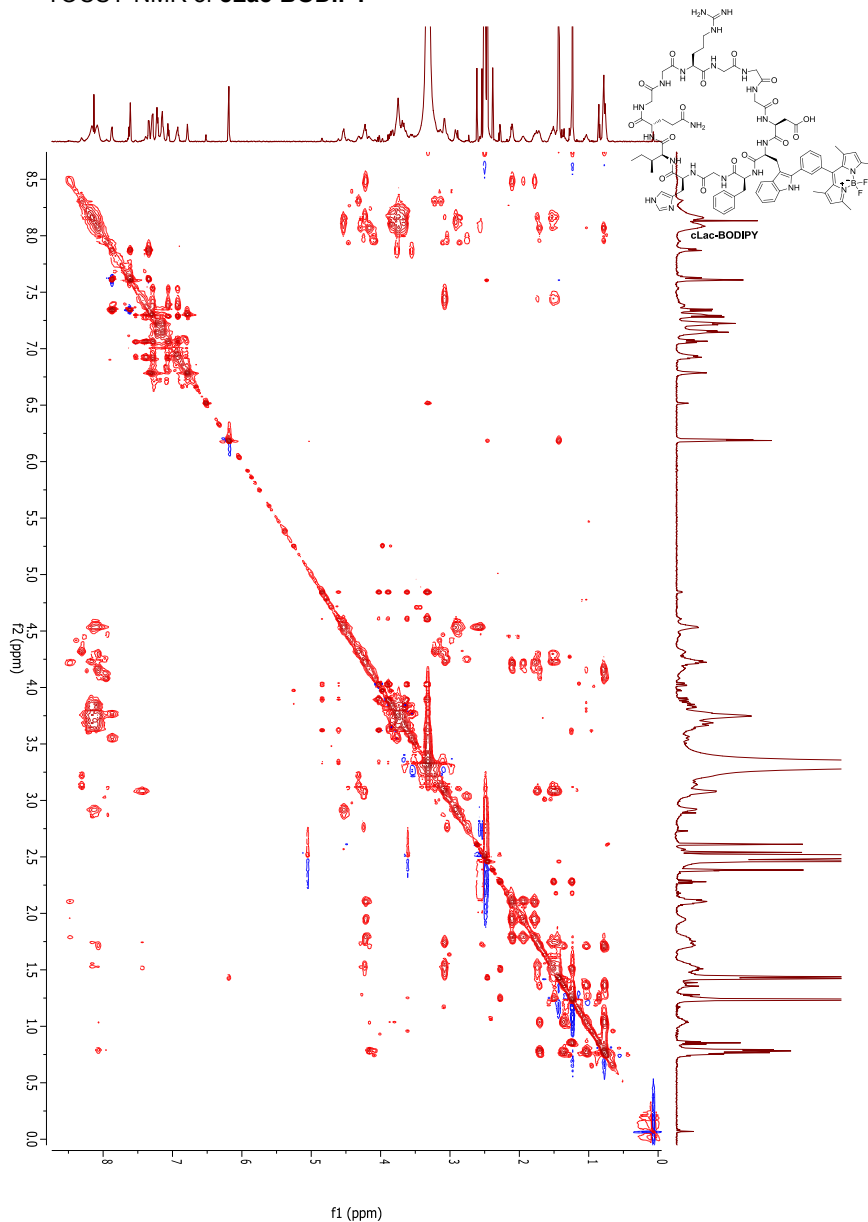
HSQC-NMR of cLac-BODIPY



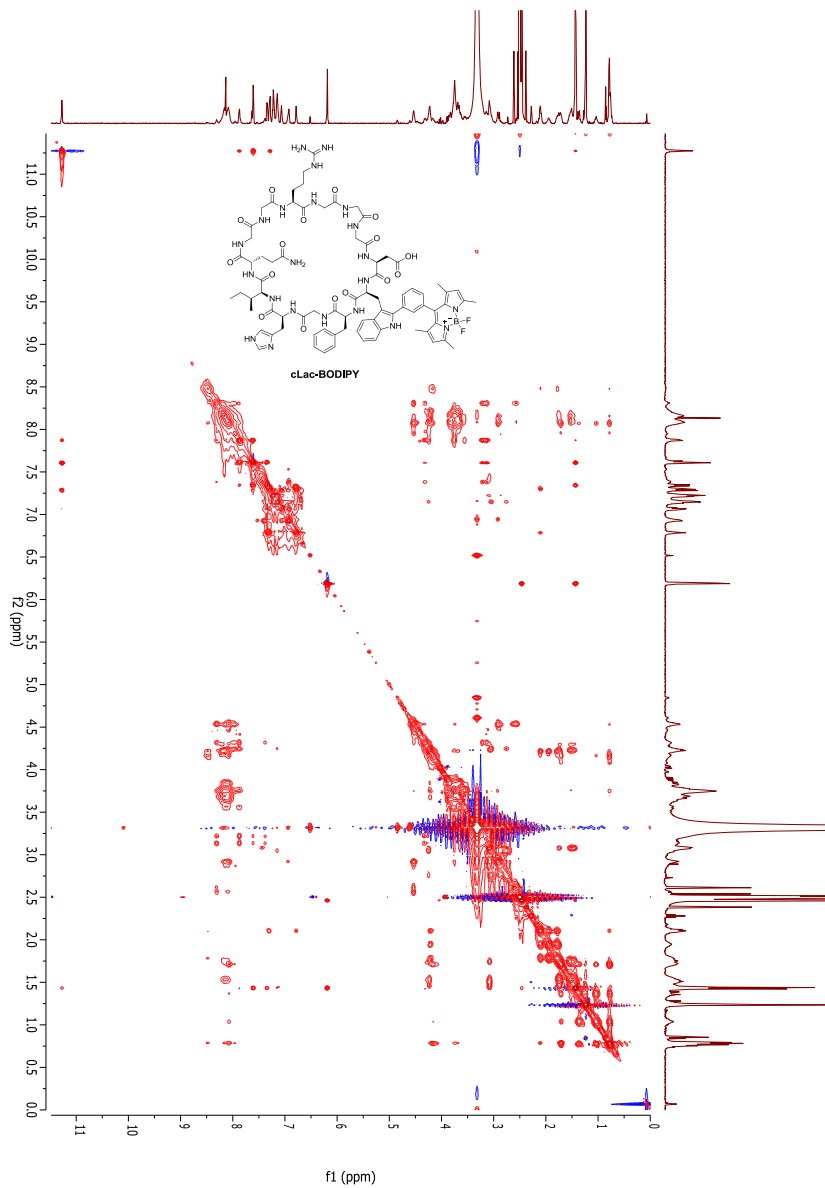
COSY-NMR of cLac-BODIPY



TOCSY-NMR of cLac-BODIPY



NOESY-NMR of cLac-BODIPY



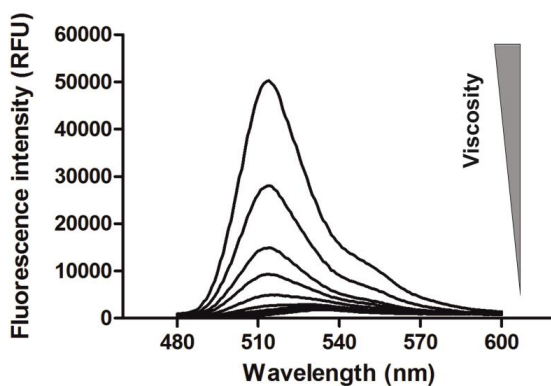
Supplementary Figures

Fig. S1. Fluorogenic behaviour of the Trp-BODIPY amino acid.

Fluorescence spectra of the Trp-BODIPY amino acid showing enhanced emission upon fluorophore rigidification in mixtures of glycerol: H₂O (10% steps) with increased viscosity. $\lambda_{exc.}$: 450 nm.

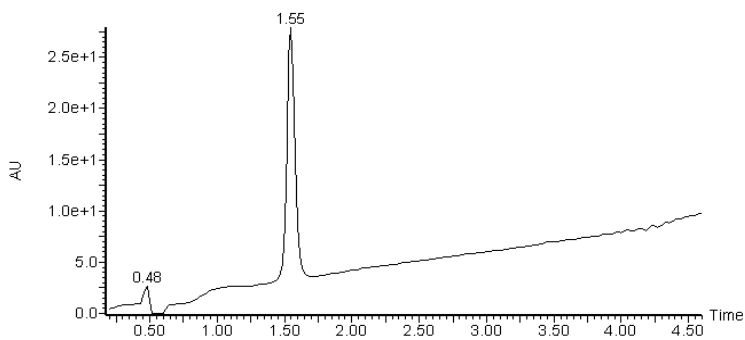


Fig. S2. HPLC trace of cLac-1. Eluents: H₂O (0.1% FA) and ACN (0.1% FA).

Flow: 1.6 mL min⁻¹. Linear gradient from 5% to 100% ACN (0.1% FA) over 3.5 min. The plot corresponds to the integrated absorbance signal from 210 to 400 nm.

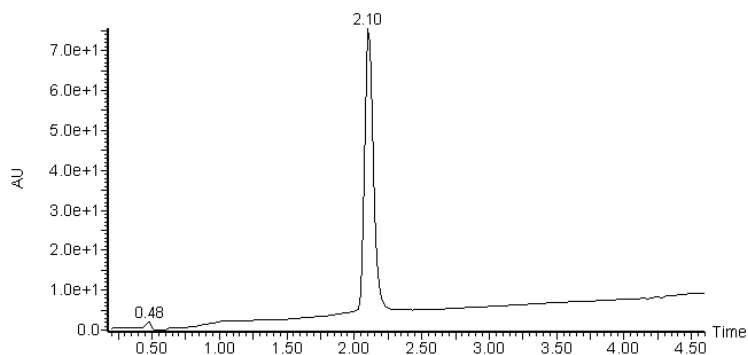


Fig. S3. HPLC trace of cLac-BODIPY. Eluents: H₂O (0.1% FA) and ACN (0.1% FA). Flow: 1.6 mL min⁻¹. Linear gradient from 5% to 100% ACN (0.1% FA) over 3.5 min. The plot corresponds to the integrated absorbance signal from 210 to 400 nm.

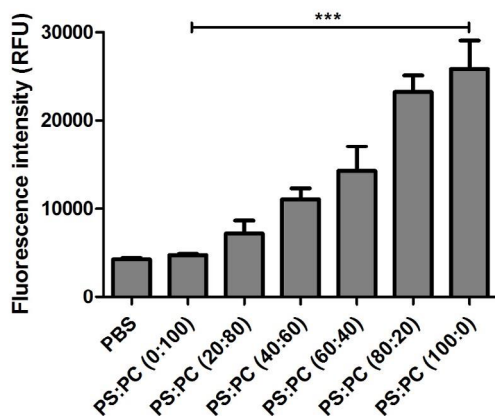


Fig. S4. Fluorescence intensity values of cLac-BODIPY (5 μM) after incubation with different PS: PC films. Values are represented as means and error bars as SD (n = 3). *** for p < 0.001.

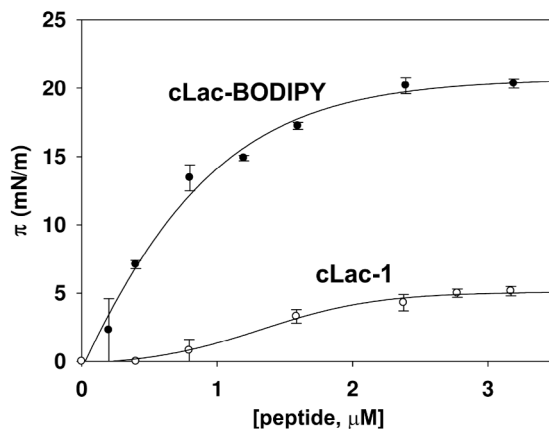


Fig. S5. Determination of the tensioactivity of **cLac-1** and **cLac-BODIPY**. **cLac-BODIPY** shows high tensioactivity with a saturation pressure (π_s) of 20.4 mN m⁻¹ and a saturation concentration (C_s) of 3 μM . The π_s for **cLac-1** is 5 mN m⁻¹. Values represented as means and error bars as SD ($n = 3$).

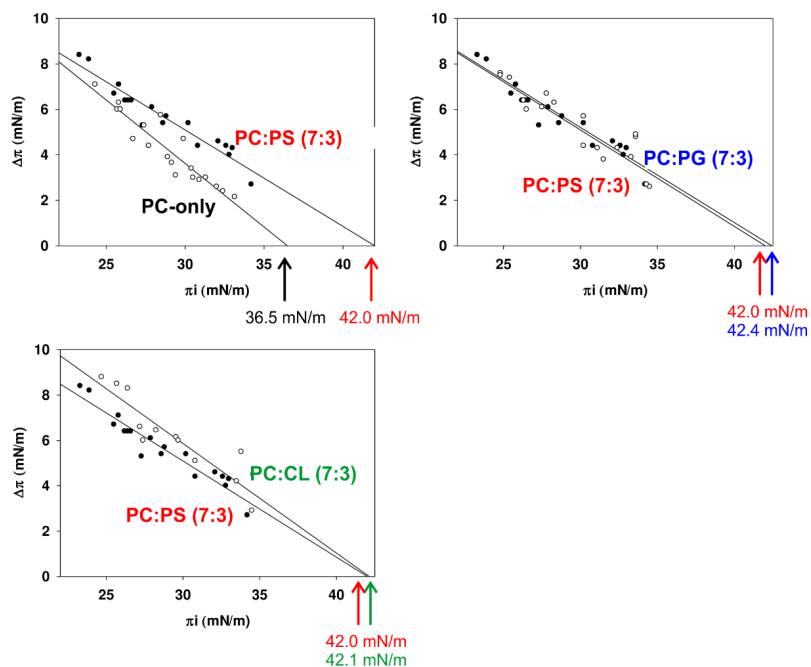


Fig. S6. Quantitative binding assays of **cLac-BODIPY** to monolayers with variable lipid composition. Arrows point at the π_c values for every lipid composition. PC: phosphatidylcholine, PS: phosphatidylserine, PG: phosphatidylglycine, CL: cardiolipin. Values represented as means from $n = 3$.

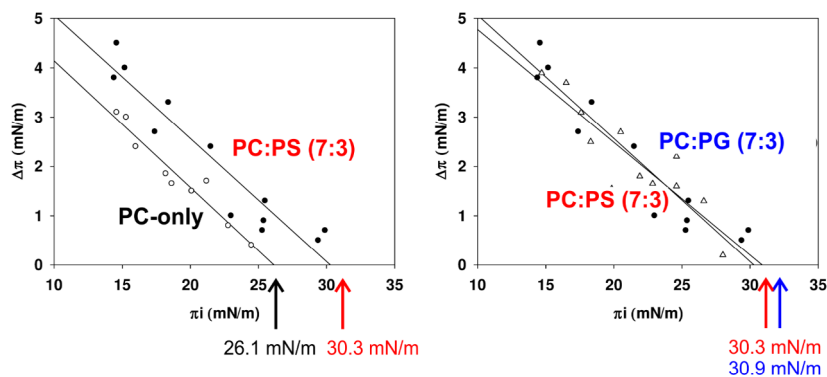


Fig. S7. Quantitative binding assays of **cLac-1** to monolayers with variable lipid composition. Arrows point at the π_c values for every lipid composition. PC: phosphatidylcholine, PS: phosphatidylserine, PG: phosphatidylglycine. Values represented as means from $n = 3$.

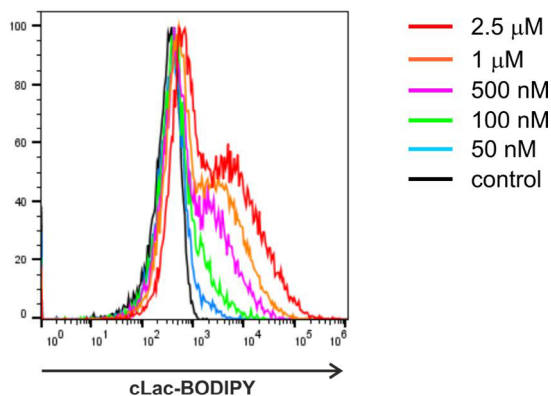


Fig. S8. Flow cytometry analysis of the fluorescence labelling of apoptotic bodies after incubation with different concentrations of **cLac-BODIPY**.

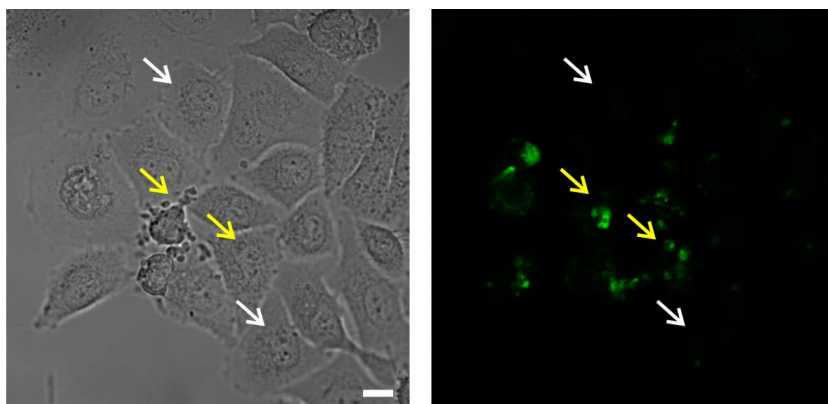


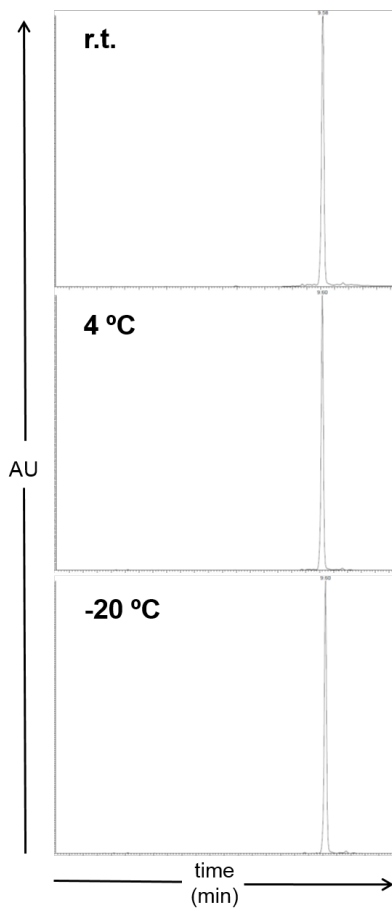
Fig S9. Brightfield and fluorescence microscopy images of human epithelial A549 cells upon induction of apoptosis and treatment with **cLac-BODIPY** (1 mM). Subcellular bodies derived from apoptotic cells (yellow arrows) are brightly stained whereas viable cells (white arrows) are not stained by **cLac-BODIPY**. Scale bar: 10 μm .

References

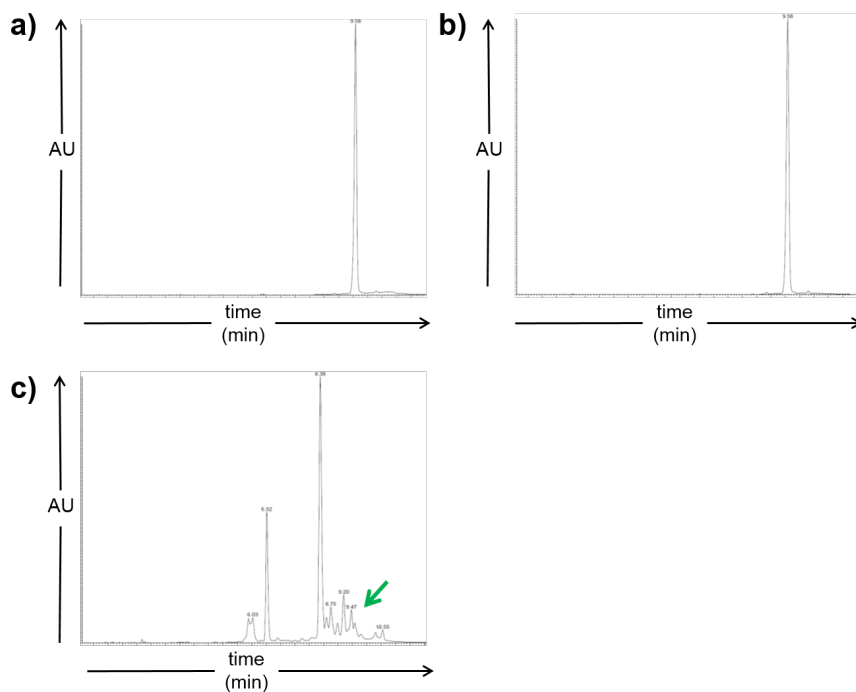
- [1] Mendive-Tapia, L.; Zhao, C.; Akram, A.R.; Preciado, S.; Albericio, F.; Lee, M.; Serrels, A.; Kielland, N.; Read, N. D.; Lavilla, R.; Vendrell, M. *Nat. Commun.* 2016, **7**, 10940.
- [2] Magde, D.; Wong, R.; Seybold, P. G. *Photochem. Photobiol.* 2002, **75**, 327.
- [3] Angelova, M. I.; Dimitrov, D. S. *Faraday Discuss. Chem. Soc.* 1986, **81**, 303.
- [4] Dimitrov, D. S.; Angelova, M. I. *Bioelectrochem. Bioenerg.* 1988, **19**, 323.
- [5] Montes, L. R.; Ahyyauch, H.; Ibarguren, M.; Sot J.; Alonso, A.; Bagatolli, L. A.; Goñi, F. M. *Methods Mol. Biol.* 2010, **606**, 105.
- [6] Kim, D. M.; Koo, S. Y.; Jeon, K.; Kim, M. H.; Lee, J.; Hong, C. Y.; Jeong, S. *Cancer Res.* 2003, **63**, 621.



FULL SUPPORTING INFORMATION PUBLICATION VI

Supplementary Information

Supplementary Figure 1. Analysis of the long-term stability of the amino acid 1 when stored as a solid at different temperatures. HPLC-MS traces of the amino acid 1 after being stored in the dark for 4 months at r.t., 4 °C, and -20 °C. UV detection: 500 nm.



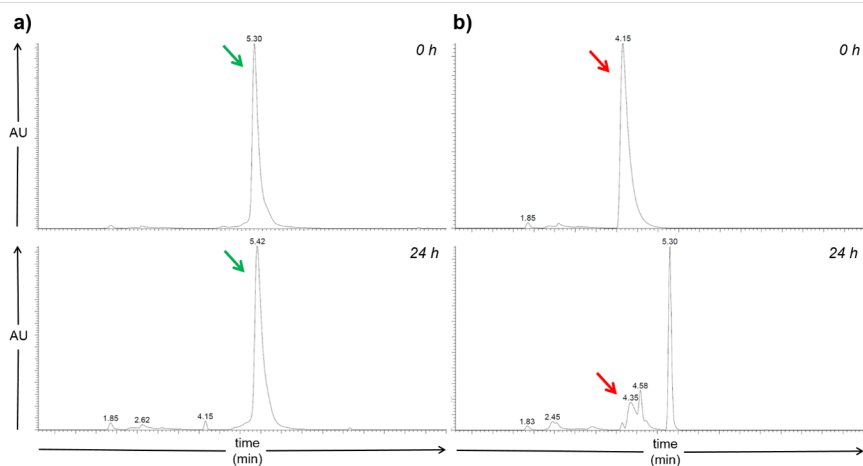
Supplementary Figure 2. Analysis of the long-term stability of the amino acid 1 when dissolved in organic solvents at different temperatures. HPLC-MS traces of the amino acid 1 after being stored in the dark for 4 months in: a) DCM at -20 °C, b) MeOH at 4 °C, c) DMF at r.t. In c), the green arrow points at the remaining amino acid 1 and the main peaks correspond to Fmoc-deprotection side products. UV detection: 500 nm.

Supplementary Table 1. Cellular activity of BODIPY-cPAF26 and PAF26 in different fungal species. Cell viability was measured after 16 h incubation with different concentrations of **BODIPY-cPAF26** or PAF26 peptides at 25 °C for *N. crassa* or 37 °C for *A. fumigatus*. IC₅₀ values (μM) are represented as means ± s.d. (n=3).

	IC ₅₀ (<i>N. crassa</i>)	IC ₅₀ (<i>A. fumigatus</i>)
BODIPY-cPAF26	1.4 ± 0.1	2.2 ± 0.1
PAF26	3.7 ± 0.1	7.9 ± 0.3

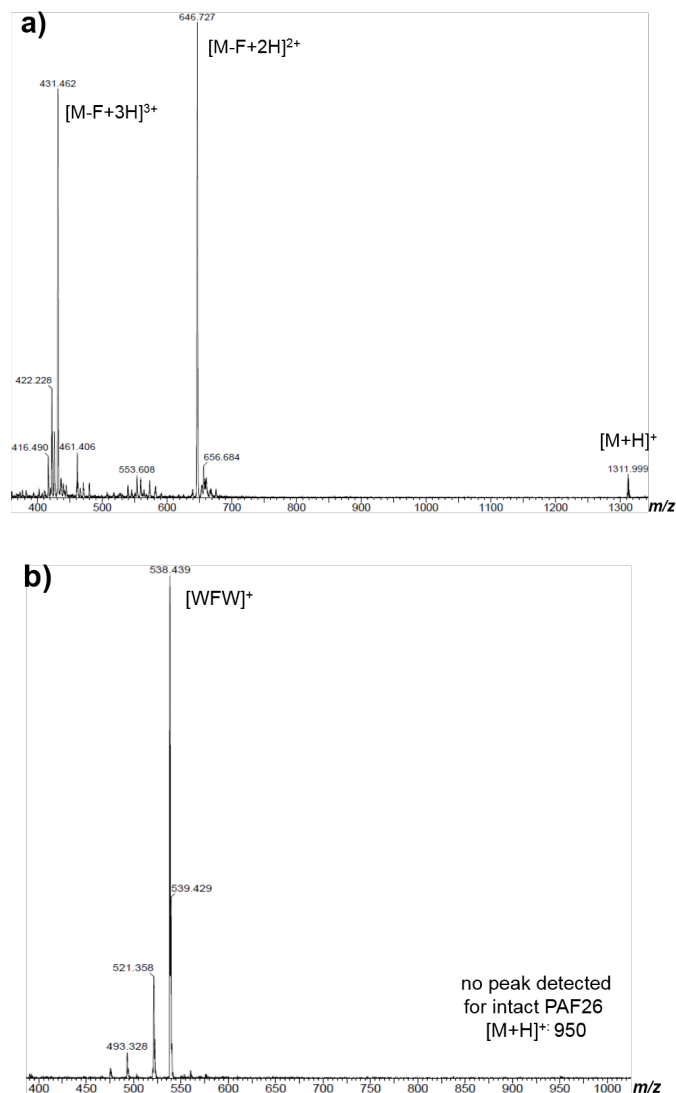
Supplementary Table 2. Fluorescence quantum yields of BODIPY-cPAF26 in PC: cholesterol (7:1) liposome suspensions in PBS with increasing hydrophobicity. PBS alone was used as a negative control. Quantum yields were determined by comparing the integrated emission area of the fluorescence spectra to the emission area of fluorescein in basic EtOH (QY: 0.97), λ_{exc.}: 450 nm. Data represented as means ± s.d. (n=3).

PC (mg mL ⁻¹) content on liposomes	Quantum yield
3.75	0.32 ± 0.04
1.88	0.27 ± 0.04
0.94	0.20 ± 0.02
0.47	0.14 ± 0.02
0.23	0.09 ± 0.01
0.12	0.06 ± 0.01
0.06	0.04 ± 0.01
0.03	0.02 ± 0.004
0.02	0.02 ± 0.003
0.007	0.01 ± 0.002
PBS	0.01 ± 0.002



Time (h)	Purity (% of intact peptide left)	
	BODIPY-cPAF26	Unlabeled PAF26
0.25	99%	83%
1	99%	79%
4	99%	73%
8	99%	63%
24	98%	20%

Supplementary Figure 3. Time-course analysis of the chemical integrity of BODIPY-cPAF26 and unlabeled linear PAF26 in proteolytic environments. HPLC traces of **BODIPY-cPAF26** (a) and unlabeled PAF26 (b) before incubation (*top*) and after incubation (*bottom*) at a concentration of 200 μM in a protease cocktail (1 mg L^{-1}). Green arrows point at the peaks of intact **BODIPY-cPAF26** and red arrows point at intact PAF26. UV detection: 280 nm. Purities were determined by integration of the peak areas in respective HPLC chromatograms at 280 nm.



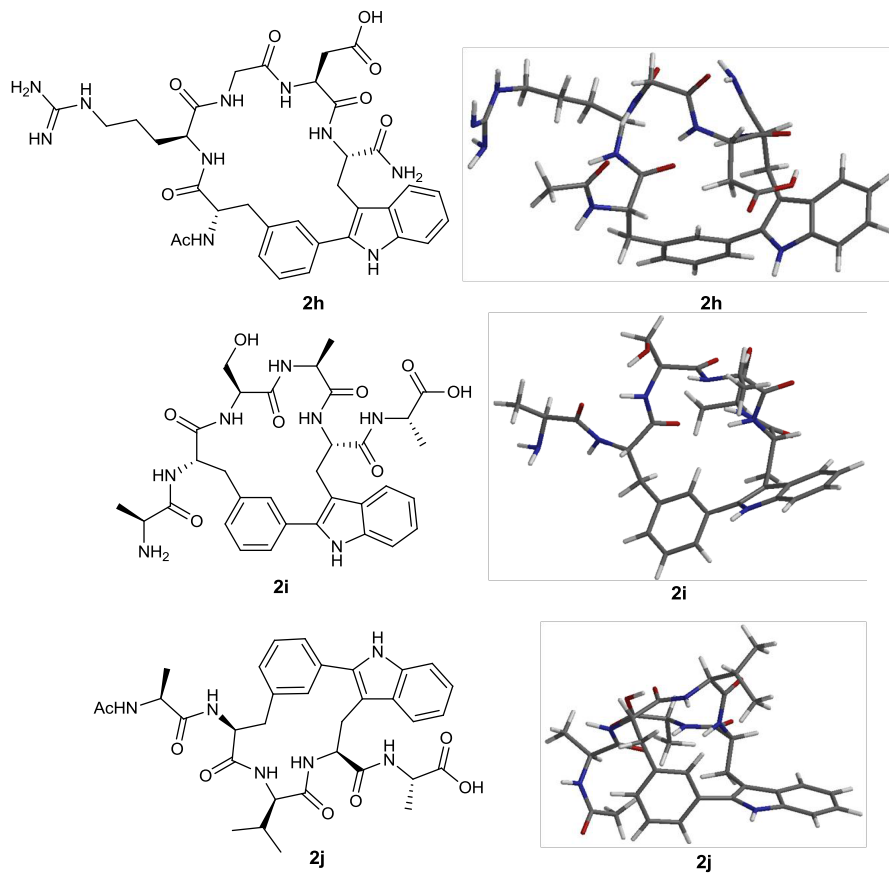
Supplementary Figure 4. Electrospray analysis of BODIPY-cPAF26 and unlabeled PAF26 after 24 h incubation in a protease cocktail. Both peptides (200 μ M) were incubated in 1 mg L⁻¹ of the protease cocktail, and their respective mass spectra were recorded on a Waters Micromass ZQ mass spectrometer (ESI positive mode). a) MS analysis of **BODIPY-cPAF26** (exact mass: 1311 Da); b) MS analysis of unlabeled PAF26 (exact mass: 949 Da).

Supplementary Video 1. Time-course high-resolution imaging of *A. fumigatus* upon treatment with BODIPY-cPAF26. *A. fumigatus* were pre-treated with a cell membrane counterstain (*red*) and imaged under the confocal microscope. Cells were then treated with **BODIPY-cPAF26** (2 μ M, *green*) and further imaged without any washing steps. The movie shows the rapid fluorogenic response of **BODIPY-cPAF26** upon interaction with the cell membrane of *A. fumigatus*. Scale bar: 5 μ m.

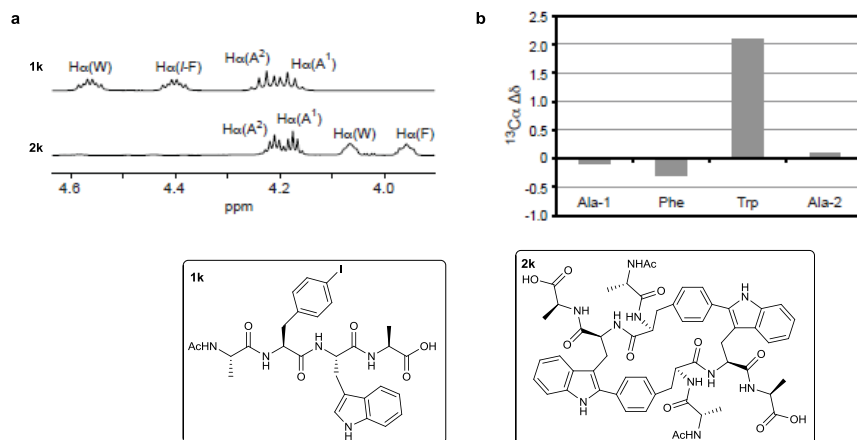


FULL SUPPORTING INFORMATION PUBLICATION VII

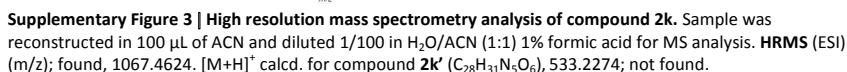
Supplementary Figures

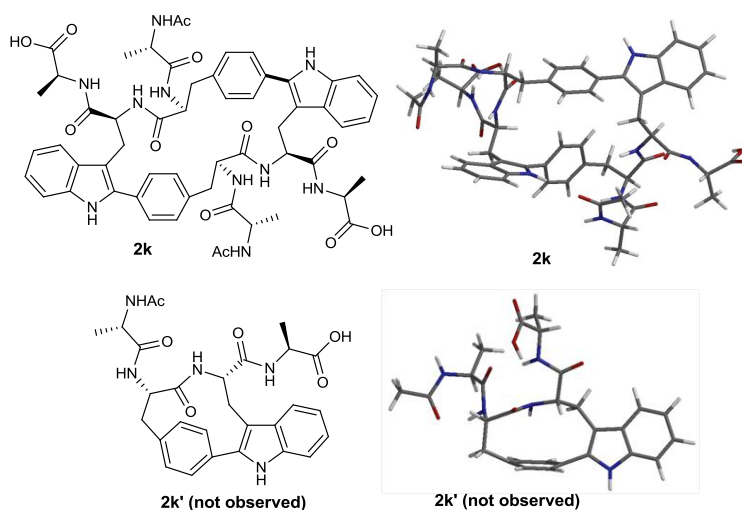


Supplementary Figure 1 | Minimized geometries of compounds 2h-j generated by the Spartan '14 suite (molecular mechanics, MMFF94).⁸

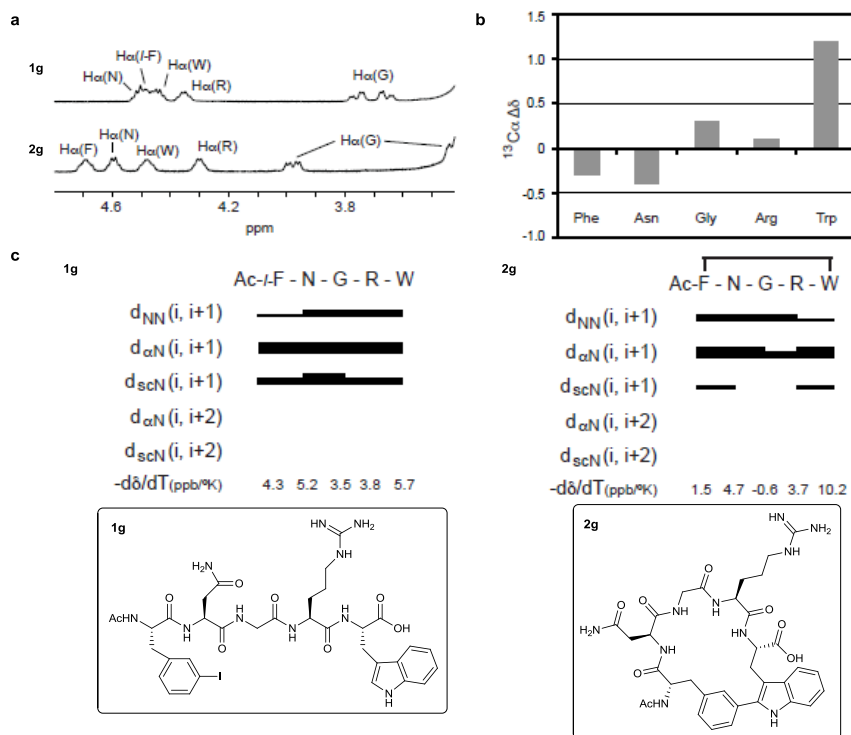


Supplementary Figure 2 | Peptide NMR spectra comparison between compounds 2k and 1k. a, NMR H_{α} region of peptide **2k** and its linear precursor **1k**. **b**, Plot of the $^{13}C_{\alpha}$ chemical shift differences ($^{13}C_{\alpha} \Delta\delta_{\text{cyclic-linear}}$) between cyclodimer **2k** and its linear counterpart **1k**. Temperature coefficients of the NH amide protons, $\Delta\delta/\Delta T$ (ppb/ $^{\circ}K$), were -3.5 (A^1), -2.8 ($I-F$), -3.8 (W), -5.9 (A^2) and -4.1 (A^1), -5.6 (F), 0.7 (W), -5.3 (A^2) for peptide **1k** and **2k**, respectively.

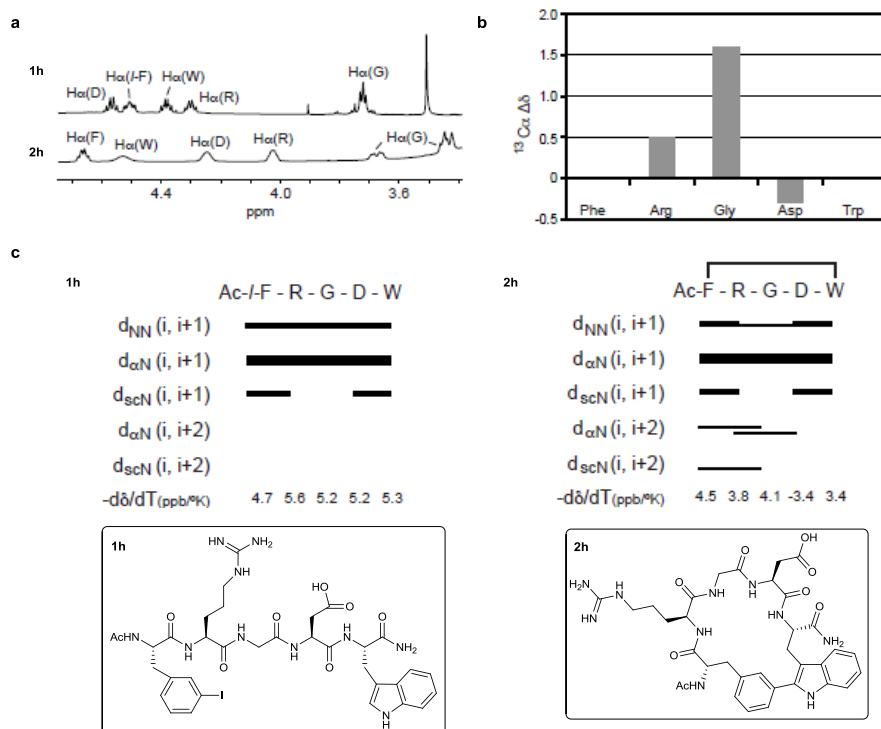




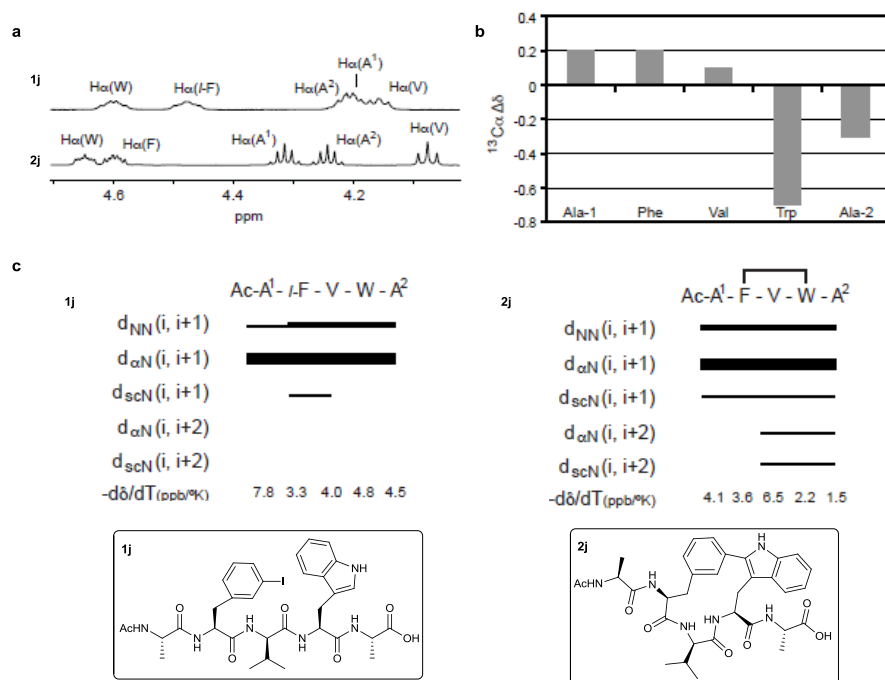
Supplementary Figure 4 | Minimized geometries of compound **2k (left) and its monomeric analog **2k'** (right) generated by the Spartan '14 suite.⁸ Structure **2k** display planar phenyl rings in contrast with the constrained monomeric structure **2k'**, where a phenyl ring is severely distorted.**



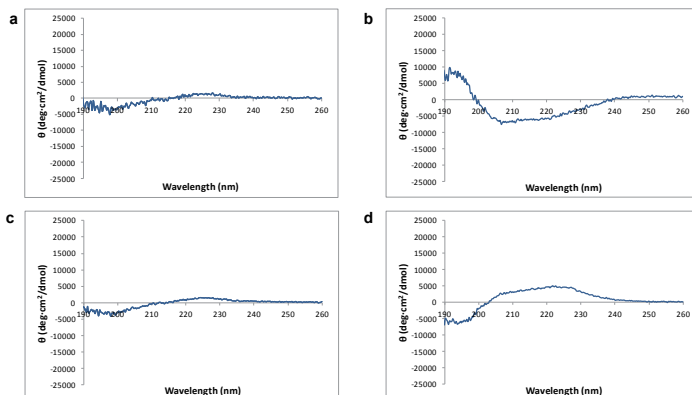
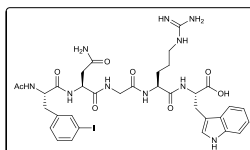
Supplementary Figure 5 | Peptide NMR spectra comparison between compounds **2g and **1g**.** **a**, NMR H_α region of peptide **2g** and its linear precursor **1g**. **b**, Plot of the $^{13}\text{C}_\alpha$ chemical shift differences ($^{13}\text{C}_\alpha \Delta\delta_{\text{cyclic-linear}}$) between stapled peptide **2g** and its linear counterpart **1g**. **c**, Summary of NOE connectivities and temperature coefficients of the NH amide protons ($\Delta\delta/\Delta T$) of peptide **1g** (bottom left) and **2g** (bottom right). The thickness of the bars reflects the intensity of the NOEs, i.e. weak (—), medium (▬) and strong (▮). I-F: *m*-iodophenylalanine.



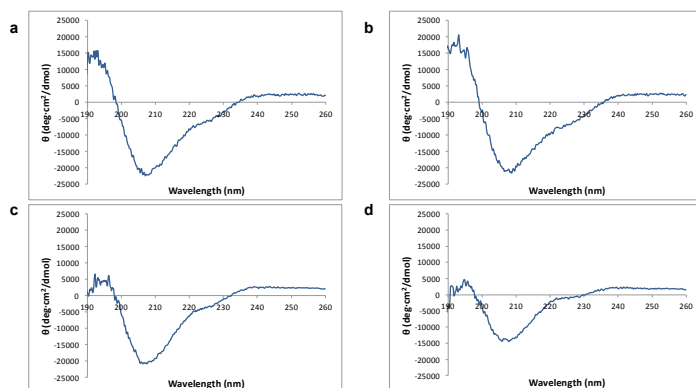
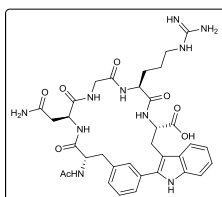
Supplementary Figure 6 | Peptide NMR spectra comparison between compounds 2h and 1h. **a**, NMR H_α region of peptide 2h and its linear precursor 1h. **b**, Plot of the $^{13}\text{C}_\alpha$ chemical shift differences ($^{13}\text{C}_\alpha \Delta\delta_{\text{cyclic-linear}}$) between stapled peptide 2h and its linear counterpart 1h. **c**, Summary of NOE connectivities and temperature coefficients of the NH amide protons ($\Delta\delta/\Delta T$) of peptide 1h (bottom left) and 2h (bottom right). The thickness of the bars reflects the intensity of the NOEs, i.e. weak (—), medium (▬) and strong (▮). I-F: *m*-iodophenylalanine.



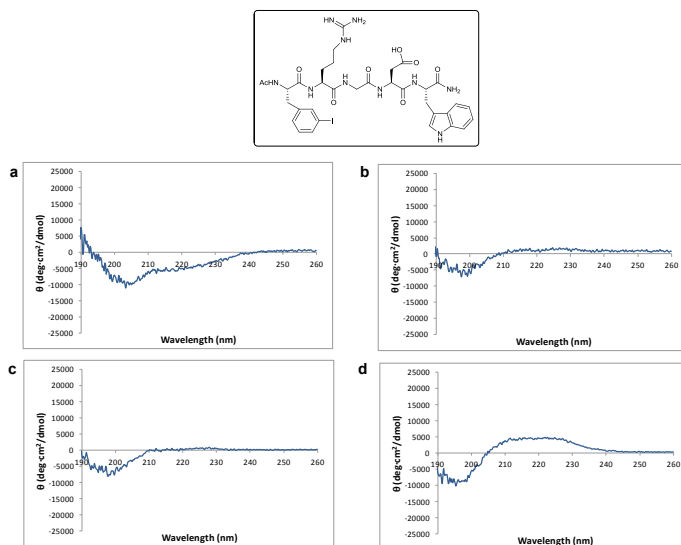
Supplementary Figure 7 | Peptide NMR spectra comparison between compounds **2j and **1j**.** **a**, NMR H_{α} region of peptide **2j** and its linear precursor **1j**. **b**, Plot of the $^{13}C_{\alpha}$ chemical shift differences ($^{13}C_{\alpha} \Delta\delta_{cyclic-linear}$) between stapled peptide **2j** and its linear counterpart **1j**. **c**, Summary of NOE connectivities and temperature coefficients of the NH amide protons ($\Delta\delta/\Delta T$) of peptide **1j** (bottom left) and **2j** (bottom right). The thickness of the bars reflects the intensity of the NOEs, i.e. weak (—), medium (■) and strong (■). I-F: *m*-iodophenylalanine.



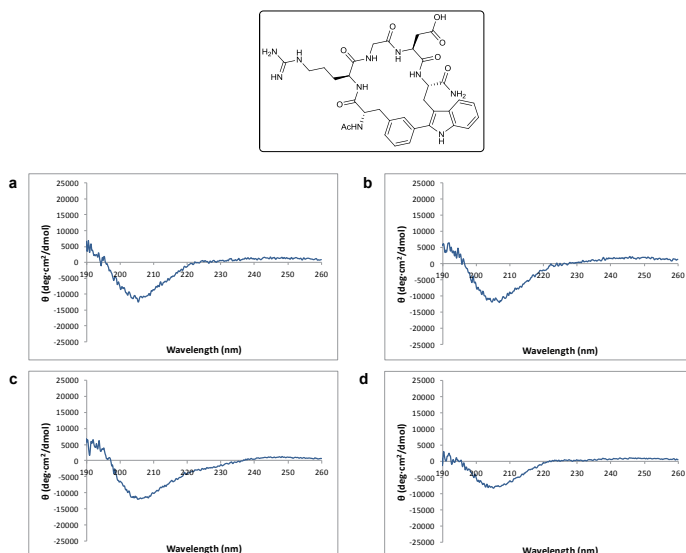
Supplementary Figure 8 | Circular dichroism spectra of 1g. **a**, At 100 μM in a buffer of 25 mM Na_2HPO_4 (pH 7). **b**, At 100 μM in a buffer of 25 mM Na_2HPO_4 (pH 7) (90%) and 10% of TFE. **c**, At 200 μM in a buffer of 25 mM Na_2HPO_4 (pH 7). **d**, At 200 μM in PBS (90%) and TFE (10%).



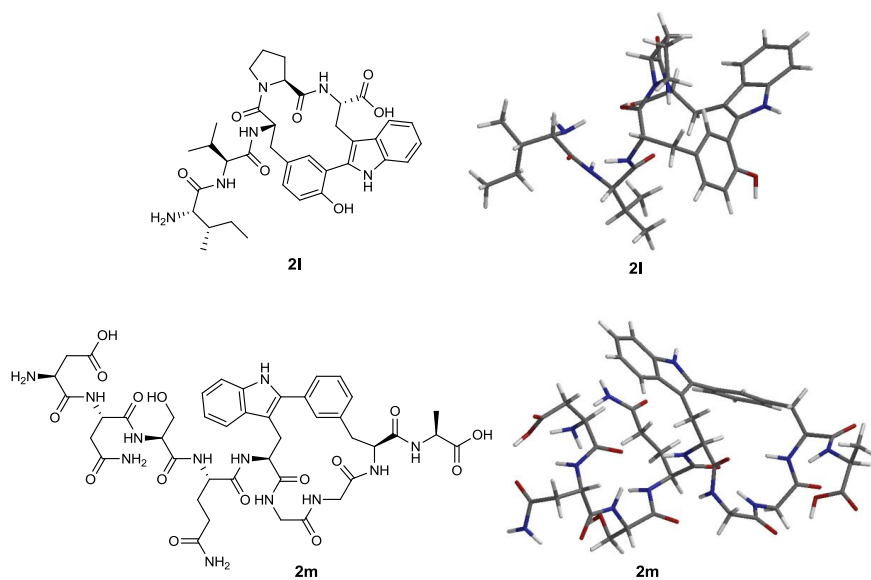
Supplementary Figure 9 | Circular dichroism spectra of 2g. **a**, At 100 μM in a buffer of 25 mM Na_2HPO_4 (pH 7). **b**, At 100 μM in a buffer of 25 mM Na_2HPO_4 (pH 7) (90%) and 10% of TFE. **c**, At 200 μM in a buffer of 25 mM Na_2HPO_4 (pH 7). **d**, At 200 μM in PBS (90%) and TFE (10%).



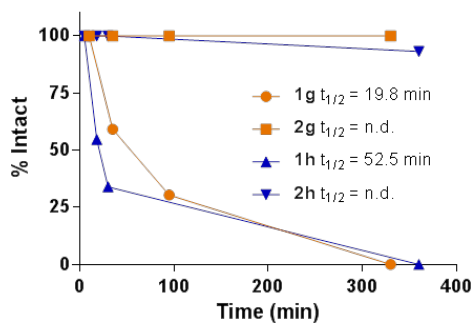
Supplementary Figure 10 | Circular dichroism spectra of 1h. a, At 100 μ M in a buffer of 25 mM Na₂HPO₄ (pH 7). b, At 100 μ M in a buffer of 25 mM Na₂HPO₄ (pH 7) (90%) and 10% of TFE. c, At 200 μ M in a buffer of 25 mM Na₂HPO₄ (pH 7). d, At 200 μ M in PBS (90%) and TFE (10%).



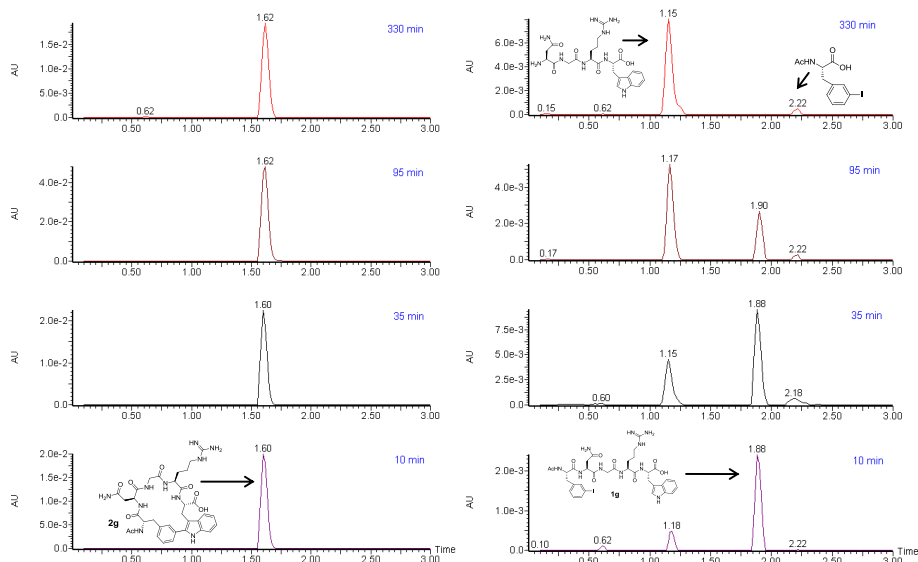
Supplementary Figure 11 | Circular dichroism spectra of 2h. a, At 100 μ M in a buffer of 25 mM Na₂HPO₄ (pH 7). b, At 100 μ M in a buffer of 25 mM Na₂HPO₄ (pH 7) (90%) and 10% of TFE. c, At 200 μ M in a buffer of 25 mM Na₂HPO₄ (pH 7). d, At 200 μ M in PBS (90%) and TFE (10%).



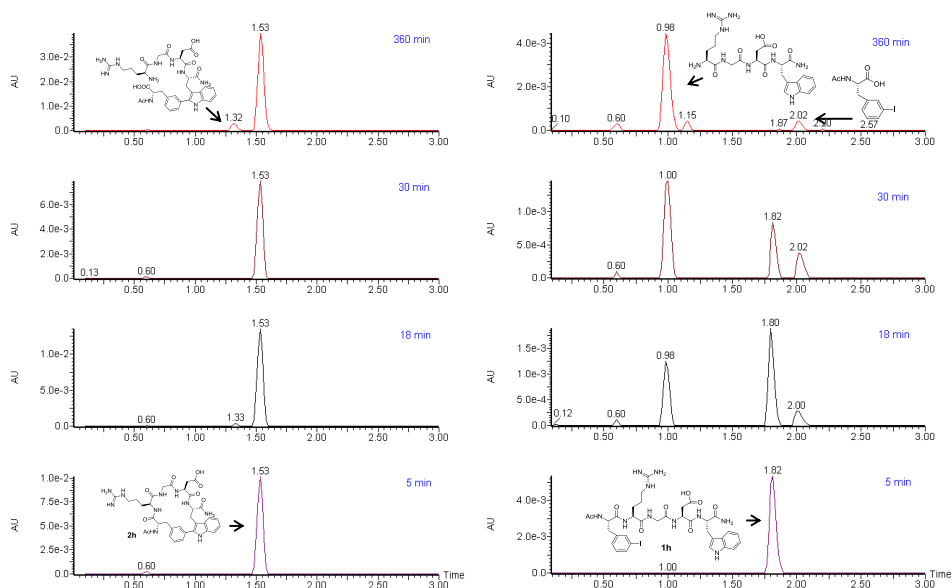
Supplementary Figure 12 | Minimized geometries of compounds 2l and 2m generated by the Spartan '14 suite (molecular mechanics, MMFF94).⁸



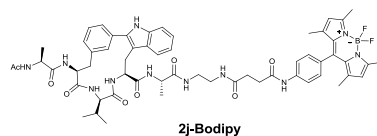
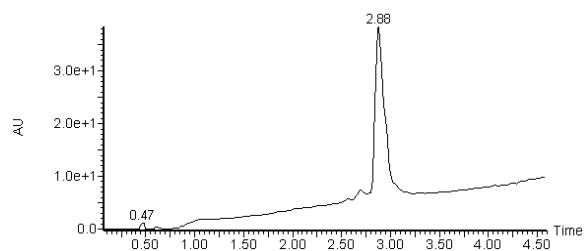
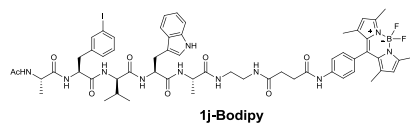
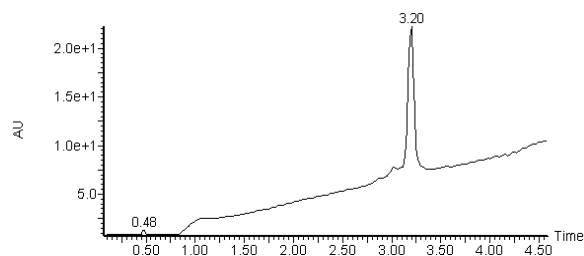
Supplementary Figure 13 | Proteolytic degradation assay of stapled peptides 2g and 2h and their linear precursors 1g and 1h. With respect to the linear compounds **1g** and **1h**, α -chymotrypsin cleavage products (from the hydrolysis on the C-terminal side of *I*-phenylalanine)¹² were observed, being the degradation complete after 6 h. Significant different behavior was observed for the corresponding stapled peptides **2g** and **2h**, which remained unaltered and only traces of the corresponding C-terminal hydrolysis of *I*-phenylalanine were detected.



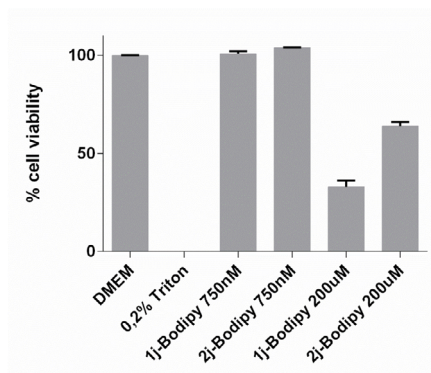
Supplementary Figure S14 | HPLC-MS chromatograms of stapled peptide **2g (left) and its linear precursor **1g** (right) monitored by at 300 and 280 nm, respectively.**



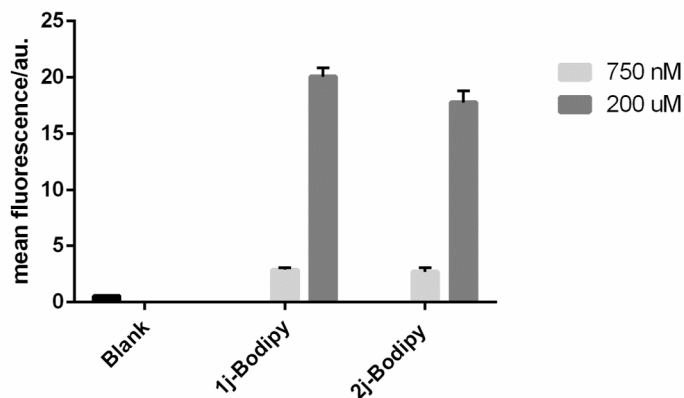
Supplementary Figure S15 | HPLC-MS chromatograms of stapled peptide **2h (left) and its linear precursor **1h** (right) monitored at 300 and 280 nm, respectively.**



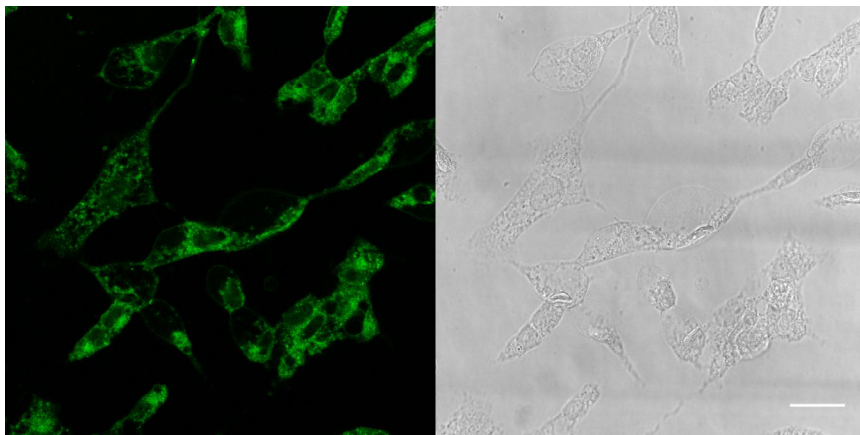
Supplementary Figure 16 | HPLC-MS chromatograms of BODIPY-labelled peptides 1j-BODIPY (above) and 2j-BODIPY (down).



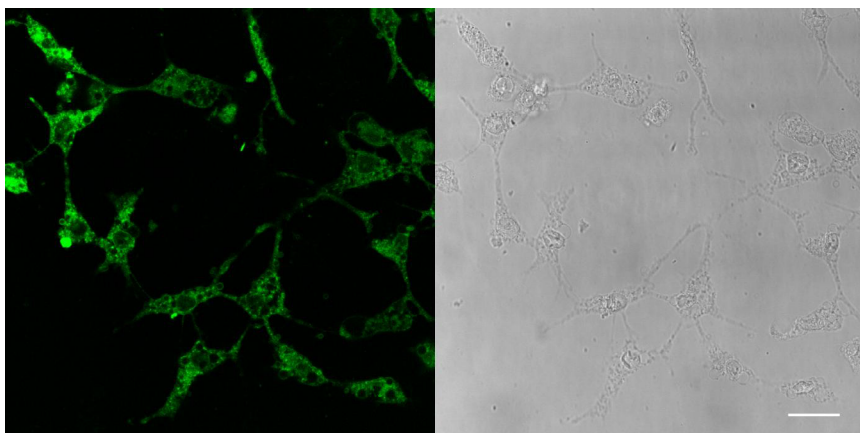
Supplementary Figure 17 | Cytotoxicity of 1j-Bodipy and 2j-Bodipy peptides using the MTT assay. The toxicity assay was carried out as described in the literature.¹³ SH-SY5Y cells were transferred to 96-well plates (100 μ L medium/well) at a density of 5000 cell/well. After 24 h, cells in triplicate were treated either with **1j-Bodipy** or **2j-Bodipy** (750 nM and 50 μ M) or TRITON 0.2% as positive control for 24 h. Values are represented as means \pm SD from three independent experiments.



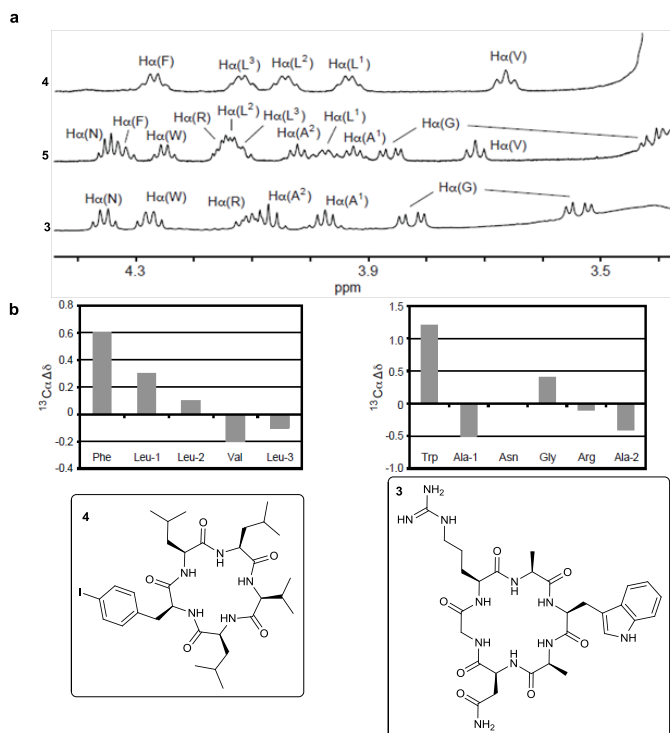
Supplementary Figure 18 | FACS analysis of SH-SY5Y cells upon incubation with 1j-Bodipy and 2j-Bodipy. For FACS analysis, SH-SY5Y cells were seeded on a plastic 24 well plate and cultured for 24 h. The culture medium was discarded, and cells were incubated for 30 min at 37 $^{\circ}$ C under 5% CO_2 with fresh medium containing either **1j-Bodipy** or **2j-Bodipy**. Cells were then rinsed, treated with trypsin, collected, centrifuged at 4 $^{\circ}$ C, filtered and re-suspended in cold medium. Fluorescence sorting was performed with a Gallios Beckman Coulter flow cytometer.



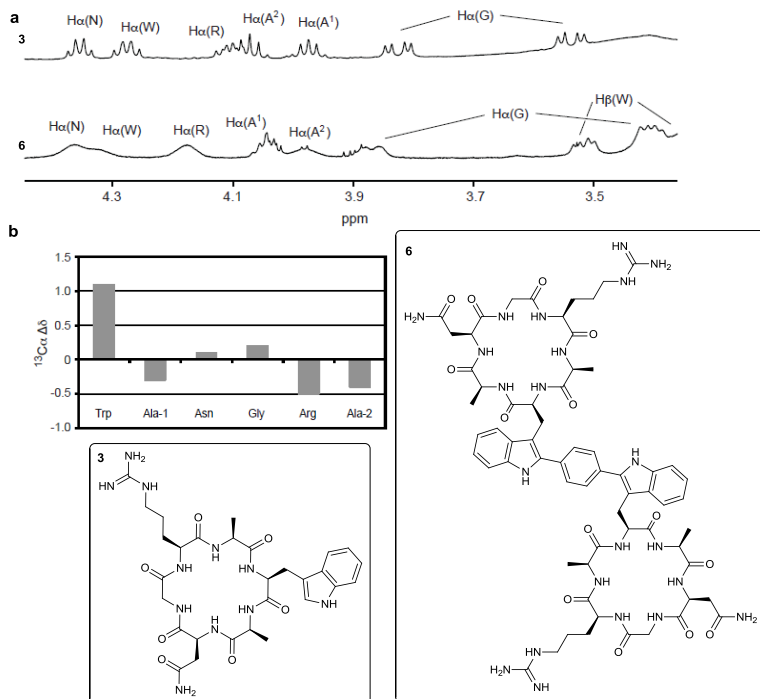
Supplementary Figure 19 | Spontaneous internalization of 1j-Bodipy in SH-SY5Y cells (scale bar, 25 μm).



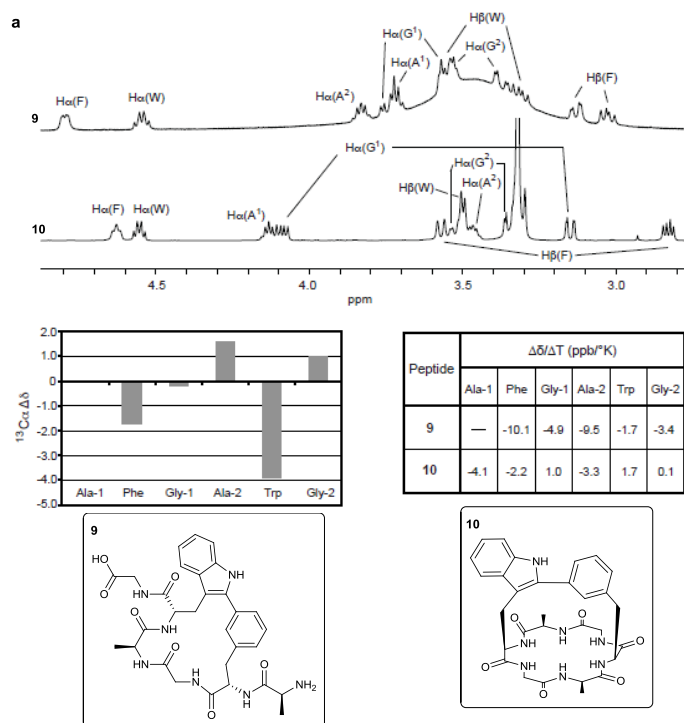
Supplementary Figure 20 | Spontaneous internalization of 2j-Bodipy in SH-SY5Y cells (scale bar, 25 μm).



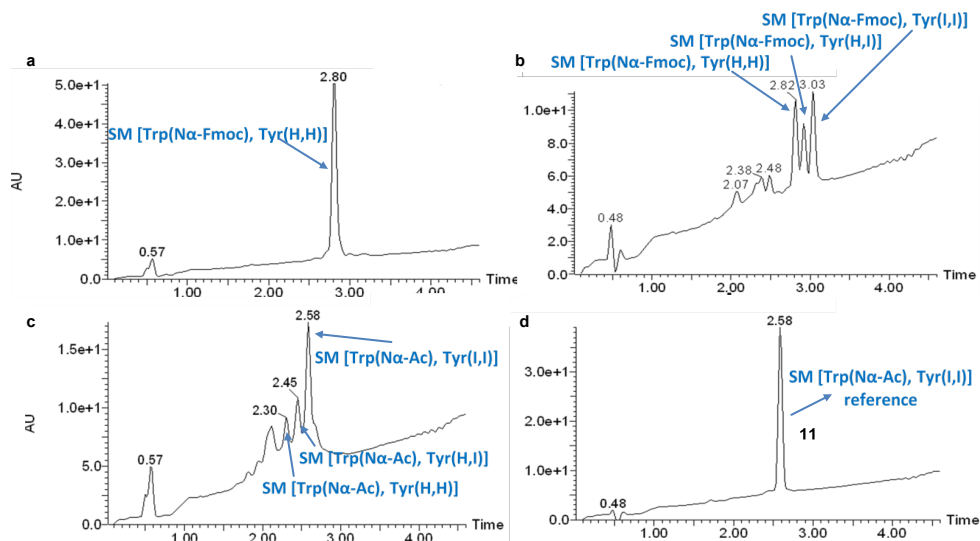
Supplementary Figure 21 | Peptide NMR spectra comparison between compounds 3 and 4. **a**, NMR H_{α} region of peptides 3, 4 and 5. **b**, Plot of the $^{13}C_{\alpha}$ chemical shift differences between conjugated peptide 5 and its macrocyclic precursors 3 and 4 ($^{13}C_{\alpha} \Delta\delta_{5-x}$ where $x=3$ or 4).



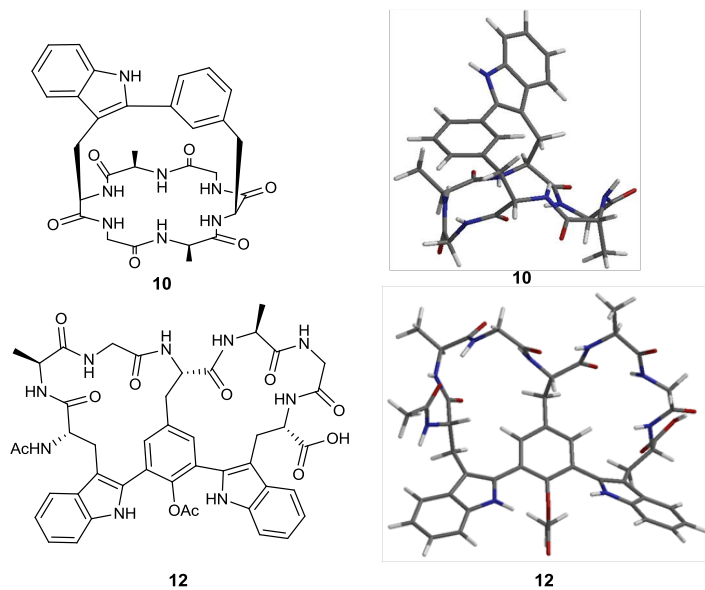
Supplementary Figure 22 | Peptide NMR spectra comparison between compounds 3 and 6. a, NMR H_α region of peptides 3 and 6. **b,** Plot of the $^{13}\text{C}_\alpha$ chemical shift differences between conjugated peptide 6 and its macrocyclic precursor 3 ($^{13}\text{C}_\alpha \Delta\delta_{6-3}$).



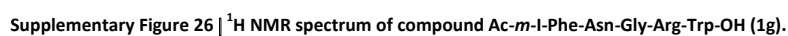
Supplementary Figure 23 | Peptide NMR spectra comparison between compounds 9 and 10. a, NMR H_{α} region of peptides 9 and 10. **b,** Plot of the $^{13}C_{\alpha}$ chemical shift differences between peptides 9 and 10 ($^{13}C_{\alpha} \Delta\delta_{10-9}$). **c,** Summary of temperature coefficients of the NH amide protons ($\Delta\delta/\Delta T$) of peptides 9 and 10.

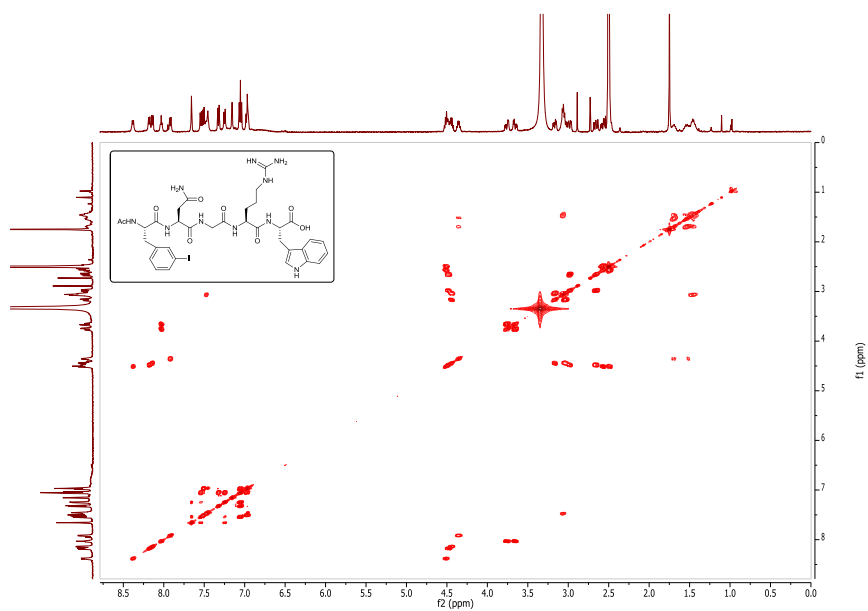


Supplementary Figure 24 || HPLC-MS chromatograms relative to diiodination of the corresponding non-halogenated N-terminal Fmoc-protected linear sequence of **11** on resin. In a preliminary procedure the corresponding non-halogenated linear sequence of **11** anchored to TentaGel resin provided with HMPPA linker was treated with IPy_2BF_4 in DCM. Although this approach is not free from byproducts relative to the halogenation of the linker, it clearly shows the feasibility of the methodology. **a**, Non-halogenated linear precursor of compound **11** obtained through routine amide couplings. **b**, On-resin iodination of the Tyr residue to yield derivative N-terminal Fmoc-protected of **11** (41% conversion). Reaction conditions: IPy_2BF_4 (2.2 eq.), DCM, r.t. (1 x 10 min, 1 x 50 min). **c**, On-resin iodination of the Tyr residue followed by Fmoc protecting group removal and N-terminal acetylation. Reaction conditions: (i) IPy_2BF_4 (4.4 eq.), DCM, r.t. (1 x 1 h), (ii) piperidine-DMF (1:4) (1 x 1 min, 2 x 5 min), (iii) DIEA (10.0 eq.), acetic anhydride (10.0 eq.), DMF, r.t., 30 min. **d**, HPLC-MS chromatogram reference of the halogenated compound **11**. All the peptides were cleaved from the resin with TFA-DCM (95:5), r.t, 1h to be analyzed by HPLC-MS. Gradient from 5 to 100% ACN (0,1% FA).

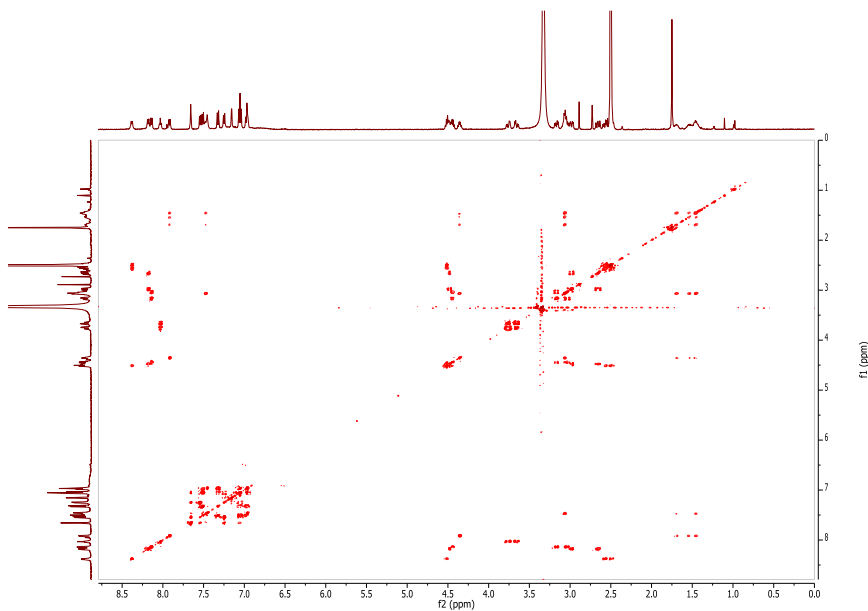


Supplementary Figure 25 | Minimized geometries of compounds 10 and 12 generated by the Spartan '14 suite.⁸

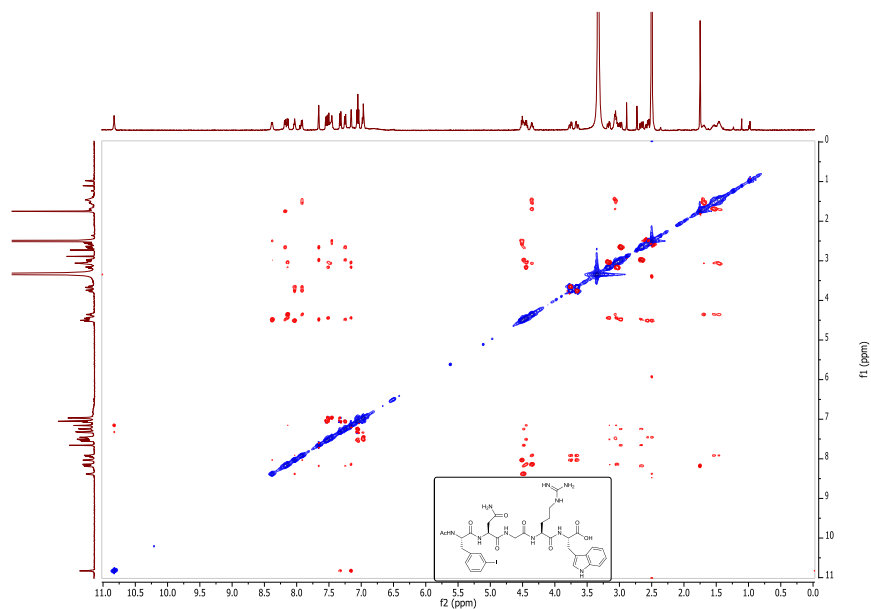




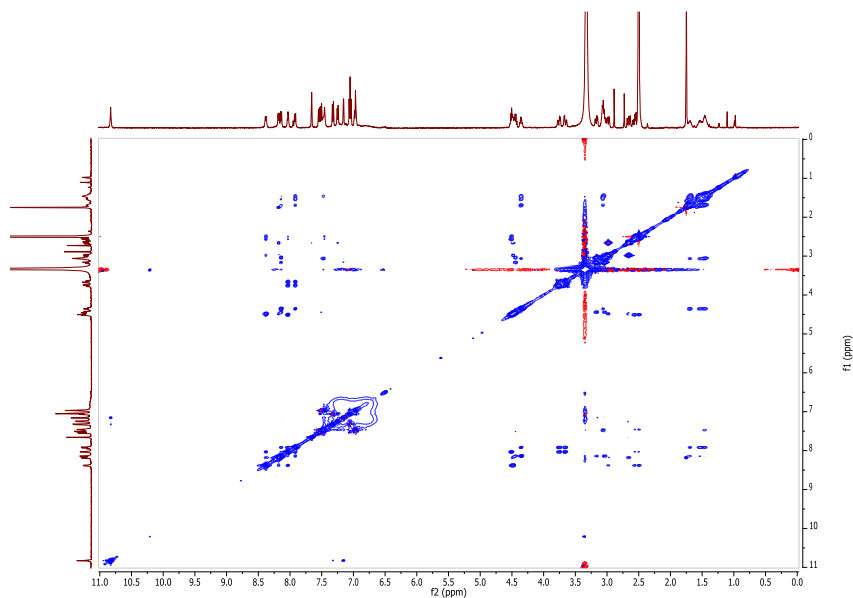
Supplementary Figure 28 | COSY NMR spectrum of compound Ac-*m*-I-Phe-Asn-Gly-Arg-Trp-OH (1g).



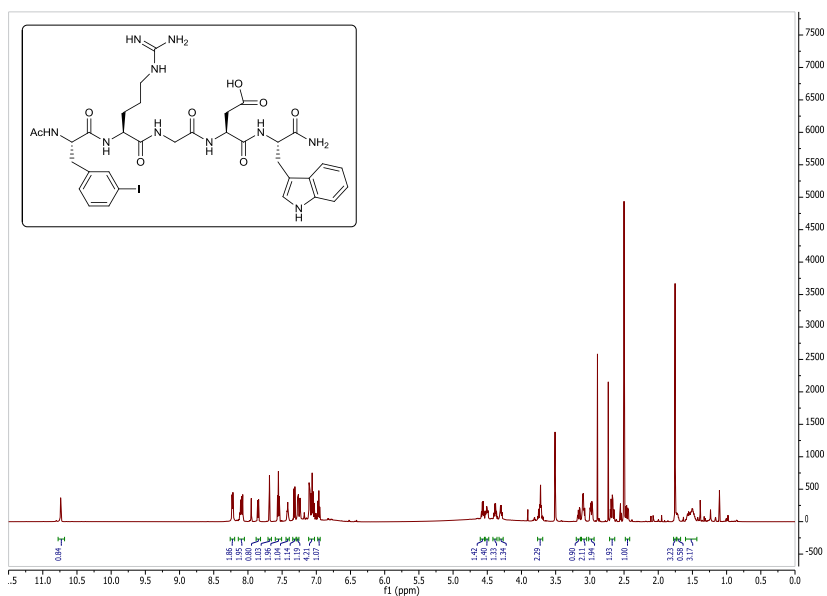
Supplementary Figure 29 | TOCSY NMR spectrum of compound Ac-*m*-I-Phe-Asn-Gly-Arg-Trp-OH (1g).



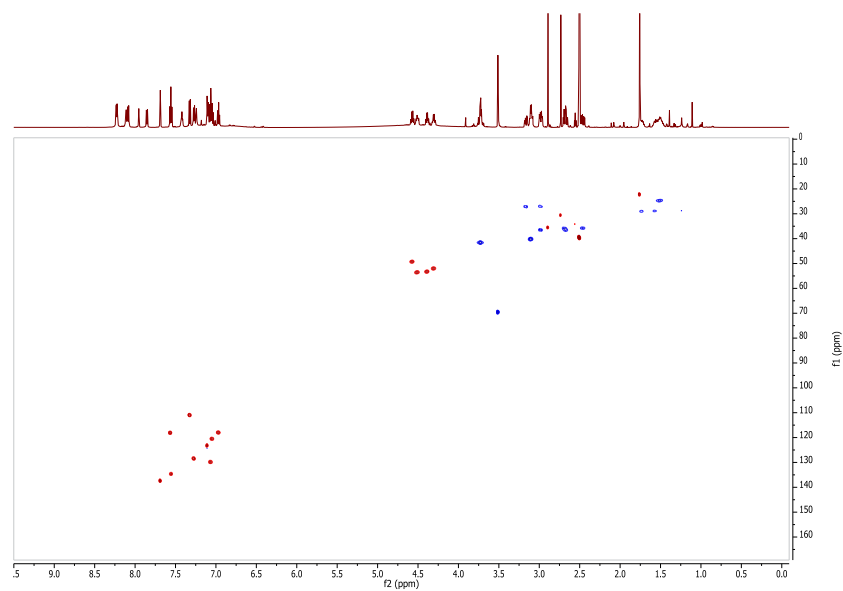
Supplementary Figure 30 | ROESY NMR spectrum of compound Ac-*m*-I-Phe-Asn-Gly-Arg-Trp-OH (1g).



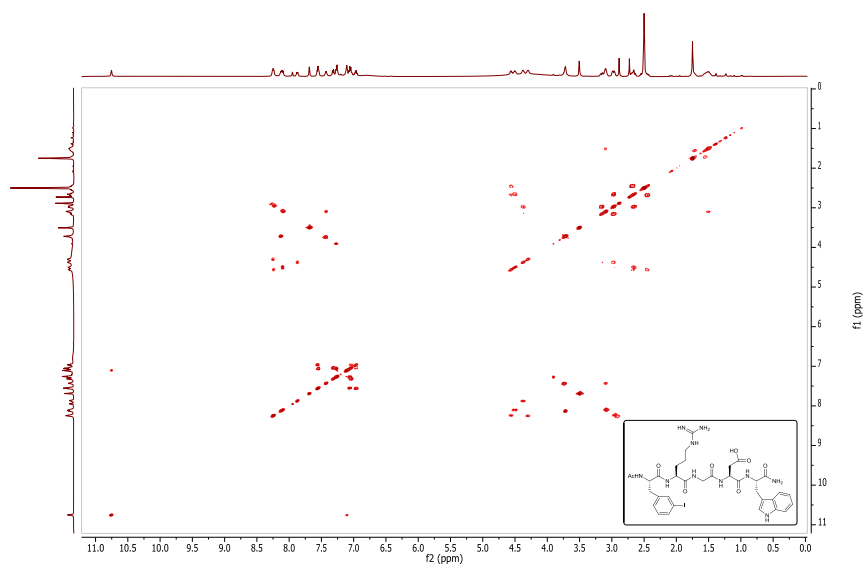
Supplementary Figure 31 | NOESY NMR spectrum of compound Ac-*m*-I-Phe-Asn-Gly-Arg-Trp-OH (1g).



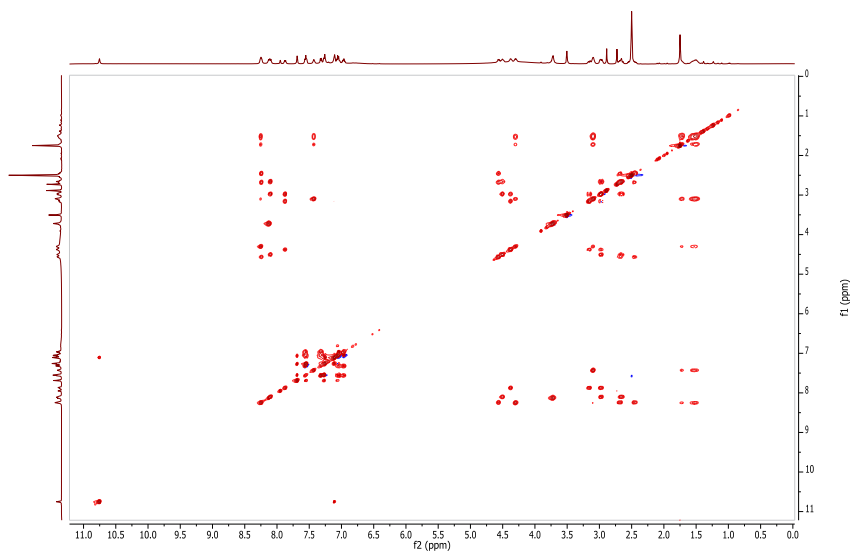
Supplementary Figure 32 | ^1H NMR spectrum of compound Ac-m-I-Phe-Arg-Gly-Asp-Trp-OH (1h).



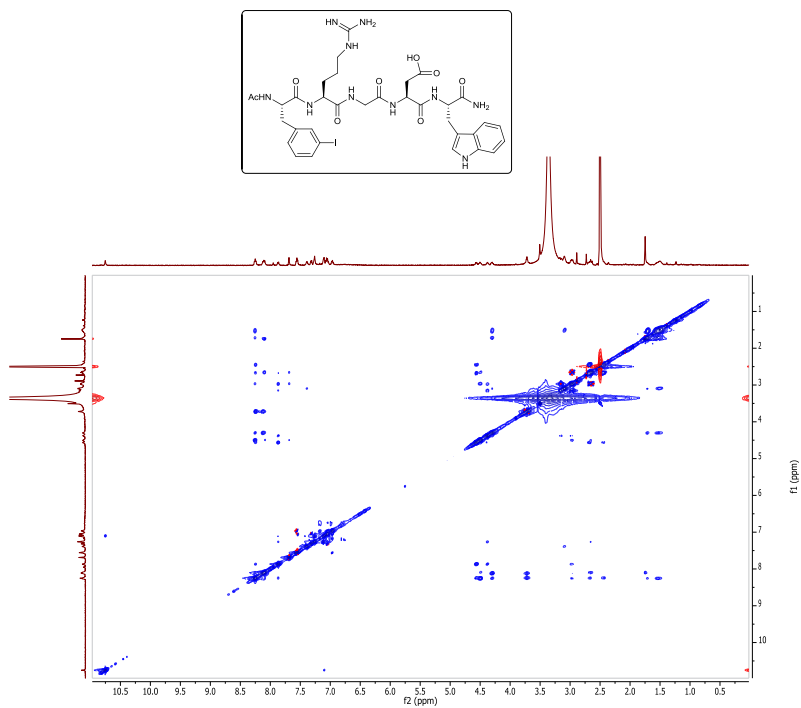
Supplementary Figure 33 | ^1H - ^{13}C HSQC NMR spectrum of compound Ac-m-I-Phe-Arg-Gly-Asp-Trp-OH (1h).



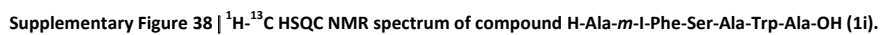
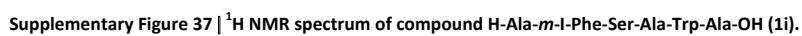
Supplementary Figure 34 | COSY NMR spectrum of compound Ac-*m*-I-Phe-Arg-Gly-Asp-Trp-OH (1h).

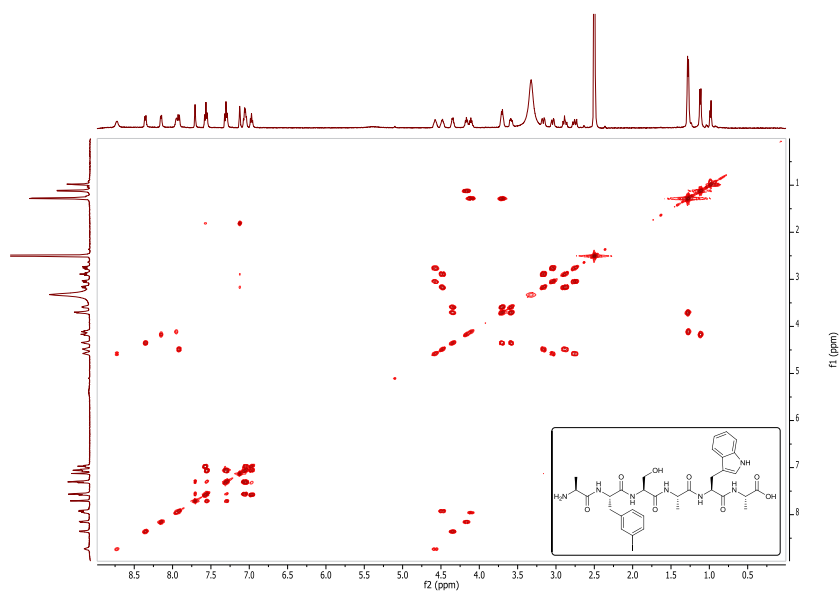


Supplementary Figure 35 | TOCSY NMR spectrum of compound Ac-*m*-I-Phe-Arg-Gly-Asp-Trp-OH (1h).

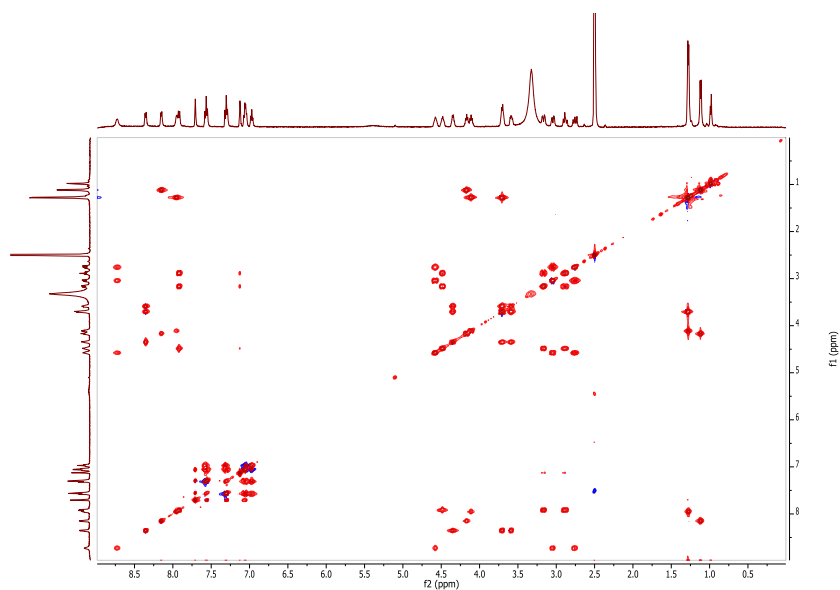


Supplementary Figure 36 | NOESY NMR spectrum of compound Ac-*m*-I-Phe-Arg-Gly-Asp-Trp-OH (1h).

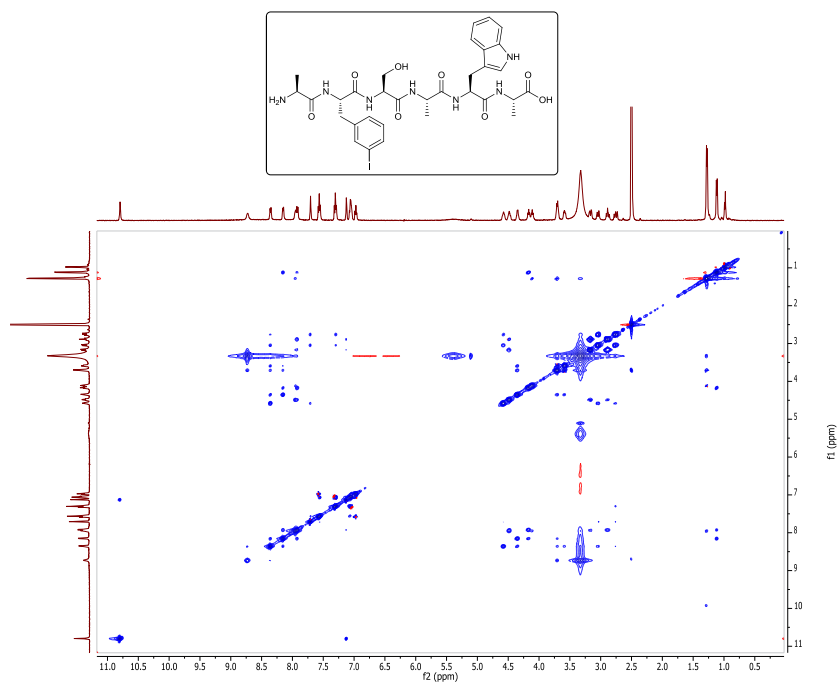




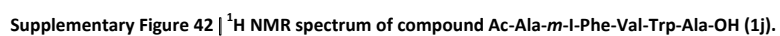
Supplementary Figure 39 | COSY NMR spectrum of compound H-Ala-*m*-I-Phe-Ser-Ala-Trp-Ala-OH (1i).

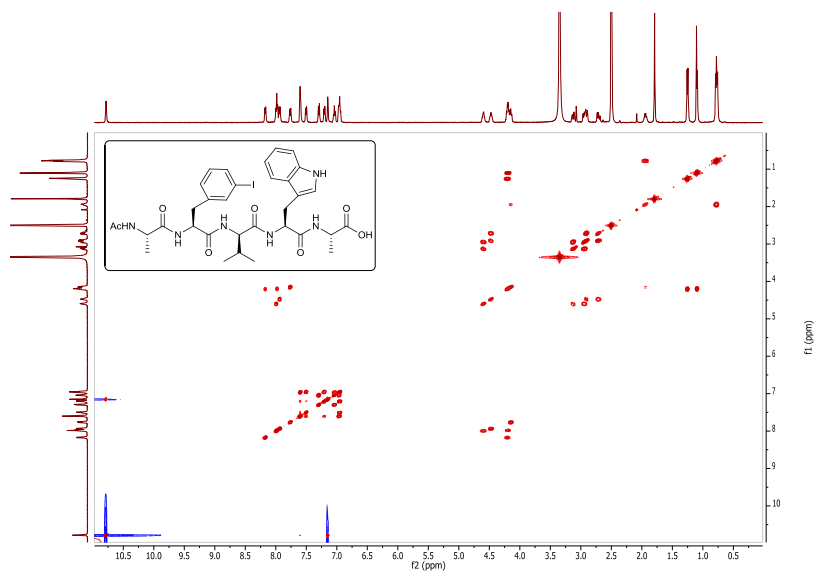


Supplementary Figure 40 | TOCSY NMR spectrum of compound H-Ala-*m*-I-Phe-Ser-Ala-Trp-Ala-OH (1i).

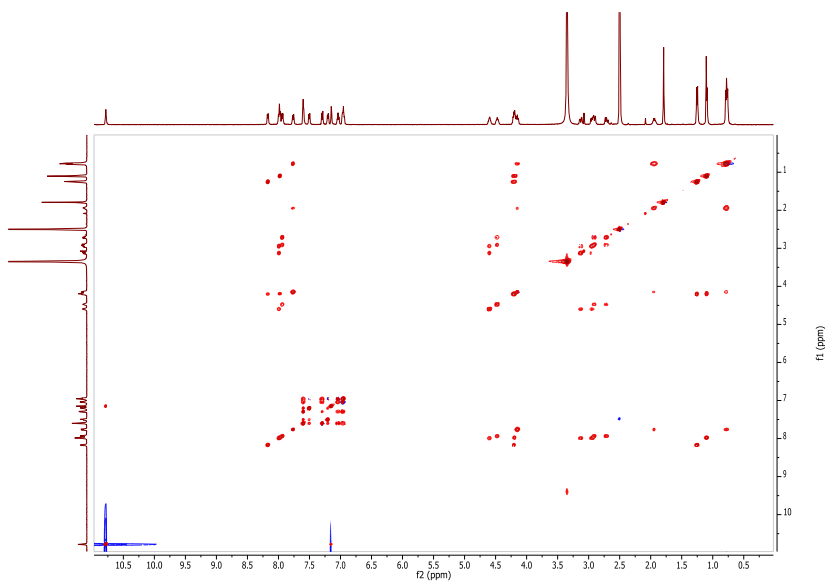


Supplementary Figure 41 | NOESY NMR spectrum of compound H-Ala-*m*-I-Phe-Ser-Ala-Trp-Ala-OH (1i).

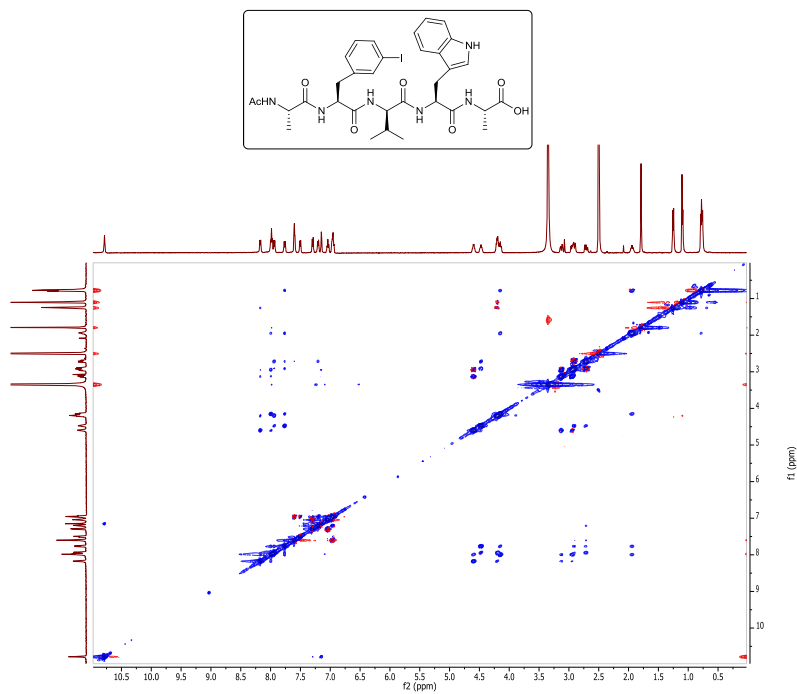




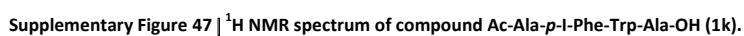
Supplementary Figure 44 | COSY NMR spectrum of compound Ac-Ala-*m*-I-Phe-Val-Trp-Ala-OH (1j).

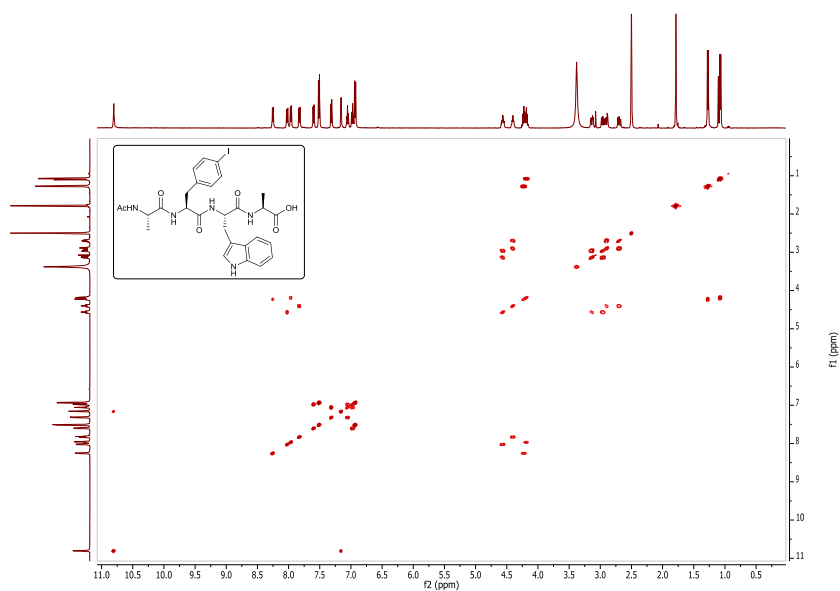


Supplementary Figure 45 | TOCSY NMR spectrum of compound Ac-Ala-*m*-I-Phe-Val-Trp-Ala-OH (1j).

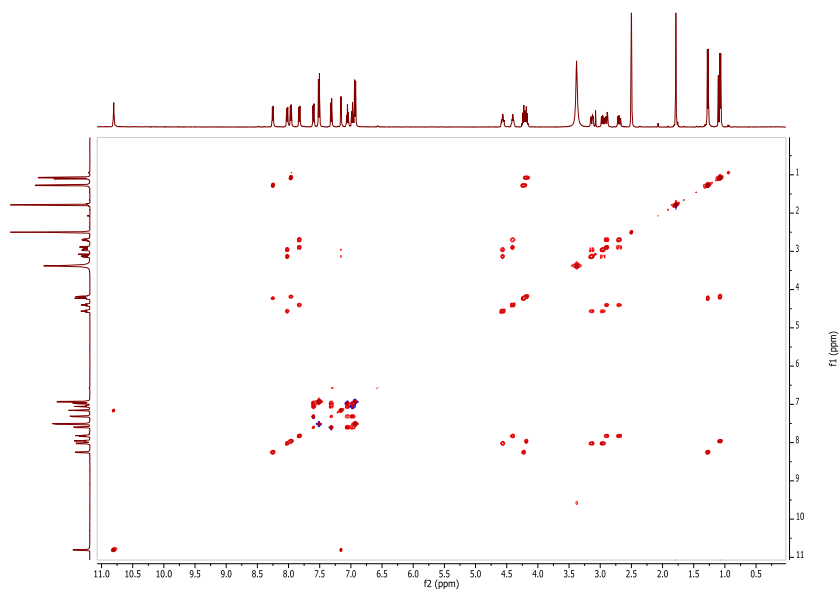


Supplementary Figure 46 | NOESY NMR spectrum of compound Ac-Ala-*m*-I-Phe-Val-Trp-Ala-OH (1j).

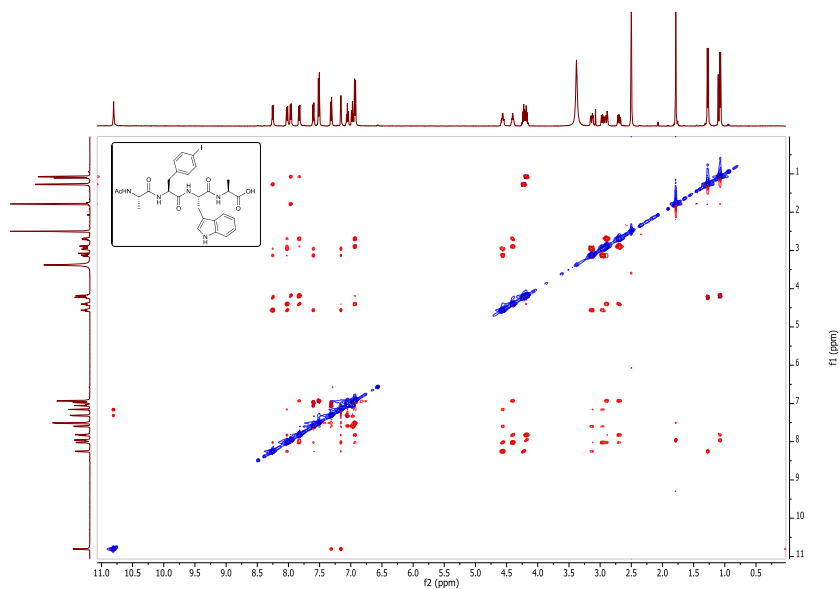




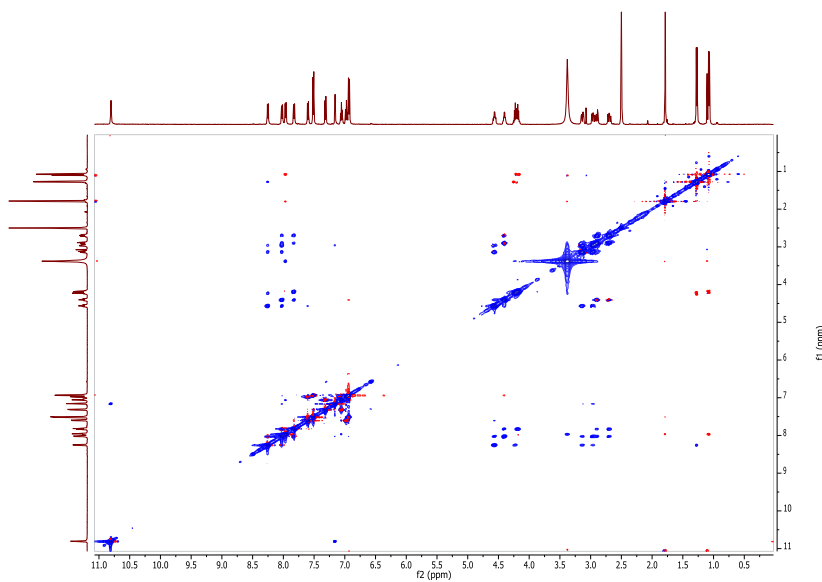
Supplementary Figure 49 | COSY NMR spectrum of compound Ac-Ala-*p*-I-Phe-Trp-Ala-OH (1k).



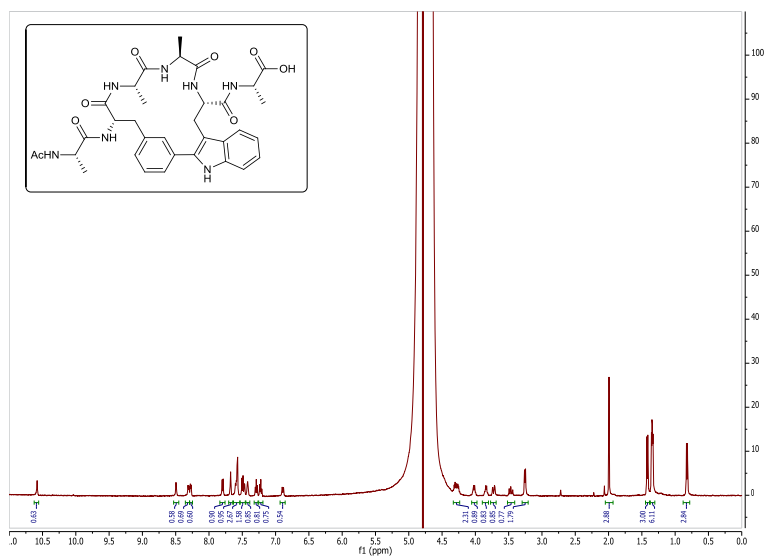
Supplementary Figure 50 | TOCSY NMR spectrum of compound Ac-Ala-*p*-I-Phe-Trp-Ala-OH (1k).



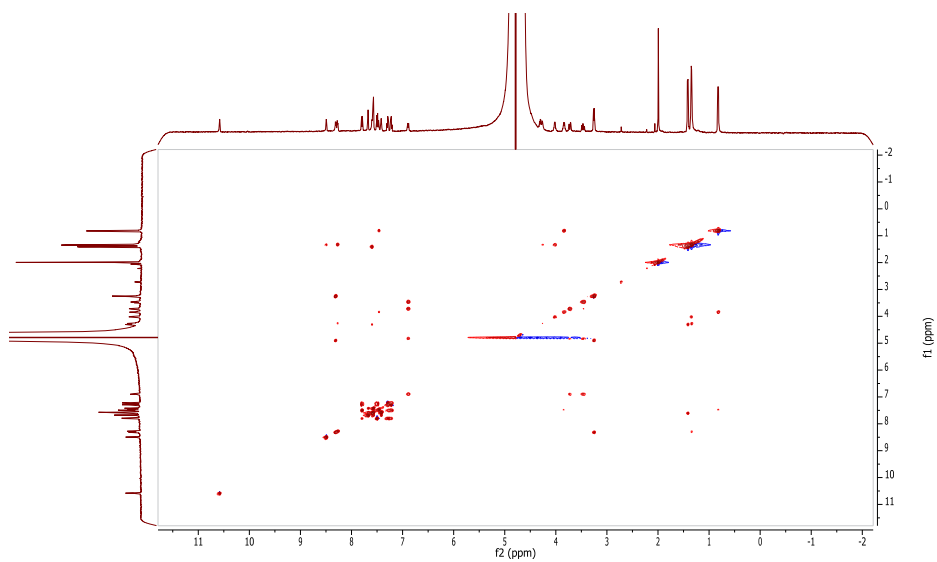
Supplementary Figure 51 | ROESY NMR spectrum of compound Ac-Ala-*p*-I-Phe-Trp-Ala-OH (1k).



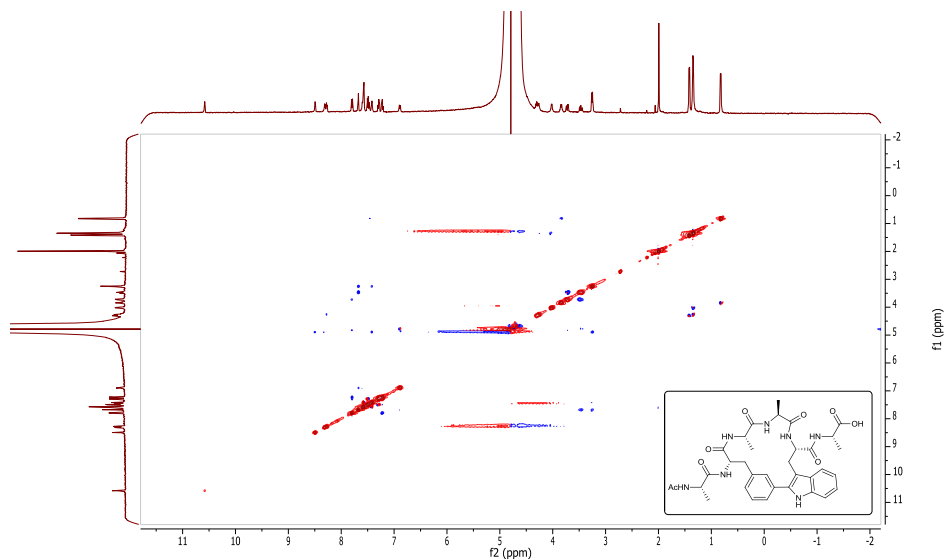
Supplementary Figure 52 | NOESY NMR spectrum of compound Ac-Ala-*p*-I-Phe-Trp-Ala-OH (1k).



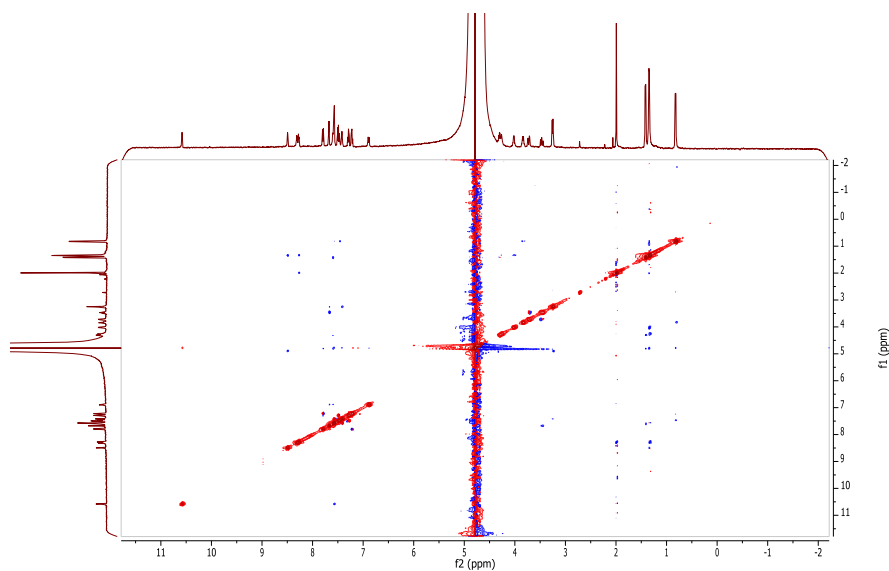
Supplementary Figure 53 | ^1H NMR spectrum of compound Ac-Ala-(Cyclo-*m*)-[Phe-Ala-Ala-Trp]-Ala-OH (**2b**).



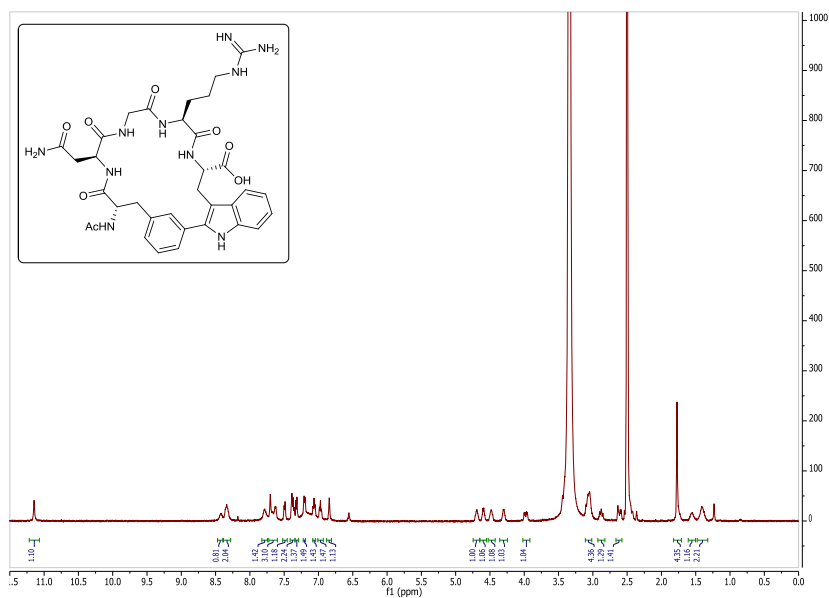
Supplementary Figure 54 | TOCSY NMR spectrum of compound Ac-Ala-(Cyclo-*m*)-[Phe-Ala-Ala-Trp]-Ala-OH (**2b**).



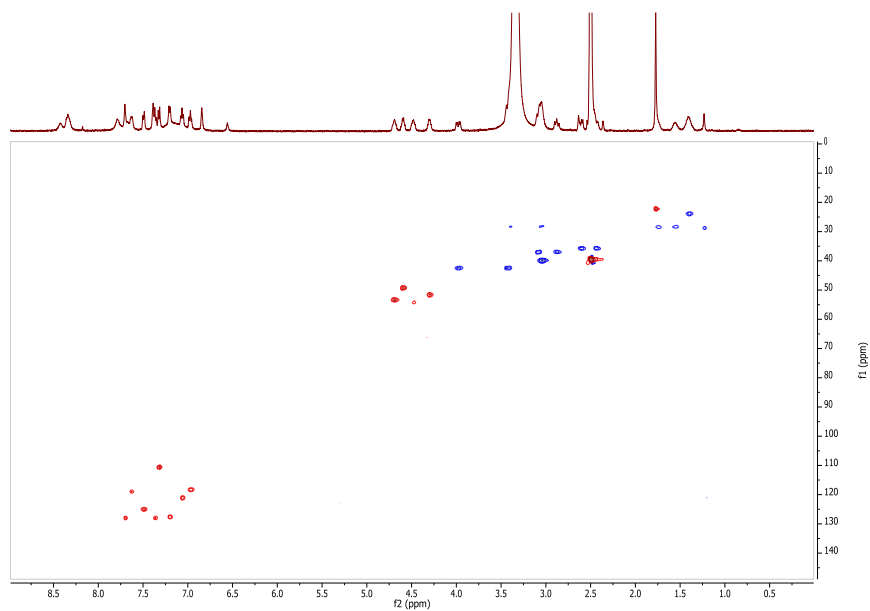
Supplementary Figure 55 | ROESY NMR spectrum of compound Ac-Ala-(Cyclo-*m*)-[Phe-Ala-Ala-Trp]-Ala-OH (2b).



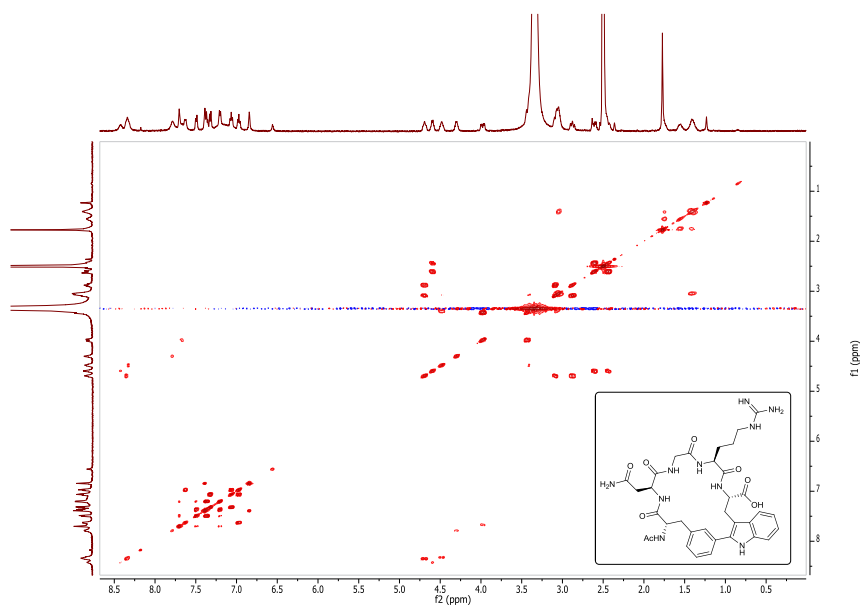
Supplementary Figure 56 | NOESY NMR spectrum of compound Ac-Ala-(Cyclo-*m*)-[Phe-Ala-Ala-Trp]-Ala-OH (2b).



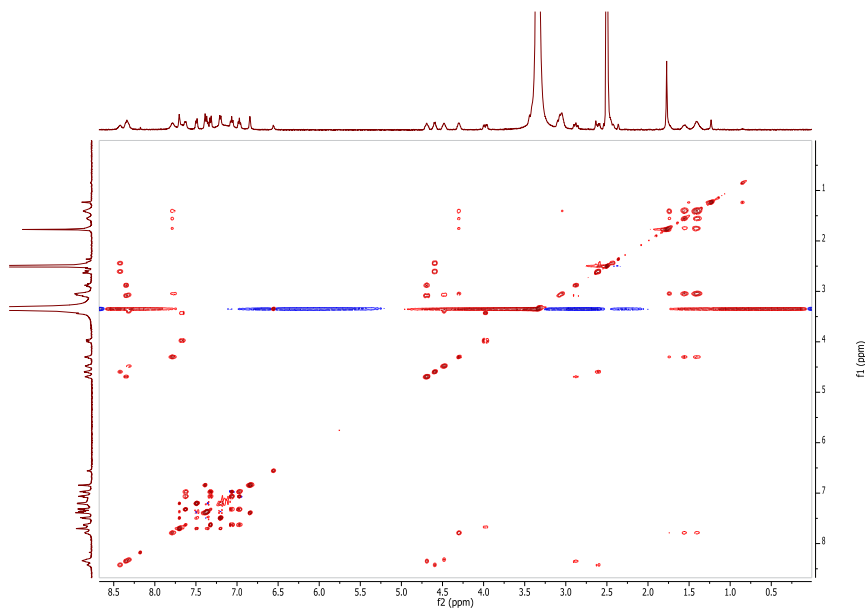
Supplementary Figure 57 | ^1H NMR spectrum of compound Ac-(Cyclo-m)-[Phe-Asn-Gly-Arg-Trp]-OH (2g).



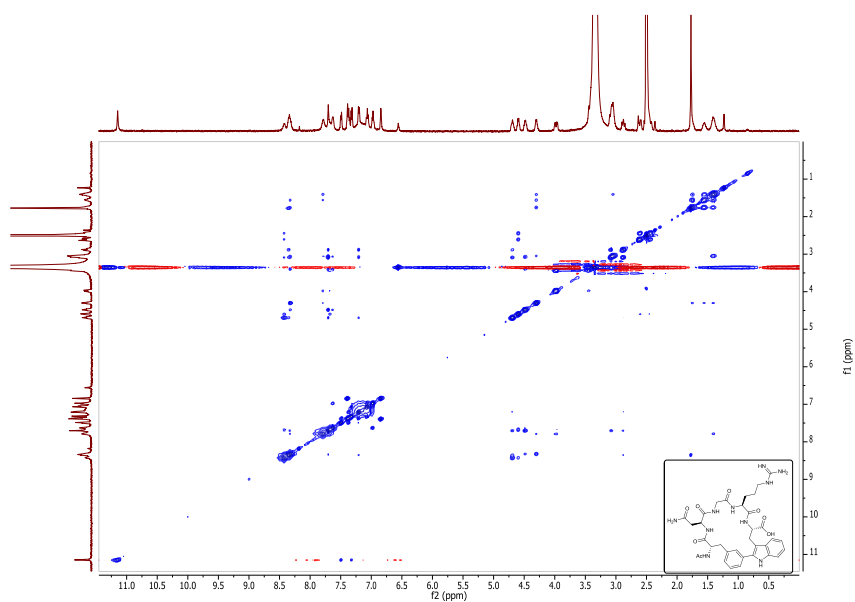
Supplementary Figure 58 | ^1H - ^{13}C HSQC NMR spectrum of compound Ac-(Cyclo-m)-[Phe-Asn-Gly-Arg-Trp]-OH (2g).



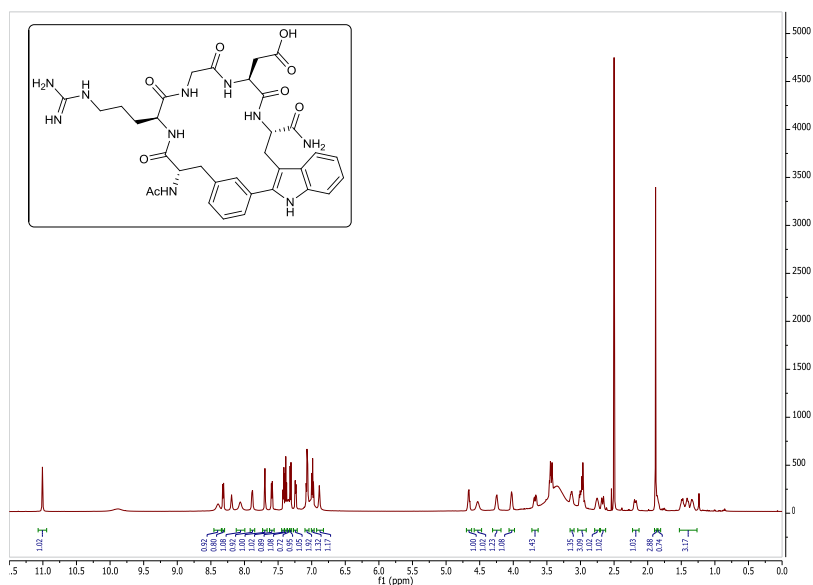
Supplementary Figure 59 | COSY NMR spectrum of compound Ac-(Cyclo-*m*)-[Phe-Asn-Gly-Arg-Trp]-OH (2g).



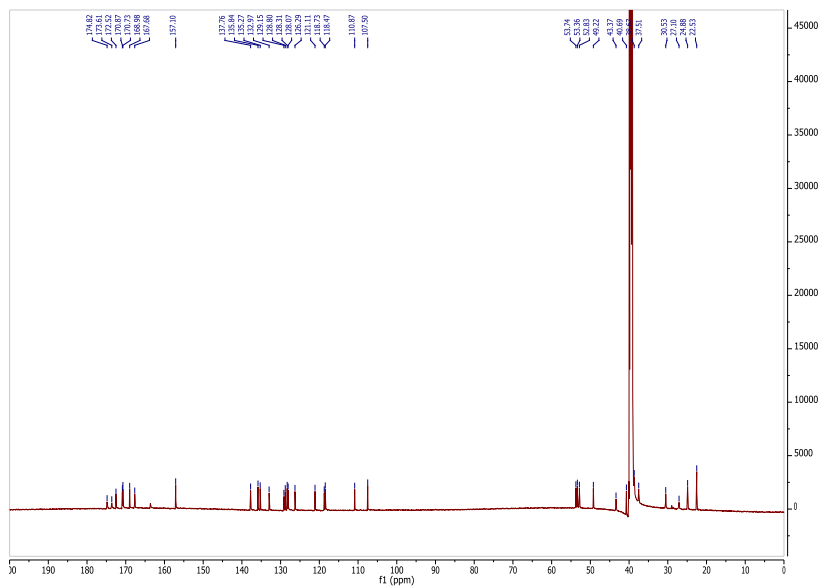
Supplementary Figure 60 | TOCSY NMR spectrum of compound Ac-(Cyclo-*m*)-[Phe-Asn-Gly-Arg-Trp]-OH (2g).



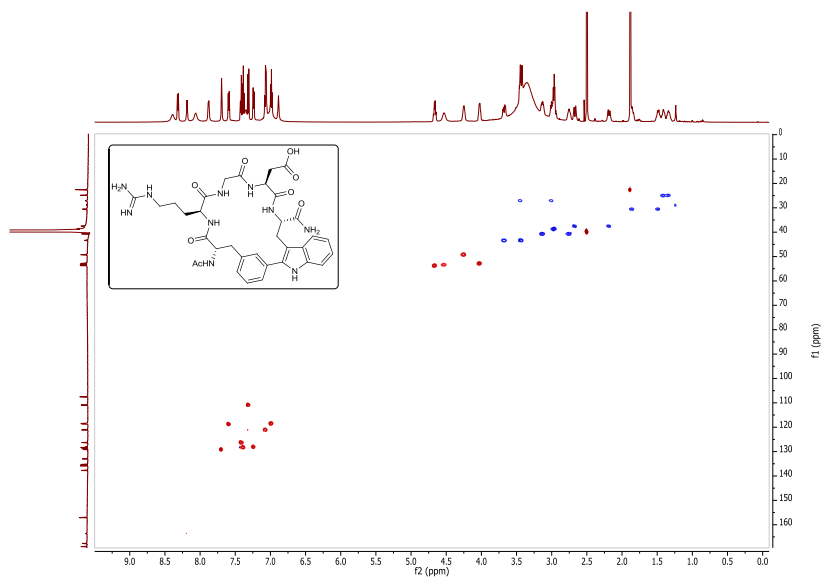
Supplementary Figure 61 | NOESY NMR spectrum of compound Ac-(Cyclo-*m*)-[Phe-Asn-Gly-Arg-Trp]-OH (2g).



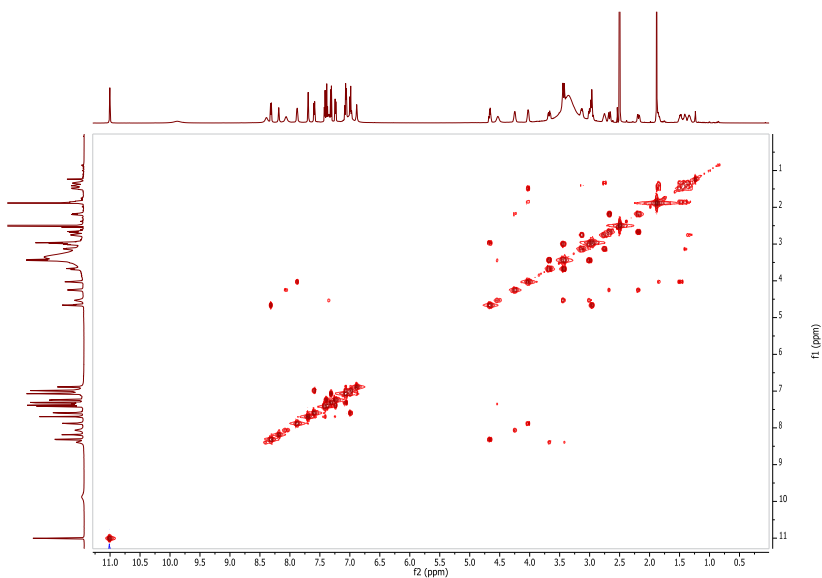
Supplementary Figure 62 | ^1H NMR spectrum of compound Ac-(Cyclo-*m*)-[Phe-Arg-Gly-Asp-Trp]-NH₂ (2h).



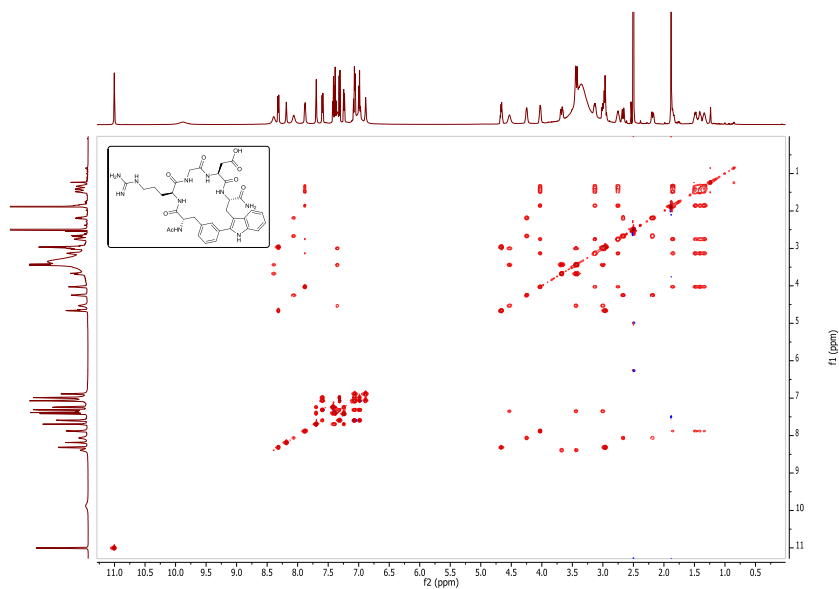
Supplementary Figure 63 | ^{13}C NMR spectrum of compound Ac-(Cyclo-*m*)-[Phe-Arg-Gly-Asp-Trp]-NH₂ (2h).



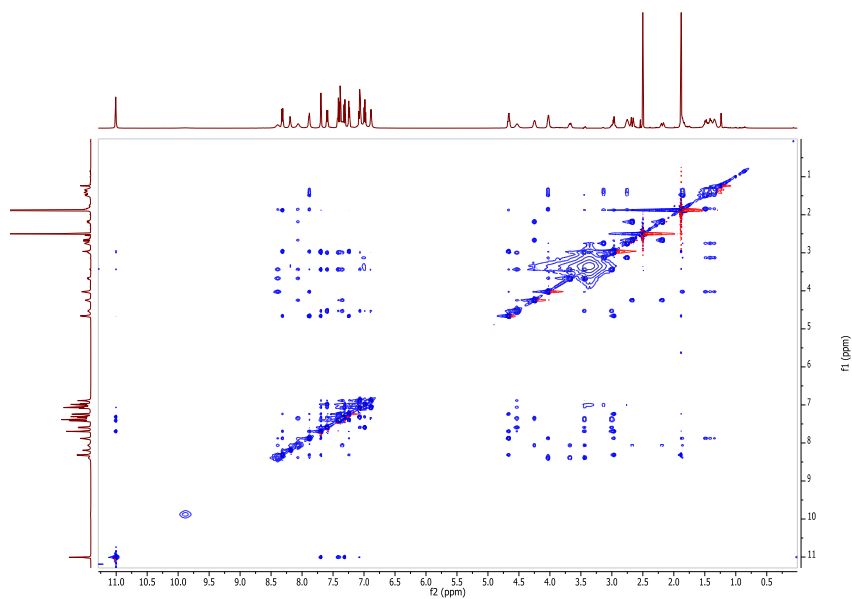
Supplementary Figure 64 | ^1H - ^{13}C HSQC NMR spectrum of compound Ac-(Cyclo-*m*)-[Phe-Arg-Gly-Asp-Trp]-NH₂ (2h).



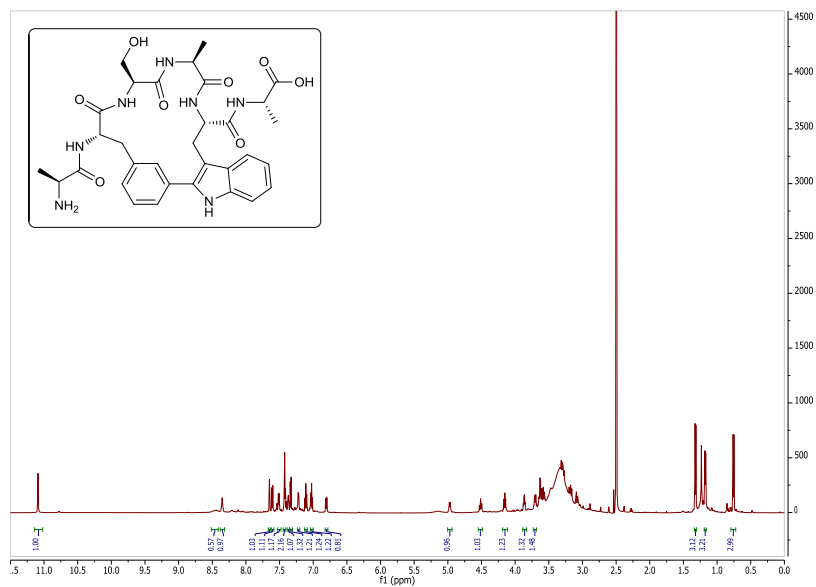
Supplementary Figure 65 | COSY NMR spectrum of compound Ac-(Cyclo-*m*)-[Phe-Arg-Gly-Asp-Trp]-NH₂ (2h).



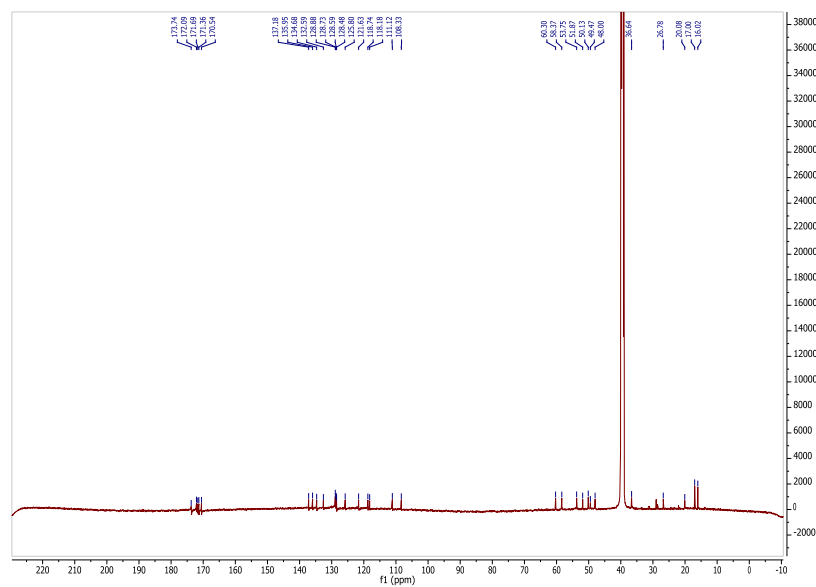
Supplementary Figure 66 | TOCSY NMR spectrum of compound Ac-(Cyclo-*m*)-[Phe-Arg-Gly-Asp-Trp]-NH₂ (2h).



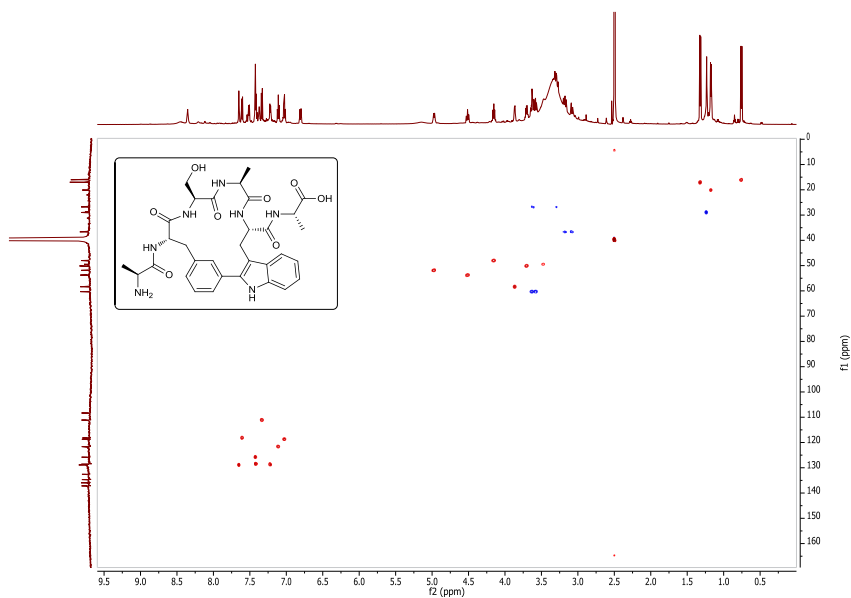
Supplementary Figure 67 | NOESY NMR spectrum of compound Ac-(Cyclo-*m*)-[Phe-Arg-Gly-Asp-Trp]-NH₂ (2h).



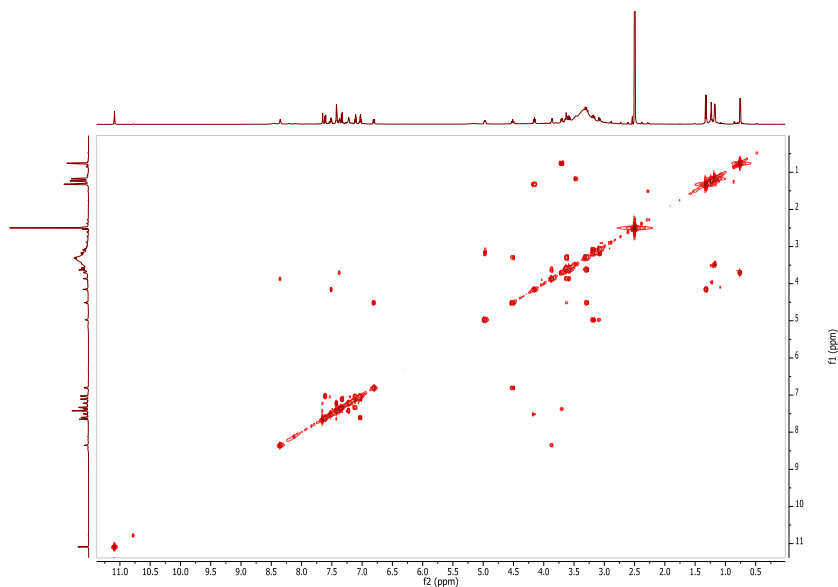
Supplementary Figure 68 | ^1H NMR spectrum of compound H-Ala-(Cyclo-m)-[Phe-Ser-Ala-Trp]-Ala-OH (2i).



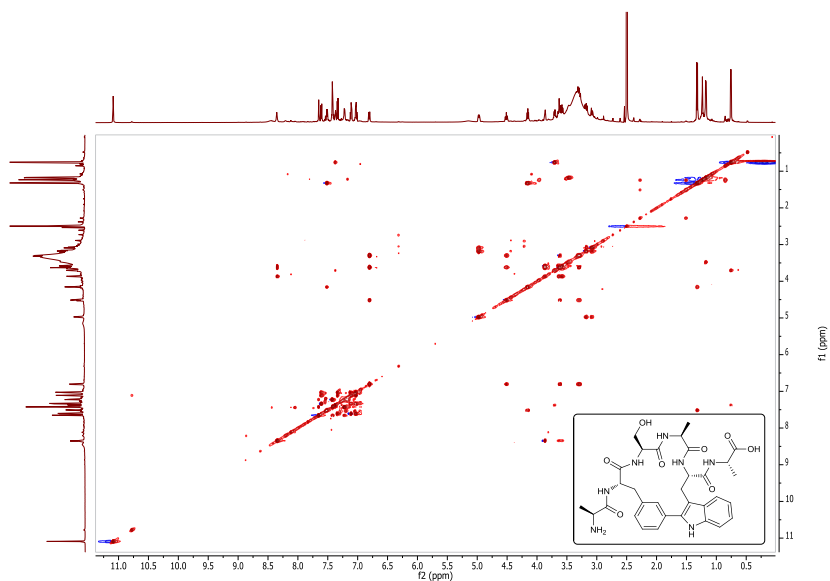
Supplementary Figure 69 | ^{13}C NMR spectrum of compound H-Ala-(Cyclo-m)-[Phe-Ser-Ala-Trp]-Ala-OH (2i).



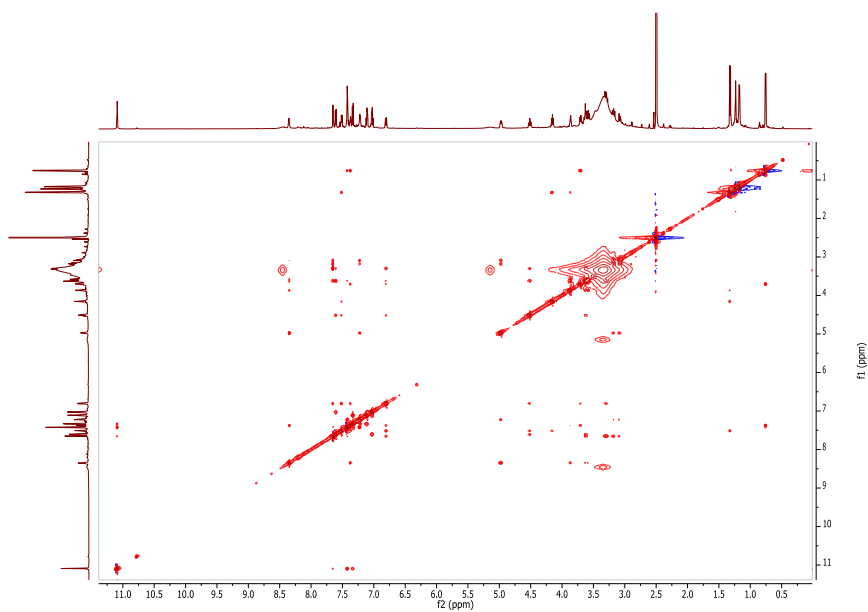
Supplementary Figure 70 | ^1H - ^{13}C HSQC NMR spectrum of compound H-Ala-(Cyclo-*m*)-[Phe-Ser-Ala-Trp]-Ala-OH (2i).



Supplementary Figure 71 | COSY NMR spectrum of compound H-Ala-(Cyclo-*m*)-[Phe-Ser-Ala-Trp]-Ala-OH (2i).

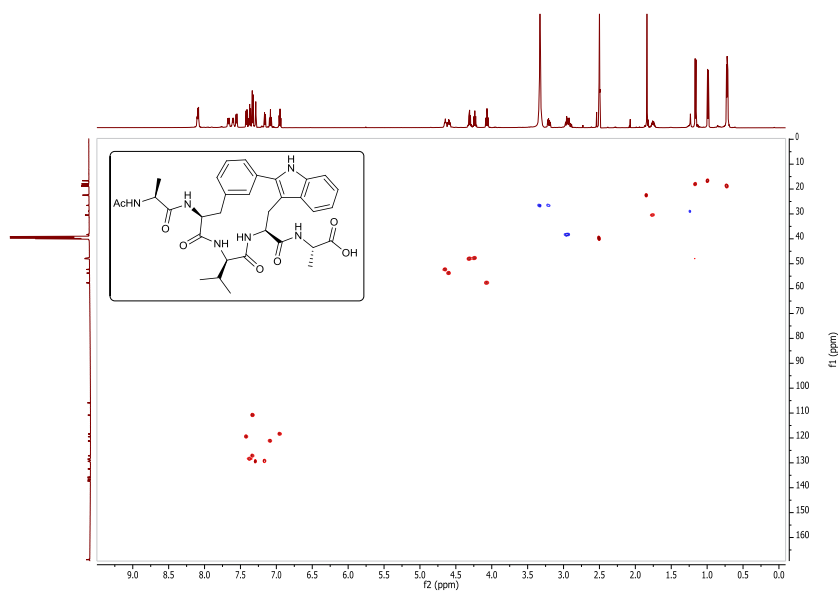


Supplementary Figure 72 | TOCSY NMR spectrum of compound H-Ala-(Cyclo-*m*)-[Phe-Ser-Ala-Trp]-Ala-OH (2i).

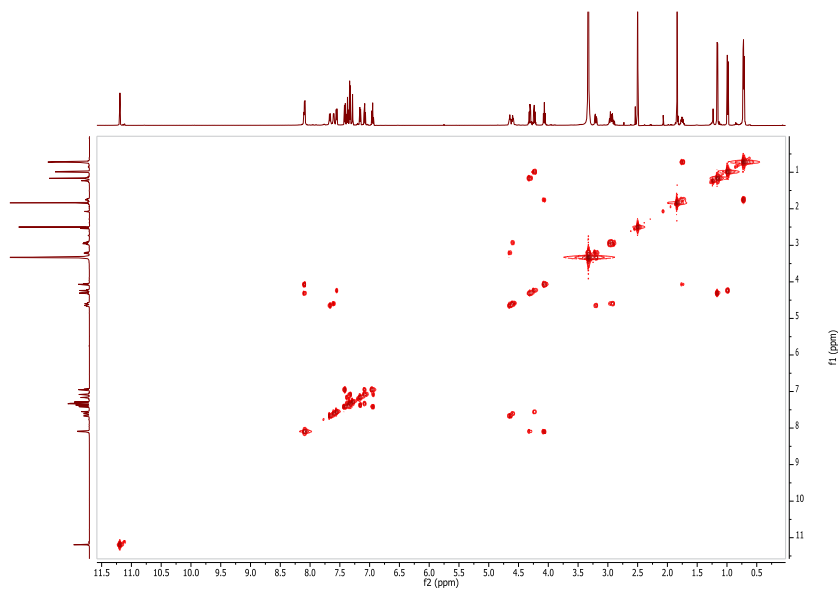


Supplementary Figure 73 | NOESY NMR spectrum of compound H-Ala-(Cyclo-*m*)-[Phe-Ser-Ala-Trp]-Ala-OH (2i).

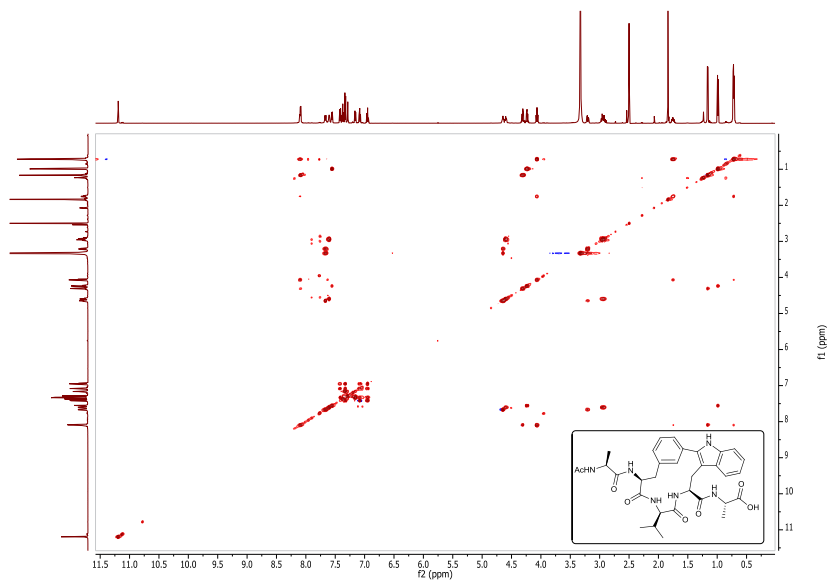




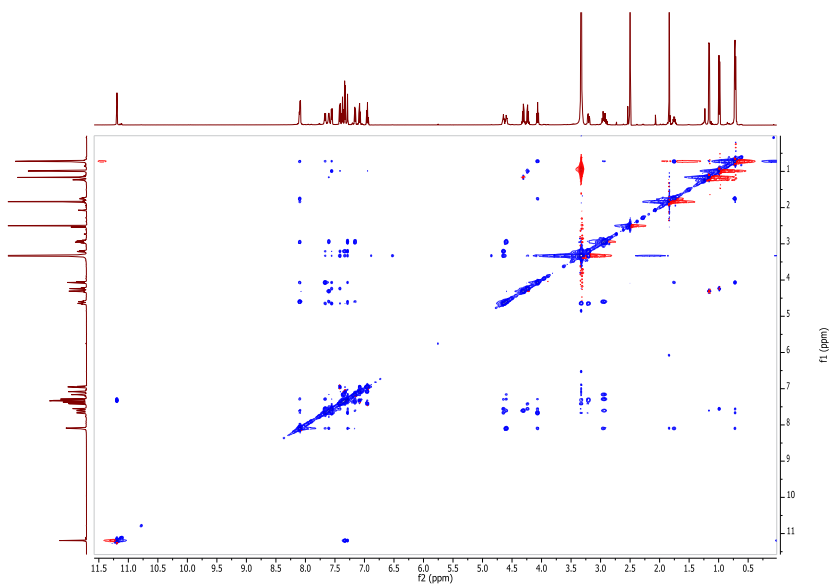
Supplementary Figure 76 | ^1H - ^{13}C HSQC NMR spectrum of compound Ac-Ala-(Cyclo-*m*)-[Phe-Val-Trp]-Ala-OH (**2j**).



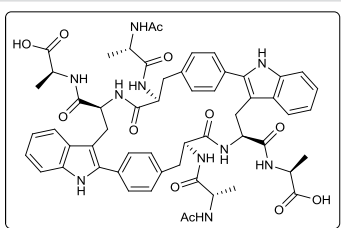
Supplementary Figure 77 | COSY NMR spectrum of compound Ac-Ala-(Cyclo-*m*)-[Phe-Val-Trp]-Ala-OH (**2j**).



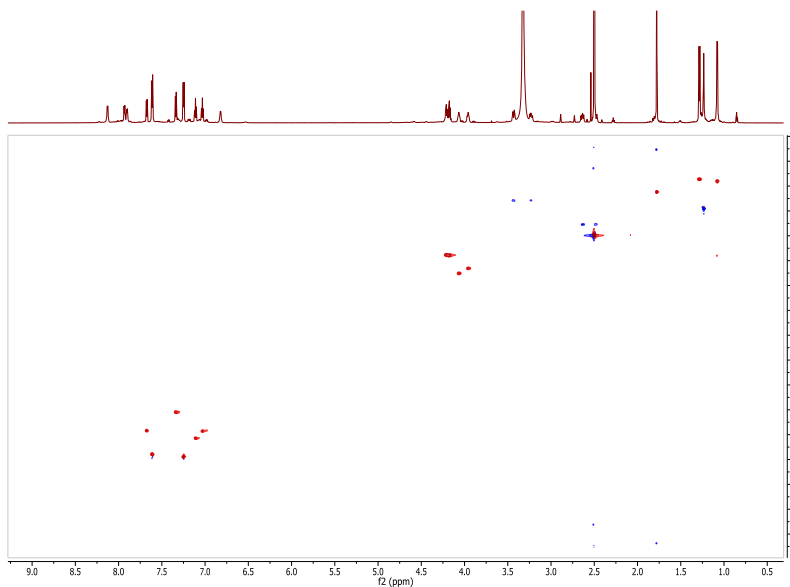
Supplementary Figure 78 | TOCSY NMR spectrum of compound Ac-Ala-(Cyclo-*m*)-[Phe-Val-Trp]-Ala-OH (2j).



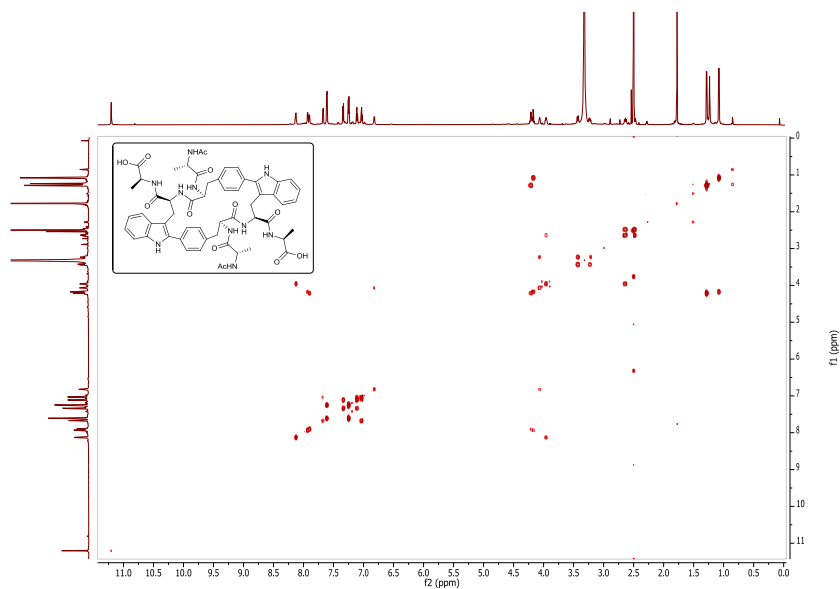
Supplementary Figure 79 | NOESY NMR spectrum of compound Ac-Ala-(Cyclo-*m*)-[Phe-Val-Trp]-Ala-OH (2j).



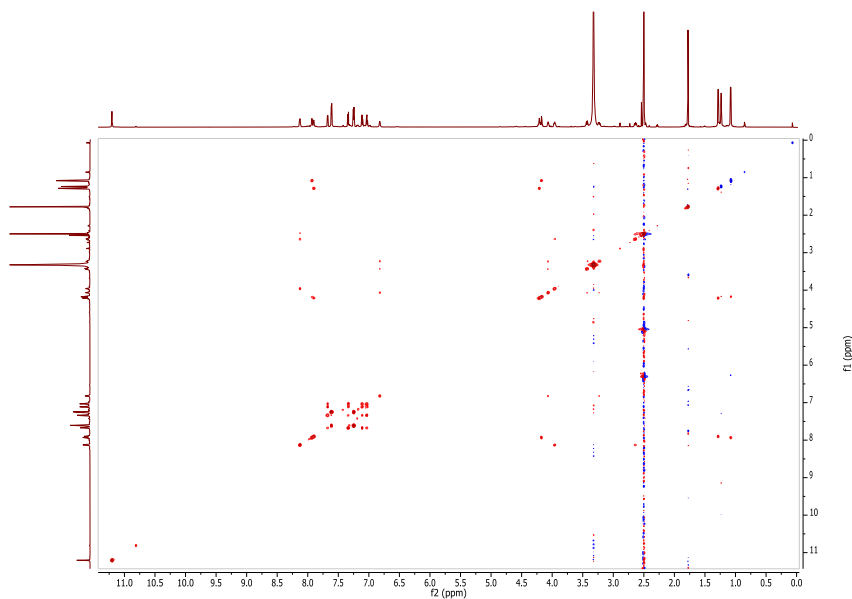
Supplementary Figure 80 | ¹H NMR spectrum of compound (Cyclo-*p,p*)bis-[Phe-Trp]-(Ac-Ala-Phe-Trp-Ala-OH) (2k).



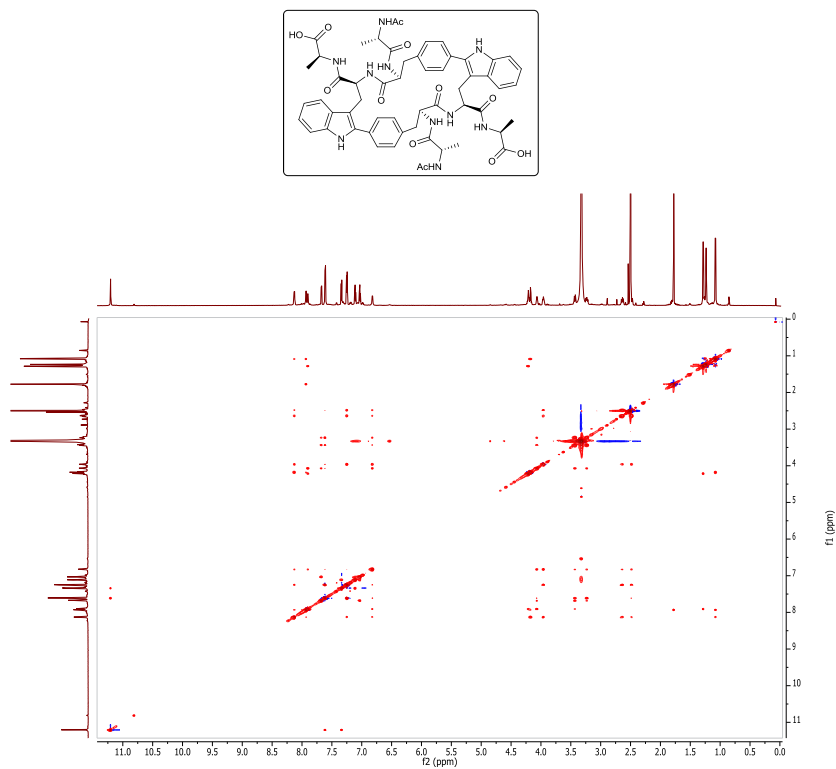
Supplementary Figure 81 | ^1H - ^{13}C HSQC NMR spectrum of compound (Cyclo-*p,p*)bis-[Phe-Trp]-(Ac-Ala-Phe-Trp-Ala-OH) (2k).



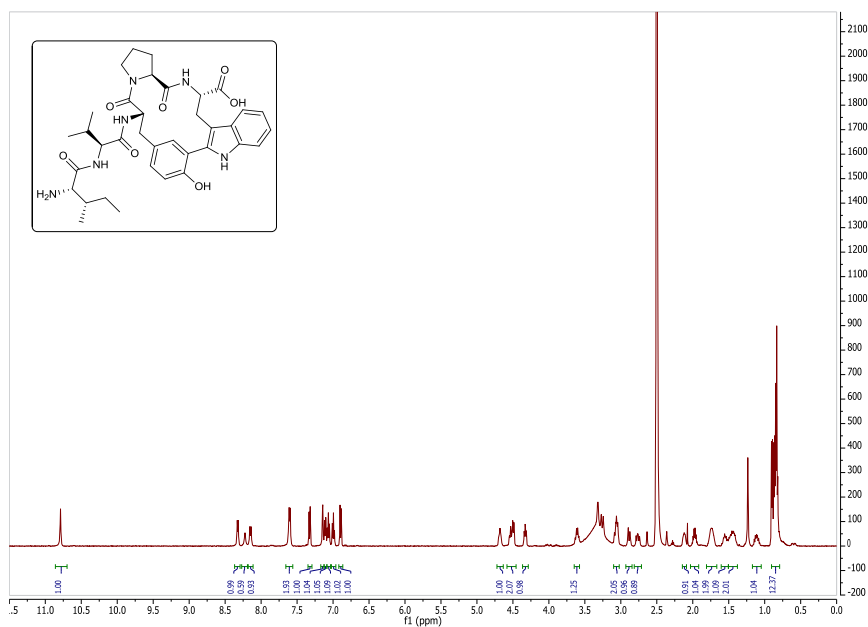
Supplementary Figure 82 | COSY NMR spectrum of compound (Cyclo-*p,p*)bis-[Phe-Trp]-(Ac-Ala-Phe-Trp-Ala-OH) (2k).



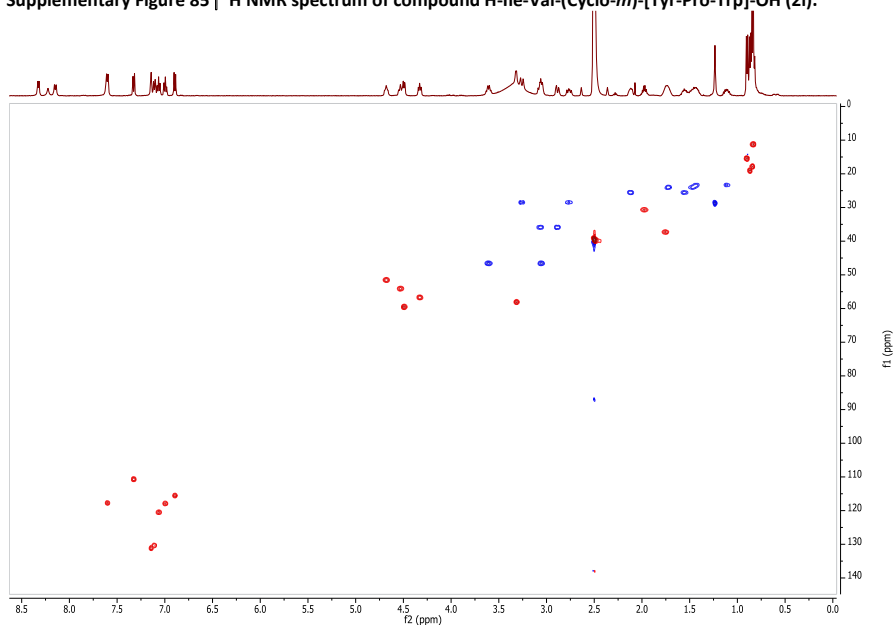
Supplementary Figure 83 | TOCSY NMR spectrum of compound (Cyclo-*p,p*)bis-[Phe-Trp]-(Ac-Ala-Phe-Trp-Ala-OH) (2k).



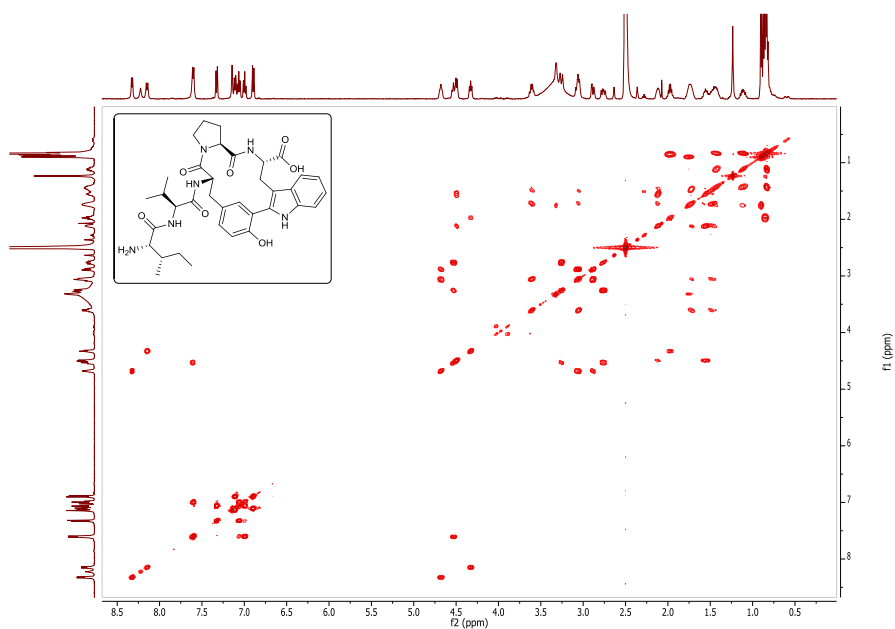
Supplementary Figure 84 | NOESY NMR spectrum of compound (Cyclo-*p,p*)bis-[Phe-Trp]-(Ac-Ala-Phe-Trp-Ala-OH) (2k).



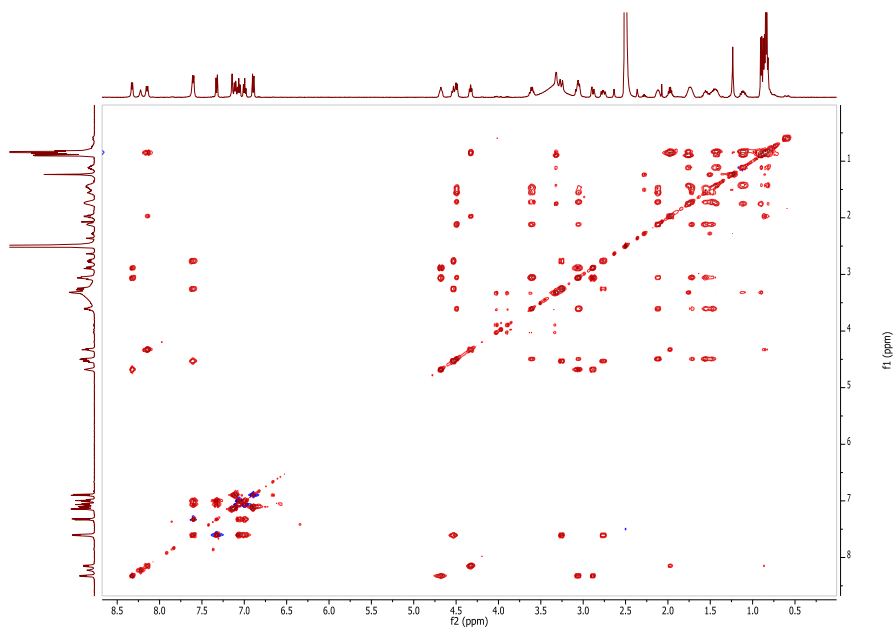
Supplementary Figure 85 | ^1H NMR spectrum of compound H-Ile-Val-(Cyclo-*m*)-[Tyr-Pro-Trp]-OH (**21**).



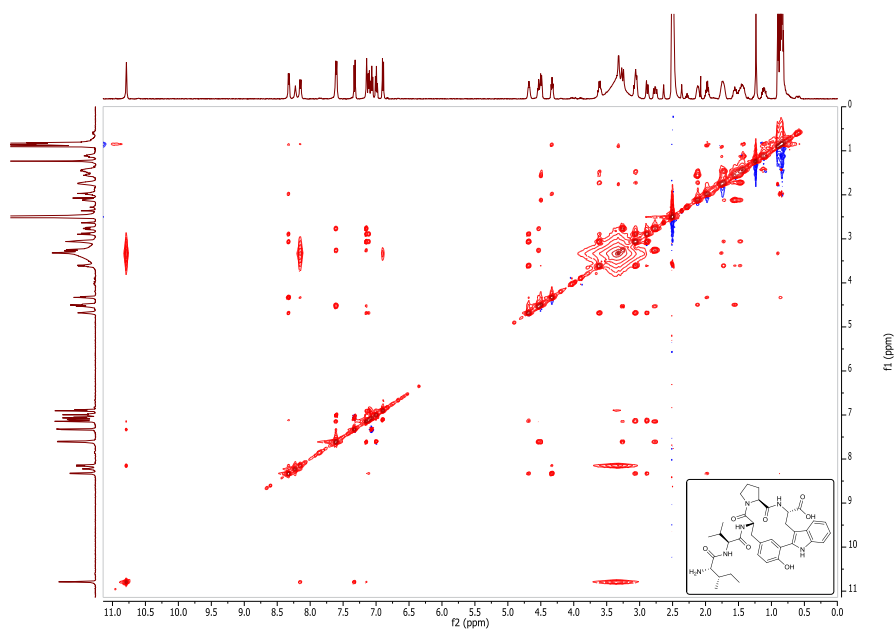
Supplementary Figure 86 | ^1H - ^{13}C HSQC NMR spectrum of compound H-Ile-Val-(Cyclo-*m*)-[Tyr-Pro-Trp]-OH (**21**).



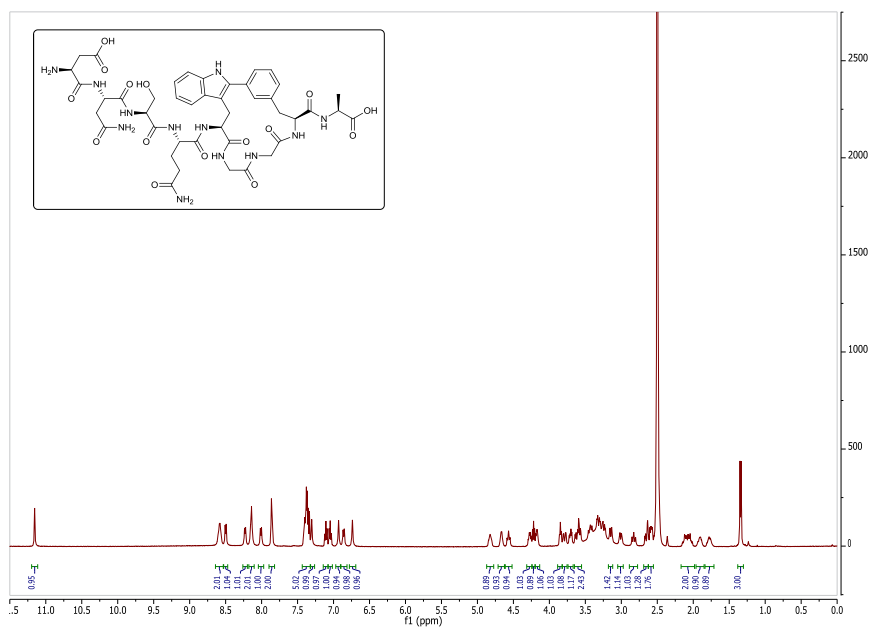
Supplementary Figure 87 | COSY NMR spectrum of compound H-Ile-Val-(Cyclo-*m*)-[Tyr-Pro-Trp]-OH (21).



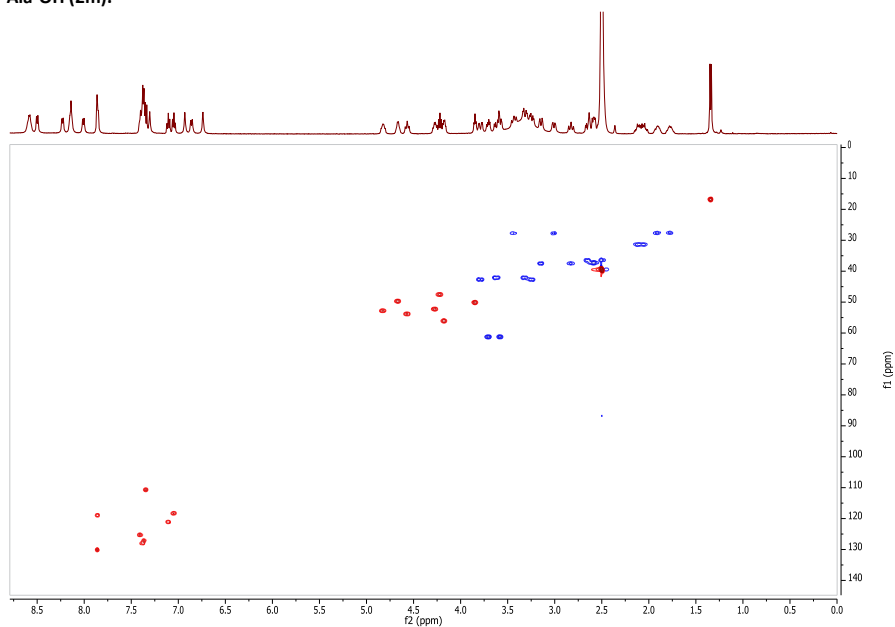
Supplementary Figure 88 | TOCSY NMR spectrum of compound H-Ile-Val-(Cyclo-*m*)-[Tyr-Pro-Trp]-OH (21).



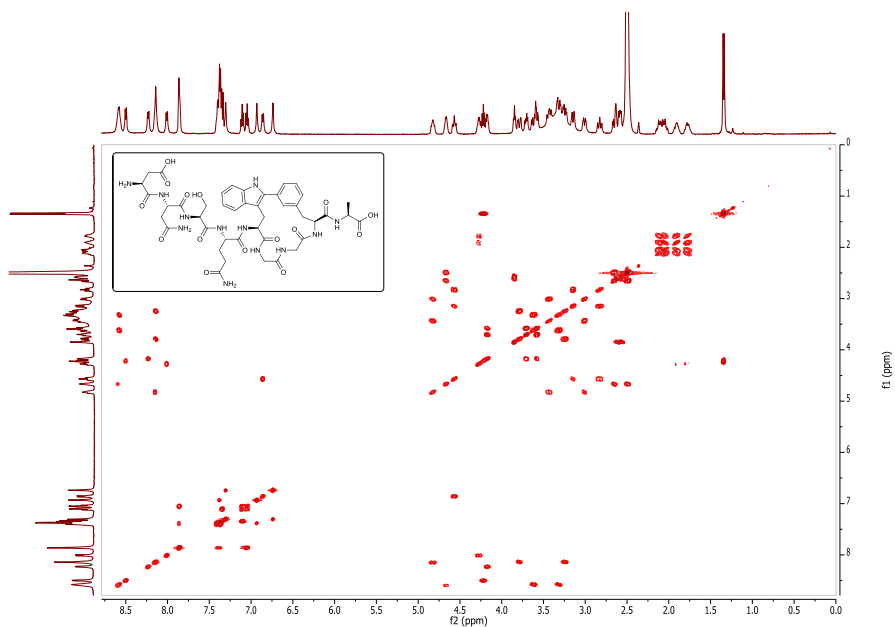
Supplementary Figure 89 | NOESY NMR spectrum of compound H-Ile-Val-(Cyclo-*m*)-[Tyr-Pro-Trp]-OH (21).



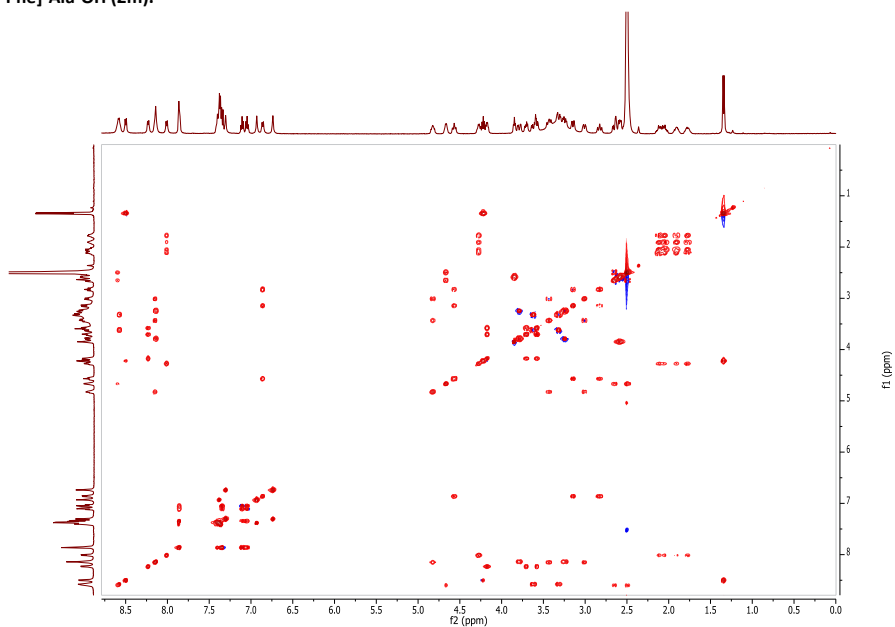
Supplementary Figure 90 | ^1H NMR spectrum of compound H-Asp-Asn-Ser-Gln-(Cyclo-*m*)-[Trp-Gly-Gly-Phe]-Ala-OH (2m).



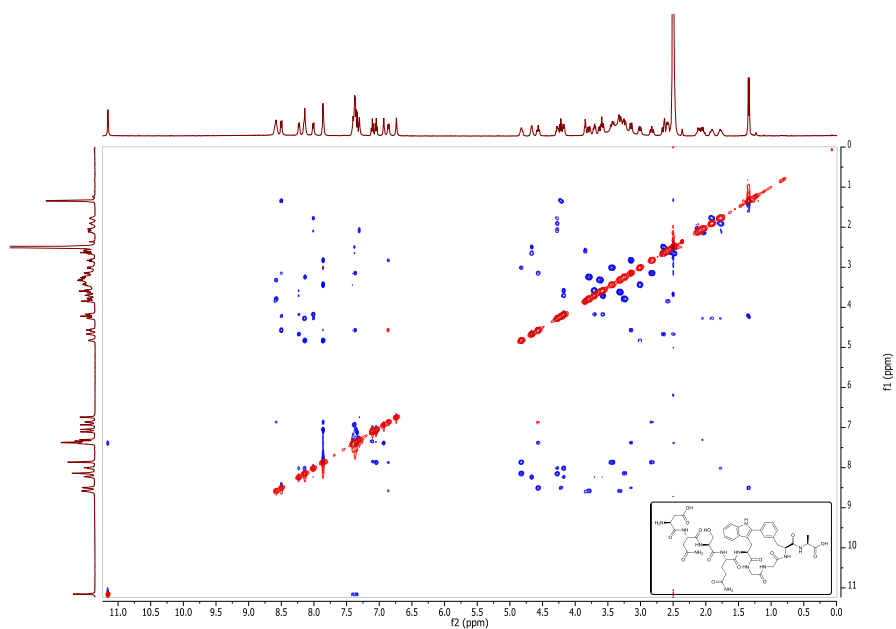
Supplementary Figure 91 | ^1H - ^{13}C HSQC NMR spectrum of compound H-Asp-Asn-Ser-Gln-(Cyclo-*m*)-[Trp-Gly-Gly-Phe]-Ala-OH (2m).



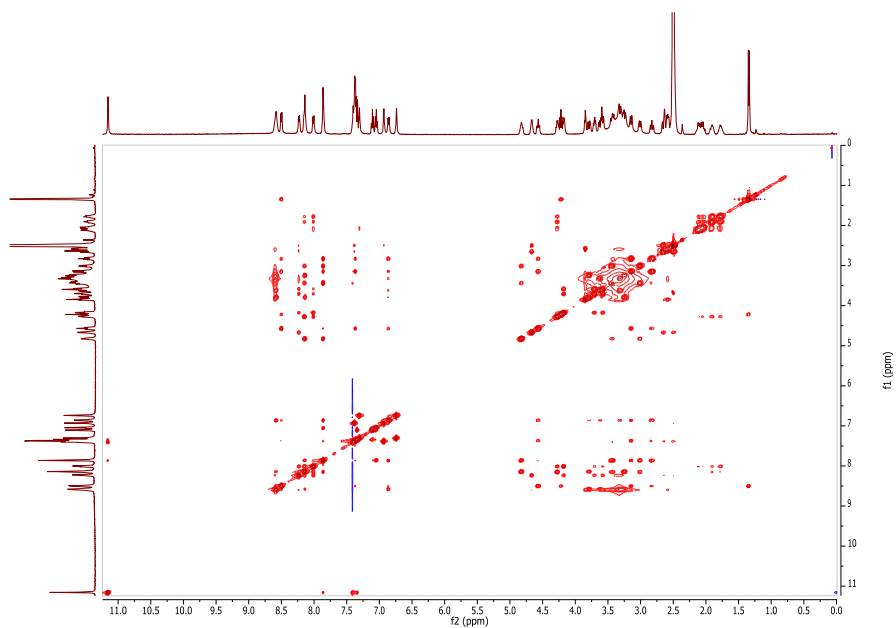
Supplementary Figure 92 | COSY NMR spectrum of compound H-Asp-Asn-Ser-Gln-(Cyclo-*m*)-[Trp-Gly-Gly-Phe]-Ala-OH (2m).



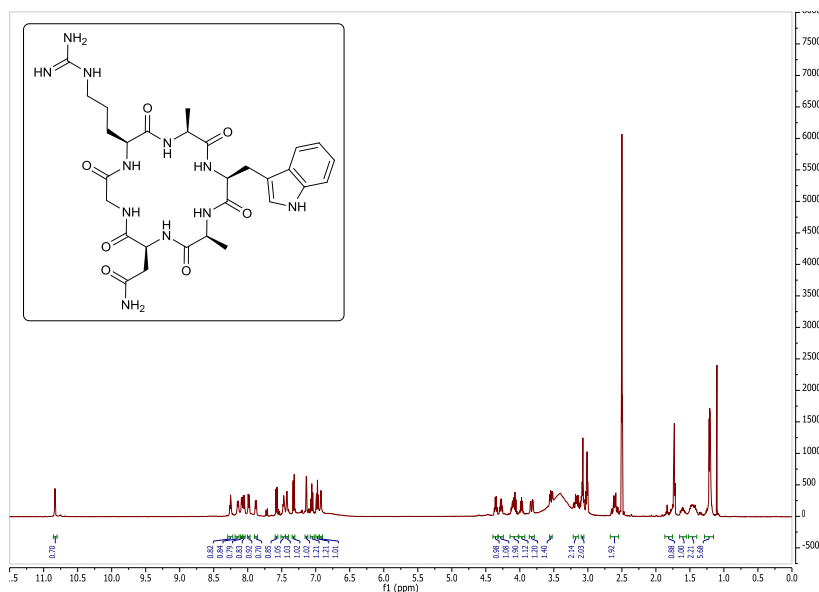
Supplementary Figure 93 | TOCSY NMR spectrum of compound H-Asp-Asn-Ser-Gln-(Cyclo-*m*)-[Trp-Gly-Gly-Phe]-Ala-OH (2m).



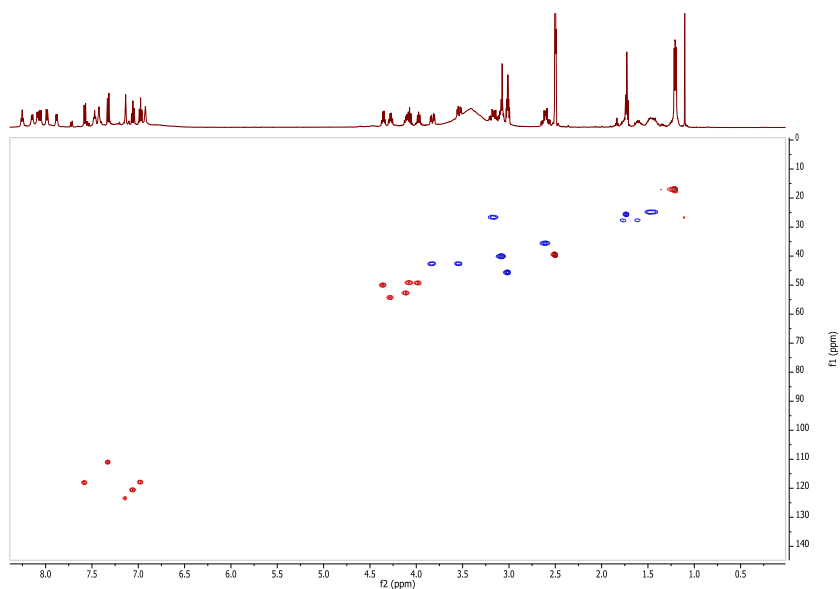
Supplementary Figure 94 | ROESY NMR spectrum of compound H-Asp-Asn-Ser-Gln-(Cyclo-m)-[Trp-Gly-Gly-Phe]-Ala-OH (2m).



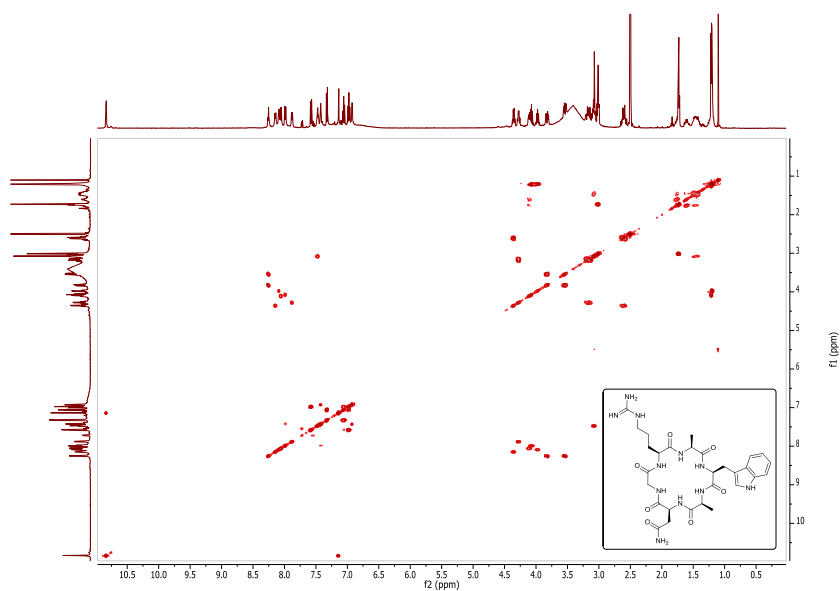
Supplementary Figure 95 | NOESY NMR spectrum of compound H-Asp-Asn-Ser-Gln-(Cyclo-m)-[Trp-Gly-Gly-Phe]-Ala-OH (2m).



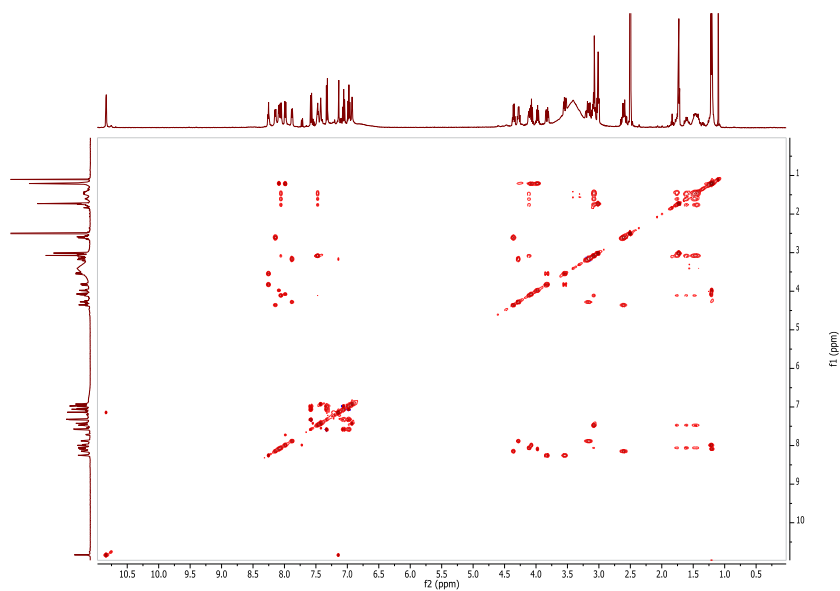
Supplementary Figure 96 | ^1H NMR spectrum of compound Cyclo(-Arg-Ala-Trp-Ala-Asn-Gly-) (3).



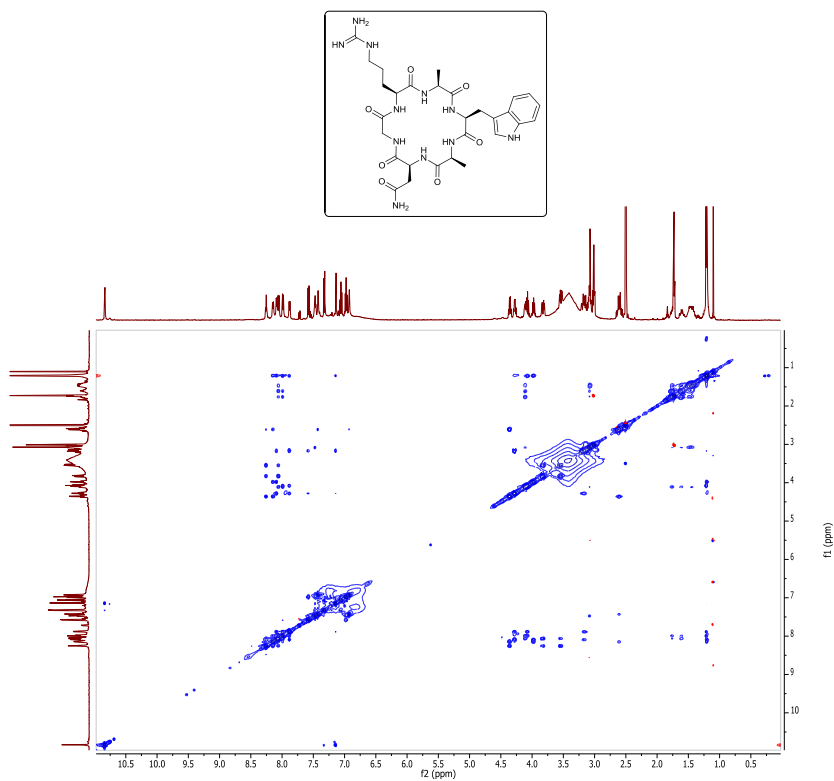
Supplementary Figure 97 | ^1H - ^{13}C HSQC NMR spectrum of compound Cyclo(-Arg-Ala-Trp-Ala-Asn-Gly-) (3).



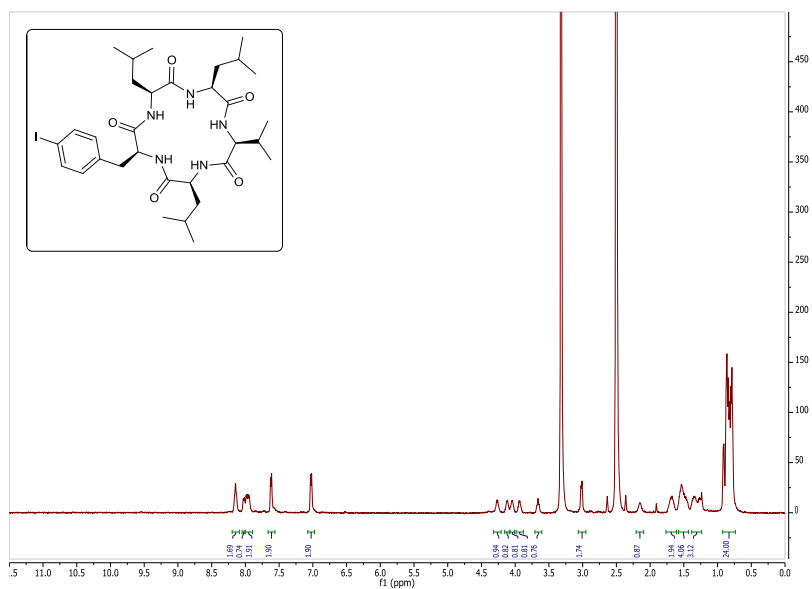
Supplementary Figure 98 | COSY NMR spectrum of compound Cyclo(-Arg-Ala-Trp-Ala-Asn-Gly-) (3).



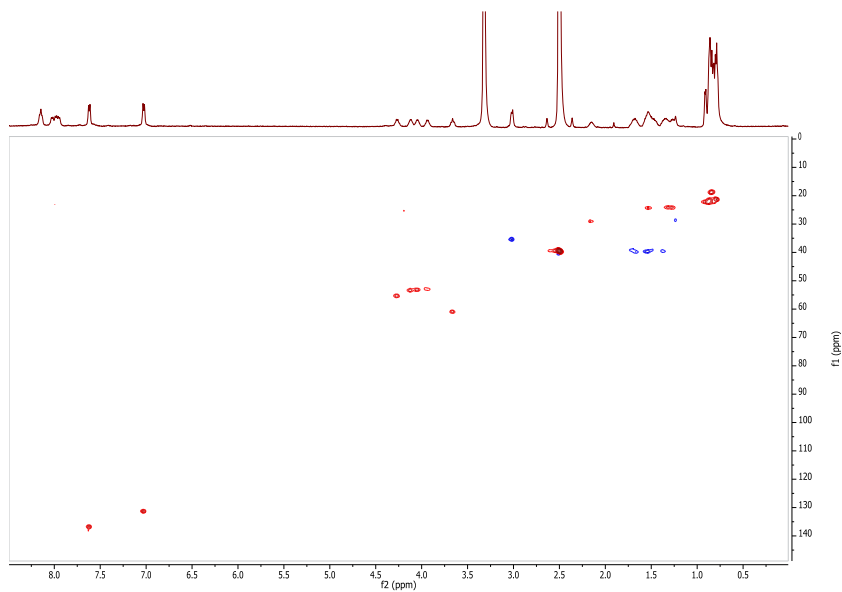
Supplementary Figure 99 | TOCSY NMR spectrum of compound Cyclo(-Arg-Ala-Trp-Ala-Asn-Gly-) (3).



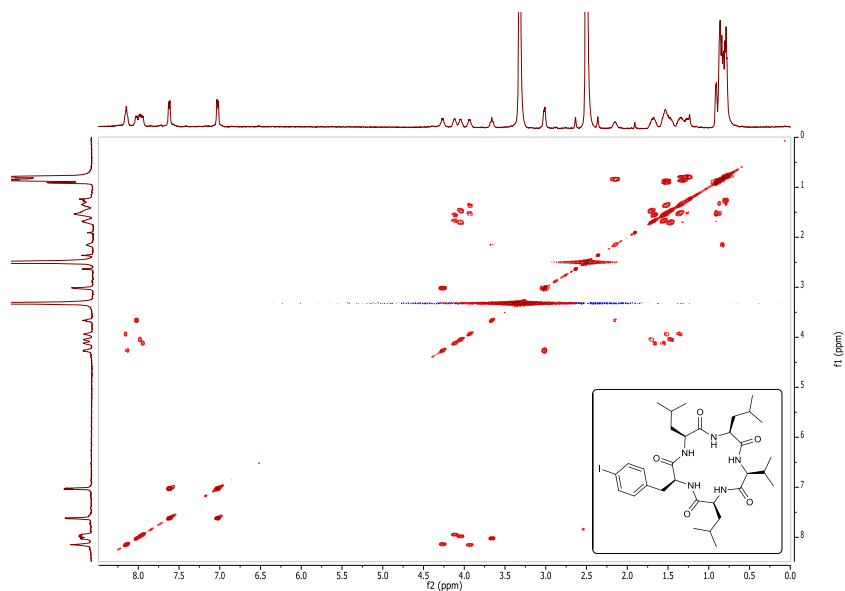
Supplementary Figure 100 | NOESY NMR spectrum of compound $\text{Cyclo}(-\text{Arg-Ala-Trp-Ala-Asn-Gly}-)$ (3).



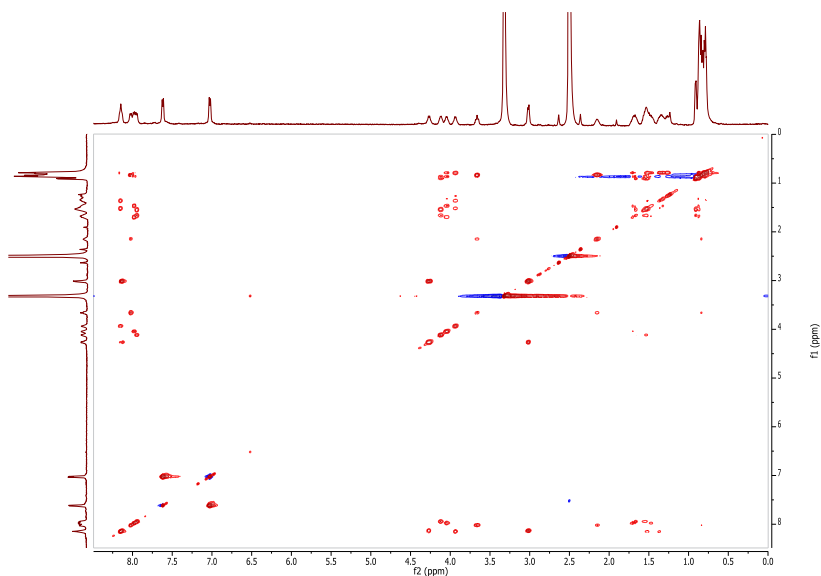
Supplementary Figure 101 | ^1H NMR spectrum of compound Cyclo(-Leu-Leu-Val-Leu-p-I-Phe-) (4).



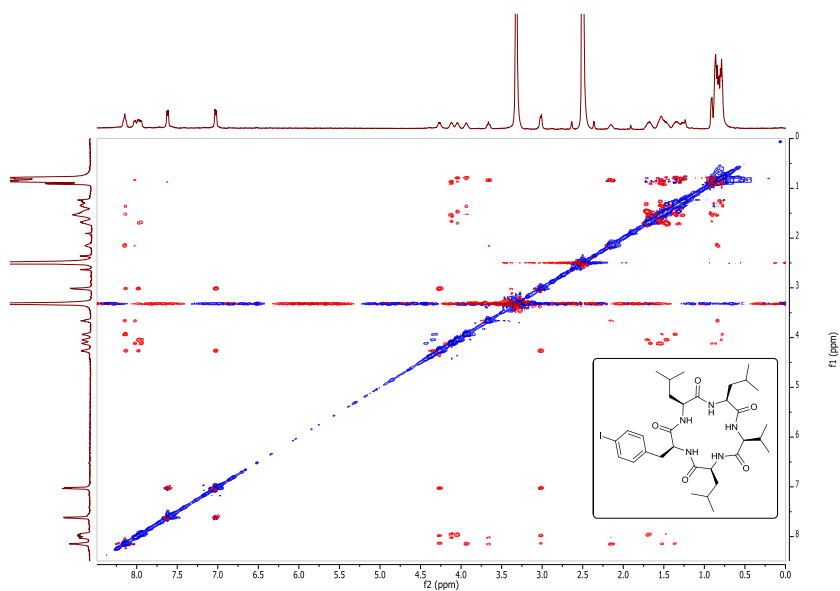
Supplementary Figure 102 | ^1H - ^{13}C HSQC NMR spectrum of compound Cyclo(-Leu-Leu-Val-Leu-p-I-Phe-) (4).



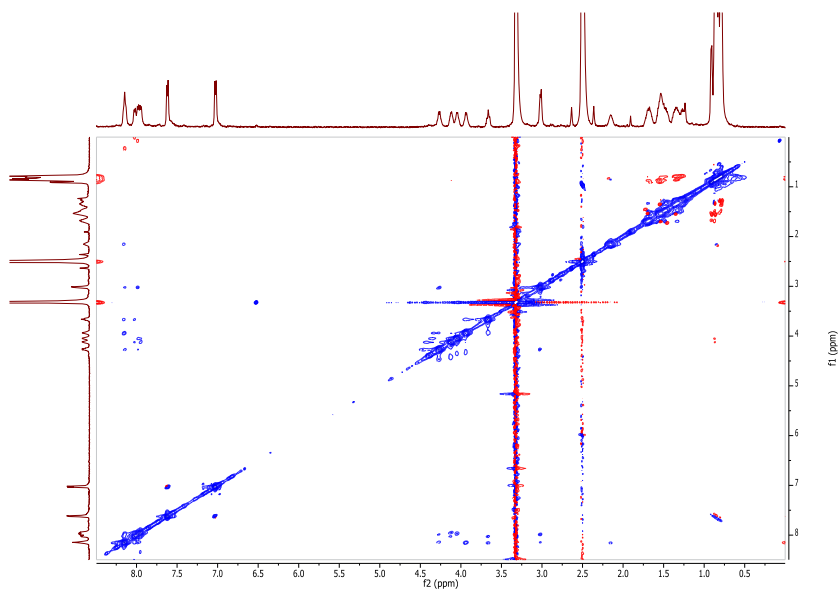
Supplementary Figure 103 | COSY NMR spectrum of compound Cyclo(-Leu-Leu-Val-Leu-*p*-I-Phe-) (4).



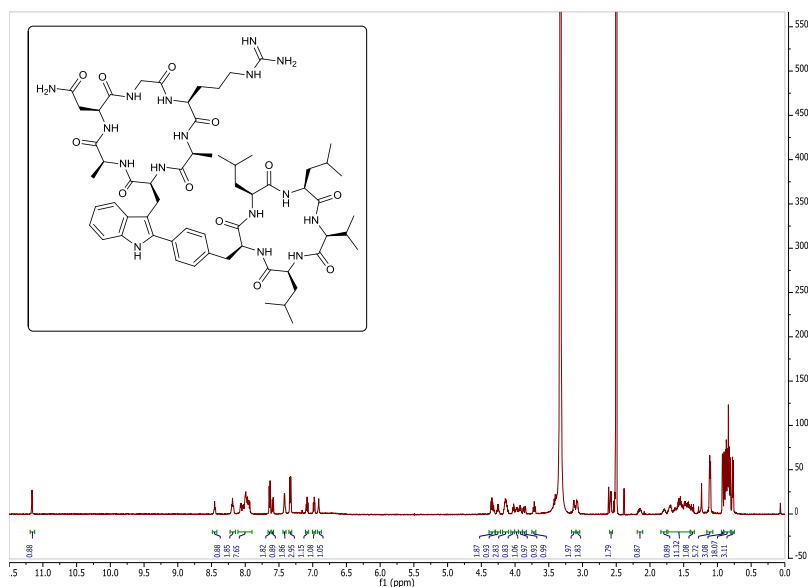
Supplementary Figure 104 | TOCSY NMR spectrum of compound Cyclo(-Leu-Leu-Val-Leu-*p*-I-Phe-) (4).



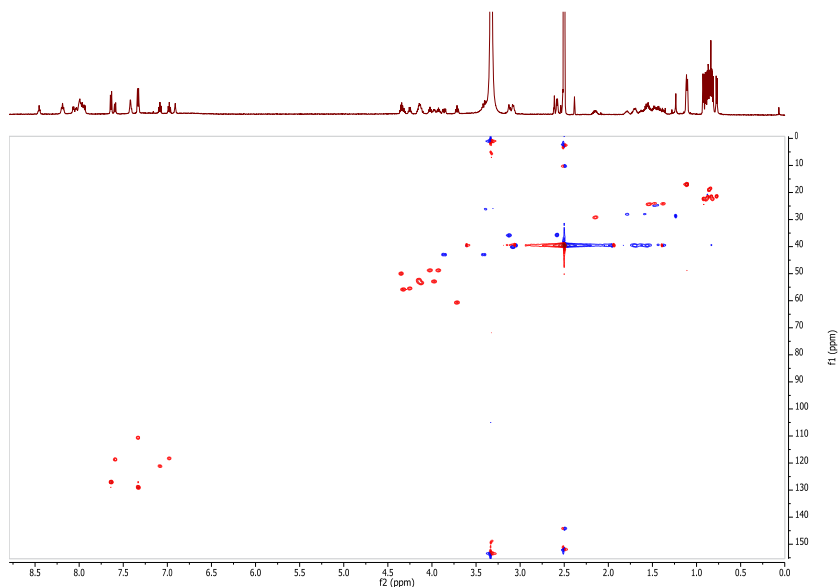
Supplementary Figure 105 | ROESY NMR spectrum of compound Cyclo(-Leu-Leu-Val-Leu-*p*-I-Phe-) (4).



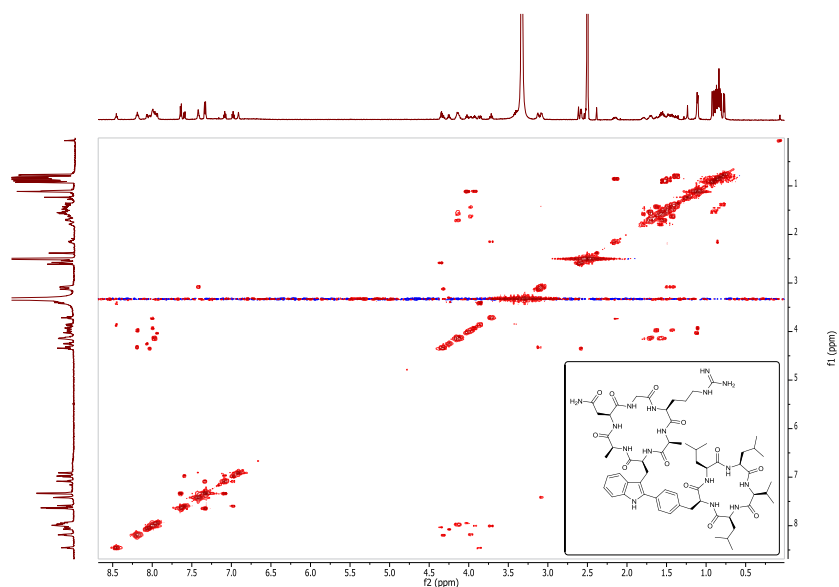
Supplementary Figure 106 | NOESY NMR spectrum of compound Cyclo(-Leu-Leu-Val-Leu-*p*-I-Phe-) (4).



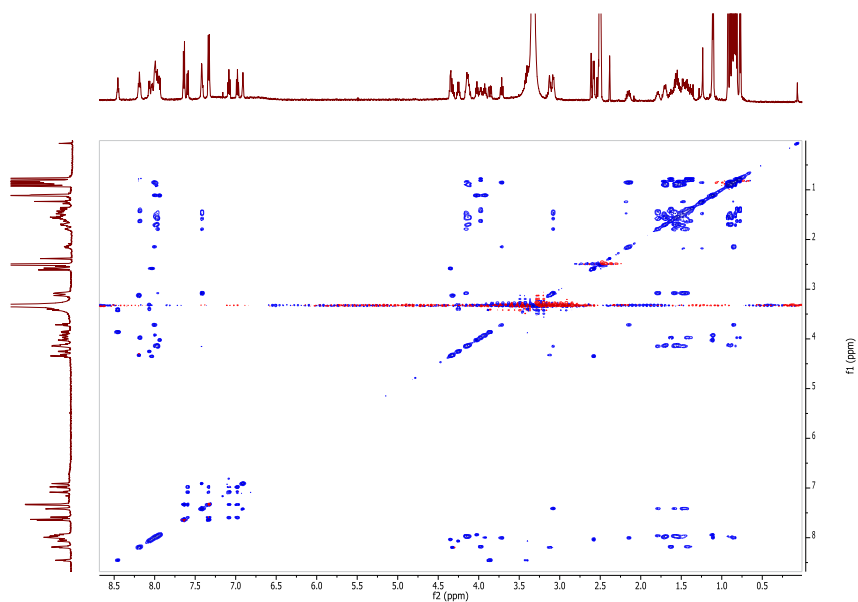
Supplementary Figure 107 | ^1H NMR spectrum of compound Cyclo(Ala-Asn-Gly-Arg-Ala-C2-Trp-)—Cyclo(C4-Phe-Leu-Leu-Val-Leu-) (5).



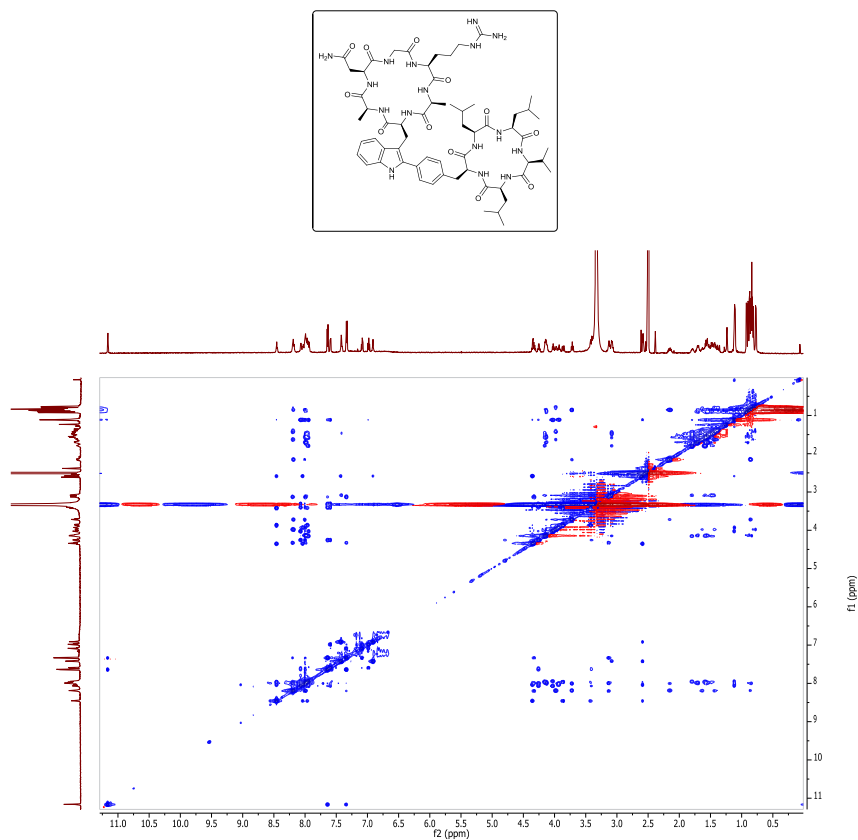
Supplementary Figure 108 | ^1H - ^{13}C HSQC NMR spectrum of compound Cyclo(Ala-Asn-Gly-Arg-Ala-C2-Trp-)—Cyclo(C4-Phe-Leu-Leu-Val-Leu-) (5).



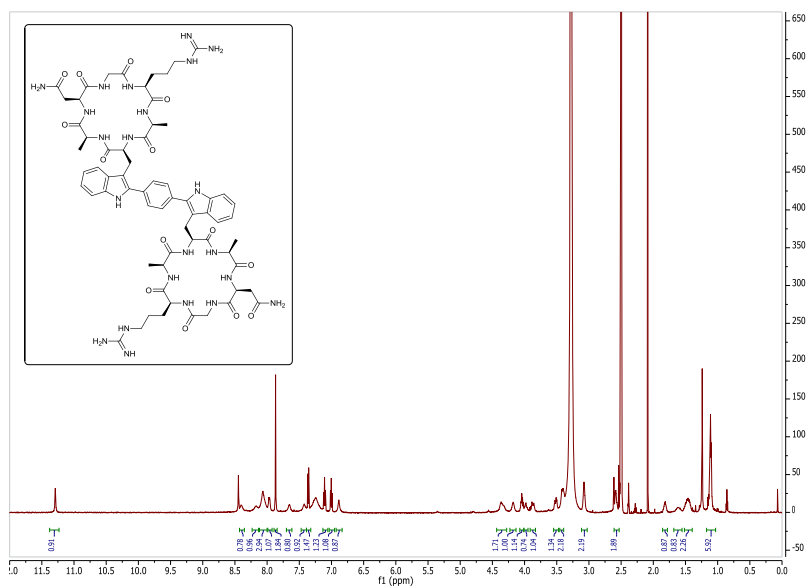
Supplementary Figure 109 | COSY NMR spectrum of compound Cyclo(Ala-Asn-Gly-Arg-Ala-C2-Trp)-Cyclo(C4-Phe-Leu-Leu-Val-Leu-) (5).



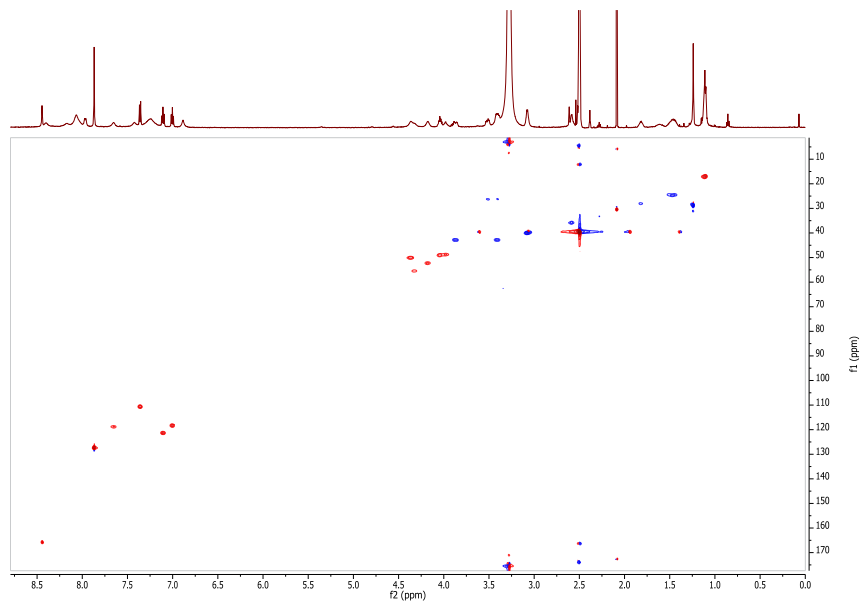
Supplementary Figure 110 | TOCSY NMR spectrum of compound Cyclo(Ala-Asn-Gly-Arg-Ala-C2-Trp)-Cyclo(C4-Phe-Leu-Leu-Val-Leu-) (5).



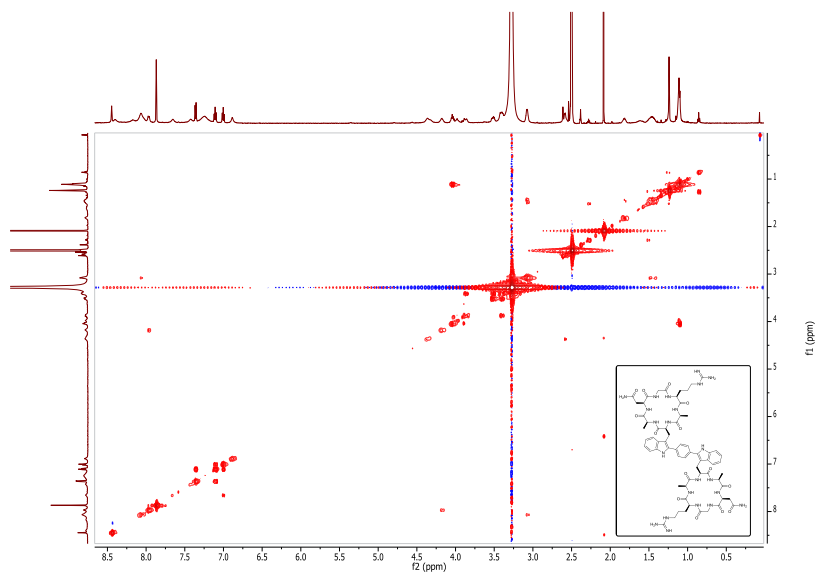
Supplementary Figure 111 | NOESY NMR spectrum of compound Cyclo(Ala-Asn-Gly-Arg-Ala-C2-Trp-)-Cyclo(C4-Phe-Leu-Leu-Val-Leu-) (5).



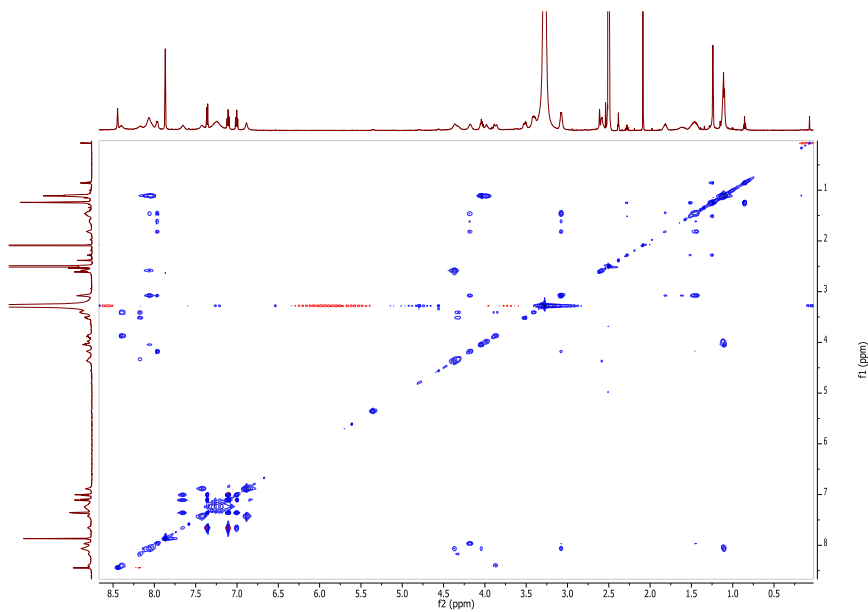
Supplementary Figure 112 | ^1H NMR spectrum of compound Bis[cyclo(-Arg-Ala-Trp-Ala-Asn-Gly-)] adduct (6).



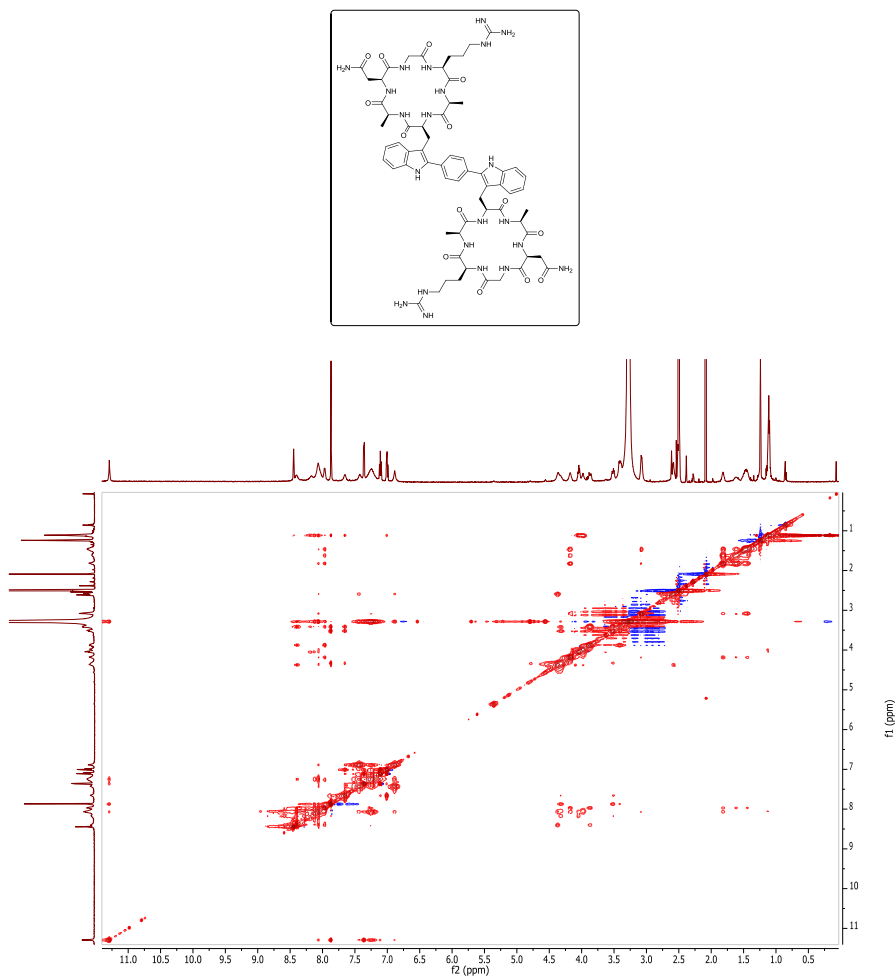
Supplementary Figure 113 | ^1H - ^{13}C HSQC NMR spectrum of compound Bis[cyclo(-Arg-Ala-Trp-Ala-Asn-Gly-)] adduct (6).



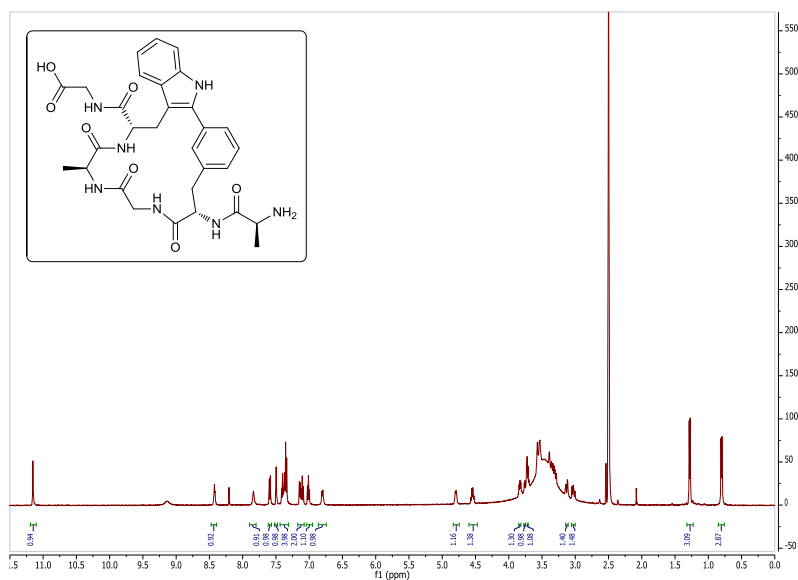
Supplementary Figure 114 | COSY NMR spectrum of compound Bis[cyclo(-Arg-Ala-Trp-Ala-Asn-Gly-)] adduct (6).



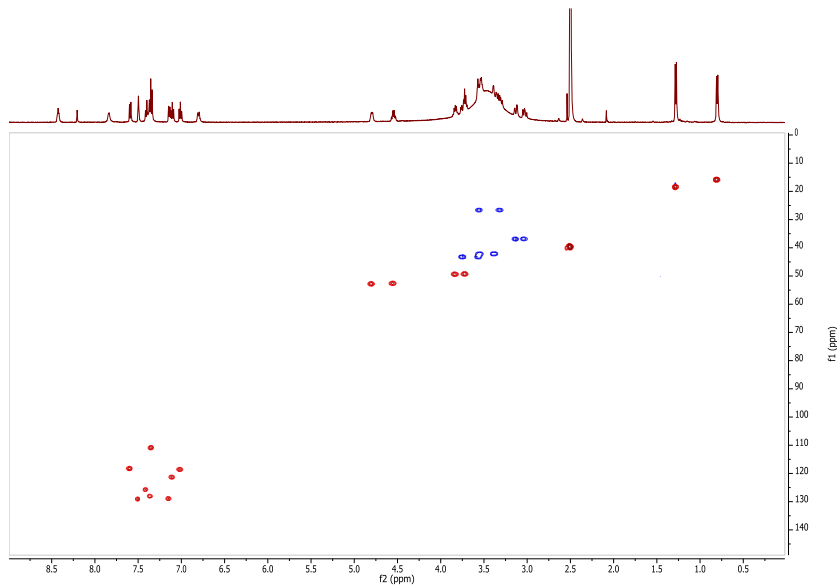
Supplementary Figure 115 | TOCSY NMR spectrum of compound Bis[cyclo(-Arg-Ala-Trp-Ala-Asn-Gly-)] adduct (6).



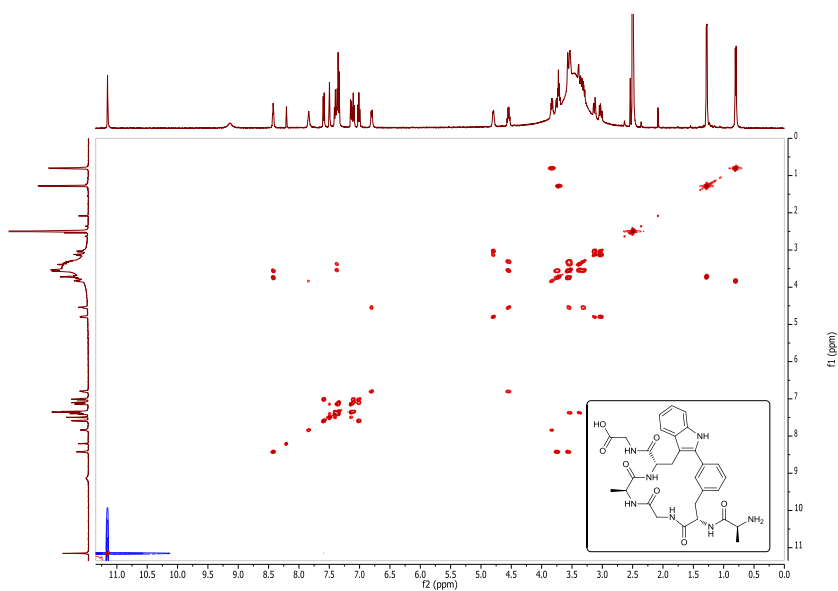
Supplementary Figure 116 | NOESY NMR spectrum of compound Bis[cyclo(-Arg-Ala-Trp-Ala-Asn-Gly-)] adduct (6).



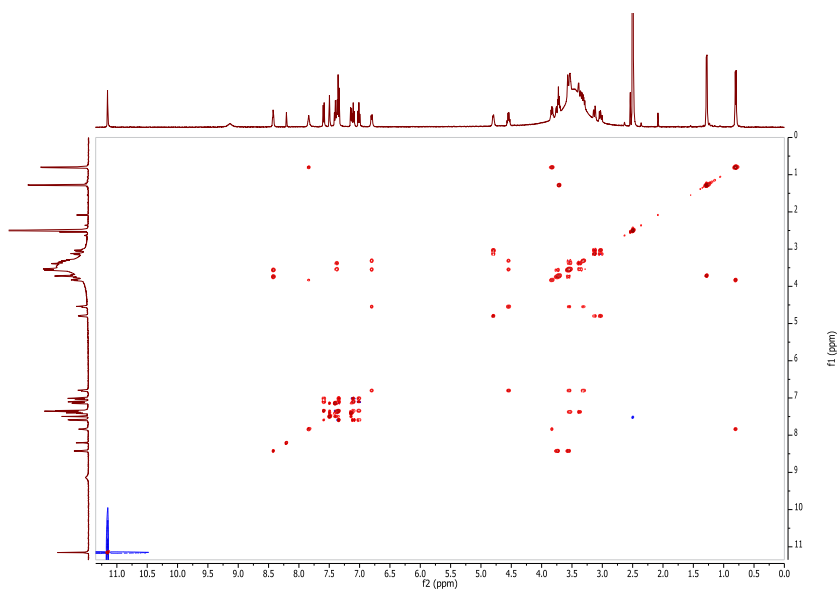
Supplementary Figure 117 | ^1H NMR spectrum of compound H-Ala-(Cyclo-*m*)-[Phe-Gly-Ala-Trp]-Gly-OH (9).



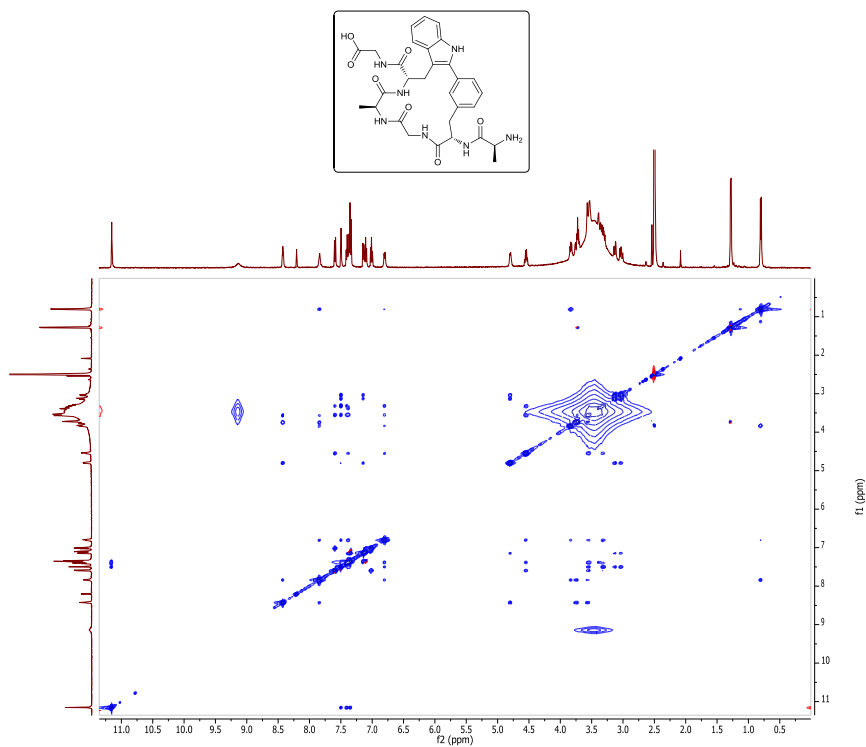
Supplementary Figure 118 | ^1H - ^{13}C HSQC NMR spectrum of compound H-Ala-(Cyclo-*m*)-[Phe-Gly-Ala-Trp]-Gly-OH (9).



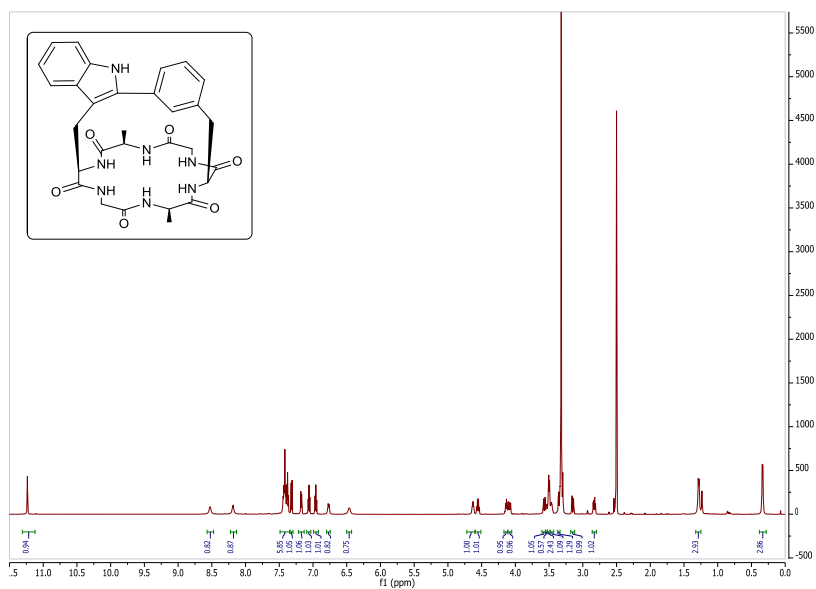
Supplementary Figure 119 | COSY NMR spectrum of compound H-Ala-(Cyclo-*m*)-[Phe-Gly-Ala-Trp]-Gly-OH (9).



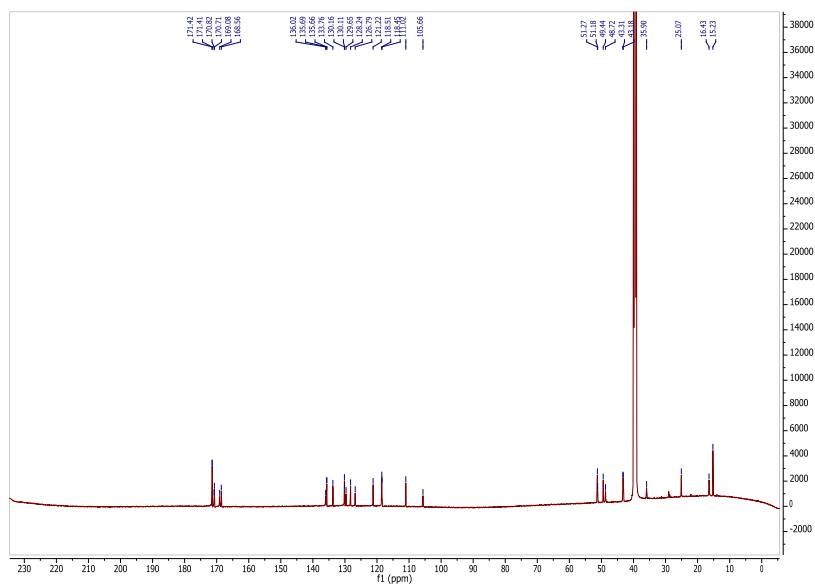
Supplementary Figure 120 | TOCSY NMR spectrum of compound H-Ala-(Cyclo-*m*)-[Phe-Gly-Ala-Trp]-Gly-OH (9).



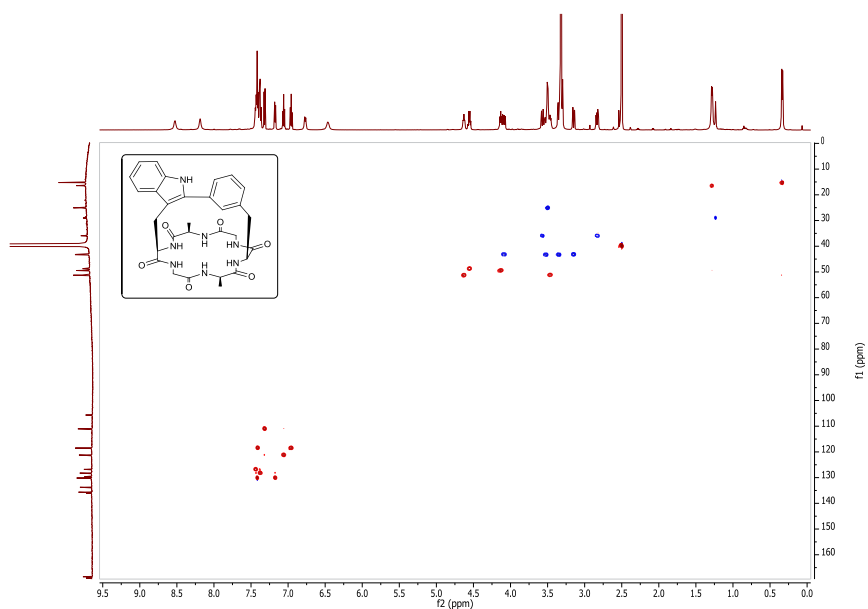
Supplementary Figure 121 | NOESY NMR spectrum of compound H-Ala-(Cyclo-*m*)-[Phe-Gly-Ala-Trp]-Gly-OH (9).



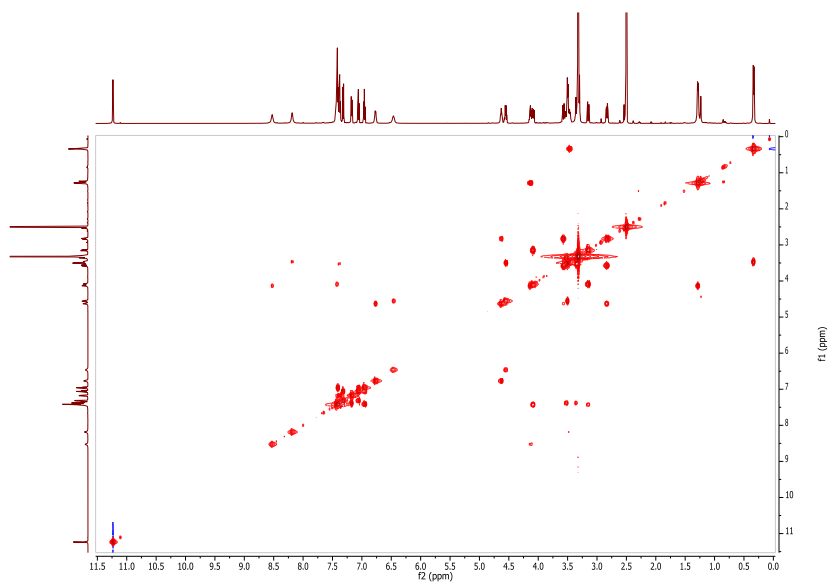
Supplementary Figure 122 | ^1H NMR spectrum of compound Cyclo[-Ala-(Cyclo-*m*)-[Phe-Gly-Ala-Trp]-Gly-] (10).



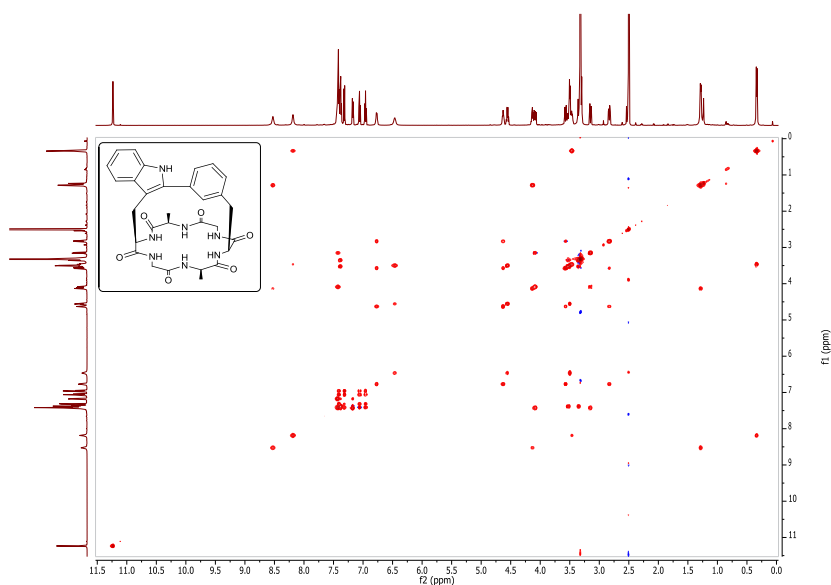
Supplementary Figure 123 | ^{13}C NMR spectrum of compound Cyclo[-Ala-(Cyclo-*m*)-[Phe-Gly-Ala-Trp]-Gly-] (10).



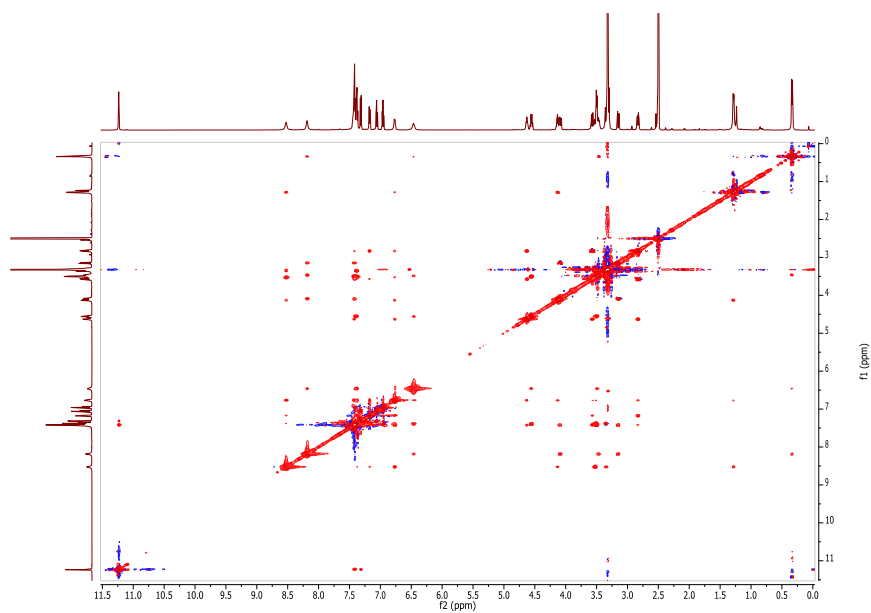
Supplementary Figure 124 | ^1H - ^{13}C HSQC NMR spectrum of compound Cyclo[-Ala-(Cyclo-*m*)-[Phe-Gly-Ala-Trp]-Gly-] (10).



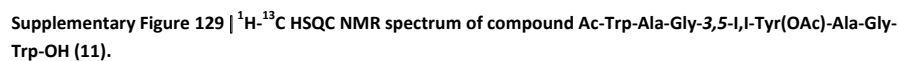
Supplementary Figure 125 | COSY NMR spectrum of compound Cyclo[-Ala-(Cyclo-*m*)-[Phe-Gly-Ala-Trp]-Gly-] (10).

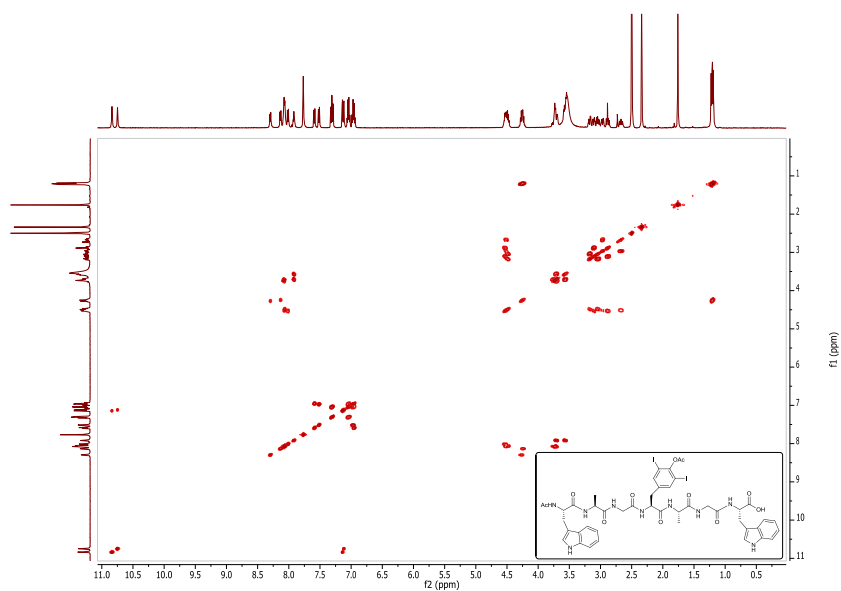


Supplementary Figure 126 | TOCSY NMR spectrum of compound Cyclo[-Ala-(Cyclo-*m*)-[Phe-Gly-Ala-Trp]-Gly-] (10).

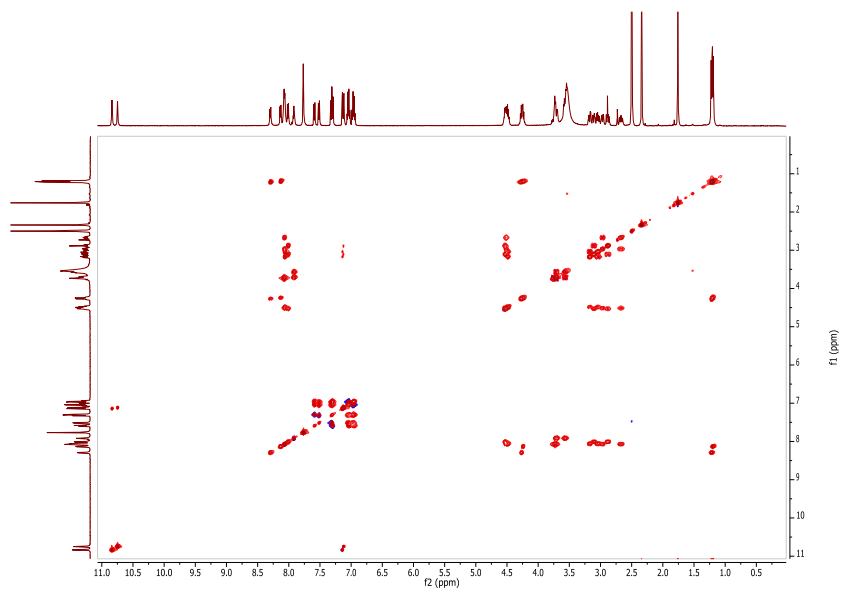


Supplementary Figure 127 | NOESY NMR spectrum of compound Cyclo[-Ala-(Cyclo-*m*)-[Phe-Gly-Ala-Trp]-Gly-] (10).

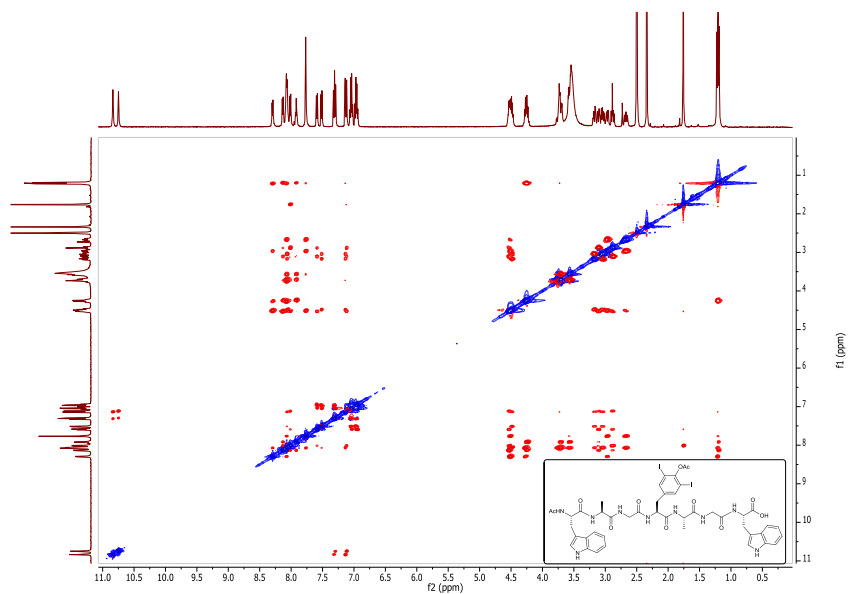




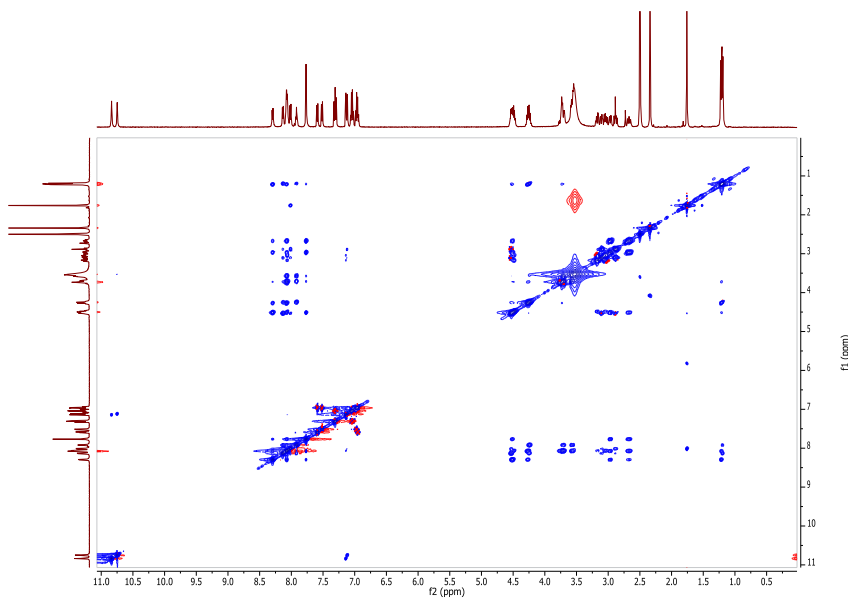
Supplementary Figure 130 | COSY NMR spectrum of compound Ac-Trp-Ala-Gly-3,5-I,I-Tyr(OAc)-Ala-Gly-Trp-OH (11).



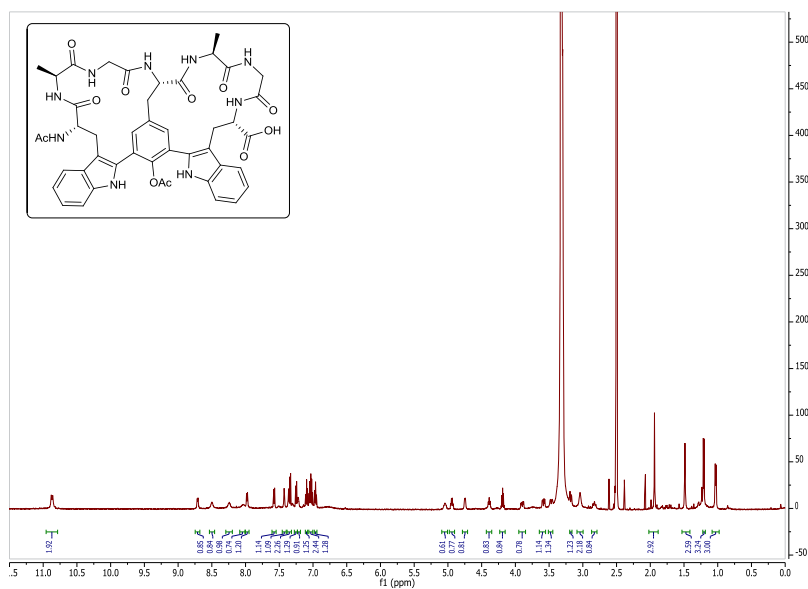
Supplementary Figure 131 | TOCSY NMR spectrum of compound Ac-Trp-Ala-Gly-3,5-I,I-Tyr(OAc)-Ala-Gly-Trp-OH (11).



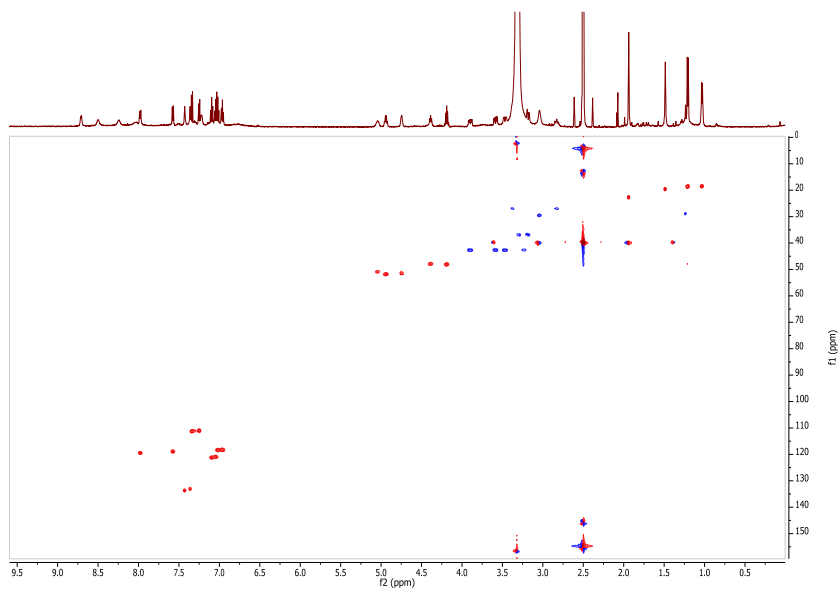
Supplementary Figure 132 | ROESY NMR spectrum of compound Ac-Trp-Ala-Gly-3,5-I-Tyr(OAc)-Ala-Gly-Trp-OH (11).



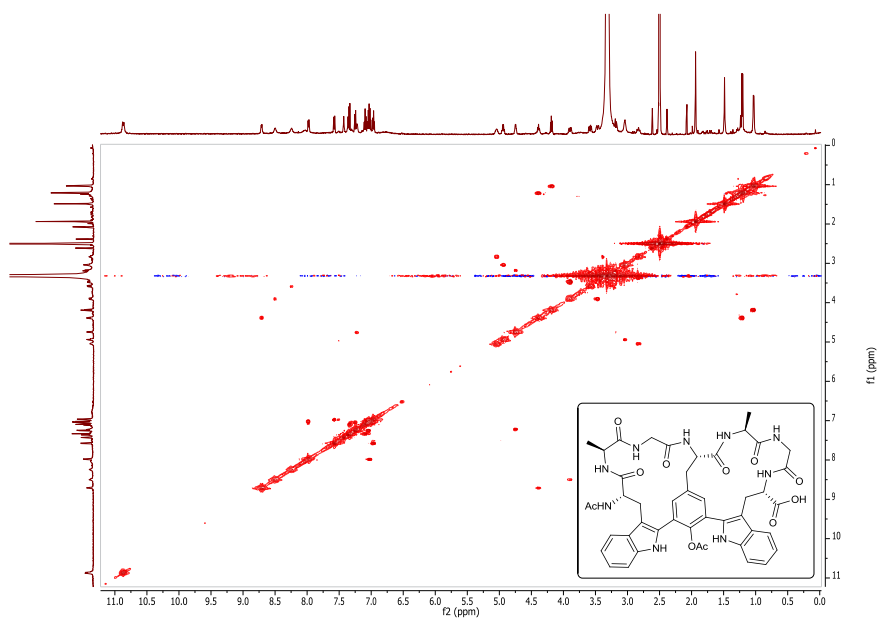
Supplementary Figure 133 | NOESY NMR spectrum of compound Ac-Trp-Ala-Gly-3,5-I-Tyr(OAc)-Ala-Gly-Trp-OH (11).



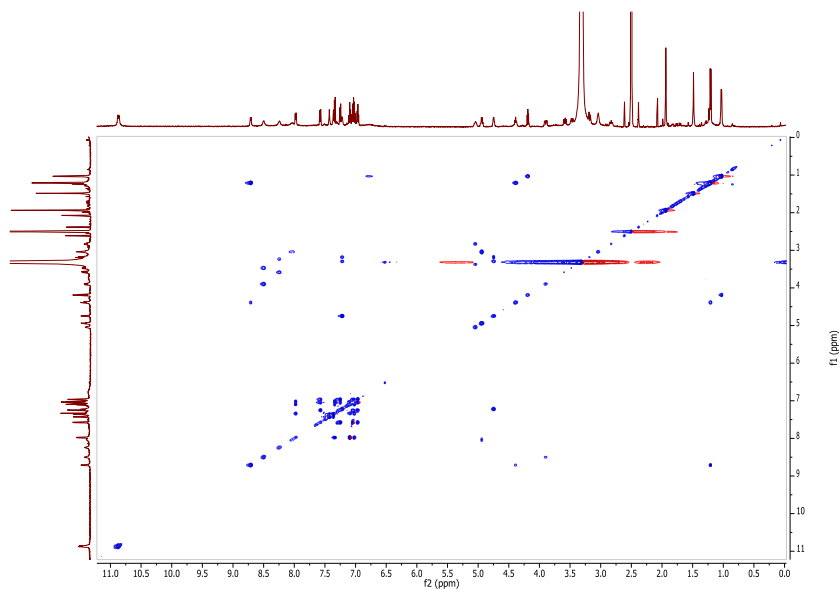
Supplementary Figure 134 | ^1H NMR spectrum of compound Ac-(bicyclo-*m,m*)-[Trp-Ala-Gly-Tyr(OAc)]-[Tyr(OAc)-Ala-Gly-Trp]-OH (12).



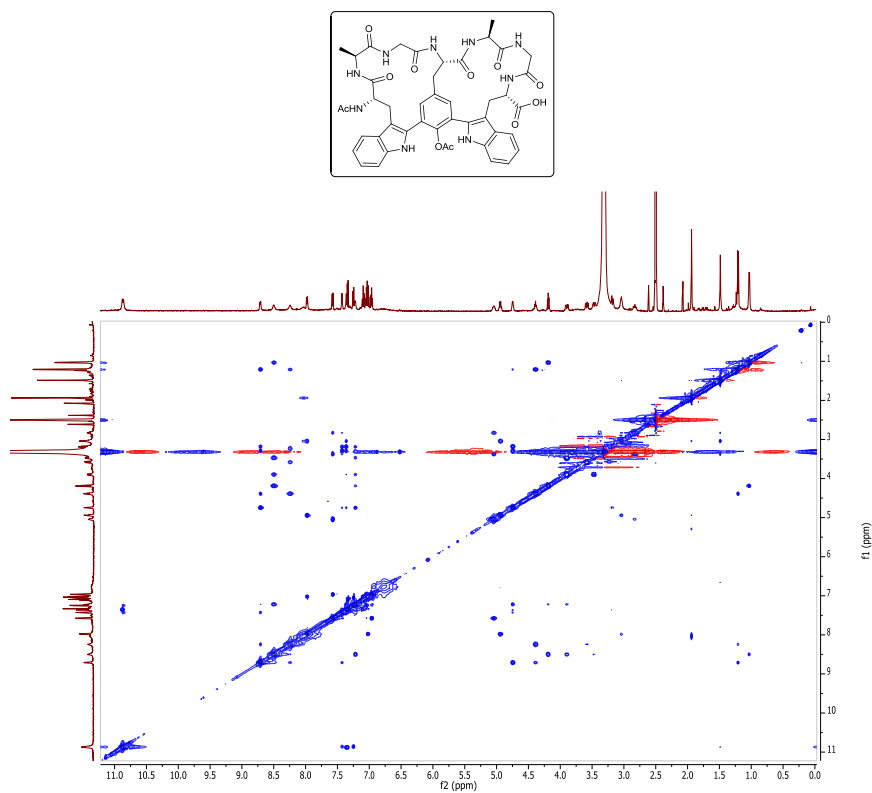
Supplementary Figure 135 | ^1H - ^{13}C HSQC NMR spectrum of compound Ac-(bicyclo-*m,m*)-[Trp-Ala-Gly-Tyr(OAc)]-[Tyr(OAc)-Ala-Gly-Trp]-OH (12).



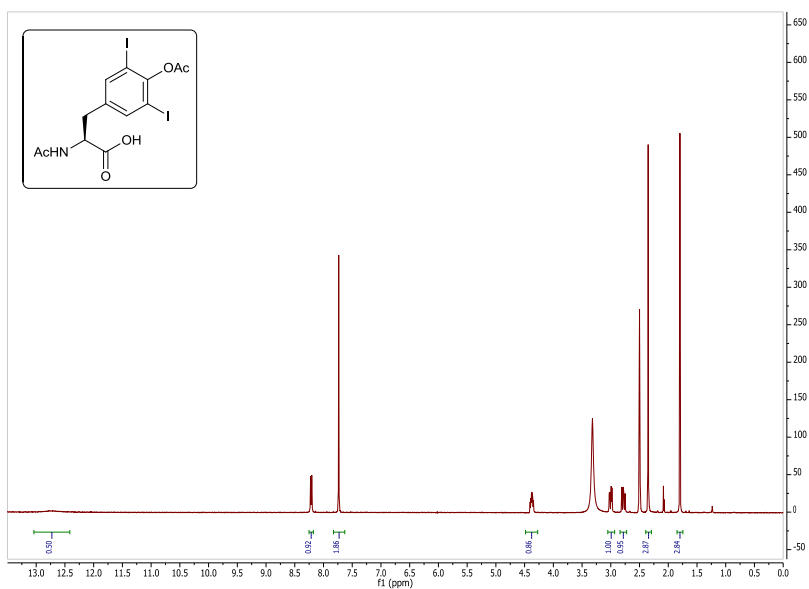
Supplementary Figure 136 | COSY NMR spectrum of compound Ac-(bicyclo-*m,m*)-[Trp-Ala-Gly-Tyr(OAc)]-[Tyr(OAc)-Ala-Gly-Trp]-OH (12).



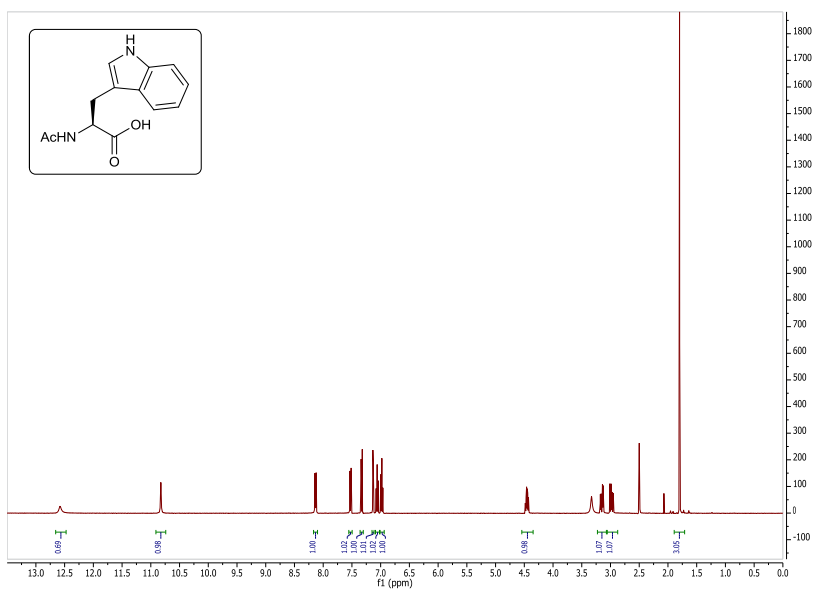
Supplementary Figure 137 | TOCSY NMR spectrum of compound Ac-(bicyclo-*m,m*)-[Trp-Ala-Gly-Tyr(OAc)]-[Tyr(OAc)-Ala-Gly-Trp]-OH (12).



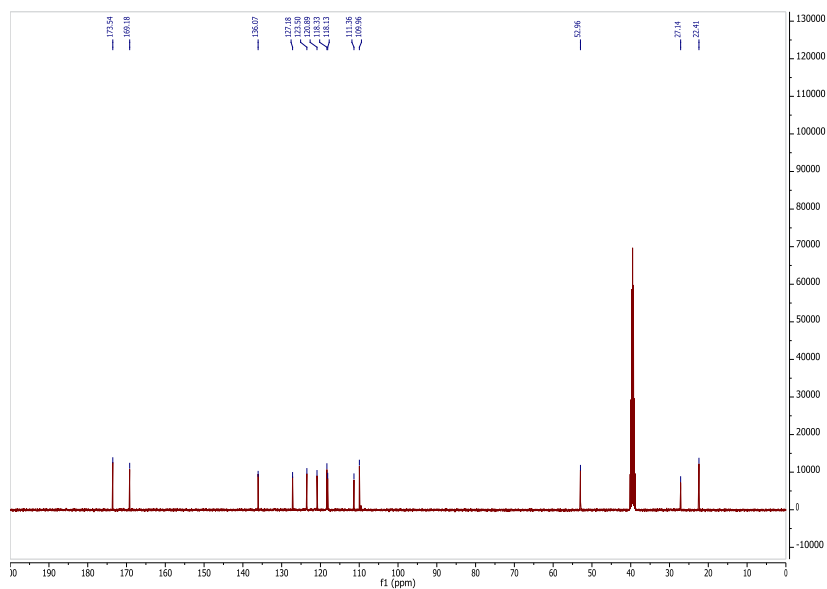
Supplementary Figure 138 | NOESY NMR spectrum of compound Ac-(bicyclo-*m,m*)-[Trp-Ala-Gly-Tyr(OAc)]-[Tyr(OAc)-Ala-Gly-Trp]-OH (12).



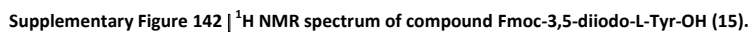
Supplementary Figure 139 | ^1H NMR spectrum of compound Ac-*m,m'*-I,I-Tyr(OAc)-OH (13).



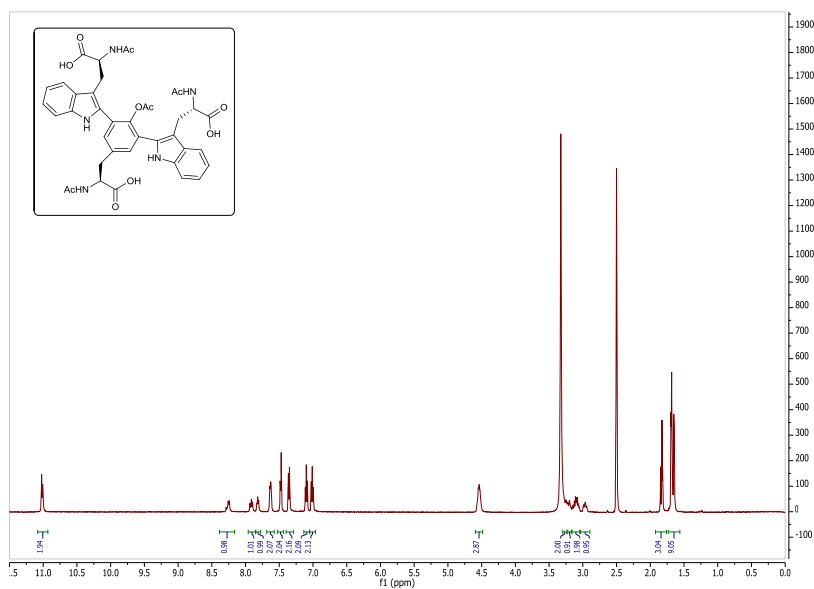
Supplementary Figure 140 | ¹H NMR spectrum of compound Ac-Trp-OH (14).



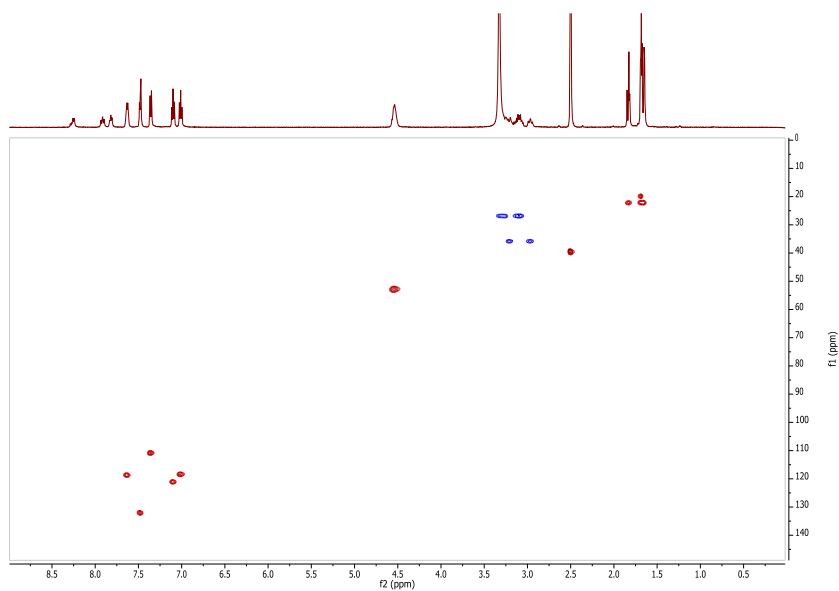
Supplementary Figure 141 | ¹³C NMR spectrum of compound Ac-Trp-OH (14).



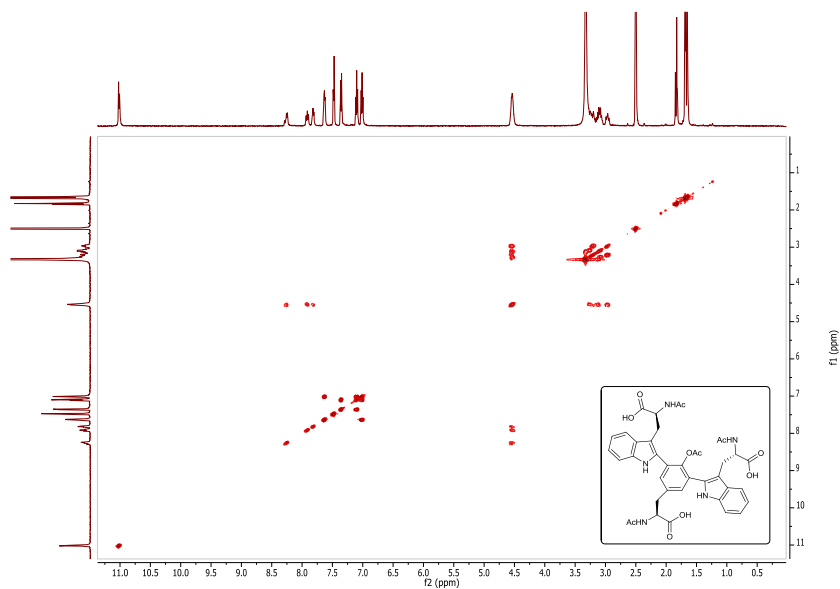
Supplementary Figure 142 | ^1H NMR spectrum of compound Fmoc-3,5-diiodo-L-Tyr-OH (15).



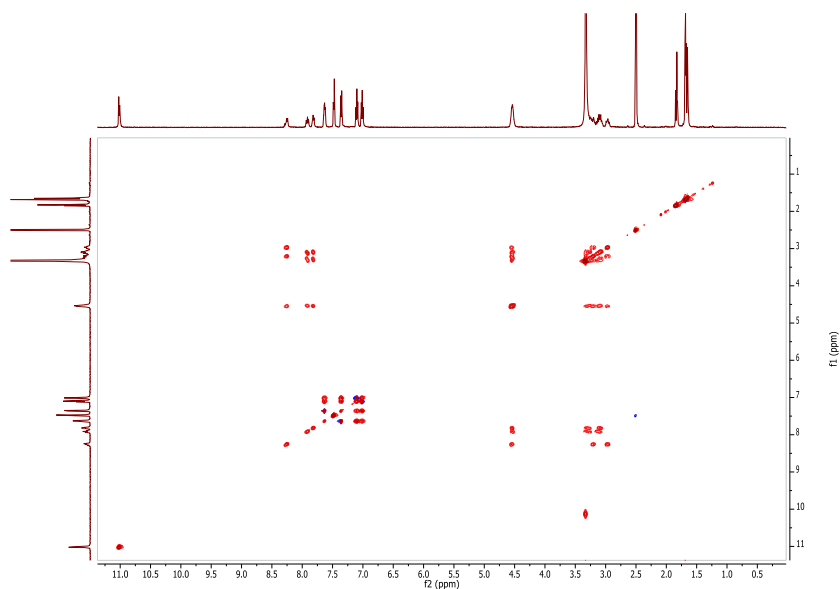
Supplementary Figure 143 | ^1H NMR spectrum of compound Ac-3,5-di-(Ac-Trp-OH)-Tyr(OAc)-OH (16).



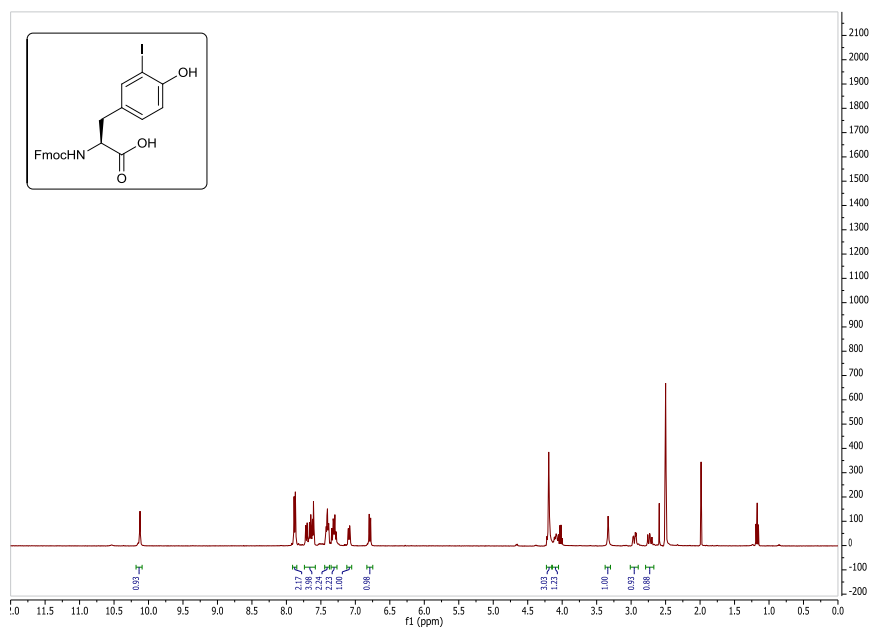
Supplementary Figure 144 | ^1H - ^{13}C HSQC NMR spectrum of compound Ac-3,5-di-(Ac-Trp-OH)-Tyr(OAc)-OH (16).



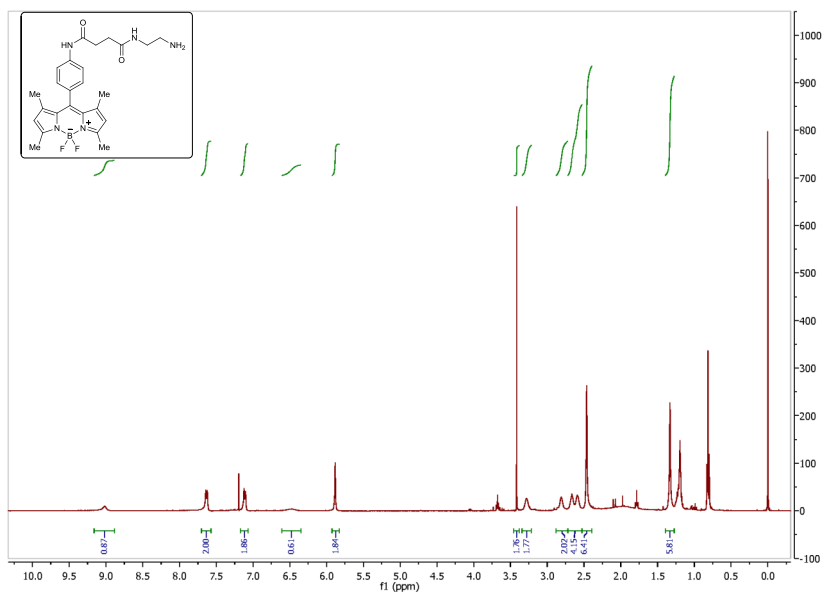
Supplementary Figure 145 | COSY NMR spectrum of compound Ac-3,5-di-(Ac-Trp-OH)-Tyr(OAc)-OH (16).



Supplementary Figure 146 | TOCSY NMR spectrum of compound Ac-3,5-di-(Ac-Trp-OH)-Tyr(OAc)-OH (16).

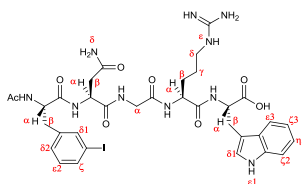


Supplementary Figure 147 | ^1H NMR spectrum of compound Fmoc-3-iodo-Tyr-OH (17).



Supplementary Figure 148 | ^1H NMR spectrum of compound 10-(4-(2-aminoethylamino)-4-oxobutanamido)phenyl)-5,5-difluoro-1,3,7,9-tetramethyl-5*H*-dipyrrolo[1,2-*c*:1',2'-*f*][1,3,2]diazaborinin-4-ium-5-uide (19).

Supplementary Tables

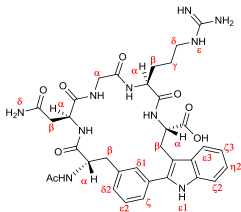


1g (¹ H)		δ (ppm)											
AA	NH	α	β	γ	δ1	δ2	ε2	ζ	ε1	ζ2	η2	ζ3	ε3
Phe	8.18	4.47	2.98/ 2.66	-	7.66	7.25	7.05	7.54	-	-	-	-	-
Asn	8.38	4.51	2.57/ 2.50	-	7.46/6.96	-	-	-	-	-	-	-	-
Gly	8.03	3.76/ 3.66	-	-	-	-	-	-	-	-	-	-	-
Arg	7.92	4.36	1.68/ 1.54	1.46	3.07	-	-	-	7.46	-	-	-	-
Trp	8.14	4.45	3.17/ 3.07	-	7.16	-	-	-	10.83	7.32	7.05	6.97	7.51

Supplementary Table 1 | ¹H chemical shifts assignments of compound Ac-*m*-I-Phe-Asn-Gly-Arg-Trp-OH (1g).

1g (¹³ C)				δ (ppm)							
AA	α	β	γ	δ1	δ2	ε2	ζ	ζ2	η2	ζ3	ε3
Phe	53.6	36.5	-	137.4	128.4	130.0	134.8	-	-	-	-
Asn	49.6	36.7	-	-	-	-	-	-	-	-	-
Gly	42.2	-	-	-	-	-	-	-	-	-	-
Arg	51.5	28.9	24.7	40.2	-	-	-	-	-	-	-
Trp	53.0	26.9	-	123.4	-	-	-	111.1	120.7	118.1	117.9

Supplementary Table 2 | ¹³C chemical shifts assignments of compound Ac-*m*-I-Phe-Asn-Gly-Arg-Trp-OH (1g).

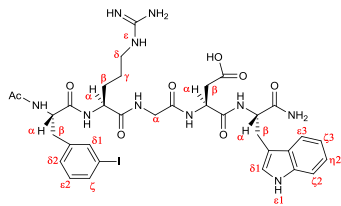


2g (¹ H)					δ (ppm)								
AA	NH	α	β	γ	δ1	δ2	ε2	ζ	ε1	ζ2	η2	ζ3	ε3
Phe	8.36	4.68	3.09/2.88	-	7.70	7.20	7.37	7.49	-	-	-	-	-
Asn	8.42	4.60	2.62/2.44	-	7.38/6.85	-	-	-	-	-	-	-	-
Gly	7.67	3.98/3.43	-	-	-	-	-	-	-	-	-	-	-
Arg	7.79	4.30	1.74/1.55	1.41	3.04	-	-	-	-	-	-	-	-
Trp	8.33	4.48	3.42/3.06	-	-	-	-	-	11.15	7.32	7.06	6.97	7.63

Supplementary Table 3 | ¹H chemical shifts assignments of compound Ac-(Cyclo-*m*)-[Phe-Asn-Gly-Arg-Trp]-OH (2g).

2g (¹³ C)				δ (ppm)							
AA	α	β	γ	δ1	δ2	ε2	ζ	ζ2	η2	ζ3	ε3
Phe	53.4	37.0	-	128.0	127.6	127.9	125.0	-	-	-	-
Asn	49.2	35.7	-	-	-	-	-	-	-	-	-
Gly	42.5	-	-	-	-	-	-	-	-	-	-
Arg	51.6	28.4	23.9	39.9	-	-	-	-	-	-	-
Trp	54.2	28.2	-	-	-	-	-	110.6	121.1	118.3	119.0

Supplementary Table 4 | ¹³C chemical shifts assignments of compound Ac-(Cyclo-*m*)-[Phe-Asn-Gly-Arg-Trp]-OH (2g).

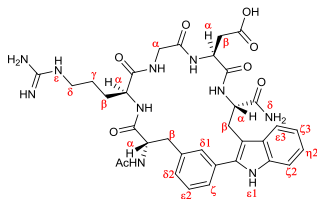


1h (¹ H)		δ (ppm)											
AA	NH	α	β	γ	δ1	δ2	ε2	ζ	ε1	ζ2	η2	ζ3	ε3
Phe	8.10	4.51	2.98/2.67	-	7.69	7.27	7.05	7.55	-	-	-	-	-
Arg	8.23	4.31	1.72/1.57	1.51	3.10	-	-	-	7.42	-	-	-	-
Gly	8.10	3.72	-	-	-	-	-	-	-	-	-	-	-
Asp	8.23	4.57	2.69/2.46	-	-	-	-	-	-	-	-	-	-
Trp	7.85	4.39	3.16/2.98	-	7.10	-	-	-	10.74	7.32	7.05	6.97	7.55

Supplementary Table 5 | ¹H chemical shifts assignments of compound Ac-*m*-I-Phe-Arg-Gly-Asp-Trp-OH (1h).

1h (¹³ C)		δ (ppm)											
AA	α	β	γ	δ1	δ2	ε2	ζ	ζ2	η2	ζ3	ε3		
Phe	53.5	36.5	-	137.3	128.4	129.8	134.6	-	-	-	-	-	-
Arg	52.0	28.9	24.5	40.1	-	-	-	-	-	-	-	-	-
Gly	41.5	-	-	-	-	-	-	-	-	-	-	-	-
Asp	49.2	35.8	-	-	-	-	-	-	-	-	-	-	-
Trp	53.1	27.1	-	123.2	-	-	-	110.9	120.5	117.9	118.0		

Supplementary Table 6 | ¹³C chemical shifts assignments of compound Ac-*m*-I-Phe-Arg-Gly-Asp-Trp-OH (1h).

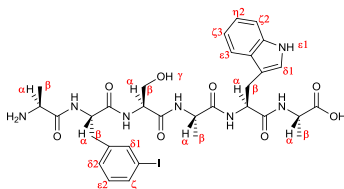


2h (¹ H)					δ (ppm)								
AA	NH	α	β	γ	δ1	δ2	ε2	ζ	ε1	ζ2	η2	ζ3	ε3
Phe	8.32	4.66	2.97	-	7.69	7.24	7.39	7.42	-	-	-	-	-
Arg	7.88	4.03	1.84/ 1.49	1.41/ 1.34	3.14/ 2.75	-	-	-	-	-	-	-	-
Gly	8.39	3.68/3.43	-	-	-	-	-	-	-	-	-	-	-
Asp	8.06	4.25	2.67/2.18	-	-	-	-	-	-	-	-	-	-
Trp	7.35	4.53	3.43/2.97	-	7.07/6.89	-	-	-	11.00	7.31	7.07	6.99	7.59

Supplementary Table 7 | ¹H chemical shifts assignments of compound Ac-(Cyclo-*m*)-[Phe-Arg-Gly-Asp-Trp]-NH₂ (2h).

2h (¹³ C)				δ (ppm)							
AA	α	β	γ	δ1	δ2	ε2	ζ	ζ2	η2	ζ3	ε3
Phe	53.5	38.4	-	128.8	127.8	128.0	126.0	-	-	-	-
Arg	52.5	30.3	24.6	40.4	-	-	-	-	-	-	-
Gly	43.1	-	-	-	-	-	-	-	-	-	-
Asp	48.9	37.2	-	-	-	-	-	-	-	-	-
Trp	53.1	26.8	-	-	-	-	-	110.6	120.8	118.2	118.5

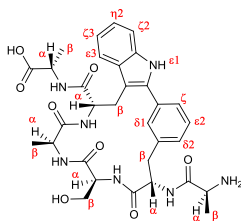
Supplementary Table 8 | ¹³C chemical shifts assignments of compound Ac-(Cyclo-*m*)-[Phe-Arg-Gly-Asp-Trp]-NH₂ (2h).



1i (¹ H)			δ (ppm)										
AA	NH	α	β	δ1	δ2	ε2	ζ	ε1	ζ2	η2	ζ3	ε3	γ
Ala1	-	3.70	1.31-1.21	-	-	-	-	-	-	-	-	-	-
<i>m</i> -I-Phe	8.73	4.58	3.04/2.76	7.71	7.3	7.06	7.57	-	-	-	-	-	-
Ser	8.36	4.35	3.7/3.59	-	-	-	-	-	-	-	-	-	5.39
Ala2	8.15	4.17	1.12	-	-	-	-	-	-	-	-	-	-
Trp	7.94	4.48	3.17/2.88	7.12	-	-	-	10.8	7.30	7.06	6.97	7.57	-
Ala3	7.94	4.10	1.31-1.21	-	-	-	-	-	-	-	-	-	-

Supplementary Table 9 | ¹H chemical shifts assignments of compound H-Ala-*m*-I-Phe-Ser-Ala-Trp-Ala-OH (1i).

1i (¹³ C)			δ (ppm)								
AA	α	β	δ1	δ2	ε2	ζ	ζ2	η2	ζ3	ε3	γ
Ala1	48.0	17.4	-	-	-	-	-	-	-	-	-
<i>m</i> -I-Phe	53.8	36.5	137.4	128.5	129.9	134.7	-	-	-	-	-
Ser	54.3	61.7	-	-	-	-	-	-	-	-	-
Ala2	48.6	17.5	-	-	-	-	-	-	-	-	-
Trp	53.0	27.4	123.1	-	-	-	110.9	120.5	117.9	118.0	-
Ala3	48.0	17.4	-	-	-	-	-	-	-	-	-

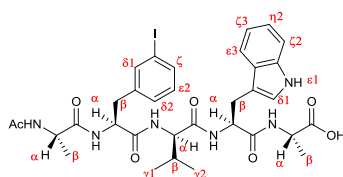
Supplementary Table 10 | ¹³C chemical shifts assignments of compound H-Ala-*m*-I-Phe-Ser-Ala-Trp-Ala-OH (1i).

2i (¹ H)		δ (ppm)										
AA	NH	α	β	δ1	δ2	ε2	ζ	ε1	ζ2	η2	ζ3	ε3
Ala1	-	3.48	1.17	-	-	-	-	-	-	-	-	-
Phe	8.46	4.97	3.18/3.08	7.65	7.22	7.42	7.42	-	-	-	-	-
Ser	8.35	3.87	3.63/3.58	-	-	-	-	-	-	-	-	-
Ala2	7.37	3.70	0.76	-	-	-	-	-	-	-	-	-
Trp	6.81	4.51	3.63/3.30	-	-	-	-	11.1	7.34	7.11	7.02	7.61
Ala3	7.51	4.15	1.32	-	-	-	-	-	-	-	-	-

Supplementary Table 11 | ¹H chemical shifts assignments of compound H-Ala-(Cyclo-*m*)-[Phe-Ser-Ala-Trp]-Ala-OH (2i).

2i (¹³ C)			δ (ppm)							
AA	α	β	δ1	δ2	ε2	ζ	ζ2	η2	ζ3	ε3
Ala1	49.1	19.8	-	-	-	-	-	-	-	-
Phe	51.5	36.3	128.5	128.3	128.1	125.4	-	-	-	-
Ser	58.0	59.9	-	-	-	-	-	-	-	-
Ala2	49.8	15.7	-	-	-	-	-	-	-	-
Trp	53.4	26.6	-	-	-	-	110.8	121.3	118.4	117.8
Ala3	47.6	16.6	-	-	-	-	-	-	-	-

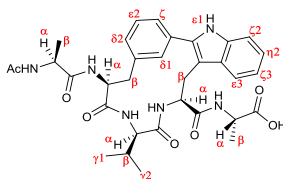
Supplementary Table 12 | ¹³C chemical shifts assignments of compound H-Ala-(Cyclo-*m*)-[Phe-Ser-Ala-Trp]-Ala-OH (2i).



1j (1H)			δ (ppm)										
AA	NH	α	β	δ1	δ2	ε2	ζ	ε1	ζ2	η2	ζ3	ε3	γ
Ala1	7.99	4.19	1.10	-	-	-	-	-	-	-	-	-	-
m-I-Phe	7.94	4.47	2.92/2.71	7.60	7.20	6.96	7.50	-	-	-	-	-	-
Val	7.76	4.15	1.94	-	-	-	-	-	-	-	-	-	0.77
Trp	7.99	4.60	3.13/2.92	7.15	-	-	-	10.78	7.29	7.04	6.96	7.60	-
Ala2	8.17	4.20	1.25	-	-	-	-	-	-	-	-	-	-

Supplementary Table 13 | ¹H chemical shifts assignments of compound Ac-Ala-*m*-I-Phe-Val-Trp-Ala-OH (1j).

1j (¹³ C)			δ (ppm)								
AA	α	β	δ1	δ2	ε2	ζ	ζ2	η2	ζ3	ε3	γ
Ala1	47.5	17.9	-	-	-	-	-	-	-	-	-
<i>m</i> -I-Phe	53.2	36.3	137.4	128.5	129.9	134.7	-	-	-	-	-
Val	57.3	30.5	-	-	-	-	-	-	-	-	18.9/17.7
Trp	52.7	27.4	123.3	-	-	-	110.9	120.6	117.9	118.2	-
Ala2	47.7	17.0	-	-	-	-	-	-	-	-	-

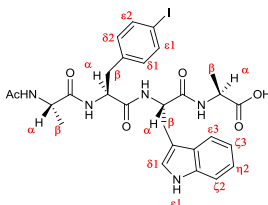
Supplementary Table 14 | ¹³C chemical shifts assignments of compound Ac-Ala-*m*-I-Phe-Val-Trp-Ala-OH (1j).

2j (¹H)			δ (ppm)										
AA	NH	α	β	δ1	δ2	ε2	ζ	ε1	ζ2	η2	ζ3	ε3	γ
Ala1	8.09	4.31	1.16	-	-	-	-	-	-	-	-	-	-
<i>m</i> -I-Phe	7.60	4.60	2.93	7.29	7.16	7.37	7.33	-	-	-	-	-	-
Val	8.09	4.07	1.75	-	-	-	-	-	-	-	-	-	0.72
Trp	7.67	4.65	3.34/3.20	-	-	-	-	11.19	7.33	7.08	6.95	7.42	-
Ala2	7.56	4.24	0.99	-	-	-	-	-	-	-	-	-	-

Supplementary Table 15 | ¹H chemical shifts assignments of compound Ac-Ala-(Cyclo-*m*)-[Phe-Val-Trp]-Ala-OH (2j).

2j (¹³ C)			δ (ppm)								
AA	α	β	δ1	δ2	ε2	ζ	ζ2	η2	ζ3	ε3	γ
Ala1	47.7	17.7	-	-	-	-	-	-	-	-	-
<i>m</i> -I-Phe	53.4	38.0	129.1	128.9	128.1	126.8	-	-	-	-	-
Val	57.4	30.1	-	-	-	-	-	-	-	-	18.5
Trp	52.0	26.2	-	-	-	-	110.5	120.9	118.0	119.2	-
Ala2	47.4	16.4	-	-	-	-	-	-	-	-	-

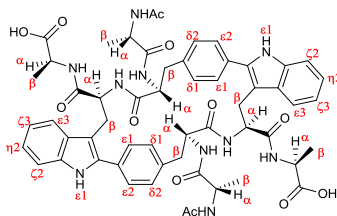
Supplementary Table 16 | ¹³C chemical shifts assignments of compound Ac-Ala-(Cyclo-*m*)-[Phe-Val-Trp]-Ala-OH (2j).



1k (¹ H)		δ (ppm)									
AA	NH	α	β	δ1	δ2	ε2	ε1	ζ2	η2	ζ3	ε3
Ala1	7.96	4.19	1.07	-	-	-	-	-	-	-	-
<i>p</i> -I-Phe	7.83	4.40	2.90/2.70	6.93	6.93	7.51	7.51	-	-	-	-
Trp	8.02	4.56	3.13/2.95	7.16	-	-	10.81	7.32	7.05	6.97	7.60
Ala2	8.25	4.23	1.27	-	-	-	-	-	-	-	-

Supplementary Table 17 | ¹H chemical shifts assignments of compound Ac-Ala-*p*-I-Phe-Trp-Ala-OH (1k).

1k(¹³ C)		δ (ppm)								
AA	α	β	δ1	δ2	ε2	ε1	ζ2	η2	ζ3	ε3
Ala1	47.8	17.6	-	-	-	-	-	-	-	-
<i>p</i> -I-Phe	53.2	36.6	131.4	131.4	136.3	136.3	-	-	-	-
Trp	52.8	27.5	123.3	-	-	-	111.0	120.6	117.9	118.2
Ala2	47.4	17.0	-	-	-	-	-	-	-	-

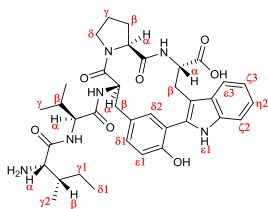
Supplementary Table 18 | ¹³C chemical shifts assignments of compound Ac-Ala-*p*-I-Phe-Trp-Ala-OH (1k).

2k (¹ H)		δ (ppm)									
AA	NH	α	β	δ1	δ2	ε2	ε1	ζ2	η2	ζ3	ε3
Ala1	7.93	4.18	1.08	-	-	-	-	-	-	-	-
<i>p</i> -I-Phe	8.13	3.96	2.64/2.48	7.25	7.25	7.61	7.61	-	-	-	-
Trp	6.82	4.07	3.43/3.43	-	-	-	11.20	7.34	7.11	7.03	7.67
Ala2	7.90	4.21	1.28	-	-	-	-	-	-	-	-

Supplementary Table 19 | ¹H chemical shifts assignments of compound Cyclo-*p,p*/bis-[Phe-Trp]-(Ac-Ala-Phe-Trp-Ala-OH) (2k).

2k (¹³ C)			δ (ppm)							
AA	α	β	δ1	δ2	ε2	ε1	ζ2	η2	ζ3	ε3
Ala1	47.7	17.8	-	-	-	-	-	-	-	-
<i>p</i> -I-Phe	52.9	35.2	128.8	128.8	127.9	127.9	-	-	-	-
Trp	54.9	25.55	-	-	-	-	110.9	121.4	118.5	118.3
Ala2	47.5	17.0	-	-	-	-	-	-	-	-

Supplementary Table 20 | ¹³C chemical shifts assignments of compound Cyclo-*p,p*/bis-[Phe-Trp]-(Ac-Ala-Phe-Trp-Ala-OH) (2k). Due to the symmetric nature of peptide 2k', both tetrapeptide moieties (A¹-F-W-A²) are equivalent and have identical NMR signals.

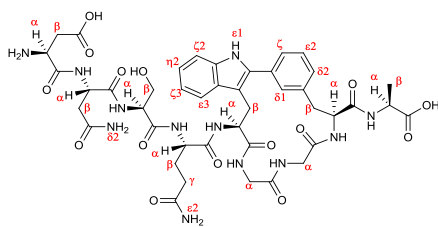


2I (¹ H)												
AA	NH	α	β	δ1	δ2	ε1	ζ2	η2	ζ3	ε3	γ1	γ2
Ile	8.22	3.31	1.75	0.85	-	-	-	-	-	-	1.43/1.11	0.85
Val	8.15	4.33	1.97	-	-	-	-	-	-	-	0.85	-
<i>m</i> - <i>l</i> -Tyr	8.32	4.68	3.07/2.89	7.11	7.14	6.89	-	-	-	-	-	-
Pro	-	4.49	2.12/1.56	3.61/3.06	-	-	-	-	-	-	1.72/1.47	-
Trp	7.60	4.53	3.26/2.77	-	-	10.79	7.32	7.06	6.99	7.60	-	-

Supplementary Table 21 | ¹H chemical shifts assignments of compound H-Ile-Val-(Cyclo-*m*)-[Tyr-Pro-Trp]-OH (2I).

2I (¹³ C)											
AA	α	β	δ1	δ2	ε1	ζ2	η2	ζ3	ε3	γ1	γ2
Ile	58.1	37.3	-	-	-	-	-	-	-	23.3	-
Val	56.7	30.7	-	-	-	-	-	-	-	-	-
<i>m</i> - <i>l</i> -Tyr	51.5	35.9	130.3	131.2	115.6	-	-	-	-	-	-
Pro	59.5	25.6	46.6	-	-	-	-	-	-	24.1	-
Trp	54.1	28.5	-	-	-	110.7	120.5	117.9	117.8	-	-

Supplementary Table 22 | ¹³C chemical shifts assignments of compound H-Ile-Val-(Cyclo-*m*)-[Tyr-Pro-Trp]-OH (2I). Based on NOE interactions and ¹³C chemical shift differences of Pro, it was assigned a *trans* type configuration to this amino acid (¹³C Δδ_{β-α} = 1.6 and ¹H_α-¹H_δ NOE correlation identified).^{6,7}

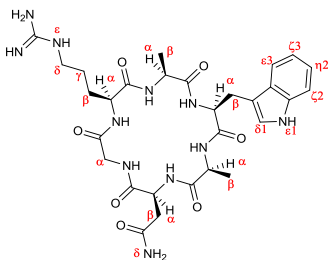


2m (¹ H)		δ (ppm)										
AA	NH	α	β	δ1	δ2	ε2	ε1	ζ/ ζ2	η2	ζ3	ε3	γ1
Asp	-	3.85	2.59	-	-	-	-	-	-	-	-	-
Asn	8.58	4.67	2.65/2.50	-	7.38/6.93	-	-	-	-	-	-	-
Ser	8.23	4.18	3.71/3.58	-	-	-	-	-	-	-	-	-
Gln	8.01	4.27	1.91/1.78	-	-	7.30/6.74	-	-	-	-	-	2.12/2.06
Trp	8.15	4.83	3.45/3.01	-	-	-	11.16	7.86	7.05	7.11	7.35	-
Gly	8.15	3.79/3.24	-	-	-	-	-	-	-	-	-	-
Gly	8.58	3.62/3.32	-	-	-	-	-	-	-	-	-	-
m-I-Phe	6.86	4.57	3.15/2.83	7.36	7.86	7.38	-	7.41	-	-	-	-
Ala	8.50	4.22	1.34	-	-	-	-	-	-	-	-	-

Supplementary Table 23 | ¹H chemical shifts assignments of compound H-Asp-Asn-Ser-Gln-(Cyclo-m)-[Trp-Gly-Gly-Phe]-Ala-OH (2m).

2m (¹³ C)			δ (ppm)								
AA	α	β	δ1	δ2	ε2	ε1	ζ/ ζ2	η2	ζ3	ε3	γ1
Asp	50.1	37.3	-	-	-	-	-	-	-	-	-
Asn	49.8	36.5	-	-	-	-	-	-	-	-	-
Ser	56.0	61.2	-	-	-	-	-	-	-	-	-
Gln	52.3	27.5	-	-	-	-	-	-	-	-	31.4
Trp	52.7	27.7	-	-	-	-	118.9	118.3	121.1	110.7	-
Gly	42.7	-	-	-	-	-	-	-	-	-	-
Gly	42.1	-	-	-	-	-	-	-	-	-	-
<i>m</i> -I-Phe	53.8	37.5	127.2	130.1	127.9	-	125.2	-	-	-	-
Ala	47.5	16.76	-	-	-	-	-	-	-	-	-

Supplementary Table 24 | ¹³C chemical shifts assignments of compound H-Asp-Asn-Ser-Gln-(Cyclo-m)-[Trp-Gly-Gly-Phe]-Ala-OH (2m).

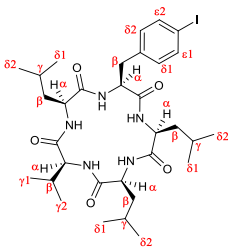


3 (¹ H)		δ (ppm)								
AA	NH	α	β	δ1	ε1	ζ2	η2	θ3	ε3	γ
Trp	7.88	4.28	3.18	7.14	10.83	7.32	7.06	6.97	7.58	-
Ala1	8.09	3.97	1.21	-	-	-	-	-	-	-
Asn	8.14	4.35	2.61	7.42/6.92	-	-	-	-	-	-
Gly	8.25	3.84/3.55	-	-	-	-	-	-	-	-
Arg	8.06	4.12	1.87/1.60	3.08	7.47	-	-	-	7.47	1.47
Ala2	7.99	4.08	1.21	-	-	-	-	-	-	-

Supplementary Table 25 | ¹H chemical shifts assignments of compound Cyclo(-Arg-Ala-Trp-Ala-Asn-Gly-) (3).

3 (¹³ C)		δ (ppm)								
AA	α	β	δ1	ζ2	η2	θ3	ε3	γ		
Trp	54.3	26.6	123.5	111.0	120.6	117.9	118.1	-	-	-
Ala1	49.3	17.0	-	-	-	-	-	-	-	-
Asn	50.0	35.6	-	-	-	-	-	-	-	-
Gly	42.6	-	-	-	-	-	-	-	-	-
Arg	52.7	27.7	40.1	-	-	-	-	24.8	-	-
Ala2	49.2	17.0	-	-	-	-	-	-	-	-

Supplementary Table 26 | ¹³C chemical shifts assignments of compound Cyclo(-Arg-Ala-Trp-Ala-Asn-Gly-) (3).

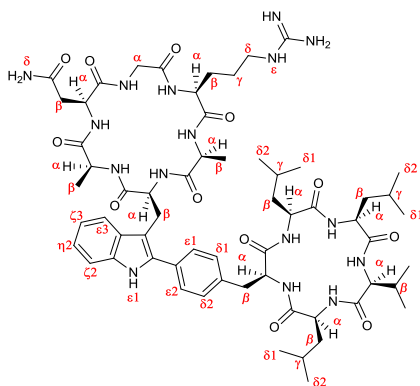


4 (¹ H)		δ (ppm)						
AA	NH	α	β	γ	δ	ε		
Leu1	8.15	3.94	1.52/1.35	1.28	0.83	-	-	-
p-I-Phe	8.14	4.27	3.02	-	7.03	7.62	-	-
Leu2	7.98	4.05	1.72/1.48	1.33	0.83	-	-	-
Leu3	7.95	4.12	1.68/1.55	1.53	0.83	-	-	-
Val	8.02	3.66	2.15	0.83	-	-	-	-

Supplementary Table 27 | ¹H chemical shifts assignments of compound Cyclo(-Leu-Leu-Val-Leu-p-I-Phe-) (4).

4 (¹³ C)		δ (ppm)				
AA	α	β	γ	δ	ε	
Leu1	53.0	39.5	24.1	-	-	-
p-I-Phe	55.3	35.4	-	131.3	136.7	-
Leu2	53.2	39.2	24.1	-	-	-
Leu3	53.4	39.7	24.4	-	-	-
Val	60.9	29.0	-	-	-	-

Supplementary Table 28 | ¹³C chemical shifts assignments of compound Cyclo(-Leu-Leu-Val-Leu-p-I-Phe-) (4).

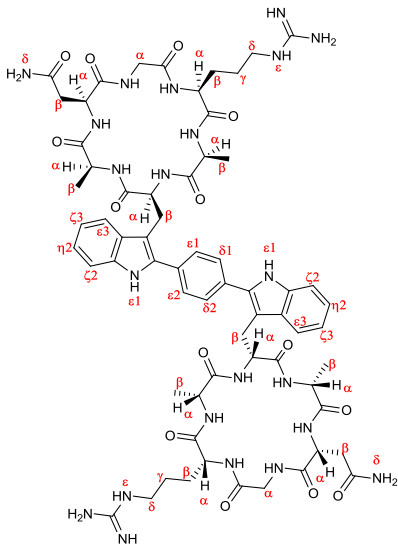


5 (¹ H)			δ (ppm)									
AA	NH	α	β	δ1	δ2	ε2	ε1	ζ2	η2	ζ3	ε3	γ
Trp	8.07	4.25	3.40/3.32	-	-	-	11.16	7.33	7.08	6.98	7.59	-
Ala1	8.00	3.92	1.11	-	-	-	-	-	-	-	-	-
Asn	8.04	4.35	2.58	7.42/6.91	-	-	-	-	-	-	-	-
Gly	8.45	3.86/3.41	-	-	-	-	-	-	-	-	-	-
Arg	7.98	4.15	1.79/1.59	3.08	-	-	7.42	-	-	-	-	1.47
Ala2	7.94	4.02	1.11	-	-	-	-	-	-	-	-	-
Leu1	8.18	3.97	1.63	0.85	0.85	-	-	-	-	-	-	1.37
p-I-Phe	8.19	4.33	3.12	7.33	7.33	7.64	7.64	-	-	-	-	-
Leu2	7.98	4.13	1.56	0.85	0.85	-	-	-	-	-	-	1.47
Leu3	7.98	4.13	1.71	0.85	0.85	-	-	-	-	-	-	1.54
Val	8.00	3.72	2.15	-	-	-	-	-	-	-	-	0.85

Supplementary Table 29 | ¹H chemical shifts assignments of compound Cyclo(Ala-Asn-Gly-Arg-Ala-C2-Trp)-Cyclo(C4-Phe-Leu-Leu-Val-Leu-) (5).

5 (¹³ C)	δ (ppm)										
AA	α	β	δ1	δ2	ε2	ε1	ζ2	η2	ζ3	ε3	γ
Trp	55.5	26.2	-	-	-	-	110.7	121.2	118.3	118.8	-
Ala1	48.8	17.0	-	-	-	-	-	-	-	-	-
Asn	50.0	35.7	-	-	-	-	-	-	-	-	-
Gly	43.0	-	-	-	-	-	-	-	-	-	-
Arg	52.6	28.1	40.1	-	-	-	-	-	-	-	24.9
Ala2	48.8	17.0	-	-	-	-	-	-	-	-	-
Leu1	52.9	39.4	-	-	-	-	-	-	-	-	24.2
<i>p</i> -I-Phe	55.9	35.9	129.0	129.0	127.1	127.1	-	-	-	-	-
Leu2	53.5	39.6	-	-	-	-	-	-	-	-	24.1
Leu3	53.5	39.5	-	-	-	-	-	-	-	-	24.4
Val	60.7	29.2	-	-	-	-	-	-	-	-	-

Supplementary Table 30 | ¹³C chemical shifts assignments of compound Cyclo(Ala-Asn-Gly-Arg-Ala-C2-Trp)-Cyclo(C4-Phe-Leu-Leu-Val-Leu-) (5).

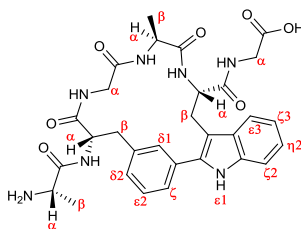


6 (¹ H)		δ (ppm)										
AA	NH	α	β	δ1	δ2	ε2	ε1	ζ2	η2	ζ3	ε3	γ
Trp	8.17	4.36	3.51/3.40	-	-	-	11.29	7.36	7.11	7.00	7.65	-
Ala1	8.06	4.04	1.11	-	-	-	-	-	-	-	-	-
Asn	8.06	4.36	2.63-2.56	7.42/6.89	-	-	-	-	-	-	-	-
Gly	8.40	3.86/3.42	-	-	-	-	-	-	-	-	-	-
Arg	7.97	4.18	1.81/1.62	3.08	-	-	-	-	-	-	-	1.47
Ala2	8.06	3.98	1.11	-	-	-	-	-	-	-	-	-
Ph	-	-	-	7.87	7.87	7.87	7.87	-	-	-	-	-

Supplementary Table 31 | ¹H chemical shifts assignments of compound Bis[cyclo(-Arg-Ala-Trp-Ala-Asn-Gly-)] adduct (6).

6 (¹³ C)			δ (ppm)								
AA	α	β	δ1	δ2	ε2	ε1	ζ2	η2	ζ3	ε3	γ
Trp	55.4	26.3	-	-	-	-	110.7	121.3	118.3	118.1	-
Ala1	49.0	17.0	-	-	-	-	-	-	-	-	-
Asn	50.1	35.8	-	-	-	-	-	-	-	-	-
Gly	42.8	-	-	-	-	-	-	-	-	-	-
Arg	52.2	28.0	39.9	-	-	-	-	-	-	-	24.6
Ala2	48.8	17.0	-	-	-	-	-	-	-	-	-
Ph	-	-	127.3	127.3	127.3	127.3	-	-	-	-	-

Supplementary Table 32 | ¹³C chemical shifts assignments of compound Bis[cyclo(-Arg-Ala-Trp-Ala-Asn-Gly-)] adduct (6).

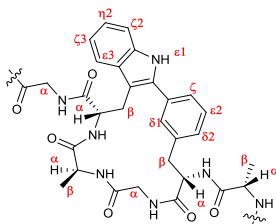


9 (^1H)		δ (ppm)										
AA	NH	α	β	$\delta 1$	$\delta 2$	$\epsilon 2$	ζ	$\epsilon 1$	$\zeta 2$	$\eta 2$	$\zeta 3$	$\epsilon 3$
Ala1	-	3.71	1.28	-	-	-	-	-	-	-	-	-
<i>m</i> -I-Phe	9.14	4.79	3.14/3.03	7.50	7.14	7.35	7.40	-	-	-	-	-
Gly1	8.43	3.76/3.57	-	-	-	-	-	-	-	-	-	-
Ala2	7.84	3.83	0.80	-	-	-	-	-	-	-	-	-
Trp	6.80	4.55	3.56/3.32	-	-	-	-	11.15	7.34	7.11	7.01	7.59
Gly2	7.38	3.55/3.38	-	-	-	-	-	-	-	-	-	-

Supplementary Table 33 | ^1H chemical shifts assignments of compound H-Ala-(Cyclo-*m*)-[Phe-Gly-Ala-Trp]-Gly-OH (9).

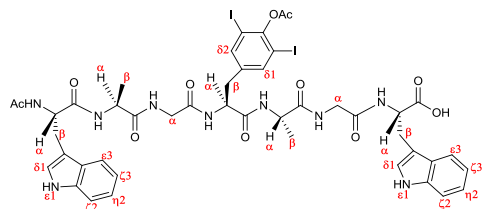
9 (¹³ C)			δ (ppm)							
AA	α	β	δ1	δ2	ε2	ζ	ζ2	η2	ζ3	ε3
Ala1	49.2	18.3	-	-	-	-	-	-	-	-
<i>m</i> -I-Phe	52.7	36.8	129.0	128.9	128.0	128.7	-	-	-	-
Gly1	43.1	-	-	-	-	-	-	-	-	-
Ala2	49.3	15.8	-	-	-	-	-	-	-	-
Trp	52.4	26.6	-	-	-	-	110.9	121.3	118.5	118.2
Gly2	42.1	-	-	-	-	-	-	-	-	-

Supplementary Table 34 | ^{13}C chemical shifts assignments of compound H-Ala-(Cyclo-*m*)-[Phe-Gly-Ala-Trp]-Gly-OH (9).



Supplementary Table 35 | ¹H chemical shifts assignments of compound Cyclo[-Ala-(Cyclo-*m*)-[Phe-Gly-Ala-Trp]-Gly-] (10).

Supplementary Table 36 | ¹³C chemical shifts assignments of compound Cyclo[-Ala-(Cyclo-*m*)-[Phe-Gly-Ala-Trp]-Gly-] (10).

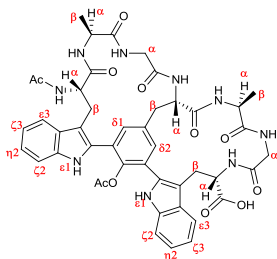


11 (¹ H)		δ (ppm)								
AA	NH	α	β	δ1	δ2	ε1	ζ2	η2	ζ3	ε3
Trp1	8.01	4.53	3.11/2.89	7.12	-	10.75	7.29	7.05	6.94	7.52
Ala1	8.13	4.24	1.20	-	-	-	-	-	-	-
Gly1	7.92	3.70/3.56	-	-	-	-	-	-	-	-
Tyr	8.07	4.56-4.45*	2.97/2.67	7.77	7.77	-	-	-	-	-
Ala2	8.30	4.27	1.21	-	-	-	-	-	-	-
Gly2	8.08	3.73	-	-	-	-	-	-	-	-
Trp2	8.06	4.48	3.18/3.04	7.14	-	10.84	7.32	7.07	6.97	7.59

Supplementary Table 37 | ¹H chemical shifts assignments of compound Ac-Trp-Ala-Gly-3,5-I,I-Tyr(OAc)-Ala-Gly-Trp-OH (11).

11 (¹³ C)			δ (ppm)					
AA	α	β	δ1	δ2	ζ2	η2	ζ3	ε3
Trp1	53.1	27.4	123.4	-	110.9	120.6	117.9	117.8
Ala1	48.1	17.9	-	-	-	-	-	-
Gly1	41.4	-	-	-	-	-	-	-
Tyr	53.1	35.7	139.4	139.4	-	-	-	-
Ala2	48.1	17.9	-	-	-	-	-	-
Gly2	41.5	-	-	-	-	-	-	-
Trp2	52.8	27.1	123.4	-	110.9	120.6	117.9	118.4

Supplementary Table 38 | ¹³C chemical shifts assignments of compound Ac-Trp-Ala-Gly-3,5-I,I-Tyr(OAc)-Ala-Gly-Trp-OH (11).



12 (¹ H)		δ (ppm)								
AA	NH	α	β	δ1	δ2	ε1	ζ2	η2	ζ3	ε3
Trp1	8.03	4.94	3.04	-	-	10.87	7.34	7.09	7.03	7.98
Ala1	6.79	4.19	1.03	-	-	-	-	-	-	-
Gly1	8.50	3.90/3.47	-	-	-	-	-	-	-	-
Tyr	7.22	4.75	3.30/3.19	7.43	7.36	-	-	-	-	-
Ala2	8.71	4.39	1.21	-	-	-	-	-	-	-
Gly2	8.24	3.58/3.24	-	-	-	-	-	-	-	-
Trp2	6.79	5.04	3.38/2.83	-	-	10.87	7.25	7.03	6.96	7.58

Supplementary Table 39 | ¹H chemical shifts assignments of compound Ac-(bicyclo-*m,m*)-[Trp-Ala-Gly-Tyr(OAc)]-[Tyr(OAc)-Ala-Gly-Trp]-OH (12).

12 (¹³ C)		δ (ppm)							
AA	α	β	δ1	δ2	ζ2	η2	ζ3	ε3	
Trp1	51.5	29.2	-	-	111.0	120.9	118.1	119.2	
Ala1	47.8	18.2	-	-	-	-	-	-	
Gly1	42.4	-	-	-	-	-	-	-	
Tyr	51.2	36.6	132.8	133.4	-	-	-	-	
Ala2	47.6	18.4	-	-	-	-	-	-	
Gly2	42.4	-	-	-	-	-	-	-	
Trp2	50.6	26.7	-	-	110.8	120.7	118.0	118.7	

Supplementary Table 40 | ¹³C chemical shifts assignments of compound Ac-(bicyclo-*m,m*)-[Trp-Ala-Gly-Tyr(OAc)]-[Tyr(OAc)-Ala-Gly-Trp]-OH (12).

Supplementary Methods

1. Abbreviations

Abbreviation used for amino acids and designations of peptides follow the rules of the IUPAC-IUB Commission of Biochemical Nomenclature in *J. Biol. Chem.* 247, 977-983 (1982). The following additional abbreviations are used: ACN: acetonitrile, DMF: *N,N*-dimethylformamide, DCM: dichloromethane, Fmoc: 9*H*-fluorenylmethyloxycarbonyl, TFA: trifluoroacetic acid, PBS: phosphate buffered saline, SPPS: solid phase peptide synthesis, DIEA: *N,N*-diisopropylethylamine, DIPCDI: *N,N*-diisopropylcarbodiimide, HOBt: hydroxybenzotriazole, HBTU: *o*-benzotriazole-*N,N,N',N'*-tetramethyl-uronium-hexafluoro-phosphate, TIS: triisopropylsilane, PyBOP: (benzotriazol-1-yl)oxytripyrrolidinophosphonium hexafluorophosphate, PyAOP: (7-azabenzotriazol-1-yl)oxytripyrrolidinophosphonium hexafluorophosphate, TBTU: *o*-(benzotriazol-1-yl)-*N,N,N',N'*-tetramethyluronium tetrafluoroborate, TFE: 2,2,2-trifluoroethanol, PivOH: pivalic acid, DMAP: 4-(dimethylamino)pyridine, Trt: trityl, Pbf: 2,2,4,6,7-pentamethyldihydrobenzofuran-5-sulfonyl, AB linker: 2-(4-hydroxymethylphenoxy)-propionic acid, IR: infrared spectroscopy, HPLC-MS: high performance liquid chromatography mass spectrometry, HRMS(ESI): high-resolution mass spectrometry (electrospray ionization), RP-HPLC; reversed phase-high performance liquid chromatography, NMR: nuclear magnetic resonance. HUVEC: human umbilica vein endothelial cell, Fb: fibrinogen, Vn: vitronectin.

2. General experimental information

Reactions were monitored by HPLC-MS at 220 nm using a HPLC Waters Alliance HT comprising a pump (Edwards RV12) with degasser, an autosampler and a diode array detector. Flow from the column was split to a MS spectrometer. The MS detector was configured with an eletrospray ionization source (micromass ZQ4000) and nitrogen was used as the nebulizer gas. Data acquisition was performed with MassLynx software. For compounds **2a-2c**, **2l**, **2m**, **1j-BODIPY**, **5**, **6**, and **16**, yields are estimated from the integration of the peak areas in the HPLC-MS crude. Other yields are for the isolated pure compound. All microwave reactions were carried out in 10 mL sealed glass tubes in a focused mono-mode microwave oven ("Discover" by CEM Corporation) featured with a surface sensor for internal temperature determination. Cooling was provided by compressed air ventilating the microwave chamber during the reaction. When stated, the final crude was purified via flash column chromatography Combi Flash ISCO RF provided with dual UV detection.

NMR spectra of peptides in DMSO-*d*₆ were acquired with either a Bruker DMX-500 MHz spectrometer or Bruker Avance III 600 MHz and Bruker Avance 800 MHz spectrometers equipped with TCI cryoprobes. The spectra were referenced relative to the residual DMSO signal (¹H, 2.49 ppm; ¹³C, 39.5 ppm). ¹H resonances were unequivocally assigned by two-dimensional NMR

experiments (COSY, TOCSY and NOESY and/or ROESY). Then, the ^{13}C resonances were straightforwardly assigned on the basis of the cross-correlations observed in the ^1H - ^{13}C HSQC spectra. Mixing times for TOCSY spectra were 70 ms, for NOESY spectra 300-450 ms and for ROESY experiments were 200 ms. The temperature coefficients for the amide protons of each peptide were determined via ^1H spectra in the range 298-313 K with a step size of 5 K. Chemical shifts (δ) are reported in ppm. Multiplicities are referred by the following abbreviations: s = singlet, d = doublet, t = triplet, dd = double doublet, dt = double triplet, q = quartet, p = pentuplet and m = multiplet. HRMS (ESI positive) were obtained with a LTQ-FT Ultra (Thermo Scientific) mass Spectrometer. IR spectra were obtained on a Thermo Nicolet NEXUS.

CD Spectroscopy. Circular dichroism (CD) measurements were performed using a Jasco J-815 spectrophotometer. The spectra were recorded from 260 to 170 nm using a 1.0 mm path-length quartz cuvette at 2 nm bandwidth, 50 nm/min scan speed, 0.5 s response time, 0.2 nm data pitch and three accumulations. The background signal of the buffer alone was subtracted for each spectrum. CD spectra were converted from raw ellipticity (θ , mdeg) to mean molar ellipticity per residue ($[\theta]$, deg $\text{cm}^2 \text{dmol}^{-1}$).

All the samples were dissolved in a buffer of 25 mM Na_2HPO_4 (pH 7) at both 100 and 200 μM final peptide concentration. Additionally, new determinations were made in 10% of 2,2,2-trifluoroethanol (TFE) to increase the propensity to form secondary structures. To ensure no interference of peptide aromatic moiety on the spectra profiles, the previously reported 3-(2-Phenyl-1*H*-indol-3-yl)propanoic acid¹ was also analysed at identical conditions as for the tested compounds.

General procedure for SPPS.² All peptides were manually synthesized in polystyrene syringes fitted with a polyethylene porous disc using Fmoc-based SPPS. Solvents and soluble reagents were removed by suction. The Fmoc group was removed with piperidine-DMF (1:4) (1 \times 1 min, 2 \times 5 min). Peptide synthesis transformations and washes were performed at r.t.

Resin loading (only for 2-Chlorotrityl resin). Fmoc-XX-OH (1.0 eq.) was attached to the resin (1.0 eq.) with DIEA (3.0 eq.) in DCM at r.t for 10 min and then DIEA (7.0 eq.) for 40 min. The remaining trityl groups were capped adding 0.8 μL MeOH/mg resin for 10 minutes. After that, the resin was

filtered and washed with DCM (4 x 1 min), DMF (4 x 1 min). The loading of the resin was determined by titration of the Fmoc group.²

Peptide elongation. After the Fmoc group was eliminated, the resin was washed with DMF (4 x 1 min), DCM (3 x 1 min), DMF (4 x 1 min). The completion of the coupling was monitored with the ninhydrin (free primary amine) or chloranil (free secondary amine) tests.³ Then, the resin was filtered and washed with DCM (4 x 1 min) and DMF (4 x 1 min) and the Fmoc group was eliminated.

Acetylation. When indicated, once the peptide was fully elongated, N-terminal acetylation was performed with acetic anhydride (10 eq.), DIEA (10 eq.) in DMF (30 min).

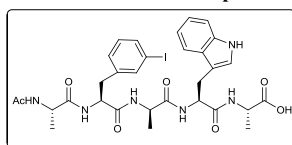
Final cleavage. The resin bound peptide was treated with the corresponding TFA cleavage cocktail. Then, the resin was washed with DCM and the combined eluates were evaporated under vacuum. Then, the residue was washed with Et₂O, dissolved in ACN:H₂O and lyophilized furnishing the corresponding peptide.

3. Experimental procedures and peptide characterization

Synthesis and peptide characterization of linear peptides 1a-1f

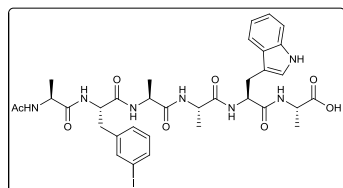
2-Chlorotrityl resin (1 mmol/g). Amino acid coupling. Fmoc-XX-OH (3.0 eq.) were incorporated with a 5-min pre-activation with DIPCDI (3.0 eq.) and HOBt (3.0 eq.) in DMF for 1h. The N-terminal was acetylated, and then the resin bound peptide was treated with a 5% (v/v) TFA/DCM solution (5 x 1 min).

Ac-Ala-*m*-Phe-Ala-Trp-Ala-OH (1a). HRMS (ESI) (m/z): [M] calcd. for C₃₁H₃₇IN₆O₇, 732.1768;



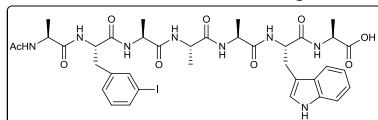
[M+H]⁺ found, 733.1836.

Ac-Ala-*m*-Phe-Ala-Ala-Trp-Ala-OH (1b). HRMS (ESI) (m/z): [M] calcd. for C₃₄H₄₂IN₇O₈,



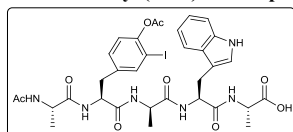
803.2140; [M+H]⁺ found, 804.2215.

Ac-Ala-*m*-Phe-Ala-Ala-Ala-Trp-Ala-OH (1c). HRMS (ESI) (m/z): [M] calcd. for $C_{37}H_{47}IN_8O_9$,



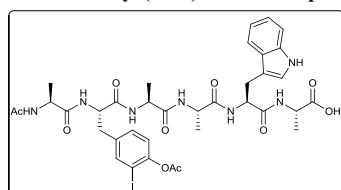
874.2511; $[M+H]^+$ found, 875.2583.

Ac-Ala-*m*-Tyr(OAc)-Ala-Trp-Ala-OH (1d). HPLC-MS (m/z): [M] calcd. for $C_{33}H_{39}IN_6O_9$,



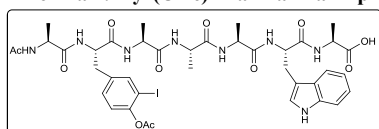
790.18; $[M+H]^+$ found, 791.06.

Ac-Ala-*m*-Tyr(OAc)-Ala-Ala-Trp-Ala-OH (1e). HPLC-MS (m/z): [M] calcd. for $C_{36}H_{44}IN_7O_{10}$,



861.22; $[M+H]^+$ found, 862.15.

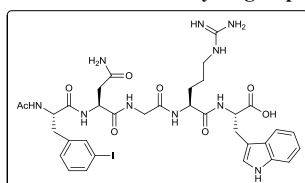
Ac-Ala-*m*-Tyr(OAc)-Ala-Ala-Ala-Trp-Ala-OH (1f). HPLC-MS (m/z): [M] calcd. for



$C_{39}H_{49}IN_8O_{11}$, 932.26; $[M+H]^+$ found, 933.17.

Synthesis and peptide characterization of linear peptides 1g-1k

Ac-*m*-I-Phe-Asn-Gly-Arg-Trp-OH (1g). 2-Chlorotrityl resin (0.94 mmol/g). Amino acid coupling.

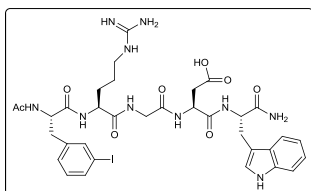


Fmoc-XX-OH (3.0 eq.) were incorporated with a 5-min pre-activation with DIPCDI (3.0 eq.) and OxymaPure (3.0 eq.) in DMF for 1h. Fmoc-XX-OH: Fmoc-Trp(Boc)-OH, Fmoc-Arg(Pbf)-OH, Fmoc-Gly-OH, Fmoc-Asn(Trt)-OH. Fmoc-*m*-I-

Phe-OH (1.5 eq.) was incorporated with HBTU (1.5 eq.), HOBT (1.5 eq.) and DIEA (3.0 eq.) in DMF for 1h. The resin bound peptide was treated with a 95% TFA, 2.5% TIS, 2.5% H_2O cocktail (1h). Pale solid (90-92% purity, estimated by HPLC-MS). 1H NMR (500 MHz, $DMSO-d_6$): δ 10.83 (m, 1H), 8.38 (d, $J = 7.7$ Hz, 1H), 8.18 (d, $J = 8.2$ Hz, 1H), 8.14 (d, $J = 7.5$ Hz, 1H), 8.03 (t, $J = 5.7$ Hz, 1H), 7.92 (d, $J = 8.2$ Hz, 1H), 7.66 (d, $J = 1.7$ Hz, 1H), 7.54 (d, $J = 7.9$ Hz, 1H), 7.51 (d, $J = 7.9$ Hz, 1H),

7.46 (m, 2H), 7.32 (d, $J = 8.1$ Hz, 1H), 7.25 (d, $J = 7.7$ Hz, 1H), 7.16 (d, $J = 2.4$ Hz, 1H), 7.05 (t, $J = 7.7$ Hz, 2H), 7.00 – 6.94 (m, 2H), 4.55 – 4.41 (m, 3H), 4.36 (td, $J = 8.4, 5.2$ Hz, 1H), 3.76 (dd, $J = 16.9, 5.9$ Hz, 1H), 3.66 (dd, $J = 16.8, 5.5$ Hz, 1H), 3.17 (dd, $J = 14.7, 5.5$ Hz, 1H), 3.07 (m, 3H), 2.98 (dd, $J = 13.7, 4.1$ Hz, 1H), 2.66 (dd, $J = 13.7, 10.3$ Hz, 1H), 2.57 (dd, $J = 15.5, 6.0$ Hz, 1H), 2.50 (1H), 1.75 (s, 3H), 1.68 (m, 1H), 1.58 – 1.40 (m, 3H) ppm. **HPLC-MS** (m/z): $[M+H]^+$ calcd. for $C_{34}H_{43}IN_{10}O_8$, 847.7; found, 847.1.

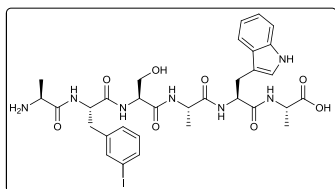
Ac-*m*-I-Phe-Arg-Gly-Asp-Trp-OH (1h). H-Rink-Amide Chemmatrix resin (0.53 mmol/g). Amino



acid coupling. Fmoc-XX-OH (3.0 eq.) were incorporated with a 5-min pre-activation with DIPCDI (3.0 eq.) and HOBt (3.0 eq.) in DMF for 1h (2h of coupling were carried out in the case of Fmoc-Trp(Boc)-OH). Fmoc-XX-OH: Fmoc-Trp(Boc)-OH,

Fmoc-Asp(Or-Bu)-OH, Fmoc-Gly-OH, Fmoc-Arg(Pbf)-OH, Fmoc-*m*-I-Phe-OH. The N-terminal was acetylated, and then the resin bound peptide was treated with a 95% TFA, 2.5% TIS, 2.5% H_2O cocktail (3h). Pale solid (>99% purity, estimated by HPLC-MS). **1H NMR** (600 MHz, $DMSO-d_6$): δ 10.74 (d, $J = 2.4$ Hz, 1H), 8.23 (dd, $J = 7.9, 2.4$ Hz, 2H), 8.14 – 8.05 (m, 2H), 7.85 (d, $J = 8.0$ Hz, 1H), 7.69 (d, $J = 1.7$ Hz, 1H), 7.60 – 7.51 (m, 2H), 7.42 (m, 1H), 7.32 (dt, $J = 8.1, 0.9$ Hz, 1H), 7.27 (dt, $J = 7.6, 1.3$ Hz, 1H), 7.12 – 7.03 (m, 4H), 6.97 (ddd, $J = 7.9, 6.9, 1.0$ Hz, 1H), 4.57 (td, $J = 7.7, 6.0$ Hz, 1H), 4.51 (ddd, $J = 10.5, 8.3, 4.0$ Hz, 1H), 4.39 (td, $J = 8.1, 5.0$ Hz, 1H), 4.31 (td, $J = 8.0, 5.6$ Hz, 1H), 3.77 – 3.69 (m, 2H), 3.16 (dd, $J = 14.7, 5.0$ Hz, 1H), 3.10 (dt, $J = 11.5, 5.7$ Hz, 2H), 2.98 (ddd, $J = 14.8, 6.6, 2.7$ Hz, 2H), 2.71 – 2.64 (m, 2H), 2.46 (dd, $J = 16.6, 7.7$ Hz, 1H), 1.76 (s, 3H), 1.72 (q, $J = 6.0, 4.3$ Hz, 1H), 1.60 – 1.44 (m, 3H) ppm. **HPLC-MS** (m/z): $[M+H]^+$ calcd. for $C_{34}H_{43}IN_{10}O_8$, 847.7; found, 847.2.

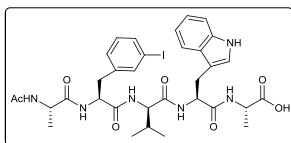
H-Ala-*m*-I-Phe-Ser-Ala-Trp-Ala-OH (1i). 2-Chlorotrityl resin (0.94 mmol/g). Amino acid



coupling. Fmoc-XX-OH (3.0 eq.) were incorporated with a 5-min pre-activation with DIPCDI (3.0 eq.) and HOBt (3.0 eq.) in DMF for 1h. Fmoc-XX-OH: Fmoc-Ala-OH, Fmoc-

Trp(Boc)-OH, Fmoc-Ser(*t*-Bu)-OH, Fmoc-*m*-I-Phe-OH. The resin bound peptide was treated with a 95% TFA, 2.5% TIS, 2.5% cocktail (1h). Pale solid (>99% purity, estimated by HPLC-MS). **¹H NMR** (500 MHz, DMSO-*d*₆): δ 10.80 (d, *J* = 2.8 Hz, 1H), 8.73 (s, 1H), 8.36 (d, *J* = 7.7 Hz, 1H), 8.15 (d, *J* = 6.7 Hz, 1H), 7.94 (dd, *J* = 16.4, 7.4 Hz, 2H), 7.71 (s, 1H), 7.57 (t, *J* = 8.5 Hz, 2H), 7.30 (t, *J* = 8.5 Hz, 2H), 7.12 (d, *J* = 2.6 Hz, 1H), 7.06 (m, 2H), 6.97 (t, *J* = 7.5 Hz, 1H), 5.39 (s, 1H), 4.58 (m, 1H), 4.48 (td, *J* = 9.1, 4.5 Hz, 1H), 4.35 (q, *J* = 6.3 Hz, 1H), 4.17 (q, *J* = 7.0 Hz, 1H), 4.10 (q, *J* = 7.1 Hz, 1H), 3.70 (m, 2H), 3.59 (dd, *J* = 10.6, 5.7 Hz, 1H), 3.17 (dd, *J* = 14.7, 4.3 Hz, 1H), 3.04 (dd, *J* = 14.2, 3.8 Hz, 1H), 2.88 (dd, *J* = 14.8, 9.6 Hz, 1H), 2.76 (dd, *J* = 14.2, 10.7 Hz, 1H), 1.31 – 1.21 (m, 6H), 1.12 (d, *J* = 7.2 Hz, 3H) ppm. **HPLC-MS** (m/z): [M+H]⁺ calcd. for C₃₂H₄₀IN₇O₈, 778.6; found, 778.2.

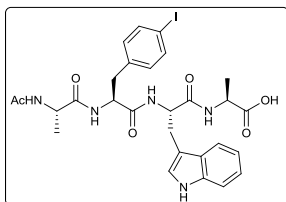
Ac-Ala-*m*-I-Phe-Val-Trp-Ala-OH (1j). 2-Chlorotrityl resin (1.0 mmol/g). Amino acid coupling.



Fmoc-XX-OH (3.0 eq.) were incorporated with a 5-min pre-activation with DIPCDI (3.0 eq.) and HOBt (3.0 eq.) in DMF for 1h. Fmoc-XX-OH: Fmoc-Ala-OH, Fmoc-Trp-OH, Fmoc-Val-OH.

Fmoc-*m*-I-Phe-OH (1.5 eq.) was incorporated with PyBOP (1.5 eq.), HOBt (1.5 eq.) and DIEA (3.0 eq.) in DMF for 1h. The N-terminal was acetylated, and then the resin bound peptide was treated with a 5% (v/v) TFA/DCM solution (5 x 1 min). Pale solid (>99% purity, estimated by HPLC-MS). **¹H NMR** (500 MHz, DMSO-*d*₆): δ 10.78 (d, *J* = 2.8 Hz, 1H), 8.17 (d, *J* = 7.1 Hz, 1H), 7.99 (t, *J* = 7.5 Hz, 2H), 7.94 (d, *J* = 8.2 Hz, 1H), 7.76 (d, *J* = 8.7 Hz, 1H), 7.60 (m, 2H), 7.50 (d, *J* = 7.9 Hz, 1H), 7.29 (d, *J* = 8.1 Hz, 1H), 7.20 (d, *J* = 7.7 Hz, 1H), 7.15 (d, *J* = 2.5 Hz, 1H), 7.04 (t, *J* = 7.5 Hz, 1H), 6.96 (td, *J* = 7.6, 3.4 Hz, 2H), 4.60 (td, *J* = 8.5, 4.8 Hz, 1H), 4.47 (td, *J* = 9.3, 8.7, 3.9 Hz, 1H), 4.25 – 4.11 (m, 3H), 3.13 (dd, *J* = 14.9, 4.7 Hz, 1H), 2.92 (ddd, *J* = 19.8, 10.3, 5.4 Hz, 2H), 2.76 – 2.67 (m, 1H), 1.94 (h, *J* = 6.8 Hz, 1H), 1.79 (s, 3H), 1.25 (d, *J* = 7.3 Hz, 3H), 1.10 (d, *J* = 7.2 Hz, 3H), 0.77 (dd, *J* = 9.8, 6.6 Hz, 6H) ppm. **HPLC-MS** (m/z): [M+H]⁺ calcd. for C₃₃H₄₁IN₆O₇, 761.6; found, 761.3.

Ac-Ala-*p*-I-Phe-Trp-Ala-OH (1k). 2-Chlorotrityl resin (1.0 mmol/g). Amino acid coupling. Fmoc-



XX-OH (3.0 eq.) were incorporated with a 5-min pre-activation with DIPCDI (3.0 eq.) and HOBt (3.0 eq.) in DMF for 1h. Fmoc-XX-OH: Fmoc-Ala-OH, Fmoc-Trp-OH. Fmoc-*p*-I-Phe-OH (1.5 eq.) was incorporated with HBTU (1.5 eq.), HOBt (1.5 eq.) and

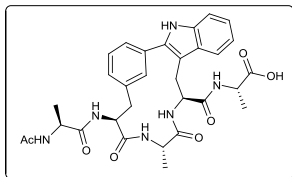
DIEA (3.0 eq.) in DMF for 1h. The N-terminal was acetylated, and the resin bound peptide was treated with a 5% (v/v) TFA/DCM solution (5 x 1 min). Pale solid (>99% purity, estimated by HPLC-MS). ¹H NMR (500 MHz, DMSO-*d*₆): δ 10.81 (d, *J* = 2.5 Hz, 1H), 8.25 (d, *J* = 7.2 Hz, 1H), 8.02 (d, *J* = 8.1 Hz, 1H), 7.96 (d, *J* = 7.4 Hz, 1H), 7.83 (d, *J* = 8.1 Hz, 1H), 7.60 (d, *J* = 7.9 Hz, 1H), 7.56 – 7.45 (m, 2H), 7.32 (d, *J* = 8.1 Hz, 1H), 7.16 (d, *J* = 2.4 Hz, 1H), 7.05 (dd, *J* = 8.2, 6.9 Hz, 1H), 6.97 (t, *J* = 7.4, 6.9 Hz, 1H), 6.95 – 6.90 (m, 2H), 4.56 (td, *J* = 8.5, 4.7 Hz, 1H), 4.40 (td, *J* = 8.5, 4.6 Hz, 1H), 4.21 (dp, *J* = 21.4, 7.1 Hz, 2H), 3.13 (dd, *J* = 14.9, 4.7 Hz, 1H), 3.01 – 2.81 (m, 2H), 2.70 (dd, *J* = 13.9, 8.9 Hz, 1H), 1.79 (s, 3H), 1.27 (d, *J* = 7.3 Hz, 3H), 1.07 (d, *J* = 7.1 Hz, 3H). ppm. HPLC-MS (*m/z*): [M+H]⁺ calcd. for C₂₈H₃₂N₅O₆, 662.5; found, 662.2.

General procedure for the C-H activation process of peptides 2a-2f

Unless stated otherwise, the linear peptide (50 mg), AgBF₄ (1.0 eq.), 2-nitrobenzoic acid (1.5 eq) and Pd(OAc)₂ (0.05 eq) were placed in a microwave reactor vessel in DMF or in a 1:1 mixture of DMF:PBS. The mixture was heated under microwave irradiation (80 W) at 80 °C for 15 min. Water was added and the resulting suspension was filtered through Celite. The filtrate was successively washed with Et₂O, and the aqueous phase was lyophilized. The residue was purified by semi-preparative RP-HPLC (XBRIDGETM Pref C18 5μM 19x100 mm column), using gradients of 25% of B to 60% B [solvent A (0.1% TFA in H₂O) and solvent B (0.07% TFA in ACN)], in 20 min, flux: 16 mL·min⁻¹, detection at λ=220 nm.

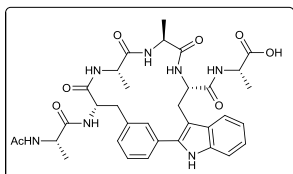
Synthesis and peptide characterization of locked peptides 2a-2f

Ac-Ala-(Cyclo-*m*)-[Phe-Ala-Trp]-Ala-OH (2a). Starting from peptide **1a** (27 mg, 0.037 mmol) in



a 1:1 mixture of DMF:PBS (total volume of 600 μ L). Pale solid (38% conversion, estimated by HPLC-MS, 32% yield). **HRMS** (ESI) (m/z): $[M+H]^+$ calcd. for $C_{31}H_{36}N_6O_7$, 605.27182; found, 605.27400.

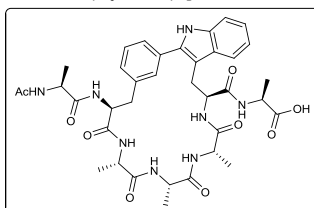
Ac-Ala-(Cyclo-*m*)-[Phe-Ala-Ala-Trp]-Ala-OH (2b). Starting from peptide **1b** (50 mg, 0.062



mmol) in a 1:1 mixture of DMF:PBS (total volume of 400 μ L). Pale solid (total conversion, estimated by HPLC-MS, 26% yield). **HRMS** (ESI) (m/z): $[M+H]^+$ calcd. for $C_{34}H_{41}N_7O_8$, 676.30894; found, 676.31130. **1H NMR** (500 MHz, D_2O): δ 10.58 (s, 1H),

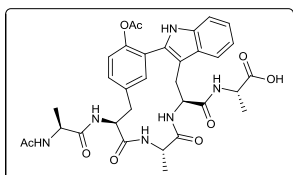
8.49 (d, $J = 3.2$ Hz, 1H), 8.29 (m, 2H), 7.79 (d, $J = 8.0$ Hz, 1H), 7.68 (s, 1H), 7.59 (dd, $J = 11.3, 5.5$ Hz, 3H), 7.48 (m, 2H), 7.44 – 7.39 (m, 1H), 7.29 (t, $J = 7.5$ Hz, 1H), 7.22 (t, $J = 7.5$ Hz, 1H), 6.89 (d, $J = 9.5$ Hz, 1H), 4.89 (1H), 4.82 (1H), 4.37 – 4.22 (m, 2H), 4.02 (dd, $J = 7.3, 3.0$ Hz, 1H), 3.84 (qd, $J = 7.3, 3.6$ Hz, 1H), 3.73 (dd, $J = 15.2, 3.4$ Hz, 1H), 3.47 (dd, $J = 15.1, 11.5$ Hz, 1H), 3.25 (d, $J = 7.3$ Hz, 2H), 1.99 (s, 3H), 1.42 (d, $J = 7.3$ Hz, 3H), 1.34 (m, 6H), 0.82 (d, $J = 7.4$ Hz, 3H) ppm.

Ac-Ala-(Cyclo-*m*)-[Phe-Ala-Ala-Ala-Trp]-Ala-OH (2c). Starting from peptide **1c** (25 mg, 0.029



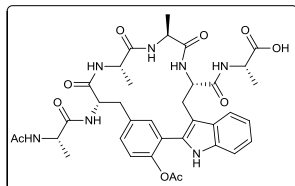
mmol) in a 1:1 mixture of DMF:PBS (total volume of 600 μ L). Pale solid (total conversion, estimated by HPLC-MS, 54% yield). **HRMS** (ESI) (m/z): $[M+H]^+$ calcd. for $C_{37}H_{46}N_8O_9$, 747.34605; found, 747.34752.

Ac-Ala-(Cyclo-*m*)-[Tyr(OAc)-Ala-Trp]-Ala-OH (2d). Starting from peptide **1d** (50 mg, 0.063



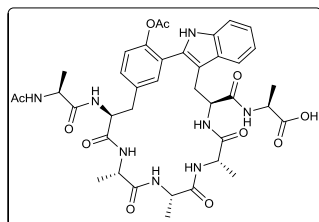
mmol) in a 1:1 mixture of DMF:PBS (total volume of 400 μ L) (total conversion, estimated by HPLC-MS). **HPLC-MS** (m/z): $[M+H]^+$ calcd. for $C_{33}H_{38}N_6O_9$, 663.69; found, 663.14.

Ac-Ala-(Cyclo-*m*)-[Tyr(OAc)-Ala-Ala-Trp]-Ala-OH (2e). Starting from peptide **1e** (50 mg, 0.058



mmol) in a 1:1 mixture of DMF:PBS (total volume of 400 μ L). (total conversion, estimated by HPLC-MS). **HRMS** (ESI) (m/z): $[M+H]^+$ calcd. for $C_{36}H_{43}N_7O_{10}$, 734.31442; found, 734.31681.

Ac-Ala-(Cyclo-*m*)-[Tyr(OAc)-Ala-Ala-Ala-Trp]-Ala-OH (2f). Starting from peptide **1f** (50 mg,



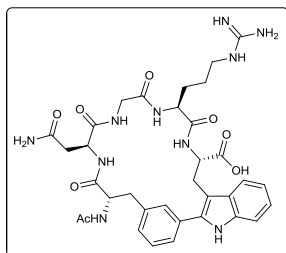
0.053 mmol) in a 1:1 mixture of DMF:PBS (total volume of 400 μ L). (total conversion, estimated by HPLC-MS). **HPLC-MS** (m/z): $[M+H]^+$ calcd. for $C_{39}H_{48}N_8O_{11}$, 805.85; found, 805.34.

General procedure for the C-H activation process of peptides 2g-2k

Unless stated otherwise, the linear peptide (50 mg), $AgBF_4$ (2.0 eq.), trifluoroacetic acid (1.0 eq.) and $Pd(OAc)_2$ (0.05 eq.) were placed in a microwave reactor vessel in DMF. The mixture was heated under microwave irradiation (250 W) at 90 $^{\circ}C$ for 20 min. The residue was filtered and purified by semi-preparative RP-HPLC (XBRIDGETM BEH 130, C18, 5 μ M OBD 19x50 mm column) [solvent A (0.1% FA in H_2O) and solvent B (0.1% FA in ACN)], in 10 min, flux: 20 mL \cdot min⁻¹, detection at $\lambda=220$ nm.

Synthesis and peptide characterization of locked peptides 2g-2m

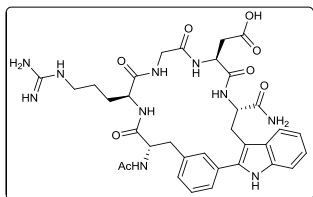
Ac-(Cyclo-*m*)-[Phe-Asn-Gly-Arg-Trp]-OH (2g). Starting from peptide **1g** (186 mg, 0.220 mmol)



(77% conversion, estimated by HPLC-MS). Semi-preparative RP-HPLC gradient: 15-30% of B. Pale solid (45.3 mg, 29%). **¹H NMR** (500 MHz, $DMSO-d_6$): δ 11.15 (s, 1H), 8.42 (s, 1H), 8.35 (m, 2H), 7.79 (d, $J = 8.2$ Hz, 1H), 7.72 – 7.60 (m, 3H), 7.49 (d, $J = 7.7$ Hz, 1H), 7.38 (m, 2H), 7.32 (d, $J = 8.1$ Hz, 1H), 7.20 (d, $J = 7.7$ Hz, 1H), 7.06 (t, $J = 7.6$ Hz, 1H), 6.97 (t, $J = 7.5$ Hz, 1H), 6.85 (m, 1H), 4.68 (m, 1H), 4.60 (m, 1H), 4.48

(m, 1H), 4.30 (m, 1H), 3.98 (dd, $J = 16.4, 6.8$ Hz, 1H), 3.43 (1H), 3.42 (1H), 3.14-2.99 (4H), 2.88 (t, $J = 12.4$ Hz, 1H), 2.66 – 2.58 (m, 1H), 2.44 (1H), 1.77 (m, 4H), 1.55 (m, 1H), 1.41 (m, 2H) ppm. **IR** (Film, cm^{-1}) $\nu = 3417.08, 3276.16, 3064.77, 2911.03, 1623.49, 1533.81$ cm^{-1} . **HRMS** (ESI) (m/z): $[M+H]^+$ calcd. for $\text{C}_{34}\text{H}_{42}\text{N}_{10}\text{O}_8$, 719.8; found, 720.1.

Ac-(Cyclo-*m*)-[Phe-Arg-Gly-Asp-Trp]-NH₂ (2h). Starting from peptide **1h** (190 mg, 0.224 mmol)



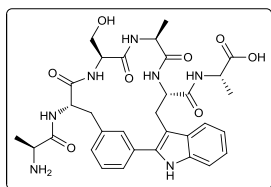
(70% conversion, estimated by HPLC-MS). Semi-preparative

RP-HPLC gradient: 15-20% of B. Pale solid (28.9 mg, 18%). **¹H**

NMR (600 MHz, DMSO- d_6): δ 11.00 (s, 1H), 9.88 (s, 1H), 8.39 (s, 1H), 8.32 (d, $J = 7.8$ Hz, 1H), 8.06 (s, 1H), 7.88 (d, $J = 5.5$

Hz, 1H), 7.69 (s, 1H), 7.59 (d, $J = 8.0$ Hz, 1H), 7.42 (dt, $J = 7.8, 1.4$ Hz, 1H), 7.39 (t, $J = 7.5$ Hz, 1H), 7.35 (s, 1H), 7.31 (d, $J = 8.0$ Hz, 1H), 7.24 (d, $J = 7.4$ Hz), 7.10 – 7.04 (m, 2H), 7.01 – 6.97 (t, $J = 7.2$ Hz, 1H), 6.89 (s, 1H), 4.66 (td, $J = 7.9, 5.4$ Hz, 1H), 4.53 (m, 1H), 4.25 (dt, $J = 9.4, 4.4$ Hz, 1H), 4.06 – 3.99 (m, 1H), 3.68 (dd, $J = 16.7, 6.6$ Hz, 1H), 3.46 – 3.42 (m, 2H), 3.14 (m, 1H), 3.04 – 2.93 (m, 3H), 2.75 (m, 1H), 2.67 (dd, $J = 16.5, 4.0$ Hz, 1H), 2.18 (dd, $J = 16.9, 5.7$ Hz, 1H), 1.88 (s, 3H), 1.86 – 1.82 (m, 1H), 1.49 (m, 1H), 1.41 (m, 1H), 1.34 (m, 1H) ppm. **¹³C NMR** (151 MHz, DMSO- d_6): δ 174.82, 173.61, 172.52, 170.87, 170.73, 168.98, 167.68, 157.10, 137.76, 135.84, 135.27, 132.97, 129.15, 128.80, 128.31, 128.07, 126.29, 121.11, 118.73, 118.47, 110.87, 107.50, 53.74, 53.36, 52.83, 49.22, 43.37, 40.69, 38.67, 37.51, 30.53, 27.10, 24.88, 22.53 ppm. **IR** (Film): $\nu = 3423.49, 3269.75, 2923.84, 1649.11, 1629.89, 1540.21$ cm^{-1} . **HRMS** (ESI) (m/z): $[M+H]^+$ calcd. for $\text{C}_{34}\text{H}_{42}\text{N}_{10}\text{O}_8$, 719.32598; found, 719.32718.

H-Ala-(Cyclo-*m*)-[Phe-Ser-Ala-Trp]-Ala-OH (2i). Starting from peptide **1i** (145 mg, 0.186



mmol). Additional microwave irradiation cycles were necessary to

perform until obtain the desired product as the main peak by HPLC-

MS (39% conversion, estimated by HPLC-MS). Semi-preparative

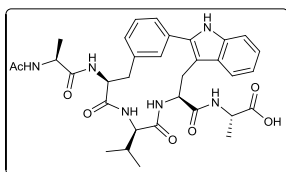
RP-HPLC gradient: 12-32% of B. Pale solid (11.5 mg, 10%). **¹H**

NMR (600 MHz, DMSO- d_6): δ 11.09 (s, 1H), 8.46 (m, 1H), 8.35 (t,

$J = 4.7$ Hz, 1H), 7.65 (s, 1H), 7.61 (d, $J = 7.9$ Hz, 1H), 7.53 – 7.48 (m, 1H), 7.45 – 7.39 (m, 2H), 7.39

– 7.35 (m, 1H), 7.34 (d, $J = 8.0$ Hz, 1H), 7.22 (dt, $J = 6.4, 1.9$ Hz, 1H), 7.11 (t, $J = 7.6$ Hz, 1H), 7.04 – 7.00 (t, $J = 7.6$ Hz, 1H), 6.81 (d, $J = 9.5$ Hz, 1H), 4.97 (dd, $J = 10.4, 3.6$ Hz, 1H), 4.51 (ddd, $J = 13.3, 8.5, 2.5$ Hz, 1H), 4.15 (p, $J = 7.3$ Hz, 1H), 3.87 (dt, $J = 5.9, 4.4$ Hz, 1H), 3.70 (qd, $J = 7.3, 4.1$ Hz, 1H), 3.65 – 3.58 (m, 3H), 3.48 (1H), 3.30 (1H), 3.18 (dd, $J = 13.6, 10.3$ Hz, 1H), 3.08 (dd, $J = 13.7, 3.5$ Hz, 1H), 1.32 (d, $J = 7.3$ Hz, 3H), 1.17 (d, $J = 6.9$ Hz, 3H), 0.76 (d, $J = 7.3$ Hz, 3H). ^{13}C NMR (151 MHz, DMSO- d_6): δ 173.74, 172.09, 171.69, 171.36, 170.54, 137.18, 135.95, 134.68, 132.59, 128.88, 128.73, 128.59, 128.48, 125.80, 121.63, 118.74, 118.18, 111.12, 108.33, 60.30, 58.37, 53.75, 51.87, 50.13, 49.47, 48.00, 36.64, 26.78, 20.08, 17.00, 16.02 ppm. IR (Film): $\nu = 3321.00, 2917.44, 3064.77, 2846.98, 1655.52, 1597.86$ cm $^{-1}$. HRMS (ESI) (m/z): $[\text{M}+\text{H}]^+$ calcd. for $\text{C}_{32}\text{H}_{39}\text{N}_7\text{O}_8$, 650.29329; found, 650.29471.

Ac-Ala-(Cyclo-*m*)-[Phe-Val-Trp]-Ala-OH (2j). Starting from peptide **1j** (207 mg, 0.374 mmol)



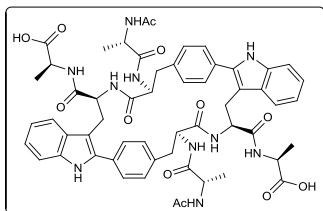
(71% conversion, estimated by HPLC-MS). Semi-preparative RP-

HPLC gradient: 20-40% of B. Pale solid (55.2 mg, 32%). ^1H NMR

(600 MHz, DMSO- d_6): δ 11.19 (s, 1H), 8.09 (m, 2H), 7.67 (d, $J = 9.6$ Hz, 1H), 7.60 (d, $J = 7.3$ Hz, 1H), 7.56 (d, $J = 7.0$ Hz, 1H), 7.42

(d, $J = 8.0$ Hz, 1H), 7.37 (t, $J = 7.5$ Hz, 1H), 7.33 (dd, $J = 7.9, 1.3$ Hz, 2H), 7.29 (t, $J = 1.7$ Hz, 1H), 7.16 (dt, $J = 7.5, 1.5$ Hz, 1H), 7.08 (ddd, $J = 8.1, 6.9, 1.1$ Hz, 1H), 6.95 (ddd, $J = 7.9, 6.9, 1.1$ Hz, 1H), 4.65 (ddd, $J = 9.7, 6.4, 3.2$ Hz, 1H), 4.60 (ddd, $J = 8.8, 7.2, 4.4$ Hz, 1H), 4.31 (p, $J = 7.2$ Hz, 1H), 4.24 (p, $J = 7.3$ Hz, 1H), 4.07 (t, $J = 9.5$ Hz, 1H), 3.34 (1H), 3.20 (dd, $J = 14.7, 6.6$ Hz, 1H), 3.01 – 2.85 (m, 2H), 1.84 (s, 3H), 1.75 (m, 1H), 1.16 (d, $J = 7.1$ Hz, 3H), 0.99 (d, $J = 7.3$ Hz, 3H), 0.72 (dd, $J = 6.7, 4.3$ Hz, 6H) ppm. ^{13}C NMR (151 MHz, DMSO- d_6): δ 173.66, 171.79, 171.26, 169.91, 169.79, 168.93, 137.29, 136.51, 135.78, 132.48, 129.45, 129.29, 128.56, 128.46, 127.18, 121.23, 119.51, 118.40, 110.83, 105.92, 57.69, 53.78, 52.32, 48.02, 47.76, 38.33, 30.44, 26.59, 22.45, 18.87, 18.53, 17.95, 16.67 ppm. IR (Film, cm $^{-1}$) $\nu = 3295.37, 3051.96, 2962.28, 1642.70, 1617.08, 1514.59$ cm $^{-1}$. HRMS (ESI) (m/z): $[\text{M}+\text{H}]^+$ calcd. for $\text{C}_{33}\text{H}_{40}\text{N}_6\text{O}_7$, 633.30312; found, 633.30487.

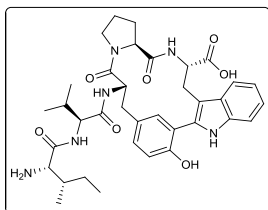
(Cyclo-*p,p*)bis-[Phe-Trp]-(Ac-Ala-Phe-Trp-Ala-OH) (2k). Starting from peptide **1k** (600 mg,



0.907 mmol) (60% conversion, estimated by HPLC-MS). Semi-preparative RP-HPLC gradient: 25-30% of B. Pale solid (3.8 mg, 1%). ¹H NMR (800 MHz, DMSO-*d*₆): δ 11.20 (s, 1H), 8.13 (d, *J* = 7.7 Hz, 1H), 7.93 (d, *J* = 7.3 Hz, 1H), 7.90 (d, *J* = 7.0 Hz, 1H), 7.67 (d, *J* = 7.9 Hz, 1H), 7.61 (d, *J* = 7.6 Hz, 2H),

7.34 (d, *J* = 7.9 Hz, 1H), 7.25 (d, *J* = 7.7 Hz, 2H), 7.11 (t, *J* = 7.5 Hz, 1H), 7.03 (t, *J* = 7.5 Hz, 1H), 6.82 (d, *J* = 6.9 Hz, 1H), 4.24 – 4.15 (dp, *J* = 28.2, 7.1 Hz, 2H), 4.07 (ddd, *J* = 10.4, 6.9, 3.8 Hz, 1H), 3.96 (m, 1H), 3.43 (dd, *J* = 15.1, 3.7 Hz, 1H), 3.23 (dd, *J* = 15.2, 9.4 Hz, 1H), 2.64 (dd, *J* = 15.1, 10.6 Hz, 1H), 2.48 (m, 1H), 1.78 (s, 3H), 1.28 (d, *J* = 7.3 Hz, 3H), 1.08 (d, *J* = 7.0 Hz, 3H) ppm. IR (Film, cm⁻¹) ν = 3404.27, 2911.03, 1655.52 cm⁻¹. HRMS (ESI) (*m/z*): [M+H]⁺ calcd. for C₅₆H₆₂N₁₀O₁₂, 1067.4621; found, 1067.4624.

H-Ile-Val-(Cyclo-*m*)-[Tyr-Pro-Trp]-OH (2l). AB linker incorporation for TentaGel S NH₂ resin.

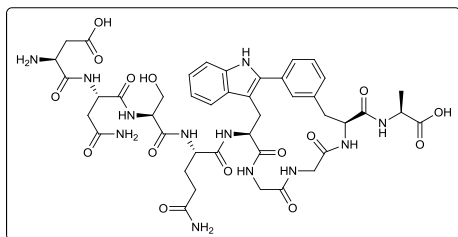


AB linker (3.0 eq.) was attached to the resin (1.0 eq.) with DIPCDI (3.0 eq.), OxymaPure (3.0 eq.) in DMF at r.t for 1h. *First amino acid incorporation.* Fmoc-Trp-OH (4.0 eq.) was attached to the resin (1.0 eq.) with DIPCDI (2.0 eq.), DMAP (0.4 eq.) in DCM at r.t (1 x 2h, 1

x 16h). *End-capping of resin to block any remaining unreacted active resin sites.* Anhydride acetic (5.0 eq.) and DIEA (5.0 eq.) in DMF were added for 30 min. Peptide elongation. Fmoc-XX-OH (3.0 eq.) were incorporated with a 5-min pre-activation with DIPCDI (3.0 eq.) and OxymaPure (3.0 eq.) in DMF for 1h. Fmoc-XX-OH: Fmoc-Pro-OH, Fmoc-3-iodo-Tyr-OH, Fmoc-Val-OH, Fmoc-Ile-OH. *Stapled bond formation on solid-phase.* The resulting peptide anchored to the resin (67 mg, 0.065 mmol), AgBF₄ (13 mg, 0.065 mmol, 1.0 eq.), 2-nitrobenzoic acid (16 mg, 0.098 mmol, 1.5 eq.) and Pd(OAc)₂ (0.7 mg, 3.3 μmol, 0.05 eq.) were placed in a microwave reactor vessel in 900 μL of DMF. The mixture was heated under microwave irradiation (250 W) at 90 °C for 20 min. Three more batches were carried out following the same procedure and were combined. The peptide anchored to the resin was treated with 1% DCC in DMF and after removing the Fmoc group it was cleaved from the resin with a 95% TFA, 2.5% TIS, 2.5% H₂O cocktail (1h). Pale solid (76.7 mg, 79% purity estimated by

HPLC-MS, 32% yield). A pure fraction was obtained by semi-preparative RP-HPLC (XBRIDGE, PrepC18, 5 μ M OBDTM 19x150 mm column) [solvent A (0.1% FA in H₂O) and solvent B (0.1% FA in ACN)], in 20 min, flux: 16 mL·min⁻¹, detection at λ =220 nm (gradient: 20-25% of B). ¹H NMR (500 MHz, DMSO-*d*₆): δ 10.79 (s, 1H), 8.32 (d, *J* = 6.7 Hz, 1H), 8.22 (s, 1H), 8.15 (d, *J* = 8.9 Hz, 1H), 7.66 – 7.56 (m, 2H), 7.33 (d, *J* = 8.0 Hz, 1H), 7.14 (d, *J* = 2.2 Hz, 1H), 7.11 (dd, *J* = 8.3, 2.2 Hz, 1H), 7.07 (t, *J* = 7.5 Hz, 1H), 6.99 (t, *J* = 7.4 Hz, 1H), 6.89 (d, *J* = 8.2 Hz, 1H), 4.68 (td, *J* = 8.0, 6.4, 3.6 Hz, 1H), 4.58 – 4.46 (m, 2H), 4.33 (dd, *J* = 8.7, 6.3 Hz, 1H), 3.61 (q, *J* = 8.5 Hz, 1H), 3.06 (td, *J* = 12.7, 11.0, 4.9 Hz, 2H), 2.88 (dd, *J* = 13.6, 3.3 Hz, 1H), 2.76 (dd, *J* = 14.8, 9.0 Hz, 1H), 2.14 – 2.09 (m, 1H), 1.98 (h, *J* = 6.7 Hz, 1H), 1.75 (tq, *J* = 14.0, 5.8, 4.5 Hz, 2H), 1.55 (dtd, *J* = 16.1, 11.9, 6.2 Hz, 1H), 1.50 – 1.38 (m, 2H), 1.23 (s, 2H), 1.11 (ddd, *J* = 13.4, 9.5, 7.0 Hz, 1H), 0.91 – 0.79 (m, 12H) ppm. HRMS (ESI) (*m/z*): [*M*+*H*]⁺ calcd. for C₃₆H₄₆N₆O₇, 675.35007; found, 675.35096.

H-Asp-Asn-Ser-Gln-(Cyclo-*m*)-[Trp-Gly-Gly-Phe]-Ala-OH (2m). *AB linker incorporation for*



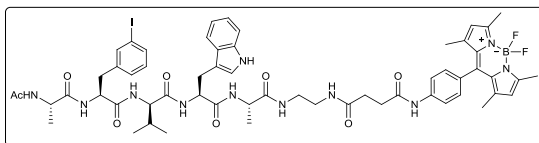
TentaGel S NH₂ resin. AB linker (3.0 eq.) was attached to the resin (1.0 eq.) with DIPCPI (3.0 eq.), OxymaPure (3.0 eq.) in DMF at r.t for 1h. *First amino acid incorporation.* Fmoc-Trp-OH (4.0 eq.) was attached to the resin (1.0 eq.) with

DIPCPI (2.0 eq.), DMAP (0.4 eq.) in DCM at r.t (1 x 2h, 1 x 16h). *End-capping of resin to block any remaining unreacted active resin sites.* Anhydride acetic (5.0 eq.) and DIEA (5.0 eq.) in DMF were added for 30 min. *Peptide elongation until fifth amino acid incorporation.* Fmoc-XX-OH (3.0 eq.) were incorporated with a 5-min pre-activation with DIPCPI (3.0 eq.) and OxymaPure (3.0 eq.) in DMF for 1h. Fmoc-XX-OH: Fmoc-Ala-OH, Fmoc-Gly-OH, Fmoc-Trp-OH. Fmoc-*m*-I-Phe-OH (1.5 eq.) was incorporated with HBTU (1.5 eq.), HOBt (1.5 eq.) and DIEA (3.0 eq.) in DMF for 1h. *Stapled bond formation on solid-phase.* The resulting peptide anchored to the resin (64 mg, 0.072 mmol), AgBF₄ (14 mg, 0.072 mmol, 1.0 eq.), 2-nitrobenzoic acid (18 mg, 0.108 mmol, 1.5 eq.) and Pd(OAc)₂ (0.8 mg, 3.6 μ mol, 0.05 eq.) were placed in a microwave reactor vessel in 980 μ L of DMF. The mixture was heated under microwave irradiation (250 W) at 90 °C for 20 min. Three more batches

were carried out following the same procedure and were combined. *Peptide elongation until ninth amino acid incorporation.* The peptide anchored to the resin was treated with 1% DDC in DMF and Fmoc-XX-OH (3.0 eq.) were incorporated with a 5-min pre-activation with DIPCDI (3.0 eq.) and OxymaPure (3.0 eq.) in DMF for 1h. Fmoc-XX-OH: Fmoc-Gln(Trt)-OH, Fmoc-Ser(*t*-Bu)-OH, Fmoc-Asn(Trt)-OH, Fmoc-Asp(*Or*-Bu)-OH. After removing the Fmoc group, the final peptide sequence was cleaved from the resin with a 95% TFA, 2.5% TIS, 2.5% H₂O cocktail (1h). Pale solid (86.3 mg, 85% purity estimated by HPLC-MS, 26% yield). A pure fraction was obtained by semi-preparative RP-HPLC (XBRIDGE, PrepC18, 5 μ M OBD™ 19x150 mm column) [solvent A (0.1% FA in H₂O) and solvent B (0.1% FA in ACN)], in 20 min, flux: 16 mL·min⁻¹, detection at λ =220 nm (gradient: 10-25% of B). ¹H NMR (500 MHz, DMSO-*d*₆): δ 11.16 (s, 1H), 8.58 (q, *J* = 6.7, 6.2 Hz, 2H), 8.50 (d, *J* = 7.2 Hz, 1H), 8.23 (d, *J* = 7.2 Hz, 1H), 8.15 (m, 2H), 8.01 (d, *J* = 7.9 Hz, 1H), 7.90 – 7.82 (m, 2H), 7.38 (m, 5H), 7.32 – 7.26 (m, 1H), 7.11 (t, *J* = 7.5 Hz, 1H), 7.05 (t, *J* = 7.4 Hz, 1H), 6.97 – 6.90 (m, 1H), 6.86 (d, *J* = 8.4 Hz, 1H), 6.78 – 6.69 (m, 1H), 4.87 – 4.77 (m, 1H), 4.67 (q, *J* = 6.2 Hz, 1H), 4.57 (ddd, *J* = 11.2, 8.3, 2.8 Hz, 1H), 4.27 (td, *J* = 8.8, 5.1 Hz, 1H), 4.22 (t, *J* = 7.3 Hz, 1H), 4.17 (q, *J* = 5.8 Hz, 1H), 3.85 (t, *J* = 5.8 Hz, 1H), 3.79 (dd, *J* = 15.8, 4.6 Hz, 1H), 3.71 (dd, *J* = 11.5, 5.8 Hz, 1H), 3.65 – 3.55 (m, 2H), 3.15 (d, *J* = 13.3 Hz, 1H), 3.01 (dd, *J* = 14.1, 4.5 Hz, 1H), 2.83 (dd, *J* = 13.7, 11.1 Hz, 1H), 2.58 (dd, *J* = 10.6, 5.9 Hz, 2H), 2.17 – 1.98 (m, 2H), 1.91 (ddt, *J* = 15.7, 10.7, 5.4 Hz, 1H), 1.77 (dtd, *J* = 14.8, 9.7, 5.3 Hz, 1H), 1.34 (d, *J* = 7.3 Hz, 3H) ppm. HRMS (ESI) (*m/z*): [*M*+H]⁺ calcd. for C₄₃H₅₄N₁₂O₅, 979.39044; found, 979.39270.

Synthesis and peptide characterization of peptides 1j-Bodipy and 2j-Bodipy

Ac-Ala-*m*-I-Phe-Val-Trp-Ala-linker-BODIPY (1j-Bodipy). The linear peptide sequence **1j** (16.9



mg, 0.022 mmol, 1.2 eq.), EDC·HCl

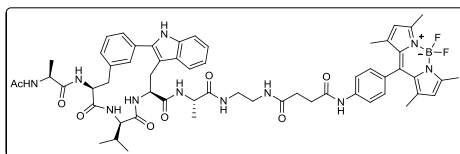
(5.3 mg, 0.028 mmol, 1.5 eq.) and

HOBT·H₂O (4.2 mg, 0.028 mmol, 1.5

eq.) were dissolved in 0.5 mL of DMF. Then, compound **19** (8.9 mg, 0.018 mmol, 1.0 eq.) dissolved in 1 mL of DMF and DIEA (9.7 μ L, 0.055 mmol, 3.0 eq.) were added to give a final peptide concentration of 0.01 M and the solution was stirred for 16 h at r.t. Workup was done by removing the

DMF under vacuum, dissolving the crude in EtOAc and extracting with $\text{NaHCO}_{3\text{sat}}$. Organic layers were combined, dried over sodium sulfate, filtered and concentrated under vacuum to afford 18.0 mg of the crude peptide (58% yield estimated by HPLC-MS conversion). A highly pure fraction of the linear peptide was obtained by purification of 11.0 mg of crude in a PoraPak Rxn RP 60 cc reverse phase column (2 g) [solvent A (0.1% FA in H_2O) and solvent B (0.1% FA in ACN)]. Red solid (95% purity by HPLC-MS). **HRMS** (ESI) (m/z): $[\text{M}+\text{H}]^+$ calcd. for $\text{C}_{58}\text{H}_{69}\text{BF}_2\text{IN}_{11}\text{O}_8$, 1224.45091; found, 1224.45351.

Ac-Ala-(Cyclo-*m*)-[Phe-Val-Trp]-Ala-OH-linker-BODIPY (2j-Bodipy). The staple peptide **2j**

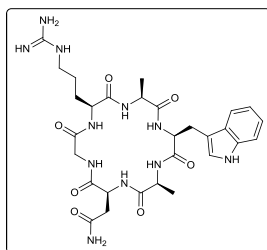


(16.1 mg, 0.021 mmol, 1.2 eq.), EDC-HCl (5.1 mg, 0.026 mmol, 1.5 eq.) and HOBt-H₂O (4.1 mg, 0.026 mmol, 1.5 eq.) were dissolved in

0.6 mL of DMF. Then, compound **19** (8.5 mg, 0.018 mmol, 1.0 eq.) dissolved in 1 mL of DMF and DIEA (9.2 μL , 0.053 mmol, 3.0 eq.) were added to give a final peptide concentration of 0.01 M and the solution was stirred for 16 h at r.t. Workup was done by removing the DMF under vacuum and purifying the crude in a PoraPak Rxn RP 60 cc reverse phase column (2 g) [solvent A (0.1% FA in H_2O) and solvent B (0.1% FA in ACN)]. Red solid (10.2 mg, 97% purity by HPLC-MS, 53% yield). **HRMS** (ESI) (m/z): $[\text{M}+\text{H}]^+$ calcd. for $\text{C}_{58}\text{H}_{68}\text{BF}_2\text{N}_{11}\text{O}_8$, 1096.53862; found, 1096.54044.

Synthesis and characterization of compounds 3-19

Cyclo(-Arg-Ala-Trp-Ala-Asn-Gly-) (3). 2-Chlorotrityl resin (1.0 mmol/g). Amino acid coupling.

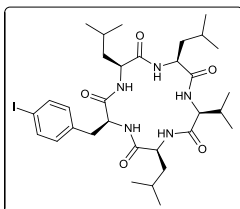


Fmoc-XX-OH (3.0 eq.) were incorporated with a 5-min pre-activation with DIPCDI (3.0 eq.) and OxymaPure (3.0 eq.) in DMF for 1h. Fmoc-XX-OH: Fmoc-Gly-OH, Fmoc-Asn(Trt)-OH, Fmoc-Ala-OH, Fmoc-Trp(Boc)-OH, Fmoc-Arg(Pbf)-OH. The resin bound peptide was treated with a 1% (v/v) TFA/DCM solution (5 x 1 min).

Pale solid (94% purity, HPLC). Cyclization in solution. The free-amine free-acid protected linear peptide (1.5 g, 1.18 mmol) was dissolved in 395 mL of ACN/DMF (14:1) solution (0.003 M) and DIEA (6.0 eq.), PyBOP (3.0 eq.) and HOBt (3.0 eq.) were added. The solution was stirred at r.t until

the cyclization was complete (1h). Workup was done by extracting with $\text{NH}_4\text{Cl}_{\text{sat}}$ and $\text{NaHCO}_{3\text{sat}}$. Organic layers were combined, dried over sodium sulfate, filtered and concentrated under vacuum. Then, the macrocycle was treated with a 95% TFA, 2.5% TIS, 2.5% H_2O cocktail (3h), washed with Et_2O , dissolved in $\text{ACN}:\text{H}_2\text{O}$ and lyophilized furnishing the corresponding peptide. Pale solid (436 mg, 33%). $^1\text{H NMR}$ (500 MHz, $\text{DMSO}-d_6$): δ 10.83 (d, $J = 2.4$ Hz, 1H), 8.25 (t, $J = 5.6$ Hz, 1H), 8.14 (d, $J = 7.3$ Hz, 1H), 8.09 (d, $J = 6.1$ Hz, 1H), 8.06 (d, $J = 8.1$ Hz, 1H), 8.00 – 7.97 (d, $J = 7.4$ Hz, 1H), 7.88 (d, $J = 6.9$ Hz, 1H), 7.60 – 7.56 (d, $J = 7.9$ Hz, 1H), 7.47 (t, $J = 5.7$ Hz, 1H), 7.42 (m, 1H), 7.32 (dt, $J = 8.1, 0.9$ Hz, 1H), 7.14 (d, $J = 2.4$ Hz, 1H), 7.06 (ddd, $J = 8.2, 6.9, 1.2$ Hz, 1H), 6.97 (ddd, $J = 7.9, 6.9, 1.0$ Hz, 1H), 6.92 (m, 1H), 4.35 (q, $J = 6.4$ Hz, 1H), 4.32 – 4.24 (m, 1H), 4.15 – 4.02 (m, 2H), 3.97 (p, $J = 7.0$ Hz, 1H), 3.83 (dd, $J = 16.1, 5.5$ Hz, 1H), 3.56 – 3.52 (m, 1H), 3.18 (m, 2H), 3.10 – 3.06 (m, 2H), 2.67 – 2.55 (m, 2H), 1.87 – 1.76 (m, 1H), 1.60 (m, 1H), 1.52 – 1.40 (m, 2H), 1.28 – 1.15 (m, 6H) ppm. **IR** (Film, cm^{-1}) $\nu = 3276.16, 3186.48, 3051.96, 2917.44, 1642.70, 1508.19$ cm^{-1} . **HRMS** (ESI) (m/z): $[\text{M}+\text{H}]^+$ calcd. for $\text{C}_{29}\text{H}_{41}\text{N}_{11}\text{O}_7$, 656.32632; found, 656.32680.

Cyclo(-Leu-Leu-Val-Leu-*p*-I-Phe-) (4). 2-Chlorotrityl resin (0.94 mmol/g). Amino acid coupling.

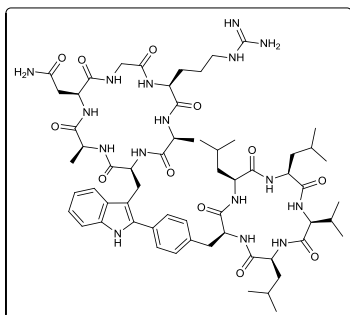


Fmoc-XX-OH (3.0 eq.) were incorporated with a 5-min pre-activation with DIPCDI (3.0 eq.) and OxymaPure (3.0 eq.) in DMF for 1h. Fmoc-XX-OH: Fmoc-*p*-I-Phe-OH, Fmoc-Leu-OH, Fmoc-Val-OH. The resin bound peptide was treated with a 5% (v/v) TFA/DCM solution (5 x 2

min). Pale solid (85% purity, HPLC). Cyclization in solution. The free-amine free-acid linear peptide (119 mg, 0.163 mmol) was dissolved in 55 mL of $\text{ACN}:\text{DCM}$ (1:9) solution (0.003 M) and DIEA (6.0 eq.), HATU (1.5 eq.) and TBTU (1.5 eq.) were added. The solution was stirred at r.t until the cyclization was complete (3h). Workup was done by extracting with $\text{NH}_4\text{Cl}_{\text{sat}}$ and $\text{NaHCO}_{3\text{sat}}$. Organic layers were combined, dried over sodium sulfate, filtered and concentrated under vacuum. Then, the macrocycle was purified via flash column chromatography using and $\text{EtOAc}:\text{hexane}$ gradient on silica gel furnishing the corresponding peptide. Pale solid (28.1 mg, 24%). $^1\text{H NMR}$ (500 MHz, $\text{DMSO}-d_6$): δ 8.15 (t, $J = 7.7$ Hz, 2H), 8.02 (d, $J = 8.4$ Hz, 1H), 8.00 – 7.89 (m, 2H), 7.62 (d, $J = 7.7$ Hz, 2H), 7.03 (d, $J = 7.9$ Hz, 2H), 4.27 (q, $J = 8.0$ Hz, 1H), 4.12 (q, $J = 8.4, 6.2$ Hz, 1H), 4.05 (m, 1H), 3.94 (q, $J =$

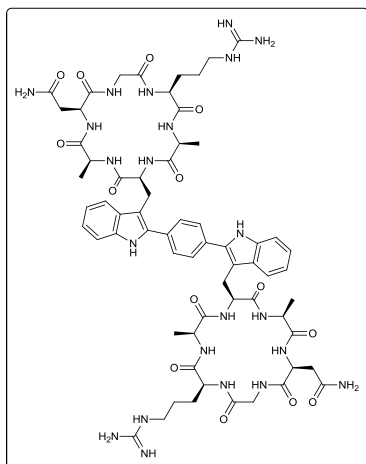
8.4 Hz, 1H), 3.66 (t, $J = 9.5$ Hz, 1H), 3.07 – 2.95 (m, 2H), 2.15 (m, 1H), 1.68 (m, 2H), 1.58 – 1.43 (m, 4H), 1.38 – 1.24 (m, 3H), 0.92 – 0.74 (m, 24H) ppm. **IR** (Film, cm^{-1}) $\nu = 3295.37, 3077.58, 2962.28, 1655.52, 1540.21 \text{ cm}^{-1}$. **HRMS** (ESI) (m/z): $[M+H]^+$ calcd. for $\text{C}_{32}\text{H}_{50}\text{N}_5\text{O}_5$, 712.29294; found, 712.29392.

Cyclo(Ala-Asn-Gly-Arg-Ala-C2-Trp)—Cyclo(C4-Phe-Leu-Leu-Val-Leu-) (5). Macrocycle



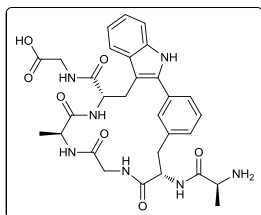
4 (40.0 mg, 0.056 mmol), macrocycle **3** (55.3 mg, 0.084 mmol, 1.5 eq.), AgBF_4 (43.8 mg, 0.225 mmol, 4.0 eq.), pivalic acid (5.7 mg, 0.056 mmol, 1.0 eq.) and $\text{Pd}(\text{OAc})_2$ (1.4 mg, 0.077 mmol, 0.1 eq.) were placed in a microwave reactor vessel in 2 mL of PBS:DMF (1:1). The mixture was heated under microwave irradiation (250 W) at 90 °C for

20 min. The irradiation cycle was repeated by adding a new portion of $\text{Pd}(\text{OAc})_2$ and AgBF_4 . The residue was filtered and partially purified in a PoraPak Rxn RP 60 cc reverse phase column (5 g) [solvent A (0.1% FA in H_2O) and solvent B (0.1% FA in ACN)]. Pale solid (1.63 mg, 2% yield estimated by HPLC-MS conversion). A pure fraction was obtained by analytic RP-HPLC (XBRIDGE™ BEH 130, C18, 5 μM 10x100 mm column) [solvent A (0.045% TFA in H_2O) and solvent B (0.036% TFA in ACN)], in 30 min, flux: 3 $\text{mL} \cdot \text{min}^{-1}$, detection at $\lambda = 220 \text{ nm}$ (gradient: 30–50% of B). **^1H NMR** (600 MHz, $\text{DMSO}-d_6$): δ 11.16 (s, 1H), 8.45 (t, $J = 5.9$ Hz, 1H), 8.19–8.18 (t, $J = 7.9$ Hz, 2H), 8.11 – 7.90 (m, 8H), 7.64 (d, $J = 8.1$ Hz, 2H), 7.59 (d, $J = 8.0$ Hz, 1H), 7.44 – 7.40 (m, 2H), 7.35 – 7.31 (m, 3H), 7.11 – 7.06 (m, 1H), 7.00 – 6.96 (m, 1H), 6.91 (m, 1H), 4.39 – 4.29 (m, 2H), 4.25 (q, $J = 7.0$ Hz, 1H), 4.19 – 4.09 (m, 3H), 4.02 (m, 1H), 3.97 (q, $J = 8.7$ Hz, 1H), 3.92 (q, $J = 6.6, 6.1$ Hz, 1H), 3.86 (dd, $J = 15.8, 5.8$ Hz, 1H), 3.72 (t, $J = 9.0$ Hz, 1H), 3.41 (1H), 3.40–3.32 (2H), 3.12 (m, 2H), 3.10 – 3.04 (m, 2H), 2.58 (d, $J = 6.2$ Hz, 2H), 2.19 – 2.11 (m, 1H), 1.79 (m, 1H), 1.73 – 1.41 (m, 11H), 1.39 – 1.34 (m, 1H), 1.11 (dd, $J = 7.1, 3.2$ Hz, 6H), 0.92 (d, $J = 6.3$ Hz, 3H), 0.90 – 0.81 (m, 18H), 0.77 (d, $J = 6.3$ Hz, 3H) ppm. **IR** (Film, cm^{-1}) $\nu = 3321.00, 3199.29, 2962.28, 2923.84, 1655.52, 1533.81 \text{ cm}^{-1}$. **HRMS** (ESI) (m/z): $[M+H]^+$ calcd. for $\text{C}_{61}\text{H}_{91}\text{N}_{16}\text{O}_{12}$, 1239.69969; found, 1239.70241.

Bis[cyclo(-Arg-Ala-Trp-Ala-Asn-Gly-)] adduct (6).

1,4-diiodobenzene (35 mg, 0.106 mmol), macrocycle **3** (209 mg, 0.318 mmol, 3.0 eq.), AgBF_4 (124 mg, 0.637 mmol, 6.0 eq.), pivalic acid (16.3 mg, 0.159 mmol, 1.5 eq.) and $\text{Pd}(\text{OAc})_2$ (9.5 mg, 0.042 mmol, 0.4 eq.) were placed in a microwave reactor vessel in 2 mL of PBS:DMF (1:1). The mixture was heated under microwave irradiation (250 W) at 90 °C for 20 min. The crude was filtered and the workup was done by washing with AcOEt and then precipitating by adding ACN to the aqueous phase. The precipitated was washed with ACN,

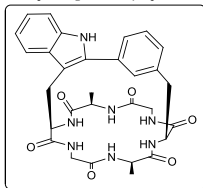
decanted and dried, obtaining 159 mg of crude (pale solid, 42%, yield estimated by HPLC-MS conversion). A pure fraction was obtained by semi-preparative RP-HPLC (Phenomenex Jupiter, C18, 10 μM , 21.20x100 mm column, [solvent A (0.1% FA in H_2O) and solvent B (0.05% FA in ACN)], in 20 min, flux: 20 mL $\cdot\text{min}^{-1}$, detection at $\lambda=220$ nm (gradient: 15-20% of B). ^1H NMR (600 MHz, $\text{DMSO}-d_6$): δ 11.29 (s, 2H), 8.40 (s, 2H), 8.17 (s, 2H), 8.06 (m, 6H), 7.97 (d, $J = 8.7$ Hz, 2H), 7.87 (s, 4H), 7.65 (m, 2H), 7.42 (s, 2H), 7.36 (d, $J = 8.0$ Hz, 2H), 7.32 – 7.16 (m, 6H), 7.13 – 7.08 (m, 2H), 7.00 (t, $J = 7.3$ Hz, 2H), 6.89 (s, 2H), 4.36 (m, 4H), 4.18 (m, 2H), 4.09 – 4.02 (m, 2H), 3.98 (m, 2H), 3.86 (m, 2H), 3.56 – 3.48 (m, 2H), 3.44 – 3.39 (m, 4H), 3.08 (q, $J = 6.4$ Hz, 4H), 2.63 – 2.56 (m, 4H), 1.81 (dd, $J = 13.4, 6.9$ Hz, 2H), 1.62 (m, 2H), 1.47 (m, 4H), 1.11 (m, 12H) ppm. IR (Film, cm^{-1}) $\nu =$ 3314.59, 3199.29, 3051.96, 2911.03, 1661.92, 1533.81 cm^{-1} . HRMS (ESI) (m/z): [M] calcd. for $\text{C}_{64}\text{H}_{84}\text{N}_{22}\text{O}_{14}$, 1384.65373; found, 1384.65505.

H-Ala-(Cyclo-*m*)-[Phe-Gly-Ala-Trp]-Gly-OH (9).

resin. AB linker (3.0 eq.) was attached to the resin (1.0 eq.) with DIPCDI (3.0 eq.), OxymaPure (3.0 eq.) in DMF at r.t for 1h. *First amino acid incorporation*. Fmoc-Gly-OH (4.0 eq.) was attached to the resin (1.0 eq.) with DIPCDI (2.0 eq.), DMAP (0.4 eq.) in DCM at r.t

(1 x 2h, 1 x 16h). *End-capping of resin to block any remaining unreacted active resin sites.* Anhydride acetic (5.0 eq.) and DIEA (5.0 eq.) in DMF were added for 30 min. *Peptide elongation.* Fmoc-XX-OH (3.0 eq.) were incorporated with a 5-min pre-activation with DIPCDI (3.0 eq.) and OxymaPure (3.0 eq.) in DMF for 1h. Fmoc-XX-OH: Fmoc-Trp-OH, Fmoc-Ala-OH, Fmoc-Gly-OH. Fmoc-*m*-I-Phe-OH (1.5 eq.) was incorporated with HBTU (1.5 eq.), HOBT (1.5 eq.) and DIEA (3.0 eq.) in DMF for 1h. *Stapled bond formation on solid-phase.* The resulting peptide **7** anchored to the resin (139 mg, 0.145 mmol), AgBF₄ (28 mg, 0.144 mmol, 1.0 eq.), 2-nitrobenzoic acid (36 mg, 0.215 mmol, 1.5 eq.) and Pd(OAc)₂ (1.6 mg, 7.1 μmol, 0.05 eq.) were placed in a microwave reactor vessel in 2 mL of DMF. The mixture was heated under microwave irradiation (250 W) at 90 °C for 20 min. Eight more batches were carried out following the same procedure and were combined. The peptide **8** anchored to the resin was treated with 1% DDC in DMF and after removing the Fmoc group it was cleaved from the resin with a 95% TFA, 2.5% TIS, 2.5% H₂O cocktail (1h). (85% purity, estimated by HPLC-MS). ¹H NMR (500 MHz, DMSO-*d*₆): δ 11.15 (s, 1H), 8.43 (t, *J* = 5.1 Hz, 1H), 7.84 (s, 1H), 7.59 (d, *J* = 7.9 Hz, 1H), 7.50 (s, 1H), 7.41-7.35 (m, 4H), 7.17 – 7.08 (m, 2H), 7.01 (t, *J* = 7.4 Hz, 1H), 6.80 (d, *J* = 8.4 Hz, 1H), 4.83 – 4.74 (m, 1H), 4.55 (q, *J* = 8.2 Hz, 1H), 3.83 (m, 1H), 3.76 (m, 1H), 3.71 (m, 1H), 3.57 – 3.53 (m, 3H), 3.38-3.32 (m, 2H), 3.14 – 3.11 (m, 1H), 3.03 (dd, *J* = 13.5, 8.8 Hz, 1H), 1.28 (d, *J* = 6.9 Hz, 3H), 0.80 (d, *J* = 7.2 Hz, 3H) ppm. IR (Film, cm⁻¹) ν = 3288.97, 3051.96, 2923.84, 1649.11, 1527.40 cm⁻¹. HRMS (ESI) (*m/z*): [M+H]⁺ calcd. for C₃₀H₃₅N₇O₇, 606.26707; found, 606.26754.

Cyclo[-Ala-(Cyclo-*m*)-[Phe-Gly-Ala-Trp]-Gly-] (10). The free-amine free-acid stapled peptide **9**

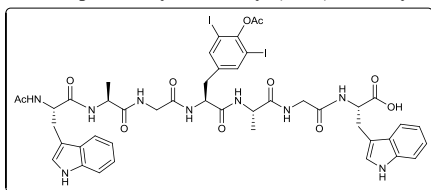


(92.2 mg, 0.152 mmol) was dissolved in 152 mL of DMF (0.001 M) and DIEA (6.0 eq.) and PyAOP (2.0 eq.) were added. The solution was stirred at r.t until the cyclization was complete (1.5h). DMF was removed under vacuum, and the crude was dissolved in EtOAc and extracted with NH₄Cl_{sat}

and NaHCO_{3sat}. Organic layers were combined, dried over sodium sulfate, filtered and concentrated under vacuum. The crude was purified by semi-preparative RP-HPLC (XBRIDGETM BEH 130, C18, 5μM OBD 19x50 mm column) [solvent A (0.1% FA in H₂O) and solvent B (0.1% FA in ACN)], in 10 min, flux: 20 mL·min⁻¹, detection at λ=220 nm (gradient: 20-30% of B). Pale solid (16.0 mg, 18%).

¹H NMR (600 MHz, DMSO-*d*₆): δ 11.23 (s, 1H), 8.53 (s, 1H), 8.19 (s, 1H), 7.49 – 7.35 (m, 6H), 7.32 (d, *J* = 8.0 Hz, 1H), 7.17 (dt, *J* = 7.7, 1.4 Hz, 1H), 7.06 (ddd, *J* = 8.0, 6.9, 1.2 Hz, 1H), 6.96 (ddd, *J* = 8.0, 6.8, 1.0 Hz, 1H), 6.77 (d, *J* = 8.9 Hz, 1H), 6.46 (s, 1H), 4.72 – 4.60 (m, 1H), 4.55 (dt, *J* = 8.6, 6.7 Hz, 1H), 4.14 (m, 1H), 4.11 – 4.05 (m, 1H), 3.57 (dd, *J* = 13.4, 1.9 Hz, 1H), 3.54 (d, *J* = 4.9 Hz, 1H), 3.50 (m, 2H), 3.49 – 3.43 (m, 1H), 3.37 – 3.34 (m, 1H), 3.15 (dd, *J* = 14.1, 2.6 Hz, 1H), 2.83 (dd, *J* = 13.7, 6.7 Hz, 1H), 1.28 (d, *J* = 7.4 Hz, 3H), 0.34 (d, *J* = 7.3 Hz, 3H) ppm. **¹³C NMR** (151 MHz, DMSO-*d*₆): δ 171.42, 171.41, 170.82, 170.71, 169.08, 168.56, 136.02, 135.69, 135.66, 133.76, 130.16, 130.11, 129.65, 128.24, 126.79, 121.22, 118.51, 118.45, 111.02, 105.66, 51.27, 51.18, 49.44, 48.72, 43.31, 43.18, 35.90, 25.07, 16.43, 15.23 ppm. **IR** (Film, cm⁻¹) ν = 3378.65, 3301.78, 3051.96, 2930.25, 1649.11, 1533.81 cm⁻¹. **HRMS** (ESI) (*m/z*): [*M*+H]⁺ calcd. for C₃₀H₃₃N₇O₆, 588.25651; found, 588.25770.

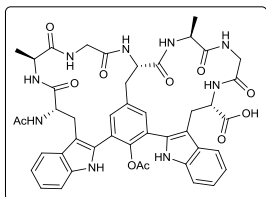
Ac-Trp-Ala-Gly-3,5-I-I-Tyr(OAc)-Ala-Gly-Trp-OH (11). 2-Chlorotrityl resin (0.8 mmol/g).



Amino acid coupling. Fmoc-XX-OH (3.0 eq.) were incorporated with a 5-min pre-activation with DIPCDI (3.0 eq.) and OxymaPure (3.0 eq.) in DMF for 1h. Fmoc-XX-OH: Fmoc-Gly-OH,

Fmoc-Ala-OH, Fmoc-*m,m*-I,I-Tyr-OH, Fmoc-Trp-OH. The N-terminal was acetylated, and the resin bound peptide was treated with a 5% (v/v) TFA/DCM solution (5 x 2 min). Pale solid (>99% purity, estimated by HPLC-MS). **¹H NMR** (500 MHz, DMSO-*d*₆): δ 10.84 (d, *J* = 2.5 Hz, 1H), 10.75 (d, *J* = 2.5 Hz, 1H), 8.30 (d, *J* = 7.2 Hz, 1H), 8.13 (d, *J* = 7.2 Hz, 1H), 8.10 – 8.03 (m, 3H), 8.01 (d, *J* = 8.0 Hz, 1H), 7.92 (t, *J* = 5.7 Hz, 1H), 7.77 (s, 2H), 7.59 (d, *J* = 7.9 Hz, 1H), 7.52 (d, *J* = 7.9 Hz, 1H), 7.31 (dd, *J* = 9.7, 8.3 Hz, 2H), 7.13 (dd, *J* = 12.0, 2.4 Hz, 2H), 7.09 – 7.00 (m, 2H), 6.96 (dddd, *J* = 8.9, 7.8, 6.9, 1.1 Hz, 2H), 4.56 – 4.50 (m, 2H), 4.48 (dt, *J* = 7.8, 3.8 Hz, 1H), 4.33 – 4.18 (m, 2H), 3.79 – 3.68 (m, 3H), 3.56 (1H), 3.18 (dd, *J* = 14.7, 5.3 Hz, 1H), 3.11 (dd, *J* = 14.7, 4.7 Hz, 1H), 3.04 (dd, *J* = 14.6, 8.0 Hz, 1H), 2.97 (dd, *J* = 14.1, 3.8 Hz, 1H), 2.93 – 2.84 (m, 1H), 2.67 (dd, *J* = 13.9, 10.0 Hz, 1H), 2.34 (s, 3H), 1.76 (s, 3H), 1.21 (dd, *J* = 10.6, 7.0 Hz, 6H) ppm. **HPLC-MS** (*m/z*): [*M*+H]⁺ calcd. for C₄₅H₄₉I₂N₉O₁₁, 1146.7; found, 1146.9.

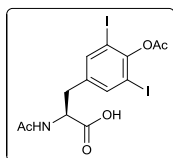
Ac-(bicyclo-*m,m*)-[Trp-Ala-Gly-Tyr(OAc)]-[Tyr(OAc)-Ala-Gly-Trp]-OH (12). The linear



peptide **11** (50 mg, 0.044 mmol), AgBF_4 (51 mg, 0.262 mmol, 6.0 eq.), pivalic acid (6.7 mg, 0.066 mmol, 1.5 eq.) and $\text{Pd}(\text{OAc})_2$ (3.9 mg, 0.018 mmol, 0.4 eq.) were placed in a microwave reactor vessel in 500 μL of DMF. The mixture was heated under microwave

irradiation (250 W) at 90 °C for 20 min. Three more batches were carried out following the same procedure. All the crudes were filtered and combined (25% conversion, estimated by HPLC-MS). The crude was purified by semi-preparative RP-HPLC (XBRIDGE™ BEH 130, C18, 5 μM OBD 19x50 mm column, [solvent A (0.1% FA in H_2O) and solvent B (0.1% FA in ACN)], in 10 min, flux: 20 mL·min⁻¹, detection at $\lambda=220$ nm, gradient: 25-30% of B. **¹H NMR** (600 MHz, $\text{DMSO}-d_6$): δ 10.87 (d, J = 12.6 Hz, 2H), 8.71 (d, J = 8.0 Hz, 1H), 8.50 (s, 1H), 8.24 (s, 1H), 8.03 (m, 1H), 7.98 (d, J = 8.0 Hz, 1H), 7.58 (d, J = 8.0 Hz, 1H), 7.43 (s, 1H), 7.38 – 7.32 (m, 2H), 7.25 (d, J = 8.2 Hz, 1H), 7.22 (d, J = 7.0 Hz, 1H), 7.09 (ddd, J = 8.1, 6.9, 1.1 Hz, 1H), 7.03 (dt, J = 15.7, 7.6 Hz, 2H), 6.96 (t, J = 7.8 Hz, 1H), 6.79 (2H), 5.04 (m, 1H), 4.94 (q, J = 7.4 Hz, 1H), 4.75 (m, 1H), 4.43 – 4.35 (m, 1H), 4.19 (p, J = 6.9 Hz, 1H), 3.90 (dd, J = 17.0, 7.1 Hz, 1H), 3.58 (dd, J = 16.7, 7.0 Hz, 1H), 3.51 – 3.44 (m, 1H), 3.38 (1H), 3.30 (1H), 3.24 (1H), 3.19 (m, 1H), 3.04 (s, 2H), 2.83 (t, J = 13.2 Hz, 1H), 1.94 (s, 3H), 1.49 (s, 3H), 1.21 (d, J = 7.2 Hz, 3H), 1.03 (d, J = 7.0 Hz, 3H) ppm. **HRMS** (ESI) (m/z): $[\text{M}+\text{H}]^+$ calcd. for $\text{C}_{45}\text{H}_{47}\text{N}_9\text{O}_{11}$, 890.34678; found, 890.34796.

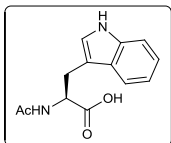
Ac-*m,m'*-I,I-Tyr(OAc)-OH (13). To a vigorously stirred suspension of commercially available H-



3,5-*I,I*-Tyr-OH·2 H_2O (2.17 g, 4.62 mmol) in H_2O (14.2 mL) at 0°C was added Et_3N (1.29 mL, 9.24 mmol). Acetic anhydride (1.05 mL, 11.1 mmol) was added dropwise at 0°C and Et_3N was added to maintain the pH between 6 and 8. After the addition was complete, the reaction was warmed to rt and stirred vigorously. After 5 min of reaction, a new portion of acetic anhydride and Et_3N was added. Once the reaction was completed (30 min), The solution was then carefully acidified to pH 2 with 1.2M $\text{HCl}_{(\text{aq})}$. The white precipitate formed was dissolved in EtOAc and subsequent extractions with H_2O afforded the desired product as a white solid (2.41 g, 90%). **¹H NMR** (400 MHz, $\text{DMSO}-d_6$): δ 12.76 (s, 1H), 8.21 (d, J = 8.1 Hz, 1H),

7.73 (s, 2H), 4.38 (ddd, $J = 9.5, 8.0, 4.9$ Hz, 1H), 3.00 (dd, $J = 13.9, 4.9$ Hz, 1H), 2.78 (dd, $J = 13.9, 9.5$ Hz, 1H), 2.35 (s, 3H), 1.80 (s, 3H) ppm.

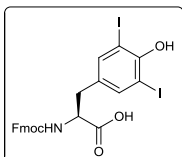
Ac-Trp-OH (14).⁴ To a solution of tryptophan (2.5 g, 12.2 mmol) and NaOH (0.588 g, 14.7 mmol)



in 75 mL of H₂O was added acetic anhydride (15 mL, 159 mmol) and was stirred for 2 h, resulting in a white solid precipitate. The precipitate was filtered from the reaction mixture and rinsed with cold water. The residue was suspended

in 50 mL of 0.2 M HCl, cooled, filtered and washed with cold water and dried to give a white solid (1.46 g, 48%). ¹H NMR (400 MHz, DMSO-*d*₆): δ 12.58 (s, 1H), 10.91 – 10.74 (m, 1H), 8.13 (d, $J = 7.8$ Hz, 1H), 7.52 (d, $J = 7.9$ Hz, 1H), 7.33 (d, $J = 8.1$ Hz, 1H), 7.13 (d, $J = 2.4$ Hz, 1H), 7.06 (ddd, $J = 8.2, 7.0, 1.2$ Hz, 1H), 6.98 (ddd, $J = 7.9, 7.0, 1.1$ Hz, 1H), 4.45 (ddd, $J = 8.6, 7.8, 5.1$ Hz, 1H), 3.15 (ddd, $J = 14.6, 5.1, 0.9$ Hz, 1H), 3.06 – 2.87 (m, 1H), 1.80 (s, 3H) ppm. ¹³C NMR (101 MHz): δ 173.54, 169.18, 136.07, 127.18, 123.50, 120.89, 118.33, 118.13, 111.36, 109.96, 52.96, 27.14, 22.41 ppm.

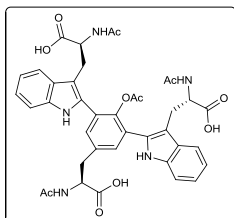
Fmoc-3,5-diiodo-Tyr-OH (15). To a suspension of 9.0 g (20.8 mmol) of H-3,5-I₂-Tyr-OH in 31.2



mL of 10% NaHCO₃ was added 7.7 g (22.9 mmol) of Fmoc-OSu in 63 mL of acetone. The resulting mixture was stirred at room temperature for 23 h and acetone was removed by rotary evaporation. Upon extraction with ether, the

sodium salt of Fmoc-diiodotyrosine precipitated and was collected by filtration; the solid was washed thoroughly with H₂O then EtOAc and dried. This sodium salt was suspended in 60 mL of H₂O and acidified with 12M HCl. The free acid was extracted with EtOAc. The organic layers were combined, dried over sodium sulfate, filtered and concentrated under vacuum. White solid (11.4 g, 84%). ¹H NMR (400 MHz, DMSO-*d*₆): δ 12.73 (s, 1H), 9.38 (s, 1H), 7.88 (d, $J = 7.8$ Hz, 2H), 7.75 (d, $J = 8.5$ Hz, 1H), 7.68 (s, 2H), 7.67 – 7.61 (m, 2H), 7.41 (tdd, $J = 7.5, 2.6, 1.1$ Hz, 2H), 7.31 (dtd, $J = 9.7, 7.5, 1.2$ Hz, 2H), 4.20 (m, 3H), 4.10 (ddd, $J = 10.6, 8.4, 4.3$ Hz, 1H), 2.96 (dd, $J = 13.9, 4.4$ Hz, 1H), 2.71 (dd, $J = 13.8, 10.6$ Hz, 1H) ppm.

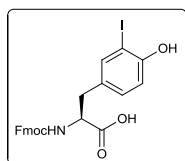
Ac-3,5-di-(Ac-Trp-OH)-Tyr(OAc)-OH (16). Ac-3,5-diiodo-Tyr(OAc)-OH (100 mg, 0.087 mmol),



Ac-Trp-OH (286 mg, 1.16 mmol, 6.0 eq.), AgBF_4 (226 mg, 1.16 mmol, 6.0 eq.), pivalic acid (30 mg, 0.290 mmol, 1.5 eq.) and $\text{Pd}(\text{OAc})_2$ (17 mg, 0.077 mmol, 0.4 eq.) were placed in a microwave reactor vessel in 1200 μL of DMF. The mixture was heated under microwave irradiation (250 W) at 90 $^\circ\text{C}$ for 20 min. The residue was filtered and partially purified in

a PoraPak Rxn RP 60 cc reverse phase column (5 g) [solvent A (0.1% FA in H_2O) and solvent B (0.1% FA in ACN)]. Pale solid (28.5 mg, 20% yield estimated by HPLC-MS conversion). A pure fraction was obtained by semi-preparative RP-HPLC (XBRIDGETM, C18, 5 μM OBD 19x100 mm column, [solvent A (0.1% FA in H_2O) and solvent B (0.05% FA in ACN)], in 20 min, flux: 16 $\text{mL}\cdot\text{min}^{-1}$, detection at $\lambda=220$ nm (gradient: 25-30% of B). ¹H NMR (500 MHz, $\text{DMSO}-d_6$): δ 12.62 (s, 3H), 11.08 – 10.93 (m, 2H), 8.26 (dd, $J = 15.5, 7.9$ Hz, 1H), 7.91 (dd, $J = 10.8, 8.0$ Hz, 1H), 7.82 (t, $J = 6.9$ Hz, 1H), 7.63 (dt, $J = 7.8, 3.8$ Hz, 2H), 7.53 – 7.44 (m, 2H), 7.36 (d, $J = 8.0$ Hz, 2H), 7.10 (t, $J = 7.5$ Hz, 2H), 7.01 (t, $J = 7.5$ Hz, 2H), 4.54 (m, 3H), 3.26 (dd, $J = 9.2, 6.2$ Hz, 2H), 3.22 – 3.17 (m, 1H), 3.16 – 3.05 (m, 2H), 2.96 (m, 1H), 1.92 – 1.76 (m, 3H), 1.73 – 1.56 (m, 9H) ppm. IR (Film, cm^{-1}) $\nu = 3353.02, 3051.96, 2923.84, 1732.38, 1649.11, 1527.40$ cm^{-1} . HRMS (ESI) (m/z): $[\text{M}+\text{H}]^+$ calcd. for $\text{C}_{39}\text{H}_{39}\text{N}_5\text{O}_{11}$, 754.27188; found, 754.27292.

Fmoc-3-iodo-Tyr-OH (17). To a suspension of 2.0 g (6.5 mmol) of H-3-I-Tyr-OH in 10.0 mL of



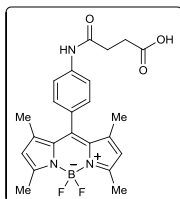
10% NaHCO_3 was added 2.4 g (7.2 mmol) of Fmoc-OSu in 20 mL of acetone.

The resulting mixture was stirred at room temperature for 20 h and acetone was removed by rotary evaporation. Upon extraction with ether, the sodium salt of Fmoc-diiodotyrosine precipitated and was collected by filtration; the solid was washed thoroughly

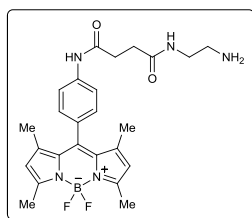
with H_2O and dried. This sodium salt was suspended in 20 mL of H_2O and acidified with 12M HCl. The free acid was extracted with EtOAc. The organic layers were combined, dried over sodium sulfate, filtered and concentrated under vacuum. The residue was recrystallized from EtOAc/hexane to give a white solid (2.8 g, 81%). ¹H NMR (400 MHz, $\text{DMSO}-d_6$): δ 10.12 (s, 1H), 7.88 (d, $J = 7.5$ Hz, 2H), 7.74 – 7.58 (m, 4H), 7.41 (dddd, $J = 7.7, 5.0, 3.8, 2.0$ Hz, 2H), 7.31 (dtd, $J = 10.6, 7.4, 1.2$

Hz, 2H), 7.09 (dd, $J = 8.3, 2.1$ Hz, 1H), 6.79 (d, $J = 8.2$ Hz, 1H), 4.19 (d, $J = 4.3$ Hz, 3H), 4.14 – 4.05 (m, 1H), 3.33 (s, 1H), 2.95 (dd, $J = 13.8, 4.4$ Hz, 1H), 2.73 (dd, $J = 13.9, 10.5$ Hz, 1H) ppm.

10-(4-(3-carboxypropanamido)phenyl)-5,5-difluoro-1,3,7,9-tetramethyl-5H-dipyrrolo[1,2-c:1',2'-f][1,3,2]diazaborinin-4-ium-5-uide (18). Compound **18** was prepared as described in the literature.⁵



10-(4-(2-aminoethylamino)-4-oxobutanamido)phenyl)-5,5-difluoro-1,3,7,9-tetramethyl-5H-dipyrrolo[1,2-c:1',2'-f][1,3,2]diazaborinin-4-ium-5-uide (19). Bodipy derivative **18** (100 mg, 0.228



mmol) and ethylenediamine (76 μ L, 1.14 mmol, 5.0 eq.) were dissolved in DCM (5 mL), EDC-HCl (52 mg, 0.271 mmol, 1.2 eq.) and HOBT (37 mg, 0.274 mmol, 1.2 eq.) were added, and the mixture was stirred for 16 h. Another portion of EDC-HCl (52 mg, 0.271 mmol, 1.2 eq.) and HOBT (37 mg, 0.274 mmol, 1.2 eq.) were added, and the

reaction further stirred for 24 h. 10 mL of DCM were added, and the mixture was extracted with $\text{Na}_2\text{CO}_{3\text{aq}}$ (3 x 15 mL). The organic layers were combined, dried over Na_2SO_4 , filtered and evaporated under vacuum. The residue was dissolved in MeOH and loaded into a SCX-2 isolate (500 mg) column, washed with MeOH (30 mL) and released with NH_3 solution (4M) in MeOH (10 mL). After removal of the solvents, amino bodipy derivative **19** was recovered as an orange solid (67 mg, 62%). ¹H NMR (400 MHz, CDCl_3): δ 9.02 (s, 1H), 7.63 (d, $J = 8.1$ Hz, 2H), 7.11 (d, $J = 8.2$ Hz, 2H), 6.48 (s, 1H), 5.88 (s, 2H), 3.42 (s, 2H), 3.28 (s, 2H), 2.85 – 2.53 (m, 6H), 2.46 (s, 6H), 1.33 (s, 6H) ppm. **HPLC-MS** (m/z): [M] calcd. for $\text{C}_{25}\text{H}_{30}\text{BF}_2\text{N}_5\text{O}_2$, 481.25; [M] found, 481.78.

4. Biochemical and cellular studies

Proteolytic degradation assay

Stock solutions of α -chymotrypsin (from bovine pancreas type II, ≥ 40 U/mg) were freshly prepared in 1 mM HCl (placed on ice), and stock solutions of peptides (500 μ M) were dissolved in DMSO. Reactions were conducted in glass vials by dilution of α -chymotrypsin solution into assay buffer (56 mM Tris pH 7.8, 560 μ M CaCl_2 , 0.1 %v Tween-80) and subsequent addition of the peptide stock solution to give a final substrate concentration of 50 μ M, 50 μ g/mL α -chymotrypsin, and 10 %v DMSO. Aliquots were removed at different times and diluted 1:1 with H_2O containing 1 %v TFA, which resulted in a pH < 2 . The rate of peptide degradation was monitored by HPLC-MS analysis at the corresponding wavelength where the UV absorption was maximum. No loss was observed in control reactions which contained BSA instead of α -chymotrypsin.

Cell adhesion assays of RGD-containing compound 2h

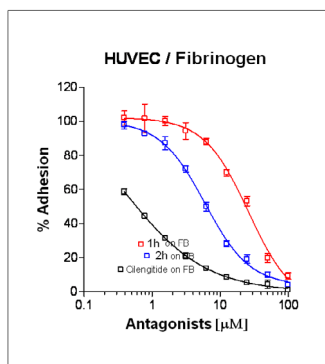
As the signaling peptides specifically bind to integrins (transmembrane receptors, directly involved in tumor metastasis and tumor-induced angiogenesis) acting as mild antagonists,⁹ we tested whether the rigidified analog conserved this property. The inhibition of the cellular adhesion of the RGD-containing compound **2h** and its linear precursor **1h** were evaluated against Human Umbilical Vein Endothelial Cell cancer cell line, with coating of fibrinogen (Fb) and vitronectin (Vn) as integrin ligands and using cilengitide® as a positive control. The tested compounds selectively block $\alpha v \beta 3$ -mediated cell adhesion with Fb but do not have blocking activity of Vn against integrin $\alpha v \beta 5$.

Non-tissue culture treated ELISA plates [NUNC, Maxisorp 442404] were coated ON at 4 °C with the specific concentration of the ligand. Coating solution was discarded and wells were blocked with blocking solution (PBS + BSA 1.5%; 60 minutes at 37 °C). Blocking solution was discarded by flicking and serial dilutions of the compounds were plated in quadruplicates. Immediately, harvested cells are plated at a given concentration (20000-25000 / well for HUVEC and DAOY and 50000 for HT-29) to the same plate. Plates were incubated for 90 minutes at 37 °C/5%CO₂ to allow cell adhesion on the ligand. After then, non-adhered cells were removed and hexosaminidase substrate (N-acetyl- β -

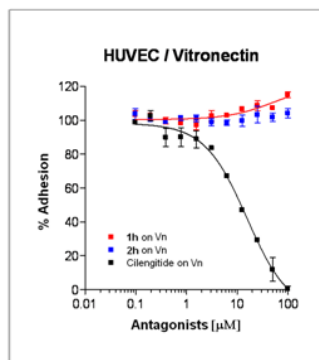
D-glucosaminide) was added to each well and incubated for 3 hours (37°C/5%CO₂ for VN and O/N for de FB). Optical density was read at 405 nm. The proliferation inhibition EC₅₀ was calculated using the Prism-4 software based on the sigmoidal dose-response (variable slope) equation.

Each plate contains positive and negative controls and peptides are tested as duplicates. Each assay has been repeated at least twice and the adhesion inhibition EC₅₀ is calculated, when possible, using the Prism-4 software based on the sigmoidal dose-response (variable slope) equation.

Cell adhesion inhibition curves for compounds **1h** and **2h** using Vn and Fb as ligands in HUVEC cell line.



HUVEC / Fb	EC ₅₀ (μM)
1h	26
2h	6
Cilengitide	0.08



HUVEC / Vn	EC ₅₀ (μM)
1h	—
2h	—
Cilengitide	16

Cytotoxicity determination of RGD-containing compound **2h**

The cytotoxicity of the conjugated peptide **5** and its macrocyclic precursors **3** and **4** were evaluated against three human cancer cell lines: lung carcinoma A549, breast cancer MCF-7 and MCF-10A cell lines. Cytotoxicity experiments were performed following the methods indicated elsewhere.¹⁰ Only the macrocycle **4** showed activity (IC₅₀ <10 μM) in line with the expected activity for the parent compound (sansalvamide).¹¹

Live imaging of SH-SY5Y cells upon incubation with 1j-Bodipy and 2j-Bodipy

For confocal microscopy analysis, cells were seeded ($4 \div 12 \times 10^3$ per cm^2) on glass chamber coverslips and cultured for 24 h before being incubated for 30 min in fresh medium containing **1j-Bodipy** (750 nM) or **2j-Bodipy** (750 nM). Cells were washed, and fresh medium was introduced to perform experiments with living cells in CO_2 and temperature-controlled conditions. Images were collected with a Leica SP5 Spectral confocal microscope attached to an inverted DMI 6000, using a $63\times/1.3$ Glyc HCX PL APO objective.

Supplementary References

1. Preciado, S., Mendive-Tapia, L., Albericio, F. & Lavilla, R. Synthesis of C-2 arylated tryptophan amino acids and related compounds through palladium-catalyzed C-H activation. *J. Org. Chem.* **78**, 8129–8135 (2013).
2. Chan, W. C. & White, P. D. *Fmoc solid phase peptide synthesis*. 376 (Oxford University Press, New York, 2000).
3. E. Kaiser, R. L. Colosco, C. D. Bossinger, P. I. C. Color test for detection of free terminal amino groups in the solid-phase synthesis of peptides. *Anal. Biochem.* **34**, 595–598 (1970).
4. Seim, K. L., Obermeyer, A. C. & Francis, M. B. Oxidative modification of native protein residues using cerium (IV) ammonium nitrate. *J. Am. Chem. Soc.* **133**, 16970–16976 (2011).
5. Cui, A. *et al.* Synthesis, spectral properties and photostability of novel boron–dipyromethene dyes. *J. Photoch. Photobio. A.* **186**, 85–92 (2007).
6. Schubert, M., Labudde, D., Oschkinat, H. & Schmieder, P. A software tool for the prediction of Xaa-Pro peptide bond conformations in proteins based on ^{13}C chemical shift statistics. *J. Biomol. NMR.* **24**, 149–154 (2002).
7. Shen, Y. & Bax, A. Prediction of Xaa-Pro peptide bond conformation from sequence and chemical shifts. *J. Biomol. NMR.* **46**, 199–204 (2010).
8. Spartan'14 for Windows, Macintosh and Linux, version 1.1.4, wavefunction, inc. www.wavefun.com.
9. Manzoni, L. *et al.* Cyclic RGD-containing functionalized azabicycloalkane peptides as potent integrin antagonists for tumor targeting. *Chem. Med. Chem.* **4**, 615–632 (2009).
10. Preciado, S. *et al.* Synthesis and biological evaluation of a post-synthetically modified Trp-based diketopiperazine. *Med. Chem. Comm.* **4**, 1171–1174 (2013).
11. Pan, P.-S. *et al.* A comprehensive study of Sansalvamide A derivatives: The structure-activity relationships of 78 derivatives in two pancreatic cancer cell lines. *Bioorg. Med. Chem.* **17**, 5806–5825 (2009).
12. Zhou, L., Budge, S. M., Ghaly, A. E., Brooks, M. S. & Dave, D. Extraction, purification and characterization of fish chymotrypsin: a review. **7**, 104–123 (2011).
13. Von Kleist, L. *et al.* Role of the clathrin terminal domain in regulating coated pit dynamics revealed by small molecule inhibition. *Cell* **146**, 471–484 (2011).



FULL SUPPORTING INFORMATION PUBLICATION VIII

CHEMISTRY

A **European** Journal

Supporting Information

Constrained Cyclopeptides: Biaryl Formation through Pd-Catalyzed C—H Activation in Peptides—Structural Control of the Cyclization vs. Cyclodimerization Outcome

Lorena Mendive-Tapia,^[a] Alexandra Bertran,^[a] Jesús García,^[a] Gerardo Acosta,^[b]
Fernando Albericio,^[b, c, d] and Rodolfo Lavilla^{*[b, e]}

chem_201601832_sm_miscellaneous_information.pdf

Table of contents

Abbreviations. Pag.S2

General experimental information. Pag.S2

Experimental procedures and peptide characterization. Pag.S3

NMR spectra of compounds 1, 3, 5, 6 and 7. Pag.S9

HPLC-MS chromatograms of compounds 1-7. Pag.S64

IR spectra of compounds 1 and 6. Pag.S68

^1H and ^{13}C chemical shifts assignments of compounds 5 and 7. Pag.S71

Additional comments on the NMR spectroscopy of cyclopeptides 3 and 5. Pag.S78

High resolution mass spectrometry analysis of compounds 3, 5 and 7. Pag.S79

HPLC-MS chromatograms relative to C-H activation on resin. Pag.S87

Emac values of compounds 3 and 5. Pag.S88

Preliminary absorbance host-guest complexation experiments of compounds 5b and 5c. Pag.S89

Minimized geometries of compounds 1, 3, 5 and 7 generated by the Spartan '14 suite. Pag.S91

Preliminary calculations on the relative stabilities of the cyclic/cyclodimeric peptides after the Pd-catalyzed CH activation reaction. Pag.S95

Bibliography. Pag.S98

Abbreviations

Abbreviation used for amino acids and designations of peptides follow the rules of the IUPAC-IUB Commission of Biochemical Nomenclature in *J. Biol. Chem.* 247, 977-983 (1982). The following additional abbreviations are used: FA: formic acid, ACN: acetonitrile, DMF: *N,N*-dimethylformamide, DCM: dichloromethane, Fmoc: 9*H*-fluorenylmethyloxycarbonyl, SPPS: solid phase peptide synthesis, DIEA: *N,N*-diisopropylethylamine, DIPCDI: *N,N*-diisopropylcarbodiimide, HOBT: hydroxybenzotriazole, HBTU: *o*-benzotriazole-*N,N,N',N'*-tetramethyl-uronium-hexafluoro-phosphate, TIS: triisopropylsilane, IR: infrared spectroscopy, NMR: nuclear magnetic resonance, RP-HPLC: reverse-phase high performance liquid chromatography, HPLC-MS high performance liquid chromatography mass spectrometry, HRMS(ESI): high-resolution mass spectrometry (electrospray ionization).

General experimental information

Reactions were monitored by HPLC-MS at 220 nm using a HPLC Waters Alliance HT comprising a pump (Edwards RV12) with degasser, an autosampler and a diode array detector. Flow from the column was split to a MS spectrometer. The MS detector was configured with an electrospray ionization source (micromass ZQ4000) and nitrogen was used as the nebulizer gas. Mass scans were acquired in positive ion mode, and linear gradients of ACN (+0.05% formic acid) into H₂O (+0.1% formic acid) were run at a flow rate of 1.6 mL·min⁻¹ over 3.5 min. Data acquisition was performed with MassLynx software. High resolution mass spectrometry analyses were conducted on an LTQ-FT Ultra (Thermo Scientific) spectrometer with a NanoESI positive ionization. Data was acquired with Xcalibur software, vs.2.0SR2 (ThermoScientific) and elemental compositions from experimental exact mass monoisotopic values were obtained with a dedicated algorithm integrated in Xcalibur. All microwave reactions were carried out in 10 mL sealed glass tubes in a focused mono-mode microwave oven ("Discover" by CEM Corporation) featured with a surface sensor for internal temperature determination. Cooling was provided by compressed air ventilating the microwave chamber during the reaction.

When stated, final crudes were purified on a semi-preparative RP-HPLC provided of a RP-HPLC XBRIDGE™ Prep C18, 5μM OBD 19 x 50 mm column, a Waters Delta 600 system comprising a sample manager (Waters 2700), a controller (Waters 600), a dual λ absorbance detector (Waters 2487), a fraction collector II, and a software system controller (MassLynx). Linear gradients of ACN (+0.05% FA) into H₂O (+0.1% FA) were run at a flow rate of 16 mL·min⁻¹ over 20 min. Otherwise, the final crude was purified via flash column chromatography Combi Flash ISCO RF provided with dual UV detection. Normal mode: crude residue and silica media were dissolved in CH₂Cl₂, concentrated, and the resultant solid samples were eluted on a RediSep Rf silica column. Reverse mode: crude residues and Celite were dissolved in CH₂Cl₂, concentrated, and the resultant solid samples were eluted on a RediSep Rf GOLD C18 column.

NMR spectra of peptides in [D₆]DMSO were acquired with either a Varian Mercury 400 MHz, Bruker DMX-500 MHz or Bruker Avance III 600 MHz spectrometers equipped with TCI cryoprobes. The spectra were referenced relative to the residual DMSO signal (¹H, 2.49 ppm; ¹³C, 39.5 ppm). For peptides **5a-c** and **7b-c**, ¹H resonances were unequivocally assigned by two-dimensional NMR experiments (COSY, TOCSY and NOESY and/or ROESY). Then, the ¹³C resonances were straightforwardly assigned on the basis of the cross-correlations observed in the ¹H-¹³C HSQC spectra. Mixing times for TOCSY spectra were 70 ms, for NOESY spectra 300-450 ms and for ROESY experiments were 200 ms. Chemical shifts (δ) are reported in ppm. Multiplicities are referred by the

following abbreviations: s = singlet, d = doublet, t = triplet, dd = double doublet, dt = double triplet, q = quartet and m = multiplet. HRMS (ESI positive) were obtained with a LTQ-FT Ultra (Thermo Scientific) mass Spectrometer. IR spectra were obtained on a Thermo Nicolet NEXUS.

General procedure for SPPS.¹ All peptides were manually synthesized in polystyrene syringes fitted with a polyethylene porous disc using Fmoc-based SPPS. Solvents and soluble reagents were removed by suction. The Fmoc group was removed with piperidine-DMF (1:4) (1×1 min, 2×5 min). Peptide synthesis transformations and washes were performed at r.t.

Resin loading (2-Chlorotriyl resin 1 mmol/g). Fmoc-XX-OH (1.0 eq.) was attached to the resin (1.0 eq.) with DIEA (3.0 eq.) in DCM at r.t for 10 min and then DIEA (7.0 eq.) for 40 min. The remaining trityl groups were capped adding 0.8 μ L MeOH/mg resin for 10 min. After that, the resin was filtered and washed with DCM (4 x 1 min), DMF (4 x 1 min). The loading of the resin was determined by titration of the Fmoc group.¹

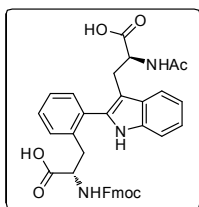
Peptide elongation. After the Fmoc group was eliminated, the resin was washed with DMF (4 x 1 min), DCM (3 x 1 min), DMF (4 x 1 min). Amino acid coupling. Fmoc-XX-OH (3.0 eq.) were incorporated with a 5-min pre-activation with DIPCDI (3.0 eq.) and OxymaPure (3.0 eq.) in DMF for 1h. To ensure the coupling of Fmoc-x-I-Phe (x: 2, 3 or 4), it was incorporated with HBTU (1.5 eq.), HOBT (1.5 eq.) and DIEA (3.0 eq.) in DMF for 1h. The completion of the coupling was monitored with the ninhydrin (free primary amine) test.² Then, the resin was filtered and washed with DCM (4 x 1 min) and DMF (4 x 1 min) and the Fmoc group was eliminated.

Acetylation. Once the peptide sequence was fully elongated, N-terminal acetylation was performed with acetic anhydride (10 eq.), DIEA (10 eq.) in DMF (30 min).

Final cleavage. The resin bound peptide was treated with a 95% TFA, 2.5% TIS, 2.5% H₂O cleavage cocktail (1h) and the eluates were evaporated under vacuum. Then, the residue was washed with Et₂O, dissolved in ACN:H₂O and lyophilized furnishing the corresponding deprotected peptide.

Experimental procedures and peptide characterization

[Ac-C2-Trp-OH]—(Fmoc-o-Phe-OH) adduct (1a). Fmoc-Phe(2-I)-OH (50 mg, 0.097 mmol, 1.0 eq.),

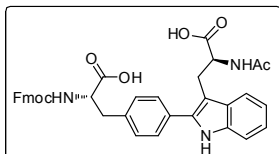


Ac-Trp-OH³ (24 mg, 0.097 mmol, 1.0 eq.), AgBF₄ (38 mg, 0.195 mmol, 2.0 eq.), trifluoroacetic acid (7.5 μ L, 0.195 mmol, 1.0 eq.) and Pd(OAc)₂ (4.4 mg, 0.012 mmol, 0.20 eq.) were placed in a microwave reactor vessel in DMF (0.60 mL). The mixture was heated under microwave irradiation (250 W) at 90 °C for 20 min. Then, Pd(OAc)₂ (4.4 mg, 0.012 mmol, 0.20 eq.) and AgBF₄ (38 mg, 0.195 mmol, 2.0 eq.) were added again, and a second irradiation cycle was performed. The resulting suspension was filtered through Celite and the filtrate was evaporated under vacuum. The crude residue was

purified by flash chromatography on Silica using DCM/EtOH to obtain the final adduct **1b** as a pale solid (23 mg, 37%). A highly pure fraction was obtained by PoraPak Rxn RP 20 cc reverse phase column purification. Mobile phase: ACN (0.1% HCOOH)/H₂O (0.1% HCOOH). Pure fractions were lyophilized furnishing the final adduct **1a** as a pale solid (10 mg, 15%). ¹H NMR (400 MHz, [D₆]DMSO): δ 12.50 (s, 2H), 11.01 (d, J = 9.3 Hz, 1H), 8.01 (t, J = 7.5 Hz, 1H), 7.88 (d, J = 7.5 Hz, 2H), 7.65 (t, J = 6.6 Hz, 4H), 7.40 (m, 4H), 7.31 (m, 5H), 7.07 (t, J = 7.5 Hz, 1H), 7.00 (t, J = 7.4 Hz, 1H), 4.58 – 4.43 (m, 1H), 4.19 (m, 5H), 3.15 – 3.06 (m, 1H), 2.89 (m, 2H), 2.85 – 2.73 (m, 1H), 1.68 (d, J = 12.5 Hz, 3H) ppm. IR (Film, cm⁻¹): ν = 3406.75, 3322.83, 3062.38, 2955.31, 2920.58, 2848.23, 1719.61, 1708.04, 1661.74,

1528.62, 1450.48 cm^{-1} . **HPLC-MS**: t_R 2.83 min (gradient 5-100% ACN). **HRMS (ESI)**: (M: $\text{C}_{37}\text{H}_{33}\text{N}_3\text{O}_7$) m/z calcd. 632.23913, found 632.23916 (M+H) $^+$.

[Ac-C2-Trp-OH]—(Fmoc-*p*-Phe-OH) adduct (1b). Fmoc-Phe(4-I)-OH (50 mg, 0.097 mmol, 1.0 eq.), Ac-



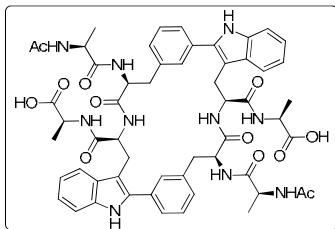
Trp-OH (24 mg, 0.097 mmol, 1.0 eq.), AgBF_4 (38 mg, 0.195 mmol, 2.0 eq.), trifluoroacetic acid (7.5 μL , 0.195 mmol, 1.0 eq.) and $\text{Pd}(\text{OAc})_2$ (4.4 mg, 0.012 mmol, 0.20 eq.) were placed in a microwave reactor vessel in DMF (0.60 mL). The mixture was heated under microwave irradiation (250 W) at 90 $^\circ\text{C}$ for 20 min.

The resulting suspension was filtered through Celite and the filtrate was evaporated under vacuum. The crude residue was purified by flash chromatography on Silica using DCM/EtOH to obtain the final adduct **1b** as a pale solid (39 mg, 63%). **^1H NMR** (400 MHz, $[\text{D}_6]\text{DMSO}$): δ 11.17 (s, 1H), 8.21 (dd, $J = 8.2, 3.6$ Hz, 1H), 7.87 (d, $J = 7.5$ Hz, 2H), 7.80 (d, $J = 8.3$ Hz, 1H), 7.67 (dd, $J = 14.0, 7.1$ Hz, 3H), 7.60 (d, $J = 6.8$ Hz, 2H), 7.39 (dd, $J = 10.2, 6.0$ Hz, 4H), 7.30 (m, 3H), 7.08 (dd, $J = 11.1, 4.0$ Hz, 1H), 6.99 (dd, $J = 11.4, 4.4$ Hz, 1H), 4.57 (dd, $J = 15.0, 7.5$ Hz, 1H), 4.25 (m, 4H), 3.35 – 3.26 (m, 1H), 3.19 – 3.08 (m, 2H), 3.01 – 2.91 (m, 1H), 1.75 (s, 3H) ppm. **^{13}C NMR** (101 MHz, $[\text{D}_6]\text{DMSO}$): δ 173.5, 173.3, 169.0, 162.3, 156.0, 143.7, 140.7, 137.2, 135.8, 135.0, 130.9, 129.4, 128.9, 127.7, 127.6, 127.1, 125.2, 121.4, 120.1, 118.9, 118.7, 111.0, 107.5, 107.4, 65.6, 55.5, 53.1, 46.6, 36.1, 27.4, 22.4 ppm. **IR** (Film, cm^{-1}): $\nu = 3406.75, 3325.72, 3056.59, 2952.41, 2917.68, 2848.23, 1728.30, 1664.63, 1525.72, 1450.48$ cm^{-1} . **HPLC-MS**: t_R 2.82 min (gradient 5-100% ACN). **HRMS (ESI)**: (M: $\text{C}_{37}\text{H}_{33}\text{N}_3\text{O}_7$) m/z calcd. 632.23913, found 632.23820 (M+H) $^+$.

General procedure for the C-H activation process of peptides **3** and **5**

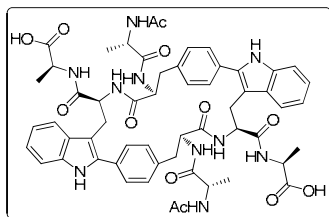
Unless stated otherwise, the linear peptide, AgBF_4 (2.0 eq.), trifluoroacetic acid (1.0 eq.) and $\text{Pd}(\text{OAc})_2$ (0.20 eq.) were placed in a microwave reactor vessel in DMF. The mixture was heated under microwave irradiation (250 W) at 90 $^\circ\text{C}$ for 20 min. The resulting suspension was filtered through Celite and the filtrate was evaporated under vacuum. The crude residue was purified by semi-preparative RP-HPLC (XBRIDGETM Prep C18, 5 μM OBD 19 x 50 mm column) [solvent A (0.1% FA in H_2O) and solvent B (0.1% FA in ACN)], in 10 min, flux: 20 $\text{mL}\cdot\text{min}^{-1}$, detection at $\lambda = 220$ nm.

(Cyclo-*m,m*)-bis-[Phe-Trp]-(Ac-Ala-Phe-Trp-Ala-OH) (3). Starting from peptide **2** (200 mg, 0.302



mmol, 1.0 eq.), AgBF_4 (118 mg, 0.605 mmol, 2.0 eq.), trifluoroacetic acid (23 μL , 0.302 mmol, 1.0 eq.) and $\text{Pd}(\text{OAc})_2$ (3.4 mg, 0.015 mmol, 0.20 eq.) were placed in a microwave reactor vessel in DMF (2.0 mL). Then, $\text{Pd}(\text{OAc})_2$ (3.4 mg, 0.015 mmol, 0.20 eq.) and AgBF_4 (3.4 mg, 0.015 mmol, 0.20 eq.) were added again, and a second irradiation cycle was performed. The resulting suspension was filtered through Celite and the filtrate was precipitated in H_2O (40% conversion estimated by HPLC-MS, 28% yield estimated by HPLC-MS conversion). A crude fraction was purified by flash chromatography on Celite using H_2O (0.1% FA)/ACN (0.1% FA) to obtain the final dimeric compound **3**. Pale solid (10 mg, 13% isolated yield). **HPLC-MS**: t_R 2.28 min (gradient 5-100% ACN). **HRMS (ESI)** (m/z): [M] calcd. for $\text{C}_{56}\text{H}_{62}\text{N}_{10}\text{O}_{12}$, 1066.45487; found, 1067.45620.

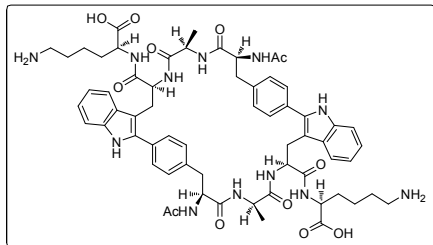
(Cyclo-*p,p*)bis-[Phe-Trp]-(Ac-Ala-Phe-Trp-Ala-OH) (5a). Starting from peptide **4a** (600 mg, 0.907



mmol) (60% conversion estimated by HPLC-MS). An analytically pure sample was obtained by semi-preparative RP-HPLC purification. Gradient: 25-30% of B (pale solid). ^1H NMR (800 MHz, $[\text{D}_6]\text{DMSO}$): δ 11.20 (s, 1H), 8.13 (d, $J = 7.7$ Hz, 1H), 7.93 (d, $J = 7.3$ Hz, 1H), 7.90 (d, $J = 7.0$ Hz, 1H), 7.67 (d, $J = 7.9$ Hz, 1H), 7.61 (d, $J = 7.6$ Hz, 2H), 7.34 (d, $J = 7.9$ Hz, 1H), 7.25 (d, $J = 7.7$ Hz, 2H), 7.11 (t, $J = 7.5$ Hz, 1H), 7.03 (t, $J = 7.5$ Hz, 1H), 6.82 (d, $J = 6.9$ Hz, 1H), 4.24 – 4.15 (dp, $J = 28.2$, 7.1

Hz, 2H), 4.07 (ddd, $J = 10.4$, 6.9, 3.8 Hz, 1H), 3.96 (m, 1H), 3.43 (dd, $J = 15.1$, 3.7 Hz, 1H), 3.23 (dd, $J = 15.2$, 9.4 Hz, 1H), 2.64 (dd, $J = 15.1$, 10.6 Hz, 1H), 2.48 (m, 1H), 1.78 (s, 3H), 1.28 (d, $J = 7.3$ Hz, 3H), 1.08 (d, $J = 7.0$ Hz, 3H) ppm. IR (Film, cm^{-1}): $\nu = 3404.27$, 2911.03, 1655.52 cm^{-1} . HPLC-MS: t_R 2.32 min (gradient 5-100% ACN). HRMS (ESI) (m/z): $[\text{M}+\text{H}]^+$ calcd. for $\text{C}_{56}\text{H}_{62}\text{N}_{10}\text{O}_{12}$, 1067.4621; found, 1067.4624.

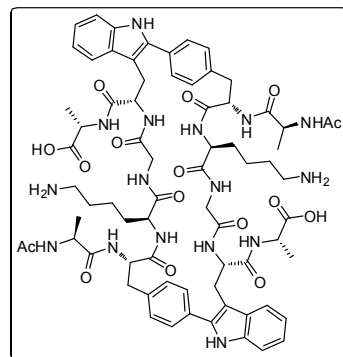
(Cyclo-*p,p*)bis-[Phe-Trp]-(Ac-Phe-Ala-Trp-Lys-OH) (5b). Starting from peptide **4b** (0.15 g, 0.209 mmol,



1.0 eq.), AgBF_4 (81 mg, 0.417 mmol, 2.0 eq.), trifluoroacetic acid (16 μL , 0.209 mmol, 1.0 eq.) and $\text{Pd}(\text{OAc})_2$ (9.4 mg, 0.042 mmol, 0.20 eq.) were placed in a microwave reactor vessel in DMF (0.87 mL) (54% conversion estimated by HPLC-MS). A highly pure fraction was obtained by semi-preparative RP-HPLC purification. Gradient: 19-22% of B (pale solid). ^1H NMR (500 MHz, $[\text{D}_6]\text{DMSO}$): δ 10.92 (s, 1H), 8.14 (s, 1H),

8.04 (d, $J = 8.0$ Hz, 1H), 7.72 (d, $J = 8.0$ Hz, 1H), 7.49 (s, 1H), 7.43 (m, 2H), 7.34 – 7.26 (m, 4H), 7.08 (t, $J = 7.6$ Hz, 1H), 7.01 (m, 1H), 4.59 (m, 2H), 4.14 (m, 1H), 3.86 (m, 1H), 3.32 (1H), 3.13 (1H), 3.01 (1H), 2.81 (m, 1H), 2.66 (m, 2H), 1.81 (s, 3H), 1.63 (m, 1H), 1.53 (m, 1H), 1.46 (m, 2H), 1.26 (m, 2H), 1.08 (d, $J = 6.9$ Hz, 3H) ppm. HPLC-MS: t_R 1.42 min (gradient 20-60% ACN). HRMS (ESI): (M : $\text{C}_{62}\text{H}_{76}\text{O}_{12}\text{N}_{12}$) m/z calcd 591.29390, found 591.29388 $[(\text{M}+2\text{H})/2]^{2+}$.

(Cyclo-*p,p*)bis-[Phe-Trp]-(Ac-Ala-Phe-Lys-Gly-Trp-Ala-OH) (5c). Starting from peptide **4c** (0.20 g,

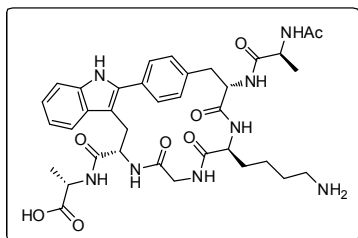


0.236 mmol, 1.0 eq.), AgBF_4 (92 mg, 0.472 mmol, 2.0 eq.), trifluoroacetic acid (18 μL , 0.236 mmol, 1.0 eq.) and $\text{Pd}(\text{OAc})_2$ (10 mg, 0.047 mmol, 0.20 eq.) were placed in a microwave reactor vessel in DMF (1.0 mL) (23% conversion estimated by HPLC-MS). A highly pure fraction was obtained by semi-preparative RP-HPLC purification. Gradient: 15-20% of B (pale solid). ^1H NMR (500 MHz, $[\text{D}_6]\text{DMSO}$): δ 11.10 (s, 1H), 8.35 – 7.86 (m, 6H), 7.70 (m, 1H), 7.51 (d, $J = 6.7$ Hz, 2H), 7.37 – 7.24 (m, $J = 8.4$ Hz, 3H), 7.06 (t, $J = 7.4$ Hz, 1H), 6.99 (t, $J = 7.2$ Hz, 1H), 4.50 (m, 2H), 4.29 (m, 1H), 4.20 (m, 1H), 3.83 (m, 1H), 3.77 – 3.44 (m, $J = 57.6$ Hz, 2H), 3.43 (1H), 3.05 (m, 2H), 2.88 (m, 1H), 2.76 (m,

2H), 1.81 (s, $J = 6.8$ Hz, 3H), 1.68 (m, 1H), 1.58 – 1.45 (m, 3H), 1.37 – 1.27 (m, 2H), 1.19 (d, $J = 6.6$ Hz,

3H), 1.12 (d, $J = 6.6$ Hz, 3H) ppm. **HPLC-MS**: t_R 1.07 min (gradient 20-60% ACN). **HRMS (ESI)**: (M: $C_{72}H_{92}N_{16}O_{16}$) m/z calcd. 1436.68772, found 1436.68351 (M).

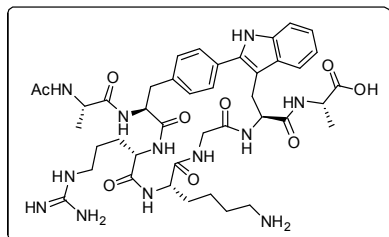
Ac-Ala-(Cyclo-*p*)-[Phe-Lys-Gly-Trp]-Ala-OH (5c'). Starting from peptide **4c** (0.20 g, 0.236 mmol, 1.0



eq.), $AgBF_4$ (92 mg, 0.472 mmol, 2.0 eq.), trifluoroacetic acid (18 μ L, 0.236 mmol, 1.0 eq.) and $Pd(OAc)_2$ (10 mg, 0.047 mmol, 0.20 eq.) were placed in a microwave reactor vessel in DMF (1.0 mL) (51% conversion estimated by HPLC-MS). A highly pure fraction was obtained by semi-preparative RP-HPLC purification. Gradient: 15-20% of B (pale solid). **1H NMR** (500 MHz, $[D_6]DMSO$): δ 11.05 (s, 1H), 8.35 (d, $J = 8.5$ Hz, 1H), 8.18 (d, $J = 6.2$ Hz, 1H), 8.11 (m, 1H), 8.08 (d, $J = 7.3$ Hz, 1H), 7.61 (d, $J = 8.3$ Hz, 1H),

7.51 (d, $J = 7.9$ Hz, 2H), 7.36 – 7.26 (m, $J = 7.3, 4.6$ Hz, 3H), 7.07 (t, $J = 8.1$ Hz, 1H), 7.00 (m, 1H), 6.96 (t, $J = 7.2$ Hz, 1H), 6.40 (m, 1H), 4.68 (m, 1H), 4.48 (m, 1H), 4.34 (m, 1H), 4.19 (m, 1H), 4.14 (m, 1H), 3.56 (dd, $J = 17.7, 6.8$ Hz, 1H), 3.45 (m, 1H), 3.27 (1H), 3.26 (1H), 2.96 (m, 2H), 2.72 (m, 2H), 1.86 (s, 3H), 1.68 (m, 1H), 1.49-1.39 (m, 3H), 1.36 (m, 1H), 1.18 (m, 7H) ppm. **HPLC-MS**: t_R 1.00 min (gradient 20-60% ACN). **HRMS (ESI)**: (M: $C_{36}H_{46}N_8O_8$) m/z calcd. 719.35114, found 719.35134 (M+H) $^+$.

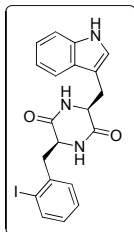
Ac-Ala-(Cyclo-*p*)-[Phe-Arg-Lys-Gly-Trp]-Ala-OH (5d'). Starting from peptide **4d** (200 mg, 0.199 mmol,



1.0 eq.), $AgBF_4$ (79 mg, 0.399 mmol, 2.0 eq.), trifluoroacetic acid (16 μ L, 0.199 mmol, 1.0 eq.) and $Pd(OAc)_2$ (9.1 mg, 0.040 mmol, 0.20 eq.) were placed in a microwave reactor vessel in DMF (2.0 mL). Then, $Pd(OAc)_2$ (49.1 mg, 0.040 mmol, 0.20 eq.) and $AgBF_4$ (79 mg, 0.399 mmol, 2.0 eq.) were added again, and a second irradiation cycle was performed (81% conversion estimated by HPLC-MS). An analytically pure sample was obtained by semi-preparative RP-

HPLC purification. Gradient: 10-20% of B (pale solid)). **1H NMR** (500 MHz, $[D_6]DMSO$): δ 10.89 (s, 1H), 8.36 (m, 1H), 8.02 (m, 3H), 7.64 (m, 1H), 7.58 (d, $J = 7.8$ Hz, 1H), 7.50 (d, $J = 7.8$ Hz, 2H), 7.32 (d, $J = 8.1$ Hz, 1H), 7.23 (d, $J = 7.8$ Hz, 2H), 7.06 (t, $J = 7.5$ Hz, 1H), 6.99 (t, $J = 7.9$ Hz, 1H), 6.95 (m, 1H), 4.56 (m, 1H), 4.30 (m, 2H), 4.22 (m, 1H), 4.04 – 3.89 (m, 2H), 3.79 (m, 1H), 3.56 (m, 1H), 3.24 (1H), 3.13 (2H), 3.12 (1H), 3.05 (1H), 2.94 (m, 2H), 2.78 (m, 2H), 1.84 (s, 3H), 1.77 (m, 1H), 1.71 – 1.47 (m, 7H), 1.40 (m, 2H), 1.23 (d, $J = 7.2$ Hz, 3H), 1.13 (d, $J = 6.9$ Hz, 3H) ppm. **HPLC-MS**: t_R 2.50 min (gradient 5-30% ACN). **HRMS (ESI)**: (M: $C_{42}H_{58}N_{12}O_9$) m/z calcd. 875.44822, found 875.45014 (M+H) $^+$.

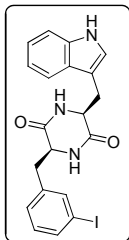
Cyclo(2-I-Phe-Trp) (6a). Compound **6a** was prepared using Fmoc-Phe(2-I)-OH (1.5 g, 2.93 mmol, 1.0



eq.), H-Trp-OMe.HCl (0.73 g, 2.93 mmol, 98%, 1.0 eq.), HBTU (1.1 g, 2.93 mmol, 1.0 eq.), DIEA (1.0 mL, 5.86 mmol, 2.0 eq.) which were dissolved in DMF (3.3 mL). The pale yellow solution was stirred at r.t. for 24 h. The resulting solution was precipitated over 10 mL of cold water and centrifugated (RPM: 2000, t: 5 min, T= 4 $^{\circ}C$). Precipitation cycles in cold water and centrifugation were repeated 8 times obtaining the desired adduct (2.6 g, 89%). The white solid was suspended in 20% piperidine/ACN (15 mL) and stirred for 22 h and the resulting solution was

precipitated over 10 mL of cold water and centrifugated (RPM: 2000, t: 5 min, T= 4 °C). Precipitation cycles in cold water and centrifugation were repeated 2 times. The crude was purified by flash chromatography on silica using DCM/MeOH:DCM (1:5) to yield the pure product **6a** (1.0 g, 85% isolated yield). **¹H NMR** (400 MHz, [D₆]DMSO): δ 10.97 (d, J = 2.4 Hz, 1H), 8.21 (d, J = 2.7 Hz, 1H), 7.66 (dd, J = 7.9, 1.3 Hz, 1H), 7.62 (dd, J = 7.5, 1.3 Hz, 1H), 7.44 (d, J = 3.2 Hz, 1H), 7.29 (m, 1H), 7.11 (d, J = 2.3 Hz, 1H), 7.07 (ddd, J = 8.1, 7.0, 1.4 Hz, 1H), 7.03 (ddd, J = 8.1, 7.0, 1.3 Hz, 1H), 6.94 (td, J = 7.5, 1.3 Hz, 1H), 6.82 (td, J = 7.6, 1.7 Hz, 1H), 5.56 (dd, J = 7.6, 1.7 Hz, 1H), 4.11 (m, 1H), 3.69 (dt, J = 9.3, 3.9 Hz, 1H), 3.27 (m, 1H), 2.97 (dd, J = 14.3, 4.6 Hz, 1H), 2.44 (dd, J = 13.3, 4.4 Hz, 1H), 1.12 (dd, J = 13.4, 9.9 Hz, 1H) ppm. **¹³C NMR** (100 MHz, [D₆]DMSO): δ 166.9, 166.1, 138.9, 138.6, 136.0, 131.8, 128.5, 127.8, 124.9, 121.1, 119.3, 118.6, 111.5, 108.6, 100.6, 55.7, 53.4, 45.2, 29.2 ppm. **IR** (Film, cm⁻¹): ν = 3389.39, 3175.24, 3047.91, 2952.41, 2914.79, 2848.23, 1681.99, 1453.38 cm⁻¹. **HPLC-MS**: t_R 2.40 min (gradient 5-100% ACN). **HRMS (ESI)**: (M: C₂₀H₁₈O₂N₃I) m/z calcd. 460.0516, found 460.0519 (M+H)⁺.

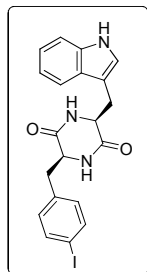
Cyclo(3-I-Phe-Trp) (6b). Compound **6b** was prepared using Fmoc-Phe(3-I)-OH (0.22 g, 0.435 mmol,



1.0 eq.), H-Trp-OMe.HCl (0.11 g, 0.435 mmol, 98%, 1.0 eq.), HBTU (0.17 g, 0.435 mmol, 1.0 eq.), DIEA (0.15 mL, 0.871 mmol, 2.0 eq.) which were dissolved in 0.94 mL of DMF. The pale yellow solution was stirred at r.t. for 22 h followed by the evaporation under vacuum of the obtained suspension. The solid was dissolved in ethyl acetate and was washed with saturated aqueous solution of NaHCO₃ (3 x 20 mL). Then, the organic phase was dried over Na₂SO₄, filtered and the solvent was removed under vacuum obtaining the desired adduct (0.31 g, 99%). The white solid was suspended in 20% piperidine/ACN (10 mL) and stirred for 20 h. The resulting suspension was concentrated under vacuum and diethyl ether was added over the

solid. The suspension was stirred for 10 min, filtered and washed with diethyl ether (3 x 10 mL). The white solid obtained was lyophilized to yield the pure product (0.16 g, 81% isolated yield). **¹H NMR** (400 MHz, [D₆]DMSO): δ 10.90 (m, 1H), 7.99 (d, J = 2.7 Hz, 1H), 7.79 (m, 1H), 7.50 (dd, J = 3.1, 1.7 Hz, 1H), 7.48 (m, 1H), 7.32 (dt, J = 8.1, 0.9 Hz, 1H), 7.09 (ddd, J = 8.2, 7.0, 1.2 Hz, 1H), 7.02 (m, 1H), 6.98 (m, 1H), 6.94 (t, J = 7.7 Hz, 1H), 6.87 (t, J = 1.7 Hz, 1H), 6.68 (dt, J = 7.7, 1.3 Hz, 1H), 3.99 (td, J = 4.9, 1.9 Hz, 1H), 3.79 (m, 1H), 2.82 (d, J = 4.6 Hz, 1H), 2.68 (m, 1H), 2.30 (dd, J = 13.4, 4.8 Hz, 1H), 1.61 (dd, J = 13.4, 7.3 Hz, 1H) ppm. **¹³C NMR** (100 MHz, [D₆]DMSO): δ 167.3, 166.4, 139.8, 138.4, 136.4, 135.6, 130.6, 129.4, 127.9, 125.0, 121.6, 119.3, 119.1, 111.8, 109.2, 95.1, 55.8, 45.3, 30.1, 24.3 ppm. **IR** (Film, cm⁻¹): ν = 3345.98, 3172.35, 3050.80, 2961.09, 2914.79, 2868.49, 1679.10, 1462.06 cm⁻¹. **HRMS (ESI)**: (M: C₂₀H₁₈O₂N₃I) m/z calcd. 460.0516, found 460.0518 (M+H)⁺.

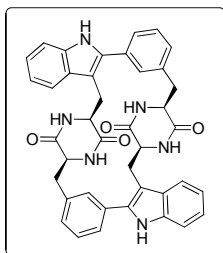
Cyclo(4-I-Phe-Trp) (6c). Compound **6c** was prepared using Fmoc-Phe(4-I)-OH (1.0 g, 1.95 mmol, 1.0



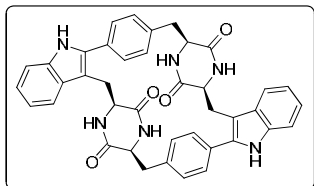
eq.), H-Trp-OMe.HCl (0.47 g, 1.95 mmol, 98%, 1.0 eq.), HBTU (0.7 g, 1.95 mmol, 1.0 eq.), DIEA (0.68 mL, 3.90 mmol, 2.0 eq.) which were dissolved in 1.5 mL of DMF. The pale yellow solution was stirred at 0 °C for 24 h followed by precipitation over 10 mL of cold water and centrifugation (RPM: 2000, t: 5 min, T= 4 °C). Precipitation cycles in cold water and centrifugation were repeated 4 times obtaining the desired adduct (1.3 g, 97% isolated yield). The white solid was suspended in 20% piperidine/ACN (10 mL) and stirred for 30 min at r.t. The resulting suspension was precipitated over 10 mL of cold water and centrifuged (RPM: 2000, t: 5 min, T= 4 °C). Precipitation cycles in cold water and centrifugation were repeated 2 times. The white solid obtained was lyophilized to

yield the pure product (0.82 g, 94% isolated yield). **¹H NMR** (400 MHz, [D₆]DMSO): δ 10.93 (s, 1H), 7.98 (s, 1H), 7.71 (s, 1H), 7.50 (dt, J = 7.9, 0.9 Hz, 1H), 7.45 (m, 2H), 7.31 (dt, J = 8.1, 0.9 Hz, 1H), 7.07 (ddd, J = 8.1, 7.0, 1.2 Hz, 1H), 7.01 (s, 1H), 6.99 (ddd, J = 8.0, 7.0, 1.1 Hz, 1H), 6.34 (m, 2H), 4.01 (ddd, J = 4.7, 5.3, 2.3 Hz, 1H), 3.75 (ddd, J = 7.6, 4.8, 2.3 Hz, 1H), 2.85 (dd, J = 14.4, 4.7 Hz, 1H), 2.73 (dd, J = 14.4, 5.3 Hz, 1H), 2.30 (dd, J = 13.4, 4.8 Hz, 1H), 1.57 (dd, J = 13.4, 7.6 Hz, 1H) ppm. **¹³C NMR** (100 MHz, [D₆]DMSO): δ 167.2, 166.5, 137.1, 136.8, 136.5, 132.4, 128.0, 125.0, 121.4, 119.4, 119.0, 111.8, 109.1, 92.7, 55.8, 55.7, 40.0, 30.1 ppm. **IR** (Film, cm⁻¹): ν = 3186.82, 3050.80, 2961.09, 2917.68, 2845.34, 1664.63, 1459.16 cm⁻¹. **HRMS (ESI)**: (M: C₂₀H₁₈O₂N₃l) m/z calcd. 460.0516, found 460.0522 (M+H)⁺. **IR** (Film, cm⁻¹): ν = 3408.41 (s), 1664.77 (s), 1459.39 (s) cm⁻¹.

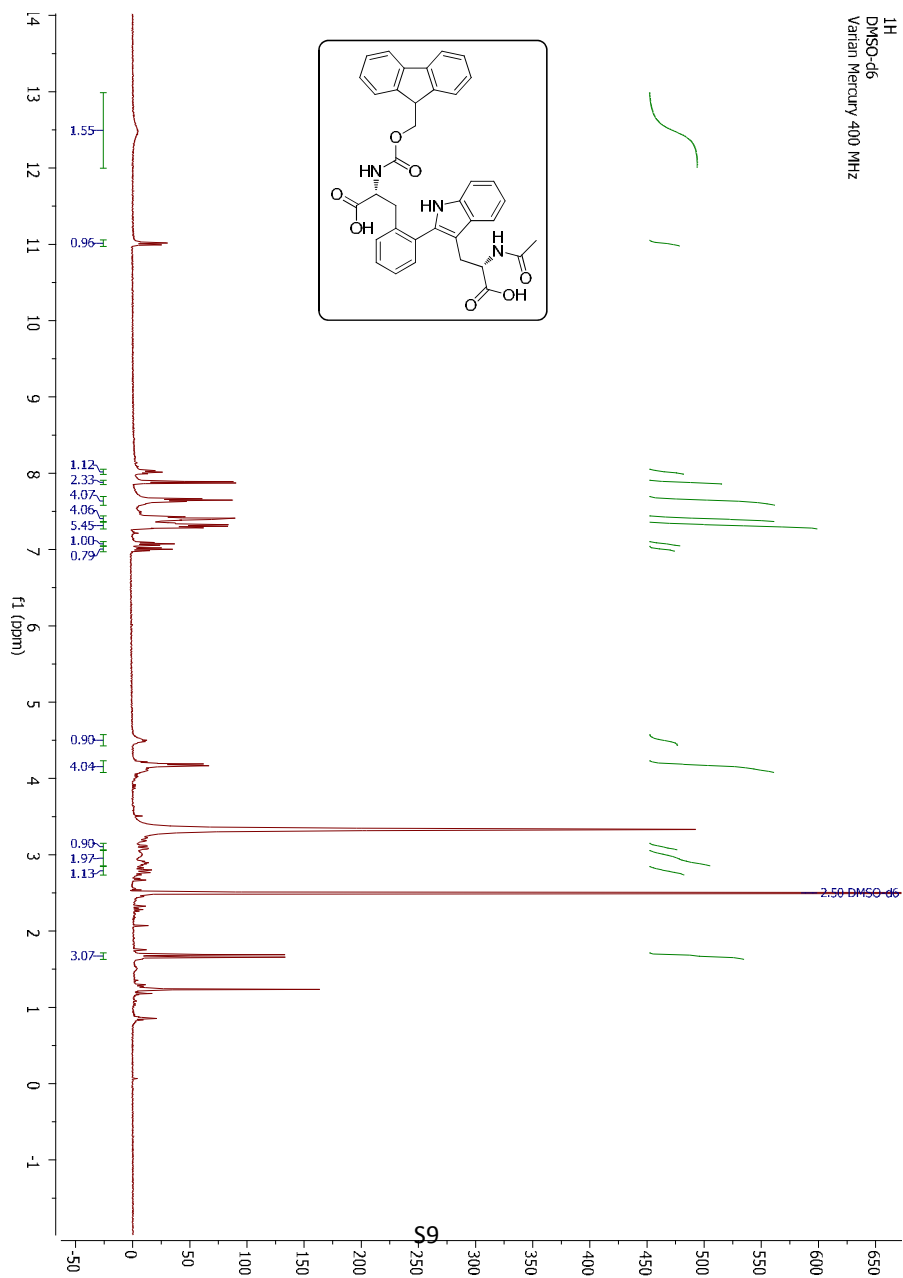
(Cyclo-*m,m*)-bis-[Phe-Trp]-cyclo(Phe-Trp) (7b). Compound **6b** (91 mg, 0.198 mmol), AgBF₄ (77 mg, 0.396 mmol, 2.0 eq.), trifluoroacetic acid (15.2 μ L, 0.198 mmol, 1.0 eq.) and Pd(OAc)₂ (2.2 mg, 0.010 mmol, 0.05 eq.) were dissolved in 2 mL of DMF and placed in a microwave reactor vessel. The mixture was heated under microwave irradiation (250W) at 90 °C for 20 min. The resulting suspension was filtered through Celite and the filtrate was evaporated under vacuum (28% yield estimated by HPLC-MS conversion). An analytically pure sample was obtained by semi-preparative RP-HPLC. **¹H NMR** (500 MHz, [D₆]DMSO): δ 11.24 (s, 1H), 8.51 (s, 1H), 8.26 (s, 1H), 7.71 (d, J = 7.8 Hz, 1H), 7.33 (m, 2H), 7.20 (d, J = 7.5 Hz, 1H), 7.08 (t, J = 7.6 Hz, 1H), 7.04 – 6.97 (m, 2H), 6.86 (s, 1H), 3.97 (s, 1H), 3.38(1H), 3.24 (m, 1H), 2.99 (m, 1H), 2.20 (m, 1H), 0.24 (m, 1H) ppm. **HPLC-MS**: t_R 2.38 min (gradient 5-100% ACN). **HRMS (ESI)**: (M: C₄₀H₃₄O₄N₆) m/z calcd 663.2707, found 663.2714 (M+H)⁺.

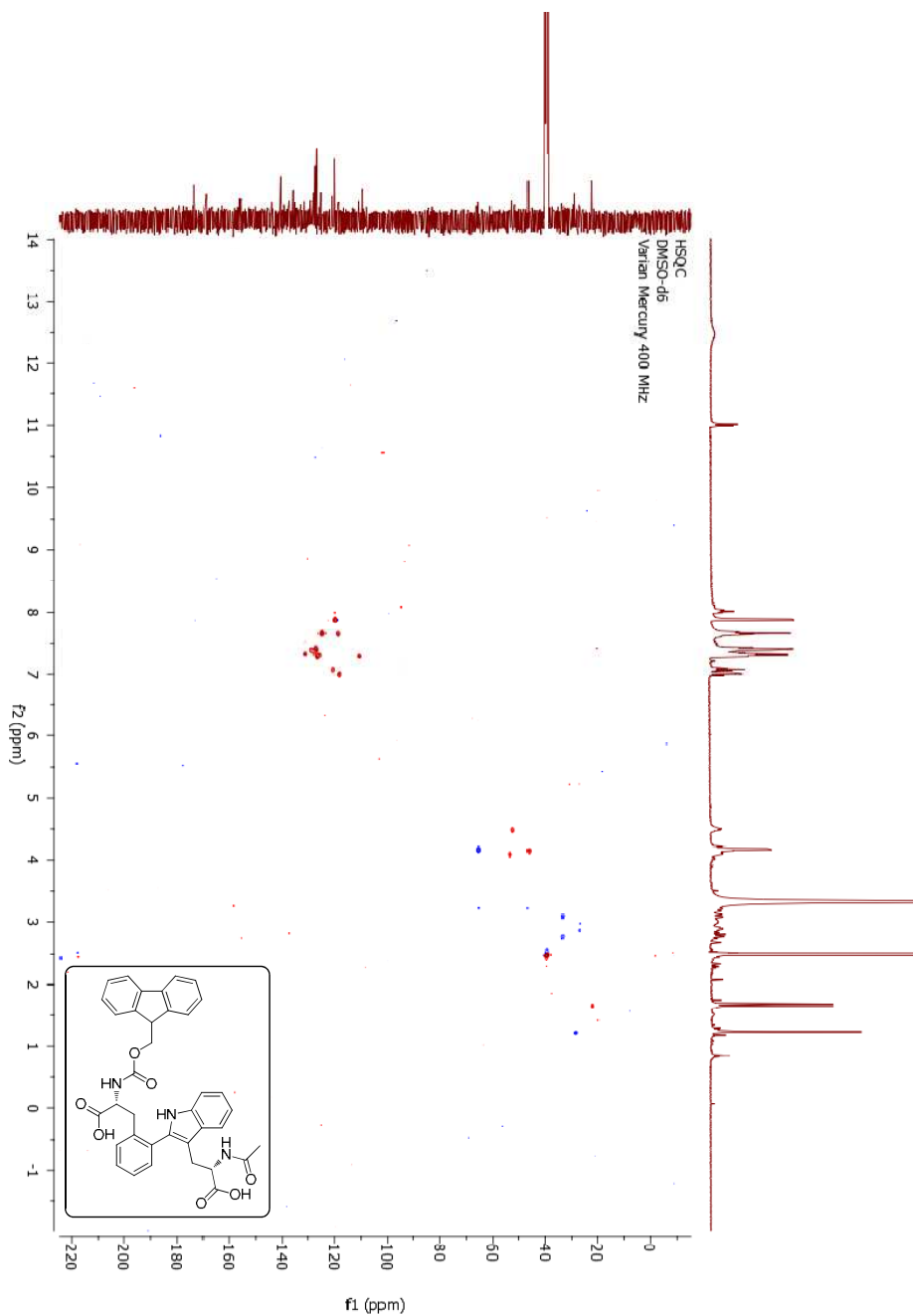


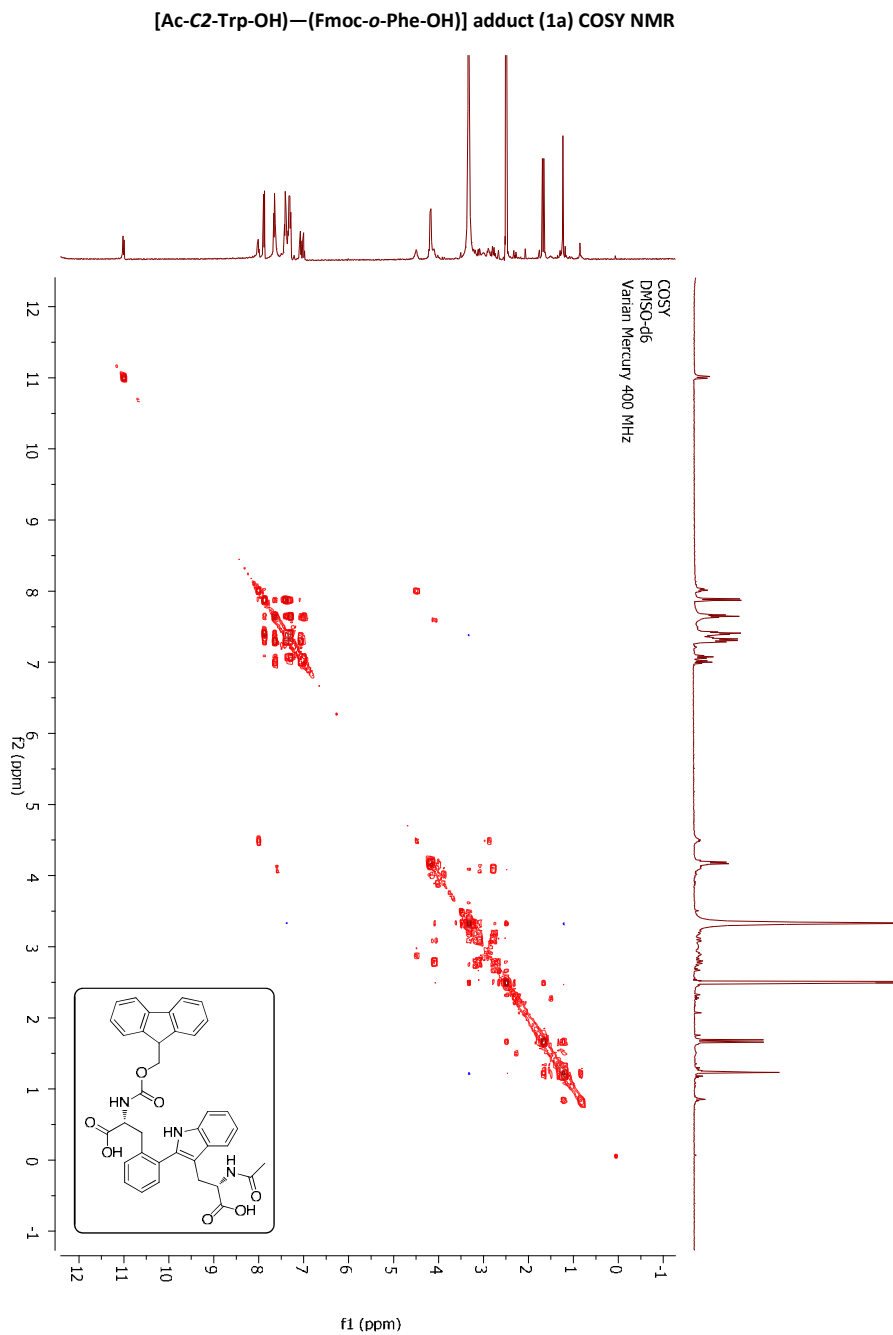
(Cyclo-*p,p*)-bis-[Phe-Trp]-cyclo(Phe-Trp) (7c). Compound **6c** (80 mg, 0.175 mmol), AgBF₄ (68 mg, 0.350 mmol, 2.0 eq.), trifluoroacetic acid (13 μ L, 0.175 mmol, 1.0 eq.) and Pd(OAc)₂ (2 mg, 0.009 mmol, 0.2 eq.) were dissolved in 2 mL of DMF and placed in a microwave reactor vessel. The mixture was heated under microwave irradiation (250W) at 90 °C for 1 h. Then, Pd(OAc)₂ (2.0 mg, 0.009 mmol, 0.2 eq.) and AgBF₄ (68 mg, 2.0 eq.) were added again, and a second irradiation cycle of 20 min was performed. The same procedure was repeated and both fractions were mixed. The resulting suspension was filtered through Celite and the filtrate was evaporated under vacuum (24% yield estimated by HPLC-MS conversion). An analytically pure sample was obtained by flash chromatography on Celite using H₂O (0.1% FA)/ACN (0.1% FA) (4.1 mg, 2% isolated yield). **¹H NMR** (800 MHz, [D₆]DMSO): δ 10.99 (s, 1H), 8.54 (d, J = 2.5 Hz, 1H), 8.32 (s, 1H), 7.58 (d, J = 8.1 Hz, 2H), 7.46 (d, J = 8.0 Hz, 1H), 7.38 (d, J = 8.0 Hz, 2H), 7.27 (d, J = 8.0 Hz, 1H), 7.04 (m, 1H), 6.92 (m, 1H), 4.38 (dt, J = 5.3, 2.7 Hz, 1H), 3.78 (dt, J = 9.0, 2.9 Hz, 1H), 3.36 (m, 1H), 3.00 (dd, J = 13.3, 5.4 Hz, 1H), 2.70 (m, 1H), 1.33 (m, 1H) ppm. **HPLC-MS**: t_R 2.18 min (gradient 5-100% ACN). **HRMS (ESI)**: (M: C₄₀H₃₄O₄N₆) m/z calcd 663.2726, found 663.2714 (M+H)⁺.

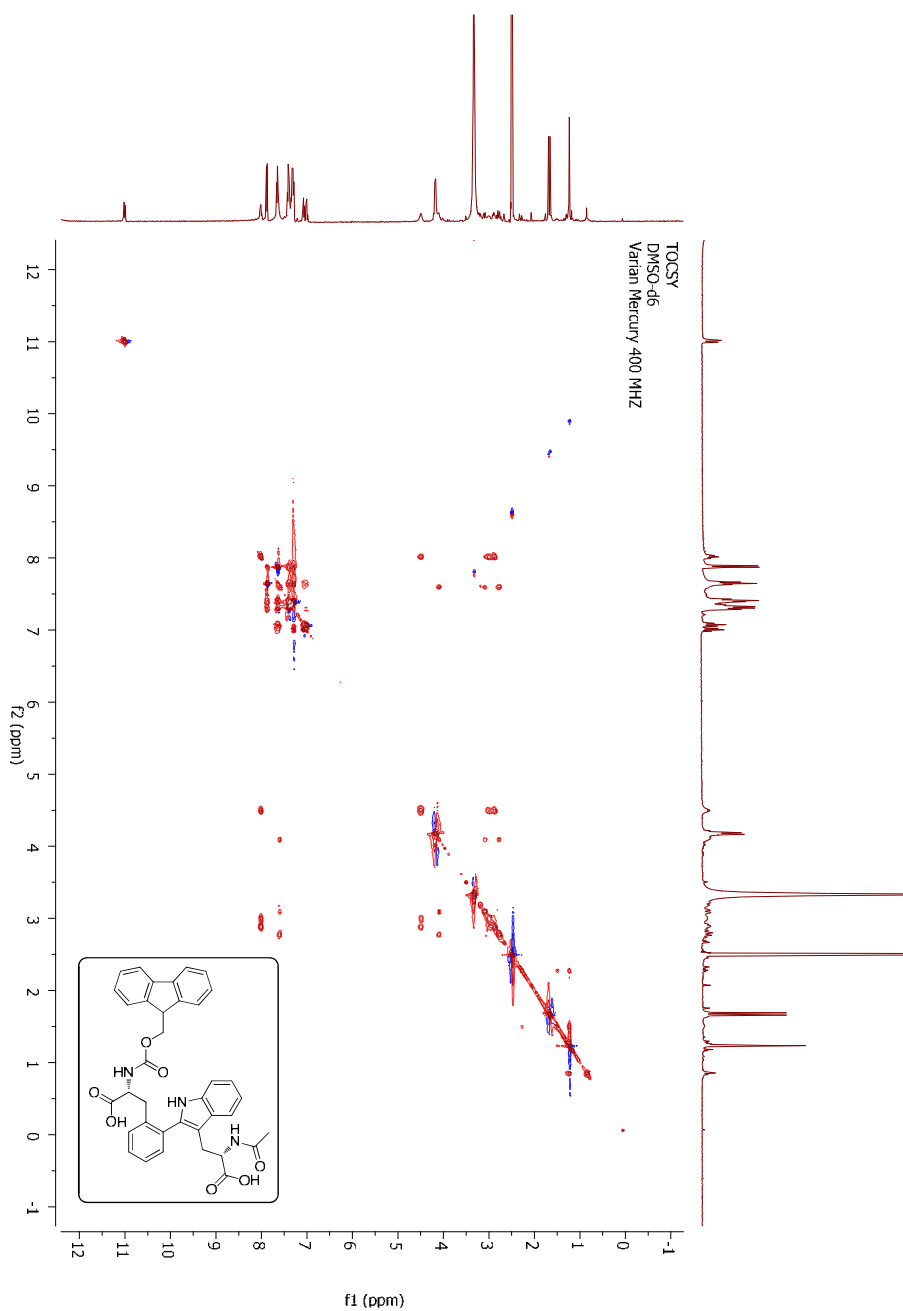


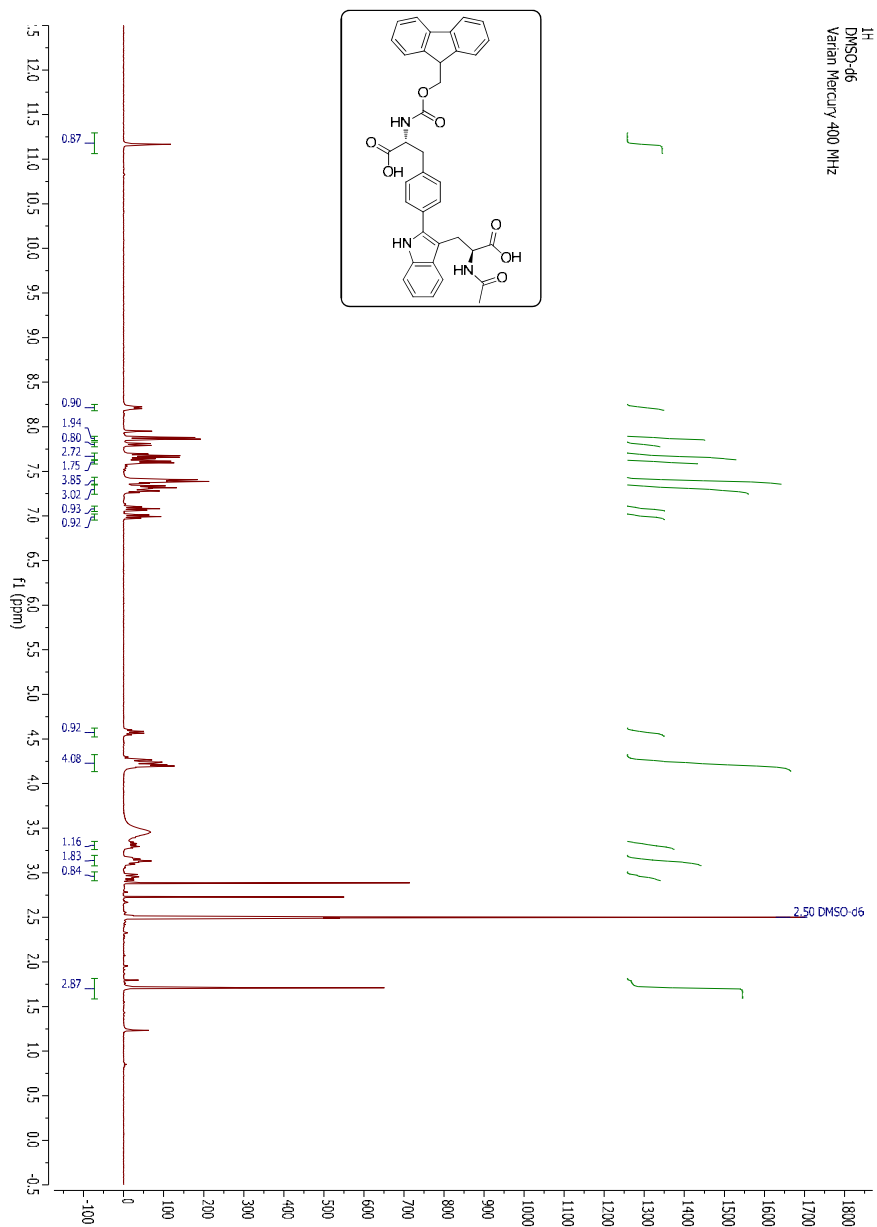
NMR spectra of compounds 1, 3, 5, 6 and 7

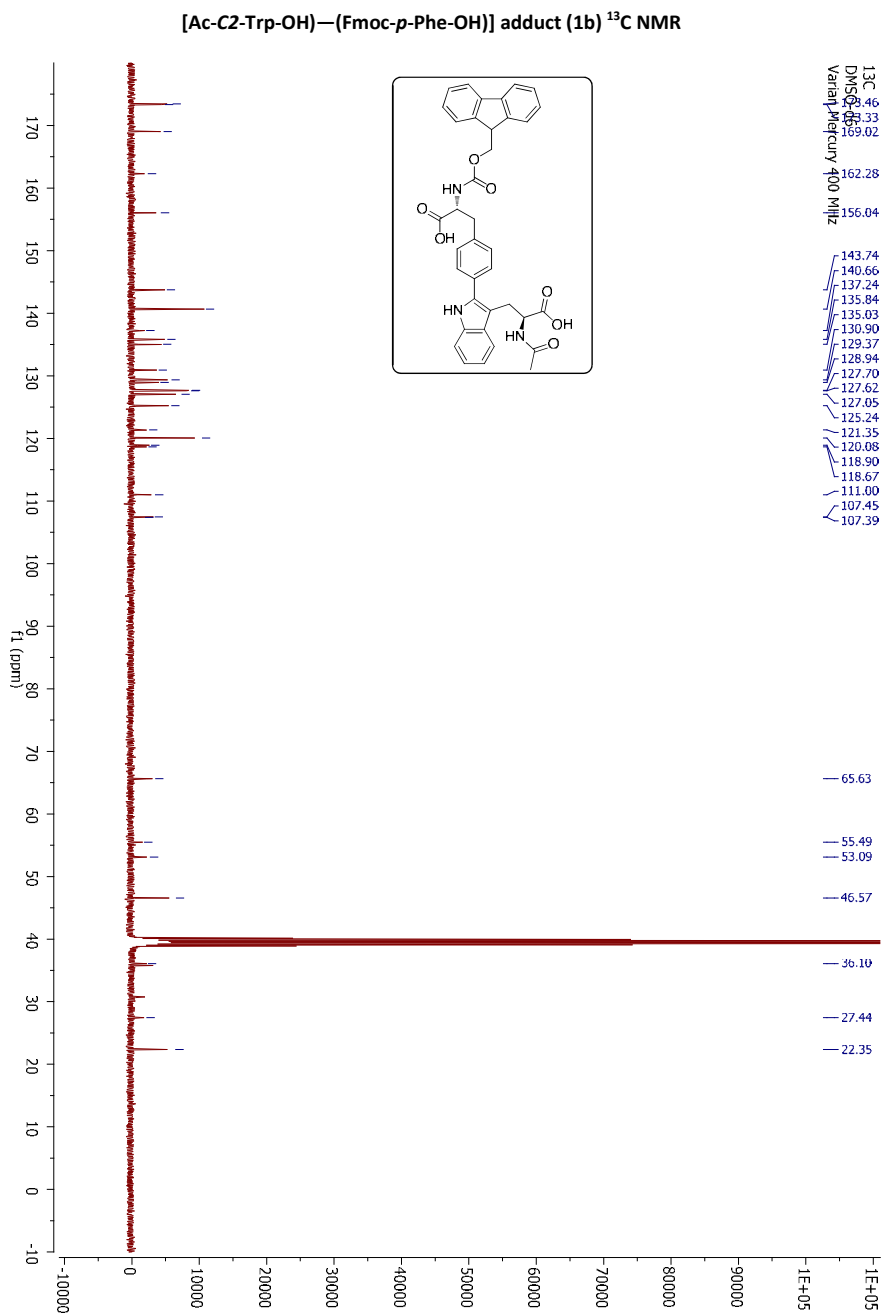
[Ac-C2-Trp-OH]—(Fmoc-o-Phe-OH) adduct (1a) ^1H NMR

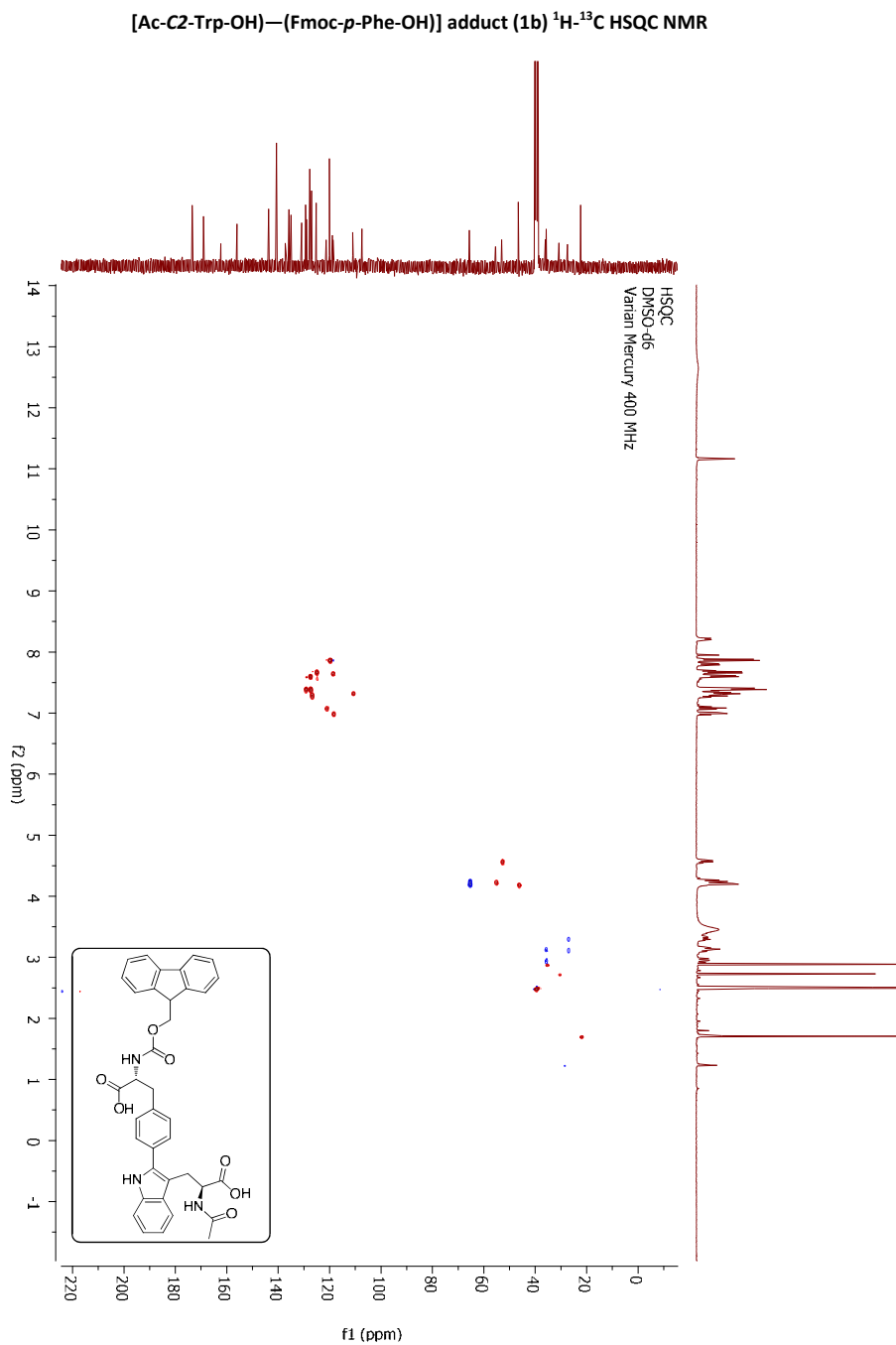
[Ac-C2-Trp-OH)—(Fmoc-*o*-Phe-OH)] adduct (1a) ^1H - ^{13}C HSQC NMR

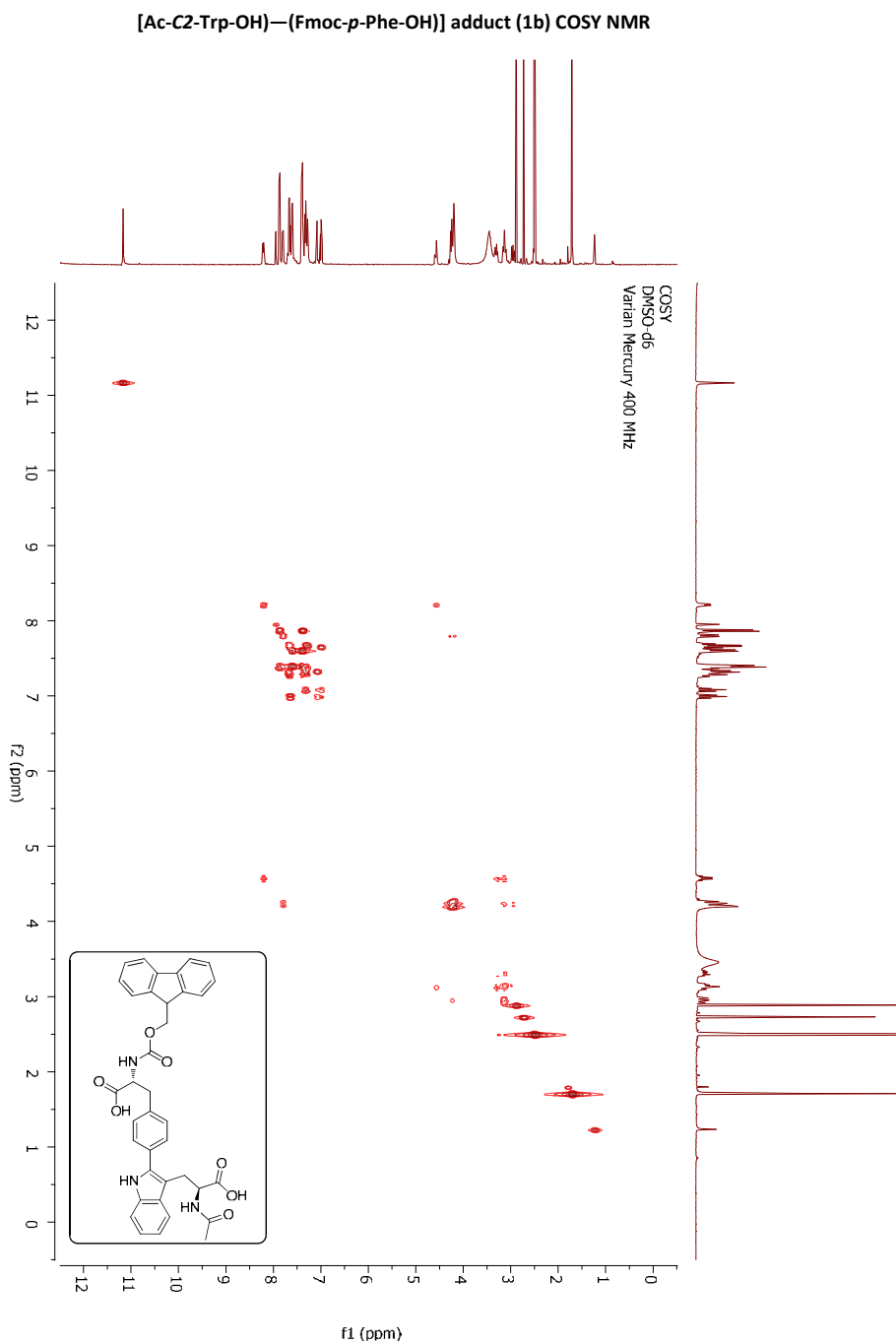


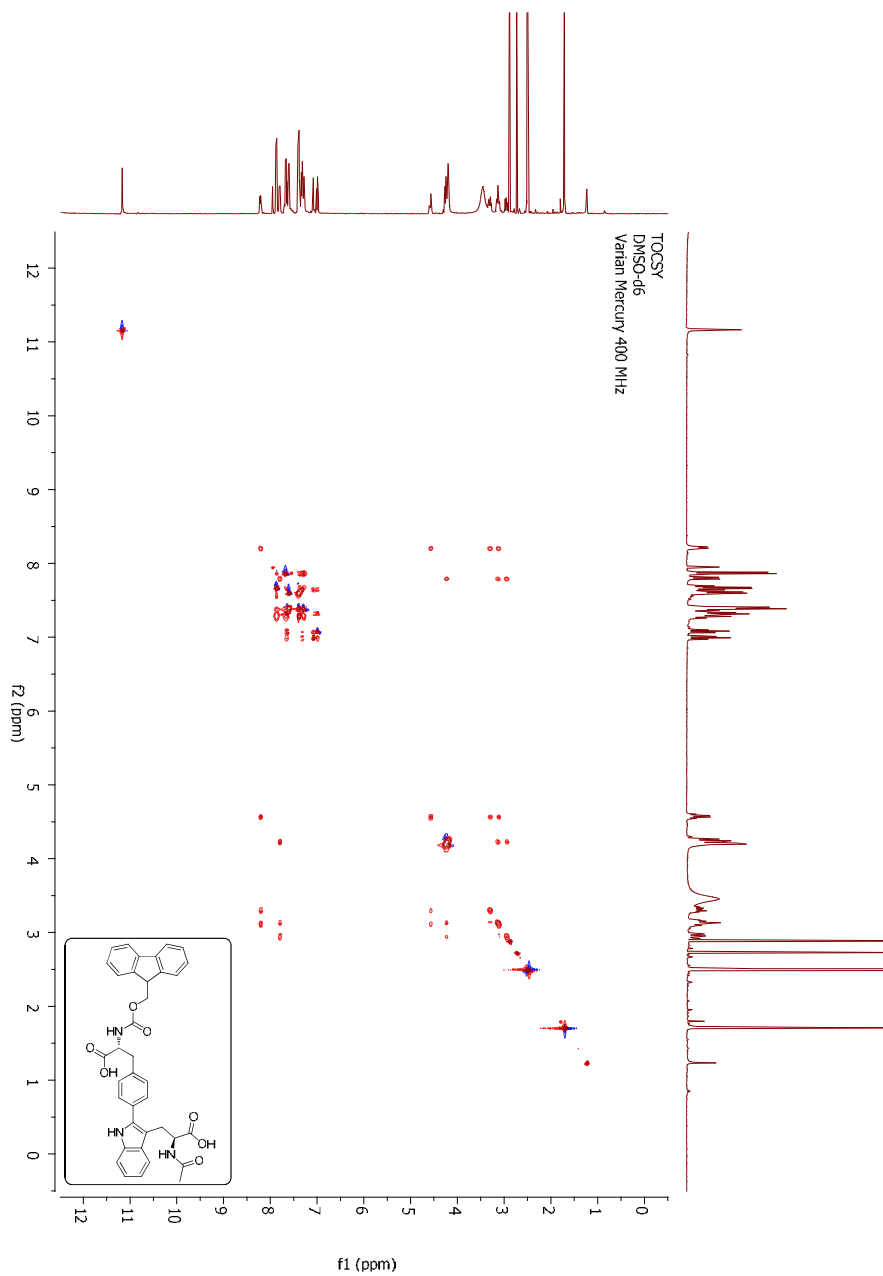
[Ac-C2-Trp-OH)—(Fmoc-*o*-Phe-OH)] adduct (1a) TOCSY NMR

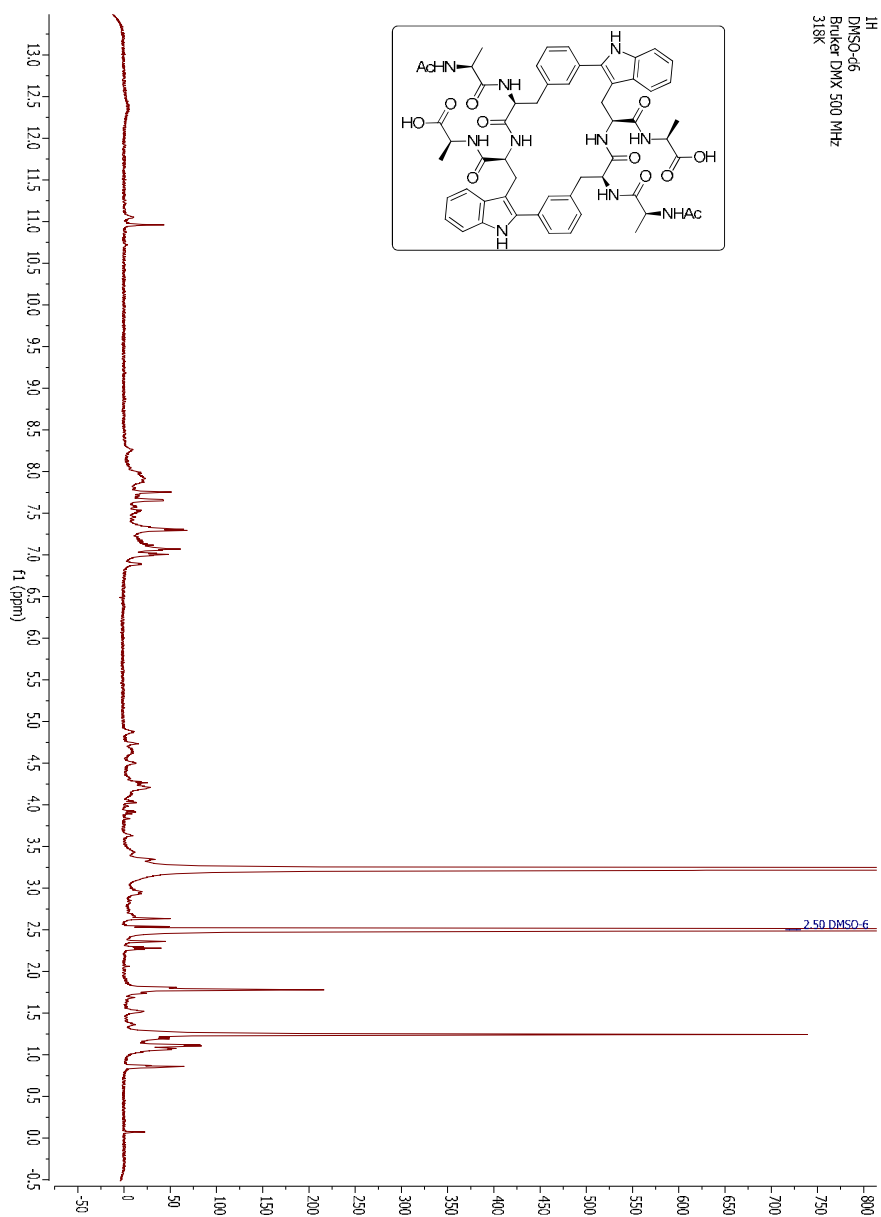
[Ac-C2-Trp-OH]—(Fmoc-p-Phe-OH)] adduct (1b) ^1H NMR

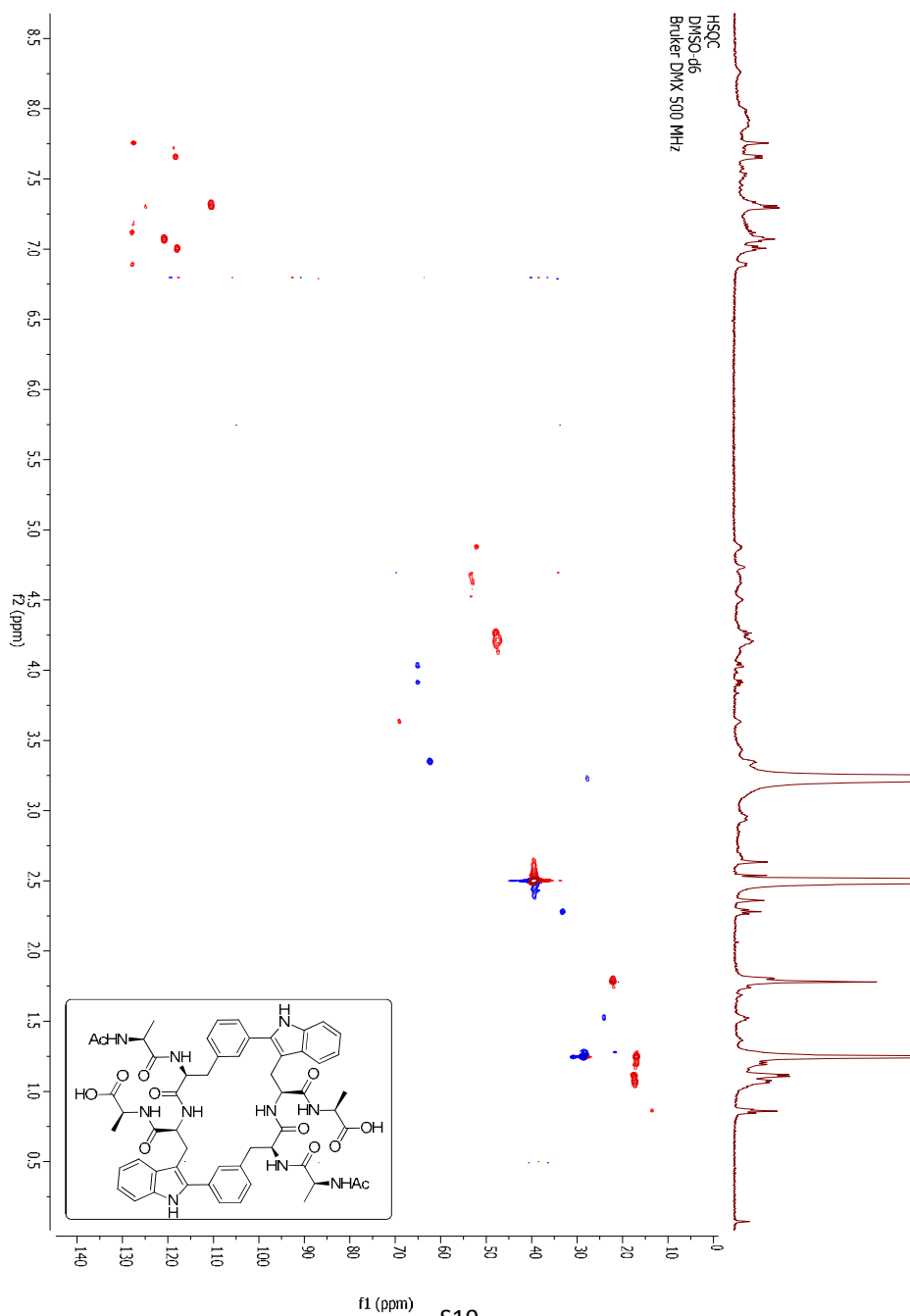


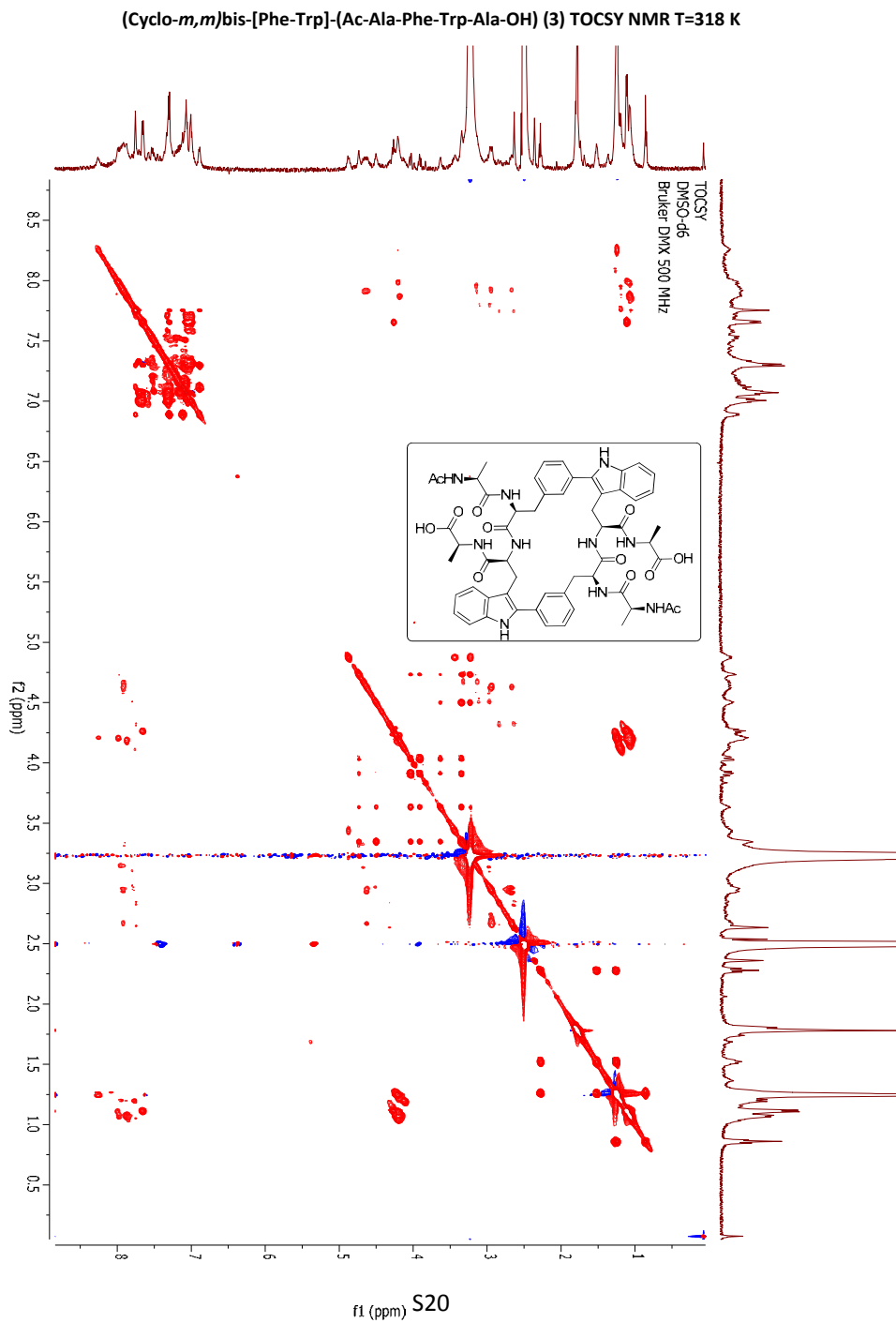


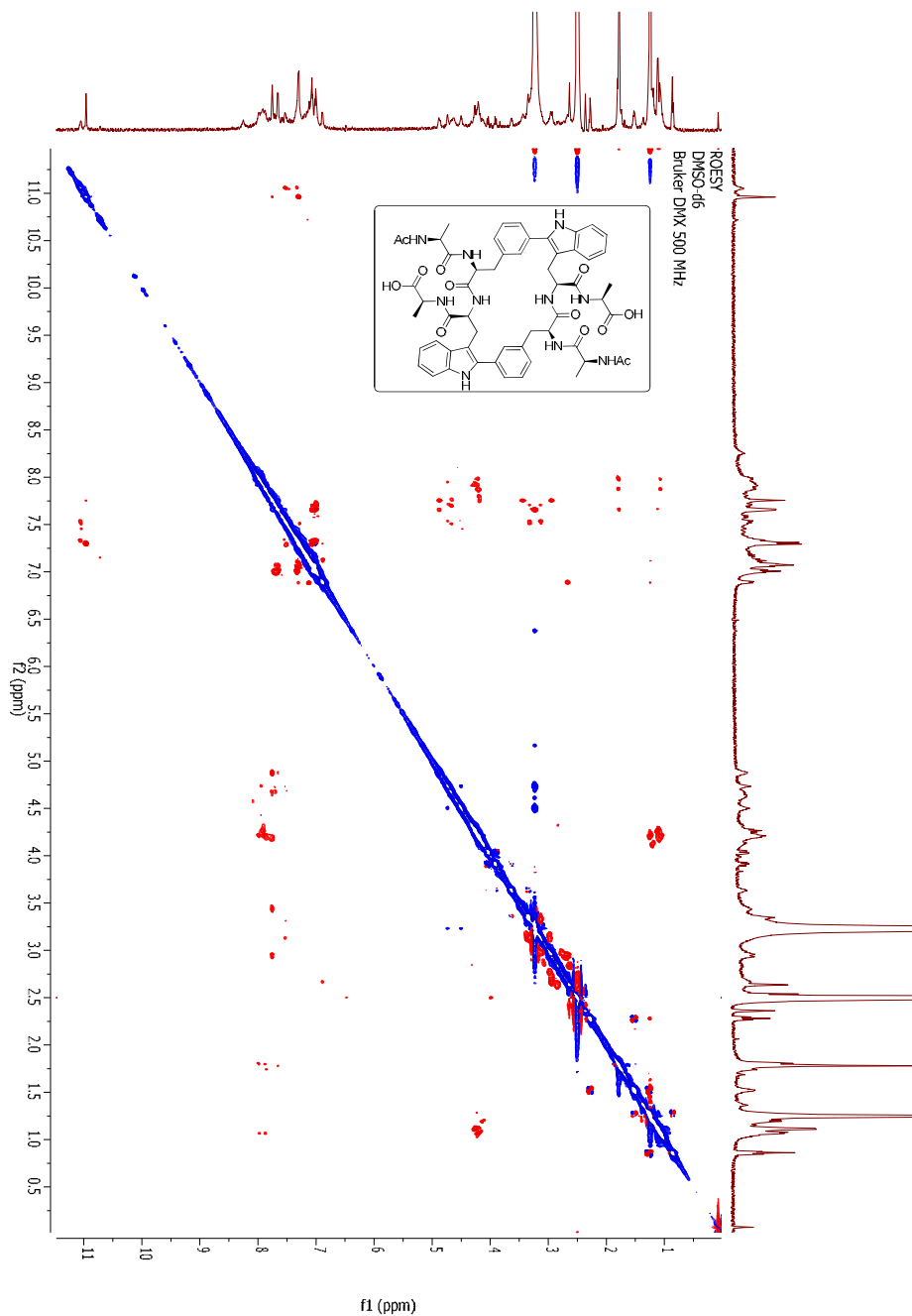


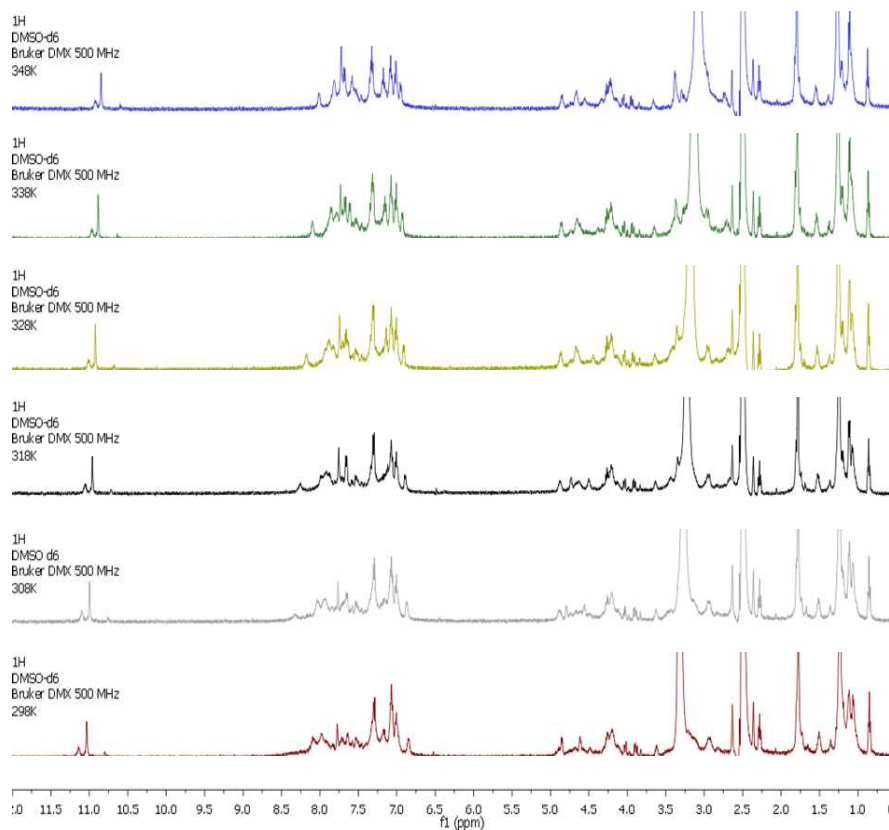
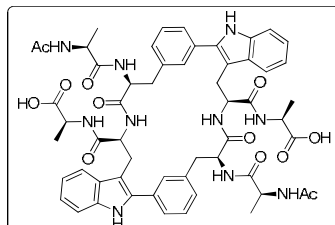
[Ac-C2-Trp-OH)—(Fmoc-*p*-Phe-OH)] adduct (1b) TOCSY NMR

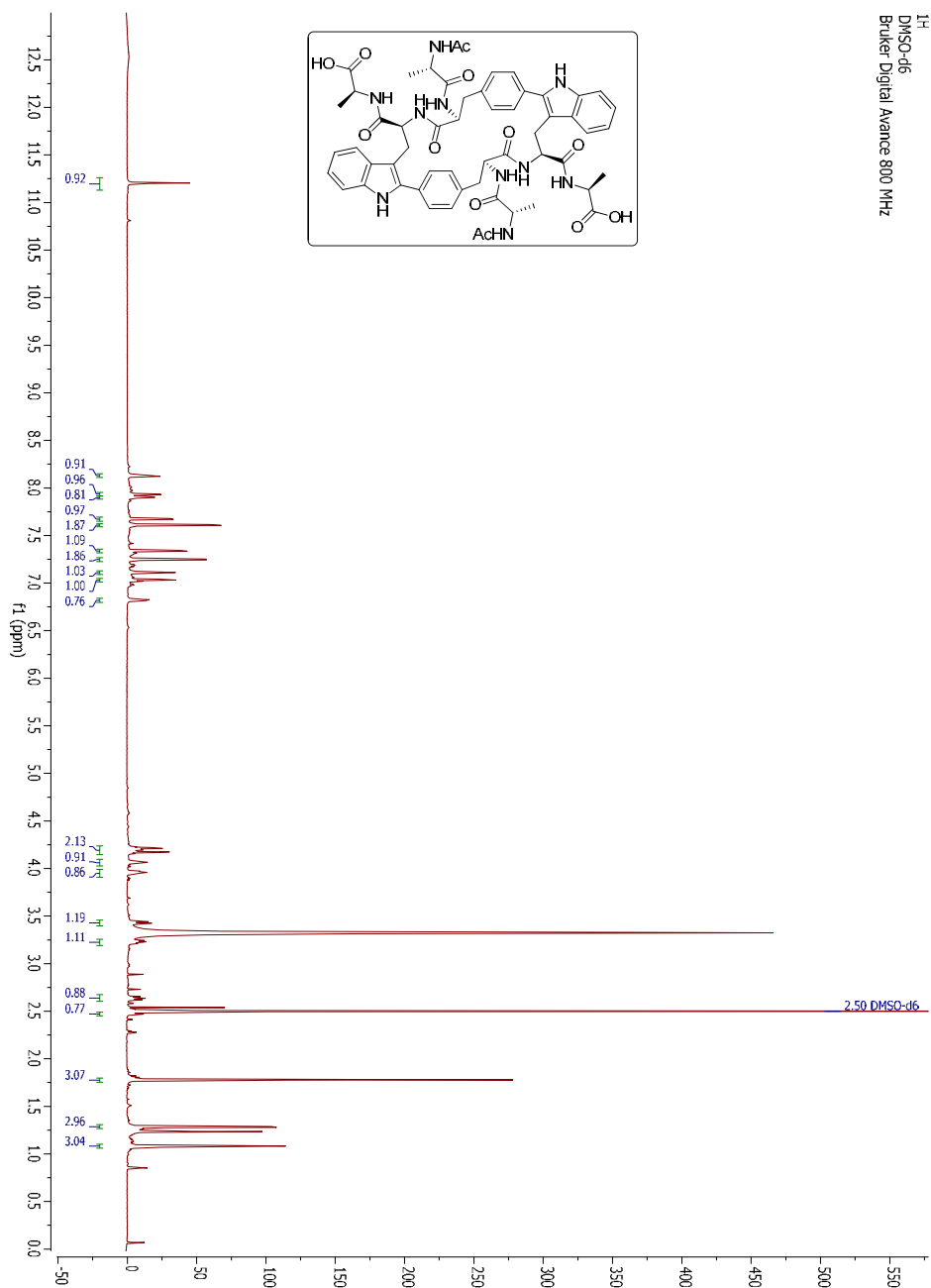
(Cyclo-*m,m*)bis-[Phe-Trp]-(Ac-Ala-Phe-Trp-Ala-OH) (3) ^1H NMR T=318 K

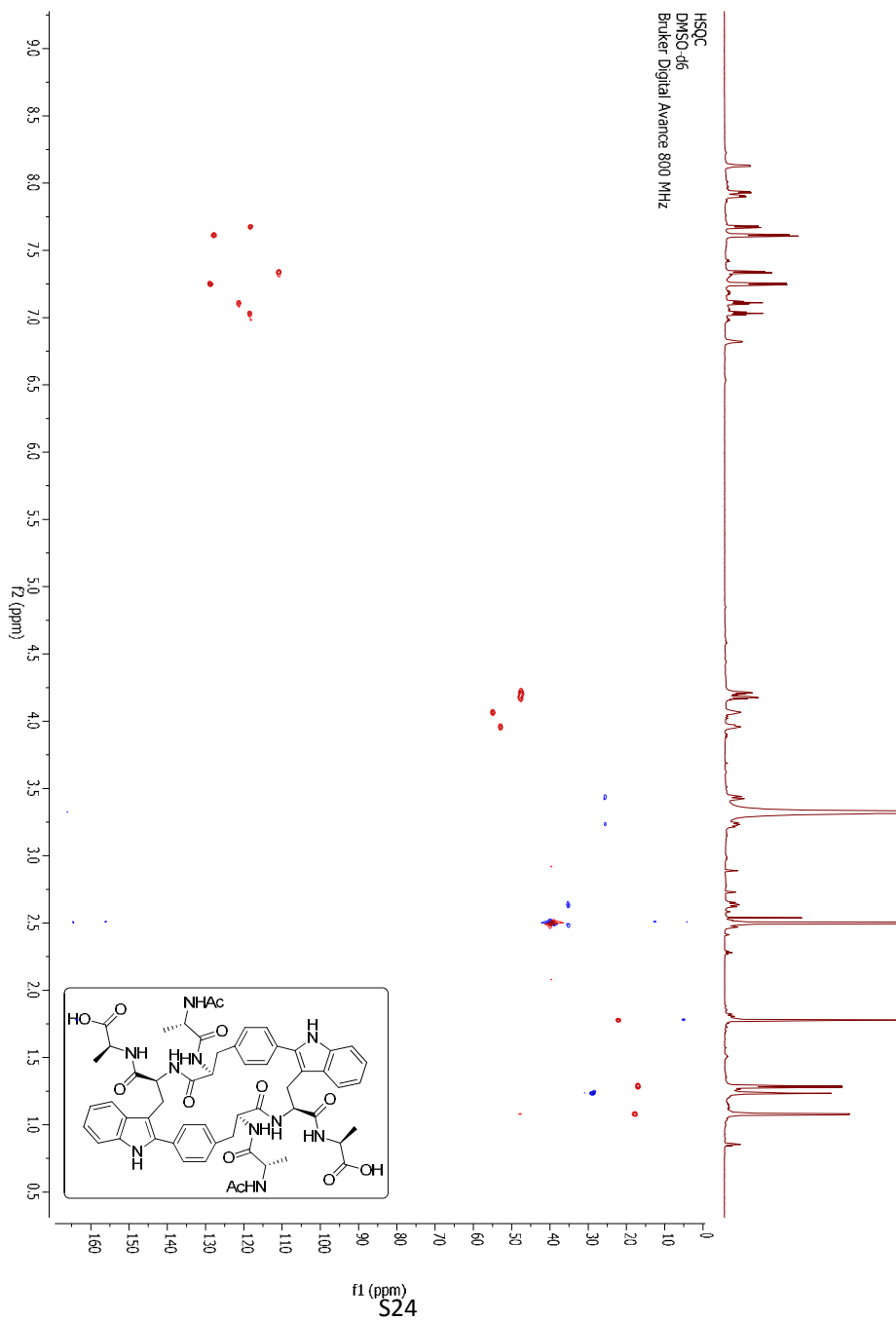
(Cyclo-*m,m*)bis-[Phe-Trp]-(Ac-Ala-Phe-Trp-Ala-OH) (3) ^1H - ^{13}C HSQC NMR T=318 K

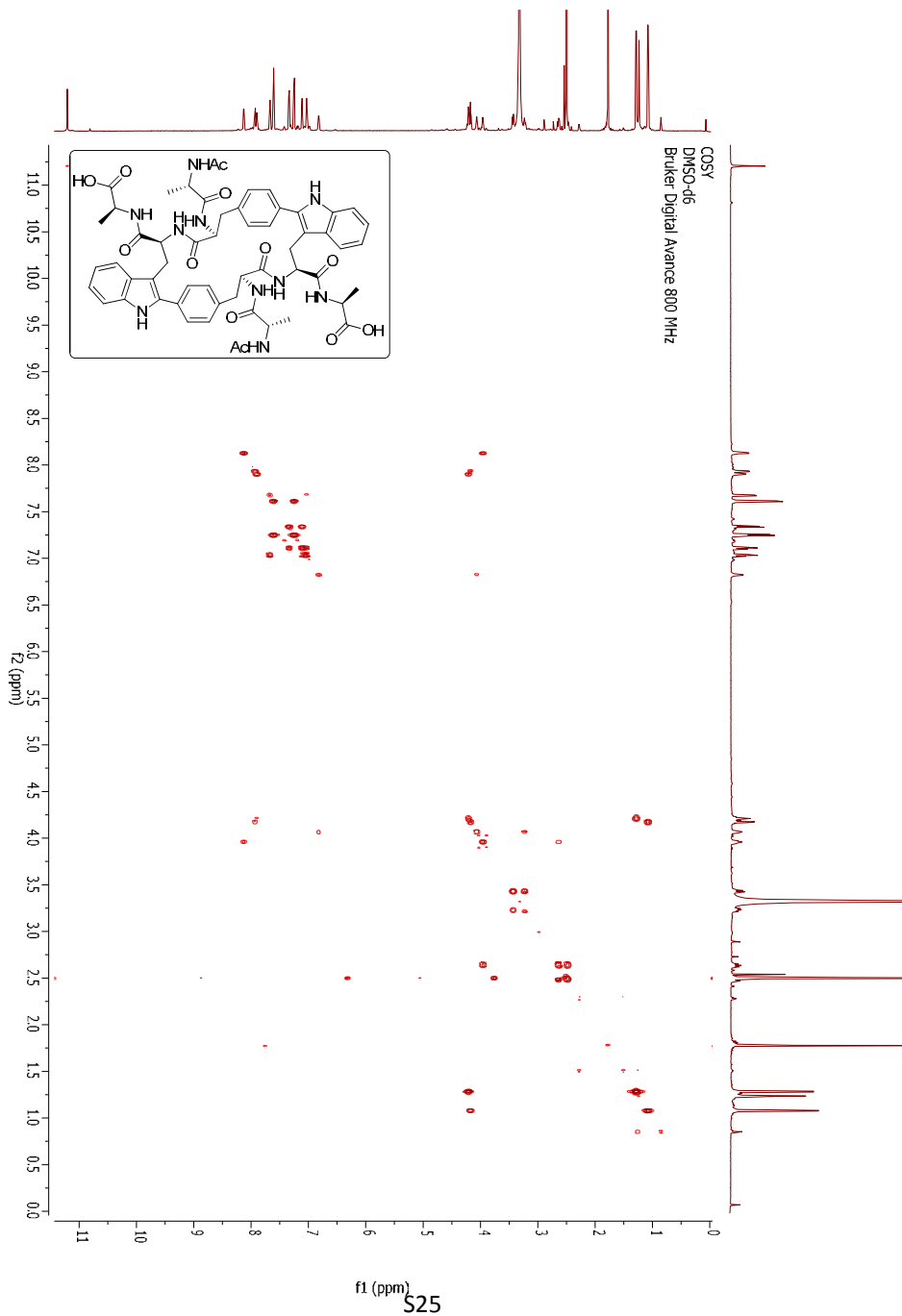


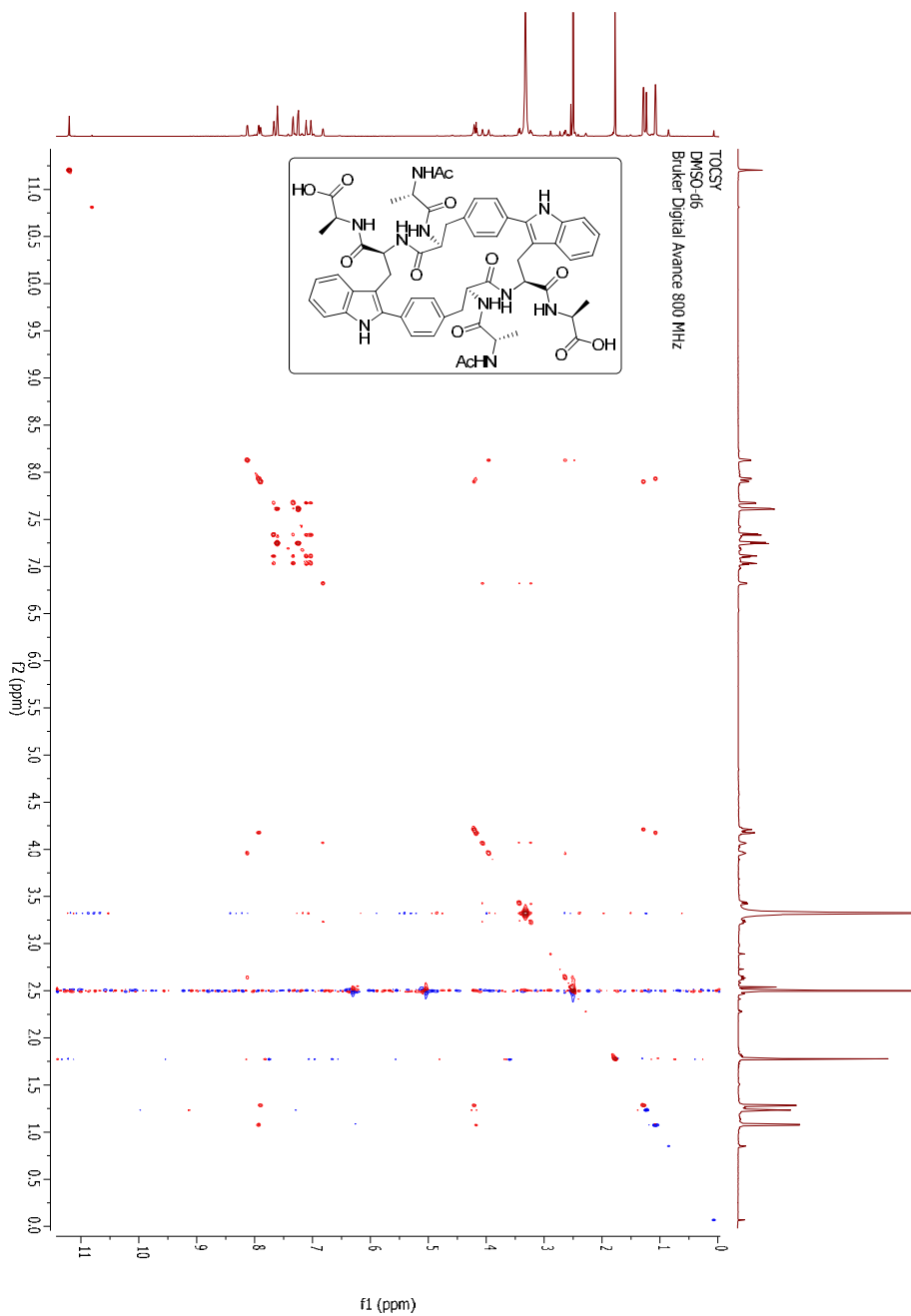
(Cyclo-*m,m*)bis-[Phe-Trp]-(Ac-Ala-Phe-Trp-Ala-OH) (3) ROESY NMR T=318 K

(Cyclo-*m,m*)bis-[Phe-Trp]-(Ac-Ala-Phe-Trp-Ala-OH) (3) ^1H NMR T=298-348 K

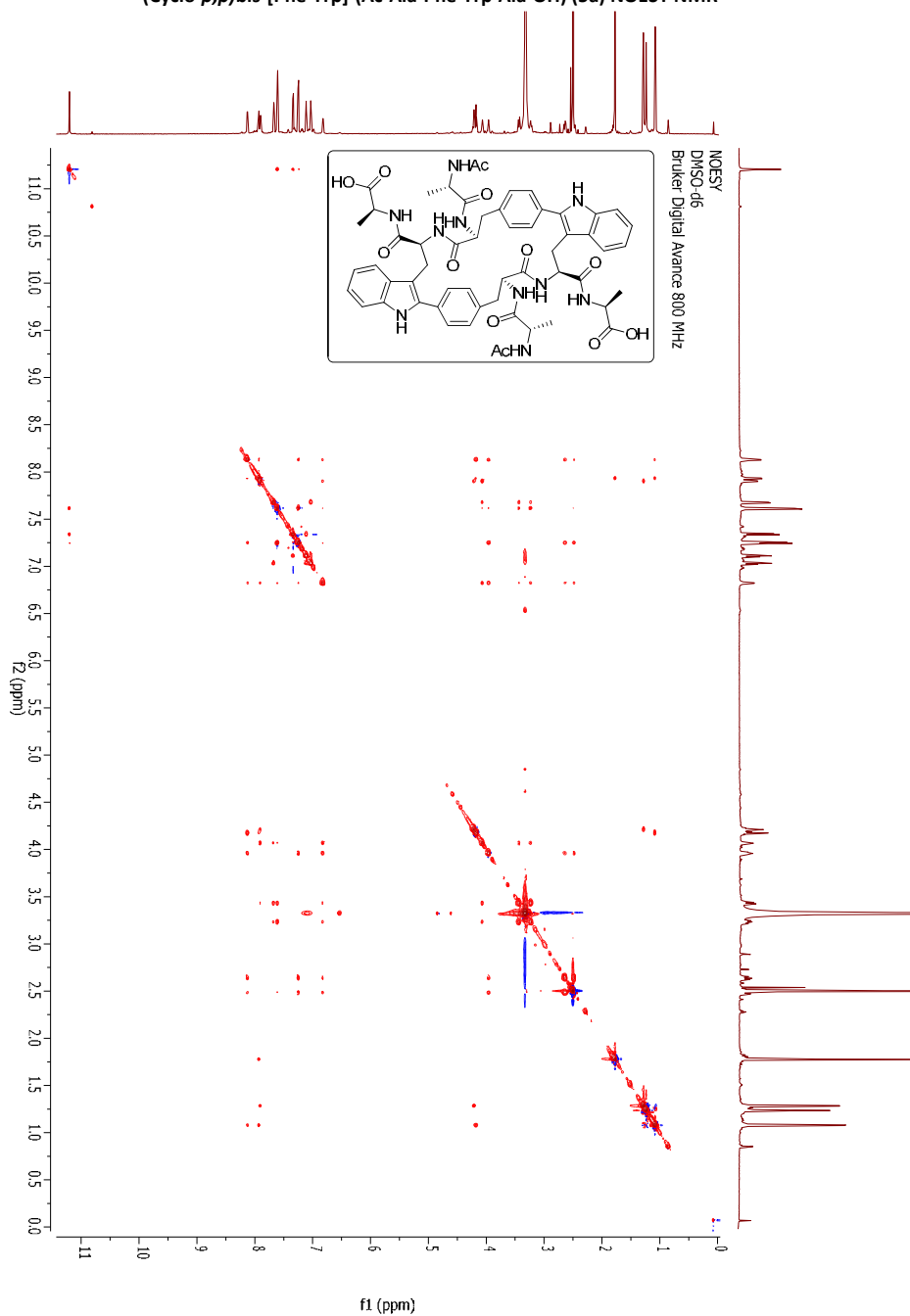
(Cyclo-*p,p*)bis-[Phe-Trp]-(Ac-Ala-Phe-Trp-Ala-OH) (5a) ^1H NMR

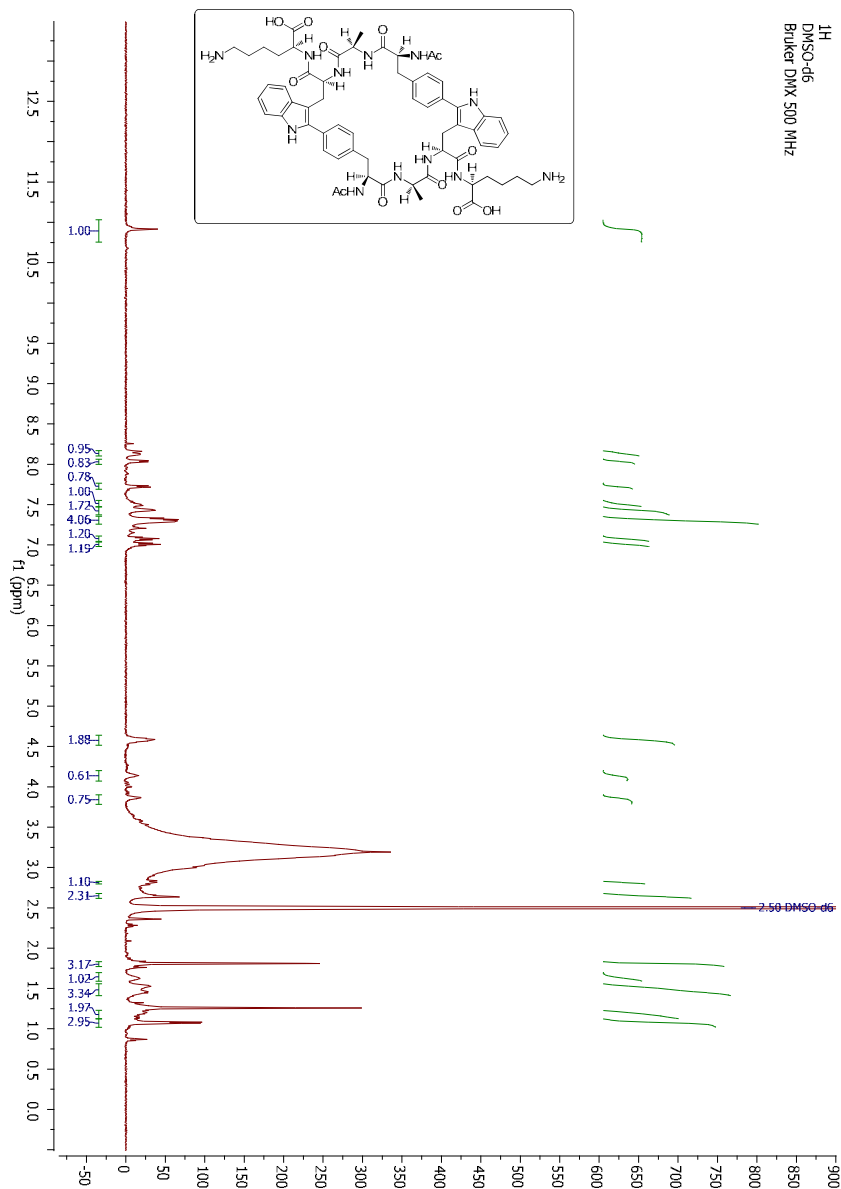
(Cyclo-*p,p*)bis-[Phe-Trp]-(Ac-Ala-Phe-Trp-Ala-OH) (5a) ^1H - ^{13}C HSQC NMR

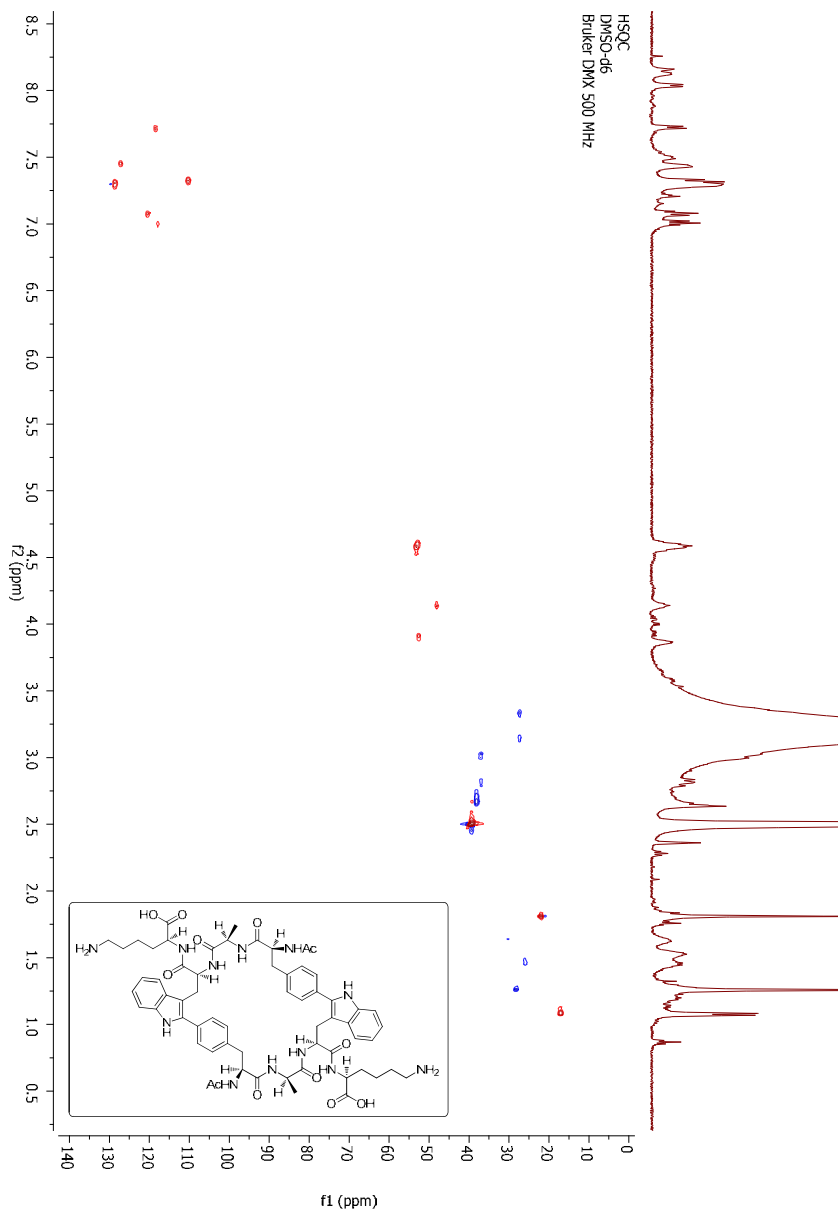
(Cyclo-*p,p*)bis-[Phe-Trp]-(Ac-Ala-Phe-Trp-Ala-OH) (5a) COSY NMR

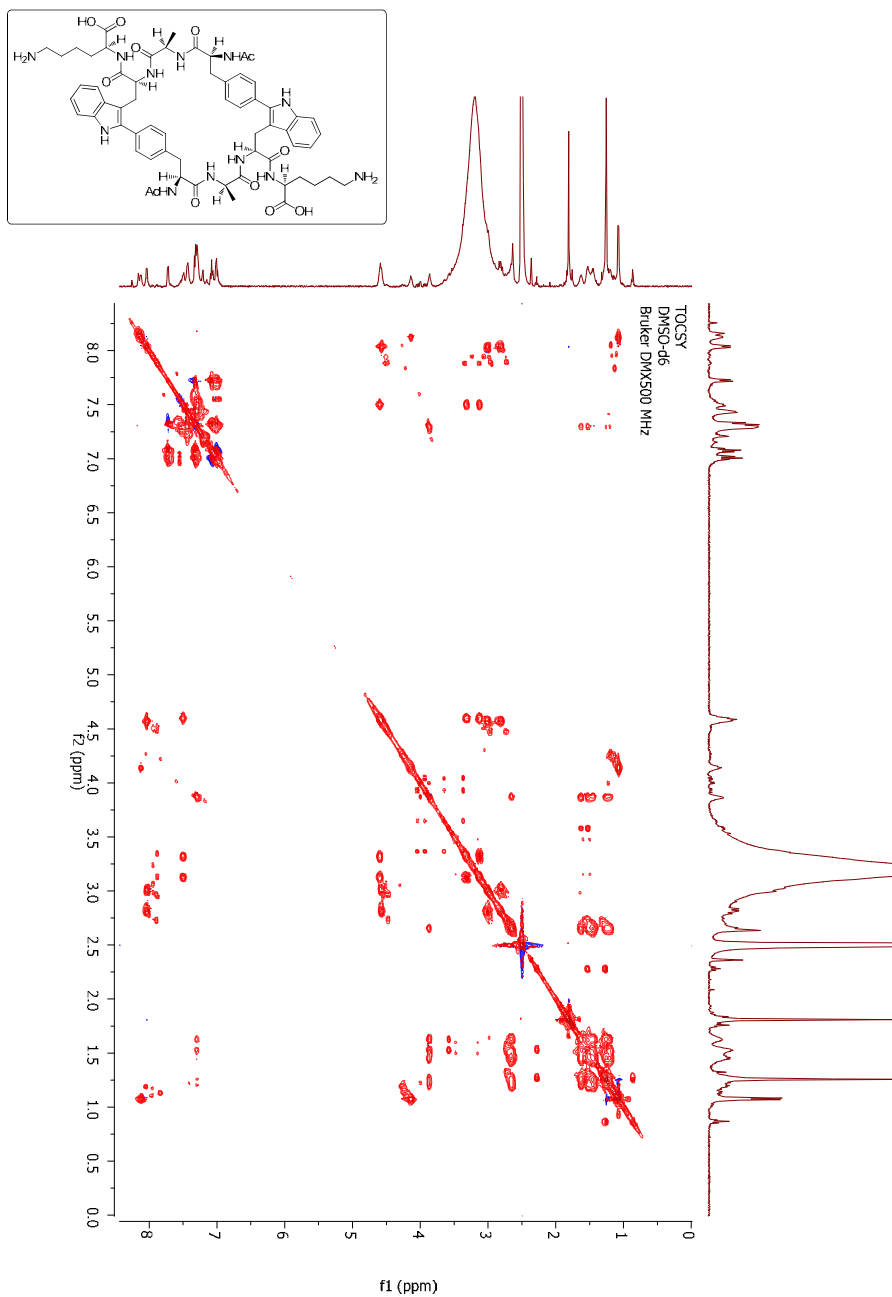
(Cyclo-*p,p*)bis-[Phe-Trp]-(Ac-Ala-Phe-Trp-Ala-OH) (5a) TOCSY NMR

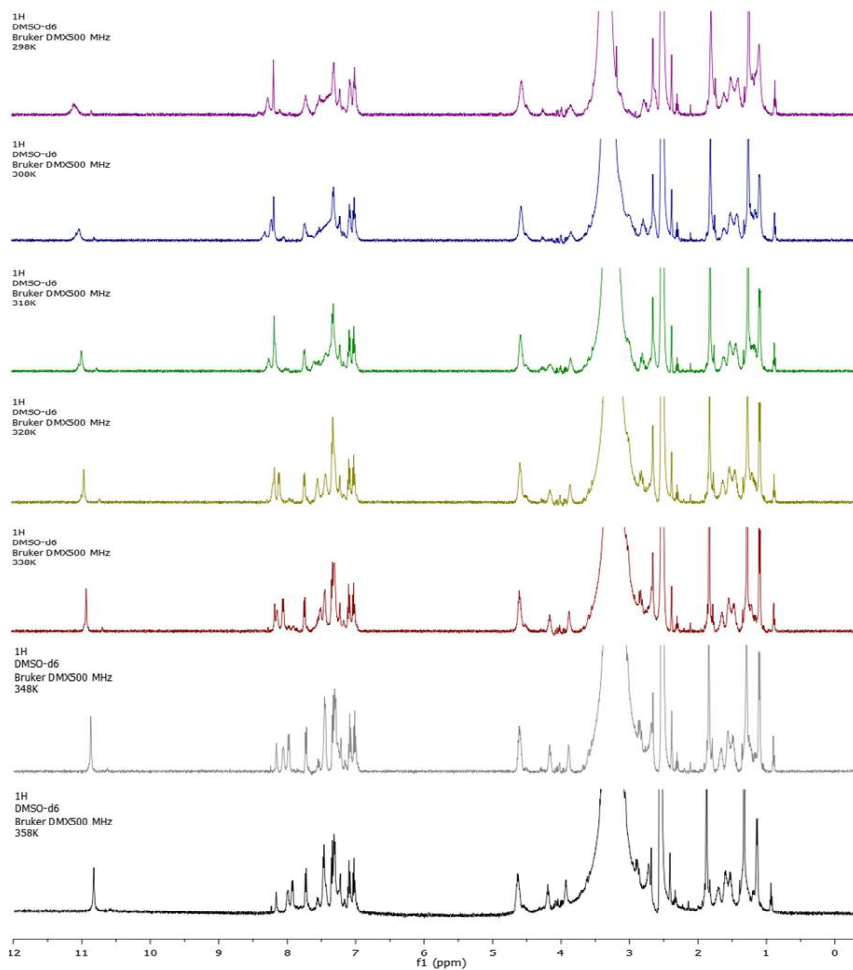
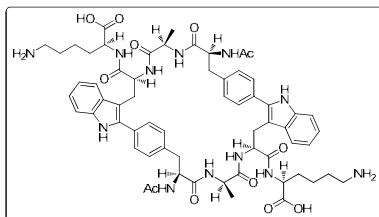
(Cyclo-*p,p*)bis-[Phe-Trp]-(Ac-Ala-Phe-Trp-Ala-OH) (5a) NOESY NMR

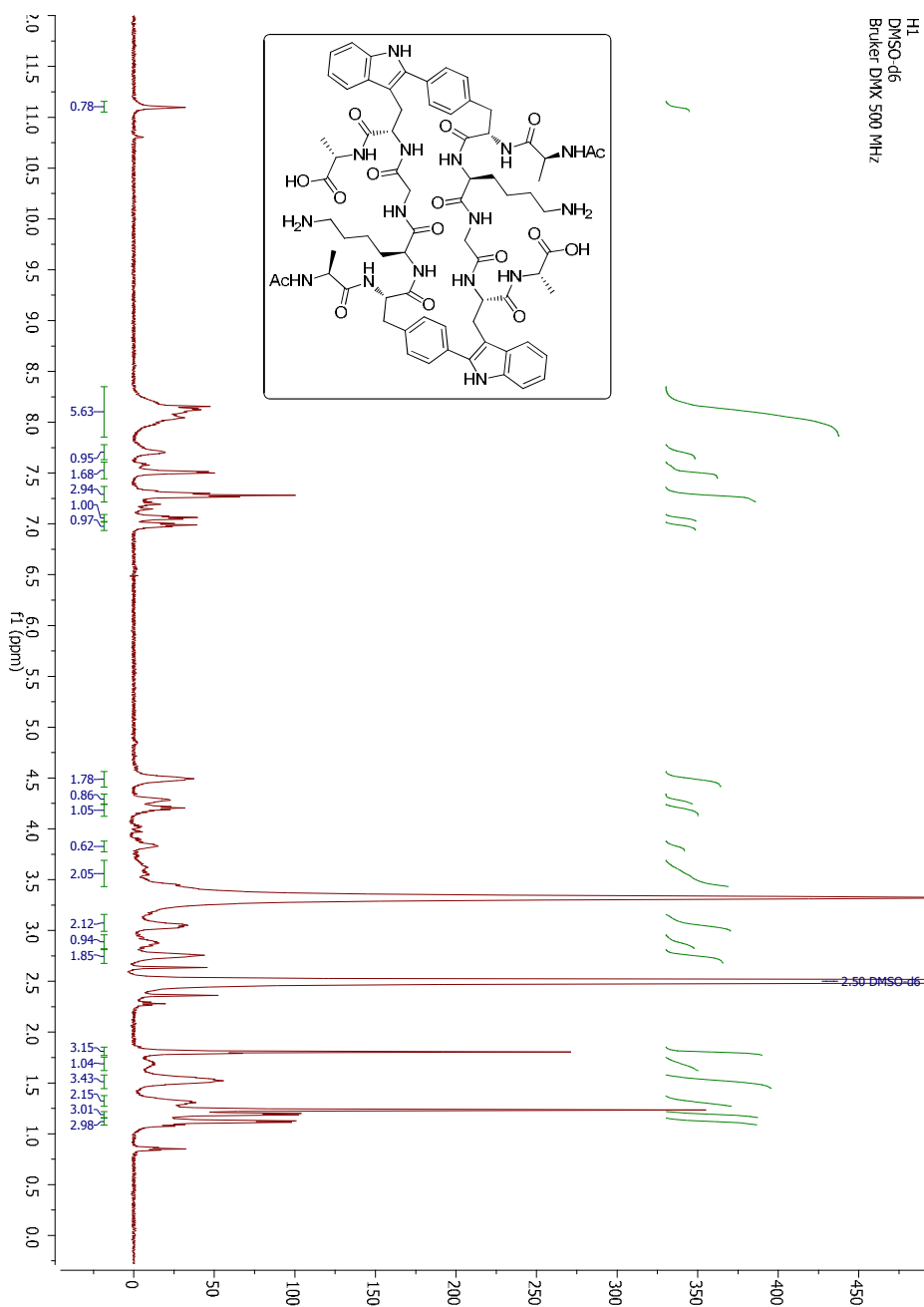


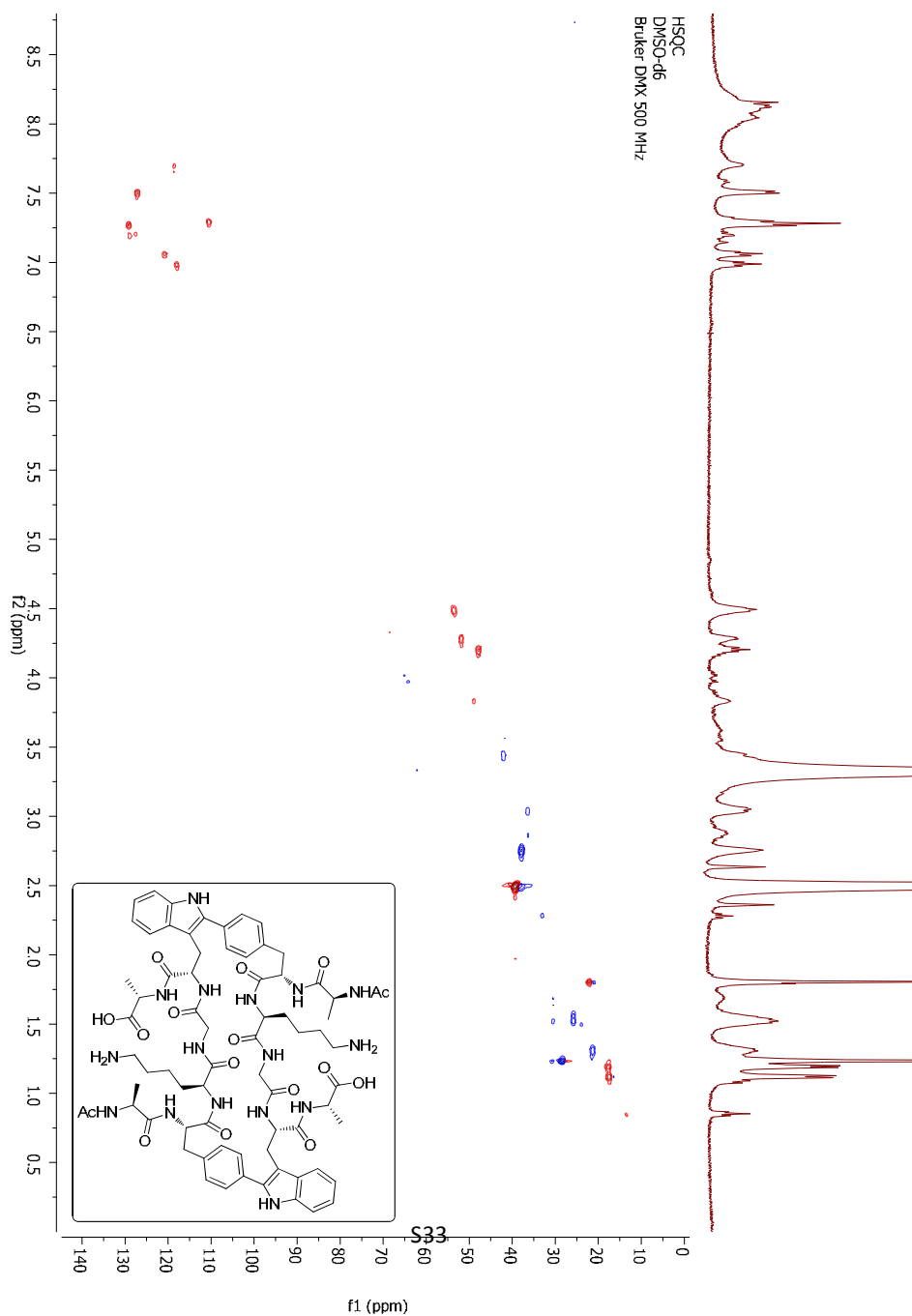
(Cyclo-*p,p*)bis-[Phe-Trp]-(Ac-Phe-Ala-Trp-Lys-OH) (5b) ^1H NMR T=338 K

(Cyclo-*p,p*)bis-[Phe-Trp]-(Ac-Phe-Ala-Trp-Lys-OH) (5b) ^1H - ^{13}C HSQC NMR T=338 K

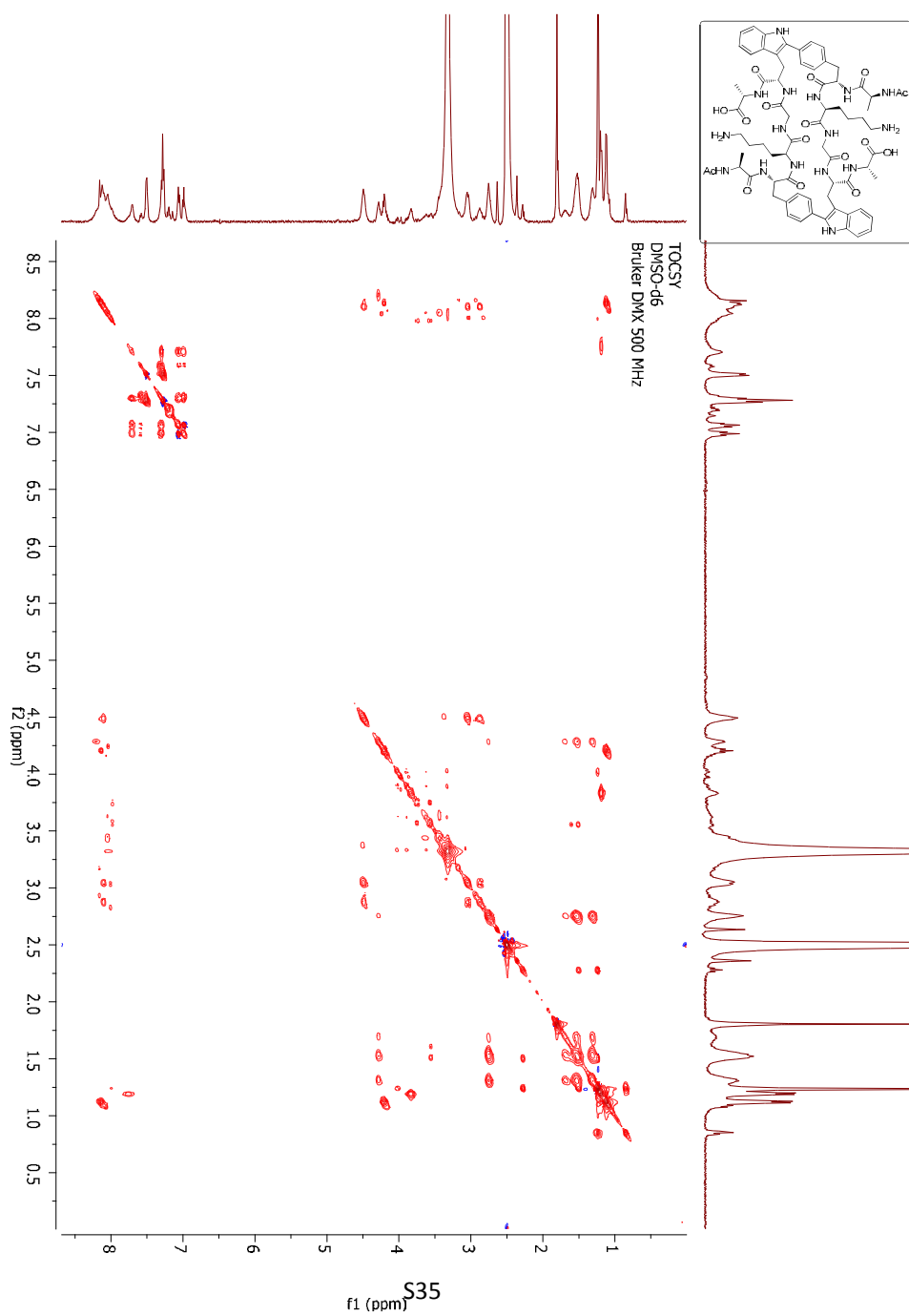
(Cyclo-*p,p*)bis-[Phe-Trp]-(Ac-Phe-Ala-Trp-Lys-OH) (5b) TOCSY NMR T=338 K

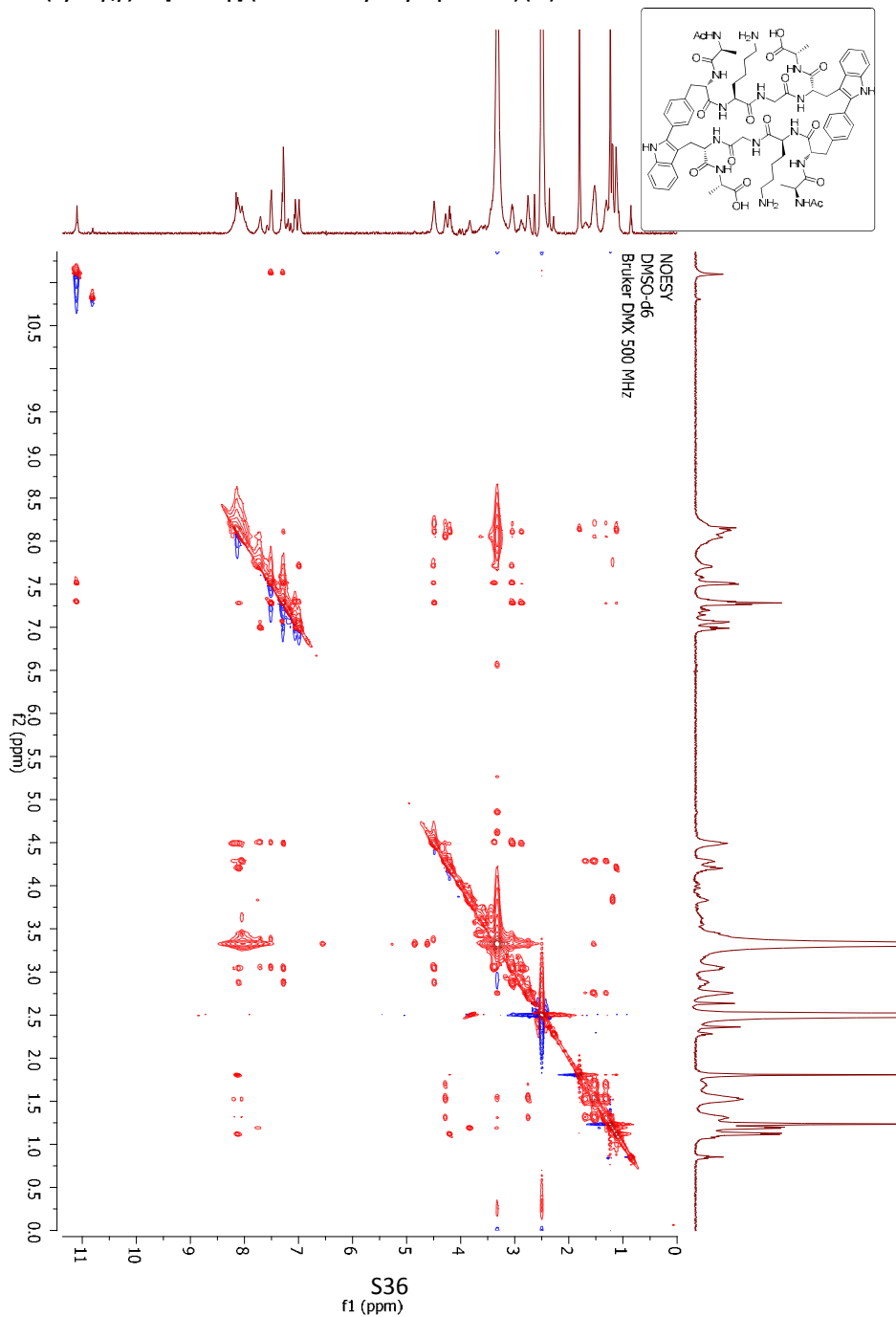
(Cyclo-*p,p*)bis-[Phe-Trp]-(Ac-Phe-Ala-Trp-Lys-OH) (5b) ^1H NMR T=298-358 K

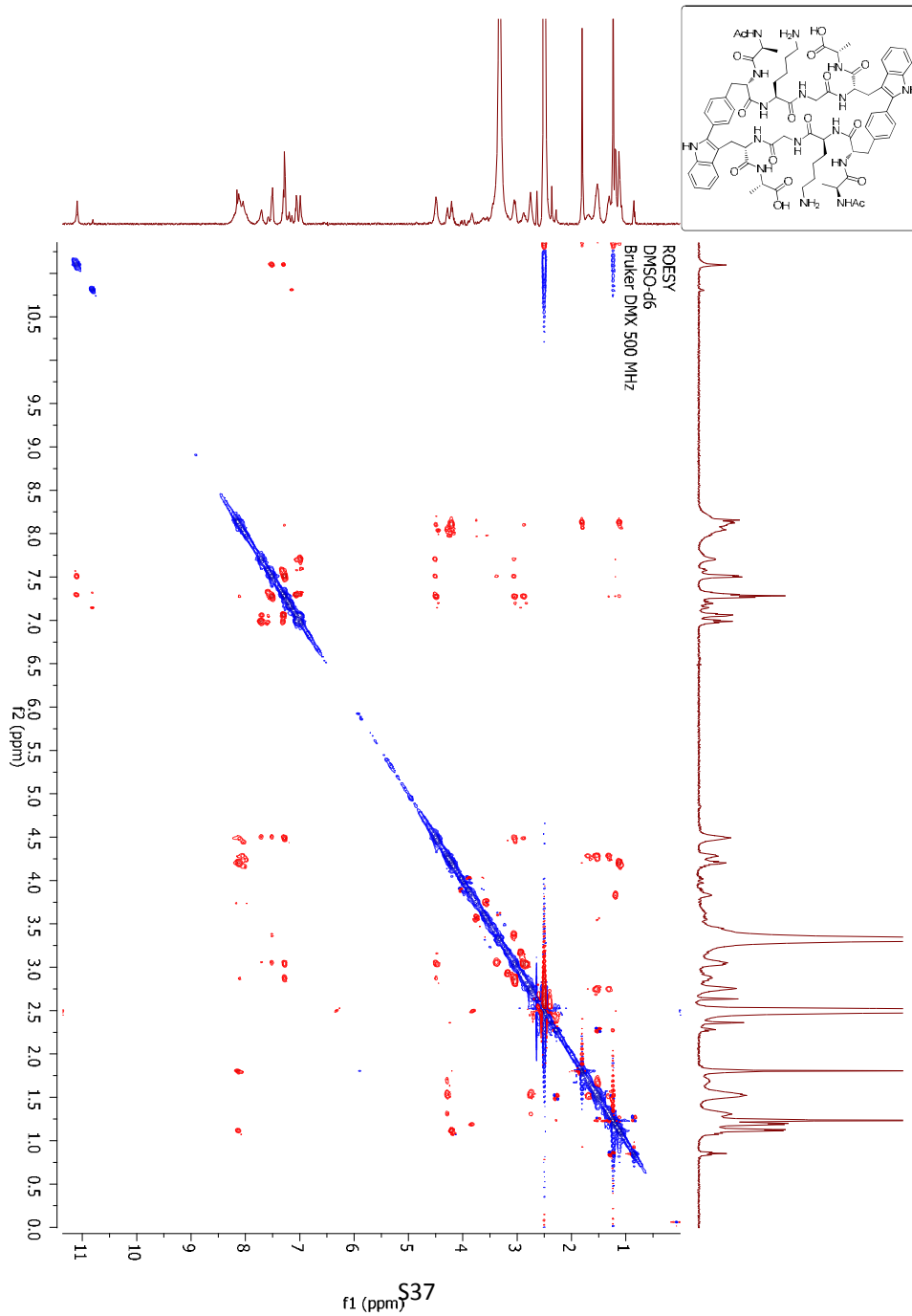
Cyclo-*p,p*)-bis-[Phe-Trp]-(Ac-Ala-Phe-Lys-Gly-Trp-Ala-OH) (5c) ^1H NMR T=338 K

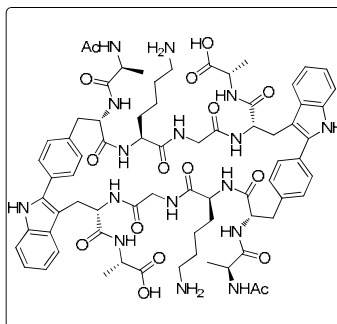
(Cyclo-*p,p*)bis-[Phe-Trp]-(Ac-Ala-Phe-Lys-Gly-Trp-Ala-OH) (5c) ^1H - ^{13}C HSQC NMR T=338 K

2D COSY NMR spectrum of compound 334. The x-axis (f1) and y-axis (f2) both range from 0.5 to 8.5 ppm. The spectrum shows diagonal peaks representing 1D ^1H NMR and off-diagonal cross-peaks indicating scalar coupling between protons. Key cross-peaks are observed in the aromatic region (6.5–8.5 ppm) and the aliphatic region (1.0–4.5 ppm). An inset shows the chemical structure of compound 334, a complex polycyclic molecule with multiple amide and carboxylic acid groups.

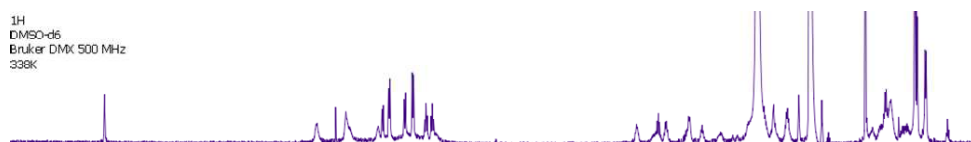
(Cyclo-*p,p*)bis-[Phe-Trp]-(Ac-Ala-Phe-Lys-Gly-Trp-Ala-OH) (5c) TOCSY NMR T=338 K

(Cyclo-*p,p*)bis-[Phe-Trp]-(Ac-Ala-Phe-Lys-Gly-Trp-Ala-OH) (5c) NOESY NMR T=338 K

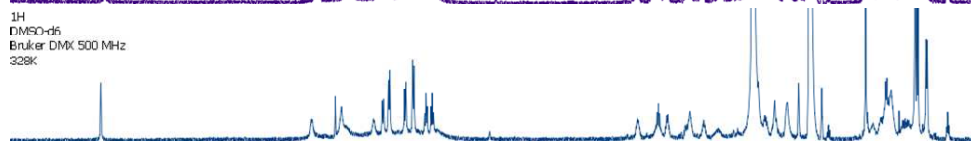
(Cyclo-*p,p*)bis-[Phe-Trp]-(Ac-Ala-Phe-Lys-Gly-Trp-Ala-OH) (5c) ROESY NMR T=338 K

(Cyclo-*p,p*)bis-[Phe-Trp]-(Ac-Ala-Phe-Lys-Gly-Trp-Ala-OH) (5c) ^1H NMR T=298-338 K

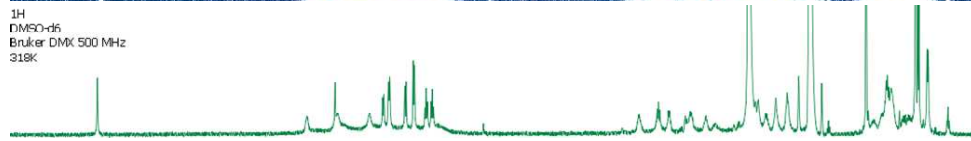
^1H
DMSO- d_6
Bruker DMX 500 MHz
338K



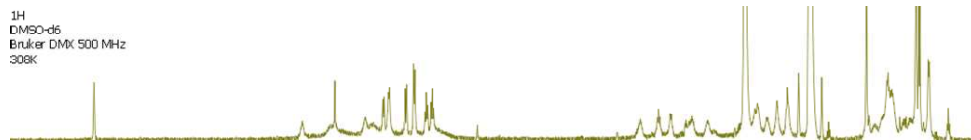
^1H
DMSO- d_6
Bruker DMX 500 MHz
328K



^1H
DMSO- d_6
Bruker DMX 500 MHz
318K



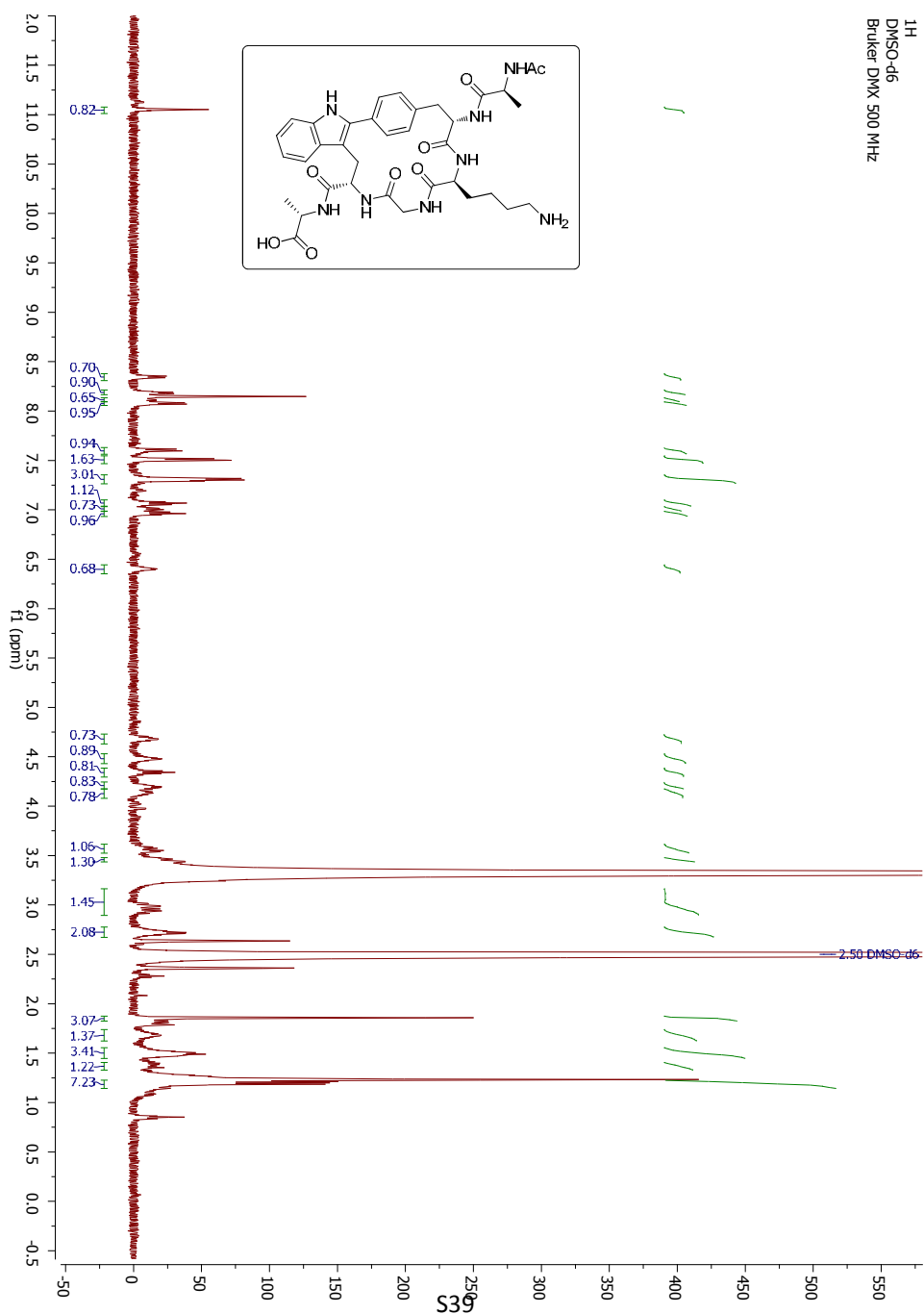
^1H
DMSO- d_6
Bruker DMX 500 MHz
308K



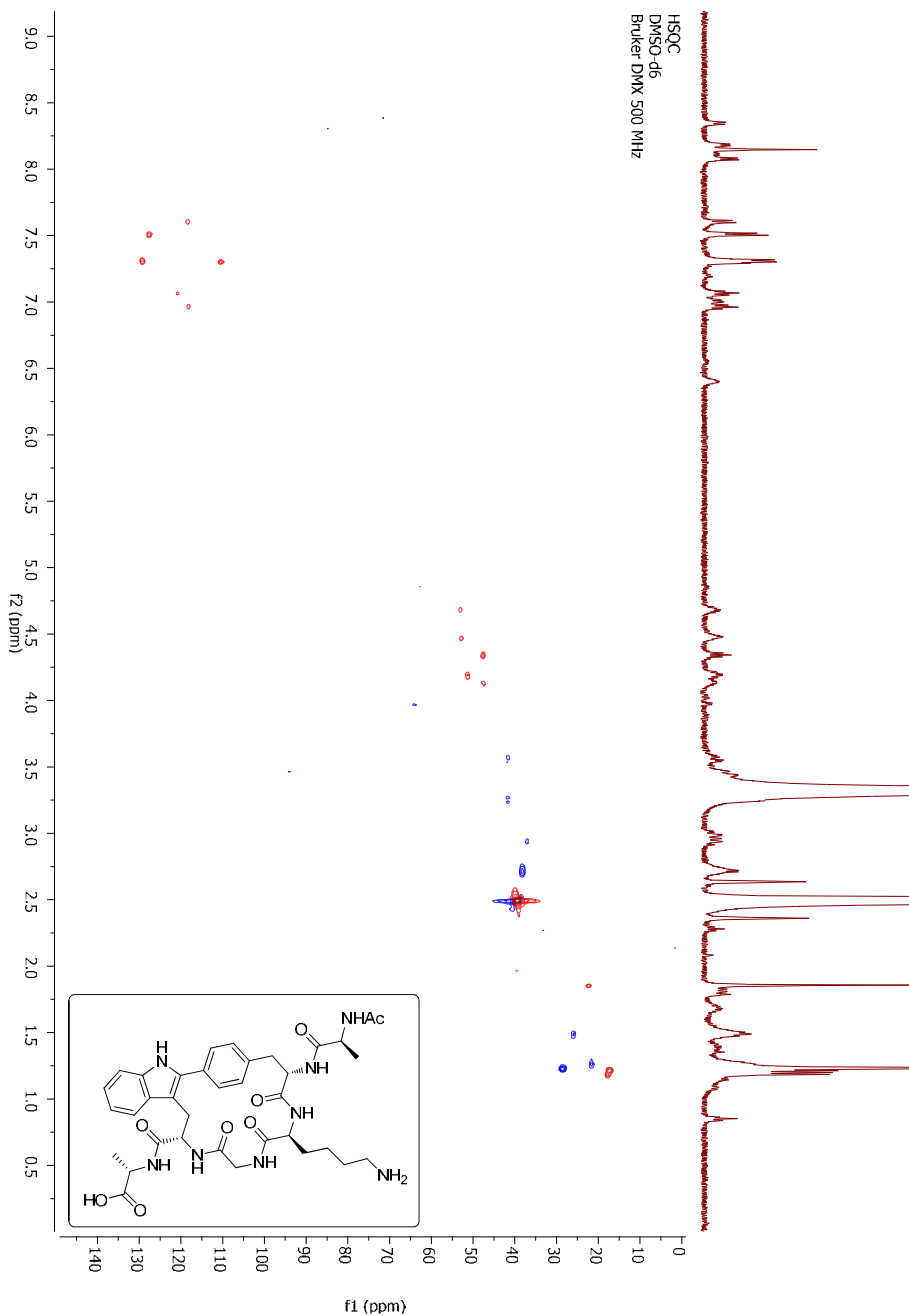
^1H
DMSO- d_6
Bruker DMX 500 MHz
298K

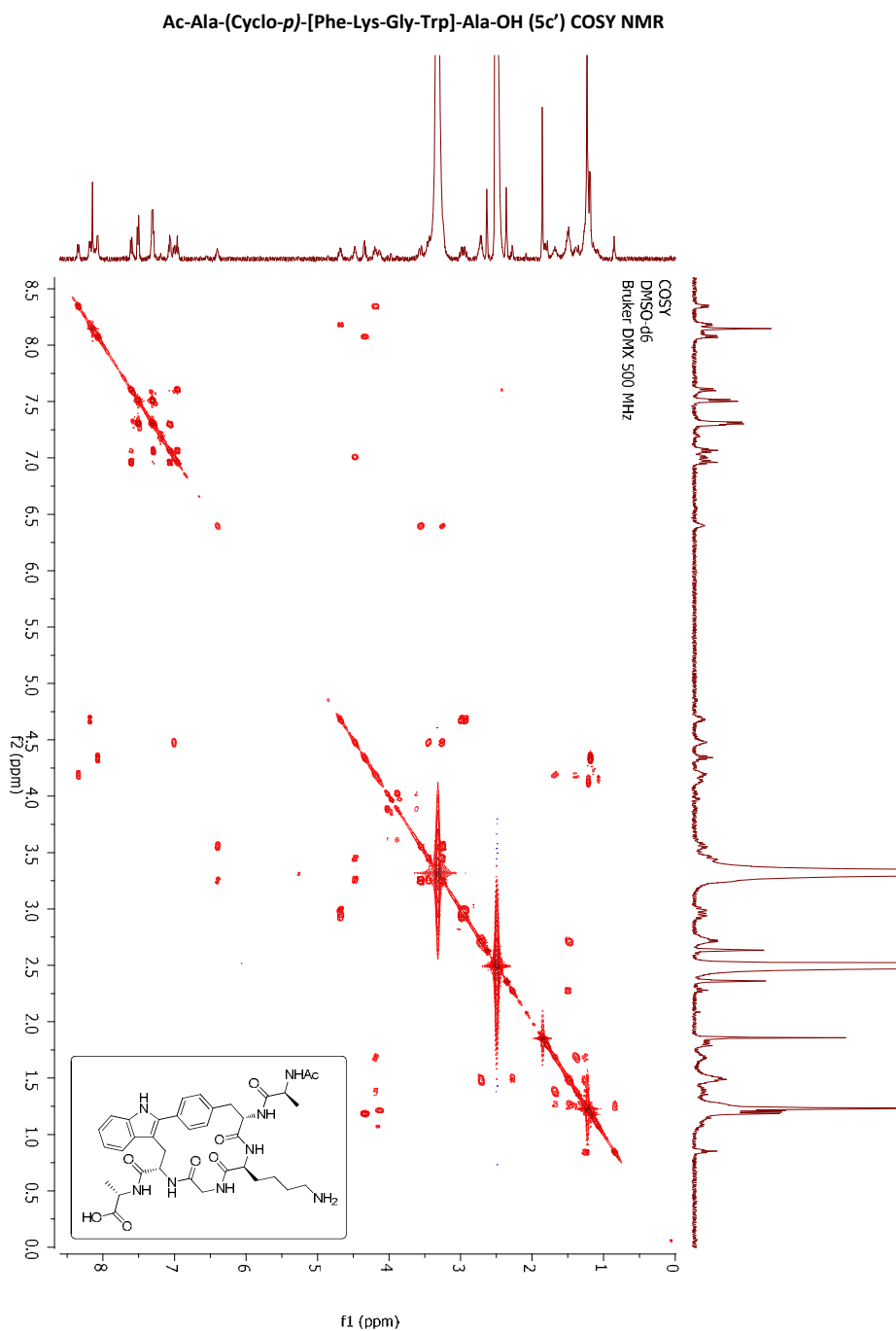


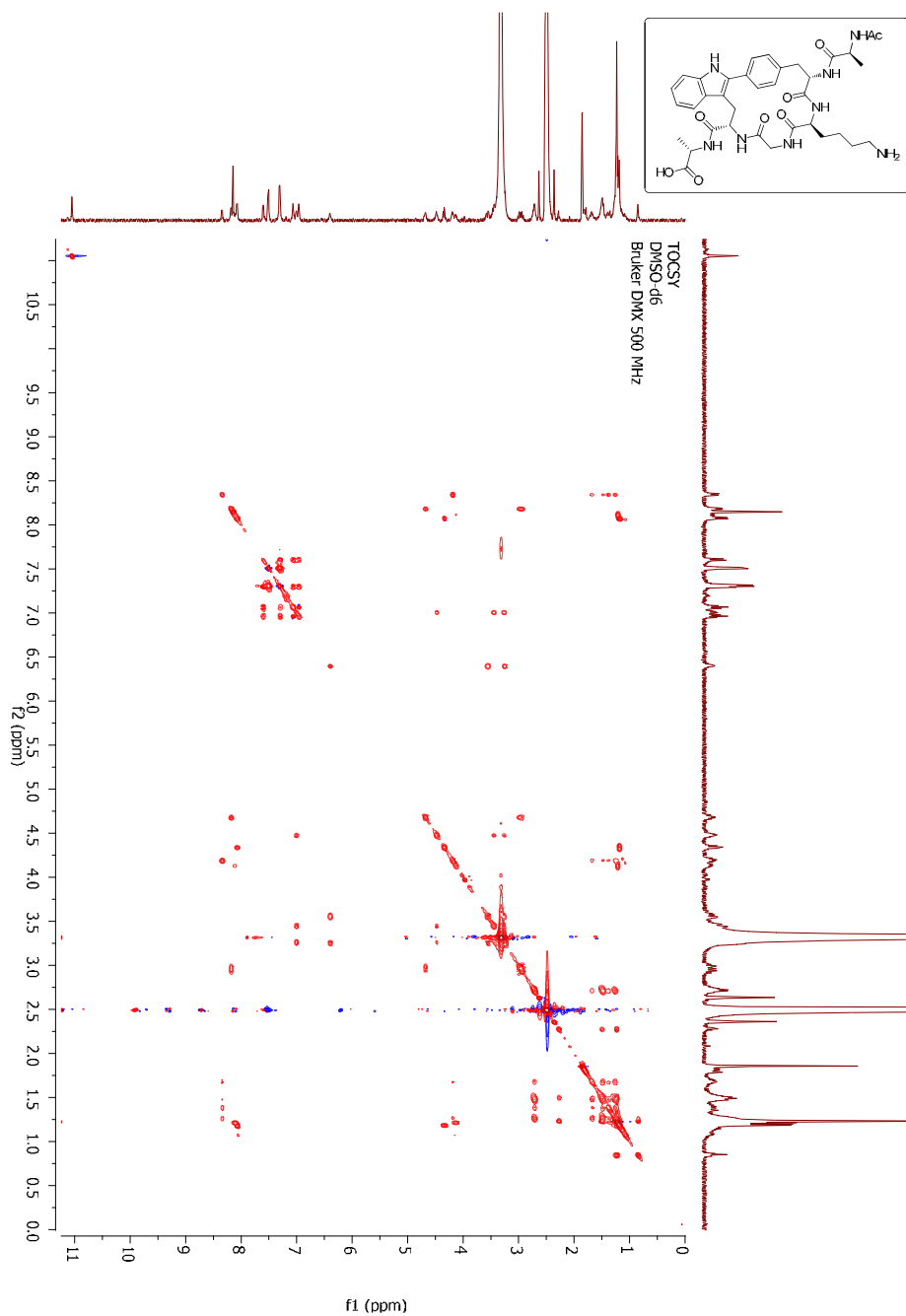
¹H
DMSO-d₆
Bruker DMX 500 MHz

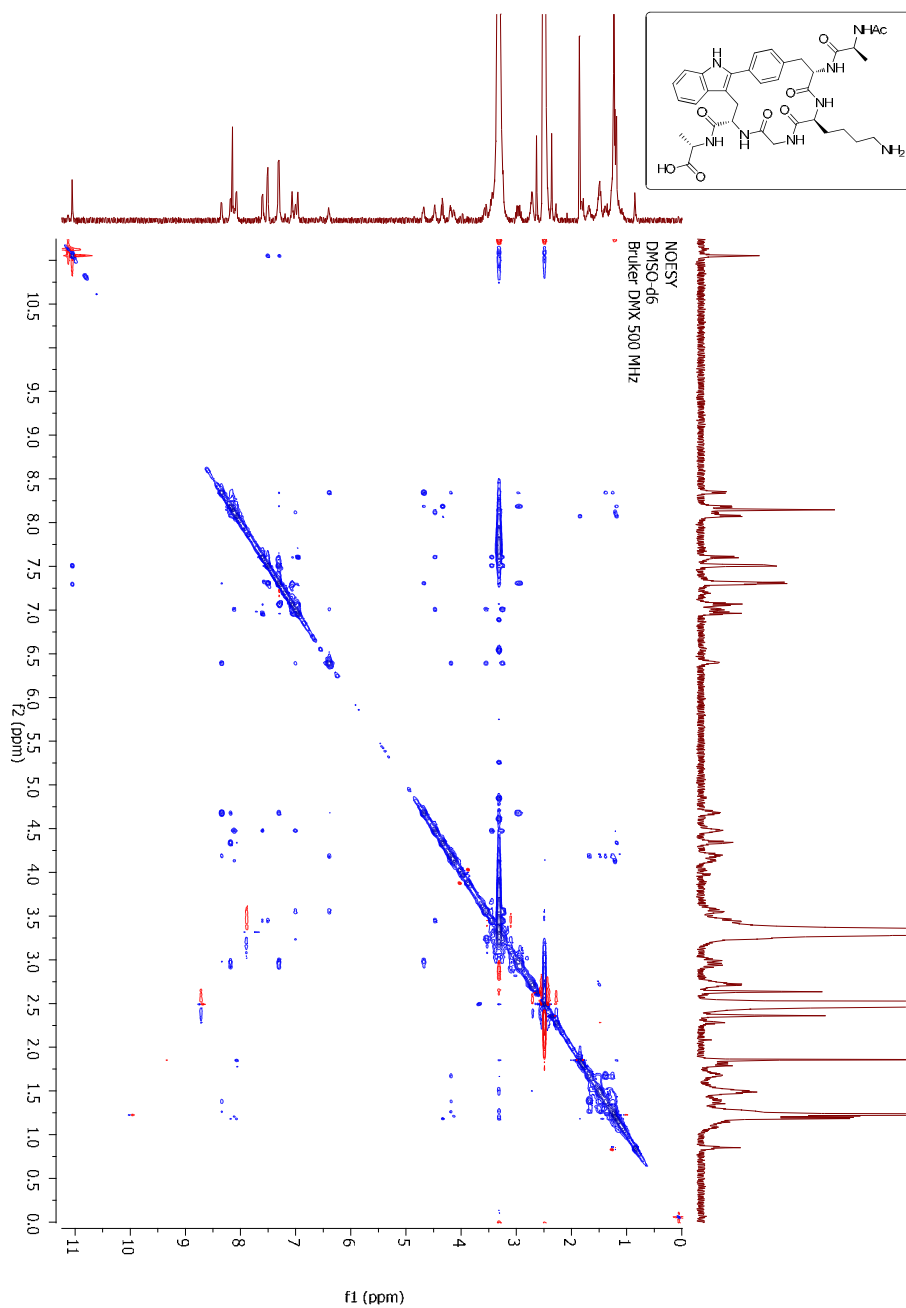


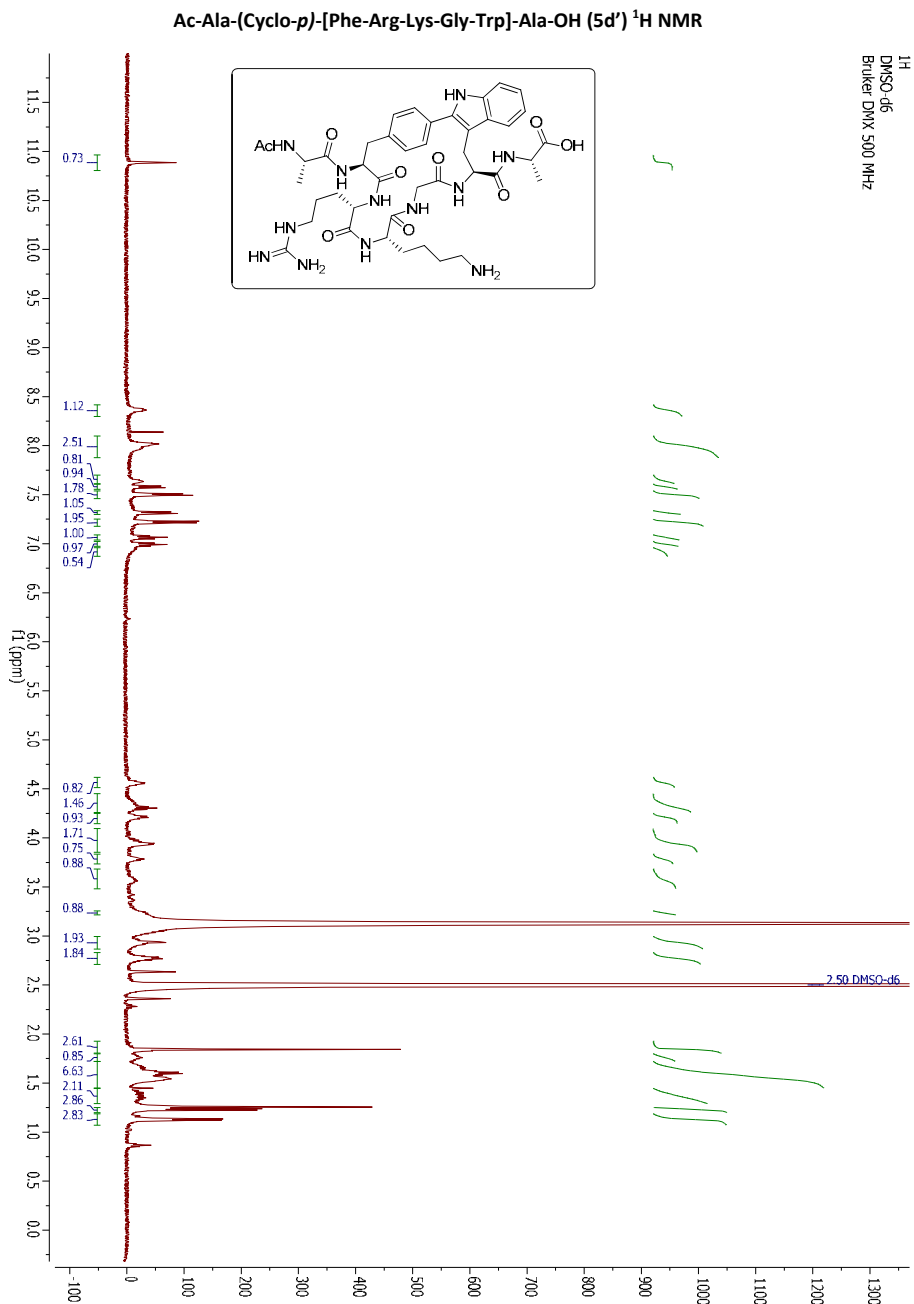
Ac-Ala-(Cyclo-*p*)-[Phe-Lys-Gly-Trp]-Ala-OH (5c') ^1H - ^{13}C HSQC NMR

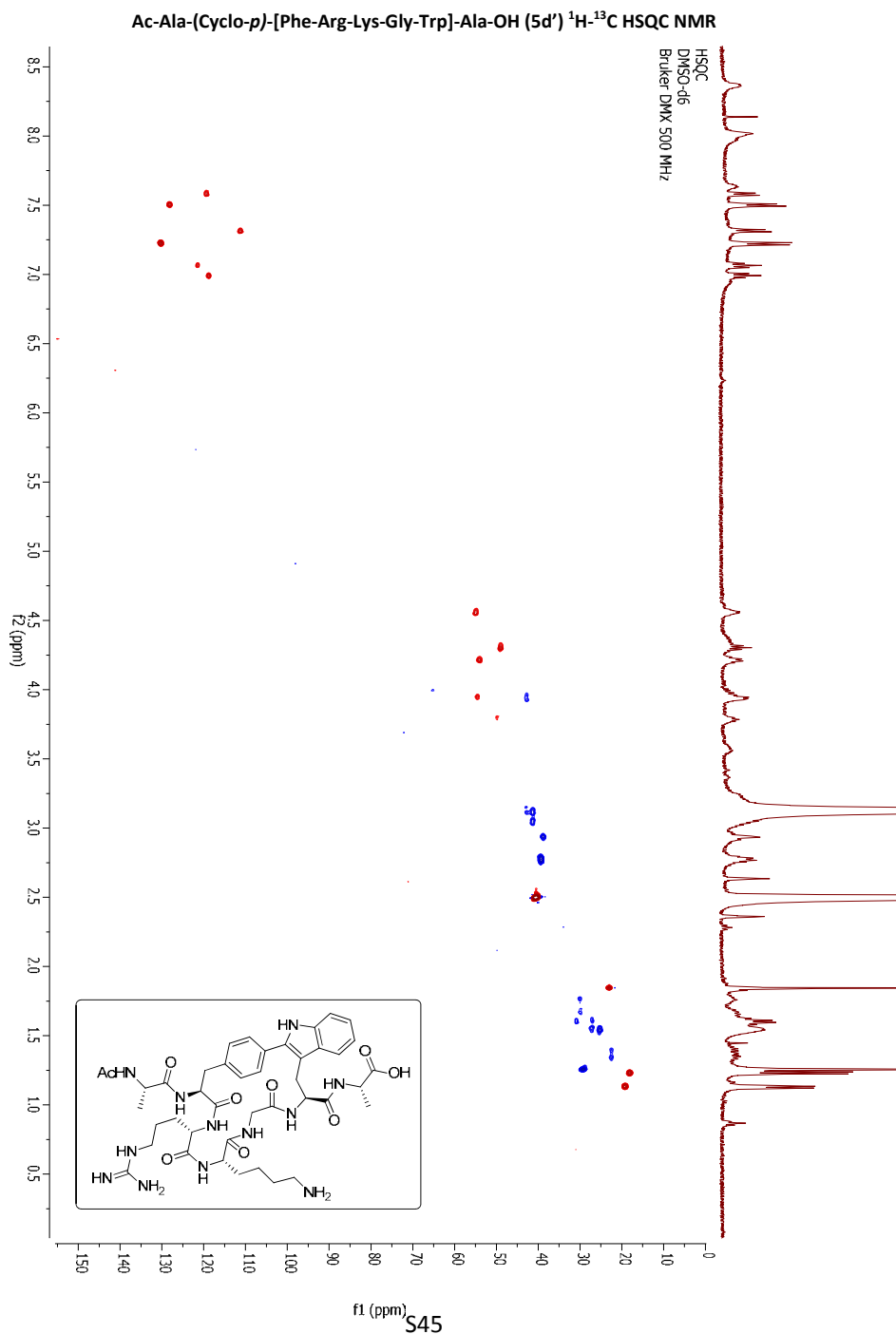


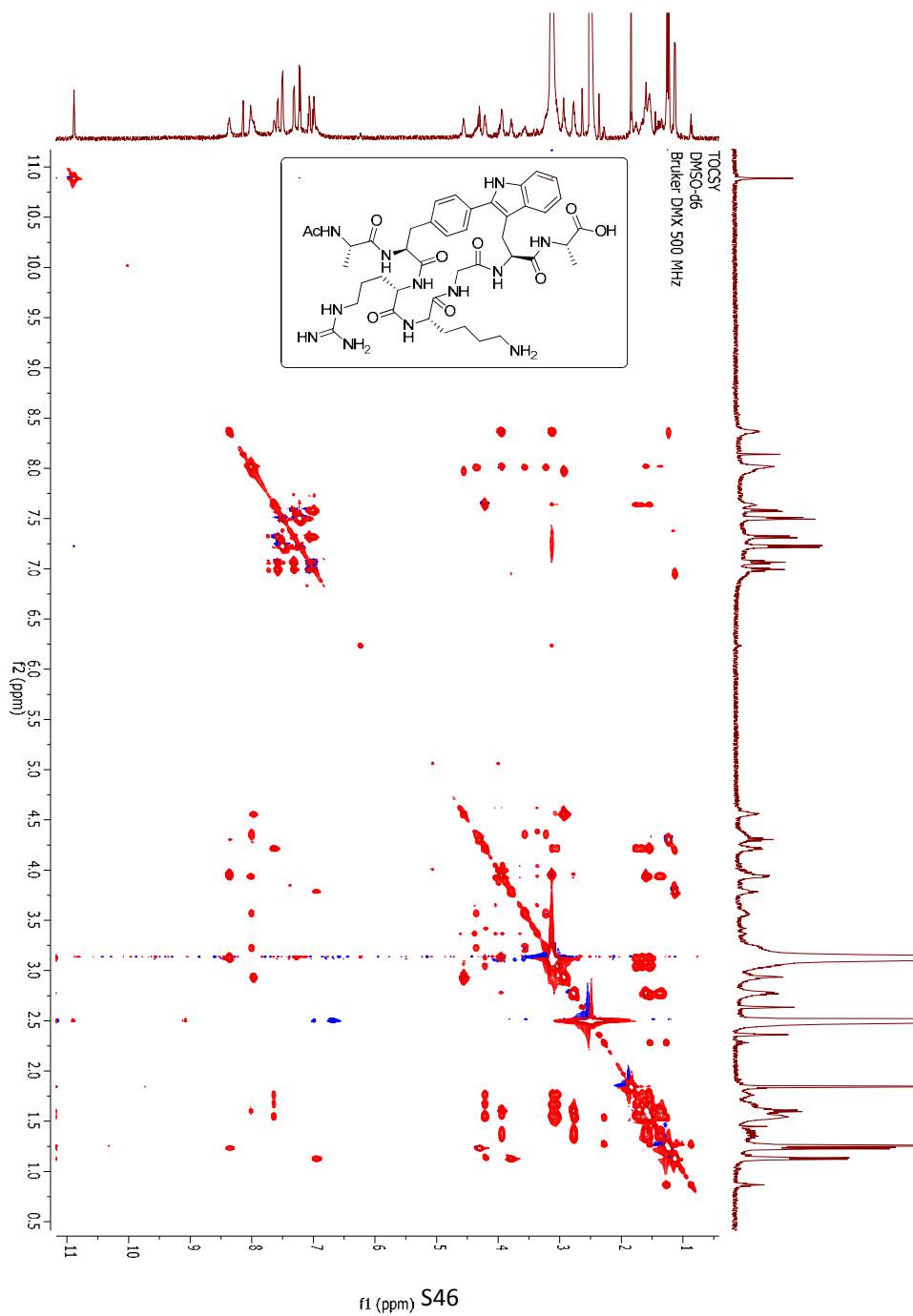


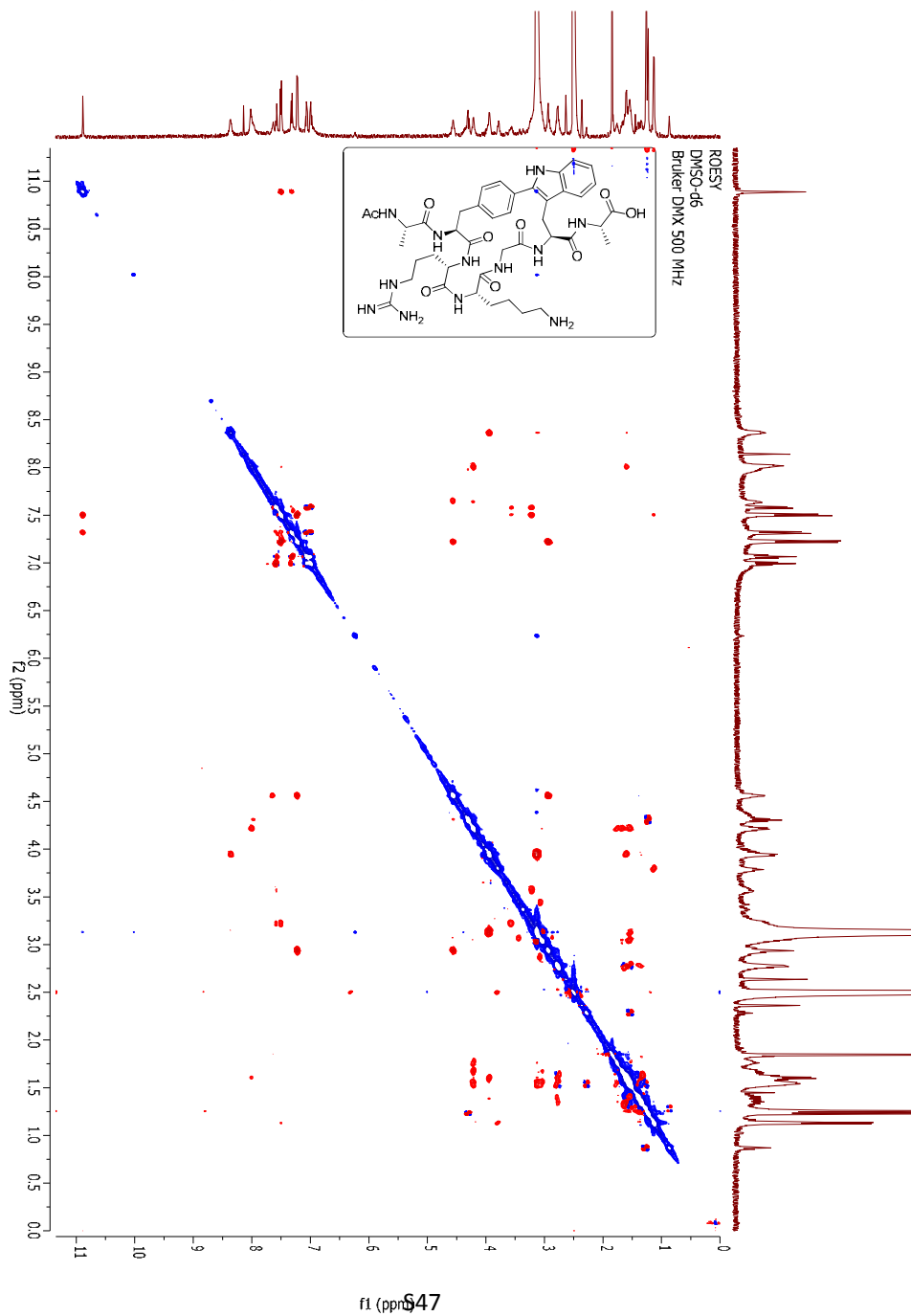
Ac-Ala-(Cyclo-*p*)-[Phe-Lys-Gly-Trp]-Ala-OH (5c') TOCSY NMR

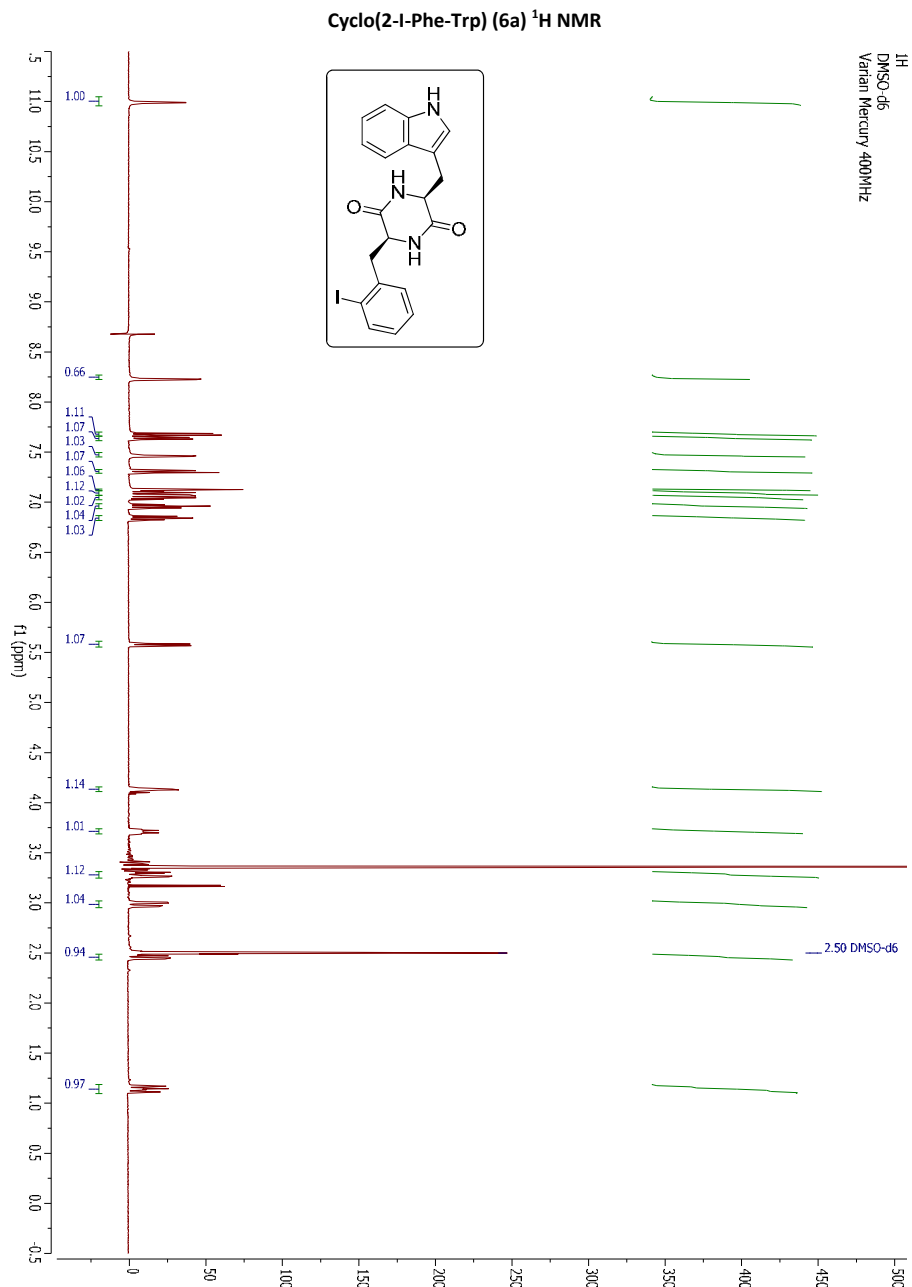
Ac-Ala-(Cyclo-*p*)-[Phe-Lys-Gly-Trp]-Ala-OH (5c') NOESY NMR

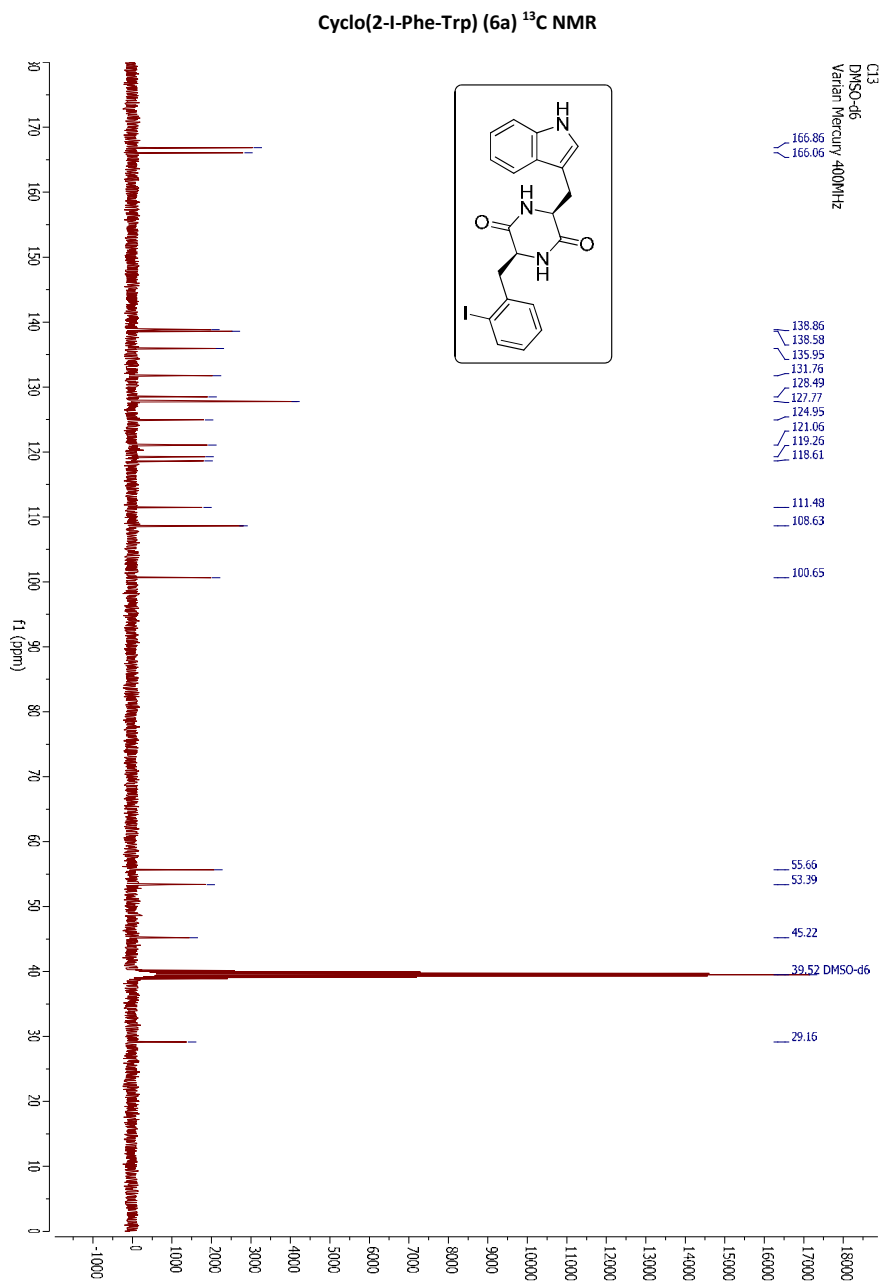


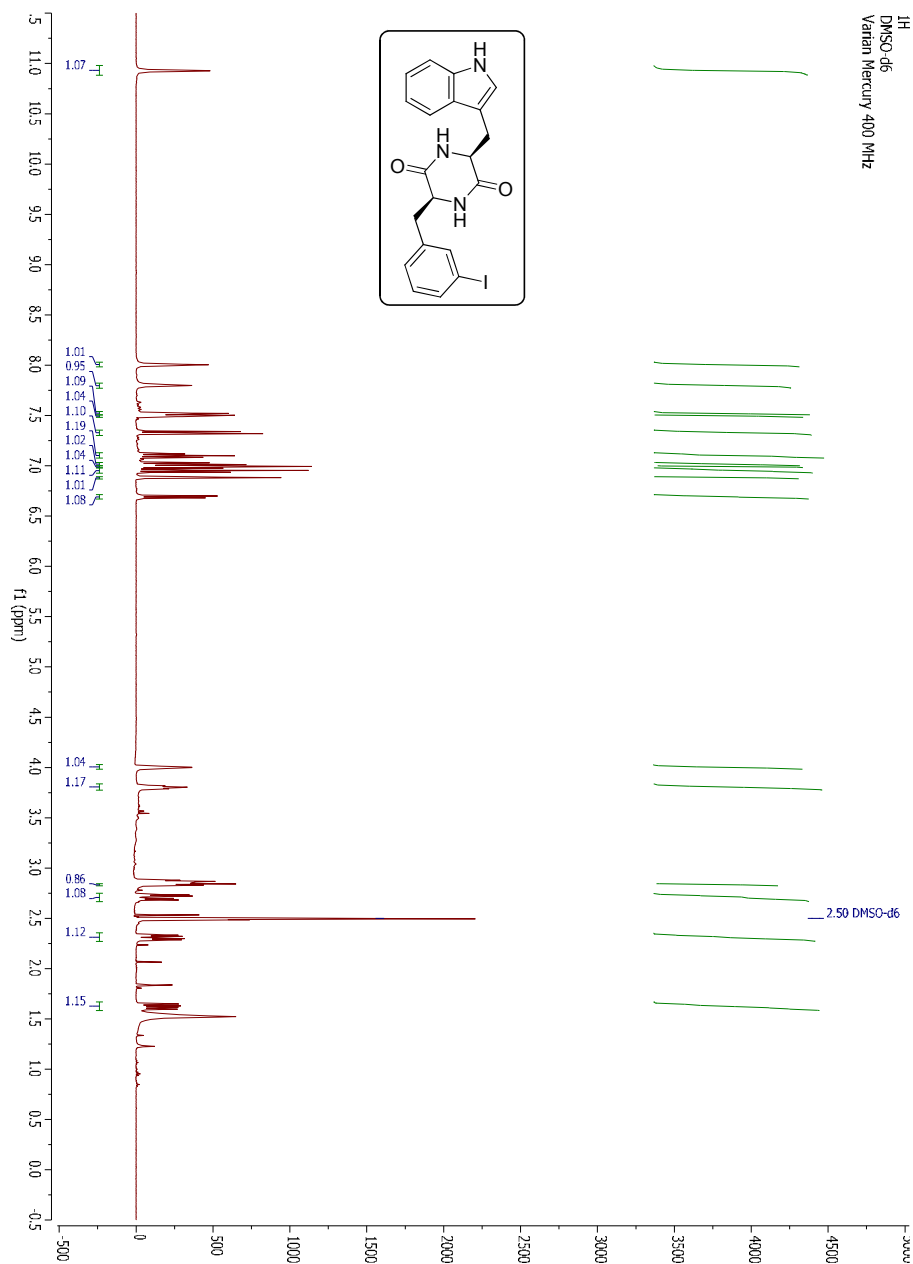


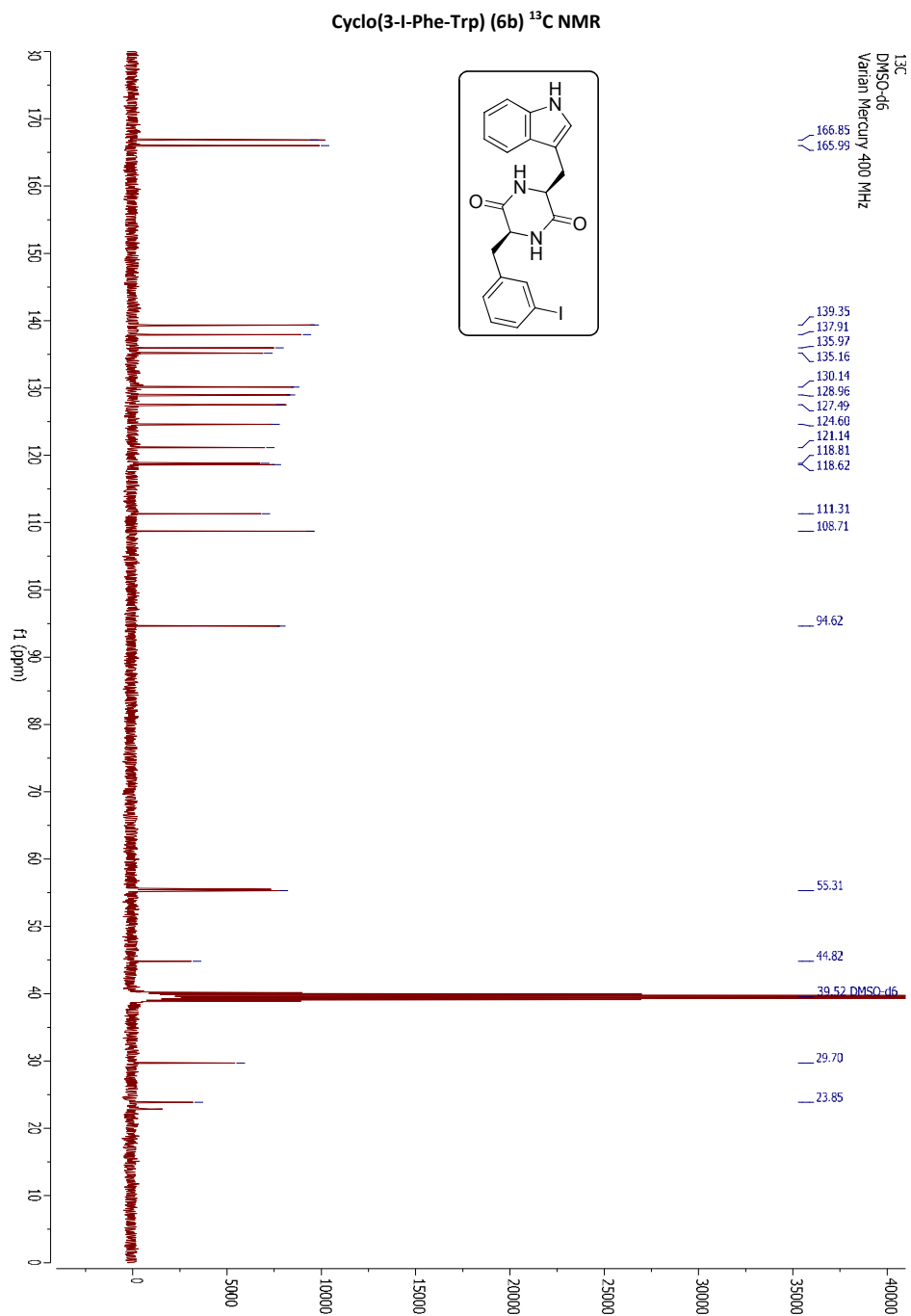
Ac-Ala-(Cyclo-*p*)-[Phe-Arg-Lys-Gly-Trp]-Ala-OH (5d') TOCSY NMR

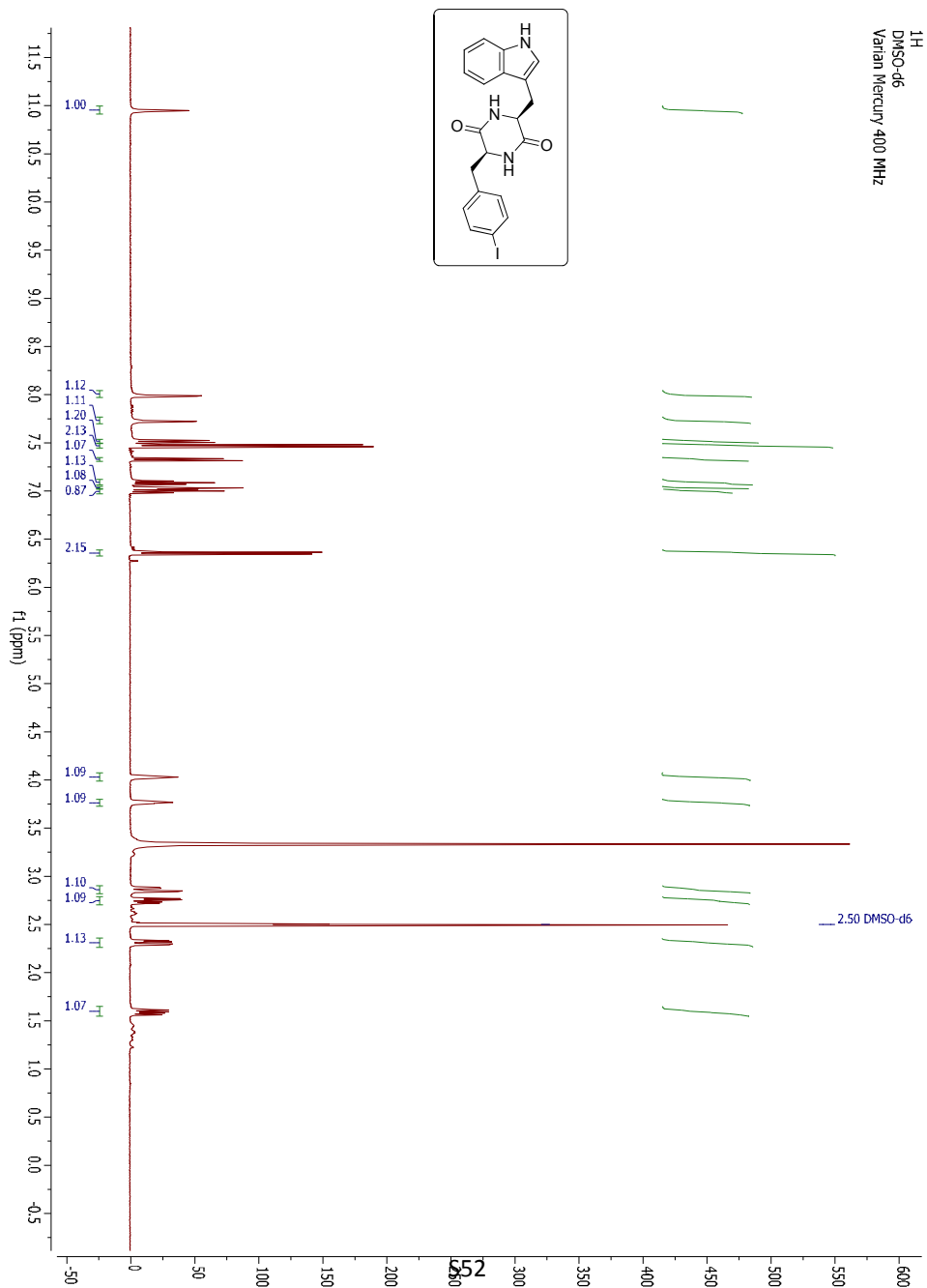
Ac-Ala-(Cyclo-*p*)-[Phe-Arg-Lys-Gly-Trp]-Ala-OH (5d') ROESY NMR

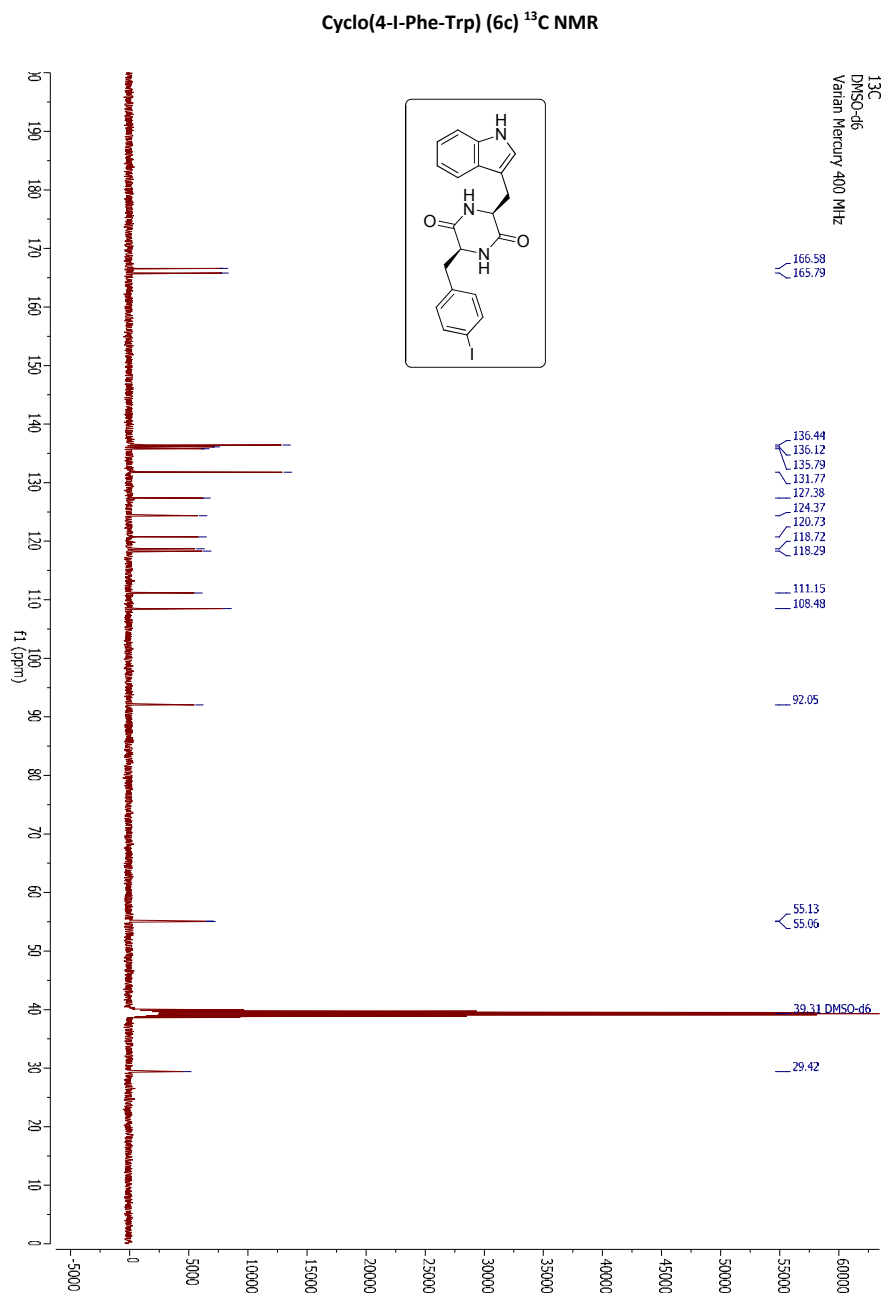


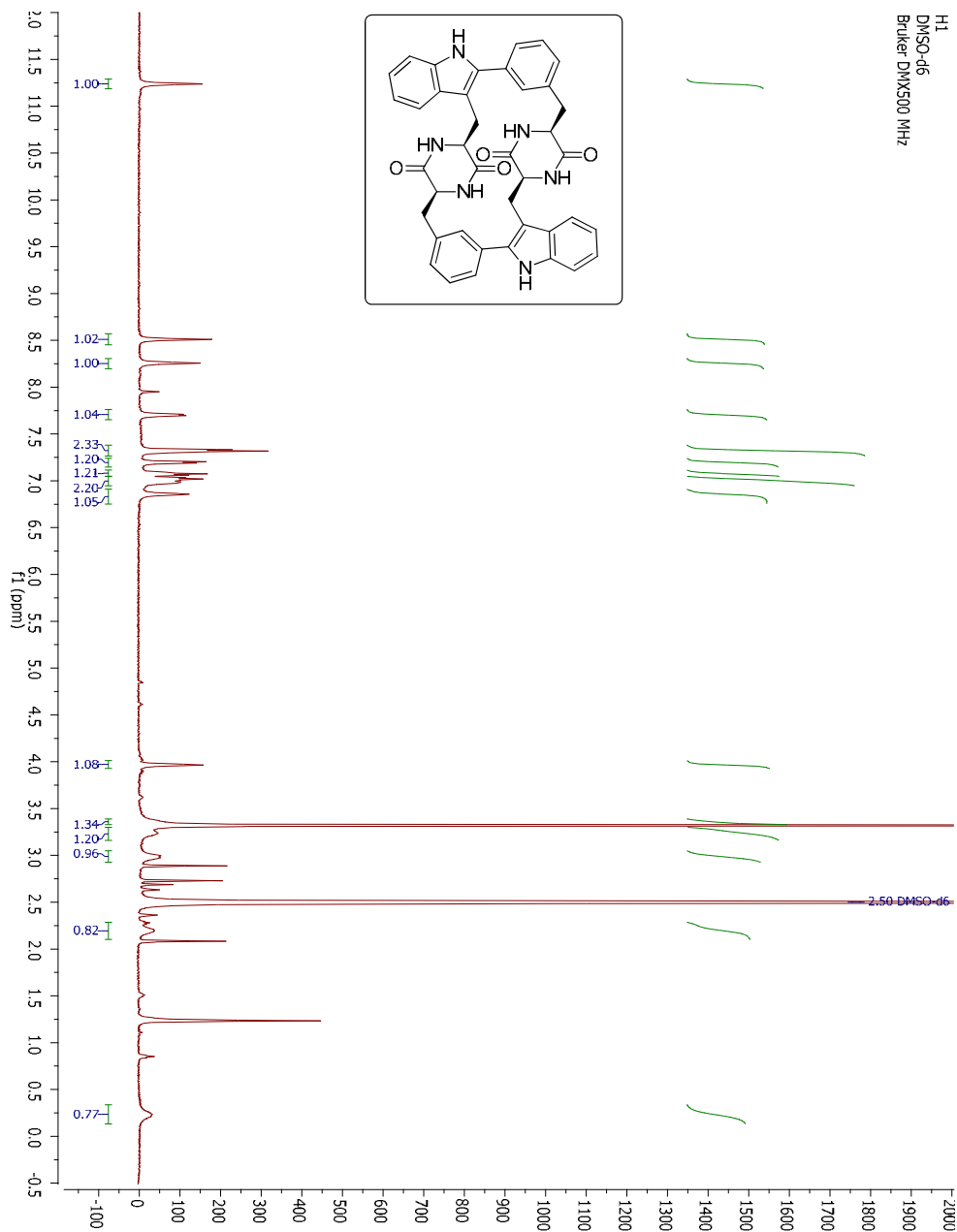


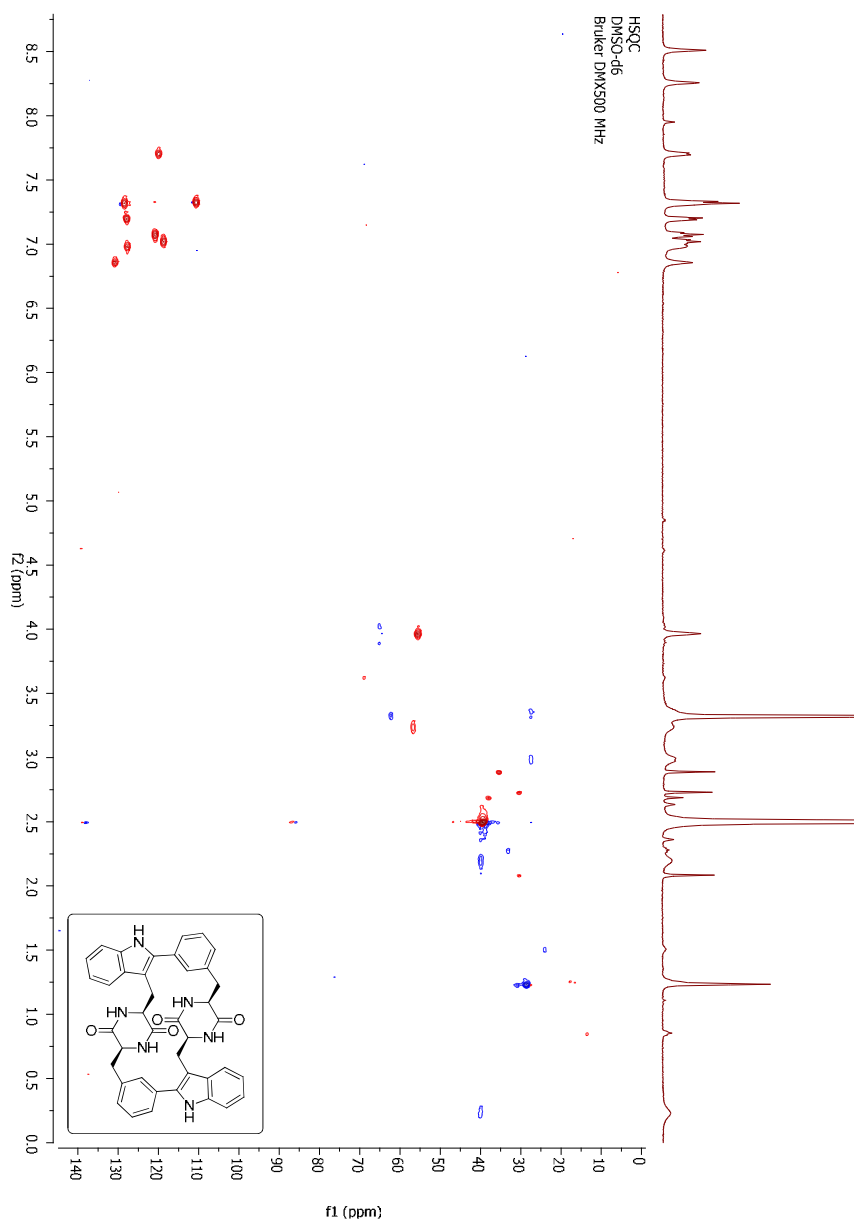
Cyclo(3-I-Phe-Trp) (6b) ^1H NMR



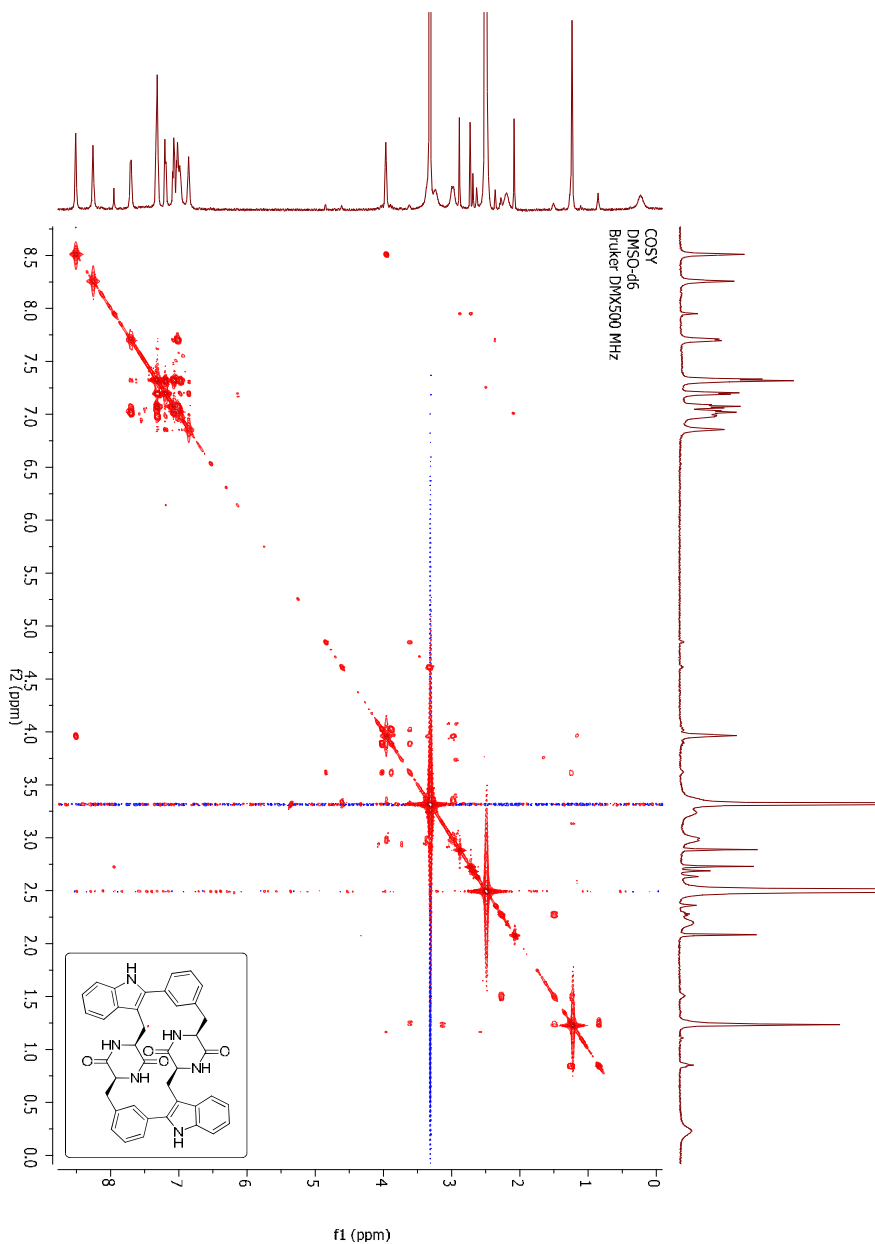
Cyclo(4-I-Phe-Trp) (6c) ^1H NMR

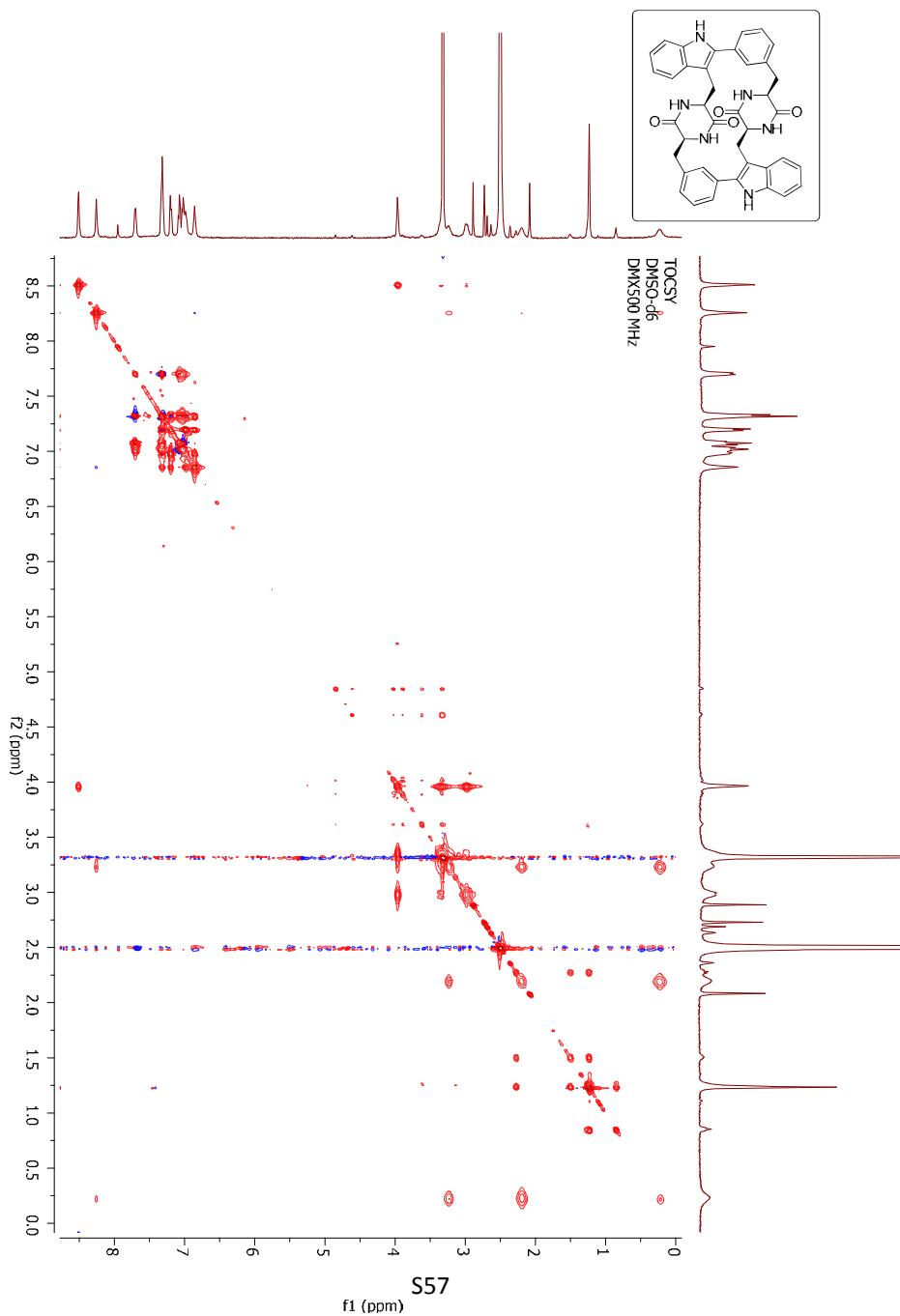


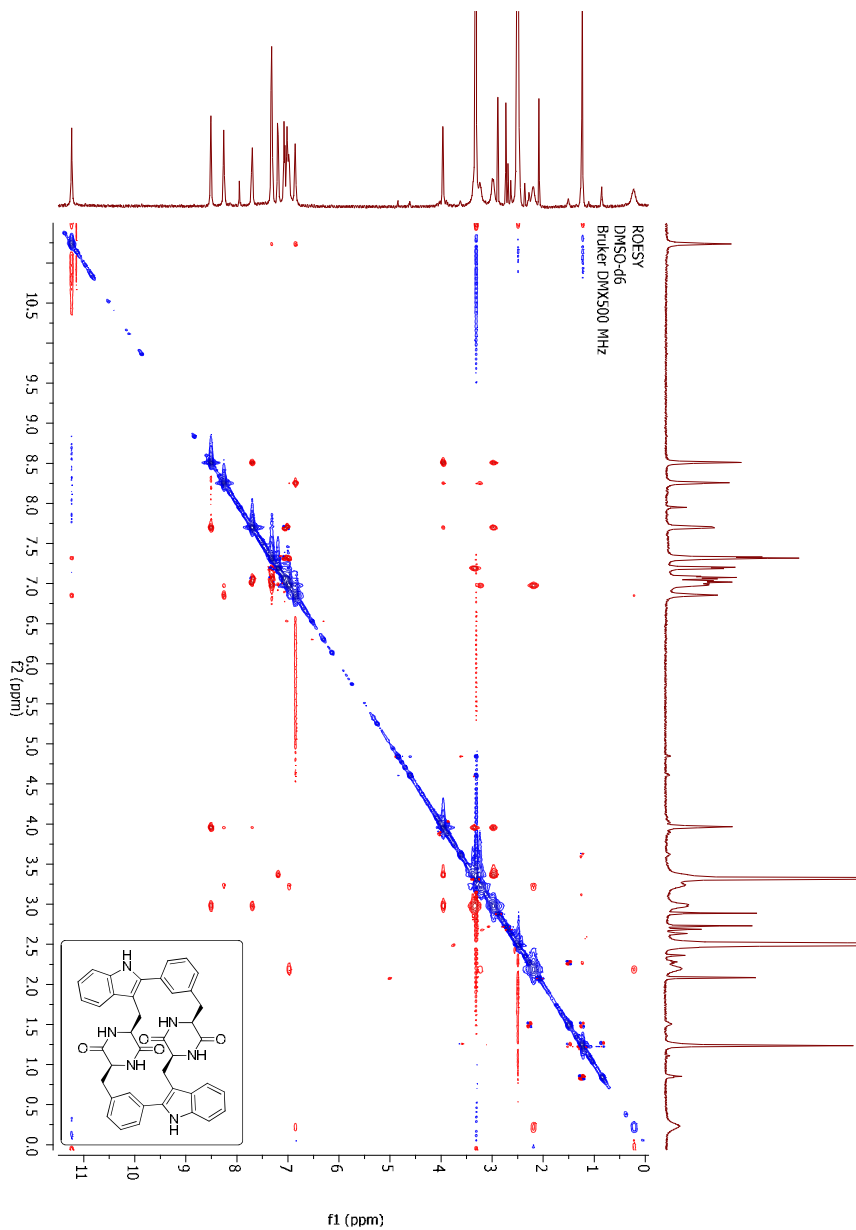
(Cyclo-*m,m*)bis-[Phe-Trp]-cyclo(Phe-Trp) (7b) ^1H NMR

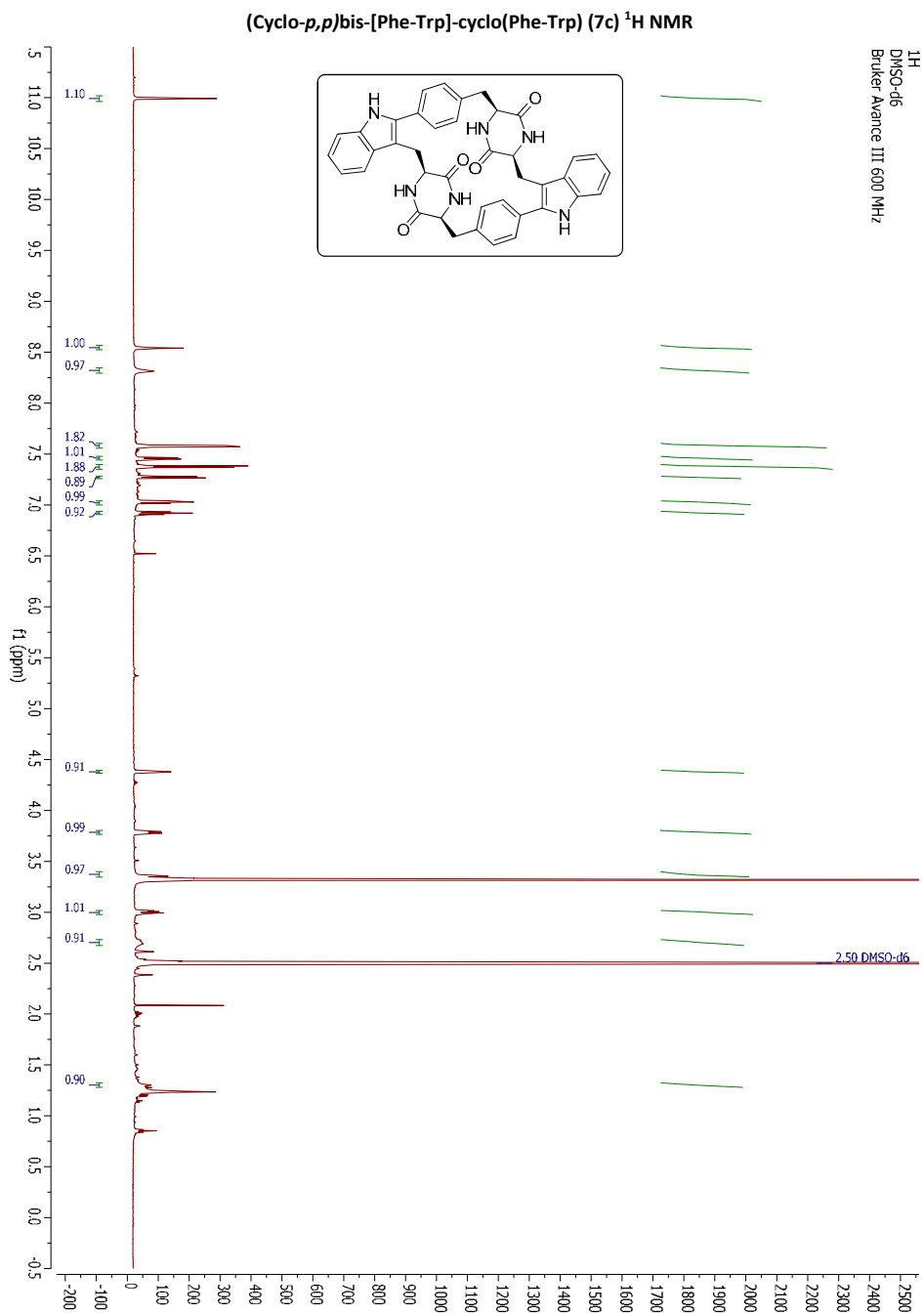
(Cyclo-*m,m*)bis-[Phe-Trp]-cyclo(Phe-Trp) (7b) ^1H - ^{13}C HSQC NMR

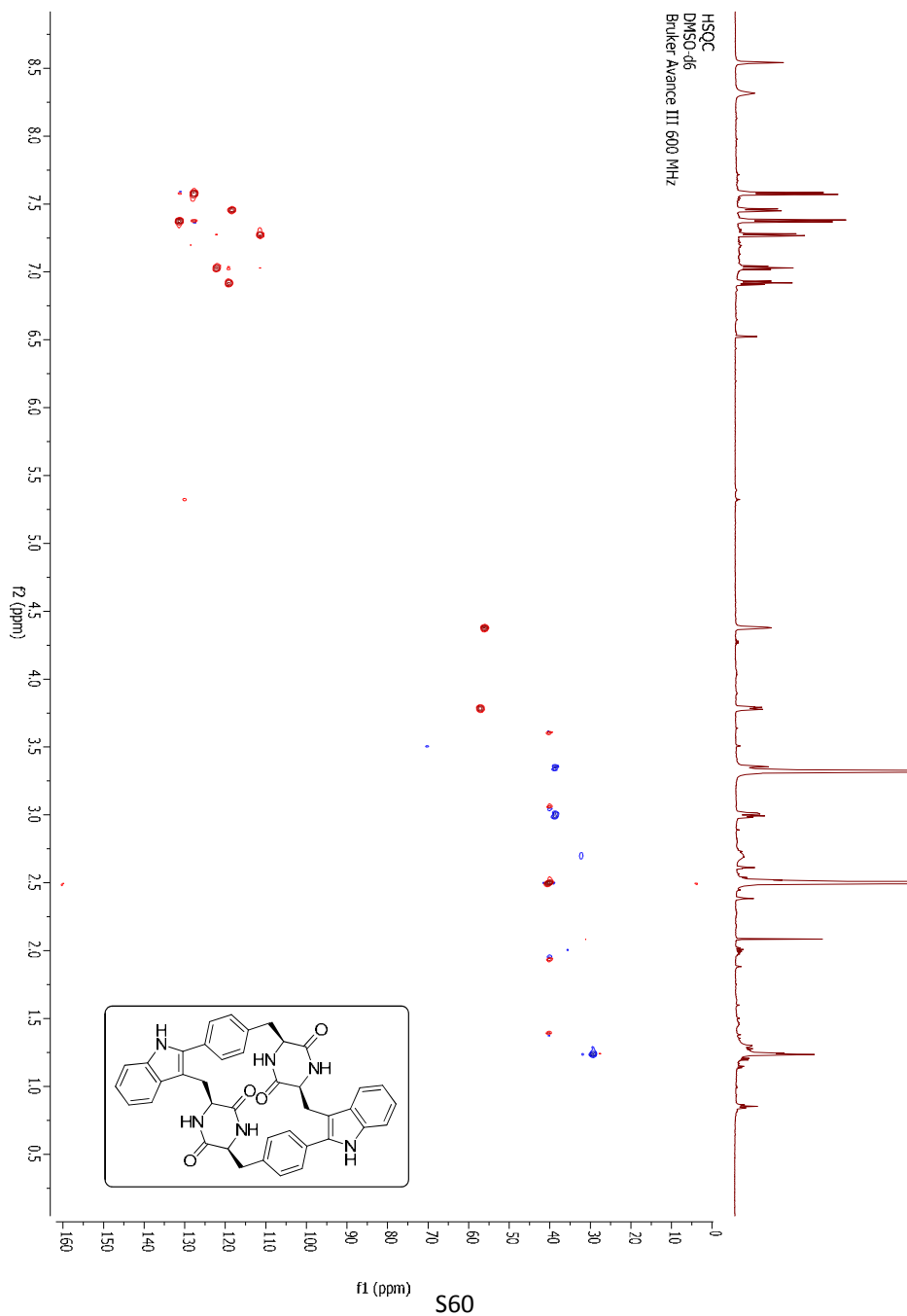
(Cyclo-*m,m*)bis-[Phe-Trp]-cyclo(Phe-Trp) (7b) COSY NMR

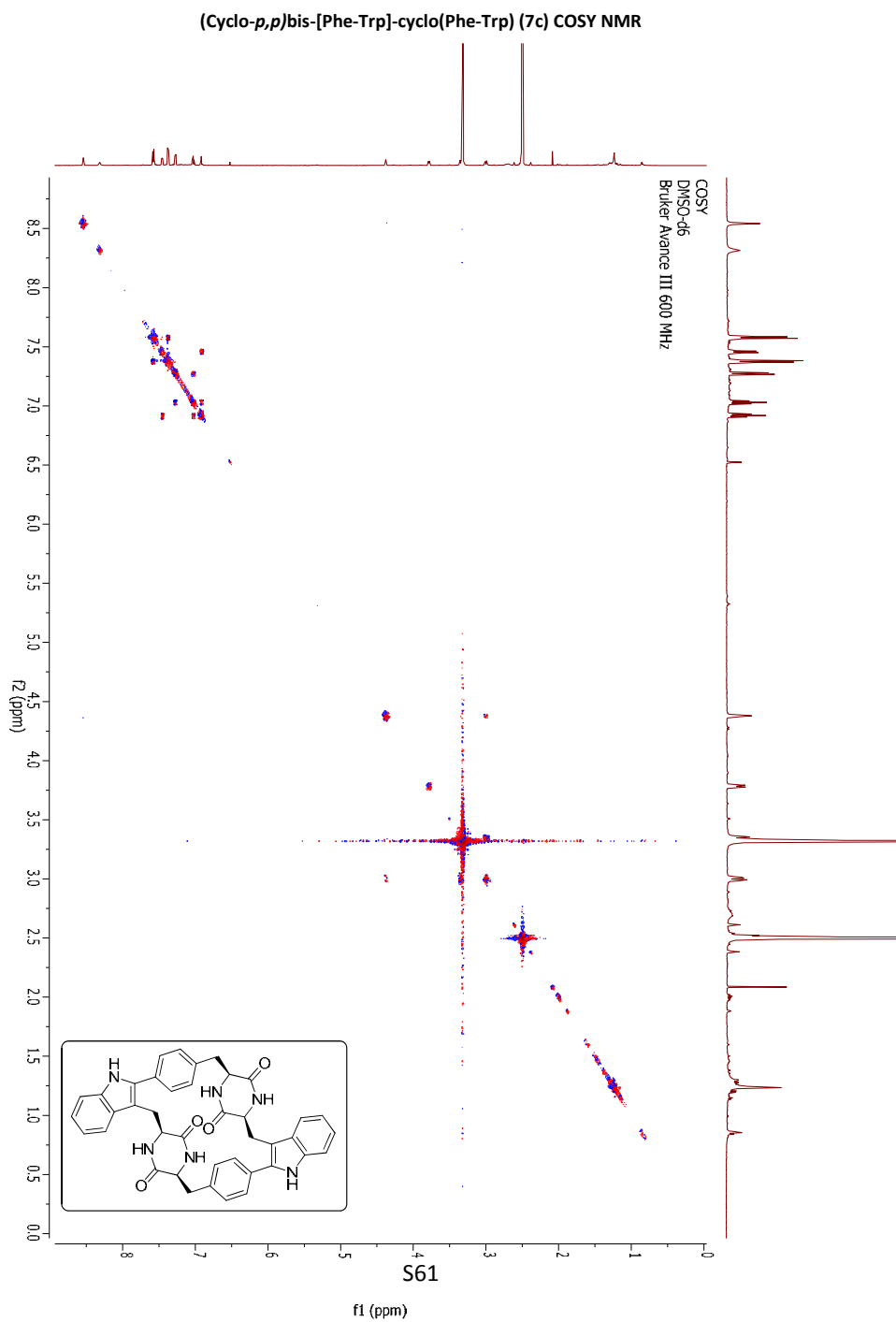


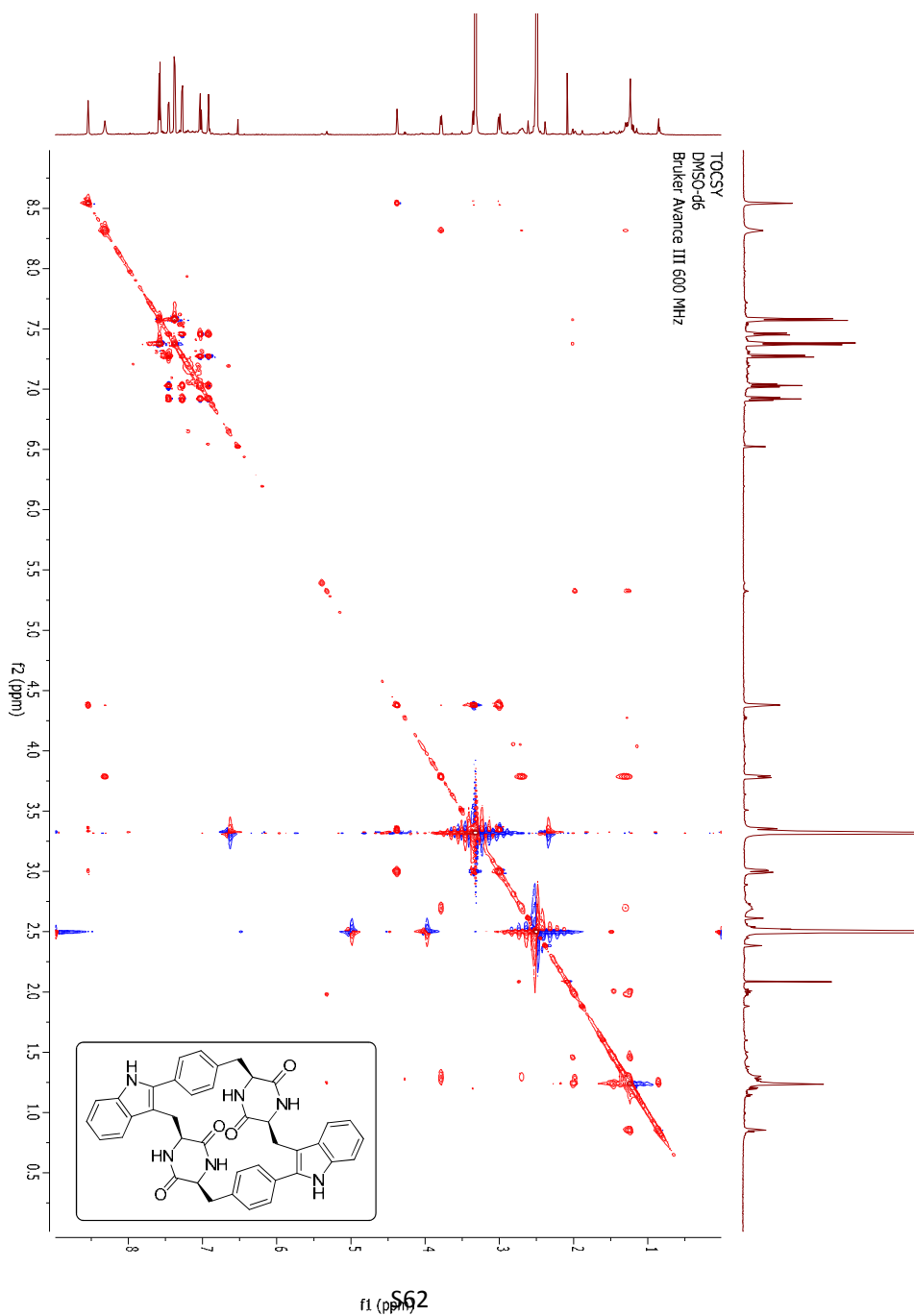
(Cyclo-*m,m*)bis-[Phe-Trp]-cyclo(Phe-Trp) (7b) TOCSY NMR

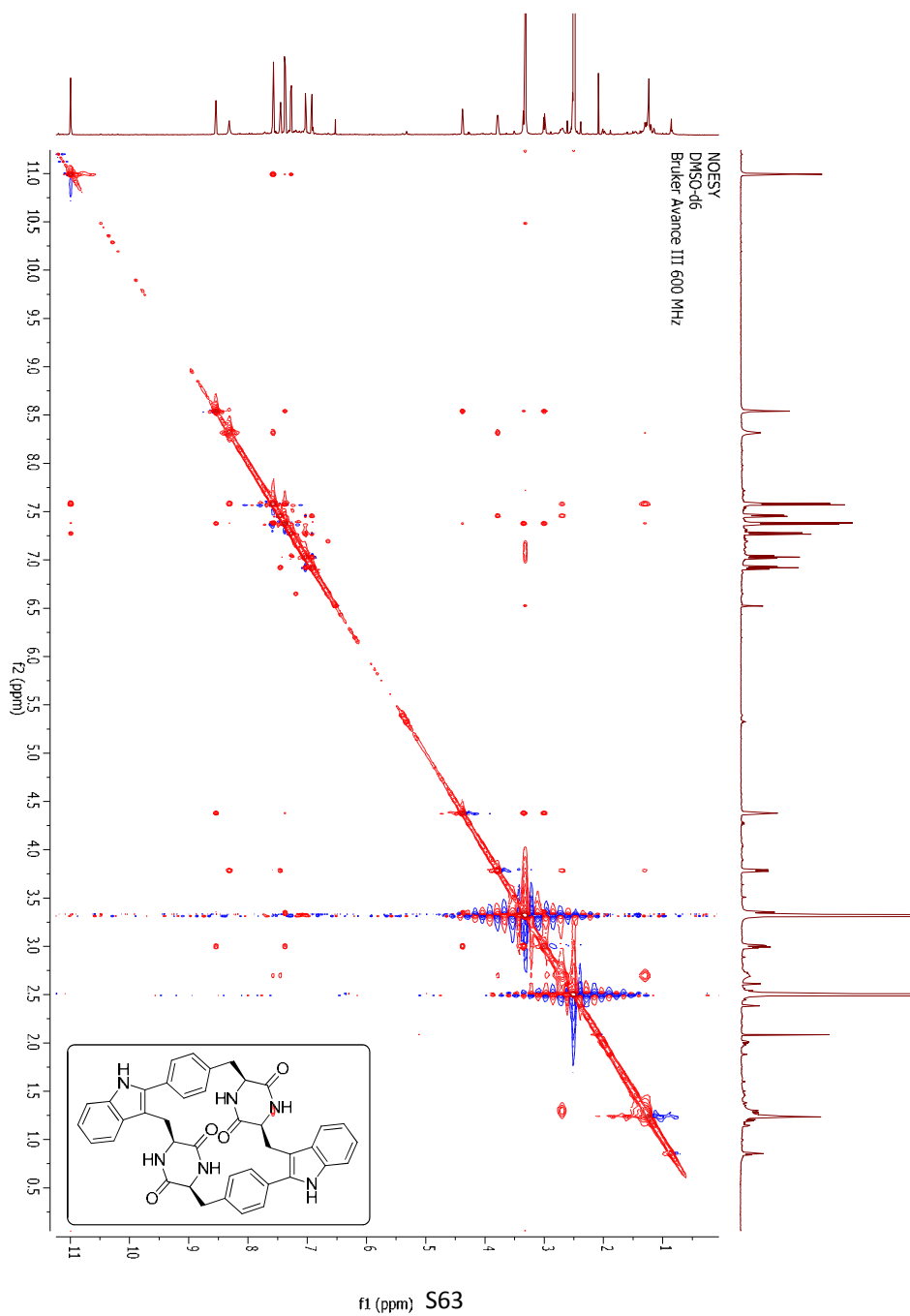
(Cyclo-*m,m*)bis-[Phe-Trp]-cyclo(Phe-Trp) (7b) ROESY NMR



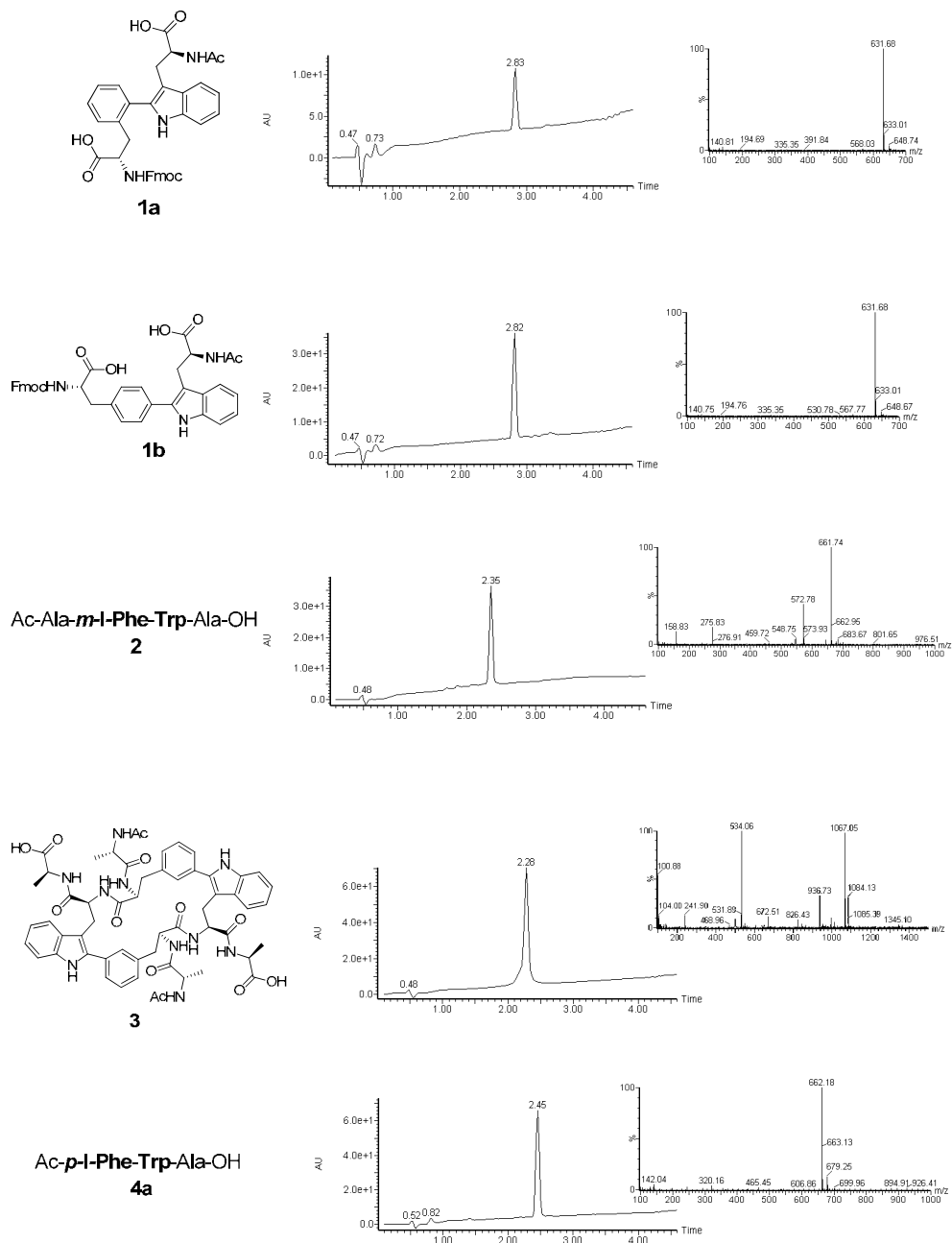
(Cyclo-*p,p*)bis-[Phe-Trp]-cyclo(Phe-Trp) (7c) ^1H - ^{13}C HSQC NMR



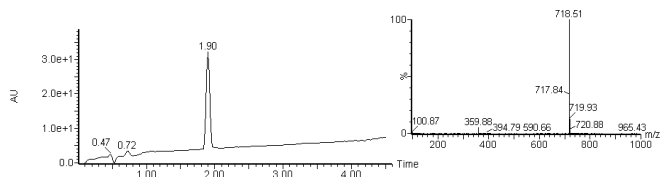
(Cyclo-*p,p*)-bis-[Phe-Trp]-cyclo(Phe-Trp) (7c) TOCSY NMR

(Cyclo-*p,p*)-bis-[Phe-Trp]-cyclo(Phe-Trp) (7c) NOESY NMR

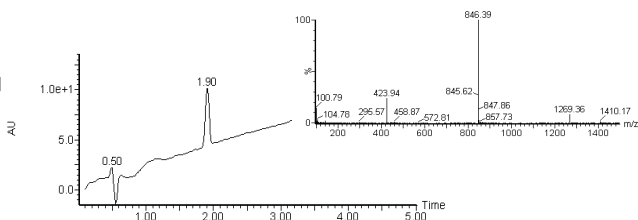
HPLC-MS chromatograms of compounds 1-7



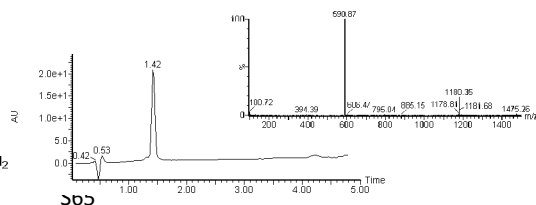
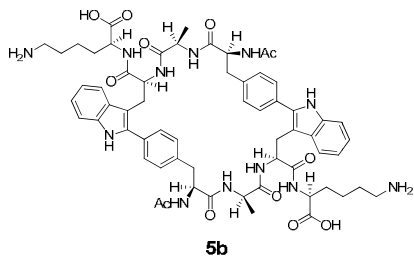
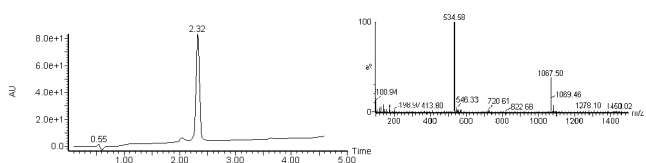
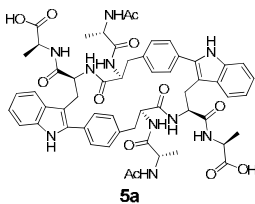
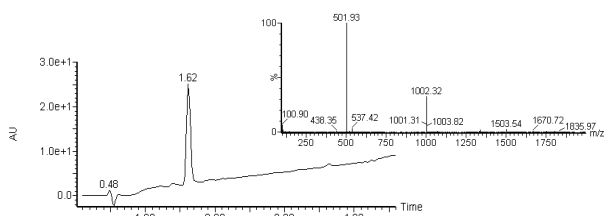
Ac-*p*-I-Phe-Ala-Trp-Lys-OH
4b

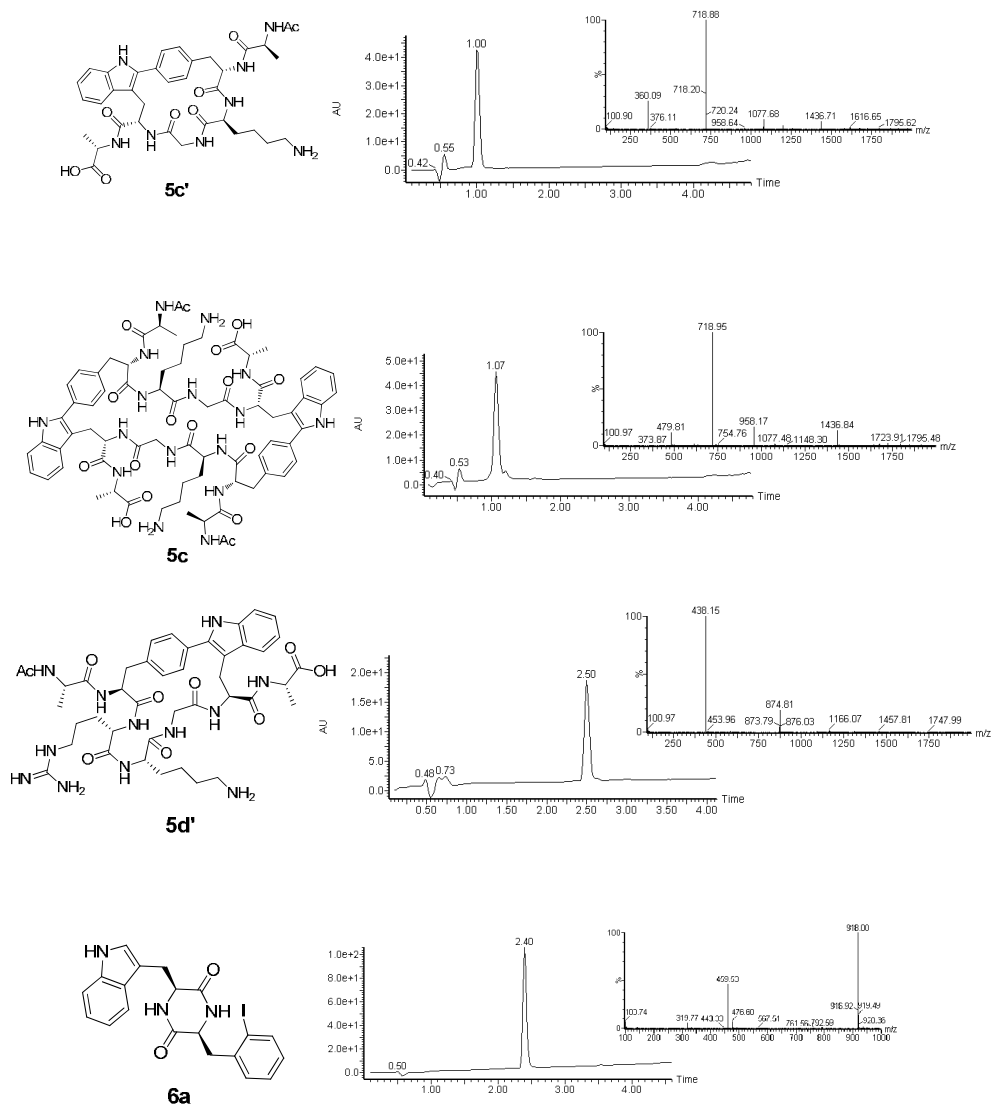


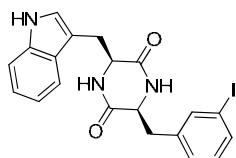
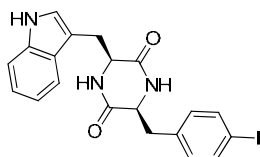
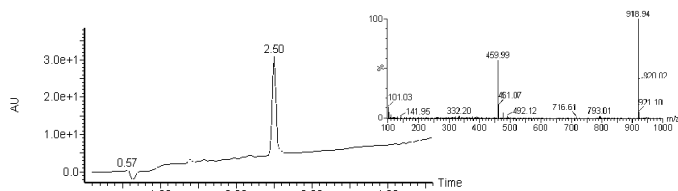
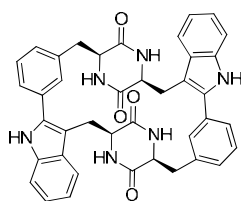
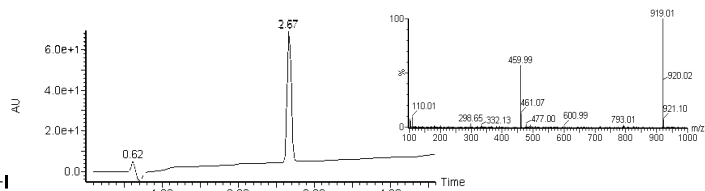
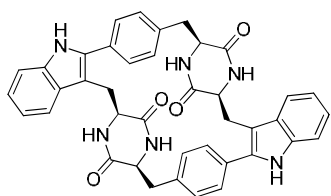
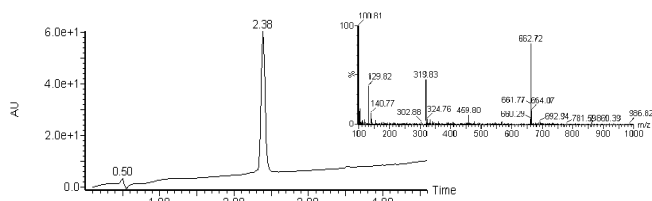
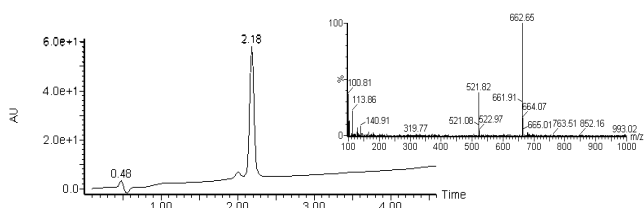
Ac-Ala-*p*-I-Phe-Lys-Gly-Trp-Ala-OH
4c



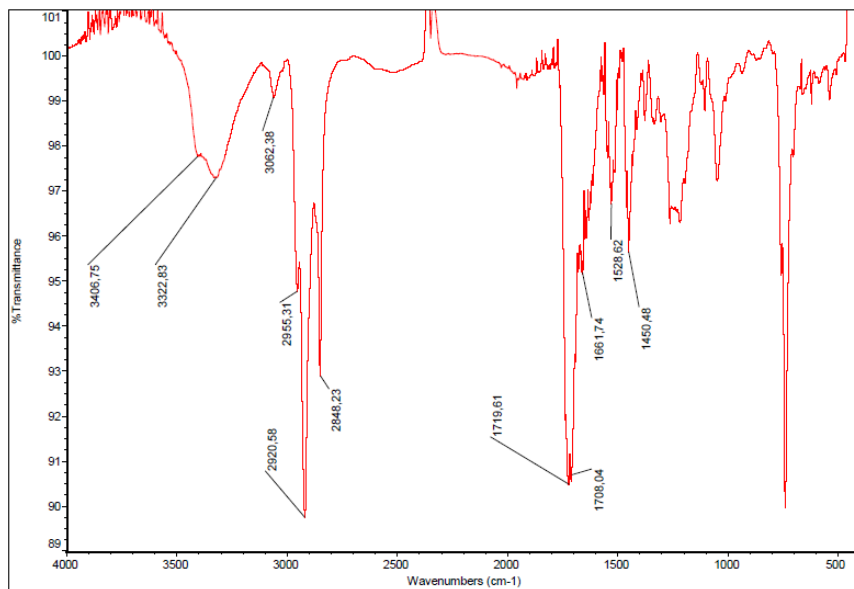
Ac-*p*-I-Phe-Arg-Lys-Gly-Trp-Ala-OH
4d

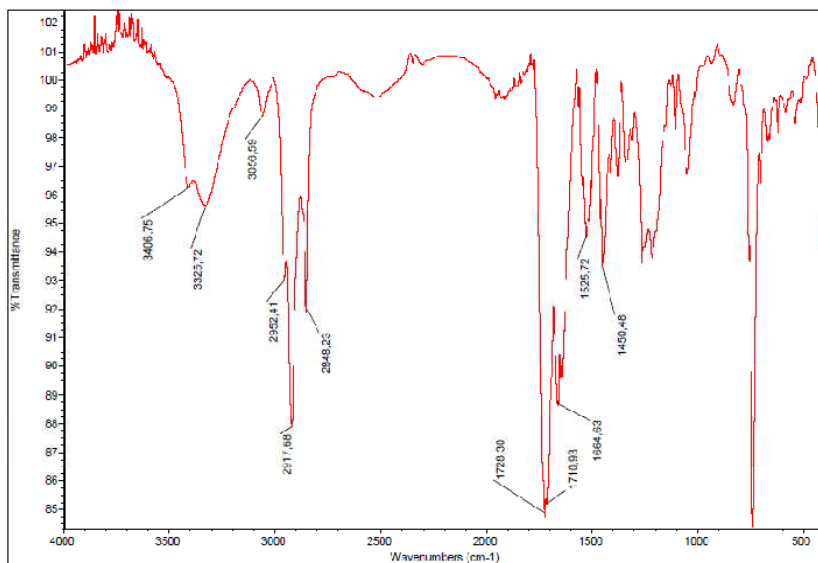
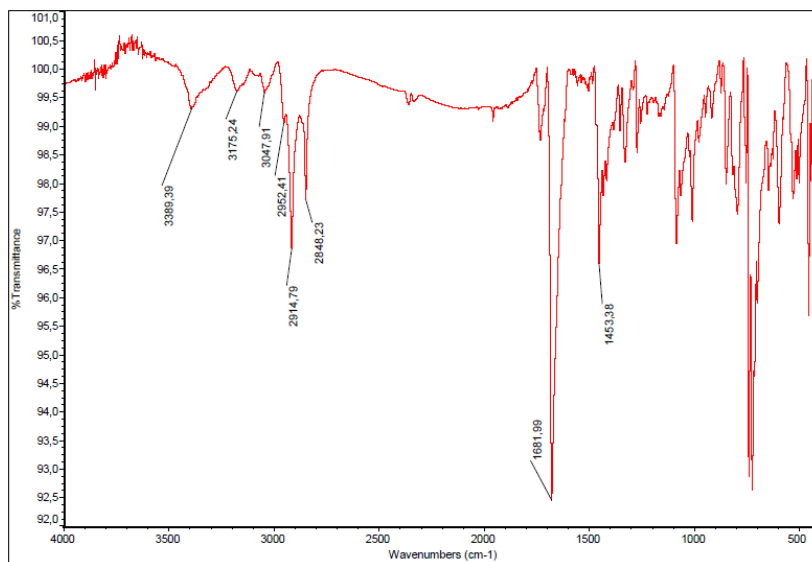


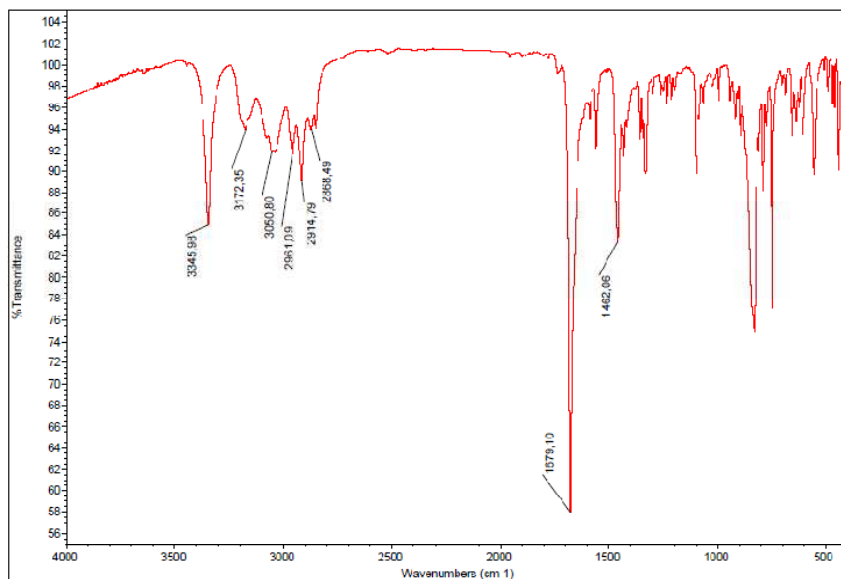
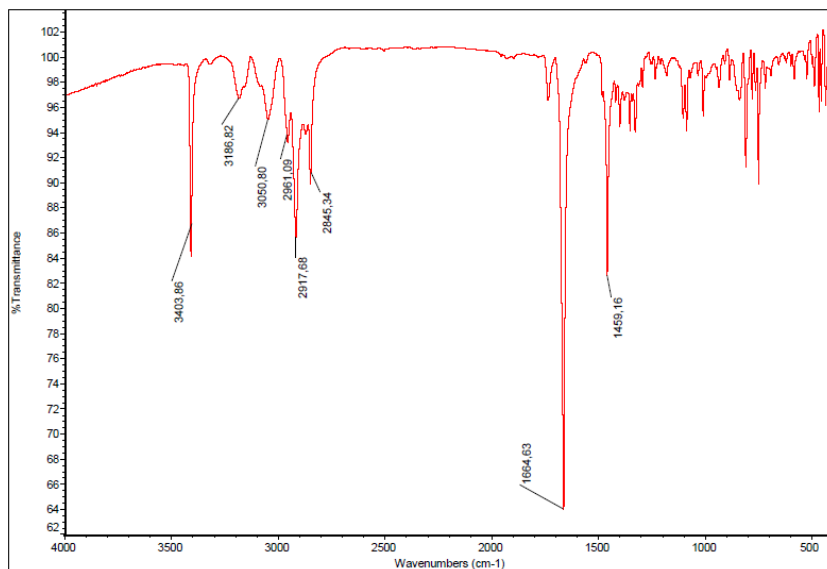


**6b****6c****7b****7c**

Linear gradients of ACN (+0.05% formic acid) into H₂O (+0.1% formic acid) were run at a flow rate of 1.6 mL·min⁻¹ over 3.5 min from 5-100% ACN for compounds **1-4**, **5a** and **6-7**, 20-60% ACN for compounds **5b-c** and 5-30% for compound **5d**.

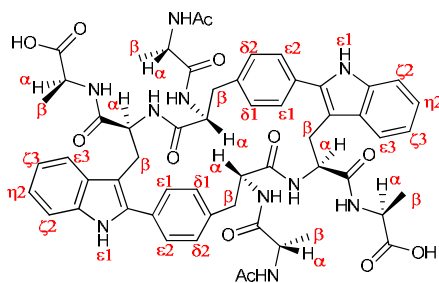
IR spectra of compounds 1 and 6**[Ac-C2-Trp-OH)—(Fmoc-*o*-Phe-OH)] adduct (1a)**

[Ac-C2-Trp-OH]—(Fmoc-*p*-Phe-OH)] adduct (1b)**Cyclo(2-I-Phe-Trp) (6a)**

Cyclo(3-I-Phe-Trp) (6b)**Cyclo(4-I-Phe-Trp) (6c)**

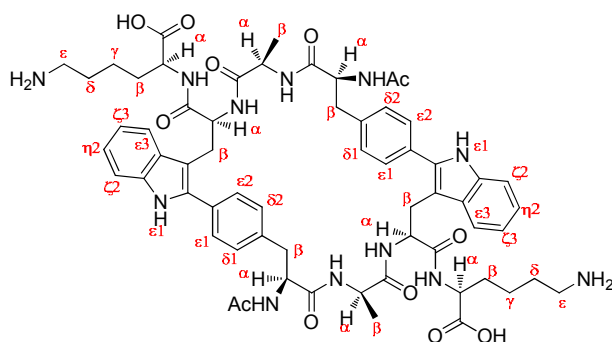
^1H and ^{13}C chemical shifts assignments of compounds 5 and 7

Due to the symmetric nature of dimeric peptides, both peptide moieties are chemically equivalent and have identical NMR signals.



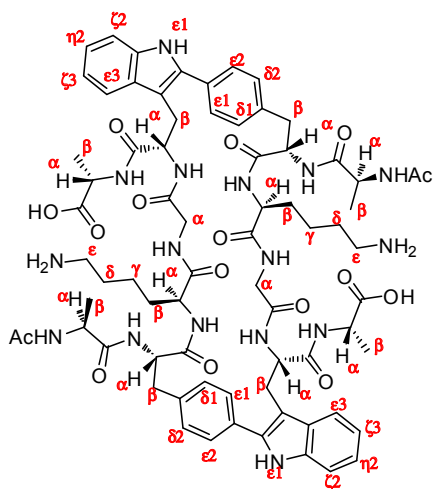
5a (^1H)		δ (ppm)									
AA	NH	α	β	δ 1	δ 2	ϵ 2	ϵ 1	ζ 2	η 2	ζ 3	ϵ 3
Ala1	7.93	4.18	1.08	-	-	-	-	-	-	-	-
<i>p</i> - <i>t</i> -Phe	8.13	3.96	2.64/2.48	7.25	7.25	7.61	7.61	-	-	-	-
Trp	6.82	4.07	3.43/3.43	-	-	-	11.20	7.34	7.11	7.03	7.67
Ala2	7.90	4.21	1.28	-	-	-	-	-	-	-	-

5a (¹³ C)			δ (ppm)							
AA	α	β	δ1	δ2	ε2	ε1	ζ2	η2	ζ3	ε3
Ala1	47.7	17.8	-	-	-	-	-	-	-	-
<i>p</i> - <i>I</i> -Phe	52.9	35.2	128.8	128.8	127.9	127.9	-	-	-	-
Trp	54.9	25.6	-	-	-	-	110.9	121.4	118.5	118.3
Ala2	47.5	17.0	-	-	-	-	-	-	-	-



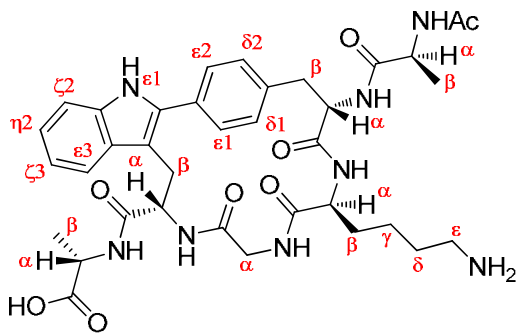
5b (¹ H)		δ (ppm) (T:338 K)										
AA	NH	α	β	δ1	δ2	ε1	ε2	ζ2	η2	ζ3	ε3	γ1
Phe	8.04	4.59	3.01/2.81	7.30	7.30	7.43	7.43	-	-	-	-	-
Ala	8.14	4.14	1.08	-	-	-	-	-	-	-	-	-
Trp	7.49	4.59	3.32/3.13	-	-	10.92	-	7.32	7.08	7.01	7.72	-
Lys	7.29	3.86	1.63-1.16	1.63-1.16	-	2.66	-	-	-	-	-	1.63-1.16

5b (¹³ C)			δ (ppm) (T:338 K)								
AA	α	β	δ1	δ2	ε1	ε2	ζ2	η2	ζ3	ε3	γ1
Phe	53.2	37.2	128.9	128.9	127.4	127.4	-	-	-	-	-
Ala	48.3	17.2	-	-	-	-	-	-	-	-	-
Trp	53.2	27.5	-	-	-	-	110.6	120.6	118.1	119.0	-
Lys	52.8	30.6-26.1	30.6-26.1	-	38.3	-	-	-	-	-	30.6-26.1



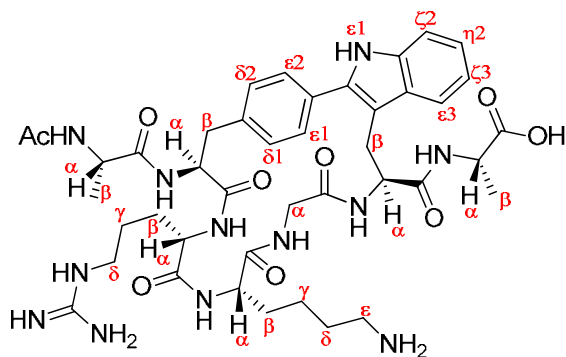
5c (¹ H)		δ (ppm) (T:338 K)											
AA	NH	α	β	δ1	δ2	ε1	ε2	ζ2	η2	ζ3	ε3	γ1	
Ala	8.35 – 7.86	4.20-3.83	1.20-1.11	-	-	-	-	-	-	-	-	-	-
Phe	8.35 – 7.86	4.50	3.05/2.88	7.27	7.27	7.51	7.51	-	-	-	-	-	-
Lys	8.35 – 7.86	4.29	1.68/1.53	1.55	-	2.76	-	-	-	-	-	1.30	-
Gly	8.35 – 7.86	3.76/3.56	-	-	-	-	-	-	-	-	-	-	-
Trp	8.35 – 7.86	4.50	3.43/3.05	-	-	11.10	-	7.29	7.06	6.99	7.70	-	-
Ala	8.35 – 7.86	4.20-3.83	1.20-1.11	-	-	-	-	-	-	-	-	-	-

5c (¹³ C)		δ (ppm) (T:338 K)											
AA	α	β	δ1	δ2	ε1	ε2	ζ2	η2	ζ3	ε3	γ1		
Ala	47.9-48.8	17.6-17.7	-	-	-	-	-	-	-	-	-	-	-
Phe	53.7	36.5	129.2	129.2	127.3	127.3	-	-	-	-	-	-	-
Lys	51.9	30.9	25.7	-	37.4	-	-	-	-	-	-	21.6	-
Gly	42.0	-	-	-	-	-	-	-	-	-	-	-	-
Trp	53.7	42.2	-	-	-	-	110.5	120.8	118.2	118.7	-	-	-
Ala	47.9-48.8	17.6-17.7	-	-	-	-	-	-	-	-	-	-	-



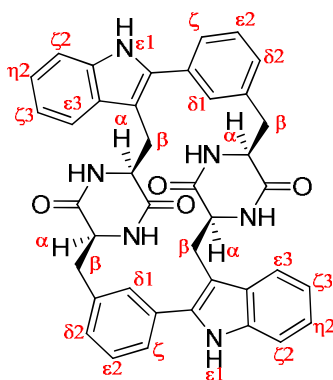
5c' (¹ H)		δ (ppm)										
AA	NH	α	β	δ1	δ2	ε1	ε2	ζ2	η2	ζ3	ε3	γ1
Ala	8.08	4.34	1.19	-	-	-	-	-	-	-	-	-
Phe	8.18	4.68	2.96	7.31	7.31	7.51	7.51	-	-	-	-	-
Lys	8.35	4.19	1.68/1.36	1.49	-	2.72	-	-	-	-	-	1.39/1.26
Gly	6.40	3.56/3.26	-	-	-	-	-	-	-	-	-	-
Trp	7.00	4.48	3.45/3.27	-	-	11.05	-	7.30	7.07	6.96	7.61	-
Ala	8.11	4.14	1.22	-	-	-	-	-	-	-	-	-

5c' (¹³ C)			δ (ppm)								
AA	α	β	δ1	δ2	ε1	ε2	ζ2	η2	ζ3	ε3	γ1
Ala	47.7	17.8	-	-	-	-	-	-	-	-	-
Phe	53.1	37.2	129.3	129.3	127.7	127.7	-	-	-	-	-
Lys	51.4	unknown	26.1	-	38.4	-	-	-	-	-	21.9
Gly	41.8	-	-	-	-	-	-	-	-	-	-
Trp	52.9	unknown	-	-	-	-	110.5	120.8	118.2	118.4	-
Ala	47.6	17.4	-	-	-	-	-	-	-	-	-



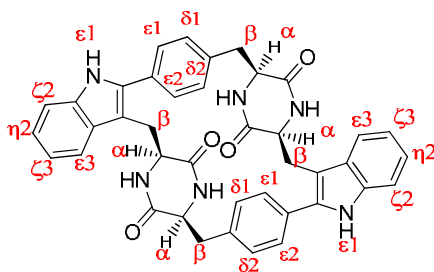
5d' (¹ H)		δ (ppm)										
AA	NH	α	β	δ1	δ2	ε1	ε2	ζ2	η2	ζ3	ε3	γ1
Ala	6.95	3.79	1.13	-	-	-	-	-	-	-	-	-
Phe	7.97	4.56	2.94	7.23	7.23	7.50	7.50	-	-	-	-	-
Arg	7.64	4.22	1.77/1.67	3.12/3.05	-	-	-	-	-	-	-	1.54
Lys	8.02	3.95	1.60	1.61/1.55	-	2.78	-	-	-	-	-	1.40
Gly	8.36	3.95/3.13	-	-	-	-	-	-	-	-	-	-
Trp	8.10	4.30	3.56/3.24	-	-	10.89	-	7.32	7.06	6.99	7.58	-
Ala	8.36	4.30	1.23	-	-	-	-	-	-	-	-	-

5d' (¹³ C)			δ (ppm)								
AA	α	β	δ1	δ2	ε1	ε2	ζ2	η2	ζ3	ε3	γ1
Ala	49.9	19.0	-	-	-	-	-	-	-	-	-
Phe	54.9	38.7	130.3	130.3	128.2	128.2	-	-	-	-	-
Arg	54.1	30.1	41.2	-	-	-	-	-	-	-	25.2
Lys	54.6	30.8	27.1	-	39.2	-	-	-	-	-	22.4
Gly	42.8	-	-	-	-	-	-	-	-	-	-
Trp	49.0	unknown	-	-	-	-	111.3	121.4	118.8	119.3	-
Ala	49.0	18.1	-	-	-	-	-	-	-	-	-



7b (¹H)		δ (ppm)										
AA	NH	α	β	δ1	δ2	ε1	ε2	ζ/ζ2	η2	ζ3	ε3	
Phe	8.26	3.24	2.20/0.24	6.86	6.98	-	7.32	7.20	-	-	-	
Trp	8.51	3.97	3.38/2.99	-	-	11.24	-	7.33	7.08	7.02	7.71	

7b (¹³C)		δ (ppm)							
AA	α	β	δ1	δ2	ε2	ζ/ζ2	η2	ζ3	ε3
Phe	56.6	40.0	130.8	127.7	128.5	127.9	-	-	-
Trp	55.4	27.6	-	-	-	110.7	120.8	118.7	120.0



γ_c (^1H)		δ (ppm)									
AA	NH	α	β	$\delta 1$	$\delta 2$	$\epsilon 1$	$\epsilon 2$	$\zeta 2$	$\eta 2$	$\zeta 3$	$\epsilon 3$
Phe	8.54	4.38	3.36/3.00	7.38	7.38	7.58	7.58	-	-	-	-
Trp	8.32	3.78	2.70/1.33	-	-	10.99	-	7.27	7.04	6.92	7.46

γ_c (^{13}C)		δ (ppm)								
AA	α	β	$\delta 1$	$\delta 2$	$\epsilon 1$	$\epsilon 2$	$\zeta 2$	$\eta 2$	$\zeta 3$	$\epsilon 3$
Phe	55.5	38.2	130.6	130.6	127.0	127.0		-	-	-
Trp	56.2	31.7	-		-	-	110.7	121.5	118.4	117.6

Additional comments on the NMR spectroscopy of cyclopeptides **3** and **5**

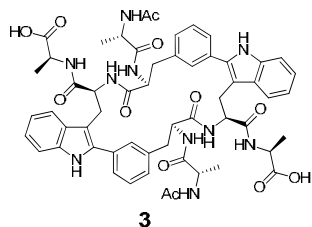
Cyclodimer peptides **3** and **5a-c** were characterized by NMR and indicated a C₂-symmetric structure. Aromatic ring flipping was observed for Phe residues in all peptides. Rapid reorientation about the C β -C γ bond renders the H δ 1/H δ 2 protons on one side and the H ϵ 1/H ϵ 2 protons on the other side, equivalent on the NMR timescale. In agreement with this observation, **5a** was the peptide that showed the largest chemical shift dispersion on the amide NH region at 298 K in all the series. Peptide **5b** showed moderate chemical shift dispersion on the amide region. In contrast, the six amide NH signals of **5c** overlapped at 7.9-8.3 ppm, indicating a significant flexibility.

With respect to cyclopeptides, the Gly residue of peptide **5c'** exhibited significant upfield shifted resonances with chemical shifts of 6.40 (NH) and 3.56/3.26 ppm (H α). Some amide NH resonances of **5b** appear as broad signals at room temperature and sharpen as the temperature was increased.

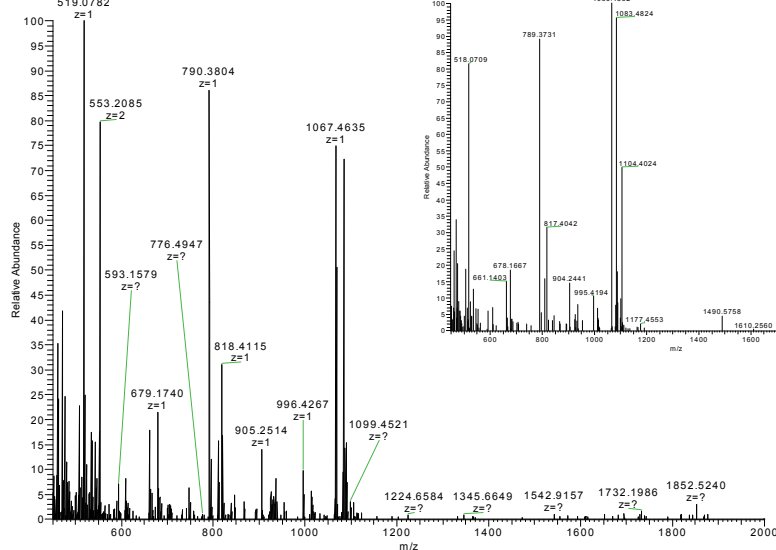
Regarding the DKP structure, cyclodimer formation was characterized by a large diastereotopic splitting of geminal H β protons. This effect was especially pronounced in the Phe H β protons of **7b**, where one Phe H β resonated at 2.20 ppm and the second H β was upfield shifted and appeared at 0.24 ppm.

High resolution mass spectrometry analysis of compounds 3, 5 and 7

Samples were reconstituted in CH₃CN or H₂O/CH₃CN (1:1) 1% Formic acid and diluted in H₂O/CH₃CN (1:1) 1% Formic acid for MS analysis. Ion deconvolution to zero charged monoisotopic masses was performed using Xtract algorithm in Xcalibur software.

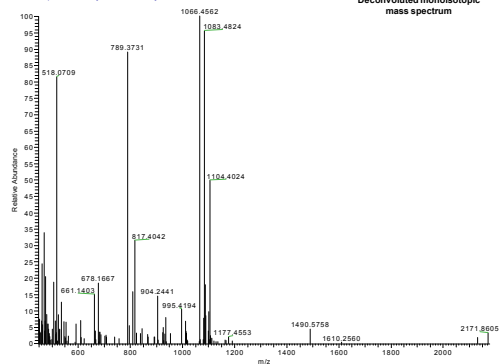


LMT_246.7.2_av25 #1 RT: 2.27 AV: 1 NL: 3.24E4
T: FTMS + p NSI Full ms [450.00-2000.00]
519.0782



LMT_246.7.2_av25.XT.00001.M.#2 RT: 2.00 AV: 1 NL: 5.12E4
T: FTMS + p NSI Full ms [450.00-2000.00]

Deconvoluted monoisotopic mass spectrum

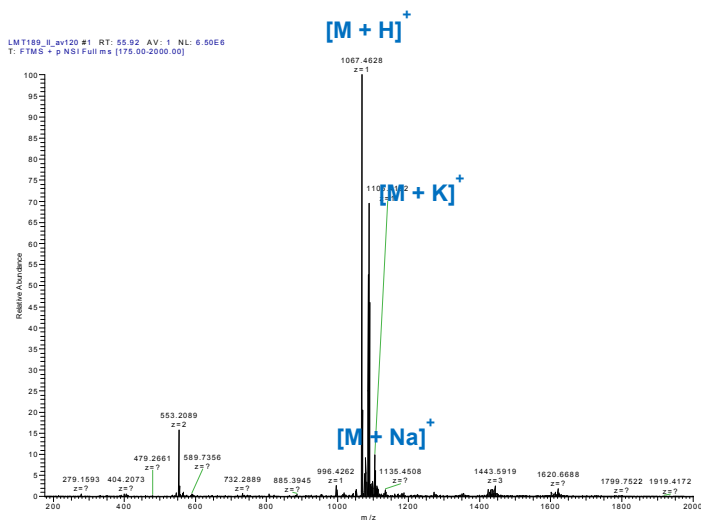
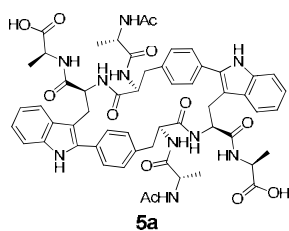


Elemental composition search on mass 1066.46

m/z = 1061.46-1071.46

m/z	Theo. Mass	Delta (ppm)	RDB equiv.	Composition
1066.45620	1066.45621	-0.01	30.5	C ₅₈ H ₆₄ O ₁₃ N ₇
	1066.45487	1.25	31.0	C ₅₆ H ₆₂ O ₁₂ N ₁₀
	1066.45755	-1.26	35.5	C ₅₉ H ₆₀ O ₉ N ₁₁
	1066.45755	-1.27	30.0	C ₆₀ H ₆₆ O ₁₄ N ₄
	1066.45084	5.02	27.0	C ₅₁ H ₆₂ O ₁₄ N ₁₂
	1066.46342	-6.77	26.5	C ₅₂ H ₆₄ O ₁₄ N ₁₁
	1066.44631	9.27	35.5	C ₆₀ H ₆₀ O ₁₀ N ₉
	1066.46610	-9.28	31.0	C ₅₅ H ₆₂ O ₁₁ N ₁₂

HRMS (ESI) (m/z): [M] calcd. for C₅₆H₆₂N₁₀O₁₂, 1066.45487; found, 1067.45620.



Elemental composition search on mass 1067.46

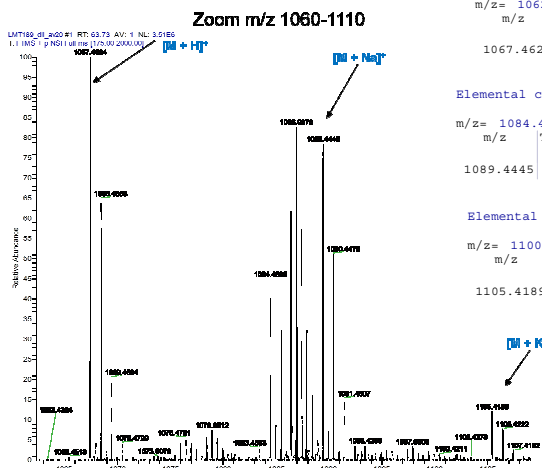
m/z	Theo. Mass	Delta (ppm)	RDB equiv.	Composition
1067.4624	1067.4621	0.22	30.5	$^{12}C_{56}H_{62}O_{12}N_{10}$
$[M + H]^+$				

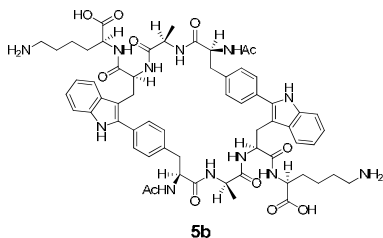
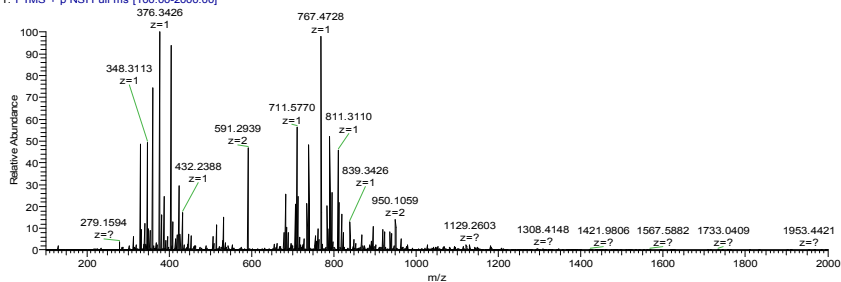
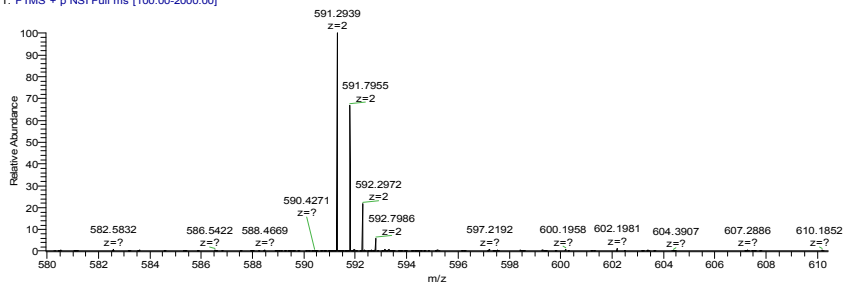
Elemental composition search on mass 1089.44

m/z	Theo. Mass	Delta (ppm)	RDB equiv.	Composition
1089.4445	1089.4441	0.42	30.5	$^{12}C_{56}H_{62}O_{12}N_{10}^{23}Na_1$
$[M + Na]^+$				

Elemental composition search on mass 1105.42

m/z	Theo. Mass	Delta (ppm)	RDB equiv.	Composition
1105.4189	1105.4180	0.76	30.5	$^{12}C_{56}H_{62}O_{12}N_{10}^{39}K_1$
$[M + K]^+$				

HRMS (ESI) (m/z): $[M + H]^+$ calcd. for $C_{56}H_{62}N_{10}O_{12}$, 1067.4621; found, 1067.4624.

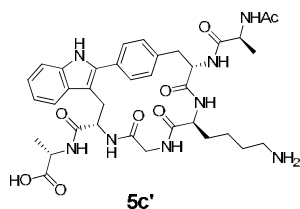
H₂O/ACN 1%FALMT253A_av150 #1 RT: 49.66 AV: 1 NL: 7.31E5
T: FTMS + p NSI Full ms [100.00-2000.00]LMT253A_av150 #1 RT: 49.66 AV: 1 NL: 3.41E5
T: FTMS + p NSI Full ms [100.00-2000.00]

Elemental composition search on mass 591.29

m/z = 586.29-596.29

m/z	Theo. Mass	Delta (ppm)	RDB equiv.	Composition
591.29388	591.29390	-0.03	34.5	C ₆₅ H ₇₆ O ₉ N ₁₃
	591.29323	1.10	29.5	C ₆₄ H ₈₀ O ₁₃ N ₉
	591.29256	2.23	30.0	C ₆₂ H ₇₈ O ₁₂ N ₁₂
	591.29684	-5.00	25.5	C ₅₈ H ₈₀ O ₁₄ N ₁₃
	591.29055	5.64	26.0	C ₅₇ H ₇₈ O ₁₄ N ₁₄
	591.29818	-7.27	30.0	C ₆₁ H ₇₈ O ₁₁ N ₁₄
	591.29885	-8.40	29.5	C ₆₃ H ₈₀ O ₁₂ N ₁₁
	591.29952	-9.54	29.0	C ₆₅ H ₈₂ O ₁₃ N ₈

← [M+2H]²⁺HRMS (ESI): (M: C₆₂H₇₆O₁₂N₁₂) m/z calcd 591.29390, found 591.29388 [(M+2H)/2]²⁺.

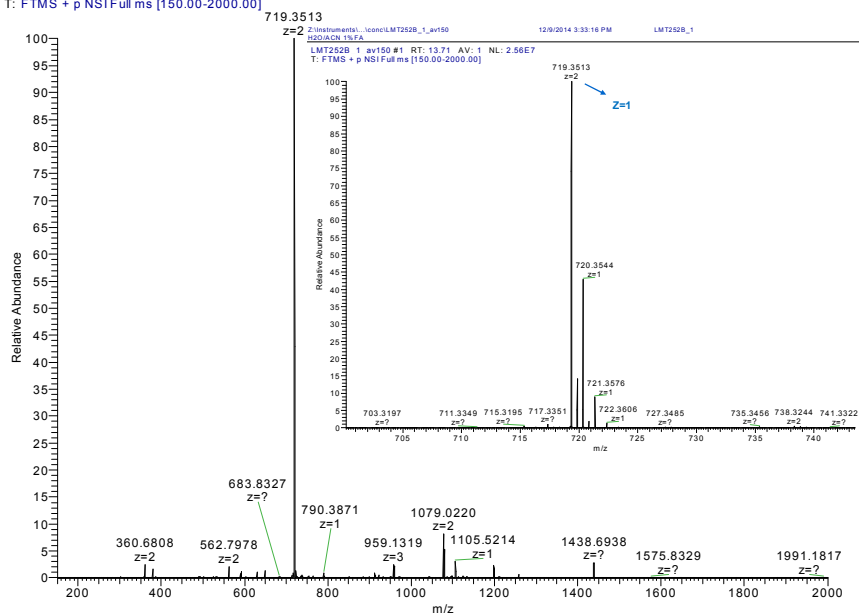


Z:\Instruments\...lconcl\MT252B_1_av150
H2O/ACN 1%FA

12/9/2014 3:33:16 PM

LMT252B_1

LMT252B_1_av150 #1 RT: 13.71 AV: 1 NL: 2.56E7
T: FTMS + p NSI Full ms [150.00-2000.00]

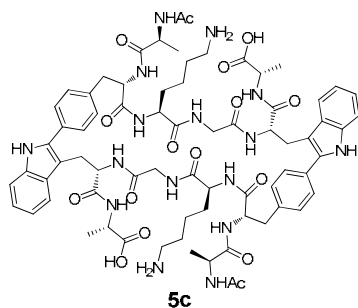


Elemental composition search on mass 719.35

m/z = 714.35-724.35

m/z	Theo. Mass	Delta (ppm)	RDB equiv.	Composition
719.35134	719.35114	0.28	17.5	C ₃₆ H ₄₇ O ₈ N ₈ ← [M+H] ⁺
	719.35248	-1.58	17.0	C ₃₈ H ₄₉ O ₉ N ₅
	719.35382	-3.44	22.0	C ₃₉ H ₄₅ O ₅ N ₉

HRMS (ESI): (M: C₃₆H₄₆N₈O₈) m/z calcd. 719.35114, found 719.35134 (M+H)⁺.



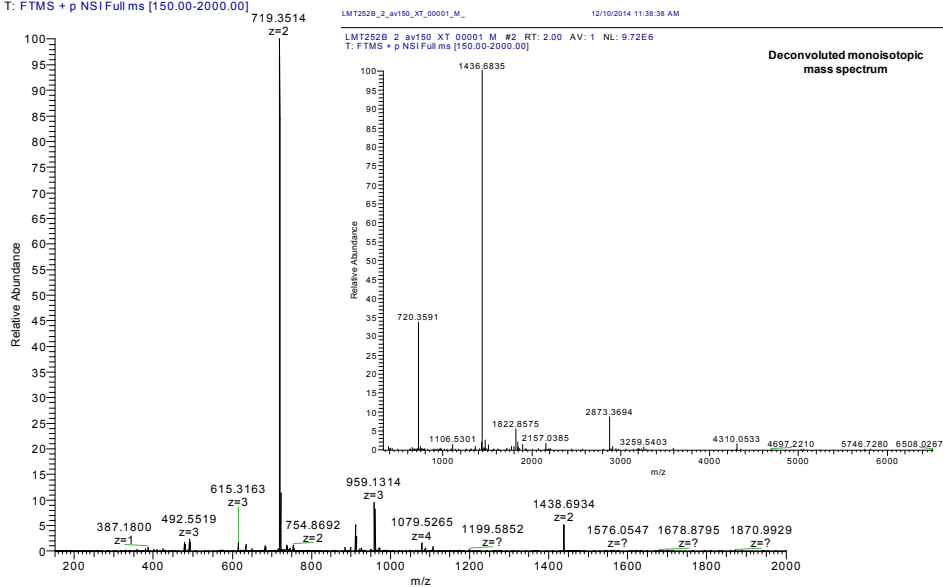
Z:\Instrumental\...lconcl\MT252B_2_av150
H2O/ACN 1%FA

12/9/2014 3:36:32 PM

LMT252B_2

LMT252B_2_av150 #1 RT: 16.99 AV: 1 NL: 7.36E6
T: FTMS + p NSI Full ms [150.00-2000.00]

LMT252B_2_av150_XT_00001_M_ 12/10/2014 11:38:38 AM
LMT252B_2_av150 XT_00001 M #2 RT: 2.00 AV: 1 NL: 9.72E6
T: FTMS + p NSI Full ms [150.00-2000.00]

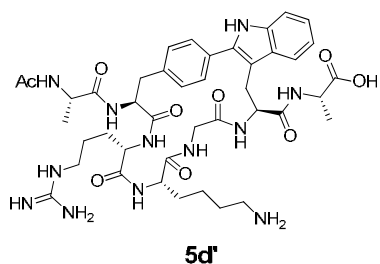


Elemental composition search on mass 1436.68

m/z = 1431.68-1441.68

m/z	Theo. Mass	Delta (ppm)	RDB equiv.	Composition
1436.68351	1436.68772	-2.93	35.0	C ₇₂ H ₉₂ O ₁₆ N ₁₆ ← [M]
	1436.68906	-3.87	34.5	C ₇₄ H ₉₄ O ₁₇ N ₁₃
	1436.67649	4.89	35.0	C ₇₃ H ₉₂ O ₁₇ N ₁₄
	1436.67514	5.82	35.5	C ₇₁ H ₉₀ O ₁₆ N ₁₇

HRMS (ESI): (M: C₇₂H₉₂N₁₆O₁₆) m/z calcd. 1436.68772, found 1436.68351 (M).

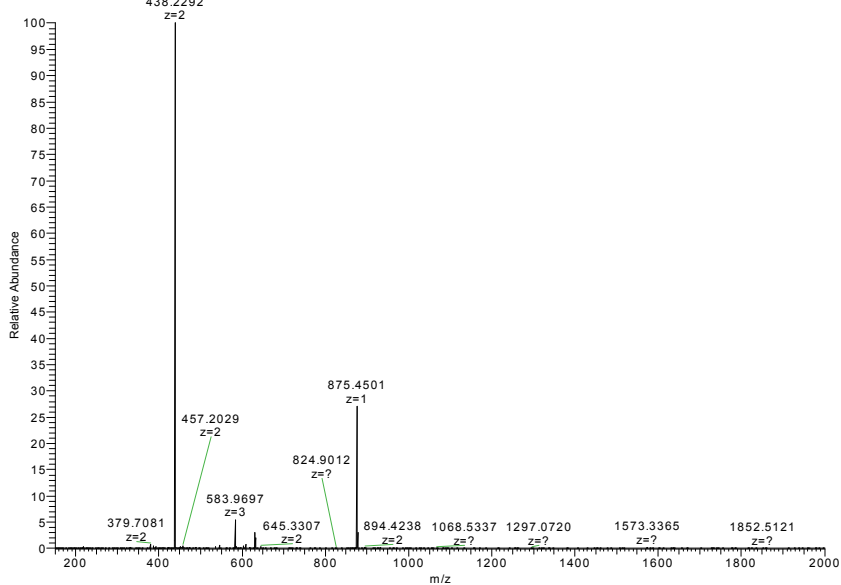


Z:\Instruments\...Iconc\LMT252C_av50
H2O/ACN 1%FA

12/9/2014 3:38:17 PM

LMT252C

LMT252C_av50 #1 RT: 18.75 AV: 1 NL: 9.02E6
T: FTMS + p NSI Full ms [150.00-2000.00]
438.2292



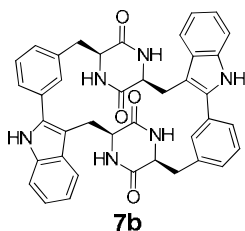
Elemental composition search on mass 875.45

m/z = 870.45-880.45

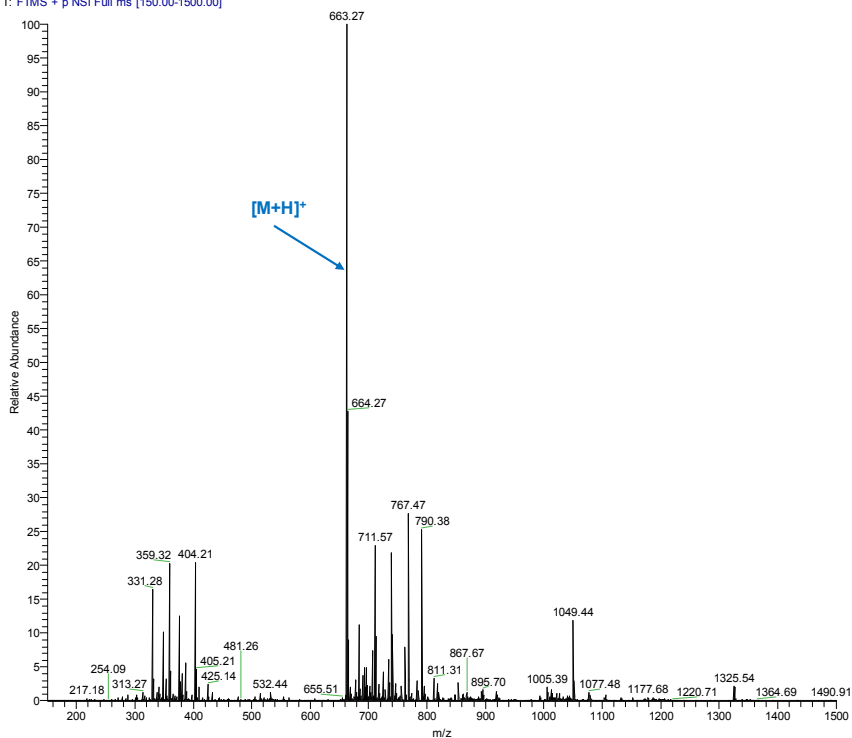
m/z	Theo. Mass	Delta (ppm)	RDB equiv.	Composition
875.45014	875.44822	2.19	15.5	C ₃₇ H ₅₉ O ₁₁ N ₁₄
	875.45225	-2.41	19.5	C ₄₂ H ₅₉ O ₉ N ₁₂
	875.45359	-3.94	19.0	C ₄₄ H ₆₁ O ₁₀ N ₉
	875.44235	8.90	24.5	C ₄₄ H ₅₅ O ₆ N ₁₄

← [M]

HRMS (ESI): (M: C₄₂H₅₈N₁₂O₉) m/z calcd. 875.44822, found 875.45014 (M+H)⁺.



2066_LM_ABJ2q_150_1500 #1 RT: 52.06 AV: 1 NL: 6.36E6
T: FTMS + p NSI Full ms [150.00-1500.00]

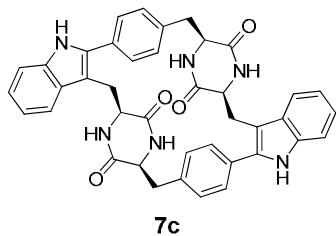


Elemental composition search on mass 663.27

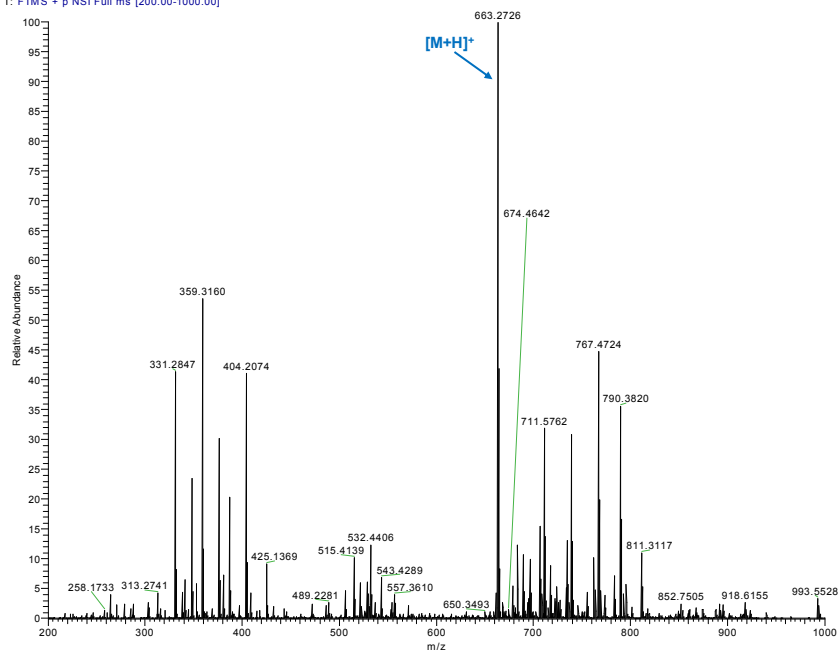
m/z = 658.27-668.27

m/z	Theo. Mass	Delta (ppm)	RDB equiv.	Composition
663.2707	663.2714	-1.12	26.5	$^{12}\text{C}_{40}\text{H}_{35}\text{O}_4\text{N}_6$ [M+H]⁺

HRMS (ESI): (M: $\text{C}_{40}\text{H}_{34}\text{O}_4\text{N}_6$) m/z calcd 663.2707, found 663.2714 (M+H)⁺.



2085_LM_ABJ11m_av60 #1 RT: 2.22 AV: 1 NL: 1.91E6
T: FTMS + p NSI Full ms [200.00-1000.00]



Elemental composition search on mass 663.27

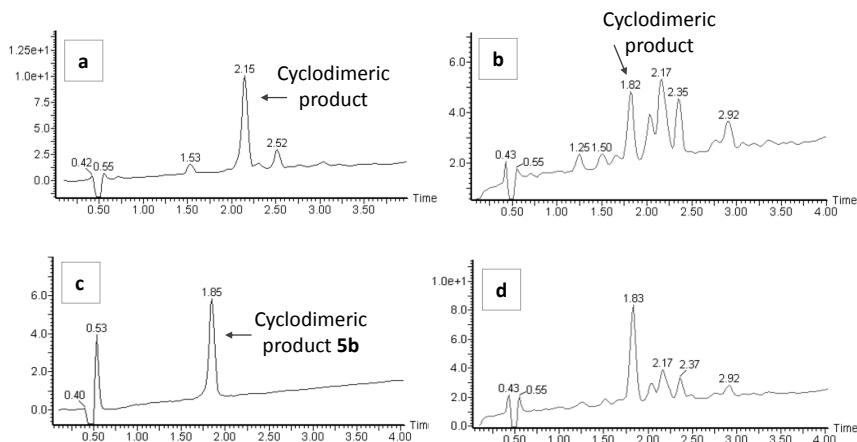
m/z = 658.27-668.27

m/z	Theo. Mass	Delta (ppm)	RDB equiv.	Composition
663.2726	663.2714	1.69	26.5	¹² C ₄₀ H ₃₅ O ₄ N ₆ [M+H] ⁺

HRMS (ESI): (M: C₄₀H₃₄O₄N₆) m/z calcd 663.2726, found 663.2714 (M+H)⁺.

HPLC-MS chromatograms relative to C-H activation on resin

In a preliminary procedure, N-terminal acetylated Ala-*m*-*p*-I-Phe-Trp-Ala sequences anchored to a low functionalized TentaGel resin (f: 0.9 mmol/g resin) provided with (3-(4-hidroxymethylphenoxy)-propionic acid linker were subjected to a Pd-catalyzed coupling on-resin. The same trends were obtained compared to solution C-H arylation procedure and the corresponding cyclodimers were detected.



[a] Intermolecular C-H activation of Ala-*m*-I-Phe-Trp-Ala sequence on-resin to yield presumably the corresponding cyclodimeric product. [b] C-H activation of Ala-*p*-I-Phe-Trp-Ala sequence on-resin to yield the corresponding cyclodimeric product. [c] Isolated cyclodimeric product **5a**. [d] Co-elution of the crude relative to Ala-*p*-I-Phe-Trp-Ala C-H activation reaction with the isolated cyclodimeric product **5a**. Reaction conditions: 5 mol % Pd(OAc)₂, AgBF₄ (1.0 eq.), 2-nitrobenzoic acid (1.5 eq.) in DMF, MW 90 °C, 20 min. All the peptides were cleaved from the resin with TFA-DCM (95:5), r.t, 1h to be analyzed by HPLC-MS. Gradient from 30 to 50% ACN (0,1% FA).

Emac values of compounds 3 and 5

Recently, James group reported a quantitative index for the macrocyclization efficiency (Emac) which is proportional to the concentration and the yield of the reaction:⁵

$$\text{Emac} = \log_{10}[Y^3 \times C]$$

where, Y = yield in %; C = concentration in mM

We calculated the Emac values for the following peptides:

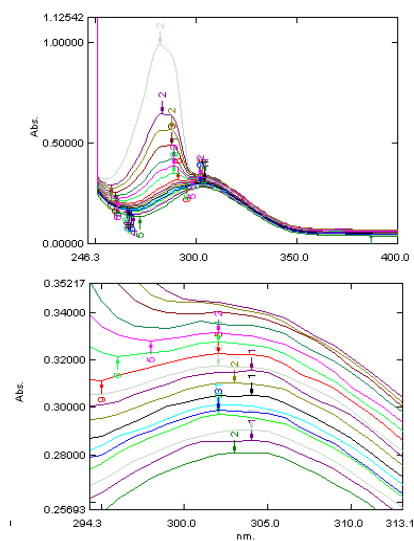
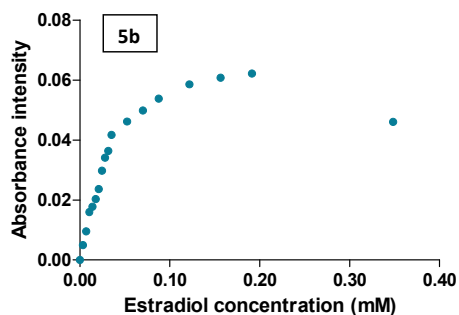
Compound	[C] (mM)	Yield (%) ^a	Emac
Ac-(Cyclo- <i>m</i>)-[Phe -Asn-Gly-Arg- Trp]-OH ³	110	77	7.70
Ac-(Cyclo- <i>m</i>)-[Phe -Arg-Gly-Asp- Trp]-NH ₂ ³	112	70	7.58
H-Ala-(Cyclo- <i>m</i>)-[Phe -Ser-Ala- Trp]-Ala-OH ³	78	39	6.66
Ac-Ala-(Cyclo- <i>m</i>)-[Phe -Val- Trp]-Ala-OH ³	187	71	7.83
(Cyclo- <i>m,m</i>)bis-[Phe-Trp]-(Ac-Ala- Phe - Trp -Ala-OH) (3)	151	48	7.22
(Cyclo- <i>p,p</i>)bis-[Phe-Trp]-(Ac-Ala- Phe - Trp -Ala-OH) (5a)	151	41	7.02
(Cyclo- <i>p,p</i>)bis-[Phe-Trp]-(Ac- Phe -Ala- Trp -Lys-OH) (5b)	240	54	7.58
(Cyclo- <i>p,p</i>)bis-[Phe-Trp]-(Ac-Ala- Phe -Lys-Gly- Trp -Ala-OH) (5c)	236	23	6.46
Ac-Ala-(Cyclo- <i>p</i>)-[Phe -Lys-Gly- Trp]-Ala-OH (5c')	236	51	7.50
Ac-Ala-(Cyclo- <i>p</i>)-[Phe -Arg-Lys-Gly- Trp]-Ala-OH (5d')	100	81	7.72

^a Yields are from conversions estimated by HPLC-MS.

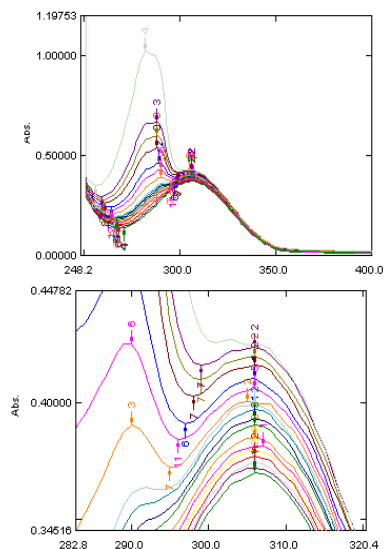
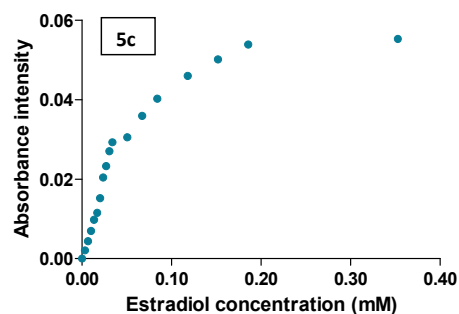
Preliminary absorbance host-guest complexation experiments of compounds **5b** and **5c**

Increasing amounts of estradiol were added to **5b** or **5c** 0.01 mM solutions in MeOH and the corresponding absorbance intensity changes were measured with a UV-VIS.

a)

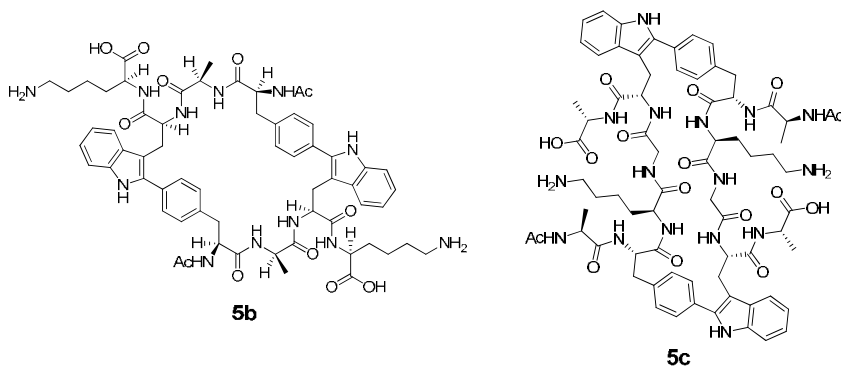


b)

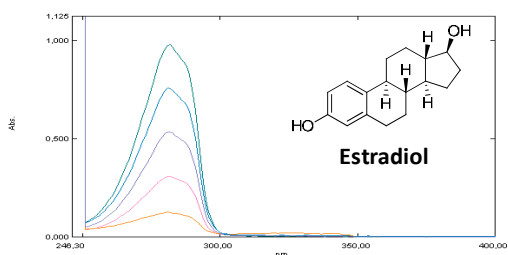
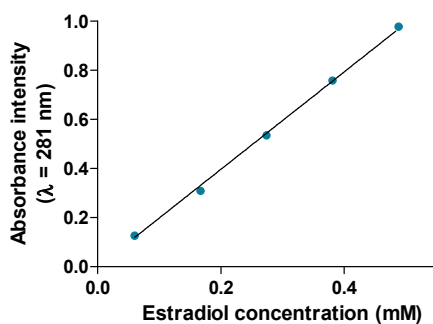


Absorbance intensity changes in MeOH of (a) **5b** (0.015 mM) at $\lambda = 303$ nm upon the addition of estradiol (from 0 to 0.35 mM) and (b) **5c** (0.014 mM) at $\lambda = 306$ nm upon the addition of estradiol (from 0 to 0.35 mM).

Taking into account that the presence of charged or hydrophilic amino acids (i.e. Lys) in the hosts may improve the binding with anionic guests,⁵ we have prepared the cyclodimers **5b** and **5c**. However, the study of the interaction with cholic acid did not show strong evidences of binding.

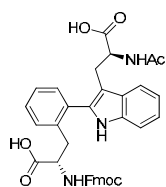
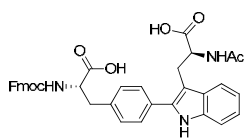
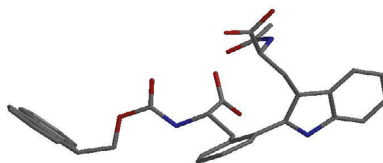
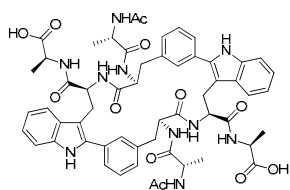
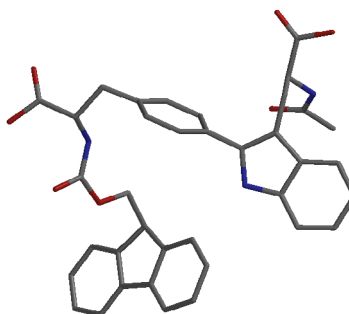
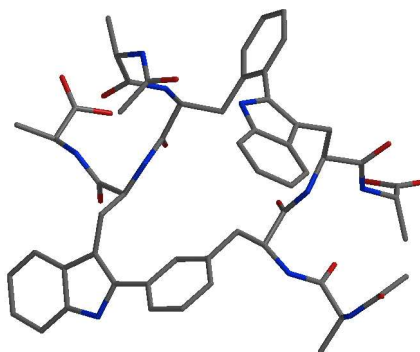


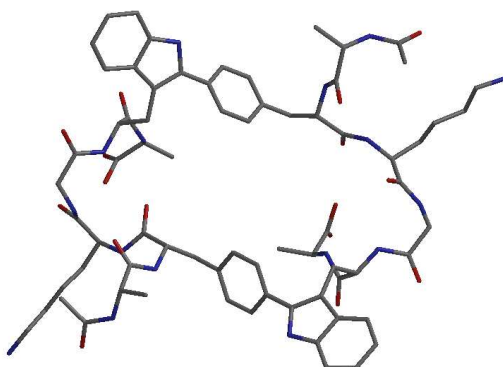
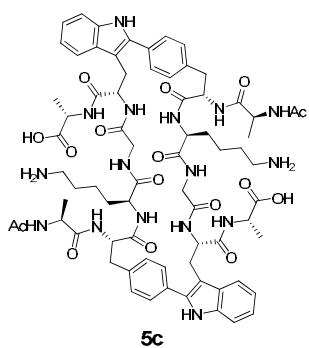
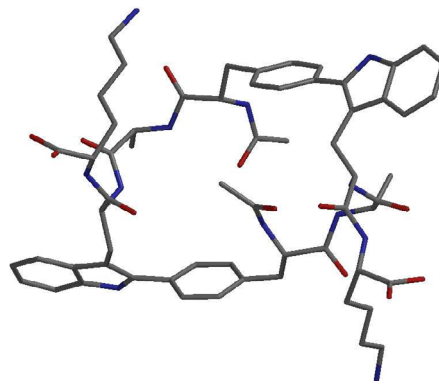
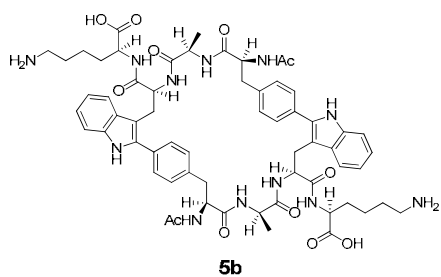
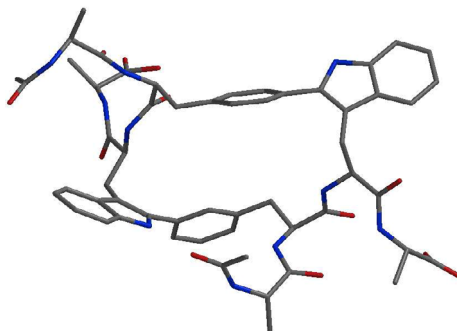
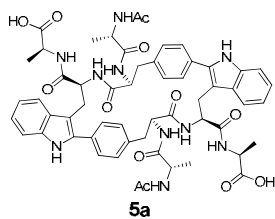
As a negative control, the absorbance intensity of Increasing estradiol solutions was measured at $\lambda = 281, 303$ and 306 nm.

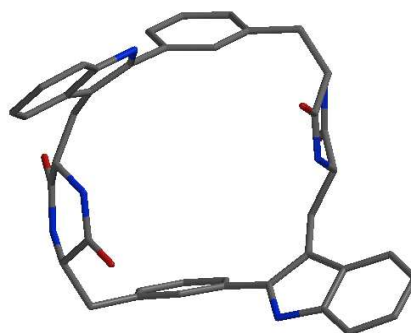
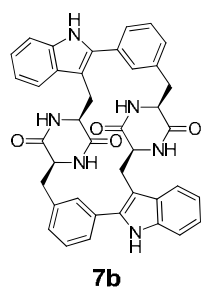
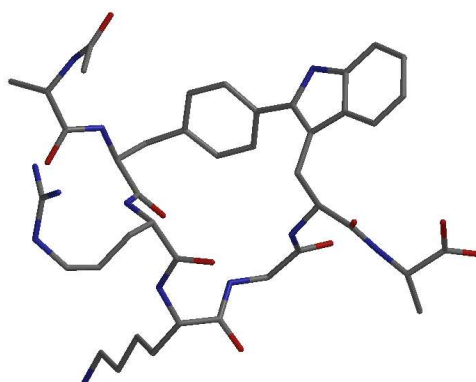
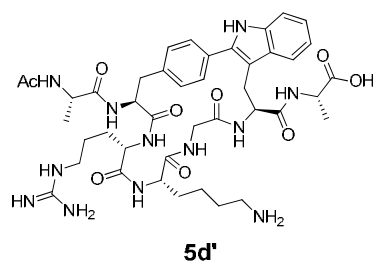
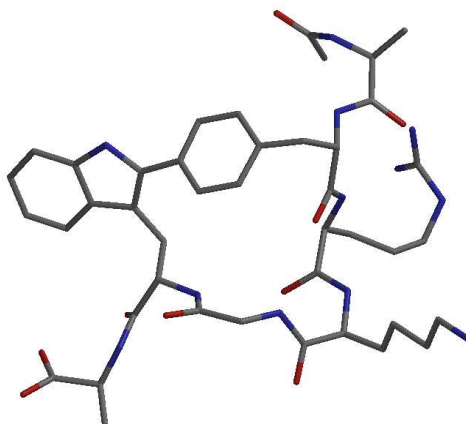
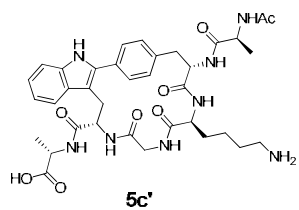


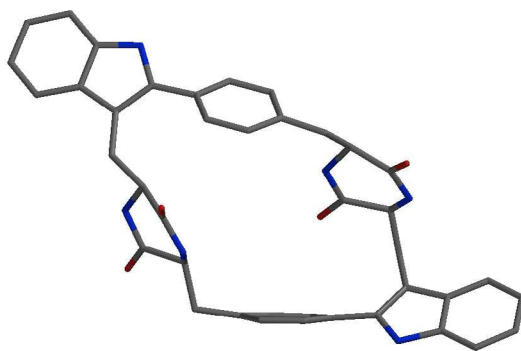
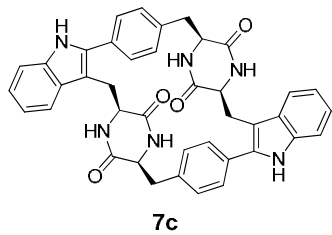
[estradiol] mM	A (λ: 281 nm)	A (λ: 303 nm)	A (λ: 306 nm)
0.488	0.977	0.005	0.014
0.381	0.758	0.009	0.016
0.274	0.535	0.006	0.011
0.167	0.309	0.007	0.010
0.060	0.126	0.015	0.015

Minimized geometries of compounds 1, 3, 5 and 7 generated by the Spartan '14 suite (Semi-Empirical, AM1)⁴ Hydrogens omitted for clarity.

**1a****1b****3**

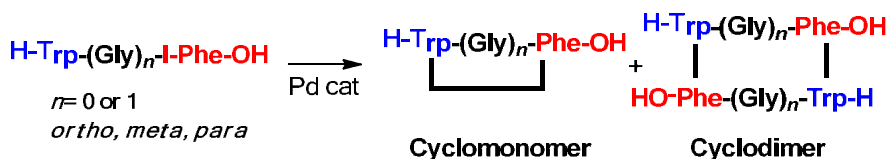






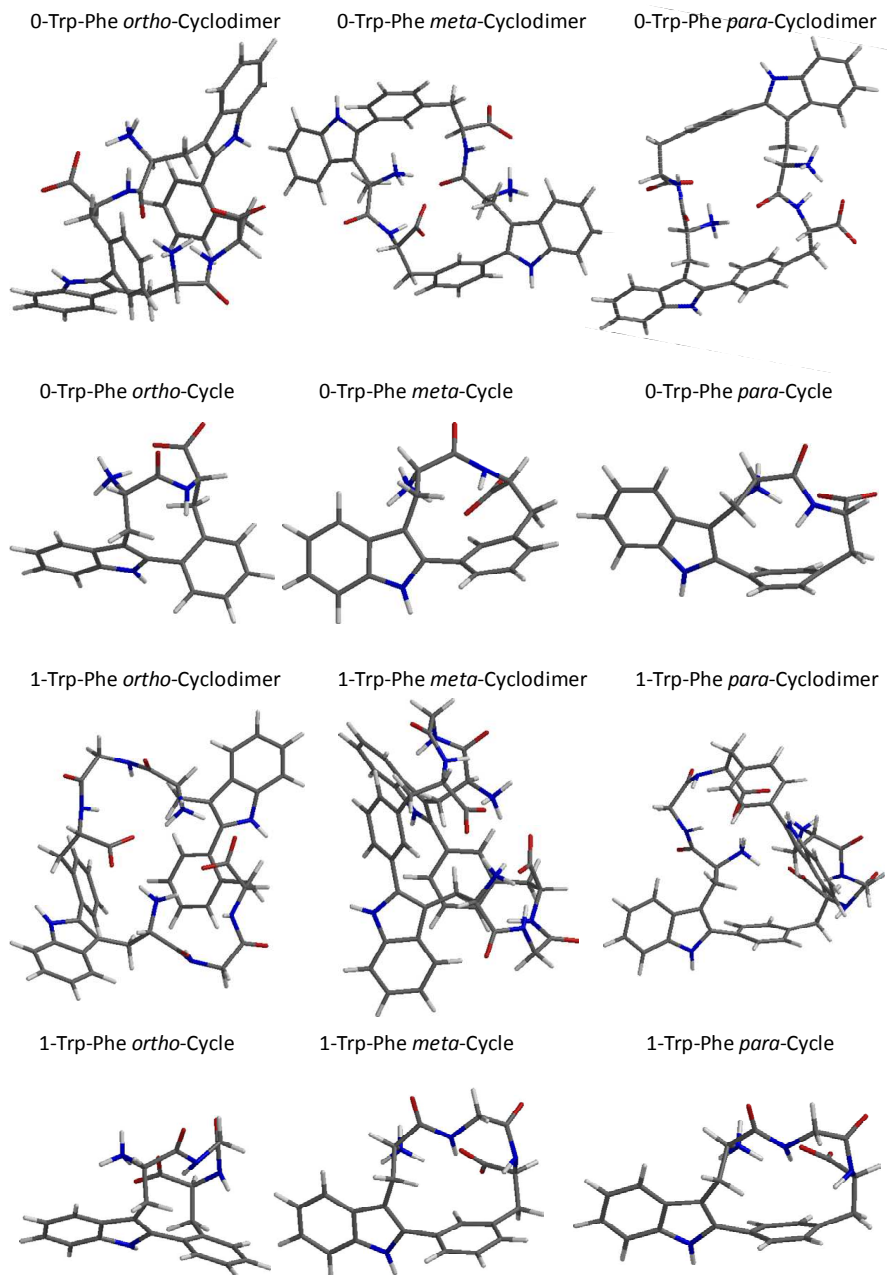
Preliminary calculations on the relative stabilities of the cyclic/cyclodimeric peptides after the Pd-catalyzed CH activation reaction

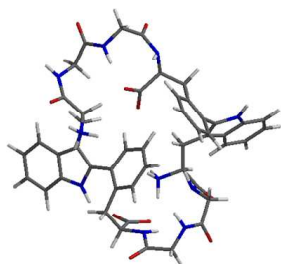
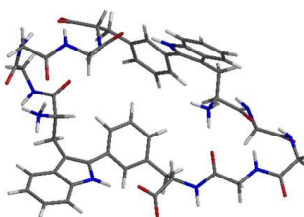
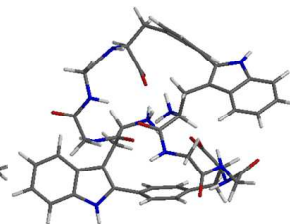
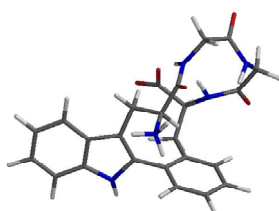
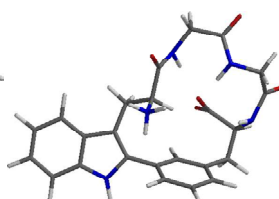
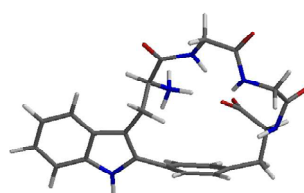
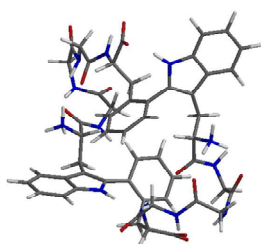
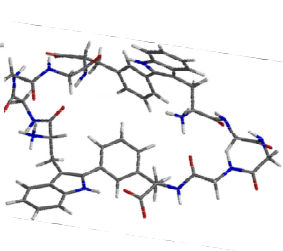
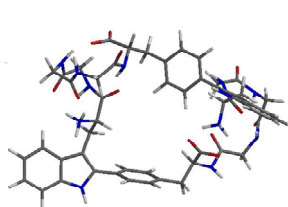
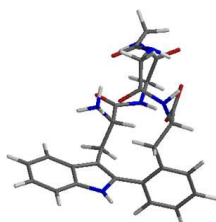
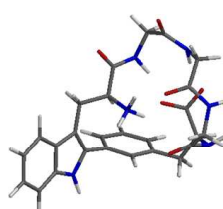
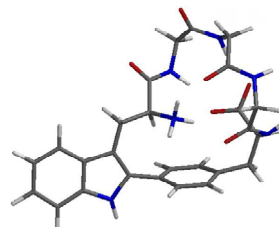
Estimation of the stabilities of the putative cyclic and cyclodimeric peptides arising from the Pd-catalyzed C-H activation upon the parent Trp-(Gly)_n-(I)Phe peptides, displaying different spacer lengths ($n=0$ or 1) and regiochemistries (*ortho*, *meta* and *para*).



Data referring to the equilibrium geometries of the products, optimized through molecular mechanics (MMFF) and semiempirical methods (PM3), implemented in a Spartan suite.⁴ For the sake of comparison, and as a rule of thumb, the cyclodimers may account for twice the enthalpy barrier to formation of their cyclic counterparts.

SIZE/Regio	CYCLOMONOMER calc. Enthalpy barrier to fotation (kJ/mol)	CYCLOMONOMER exp. Detection	CYCLODIMER calc. Enthalpy barrier to formation (kJ/mol)	CYCLODIMER exp. Detection
0-ortho	-58.451	×	-222.670	×
0-meta	-74.395	×	-283.809	ISOLATED
0-para	-26.863	×	-286.967	ISOLATED
1-ortho	-237.066	×	-709.951	×
1-meta	-273.213	ISOLATED	-708.951	×
1-para	-251.280	×	-737.138	ISOLATED



2-Trp-Phe *ortho*-Cyclodimer2-Trp-Phe *meta*-Cyclodimer2-Trp-Phe *para*-Cyclodimer2-Trp-Phe *ortho*-pCycle2-Trp-Phe *meta*-Cycle2-Trp-Phe *para*-Cycle3-Trp-Phe *ortho*-Cyclodimer3-Trp-Phe *meta*-Cyclodimer3-Trp-Phe *para*-Cyclodimer3-Trp-Phe *ortho*-Cycle3-Trp-Phe *meta*-Cycle3-Trp-Phe *para*-Cycle

Although qualitatively, the preliminary estimations fit quite reasonably with the observed results for the models with smaller size ($n=0, 1$).

Additional calculations on the remaining series ($n=2, 3$) are not conclusive at this point due to the fact that the conformational space relative to these compounds is much bigger and the possibility of dealing with local minima may bias the calculations. This makes difficult an appraisal of the chemical evolution regarding cyclization or cyclodimerization. Even so, it has to be said, that for these species, if the cyclization is energetically accessible, although it may not be as stable as the cyclodimer, likely it may be generated at faster rates because of entropic factors.

Ortho-regiochemistries seem to lead to strained geometries, which for the cases analyzed ($n=0, 1$), no adducts have been detected (neither cyclomonomers nor cyclodimers). On the other hand, *meta*-arrangements, lead to very strained unstable structures on the peptide featuring adjacent amino acids ($n=0$), then leading to cyclodimer; whereas for the spacer of 1 Gly, the corresponding cyclic peptide has been isolated. The *para* isomers lead to the more stable cyclodimers for both $n=0$ and 1, likely because the putative cyclic peptides should be very unstable, featuring clearly non-planar benzene rings.

It has to be said that these processes are formally irreversible, and arise from a complex palladium-catalytic cycle, therefore the estimation of the activation barriers for the key steps, although relevant for the physicochemical interpretation of the process, should be extremely challenging. Furthermore, these barriers probably may display similar trends than the relative stabilities of the compounds.

The evidence that compounds **5b** and **5c** show broad ^1H NMR spectrum in contrast with **5a** which displayed sharp peaks, which suggests that backbone flexibility increases with the size of the polypeptide chain, reinforces the computational problems seen in this section.

Bibliography

- (1) W. C. Chan and P. D. White, *Fmoc solid phase peptide synthesis.*, Oxford University Press, New York, New York, 2000.
- (2) P. I. C. E. Kaiser, R. L. Colescott, C. D. Bossinger, *Anal. Biochem.* **1970**, *34*, 595–598.
- (3) L. Mendive-Tapia, S. Preciado, J. García, R. Ramón, N. Kielland, F. Albericio and R. Lavilla, *Nat. Commun.*, Published online May, 2015; DOI:10.1038/ncomms8160.
- (4) Spartan '14. Wavefunction, Inc. 18401 Von Karman Ave., Suite 370. Irvine, CA 92612, USA.
- (5) Bom, A.; Bradley, M.; Cameron, K.; Clark, J. K.; Egmond, J. Van; Feilden, H.; Maclean, E. J.; Muir, A. W.; Palin, R.; Rees, D. C.; Zhang, M. *Angew. Chem. Int. Ed.* **2002**, *41*, 265–270.
- (6) Collins, J. C.; James, K. *Med. Chem. Commun.* **2012**, *3*, 1489–1495.



FULL SUPPORTING INFORMATION PUBLICATION IX

Cross-dehydrogenative couplings on tryptophan-based diketopiperazines: access to new scaffolds

Lorena Mendive-Tapia, Arantxa Albornoz Grados, Alexandra Bertran,
Fernando Albericio and Rodolfo Lavilla*

INDEX

<i>Abbreviations</i>	<i>1</i>
<i>General experimental information</i>	<i>1</i>
<i>Experimental procedures and peptide characterization</i>	<i>2</i>
<i>NMR spectra of compounds 1-4</i>	<i>8</i>
<i>Oxidative screening experiments. Supplementary tables.....</i>	<i>29</i>
<i>Chiral chromatography of oxidized DKPs (4g-h)</i>	<i>31</i>
<i>Proposed mechanism for the decarboxylation of Asp-containing DKP.....</i>	<i>32</i>
<i>Proposed 1,4-hydride shift within iminium forms for the CDC.....</i>	<i>32</i>
<i>Bibliography</i>	<i>33</i>

Abbreviations

Abbreviation used for amino acids and designations of peptides follow the rules of the IUPAC-IUB Commission of Biochemical Nomenclature in J. Biol. Chem. 247, 977-983 (1982). The following additional abbreviations are used: ACN: acetonitrile, Ala: alanine, Asp: aspartic acid, BQ: 1,4-benzoquinone, CD: circular dichroism, DCM: dichloromethane, DDQ: 2,3-Dichloro-5,6-dicyano-1,4-benzoquinone, DIEA: N,N-diisopropylethylamine, DKP: diketopiperazine, DLP: Dilauroyl peroxide, DMF: N,N-dimethylformamide, DMSO: dimethyl sulfoxide, DTBP: Di-*tert*-butyl peroxide, Gly: glycine, HBTU: *o*-benzotriazole-*N,N,N',N'*-tetramethyl-uronium-hexafluoro-phosphate, HPLC-MS: high performance liquid chromatography mass spectrometry, HRMS(ESI): high-resolution mass spectrometry (electrospray ionization), Fmoc: 9H-fluorenylmethyloxycarbonyl, Leu: leucine, Lys: lysine, MW: microwave, NMR: nuclear magnetic resonance, Phe: phenylalanine, PIFA: bis(trifluoroacetoxy)iodobenzene, Pro: proline, TBH: *tert*-Butyl hydroperoxide, TFA: trifluoroacetic acid, Trp: tryptophan, Z: benzyloxycarbonyl.

General experimental information

Reactions were monitored by HPLC-MS using a HPLC Waters Alliance HT comprising a pump (Edwards RV12) with degasser, an autosampler and a diode array detector. Flow from the column was split to a MS spectrometer. The MS detector was configured with an electrospray ionization source (micromass ZQ4000) and nitrogen was used as the nebulizer gas. Data acquisition was performed with MassLynx software. Unless otherwise stated, yields are for the isolated pure compound. All microwave reactions were carried out in 10 mL sealed glass tubes in a focused mono-mode microwave oven ("Discover" by CEM Corporation) featured with a surface sensor for internal temperature determination. Cooling was provided by compressed air ventilating the microwave chamber during the reaction. When stated, the final crude was purified via flash column chromatography Combi Flash ISCO RF provided with dual UV detection.

NMR spectra of peptides in DMSO- d_6 were acquired with either a Varian Mercury 400 MHz or a Bruker DMX-500 MHz spectrometer. The spectra were referenced relative to the residual DMSO signal (^1H , 2.50 ppm; ^{13}C , 39.5 ppm). Chemical shifts (δ) are reported in ppm. Multiplicities are referred by the following abbreviations: s = singlet, d = doublet, t = triplet, dd = doublet of doublets, ddd: doublet of doublet of doublets, dt = doublet of triplets, td: triplet of doublets, and m = multiplet. HRMS (ESI positive) were obtained with a LTQ-FT Ultra (Thermo Scientific) mass Spectrometer.

CD spectroscopy. Circular dichroism (CD) measurements were performed using a Jasco J-815 spectrophotometer. The spectra were recorded from 300 to 190 nm using a 1.0 mm path-length quartz cuvette at 2 nm bandwidth, 50 nm·min⁻¹ scan speed, 0.5 s response time, 0.2 nm data pitch and four-scan accumulations. The background signal of the buffer alone was subtracted for each spectrum. CD spectra were converted from raw ellipticity (θ , mdeg) to molar ellipticity ($[\theta]$, deg·cm⁻²·dmol⁻¹). All the samples were dissolved in MeOH at 0.3 mM final concentration.

Chiral chromatography. The chiral chromatography was performed in a chiral HPLC column (Chiralpak ia, Amylose tris(3,5-dimethylphenylcarbamate) immobilized on 5 μm silica gel, 250 \times

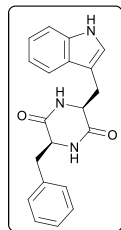
4.6 mm), at a flow rate of 1 mL·min⁻¹ and a linear gradient of ACN (+0.036% TFA) into H₂O (+0.045% TFA) from 50% to 70% ACN for 30 min.

Experimental procedures and peptide characterization

General procedure for the synthesis of 2,5-Diketopiperazines 1a-j

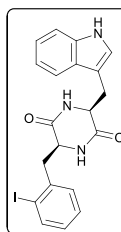
Unless stated otherwise, all DKPs were synthesized using the following procedure. Fmoc-AA-OH (1.0 eq), H-Trp-OMe·HCl (1.0 eq), HBTU (1.0 eq) and DIEA (2.0 eq) were dissolved in DMF and the solution was stirred at r.t. for 24 h followed by evaporation under vacuum. The resulting suspension was dissolved in ethyl acetate and washed with saturated aqueous solution of NaHCO₃ (×5). Then, the organic phase was dried over Na₂SO₄, filtered and the solvent was removed under vacuum obtaining the desired dipeptide. The resulting white solid was suspended in 20% piperidine/ACN and stirred for 16 h. The resulting suspension was concentrated under vacuum and washed with diethyl ether (×5). The white solid obtained was dried to yield the corresponding pure product (66-93% isolated yields). Cyclo(Pro-Trp) stereoisomers **1g-i** were prepared according to a previously published procedure on brevianamide arylation disclosed by the group.¹

Cyclo(Phe-Trp) (1a). Compound **1a** was prepared using Fmoc-Phe-OH (2.32 g, 5.99 mmol, 1.0



eq), following the general procedure for the synthesis of DKPs to obtain the desired product as a white solid (1.86 g, 93%). ¹H NMR (400 MHz, DMSO-d₆): δ 10.87 (s, 1H), 7.89 (d, *J* = 2.7 Hz, 1H), 7.68 (d, *J* = 1.7 Hz, 1H), 7.47 (d, *J* = 7.9 Hz, 1H), 7.30 (d, *J* = 8.0 Hz, 1H), 7.15 (m, 3H), 7.05 (t, *J* = 7.5 Hz, 1H), 6.98 (d, *J* = 7.6 Hz, 1H), 6.94 (d, *J* = 2.6 Hz, 1H), 6.69 (dd, *J* = 6.7 Hz, 2H), 3.96 (m, 1H), 3.84 (m, 1H), 2.79 (dd, *J* = 14.5, 4.4 Hz, 1H), 2.53 (m, 1H), 2.43 (d, *J* = 4.6 Hz, 1H), 1.84 (dd, *J* = 13.4, 7.0 Hz, 1H) ppm. ¹³C NMR (100 MHz, DMSO-d₆): δ 166.8, 166.2, 136.5, 136.0, 129.7, 128.0, 127.5, 126.4, 124.4, 120.9, 118.8, 118.4, 111.3, 108.8, 55.6, 55.3, 29.7 ppm.

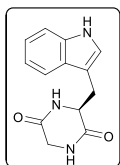
Cyclo(2-I-Phe-Trp) (1b). Compound **1b** was prepared using Fmoc-Phe(2-I)-OH (1.50 g, 2.93



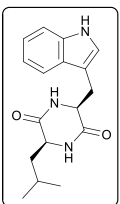
mmol, 1.0 eq), H-Trp-OMe·HCl (730 mg, 2.93 mmol, 98%, 1.0 eq), HBTU (1.10 g, 2.93 mmol, 1.0 eq), DIEA (1.0 mL, 5.86 mmol, 2.0 eq) which were dissolved in DMF (3.3 mL). The pale yellow solution was stirred at r.t. for 24 h. The resulting solution was precipitated over 10 mL of cold water and centrifugated (RPM: 2000, t: 5 min, T= 4 °C). Precipitation cycles in cold water and centrifugation were repeated 8 times obtaining the desired adduct (2.6 g, 89%). The white solid was suspended in 20% piperidine/ACN (15 mL) and stirred for 22 h and the resulting solution was precipitated over 10 mL of cold water and centrifugated (RPM: 2000, t: 5 min, T= 4 °C). Precipitation cycles in cold water and centrifugation were repeated 2 times. The crude was purified by flash chromatography on silica using DCM/MeOH:DCM (1:5) to yield the pure product **1b** as a white solid (1.0 g, 85% yield). ¹H NMR (400 MHz, DMSO-d₆): δ 10.97 (d, *J* = 2.4 Hz, 1H), 8.21 (d, *J* = 2.7 Hz, 1H), 7.66 (dd, *J* = 7.9, 1.3 Hz, 1H), 7.62 (dd, *J* = 7.5, 1.3 Hz, 1H), 7.44 (d, *J* = 3.2 Hz, 1H), 7.29 (d, *J* = 7.6 Hz, 1H), 7.11 (d, *J* = 2.3 Hz, 1H), 7.13-7.02 (m, 2H), 6.94 (td, *J* = 7.5, 1.3 Hz, 1H), 6.82 (td, *J* = 7.6, 1.7

Hz, 1H), 5.56 (dd, $J = 7.6, 1.7$ Hz, 1H), 4.11 (m, 1H), 3.69 (dt, $J = 9.3, 3.9$ Hz, 1H), 3.27 (dd, $J = 14.4, 3.8$ Hz, 1H), 2.97 (dd, $J = 14.3, 4.6$ Hz, 1H), 2.44 (dd, $J = 13.3, 4.4$ Hz, 1H), 1.12 (dd, $J = 13.4, 9.9$ Hz, 1H) ppm. ^{13}C NMR (100 MHz, DMSO- d_6): δ 166.9, 166.1, 138.9, 138.6, 136.0, 131.8, 128.5, 127.8, 124.9, 121.1, 119.3, 118.6, 111.5, 108.6, 100.6, 55.7, 53.4, 45.2, 29.2 ppm. HRMS (ESI): (M: $\text{C}_{20}\text{H}_{18}\text{O}_2\text{N}_3$) m/z calcd. 460.0516, found 460.0519 (M+H) $^+$.

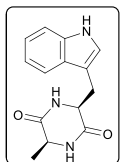
Cyclo(Gly-Trp) (1c). Compound **1c** was prepared using Fmoc-Gly-OH (1.78 g, 5.99 mmol, 1.0 eq), following the general procedure for the synthesis of DKPs to obtain the desired product as a white solid (1.23 g, 85%). ^1H NMR (400 MHz, DMSO- d_6): δ 10.92 (s, 1H), 8.09 (d, $J = 1.9$ Hz, 1H), 7.76 (br s, 1H), 7.54 (dd, $J = 7.9, 1.1$ Hz, 1H), 7.33 (dt, $J = 8.1, 0.9$ Hz, 1H), 7.08–7.01 (m, 2H), 6.95 (ddd, $J = 8.0, 7.0, 1.1$ Hz, 1H), 4.02 (m, 1H), 3.31 (dd, $J = 17.2, 2.8$ Hz, 1H), 3.24 (dd, $J = 14.4, 4.7$ Hz, 1H), 3.02 (dd, $J = 14.4, 4.6$ Hz, 1H), 2.79 (d, $J = 17.3$ Hz, 1H) ppm.



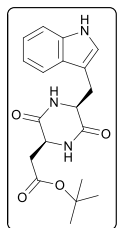
Cyclo(Leu-Trp) (1d). Compound **1d** was prepared using Fmoc-Leu-OH (710 mg, 2.01 mmol, 1.0 eq), following the general procedure for the synthesis of DKPs to obtain the desired product as a white solid (470 mg, 78%). ^1H NMR (400 MHz, DMSO- d_6): δ 10.90 (s, 1H), 8.04 (s, 1H), 7.94 (s, 1H), 7.55 (d, $J = 7.8$ Hz, 1H), 7.30 (d, $J = 8.0$ Hz, 1H), 7.02 (m, 2H), 6.92 (t, $J = 7.4$ Hz, 1H), 4.09 (m, 1H), 3.46–3.36 (m, 1H), 3.26 (dd, $J = 14.3, 3.8$ Hz, 1H), 2.98 (dd, $J = 14.3, 4.5$ Hz, 1H), 1.19 (m, 1H), 0.64 (m, 1H), 0.53 (d, $J = 6.5$ Hz, 3H), 0.42 (d, $J = 6.6$ Hz, 3H), -0.01 (m, 1H) ppm.



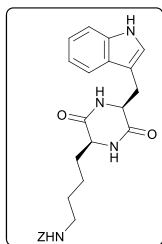
Cyclo(Ala-Trp) (1e). Compound **1e** was prepared using Fmoc-Ala-OH (1.87 g, 6.01 mmol, 1.0 eq), following the general procedure for the synthesis of DKPs to obtain the desired product as a white solid (1.57 g, 83%). ^1H NMR (400 MHz, DMSO- d_6): δ 10.88 (s, 1H), 8.00 (s, 1H), 7.90 (s, 1H), 7.56 (d, $J = 7.9$ Hz, 1H), 7.31 (d, $J = 8.0$ Hz, 1H), 7.08–6.98 (m, 2H), 6.94 (t, $J = 7.4$ Hz, 1H), 4.10 (m, 1H), 3.59 (q, $J = 6.5$ Hz, 1H), 3.24 (dd, $J = 14.4, 4.1$ Hz, 1H), 3.01 (dd, $J = 14.4, 4.6$ Hz, 1H), 0.42 (d, $J = 7.0$ Hz, 3H) ppm.



Cyclo[Asp(t Bu)-Trp] (1f). Compound **1f** was prepared using Fmoc-Asp(t Bu)-OH (2.47 g, 6.00 mmol, 1.0 eq), following the general procedure for the synthesis of DKPs to obtain the desired product as a pale yellow solid (2.18 g, 66%). ^1H NMR (400 MHz, DMSO- d_6): δ 10.92 (s, 1H), 7.98 (s, 1H), 7.76 (s, 1H), 7.55 (d, $J = 7.9$ Hz, 1H), 7.33 (d, $J = 8.1$ Hz, 1H), 7.10 (d, $J = 2.3$ Hz, 1H), 7.05 (t, $J = 7.1$ Hz, 1H), 6.94 (t, $J = 7.1$ Hz, 1H), 4.16 (t, $J = 4.2$ Hz, 1H), 3.97 (t, $J = 6.2$ Hz, 1H), 3.22 (dd, $J = 14.5, 4.9$ Hz, 1H), 3.08 (dd, $J = 14.6, 4.5$ Hz, 1H), 1.95 (dd, $J = 16.4, 5.5$ Hz, 1H), 1.50 (dd, $J = 16.4, 6.9$ Hz, 1H), 1.32 (s, $J = 4.3$ Hz, 9H) ppm. ^{13}C NMR (100 MHz, DMSO- d_6): δ 169.1, 167.3, 166.6, 135.9, 127.5, 124.5, 120.9, 118.8, 118.4, 111.2, 108.6, 80.1, 55.1, 51.0, 44.3, 27.7, 23.1 ppm.

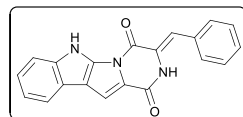


Cyclo[Lys(z)-Trp] (1j). Compound **1j** was prepared using Fmoc-Lys(z)-OH (1.00 g, 1.99 mmol,



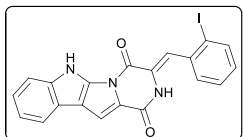
1.0 eq), following the general procedure for the synthesis of DKPs to obtain the desired product as a white solid (725 mg, 93%). **¹H NMR** (400 MHz, DMSO-*d*₆): δ 10.85 (s, 1H), 8.02 (d, *J* = 1.5 Hz, 1H), 7.91 (d, *J* = 1.4 Hz, 1H), 7.57 (d, *J* = 7.9 Hz, 1H), 7.41 – 7.26 (m, 6H), 7.09 – 6.98 (m, 3H), 6.92 (t, *J* = 7.4 Hz, 1H), 4.99 (s, 2H), 4.10 (m, 1H), 3.55 – 3.46 (m, 1H), 3.24 (dd, *J* = 14.4, 4.2 Hz, 1H), 3.00 (dd, *J* = 14.4, 4.7 Hz, 1H), 2.71 (q, *J* = 6.9 Hz, 2H), 1.07 – 0.89 (m, 3H), 0.68 – 0.47 (m, 3H) ppm.

(Z)-3-benzylidene-2,3-dihydro-1H-pyrazino[1',2':1,5]pyrrolo[2,3-*b*]indole-1,4(6H)-dione (2a).



Compound **2a** (150 mg, 0.450 mmol, 1.0 eq) and DDQ (306 mg, 1.35 mmol, 3.0 eq) were dissolved in 100 mL of DMF and the solution was stirred at 120 °C for 24h. Then, the resulting crude was concentrated under vacuum, dissolved in ethyl acetate and washed with saturated aqueous solution of NaHCO₃ (3 x 20 mL); the aqueous solution was back-extracted with ethyl acetate. Then, the organic layers were combined, dried over Na₂SO₄, filtered and concentrated under vacuum (17% yield estimated by HPLC-MS conversion). An analytically pure sample was obtained by via flash column chromatography on Celite using H₂O (0.1% formic acid)/ACN (0.1% formic acid). The expected compound was isolated as an orange solid (2.6 mg, 2%). **¹H NMR** (500 MHz, DMSO-*d*₆): δ 12.31 (s, 1H), 9.89 (s, 1H), 7.82 (d, *J* = 7.7 Hz, 1H), 7.68 (d, *J* = 7.4 Hz, 2H), 7.59 – 7.51 (m, *J* = 11.9 Hz, 2H), 7.48 (t, *J* = 7.4 Hz, 2H), 7.40 (t, *J* = 7.3 Hz, 1H), 7.26 (t, *J* = 7.6 Hz, 1H), 7.18 (t, *J* = 7.3 Hz, 1H), 7.13 (s, 1H) ppm. **HRMS (ESI):** (M: C₂₀H₁₃O₂N₃) *m/z* calcd 328.10805, found 328.10800 (M+H)⁺.

(Z)-3-(2-iodobenzylidene)-2,3-dihydro-1H-pyrazino[1',2':1,5]pyrrolo[2,3-*b*]indole-1,4(6H)-dione (2b).

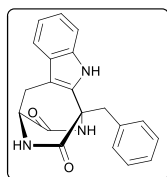


Compound **2a** (150 mg, 0.327 mmol, 1.0 eq) and DDQ (222 mg, 0.980 mmol, 3.0 eq) were dissolved in 3 mL of DMF and placed in a microwave reactor vessel. The mixture was heated under microwave irradiation (250W) at 120 °C for 20 min. The resulting crude was dissolved in ethyl acetate and washed with saturated aqueous solution of NaHCO₃ (4 x 20 mL); the aqueous solution was back-extracted with ethyl acetate. Then, the organic layers were combined, dried over Na₂SO₄, filtered and concentrated under vacuum (24% yield estimated by HPLC-MS conversion). An analytically pure sample was obtained by via flash column chromatography on Celite using H₂O (0.1% formic acid)/ACN (0.1% formic acid). The expected compound was isolated as an orange solid (3.1 mg, 2%). **¹H NMR** (500 MHz, DMSO-*d*₆): δ 12.33 (s, 1H), 10.05 (s, 1H), 7.98 (d, *J* = 7.6 Hz, 1H), 7.82 (d, *J* = 7.9 Hz, 1H), 7.61 (d, *J* = 7.4 Hz, 1H), 7.57 (d, *J* = 8.2 Hz, 1H), 7.54 (s, 1H), 7.51 (t, *J* = 7.5 Hz, 1H), 7.27 (t, *J* = 7.2 Hz, 1H), 7.19 (t, *J* = 7.2 Hz, 1H), 7.13 (t, *J* = 7.6 Hz, 1H), 6.99 (s, 1H) ppm. **HRMS (ESI):** (M: C₂₀H₁₂O₂N₃I) *m/z* calcd 454.00470, found 454.00468 (M+H)⁺.

General procedure for the cross-dehydrogenative coupling (CDC) of DKPs 1a-j

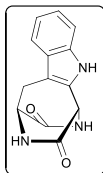
Unless stated otherwise, cyclo(AA-Trp) (0.2 mmol, 1.0 eq) and $\text{Cu}(\text{OCOCF}_3)_2$ (4.0 eq) were placed in a microwave reactor vessel and dissolved in DMF (1 mL). Afterwards, TFA (4.0 eq) was added to the solution and the mixture was heated under microwave irradiation (250 W) at 120 °C for 30 min. The resulting crude was diluted in ethyl acetate, filtered through Celite and evaporated under vacuum. Then, the crude was dissolved again in ethyl acetate and washed with NaCl ($\times 3$); the aqueous solution was back-extracted. Then, all the organic layers were mixed, dried over Mg_2SO_4 , filtered and concentrated under vacuum. The crude was purified by flash chromatography on silica using DCM/DCM:MeOH (8:2) to yield the pure products **4a-i**.

Oxidized cyclo(Phe-Trp) (4a). Compound **4a** was prepared using compound **1a** (67 mg, 0.201 mmol, 1.0 eq), following the general procedure for the synthesis of oxidized DKPs to obtain the pure product **4a** as a yellow solid (30% yield estimated by HPLC-MS conversion).



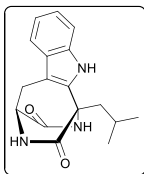
^1H NMR (500 MHz, $\text{DMSO}-d_6$): δ 11.28 (s, 1H), 8.59 (s, 1H), 8.35 (d, $J = 4.0$ Hz, 1H), 7.55 (d, $J = 7.1$ Hz, 2H), 7.44 (d, $J = 8.0$ Hz, 1H), 7.41 (d, $J = 8.1$ Hz, 1H), 7.29 (t, $J = 7.4$ Hz, 2H), 7.23 (t, $J = 7.3$ Hz, 1H), 7.14 (t, $J = 7.2$ Hz, 1H), 7.03 (t, $J = 7.2$ Hz, 1H), 4.02 (m, 1H), 3.91 (d, $J = 13.7$ Hz, 1H), 3.32 (1H), 3.15 (dd, $J = 17.0$, 1.8 Hz, 1H), 2.99 (dd, $J = 17.0$, 3.9 Hz, 1H) ppm. **HRMS (ESI)**: (M: $\text{C}_{20}\text{H}_{17}\text{O}_2\text{N}_3$) m/z calcd 332.13935, found 332.13922 (M+H) $^+$.

Oxidized cyclo(Gly-Trp) (4c). Compound **4c** was prepared using compound **1c** (50 mg, 0.206 mmol, 1.0 eq), following the general procedure for the synthesis of oxidized DKPs to obtain the pure product **4c** as a pale brown solid (16.6 mg, 33%).



^1H NMR (400 MHz, $\text{DMSO}-d_6$): δ 11.33 (s, 1H), 9.05 (d, $J = 4.9$ Hz, 1H), 8.43 (d, $J = 3.9$ Hz, 1H), 7.43 (d, $J = 7.8$ Hz, 1H), 7.36 (d, $J = 8.1$ Hz, 1H), 7.12 (t, $J = 7.5$ Hz, 1H), 7.01 (t, $J = 7.4$ Hz, 1H), 4.47 (dd, $J = 5.1$, 1.9 Hz, 1H), 4.11 – 4.05 (m, 1H), 3.14 (dd, $J = 17.0$, 2.5 Hz, 1H), 2.97 (dd, $J = 17.0$, 4.5 Hz, 1H) ppm. ^{13}C NMR (100 MHz, $\text{DMSO}-d_6$): δ 171.7, 169.3, 134.6, 131.7, 127.7, 121.8, 119.2, 118.0, 111.5, 105.8, 54.5, 52.3, 27.3 ppm. **HRMS (ESI)**: (M: $\text{C}_{13}\text{H}_{11}\text{O}_2\text{N}_3$) m/z calcd 242.09240, found 242.09228 (M+H) $^+$.

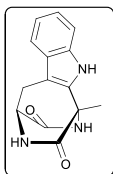
Oxidized cyclo(Leu-Trp) (4d). Compound **1d** (180 mg, 0.601 mmol, 1.0 eq) and $\text{Cu}(\text{OCOCF}_3)_2$



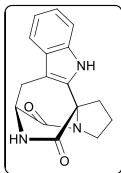
(6.0 eq) were placed in a microwave reactor vessel and dissolved in DMF (3 mL). Afterwards, TFA (4.0 eq) was added to the solution and the mixture was heated at 200 °C for 18 h. The resulting crude was diluted in ethyl acetate, filtered through Celite and evaporated under vacuum. Then, the crude was dissolved again in ethyl acetate and washed with NaCl ($\times 3$) and 5% aqueous LiCl ($\times 3$); the aqueous solution was back-extracted. Then, all the organic layers were mixed, dried over Mg_2SO_4 , filtered and concentrated under vacuum. The crude was purified by flash chromatography on silica using DCM/DCM:MeOH (8:2) to yield the pure product **4d** as a pale yellow solid (36.4 mg, 20%). ^1H NMR (400 MHz, $\text{DMSO}-d_6$): δ 11.02 (s, 1H), 8.68 (s, 1H), 8.27 (d, $J = 4.5$ Hz, 1H), 7.40 (d, $J = 7.9$ Hz, 1H), 7.35 (d, $J = 8.1$ Hz, 1H), 7.10 (t, $J = 7.6$ Hz, 1H), 6.99 (t, $J = 7.6$ Hz, 1H), 4.07 (m, 1H), 3.13 (dd, $J = 17.0$, 2.4 Hz, 1H), 2.95 (dd, $J = 17.1$, 4.5 Hz, 1H), 2.41 (dd, $J = 15.5$, 9.4 Hz, 1H), 2.02

(m, 2H), 1.04 (d, $J = 6.3$ Hz, 3H), 0.95 (d, $J = 6.5$ Hz, 3H). **^{13}C NMR** (100 MHz, DMSO- d_6): δ 171.9, 169.7, 135.0, 134.6, 127.8, 121.8, 119.2, 117.8, 111.7, 105.7, 57.6, 54.1, 36.2, 27.9, 24.1, 23.9, 23.0 ppm. **HRMS (ESI)**: (M: $\text{C}_{17}\text{H}_{19}\text{O}_2\text{N}_3$) m/z calcd 298.1556, found 298.1559 (M+H) $^+$.

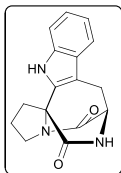
Oxidized cyclo(Ala-Trp) (4e). Compound **4e** was prepared using compound **1f** (73 mg, 0.204 mmol, 1.0 eq), following the general procedure for the synthesis of oxidized DKPs to obtain the pure product **4e** as a brown-orange solid (15.2 mg, 43%). Although formed in a reasonable extent, the isolation of the product **4e** from DKP **1e** was not feasible due to the similarity by HPLC of the different crude compounds. **^1H NMR** (400 MHz, DMSO- d_6): δ 11.02 (s, 1H), 8.91 (s, 1H), 8.42 (d, $J = 5.1$ Hz, 1H), 7.42 (d, $J = 7.8$ Hz, 1H), 7.36 (d, $J = 8.1$, 1H), 7.12 (ddd, $J = 8.2$, 7.0, 1.2 Hz, 1H), 7.01 (ddd, $J = 7.9$, 7.1, 1.1 Hz, 1H), 4.07 (m, 1H), 3.14 (dd, $J = 16.9$, 2.5 Hz, 1H), 2.97 (dd, $J = 16.9$, 4.6 Hz, 1H), 1.69 (s, 3H) ppm. **^{13}C NMR** (100 MHz, DMSO- d_6): δ 171.8, 170.8, 134.6, 134.3, 127.9, 121.9, 119.2, 117.9, 111.7, 106.2, 54.6, 54.5, 27.5, 17.1 ppm. **HRMS (ESI)**: (M: $\text{C}_{14}\text{H}_{13}\text{O}_2\text{N}_3$) m/z calcd 256.1086, found 256.1085 (M+H) $^+$.



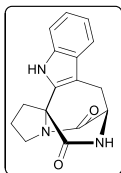
Oxidized cyclo(ProL-Trp) (4g). Compound **4g** was prepared using compound **1g** (58 mg, 0.205 mmol, 1.0 eq), following the general procedure for the synthesis of oxidized DKPs to obtain the pure product **4g** as a pale brown solid (34.8 mg, 60%). **^1H NMR** (400 MHz, DMSO- d_6): δ 11.20 (s, 1H), 8.46 (d, $J = 5.1$ Hz, 1H), 7.41 (d, $J = 7.9$ Hz, 1H), 7.36 (d, $J = 8.1$, 1H), 7.13 (ddd, $J = 8.2$, 7.0, 1.2 Hz, 1H), 7.01 (ddd, $J = 8.0$, 7.0, 1.0 Hz, 1H), 4.16 (td, $J = 4.9$, 2.3 Hz, 1H), 3.46 – 3.35 (m, 2H), 3.14 (dd, $J = 17.1$, 2.4 Hz, 1H), 3.00 (dd, $J = 17.1$, 4.8 Hz, 1H), 2.80 (ddd, $J = 13.4$, 6.3, 4.2 Hz, 1H), 2.48 – 2.41 (m, 1H), 2.04 – 1.89 (m, 2H) ppm. **^{13}C NMR** (100 MHz, DMSO- d_6): δ 170.8, 167.6, 134.7, 131.7, 128.0, 122.0, 119.2, 117.9, 111.6, 106.9, 64.1, 55.0, 44.5, 28.4, 27.2, 23.0 ppm. $[\alpha]_D^{25} +24.6$ (c 0.5, MeOH). **HRMS (ESI)**: (M: $\text{C}_{16}\text{H}_{15}\text{O}_2\text{N}_3$) m/z calcd 282.1243, found 282.1243 (M+H) $^+$.



Oxidized cyclo(ProD-Trp) (4h). Compound **4h** was prepared using compound **1h** (58 mg, 0.205 mmol, 1.0 eq), following the general procedure for the synthesis of oxidized DKPs to obtain the pure product **4h** as a brown-orange solid (41.0 mg, 71%). **^1H NMR** (400 MHz, DMSO- d_6): δ 11.20 (s, 1H), 8.46 (d, $J = 5.1$ Hz, 1H), 7.41 (d, $J = 7.9$ Hz, 1H), 7.36 (dt, $J = 8.1$, 0.8 Hz, 1H), 7.13 (ddd, $J = 8.2$, 7.0, 1.2 Hz, 1H), 7.01 (ddd, $J = 8.0$, 7.1, 1.0 Hz, 1H), 4.16 (td, $J = 4.9$, 2.4 Hz, 1H), 3.46 – 3.35 (m, $J = 9.7$, 8.0, 5.6 Hz, 2H), 3.14 (dd, $J = 17.1$, 2.3 Hz, 1H), 3.00 (dd, $J = 17.1$, 4.8 Hz, 1H), 2.80 (ddd, $J = 13.6$, 6.3, 4.2 Hz, 1H), 2.48 – 2.42 (m, 1H), 2.02 – 1.88 (m, 2H) ppm. $[\alpha]_D^{25} -26.0$ (c 0.5, MeOH). **HRMS (ESI)**: (M: $\text{C}_{16}\text{H}_{15}\text{O}_2\text{N}_3$) m/z calcd 282.1243, found 282.1241 (M+H) $^+$.

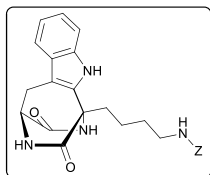


Oxidized cyclo(ProL-Trp) (4i). Compound **4i** was prepared using compound **1i** (58 mg, 0.205 mmol, 1.0 eq), following the general procedure for the synthesis of oxidized DKPs to obtain the pure product **4i** as a brown-orange solid (9.6 mg, 17%). **^1H NMR** (400 MHz, DMSO- d_6): δ 11.20 (s, 1H), 8.46 (d, $J = 5.1$ Hz, 1H), 7.41 (d, $J = 7.9$ Hz, 1H), 7.36 (d, $J = 8.1$ Hz, 1H), 7.13 (ddd, $J = 8.2$, 7.1, 1.1 Hz, 1H), 7.01 (ddd, $J = 7.9$, 7.2, 0.9 Hz, 1H), 4.16 (td, $J = 4.9$, 2.3 Hz, 1H), 3.43 – 3.35 (m, 2H), 3.14 (dd, $J = 17.1$, 2.3 Hz, 1H), 3.00 (dd, $J = 17.1$, 4.8 Hz, 1H), 2.80 (ddd, $J =$



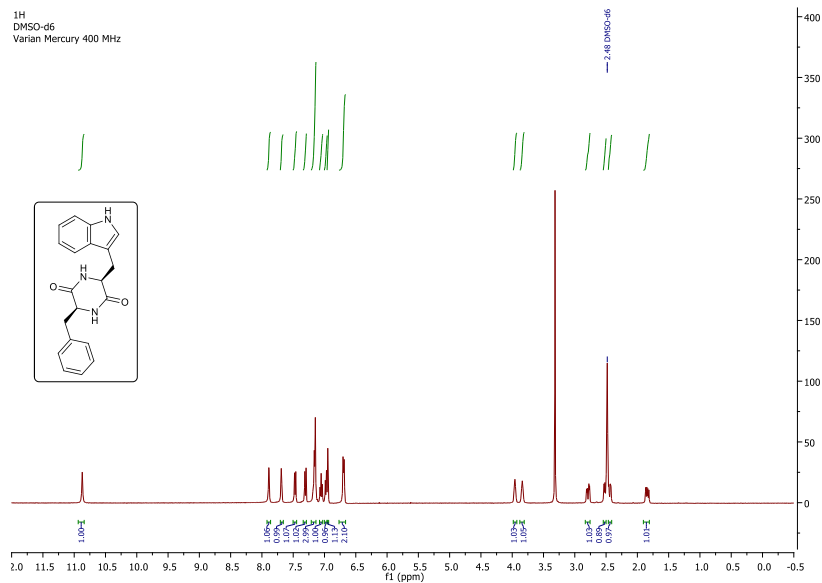
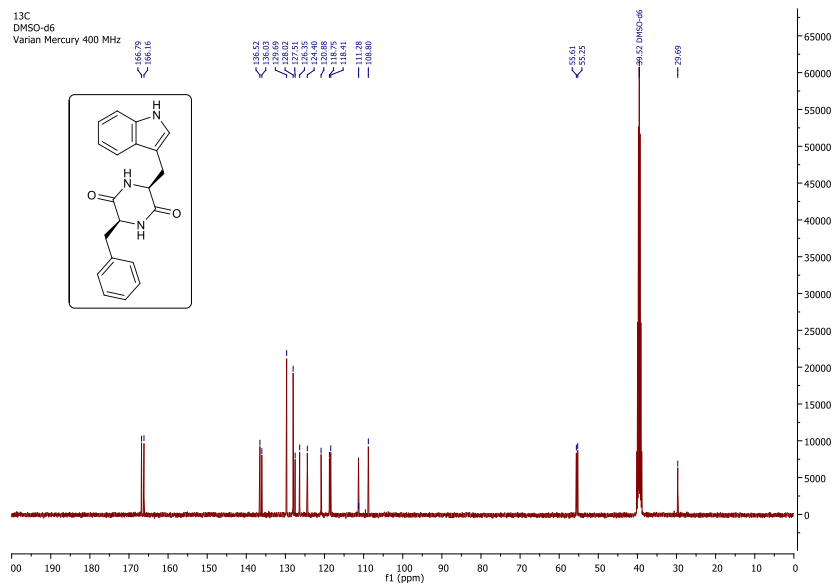
13.4, 6.3, 4.2 Hz, 1H), 2.48 – 2.43 (m, $J = 8.0, 5.4$ Hz, 1H), 2.03 – 1.88 (m, 2H) ppm. **HRMS (ESI)**: (M: $C_{16}H_{15}O_2N_3$) m/z calcd 282.1243, found 282.1242 (M+H)⁺.

Oxidized cyclo[Lys(z)-Trp] (4i). Compound **4i** was prepared using compound **1j** (90 mg, 0.201 mmol, 1.0 eq) and $Cu(OSO_2CF_3)_2$ (4.0 eq) instead of $Cu(OCOCF_3)_2$, following the general procedure for the synthesis of oxidized DKPs.



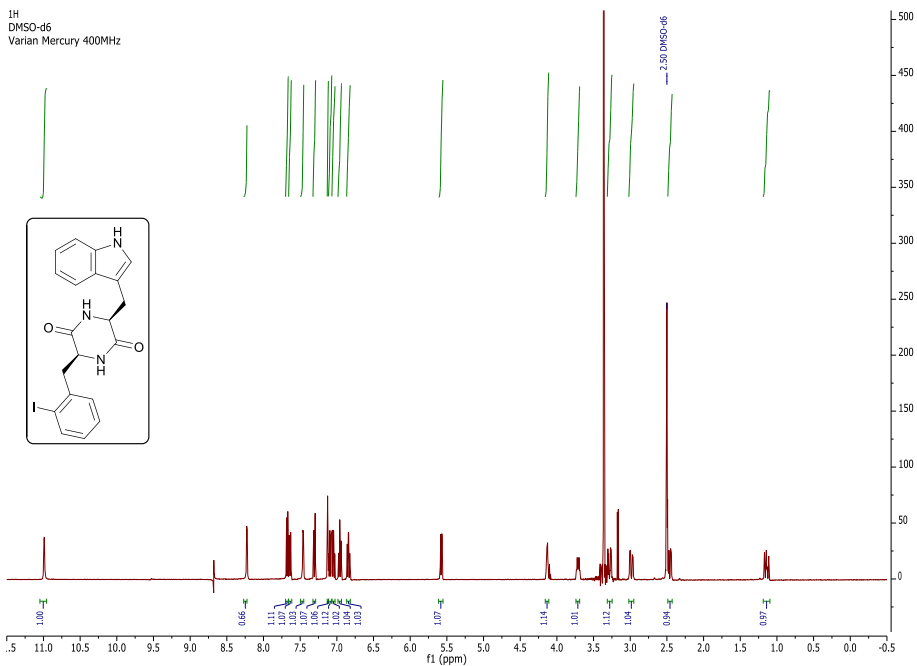
The crude was purified by flash chromatography on silica using hexane/ethyl acetate to yield the pure product **4i** as a yellow solid (18.5 mg, 20%). **¹H NMR** (400 MHz, DMSO- d_6): δ 11.03 (s, 1H), 8.79 (s, 1H), 8.37 (d, $J = 4.7$ Hz, 1H), 7.41 (d, $J = 7.9$ Hz, 1H), 7.39 – 7.26 (m, 7H), 7.11 (ddd, $J = 8.2, 7.1, 1.1$ Hz, 1H), 7.00 (ddd, $J = 8.0, 7.1, 1.0$ Hz, 1H), 5.03 (s, 2H), 4.06 (m, 1H), 3.19 – 3.04 (m, 3H), 2.95 (dd, $J = 17.1, 4.6$ Hz, 1H), 2.41 – 2.30 (m, 1H), 2.06 – 1.91 (m, 1H), 1.60 – 1.43 (m, 4H) ppm. **HRMS (ESI)**: (M: $C_{25}H_{26}O_4N_4$) m/z calcd 447.2032, found 447.2036 (M+H)⁺.

NMR spectra of compounds 1-4

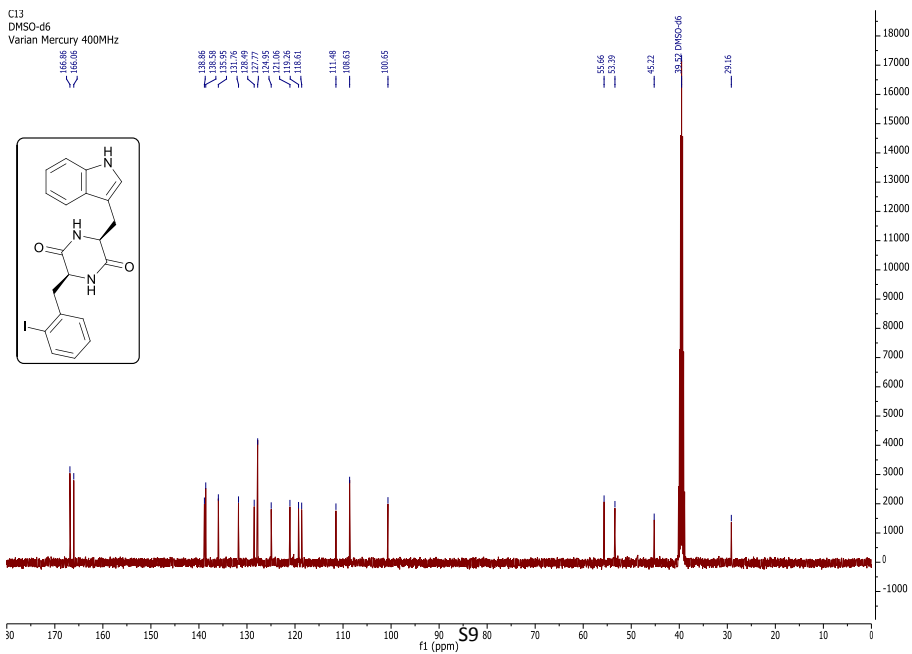
Cyclo(Phe-Trp) (1a) ^1H NMRCyclo(Phe-Trp) (1a) ^{13}C NMR

Cyclo(2-I-Phe-Trp) (1b) ^1H NMR

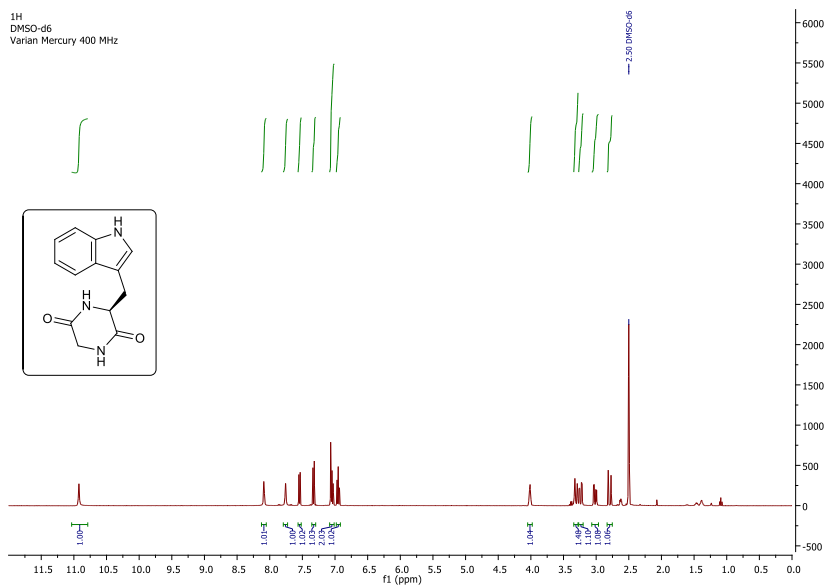
^1H
DMSO- d_6
Varian Mercury 400MHz

Cyclo(2-I-Phe-Trp) (1b) ^{13}C NMR

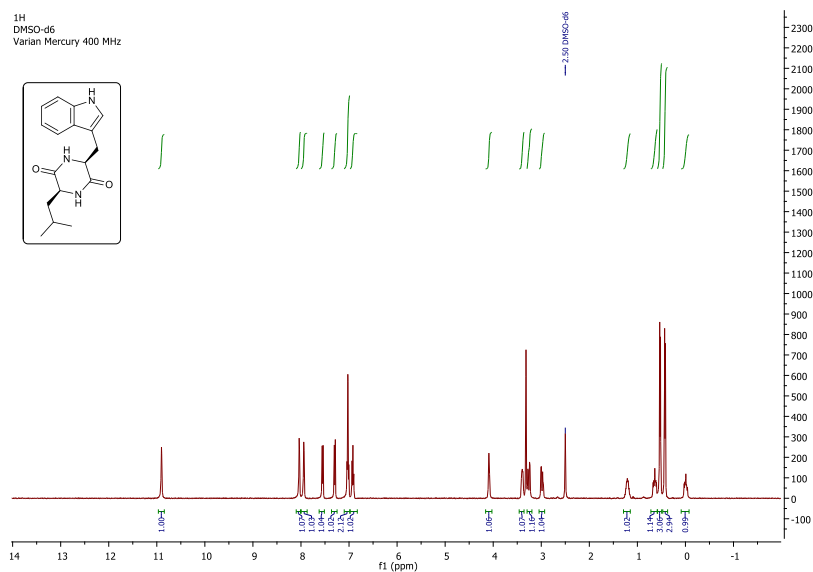
^{13}C
DMSO- d_6
Varian Mercury 400MHz

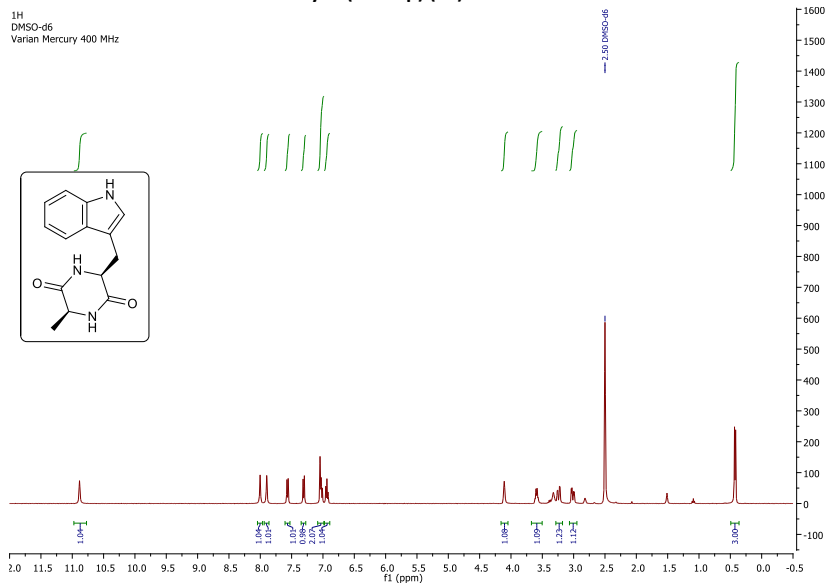
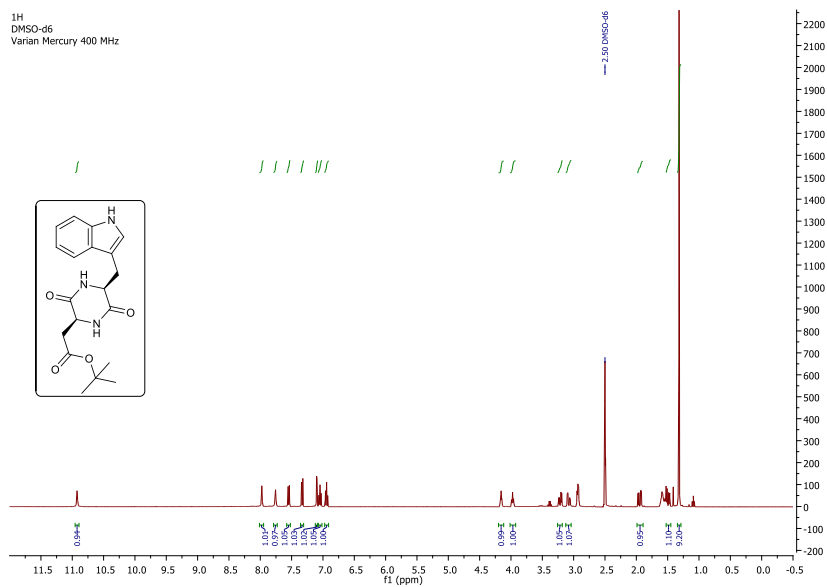


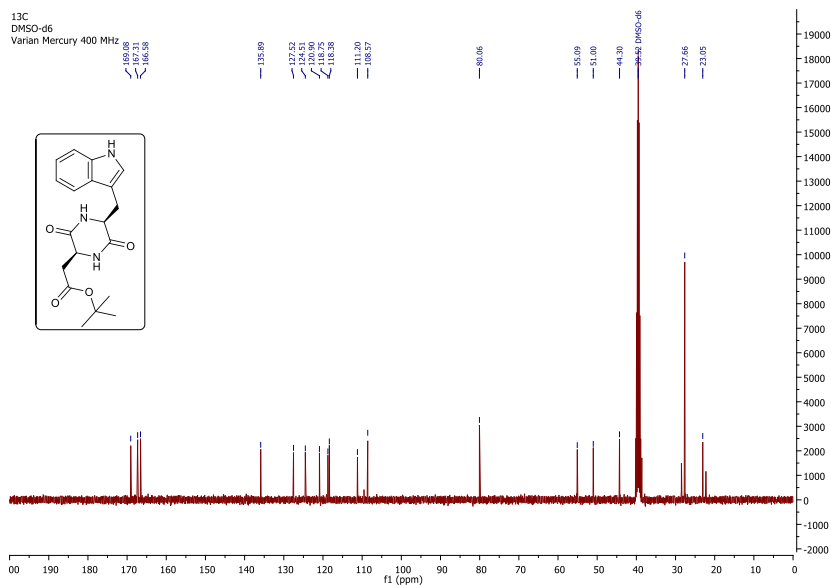
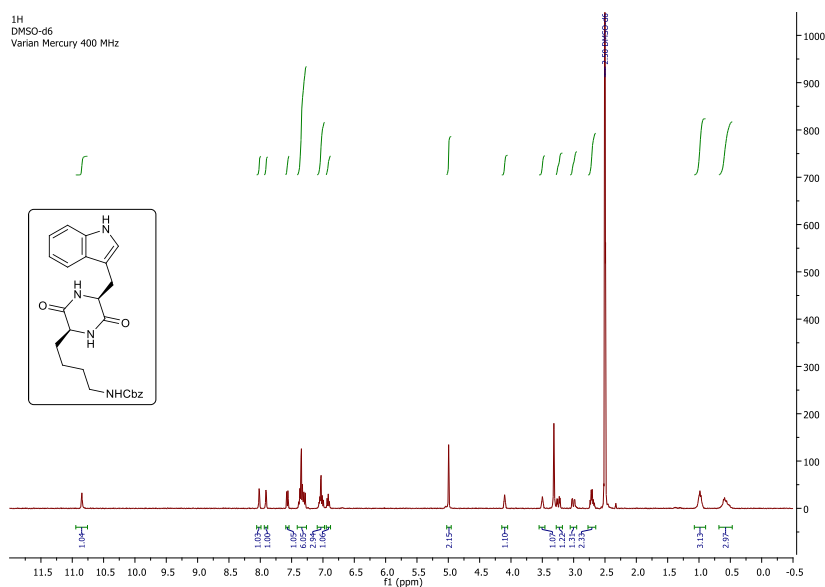
Cyclo(Gly-Trp) (1c) ¹H NMR



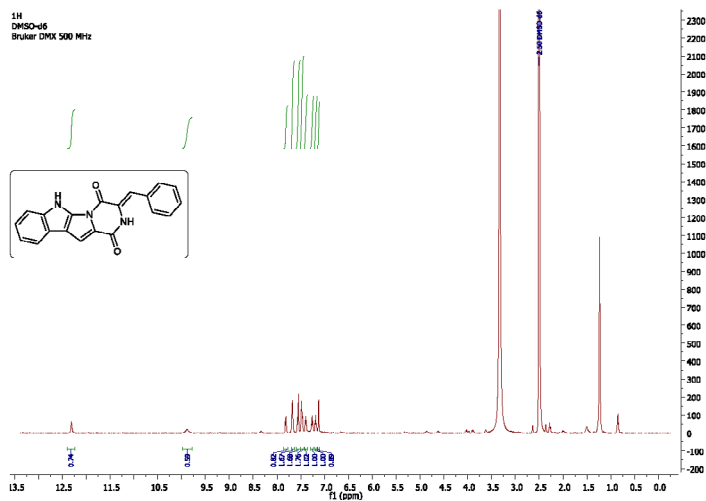
Cyclo(Leu-Trp) (1d) ¹H NMR



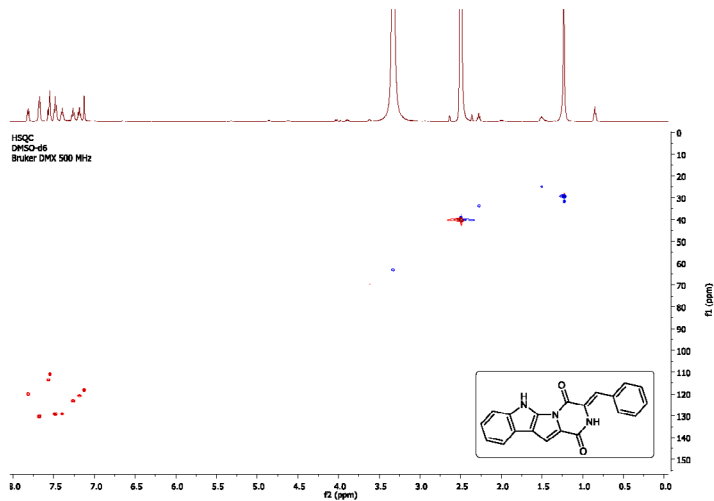
Cyclo(Ala-Trp) (1e) ^1H NMRCyclo[Asp(^tBu)-Trp] (1f) ^1H NMR

Cyclo[Asp(^tBu)-Trp] (1f) ¹³C NMRCyclo[Lys(z)-Trp] (1j) ¹H NMR

(Z)-3-benzylidene-2,3-dihydro-1H-pyrazino[1',2':1,5]pyrrolo[2,3-b]indole-1,4(6H)-dione (2a)
¹H NMR

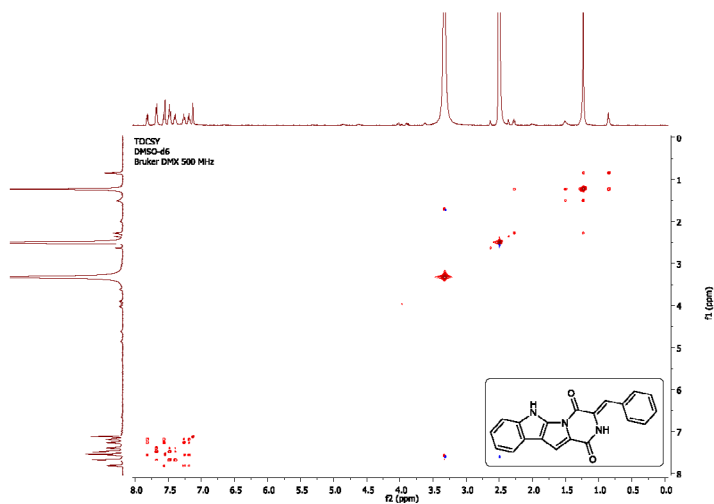


(Z)-3-benzylidene-2,3-dihydro-1H-pyrazino[1',2':1,5]pyrrolo[2,3-b]indole-1,4(6H)-dione (2a)
¹H-¹³C HSQC NMR

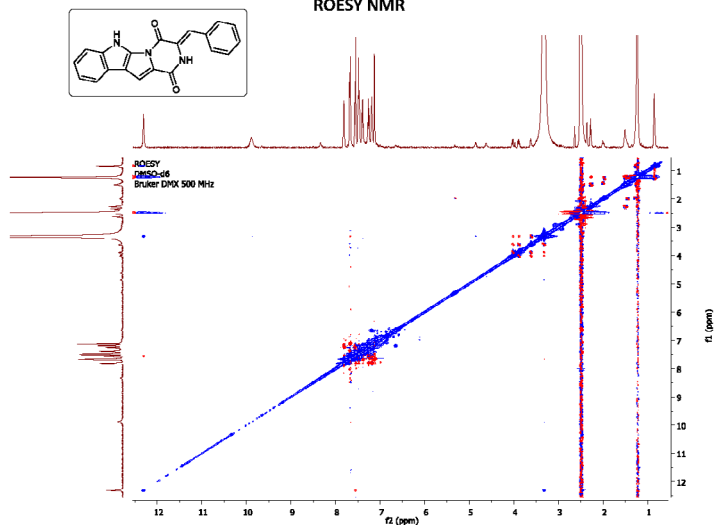


(Z)-3-benzylidene-2,3-dihydro-1H-pyrazino[1',2':1,5]pyrrolo[2,3-b]indole-1,4(6H)-dione (2a)

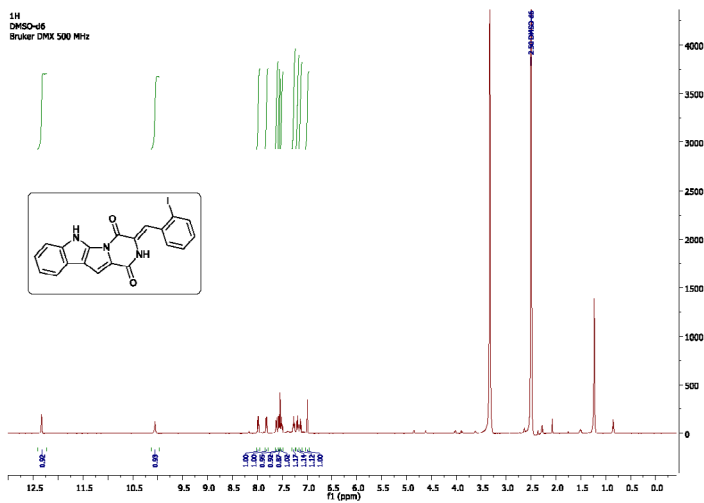
TOCSY NMR

**(Z)-3-benzylidene-2,3-dihydro-1H-pyrazino[1',2':1,5]pyrrolo[2,3-b]indole-1,4(6H)-dione (2a)**

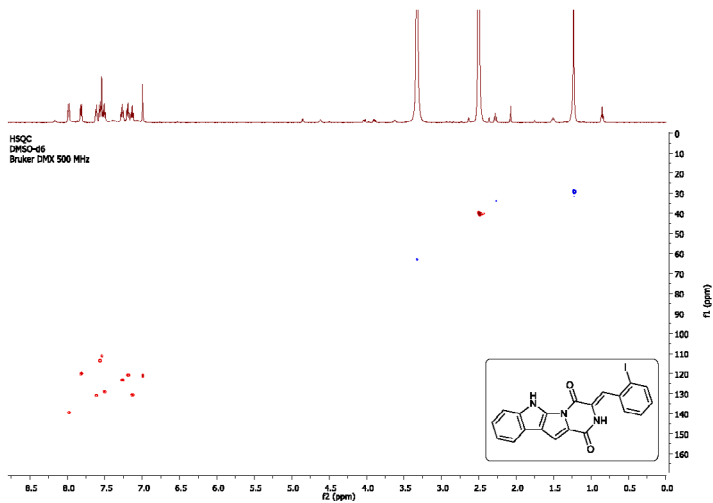
ROESY NMR



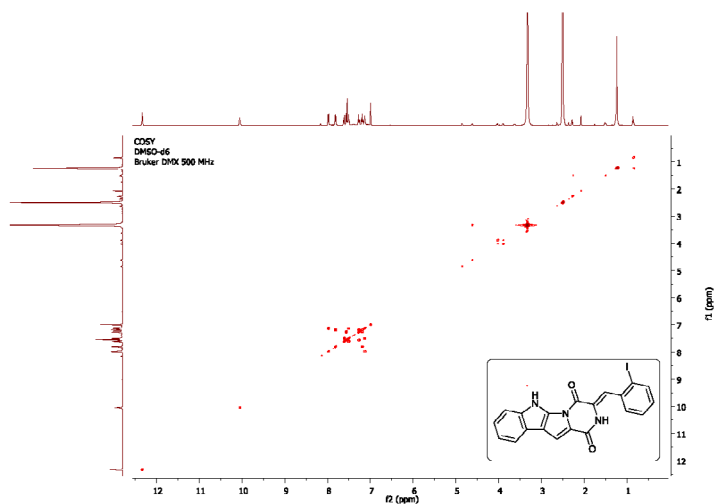
(Z)-3-[2-iodobenzylidene]-2,3-dihydro-1H-pyrazino[1',2':1,5]pyrrolo[2,3-b]indole-1,4(6H)-dione (2b) ^1H NMR



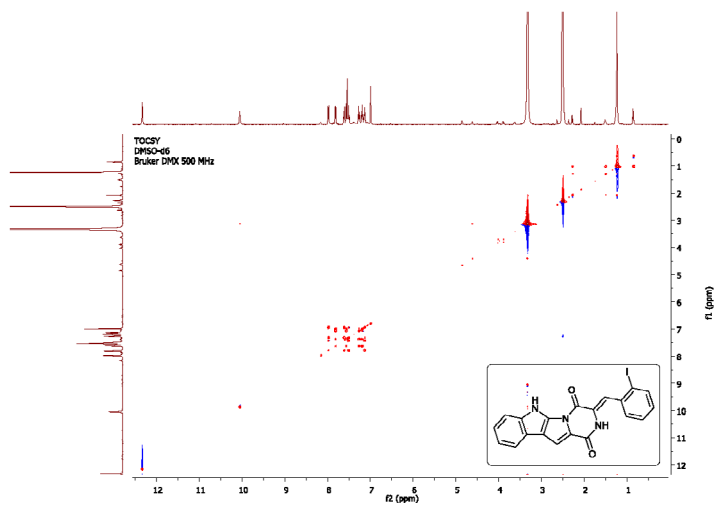
(Z)-3-[2-iodobenzylidene]-2,3-dihydro-1H-pyrazino[1',2':1,5]pyrrolo[2,3-b]indole-1,4(6H)-dione (2b) ^1H - ^{13}C HSQC NMR



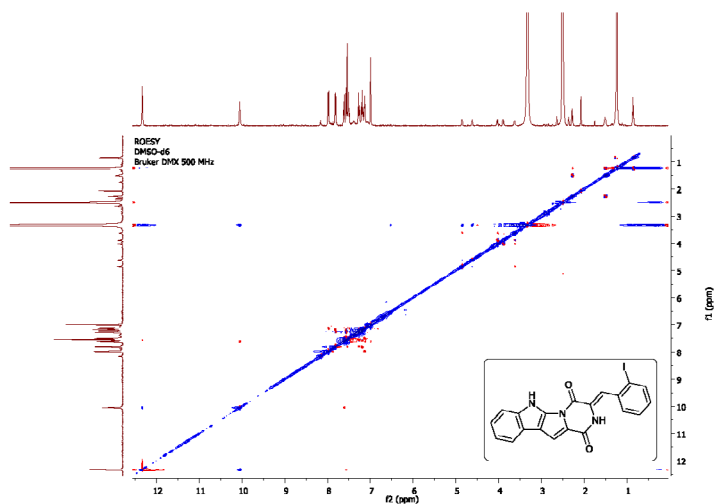
(Z)-3-[2-iodobenzylidene]-2,3-dihydro-1H-pyrazino[1',2':1,5]pyrrolo[2,3-b]indole-1,4(6H)-dione (2b) COSY NMR



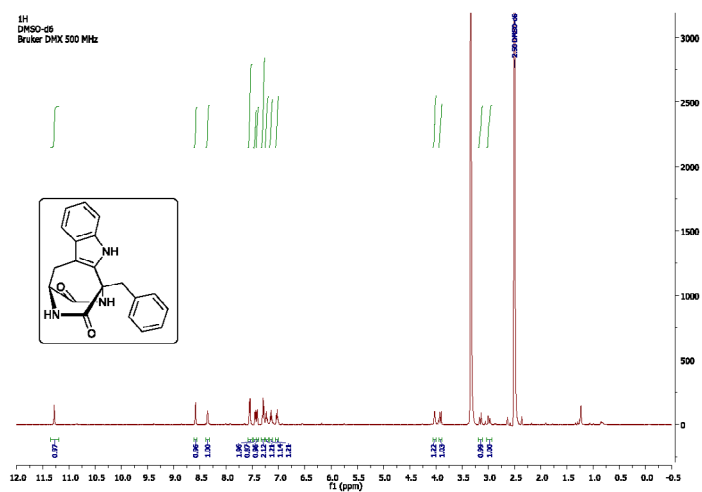
(Z)-3-[2-iodobenzylidene]-2,3-dihydro-1H-pyrazino[1',2':1,5]pyrrolo[2,3-b]indole-1,4(6H)-dione (2b) TOCSY NMR

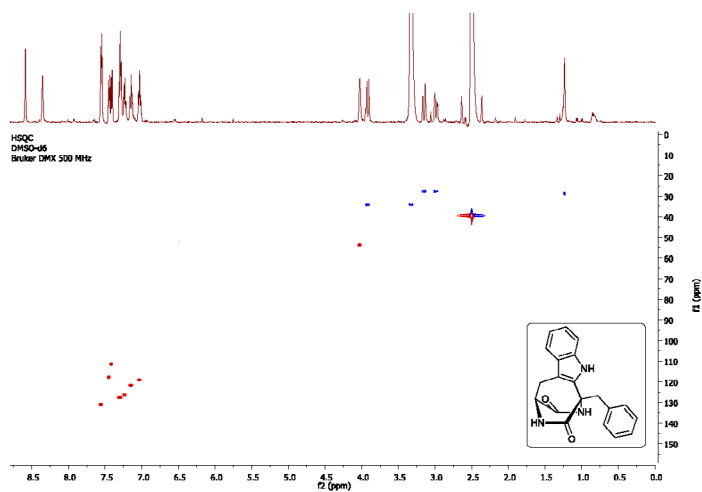


(Z)-3-(2-iodobenzylidene)-2,3-dihydro-1H-pyrazino[1',2':1,5]pyrrolo[2,3-b]indole-1,4(6H)-dione (2b) ROESY NMR

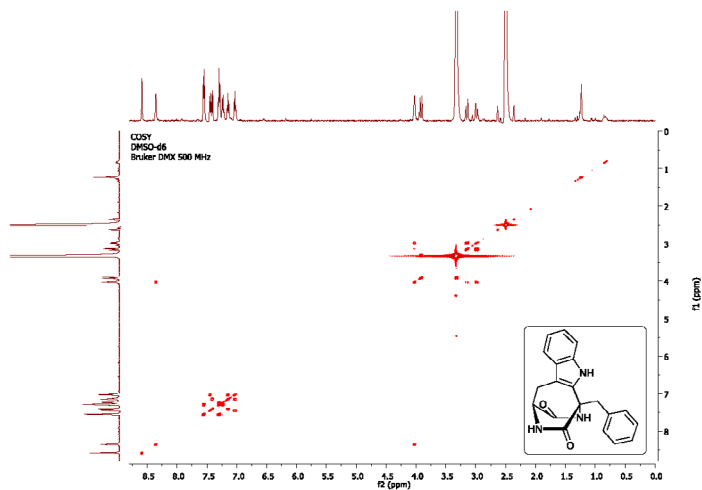


Oxidized cyclo(Phe-Trp) (4a) ^1H NMR

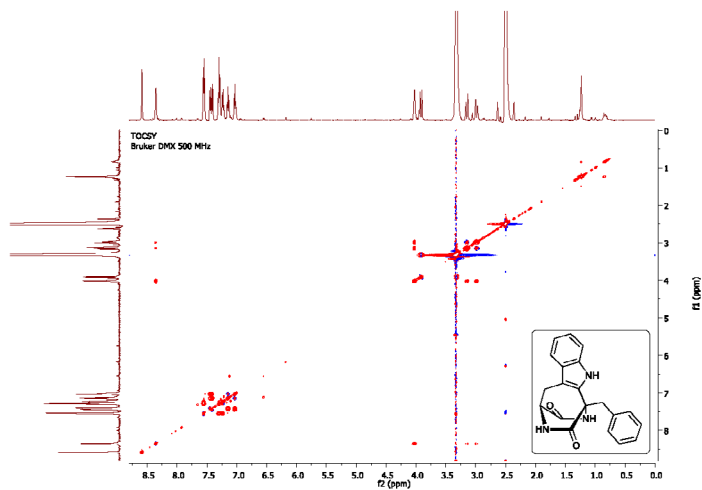


Oxidized cyclo(Phe-Trp) (4a) ^1H - ^{13}C HSQC NMR

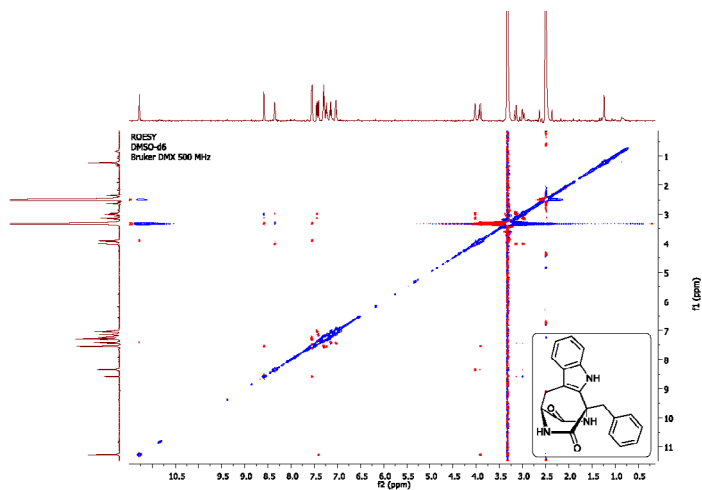
Oxidized cyclo(Phe-Trp) (4a) COSY NMR

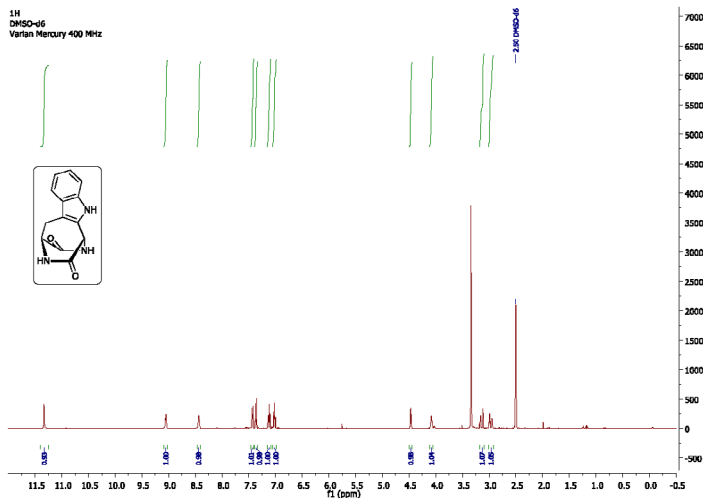
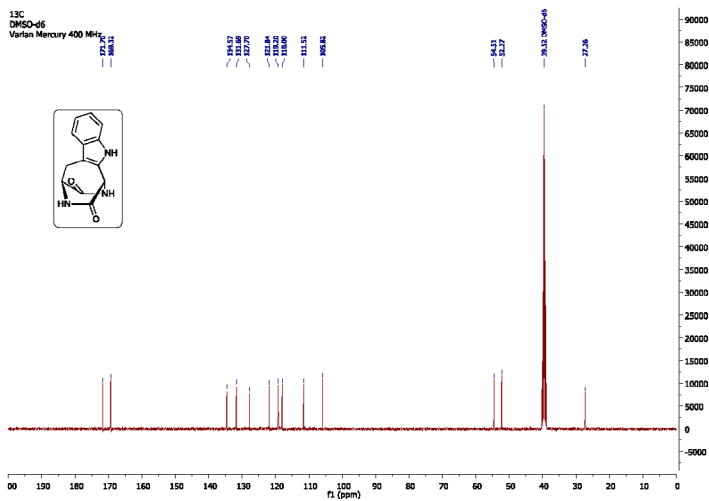


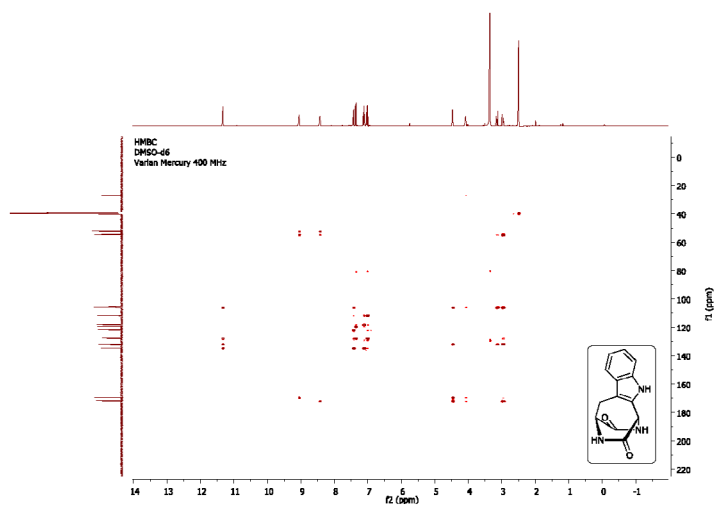
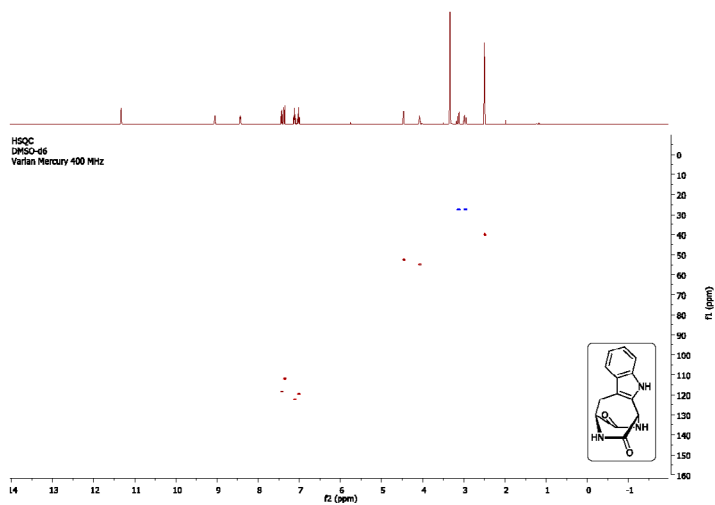
Oxidized cyclo(Phe-Trp) (4a) TOCSY NMR



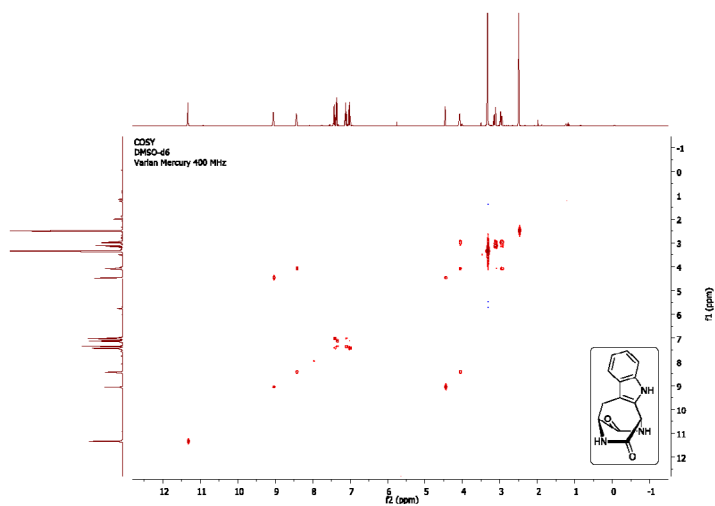
Oxidized cyclo(Phe-Trp) (4a) ROESY NMR



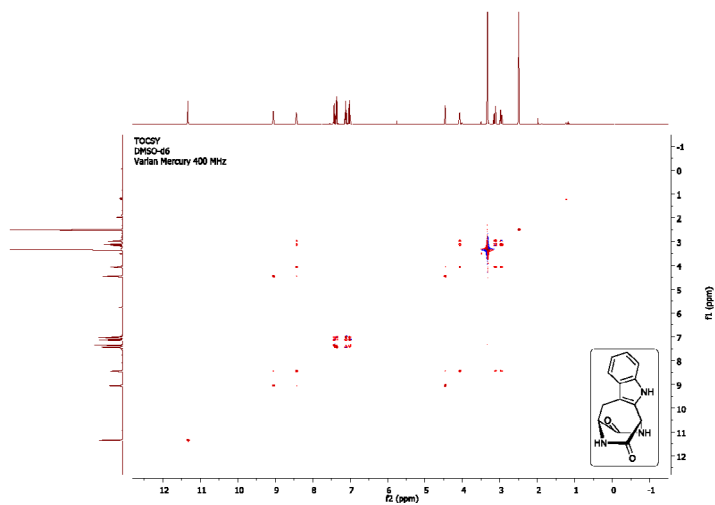
Oxidized cyclo(Gly-Trp) (4c) ^1H NMROxidized cyclo(Gly-Trp) (4c) ^{13}C NMR

Oxidized cyclo(Gly-Trp) (4c) ^1H - ^{13}C HMBC NMROxidized cyclo(Gly-Trp) (4c) ^1H - ^{13}C HSQC NMR

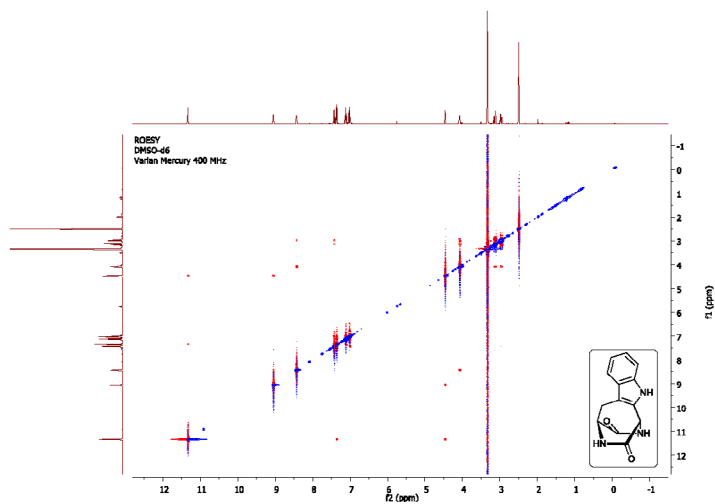
Oxidized cyclo(Gly-Trp) (4c) COSY NMR



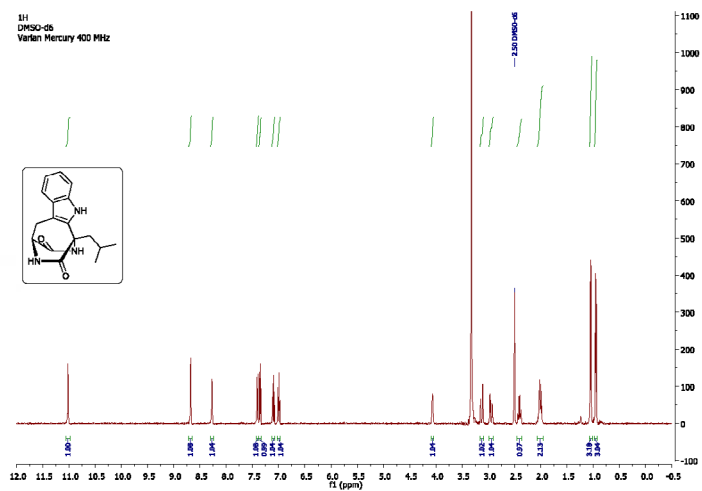
Oxidized cyclo(Gly-Trp) (4c) TOCSY NMR

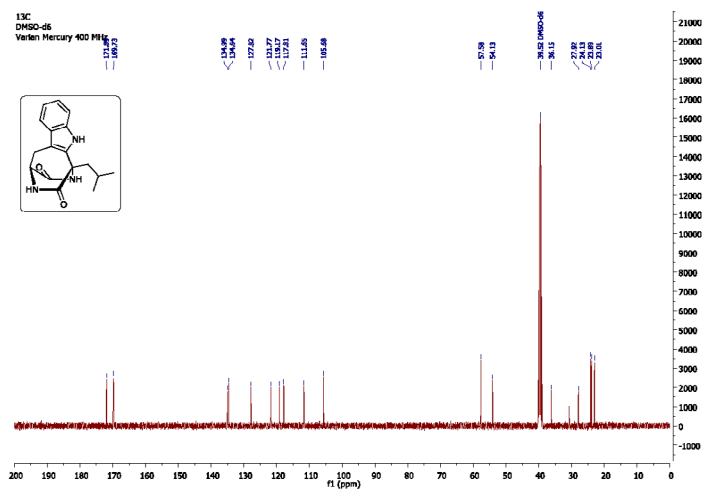
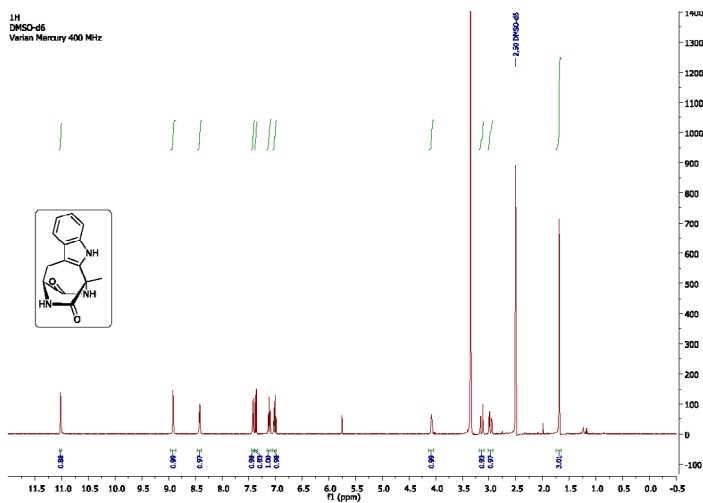


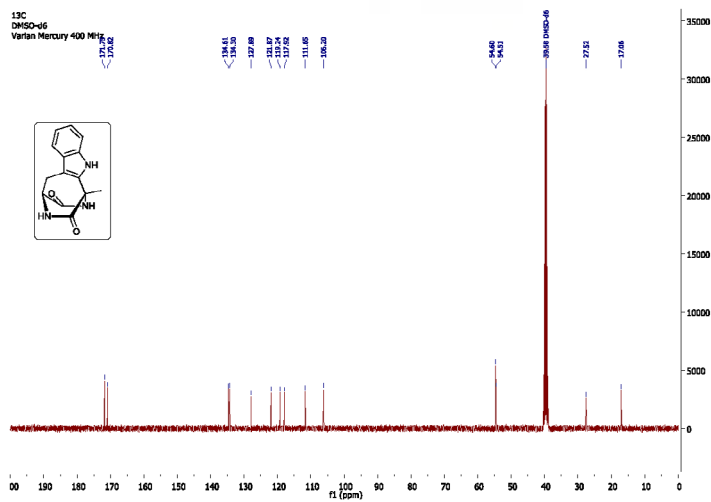
Oxidized cyclo(Gly-Trp) (4c) ROESY NMR



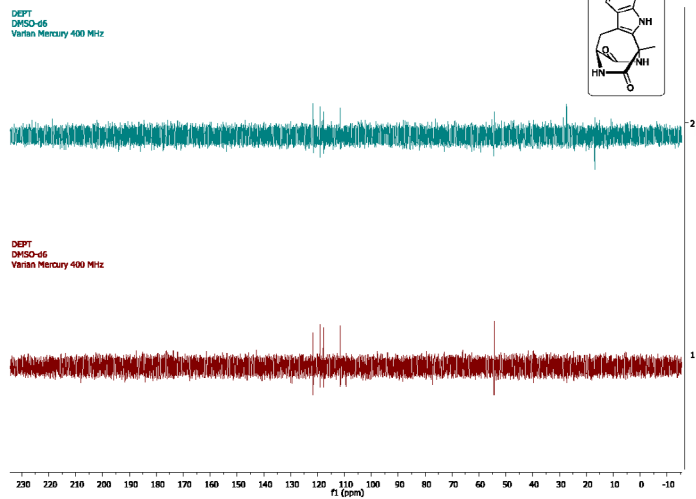
Oxidized cyclo(Leu-Trp) (4d) ¹H NMR



Oxidized cyclo[Leu-Trp] (4d) ^{13}C NMROxidized cyclo[Ala-Trp] (4e) ^1H NMR

Oxidized cyclo(Ala-Trp) (4e) ^{13}C NMR

Oxidized cyclo(Ala-Trp) (4e) DEPT NMR



14
DMSO-d₆
Varian Mercury 400 MHz

Chemical structure of compound 14 is shown in the top left. The structure is a complex polycyclic molecule with a benzene ring fused to a pyrrole ring, which is further fused to a bicyclic system containing a carbonyl group and a nitrogen atom.

The ¹H NMR spectrum (DMSO-d₆, 400 MHz) shows the following peaks and integrations:

- Peak at ~11.2 ppm (integration: 0.05)
- Peak at ~8.2 ppm (integration: 1.00)
- Peak at ~7.2 ppm (integration: 1.03)
- Peak at ~7.0 ppm (integration: 1.00)
- Peak at ~6.8 ppm (integration: 1.00)
- Peak at ~5.8 ppm (integration: 1.00)
- Peak at ~4.0 ppm (integration: 1.00)
- Peak at ~3.5 ppm (integration: 1.00)
- Peak at ~3.2 ppm (integration: 1.00)
- Peak at ~3.0 ppm (integration: 1.00)
- Peak at ~2.8 ppm (integration: 1.00)
- Peak at ~2.5 ppm (integration: 1.00)
- Peak at ~2.2 ppm (integration: 1.00)
- Peak at ~2.0 ppm (integration: 1.00)

13C
DMSO-d6
Varian Mercury 400 MHz

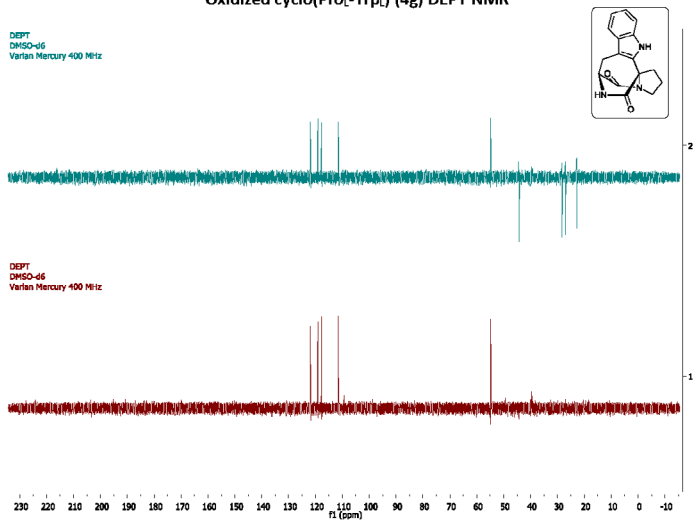
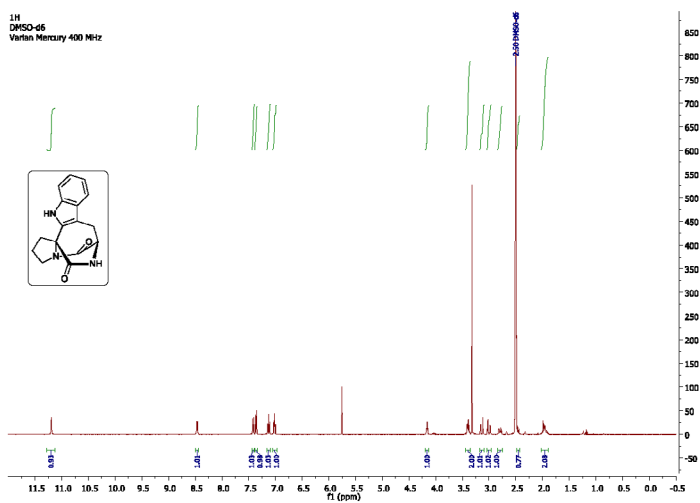
Chemical structure of the compound is shown in the inset.

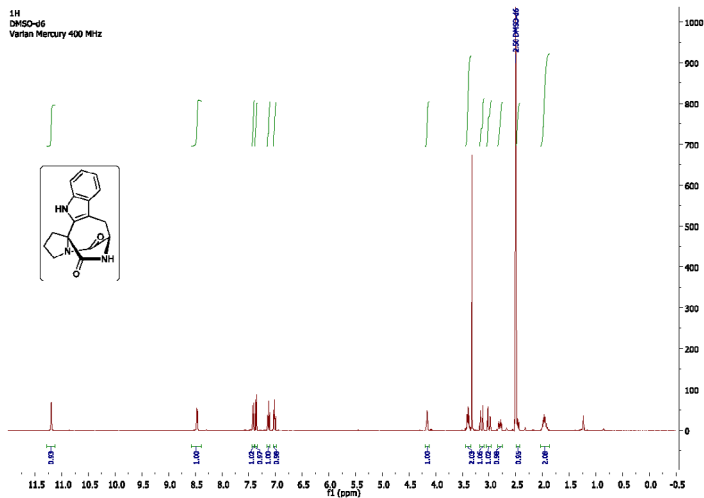
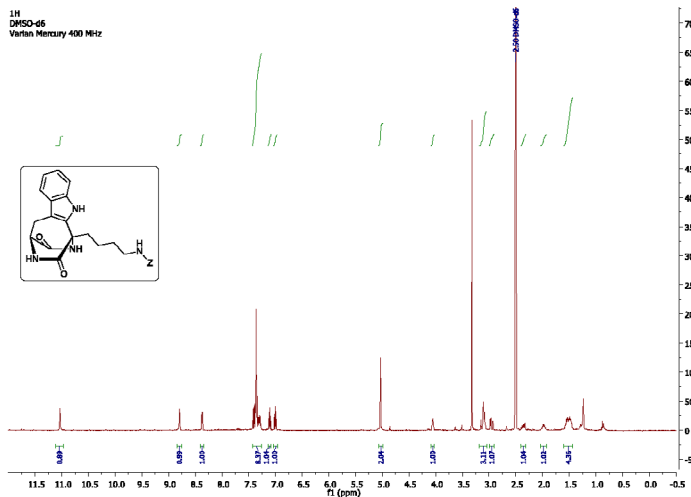
Chemical shift (ppm) values (from left to right):

- 176.77, 163.27
- 139.71, 139.03, 138.03
- 132.04, 129.88, 119.88
- 113.87, 98.94
- 64.10, 64.06
- 44.17
- 39.83, 39.60, 39.50
- 22.18, 22.06, 21.98

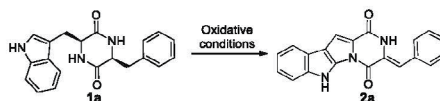
Intensity (Y-axis) ranges from 0 to 40,000.

Chemical shift (ppm) ranges from 0 to 200.

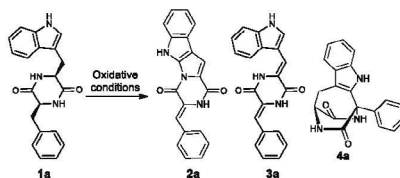
Oxidized cyclo(Pro_L-Trp_L) (4g) DEPT NMROxidized cyclo(Pro_D-Trp_D) (4h) ¹H NMR

Oxidized cyclo(Pro_L-Trp_O) (4h) ¹H NMROxidized cyclo[Lys(z)-Trp] (4i) ¹H NMR

Oxidative screening experiments. Supplementary tables

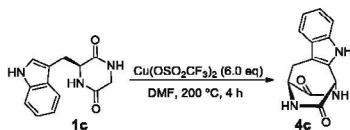
Table S1. First oxidative screening upon c(Phe-Trp) diketopiperazine **1a**.

T (°C)	Oxidant (eq)	Solvent	Time (h)	2a (HPLC-MS conversion %)
120	TBH (3.0)	1-butanol	26	-
RT	FeCl ₃ (3.0)	CH ₂ Cl ₂	24	-
RT	PIFA (3.0)	DMSO	23	-
120	BQ (3.0)	DMF	25	-
reflux	DLP (3.0)	CH ₂ Cl ₂ :H ₂ O (1:0.2)	30	-
170	DLP (3.0)	DMSO	24	< 5
77	MnO ₂ (100)	AcOEt	20	< 5
70	DTBP (3.0)	CHCl ₃ :DMF (1:0.1)	18	-
140	DTBP (4.0)	DMF	48	< 5
140	DTBP:FeCl ₃ (4.0:0.2)	DMF	24	-
120	DDQ:FeCl ₃ (3.0:0.1)	DMF	37	16
80	DDQ (3.0)	^t BuOH	27	-
120	DDQ (3.0)	DMF	39	25

Table S2. Oxidative screening upon c(Phe-Trp) diketopiperazine **1a**.^a

Entry	Oxidant (eq)	Additive (eq)	Time	2a ^b	3a	4a
1 ^b	PhI(OAc) ₂ (1.1)	-	4 h	-	-	-
2	PdCl ₂ (3.0)	2,5-lutidine (6.0) Ag ₂ CO ₃ (3.0)	4 h	-	19	5
3	CuCl ₂ (6.0)	-	4 h	-	-	-
4	Cu(OAc) ₂ (6.0)	-	4 h	14	59	3
5	Cu(OCOCF ₃) ₂ (6.0)	-	4 h	1	42	28
6	Cu(OSO ₂ CF ₃) ₂ (6.0)	-	4 h	-	4	71
7	Cu(OAc) ₂ (6.0)	DDQ (1.0)	4 h	3	45	4
8	Mn(OAc) ₃ (6.0)	DDQ (1.0)	4 h	-	12	4
9	Mn(OAc) ₃ (6.0)	Cu(OAc) ₂ (1.0)	4 h	-	6	20
10	MnO ₂ (6.0)	Cu(OAc) ₂ (1.0)	4 h	-	-	-
11	Cu(OAc) ₂ (6.0)	TFA (3.0)	4 h	-	32	31
12	Cu(OAc) ₂ (6.0)	2,5 lutidine (6.0)	4 h	1	44	4

^a 30 mg of DKP (0.09 mmol), C:0.2-0.3M, DMF, T: 200 °C, ^b T: r.t, HPLC. ^b Values are given in (%).

Table S3. Optimization of Cu(II)-based oxidation upon c(Gly-Trp) diketopiperazine **1c**.^a

T (°C)	Oxidant (eq)	Additive (eq)	Solvent	Time	Product (%) ^b
200	Cu(OCOCF ₃) ₂ (6.0)	-	DMF	4 h	90
200	Cu(OAc) ₂ (6.0)	-	DMF	4 h	75
200	Cu(OSO ₂ CF ₃) ₂ (6.0)	-	DMF	4 h	40
200	Cu(OCOCF ₃) ₂ (6.0)	-	DMF	2 h	74
200	Cu(OCOCF ₃) ₂ (4.0)	-	DMF	4 h	70
150	Cu(OCOCF ₃) ₂ (6.0)	-	DMF	16 h	68
150 (MW)	Cu(OCOCF ₃) ₂ (6.0)	-	DMF	30 min	49
150 (MW)	Cu(OCOCF ₃) ₂ (2.0)	TFA (4.0)	DMF	30 min	66
150 (MW)	Cu(OCOCF ₃) ₂ (2.0)	-	DMF	30 min	54
120 (MW)	Cu(OCOCF ₃) ₂ (2.0)	TFA (4.0)	DMF	30 min	69
120 (MW)	Cu(OCOCF ₃) ₂ (4.0)	TFA (4.0)	DMF	30 min	92
120 (MW)	Cu(OCOCF ₃) ₂ (4.0)	TFA (2.0)	DMF	30 min	86

^a 30 mg of DKP (0.12 mmol), C: 0.2 M. ^b Conversion estimated by HPLC-MS. ^c C: 0.4 M.

Chiral chromatography of oxidized DKPs (4g-h)

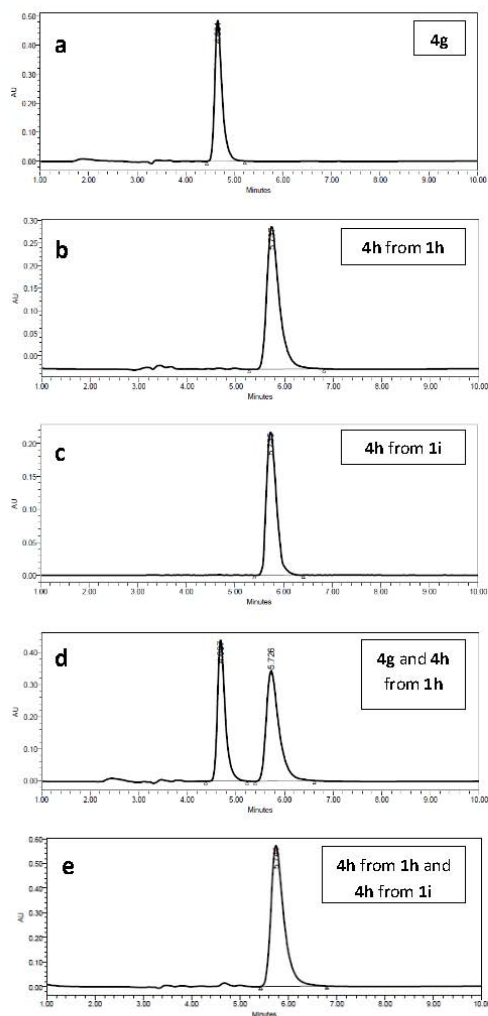


Figure S1. Chiral chromatograms of a) **4g**, b) **4h** from **1h**, c) **4h** from **1i**, d) co-injection of **4g** from **1g** and **4h** from **1h**, e) co-injection of **4h** from **1h** and **4h** from **1i**. Linear gradient of ACN (+0.036% TFA) into H₂O (+0.045% TFA) from 50% to 70% ACN for 30 min.

Proposed mechanism for the decarboxylation of Asp-containing DKP

Asp(^tBu)-containing DKP **1f** underwent decarboxylation to yield the oxidized c(Ala-Trp) **4e**. Since no traces of decarboxylated starting DKP **1f** were detected by HPLC-MS analysis, it was proposed a mechanism where the initial DKP undergoes decarboxylation once the dehydrogenative C-C bond is formed to yield compound **4e** (Fig. S2). Incidentally, use of alternative non-acid labile protecting groups for Asp (*i.e.* -Allyl, -Bzl) was detrimental for the outcome of the CDC reaction.

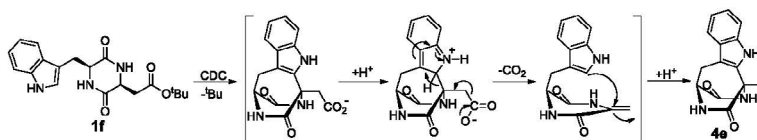


Figure S2. Plausible mechanism for the decarboxylation of compound **4e**.

Proposed 1,4-hydride shift within iminium forms for the CDC

The high conversion observed for different DKPs suggests a high α -C selectivity for the C-C bond formation, which is remarkable taking into consideration that two N-iminium intermediates are possible. This may be attributed to an hypothetical 1,4-hydride shift within the two iminium forms. The following mechanism proposal was based on other 1,4-hydride shifts reported in the literature²⁻⁵ as well as hydrogen tunneling and relay mechanisms^{6,7} (Fig. S3). Moreover, the cyclization via the nucleophilic attack of the indole ring to the N-iminium of Trp residue would arise a highly strained four-member cycle.

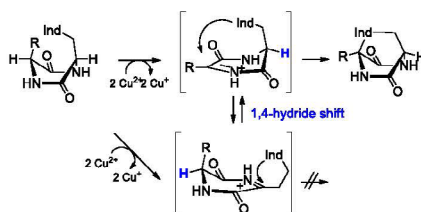


Figure S3. Hypothetical 1,4-hydride shift within iminium intermediates generated during CDC.

Bibliography

- 1 S. Preciado, L. Mendive-Tapia, C. Torres-García, R. Zamudio-Vázquez, V. Soto-Cerrato, R. Pérez-Tomás, F. Albericio, E. Nicolás and R. Lavilla, *Med. Chem. Comm.*, 2013, **4**, 1171–1174.
- 2 D. Vasu, S. K. Pawar and R. S. Liu, *Beilstein J. Org. Chem.*, 2013, **9**, 1751–1756.
- 3 T. Suzuki, Y. Yoshimoto, T. Takeda, H. Kawai and K. Fujiwara, *Chem. Eur. J.*, 2009, **15**, 2210–2216.
- 4 J. Ben Ari, M. Karni, Y. Apeloig and A. Mandelbaum, *Int. J. Mass Spectrom.*, 2003, **228**, 297–306.
- 5 J. M. Veauthier, A. Chow, G. Fraenkel, S. J. Geib and N. J. Cooper, *Organometallics*, 2000, **19**, 3942–3947.
- 6 L. Cheng, C. Doubleday and R. Breslow, *Proc. Natl. Acad. Sci. U. S. A.*, 2015, **112**, 4218–4220.
- 7 P. K. Agarwal, S. P. Webb and S. Hammes-Schiffer, *J. Am. Chem. Soc.*, 2000, **122**, 4803–4812.

SOBRE LA AUTORA



EDUCACIÓN

15/01/2013-24/02/2017. Doctorado en Química Organica. Universidad de Barcelona, España. Sobresaliente Cum Laude con Mención Internacional.

03/10/2011-21/12/2012. Máster en Química Avanzada (especialidad Química Orgánica). Universidad de Barcelona, España. Nota ponderada: 8.9 (escala 1-10).

15/09/2007-15/06/2011. Licenciatura en Química. Universidad de Barcelona, España. Nota ponderada: 8.7 (escala 1-10).

EXPERIENCIA PROFESIONAL

- Posición actual:

02/10/2017-actualidad. Postdoctoral Research Associate, Centre for Inflammation Research, University of Edinburgh, UK.

- Posiciones previas:

01/07/2012-17/03/2017. Investigadora en Química Orgánica, Parque Científico de Barcelona, España.

Desarrollo de nuevas metodologías sintéticas para la preparación de compuestos bioactivos.

01/07/2011-30/06/2012. Investigadora en Química Orgánica, Instituto de Investigación Biomédica, España.

Desarrollo de nuevos grupos funcionales para la síntesis de péptidos.

- Estancias de investigación:

01/05/2015-31/07/2015. Estancia doctoral, University of Edinburgh, UK.

Sondas químicas para la detección de apoptosis.

01/07/2011-31/07/2011. Estancia pregraduado, Departamento de Química Orgánica, Universidad de Barcelona, España.

BECAS Y RECONOCIMIENTOS

2018 Premio Enrique Fuentes Quintana Tesis Doctoral
 2018 Beca Alfonso Martín Escudero
 2017 Premio extraordinario Tesis Doctoral – UB
 2013 Beca de doctorado FPU–MECD (2013-2017)
 2012 Beca de máster (Instituto de Investigación Biomédica)
 2011 Estancia en prácticas Parque Científico de Barcelona.
 2007-2011 Beca de estudios universitarios - MECD

PUBLICACIONES

Mendive-Tapia, L.; Subiros-Funosas, R.; Zhao, C.; Albericio, F.; Read, N. D.; Lavilla, R.; Vendrell, M., *Nat. Protoc.* 2017, 12, 1588–1619.

Subiros-Funosas, R.[#]; **Mendive-Tapia, L.[#]**; Sot, J.; Pound, J. D.; Barth, N.; Varela, Y.; Goñi, F. M.; Paterson, M.; Gregory, C. D.; Albericio, F.; Dransfield, I.; Lavilla, R.; Vendrell, M., *Chem. Commun.*, 2017, 53, 945–948. [#] Both researchers contributed equally to this work.

Mendive-Tapia, L.; Albornoz-Grados, A.; Bertran, A.; Albericio, F.; Lavilla, R., *Chem. Commun.*, 2017, 53, 2740–2743.

Mendive-Tapia, L.; Zhao, C.; Akram, A. R.; Preciado, S.; Albericio, F.; Lee, M.; Serrels, A.; Kielland, N.; Read, N. D.; Lavilla, R.; Vendrell, M., *Nat. Commun.* 2016, 7: 10940.

Mendive-Tapia, L.; Bertran, A.; García, J.; Acosta, G.; Albericio, F.; Lavilla, R., *Chem. Eur. J.*, 2016, 22, 1–7.

González, R.; **Mendive-Tapia, L.**; Pastian, M. B.; Albericio, F.; Lavilla, R.; Cascone, O.; Iannucci, N. B., *J. Pept. Sci.* 2016, 22, 123–128.

Mendive-Tapia, L.; Preciado, S.; García, J.; Ramón, R.; Kielland, N.; Albericio, F.; Lavilla, R., *Nat. Commun.* 2015, 6: 7160.

Preciado, S.[#]; Mendive-Tapia, L.[#]; Albericio, F.; Lavilla, R., *J. Org. Chem.* 2013, 78, 8129–8135. [#] Both researchers contributed equally to this work.

Preciado, S.; **Mendive-Tapia, L.**; Torres García C.; Zamudio-Vázquez R.; Soto-Cerrato, V.; Pérez-Tomás, R.; Albericio, F.; Nicolás E.; Lavilla, R., *Med. Chem. Comm.* 2013, 4, 1171–1174.

Ramos-Tomillero, I.[#]; **Mendive-Tapia, L.[#]**; Góngora Benítez, M.; Nicolás, E.; Tulla-Puche, J.; Albericio, F., *Molecules*, 2013, 18, 5155–5162. [#] Both researchers contributed equally to this work.

Góngora Benítez, M.; **Mendive-Tapia, L.**; Ramos-Tomillero, I.; Breman, A. C.; Tulla-Puche, J.; Albericio, F., *Org. Lett.* 2012, 14, 5472–5475.

PATENTE

- Fluorogenic compounds, process of preparation thereof and methods of use.

WO 2016207626 (PCT/GB2016/051864). Acuerdos de licencias: Merck y Cambridge Research Biomedicals (CRB)

ORGANIZACIÓN Y SUPERVISIÓN

2016-2017. Profesor asistente de Prácticas Avanzadas de Laboratorio, como miembro en el Departamento de Química Orgánica (Universidad de Barcelona).

2016-2017. Miembro del Comité Organizador del III y IV Simposio de Jóvenes Investigadores de la Sociedad Española de Química Terapéutica (SEQT), junio 2016 y mayo 2017, España.

EVENTOS ACADÉMICOS Y PRESENTACIONES EN CONFERENCIAS INTERNACIONALES

- XXXVI Reunión Bienal de la Real Sociedad Española de Química (RSEQ). Comunicación oral, Sitges, junio 2017.
- Curso de química médica (Drug Discovery Workshop), empresa Lilly, Madrid, 2015.
- Institute for Research in Biomedicine (IRB) retreat. Comunicación oral, Hospital de Sant Pau, Barcelona, febrero 2015.
- VII International School on Organometallic Chemistry Marcial Moreno Mañas. Comunicación oral, Universidad Autónoma de Barcelona (UAB), Junio 2014.

Últimos números publicados

N.º 1. GRAPHENE-BASED NANOMATERIALS INNOVATIVE TOOLS IN ELECTROCHEMICAL AND MICROFLUIDIC (BIO-)-SENSING AND IN MICROMOTORS DESIGN (*Serie Ciencias de la Salud*)

Por Aída Martín Galán

N.º 2. CONICAL REFRACTION: FUNDAMENTALS AND APPLICATIONS (*Serie Ingeniería, Matemáticas, Arquitectura y Física*)

Por Alejandro Turpin Avilés

N.º 3. LAS VERSIONES CASTELLANAS MEDIEVALES DE LA CONSOLATIO PHILOSOPHIAE DE BOECIO (*Serie Humanidades*)

Por Antonio Doñas Beleña

N.º 4. ESSAYS ON FAMILIARITY AND CHOICE (*Serie Ciencias Sociales*)

Por Francesco Cerigioni

N.º 5. DISTRIBUTIONAL ANALYSIS OF CLIMATE CHANGE MITIGATION POLICIES (*Serie Ciencias Sociales*)

Por Xaquín García-Muros

N.º 6. TOPOLOGICAL PHASES OF MATTER AND OPEN QUANTUM SYSTEMS (*Serie Ingeniería, Matemáticas, Arquitectura y Física*)

Por Oscar Viyuela García

 funcas

PREMIOS
ENRIQUE
FUENTES
QUINTANA

2018

Pedidos e información:

Funcas

Caballero de Gracia, 28

28013 Madrid

Teléfono: 91 596 54 81

Fax: 91 596 57 96

publica@funcas.es

www.funcas.es

P.V.P.: Edición papel, 12€ (IVA incluido)

P.V.P.: Edición digital, gratuita

ISBN 978-84-17609-12-2

